frontiers | Research Topics

Combinational immunotherapy of cancer: Novel targets, mechanisms, and strategies

Edited by
Xuyao Zhang, Xian Zeng, Yubin Li and Dianwen Ju

Published in
Frontiers in Immunology
Frontiers in Oncology

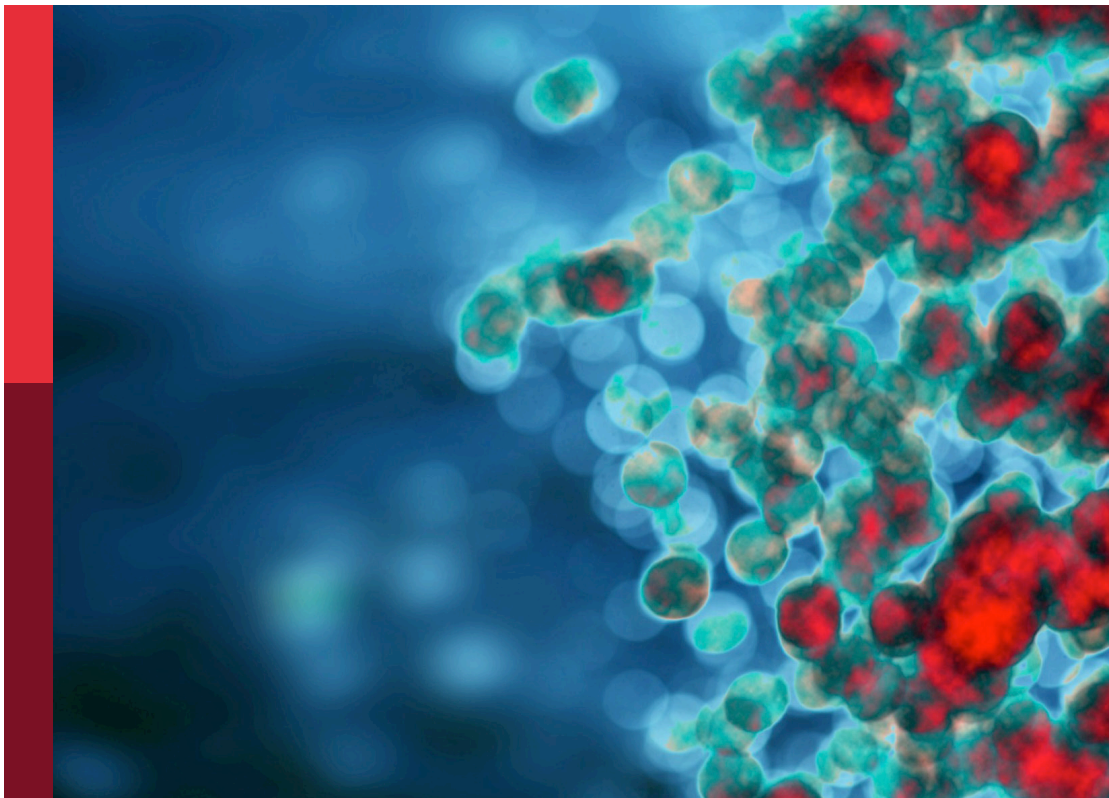

ISSN 1664-8714
ISBN 978-2-8325-3972-9
DOI 10.3389/978-2-8325-3972-9

About Frontiers

Frontiers is more than just an open access publisher of scholarly articles: it is a pioneering approach to the world of academia, radically improving the way scholarly research is managed. The grand vision of Frontiers is a world where all people have an equal opportunity to seek, share and generate knowledge. Frontiers provides immediate and permanent online open access to all its publications, but this alone is not enough to realize our grand goals.

Frontiers journal series

The Frontiers journal series is a multi-tier and interdisciplinary set of open-access, online journals, promising a paradigm shift from the current review, selection and dissemination processes in academic publishing. All Frontiers journals are driven by researchers for researchers; therefore, they constitute a service to the scholarly community. At the same time, the *Frontiers journal series* operates on a revolutionary invention, the tiered publishing system, initially addressing specific communities of scholars, and gradually climbing up to broader public understanding, thus serving the interests of the lay society, too.

Dedication to quality

Each Frontiers article is a landmark of the highest quality, thanks to genuinely collaborative interactions between authors and review editors, who include some of the world's best academicians. Research must be certified by peers before entering a stream of knowledge that may eventually reach the public - and shape society; therefore, Frontiers only applies the most rigorous and unbiased reviews. Frontiers revolutionizes research publishing by freely delivering the most outstanding research, evaluated with no bias from both the academic and social point of view. By applying the most advanced information technologies, Frontiers is catapulting scholarly publishing into a new generation.

What are Frontiers Research Topics?

Frontiers Research Topics are very popular trademarks of the *Frontiers journals series*: they are collections of at least ten articles, all centered on a particular subject. With their unique mix of varied contributions from Original Research to Review Articles, Frontiers Research Topics unify the most influential researchers, the latest key findings and historical advances in a hot research area.

Find out more on how to host your own Frontiers Research Topic or contribute to one as an author by contacting the Frontiers editorial office: frontiersin.org/about/contact

Combinational immunotherapy of cancer: Novel targets, mechanisms, and strategies

Topic editors

Xuyao Zhang — Fudan University, China
Xian Zeng — Fudan University, China
Yubin Li — GlaxoSmithKline, United States
Dianwen Ju — Fudan University, China

Citation

Zhang, X., Zeng, X., Li, Y., Ju, D., eds. (2023). *Combinational immunotherapy of cancer: Novel targets, mechanisms, and strategies*. Lausanne: Frontiers Media SA. doi: 10.3389/978-2-8325-3972-9

The authors declare that the research was conducted in the absence of any commercial or financial relationships that could be construed as a potential conflict of interest.

Table of contents

frontiers | Frontiers in Immunology

ORIGINAL RESEARCH
published: 01 July 2022
doi: 10.3389/fimmu.2022.912180

Peripheral Blood Lymphocyte Subsets Predict the Efficacy of Immune Checkpoint Inhibitors in Non–Small Cell Lung Cancer

Kang Miao, Xiaotong Zhang, Hanping Wang, Xiaoyan Si, Jun Ni, Wei Zhong, Jing Zhao, Yan Xu, Minjiang Chen, Ruili Pan, Mengzhao Wang†† and Li Zhang*††*

Department of Pulmonary and Critical Care Medicine, Peking Union Medical College Hospital, Chinese Academy of Medical Sciences & Peking Union Medical College, Beijing, China

OPEN ACCESS

Edited by:
Xuyao Zhang,
Fudan University, China

Reviewed by:
Dongqing Wei,
Shanghai Jiao Tong University, China
Jun-Ling Li,
Chinese Academy of Medical Sciences and Peking Union Medical College, China
Shucai Zhang,
Capital Medical University, China

***Correspondence:**
Li Zhang
zhanglipumch1026@sina.com
Mengzhao Wang
mengzhaowang@sina.com

†These authors share last authorship

Specialty section:
This article was submitted to Cancer Immunity and Immunotherapy, a section of the journal Frontiers in Immunology

Received: *04 April 2022*
Accepted: *02 June 2022*
Published: *01 July 2022*

Citation:
Miao K, Zhang X, Wang H, Si X, Ni J, Zhong W, Zhao J, Xu Y, Chen M, Pan R, Wang M and Zhang L (2022) Peripheral Blood Lymphocyte Subsets Predict the Efficacy of Immune Checkpoint Inhibitors in Non–Small Cell Lung Cancer. Front. Immunol. 13:912180. doi: 10.3389/fimmu.2022.912180

Background: Non–small cell lung cancer (NSCLC) has entered the era of immunotherapy. However, only partial patients were able to benefit from immune checkpoint inhibitors (ICIs). Currently, biomarkers for predicting patients' response to ICIs are primarily tumor tissue dependent and have limited accuracy. There is an urgent need to explore peripheral blood-based biomarkers to predict the efficacy and safety of ICI therapy.

Methods: To explore the correlation between lymphocyte subsets and the efficacy and safety of ICIs, we retrospectively analyzed peripheral blood lymphocyte subsets and survival prognosis data of 136 patients with stage IV NSCLC treated with ICIs.

Results: The two factors that had the greatest impact on the prognosis of patients with NSCLC treated with ICIs were $CD4^+CD45RA^-$ T cell (HR = 0.644, P = 0.047) and $CD8^+$ T/lymphocyte (%) (HR = 1.806, P = 0.015). $CD4^+CD45RA^-$ T cell showed excellent predictive efficacy (AUC = 0.854) for ICIs monotherapy, with a sensitivity of 75.0% and specificity of 91.7% using $CD4^+CD45RA^-$ T cell >311.3 × 10^6/L as the threshold. In contrast, $CD8^+$ T/lymphocyte (%) was only associated with the prognosis but had no predictive role for ICI efficacy. $CD4^+$ T cell and its subsets were significantly higher in patients with mild (grades 1–2) immune-related adverse events (irAEs) than those without irAEs. $CD8^+CD38^+$ T cell was associated with total irAEs and severe (grades 3–4) irAEs but was not suitable to be a predictive biomarker.

Conclusion: Peripheral blood $CD4^+CD45RA^-$ T cell was associated with the prognosis of patients with NSCLC applying ICIs, whereas $CD8^+CD38^+$ T cell was associated with irAEs and severe irAEs.

Keywords: immune checkpoint inhibitors (ICIs), lymphocyte subsets, $CD4^+CD45RA^-$ T cell, biomarker, $CD8^+CD38^+$ T cell

Abbreviations: NSCLC, non–small cell lung cancer; ICIs, immune checkpoint inhibitors; irAEs, immune-related adverse events; ORR, objective response rate; ECOG PS, eastern Cooperative Oncology Group performance status; PFS, progression-free survival; IQR, interquartile range; ROC, receiver operating characteristic curve; PD, progressive disease; AUC, area under the curve; TMB, tumor mutational burden; MSI, microsatellite instability; TIL, tumor-infiltrating lymphocytes; OS, overall survival.

BACKGROUND

Immune checkpoint inhibitors (ICIs), represented by cytotoxic T lymphocyte-associated antigen 4 (CTLA-4) inhibitors, programmed cell death protein 1 (PD-1) inhibitors, and programmed cell death protein ligand 1 (PD-L1) inhibitors, have transformed cancer treatment since ipilimumab was first approved for melanoma in 2011 (1). ICIs bring lasting objective remission to patients with cancer by activating autologous lymphocytes. Currently, they have been approved for multiple indications including melanoma, non–small cell lung cancer (NSCLC), and head and neck squamous carcinoma. The approved ICIs in NSCLC are mainly PD-1 inhibitors, including pembrolizumab, nivolumab, camrelizumab, and tislelizumab (2). Although PD-L1 is currently the best biomarker for predicting the efficacy of ICIs in patients with NSCLC, the accuracy is still limited. However, not all patients with NSCLC can benefit from ICI therapy. Keynote-042 study showed that only 27.3% patients with positive PD-L1 were able to achieve an objective response from pembrolizumab monotherapy. In addition, the objective response rate (ORR) was only 39.1% even in those with PD-L1 ≥ 50% (3). Nevertheless, patients with low or negative PD-L1 expression may also achieve favorable efficacy from immunotherapy (4). In addition, current biomarkers for predicting patients' response to ICIs are primarily tumor tissue dependent. Therefore, exploring new biomarkers that can predict the efficacy and safety of ICIs has become an urgent need.

The key factor for immunotherapy is to activate the lymphocytes; thus, the quantity and subset of lymphocytes are closely related to the efficacy of ICIs. T cell constitute the main effector cells involved in the immune response, which can be generally classified into cytotoxic T cell ($CD8^+$) and regulatory T cell ($CD4^+$). By detecting CD45RA, CD28, and CD38 molecules on the surface of T cell, they can be further categorized into memory subsets, functional subsets, and activated subsets (5). $CD8^+$ T cells are essential participants in the anti-tumor immune response for their cytotoxicity and ability to migrate from peripheral blood into tumor tissues (6). Studies have shown that the counts of infiltrating $CD8^+$ T cell were intimately associated with the antitumor efficacy of PD-1 inhibitors (7). In contrast to the direct tumor-killing effect of $CD8^+$ T cells, $CD4^+$ T cells play more of an immune-modulatory and paracrine role. $CD4^+$ Th1 cells promote the differentiation of initial $CD8^+$ T cell into cytotoxic T lymphocytes (CTL) through the CD70-CD27 pathway and secreting cytokines, such as interferon γ (IFN-γ) and interleukin 2 (IL-2) (8). Recently, several clinical studies have shown that the peripheral blood $CD4^+$ T subsets may be associated with tumor objective response for immunotherapy (9, 10).

Herein, we conducted a retrospective study to analyze the correlation between baseline peripheral blood lymphocyte subsets and tumor regression after ICI therapy to explore the applicability of lymphocyte subsets to be a potential biomarker.

METHODS

Study Objectives and Ethics Approval Statement

Our retrospective study collected baseline lymphocyte subset data and the follow-up information of 136 patients with stage IV NSCLC treated with ICIs. The aim was to explore the correlation between lymphocyte subsets and the therapeutic effect of ICIs and to find a new biomarker for ICI therapy. The study design was in accordance with the ethical guidelines of the Declaration of Helsinki, and ethical approval was obtained from the Ethical Review Committee of Peking Union Medical College Hospital. Informed consent was waived due to the retrospective character.

Inclusion and Exclusion Criteria

Inclusion criteria: (i) patients were pathologically confirmed NSCLC; (ii) the disease stage was stage IV; (iii) patients utilized ICIs during the course of treatment; and (iv) lymphocyte subsets were detected within 28 days before the first dose of ICIs. Exclusion criteria: (i) the follow-up period after ICI therapy <6 months; and (ii) received two or more types of ICI therapy.

Data Collection

For each patient who met the inclusion criteria, we obtained the following information separately: (i) baseline lymphocyte subset data, including total lymphocytes, B cell, T cell, NK cells, $CD4^+$ T cell, $CD8^+$ T cell, $CD4^+CD45RA^-$ T cell, $CD4^+CD45RA^+$ T cell, $CD4^+CD28^+$ T cell, $CD8^+CD28^+$ T cell, $CD8^+DR^+$ T cell, $CD8^+CD38^+$ T cell, $CD4^+$ T cell/lymphocyte (%), and $CD8^+$ T cell/lymphocyte (%); (ii) patient basic information, including gender, age, tumor pathology, history of smoking, history of alcohol consumption, and eastern Cooperative Oncology Group performance status (ECOG PS) score; (iii) treatment details, including the lines of ICIs applied and whether combined with chemotherapy; (iv) efficacy and safety assessment, including ORR, progression-free survival (PFS), and irAEs.

Data Analysis

IBM SPSS version 24.0 was used for statistical analysis, and GraphPad Prism version 8.0.1 was used to graph the statistics. Median and interquartile range (IQR) were used for description of baseline lymphocyte subsets due to non-conformance with normal distribution. Patients with disease control and PFS ≥6 months were recorded as benefit group, whereas those with progressive disease (PD) or PFS <6 months were recorded as non-benefit group. Comparisons of the average values were analyzed using the Mann–Whitney test. Patient basic information and treatment details were described as count values and percentages. The receiver operating characteristic (ROC) curve was established to assess the value of efficacy prediction. $CD4^+CD45RA^-$ T cell and $CD8^+$ T/lymphocyte (%) were divided into high-level group and low-level group according to the median. Correlations between them and patient basic information were analyzed by the chi-square test. Kaplan–Meier survival curves were used to reflect differences in survival benefit. Log-rank test was used to explore the effect of basic

information, treatment details, and baseline lymphocyte subsets on the efficacy of ICIs. Logistic regression was used to analyze the risk factors for irAEs and severe irAEs. All independent variables were included in the univariate regression, and then indicators that reached the threshold ($P < 0.2$) were included into multivariate regression. $P < 0.05$ was determined to be with statistical difference.

RESULTS

Basic Characteristics of the Patients

A total of 136 patients with stage IV NSCLC met the inclusion and exclusion criteria. Among them, 94 were male and 42 were female, with a median age of 64 years old. There were more patients with non-squamous NSCLC (75 patients) than squamous NSCLC (61 patients). The majority of patients (71 patients) chose ICIs for first-line treatment, whereas 47 patients (34.6%) for the second line and 10 patients (13.2%) for the third line and beyond. Only a quarter of patients chose ICIs as monotherapy (de-chemotherapy), which means that most of patients applied ICIs combined with chemotherapy. There were 61.8% patients had smoking history and 29.4% had alcohol consumption history. Most of patients were in good physical condition on ICIs, 90.5% patients were of 0-1 ECOG PS scores **(Table 1)**. The overall ORR of the patients was 42.6%, with a median PFS of 8.5 months. Immune-related adverse events (irAEs) occurred in 49 (36.0%) patients, of which 24 (17.6%) were grade 3 or higher.

Correlation of Lymphocyte Subsets With the Efficacy of ICIs

To explore the relationship between baseline lymphocyte subsets and the efficacy of ICIs, patients were divided into two groups based on survival benefit. Patients with disease control and PFS ≥6 months were recorded as benefit group, whereas those with PD or PFS <6 months were recorded as non-benefit group. The counts of total lymphocytes and all lymphocyte subsets were higher in the benefit group than in the non-benefit group. Among them, total lymphocytes, B cell, T cell, $CD4^+$ T cell, various $CD4^+$ T cell subsets ($CD4^+CD45RA^-$ T cell, $CD4^+CD45RA^+$ T cell, and $CD4^+CD28^+$ T cell), and $CD8^+CD28^+$ T cell showed statistical differences ($P < 0.05$) **(Figure S1)**. In addition, we explored changes in lymphocyte subsets after two cycles of ICI treatment. However, only total T cells showed a decreasing trend in the benefit group **(Figure S2)**. Patient basic information was included into univariate cox regression analysis together with baseline lymphocyte subsets **(Table 2)**. The results showed that gender ($P = 0.196$), age ($P = 0.191$), type of pathology ($P = 0.080$), lines of ICIs usage ($P = 0.199$), ECOG PS score ($P = 0.064$), B cell ($P = 0.174$), $CD4^+CD45RA^-$ T cell ($P = 0.016$), and $CD8^+$ T/lymphocyte (%) ($P = 0.006$) may contribute to the prognosis (threshold: $P < 0.2$). Multivariate cox regression showed that the two factors with the greatest impact were $CD4^+CD45RA^-$ T cell (HR = 0.644, $P = 0.047$) and $CD8^+$ T/lymphocyte (%) (HR = 1.806, $P = 0.015$), respectively **(Table 3)**.

Further, we performed a systematic analysis for these two biomarkers. Baseline $CD4^+CD45RA^-$ T cells ($P = 0.001$) were significantly higher in the benefit group, whereas $CD8^+$ T/lymphocytes (%) were lower in the benefit group ($P = 0.09$) **(Figures 1A, D)**. However, they were not ideal biomarker for predicting the prognosis of patients with NSCLC, with the area under the curve (AUC) of the ROC being just 0.657 and 0.592 **(Figures 1B, E)**. Kaplan–Meier survival curve showed that the high $CD4^+CD45RA^-$ T-cell group (median PFS: 11.8 months) had a significantly better PFS benefit than the low $CD4^+CD45RA^-$ T-cell group (median PFS: 5.9 months) ($P = 0.016$). There was also a difference in survival prognosis between the high $CD8^+$ T/lymphocyte (%) group (median PFS: 6.3 months) and the low $CD8^+$ T/lymphocyte (%) group (median PFS: 11.8 months) ($P = 0.006$) but showing an opposite trend to $CD4^+CD45RA^-$ T cell **(Figures 1C, F)**.

Subgroup Analysis

Considering that the patients included in this study were treated with ICIs monotherapy and ICIs combined with chemotherapy. The analysis of total population only represents the survival

TABLE 1 | Basic information.

Basic Information	Number
Patients	136
Sex	
male	94 (69.1%)
female	42 (30.9%)
Age	64 (60–70)
<60	33 (24.3%)
≥60	103 (75.7%)
Histology	
Non-squamous carcinoma	75 (55.1%)
Squamous carcinoma	61 (44.9%)
Line of therapy	
First line	71 (52.2%)
Second line	47 (34.6%)
Third line and beyond	10 (13.2%)
Combined chemotherapy	
No	32 (23.5%)
Yes	104 (76.5%)
Smoking status	
No	52 (38.2%)
Yes	84 (61.8%)
Drinking status	
no	96 (70.6%)
yes	40 (29.4%)
ECOG PS	
0	70 (51.5%)
1	53 (39.0%)
2–4	13 (9.6%)
Total lymphocyte ($\times10^6$/L)	1295.2 (973.1–1728.4)
B cell ($\times10^6$/L)	94.7 (57.1–175.6)
T cell ($\times10^6$/L)	916.6 (639.4–1221.1)
NK cell ($\times10^6$/L)	258 (164.4–360.1)
$CD4^+$ T ($\times10^6$/L)	475.9 (302.4 - 668)
$CD8^+$ T ($\times10^6$/L)	340.1 (237.5 - 493.3)
$CD4^+CD45RA^-$ T ($\times10^6$/L)	348.3 (218.3 - 510.1)
$CD4^+CD45RA^+$ T ($\times10^6$/L)	109.1 (49.4 - 189.1)
$CD4^+CD28^+$ T ($\times10^6$/L)	413.1 (257.7 - 613.7)
$CD8^+CD28^+$ T ($\times10^6$/L)	152.2 (94.9 - 219.7)
$CD8^+DR^+$ T ($\times10^6$/L)	176.3 (112.3 - 264.2)
$CD8^+CD38^+$ T ($\times10^6$/L)	151.7 (91.3 - 208.9)
$CD4^+$ T/lymphocyte (%)	36.1 (29.1 - 45.4)
$CD8^+$ T/lymphocyte (%)	26.9 (21.7 - 35.4)

prognosis, but not the efficacy of ICIs. Therefore, a subgroup of 32 patients treated with ICIs monotherapy was selected for further analysis. In this subgroup, $CD4^+CD45RA^-$ T cell showed a more significant difference (p = 0.002) between the benefit and non-benefit groups (**Figure 2A**). Notably, its efficacy as a biomarker to predict the therapeutic benefit of ICIs is also excellent (AUC = 0.854), with a sensitivity of 75.0% and specificity of 91.7% using $CD4^+CD45RA^-$ T cell >311.3 × 10^6/L as the threshold (**Figure 2B**). The results of Kaplan–Meier survival curves also demonstrated close relationship between $CD4^+CD45RA^-$ T cell and the efficacy of ICIs. The median PFS was not reached in the $CD4^+CD45RA^-$ T-cell high group and 5.2 months in the $CD4^+CD45RA^-$ T-cell low group (P < 0.001) (**Figure 2C**). However, $CD8^+$ T/lymphocyte (%) did not show a better correlation with the efficacy of ICIs, with no significant difference (P = 0.075) (**Figure 2D**). In addition, the AUC was only 0.673 of $CD8^+$ T/lymphocyte (%), which was considerably lower than that of CD4+$CD45RA^-$ T cell (**Figure 2E**). There was also no meaningful discrepancy observed between the high-level group and the low-level group of $CD8^+$ T/lymphocyte (%) on the Kaplan–Meier survival curve (P = 0.198) (**Figure 2F**).

Further, we analyzed $CD4^+CD45RA^-$ T cell and $CD8^+$ T/lymphocyte (%) with patient basic information, separately. The results showed that $CD8^+$ T/lymphocytes (%) were well matched for all basic information, whereas $CD4^+CD45RA^-$ T cells were matched for gender, age, pathology type, combination of chemotherapy, smoking history, alcohol consumption history, and ECOG PS score but had strong relevance with lines of ICIs usage (p = 0.003) (**Table 4**). The count of $CD4^+CD45RA^-$ T cell was higher in the first-line treatment than in the second line and beyond (P < 0.001) (**Figure S3**).

In the population of first-line treatment, there was no remarkable difference in $CD4^+CD45RA^-$ T cell between the benefit and non-benefit groups (P = 0.154) (**Figure 3A**). ROC curves showed that $CD4^+CD45RA^-$ T-cell count was not an ideal biomarker (AUC = 0.585) (**Figure 3B**). Kaplan–Meier survival curves also indicated no significant prognostic difference between the high $CD4^+CD45RA^-$ T-cell group and the low $CD4^+CD45RA^-$ T-cell group (P = 0.828) (**Figure 3C**). These findings differ dramatically from those of total population. Therefore, we considered whether the survival benefit in the high $CD4^+CD45RA^-$ T-cell group was more likely to originate from the second-line and beyond population. In this subgroup, $CD4^+CD45RA^-$ T-cell count was significantly higher in the benefit group than in the non-benefit group (P = 0.006) (**Figure 3D**). The AUC was 0.713, at the threshold of $CD4^+CD45RA^-$ T cell >339.9 × 106/L, the sensitivity was 51.6%, and the specificity was 84.6% (**Figure 3E**). The high $CD4^+CD45RA^-$ T-cell group exhibited a notable PFS benefit (median PFS: undefined) compared with the low $CD4^+CD45RA^-$ T-cell group (median PFS: 5.2 months), P = 0.003 (**Figure 3F**).

Correlation of Lymphocyte Subsets With irAEs

In addition, we explored the correlation between peripheral blood lymphocyte subsets and all kinds of irAEs (**Figure S4**). We found that baseline counts of total lymphocytes, T cell, $CD4^+$ T cell, and various $CD4^+$ T-cell subsets ($CD4^+CD45RA^-$ T cell, $CD4^+CD45RA^+$ T cell, and $CD4^+CD28^+$ T cell) were higher in the mild (grades 1–2) irAEs group than in the non-irAEs group. However, the expression of these lymphocyte subsets in the severe (grades 3–4) irAEs group remained at a low level, similar to that in the non-irAEs group. $CD8^+CD38^+$ T cells were the only cell subset that showed statistical differences in the populations of severe irAEs and non-irAEs. Logistic

TABLE 2 | Univariate Cox regression of PFS.

		HR	95% CI	P-value
Sex	Male/female	1.337	0.861-2.075	0.196
Age	<60/≥60	1.412	0.842-2.37	0.191
Histology	Non-squamous/squamous	0.686	0.45-1.046	0.080
Line of therapy	First/second/third and beyond	1.220	0.883-1.686	0.199
Combined chemotherapy	No/yes	1.155	0.696-1.919	0.577
Smoking status	No/yes	0.782	0.513-1.193	0.254
Drinking status	No/yes	1.062	0.683-1.652	0.789
ECOG PS	0/1/2-4	1.338	0.984-1.819	0.064
Total lymphocyte	×10^6	0.788	0.519-1.197	0.264
B cell	×10^6	0.749	0.493-1.136	0.174
T cell	×10^6	0.972	0.641-1.475	0.894
NK cell	×10^6	0.781	0.517-1.178	0.238
$CD4^+$ T	×10^6	0.785	0.517-1.191	0.255
$CD8^+$ T	×10^6	1.150	0.758-1.745	0.511
$CD4^+CD45RA^-$ T	×10^6	0.599	0.395-0.907	0.016
$CD4^+CD45RA^+$ T	×10^6	1.016	0.67-1.54	0.941
$CD4^+CD28^+$ T	×10^6	0.803	0.53-1.216	0.300
$CD8^+CD28^+$ T	×10^6	0.842	0.556-1.274	0.416
$CD8^+DR^+$ T	×10^6	1.021	0.673-1.549	0.922
$CD8^+CD38^+$ T	×10^6	1.049	0.691-1.591	0.823
$CD4^+$ T/lymphocyte	×100%	0.825	0.548-1.248	0.363
$CD8^+$ T/lymphocyte	×100%	1.803	1.182-2.750	0.006

TABLE 3 | Multivariate Cox regression of PFS.

		Median PFS	HR	95% CI	P-value
Sex	Male	8.6 months		Reference	
	Female	7.5 months	1.203	0.718–2.015	0.483
Age	<60	11.8 months		Reference	
	≥60	8.1 months	1.252	0.726–2.161	0.419
Histology	Non-squamous	7.5 months		Reference	
	Squamous	11.7 months	0.793	0.483–1.303	0.360
Line of therapy	First line	10.5 months		Reference	
	Second line	7 months	0.938	0.558–1.576	0.810
	Third line and beyond	5.9 months	1.380	0.603–3.157	0.446
ECOG PS	0	11.5 months		Reference	
	1	7.5 months	1.219	0.775–1.918	0.392
	2–4	5.5 months	1.131	0.510–2.508	0.762
B cell	Low	6.2 months		Reference	
	High	11.2 months	1.035	0.642–1.668	0.887
$CD4^+CD45RA^-$ T	Low	5.9 months		Reference	
	High	11.8 months	0.644	0.417–0.994	0.047
$CD8^+$ T/lymphocyte (%)	Low	11.8 months		Reference	
	High	6.3 months	1.806	1.122–2.905	0.015

regression analysis showed that the total T cells and $CD8^+CD38^+$ T cells were strongly associated with the development of irAEs, whereas $CD4^+$ T-cell subsets did not show statistical contributions to irAEs. In addition, $CD8^+CD38^+$ T cells were also associated with the development of severe irAEs, P = 0.05 (**Table 5**). However, the ROC curve constructed with $CD8^+CD38^+$ T predicting the occurrence of severe irAEs had an AUC of only 0.535, which was not suitable to be a predictive biomarker (**Figure S5**).

DISCUSSION

Currently, biomarkers for predicting the efficacy of ICIs mainly include PD-L1, tumor mutational burden (TMB), microsatellite instability (MSI), and gene expression profile of tumor-infiltrating lymphocytes (TILs) (11). In the field of NSCLC, PD-L1 is currently the only biomarker approved by the Food and Drug Administration (FDA) (12). However, its credibility remains to be controversial. In addition, mainstream biomarkers are based on the acquisition of

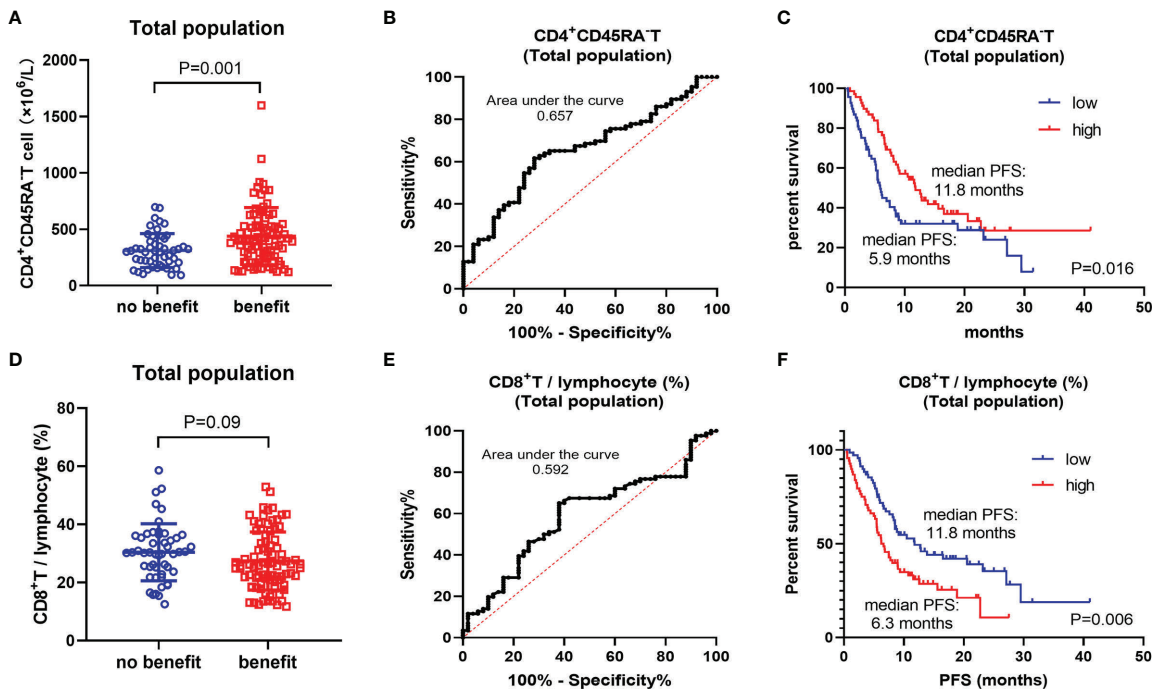

FIGURE 1 | Total population analysis. **(A)** Differences of $CD4^+CD45RA^-$ T cell between benefit group and non-benefit group. **(B)** ROC curve of $CD4^+CD45RA^-$ T cell. **(C)** Kaplan–Meier survival curve of different levels of $CD4^+CD45RA^-$ T cell. **(D)** Differences of $CD8^+$ T/lymphocyte (%) between benefit group and non-benefit group. **(E)** ROC curve of $CD8^+$ T/lymphocyte (%). **(F)** Kaplan–Meier survival curve of different levels of $CD8^+$ T/lymphocyte (%).

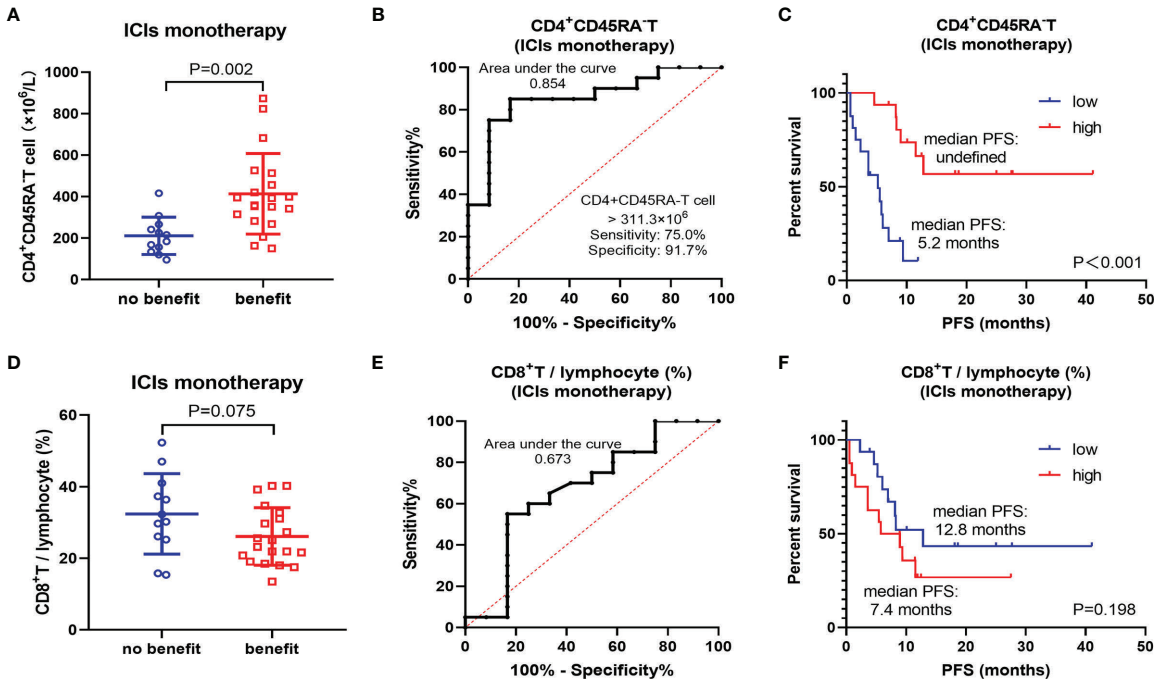

FIGURE 2 | Subgroup analysis of ICIs monotherapy. **(A)** Differences of $CD4^+CD45RA^-$ T cell between benefit group and non-benefit group. **(B)** ROC curve of $CD4^+CD45RA^-$ T cell. **(C)** Kaplan–Meier survival curve of different levels of $CD4^+CD45RA^-$ T cell. **(D)** Differences of $CD8^+$ T/lymphocyte (%) between benefit group and non-benefit group. **(E)** ROC curve of $CD8^+$ T/lymphocyte (%). **(F)** Kaplan–Meier survival curve of different levels of $CD8^+$ T/lymphocyte (%).

TABLE 4 | Basic information matching analysis.

	$CD4^+CD45RA^-$ T cell		P-value	$CD8^+$ T/lymphocyte (%)		P-value
	Low	High		Low	High	
Patients	68	68		68	68	
Sex			1.000			0.710
Male	47 (69.1%)	47 (69.1%)		46 (67.6%)	48 (70.6%)	
Female	21 (30.9%)	21 (30.9%)		22 (32.4%)	20 (29.4%)	
Age			0.424			0.161
<60	14 (20.6%)	19 (27.9%)		20 (29.4%)	13 (19.1%)	
≥60	54 (79.4%)	49 (72.1%)		48 (70.6%)	55 (80.9%)	
Histology			0.168			0.605
Non-squamous carcinoma	42 (61.8%)	33 (48.5%)		39 (57.4%)	36 (52.9%)	
Squamous carcinoma	26 (38.2%)	35 (51.5%)		29 (42.6%)	32 (47.1%)	
Line of therapy			0.003			0.765
First line	30 (44.1%)	49 (72.1%)		38 (55.9%)	41 (60.3%)	
Second line	30 (44.1%)	17 (25.0%)		24 (35.3%)	23 (33.8%)	
Third line and beyond	8 (11.8%)	2 (2.9%)		6 (8.8%)	4 (5.9%)	
Combined chemotherapy			0.419			1.000
No	18 (26.5%)	14 (20.6%)		16 (23.5%)	16 (23.5%)	
Yes	50 (73.5%)	54 (79.4%)		52 (76.5%)	52 (76.5%)	
Smoking status			0.217			0.158
No	30 (44.1%)	22 (32.4%)		30 (44.1%)	22 (32.4%)	
Yes	38 (55.9%)	46 (67.6%)		38 (55.9%)	46 (67.6%)	
Drinking status			0.572			0.707
No	50 (73.5%)	46 (67.6%)		49 (72.1%)	47 (69.1%)	
Yes	18 (26.5%)	22 (32.4%)		19 (27.9%)	21 (30.9%)	
ECOG PS			0.625			0.293
0	33 (48.5%)	37 (54.5%)		38 (55.9%)	32 (47.1%)	
1	27 (39.7%)	26 (38.2%)		26 (38.2%)	27 (39.7%)	
2–4	8 (11.8%)	5 (7.4%)		4 (5.9%)	9 (13.2%)	

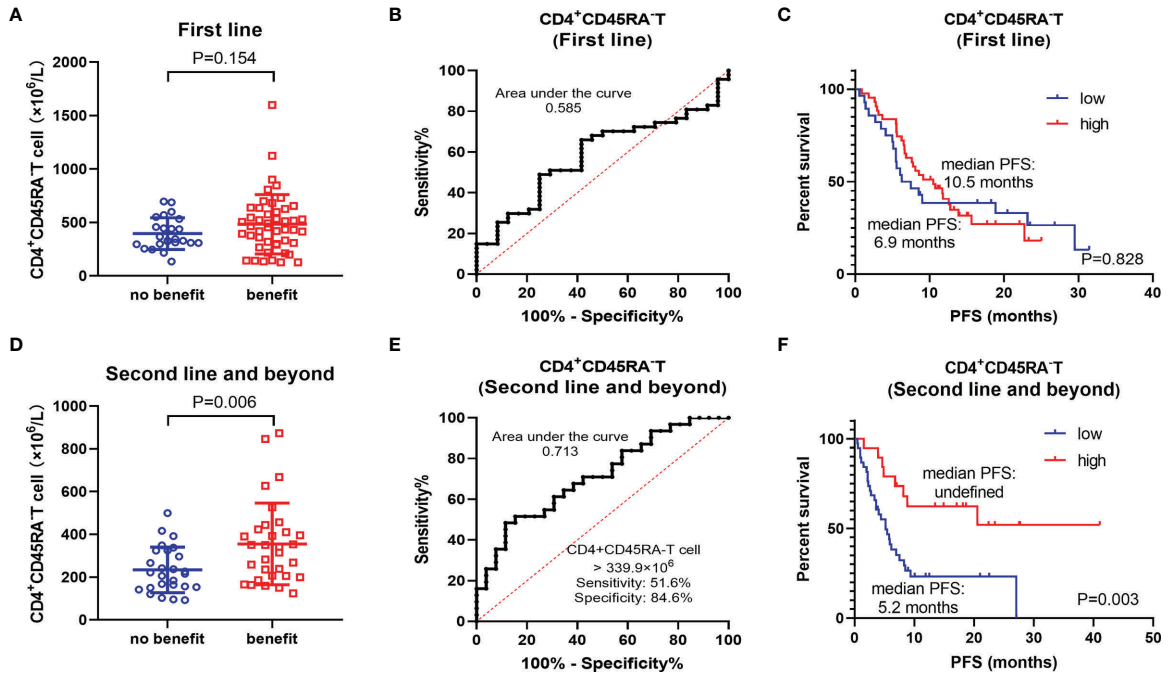

FIGURE 3 | Subgroup analysis of different treatment lines. **(A)** Differences of $CD4^+CD45RA^-$ T cell between benefit group and non-benefit group in the first-line patients. **(B)** ROC curve of $CD4^+CD45RA^-$ T cell in the first-line patients. **(C)** Kaplan–Meier survival curve of different levels of $CD4^+CD45RA^-$ T cell in the first-line patients. **(D)** Differences of $CD4^+CD45RA^-$ T cell between the benefit group and the non-benefit group in the second-line and beyond patients. **(E)** ROC curve of $CD4^+CD45RA^-$ T cell in the second-line and beyond patients. **(F)** Kaplan–Meier survival curve of different levels of $CD4^+CD45RA^-$ T cell in the second-line and beyond patients.

tumor tissues. No relevant peripheral blood biomarkers have been approved by the FDA, European Medicines Agency (EMA), and Pharmaceuticals and Medical Devices Agency (PMDA) (13, 14). However, the accessibility of tissue is limited, especially for patients of second line and beyond. Therefore, peripheral blood lymphocyte may be a promising non-invasive biomarker for patients treated with ICIs.

In this study, we explored the predictive effect of peripheral blood lymphocyte subsets on the efficacy of ICIs. We found that $CD4^+CD45RA^-$ T cells and $CD8^+$ T/lymphocytes (%) were associated with the prognosis of patients with NSCLC treated with ICIs. Low $CD4^+CD45RA^-$ T cell was associated with poor prognosis, whereas low $CD8^+$ T/lymphocyte (%) represented better prognosis. In the further subgroup analysis of the ICIs monotherapy population, we observed that only $CD4^+CD45RA^-$ T cell reflected the efficacy of ICIs, whereas $CD8^+$ T/lymphocyte (%) merely correlated with the prognosis. In addition, we explored the correlation between lymphocyte subsets and irAEs. The results showed that $CD4^+$ T-cell subsets were higher in the mild-irAEs group than in the non-irAEs group but did not contribute significantly in logistic regression. $CD8^+CD38^+$ T cell was associated with irAEs and severe irAEs but was not suitable as a predictive marker.

After activation by specific antigens, T cell would form two subtypes that differ in function, called effector T cell and memory T cell. Memory T cell, after secondary activated by antigen, would infiltrate into tumor tissue and express perforin to induce tumor cells apoptosis (15). CD45RA, one of the surface features of initial T cell, is expressed by initial T cell in the thymus and would disappear after antigen stimulation (16). It means that $CD45RA^-$ is the characteristic of memory T cell. CD62L, the characteristic of peripheral memory T cell, is expressed by central memory T cell but peripheral memory T cell (17). Kagamu et al. concluded that $CD4^+CD62L^-$ T cell presented in higher baseline counts in the responders to ICIs. In addition, patients who maintained high levels of $CD62L^-CD4^+$ T cell had a prolonged survival, compared with those patients whose $CD62L^-CD4^+$ T-cell counts decreased after ICI therapy (18). Similar conclusion was obtained by Zuazo et al. that patients with large amounts of highly differentiated ($CD27^-CD28^-$) $CD4^+$ T cell responded well to ICI therapy. ROC curves constructed with it were of good predictive value for the efficacy of ICIs (AUC = 0.85) (19). The above two studies demonstrated from two perspectives of peripheral memory T cell and highly differentiated T cell, respectively. We reaffirmed this idea from the third perspective that baseline memory $CD4^+$ T cell (central and peripheral) can reflect the efficacy of ICIs. In the subgroup of ICIs monotherapy patients, the ROC curve of $CD45RA^-CD4^+$ T cell had an AUC of 0.854, which was in favorable consistency with the study of Zuazo et al.

TABLE 5 | Logistic regression of irAEs.

		irAEs (P-value)		Severe irAEs (P-value)
		Univariate	Multivariate	Univariate
Sex	Male/female	0.110	0.579	0.492
Age	<60/≥60	0.229		0.138
Histology	Non-squamous/squamous	0.765		0.188
Line of therapy	First/second/third and beyond	0.191	0.412	0.779
Combined chemotherapy	No/yes	0.603		0.500
Smoking status	No/yes	0.170	0.750	0.586
Drinking status	No/yes	0.534		0.977
ECOG PS	0/1/2–4	0.453		0.529
Total lymphocyte	$\times10^6$	0.090	0.229	0.536
B cell	$\times10^6$	0.332		0.925
T cell	$\times10^6$	0.120	0.017	0.502
NK cell	$\times10^6$	0.410		0.870
$CD4^+$ T	$\times10^6$	0.050	0.123	0.552
$CD8^+$ T	$\times10^6$	0.777		0.607
$CD4^+CD45RA^-$ T	$\times10^6$	0.213		0.415
$CD4^+CD45RA^+$ T	$\times10^6$	0.009	0.206	0.911
$CD4^+CD28^+$ T	$\times10^6$	0.101	0.599	0.747
$CD8^+CD28^+$ T	$\times10^6$	0.678		0.540
$CD8^+DR^+$ T	$\times10^6$	0.538		0.699
$CD8^+CD38^+$ T	$\times10^6$	0.036	0.011	0.050
$CD4^+$ T/lymphocyte	×100%	0.905		0.491
$CD8^+$ T/lymphocyte	×100%	0.219		0.924

With the widespread application of ICIs in multiple tumor types, the indications approved have been gradually pushed to the first line from the second line and beyond (20). However, it remains to be unclear whether the application of ICIs in the first line brings better overall survival (OS) benefit. Chemotherapy and other anti-neoplastic therapy would cause myelosuppression, which include the depression of lymphocytes (21). We found that not only total lymphocyte counts but also $CD4^+CD45RA^-$ T-cell counts were significantly lower in the second line and beyond patients. We speculated that the efficacy of ICIs in the second line and beyond would be affected by the previous treatments as and $CD4^+CD45RA^-$ T-cell counts. The results demonstrated that the correlation between $CD4^+CD45RA^-$ T cell and patients' prognosis after ICIs was significantly higher in the second line and beyond (P = 0.006) than in the first line (P = 0.154). Therefore, the application of ICIs in the first-line therapy may help to better activate immune cells for anti-tumor efficacy.

Increased density of $CD8^+$ TILs is an indicator of favorable prognosis for ICI treatment (22). Kamphorst et al. showed that patients with high levels of $CD8^+$ T cell at baseline were strongly associated with OS benefit after receiving nivolumab (23). However, our study found no correlation between the absolute value of baseline $CD8^+$ T cell and the prognosis of NSCLC. Notably, lower proportions of baseline $CD8^+$ T/lymphocyte (%) were associated with better prognosis but did not affect the efficacy of ICIs. We hypothesized that patients responding well to treatment hold more CTL infiltrated into the tumor tissue. Therefore, less proportion of $CD8^+$ T cell can be detected in peripheral blood. In addition to baseline expression status, early expansion of peripheral blood $PD\text{-}1^+CD8^+$ T cell may also correlate with anti-PD-1 inhibitors clinical efficacy (23). PD-1 inhibitors can interfere the PD-1 signaling and depress the upregulation of CBL-b ubiquitin ligase, thus boosting the proliferation of $CD8^+$ T cell (24). PD-1 expressing peripheral blood $CD8^+$ T cell, who possess highly similar TCR clones to TIL, had the ability to be activated by tumor cells and kill them (25, 26). We also explored the correlation between the changes of peripheral blood $CD8^+$ T cell before and after ICI treatment. However, we did not find any correlation between the changes in $CD8^+$ T cell and the prognosis. This may be explained by the fact that $PD\text{-}1^+$ T cell represent only a small proportion of overall peripheral blood $CD8^+$ T cell, whereas the proliferative burst of $CD8^+$ T cell after PD-1 blockade was almost exclusively derived from the $PD\text{-}1^+CD8^+$ T-cell subset (27, 28).

The correlation between lymphocyte subsets and irAEs was also a research focus. Chaput et al. suggested that high levels of $CD4^+$ T cell at baseline may predict a higher incidence of immune-associated colitis (29). Subudhi et al. found that high levels of $CD8^+$ T cell may indicate an increased risk of irAEs (30). However, all of these findings suffered from small sample sizes and poor rigor. Our exploratory analysis results showed that patients who developed mild irAEs had higher levels of baseline $CD4^+$ T cell and various $CD4^+$ T cell subsets. In addition, the population of mild irAEs was highly overlapped with the population who obtained survival benefit. It validated the high correlation between the occurrence of irAEs and the efficacy of ICIs (31). In contrast to patients with mild irAEs, $CD4^+$ T-cell levels in patients with severe irAEs, surprisingly, did not increase further but decreased to the level of non-irAE patients. The currently available mechanisms of irAEs include off-target of ICIs, cross-antigen reactions of T cells, and injury mediated by

autoantibodies or cytokine (32). We ventured the hypothesis that severe irAEs and mild irAEs are mediated by two separate mechanisms, which needs to be explored and verified by further studies. Among all lymphocyte subsets we analyzed, only $CD8^+CD38^+$ T cell was positively correlated with the severity of irAEs. However, it did not show good predictive efficacy for severe irAEs.

This study was a retrospective research and inevitably existed with some deficiencies. First, the basic information of patients could not be well matched. For example, there was a significant correlation between the counts of $CD4^+CD45RA^-$ T cell and treatment lines. Although we tried to minimize them by performing subgroup analyses, they could not be completely eliminated. Second, the number of patients was insufficient, especially after performing the subgroup analyses. For instance, the immune monotherapy subgroup only contained 32 patients. Third, prolonging OS is the fundamental of oncology treatment. However, because of the lack of patients' OS data, we evaluated the survival benefit only by ORR and PFS. In the future, a prospective study with large sample size is needed to further explore whether lymphocyte subsets can serve as the biomarker to predict the survival benefit and irAEs of ICI therapy.

Overall, NSCLC has entered the era of immunotherapy, but current biomarkers to predict patient response to ICIs are limited. Peripheral blood biomarkers provide a convenient, rapid, and non-invasive method for clinical diagnosis and disease prognosis. We propose that baseline peripheral blood $CD4^+CD45RA^-$ T-cell counts can be used as a biomarker for predicting the efficacy of ICIs, especially for the second line and beyond patients, whose tumor tissue acquisition is difficult. In addition, $CD8^+CD38^+$ T cell may be suggestive for the predicting the occurrence of irAEs. This study will pave the way for further prospective studies to use peripheral blood lymphocyte subsets as a non-invasive biomarker basis for ICI treatment in patients with NSCLC.

DATA AVAILABILITY STATEMENT

The original contributions presented in the study are included in the article/**Supplementary Material**. Further inquiries can be directed to the corresponding authors.

ETHICS STATEMENT

The studies involving human participants were reviewed and approved by Ethics Review Committee of Peking Union Medical College Hospital. The patients/participants provided their written informed consent to participate in this study.

AUTHOR CONTRIBUTIONS

KM: Drafting the manuscript and revising it for important intellectual content. XZ, HW, XS, JN, WZ, JZ, YX, MC, and RP: Provision of clinical data, article revision, and correction. LZ and MZ: Substantial contributions to the conception or design of the work and final approval of the version to be published. All authors contributed to the article and approved the submitted version.

ACKNOWLEDGMENTS

The authors would like to thank all medical staff at the Lung Cancer Center of Peking Union Medical College Hospital.

SUPPLEMENTARY MATERIAL

The Supplementary Material for this article can be found online at: https://www.frontiersin.org/articles/10.3389/fimmu.2022.912180/full#supplementary-material

Supplementary Figure 1 | Absolute value of different lymphocyte subsets in benefit and non-benefit groups.

Supplementary Figure 2 | Lymphocyte subsets changes after two cycles ICI therapy in benefit and non-benefit groups.

Supplementary Figure 3 | Differences of $CD4^+CD45RA^-$ T cell between different treatment lines.

Supplementary Figure 4 | Absolute value of different lymphocyte subsets in non-irAEs, mild-irAEs and severe-irAEs groups.

Supplementary Figure 5 | ROC curve of $CD8^+CD38^+$ T cell for predicting severe irAEs.

REFERENCES

1. Vafaei S, Zekiy AO, Khanamir RA, Zaman BA, Ghayourvahdat A, Azimizonuzi H, et al. Combination Therapy With Immune Checkpoint Inhibitors (ICIs); A New Frontier. *Cancer Cell Int* (2022) 22:2. doi: 10.1186/s12935-021-02407-8
2. Doroshow DB, Sanmamed MF, Hastings K, Politi K, Rimm DL, Chen L, et al. Immunotherapy in Non-Small Cell Lung Cancer: Facts and Hopes. *Clin Cancer Res* (2019) 25:4592–602. doi: 10.1158/1078-0432.Ccr-18-1538
3. Mok TSK, Wu YL, Kudaba I, Kowalski DM, Cho BC, Turna HZ, et al. Pembrolizumab Versus Chemotherapy for Previously Untreated, PD-L1-Expressing, Locally Advanced or Metastatic non-Small-Cell Lung Cancer (KEYNOTE-042): A Randomised, Open-Label, Controlled, Phase 3 Trial. *Lancet* (2019) 393:1819–30. doi: 10.1016/s0140-6736(18)32409-7
4. Shen X, Zhao B. Efficacy of PD-1 or PD-L1 Inhibitors and PD-L1 Expression Status in Cancer: Meta-Analysis. *Bmj* (2018) 362:k3529. doi: 10.1136/bmj.k3529
5. Muroyama Y, Wherry EJ. Memory T-Cell Heterogeneity and Terminology. *Cold Spring Harb Perspect Biol* (2021) 13(10):a037929. doi: 10.1101/cshperspect.a037929
6. Reina-Campos M, Scharping NE, Goldrath AW. CD8(+) T Cell Metabolism in Infection and Cancer. *Nat Rev Immunol* (2021) 21:718–38. doi: 10.1038/s41577-021-00537-8
7. Tumeh PC, Harview CL, Yearley JH, Shintaku IP, Taylor EJ, Robert L, et al. PD-1 Blockade Induces Responses by Inhibiting Adaptive Immune Resistance. *Nature* (2014) 515:568–71. doi: 10.1038/nature13954

8. Bos R, Sherman LA. CD4+ T-Cell Help in the Tumor Milieu is Required for Recruitment and Cytolytic Function of CD8+ T Lymphocytes. *Cancer Res* (2010) 70:8368–77. doi: 10.1158/0008-5472.Can-10-1322
9. Manjarrez-Orduño N, Menard LC, Kansal S, Fischer P, Kakrecha B, Jiang C, et al. Circulating T Cell Subpopulations Correlate With Immune Responses at the Tumor Site and Clinical Response to PD1 Inhibition in Non-Small Cell Lung Cancer. *Front Immunol* (2018) 9:1613. doi: 10.3389/fimmu.2018.01613
10. Zuazo M, Arasanz H, Bocanegra A, Fernandez G, Chocarro L, Vera R, et al. Systemic CD4 Immunity as a Key Contributor to PD-L1/PD-1 Blockade Immunotherapy Efficacy. *Front Immunol* (2020) 11:586907. doi: 10.3389/fimmu.2020.586907
11. Indini A, Rijavec E, Grossi F. Circulating Biomarkers of Response and Toxicity of Immunotherapy in Advanced Non-Small Cell Lung Cancer (NSCLC): A Comprehensive Review. *Cancers (Basel)* (2021) 13(8):1794. doi: 10.3390/cancers13081794
12. Honrubia-Peris B, Garde-Noguera J, García-Sánchez J, Piera-Molons N, Llombart-Cussac A, Fernández-Murga ML. Soluble Biomarkers With Prognostic and Predictive Value in Advanced Non-Small Cell Lung Cancer Treated With Immunotherapy. *Cancers (Basel)* (2021) 13(17):4280. doi: 10.3390/cancers13174280
13. Cristescu R, Mogg R, Ayers M, Albright A, Murphy E, Yearley J, et al. Pan-Tumor Genomic Biomarkers for PD-1 Checkpoint Blockade-Based Immunotherapy. *Science* (2018) 362(6411):eaar3593. doi: 10.1126/science.aar3593
14. Rizvi NA, Hellmann MD, Snyder A, Kvistborg P, Makarov V, Havel JJ, et al. Cancer Immunology. Mutational Landscape Determines Sensitivity to PD-1 Blockade in non-Small Cell Lung Cancer. *Science* (2015) 348:124–8. doi: 10.1126/science.aaa1348
15. Behr FM, Chuwonpad A, Stark R, van Gisbergen K. Armed and Ready: Transcriptional Regulation of Tissue-Resident Memory CD8 T Cells. *Front Immunol* (2018) 9:1770. doi: 10.3389/fimmu.2018.01770
16. Tian Y, Babor M, Lane J, Schulten V, Patil VS, Seumois G, et al. Unique Phenotypes and Clonal Expansions of Human CD4 Effector Memory T Cells Re-Expressing CD45RA. *Nat Commun* (2017) 8:1473. doi: 10.1038/s41467-017-01728-5
17. Nakajima Y, Chamoto K, Oura T, Honjo T. Critical Role of the CD44(low) CD62L(low) CD8(+) T Cell Subset in Restoring Antitumor Immunity in Aged Mice. *Proc Natl Acad Sci U S A* (2021) 118(23):e2103730118. doi: 10.1073/pnas.2103730118
18. Kagamu H, Kitano S, Yamaguchi O, Yoshimura K, Horimoto K, Kitazawa M, et al. CD4(+) T-Cell Immunity in the Peripheral Blood Correlates With Response to Anti-PD-1 Therapy. *Cancer Immunol Res* (2020) 8:334–44. doi: 10.1158/2326-6066.Cir-19-0574
19. Zuazo M, Arasanz H, Fernández-Hinojal G, García-Granda MJ, Gato M, Bocanegra A, et al. Functional Systemic CD4 Immunity is Required for Clinical Responses to PD-L1/PD-1 Blockade Therapy. *EMBO Mol Med* (2019) 11:e10293. doi: 10.15252/emmm.201910293
20. Xia L, Liu Y, Wang Y. PD-1/PD-L1 Blockade Therapy in Advanced Non-Small-Cell Lung Cancer: Current Status and Future Directions. *Oncologist* (2019) 24:S31–s41. doi: 10.1634/theoncologist.2019-IO-S1-s05
21. Newman NB, Sidhu MK, Baby R, Moss RA, Nissenblatt MJ, Chen T, et al. Long-Term Bone Marrow Suppression During Postoperative Chemotherapy in Rectal Cancer Patients After Preoperative Chemoradiation Therapy. *Int J Radiat Oncol Biol Phys* (2016) 94:1052–60. doi: 10.1016/j.ijrobp.2015.12.374
22. Li F, Li C, Cai X, Xie Z, Zhou L, Cheng B, et al. The Association Between CD8+ Tumor-Infiltrating Lymphocytes and the Clinical Outcome of Cancer Immunotherapy: A Systematic Review and Meta-Analysis. *E Clinical Medicine* (2021) 41:101134. doi: 10.1016/j.eclinm.2021.101134
23. Kamphorst AO, Pillai RN, Yang S, Nasti TH, Akondy RS, Wieland A, et al. Proliferation of PD-1+ CD8 T Cells in Peripheral Blood After PD-1-Targeted Therapy in Lung Cancer Patients. *Proc Natl Acad Sci U S A.* (2017) 114:4993–8. doi: 10.1073/pnas.1705327114
24. Huang AC, Postow MA, Orlowski RJ, Mick R, Bengsch B, Manne S, et al. T-Cell Invigoration to Tumour Burden Ratio Associated With Anti-PD-1 Response. *Nature* (2017) 545:60–5. doi: 10.1038/nature22079
25. Stevanović S, Pasetto A, Helman SR, Gartner JJ, Prickett TD, Howie B, et al. Landscape of Immunogenic Tumor Antigens in Successful Immunotherapy of Virally Induced Epithelial Cancer. *Science* (2017) 356:200–5. doi: 10.1126/science.aak9510
26. Gros A, Robbins PF, Yao X, Li YF, Turcotte S, Tran E, et al. PD-1 Identifies the Patient-Specific $CD8^+$ Tumor-Reactive Repertoire Infiltrating Human Tumors. *J Clin Invest* (2014) 124:2246–59. doi: 10.1172/jci73639
27. Im SJ, Hashimoto M, Gerner MY, Lee J, Kissick HT, Burger MC, et al. Defining CD8+ T Cells That Provide the Proliferative Burst After PD-1 Therapy. *Nature* (2016) 537:417–21. doi: 10.1038/nature19330
28. Li T, Zhao L, Yang Y, Wang Y, Zhang Y, Guo J, et al. T Cells Expanded From PD-1(+) Peripheral Blood Lymphocytes Share More Clones With Paired Tumor-Infiltrating Lymphocytes. *Cancer Res* (2021) 81:2184–94. doi: 10.1158/0008-5472.Can-20-2300
29. Chaput N, Lepage P, Coutzac C, Soularue E, Le Roux K, Monot C, et al. Baseline Gut Microbiota Predicts Clinical Response and Colitis in Metastatic Melanoma Patients Treated With Ipilimumab. *Ann Oncol* (2017) 28:1368–79. doi: 10.1093/annonc/mdx108
30. Subudhi SK, Aparicio A, Gao J, Zurita AJ, Araujo JC, Logothetis CJ, et al. Clonal Expansion of CD8 T Cells in the Systemic Circulation Precedes Development of Ipilimumab-Induced Toxicities. *Proc Natl Acad Sci U S A.* (2016) 113:11919–24. doi: 10.1073/pnas.1611421113
31. Das S, Johnson DB. Immune-Related Adverse Events and Anti-Tumor Efficacy of Immune Checkpoint Inhibitors. *J Immunother Cancer* (2019) 7:306. doi: 10.1186/s40425-019-0805-8
32. Sullivan RJ, Weber JS. Immune-Related Toxicities of Checkpoint Inhibitors: Mechanisms and Mitigation Strategies. *Nat Rev Drug Discovery* (2021). doi: 10.1038/s41573-021-00259-5

Conflict of Interest: The authors declare that the research was conducted in the absence of any commercial or financial relationships that could be construed as a potential conflict of interest.

The reviewer J-LL declared a shared parent affiliation with the authors to the handling editor at the time of review.

Publisher's Note: All claims expressed in this article are solely those of the authors and do not necessarily represent those of their affiliated organizations, or those of the publisher, the editors and the reviewers. Any product that may be evaluated in this article, or claim that may be made by its manufacturer, is not guaranteed or endorsed by the publisher.

frontiers | Frontiers in Immunology

TYPE Correction
PUBLISHED 08 December 2022
DOI 10.3389/fimmu.2022.1111230

OPEN ACCESS

APPROVED BY
Frontiers Editorial Office, Frontiers Media SA, Switzerland

*CORRESPONDENCE
Li Zhang
zhanglipumch1026@sina.com
Mengzhao Wang
mengzhaowang@sina.com

†These authors share last authorship

SPECIALTY SECTION
This article was submitted to Cancer Immunity and Immunotherapy, a section of the journal Frontiers in Immunology

RECEIVED 29 November 2022
ACCEPTED 30 November 2022
PUBLISHED 08 December 2022

CITATION
Miao K, Zhang X, Wang H, Si X, Ni J, Zhong W, Zhao J, Xu Y, Chen M, Pan R, Wang M and Zhang L (2022) Corrigendum: Peripheral blood lymphocyte subsets predict the efficacy of immune checkpoint inhibitors in non– small cell lung cancer.
Front. Immunol. 13:1111230.
doi: 10.3389/fimmu.2022.1111230

Corrigendum: Peripheral blood lymphocyte subsets predict the efficacy of immune checkpoint inhibitors in non– small cell lung cancer

Kang Miao, Xiaotong Zhang, Hanping Wang, Xiaoyan Si, Jun Ni, Wei Zhong, Jing Zhao, Yan Xu, Minjiang Chen, Ruili Pan, Mengzhao Wang*† and Li Zhang*†

Department of Pulmonary and Critical Care Medicine, Peking Union Medical College Hospital, Chinese Academy of Medical Sciences & Peking Union Medical College, Beijing, China

KEYWORDS

immune checkpoint inhibitors (ICIs), lymphocyte subsets, CD4$^+$CD45RA$^-$ T cell, biomarker, CD8$^+$CD38$^+$ T cell

A Corrigendum on

Peripheral blood lymphocyte subsets predict the efficacy of immune checkpoint inhibitors in non–small cell lung cancer

by Miao K, Zhang X, Wang H, Si X, Ni J, Zhong W, Zhao J, Xu Y, Chen M, Pan R, Wang M and Zhang L (2022) Front. Immunol. 13:912180. doi: 10.3389/fimmu.2022.912180

In the published article, there was an error in affiliation 1. Instead of "Department of Pulmonary and Critical Care Medicine, Peking Union Medical Hospital, Chinese Academy of Medical Science and Peking Union Medical College, Beijing, China", it should be "Department of Pulmonary and Critical Care Medicine, Peking Union Medical College Hospital, Chinese Academy of Medical Sciences & Peking Union Medical College, Beijing, China".

The authors apologize for this error and state that this does not change the scientific conclusions of the article in any way. The original article has been updated.

Publisher's note

All claims expressed in this article are solely those of the authors and do not necessarily represent those of their affiliated organizations, or those of the publisher, the editors and the reviewers. Any product that may be evaluated in this article, or claim that may be made by its manufacturer, is not guaranteed or endorsed by the publisher.

frontiers | Frontiers in Immunology

ORIGINAL RESEARCH
published: 01 July 2022
doi: 10.3389/fimmu.2022.921761

Increased Tumor Intrinsic Growth Potential and Decreased Immune Function Orchestrate the Progression of Lung Adenocarcinoma

Yue Zhao[1,2,3†], Jun Shang[4†], Jian Gao[1,2,5†], Han Han[1,2,3], Zhendong Gao[1,2,3], Yueren Yan[1,2,3], Qiang Zheng[3,6], Ting Ye[1,2,3], Fangqiu Fu[1,2,3], Chaoqiang Deng[1,2,3], Zelin Ma[1,2,3], Yang Zhang[1,2,3], Difan Zheng[1,2,3], Shanbo Zheng[1,2,3], Yuan Li[3,6], Zhiwei Cao[7‡], Leming Shi[2,4*‡] and Haiquan Chen[1,2,3*‡]*

[1] Department of Thoracic Surgery and State Key Laboratory of Genetic Engineering, Fudan University Shanghai Cancer Center, Shanghai, China, [2] Institute of Thoracic Oncology, Fudan University, Shanghai, China, [3] Department of Oncology, Shanghai Medical College, Fudan University, Shanghai, China, [4] State Key Laboratory of Genetic Engineering, Human Phenome Institute, School of Life Sciences and Shanghai Cancer Center, Fudan University, Shanghai, China, [5] International Human Phenome Institutes (Shanghai), Shanghai, China, [6] Department of Pathology, Fudan University Shanghai Cancer Center, Shanghai, China, [7] School of Life Sciences, Fudan University, Shanghai, China

Background: The overall 5-year survival of lung cancer was reported to be only ~15%, with lung adenocarcinoma (LUAD) as the main pathological subtype. Before developing into invasive stages, LUAD undergoes pre-invasive stages of adenocarcinoma *in situ* (AIS) and minimally invasive adenocarcinoma (MIA), where surgical resection gives an excellent 5-year survival rate. Given the dramatic decline of prognosis from pre-invasive to invasive stages, a deeper understanding of key molecular changes driving the progression of LUAD is highly needed.

Methods: In this study, we performed whole-exome sequencing and RNA sequencing on surgically resected 24 AIS, 74 MIA, 99 LUAD specimens, and their adjacent paired normal tissues. Survival data were obtained by follow-up after surgery. Key molecular events were found by comparing the gene expression profiles of tumors with different stages. Finally, to measure the level of imbalance between tumor intrinsic growth potential and immune microenvironment, a tumor progressive (TP) index was developed to predict tumor progression and patients' survival outcome and validated by external datasets.

Results: As tumors progressed to more invasive stages, they acquired higher growth potential, mutational frequency of tumor suppressor genes, somatic copy number alterations, and tumor mutation burden, along with suppressed immune function. To better predict tumor progression and patients' outcome, TP index were built to measure the imbalance between tumor intrinsic growth potential and immune microenvironment. Patients with a higher TP index had significantly worse recurrence-free survival [Hazard ratio (HR), 10.47; 95% CI, 3.21–34.14; $p < 0.0001$] and overall survival (OS) [Hazard ratio

OPEN ACCESS

Edited by:
Yubin Li,
University of Pennsylvania,
United States

Reviewed by:
Xin Chen,
Zhejiang University, China
Yuwei Liu,
Jiangsu University, China

***Correspondence:**
Haiquan Chen
hqchen1@yahoo.com
Leming Shi
lemingshi@fudan.edu.cn
Zhiwei Cao
zwcao@fudan.edu.cn

†These authors have contributed equally to this work and share first authorship

‡These authors have contributed equally to this work

Specialty section:
This article was submitted to Cancer Immunity and Immunotherapy, a section of the journal Frontiers in Immunology

Received: 16 April 2022
Accepted: 01 June 2022
Published: 01 July 2022

Citation:
Zhao Y, Shang J, Gao J, Han H, Gao Z, Yan Y, Zheng Q, Ye T, Fu F, Deng C, Ma Z, Zhang Y, Zheng D, Zheng S, Li Y, Cao Z, Shi L and Chen H (2022) Increased Tumor Intrinsic Growth Potential and Decreased Immune Function Orchestrate the Progression of Lung Adenocarcinoma. Front. Immunol. 13:921761. doi: 10.3389/fimmu.2022.921761

(HR), 4.83e8; 95% CI, 0–Inf; p = 0.0013]. We used The Cancer Genome Atlas (TCGA)-LUAD dataset for validation and found that patients with a higher TP index had significantly worse OS (HR, 1.10; 95% CI, 0.83–1.45; p = 0.048), demonstrating the prognostic value of the TP index for patients with LUAD.

Conclusions: The imbalance of tumor intrinsic growth potential and immune function orchestrate the progression of LUAD, which can be measured by TP index. Our study provided new insights into predicting survival of patients with LUAD and new target discovery for LUAD through assessing the imbalance between tumor intrinsic growth potential and immune function.

Keywords: imbalance, tumor intrinsic growth potential, immune response, progression, lung adenocarcinoma

INTRODUCTION

Lung cancer is one of the deadliest disease worldwide, with a 5-year survival of only ~19% (1). Lung adenocarcinoma (LUAD) is the most common pathological subtype. Pre-invasive stages of LUAD, namely, adenocarcinoma *in situ* (AIS) and minimally invasive adenocarcinoma (MIA), have a nearly 100% 5-year survival rate after complete surgery (2, 3). The prognosis of patients would downslide dramatically once the disease progressed to invasive stages. Therefore, it is necessary to study the evolution of LUAD for discovering new targets and developing new treatments. Although there have been studies on genomic and immune profiling of patients with AIS, MIA, and LUAD, there lack a systematic study focusing on key molecular events that drive the evolution of LUAD (4–8).

As tumors progress, their radiological manifestations change. With the development of thoracic computed tomography (CT) scanning and the application of low-dose CT screening, an increasing number of small pulmonary nodules, especially subsolid nodules have been detected (9–12). The prognostic impact of solid components for LUADs presented as ground-glass opacities (GGOs) on CT scanning has been under extensive investigation, where tumors manifesting as GGOs were found to have indolent clinical course (13, 14). Our two previous studies further provided evidence on the prognostic value of LUADs, manifesting as GGOs on CT scan (15, 16). However, there still lack comprehensive genomic and transcriptomic studies comparing the differences between LUADs having GGO components and their counterparts not having GGO components on CT scan.

In this study, we performed whole-exome sequencing and RNA sequencing (RNA-seq) on 197 surgically resected LUADs and divided them into different groups by pathological characteristics and radiological manifestations, aiming to find key genetic factors that drive the evolution of LUAD. Twelve expression patterns were identified based on expression profiles, and pathway analysis was performed to reveal the biological functions for each pattern. Tumor intrinsic growth potential and immune microenvironment were assessed, and immune cell infiltration was calculated. Finally, to better predict tumor progression and patients' outcome, we developed a tumor progressive (TP) index to measure the level of imbalance between tumor intrinsic growth potential and immune microenvironment and validated the index by external datasets.

MATERIALS AND METHODS

Study Cohort

A total of 197 patients with LUAD who underwent surgery between September 2011 and May 2016 at the Department of Thoracic Surgery, Fudan University Shanghai Cancer Center, were retrospectively included in this study (**Figure 1A**). None of the patients received neoadjuvant therapy. This study was approved by the Committee for Ethical Review of Research (Fudan University Shanghai Cancer Center Institutional Review Board, No. 090977-1). Informed consents of all patients for donating their samples to the tissue bank of Fudan University Shanghai Cancer Center were obtained from patients themselves or their relatives.

Radiological and Histological Evaluation

Whole-lung CT scans were performed on each patient included before surgery as previously described (15). For each nodule, the maximum diameter of both the entire nodule and solid component on the single largest axial dimension was recorded on lung window. Pulmonary nodules were further divided into three groups: pure GGOs, where there was no solid component in one pulmonary nodule; subsolid nodules, where both solid and GGO components existed in one pulmonary nodule; and solid nodules, where the pulmonary nodule contained only solid component (**Figure 1A**). CT scans were reviewed by two radiologists independently, and interobserver and intraobserver agreements were measured to quantify the reproducibility and accuracy between the two radiologists as previously described (15).

Intraoperative frozen section diagnosis was made after the tumor was resected, and postoperative diagnosis was made after surgery by two independent pathologists. According to the IASLC/ATS/ERS classification, tumors were classified as AIS, MIA, or invasive LUAD based on their histological presentations. Invasive LUAD subtypes were further analyzed in a semi-quantitative manner, where the components of different subtypes (lepidic, acinar, papillary, micropapillary,

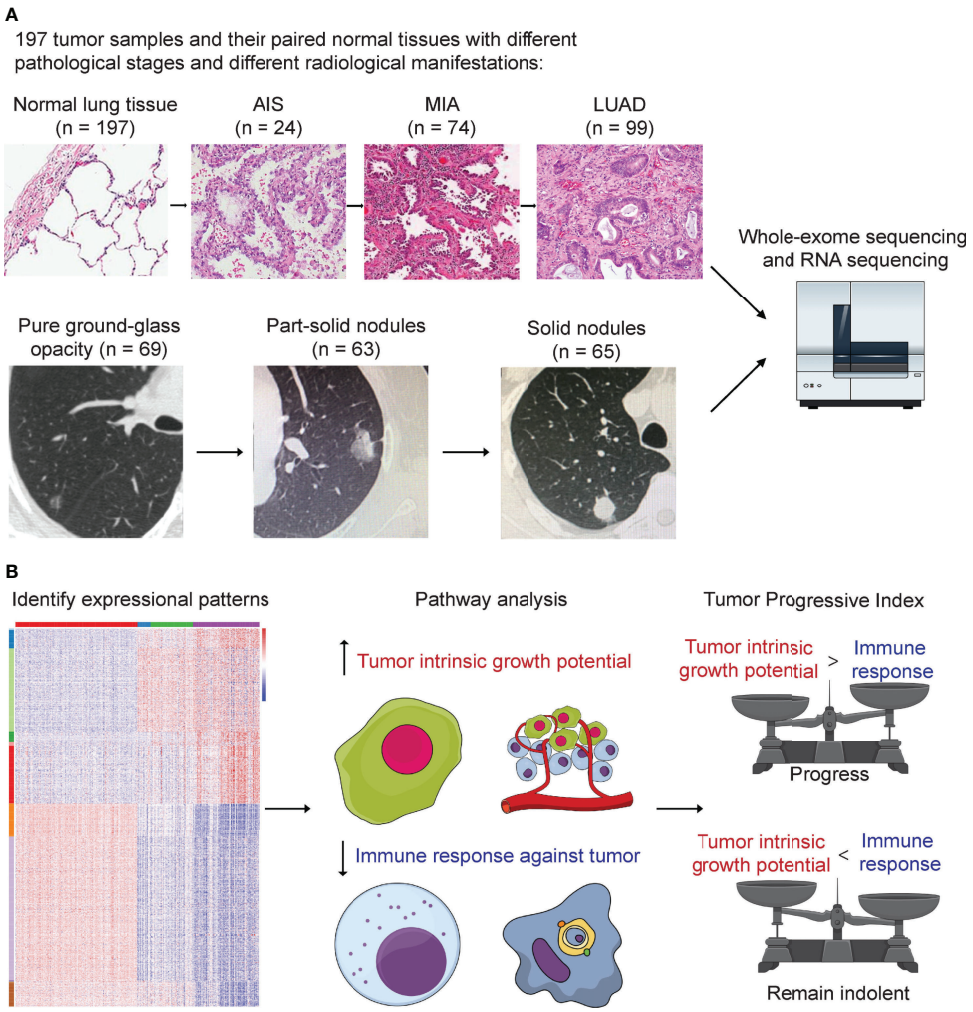

FIGURE 1 | Study design. **(A)** A total number of 197 tumor samples, including 24 adenocarcinoma *in situ* (AIS), 74 minimally invasive adenocarcinoma (MIA), 99 lung adenocarcinoma (LUAD), and their paired adjacent normal lung tissue underwent whole-exome sequencing and RNA sequencing. Genomic and transcriptomic data were analyzed and compared among different groups. Samples were further divided into three groups according to their radiological manifestations: 69 pure ground-glass opacities (GGOs), 63 subsolid nodules, and 65 solid nodules. **(B)** Identification of 12 expressional patterns and development of tumor progressive index based on genomic and transcriptomic data.

solid, and invasive mucinous) were recorded in 5% increments. The predominant subtype was the one with the largest percentage (not necessarily 50% or higher) (17). Pathological stage of disease was determined according to the eighth TNM staging system.

Follow-Up Protocol

Patients were followed up regularly after surgery as we previously described (15). Briefly, patients were followed up every 3 months after surgery for the first 2 years, where physical examination, chest CT scans, and abdominal ultrasonography were performed every 3 to 6 months. The follow-up interval was changed to every 6 months for the third year and once a year from then on. Brain CT or magnetic resonance imaging (MRI) and bone scintigraphy were performed every 6 months for patients with invasive adenocarcinoma in the first 3 years. In addition, positron emission tomography (PET)–CT scans were performed if necessary. Recurrence-free survival (RFS) was defined as the time between surgery and first recurrence or last follow-up. Patients with no recurrence but died from other causes were censored on that date. Overall survival (OS) was defined as the time between surgery and death or last follow-up.

Whole-Exome Sequencing

Genomic DNA from tumors and paired adjacent normal tissues were extracted and prepared using the QIAamp DNA Mini Kit (Qiagen, Germany) following the manufacturer's instructions. Exon libraries were constructed using the SureSelect XT Target Enrichment System. A total amount of 1–3 μg of genomic DNA for each samples was fragmented into an average size of ~200 bp. DNA was hybridized, captured, and amplified using SureSelect XT reagents and protocols to generate indexed, target-enriched

library amplicons. Constructed libraries were then sequenced on the Illumina HiSeq X Ten platform and 150-bp paired-end reads were generated.

Alignment, Mutation Calling, and Somatic Copy Number Alteration Calling

Sequence reads from the exome capture libraries were aligned to the reference human genome (hg19) using BWA-MEM (18). Picard tools were then used for marking Polymerase Chain Reaction (PCR) duplicated, and the Genome Analysis Toolkit was used to perform base quality recalibration and local indel re-alignments (19). Single-nucleotide variants (SNVs) were called using MuTect and MuTect2 (20). Indels were called using MuTect2 and Strelka v2.0.13 (21). Variantes were filtered if called by only one tool. After the variants were called, Oncotator v1.9.1 was used for annotating somatic mutations (22), and significantly mutated genes were identified using MutSig2CV (23). Tumor mutation burden (TMB) was calculated as the total number of non-synonymous SNVs and indels per sample divided by 30, given the total coverage of ~30 Mb. CNVkit v0.9.7 with default parameters was used to perform somatic copy number alteration (SCNA) analysis for alignment reads (24). Amplification and deletion peaks were identified using GISTIC2.0 from segment files (25). Amplification and deletion thresholds were set 0.1 and −0.1, respectively. Frequency distribution of amplification and deletion was shown using R package copy number v1.26.0 (26).

RNA Sequencing and Calculation of Expression

Total RNA from tumors and paired adjacent normal tissues was extracted and prepared using NucleoZOL (Macherey-Nagel, Germany) and NucleoSpin RNA Set for NucleoZOL (Macherey-Nagel, Germany) following the manufacturer's instructions. A total amount of 3 μg of RNA per sample was used as initial material for RNA sample preparations. Ribosomal RNA was removed using Epicenter Ribo-Zero Gold Kits (Epicenter, USA). Sequencing libraries were generated using NEBNext Ultra Directional RNA Library Prep Kit for Illumina (NEB, Ipswich, USA) according to the manufacturer's instructions. Libraries were then sequenced on the Illumina HiSeq X Ten platform and 150-bp paired-end reads were generated. As a quality-control step, only those samples with RNA integrity number (RIN) ≥ 5.0 were included in this study.

After the data were obtained, RNA-seq reads were aligned to the reference human genome (hg19) using STAR v2.5.3 (27). Expression values were normalized to the transcripts per million (TPM) estimates using RSEM v1.3.0 (28).

Identification of Gene Expression Patterns

One-hundred fifty samples with RIN ≥ 5.0 were divided into four groups: normal (n = 150), AIS (n = 16), MIA (n = 52), and LUAD (n = 82). Analysis of variance (ANOVA) was used to determine differentially expressed genes. First, paired comparison was performed between two adjacent groups (normal vs. AIS, AIS vs. MIA, and MIA vs. LUAD), and then, genes with $p < 0.0001$ and $|\text{fold change}| \geq 2$ in at least one of three comparisons were considered significant and put into downstream analyses. Twelve patterns of gene expression were then identified based on their trends of expression between each two adjacent groups in the study cohort (up trend, no significant change or down trend; **Figures 1B**, **3**). Finally, KOBAS was used to perform KEGG pathway enrichment analysis for the patterns identified in the study cohort (29).

Development of Tumor Progressive Index

TP index was developed for quantitatively measuring the level of imbalance between tumor intrinsic growth potential and immune response. To minimize the possible confounding effect introduced by genes with low expression, we first filtered out genes with mean TPM < 1.0 across all samples. Next, genes for calculating the tumor index were selected from pattern 1, where there was a significant increase between each two adjacent groups. Genes for calculating the immune index were selected from pattern 8 where there was a significant decrease from normal tissue to AIS and from MIA to LUAD. Those genes that were both selected from pattern 8 and were in an *a priori* immune-related gene list containing 730 genes were used to calculate the immune index (7). For both tumor index and immune index, first, expression for those genes for each sample was log2-transformed; then, for each sample, tumor index was calculated as the mean value of log2-transformed expression of *BCL2L15*, *COMP*, *CST1*, and *FAM83A*, whereas immune index was calculated as the mean value of log2-transformed expression of *ITLN2*, *MARCO*, *C8B*, *MASP1*, *CD36*, *TAL1*, *PPBP*, and *CDH5*. Finally, TP index was calculated as the subtraction of tumor index by immune index:

Tumor progressive index = tumor index − immune index

Statistical Analysis

Clinical and pathological characteristics were recorded and compared among three groups. Pearson χ (2) test and Fisher's exact test were used to compare categorical variables wherever applicable. Non-parametric Wilcoxon signed-rank test was used to compare medians of groups of continuous variables. Kaplan–Meier survival curves and log-rank p-values were calculated for patients' RFS and OS. All statistical analyses and graphing work were performed using R (version 3.6.0, R Foundation for Statistical Computing, Vienna, Austria). Two-tailed $p < 0.05$ was considered significant for all statistical analyses unless stated otherwise.

RESULTS

Pathological and Radiological Characteristics of 197 Lung Adenocarcinoma

Tumor samples were divided into three groups based on their pathological characteristics: 24 AIS, 74 MIA, and 99 LUAD, and into three groups based on their radiological manifestations: 69 pure GGOs, 63 subsolid nodules, and 65 solid nodules (**Figure 1A**). Clinical and pathological characteristics, including sex, smoking status, tumor location, pathology, and

adenocarcinoma subtypes, were compared (**Table 1**). Of note, we found that there was an association between radiological and pathological presentations. Sixty-six of the 69 (95.7%) of pulmonary nodules manifesting as pure GGOs on CT scan were either AIS or MIA, whereas for pulmonary nodules manifesting as pure solid nodules, only one of 65 (1.5%) was either AIS or MIA (MIA in this case). For pulmonary nodules manifesting as subsolid nodules on CT scan, 31 of 63 (49.2%) were either AIS or MIA, and 32 (50.8%) were invasive adenocarcinoma. Compared with male patients, female patients had significantly higher frequency of pure GGO lesions ($p = 0.025$). For predominant adenocarcinoma subtypes, lepidic subtype was significantly enriched in the pure GGO group ($p < 0.001$), whereas papillary subtype was significantly enriched in the pure solid group ($p = 0.004$). Solid subtype was only found predominant in the pure solid group. Moreover, for presenting subtypes, lepidic subtype was significantly enriched in the pure GGO group ($p = 0.001$), and solid subtype was significantly enriched in the pure solid group ($p = 0.014$). Micropapillary subtype was also more likely to be found in the pure solid group, although without a significant difference (pure GGO vs. subsolid vs. solid: 0.0% vs. 3.1% vs. 9.4%, $p = 0.472$). Taken together, these results demonstrated there was a link between radiological and pathological findings; therefore, radiological manifestations can, at least partly, help predict the invasiveness of LUAD.

Mutation Frequency of Tumor Suppressor Gene Increased With Tumor Progression

We next assessed the genomic alterations of tumors with different radiological manifestations. The landscape of somatic mutations for all patients included in this study was shown in **Figure 2A**. The most frequently mutated genes in this cohort were *EGFR* (50%), followed by *TP53* (22%), *RBM10* (8%), *ERBB2* (5%), *BRAF* (5%), *RB1* (5%), *KRAS* (4%), and *NF1* (3%) (**Figure 2A**). A further comparison found that frequency of mutations in driver genes did not differ as tumor progressed, whereas frequency of mutations in tumor suppressor genes increased as tumor progressed. For individual driver genes, *EGFR* mutations were significantly more enriched in LUAD ($p = 0.005$), whereas *BRAF* was significantly more enriched in AIS ($p = 0.028$, **Supplementary Table 1**). *ALK* fusions were detected only in three LUAD samples, all of which were solid nodules on CT scan (3 of 65, $p = 0.045$, **Supplementary Table 2**). On the other hand, a significant difference was observed in the frequency of tumor suppressor genes. The number of mutations in common tumor suppressor genes was 2 (8.3%) for AIS, 4 (5.4%) for MIA, and 38 (38.4%) for LUAD ($p < 0.001$, **Supplementary Table 1**), and 7 (10.1%) for pure GGOs, 15 (23.8%) for subsolid nodules, and 37 (56.9%) for solid nodules ($p < 0.001$, **Supplementary Table 3**). For individual tumor suppressor genes, frequency of *TP53* mutations was found to be significantly higher in LUAD and solid nodules ($p < 0.001$ and

TABLE 1 | Clinical and pathological characteristics of the study cohort (n = 197).

	Pure GGO (n = 69)	Subsolid (n = 63)	Solid (n = 65)	P-value
Sex				0.025
Female	48 (69.6%)	41 (65.1%)	31 (47.7%)	
Male	21 (30.4%)	22 (34.9%)	34 (52.3%)	
Smoking status				0.212
Former/current	16 (23.2%)	15 (23.8%)	23 (35.4%)	
Never	53 (76.8%)	48 (76.2%)	42 (64.6%)	
Tumor location				0.661
LUL	18 (26.1%)	13 (20.6%)	11 (16.9%)	
LLL	7 (10.1%)	6 (9.5%)	10 (15.4%)	
RUL	26 (37.7%)	31 (49.2%)	23 (35.4%)	
RML	7 (10.1%)	5 (7.9%)	8 (12.3%)	
RLL	11 (15.9%)	8 (12.7%)	13 (20.0%)	
Pathology				<0.001
AIS/MIA	66 (95.7%)	31 (49.2%)	1 (1.5%)	
LUAD	3 (4.3%)	32 (50.8%)	64 (98.5%)	
Predominant subtype				
Lepidic	2 (66.7%)	9 (28.1%)	3 (4.7%)	<0.001
Acinar	1 (33.3%)	17 (53.1%)	40 (62.5%)	0.453
Papillary	0 (0.0%)	6 (9.4%)	10 (15.6%)	0.004
Micropapillary	0 (0.0%)	0 (0.0%)	0 (0.0%)	–
Solid	0 (0.0%)	0 (0.0%)	9 (14.1%)	0.067
IMA	0 (0.0%)	0 (0.0%)	2 (3.1%)	0.123
Presenting subtype				
Lepidic	2 (66.7%)	12 (37.5%)	6 (9.4%)	0.001
Acinar	2 (66.7%)	24 (75.0%)	50 (78.1%)	0.863
Papillary	0 (0.0%)	9 (28.1%)	22 (34.4%)	0.407
Micropapillary	0 (0.0%)	1 (3.1%)	6 (9.4%)	0.472
Solid	0 (0.0%)	1 (3.1%)	17 (26.6%)	0.014
IMA	0 (0.0%)	0 (0.0%)	2 (3.1%)	0.572

AIS, adenocarcinoma in situ; GGO, ground-glass opacity; IAD, invasive adenocarcinoma; IMA, invasive mucinous adenocarcinoma; MIA, minimally invasive adenocarcinoma; LLL, left lower lobe; LUL, left upper lobe; RLL, right lower lobe; RML, right middle lobe; RUL, right upper lobe.

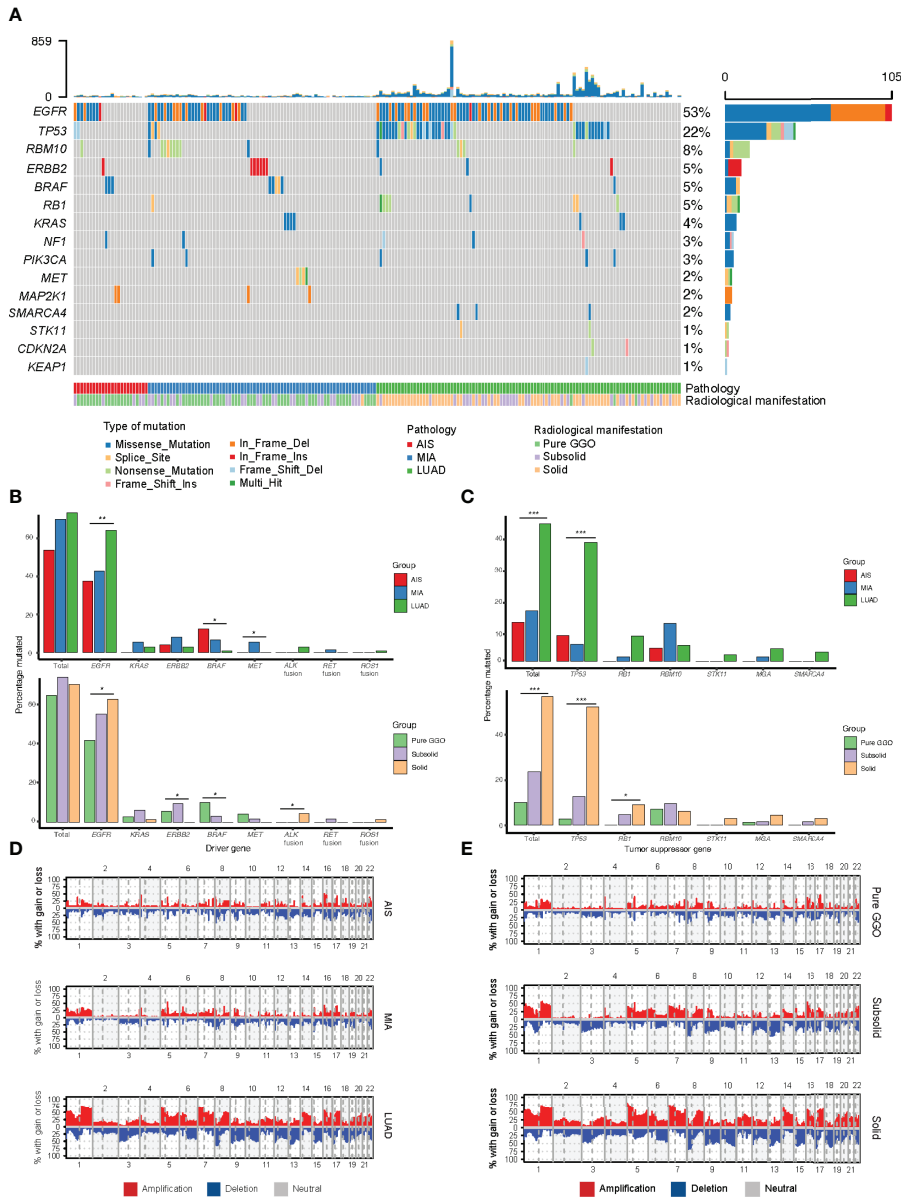

FIGURE 2 | Comparison of genomic alterations for different pathological and radiological groups. **(A)** Waterfall plot showing the landscape of genomic alterations in each group. **(B)** Comparison of mutation frequency in major driver genes among different groups. **(C)** Comparison of mutation frequency in major tumor suppressor genes among different groups. **(D)** Comparison of somatic copy number alterations among different pathological groups. **(E)** Comparison of somatic copy number alterations among different radiological groups. *, p<0.05; **, p<0.01; ***, p<0.001.

$p < 0.001$, respectively, **Figures 2B, C** and **Supplementary Tables 1, 2**), whereas frequency of *RB1* mutations was significantly higher in solid nodules ($p = 0.038$) and marginally significantly higher in LUAD ($p = 0.058$). TMB was significantly higher in LUAD compared with AIS/MIA, and solid nodules compared with GGOs/subsolid nodules on CT scan (**Supplementary Figures 1**, **2**).

Frequency of Somatic Copy Number Alterations Increased as Tumors Progressed

To explore the SCNAs of different stages of LUAD, we identified SCNAs from raw sequencing reads of samples of different pathological and radiological groups. Notably, the SCNA frequency including amplification and deletion increased as

tumors progressed (**Figures 2D, E**). We used GISTIC2.0 to identify significant arm-level SCNAs in samples of different groups, and the union of significant arm-level event of the three groups was used for further analysis. As a result, the ratio of amplification and deletion in arm-level SCNAs increased from AIS to MIA and LUAD and from pure GGOs to subsolid and solid nodules. These results indicated that the frequency of SCNA burden was higher as tumors progressed.

Decreased Cytotoxic CD8+ T Cells and Increased Tregs as Tumors Progressed

To explore whether there are any differences in immune cell infiltration as tumors progress to different stages, we next used CIBERSORT, a deconvolution method to estimate the infiltration of immune cells in different pathological stages (30). We found that the number of CD8+ T cells decreased as tumor stage increased (**Figure 3A**), which was consistent with Dejima et al. on the immune evolution from neoplasia to invasive lung adenocarcionma (7). Furthermore, we found that the number of Tregs increased as tumor stage increased, suggesting an enhanced immunosuppression as disease progressed (**Figure 3B**), which was also validated by the Dejima dataset (**Figure 3C**). Interestingly, we found an increased number of activated NK cells and a decreased number of resting NK cells as disease progressed and validated this result using the Dejima dataset, suggesting that NK cells might be important in the progression of LUAD (**Figures 3D, E**). A more detailed staging of LUAD also showed similar results, with tumors at earlier stages having more CD8+ T cells and less Tregs, whereas tumors at later stages having less CD8+ T cells and more Tregs (**Supplementary Figure 3**). Taken together, our findings showed that a suppressed immune microenvironment plays an important role in the progression of LUAD.

Expression Patterns Correlated With Tumor Intrinsic Growth Potential and Immune Function

Next, we defined expression patterns that correlated with tumor progression using RNA-seq data. One-hundred fifty samples with RIN ≥ 5.0 were included in this part. We developed an ANOVA model with pathological stage (normal tissue, AIS, MIA, and LUAD) as a factor and patient as a random effect. A total of 2023 genes with $p < 0.0001$ and $|\text{fold change}| > 2$ in pairwise comparisons of two adjacent groups of patients (normal tissue vs. AIS, AIS vs. MIA, and MIA vs. LUAD, respectively) were divided into 12 following patterns: pattern 1 (nine genes): increase from normal to AIS, from AIS to MIA and from MIA to LUAD; pattern 2 (97 genes): increase from normal to AIS and from MIA to LUAD, no change from AIS to MIA; pattern 3 (446 genes): increase from normal to AIS alone; pattern 4 (54 genes): no change from normal to AIS, increase from AIS to MIA and from MIA to LUAD; pattern 5 (20 genes): increase from AIS to MIA alone; pattern 6 (309 genes): increase from MIA to LUAD alone; pattern 7 (three genes): decrease from normal to AIS, from AIS to MIA and from MIA to LUAD; pattern 8 (175 genes): decrease from normal to AIS and from MIA to LUAD, no change from AIS to MIA; pattern 9 (771 genes): decrease from normal to AIS alone; pattern 10 (6 genes): no change from normal to AIS, decrease from AIS to MIA and from MIA to LUAD; pattern 11 (three genes): decrease from AIS to MIA alone; pattern 12 (130 genes): decrease from MIA to LUAD alone (**Figure 4** and **Supplementary Table 3**). Pathway enrichment analysis showed that pathways associated with tumor invasiveness and cell growth were enriched in up-trend patterns (patterns 1 to 6). Of note, Phosphatidylinositol 3-Kinase - Protein Kinase B (PI3K-AKT) signaling pathway and NF-κB signaling pathway were upregulated in AIS compared with normal tissue, suggesting that malignant

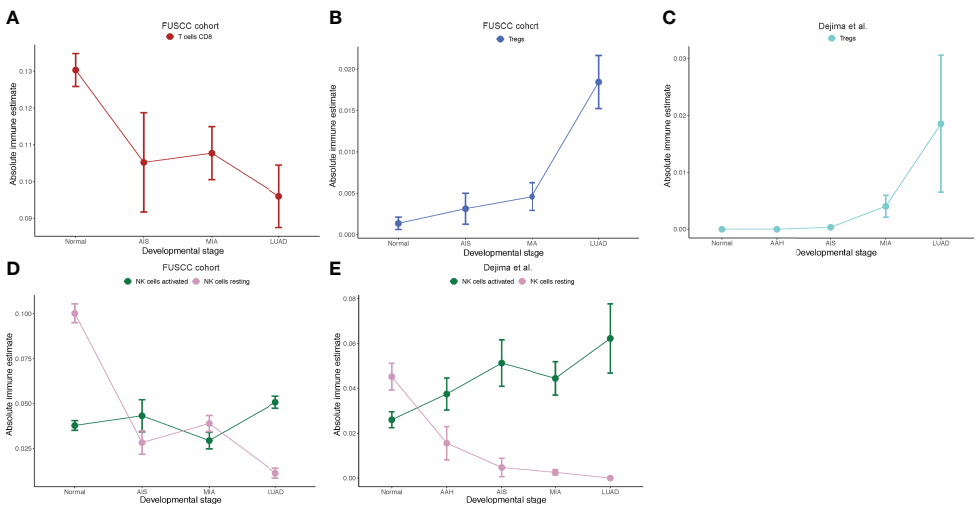

FIGURE 3 | Immune cell infiltration inferred by CIBERSORT. **(A)** Prediction of number of CD8+ T cells in the Fudan University Shanghai Cancer Center (FUSCC) cohort. **(B)** Prediction of number of Tregs in the FUSCC cohort. **(C)** Prediction of number of Tregs in Dejima's cohort. **(D)** Prediction of number of activated and resting natural killer (NK) cells in the FUSCC cohort. **(E)** Prediction of number of activated and resting NK cells in Dejima's cohort.

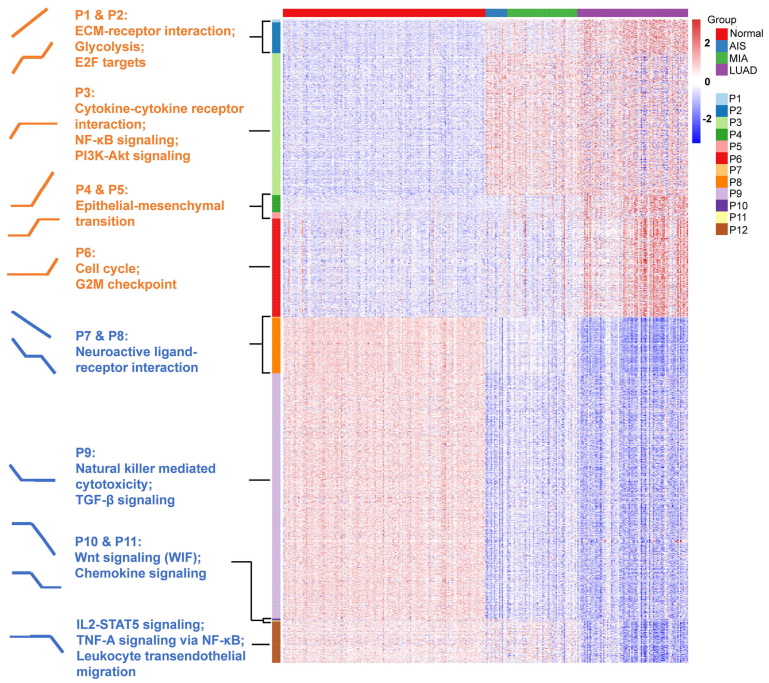

FIGURE 4 | Identification of 12 expression patterns and prediction of immune cell infiltration. Pattern 1 (nine genes): increase from normal to AIS, from AIS to MIA and from MIA to LUAD; pattern 2 (97 genes): increase from normal to AIS and from MIA to LUAD, no change from AIS to MIA; pattern 3 (446 genes): increase from normal to AIS alone; pattern 4 (54 genes): no change from normal to AIS, increase from AIS to MIA and from MIA to LUAD; pattern 5 (20 genes): increase from AIS to MIA alone; pattern 6 (309 genes): increase from MIA to LUAD alone; pattern 7 (three genes): decrease from normal to AIS, from AIS to MIA and from MIA to LUAD; pattern 8 (175 genes): decrease from normal to AIS and from MIA to LUAD, no change from AIS to MIA; pattern 9 (771 genes): decrease from normal to AIS alone; pattern 10 (six genes): no change from normal to AIS, decrease from AIS to MIA and from MIA to LUAD; pattern 11 (three genes): decrease from AIS to MIA alone; pattern 12 (130 genes): decrease from MIA to LUAD alone. Gene set enrichment analysis (GSEA) was performed to assess the functional significance for those patterns.

behaviors could exist in as early as AIS. Epithelial–mesenchymal transition, which was highly associated with tumor metastasis, was also found to be increased from AIS to MIA, suggesting an acquisition of metastatic potential as invasive subtypes of LUAD emerge (31). Moreover, cell cycle was found to be increased from MIA to LUAD, consistent with the fact that AIS/MIA behaved more indolent than LUAD. On the other hand, for down-trend patterns, natural killer–mediated cytotoxicity and Transforming Growth Factor-beta (TGF- β) signaling pathway were found to be decreased from normal lung tissue to AIS, suggesting an inhibited immune response against tumor. Chemokine signaling, Interleukin2-Signal Transducer and Activator of Transcription 5 (IL2-STAT5) signaling, TNF-A signaling *via* NF-κB and leukocyte transendothelial migration were also found to be enriched in down-trend patterns, further suggesting an impaired immune function in tumor microenvironment. Interestingly, Wnt signaling pathway, which was often upregulated in cancer, was found to be decreased from AIS to MIA and from MIA to LUAD. A deeper look into pattern 10 showed that this finding was contributed by WIF1 (Wnt inhibiting factor 1), which was an inhibitor of Wnt signaling pathway. Taken together, our results suggest that both an increased tumor intrinsic growth potential and an inhibited immune microenvironment contributed to the development and progression of LUAD.

TP Index Measured the Imbalance Between Tumor Intrinsic Growth Potential and Immune Microenvironment

To better predict tumor progression and outcome of patients, TP index were built to measure the imbalance between tumor intrinsic growth potential and immune microenvironment. On the basis of our previous findings, we used the genes in pattern 1 and immune-related genes in patterns 7 and 8 with mean TPM ≥ 1 across all samples (methods). Four genes that were associated with apoptosis, tumor metastasis and progression (*BCL2L15*, *COMP*, *CST1*, and *FAM83A*) reflected tumor intrinsic growth potential, whereas eight genes (*ITLN2*, *MARCO*, *C8B*, *MASP1*, *CD36*, *TAL1*, *PPBP*, and *CDH5*) that were associated with immune microenvironment reflected immune response against tumors. A negative TP index indicates that the immune system is competent enough to suppress the progression of tumors, whereas a positive TP index indicates that the immune system can no longer suppress the growth of tumor cells. In our study cohort, TP index was negative in normal tissues but positive in AIS and stages onward, indicating that immune escape already existed in AIS, the precursor stage of LUAD, and became more severe with the progression of disease (**Figure 5A**). Same increasing trend was observed in another dataset, which showed a significant increase of TP index from normal tissue

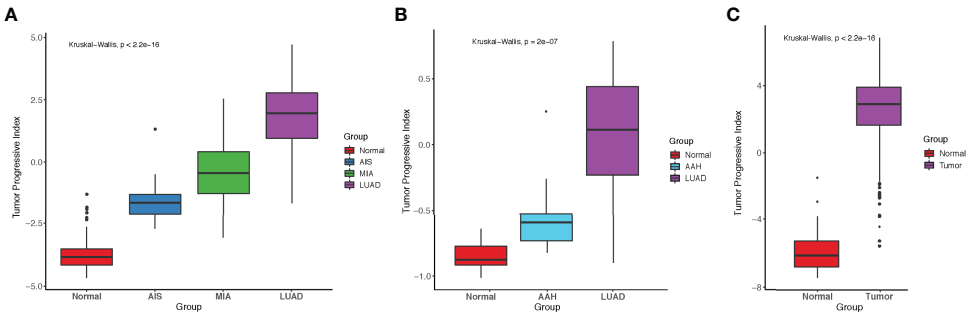

FIGURE 5 | Comparison of tumor progressive index for different datasets. **(A)** Boxplot showing the index increased as tumor progressed in the FUSCC cohort. **(B)** Boxplot showing the index increased as tumor progressed in Dejima's cohort. **(C)** Boxplot showing the difference of tumor progressive index between normal and tumor samples in the TCGA-LUAD cohort.

to atypical adenomatous hyperplasia (AAH) then to LUAD (**Figure 5B**) (32). Interestingly, there was a negative TP index in the stage of AAH, where tumors could not overcome the immune system to metastasize further. Although the TCGA-LUAD dataset does not contain pre-invasive stages of LUAD, we still calculated the TP index for each sample and compared it between normal and tumor samples. Not surprisingly, tumor samples had significantly higher TP index than normal samples (**Figure 5C**).

TP Index Effectively Predicted the Prognosis in Patients With Lung Adenocarcinoma

To investigate whether our TP index had prognostic value for patients with LUAD, survival analysis was performed on both our dataset and TCGA-LUAD dataset. Our results showed that in our dataset, patients with a high TP index had poorer RFS (HR, 10.47; 95% CI, 3.21–34.14) and OS (HR, 4.83e8; 95% CI, 0–Inf; **Figures 6A, B**), whereas in the TCGA-LUAD dataset, patients with a higher TP index had poorer OS (HR, 1.35; 95% CI, 1.00–1.81) but progression-free survival (PFS) was comparable for the two groups (HR, 1.10; 95% CI, 0.83–1.45; **Figures 6C, D**). Taken together, our results suggested that increased tumor intrinsic growth potential and impaired immune response against tumor work together to drive the progression of LUAD, and our TP index, which measures the level of imbalance between tumor intrinsic growth potential and tumor immune microenvironment, is of prognostic value for patients with LUAD (**Figure 6E**).

DISCUSSION

In this study, we provided a comprehensive analysis integrating clinical, radiological, pathological, genomic, and transcriptomic analysis of 197 pulmonary lesions with different radiological and pathological manifestations.

We first assessed the transcriptomic profiles of our cohort. On the basis of the differentially expressed genes between each two adjacent groups, 12 expression patterns were identified (**Figure 4**). Genes associated with cell cycle and G2M checkpoint were found to be significantly upregulated from MIA to LUAD, but not different from normal tissue to MIA. This indicates that pre-invasive stages of LUAD had more indolent behaviors, which might explain why AIS and MIA had a nearly 100% 5-year survival rate after surgical resection. Histologically, AIS is defined as a ≤3-cm adenocarcinoma lacking invasive patterns, whereas MIA is a ≤3-cm adenocarcinoma with invasive patterns of no more than 5 mm in size (31). PI3K-AKT signaling pathway, a classical pathway that was upregulated in various cancer types, was found to be increased from normal tissue to AIS (33). Although AIS is the precursor of LUAD, this finding shows that cells in this stage already have an increased potential for growth. On the other hand, we found that epithelial–mesenchymal transition, a biological process known to increase metastatic potential of cancer cells (34), was found to be significantly increased from AIS to MIA, consistent with histological differences between AIS and MIA. Although AIS and MIA both have a nearly perfect prognosis, our results suggest that MIA should be surgically intervened before it progresses to the next stage as invasive patterns already exist. To our surprise, several immune-related pathways were found in down-trend expression patterns, indicating a decreased or impaired immune response as tumors progress. Consistent with this finding, using CIBERSORT to deconvolute our bulk-sequencing data, we found a decrease in the number of CD8+ cytotoxic T cells and an increase in the number of Treg cells, which was also validated by another dataset that compared immune cells among normal tissue, AAH, AIS, MIA, and LUAD (7). Taken together, our results demonstrated that increased tumor intrinsic growth signals and decreased immune response orchestrate the evolution of LUAD.

We next demonstrated that there was an association between radiological and pathological presentations. Most nodules that were GGOs on CT scan were AIS or MIA, whereas most solid nodules were invasive LUAD (**Table 1**). This might provide explanation of why pulmonary nodules manifesting as GGOs on CT scan usually have indolent clinical courses. This result was

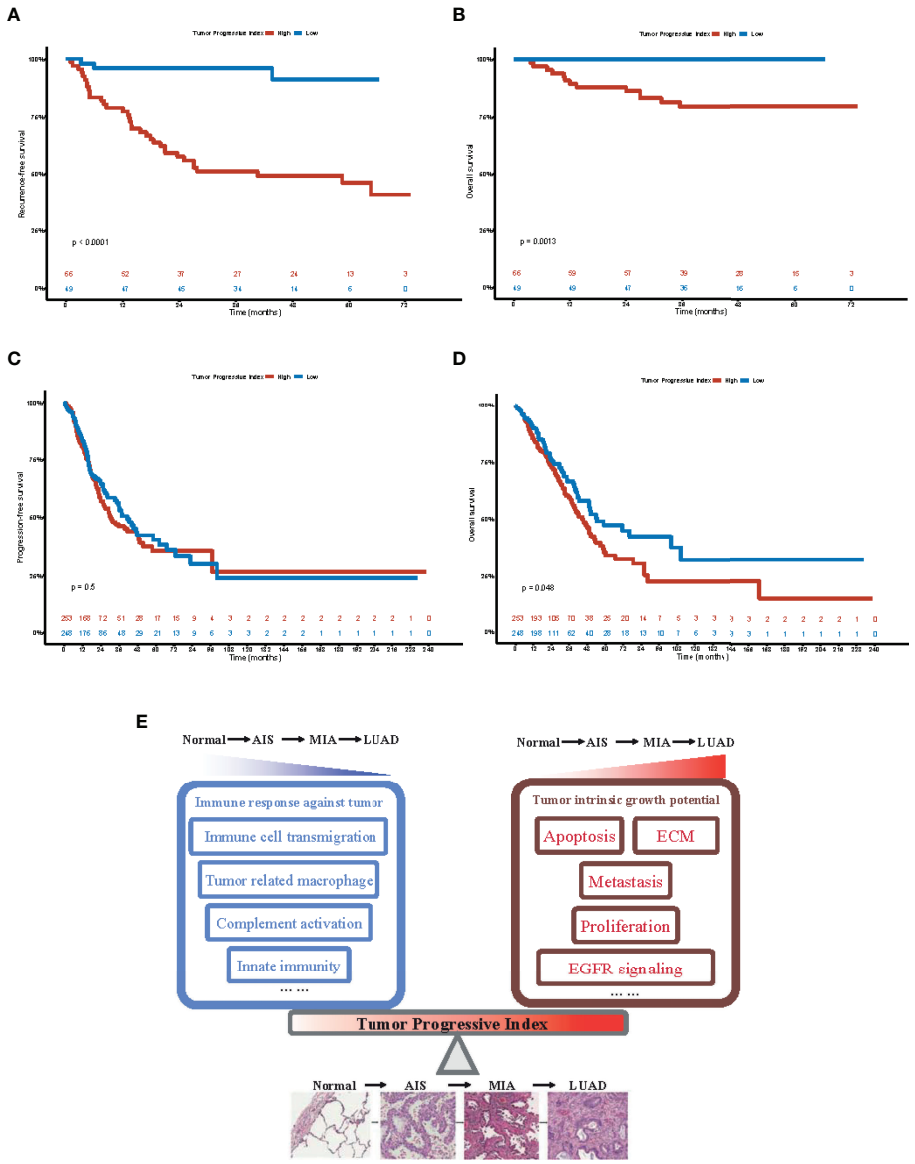

FIGURE 6 | Prognostic value of tumor progressive index for patients with lung adenocarcinoma. **(A)** Recurrence-free survival for patients with tumor progressive index higher and lower than the median value across the Fudan University Shanghai Cancer Center (FUSCC) cohort. **(B)** Overall survival for patients with tumor progressive index higher and lower than the median value across the Fudan University Shanghai Cancer Center (FUSCC) cohort. **(C)** Recurrence-free survival for patients with tumor progressive index higher and lower than the median value across the TCGA-LUAD cohort. **(D)** Overall survival for patients with tumor progressive index higher and lower than the median value across the TCGA-LUAD cohort. **(E)** Schematic demonstration showing the imbalance between tumor intrinsic growth potential and immune response against tumor, which can be measured by tumor progressive index, leads to the evolution and progression of lung adenocarcinoma.

also consistent with previous studies and provided a link between histological and radiological manifestations (35, 36). For major driver mutations, we found that frequency of neither *EGFR* nor *KRAS* mutations was significantly different among the three groups (**Figure 2B** and **Supplementary Table 2**). *BRAF* mutations were more enriched in the pure GGO group, whereas *ALK* fusion was only seen in the solid group. On the other hand, the frequency of mutations in tumor suppressor genes was significantly different among the three groups, with a sharp increase from 2 (2.9%) in the pure GGO group, to 8 (12.7%) in the subsolid group, and 33 (50.8%) in the solid group (**Figure 2C** and **Supplementary Table 2**), suggesting a pivotal role that tumor suppressor genes play in the progression of LUAD. For individual tumor suppressor genes, *TP53* and *RB1* were significantly different among the three groups ($p < 0.001$ and $p = 0.038$, respectively; **Figure 2C** and **Supplementary Table 2**).

Previous studies have discussed the genomic alterations in pulmonary nodules manifesting as GGO. In 2015, Kobayashi et al. evaluated *EGFR*, *KRAS*, *ALK*, and *HER2* mutations in 104 pulmonary nodules, manifesting as GGO. They found that *EGFR*

was mutated in 64% of all the 104 samples, whereas *KRAS*, *ALK*, and *HER2* were mutated in 4%, 3%, and 4% of the samples, respectively (37). In 2018, Lu et al. reported that *EGF*R was mutated in 75 of 156 (48.1%) patients with LUAD, which was similar to 50% in our cohort (38). We also observed a significant difference in *EGFR* mutation frequency among three radiological groups (**Figure 2B** and **Supplementary Table 2**). In 2020, Li et al. performed whole-exome sequencing on 154 pulmonary subsolid nodules from 120 patients and found that *EGFR* was the most frequently mutated gene, followed by *RBM10*, *TP53*, *STK11*, and *KRAS*. They also found that frequency of *EGFR*, *RBM10*, and *TP53* was significantly different between pure GGO and subsolid nodules (39). Although not significantly different for *EGFR* and *RBM10* in our cohort, there was indeed a significant difference of the frequency of *TP53* mutations (**Figure 2C** and **Supplementary Table 2**).

For SCNAs, we found that the frequency of SCNAs increased as tumors progressed. As the solid components increased, the genome became more unstable. Frequency of arm-level alterations also followed the same trend, where tumors at earlier stages and manifested as pure GGOs on CT scan had fewer significant arm-level events, whereas tumors at later stages and manifested as solid nodules had more significant arm-level events. Genomic instability was widely reported to be associated with increased rate of tumor proliferation and progression among different cancer types (40–42).

Tumor intrinsic growth potential and immune microenvironment are both associated with tumor evolution and progression (43, 44). On the basis of our findings, a TP index was designed to quantitatively measure the level of imbalance between tumor intrinsic growth potential and immune microenvironment. Interestingly, AAH, a stage of pre-cancerous hyperplasia, had a negative TP index, indicating some key alteration would be needed to activate the malignant transformation of cells. AIS, MIA, and LUAD all had a progressive index of more than 0, and the index increased as the tumor developed to the next stage. Furthermore, patients with a high TP index tended to have a poorer RFS and OS. Taken together, our data demonstrated that TP index can be used as a predictor for disease progression and prognosis, discovering new markers for predicting patients' survival and potential drug targets.

In our study, surgically resected specimens were used. However, in some cases, cytology is the only available specimens. Previous studies have shown that performing next-generation sequencing on cytological samples can yield comparable results than on histological samples (45, 46). In the context of lung transplantation, donors with suspected tumors are rarely used due to the risk of transmission (47). However, as patients needing lung transplantation are increasing and pulmonary nodules are increasingly diagnosed, pulmonary nodules that are not malignant need to be excluded from the blacklist. A fast assessment based on pathology and genomics using cytological specimens might be a possible solution, shedding light on future application of molecular testing.

In summary, this study integrates the genomic alterations, transcriptomic profiles, and histological and radiological progression of LUAD, providing deeper understandings of the evolution of this disease.

DATA AVAILABILITY STATEMENT

The datasets presented in this study can be found in online repositories. The names of the repository/repositories and accession number(s) can be found below: European Genome-phenome Archive (EGA). Accession number: EGAS00001004006 ("https://ega-archive.org/studies/EGAS00001004006)". Source data and codes for generating the figures in this study are available at https://github.com/yuezhao97/Progression_LUAD_project.

ETHICS STATEMENT

The studies involving human participants were reviewed and approved by the Committee for Ethical Review of Research (Fudan University Shanghai Cancer Center Institutional Review Board No. 090977-1). The patients/participants provided their written informed consent to participate in this study.

AUTHOR CONTRIBUTIONS

HC, LS, ZC, and YuZ designed the study. YuZ, JS, and JG performed data analysis. YuZ, HH, and ZG performed experiments. QZ and YL reviewed pathological slides. YY, TY, FF, CD, ZM, YaZ, DZ, and SZ collected samples. JS and LS helped with quality control of sequencing data. YuZ, JS, and JG drafted the manuscript. All authors contributed to the article and approved the submitted version.

FUNDING

The design of the study and collection, analysis, and interpretation of data and in writing the manuscript were supported by the National Natural Science Foundation of China (81930073), Shanghai Science and Technology Innovation Action Project (20JC1417200), Shanghai Municipal Science and Technology Major Project (2017SHZDZX01 and VBH1323001/026), Shanghai Municipal Key Clinical Specialty Project (SHSLCZDZK02104), Pilot Project of Fudan University (IDF159045), Shanghai Sailing Program (22YF1408900), and Project supported by Shanghai Municipal Science and Technology Major Project (2017SHZDZX01).

SUPPLEMENTARY MATERIAL

The Supplementary Material for this article can be found online at: https://www.frontiersin.org/articles/10.3389/fimmu.2022.921761/full#supplementary-material

Supplementary Figure 1 | Comparison of tumor mutation burden (TMB) for different pathological groups.

Supplementary Figure 2 | Comparison of tumor mutation burden (TMB) for different radiological groups.

Supplementary Figure 3 | Prediction of number of **(A)** CD8+ T cells, **(B)** Tregs, and **(C)** natural killer (NK) cells for different tumor stages.

REFERENCES

1. Siegel RL, Miller KD, Jemal A. Cancer Statistics, 2020. *CA Cancer J Clin* (2020) 70:7–30. doi: 10.3322/caac.21590
2. Maeshima AM, Tochigi N, Yoshida A, Asamura H, Tsuta K, Tsuda H. Histological Scoring for Small Lung Adenocarcinomas 2 Cm or Less in Diameter: A Reliable Prognostic Indicator. *J Thorac Oncol* (2010) 5:333–9. doi: 10.1097/JTO.0b013e3181c8cb95
3. Borczuk AC, Qian F, Kazeros A, Eleazar J, Assaad A, Sonett JR, et al. Invasive Size is an Independent Predictor of Survival in Pulmonary Adenocarcinoma. *Am J Surg Pathol* (2009) 33:462–9. doi: 10.1097/PAS.0b013e318190157c
4. Izumchenko E, Chang X, Brait M, Fertig E, Kagohara LT, Bedi A, et al. Targeted Sequencing Reveals Clonal Genetic Changes in the Progression of Early Lung Neoplasms and Paired Circulating DNA. *Nat Commun* (2015) 6:8258. doi: 10.1038/ncomms9258
5. Murphy SJ, Wigle DA, Lima JF, Harris FR, Johnson SH, Halling G, et al. Genomic Rearrangements Define Lineage Relationships Between Adjacent Lepidic and Invasive Components in Lung Adenocarcinoma. *Cancer Res* (2014) 74:3157–67. doi: 10.1158/0008-5472.CAN-13-1727
6. Hu X, Fujimoto J, Ying L, Fukuoka J, Ashizawa K, Sun W, et al. Multi-Region Exome Sequencing Reveals Genomic Evolution From Preneoplasia to Lung Adenocarcinoma. *Nat Commun* (2019) 10:2978. doi: 10.1038/s41467-019-10877-8
7. Dejima H, Hu X, Chen R, Zhang J, Fujimoto J, Parra ER, et al. Immune Evolution From Preneoplasia to Invasive Lung Adenocarcinomas and Underlying Molecular Features. *Nat Commun* (2021) 12:2722. doi: 10.1038/s41467-021-22890-x
8. Chen H, Carrot-Zhang J, Zhao Y, Hu H, Freeman SS, Yu S, et al. Genomic and Immune Profiling of Pre-Invasive Lung Adenocarcinoma. *Nat Commun* (2019) 10:5472. doi: 10.1038/s41467-019-13460-3
9. Walter JE, Heuvelmans MA, de Bock GH, Yousaf-Khan U, Groen HJM, van derAalst CM, et al. Characteristics of New Solid Nodules Detected in Incidence Screening Rounds of Low-Dose CT Lung Cancer Screening: The NELSON Study. *Thorax* (2018) 73:741–7. doi: 10.1136/thoraxjnl-2017-211376
10. Horeweg N, van Rosmalen J, Heuvelmans MA, van derAalst CM, Vliegenthart R, Scholten ET, et al. Lung Cancer Probability in Patients With CT-Detected Pulmonary Nodules: A Prespecified Analysis of Data From the NELSON Trial of Low-Dose CT Screening. *Lancet Oncol* (2014) 15:1332–41. doi: 10.1016/S1470-2045(14)70389-4
11. McWilliams A, Tammemagi MC, Mayo JR, Roberts H, Liu G, Soghrati K, et al. Probability of Cancer in Pulmonary Nodules Detected on First Screening CT. *N Engl J Med* (2013) 369:910–9. doi: 10.1056/NEJMoa1214726
12. Fu F, Zhou Y, Zhang Y, Chen H. Lung Cancer Screening Strategy for non-High-Risk Individuals: A Narrative Review. *Transl Lung Cancer Res* (2021) 10:452–61. doi: 10.21037/tlcr-20-943
13. Hattori A, Matsunaga T, Takamochi K, Oh S, Suzuki K. Prognostic Impact of a Ground Glass Opacity Component in the Clinical T Classification of non-Small Cell Lung Cancer. *J Thorac Cardiovasc Surg* (2017) 154:2102–10.e2101. doi: 10.1016/j.jtcvs.2017.08.037
14. Hattori A, Suzuki K, Takamochi K, Wakabayashi M, Aokage K, Saji H, et al. Prognostic Impact of a Ground-Glass Opacity Component in Clinical Stage IA non-Small Cell Lung Cancer. *J Thorac Cardiovasc Surg* (2021) 161:1469–80. doi: 10.1016/j.jtcvs.2020.01.107
15. Ye T, Deng L, Wang S, Xiang J, Zhang Y, Hu H, et al. Lung Adenocarcinomas Manifesting as Radiological Part-Solid Nodules Define a Special Clinical Subtype. *J Thorac Oncol* (2019) 14:617–27. doi: 10.1016/j.jtho.2018.12.030
16. Fu F, Zhang Y, Wen Z, Zheng D, Gao Z, Han H, et al. Distinct Prognostic Factors in Patients With Stage I Non-Small Cell Lung Cancer With Radiologic Part-Solid or Solid Lesions. *J Thorac Oncol* (2019) 14:2133–42. doi: 10.1016/j.jtho.2019.08.002
17. Travis WD, Brambilla E, Noguchi M, Nicholson AG, Geisinger KR, Yatabe Y, et al. International Association for the Study of Lung Cancer/American Thoracic Society/European Respiratory Society International Multidisciplinary Classification of Lung Adenocarcinoma. *J Thorac Oncol* (2011) 6:244–85. doi: 10.1097/JTO.0b013e318206a221
18. Li H. *Aligning Sequence Reads, Clone Sequences and Assembly Contigs With BWA-MEM* (2013). Available at: https://ui.adsabs.harvard.edu/abs/2013arXiv1303.3997L.
19. DePristo MA, Banks E, Poplin R, Garimella KV, Maguire JR, Hartl C, et al. A Framework for Variation Discovery and Genotyping Using Next-Generation DNA Sequencing Data. *Nat Genet* (2011) 43:491–8. doi: 10.1038/ng.806
20. Cibulskis K, Lawrence MS, Carter SL, Sivachenko A, Jaffe D, Sougnez C, et al. Sensitive Detection of Somatic Point Mutations in Impure and Heterogeneous Cancer Samples. *Nat Biotechnol* (2013) 31:213–9. doi: 10.1038/nbt.2514
21. Saunders CT, Wong WSW, Swamy S, Becq J, Murray LJ, Cheetham RK. Strelka: Accurate Somatic Small-Variant Calling From Sequenced Tumor-Normal Sample Pairs. *Bioinformatics* (2012) 28:1811–7. doi: 10.1093/bioinformatics/bts271
22. Ramos AH, Lichtenstein L, Gupta M, Lawrence MS, Pugh TJ, Saksena G, et al. Oncotator: Cancer Variant Annotation Tool. *Hum Mutat* (2015) 36:E2423–2429. doi: 10.1002/humu.22771
23. Lawrence MS, Stojanov P, Mermel CH, Robinson JT, Garraway LA, Golub TR, et al. Discovery and Saturation Analysis of Cancer Genes Across 21 Tumour Types. *Nature* (2014) 505:495–501. doi: 10.1038/nature12912
24. Talevich E, Shain AH, Botton T, Bastian BC. CNVkit: Genome-Wide Copy Number Detection and Visualization From Targeted DNA Sequencing. *PloS Comput Biol* (2016) 12:e1004873. doi: 10.1371/journal.pcbi.1004873
25. Mermel CH, Schumacher SE, Hill B, Meyerson ML, Beroukhim R, Getz G. GISTIC2.0 Facilitates Sensitive and Confident Localization of the Targets of Focal Somatic Copy-Number Alteration in Human Cancers. *Genome Biol* (2011) 12:R41. doi: 10.1186/gb-2011-12-4-r41
26. Nilsen G, Liestol K, Van Loo P, Vollan HKM, Eide MB, Rueda OM, et al. Copynumber: Efficient Algorithms for Single- and Multi-Track Copy Number Segmentation. *BMC Genomics* (2012) 13:591. doi: 10.1186/1471-2164-13-591
27. Dobin A, Davis CA, Schlesinger F, Drenkow J, Zaleski C, Jha S, et al. STAR: Ultrafast Universal RNA-Seq Aligner. *Bioinformatics* (2013) 29:15–21. doi: 10.1093/bioinformatics/bts635
28. Li B, Dewey CN. RSEM: Accurate Transcript Quantification From RNA-Seq Data With or Without a Reference Genome. *BMC Bioinf* (2011) 12:323. doi: 10.1186/1471-2105-12-323
29. Bu D, Luo H, Huo P, Wang Z, Zhang S, He Z, et al. KOBAS-I: Intelligent Prioritization and Exploratory Visualization of Biological Functions for Gene Enrichment Analysis. *Nucleic Acids Res* (2021) 49:W317–25. doi: 10.1093/nar/gkab447
30. Newman AM, Liu CL, Green MR, Gentles AJ, Feng W, Xu Y, et al. Robust Enumeration of Cell Subsets From Tissue Expression Profiles. *Nat Methods* (2015) 12:453–7. doi: 10.1038/nmeth.3337
31. Travis WD, Brambilla E, Nicholson AG, Yatabe Y, Austin JHM, Beasley MB, et al. The 2015 World Health Organization Classification of Lung Tumors: Impact of Genetic, Clinical and Radiologic Advances Since the 2004 Classification. *J Thorac Oncol* (2015) 10:1243–60. doi: 10.1097/JTO.0000000000000630
32. Sivakumar S, San Lucas FA, McDowell TL, Lang W, Xu L, Fujimoto J, et al. Genomic Landscape of Atypical Adenomatous Hyperplasia Reveals Divergent Modes to Lung Adenocarcinoma. *Cancer Res* (2017) 77:6119–30. doi: 10.1158/0008-5472.CAN-17-1605
33. Jiang N, Dai Q, Su X, Fu J, Feng X, Peng J. Role of PI3K/AKT Pathway in Cancer: The Framework of Malignant Behavior. *Mol Biol Rep* (2020) 47:4587–629. doi: 10.1007/s11033-020-05435-1
34. Dongre A, Weinberg RA. New Insights Into the Mechanisms of Epithelial-Mesenchymal Transition and Implications for Cancer. *Nat Rev Mol Cell Biol* (2019) 20:69–84. doi: 10.1038/s41580-018-0080-4
35. Zhang Y, Fu F, Chen H. Management of Ground-Glass Opacities in the Lung Cancer Spectrum. *Ann Thorac Surg* (2020) 110:1796–804. doi: 10.1016/j.athoracsur.2020.04.094

36. Sun F, Xi J, Zhan C, Yang X, Wang L, Shi Y, et al. Ground Glass Opacities: Imaging, Pathology, and Gene Mutations. *J Thorac Cardiovasc Surg* (2018) 156:808–13. doi: 10.1016/j.jtcvs.2018.02.110
37. Kobayashi Y, Mitsudomi T, Sakao Y, Yatabe Y. Genetic Features of Pulmonary Adenocarcinoma Presenting With Ground-Glass Nodules: The Differences Between Nodules With and Without Growth. *Ann Oncol* (2015) 26:156–61. doi: 10.1093/annonc/mdu505
38. Lu Q, Ma Y, An Z, Zhao T, Xu Z, Chen H. Epidermal Growth Factor Receptor Mutation Accelerates Radiographic Progression in Lung Adenocarcinoma Presented as a Solitary Ground-Glass Opacity. *J Thorac Dis* (2018) 10:6030–9. doi: 10.21037/jtd.2018.10.19
39. Li Y, Li X, Li H, Zhao Y, Liu Z, Sun K, et al. Genomic Characterisation of Pulmonary Subsolid Nodules: Mutational Landscape and Radiological Features. *Eur Respir J* (2020) 55:19014091. doi: 10.1183/13993003.01409-2019
40. Coschi CH, Dick FA. Chromosome Instability and Deregulated Proliferation: An Unavoidable Duo. *Cell Mol Life Sci* (2012) 69:2009–24. doi: 10.1007/s00018-011-0910-4
41. Endesfelder D, Burrell R, Kanu N, McGranahan N, Howell M, Parker PJ, et al. Chromosomal Instability Selects Gene Copy-Number Variants Encoding Core Regulators of Proliferation in ER+ Breast Cancer. *Cancer Res* (2014) 74:4853–63. doi: 10.1158/0008-5472.CAN-13-2664
42. Watkins TBK, Lim EL, Petkovic M, Elizalde S, Birkbak NJ, Wilson GA, et al. Pervasive Chromosomal Instability and Karyotype Order in Tumour Evolution. *Nature* (2020) 587:126–32. doi: 10.1038/s41586-020-2698-6
43. Rosenthal R, Cadieux EL, Salgado R, Al Bakir M, Moore DA, Hiley CT, et al. Neoantigen-Directed Immune Escape in Lung Cancer Evolution. *Nature* (2019) 567:479–85. doi: 10.1038/s41586-019-1032-7
44. Pitt JM, Marabelle A, Eggermont A, Soria JC, Kroemer G, Zitvogel L. Targeting the Tumor Microenvironment: Removing Obstruction to Anticancer Immune Responses and Immunotherapy. *Ann Oncol* (2016) 27:1482–92. doi: 10.1093/annonc/mdw168
45. Pepe F, Pisapia P, Gristina V, Rocco D, Micheli M, Micheli P, et al. Tumor Mutational Burden on Cytological Samples: A Pilot Study. *Cancer Cytopathol* (2021) 129:460–7. doi: 10.1002/cncy.22400
46. Pisapia P, Pepe F, Iaccarino A, Sgariglia R, Nacchio M, Conticelli F, et al. Next Generation Sequencing in Cytopathology: Focus on Non-Small Cell Lung Cancer. *Front Med (Lausanne)* (2021) 11:633923. doi: 10.3389/fmed.2021.633923
47. Mathew J, Kratzke RA. Lung Cancer and Lung Transplantation: A Review. *J Thorac Oncol* (2009) 4:753–60. doi: 10.1097/JTO.0b013e31819afdd9

Conflict of Interest: The authors declare that the research was conducted in the absence of any commercial or financial relationships that could be construed as a potential conflict of interest.

Publisher's Note: All claims expressed in this article are solely those of the authors and do not necessarily represent those of their affiliated organizations, or those of the publisher, the editors and the reviewers. Any product that may be evaluated in this article, or claim that may be made by its manufacturer, is not guaranteed or endorsed by the publisher.

frontiers | Frontiers in Immunology

ORIGINAL RESEARCH
published: 01 July 2022
doi: 10.3389/fimmu.2022.873871

SCG2: A Prognostic Marker That Pinpoints Chemotherapy and Immunotherapy in Colorectal Cancer

Siyuan Weng[1,2,3†], Zaoqu Liu[1,2,3†], Xiaofeng Ren[4†], Hui Xu[1,2,3], Xiaoyong Ge[1,2,3], Yuqing Ren[5], Yuyuan Zhang[1], Qin Dang[6], Long Liu[7], Chunguang Guo[8], Richard Beatson[9], Jinhai Deng[10] and Xinwei Han[1,2,3]*

[1] Department of Interventional Radiology, The First Affiliated Hospital of Zhengzhou University, Zhengzhou, China, [2] Interventional Institute of Zhengzhou University, Zhengzhou, China, [3] Interventional Treatment and Clinical Research Center of Henan Province, Zhengzhou, China, [4] Faculty of Engineering and Information Technology University of Technology Sydney, Sydney, NSW, Australia, [5] Department of Respiratory and Critical Care Medicine, The First Affiliated Hospital of Zhengzhou University, Zhengzhou, China, [6] Department of Colorectal Surgery, The First Affiliated Hospital of Zhengzhou University, Zhengzhou, China, [7] Department of Hepatobiliary and Pancreatic Surgery, The First Affiliated Hospital of Zhengzhou University, Zhengzhou, China, [8] Department of Endovascular Surgery, The First Affiliated Hospital of Zhengzhou University, Zhengzhou, China, [9] King's College London, School of Cancer and Pharmaceutical Sciences, Guy's Cancer Centre, London, United Kingdom, [10] Richard Dimbleby Laboratory of Cancer Research, School of Cancer and Pharmaceutical Sciences, King's College London, London, United Kingdom

Background: Fluorouracil (FU)-based chemotherapy regimens are indispensable in the comprehensive treatment of colorectal cancer (CRC). However, the heterogeneity of treated individuals and the severe adverse effects of chemotherapy results in limited overall benefit.

Methods: Firstly, Weighted gene co-expression network analysis (WGCNA) identified modules tightly associated with chemotherapy response. Then, the in-house cohort and prognostic cohorts from TCGA and GEO were subjected to Cox proportional hazards model and survival analysis to ascertain the predictable function of SCG2 on the prognosis of CRC patients. Finally, we performed *In vitro* experiments, functional analysis, somatic mutation, and copy number variation research to explore the biological characteristics of SCG2.

Results: We identified red and green as the modules most associated with chemotherapy response, in which SCG2 was considered a risky factor with higher expression predicting poorer prognosis. SCG2 expression in the APC non-mutation group was remarkably higher than in the mutation group. The mutation frequencies of amplified genes differed significantly between different SCG2 expression subgroups. Besides, CRC cell lines with SCG2 knockdown have reduced invasive, proliferative, and proliferative capacity. We discovered that the SCG2 high expression subgroup was the immune hot type and considered more suitable for immunotherapy.

Conclusion: This study demonstrates the clinical significance and biological characteristics of SCG2, which could serve as a promising biomarker to identify patients who may benefit from chemotherapy and immunotherapy.

Keywords: colorectal cancer, chemotherapy, prognosis, immunotherapy, biomarker

OPEN ACCESS

Edited by:
Xian Zeng,
Fudan University, China

Reviewed by:
Nannan Kong,
Huazhong University of Science and Technology, China
Yin Qiu Tan,
Huazhong University of Science and Technology, China

****Correspondence:***
Xinwei Han
fcchanxw@zzu.edu.cn

†These authors have contributed equally to this work

Specialty section:
This article was submitted to Cancer Immunity and Immunotherapy, a section of the journal Frontiers in Immunology

Received: *11 February 2022*
Accepted: *31 May 2022*
Published: *01 July 2022*

Citation:
Weng S, Liu Z, Ren X, Xu H, Ge X, Ren Y, Zhang Y, Dang Q, Liu L, Guo C, Beatson R, Deng J and Han X (2022) SCG2: A Prognostic Marker That Pinpoints Chemotherapy and Immunotherapy in Colorectal Cancer. Front. Immunol. 13:873871. doi: 10.3389/fimmu.2022.873871

INTRODUCTION

Colorectal cancer (CRC) accounts for approximately 10% of all annual diagnosed cancer and oncology-related deaths worldwide and is the second leading contributor of cancer death worldwide (1). Although the development of early screening methods and efficacious treatment options has contributed to a dramatic improvement in colorectal cancer patients, CRC remains a considerable health burden (2–4). Since the 90s of the 20th century, fluorouracil (FU)-based adjuvant chemotherapy has been an essential choice to decrease the risk of advanced colorectal cancer (5). For stage II patients with risk factors, fluoropyrimidine monotherapy is often used. In resected stage III colorectal cancer, adjuvant fluoropyrimidine alone reduces the risk of death by 10% to 15%, with an additional 4% to 6% diminution in the risk of death when treatment consists of oxaliplatin-based combination therapy (6). Although adjuvant chemotherapy has achieved remarkable results, the heterogeneity of the tumor and risk factors of disease make the clinical outcome and treatment response of CRC patients very different (7). However, there is considerable potential to improve the benefit ratio by adopting a more personalized approach. The noninferiority of 3-month adjuvant chemotherapy illustrates this possibility compared to 6-month standard treatment duration in patients with low-risk stage III and high-risk stage II CRC (8, 9).

The tremendous benefit achieved in the past several years with the appearance of immunotherapy and checkpoint inhibitors (ICIs) has revolutionized the field of oncology, particularly regarding the therapy of solid tumors (10). Immuno-checkpoint regimens received FDA approval in 2017 for CRC patients with defective mismatch repair (dMMR) or high-level microsatellite instability (MSI-H). In addition, more meticulous tumor biological stratification has led to successfully durable responses to PD1 and CTLA4 inhibitors in some patients, such as tumor mutation burden (TMB) and tumor environment (TME) (11). By contrast, ICIs perform tiny efficiency on tumors with mismatch repair proficient (pMMR), microsatellite-stable (MSS), or low levels of microsatellite instability (MSI-L), which account for a large proportion of CRC (12). Besides, TMB is also not the only biological marker to judge the response to immunotherapy (13). Therefore, based on the polymorphisms of tumor biology, it is imperative to investigate novelty biomarkers that can promote immunotherapy precisely in CRC.

While chemotherapy and immunotherapy exert their unique advantages in the multimodality treatment of CRC, the limitations of monotherapy with each of them make the therapeutic benefit applicable to only a minority of CRC patients. A growing body of research has shown that chemotherapy is simple tumor suppression and involves positive immune system regulation. CRC treatment with conventional chemotherapeutic agents also represents a monstrous burden for the patient's apparatus due to the high toxicity and the correspondingly low response (14). Recent advancements in deciphering the biology and drivers of early-stage disease and the microenvironment promise to translate into patient-specific therapeutic strategies (6). Stratified approach or biomarkers to guide precise treatment of CRC will prevent unnecessary burdens on patients both physically, mentally, and financially. However, there is no proposed biomarker to determine the prognosis while also predicting the efficacy of chemotherapy and immunotherapy in patients. In the present research, we integrated the chemotherapy and prognosis data analysis by bioinformatics methods to identify a marker that predicted prognosis and response to chemotherapy and discovered that the biomarker also predicted potential immunotherapeutic responding.

METHODS

Public Data Access and Proceed

Somatic mutation profiles, copy number alteration (CNA), RNA sequencing data, and correspondent clinical information of CRC sourced from The Cancer Genome Atlas (TCGA) portal. Expression microarrays datasets containing chemotherapy (GSE19860, GSE62080, GSE69657) and survival (GSE161158, GSE17536, GSE17537, GSE29621, GSE38832, GSE39582, GSE87211) cohorts were accessed from the Gene Expression Omnibus (GEO) database. Meta-GEO cohort consisted of 3 chemotherapy databases, in which raw data were acquired and further handled *via* a robust multi-array averaging algorithm (RMA) incorporated in the "affy" R package (15). We rectified batch effects using the ComBat function in the "sva" R package.

WGCNA and Identifying Key Module

Weighted Gene Co-expression Network Analysis (WGCNA) facilitates network-based gene screening, detecting markers with specific characteristics, such as treatment response. To define latent highly co-expressed clusters of genes, we developed the gene profiling of the Meta-GEO cohort into gene co-expression networks using the "WGCNA" package (16, 17). The clustering analysis of samples was achieved *via* the "hclust" function to validate and remove outliers. An appropriately elected soft power threshold that could accentuate robust associations of genes and penalize low associations ensures the scale-free network. The adjacency matrix is founded by analyzing the Pearson correlation between each extracted gene pair and transformed into a topological overlap matrix (TOM) and a corresponding dissimilarity (1-TOM). The "DynamicTreeCut" algorithm implemented network configuration and consensus module detection. The module eigengene (ME) was calculated for each *module*, representing the gene expression profiles of a given module. The modules with the high correlation coefficient between ME profiles and clinical feature information were considered candidate modules and selected for consequent analysis.

Functional Enrichment Analysis

Gene ontology (GO) and Kyoto Encyclopedia of Genes and Genomes (KEGG) combine genomic information with advanced functional information to explain the function of genes. The enrichment of GO compasses biological process (BP), cellular component (CC), and molecular function (MF). We conducted the GO term and KEGG pathway analysis with the

"clusterProfiler" R package for genes based on feature-related modules. P-value <0.05 was deemed to be statistically significant for functional annotation.

Identification and Validation of Prognostic Hub Genes

To further identify hub genes that tightly connect with chemotherapy response, we adopted the 'pROC' R package to calculate the area under the receiver operating characteristic curve (AUC) to evaluate the chemotherapy-predicted power of the candidate module genes. Gene, whose AUC >0.7 simultaneously in 3 chemotherapy cohorts, was selected to perform the univariate Cox analysis to determine prognostic genes in relapse-free and overall survival cohorts. Kaplan-Meier survival curves with log-rank tests validated the foreboding power of these genes (P <0.05). Subsequently, the results obtained by the external queue by the above method are further elaborated in the in-house chemotherapy cohort.

Validation of Gene Expression by qRT-PCR

The genes associated with both prognosis and chemotherapy were detected in quantitative real-time PCR analysis. The clinicopathological features of each patient are summarized in **Table S1**. Total RNA was extracted from the human tumor and adjacent normal tissues using TRIzol reagent (Invitrogen, Carlsbad, CA, USA) and reverse transcript using TIANScript RT kit (Servicebio, Wuhan, China). The expression value of the target genes was normalized to GAPDH and then log2 transformation for subsequent analysis. The primer sequences of the included four genes and GAPDH are shown in **Table S2**. The 2-ΔΔCT approach was applied to compute the relative RNA expression of each gene.

Immunohistochemistry

Immunohistochemistry (IHC) was performed using an anti-SCG2 (BS-1988R, 1:500) antibody. Staining percentage scores were classified as follows: 1 (1%-25%), 2 (26%-50%), 3 (51%-75%), and 4 (76%-100%), and staining intensity was scored 0 (signal less color) to 3 (light yellow, brown and dark brown). The stained tissues were scored by three individuals blinded to the clinical parameters, and the IHC scores were determined by percentage and intensity scores.

Gene Set Enrichment Analysis

For confirming the biological features of SCG2, we counted the correlations with the other genes and ordered genes based on results. The ordered gene list was input GSEA analysis to investigate whether strongly correlated genes gathered in meaningfully functional pathways. The annotated gene set chosen as the reference gene set included c5.go.v7.4.symbols.gmt and c2.cp.kegg.v7.4.symbols.gmt. False discovery rate (FDR) <0.05 and p-value <0.01 were regarded significant as described previously.

Gene Set Variation Analysis

For further investigating the differences of SCG2 about biological processes, we divided the samples from TCGA datasets into two groups depending on the median expression of SCG2 and subsequently utilized GSVA enrichment analysis to investigate whether differentially expressed genes in the two groups gathered meaningfully functional pathways. The annotated gene set hallmarks downloaded from the GSEA portal were chosen as the reference gene set. The absolute values of t >1 were considered significant as described previously (18).

The Landscape of Somatic Mutation

Tumor mutation burden (TMB) was considered the biomarker representing macroscopic alterations of genomic mutations. We calculated all base substitutions and insertions or deletions in the coding regions of the target genes. The top 30 genes in mutation frequency were defined as the driver genes by the 'maftool' R package. In accord with the expression of SCG2, the mutation landscape of the driver genes in two groups of samples was described respectively with regarding p-value <0.05 as remarked differences. Univariate and multivariate logistic regression analysis investigated the dependence of driver gene mutations on SCG2 with additional clinical information, including TMB, age, gender, and stage.

Copy Number Alteration Analysis

We conducted the GISTIC 2.0 pipeline to determine the significantly amplified and deleted genome regions. A mutational landscape map of CNA was constructed by amplifying and deleting each of the top 15 genes in copy number. We compared the expression differences of each gene in groups with different SCG2 expressions and implemented logistic regression analysis to explore the role of SCG2 in CNA. Univariate logistics used SCG2 expression as an independent variable. In multivariate logistics regression, SCG2 expression and fraction of genome gained (FGG) were included as independent variables when amplified genes were dependent variables, while SCG2 expression and fraction of genome lost (FGL) were included as independent variables when deleted genes were dependent variables.

Cell Transient Transfection, RNA Extraction and qRT-PCR

The current research used two cell lines comprising human CRC cell lines, HCT116 and SW480. CAL-27 and CAL-33 were incubated in DMEM (Solarbio, Beijing, China) containing 10% fetal bovine serum (Bioind, Kibbutz Beit Haemek, Israel), preserved in the humidified incubator with 5% CO_2, 37°C. RiboFECT^{TM} CP (RiboBio, Guangzhou, China) was used to transfect Negative Control (NC) and SCG2 siRNAs (RiboBio, Guangzhou, China) into CRC cells according to the manufacturer's instruction. The plates were placed in the incubator for 48 hours, and total RNA was extracted for qRT-PCR. The siRNA sequences were as follows:

siRNA#1 5' CCTATGCCTTGAATTCAGA dTdT 3',
siRNA#2 5' GCCGAATGGATCAGTGGAA dTdT 3',
siRNA#3 5' CCAAGTGAAGCGAGTTCCT dTdT 3'.

Wound Healing Assay

The constructed NC and SCG2 siRNA cells were seeded in 24-well culture plates (1×10^5/well) and placed at 37°C, Incubated

overnight in a 5% CO_2 incubator. Remove the medium and use a 10 μl pipette tip to scratch and mark the surface of the inoculated cells. Wash gently with PBS three times. Photograph the scratches at 0 h and 48 h. The experiment is repeated three times. Measure the distance of cell migration to the injured area during this period.

Transwell Assay

Transwell chambers were utilized to measure the invasion and migration ability of the cells. Approximately 4×10^4 transiently transfected cells were cultured in the upper chamber with serum-free medium, while a complete medium was added to the lower chamber. Cells were maintained at 37°C for 24 hours, washed with physiological saline, and fixed with methanol. After that, 0.1% crystal violet stain solution (Solarbio) was used to stain the cells. Finally, cells were photographed under a microscope, and stained cells were counted.

Colony Formation Assay

Each cell line was inoculated in a gradient of 50, 100, and 200 cells per dish, respectively, and cells were cultured in a 5% CO_2 incubator at 37°C for 2 weeks. At the end-point, the cells were washed with cold phosphate-buffered saline (PBS) twice, fixed with 4% paraformaldehyde for 15 minutes, and stained with 1% crystal violet solution for 20 minutes at room temperature. The visible colony numbers were counted. This experiment was performed in triplicate. Finally, to calculate the clone formation rate (Clone formation rate =(number of clones/ number of inoculated cells) × 100%).

Cell Counting Kit-8 Assay

Approximately 1×10^4 transiently transfected cells in 100 μL medium were maintained in 96-well plates. After 24, 48, 72, and 96 hours incubation, 10 μL cell counting kit-8 assay (CCK8) solution was added to each well. After 2 hours of additional incubation, the optical density (OD) value at 450 nm was measured with a microplate reader.

5-Ethynyl-2'-Deoxyuridine Assay

First, HCT116 and SW480 cells were grown in a 5-ethynyl-2'-deoxyuridine (EdU) solution for 2 hr. The cells were fixed with PBS containing 4% paraformaldehyde. Finally, the fixed cells were deposited in 70% ethanol, and then Cell-Light™ EdU Apollo®567 *In Vitro* Imaging Kit (RiboBio, China) was used to dye cells. Cell growth was observed by fluorescence microscopy.

Evaluation of Immune Infiltration and Immunotherapy Response

Single-sample gene set enrichment analysis (ssGSEA) quantified the infiltration level of immunity cells in individual cancer samples based on the 'ssGSEA' R package. The deconvolution method was employed in this research covering 28 immune cells in innate immunity (19). Then, we predicted clinical reactions to ICIs according to pre-treatment expression data of tumors with the Tumor Immune Dysfunction and Exclusion (TIDE) web tool (http://tide.dfci.harvard.edu/). The TIDE framework evaluates immune evasion by integrating T cell dysfunction and rejection (20). By the TIDE tool, we acquired the results of the bioinformatics evaluation of each patient's exposure to immunotherapy. The Subclass Mapping (SubMap) is an unsupervised clustering algorithm discovering shared subtypes among separate queues. With the SubMap approach, we analyzed similar transcriptome expression patterns between SCG2 differentially expressed groups and patients with distinct immunotherapy responses (21). FDR <0.05 suggested that the two subcategories were significantly similar.

The Prediction of Potential Drug

We employed the Connectivity Map (CMap), a data-driven, systematic approach for discovering associations among genes, chemicals, and biological conditions, to search for candidate compounds that might target pathways associated with CRC (22). To further investigate the mechanism of actions (MoA) and drug target, we performed specific analysis through CMap tools.

Statistical Analysis

R version 4.1.0 was employed to conduct all statistical analyses and plotting while processing data. The correlation of gene expression with gene significance for drug response was evaluated using the Person or Spearman correlation coefficient. The Wilcoxon rank-sum test and Kruskal-Wallis test were applied to test for differences between two and multiple groups. The Kaplan-Meier analysis was performed *via* the "survival" R package, and the log-rank test was applied to compare the survival differences among three phenotypes. All p-values were bilateral, and less than 0.05 were considered statistically significant.

RESULTS

Modules Relevant to Chemotherapy Response

The flow chart of this study is shown in **Figure 1**. For identifying significant modules associated with the response of Fluoropyrimidine-based chemotherapy in CRC, we removed outlying samples from the Meta-GEO cohort after batch correction (**Figures 2A, B**) and performed WGCNA. The optimal β =6 considered the soft threshold ensured that the constructed networks were scale-free (scale-free R2>0.90, **Figure 2C**). To make the segmentation of modules easier, we transformed the adjacency matrix to the topological overlap matrix (TOM), which is displayed in **Figure S1A**. Then, using a cutoff of 0.25 and a minimum module size of 50 contributed to 18 modules (**Figure 2D**). An eigengene adjacency heatmap depicted the correlations between modules (**Figure S1B**). Subsequently, we used a heatmap to explore the relationship between modules and chemotherapy response (**Figure 2E**). The red block (r =0.42, *P* =0.002) and the green block (r =-0.32, *P* =0.02) had the greatest correlations with chemotherapy response. The expression level of 623 genes in the red block was positively correlated with chemotherapy response, while 170 genes in the green block were negatively correlated with

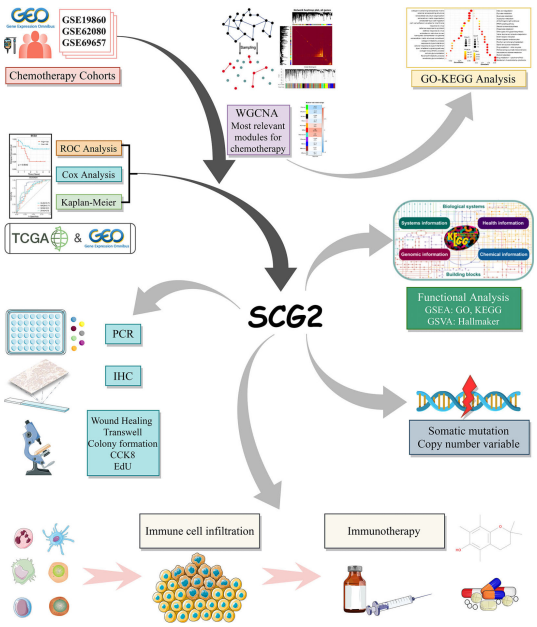

FIGURE 1 | The flow chart of this study.

chemotherapy response (**Figures 2F, G**). It implied that 793 genes serve more critical functions in the molecular mechanisms of chemotherapy response.

Functional Analysis and Identify Prognostic Genes in Modules

To further dissect the potential mechanisms of the above modules, we conducted the KEGG enrichment analysis and GO enrichment analysis of the 793 genes in the modules based on the R package "clusterProfiler". The outcomes showed that 51 GO terms and 32 KEGG pathways were significantly enriched in module genes. Some of these GO terms (extracellular matrix organization, ameboid-type cell migration, type I interferon signaling pathway), as well as part of the KEGG pathways (Metabolism of xenobiotics by cytochrome P450, Drug metabolism-cytochrome P450, ECM-receptor interaction), is displayed through the bubble diagram (**Figure 3A**). Afterward, we evaluated the area under the curve (AUC) values of all modular genes in the three chemotherapy cohorts to better identify the genes that can determine the response to CRC chemotherapy. Genes with AUC >0.7 in each chemotherapy cohort seem as core genes, which consist of 20 candidate genes shown in **Figure 3B**. One-way Cox analysis of the above genes yielded four signatures (GILS2, MAOB, SCG2, ZHX2) that consistently act as risk factors in more than half of the cohorts with relapse-free survival (RFS). Besides, in a one-way Cox analysis of samples with overall survival (OS), these signatures were still more closely related to prognosis than other genes (**Figures 3C**, **S1C**). For validating the effects of the signatures on prognosis, the patients in RFS and OS cohorts were allocated to groups according to the high or low expression of the 20 genes using the cutoff values acquired with the "survminer" package and performed Kaplan-Meier survival analyses and log-rank tests (**Figures S1D**, **S2A**). Quantitative PCR results showed that only SCG2 (P <0.001) expression in the tumor was markedly higher than that in adjacent normal tissues (**Figure 3D**). Immunohistochemical staining for SCG2 in CRC specimens showed the same trend (**Figure 3E**). In addition, in the RFS survival analysis of the internal cohort, the group with high SCG2 (P <0.01) expression suggested a poor prognosis, and there was no statistically significant difference in MOAB (P =0.12), GLIS2 (P =0.18), and ZHX2 (P =0.095) (**Figure 3F**). However, in agreement with the outcomes from external cohorts, these four genes still showed good performance in predicting chemotherapy response (**Figure S2B**). Univariate and multifactorial Cox regression analysis indicated that SCG2 could be considered an independent predictor of prognosis (**Figures 3G, H**). Therefore, SCG2 may be a latent biological marker to predict chemotherapy response and prognosis.

Exploring the Biological Characteristics of SCG2

Based on the correlation between SCG2 and other genes, the GSEA enrichment analysis revealed that SCG2 was involved in cancer invasion and growth signaling pathways. The GO terms shown in **Figure 4A** significantly enriched the genes highly related to SCG2, including cell-matrix adhesion, cell-substrate adhesion, mesenchymal cell differentiation, endothelial cell migration, and epithelial cell proliferation (**Figure 4C**). The KEGG pathways shown in **Figure 4B** include ECM receptor interaction, focal adhesion, cell adhesion molecules (CAMs), pathway in cancer, and chemokine signaling pathway (**Figure 4D**). The GSVA analysis of hallmark pathway gene signatures highlighted that, under the condition of differential

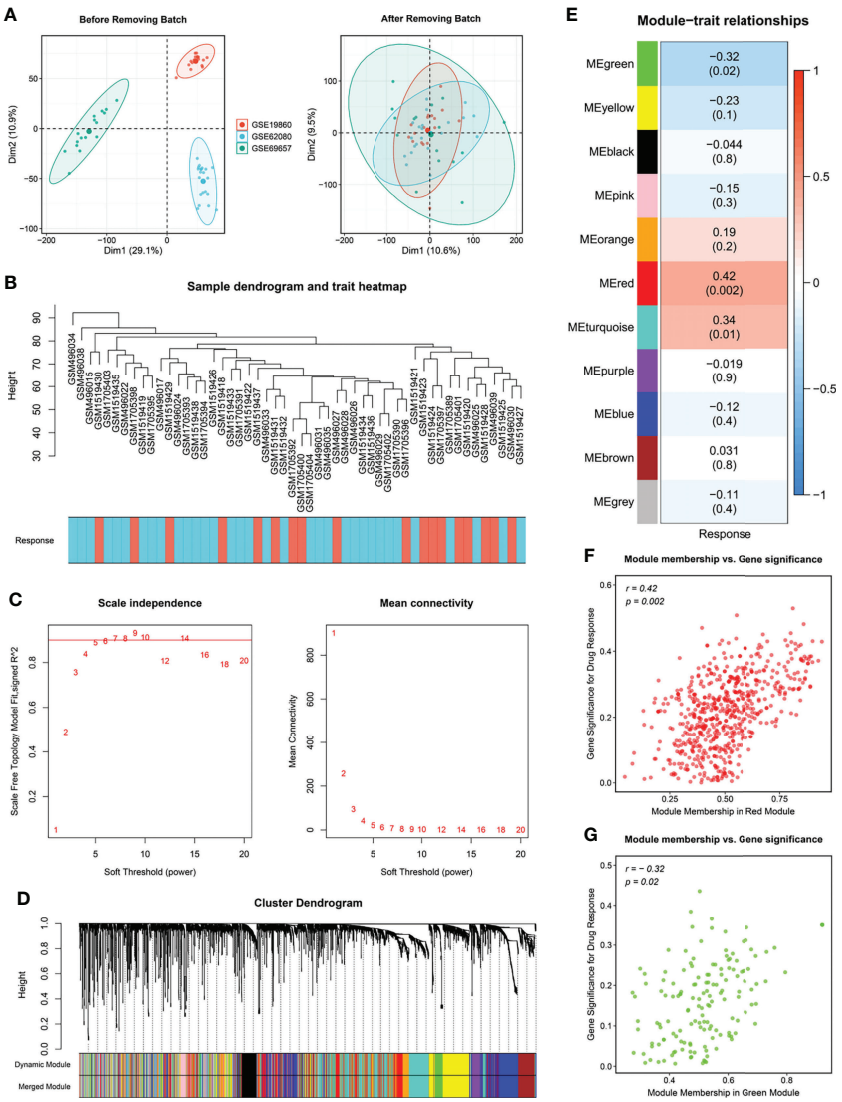

FIGURE 2 | Modules relevant to chemotherapy response. **(A)** Raw data from GSE19860, GSE62080 and GSE69657 were batch corrected to form a Meta cohort. **(B)** Remaining samples after discarding outliers. **(C)** Scale-free topological indices at various soft-thresholding powers. **(D)** Gene clustering diagram based on hierarchical clustering under optimal soft-thresholding power. **(E)** Correlations between gene modules and chemotherapy response. **(F, G)** The correlation between the key modules (red, **F**; green, **G**) memberships and the gene significance for chemotherapy response.

expression between high and low, most changes focus on cancer development and progression mechanisms, such as KRAS signaling and the TP53 pathway (**Figure 4E**). Integrative analysis of biological pathways hints that SCG2 may be engaged in meditating tumor growth and invasion.

Cell Culture and Functional Assay

Specific shRNAs (sh-Control, sh-SCG2#1/2/3) and SCG2 plasmids were transfected into HCT116 and SW480 cancer cell lines, and the expression of the SCG2 gene was verified by qRT-PCR (**Figures 5A, B**). Then, wound-healing assays showed that depletion of SCG2 significantly inhibited the healing of scratched wounds (**Figure 5C**). In line with the above outcomes, Transwell assays confirmed that SCG2 snubbing suppressed CT116 and SW480 cells (**Figures 5D–H**). On the contrary, cancer cells with SCG2 overexpression demonstrated more aggressive migratory and invasive potential.

In the study of cell proliferation, reduced SCG2 expression significantly suppressed the cell colony formation capacity in HCT116 and SW480 cells (**Figures 6A, B**). The CCK8 assay showed that significant differences in cell proliferation could be observed in HCT116 (P <0.05) and SW480 (P <0.05) cells with knockdown of SCG2 compared to control cells (**Figures 6C, D**). Further validation by EdU assay showed that knockdown of SCG2 in two cell lines markedly restrained cell proliferation, and the control group with SCG2 overexpression proliferated actively (**Figures 6E–G**). This result hints that overexpression of SCG2 is closely associated with CRC proliferation.

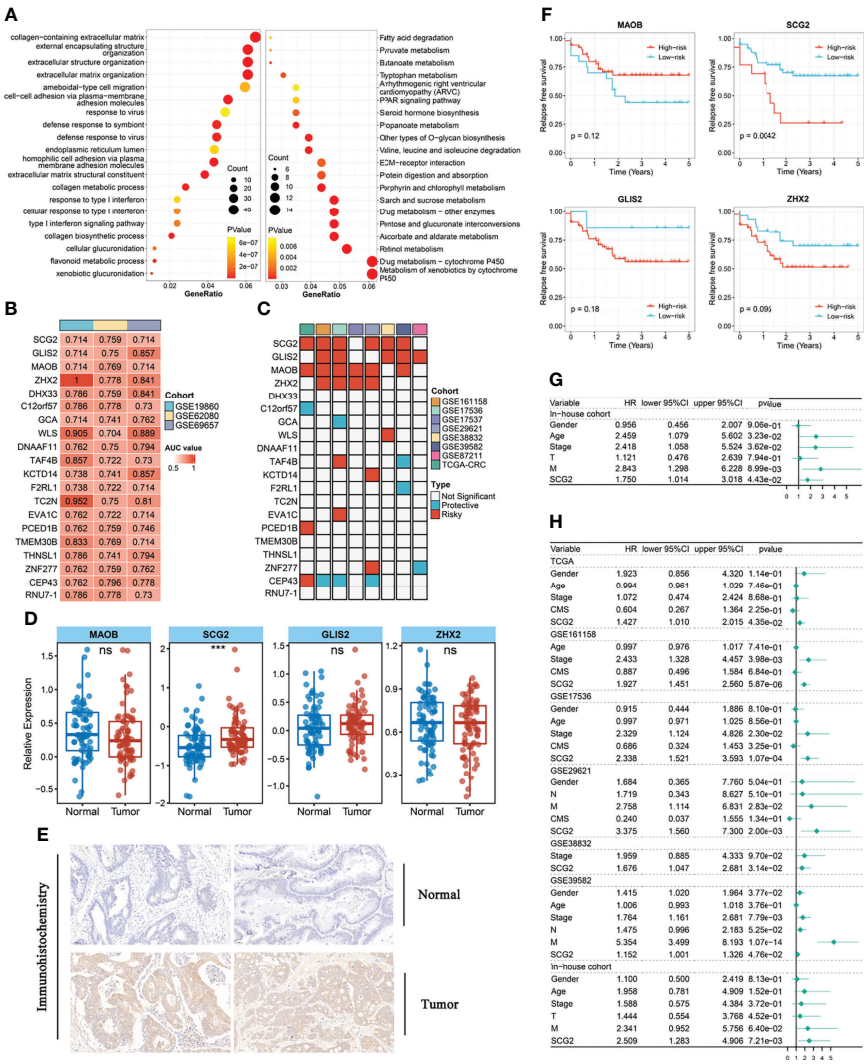

FIGURE 3 | Functional analysis and identify prognostic genes in modules. **(A)** Gene ontology (GO) and Kyoto Encyclopedia of Genes and Genomes (KEGG) enrichment analysis of genes in key modules. **(B)** The 20 module genes with AUC values >0.7 in all chemotherapy cohorts. **(C)** Univariate analysis with relapse-free survival (RFS) as the outcome event and the expression of the above 20 genes as independent variables. **(D)** Different expression of GILS2, MAOB, SCG2, ZHX2 between tumor and normal tissues in the internal cohort. **(E)** Representative IHC staining images of SCG2 between colorectal cancer and normal tissue. **(F)** Survival analysis of in-house cohort with RFS. **(G)** Univariate analysis of internal cohort with relapse-free survival (RFS) as the outcome event. **(H)** Multi-factor regression analysis of internal and external queues with relapse-free survival (RFS) as the outcome event. ns, P >0.05; ***P <0.001.

Gene Mutation and Copy Number Variation Analysis

A total of 30 frequently mutated genes (FMGs) were identified in the CRC patients from TCGA, consisting APC (78%), TP53 (61%), TTN (48%), KRAS (43%), SYNE1 (28%), MUC16 (25%), PIK3CA (25%), FAT4 (22%), RYR2 (19%), ZFHX4 (19%), OBSCN (18%), DNAH5 (17%), DNAH11 (17%), LRP1B (16%), PCLO (16%), ABCA13 (16%), FBXW7 (16%), CSMD1 (15%), FLG (15%), CSMD3 (15%), USH2A (14%), FAT3 (14%), RYR1 (14%), ADGRV1 (14%), LRP2 (14%), MUC4 (14%), SMAD4 (13%), RYR3 (13%), MUC5B (13%), NEB (13%; **Figure 7A**). Despite the high mutation frequency of FMGs in CRC, there were no significant differences in TMB between SCG2-expressing subgroups and no statistically significant correlation analysis between TMB and SCG2 (**Figures S3A, B**). Similarly, neoantigen load, which is highly related to TMB, was not significantly associated with SCG2 expression (**Figure S3C**). The mutation frequencies of APC and ABCA13 were dramatically distinct between samples from the high and low SCG2 expression groups (**Figure 7B**). Nevertheless, only APC appeared significant expression differences of SCG2 between mutation and non-mutation groups in FMGs (**Figure S3D**). Univariate logistics regression with SCG2 expression as the independent variable indicated that SCG2 expression is an important factor influencing for APC mutation (**Figure S3E**). The above results were confirmed

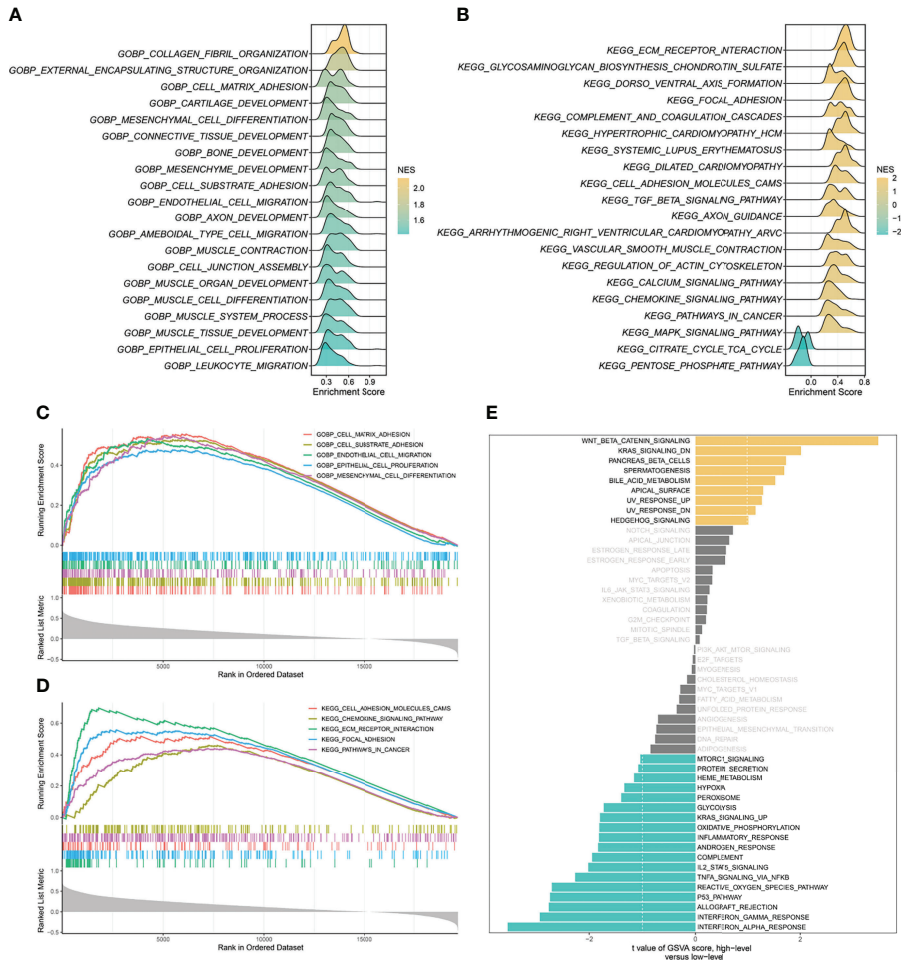

FIGURE 4 | Gene set enrichment analysis (GSEA) and gene set variation analysis (GSVA) of SCG2. **(A)** Top 20 Gene Ontology (GO) terms with significant enrichment. **(B)** Top 20 Kyoto Encyclopedia of Genes and Genomes (KEGG) pathways with significant enrichment. **(C)** Five significantly enriched GO terms associated with SCG2. **(D)** Five Significantly enriched KEGG pathways associated with SCG2. **(E)** Differences in pathway activities scored by GSVA between high and low expression of SCG2.

in multivariate logistics regression analysis covering variables of TMB, age, gender, stage, and SCG2 expression (**Figure 7C**). In the copy number variation analysis, the top 15 genes with the highest frequency of amplification and deletion, respectively, are shown in **Figure 7D**. Among them, the expression levels of SCG2 present a statistically significant difference between mutant and non-mutant subgroups of all amplified genes (**Figure 7E**). Univariate and multivariate logistic regression analysis revealed that SCG2 expression was an independent factor for all amplified genes mutation (**Figure S3G**). However, At the arm level, both the gain and loss loads were not significantly associated with SCG2 expression (**Figure S3F**).

Immune Infiltration Associated With SCG2 Expression

We utilized the ssGSEA approach to deconvolve the relative abundance of each immune cell type with transcriptome expression profiling data retrieved from the TCGA repository. Correlation analysis between SCG2 expression samples and 28 immune cell infiltration scores in CRC samples suggested that 22 cells were significantly associated with SCG2 (**Figure 8A**). According to the immune cell infiltration score, hierarchical clustering was used to stratify the samples into three groups: high, medium, and low. Samples with high SCG2 expression and APC mutation tend to be included in high immune infiltration (**Figure 8B**). There were likewise remarkable differences in SCG2 expression among samples from distinct immune infiltrate groups: SCG2 expression was highest in the high infiltration group, followed by the medium infiltration group, and lowest in the low infiltration group (**Figure 8C**).

Further study on the immune difference between high and low SCG2 groups showed the distinction of the immune landscape by ComplexHeatmap. The results showed that the immune cell score and the expression of immune-related molecular markers were

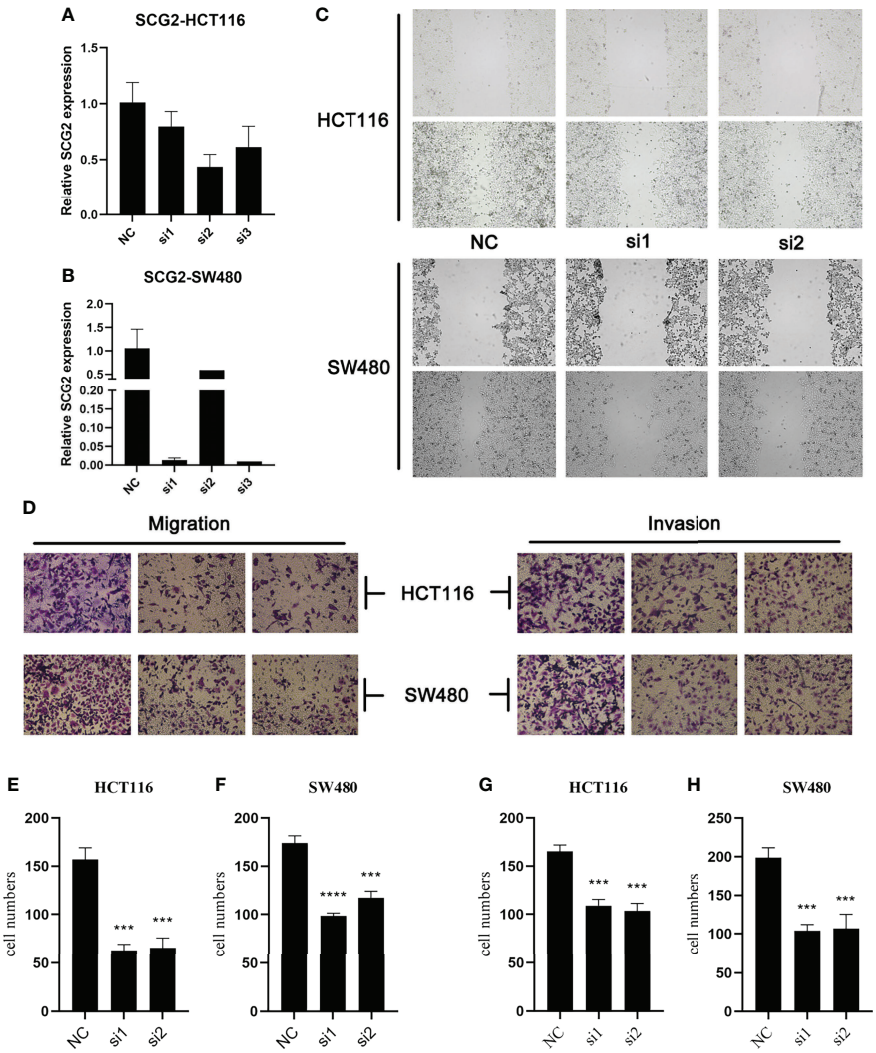

FIGURE 5 | Effects of SCG2 on CRC cells migration and invasion. **(A, B)** Expression was significantly reduced after SCG2 knockdown in in HCT116 **(A)** and SW480 **(B)** cell lines. **(C)** Wound-healing assay to detect the migratory ability of CRC cells in the control group and SCG2 downregulation group. **(D)** Transwell assay to detect the migratory and invasive ability of CRC cells in the control group and SCG2 downregulation group. **(E–H)** SCG2 knockdown significantly inhibits migration and invasion behavior in HCT119 **(E, G)** and SW480 **(F, H)** cell lines. ***P <0.001; ****P <0.0001.

significantly higher in the high SCG2 expression group than in the low expression group (**Figure 8D**). Immune checkpoints are generally overexpressed in the SCG2 high group. Molecular markers of immune checkpoints such as CD274, CD276, CTLA4, ICOS, ICOSLG, PDCD1, PDCD1LG2, TMIGD2, VTCN1, BTLA, CD27, CD40, CD70, TNFRSF9, TNFSF14, ENTPD1, HAVCR2, IDO1, LAG3, NT5E, and SIGLEC15 were significantly overexpressed in the SCG2 high group than the low group. Although the expression of HHLA2, CD40LG, TNFRSF18, FGL1, and NCR3 was not statistically different between the two groups, there was still a trend of overexpression in the high expression group (**Figure 8E**). Altogether, the molecular characterization of high SCG2 expression is of great significance for immunotherapy.

Immunotherapy and Potential Drug Targets

We found significant expression similarity between patients with high SCG2 expression treated with anti-CTLA-4 by SubMap analysis, which revealed the same subtype sensitive to immunotherapy between independent cohorts (FDR <0.05; **Figure 8F**). The result follows the preliminary finding that immunotherapy may yield a better response in the high expression group. We performed the TIDE framework to estimate the immunotherapy response of each patient and encountered the ratio of responders to immunotherapy in high SCG2 expression was bigger than low SCG2 expression (high vs. low: 55% vs. 26%; P <0.001; **Figure 8G**). We operated CMap to

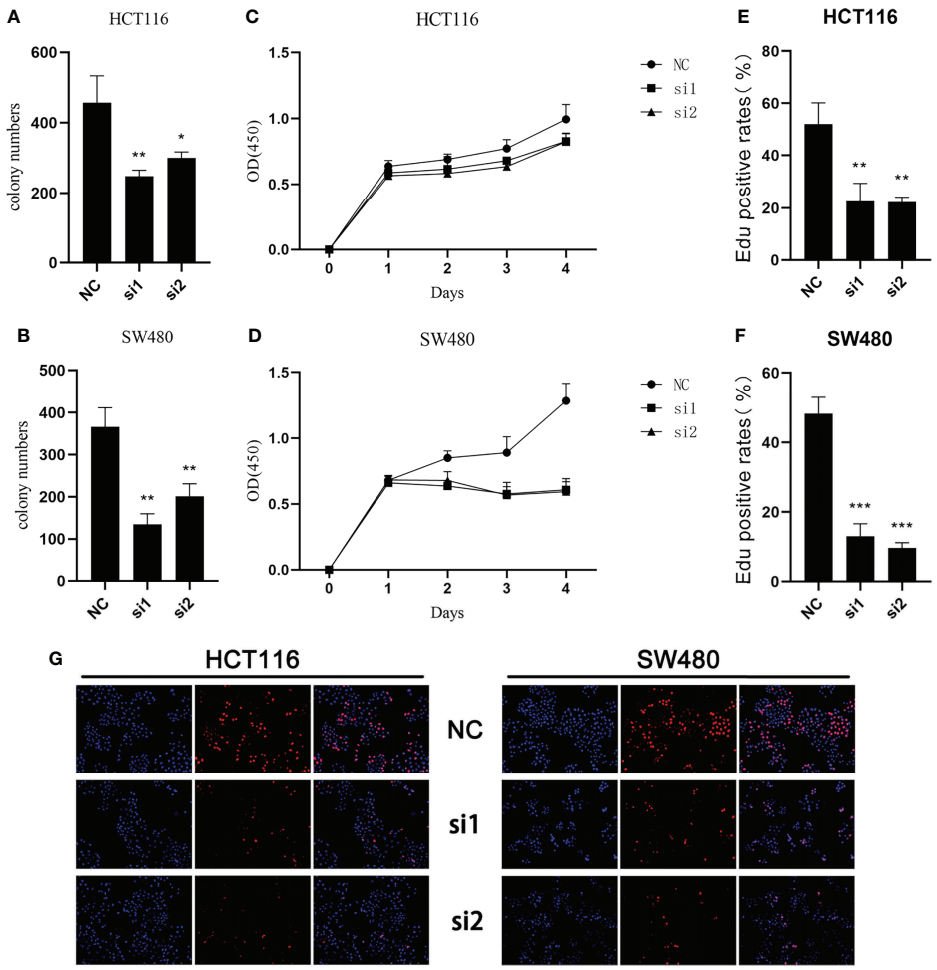

FIGURE 6 | Effects of SCG2 on CRC cells proliferation. **(A, B)** SCG2 knockdown significantly reduced colony numbers of HCT116 **(A)** and SW480 **(B)** cell lines. **(C, D)** Reduced proliferative capacity of SCG2 knockdown HCT116 **(C)** and SW480 **(D)** cell lines in CCK8 array. **(E-G)** EdU assay **(G**, left: DAPI, middle: EdU, right: Merge**)** to detect the proliferative ability of CRC cells in the control group and SCG2 downregulation group. SCG2 knockdown significantly reduced the proliferative ability of HCT116 **(E)** and SW480 **(F)** cell lines. *P <0.05; **P <0.01; ***P <0.001.

explore prospect blends that might target pathways associated with the SCG2 gene. The results showed that 107 compounds were significantly enriched, and we selected the top 20 compounds based on specificity and obtained their mechanism of action by CMap Mode-of-action (MOA) analysis (**Figures S4A, B**).

DISCUSSION

Despite the inspiring advances of CRC chemotherapy so far, the response rate in patients continues to remain low, and the treatment benefits are uneven due to the development of chemoresistance. Such inter-individual differences may stem from the unique genetic and epigenetic make-up of each individual (23). Thus, there is a pressing demand for molecular identifications to guide clinical chemotherapy. The genomic transcriptome reflects tumor heterogeneity and promises personalized therapy (7). In our research, crucial modules associated with chemotherapy response yielded after WGCNA, and the survival analysis presented a valuable biomarker. Most of the pathways enriched in module genes are associated with extracellular matrix and drug metabolism, embodying the potential value of these genes in predicting response to chemotherapy. Multiple studies have demonstrated that elevated extracellular matrix in colorectal cancer tissues promotes aggressive tumor growth or increases drug resistance (24, 25), which further suggests a potential link between modular genes with drug response and tumor progression.

Comprehensive analysis of independent cohorts with OS or RFS of CRC indicated that the overall prognosis of patients in the SCG2 high group was higher than the low group, in agreement with the results of previously published studies (26). In the study of group 3 medulloblastoma, Eric et al. have verified these results (27). Functional pathways displaying cell adhesion and migration and immune cell infiltrations were prominent in the

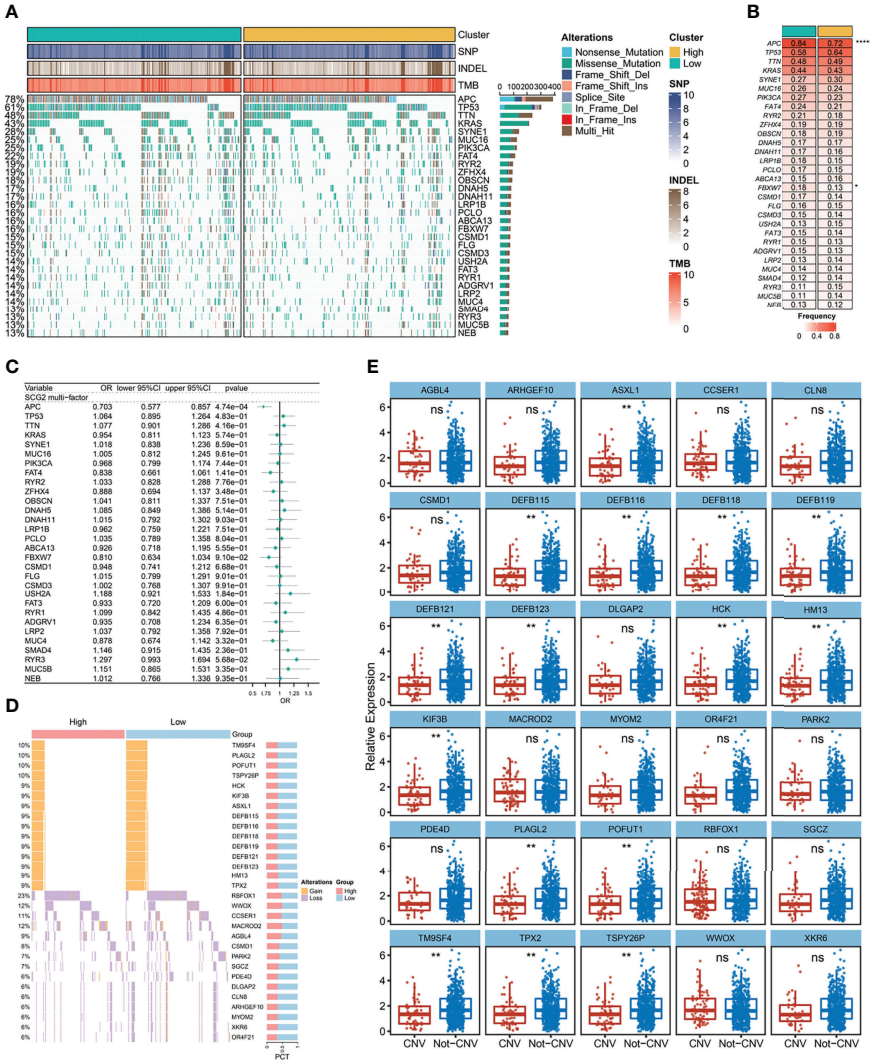

FIGURE 7 | Gene mutation and copy number variation analysis. **(A)** Mutation landscape between high and low expression groups of SCG2, including a total of 30 frequently mutated genes (FMGs). **(B)** Analysis of mutational differences in FMGs between SCG2 expression subgroups. **(C)** A multivariate logistic regression analysis of FMGs, which incorporated SCG2 expression, TMB, age, gender, and stage. **(D)** Copy number variation landscape between high and low expression groups of SCG2. **(E)** Expression differences of SCG2 between variant and non-variant groups in top 15 deletion and amplification genes of copy number variation. **P* <0.05; ***P* <0.01; *****P* <0.0001; ns, *P* >0.05.

enrichment analysis of SCG2-associated genes, which further suggested the potential mining value of SCG2 in tumor development and immune microenvironment.

Adenomatous polyposis coli (APC) is a highly mutated oncogene in colorectal cancer. This gene's mutation and inactivation are critical and premature events observed during CRC tumorigenesis (28). In our study, SCG2 expression was most closely associated with APC mutations as an independent influencing factor. APC is a critical negative regulator of the typical Wnt signaling pathway, which controls gastrointestinal cells' coordinated proliferation and differentiation (29, 30). The previous studies have shown that genomic alterations of APC conduct to activation of β-catenin/T-cell factor transcriptional activity by rising nuclear β-catenin levels and attenuating CtBP-mediated repression of the repressor complex. The activation results in the upregulation of downstream target molecules, such as the cell cycle proteins D1 and Myc, which are essential motorists of tumor appearance due to their precise functions in cell proliferation, apoptosis, and cell cycle progression (28). Deactivation of APC is similarly thought to facilitate tumorigenesis *via* misplacement of cell-cell adhesion, possibly by regulating cell adhesion through the allocation of β-catenin and E-cadherin between the cytoplasm and cell membrane. APC mutations lack the binding domain of β-catenin, leading to diminished cell adhesion (31).

Interestingly, the GSEA enrichment results in this study suggest that SCG2-related pathways are also predominantly cell adhesion and migration. In addition, the Wnt/β-catenin signaling pathway was the highest-scoring related pathway in the GSVA study of SCG2 high and low expression groups. There

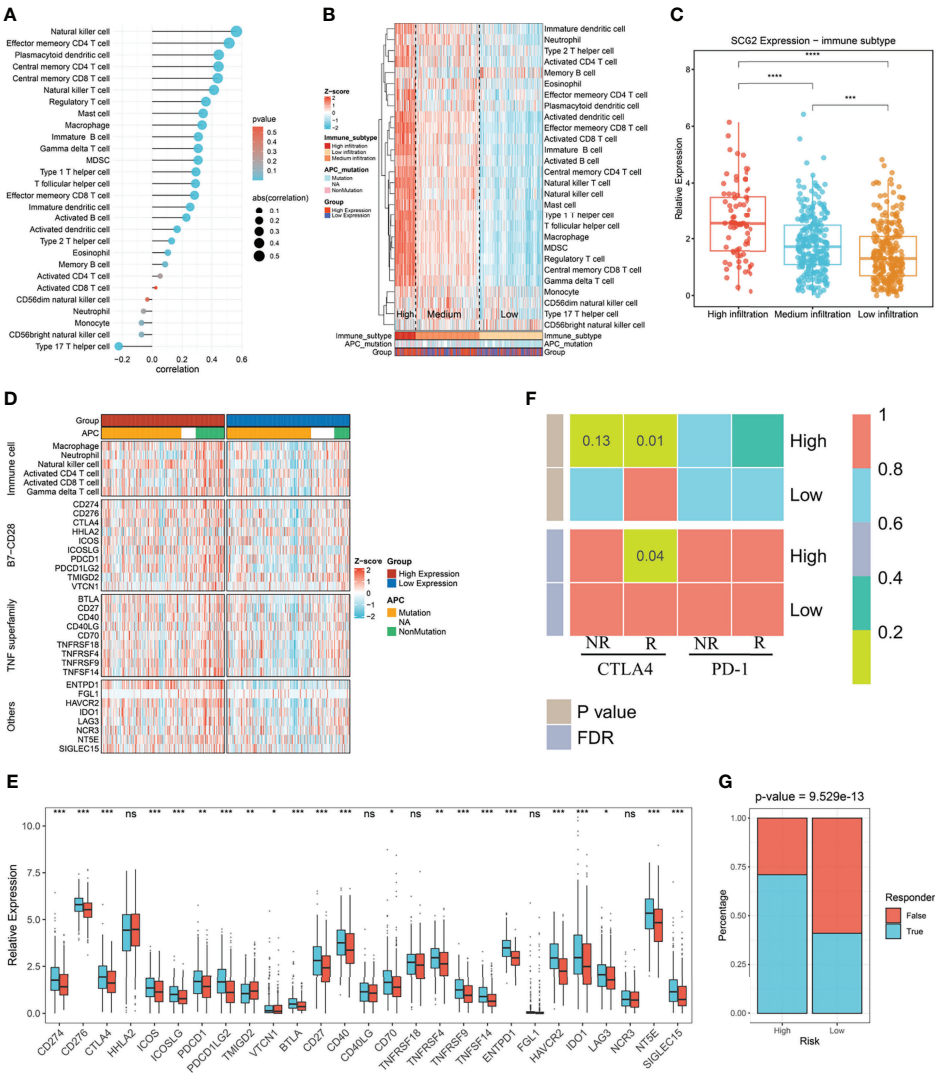

FIGURE 8 | Immune infiltration associated with SCG2 expression and immunotherapy prognosis. **(A)** Correlation of immune cell infiltration score with SCG2 expression. **(B)** Distribution of immune cell infiltration and clinical features among the three subtypes obtained by hierarchical clustering. **(C)** Significant differences in SCG2 expression among the three immune subtypes. **(D)** Differential expression analysis of molecules representing immune characteristics in different SCG2 expression subgroups. **(E)** Differences in immune checkpoint expression between high and low SCG2 expression groups. **(F)** SubMap algorithm evaluated the expression similarity between the two SCG2 expression subgroups and the patients with a different immunotherapy response. **(G)** Distribution of immunotherapy responders predicted by TIDE algorithm between high and low SCG2 expression groups. **P* <0.05; ***P* <0.01; ****P* <0.001; *****P* <0.0001; ns, *P* >0.05.

may be a link between SCG2 and APC in the development of colorectal cancer, making SCG2 play an essential role in disease progression. Besides, this finding was also evidenced in the study of CNA. In previous investigations, TM9SF4, PLAGL2, and POFUT1, the most frequently amplified genes in our study, were strongly associated with the proliferation and metastasis of CRC (32–34). In addition, studies in CRC and breast cancers have shown that high TM9SF4 expression may promote chemoresistance and that knocking down the gene is not only for inhibiting tumor progression but also for enhancing chemotherapeutic sensitivity (33, 35). Therefore, we hypothesize that SCG2 can serve as a prognostic indicator and may also have the potential to predict drug response.

The prognosis of CRC is associated with the infiltration and activation of immune cells in the tumor microenvironment (36). Follow-up bioinformatics analysis showed that SCG2 was closely associated with immune progress, indicating the role of SCG2 in the immune microenvironment of CRC. In the current investigation, we observed that the SCG2 high expression group was featured by immune activation concomitant with immunosuppression; this characterization describes why immune activation was abundant in the SCG2 high expression group without impeding tumor progression. In general, tumor cells, immune cells, stromal cells, vascular endothelial cells, and their secreted factors and extracellular matrix components form a microenvironment that promotes tumor progression (37). In

the early stages of tumor formation, these immune cells and associated stroma are recruited and activated, which creates an anti-tumor inflammatory environment that hinders tumor progression (13, 38). As tumors progress, immune cells infiltrating the tumor microenvironment, besides exerting anti-tumor effects, promote immune escape and tumor growth (13, 39). In recent decades, immunotherapy emerged as a hot spot in anti-tumor research and acted effectively on tumor treatment (40). Our study revealed that the SCG2 high expression group had an enriched immune response with significantly higher expression of CD28-B7, the co-stimulatory molecules that activate T cells, than the low expression group. The TNF superfamily, which is pivotal in the tumor microenvironment, is highly expressed in the high group. It suggests that the tumor microenvironment in the high SCG2-expressing group may incline to be immune hot compared to the low expression group. In addition, we uncovered that the SCG2 high group presented more elevated PD1, PDL1, and CTLA4 expression than the SCG2 low group, suggesting that the former is better conceivable to be in immunosuppressed circumstances, thereby suppressing the procedure of immune cells. Established on these conclusions, we scrutinized the relationship between SCG2 and immune checkpoints and the sensitivity of different expression groups of SCG2 to immunotherapeutic responses. Interestingly, TMB, as an essential biological indicator for predicting response to immunotherapy, was not significantly correlated with SCG2 expression. In CRC, high TMB is necessary but not sufficient to achieve long-lasting benefits, and above the critical threshold for hypermutation phenotypes, even CRC with very high TMB may not respond to treatment. This is different from lung cancer and melanoma, where the response is always positively correlated with TMB (41, 42). The further investigation exhibited a potent correlation between SCG2 and immune checkpoints and that a subgroup with high SCG2 expression was more sensitive to immunotherapy. Therefore, SCG2 has potential value for immunotherapy prediction. Combined with the fact that SCG2 obtained from the previous study can be considered a predictor of chemotherapy, it suggests that the combination of immune checkpoint therapy with chemotherapy in the group with high SCG2 expression may have unexpected benefits. Finally, CMap analysis provides more compounds that can be used as chemotherapy regimens for potential monotherapy or combination therapy in CRC treatment.

The biological heterogeneity of tumors has been plaguing the clinical choice of treatment options. While chemotherapy and immunotherapy serve as indispensable oncological therapeutic agents, selecting appropriate patients deserves more attention. However, there are currently no applicable clinical biomarkers to help doctors choose the appropriate treatment for CRC patients, improve the treatment effect and prolong survival, and reduce unnecessary side effects in other patients. Our study analyzed CRC chemotherapy data and validated results by *in vitro* experiments, providing a potential marker that can predict chemotherapy and immunotherapy responses, which offers the possibility to guide clinical treatment management. Moreover, treatment regimens with chemotherapy and immunotherapy are also essential in the clinic, suggesting a higher requirement for precision treatment in the future.

Despite these spottings, there remain some constraints. The sample data were accessed from the TCGA and GEO databases and did not provide precise details on the extent of surgical resection, an essential facet affecting overall survival. Data information stored in public databases is limited, and there is a lack of detailed transcriptome sequencing cohorts in this study to validate the obtained results, especially from the latest clinical samples. Therefore, more explicit clinical information should be provided for further analysis in the following study. In addition, we lacked sufficient clinical data to verify the predictive worth of SCG2 on the response to immunotherapy in CRC, which requires further efforts in our future studies. Finally, there is a lack of an internal cohort including chemotherapy and immunotherapy combination therapy to validate the conjecture of this study, which will be the emphasis of future research. While a comprehensive analysis of the multi-omics data from independent cohorts was conducted and some conclusions with clinical translation prospects were obtained, the molecular mechanism of SCG2 in the prognosis, chemotherapy, and immunotherapy of CRC should be further validated in more systematic molecular experiments.

CONCLUSIONS

Our study suggests that SCG2 can be used as a new and effective indicator for predicting chemotherapy response, prognosis, and immune response in CRC patients, which means that SCG2 holds promise as a molecular marker to guide chemotherapy and immunotherapy in the clinical management of CRC. These results have important clinical implications and will contribute to the precise treatment of CRC patients.

DATA AVAILABILITY STATEMENT

The original contributions presented in the study are included in the article/**Supplementary Material**, further inquiries can be directed to the corresponding author/s.

ETHICS STATEMENT

The studies involving human participants were reviewed and approved by Ethnics Committee of The First Affiliated Hospital of Zhengzhou University. The patients/participants provided their written informed consent to participate in this study.

AUTHOR CONTRIBUTIONS

ZQL and SYW designed the research route, and XWH performs conception, supervision, and funding acquisition. SYW executes

the majority of data collation, analysis, experimental verification, and writing. HX, XYG, XFR, YYZ, RB, and JHD contributed to some data analysis and figures. ZQL and QD supported the completion of the experiments. YQR, LL, and CGG wrote the draft paper, and all the authors reviewed and modified the manuscript. All authors read and approved the final manuscript.

ACKNOWLEDGMENTS

We are indebted and thankful to all participants for their valuable contributions. We thank the contribution of the appropriate specimen donors and research groups.

SUPPLEMENTARY MATERIAL

The Supplementary Material for this article can be found online at: https://www.frontiersin.org/articles/10.3389/fimmu.2022.873871/full#supplementary-material

Supplementary Figure 1 | Construction of co-expression network and prognostic analysis. **(A)** The topological overlap matrix (TOM) was transformed from the adjacency matrix. **(B)** The correlations between modules. **(C)** Univariate analysis with overall survival (OS) as the outcome event and the expression of the above 20 genes as independent variables. **(D)** Kaplan-Meier survival analysis of RFS cohorts from public portal.

Supplementary Figure 2 | Prognostic analysis and efficacy of predicting chemotherapy response. **(A)** Kaplan-Meier survival analysis of OS cohorts from public portal. **(B)** The receiver operating characteristic curve assesses the efficacy of genes in predicting chemotherapy response in external and internal cohorts. **(C)** Differential expression of genes between chemotherapy-responsive and non-responsive groups in an internal cohort.

Supplementary Figure 3 | Gene Mutation and Copy Number Variation Analysis. **(A)** Correlation analysis of TMB and SCG2 expression. **(B)** Differential analysis of the number of deletion and amplification mutations and TMB between high and low SCG2 expression groups. **(C)** Correlation analysis of neoantigen load and SCG2 expression. **(D)** Expression differences of SCG2 between mutation and non-mutation groups in top 30 FMGs. **(E)** A univariate logistic regression analysis of FMGs, which incorporated SCG2 expression as independent variable. **(F)** The association between the gain and loss loads with SCG2 expression at the arm level. **(G)** Univariate and multivariate logistic regression analysis revealed that SCG2 expression was an independent factor for all amplified genes mutation.

Supplementary Figure 4 | Drug prediction. **(A)** CMap algorithm predicts drugs that may target SCG2 and ranks them by their specificity. **(B)** Mechanisms associated with the above drugs.

REFERENCES

1. Sung H, Ferlay J, Siegel RL, Laversanne M, Soerjomataram I, Jemal A, et al. Global Cancer Statistics 2020: GLOBOCAN Estimates of Incidence and Mortality Worldwide for 36 Cancers in 185 Countries. *CA Cancer J Clin* (2021) 71(3):209–49. doi: 10.3322/caac.21660
2. Dekker E, Tanis PJ, Vleugels JLA, Kasi PM, Wallace MB. Colorectal Cancer. *Lancet* (2019) 394(10207):1467–80. doi: 10.1016/s0140-6736(19)32319-0
3. Doubeni CA, Corley DA, Quinn VP, Jensen CD, Zauber AG, Goodman M, et al. Effectiveness of Screening Colonoscopy in Reducing the Risk of Death From Right and Left Colon Cancer: A Large Community-Based Study. *Gut* (2018) 67(2):291–U53. doi: 10.1136/gutjnl-2016-312712
4. Levin TR, Corley DA, Jensen CD, Schottinger JE, Quinn VP, Zauber AG, et al. Effects of Organized Colorectal Cancer Screening on Cancer Incidence and Mortality in a Large Community-Based Population. *Gastroenterology* (2018) 155(5):1383–+. doi: 10.1053/j.gastro.2018.07.017
5. Allen WL, Johnston PG. Role of Genomic Markers in Colorectal Cancer Treatment. *J Clin Oncol* (2005) 23(20):4545–52. doi: 10.1200/jco.2005.19.752
6. Dienstmann R, Salazar R, Tabernero J. Personalizing Colon Cancer Adjuvant Therapy: Selecting Optimal Treatments for Individual Patients. *J Clin Oncol* (2015) 33(16):1787–+. doi: 10.1200/jco.2014.60.0213
7. Linnekamp JF, Wang X, Medema JP, Vermeulen L. Colorectal Cancer Heterogeneity and Targeted Therapy: A Case for Molecular Disease Subtypes. *Cancer Res* (2015) 75(2):245–49. doi: 10.1158/0008-5472.Can-14-2240
8. Iveson TJ, Sobrero AF, Yoshino T, Souglakos I, Ou FS, Meyers JP, et al. Duration of Adjuvant Doublet Chemotherapy (3 or 6 Months) in Patients With High-Risk Stage II Colorectal Cancer. *J Clin Oncol* (2021) 39(15):1691–91. doi: 10.1200/jco.21.00954
9. Shi Q, Paul J, Grothey A. Duration of Adjuvant Chemotherapy for Stage III Colon Cancer REPLY. *N Engl J Med* (2018) 379(4):396–97. doi: 10.1056/NEJMc1805498
10. Galon J, Bruni D. Approaches to Treat Immune Hot, Altered and Cold Tumours With Combination Immunotherapies. *Nat Rev Drug Discovery* (2019) 18(3):197–218. doi: 10.1038/s41573-018-0007-y
11. Ganesh K, Stadler ZK, Cercek A, Mendelsohn RB, Shia J, Segal NH, et al. Immunotherapy in Colorectal Cancer: Rationale, Challenges and Potential. *Nat Rev Gastroenterol Hepatol* (2019) 16(6):361–75. doi: 10.1038/s41575-019-0126-x
12. Kather JN, Halama N, Jaeger D. Genomics and Emerging Biomarkers for Immunotherapy of Colorectal Cancer. *Semin Cancer Biol* (2018) 52:189–97. doi: 10.1016/j.semcancer.2018.02.010
13. O'Donnell JS, Teng MWL, Smyth MJ. Cancer Immunoediting and Resistance to T Cell-Based Immunotherapy. *Nat Rev Clin Oncol* (2019) 16(3):151–67. doi: 10.1038/s41571-018-0142-8
14. Rejhová A, Opattová A, Čumová A, Slíva D, Vodička P. Natural Compounds and Combination Therapy in Colorectal Cancer Treatment. *Eur J Med Chem* (2018) 144:582–94. doi: 10.1016/j.ejmech.2017.12.039
15. Liu Z, Guo C, Dang Q, Wang L, Liu L, Weng S, et al. Integrative Analysis From Multi-Center Studies Identities a Consensus Machine Learning-Derived lncRNA Signature for Stage II/III Colorectal Cancer. *EBioMedicine* (2022) 75:103750. doi: 10.1016/j.ebiom.2021.103750
16. Langfelder P, Horvath S. WGCNA: An R Package for Weighted Correlation Network Analysis. *BMC Bioinf* (2008) 9:13. doi: 10.1186/1471-2105-9-559
17. Langfelder P, Horvath S. Fast R Functions for Robust Correlations and Hierarchical Clustering. *J Stat Software* (2012) 46(11):1–17. doi: 10.18637/jss.v046.i11
18. Lambrechts D, Wauters E, Boeckx B, Aibar S, Nittner D, Burton O, et al. Phenotype Molding of Stromal Cells in the Lung Tumor Microenvironment. *Nat Med* (2018) 24(8):1277–+. doi: 10.1038/s41591-018-0096-5
19. Charoentong P, Finotello F, Angelova M, Mayer C, Efremova M, Rieder D, et al. Pan-Cancer Immunogenomic Analyses Reveal Genotype-Immunophenotype Relationships and Predictors of Response to Checkpoint Blockade. *Cell Rep* (2017) 18(1):248–62. doi: 10.1016/j.celrep.2016.12.019
20. Jiang P, Gu SQ, Pan D, Fu JX, Sahu A, Hu XH, et al. Signatures of T Cell Dysfunction and Exclusion Predict Cancer Immunotherapy Response. *Nat Med* (2018) 24(10):1550–+. doi: 10.1038/s41591-018-0136-1
21. Hoshida Y, Brunet JP, Tamayo P, Golub TR, Mesirov JP. Subclass Mapping: Identifying Common Subtypes in Independent Disease Data Sets. *PloS One* (2007) 2(11):e1195. doi: 10.1371/journal.pone.0001195
22. Malta TM, Sokolov A, Gentles AJ, Burzykowski T, Poisson L, Weinstein JN, et al. Machine Learning Identifies Stemness Features Associated With Oncogenic Dedifferentiation. *Cell* (2018) 173(2):338–+. doi: 10.1016/j.cell.2018.03.034
23. Vodenkova S, Buchler T, Cervena K, Veskrnova V, Vodicka P, Vymetalkova V. 5-Fluorouracil and Other Fluoropyrimidines in Colorectal Cancer: Past, Present and Future. *Pharmacol Ther* (2020) 206:19. doi: 10.1016/j.pharmthera.2019.107447

24. Kasashima H, Duran A, Martinez-Ordonez A, Nakanishi Y, Kinoshita H, Linares JF, et al. Stromal SOX2 Upregulation Promotes Tumorigenesis Through the Generation of a SFRP1/2-Expressing Cancer-Associated Fibroblast Population. *Dev Cell* (2021) 56(1):95–+. doi: 10.1016/j.devcel.2020.10.014
25. Unterleuthner D, Neuhold P, Schwarz K, Janker L, Neuditschko B, Nivarthi H, et al. Cancer-Associated Fibroblast-Derived WNT2 Increases Tumor Angiogenesis in Colon Cancer. *Angiogenesis* (2020) 23(2):159–77. doi: 10.1007/s10456-019-09688-8
26. Sun GW, Li YL, Peng YJ, Lu DP, Zhang FQ, Cui XY, et al. Identification of a Five-Gene Signature With Prognostic Value in Colorectal Cancer. *J Cell Physiol* (2019) 234(4):3829–36. doi: 10.1002/jcp.27154
27. Thompson EM, Keir ST, Venkatraman T, Lascola C, Yeom KW, Nixon AB, et al. The Role of Angiogenesis in Group 3 Medulloblastoma Pathogenesis and Survival. *Neuro-Oncology* (2017) 19(9):1217–27. doi: 10.1093/neuonc/nox033
28. Zhang L, Shay JW. Multiple Roles of APC and its Therapeutic Implications in Colorectal Cancer. *JNCI J Natl Cancer Inst* (2017) 109(8):10. doi: 10.1093/jnci/djw332
29. Klaus A, Birchmeier W. Wnt Signalling and its Impact on Development and Cancer. *Nat Rev Cancer* (2008) 8(5):387–98. doi: 10.1038/nrc2389
30. Koni M, Pinnaro V, Brizzi MF. The Wnt Signalling Pathway: A Tailored Target in Cancer. *Int J Mol Sci* (2020) 21(20):26. doi: 10.3390/ijms21207697
31. Bienz M, Hamada F. Adenomatous Polyposis Coli Proteins and Cell Adhesion. *Curr Opin Cell Biol* (2004) 16(5):528–35. doi: 10.1016/j.ceb.2004.08.001
32. Li DJ, Lin CW, Li NP, Du YH, Yang CX, Bai Y, et al. PLAGL2 and POFUT1 are Regulated by an Evolutionarily Conserved Bidirectional Promoter and are Collaboratively Involved in Colorectal Cancer by Maintaining Stemness. *EBioMedicine* (2019) 45:124–38. doi: 10.1016/j.ebiom.2019.06.051
33. Lozupone F, Borghi M, Marzoli F, Azzarito T, Matarrese P, Iessi E, et al. TM9SF4 is a Novel V-ATPase-Interacting Protein That Modulates Tumor pH Alterations Associated With Drug Resistance and Invasiveness of Colon Cancer Cells. *Oncogene* (2015) 34(40):5163–74. doi: 10.1038/onc.2014.437
34. Wu L, Zhou ZL, Han SB, Chen JH, Liu ZY, Zhang XD, et al. PLAGL2 Promotes Epithelial-Mesenchymal Transition and Mediates Colorectal Cancer Metastasis *via* Beta-Catenin-Dependent Regulation of ZEB1. *Br J Cancer* (2020) 122(4):578–89. doi: 10.1038/s41416-019-0679-z
35. Zhu YF, Xie MX, Meng ZY, Leung LK, Chan FL, Hu X, et al. Knockdown of TM9SF4 Boosts ER Stress to Trigger Cell Death of Chemoresistant Breast Cancer Cells. *Oncogene* (2019) 38(29):5778–91. doi: 10.1038/s41388-019-0846-y
36. Liu Z, Guo C, Dang Q, Wang L, Liu L, Weng S, et al. Integrative analysis from multi-center studies identities a consensus machine learning-derived lncRNA signature for stage II/III colorectal cancer. *EBioMedicine* (2021) 75:103750. doi: 10.1016/j.ebiom.2021.103750
37. Bejarano L, Jordao MJC, Joyce JA. Therapeutic Targeting of the Tumor Microenvironment. *Cancer Discovery* (2021) 11(4):933–59. doi: 10.1158/2159-8290.Cd-20-1808
38. Ozga AJ, Chow MT, Luster AD. Chemokines and the Immune Response to Cancer. *Immunity* (2021) 54(5):859–74. doi: 10.1016/j.immuni.2021.01.012
39. Del Alcazar CRG, Aleckovic M, Polyak K. Immune Escape During Breast Tumor Progression. *Cancer Immunol Res* (2020) 8(4):422–27. doi: 10.1158/2326-6066.Cir-19-0786
40. Del Paggio JC. Immunotherapy Cancer Immunotherapy and the Value of Cure. *Nat Rev Clin Oncol* (2018) 15(5):268–+. doi: 10.1038/nrclinonc.2018.27
41. Bortolomeazzi M, Keddar MR, Montorsi L, Acha-Sagredo A, Benedetti L, Temelkovski D, et al. Immunogenomics of Colorectal Cancer Response to Checkpoint Blockade: Analysis of the KEYNOTE 177 Trial and Validation Cohorts. *Gastroenterology* (2021) 161(4):1179–93. doi: 10.1053/j.gastro.2021.06.064
42. Wood MA, Weeder BR, David JK, Nellore A, Thompson RF. Burden of Tumor Mutations, Neoepitopes, and Other Variants are Weak Predictors of Cancer Immunotherapy Response and Overall Survival. *Genome Med* (2020) 12(1):33. doi: 10.1186/s13073-020-00729-2

Conflict of Interest: The authors declare that the research was conducted in the absence of any commercial or financial relationships that could be construed as a potential conflict of interest.

Publisher's Note: All claims expressed in this article are solely those of the authors and do not necessarily represent those of their affiliated organizations, or those of the publisher, the editors and the reviewers. Any product that may be evaluated in this article, or claim that may be made by its manufacturer, is not guaranteed or endorsed by the publisher.

frontiers | Frontiers in Immunology

ORIGINAL RESEARCH
published: 06 July 2022
doi: 10.3389/fimmu.2022.905768

Dual Antigen T Cell Engagers Targeting CA9 as an Effective Immunotherapeutic Modality for Targeting CA9 in Solid Tumors

*Nazanin Tatari[1,2], Xiaoyu Zhang[3,4], Shawn C. Chafe[2,5], Dillon McKenna[2,5], Keith A. Lawson[3,4], Minomi Subapanditha[2,5], Muhammad Vaseem Shaikh[2,5], Mathieu Seyfrid[2,5], Neil Savage[1,2], Chitra Venugopal[2,5], Jason Moffat[3,4] and Sheila K. Singh[1,2,5]**

[1] Department of Biochemistry and Biomedical Sciences, McMaster University, Hamilton, ON, Canada, [2] Centre for Discovery in Cancer Research, McMaster University, Hamilton, ON, Canada, [3] Donnelly Centre, University of Toronto, Toronto, ON, Canada, [4] Department of Molecular Genetics, University of Toronto, Toronto, ON, Canada, [5] Department of Surgery, Faculty of Health Sciences, McMaster University, Hamilton, ON, Canada

OPEN ACCESS

Edited by:
Xian Zeng,
Fudan University, China

Reviewed by:
Di Yu,
Uppsala University, Sweden
Franziska Eckert,
Medical University of Vienna, Austria

***Correspondence:**
Sheila K. Singh
ssingh@mcmaster.ca

Specialty section:
This article was submitted to Cancer Immunity and Immunotherapy, a section of the journal Frontiers in Immunology

Received: 27 March 2022
Accepted: 31 May 2022
Published: 06 July 2022

Citation:
Tatari N, Zhang X, Chafe SC, McKenna D, Lawson KA, Subapanditha M, Shaikh MV, Seyfrid M, Savage N, Venugopal C, Moffat J and Singh SK (2022) Dual Antigen T Cell Engagers Targeting CA9 as an Effective Immunotherapeutic Modality for Targeting CA9 in Solid Tumors. Front. Immunol. 13:905768. doi: 10.3389/fimmu.2022.905768

Glioblastomas (GBM), the most common malignant primary adult brain tumors, are uniformly lethal and are in need of improved therapeutic modalities. GBM contain extensive regions of hypoxia and are enriched in therapy resistant brain tumor-initiating cells (BTICs). Carbonic anhydrase 9 (CA9) is a hypoxia-induced cell surface enzyme that plays an important role in maintenance of stem cell survival and therapeutic resistance. Here we demonstrate that CA9 is highly expressed in patient-derived BTICs. $CA9^+$ GBM BTICs showed increased self-renewal and proliferative capacity. To target CA9, we developed dual antigen T cell engagers (DATEs) that were exquisitely specific for CA9-positive patient-derived clear cell Renal Cell Carcinoma (ccRCC) and GBM cells. Combined treatment of either ccRCC or GBM cells with the CA9 DATE and T cells resulted in T cell activation, increased release of pro-inflammatory cytokines and enhanced cytotoxicity in a CA9-dependent manner. Treatment of ccRCC and GBM patient-derived xenografts markedly reduced tumor burden and extended survival. These data suggest that the CA9 DATE could provide a novel therapeutic strategy for patients with solid tumors expressing CA9 to overcome treatment resistance.

Keywords: glioblastoma, immunotherapy, dual antigen T cell engagers, hypoxic niche, CA9, clear cell renal cell carcinoma

INTRODUCTION

Glioblastoma (GBM), a highly aggressive astrocytic tumor (WHO grade IV), is the most common primary malignant brain tumor in adults (1, 2). Despite aggressive multi-modal treatment, including maximal safe surgical resection, chemotherapy with the alkylating agent temozolomide (TMZ) and radiotherapy, tumor re-growth and patient relapse occurs within 7-9 months post-

diagnosis (3, 4). The average survival in GBM patients is only 12-14 months (5–9) with an abysmal two-year survival rate of 16.9% and only 5.5% of patients surviving at five years and 2.9% at ten years (4), underscoring the urgent need for novel therapeutic approaches. Treatment failure and disease relapse are attributed to extensive cellular and genetic heterogeneity existing not only between patients but also within a single tumor through space and time (10–13). This cellular heterogeneity, which is associated with clonal evolution, can be explained by the existence of multiple cellular subpopulations of cancer cells, called brain tumor initiating cells (BTICs), which have acquired stem cell properties including self-renewal, proliferation and multi-lineage differentiation capacity (14–17). Increased presence of chemo- (18) and radio-resistant (19) BTICs (14) plays a significant role in development of GBM treatment resistance and eventually tumor recurrence. Therefore, development of novel therapeutic modalities targeting BTIC populations is desperately needed for the GBM field.

Components of the tumor microenvironment play key roles in BTIC maintenance. A dominant microenvironmental factor of solid tumors including GBM is hypoxia (20). Intratumoral hypoxia has a significant effect on BTIC maintenance by supporting critical stem cell features including self-renewal, multipotency, tumorigenicity, and response to radiation (21, 22). In addition, hypoxia promotes cancer progression by inducing angiogenesis, cell growth, tumor cell invasion, genomic instability, immunomodulation, and metabolic reprogramming of cancer cells and tumor stroma (22–26). Therefore, targeting the hypoxic niche would be a necessary step towards decreasing BTIC survival and therapy resistance in GBM patients.

One of the most highly expressed genes in response to hypoxia is Carbonic Anhydrase 9 (CA9). CA9 is a cell surface metalloenzyme which catalyzes the reversible hydration of CO_2 to produce protons (H^+) and bicarbonate ($HCO3^-$), permitting tumor cells to survive exposure to acidosis (25, 27–29). CA9 is highly overexpressed in response to hypoxia in many types of solid tumors including GBM (29–31). Furthermore, CA9 is also highly expressed in a large proportion of clear cell Renal Cell Carcinoma (ccRCC) (32) in a hypoxia-independent manner where it is driven by stabilization and constitutive activation of HIF-1alpha signaling as a result of mutation of the von Hippel-Lindau (VHL) tumor suppressor (33, 34). Clear cell Renal Cell Carcinoma is the most common form of renal cancer and like GBM is in need of improved therapeutic strategies. Patients with localized disease at diagnosis have a 5 year survival of 76%; however 30% of patients will present with metastatic disease which carries a dismal 5 year survival rate of 8% (35). Notably, CA9 displays limited expression in most normal tissues with the exception of gastrointestinal tract, gallbladder, and pancreatic ducts (36, 37). It has been shown that elevated CA9 expression is positively correlated with poor patient prognosis in a number of solid malignancies (29). The major therapeutic thrust targeting CA9 in solid tumors to date has been focused on small molecule inhibitors (38–40) and monoclonal antibodies such as G250 (41–43). While therapeutic benefit from single agent treatment is often quickly met with resistance (38, 44, 45), this has prompted investigation of combinatorial approaches with chemo- (38, 44, 45) and immunotherapy (46) which have enhanced therapeutic responses and expanded the possibility of therapeutic strategies to better target CA9 (47).

Here, we designed a T cell-based therapy that employs a Dual Antigen T-cell engager (DATE) antibody as a promising alternate strategy, which allows for targeting cancer cells and redirecting immune cells against tumor cells simultaneously. CA9 DATE was engineered by fusing the light chain of the CA9-Fab to OKT3, a single-chain fragment variable (scFv) construct that binds to the antigen-binding region of the mitogenic antiCD3ϵ clone. Bifunctional T cell engagers exhibiting specificity for the GBM tumor cell surface antigen CD133 (48)/EGFRvIII (49, 50) have also been shown to induce anti-tumorigenic activity in xenograft tumor models. Furthermore, we have previously demonstrated the utility of DATEs in eliminating GBM BTICs by targeting CD133 (51). Given their low molecular weight, DATEs may prove to be more efficient in localizing to the central nervous system (CNS) and this particular feature allows for maximal membrane proximity between the T cell and the cancer cell necessary for the immune response (52–55). However, DATEs are yet to be clinically translated for many solid tumors such as GBM and ccRCC.

We capitalized on the cell surface expression of CA9 and developed a DATE targeting its expression in solid tumors. To demonstrate proof-of-concept of our DATE in a model that highly expresses CA9 in a constitutive manner we utilized VHL mutant ccRCC PDX models. We demonstrate that the DATE is exquisitely specific for CA9 expressing patient-derived models of ccRCC and GBM. Simultaneous engagement of T cells and $CA9^+$ target cells led to increased activation of T cells, increased inflammatory cytokine production and increased target cell death. Treatment of patient-derived models of ccRCC and GBM *in vivo* significantly reduced tumor burden and extended survival. This technology represents a new therapeutic strategy for hard-to-treat cancers highly expressing CA9.

MATERIAL AND METHODS

Human GBM and ccRCC Sample Collection

Human GBM brain tumors (**Table S1**) and patient-derived ccRCC cell lines (**Table S2**) were obtained from consenting patients, as approved by the Hamilton Health Sciences/McMaster Health Sciences Research Ethics Board and the Princess Margaret Cancer Centre, Toronto, respectively. Moreover, normal brain cells including Neural Stem Cells (NSCs) were isolated and propagated from fetal brain samples which was approved by the Hamilton Health Sciences/McMaster Health Sciences. Normal Human Astrocytes (NHAs) were purchased from Lonza.

In Silico Analysis

Publically available databases including GEPIA2 and GlioVis were used for *in silico* validation of the target of interest across a large number of GBM samples.

Culture Conditions for Isolating and Propagating the GBM and ccRCC Tumor Cells

Human brain tumor tissue was processed as previously described (14, 16, 56). Briefly, samples were dissociated in PBS (ThermoFisher, Cat#10010049) containing 0.2 Wünsch unit/mL Liberase Blendzyme 3 (Millipore Sigma, Cat#5401119001) and incubated on a shaker at 37°C for 15 minutes. The dissociated tissue was then filtered through a 70 μm cell strainer (Falcon, Cat#08-771-2) and collected by centrifugation at 1200 rpm for 5 minutes. Red blood cells were lysed using ammonium chloride solution (STEMCELL Technologies, Cat#07850). GBM cells were resuspended in NeuroCult complete (NCC) media, a chemically defined serum-free neural stem cell medium (STEMCELL Technologies, Cat#05751), supplemented with human recombinant epidermal growth factor (hrEGF) (20ng/mL: STEMCELL Technologies, Cat#78006), basic fibroblast growth factor (bFGF) (10ng/mL; STEMCELL Technologies Cat#78006), heparin (2 mg/mL 0.2% Heparin Sodium Salt in PBS; STEMCELL technologies, Cat#07980), antibiotic-antimycotic (1X; Wisent, Cat# 450-115-EL), and plated on ultra-low attachment plates (Corning, Cat#431110) and cultured as neurospheres. GBM BTICs Neurospheres were propagated by minimally-culturing (< 20 passages) human GBM samples and plating them on polyornithine- laminin coated plates for adherent growth. Adherent cells were replated in low-binding plates and cultured as tumorspheres, which were maintained as spheres upon serial passaging *in vitro*. These cells retained their self-renewal potential and were capable of *in vivo* tumor formation.

The human ccRCC cell lines were generated by sorting CA9-positive cells from patient tumor specimens as previously described (57). The ccRCC cell lines and their derived overexpression or knockout cell lines were grown in Iscove's Modified Dulbecco's Medium (IMDM) (ThermoFisher, Cat#12440053) supplemented with 10% fetal bovine serum (FBS, Thermo Fisher, Waltham) and 1% penicillin/streptomycin (ThermoFisher, Cat#15140122) at 37°C in 5% CO_2. The murine cortical adenocarcinoma renal cell carcinoma cell line, Renca, was purchased from the American Type Culture Collection (ATCC). Renca and its derived overexpression cell lines were grown in Roswell Park Memorial Institute medium (RPMI 1640) (ThermoFisher, Cat#11875101) supplemented with 10% FBS and 1% penicillin/streptomycin at 37°C in 5% CO2.

Generation of CA9 Knockout (KO) and CA9 Over-Expressed ccRCC Cell Lines

To perturb the carbonic anhydrase IX (CA9) gene in RCC243 for the generation of CA9-KO cell line, early-passage cells were transduced with lentivirus carrying Cas9 and guide RNAs (gRNA) targeting CA9 exons. The lentiviral expression vector lentiCRISPR v.2 (lcv2, Addgene) was purchased and modified in-house for gRNA compatibility. Three CA9-targeting gRNAs were individually cloned into the lcv2 vectors for lenti-virus production and transduction of RCC243 cells. The editing efficiency of the three gRNAs were verified using flow cytometry assessing surface CA9. The final CA9 knockout cells (RCC243 CA9-KO, gRNA sequence GGGATCAACAGAGGGA GCCA) were selected by fluorescence-activated cell sorting (FACS). To over express human CA9 in Renca (Renca hCA9), the mRNA open reading frame (ORF) was amplified from the human ORF transfection library (Dharmacon) using polymerase chain reaction (PCR), and Gibson-assembled into a lentiviral expression vector designed in-house. The CA9 ORF is linked to an enhanced green fluorescence protein (EGFP) *via* a P2A peptide. Early passage Renca cells were transduced with the CA9-lentivirus and FACS sorted based on positive EGFP signals. The surface CA9 levels of the validation cell lines were profiled by flow cytometry using phycoerithrin (PE)-conjugated anti-CA9 antibody (R&D systems, Cat# FAB2188P)

Engineering and Production of CA9 DATEs

The complementarity-determining region (CDR) sequences of previously selected CA9-binders (generated by Dr. Sunandan Banerjee) were sub-cloned into the pSCSTa antibody expression vectors designed in-house, containing the OKT3-anti-CD3 single-chain variable fragment (scFv). The CDR-containing light and heavy chain variable regions of the F library phage-mids were amplified using PCR and restriction enzyme-digested to ligate with the pSCSTa backbone vectors. Both light- and heavy-chain pSCSTa expression vectors were then transfected into Expi293™ cells using the PEIpro® transfection reagents (Polyplus, New York) following the manufacturer's instruction. The transfected Expi293™ cells were cultured in the Expi293™ expression medium (Thermo Fisher, Waltham) and incubated at 37°C, 5% CO_2 on a shaker. Five days post-transfection, the supernatant was harvested, and the antibody products were extracted by incubating with protein A resin and purified by affinity chromatography (Bio-Rad Laboratories, Hercules). The antibodies were exchanged into PBS buffer using Amicon® Pro Purification tubes. The protein concentrations were measured using NanoDrop. The protein purity was verified using SDS-PAGE followed by Coomassie Blue staining.

Flow Cytometry Analysis

GBM Tumorspheres were dissociated using 0.2 Wünsch unit/mL Liberase Blendzyme 3 (Millipore Sigma, Cat#5401119001) plus 10 μL DNase (Worthington Biochemical, Cat#LK003170) and adherent cultures were dissociated using dissociation enzyme TrypLE (ThermoFisher, Cat#12605028). The single cells were resuspended in PBS+2 mM EDTA (Invitrogen, Cat# AM9260G). Cells were then stained with APC conjugated mouse monoclonal human Carbonic Anhydrase 9 antibody (1:10) (R&D, Cat#FAB2188A) or a matched isotype control and CA9 DATEs followed by goat anti human APC-Fab IgG (1:2000, Jackson ImmunoResearch, Cat#109-136-170) and incubated for

15 minutes at room temperature. T cells were stained with CA9 DATEs (15 minutes RT) followed by goat anti human APC-Fab IgG (1:2000, Jackson ImmunoResearch, Cat#109-136-170), anti-CD25 (Miltenyi Biotech, Cat#130-113-283) and anti-CD69 (BD Bioscienecs, Cat#555533). Samples were run on a MoFlo XDP Cell Sorter (Beckman Coulter). Dead cells were excluded using the viability dye 7AAD (1:10; Beckman Coulter, Cat#A07704). Compensation was performed using mouse IgG CompBeads (BD Biosciences, Cat#552843). Samples were run on a MoFlo XDP Cell Sorter (Beckman Coulter) to assess the level of CA9 surface expression.

Secondary Sphere Formation Assay (Self-Renewal Assay)

Tumorspheres were dissociated using 10 µL Liberase Blendzyme3 (0.2 Wunsch unit/mL) plus 10 µL of DNase in 1 mL PBS for 5 minutes at 37°C and adherent cultures were dissociated using dissociation enzyme TrypLE. $CA9^+$ and $CA9^-$ sorted GBM BTICs were plated at 200 cells per well in 200 µL of NCC media in a 96-well plate. Cultures were left undisturbed at 37°C, 5% CO_2. The number of secondary spheres per well was counted at day 3 to 7 every day and used to estimate the mean number of spheres per 2,000 cells.

Cell Proliferation Assay

Upon tumor culture dissociation, single cells were sorted into $CA9^+$ and $CA9^-$ population and 1,000 single cells were plated in 180 µL NCC per well in quadruplicate in a 96-well plate and incubated for five days. 20 microliters of Presto Blue (ThermoFisher, Cat#A13262), a fluorescent cell viability (metabolism) indicator, was added to each well approximately 4 hours prior to the readout time point. Fluorescence was measured using a FLUOstar Omega Fluorescence 556 Microplate reader (BMG LABTECH) at excitation and emission wavelengths of 544 nm and 590 nm, respectively. Readings were analyzed using Omega analysis software.

Cell Growth in Hypoxic Condition

$CA9^{lo}$ expressing GBM BTICs were cultured in both hypoxic and normoxic conditions. In hypoxic condition, cells were incubated in hypoxia chamber (1% O_2, 5% CO_2, 94% N_2) and in normoxic condition they were incubated in normoxia (21% O_2) for a total of 5 days. After 5 days cultures were dissociated, and single cells were resuspended in PBS + 2 mM EDTA. Cells were then stained with mouse monoclonal human Carbonic Anhydrase 9 antibody (1:10) (R&D, Cat#FAB2188A) and run on the LSRII flow cytometer (BD) to assess the effect of hypoxia on CA9 expression on GBM BTICs.

PBMC Isolation and T Cell Purification and Expansion

Peripheral blood mononuclear cells (PBMCs) from consenting healthy blood donors were obtained using SepMate™ (STEMCELL technologies, Cat#85450) or Ficoll-Paque PLUS (GE Healthcare). This study was approved by the McMaster Health Sciences Research and the University of Toronto Ethics Board for GBM and ccRCC projects, respectively. 1×10^5 cells in XSFM media (Irvine Scientific, Cat#91141) were activated with anti-CD3/CD28 beads at a 1:1 ratio (Dynabeads, Life Technologies) in a 96-well round bottom plate with 100U/mL rhIL-2 (Peprotech, Cat#200-02). T cell cultures were expanded into fresh media (XSFM media supplemented with 100U/mL rhIL-2) as required for a period of 12–15 days prior to experimentation.

Binding Assay

The specificity of CA9 DATE for GBM cells, ccRCC cells and T cells were tested using flow cytometry analysis. $CA9^{hi}$ GBMs, $CA9^-$ GBMs, ccRCCs and T cells (isolated from human PBMCs for GBM study and Jurkat cells for ccRCC study) were resuspended in PBS plus 2 mM EDTA and were stained with CA9 DATEs followed by the secondary antibody, goat anti -human APC-Fab IgG (1:2000, Jackson ImmunoResearch, Cat#109-136-170) staining. GBM and ccRCC cells were incubated for 15 minutes at room temperature and for 20 minutes on ice, respectively followed by 15 minutes incubation at room temperature for the secondary antibody staining. Dead cells were excluded using the viability dye 7AAD (1:10; Beckman Coulter, Cat#A07704) and samples were run on MoFlo XDP Cell Sorter (Beckman Coulter) to assess the level of CA9 DATE binding to each of the above-mentioned lines.

T Cell Activation Assays

In ccRCC model, RCC243 and RCC243 CA9-KO cells were plated at 200,000 cells/well in 6 well plates the night prior to treatment. Human $CD3^+$ T cells at an E:T ratio of 5:1 were added to the wells along with (1 nM) or without CA9 DATEs and incubated at 37°C in 5% CO_2 for 48 hours. The T cells were collected and stained for BV785 anti-human CD3 (BioLegend, Cat#317330), BV605 anti-human CD4 (BioLegend, Cat#317438), PE-anti-human CD8 (BioLegend, Cat#300908), and PE-CF594-anti-CD25 (BD Biosciences, Cat#562403) antibodies. Supernatants were collected and stored at -80°C for cytokine release analysis by enzyme-linked immunosorbent assay (ELISA).

In GBM models, GBM cells and T cells were co-incubated at a 1:1 ratio for 24 hours with (1µg = 13 nM) or without CA9 DATEs. The $CD3^+$ (BD Pharmingen, Cat#563423) T cells and subpopulation of T cells including $CD4^+$ (BD Pharmingen, Cat#555347) and $CD8^+$ T (BD Horizon, Cat#562428) cells were analyzed for activation markers CD25 (Miltenyi Biotech, Cat#130-113-283) and CD69 (BD Pharmingen, Cat#555533) by flow cytometry. Supernatants were collected and stored at -80°C for cytokine release analysis by enzyme-linked immunosorbent assay (ELISA).

Enzyme Linked Immunosorbent Assay (ELISA)

The concentration of TNF-α and IFN-γ were quantitated in the supernatant collected from the T cell activation assay (the T cell and GBM co-culture +/- CA9 DATE) using commercially available human TNF-α DuoSet ELISA kit (R & D Systems,

Cat#DY210-05) and IFN-γ DuoSet ELISA kit (R & D Systems, Cat#DY285B-05) respectively. The sensitivity limits of TNF-α and IFN-γ assay were 15.60 pg/ml and 9.38 pg/ml, respectively. The experiment was performed in duplicates and the OD was measured at 450 nm using the FLUOstar Omega Fluorescence 556 Microplate reader (BMG LABTECH). The IFN-γ concentration in ccRCC model was quantified using the eBioscience Ready-SET-Go human IFN-γ ELISA kit (ThermoFisher, Cat#88-7386-88).

Cytotoxicity Assay

To quantify target cell death without interfering signals from the effector cells, luciferase was overexpressed in ccRCC and GBM cells using lentiviral transduction (plasmidlenti-PGK-luciferase-GFP (Ailles Lab) for ccRCC cells and pCCL ffLuciferase for GBM cells).

ccRCC model: The RCC243 and RCC243 CA9-KO target cells were plated at 25,000 cells/well in triplicates in 96 well plate the night prior to treatment. The next morning, purified human $CD3^+$ T cells were added at an E:T ratio of 5:1, along with CA9 DATE, and anti-CD3/BCMA control antibody at 1 nM concentration in standard complete IMDM media supplemented with 100 μM beta-mercaptoethanol (Sigma-Aldrich, Cat# M3148-25ML) to reduce T cell oxidative stress. The assays were incubated for 40-48 hours at 37°C, 5% CO_2 before the microscopic images were documented and bioluminescence signals were measured. Working concentration (7.5 mg/mL) of firefly luciferin was added to the washed wells and read immediately with a spectrophotometer (BioTek plate reader).

Lactate dehydrogenase (LDH) release assays: Target cells (patient-derived ccRCC cell) were plated at 20,000 cells/well in 96 well plates (Corning, Cat#: 3628). Total PBMCs were used as effectors at an E:T ratio of 10:1. The LDH release by the damaged target cells were measured 48 hours later using the LDH cytotoxicity assay kit (Thermo Fisher, Cat# 88953). Prior to measuring, kit lysis buffer was added to three untreated wells of each cell line for the maximum LDH release controls. The assay steps were carried out as per manufacturer's instructions. Briefly, supernatant from each treatment conditions was incubated with the LDH substrate mix at room temperature in dark for 20 minutes for the colour to develop. The stop solution was added and the plates were read using a spectrophotometer at 490 and 680 nm. The absolute LDH release was calculated as sample release, effector spontaneous release, target spontaneous release and medium blank. Relative LDH levels was calculated as sample absolute release/plus-PBMC-only absolute release.

GBM model: Luciferase-expressing GBM cells ($CA9^{hi}$ GBM cells) and HEK cells at a concentration of 25,000 cells/well were plated in 96–well plates in triplicates. T cells at different effector-to-target (E:T) ratios (0:1, 0:0.25, 0.5:1, 0.75:1, 1:1, 2:1) were added to each well in the presence (1nM) and absence of CA9 DATE. The cultures were then incubated at 37°C for 18 hours. The next day 150 μg/mL firefly D-luciferin potassium salt (R&D systems, Cat#800-LN-05M) was added to each well and the BLI was measured with a luminometer (Omega) as relative luminescence units (RLU). Target cells incubated without effector cells were used to measure spontaneous death RLU. The readings from triplicates were averaged and percent lysis was calculated with the following equation:

$$\%\ \textit{Specific lysis} = 100X\ (\textit{spontaneous death RLU} - \textit{test RLU}) / (\text{spontaneous death RLU} - \text{maximal killing RLU})$$

Animal Studies

Animal studies were performed according to guidelines under Animal Use Protocols (19-01-01) of McMaster University Central Animal Facility.

In ccRCC model, 5 x 10^6 RCC243 VHL mutant cells were subcutaneously injected into the right flank of 8- to 10- week old immunocompromised NSG mice for tumor formation. After the half-maximal tumor engraftment (4 weeks post-engraftment) mice were randomly assigned into control or treatment groups based on matched-tumor size and CA9 DATE treatment started as described in **Supplementary Figure 2.** All animals received 12 doses of therapy within a 6-week time frame. The animals which were assigned to the treatment group were intratumorally injected with 50 μg CA9 DATE + 2 x10^6 T cells (isolated from the freshly thawed PBMC of healthy donors) once a week and only 50 μg (667 nM) CA9 DATE for the second treatment in the week. Mice in the control group received the same therapy regimen as treatment group; however, the CA9 DATE was replaced with CA9 DATE control. Tumor size was measured using a ruler caliper after each treatment (length x width). To study the effect of CA9 DATE treatment on tumor size, tumors were collected one week after the last treatment and the tumor size was measured using a ruler caliper. For survival studies, all the mice were kept until they reached endpoint and the number of days for survival were noted for Kaplan-Meier analysis. The endpoint criteria were defined as 20% weight loss and 1.0 cm x 1.0 cm tumor size.

In GBM model, GBM cells (1x10^6 BT935 and 2x10^5 BT241) were intracranially injected into right frontal lobes of 6- to 8-week old immunocompromised NSG mice (bred in McMaster University Central Animal Facility) for tumor formation as previously described (58). Briefly, mice were anaesthetized using 2.5% Isoflurane (gas anaesthesia). Using a 15-blade scalpel a 1.0 cm vertical midline incision was made on top of the skull. A small burr hole was then made (2-3 mm anterior to the coronal suture, 3 mm lateral to midline) using a drill held perpendicular to the skull. A Hamilton syringe (Hamilton, Cat#7635-01) was used to inject 10 μL of cell suspension (GBM cells suspended in 10 mL PBS) into the frontal lobe. The syringe was inserted through the burr hole to a 5 mm depth. The incision was closed using interrupted stitches and sutures were sealed with a tissue adhesive. After the half-maximal tumor engraftment which was confirmed by MRI imaging (6 weeks post-surgery for BT935 and 10 days post-surgery for BT241)

mice were randomly assigned into control or treatment groups and CA9 DATE treatment started as described in **Supplementary Figure 2**. All animals received 4 doses of therapy within a 2-week time frame. The animals which were assigned to the treatment group were intracranially injected with 50 μg (667 nM) CA9 DATE + 10^6 T cells and received only 50 μg (667 nM) CA9 DATE top up each once a week for 2 weeks. Mice in the control group received the same therapy regimen as treatment group; however, the CA9 DATE was replaced with CA9 DATE control. For tumor volume evaluation, animals were perfused with 10% formalin one week after the last treatment and the collected brains were sliced at 2 mm thickness using brain-slicing matrix for paraffin embedding and H&E staining. Images were captured using an Aperio Slide Scanner and analyzed using ImageScope v11.1.2.760 (Aperio) and imageJ software. For survival studies, all the mice were kept until they reached endpoint and number of days of survival were noted for Kaplan-Meier analysis. The endpoint criteria were defined as 20% body weight reduction, physical appearance deterioration, measurable clinical signs, unprovoked behavior and response to external stimuli.

Statistical Analysis

Biological replicates from at least three patient samples were compiled for each experiment, unless otherwise specified in figure legends. Respective data represent mean ± SEM, n values are listed in figure legends. Cox regression and Kaplan-Meier analysis were performed for survival analysis. Student's t-test analyses, 2-way ANOVA analysis and Kaplan-Meier analysis were performed using GraphPad Prism 6. $P<0.05$ was considered significant.

Study Approval

This study was conducted with approval from the Hamilton Integrated Research Ethics Board for human studies and the Animal Research Ethics Board at McMaster University.

RESULTS

CA9 Is a Safe Target for GBM Immunotherapy

To evaluate the potential utility of CA9 as a therapeutic target in GBM, we performed *in silico* analysis using the GEPIA2 database to assess the level of *CA9* expression in GBM versus normal tissue. This analysis revealed a significant upregulation of *CA9* in GBM tissue compared to normal tissues (**Figure 1A**). We next evaluated CA9 expression in the TCGA glioma database and identified higher expression of *CA9* in GBM (grade IV glioma) compared to low-grade glioma (**Figure S1A**). Notably, this *in silico* analysis revealed significantly higher expression of *CA9* in the mesenchymal subtype, the most aggressive GBM subtype (**Figure 1B**). Furthermore, *CA9* expression was also significantly higher in all subtypes of GBM compared to normal tissue (**Figure S1B**). Stratifying patients according to median *CA9* expression revealed patients with increased *CA9* expression survived for shorter periods (59, 60) (**Figure 1C**). We next validated our *in silico* findings at the protein level using flow cytometry analysis to evaluate cell surface CA9 expression in a cohort of our patient-derived GBM BTIC lines as well as in normal brain cell lines [Normal Human Astrocyte (NHA) and Neural Stem Cells (NSC)]. We identified very little CA9 expression on normal brain cells (NHAs and NSCs), and strong extracellular/cell surface expression in our patient-derived GBM BTIC lines (**Figure 1D**). Since this respository is linked to patient outcome data we next investigated whether CA9 expression impacted the survival of the patients from which these lines were derived. Our analysis revealed a positive correlation between CA9 expression and poor patient survival (**Figure 1E** and **Table S1**) suggesting that our findings at the mRNA level are extended to expression of the protein. Together, these data suggest that CA9 is an important therapeutic target in GBM and given its cell surface expression and limited expression in normal brain samples, immuno-therapeutic modalities targeting cells expressing CA9 have reduced risk of off-target toxicity in the brain.

CA9 Influences BTIC Stem-Like Properties

To investigate the effect of hypoxia on CA9 expression in our patient-derived GBM BTIC lines, $CA9^{lo}$ expressing GBM BTICs were cultured side by side in hypoxic (1% O_2) and normoxic conditions. Cell surface characterization by flow cytometry indicated that cells cultured in hypoxic conditions had significant elevation of CA9 expression compared to cells which were cultured in normoxic conditions (**Figure 2A**).

There is accumulating evidence about the effect of the tumor microenvironment, particularly hypoxia, on BTIC maintenance and treatment resistance (61, 62). It has also been shown that hypoxia can induce a stem-like phenotype in non-stem-like cancer cells, promoting cell growth and self-renewal (62). Moreover, CA9 has previously been implicated in BTIC survival (38). To assess the influence of CA9 on GBM BTIC stem-like properties including self-renewal and proliferation, secondary sphere formation and proliferation assays were performed. Each GBM BTIC line was sorted into $CA9^+$and $CA9^-$ fractions by FACS and plated to assess self-renewal and proliferation. The expression of CA9 significantly enhanced clonogenicity of the BTIC lines (**Figure 2B**). Moreover, in 2 out of 3 GBM BTIC lines tested, the $CA9^+$ cell population had significantly greater proliferative capacity than the $CA9^-$ cell fractions (**Figure 2C**). Altogether, these data revealed that CA9 influences stem-like properties in GBM BTICs where targeting cells expressing CA9 may be beneficial.

CA9 Dual Antigen T Cell Engager (DATE) Is Specific for CA9 and CD3

To target CA9 expressing tumor cells, we exploited the cell surface localization and generated DATEs. CA9-specific DATEs were engineered by fusing the antigen-binding portion (Fab) of the anti-CA9 antibody to the antigen-binding region of

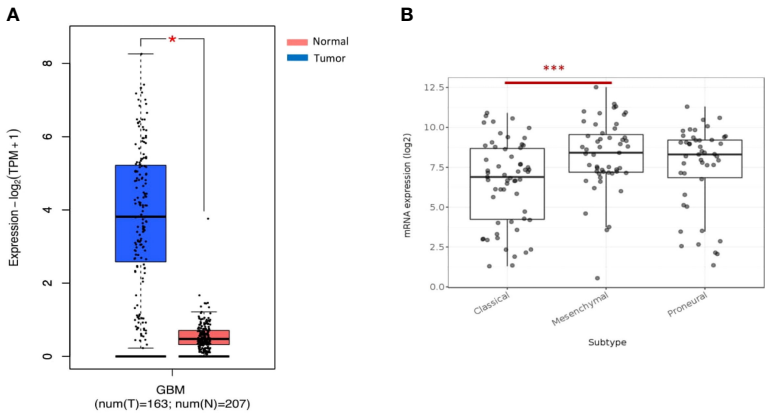

D

Cells	Percentage of CA9 expression
BT428	69.76%
BT 935	66.80%
BT241	66.17%
MBT212	48.37%
GBM08	36.68%
BT618	13.58%
MBT225	12.64
BT594	11.81%
BT 458	0.56%
BT667	0.37%
BT799	0.15%
Normal Stem Cells (NSCs)	0.99%
Normal Human Astrocytes (NHA)	2.12%

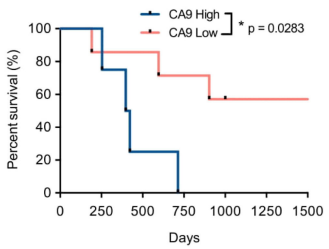

FIGURE 1 | CA9 as a therapeutic target in GBM. **(A)** Transcriptomic dataset shows significant upregulation of CA9 in GBM samples (n=163) when compared to non-tumor (n=207) (GEPIA2) (P value: * < 0.05). **(B)** CA9 has higher expression in mesenchymal (Mes) subtype (n=51) compared to proneural (PN) (n=46) and classical (Cla) (n=59) of GBM (GlioVisTCGA) (P value:***< 0.001). **(C)** Survival data from the TCGA dataset for *CA9* high (n=77) transcript expression of GBM samples illustrating a significant increase in survival when compared to *CA9* low (n=78) samples (Median *CA9* mRNA expression (log2) cut off: 7.66; HR: 0.72 (0.5-1.02); Wilcoxon p value: 0.0288). **(D)** Characterisation of surface CA9 expression of GBM samples along with normal stem cells (NSCs) and normal human astrocytes (NHAs) in normoxic condition by flow cytometry reveals varying expression of CA9 in GBM lines, but low levels in normal cells. **(E)** GBM samples (n=11) from Fig 1.D. were grouped into either CA9low (red, n=5) or CA9high (blue, n=4) expression based on a flow cytometric median of 20%. Log-rank (Mantel-Cox Test) analysis demonstrated a significant survival benefit for patients bearing CA9low tumors with a median survival of 33 and 13.5 months for patients bearing CA9low and patients bearing CA9high tumors, respectively (P value: * =0.0283).

mitogenic anti-CD3ε clone (scFv OKT3) with a short flexible amino acid linker (63). This engineered CA9 DATE consists of a ~50 kDa CA9 Fab-light chain fused to OKT3 scFv and a ~25 kDa CA9 Fab-heavy chain.

We performed binding assays to test the dual specificity of the purified DATEs for CD3 on T cells and CA9 on patient-derived tumor cells. As a proof-of-principle we first assessed DATE specificity in patient-derived models of ccRCC where CA9 is constitutively expressed, irrespective of oxygen tension, due to *VHL* loss (RCC243) and in the murine cortical adenocarcinoma renal cell carcinoma cell line (Renca) where we overexpressed CA9. Endogenous, cell surface expression of CA9 was found in

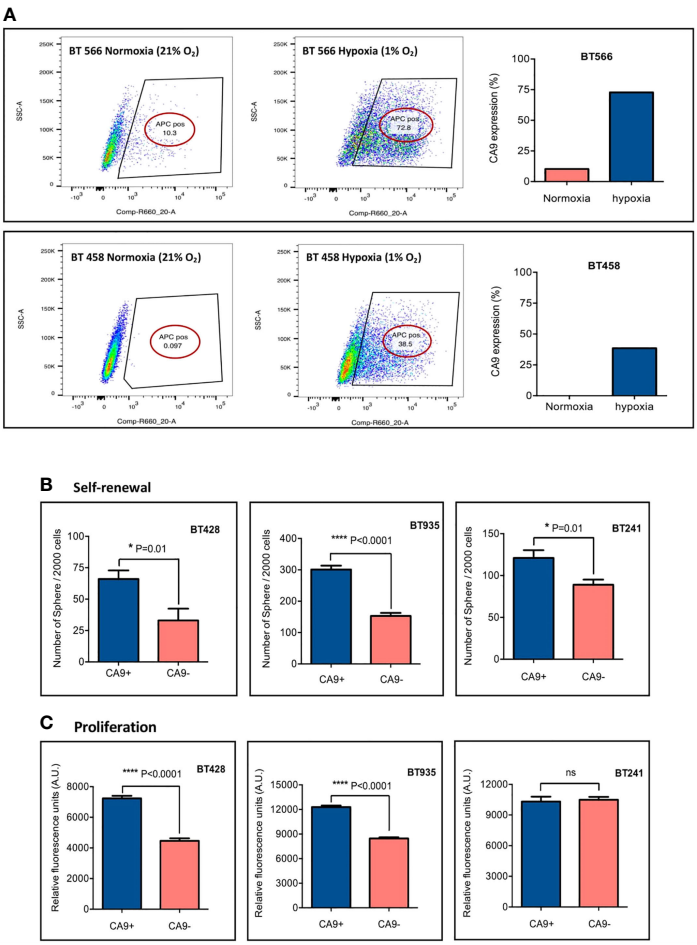

FIGURE 2 | CA9 expression elevates in hypoxic condition and is associated with higher level of self-renewal and proliferation. **(A)** CA9 surface expression was evaluated after cells were cultured in normoxia or hypoxia (1% O_2) for 5 days; and the results indicated a dramatic increase in CA9 expression on both GBM BTIC lines upon exposure to hypoxia. **(B)** Significant increase of self-renewal capacity as measured by secondary sphere formation assay and **(C)** proliferative potential as measured by PrestoBlue proliferation assay is seen in CA9+ when compared to CA9- cells. (P value: **** <~0.0001, * 0.01, ns: non-significant) (mean±SEM, two-tailed t-test).

>80% of RCC243 cells which was completely lost upon CRISPR knockout of the gene (**Figure 3A**). Similarly, overexpression of human CA9 (hCA9) in Renca cells resulted in 90% of the cells positive for cell surface expression of CA9, which was undetectable in the wild type cells (**Figure 3A**). We stained the RCC243 and RCC243 CA9 KO as well as WT and hCA9 Renca cells with varying concentrations of the CA9 DATE. CA9 binding was only observed in CA9-expressing lines (RCC243, Renca hCA9) and no binding was detected in CA9-negative lines (RCC243 CA9 KO and Renca WT) demonstrating the specificity of the CA9 DATE to bind target cells in an antigen (CA9) restricted manner (**Figures 3B, C**). We next confirmed DATE binding to T cells using Jurkat cells which were 90% positive for CD3 expression (**Figure 3D**). Again, we observed a dose-dependent increase in DATE binding to Jurkat cells (**Figure 3E**). Together, our results confirmed antigen specificity and high affinity binding of CA9 DATEs to the tumor cells and T cells.

CA9 DATE Activates T Cells and Induces Tumor Cell Lysis

The main mechanism of action for the CA9 DATE upon binding to T cells and tumor cells is T cell activation and subsequent tumor cell lysis. Upon confirming the antigen specificity of the CA9 DATE for both T cells and tumor cells, we aimed to assess the efficacy of the CA9 DATE by further investigating its ability to activate and re-direct human T-cells against antigen-expressing tumor cells. For this purpose, T cells were co-cultured with ccRCC cells in the presence and absence of DATEs. We evaluated T-cell activation by staining for CD25 and detected elevated expression of CD25 (late activation marker) in both CD4 and CD8 T cells only in the presence of

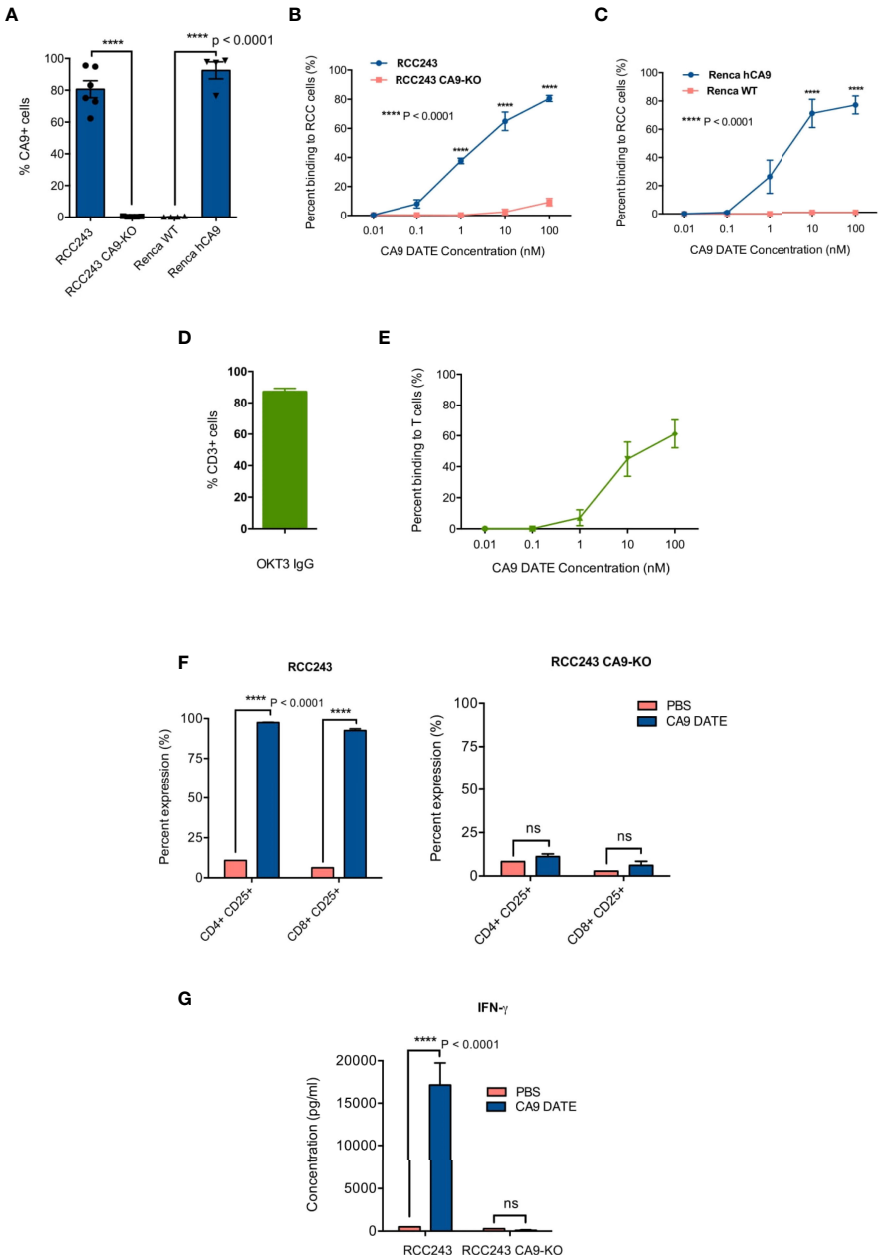

FIGURE 3 | Generation and assessment of human anti-CA9 Dual specific T cell engagers (DATEs) on Renal Cell Carcinoma (ccRCC). **(A)** CA9 expression level on RCC243, RCC243 CA9-KO, Renca and Renca hCA9 cells. **(B)** Increasing concentrations of CA9 DATE binding to RCC243 vs RCC243 CA9-KO, **(C)** Renca hCA9 vs Renca WT cells and **(E)** CD3 expressing Jurkat cells were measured using flow cytometry. Error bars: mean ± SEM. **(D)** okt3 expression level on Jurkat cells. **(F)** Addition of CA9 DATEs (1 nM) to the co-culture of human CD3+ T cells with CA9 expressing target cells (Luciferase-expressing RCC 243 cell lines and the CA9 knockout counterpart [CA9-KO]) for 48 hours at the E:T ratio, 1:5 resulted in a significant elevation of CD25 expression on both CD4+ and eng+ T cells population confirmed by flow cytometry analysis. (n=4) (P value: **** < 0.0001) (2 way ANOVA) **(G)** Enzyme-linked immunosorbent assay (ELISA) indicated increased secretion of Interferon-gamma (IFN-γ) by T cells only in the presence ofCA9 DATE and CA9 expression on target cells. (P value:**** < 0.0001) (2 way ANOVA).

CA9 DATEs (**Figure 3F**; left). Moreover, this effect was entirely dependent on the expression of CA9 by the target cells (**Figure 3F**; right), suggesting the DATE was permitting the formation of an immunological synapse between the T cells and ccRCC cells leading to T cell activation. Furthermore, T cell activation was further confirmed by the increase in IFN-γ production in the presence of the DATE in a CA9-dependent manner (**Figure 3G**). Together, these results demonstrated that the CA9 DATE has the ability to activate T cells in a strictly antigen-dependent manner.

We next assessed the efficacy and potency of CA9 DATE-directed T-cell cytotoxicity. Co-culture of RCC243 cells with T

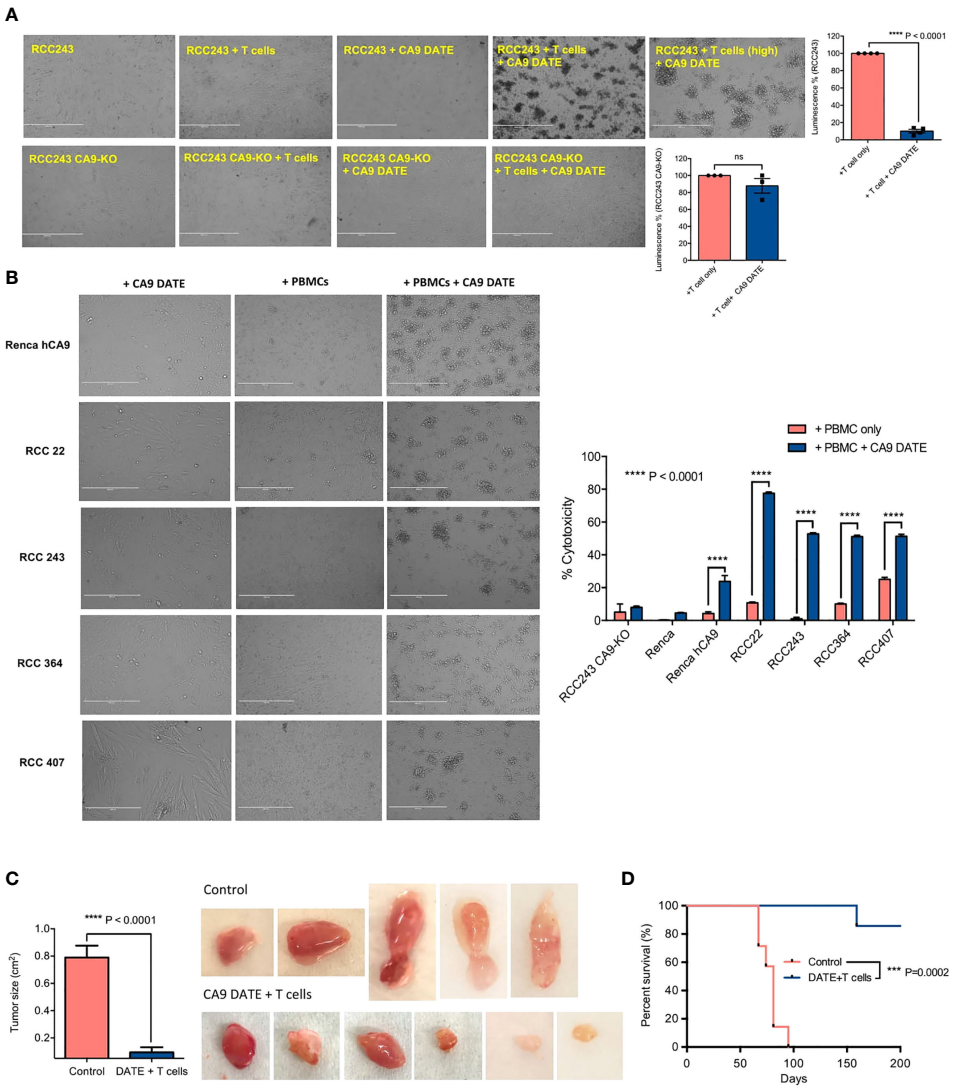

FIGURE 4 | Assessing the efficacy of CA9 DATE in therapeutic targeting of CA9 expressing RCC lines and xenografted immunocompromised mice: **(A)** CA9 DATE (1 nM) induced potent cytolysis in antigen expressing target cells when cocultured with human CD3+ T cells at an E:T ratio of 5:1 for 48 hours quantified by luminescence assay. Phase contrast images of the *in vitro* cytotoxicity assay confirmed potent cytolytic effect of CA9 DATE on CA9 antigen expression. (n=4) (Scale bar: 1000 μ) (P value: ****< 0.0001, ns, non-significant) (mean SEM, two-tailed t-test). **(B)** CA9 DATE effectively induced target lysis across a panel of kidney cancer cell lines when co-cultured with CD3+ T cells at E:T ratio of 10:1 *(In vitro* cytotoxicity assay setup as described earlier). lactate dehydrogenase (LDH) release assay on the supernatant indicated a drastic increase in target cell cytotoxicity in the presence of CA9 DATE and CA9 antigen expression. The phase contrast images of light microscope confirmed the cytolytic effect of CA9 DATE on CA9 expressing RCC lines (n=2). (P value:****< 0.0001) (2 way ANOVA). **(C)** NSG mice were subcutaneously implanted with human CA9+ RCC 243 VHL mut cells. Upon successful engraftment and having a palpable tumor, mice were intratumorally treated with $2x10^6$ T cells isolated from human PBMCs either with CA9 DATE or CA9 DATE control (50μg) for a total of 12 doses over 6 weeks. Mouse xenografts generated after CA9 DATE treatment had less tumor burden (n=6) (P value: **** < 0.0001) (mean±SEM, two-tailed t-test) and **(D)** maintained a significant survival advantage over control mice (n=7) (P value: *** < 0.0004) (Log-rank Mantel-Cox Test).

cells in the presence of the CA9 DATE resulted in significant cell death (**Figure 4A**). In contrast, no cell death was detected when RCC243 CA9 KO cells were cultured with T cells in the presence of the DATE (**Figure 4A**). We then extended our findings to 3 additional patient-derived models of ccRCC as well as the Renca-hCA9 model (**Figure 4B**). Co-culture of these lines with PBMCs resulted in significant target cell death only when the DATE was present (**Figure 4B**). Altogether, these data strongly confirmed that CA9 DATE can potently activate T cells and redirect them to tumor cells triggering robust tumor cell death.

CA9 DATE Inhibits ccRCC Tumor Growth

To evaluate the effect of the CA9 DATE on tumor growth *in vivo* we evaluated the RCC243 model where CA9 expression is highly,

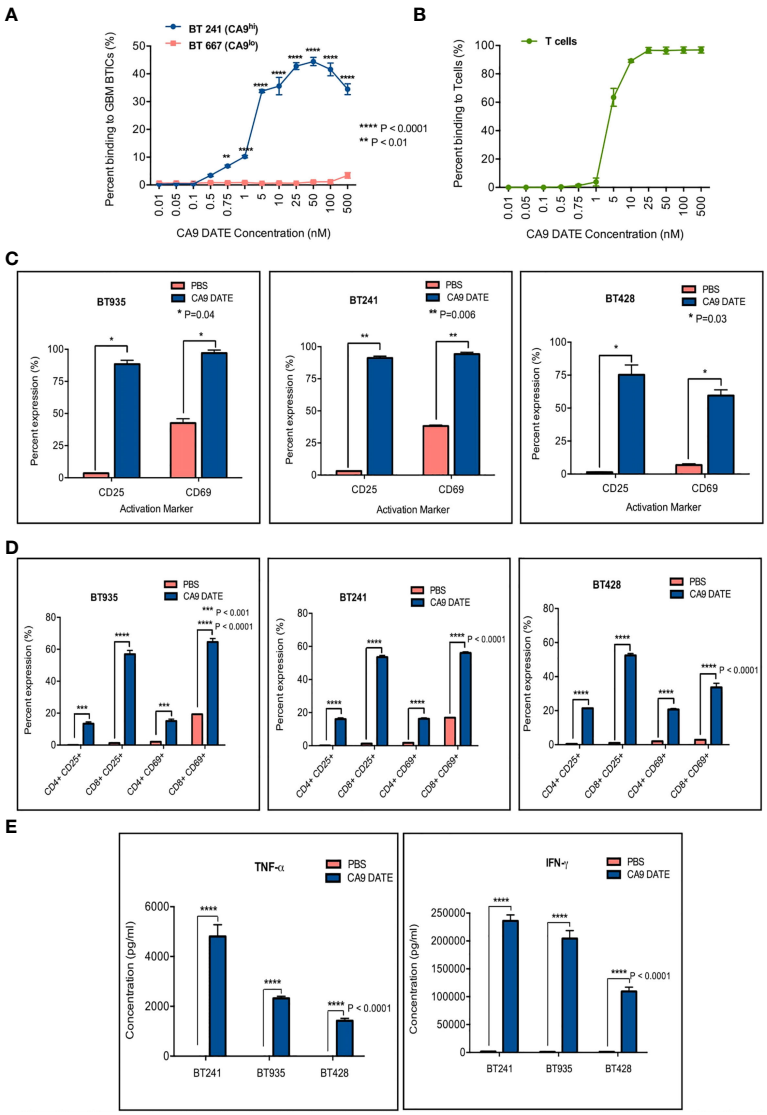

FIGURE 5 | Assessment of anti-CA9 Dual specific T cell engagers (DATEs) dual specificity and its effect on GBM model. **(A)** Dual specificity of CA9 DATEs on CA9hi GBM BTIC (BT241), CA9low GBM BTIC (BT667) and **(B)** human PBMC derived T cells by flow cytometry. (P value: **<0.01, **** <0.0001) (2-way RM AVOVA). **(C)** Addition of CA9 DATE (1μg/mL) (13nM) to the co-culture of CA9hi GBM BTICs (BT241, BT935, BT428) and T cells (E:T ratio, 1:1) (overnight incubation) caused T cells activation as confirmed by increased expression of CD25 and CD69 by flow cytometry analysis (n=2). (P value: *= 0.04, **= 0.006) (2 way ANOVA) **(D)** CD8+ T cells were the main subset of activated T cells. (P value: ***< 0.001, **** < 0.0001) (2 way ANOVA) **(E)** Enzyme-linked immunosorbent assay (ELISA) shows elevated secretion of IFN-γ and TNF-α cytokines in supernatant collected from co-cultures ofT cells and GBM BTICs treated with CA9 DATEs. (n=2) (P value: **** < 0.0001).

homogeneously expressed throughout the tumor. RCC243 *VHL* mutant lines sorted for CA9 expression and CA9^{+} cells were injected into the flank of immunocompromised NSG mice. Upon tumor formation, mice were co-injected with DATEs and isolated T cells from freshly thawed human PBMCs intratumorally (**Schematic Figure S2A**). Mice treated with CA9 DATE and T cells had significantly reduced tumor growth (**Figure 4C**) which translated to a significant survival benefit (**Figure 4D**) over the control arm. Thus, these data provide excellent evidence that the CA9 DATE can be effectively utilized to treat CA9 expressing solid tumors independent of hypoxia.

CA9 DATE Binds *CA9* on GBM BTICs, Activates T Cells and Induces Target Cell Death

We next sought to determine the efficacy of the CA9 DATE in GBM using our patient-derived GBM BTIC lines. We first

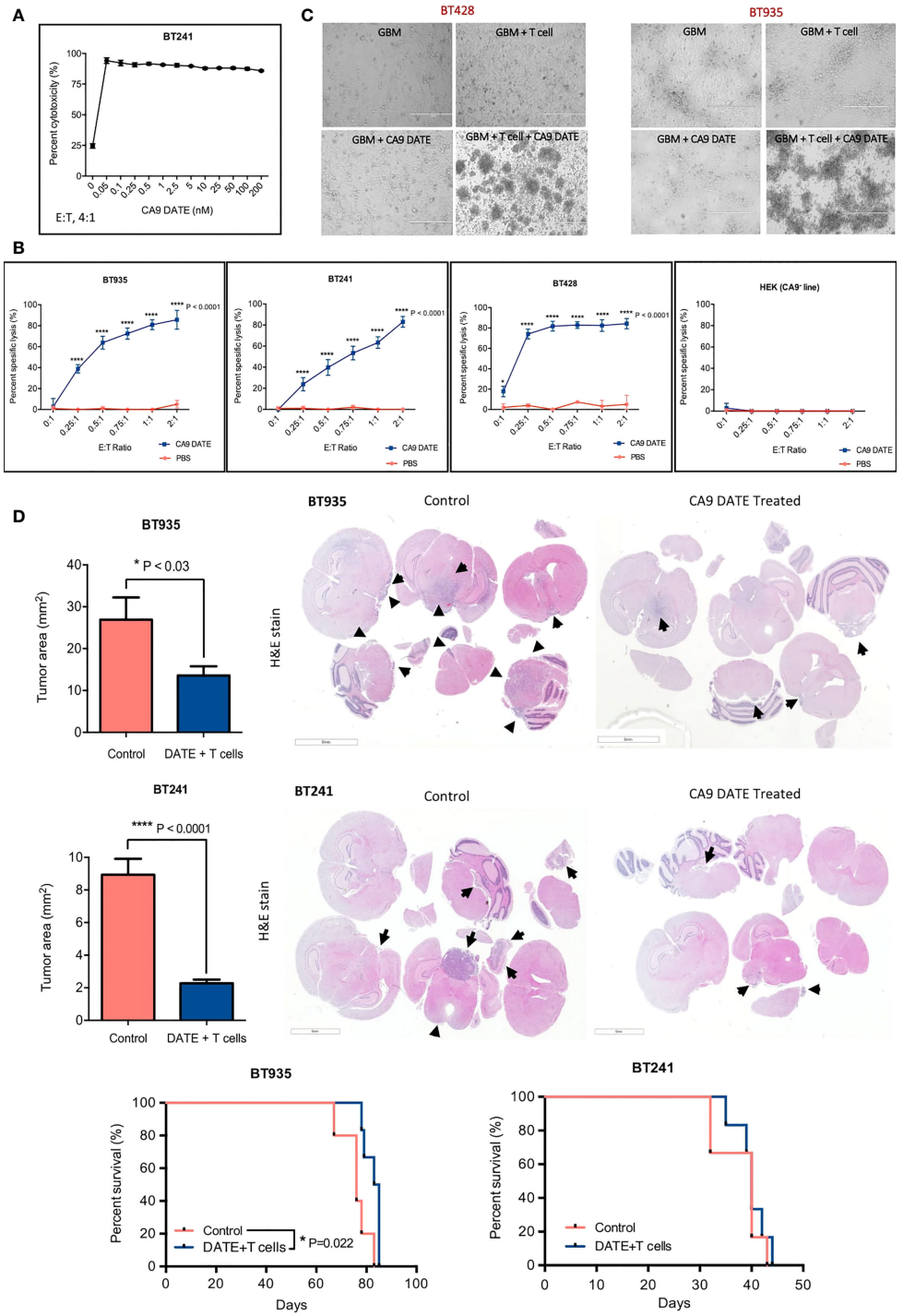

FIGURE 6 | Therapeutic targeting of CA9hi GBM BTICs using CA9 DATEs at *in vitro* level and in patient derived xenograft model of GBM. **(A)** Dose response study performed on BT 241, CA9hi GBM BTIC, identified 1 nM as the optimal dose for GBM cytotoxicity assay. **(B)** DATEs significantly induced cytotoxicity of CA9hi GBM BTICs (BT241, BT935, BT428) but not CA9- cells (HEK) when co-cultured with T cells and DATEs (1n M) for 16 hours at different E:T ratios. (n=3) (P value:*< 0.05, **** < 0.0001) (2 way ANOVA). **(C)** Micrographs of GBM BTICs and T-cell co-culture with and without DATEs. CA9hi GBM BTIC lines (BT 935 and BT 428) were incubated with either T cells (E:T ratio, 1 :2) or CA9 DATE alone or with both. GBM BTIC lysis were observed only in the presence of both T cells and CA9 DATEs (Scale bar: 400 m). **(D)** NSG mice were intracranially implanted with human CA9hi GBM BTICs (BT935 and BT241). Upon successful engraftment, mice were intracranially treated with $1x10^6$ T cells isolated from human PBMCs either with CA9 DATE or CA9 DATE control (50µg = 667nM) for a total of four doses over two weeks. Mouse xenografts generated after CA9 DATE treatment had less tumor burden (n=6) (P value: * < 0.03, **** < 0.0001) (mean±SEM, two-tailed t-test) and maintained a significant survival advantage over control mice in BT935 engrafted mice (P value: * < 0.03) (Log-rank Mantel-Cox Test); however, DATE treatment on BT241 engrafted mice only showed increased pattern of survival (n=6).

performed binding assays on $CA9^{hi}$ (BT241) and $CA9^{lo}$ (BT667) GBM lines (**Figure 5A**) to determine the DATE binding capacity in these GBM cells. Similar to our ccRCC observations (**Figure 3B**), we observed a dose-dependent increase in DATE binding to BT241 cells that was not detected in the BT667 line (**Figure 5A**) confirming the antigen specificity of the DATE. We next confirmed the ability of the DATE to bind T cells derived from human PBMC (**Figure 5B**). The DATE bound T cells in a dose-dependent, saturable manner.

We next assessed whether the co-culture of T cells and GBM cells in the presence of the DATE would also lead to activation of the T cells. We stained T cells for CD25 and CD69 after an overnight co-culture with BT935, BT241 and BT428 with or without the CA9 DATE (**Figure 5C**). T cell activation was observed in all 3 co-cultures in a DATE-dependent manner. Moreover, this activation was greatest for CD8 T cells (**Figure 5D**). Furthermore, T-cell activation was also associated with the elevated secretion of pro-inflammatory cytokines TNFα and IFNγ in a DATE-dependent manner (**Figure 5E**).

We next sought to determine whether the enhanced T cell activation following exposure to the CA9 DATE in the presence of CA9 would lead to GBM lysis. To determine the concentration at which the CA9 DATE has optimal cytotoxicity on GBM BTICs, we titrated the DATE from 0 nM to 200 nM in co-cultures of GBM BTICs and T cells (**Figure 6A**). Remarkably, even the lowest concentration of CA9 DATE (50 pM) invoked a potent cytolytic effect on GBM BTICs (**Figure 6A**). Ultimately, 1 nM was chosen as the best concentration for performing cytotoxicity assays. We then evaluated cytotoxicity across multiple E:T ratios at a constant DATE concentration and identified significant cell death was induced as low as at a E:T ratio of 0.25:1 (**Figure 6B**). Furthermore, this was only observed in the presence of DATE and CA9. In addition, microscopic examination confirmed that co-incubation of T cells (suspension) and GBM BTICs (adherent) in the presence of CA9 DATEs leads to GBM BTIC lysis. In contrast to wells without DATEs, the co-cultures with CA9 DATEs showed detachment of target GBM cells that formed rosettes, indicating clumps of dying cells (**Figure 6C**).

CA9 DATE Reduces GBM Tumor Growth and Extends Survival

We next assessed the efficacy of the CA9 DATE *in vivo* using two separate early passage patient-derived GBM cell lines enriched for BTIC populations (BT935 and BT241). BT935 cells were injected intracranially into immunocompromised NSG mice. Following engraftment, CA9 DATEs and isolated T cells from freshly thawed human PBMCs were co-injected intracranially (**Figure S2B**). Treatment with the CA9 DATE and T cells significantly reduced tumor growth upon completion of the treatment regimen, whereas tumor growth was unaffected in mice receiving the control DATE and T cells (**Figure 6D**). Furthermore, the CA9 DATE-T cell regimen led to an extension in mouse survival (**Figure 6D**). We then tested the efficacy of the DATE in a second orthotopic patient-derived GBM model. Following engraftment of BT241 tumors mice were treated with the CA9 DATE and T cell regimen (**Figure S2C**). Again, the CA9 DATE and T cell regimen led to a significant reduction in BT241 tumor growth upon completion of the treatment regimen. However, this failed to provide a survival benefit in this model (**Figure 6D**). In summary, we have developed a highly specific CA9 targeting DATE that potently activates T cells and effectively controls growth of CA9-positive solid tumors.

DISCUSSION

In the present study we developed a novel immunotherapeutic approach to target CA9 utilizing a CA9-specific DATE. The CA9 DATE was able to bind CA9 and redirect T cells to ccRCC and GBM cells in a CA9-dependent manner. Furthermore, the DATE possessed potent antitumor activity in multiple patient-derived solid tumor models of GBM and ccRCC containing both robust constitutive CA9 expression in response to *VHL* loss as well as in models with microenvironmentally-driven CA9 upregulation. While survival benefit from our studies was substantive in the ccRCC models, this was not the case in our GBM models. This is perhaps a reflection of the higher antigen levels present throughout the tumor at the initiation of dosing in the ccRCC models versus the GBM models together with the half-life of the administered DATE and the number of times it can be administered. It thus requires development of an optimized dosing regimen. Consequently, it is difficult to extrapolate these findings to the patient condition given that the dose and dosing regimen are likely to be entirely different in humans and patients will have undergone or will be undergoing standard of care treatment concurrently compared to our single agent experiments. Standard of care in GBM has left the dismal patient outcome associated with this disease unchanged over the last two decades (5). The tremendous degree of heterogeneity within GBM tumors combined with the influence of the tumor microenvironment has contributed significantly to this (64). GBMs are quite hypoxic (22, 65, 66) and BTICs are enriched in areas of hypoxia (22, 61, 62). Here we provide evidence that CA9 expression is important for BTIC self renewal and proliferation, suggesting that our CA9 DATE has the potential to eliminate BTIC cells within GBMs. These data align with previous findings demonstrating that combining a small molecule targeting CA9 activity with temozolomide reduces the GBM BTIC population (38). Since BTICs are a significant contributing factor to treatment resistance and disease recurrence (18, 19), our CA9 targeting DATE may be used to overcome treatment resistance and help prevent the recurrence of GBMs.

The development of novel immunotherapeutic strategies to engage the immune system to treat GBMs have provided renewed hope for improving patient outcomes (67, 68). GBMs are typically classified as an immunologically cold tumor (69) and contain T cells at low abundance (70, 71). Overcoming this with strategies that can direct the T cells to critical tumor associated antigens has led to the development of bifunctional T cell engagers which are currently being evaluated clinically in GBM (68). Here we propose that CA9 is an important tumor associated antigen that may be exploited using

this strategy. Our data demonstrates long term efficacy of the DATE in tumors with CA9 expressed homogeneously throughout the tumor at a high level, yet short term efficacy in models where the proportion of CA9 positivity is lower. These findings demonstrate that the DATE is very effective at eliminating antigen positive cells and that recurrence is perhaps a reflection of both regrowth driven by antigen negative cells (68) and the short half-life of the DATE (72). This suggests that the CA9-DATE treatment strategy can benefit from combinatorial tumor targeting strategies such as CAR T therapies or oncolytic viruses, including those that are engineered to secrete bifunctional T cell engagers (73–75), targeting additional GBM tumor associated antigens along with CA9. Moreover, CA9 inhibition has been shown to enhance the efficacy of immune checkpoint inhibitors (ICIs) in hypoxic solid tumors (46). While this approach has yet to provide substantial benefit in GBM, combining the ICIs with the DATE and injected T cells may be worth further exploration in this setting where some of the immunosuppressive features of the GBM have been overcome by targeting CA9.

CA9 expression while highly upregulated in solid tumors, is also present minimally in normal tissues (36, 37) which may pose on-target, off-tumor toxicity challenges. This is precisely why CAR-T strategies targeting CA9 have failed (76). However, on-target-off-tumor toxicity appears to be less of a concern in antibody mediated therapy as monoclonal antibody targeting of CA9 has been used for imaging (77) and radio-immunotherapy (78, 79) without significant GI toxicity issues. Thus, persistence of CA9 targeting may be the culprit responsible for the biliary toxicity associated with CA9 CAR-T therapies, but not antibody mediated therapies. The fact that this strategy requires both the target antigen to be expressed (CA9) and the T cells to be in the same location likely adds safety to the approach and potentially mitigates the concerns about on-target-off-tumor toxicity. Furthermore, local delivery of the DATE will further aid in eliminating systemic on-target-off-tumor toxicity. Nevertheless, this is a concern that will be evaluated, along with delivery strategies, as this therapeutic approach progresses through preclinical and clinical testing.

In summary, our data strongly supports the utility of CA9 DATEs against GBM and ccRCC tumors highly expressing CA9. This antibody-based targeted therapy may expand our arsenal of effective therapeutic approaches targeting CA9 in solid tumors and warrants further exploration.

DATA AVAILABILITY STATEMENT

The original contributions presented in the study are included in the article/**Supplementary Material**. Further inquiries can be directed to the corresponding author.

ETHICS STATEMENT

Human GBM brain tumors and patient-derived RCC cell lines were obtained from consenting patients, as approved by the Hamilton Health Sciences/McMaster Health Sciences Research Ethics Board and the Princess Margaret Cancer Centre, Toronto, respectively. The patients/participants provided their written informed consent to participate in this study. The animal studies were performed according to guidelines under Animal Use Protocols (19-01-01) of McMaster University Central Animal Facility.

AUTHOR CONTRIBUTIONS

NT, CV, XZ, JM, and SS conceived and designed overall studies. NT, DM, and NS performed animal studies. NT, XZ, MSh, and SC propagated brain tumor lines and performed *in vitro* assays. Flow studies were performed by MSu. NT, CV, XZ, and KL perfomed data interpretation. MSe helped with assessing the effect of hypoxia on target expression. NT developed and edited figures and performed statistical analyses. NT, SC, and CV drafted and edited the manuscript, with input from all authors. All authors contributed to the article and approved the submitted version.

FUNDING

This work was supported through a program project grant from the Terry Fox Research Institute Canada (#1065) (to SS and JM) and funds to SS from McMaster University Department of Surgery. NT was supported by MITACS fellowship in partnership with Center for the Commercialization of Antibodies and Biologic.

SUPPLEMENTARY MATERIAL

The Supplementary Material for this article can be found online at: https://www.frontiersin.org/articles/10.3389/fimmu.2022.905768/full#supplementary-material

ACKNOWLEDGMENTS

We thank Dr. Sachdev Sidhu and Dr. Jarret Adams from University of Toronto for helping with CA9 DATEs.

REFERENCES

1. Louis DN, Perry A, Reifenberger G, von Deimling A, Figarella-Branger D, Cavenee WK, et al. The 2016 World Health Organization Classification of Tumors of the Central Nervous System: A Summary. *Acta Neuropathol* (2016) 131(6):803–20. doi: 10.1007/s00401-016-1545-1
2. Omuro A, DeAngelis LM. Glioblastoma and Other Malignant Gliomas: A Clinical Review. *JAMA* (2013) 310(17):1842–50. doi: 10.1001/jama.2013.280319
3. Stupp R, Weber DC. The Role of Radio- and Chemotherapy in Glioblastoma. *Onkologie* (2005) 28(6-7):315–7. doi: 10.1159/000085575
4. Ostrom QT, Gittleman H, de Blank PM, Finlay JL, Gurney JG, McKean-Cowdin R, et al. American Brain Tumor Association Adolescent and Young

Adult Primary Brain and Central Nervous System Tumors Diagnosed in the United States in 2008-2012. *Neuro Oncol* (2016) 18 Suppl 1:i1–i50. doi: 10.1093/neuonc/nov297
5. Stupp R, Mason WP, van den Bent MJ, Weller M, Fisher B, Taphoorn MJ, et al. Radiotherapy Plus Concomitant and Adjuvant Temozolomide for Glioblastoma. *N Engl J Med* (2005) 352(10):987–96. doi: 10.1056/NEJMoa043330
6. Stupp R, Hegi ME, Mason WP, van den Bent MJ, Taphoorn MJ, Janzer RC, et al. Effects of Radiotherapy With Concomitant and Adjuvant Temozolomide Versus Radiotherapy Alone on Survival in Glioblastoma in a Randomised Phase III Study: 5-Year Analysis of the EORTC-NCIC Trial. *Lancet Oncol* (2009) 10(5):459–66. doi: 10.1016/S1470-2045(09)70025-7
7. Hegi ME, Diserens AC, Gorlia T, Hamou MF, de Tribolet N, Weller M, et al. MGMT Gene Silencing and Benefit From Temozolomide in Glioblastoma. *N Engl J Med* (2005) 352(10):997–1003. doi: 10.1056/NEJMoa043331
8. Noroxe DS, Poulsen HS, Lassen U. Hallmarks of Glioblastoma: A Systematic Review. *ESMO Open* (2016) 1(6):e000144. doi: 10.1136/esmoopen-2016-000144
9. Wen PY, Kesari S. Malignant Gliomas in Adults. *N Engl J Med* (2008) 359(5):492–507. doi: 10.1056/NEJMra0708126
10. Neftel C, Laffy J, Filbin MG, Hara T, Shore ME, Rahme GJ, et al. An Integrative Model of Cellular States, Plasticity, and Genetics for Glioblastoma. *Cell* (2019) 178(4):835–49.e21.
11. Yap TA, Gerlinger M, Futreal PA, Pusztai L, Swanton C . Intratumor Heterogeneity: Seeing the Wood for the Trees. *Sci Transl Med* (2012) 4(127):127ps10. doi: 10.1126/scitranslmed.3003854
12. McGranahan N, Swanton C. Biological and Therapeutic Impact of Intratumor Heterogeneity in Cancer Evolution. *Cancer Cell* (2015) 27(1):15–26. doi: 10.1016/j.ccell.2014.12.001
13. Szerlip NJ, Pedraza A, Chakravarty D, Azim M, McGuire J, Fang Y, et al. Intratumoral Heterogeneity of Receptor Tyrosine Kinases EGFR and PDGFRA Amplification in Glioblastoma Defines Subpopulations With Distinct Growth Factor Response. *Proc Natl Acad Sci U S A* (2012) 109(8):3041–6. doi: 10.1073/pnas.1114033109
14. Singh SK, Hawkins C, Clarke ID, Squire JA, Bayani J, Hide T, et al. Identification of Human Brain Tumour Initiating Cells. *Nature* (2004) 432(7015):396–401. doi: 10.1038/nature03128
15. Dalerba P, Cho RW, Clarke MF. Cancer Stem Cells: Models and Concepts. *Annu Rev Med* (2007) 58:267–84. doi: 10.1146/annurev.med.58.062105.204854
16. Singh SK, Clarke ID, Terasaki M, Bonn VE, Hawkins C, Squire J, et al. Identification of a Cancer Stem Cell in Human Brain Tumors. *Cancer Res* (2003) 63(18):5821–8.
17. Clarke MF, Fuller M. Stem Cells and Cancer: Two Faces of Eve. *Cell* (2006) 124(6):1111–5.
18. Liu G, Yuan X, Zeng Z, Tunici P, Ng H, Abdulkadir IR, et al. Analysis of Gene Expression and Chemoresistance of CD133+ Cancer Stem Cells in Glioblastoma. *Mol Cancer* (2006) 5:67.
19. Bao S, Wu Q, McLendon RE, Hao Y, Shi Q, Hjelmeland AB, et al. Glioma Stem Cells Promote Radioresistance by Preferential Activation of the DNA Damage Response. *Nature* (2006) 444(7120):756–60.
20. Cooper LA, Gutman DA, Chisolm C, Appin C, Kong J, Rong Y, et al. The Tumor Microenvironment Strongly Impacts Master Transcriptional Regulators and Gene Expression Class of Glioblastoma. *Am J Pathol* (2012) 180(5):2108–19.
21. Pistollato F, Chen HL, Schwartz PH, Basso G, Panchision DM, et al. Oxygen Tension Controls the Expansion of Human CNS Precursors and the Generation of Astrocytes and Oligodendrocytes. *Mol Cell Neurosci* (2007) 35(3):424–35. doi: 10.1016/j.mcn.2007.04.003
22. Colwell N, Larion M, Giles AJ, Seldomridge AN, Sizdahkhani S, Gilbert MR, et al. Hypoxia in the Glioblastoma Microenvironment: Shaping the Phenotype of Cancer Stem-Like Cells. *Neuro Oncol* (2017) 19(7):887–96. doi: 10.1093/neuonc/now258
23. Rankin EB, Giaccia AJ. The Role of Hypoxia-Inducible Factors in Tumorigenesis. *Cell Death Differ* (2008) 15(4):678–85. doi: 10.1038/cdd.2008.21
24. Chiche J, Brahimi-Horn MC, Pouyssegur J. Tumour Hypoxia Induces a Metabolic Shift Causing Acidosis: A Common Feature in Cancer. *J Cell Mol Med* (2010) 14(4):771–94. doi: 10.1111/j.1582-4934.2009.00994.x
25. Sedlakova O, Svastova E, Takacova M, Kopacek J, Pastorek J, Pastorekova S , et al. Carbonic Anhydrase IX, a Hypoxia-Induced Catalytic Component of the pH Regulating Machinery in Tumors. *Front Physiol* (2014) 4:400. doi: 10.3389/fphys.2013.00400
26. Agnihotri S, Zadeh G. Metabolic Reprogramming in Glioblastoma: The Influence of Cancer Metabolism on Epigenetics and Unanswered Questions. *Neuro Oncol* (2016) 18(2):160–72. doi: 10.1093/neuonc/nov125
27. Pastorekova S, Gillies RJ. The Role of Carbonic Anhydrase IX in Cancer Development: Links to Hypoxia, Acidosis, and Beyond. *Cancer Metastasis Rev* (2019) 38(1-2):65–77. doi: 10.1007/s10555-019-09799-0
28. Lee SH, Griffiths JR. How and Why Are Cancers Acidic? Carbonic Anhydrase IX and the Homeostatic Control of Tumour Extracellular pH. *Cancers (Basel)* (2020) 12(6):1616. doi: 10.3390/cancers12061616
29. McDonald PC, Winum JY, Supuran CT, Dedhar S. Recent Developments in Targeting Carbonic Anhydrase IX for Cancer Therapeutics. *Oncotarget* (2012) 3(1):84–97. doi: 10.18632/oncotarget.422
30. Proescholdt MA, Merrill MJ, Stoerr EM, Lohmeier A, Pohl F, Brawanski A, et al. Function of Carbonic Anhydrase IX in Glioblastoma Multiforme. *Neuro Oncol* (2012) 14(11):1357–66. doi: 10.1093/neuonc/nos216
31. Said HM, Supuran CT, Hageman C, Staab A, Polat B, Katzer A, et al. Modulation of Carbonic Anhydrase 9 (CA9) in Human Brain Cancer. *Curr Pharm Des* (2010) 16(29):3288–99. doi: 10.2174/138161210793429788
32. Bui MH, Seligson D, Han KR, Pantuck AJ, Dorey FJ, Huang Y, et al. Carbonic Anhydrase IX is an Independent Predictor of Survival in Advanced Renal Clear Cell Carcinoma: Implications for Prognosis and Therapy. *Clin Cancer Res* (2003) 9(2):802–11.
33. Heaton JT, Farabaugh SM, Brauth SE. Effect of Syringeal Denervation in the Budgerigar (Melopsittacus Undulatus): The Role of the Syrinx in Call Production. *Neurobiol Learn Mem* (1995) 64(1):68–82. doi: 10.1006/nlme.1995.1045
34. Soyupak B, Erdoğan S, Ergin M, Seydaoğlu G, Kuzgunbay B, Tansuğ Z, et al. CA9 Expression as a Prognostic Factor in Renal Clear Cell Carcinoma. *Urol Int* (2005) 74(1):68–73. doi: 10.1159/000082713
35. Choueiri TK, Motzer RJ. Systemic Therapy for Metastatic Renal-Cell Carcinoma. *N Engl J Med* (2017) 376(4):354–66. doi: 10.1056/NEJMra1601333
36. Liao SY, Lerman MI, Stanbridge EJ. Expression of Transmembrane Carbonic Anhydrases, CAIX and CAXII, in Human Development. *BMC Dev Biol* (2009) 9:22. doi: 10.1186/1471-213X-9-22
37. Ivanov S, Liao SY, Ivanova A, Danilkovitch-Miagkova A, Tarasova N, Weirich G, et al. Expression of Hypoxia-Inducible Cell-Surface Transmembrane Carbonic Anhydrases in Human Cancer. *Am J Pathol* (2001) 158(3):905–19. doi: 10.1016/S0002-9440(10)64038-2
38. Boyd NH, Walker K, Fried J, Hackney JR, McDonald PC, Benavides GA, et al. Addition of Carbonic Anhydrase 9 Inhibitor SLC-0111 to Temozolomide Treatment Delays Glioblastoma Growth *In Vivo*. *JCI Insight* (2017) 2(24):e92928. doi: 10.1172/jci.insight.92928
39. Supuran CT. Experimental Carbonic Anhydrase Inhibitors for the Treatment of Hypoxic Tumors. *J Exp Pharmacol* (2020) 12:603–17. doi: 10.2147/JEP.S265620
40. Pacchiano F, Carta F, McDonald PC, Lou Y, Vullo D, Scozzafava A, et al. Ureido-Substituted Benzenesulfonamides Potently Inhibit Carbonic Anhydrase IX and Show Antimetastatic Activity in a Model of Breast Cancer Metastasis. *J Med Chem* (2011) 54(6):1896–902. doi: 10.1021/jm101541x
41. Zatovicova M, Jelenska L, Hulikova A, Ditte P, Ditte Z, Csaderova L, et al. Monoclonal Antibody G250 Targeting CA: Binding Specificity, Internalization and Therapeutic Effects in a non-Renal Cancer Model. *Int J Oncol* (2014) 45(6):2455–67. doi: 10.3892/ijo.2014.2658
42. Lam JS, Pantuck AJ, Belldegrun AS, Figlin RA. G250: A Carbonic Anhydrase IX Monoclonal Antibody. *Curr Oncol Rep* (2005) 7(2):109–15. doi: 10.1007/s11912-005-0036-7
43. Zatovicova M, Jelenska L, Hulikova A, Csaderova L, Ditte Z, Ditte P, et al. Carbonic Anhydrase IX as an Anticancer Therapy Target: Preclinical Evaluation of Internalizing Monoclonal Antibody Directed to Catalytic Domain. *Curr Pharm Des* (2010) 16(29):3255–63. doi: 10.2174/138161210793429832

44. Lock FE, McDonald PC, Lou Y, Serrano I, Chafe SC, Ostlund C, et al. Targeting Carbonic Anhydrase IX Depletes Breast Cancer Stem Cells Within the Hypoxic Niche. *Oncogene* (2013) 32(44):5210–9. doi: 10.1038/onc.2012.550
45. McDonald PC, Chafe SC, Brown WS, Saberi S, Swayampakula M, Venkateswaran G, et al. Regulation of pH by Carbonic Anhydrase 9 Mediates Survival of Pancreatic Cancer Cells With Activated KRAS in Response to Hypoxia. *Gastroenterology* (2019) 157(3):823–37. doi: 10.1053/j.gastro.2019.05.004
46. Chafe SC, McDonald PC, Saberi S, Nemirovsky O, Venkateswaran G, Burugu S, et al. Targeting Hypoxia-Induced Carbonic Anhydrase IX Enhances Immune-Checkpoint Blockade Locally and Systemically. *Cancer Immunol Res* (2019) 7(7):1064–78. doi: 10.1158/2326-6066.CIR-18-0657
47. Chafe SC, Vizeacoumar FS, Venkateswaran G, Nemirovsky O, Awrey S, Brown WS, et al. Genome-Wide Synthetic Lethal Screen Unveils Novel CAIX-NFS1/xCT Axis as a Targetable Vulnerability in Hypoxic Solid Tumors. *Sci Adv* (2021) 7(35):eabj0364. doi: 10.1126/sciadv.abj0364
48. Prasad S, Gaedicke S, Machein M, Mittler G, Braun F, Hettich M, et al. Effective Eradication of Glioblastoma Stem Cells by Local Application of an AC133/CD133-Specific T-Cell-Engaging Antibody and CD8 T Cells. *Cancer Res* (2015) 75(11):2166–76. doi: 10.1158/0008-5472.CAN-14-2415
49. Choi BD, Gedeon PC, Herndon JE 2nd, Archer GE, Reap EA, Sanchez-Perez L, et al. Human Regulatory T Cells Kill Tumor Cells Through Granzyme-Dependent Cytotoxicity Upon Retargeting With a Bispecific Antibody. *Cancer Immunol Res* (2013) 1(3):163. doi: 10.1158/2326-6066.CIR-13-0049
50. Choi BD, Kuan CT, Cai M, Archer GE, Mitchell DA, Gedeon PC, et al. Systemic Administration of a Bispecific Antibody Targeting EGFRvIII Successfully Treats Intracerebral Glioma. *Proc Natl Acad Sci U S A* (2013) 110(1):270–5. doi: 10.1073/pnas.1219817110
51. Vora P, Venugopal C, Salim SK, Tatari N, Bakhshinyan D, Singh M, et al. The Rational Development of CD133-Targeting Immunotherapies for Glioblastoma. *Cell Stem Cell* (2020) 26(6):832–44.e6. doi: 10.1016/j.stem.2020.04.008
52. Klein JS, Gnanapragasam PN, Galimidi RP, Foglesong CP, West AP Jr, Bjorkman PJ, et al. Examination of the Contributions of Size and Avidity to the Neutralization Mechanisms of the Anti-HIV Antibodies B12 and 4E10. *Proc Natl Acad Sci U S A* (2009) 106(18):7385–90. doi: 10.1073/pnas.0811427106
53. Brischwein K, Parr L, Pflanz S, Volkland J, Lumsden J, Klinger M, et al. Strictly Target Cell-Dependent Activation of T Cells by Bispecific Single-Chain Antibody Constructs of the BiTE Class. *J Immunother* (2007) 30(8):798–807. doi: 10.1097/CJI.0b013e318156750c
54. Herrmann I, Baeuerle PA, Friedrich M, Murr A, Filusch S, Rüttinger D, et al. Highly Efficient Elimination of Colorectal Tumor-Initiating Cells by an EpCAM/CD3-Bispecific Antibody Engaging Human T Cells. *PLoS One* (2010) 5(10):e13474. doi: 10.1371/journal.pone.0013474
55. Hoffmann P, Hofmeister R, Brischwein K, Brandl C, Crommer S, Bargou R, et al. Serial Killing of Tumor Cells by Cytotoxic T Cells Redirected With a CD19-/CD3-Bispecific Single-Chain Antibody Construct. *Int J Cancer* (2005) 115(1):98–104. doi: 10.1002/ijc.20908
56. Venugopal C, McFarlane NM, Nolte S, Manoranjan B, Singh SK. Processing of Primary Brain Tumor Tissue for Stem Cell Assays and Flow Sorting. *J Vis Exp* (2012) 67:4111. doi: 10.3791/4111
57. Lobo NC, Gedye C, Apostoli AJ, Brown KR, Paterson J, Stickle N, et al. Efficient Generation of Patient-Matched Malignant and Normal Primary Cell Cultures From Clear Cell Renal Cell Carcinoma Patients: Clinically Relevant Models for Research and Personalized Medicine. *BMC Cancer* (2016) 16:485. doi: 10.1186/s12885-016-2539-z
58. Qazi M, Mann A, van Ommeren R, Venugopal C, McFarlane N, Vora P, et al. Generation of Murine Xenograft Models of Brain Tumors From Primary Human Tissue for *In Vivo* Analysis of the Brain Tumor-Initiating Cell. *Methods Mol Biol* (2014) 1210:37–49. doi: 10.1007/978-1-4939-1435-7_4
59. Bowman RL, Wang Q, Carro A, Verhaak RG, Squatrito M. GlioVis Data Portal for Visualization and Analysis of Brain Tumor Expression Datasets. *Neuro Oncol* (2017) 19(1):139–41. doi: 10.1093/neuonc/now247
60. Cancer Genome Atlas Research, N. Comprehensive Genomic Characterization Defines Human Glioblastoma Genes and Core Pathways. *Nature* (2008) 455(7216):1061–8. doi: 10.1038/nature07385
61. Li Z, Bao S, Wu Q, Wang H, Eyler C, Sathornsumetee S, et al. Hypoxia-Inducible Factors Regulate Tumorigenic Capacity of Glioma Stem Cells. *Cancer Cell* (2009) 15(6):501–13. doi: 10.1016/j.ccr.2009.03.018
62. Heddleston JM, Li Z, McLendon RE, Hjelmeland AB, Rich JN. The Hypoxic Microenvironment Maintains Glioblastoma Stem Cells and Promotes Reprogramming Towards a Cancer Stem Cell Phenotype. *Cell Cycle* (2009) 8(20):3274–84. doi: 10.4161/cc.8.20.9701
63. Shiheido H, Chen C, Hikida M, Watanabe T, Shimizu J. Modulation of the Human T Cell Response by a Novel non-Mitogenic Anti-CD3 Antibody. *PLoS One* (2014) 9(4):e94324. doi: 10.1371/journal.pone.0094324
64. Aldape K, Brindle KM, Chesler L, Chopra R, Gajjar A, Gilbert MR, et al. Challenges to Curing Primary Brain Tumours. *Nat Rev Clin Oncol* (2019) 16 (8):509–20. doi: 10.1038/s41571-019-0177-5
65. Patel AP, Tirosh I, Trombetta JJ, Shalek AK, Gillespie SM, Wakimoto H, et al. Single-Cell RNA-Seq Highlights Intratumoral Heterogeneity in Primary Glioblastoma. *Science* (2014) 344(6190):1396–401. doi: 10.1126/science.1254257
66. Bhandari V, Hoey C, Liu LY, Lalonde E, Ray J, Livingstone J, et al. Molecular Landmarks of Tumor Hypoxia Across Cancer Types. *Nat Genet* (2019) 51(2):308–18. doi: 10.1038/s41588-018-0318-2
67. Chokshi CR, Brakel BA, Tatari N, Savage N, Salim SK, Venugopal C, et al. Advances in Immunotherapy for Adult Glioblastoma. *Cancers (Basel)* (2021) 13(14):3400. doi: 10.3390/cancers13143400
68. Singh K, Hotchkiss KM, Mohan AA, Reedy JL, Sampson JH, Khasraw M, et al. For Whom the T Cells Troll? Bispecific T-Cell Engagers in Glioblastoma. *J Immunother Cancer* (2021) 9(11):e003679. doi: 10.1136/jitc-2021-003679
69. Jackson CM, Choi J, Lim M. Mechanisms of Immunotherapy Resistance: Lessons From Glioblastoma. *Nat Immunol* (2019) 20(9):1100–9. doi: 10.1038/s41590-019-0433-y
70. Klemm F, Maas RR, Bowman RL, Kornete M, Soukup K, Nassiri S, et al. Interrogation of the Microenvironmental Landscape in Brain Tumors Reveals Disease-Specific Alterations of Immune Cells. *Cell* (2020) 181(7):1643–60.e17.
71. Friebel E, Kapolou K, Unger S, Núñez NG, Utz S, Rushing EJ, et al. Single-Cell Mapping of Human Brain Cancer Reveals Tumor-Specific Instruction of Tissue-Invading Leukocytes. *Cell* (2020) 181(7):1626–42.e20.
72. Labrijn AF, Janmaat ML, Reichert JM, Parren PWHI. Bispecific Antibodies: A Mechanistic Review of the Pipeline. *Nat Rev Drug Discovery* (2019) 18(8):585–608. doi: 10.1038/s41573-019-0028-1
73. Choi BD, Yu X, Castano AP, Bouffard AA, Schmidts A, Larson RC, et al. CAR-T Cells Secreting BiTEs Circumvent Antigen Escape Without Detectable Toxicity. *Nat Biotechnol* (2019) 37(9):1049–58. doi: 10.1038/s41587-019-0192-1
74. Scott EM, Duffy MR, Freedman JD, Fisher KD, Seymour LW. Solid Tumor Immunotherapy With T Cell Engager-Armed Oncolytic Viruses. *Macromol Biosci* (2018) 18(1):1700187. doi: 10.1002/mabi.201700187
75. Fajardo CA, Guedan S, Rojas LA, Moreno R, Arias-Badia M, de Sostoa J, et al. Oncolytic Adenoviral Delivery of an EGFR-Targeting T-Cell Engager Improves Antitumor Efficacy. *Cancer Res* (2017) 77(8):2052–63. doi: 10.1158/0008-5472.CAN-16-1708
76. Lamers CH, Sleijfer S, Vulto AG, Kruit WH, Kliffen M, Debets R, et al. Treatment of Metastatic Renal Cell Carcinoma With Autologous T-Lymphocytes Genetically Retargeted Against Carbonic Anhydrase IX: First Clinical Experience. *J Clin Oncol* (2006) 24(13):e20–2. doi: 10.1200/JCO.2006.05.9964
77. van Oostenbrugge T, Mulders P. Targeted PET/CT Imaging for Clear Cell Renal Cell Carcinoma With Radiolabeled Antibodies: Recent Developments Using Girentuximab. *Curr Opin Urol* (2021) 31(3):249–54. doi: 10.1097/MOU.0000000000000872
78. Bleumer I, Knuth A, Oosterwijk E, Hofmann R, Varga Z, Lamers C, et al. A Phase II Trial of Chimeric Monoclonal Antibody G250 for Advanced Renal Cell Carcinoma Patients. *Br J Cancer* (2004) 90(5):985–90. doi: 10.1038/sj.bjc.6601617
79. Muselaers CH, Boers-Sonderen MJ, van Oostenbrugge TJ, Boerman OC, Desar IM, Stillebroer AB, et al. Phase 2 Study of Lutetium 177-Labeled Anti-Carbonic Anhydrase IX Monoclonal Antibody Girentuximab in Patients With Advanced Renal Cell Carcinoma. *Eur Urol* (2016) 69(5):767–70. doi: 10.1016/j.eururo.2015.11.033

Conflict of Interest: The authors declare that the research was conducted in the absence of any commercial or financial relationships that could be construed as a potential conflict of interest.

this article, or claim that may be made by its manufacturer, is not guaranteed or endorsed by the publisher.

frontiers | Frontiers in Immunology

MINI REVIEW
published: 07 July 2022
doi: 10.3389/fimmu.2022.923598

Cell Membrane-Derived Vesicle: A Novel Vehicle for Cancer Immunotherapy

Caili Xu, Dianwen Ju and Xuyao Zhang**

Department of Biological Medicines & Shanghai Engineering Research Center of Immunotherapeutics, School of Pharmacy, Fudan University, Shanghai, China

As nano-sized materials prepared by isolating, disrupting and extruding cell membranes, cellular vesicles are emerging as a novel vehicle for immunotherapeutic drugs to activate antitumor immunity. Cell membrane-derived vesicles inherit the surface characteristics and functional properties of parental cells, thus having superior biocompatibility, low immunogenicity and long circulation. Moreover, the potent antitumor effect of cellular vesicles can be achieved through surface modification, genetic engineering, hybridization, drug encapsulation, and exogenous stimulation. The capacity of cellular vesicles to combine drugs of different compositions and functions in physical space provides a promising vehicle for combinational immunotherapy of cancer. In this review, the latest advances in cellular vesicles as vehicles for combinational cancer immunotherapy are systematically summarized with focuses on manufacturing processes, cell sources, therapeutic strategies and applications, providing an insight into the potential and existing challenges of using cellular vesicles for cancer immunotherapy.

Keywords: cellular vesicle, drug delivery vehicle, cancer immunotherapy, combination therapy, membrane hybridization, drug encapsulation

OPEN ACCESS

Edited by:
Alessandra Zingoni, Sapienza University of Rome, Italy

Reviewed by:
Abhalaxmi Singh, University of Illinois at Chicago, United States

****Correspondence:***
Dianwen Ju
dianwenju@fudan.edu.cn
Xuyao Zhang
xuyaozhang@fudan.edu.cn

Specialty section:
This article was submitted to Cancer Immunity and Immunotherapy, a section of the journal Frontiers in Immunology

Received: *19 April 2022*
Accepted: *14 June 2022*
Published: *07 July 2022*

Citation:
Xu C, Ju D and Zhang X (2022) Cell Membrane-Derived Vesicle: A Novel Vehicle for Cancer Immunotherapy. Front. Immunol. 13:923598. doi: 10.3389/fimmu.2022.923598

INTRODUCTION

Immunotherapy brings great hope to cancer patients, but it also faces challenges such as low response rate, difficulty in eradication, and susceptibility to relapse. Combination therapy offers promising solutions to address these issues (1). The appropriate delivery system physically combines multiple drugs, providing an integrated solution to achieve tumor targeting, killing, and activation of immune systems simultaneously. The main problem with conventional drug delivery systems such as liposomes, polymer micelles, dendrimers and nanogels is their vulnerability to clearance by the reticuloendothelial system and other circulating immune cells, resulting in severe liver toxicity and inadequate enrichment in target sites (2). With this in mind, researchers focus on the study of biomimetic drug vehicles (3, 4). Cellular vesicle is an important area of interest within the field of biomimetic drug delivery vehicles. It mainly refers to plasma membrane structures extracted from parental cells under external intervention and prepared into nano-sized vesicles for drug delivery (5).

In this review, we seek to track the recent advances in the application of cell membrane vesicles as drug vehicles for cancer immunotherapy. We introduce the manufacturing workflow of cellular vesicles and summarize their characteristics from various parental origins. Then, the currently

reported strategies of utilizing cellular vesicles to combat tumors are comprehensively reviewed. And finally, the comparion with other nanovehicles and challenges of cellular vesicles in cancer immunotherapy are discussed in depth with the aim of accelerating the clinical applications of this novel platform for cancer immunotherapy.

MANUFACTURING OF CELLULAR VESICLES FOR CANCER IMMUNOTHERAPY

Isolation

The typical process of isolating cellular vesicles consists of several steps (**Figure 1A**). Firstly, the parental cells are harvested and resuspended in a hypotonic buffer, rendering the cytoplasm swollen and susceptible to fragmentation by external forces (6, 7). Then, if the cytoplasmic components are to be removed, cells usually need to undergo approximately five freeze-thawing cycles and dounce homogenization to release intracellular proteins (6, 7). Next, cell membranes are separated from other cellular components by continuous high-speed or density gradient centrifugation. For example, the cells were subjected to centrifugation at 1000 g, 10000 g, and 100000 g to remove the nuclei, organelles, and other impurities, respectively (6). For density gradient centrifugation, cell membranes were prepared by centrifugation through discontinuous 30-40-55% sucrose (w/v) density gradient. At the interface of the different sucrose solutions, three lipid rings could be clearly detected, where the fraction between 30% and 40% sucrose retained the most plasma membrane proteins and was then collected and prepared for vesicles (7–9). Finally, they are sonicated for several minutes and repeatedly extruded through about three layers of polycarbonate membranes with stepwise decreasing pore size to obtain cellular vesicles (6, 10). Besides, to obtain vesicles that retain cytoplastic proteins and RNAs, cellular vesicles can be purified by OptiPrep density gradient centrifugation. Briefly, the cells underwent serial

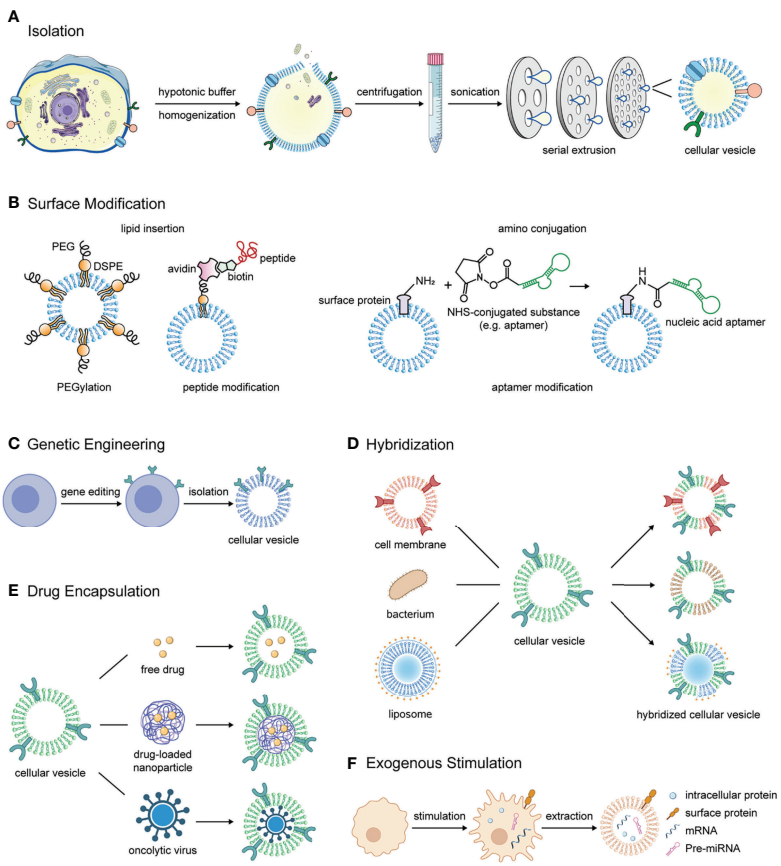

FIGURE 1 | The manufacturing process, modification methods, and application strategies of cellular vesicles in combinational immunotherapy of cancer. **(A)** The process of isolating cell membrane-derived vesicles from parental cells. **(B)** Methods for modifying substances such as polyethylene glycol, tumor targeting peptide and nucleic acid aptamer on the surface of cellular vesicles. **(C)** Cellular vesicles inherit antitumor proteins that the parental cells overexpress through gene editing. **(D)** Cellular vesicles are hybridized with different materials such as cell membranes from other sources, bacterial membranes and liposomes to obtain multiple components and functions for cancer immunotherapy. **(E)** Free drugs, drug-loaded nanoparticles or oncolytic viruses are encapsulated in cellular vesicles for delivery to the tumor lesions to activate antitumor immunity. **(F)** In response to exogenous stimulation, immune cells produce a variety of tumor growth inhibitors including surface markers, intracellular proteins, mRNA for pro-inflammatory cytokines, and certain miRNAs, which can be retained in cellular vesicles.

extrusion of the polycarbonate membranes, followed by centrifugation at 100000 g through 10% and 50% OptiPrep medium, and vesicles were harvested at the junction of the two layers (11–14). Aside from the above typical procedures, cellular vesicles can be induced by cytochalasin B or obtained by nitrogen cavitation (15–17).

Surface Modification

Surface modification of cellular vesicles is a vital strategy to improve their stability and tumor targeting ability. The modification methods include lipid insertion and amino conjugation. In terms of modification contents, they mainly include peptides, nucleic acid aptamers, and polyethylene glycol (PEG) (**Figure 1B**).

Attachment of tumor-targeting peptides is one of the most commonly used modification. One approach is to resort to lipid insertion and biotin-avidin interaction (18). Another approach is conjugation *via* N-hydroxysuccinimide (NHS) group. NHS esters are capable of covalent coupling with primary amines on proteins. Therefore, NHS-PEG-folic acid could be linked with amino groups of vesicle proteins for targeting tumors highly expressing folate receptors (19, 20). The modification of nucleic acid aptamers can also be performed by amino coupling to achieve specific targeting of tumors with high expressions of nucleolin (15). PEGylation is able to increase the dispersion stability and prolong the circulation time (21–23).

POTENTIAL OF CELLULAR VESICLES FROM DIVERSE PARENTAL CELLS IN CANCER IMMUNOTHERAPY

Tumor Cells

Tumor cell membrane-derived vesicles have some unique properties in cancer therapy including persistent existence, homotypic targeting, and antigen stimulation. Tumor cells can evade clearance by macrophages through expressing innate immune checkpoint CD47 to convey a negative signal of phagocytosis (24). This property was well preserved on its cellular vesicles and enabled a prolonged circulation *in vivo*. However, other immunosuppressive molecules expressed on tumor cells such as PD-L1, Galectin-9 and Siglec-15 may also be retained on cellular vesicles and inhibit the function of tumor-infiltrating lymphocytes (25–27).

Another important rationale for employing cancer cell vesicles as antitumor drug vehicles is homotypic targeting, which is probably through surface adhesion molecules such as N-cadherin and galectin-3 (28, 29). In a tumor self-targeting study, researchers prepared four kinds of cell membrane-encapsulated magnetic nanoparticles derived from different tumor cell lines. In the *in vivo* competition of tumor "homing", vesicles derived from heterologous tumor cells were notably weaker than that from homologous cells (28). This finding was also verified in patient-derived xenograft (PDX) models. The fluorescence intensity of tumor cell membrane-encapsulated nanoparticles at the tumor site was 3 and 10 times higher than that of erythrocyte membrane-coated nanoparticles and bare nanoparticles, respectively. For tumor cell vesicles derived from various patients, 2.5 to 10-fold higher tumor-targeting capacity was observed when the source of the donor membrane was consistent with the host compared to inconsistent cases (30).

Carrying tumor antigens is also a non-negligible advantage of tumor cell-derived cellular vesicles. Tumor cell vesicles inherit tumor-associated antigens and tumor-specific antigens and can therefore be equipped with immunological adjuvant for the preparation of cancer vaccine (21, 31–33).

Immune Cells

The advantages of selecting immune cells as the source of cellular vesicles for antitumor drug vehicles are ease of genetic modification, natural cargo of antitumor components, and the ability to evade immune surveillance, target tumor cells and present tumor antigens.

Abnormal nuclear structure in erythrocytes and platelets as well as excessively active DNA replication and mutation in tumor cells pose additional impediments to gene editing. As for the immune cells, genetic engineering technologies have been widely used in manufacturing immune cells with chimeric antigen receptors (CARs) (34–37). Coating IR780-loaded mesoporous silica nanoparticles with GPC3-specific CAR-T cell membranes enhanced tumor-targeting capability, with tumors weighing less than half the weight of normal T cell membrane-coated nanoparticle treatment group (38).

Another noteworthy point is that vesicles extruded from immune cells carry naturally expressed pro-inflammatory and antitumor substances (13). Programmed cell death-1 (PD-1) and transforming growth factor-beta receptor (TGF-βR) expressed on T cells are considered to inhibit the antitumor effects of $CD8^+$ T cells, however their retention on T-cell vesicles in turn neutralizes PD-L1 and TGF-β in the tumor microenvironment (TME). Meanwhile, antitumor substances expressed by T cells such as granzyme B and FasL can still induce apoptosis of tumor cells through their vesicles (13, 39). Studies on macrophages showed that cellular vesicles derived from M1-type macrophages contained high levels of IL-6 and tumor necrosis factor-alpha (TNF-α), which presented pro-inflammatory and tumoricidal effects *in vivo* (11, 14). Intravenous injection of M1 macrophage-derived vesicles alone was demonstrated to promote tumor-associated macrophage polarization toward M1 type and improve $CD8^+$ T cell infiltration in TME (14).

In addition, vesicles originating from certain immune cells can evade clearance, target tumor sites, recognize cancer cells and present tumor antigens. The use of monocyte- and macrophage-derived vesicles as nanovehicles emphasizes on their ability to evade clearance by the mononuclear phagocyte system and the expression of α4β1 that interacts with the vascular cell adhesion molecule-1 (VCAM-1) of metastatic tumors (8, 40, 41). It was reported that macrophage J774 membrane-encapsulated nanoparticles exhibited delayed liver accumulation, with integrity maintained for up to 40 min, which is 2-fold longer than that of naked nanoparticles. Also, 25% of adherent particles coated with macrophage membrane were not phagocytized by

Kupffer cells, significantly higher than uncoated nanoparticles (~ 9%). Drug delivery with macrophage vesicles increased the particle density at the tumor sites by approximately twofold (8). Besides, T-cell vesicles were shown to carry high levels of lymphocyte function-associated antigen-1 (LFA-1), which mediates the targeting of tumor sites *via* binding to intercellular adhesion molecule-1 (ICAM-1) highly expressed on tumor cells and inflamed endothelium (8, 39). Natural killer (NK) cell vesicles also have some degree of tumor homing ability due to aberrant expression of ligands for NK cell receptors (e.g., NKG2-D) in tumors (9). Neutrophil-derived vesicles have been shown to target tumor cells and inflammatory endothelium through three pairs of interactions including LFA-1/ICAM-1, β1 integrin/VCAM-1, and CD44/L-selectin (42). And DC vesicles could present tumor antigens to activate T cells (43, 44).

Erythrocytes and Platelets

The abundance in quantity and simplicity in composition have led to the extensive use of erythrocyte membranes as drug vehicles (45). Similar to tumor cells, erythrocytes also highly express CD47 to protect themselves from the attack of macrophages, thus prolong the circulation time (46–48).

Platelets play a significant role in tumor metastasis (49). In analogy to erythrocytes, platelets regulate self-homeostasis in the circulation by expressing phagocytic negative signal CD47 (50). Besides, it is worth noting that platelet-derived vesicles contain P-selectin protein. CD44 is highly expressed and acts as the primary P-selectin ligand on certain types of carcinoma cells. Therefore platelet-derived vesicles probably have some degree of tumor-targeting ability (51–53). However, it was also reported that platelet-derived vesicles rapidly bound to blood monocytes due to P-selectin-mediated adhesion, which would reduce their stability and half-life (54).

Other Types of Cells

In addition to the cells aforementioned, cellular vesicles obtained from fibroblasts and bacterial membrane for cancer treatment have also been reported. Fibroblast membrane-derived vesicles are superior in penetration into the TME, and bacterial membranes contribute to activation of the innate immune system (55–57).

STRATEGIES AND APPLICATIONS OF CELLULAR VESICLES IN COMBINATIONAL IMMUNOTHERAPY OF CANCER

Genetic Engineering of Cellular Vesicles

Gene editing allows cells to express proteins targeting tumor lesions or substances regulating immunity of TME, and the functionality can be perpetuated to their extruded vesicles (**Figure 1C**). For example, lentivirus carrying sequence of signal regulatory protein alpha (SIRPα), a ligand of CD47, and plasmid inserted with PD-1 sequence were transfected into different tumor cells. After being prepared into cellular vesicles separately, they were fabricated into fusion vesicles. The fusion vesicles were demonstrated to possess high levels of both SIRPα and PD-1 on the surface and have the ability to block innate and adaptive immune checkpoints simultaneously (10). To achieve targeted killing of tumor cells, CAR-T cells were extruded into cellular vesicles for hepatocellular carcinoma treatment (38). Besides, cellular vesicles were also engineered to overexpress antigens to stimulate T cell activation (58).

Hybridization of Cellular Vesicles From Different Type of Cells or With Other Materials

Hybridized cellular vesicles inherit function characteristics of both parental materials (**Figure 1D**). Fused or hybridized cellular vesicles can be produced by breaking up, mixing and then co-extruding through polycarbonate porous membranes. A large number of works have investigated the fusion of two or even more types of cell membrane vesicles to achieve multi-functionality (10, 14, 29, 59).

Bacteria are one of the most common immune stimulants, and Escherichia coli (*E. coli*) membrane vesicles have been successfully employed to transport tumor antigens and act as vaccines in the absence of adjuvants (60, 61). Researchers constructed fusion vesicles by hybridizing *E. coli* outer membrane vesicles and tumor cell vesicles in order to simultaneously augment innate and adaptive immunity for personalized tumor immunotherapy. The fusion vesicles could be effectively enriched in lymph nodes and inhibited the growth and lung metastasis of colorectal and breast tumors (57). In another similar study, tumor cell membrane and *E. coli* cytomembrane were co-extruded with nanoparticles to obtain hybrid vaccine. In 4T1 tumor model, the tumor-suppressive effect of fusion vesicles was significantly better than the simple combinational dosing of tumor vesicle-nanoparticles and *E. coli* vesicle-nanoparticles, with 60-day survival rates improved from 0 to 93% and 25%, respectively (62).

In addition, the advantages of liposomes can also be conferred to cellular vesicles by hybridization (9, 41). For instance, decoration of emtansine-carrying liposomes with macrophage membranes displayed a significant suppressing effect on lung metastasis of breast cancer (41).

Entrapping Drugs in the Hollow Cores of Cellular Vesicles

The hollow-core structure of cellular vesicles provides space for loading antitumor drugs and entrapping nanoparticles (**Figure 1E**). Encapsulation of free therapeutic agents can be achieved by co-incubation or remote loading (12, 63). And simple mixing of cellular vesicles and nanoparticles followed by co-extrusion is sufficient to prepare the desired cell membrane-coated nanoparticles (64). However, the surface charge interaction needs to be taken into account before wrapping the nanoparticles (65, 66). Studies of cellular vesicles loading chemotherapeutic drugs such as docetaxel, doxorubicin, camptothecin and oxaliplatin have been extensively reported (9, 18, 43, 48). These drugs can induce immunogenic cell death, and the combination with cellular vesicles confers an enhanced

immune response. One of the interesting attempts was the combination of mature DC vesicles with oxaliplatin-loaded nanoparticles. Chemotherapy led to immunogenic cell death, and the camouflaged mature dendrosomes initiated T cell responses by presenting tumor antigens, thus amplifying antitumor immune responses (43). Cellular vesicles were also widely applied in cancer photothermal therapy, such as membrane-camouflaged indocyanine green nanoparticles, black phosphorus quantum dot and melanin nanoparticles (20, 38, 67–69). Oncolytic viruses can also be enveloped in cellular vesicles aiming to evade antiviral neutralizing antibodies and enhance tumor-targeting ability (70).

Stimulating Production of Natural Antitumor Substances Before Vesicle Extraction

Stimulating immune cells to express endogenous antitumor substances and then extruding for vesicles is also an important strategy (**Figure 1F**). Vesicles isolated from activated or polarized immune cells were able to retain not only the membrane protein properties of the parental cells but also their intracellular proteins, mRNA and miRNA under appropriate preparation (11, 13, 14). It was reported that M1-type macrophages-derived nanovesicles contained high levels of mRNA of multiple pro-inflammatory cytokines and they could promote macrophage polarization toward M1 and infiltration of $CD8^+$ T cells into tumors (11, 14).

COMPARISON OF CELLULAR VESICLES WITH OTHER NANOVEHICLES

The advantages of non-biomimetic nanovehicles (e.g., liposomes, polymer micelles, dendrimer, nanogels, mesoporous silica, metallic nanoparticles) include high yield, diverse chemical modifications and precise regulation of physicochemical properties. For example, pH-sensitive dendrimers, temperature-responsive nanogels and magnetic nanoparticles enable specific drug release, size switching, sol-gel transition, and magnetic hyperthermia at tumor sites (71–74). In comparison with that, cellular vesicles preserved membrane characteristics and functions of parental cells, thus exhibiting better biocompatibility, low immunogenicity, negligible toxicity, long circulation, and natural targeting ability (75).

Exosome is also emerging as an important drug delivery platform for cancer immunotherapy. Compared to cell membrane vesicles, the difference between exosomal surface proteins and cytoplasmic membranes offer unique possibilities for exosome as drug vehicles. For instance, co-expression of peptides with proteins highly expressed on exosome surface (e.g., tetraspanin CD9/CD63/CD81, LAMP-2B and lactadherin) by genetic engineering allows for their enrichment on exosomes (76–81). Anchoring drugs to the exosomal marker *via* a medium such as CP05 peptide-mediated CD63 linkage simplifies drug loading approaches (82). However, for cancer therapy, exosomes are mostly administered at doses of 100-600 μg exosomal proteins per mouse, which implies consumption of approximately 1 L cell supernatant, severely hindering the application of exosomes as drug vehicles (83, 84). Cell membrane vesicles and exosomes share most of the characteristics of biomimetic nanovehicles, yet the former has superiority in terms of yield, production stability, and size homogeneity (11, 12). Cell membrane vesicles are administered at doses similar to exosomes, but with yields up to 30-300 μg vesicle proteins/10^7 cells (12, 17, 41).

FUTURE PERSPECTIVES

Through genetic modifications, membrane hybridization, drug encapsulation and exogenous stimulation, cellular vesicles were engineered to provide ideal vehicles for cancer immunotherapy drugs, including not only surface proteins but also internal nanoparticles, proteins, nucleic acids, and small-molecule drugs (**Table 1**).

TABLE 1 | Applications of cellular vesicles in cancer immunotherapy.

Strategies	Intervention	Parental cell	Mechanisms	Tumor models	References
Genetic engineering	CAR-T cell vesicle-coated nanoparticle	T cell	GPC3-specific CAR-T membrane vesicles were used to wrap IR780-loaded mesoporous silica nanoparticles for tumor targeting and photothermal therapy.	Xenograft model of human liver cancer.	(38)
	SIRPα and PD-1	Tumor cell	Tumor cells were programmed to overexpress SIRPα and PD-1 and then extracted for cellular vesicles to simultaneously block innate and adaptive immune checkpoints *in vivo*.	Breast cancer and melanoma models. Recurrence and metastasis model of breast cancer.	(10)
Membrane hybridizaiton	Various cell membranes	Two types of tumor cells; Macrophage, platelet and tumor cell	Hybridization of two or more types of cellular vesicles from tumor cells, erythrocytes, platelets and immune cells to achieve the multiple functions of escaping clearance, targeting tumor leison and activating antitumor immunity.	Primary, recurrence and metastasis tumor model of breast cancer and melanoma.	(10, 14)
		Tumor cell and bacterium		Breast and colon cancer models.	(56, 62)

(Continued)

TABLE 1 | Continued

Strategies	Intervention	Parental cell	Mechanisms	Tumor models	References
	Cell membrane and bacterial membrane		Tumor cell vesicles were fused with *E. coli* membrane vesicles to stimulate dendritic cell maturation and T cell activation for personalized cancer vaccines and immunotherapy.	Lung metastasis model of breast cancer.	
	Cell membrane and drug-loaded liposome	Macrophage; Natural killer cell	Liposomes carrying antitumor drugs (emtansine or doxorubicin) were hybridized with macrophage or NK cell vesicles for targeted cancer therapy through interactions of α4β1/VCAM-1 and NKG2-D and its ligands, respectively.	Lung metastasis model of breast cancer. Xenograft tumor model of human cancer cells.	(9, 41)
Drug encapsulation	DC vesicles, oxaliplatin-loaded nanoparticles and αPD-L1	Dendritic cell	Oxaliplatin encapsulated in cellular vesicles resulted in immunogenic cell death, followed by DC vesicle presentation of tumor antigens to initiate T-cell responses. They also displayed synergistic antitumor effect when combined with anti-PD-L1 therapy.	Mouse model of colon cancer.	(43)
	Erythrocyte vesicles and oncolytic virus	Erythrocyte	Oncolytic viruses were encapsulated into bioengineered cell vesicles to evade antiviral neutralizing antibodies, reduce systemic toxicity and enhance targeting delivery.	Human liver cancer xenograft tumor model.	(70)
	T cell vesicle-coated nanoparticle	T cell	T cell vesicles retained LFA-1, PD-1, TGF-βR and FasL. They actively targeted tumor tissues through LFA-1/ICAM-1 interaction, rescued antitumor effects of CD8+ T cells by blocking PD-1 and TGF-β, and directly induced apoptosis of tumor cells via Fas/FasL axis.	Subcutaneous tumor models of melanoma and lung cancer. Lung metastasis model of melanoma.	(39)
	Neutrophil vesicle-coated drug-loaded nanoparticle	Neutrophil	Carfilzomib-loaded nanoparticles were encapsulated in neutrophil-derived vesicles. Neutrophil vesicles targeted circulating tumor cells and premetastatic lesion through three pairs of interactions including LFA-1/ICAM-1, β1 integrin/VCAM-1, and CD44/L-selectin.	Lung metastasis and premetastatic mouse model of breast cancer.	(42)
	Monocyte vesicle-coated drug-loaded nanoparticle	Monocyte	Doxorubicin-loaded PLGA nanoparticles were coated with monocyte-derived vesicles to achieve tumor targeting through the interaction of α4β1 integrin with VCAM-1.	Human breast cancer xenograft model.	(40)
Exogenous stimulation	Granzyme B, PD-1 and TGF-β receptor	T cell	Cellular vesicles derived from activated T cells contained abundant granzyme B, PD-1 and TGF-β receptors and could exert tumoricidal effect as well as prevent T cell exhaustion.	Mouse model of lung cancer.	(13)
	mRNAs of pro-inflammatory cytokines and αPD-L1	Macrophage	Vesicles extruded from M1 macrophages carried high levels of mRNA of pro-inflammatory cytokines such as IL-6 and TNF-α. They could promote the polarization of macrophages toward M1 type and enhance antitumor efficacy of anti-PD-L1 therapy.	Mouse model of colon cancer. Recurrence and metastasis model of breast cancer and melanoma.	(11, 14)

Cellular vesicles hold great therapeutic promise as drug vehicles for combinational cancer immunotherapy, but translating these concepts into practical treatment approaches has proven challenging. Firstly, a key consideration of choosing cellular vesicles as a biomimetic cancer immunotherapy drug carrier is the low immunogenicity, but this also puts forward a requirement that donor cells have to be highly compatible with the recipient to avoid host rejection response. In the meantime, cellular vesicles homing to tumor lesions rely on homotypic recognition and targeting of tumor cells (28). The requirement for autologous cells, especially autologous tumor cells, limits their transformation to clinical applications. Currently, there are only two clinical trials using tumor cell membrane-derived vesicles for the treatment of malignant pleural effusion (NCT01854866 and NCT02657460) (85). Secondly, the hydrodynamic diameter of proteins is usually around 10 nm, while the diameter of the prepared cellular vesicles is approximately 100 to 200 nm. Therefore, the protein density and topology may need to be considered when overexpressing proteins of interest on the vesicle surface to preserve their biological activity as much as possible. Thirdly, when preparing multifunctional cellular vesicles by hybridization, it was noted that the ratio of two different membranes would affect the function of hybridized vesicles (69). In the case of mixed erythrocyte and tumor cell membrane-derived vesicles, an increase in the proportion of erythrocyte membranes displayed prolonged circulation, while an increase in the proportion of tumor cell membranes improved homotypic targeting ability (69). However, this was difficult to control as precisely as mixed liposome preparation and relied on empirical studies on most occasions. Besides, cellular vesicles are prone to spontaneous aggregation in external solutions. The extracted cell membranes can be stored at ultra-low temperature for a long time but not for extruded cellular vesicles. And there are many other problems to be solved in terms of manufacturing, storage, stability and efficiency.

In conclusion, cellular vesicles inherit the cell membrane and part of cytoplasmic components and functions of parental cells. They can serve as ideal drug vehicles for cancer combinational immunotherapy. Future research is particularly needed in the areas of engineering strategies, long-term stability and *in vivo* fate.

AUTHOR CONTRIBUTIONS

CX drafted the paper and prepared the table and figures. XZ and DJ conceived and proofread the manuscript. All authors contributed to the article and approved the submitted version.

FUNDING

This study was supported by Shanghai Sailing Program (21YF1401900), National Natural Science Foundation of China (82073752, 81773620, and 81803529), Scientific and Innovative Action Plan of Shanghai (20S11904700 and 20JC1411000).

REFERENCES

1. Colli LM, Machiela MJ, Zhang H, Myers TA, Jessop L, Delattre O, et al. Landscape of Combination Immunotherapy and Targeted Therapy to Improve Cancer Management. *Cancer Res* (2017) 77(13):3666–71. doi: 10.1158/0008-5472.Can-16-3338
2. Zhang YN, Poon W, Tavares AJ, McGilvray ID, Chan WCW. Nanoparticle-Liver Interactions: Cellular Uptake and Hepatobiliary Elimination. *J Control Release* (2016) 240:332–48. doi: 10.1016/j.jconrel.2016.01.020
3. Chen YX, Wei CX, Lyu YQ, Chen HZ, Jiang G, Gao XL. Biomimetic Drug-Delivery Systems for the Management of Brain Diseases. *Biomater Sci* (2020) 8(4):1073–88. doi: 10.1039/c9bm01395d
4. Wang H, Liu Y, He R, Xu D, Zang J, Weeranoppanant N, et al. Cell Membrane Biomimetic Nanoparticles for Inflammation and Cancer Targeting in Drug Delivery. *Biomater Sci* (2020) 8(2):552–68. doi: 10.1039/c9bm01392j
5. Thanuja MY, Anupama C, Ranganath SH. Bioengineered Cellular and Cell Membrane-Derived Vehicles for Actively Targeted Drug Delivery: So Near and Yet So Far. *Adv Drug Deliv Rev* (2018) 132:57–80. doi: 10.1016/j.addr.2018.06.012
6. Li C, Zhao Z, Luo Y, Ning T, Liu P, Chen Q, et al. Macrophage-Disguised Manganese Dioxide Nanoparticles for Neuroprotection by Reducing Oxidative Stress and Modulating Inflammatory Microenvironment in Acute Ischemic Stroke. *Adv Sci (Weinh)* (2021) 8(20):e2101526. doi: 10.1002/advs.202101526
7. Zhang L, Li R, Chen H, Wei J, Qian H, Su S, et al. Human Cytotoxic T-Lymphocyte Membrane-Camouflaged Nanoparticles Combined With Low-Dose Irradiation: A New Approach to Enhance Drug Targeting in Gastric Cancer. *Int J Nanomed* (2017) 12:2129–42. doi: 10.2147/ijn.S126016
8. Parodi A, Quattrocchi N, van de Ven AL, Chiappini C, Evangelopoulos M, Martinez JO, et al. Synthetic Nanoparticles Functionalized With Biomimetic Leukocyte Membranes Possess Cell-Like Functions. *Nat Nanotechnol* (2013) 8(1):61–8. doi: 10.1038/nnano.2012.212
9. Pitchaimani A, Nguyen TDT, Aryal S. Natural Killer Cell Membrane Infused Biomimetic Liposomes for Targeted Tumor Therapy. *Biomaterials* (2018) 160:124–37. doi: 10.1016/j.biomaterials.2018.01.018
10. Meng QF, Zhao Y, Dong C, Liu L, Pan Y, Lai J, et al. Genetically Programmable Fusion Cellular Vesicles for Cancer Immunotherapy. *Angew Chem Int Ed Engl* (2021) 60(50):26320–26. doi: 10.1002/anie.202108342
11. Choo YW, Kang M, Kim HY, Han J, Kang S, Lee JR, et al. M1 Macrophage-Derived Nanovesicles Potentiate the Anticancer Efficacy of Immune Checkpoint Inhibitors. *ACS Nano* (2018) 12(9):8977–93. doi: 10.1021/acsnano.8b02446
12. Jang SC, Kim OY, Yoon CM, Choi DS, Roh TY, Park J, et al. Bioinspired Exosome-Mimetic Nanovesicles for Targeted Delivery of Chemotherapeutics to Malignant Tumors. *ACS Nano* (2013) 7(9):7698–710. doi: 10.1021/nn402232g
13. Hong J, Kang M, Jung M, Lee YY, Cho Y, Kim C, et al. T-Cell-Derived Nanovesicles for Cancer Immunotherapy. *Adv Mater* (2021) 33(33):e2101110. doi: 10.1002/adma.202101110
14. Rao L, Wu L, Liu Z, Tian R, Yu G, Zhou Z, et al. Hybrid Cellular Membrane Nanovesicles Amplify Macrophage Immune Responses Against Cancer Recurrence and Metastasis. *Nat Commun* (2020) 11(1):4909. doi: 10.1038/s41467-020-18626-y
15. Peng LH, Zhang YH, Han LJ, Zhang CZ, Wu JH, Wang XR, et al. Cell Membrane Capsules for Encapsulation of Chemotherapeutic and Cancer Cell Targeting in Vivo. *ACS Appl Mater Interfaces* (2015) 7(33):18628–37. doi: 10.1021/acsami.5b05065
16. Gao J, Chu D, Wang Z. Cell Membrane-Formed Nanovesicles for Disease-Targeted Delivery. *J Control Release* (2016) 224:208–16. doi: 10.1016/j.jconrel.2016.01.024
17. Li R, He Y, Zhu Y, Jiang L, Zhang S, Qin J, et al. Route to Rheumatoid Arthritis by Macrophage-Derived Microvesicle-Coated Nanoparticles. *Nano Lett* (2019) 19(1):124–34. doi: 10.1021/acs.nanolett.8b03439
18. Chai Z, Ran D, Lu L, Zhan C, Ruan H, Hu X, et al. Ligand-Modified Cell Membrane Enables the Targeted Delivery of Drug Nanocrystals to Glioma. *ACS Nano* (2019) 13(5):5591–601. doi: 10.1021/acsnano.9b00661
19. Mishra PR, Jain NK. Folate Conjugated Doxorubicin-Loaded Membrane Vesicles for Improved Cancer Therapy. *Drug Deliv* (2003) 10(4):277–82. doi: 10.1080/drd_10_4_277
20. Li X, Zhao X, Pardhi D, Wu Q, Zheng Y, Zhu H, et al. Folic Acid Modified Cell Membrane Capsules Encapsulating Doxorubicin and Indocyanine Green for Highly Effective Combinational Therapy. *Vivo Acta Biomater* (2018) 74:374–84. doi: 10.1016/j.actbio.2018.05.006
21. Ochyl LJ, Bazzill JD, Park C, Xu Y, Kuai R, Moon JJ. PEGylated Tumor Cell Membrane Vesicles as a New Vaccine Platform for Cancer Immunotherapy. *Biomaterials* (2018) 182:157–66. doi: 10.1016/j.biomaterials.2018.08.016
22. Kooijmans SAA, Fliervoet LAL, van der Meel R, Fens M, Heijnen HFG, van Bergen En Henegouwen PMP, et al. PEGylated and Targeted Extracellular Vesicles Display Enhanced Cell Specificity and Circulation Time. *J Control Release* (2016) 224:77–85. doi: 10.1016/j.jconrel.2016.01.009
23. Suk JS, Xu Q, Kim N, Hanes J, Ensign LM. PEGylation as a Strategy for Improving Nanoparticle-Based Drug and Gene Delivery. *Adv Drug Deliv Rev* (2016) 99(Pt A):28–51. doi: 10.1016/j.addr.2015.09.012
24. Zhang W, Huang Q, Xiao W, Zhao Y, Pi J, Xu H, et al. Advances in Anti-Tumor Treatments Targeting the CD47/Sirpα Axis. *Front Immunol* (2020) 11:18. doi: 10.3389/fimmu.2020.00018
25. Cervantes-Villagrana RD, Albores-García D, Cervantes-Villagrana AR, García-Acevez SJ. Tumor-Induced Neurogenesis and Immune Evasion as Targets of Innovative Anti-Cancer Therapies. *Signal Transd Target Ther* (2020) 5(1):99. doi: 10.1038/s41392-020-0205-z
26. Yang R, Sun L, Li CF, Wang YH, Yao J, Li H, et al. Galectin-9 Interacts With PD-1 and TIM-3 to Regulate T Cell Death and Is a Target for Cancer Immunotherapy. *Nat Commun* (2021) 12(1):832. doi: 10.1038/s41467-021-21099-2
27. Sun J, Lu Q, Sanmamed MF, Wang J. Siglec-15 as an Emerging Target for Next-Generation Cancer Immunotherapy. *Clin Cancer Res* (2021) 27(3):680–88. doi: 10.1158/1078-0432.Ccr-19-2925
28. Zhu JY, Zheng DW, Zhang MK, Yu WY, Qiu WX, Hu JJ, et al. Preferential Cancer Cell Self-Recognition and Tumor Self-Targeting by Coating Nanoparticles With Homotypic Cancer Cell Membranes. *Nano Lett* (2016) 16(9):5895–901. doi: 10.1021/acs.nanolett.6b02786
29. Song J, Jung H, You G, Mok H. Cancer-Cell-Derived Hybrid Vesicles From MCF-7 and HeLa Cells for Dual-Homotypic Targeting of Anticancer Drugs. *Macromol Biosci* (2021) 21(7):e2100067. doi: 10.1002/mabi.202100067
30. Rao L, Yu G-T, Meng Q-F, Bu L-L, Tian R, Lin L-S, et al. Cancer Cell Membrane-Coated Nanoparticles for Personalized Therapy in Patient-Derived Xenograft Models. *Adv Funct Mater* (2019) 29(51):1905671. doi: 10.1002/adfm.201905671
31. Fang RH, Hu CM, Luk BT, Gao W, Copp JA, Tai Y, et al. Cancer Cell Membrane-Coated Nanoparticles for Anticancer Vaccination and Drug Delivery. *Nano Lett* (2014) 14(4):2181–8. doi: 10.1021/nl500618u
32. Yang R, Xu J, Xu L, Sun X, Chen Q, Zhao Y, et al. Cancer Cell Membrane-Coated Adjuvant Nanoparticles With Mannose Modification for Effective Anticancer Vaccination. *ACS Nano* (2018) 12(6):5121–29. doi: 10.1021/acsnano.7b09041

33. Liu B, Yang Y, Chao Y, Xiao Z, Xu J, Wang C, et al. Equipping Cancer Cell Membrane Vesicles With Functional DNA as a Targeted Vaccine for Cancer Immunotherapy. *Nano Lett* (2021) 21(22):9410-18. doi: 10.1021/acs.nanolett.1c02582
34. Bailey SR, Maus MV. Gene Editing for Immune Cell Therapies. *Nat Biotechnol* (2019) 37(12):1425–34. doi: 10.1038/s41587-019-0137-8
35. Sloas C, Gill S, Klichinsky M. Engineered CAR-Macrophages as Adoptive Immunotherapies for Solid Tumors. *Front Immunol* (2021) 12:783305. doi: 10.3389/fimmu.2021.783305
36. Schmidt P, Raftery MJ, Pecher G. Engineering NK Cells for CAR Therapy-Recent Advances in Gene Transfer Methodology. *Front Immunol* (2020) 11:611163. doi: 10.3389/fimmu.2020.611163
37. Xu C, Ju D, Zhang X. Chimeric Antigen Receptor T-Cell Therapy: Challenges and Opportunities in Lung Cancer. *Antib Ther* (2022) 5(1):73–83. doi: 10.1093/abt/tbac006
38. Ma W, Zhu D, Li J, Chen X, Xie W, Jiang X, et al. Coating Biomimetic Nanoparticles With Chimeric Antigen Receptor T Cell-Membrane Provides High Specificity for Hepatocellular Carcinoma Photothermal Therapy Treatment. *Theranostics* (2020) 10(3):1281–95. doi: 10.7150/thno.40291
39. Kang M, Hong J, Jung M, Kwon SP, Song SY, Kim HY, et al. T-Cell-Mimicking Nanoparticles for Cancer Immunotherapy. *Adv Mater* (2020) 32 (39):e2003368. doi: 10.1002/adma.202003368
40. Krishnamurthy S, Gnanasammandhan MK, Xie C, Huang K, Cui MY, Chan JM. Monocyte Cell Membrane-Derived Nanoghosts for Targeted Cancer Therapy. *Nanoscale* (2016) 8(13):6981–5. doi: 10.1039/c5nr07588b
41. Cao H, Dan Z, He X, Zhang Z, Yu H, Yin Q, et al. Liposomes Coated With Isolated Macrophage Membrane Can Target Lung Metastasis of Breast Cancer. *ACS Nano* (2016) 10(8):7738–48. doi: 10.1021/acsnano.6b03148
42. Kang T, Zhu Q, Wei D, Feng J, Yao J, Jiang T, et al. Nanoparticles Coated With Neutrophil Membranes Can Effectively Treat Cancer Metastasis. *ACS Nano* (2017) 11(2):1397–411. doi: 10.1021/acsnano.6b06477
43. Chen X, Ling X, Xia J, Zhu Y, Zhang L, He Y, et al. Mature Dendritic Cell-Derived Dendrosomes Swallow Oxaliplatin-Loaded Nanoparticles to Boost Immunogenic Chemotherapy and Tumor Antigen-Specific Immunotherapy. *Bioactive Mater* (2021) 15:15–28. doi: 10.1016/j.bioactmat.2021.12.020
44. Ochyl LJ, Moon JJ. Dendritic Cell Membrane Vesicles for Activation and Maintenance of Antigen-Specific T Cells. *Adv Healthc Mater* (2019) 8(4): e1801091. doi: 10.1002/adhm.201801091
45. Ihler GM, Glew RH, Schnure FW. Enzyme Loading of Erythrocytes. *Proc Natl Acad Sci USA* (1973) 70(9):2663–6. doi: 10.1073/pnas.70.9.2663
46. Lutz HU. Innate Immune and non-Immune Mediators of Erythrocyte Clearance. *Cell Mol Biol (Noisy-le-grand)* (2004) 50(2):107–16.
47. Zhang X, Fan J, Ju D. Insights Into CD47/Sirpα Axis-Targeting Tumor Immunotherapy. *Antib Ther* (2018) 1(2):37–42. doi: 10.1093/abt/tby006
48. Malhotra S, Dumoga S, Sirohi P, Singh N. Red Blood Cells-Derived Vesicles for Delivery of Lipophilic Drug Camptothecin. *ACS Appl Mater Interfaces* (2019) 11(25):22141–51. doi: 10.1021/acsami.9b04827
49. Schlesinger M. Role of Platelets and Platelet Receptors in Cancer Metastasis. *J Hematol Oncol* (2018) 11(1):125. doi: 10.1186/s13045-018-0669-2
50. Olsson M, Bruhns P, Frazier WA, Ravetch JV, Oldenborg PA. Platelet Homeostasis Is Regulated by Platelet Expression of CD47 Under Normal Conditions and in Passive Immune Thrombocytopenia. *Blood* (2005) 105 (9):3577–82. doi: 10.1182/blood-2004-08-2980
51. Hanley WD, Napier SL, Burdick MM, Schnaar RL, Sackstein R, Konstantopoulos K. Variant Isoforms of CD44 are P- and L-Selectin Ligands on Colon Carcinoma Cells. *FASEB J* (2006) 20(2):337–9. doi: 10.1096/fj.05-4574fje
52. Alves CS, Burdick MM, Thomas SN, Pawar P, Konstantopoulos K. The Dual Role of CD44 as a Functional P-Selectin Ligand and Fibrin Receptor in Colon Carcinoma Cell Adhesion. *Am J Physiol Cell Physiol* (2008) 294(4):C907–16. doi: 10.1152/ajpcell.00463.2007
53. Iannacone M. Platelet-Mediated Modulation of Adaptive Immunity. *Semin Immunol* (2016) 28(6):555–60. doi: 10.1016/j.smim.2016.10.008
54. Chimen M, Evryviadou A, Box CL, Harrison MJ, Hazeldine J, Dib LH, et al. Appropriation of Gpibα From Platelet-Derived Extracellular Vesicles Supports Monocyte Recruitment in Systemic Inflammation. *Haematologica* (2020) 105(5):1248–61. doi: 10.3324/haematol.2018.215145
55. Li J, Zhen X, Lyu Y, Jiang Y, Huang J, Pu K. Cell Membrane Coated Semiconducting Polymer Nanoparticles for Enhanced Multimodal Cancer Phototheranostics. *ACS Nano* (2018) 12(8):8520–30. doi: 10.1021/acsnano.8b04066
56. Kuerban K, Gao X, Zhang H, Liu J, Dong M, Wu L, et al. Doxorubicin-Loaded Bacterial Outer-Membrane Vesicles Exert Enhanced Anti-Tumor Efficacy in Non-Small-Cell Lung Cancer. *Acta Pharm Sin B* (2020) 10(8):1534–48. doi: 10.1016/j.apsb.2020.02.002
57. Zou MZ, Li ZH, Bai XF, Liu CJ, Zhang XZ. Hybrid Vesicles Based on Autologous Tumor Cell Membrane and Bacterial Outer Membrane To Enhance Innate Immune Response and Personalized Tumor Immunotherapy. *Nano Lett* (2021) 21(20):8609–18. doi: 10.1021/acs.nanolett.1c02482
58. Ukrainskaya V, Rubtsov Y, Pershin D, Podoplelova N, Terekhov S, Yaroshevich I, et al. Antigen-Specific Stimulation and Expansion of CAR-T Cells Using Membrane Vesicles as Target Cell Surrogates. *Small* (2021) 17 (45):e2102643. doi: 10.1002/smll.202102643
59. Dehaini D, Wei X, Fang RH, Masson S, Angsantikul P, Luk BT, et al. Erythrocyte-Platelet Hybrid Membrane Coating for Enhanced Nanoparticle Functionalization. *Adv Mater* (2017) 29(16):1606209. doi: 10.1002/adma.201606209
60. Chen DJ, Osterrieder N, Metzger SM, Buckles E, Doody AM, DeLisa MP, et al. Delivery of Foreign Antigens by Engineered Outer Membrane Vesicle Vaccines. *Proc Natl Acad Sci USA* (2010) 107(7):3099–104. doi: 10.1073/pnas.0805532107
61. Fessler J, Matson V, Gajewski TF. Exploring the Emerging Role of the Microbiome in Cancer Immunotherapy. *J Immunother Cancer* (2019) 7 (1):108. doi: 10.1186/s40425-019-0574-4
62. Chen L, Qin H, Zhao R, Zhao X, Lin L, Chen Y, et al. Bacterial Cytoplasmic Membranes Synergistically Enhance the Antitumor Activity of Autologous Cancer Vaccines. *Sci Transl Med* (2021) 13(601):eabc2816. doi: 10.1126/scitranslmed.abc2816
63. Zhang X, Angsantikul P, Ying M, Zhuang J, Zhang Q, Wei X, et al. Remote Loading of Small-Molecule Therapeutics Into Cholesterol-Enriched Cell-Membrane-Derived Vesicles. *Angew Chem Int Ed Engl* (2017) 56 (45):14075–79. doi: 10.1002/anie.201707598
64. Luk BT, Hu CM, Fang RH, Dehaini D, Carpenter C, Gao W, et al. Interfacial Interactions Between Natural RBC Membranes and Synthetic Polymeric Nanoparticles. *Nanoscale* (2014) 6(5):2730–7. doi: 10.1039/c3nr06371b
65. Hu CM, Fang RH, Luk BT, Chen KN, Carpenter C, Gao W, et al. 'Marker-Of-Self' Functionalization of Nanoscale Particles Through a Top-Down Cellular Membrane Coating Approach. *Nanoscale* (2013) 5(7):2664–8. doi: 10.1039/c3nr00015j
66. Xia Q, Zhang Y, Li Z, Hou X, Feng N. Red Blood Cell Membrane-Camouflaged Nanoparticles: A Novel Drug Delivery System for Antitumor Application. *Acta Pharm Sin B* (2019) 9(4):675–89. doi: 10.1016/j.apsb.2019.01.011
67. Han Y, Pan H, Li W, Chen Z, Ma A, Yin T, et al. T Cell Membrane Mimicking Nanoparticles With Bioorthogonal Targeting and Immune Recognition for Enhanced Photothermal Therapy. *Adv Sci (Weinh)* (2019) 6(15):1900251. doi: 10.1002/advs.201900251
68. Liang X, Ye X, Wang C, Xing C, Miao Q, Xie Z, et al. Photothermal Cancer Immunotherapy by Erythrocyte Membrane-Coated Black Phosphorus Formulation. *J Control Release* (2019) 296:150–61. doi: 10.1016/j.jconrel.2019.01.027
69. Jiang Q, Liu Y, Guo R, Yao X, Sung S, Pang Z, et al. Erythrocyte-Cancer Hybrid Membrane-Camouflaged Melanin Nanoparticles for Enhancing Photothermal Therapy Efficacy in Tumors. *Biomaterials* (2019) 192:292–308. doi: 10.1016/j.biomaterials.2018.11.021
70. Lv P, Liu X, Chen X, Liu C, Zhang Y, Chu C, et al. Genetically Engineered Cell Membrane Nanovesicles for Oncolytic Adenovirus Delivery: A Versatile Platform for Cancer Virotherapy. *Nano Lett* (2019) 19(5):2993–3001. doi: 10.1021/acs.nanolett.9b00145
71. Xia C, Yin S, Xu S, Ran G, Deng M, Mei L, et al. Low Molecular Weight Heparin-Coated and Dendrimer-Based Core-Shell Nanoplatform With Enhanced Immune Activation and Multiple Anti-Metastatic Effects for Melanoma Treatment. *Theranostics* (2019) 9(2):337–54. doi: 10.7150/thno.29026
72. Li HJ, Du JZ, Liu J, Du XJ, Shen S, Zhu YH, et al. Smart Superstructures With Ultrahigh pH-Sensitivity for Targeting Acidic Tumor Microenvironment: Instantaneous Size Switching and Improved Tumor Penetration. *ACS Nano* (2016) 10(7):6753–61. doi: 10.1021/acsnano.6b02326

73. Zhou X, He X, Shi K, Yuan L, Yang Y, Liu Q, et al. Injectable Thermosensitive Hydrogel Containing Erlotinib-Loaded Hollow Mesoporous Silica Nanoparticles as a Localized Drug Delivery System for NSCLC Therapy. *Adv Sci (Weinh)* (2020) 7(23):2001442. doi: 10.1002/advs.202001442
74. Singh A, Jain S, Sahoo SK. Magnetic Nanoparticles for Amalgamation of Magnetic Hyperthermia and Chemotherapy: An Approach Towards Enhanced Attenuation of Tumor. *Mater Sci Eng C Mater Biol Appl* (2020) 110:110695. doi: 10.1016/j.msec.2020.110695
75. Xu CH, Ye PJ, Zhou YC, He DX, Wei H, Yu CY. Cell Membrane-Camouflaged Nanoparticles as Drug Carriers for Cancer Therapy. *Acta Biomater* (2020) 105:1–14. doi: 10.1016/j.actbio.2020.01.036
76. Liang G, Kan S, Zhu Y, Feng S, Feng W, Gao S. Engineered Exosome-Mediated Delivery of Functionally Active miR-26a and Its Enhanced Suppression Effect in HepG2 Cells. *Int J Nanomed* (2018) 13:585–99. doi: 10.2147/IJN.S154458
77. Kanuma T, Yamamoto T, Kobiyama K, Moriishi E, Masuta Y, Kusakabe T, et al. CD63-Mediated Antigen Delivery Into Extracellular Vesicles *via* DNA Vaccination Results in Robust CD8(+) T Cell Responses. *J Immunol* (2017) 198(12):4707–15. doi: 10.4049/jimmunol.1600731
78. Dooley K, McConnell RE, Xu K, Lewis ND, Haupt S, Youniss MR, et al. A Versatile Platform for Generating Engineered Extracellular Vesicles With Defined Therapeutic Properties. *Mol Ther* (2021) 29(5):1729–43. doi: 10.1016/j.ymthe.2021.01.020
79. Tian Y, Li S, Song J, Ji T, Zhu M, Anderson GJ, et al. A Doxorubicin Delivery Platform Using Engineered Natural Membrane Vesicle Exosomes for Targeted Tumor Therapy. *Biomaterials* (2014) 35(7):2383–90. doi: 10.1016/j.biomaterials.2013.11.083
80. Limoni SK, Moghadam MF, Moazzeni SM, Gomari H, Salimi F. Engineered Exosomes for Targeted Transfer of siRNA to HER2 Positive Breast Cancer Cells. *Appl Biochem Biotechnol* (2019) 187(1):352–64. doi: 10.1007/s12010-018-2813-4
81. Rountree RB, Mandl SJ, Nachtwey JM, Dalpozzo K, Do L, Lombardo JR, et al. Exosome Targeting of Tumor Antigens Expressed by Cancer Vaccines Can Improve Antigen Immunogenicity and Therapeutic Efficacy. *Cancer Res* (2011) 71(15):5235–44. doi: 10.1158/0008-5472.Can-10-4076
82. Gao X, Ran N, Dong X, Zuo B, Yang R, Zhou Q, et al. Anchor Peptide Captures, Targets, and Loads Exosomes of Diverse Origins for Diagnostics and Therapy. *Sci Transl Med* (2018) 10(444):eaat0195. doi: 10.1126/scitranslmed.aat0195
83. Gupta D, Zickler AM, El Andaloussi S. Dosing Extracellular Vesicles. *Adv Drug Deliv Rev* (2021) 178:113961. doi: 10.1016/j.addr.2021.113961
84. Kimiz-Gebologlu I, Oncel SS. Exosomes: Large-Scale Production, Isolation, Drug Loading Efficiency, and Biodistribution and Uptake. *J Control Release* (2022) 347:533–43. doi: 10.1016/j.jconrel.2022.05.027
85. Patel RB, Ye M, Carlson PM, Jaquish A, Zangl L, Ma B, et al. Development of an *In Situ* Cancer Vaccine *via* Combinational Radiation and Bacterial-Membrane-Coated Nanoparticles. *Adv Mater* (2019) 31(43):e1902626. doi: 10.1002/adma.201902626

Conflict of Interest: The authors declare that the research was conducted in the absence of any commercial or financial relationships that could be construed as a potential conflict of interest.

frontiers | Frontiers in Immunology

ORIGINAL RESEARCH
published: 08 July 2022
doi: 10.3389/fimmu.2022.927635

Development and Verification of a Combined Immune- and Metabolism-Related Prognostic Signature for Hepatocellular Carcinoma

Yuanyuan Guo[1,2], *Jing Yang*[1,2], *Hua Gao*[3], *Xin Tian*[1,2*], *Xiaojian Zhang*[1,2*] *and Quancheng Kan*[1,2*]

[1] Department of Pharmacy, The First Affiliated Hospital of Zhengzhou University, Zhengzhou, China, [2] Henan Key Laboratory of Precision Clinical Pharmacy, Zhengzhou University, Zhengzhou, China, [3] Department of Radiotherapy, The First Affiliated Hospital of Zhengzhou University, Zhengzhou, China

OPEN ACCESS

Edited by:
Xuyao Zhang,
Fudan University, China

Reviewed by:
Jia Xiangqian,
Heilongjiang University, China
Qiuju Han,
Shanghai Jiao Tong University, China

***Correspondence:**
Xin Tian
tianx@zzu.edu.cn
Xiaojian Zhang
zhxj0524@hotmail.com
Quancheng Kan
kanqc@zzu.edu.cn

Specialty section:
This article was submitted to Cancer Immunity and Immunotherapy, a section of the journal Frontiers in Immunology

Received: 24 April 2022
Accepted: 10 June 2022
Published: 08 July 2022

Citation:
Guo Y, Yang J, Gao H, Tian X, Zhang X and Kan Q (2022) Development and Verification of a Combined Immune- and Metabolism-Related Prognostic Signature for Hepatocellular Carcinoma. Front. Immunol. 13:927635. doi: 10.3389/fimmu.2022.927635

Immune escape and metabolic reprogramming are becoming important characteristics of tumor biology, which play critical roles in tumor initiation and progression. However, the integrative analysis of immune and metabolic characteristics for the tumor microenvironment in hepatocellular carcinoma (HCC) remains unclear. Herein, by univariate and least absolute shrinkage and selection operator (LASSO) Cox regression analyses, a prognostic signature associated with tumor microenvironment was established based on five immune- and metabolism-related genes (IMRGs), which was fully verified and evaluated in both internal and external cohorts. The C-index was superior to previously published HCC signatures, indicating the robustness and reliability of IMRGs prognostic signature. A nomogram was built based on IMRGs prognostic signature and various clinical parameters, such as age and T stage. The AUCs of nomogram at 1-, 3-, and 5-year (AUC = 0.829, 0.749, 0.749) were slightly better than that of IMRGs signature (AUC = 0.809, 0.734, 0.711). The relationship of risk score (RS) with immune checkpoint expressions, immunophenoscore (IPS), as well as microsatellite instability (MSI) together accurately predicted the treatment efficacy. Collectively, the IMRGs signature might have the potential to better predict prognostic risk, evaluate immunotherapy efficacy, and help personalize immunotherapy for HCC patients.

Keywords: immune, metabolism, prognosis, hepatocellular carcinoma, TME

INTRODUCTION

Hepatocellular carcinoma (HCC) is one of the most frequent malignant tumors globally with a high morbidity and mortality rate (1), and the 5-year survival rate remains at just 14.1% (2). Currently, rapid progress has been made in immune checkpoint blockade strategies (3–6) (e.g., anti-PD-1, anti-PD-L1/PD-L2, and anti-CTLA-4). Nevertheless, only a small proportion of HCC patients respond positively to and

Abbreviations: HCC, hepatocellular carcinoma; TME, tumor microenvironment; MSI, microsatellite instability; IPS, immunophenoscore; AUC, area under the curve; NFM, non-negative matrix factorization; GSEA, gene set enrichment analysis; ROC, receiver operating characteristic.

benefit from these therapies (7). The main reason for differences in therapeutic efficacy might be due to the high heterogeneity of the immune microenvironment (8, 9). Consequently, the development and verification of a prognostic signature of the tumor microenvironment (TME) for HCC patients to aid immunotherapy remains of critical importance.

Immune escape (10) and metabolic reprogramming (11) are becoming important characteristics of tumor biology and play key roles in tumor initiation and progression. It is well-known that there is a strong connection between the metabolic system that provides energy and the immune system that defends against pathogens. In addition to defending against pathogens, the immune system is closely related to metabolism (12). Meanwhile, metabolic changes in the tumor microenvironment can suppress the immune system and promote tumor growth (13). Based on solely immune- or metabolism-related genes, prognosis prediction signatures were constructed. For example, Dai et al (14). found that immune-related genes signature could predict outcomes and the effectiveness of immunotherapy in HCC. Yang et al. (15) characterized the molecular features of HCC using the gene expression profile of metabolic genes. He et al. (16) constructed a metabolism-associated gene signature, which could help individualize outcome predictions. However, the liver is not only a metabolic organ, but also an immune organ, which makes the tumor microenvironment of HCC have its specificity in addition to its commonalities with other tumors. The evidences above indicate that it is urgently needed to explore the prognostic significance for the interaction between immune and metabolism.

In this study, a systematic and comprehensive integrative analysis of immune- and metabolism-related genessignature was constructed in HCC, and the prognostic value was analyzed. Moreover, a prognostic nomogram was developed to provide a quantitative analysis tool in order to predict prognostic risk in HCC patients.

MATERIALS AND METHODS

Data Acquisition and Identification of Immune- and Metabolism-Related Genes (IMRGs)

Clinical features and gene expression profilesof HCC samples were downloaded from TCGA (https://portal.gdc.cancer.gov/) and ICGC database (https://dcc.icgc.org/). According to the ratio of 7:3, the TCGA-LIHC participants were randomly assigned to two cohorts: the training cohort (N = 262) and the testing cohort (N = 108). The clinical characteristics of the two cohorts were summarized in **Supplementary Table S1**. The testing and entire TCGA-LIHC cohorts were used as internal validation sets, while the ICGC-LIRI-JP cohort was treated as an external validation set. A detailed description of the survival follow-up data for ICGC-LIRI-JP cohort could be found in **Supplementary Table S2**. In addition, the genes associated with immunity were acquired from the ImmPort database (17) (https://www.immport.org). The metabolism-related genes were extracted by downloading the "c2.cp.kegg.v7.4.symbols" from MSigDB (Version 7.4).

Non-Negative Matrix Factorization (NMF) Clustering Algorithm

The "Limma" R package (18) was used for the analysis of the differentially expressed genes (DEGs) in HCC and normal samples. The absolute value of log2 (fold change) > 1 and false discovery rate (FDR) < 0.05 were considered as the criteria to screen the DEGs, from which the differentially expressed IMRGs were extracted. HCC samples were clustered using the NMF method after a univariate Cox analysis was performed. The "nsNMF" algorithm was selected with 100 iterations performed and the number of clusters K was set in the range of 2 to 10.

Establishment of the Prognostic Signature Based on IMRGs

Univariate Cox regression analysis was conducted to identify the genes related to prognosis in the TCGA training cohort. To establish the prognosis signature, the "glmnet" R package was applied to perform the least absolute shrinkage and selection operator (LASSO) Cox regression analysis. Accordingto the median risk score (RS), the TCGA training cohort was categorized into high- and low-risk groups. The ICGC-LIRI-JP cohort was subsequently analyzed in line with the cutoff value on the TCGA training set.

Construction of Prognostic Nomogram

On the basis of IMRGs prognostic signature and various clinical parameters, a prognostic nomogram was constructed to predict the survival probability of HCC patients. The predictive performance of the nomogram was evaluated by comparing predicted and actual survival risks. The calibration curves at 1-, 3-, and 5-year were plotted *via* "rms" R package.

Evaluation of the Response to Immunotherapy

Immunophenoscore (IPS) was calculated using the four main factors, including MHC molecules, immunomodulators, effector cells, and suppressor cells, in theTCIA database (19) (https://tcia.at/home), which was used to predict the therapeutic responses to the four major immune checkpoints (including PD-1 and its two ligands, PD-L1/PD-L2 as well as CTLA-4). Moreover, we analyzed the correlation of IMRGs signature with microsatellite instability (MSI), an indicator used to reflect the efficacy of immunotherapy.

Statistical Analysis

R software (version 4.0.3) was applied to conduct the statistical analyses with P < 0.05 considered statistically significant. The correlation analysis was performed using the Pearson method *via* the "corrplot" R package. The difference between the two groups was compared by Mann–Whitney U test. The "survival" R package was used to perform univariate and multivariate Cox hazard regression analyses. The Kaplan–Meier curve was employed to compare the survival difference by log-rank test. The "time ROC" R package was used to conduct the receiver

operator characteristic (ROC) curve and the area under the curve (AUC).

RESULT

Identification of HCC Molecular Subtypes Based on NMF Algorithm

After filtering and deduplication, a total of 2,715 immune- and metabolism-associated genes (IMRGs) were included. Compared with the normal group, 546 DEGs from IMRGs were observed in HCC samples by further difference analysis, with 441 DEGs upregulation and 105 DEGs downregulation (**Supplementary Table S4**). Then a total number of 257 prognosis-related IMRGs were identified using univariate Cox regression (**Supplementary Table S5**). Afterwards, two molecular subtypes were identified based on the DEGs by the NFM clustering algorithm (**Figure 1A**, **Supplementary Table S6**). The optimal rank value was determined by the indicators of cophenetic, silhouette, and dispersion (**Supplementary Figure S1**). The Kaplan–Meier curve displayed that the overall survival (OS) and progression-free survival (PFS) of cluster 1 were significantly worse than those of cluster 2 (**Figure 1B**). There were significant differences in Immune Score, and ESTIMATE Score between cluster 1 and cluster 2, but not in Stromal Score (**Figure 1C**). Likewise, the proportions of almost 10 immune cells in cluster 1 were higher than that in cluster 2 (**Figures 1D, E**), but the prognosis was worse. It was speculated that the immunosuppressive microenvironment of cluster 1 was composed of exhaust T cells, $CD8^+$ T cells, NK cells as well as a high proportion of monocytes-macrophages and neutrophils.

Furthermore, unsupervised clustering of differential expression profiles of immune- and metabolism-related genes between the two clusters were shown in **Figure 1F**. The

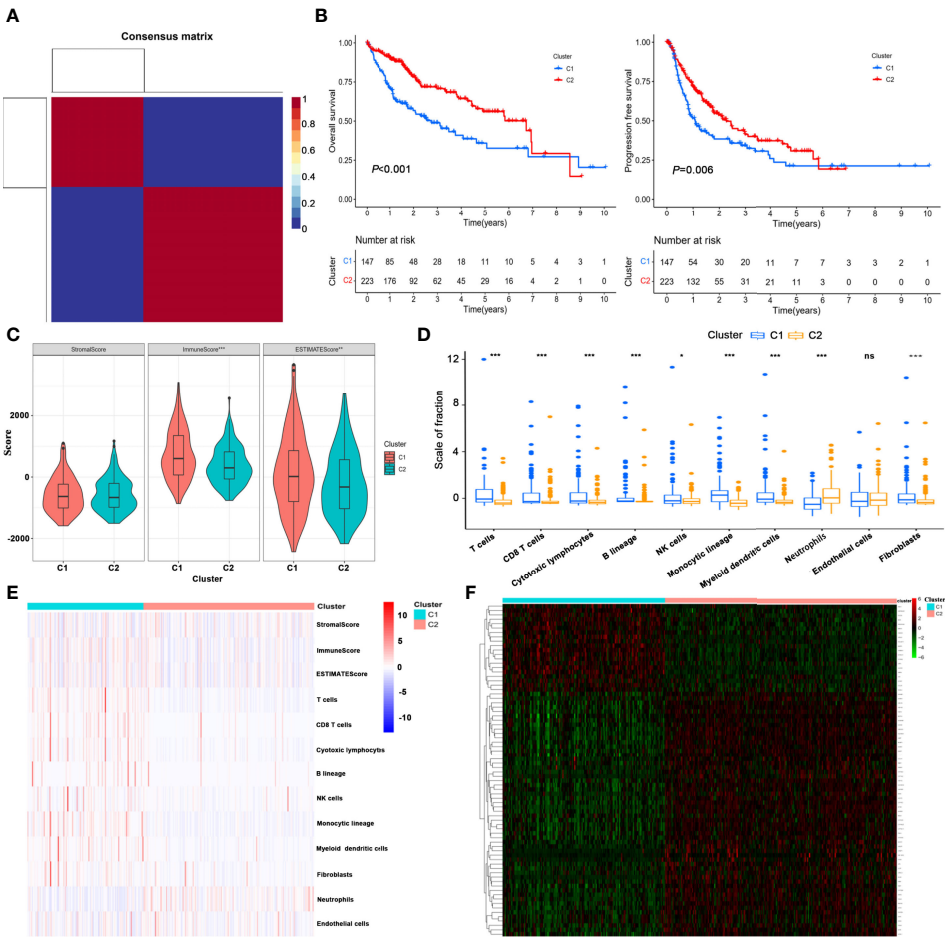

FIGURE 1 | Identification of HCC molecular subtypes based on NMF algorithm. **(A)** Heatmap of nsNMF consensus matrix of $K = 2$. **(B)** Kaplan–Meier curve of overall survival (OS) and progression-free survival (PFS) for HCC subtypes. **(C)** Comparison of immune scores between the two subtypes using estimate algorithm. **(D)** Comparison of immune scores calculated by MCP counter algorithm between the two subtypes. **(E)** Heatmap of the immune scores for ESTIMATE and MCP counter algorithms. **(F)** Unsupervised clustering of immune- and metabolism-related gene expression profiling between the two clusters. $^*P < 0.05$, $^{**}P < 0.01$, $^{***}P < 0.001$. ns, no significance.

distribution of clinical parameters between the two molecular subtypes was compared. The survival time of cluster 1 was lower than that of cluster 2, and the mortality rate was significantly higher. The proportions of patients with grade (G3–4), and T stage (T3–4) in cluster 1 were higher than those in cluster 2 (**Supplementary Figure S2**).

Construction of the IMRGs Prognostic Signature Using LASSO Cox Regression Analysis in TCGA Training Cohort

The TCGA-LIHC cohort was randomly divided into two groups in a 7:3 ratio, namely, the training cohort and testing cohort, and no significant differences in clinical features were demonstrated between the two groups (**Supplementary Table S7**). The LASSO Cox regression analysis was used to construct a prognostic prediction model based on the prognosis-related IMRGs in TCGA training cohort. Coefficients of independent variables in LASSO regression were shown in **Figure 2A**. Based on the optimal log value of lambda, we identified 8 genes (**Figure 2B**), among which PPIA and GHR were immune-associated genes, and ACYP1, ADH4, G6PD, POLR3G, PPAT, and UCK2 were metabolism-associated genes. By multivariate Cox regression analysis, a risk score (RS) that represented the comprehensive index of immune and metabolism status for IMRGs signature was calculated by each gene expression multiplied by the corresponding coefficient as follows:

$$RS = -0.148766 \times GHR + 0.286961 \times ACYP1 - 0.089981 \times ADH4 + 0.755085 \times POLR3G + 0.593780 \times PPAT .$$

The forest plot displayed that the five genes in the risk mode were closely related to prognosis (**Supplementary Figure S3A**). And Wilcoxon test showed that there were significant differences in the expression of five genes in the high- and low-risk groups. The expressions of ACYP1, POLR3G, and PPAT were higher in high-risk group, while the expressions of GHR and ADH4 were higher in low-risk group (**Supplementary Figure S3B**). Then, based on the median of RS, the HCC samples in the TCGA training cohort were divided into high- and low-risk groups to probe the association between the RS and prognosis. Scatter plot depicted the distribution of RS and their relationship to survival outcomes (**Figure 2C**). Heat map presented expression profiles of risk genes in prognostic models for high- and low-risk groups (**Figure 2D**). According to the Kaplan–Meier curve, HCC samples with high RS had a poor prognosis (**Figure 2E**). The AUCs of the prognostic model reached 0.821, 0.759, and 0.752 at 1-, 3-, and 5-year, respectively (**Figure 2F**), which exhibited good prognostic value.

Internal and External Validation of the IMRGs Prognostic Signature

To further assess the robustness and predictive ability of the IMRGs signature, both internal (TCGA testing cohort and entire TCGA-LIHC cohort) and external validations (ICGC-LIRI-JP

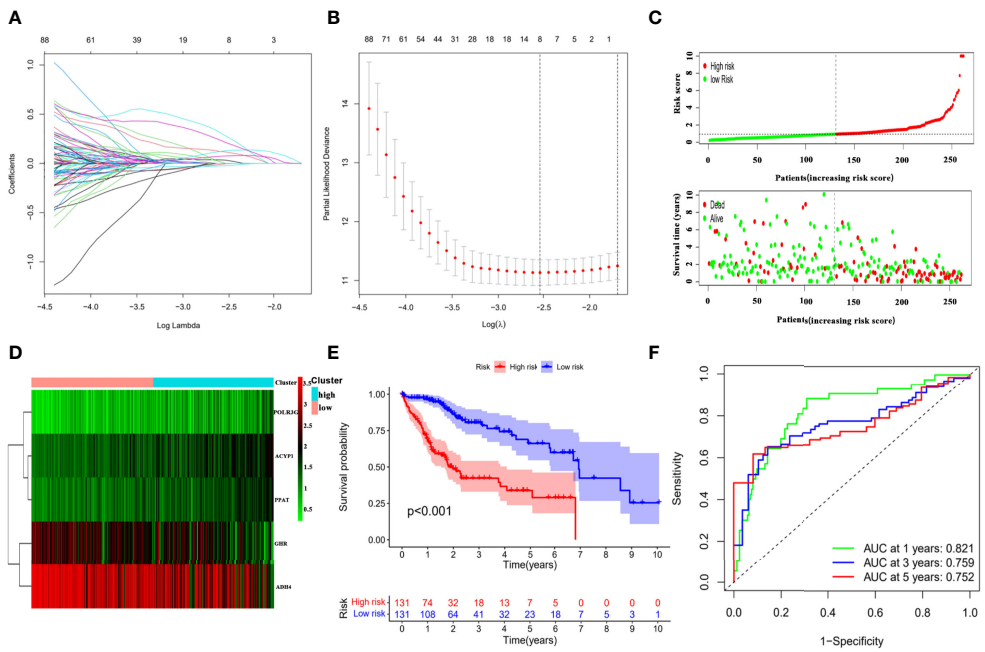

FIGURE 2 | Establishment of the IMRGs prognostic signature using LASSO Cox regression analysis in TCGA training cohort. **(A)** Coefficients of independent variables in LASSO regression. **(B)** The optimal log value of lambda was indicated by the first black dotted line from the left. **(C)** Kaplan–Meier curve analyses for the high-risk group and low-risk group were classified according to the median risk score (RS). **(D)** The ROC curves of the IMRGs prognostic signature at 1-, 3-, and 5-year. **(E)** Distribution of RS and survival status. **(F)** Heatmap of the gene-expression profiles of the IMRGs prognostic signature.

cohort) were performed. The RS of validation groups was determined according to the same formula as the TCGA training set. Likewise, the high- and low-risk groups were classified using the same cutoff value as the training group.

The distribution of the RS and their associations with survival status were illustrated in **Figure 3A**. **Figure 3B** displayed the heatmaps of gene expression profiles included in prognostic models. Significant prognostic differences were found between the high-and low-riskgroups in the TCGA testing (P = 0.002), entire TCGA-LIHC (P < 0.001), and ICGC cohorts (P = 0.045; **Figure 3C**). Additionally, the AUCs of 1-, 3-, and 5-year survival in the TCGA testing, entire TCGA-LIHC, and ICGC cohorts were shown in **Figure 3D**. These results suggested that the IMRGs signature exhibited high performance in terms of robustness and predictive ability.

Correlation of theIMRGs Prognostic Signature With Clinical Features

To investigate whether the IMRGs signature correlated with clinical features, the differences in RS were compared in the entire TCGA-LIHC cohort by independent t tests. The RS of HCC samples with tumor grade (**Figure 4A**), T stage (**Figure 4B**), and advanced pathological stage (**Figure 4C**) was higher than that of the corresponding early-stage samples. The RS of cluster 1 with a poor prognosis was higher than that of cluster 2 (**Figure 4D**). Based on subgroup analysis, significant differences in prognosis existed between high- and low-risk groups regardless of clinical features such as age (**Figure 4E**), gender (**Figure 4F**), tumor grade (**Figure 4G**), pathological stage (**Figure 4H**), and T stage (**Figure 4I**). These findings indicated that the IMRGs prognostic signature showed

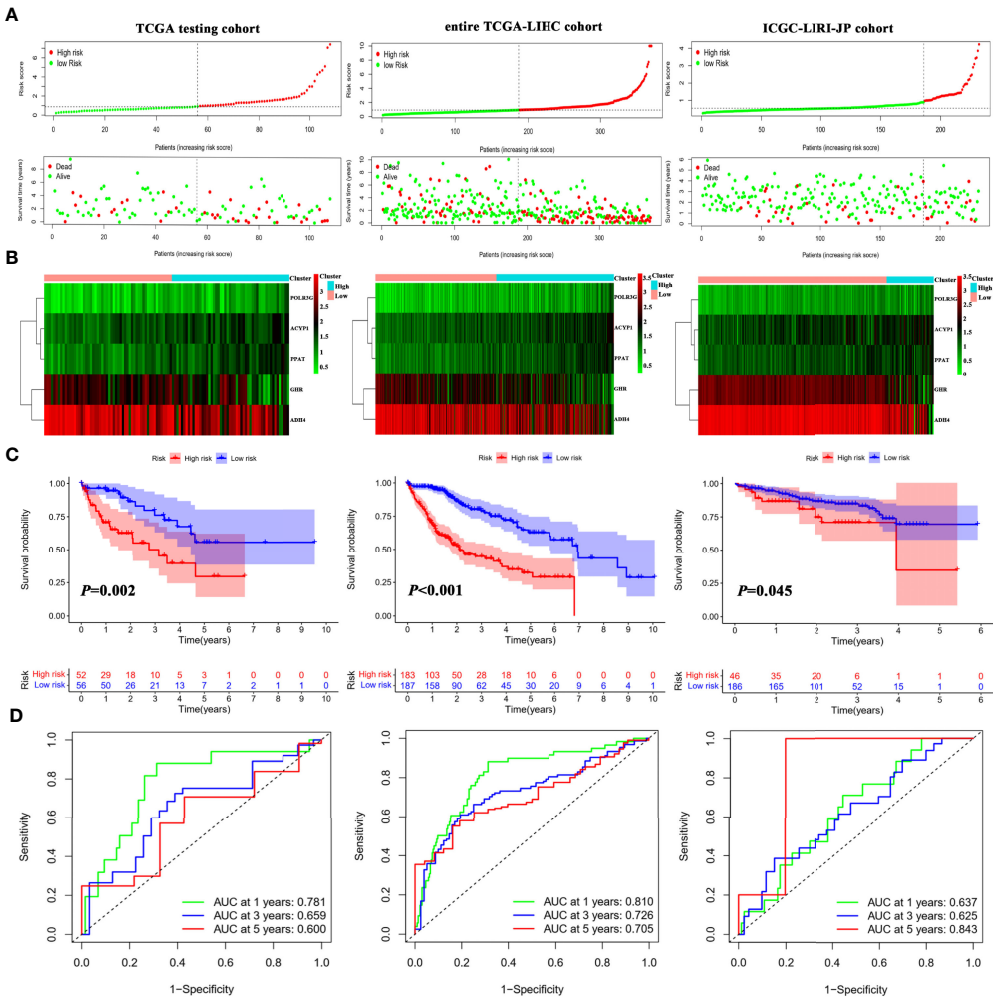

FIGURE 3 | Internal and external validation of the IMRGsprognostic signature. **(A)** Distributionof RS and survival status in internal (TCGA testing and entire TCGA-LIHC) and external (ICGC-LIRI-JP) cohorts. Heatmap of the gene-expression profiles of the IMRGs prognostic signature **(B)**, Kaplan–Meier curve analyses for high-risk group and low-risk group **(C)**, and the ROC curves of the IMRGs prognostic signature at 1-, 3-, and 5-year **(D)** in TCGA testing, entire TCGA-LIHC as well as ICGC-LIRI-JP cohorts.

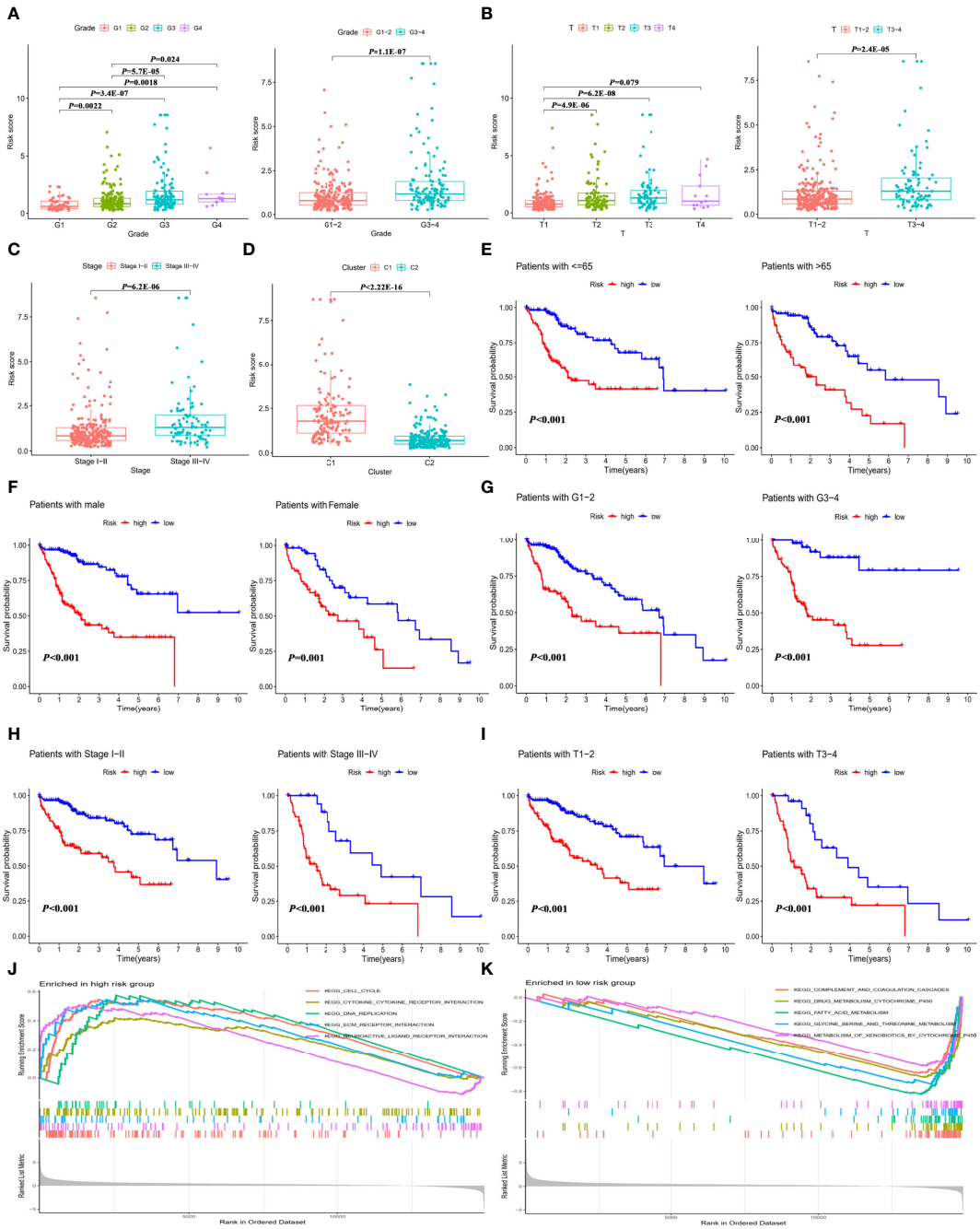

FIGURE 4 | Correlation of the IMRGs prognostic signature with clinical features in the entire TCGA-LIHC cohort. The difference in RS between different clinical features. **(A)** Tumor grade; **(B)** T stage; **(C)** tumor stage; and **(D)** cluster molecular subtypes. Kaplan–Meier curve analyses of OS in clinical subtypes in different clinical subtypes. **(E)** Age ≤65 years and age >65 years; **(F)** gender; **(G)** tumor grade 1–2 and tumor grade 3–4; **(H)** tumor stage I–II and tumor stage III–IV; and **(I)** T stage 1–2 and T stage 3–4. GSEA enrichment analysis in the high-risk group **(J)** and low-risk group **(K)**.

good prognostic predictive power according to different clinical characteristics.

Additionally, gene set enrichment analysis (GSEA) for the high-risk (**Figure 4J**) and low-risk (**Figure 4K**) groups of the entire TCGA-LIHC cohort was conducted. The results found that the genes in the low-risk group were significantly enriched in metabolism-related pathways, which were detailed in **Supplementary Table S8**. It can be inferred from the pathway enrichment analysis that alterations in metabolic pathways might lead to different immune status in the high-risk group.

Comparison of the IMRGs Prognostic Signature With the Published Signatures

To explore whether the immune- and metabolism-associated model had a superior predictive ability, we compared it with four published prognostic models, namely Tian signature (20) (a five-gene model), Fu signature (21) (a three-gene model), Lin signature (22) (an eight-gene model) and Fang signature (23) (a six-gene model). To make the signatures comparable, the same method was applied to calculate and convert the RS of the entire TCGA-LIHC cohort. All the published four signatures were able to categorize the HCC samples into a high-risk group and low-risk group with significantly different outcomes (**Figures 5A–D**). Nevertheless, ROC curve analysis found that the AUCs of the published four signatures were lower than those of our model with AUCs of 0.810, 0.726, and 0.705 for 1-, 3-, and 5-year survival, respectively (**Figures 5E–H**). Furthermore, the C-index was highest in our model at 0.717, followed by Tian signature (C-index = 0.652), Fu signature (C-index = 0.64), Lin signature (C-index = 0.635), and Fang signature (C-index = 0.6; **Figure 5I**). The findings highlighted consistently superior performance of IMRGsprognostic signature.

Construction of the Nomogram Based on the IMRGs Prognostic Signature and Evaluation of Clinical Significance

To assess the independence of the IMRGs prognostic signature for clinical application, Cox regression analyses were performed in the entire TCGA-LIHC cohort and ICGC-LIRI-JP cohort. In the entire TCGA-LIHC cohort, significant correlations between RS and prognosis were found in both univariate [hazard ratio (95% CI) = 1.201 (1.135–1.272), $P < 0.001$] (**Figure 6A**) and multivariate regression analyses [hazard ratio (95% CI) = 1.179 (1.105–

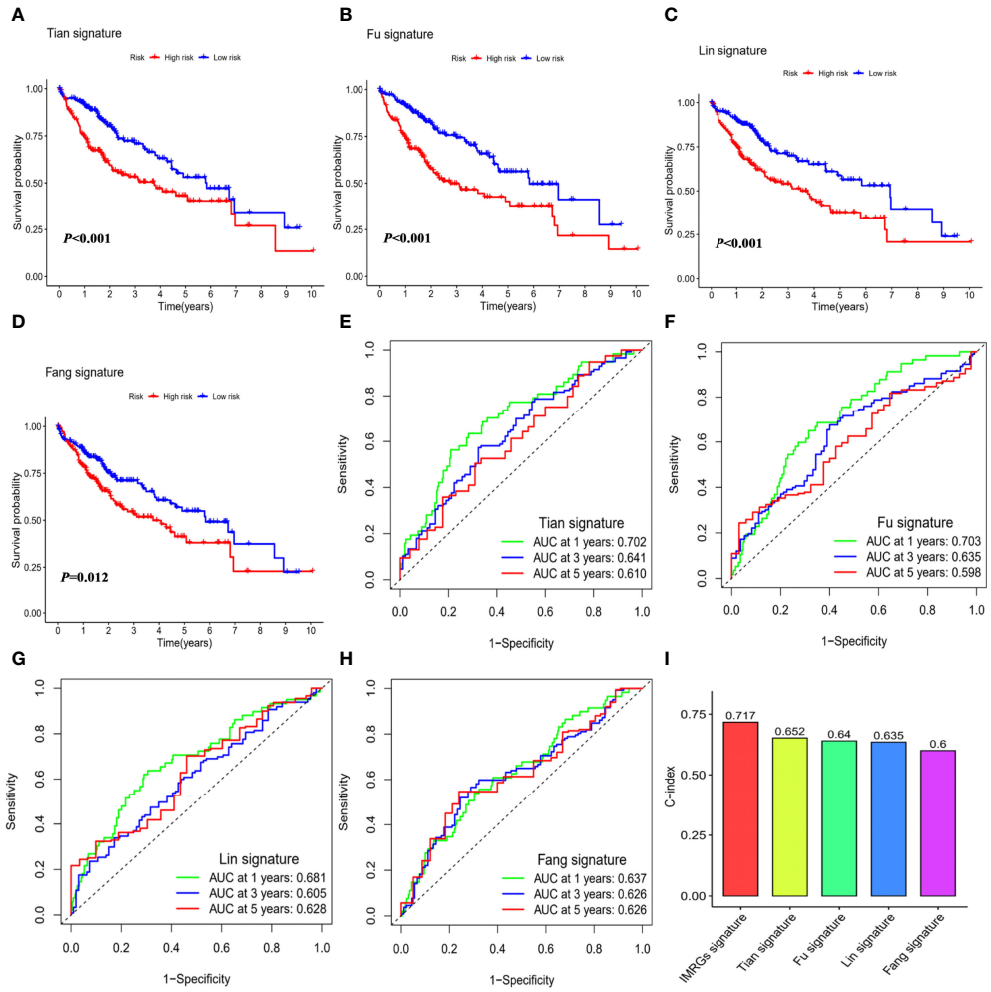

FIGURE 5 | Comparison of the IMRGs prognostic signature with the published signatures. Kaplan–Meier survival curve and ROC curve of five genes signature established by Tian et al. (Tian signature; **A**, **B**), three genes signature established by Fu et al. (Fu signature; **C**, **D**), eight genes signature established by Lin et al. (Lin signature; **E**, **F**), six genes signature established by Fang et al. (Fang signature; **G**, **H**). **(I)** Comparison of C-indexes for the five prognostic models.

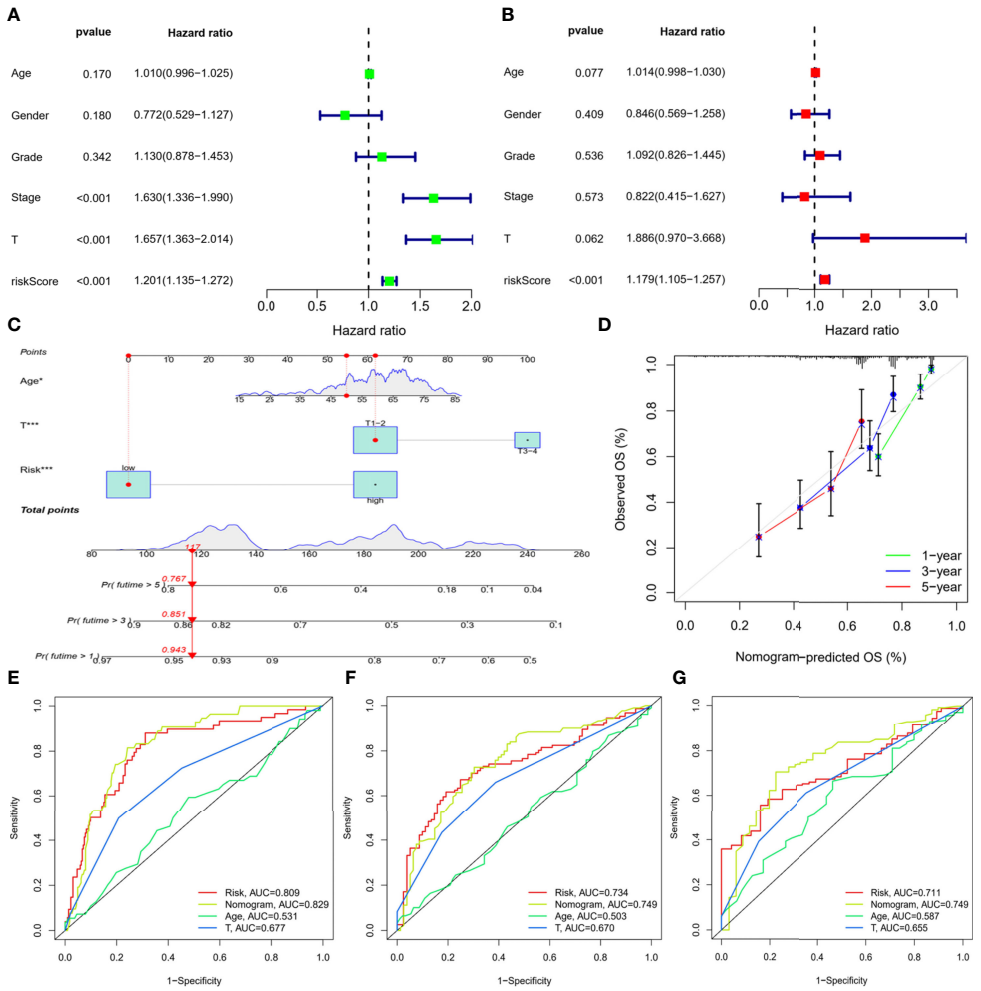

FIGURE 6 | Construction of the nomogram based on the IMRGs prognostic signature and evaluation of clinical significance in the entire TCGA-LIHC cohort. **(A, B)** Univariate and multivariate Cox regression analyses of RS and various clinical features. **(C)** Nomogram for predicting the OS in the entire TCGA-LIHC cohort at 1-, 3-, and 5-year. For each patient, the total score was calculated by adding the points determined by the point scale of each variable. Based on the total points, the bottom scale was used to predict the probability of 1-, 3-, or 5-year survival. The red line exemplified the calculation process and principle of the nomogram. **(D)** Calibration curve for consistency between 1-, 3-, or 5-year nomogram predicted survival and actual survival. **(E–G)** ROC curves of nomograms for 1-year, 3-year, and 5-year survival.

1.257), $P < 0.001$] (**Figure 6B**). The results were further verified in ICGC-LIRI-JP cohort (**Supplementary Figure S4**), suggesting that the IMRGs prognostic signature exhibited a good clinical predictive value.

Then, three variables with a P value less than 0.1 were determined by multiple regression, namely, age, T stage, and RS, and a nomogram was constructed to predict survival risk for individuals (**Figure 6C**). As shown in **Figure 6D**, the calibration curves displayed good consistency between the nomogram-predicted survival and actual survival. Moreover, the AUCs for the nomogram were 0.829, 0.749, and 0.749 at 1-, 3-, and 5-year, which were also higher than the other two variables (**Figures 6E–G**). Thus, the results indicated thatthe nomogram based on the IMRGs prognostic signature showed a significant relation to prognosis and helped predict disease progression.

Predictive Role of the IMRGs Prognostic Signature in Response to Immunotherapy

To further seek the effect of the IMRGs prognostic signature on immunotherapy efficacy, correlations between the RS and immune infiltration of TME were analyzed. As shown in **Figure 7A**, the RS was negatively associated with neutrophils, but positively associated with monocytic lineage and myeloid dendritic cells, cytotoxic lymphocytes, and fibroblasts as well MSI (24), a well-established biomarker for predicting immune efficacy. In the low-risk group, the proportions of monocytes, myeloid dendritic cells, and T cells were significantly decreased, while the proportions of neutrophils and endothelial cells were significantly increased (**Figure 7B**). Furthermore, the RS was significantly positively associated with immune checkpoint expressions (**Figure 7C**). There were significant differences in the expression of immune

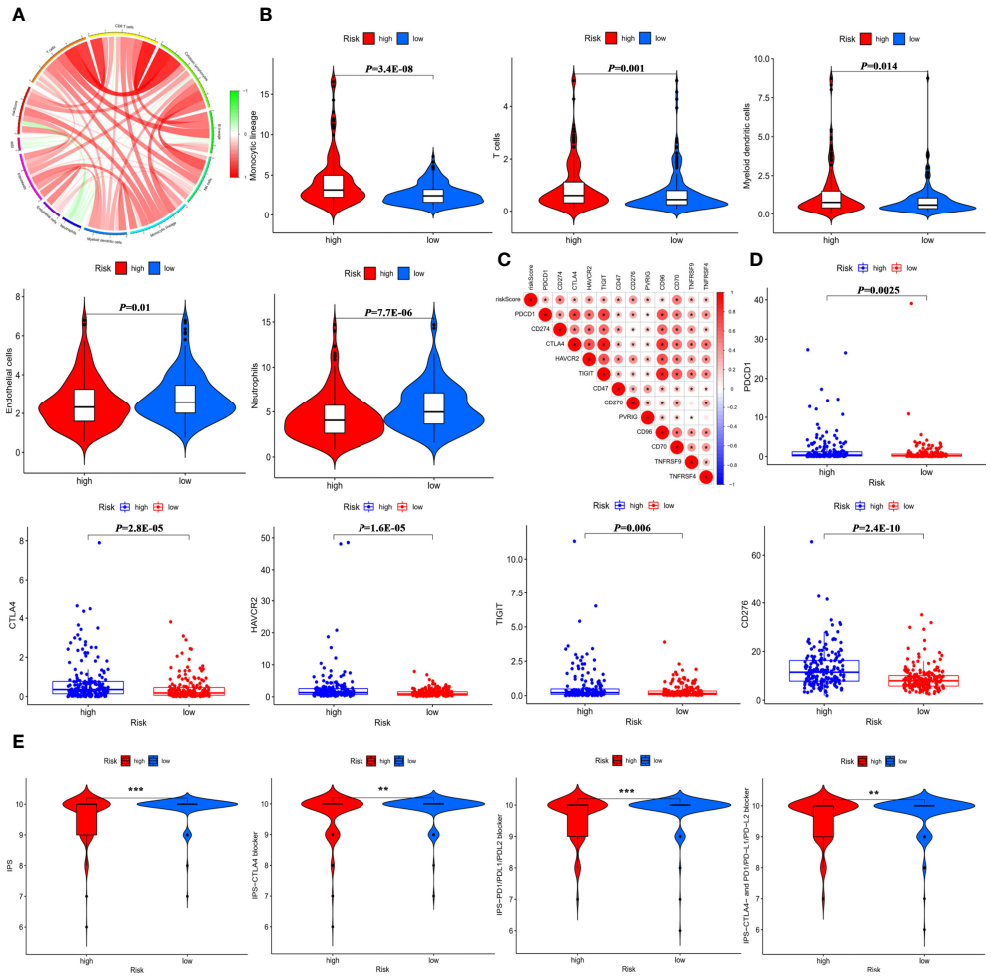

FIGURE 7 | Predictive role of the IMRGs prognosticsignature in response to immunotherapy. **(A)** Correlation of the RS, MSI, and MCP counter immune scores. **(B)** Differences in immune cell infiltration between the high-risk group and low-risk group. **(C)** Correlation of the RS and immune check point expressions. **(D)** Comparison of the difference in immune checkpoint expressions (such as PD-1/PDCD1, CTLA4, TIM-3/HAVCR2, TIGIT, B7-H3/CD276) between high- and low-risk groups. **(E)** Correlation between the RS and four IPS scores related to a single ICI or a combination of ICIs including PD-1, PD-L1/PD-L2, and CTLA-4. $^{*}P < 0.05$, $^{**}P < 0.01$, $^{***}P < 0.001$.

checkpoints such as PD-1/PDCD1, CTLA4, TIM-3/HAVCR2, TIGIT, and B7-H3/CD276 between high- and low-risk groups (**Figure 7D**). Additionally, the relationship was explored between the RS and IPS, excellent indicators in predicting the response to immunotherapy. Significant differences were found between the high-risk and low-risk groups in terms of IPS, IPS-CTLA4, IPS-PD1/PD-L1/PD-L2 blockers, and IPS-CTLA4+PD1/PD-L1/PD-L2 blockers (**Figure 7E**). The findings indicated that the IMRGs prognostic signature could potentially reflect the immune infiltration status and predict the response to immunotherapy.

DISCUSSION

The advent of the era of immunotherapy has greatly improved outcomes for HCC patients. However, not all patients can get benefit from it, which might be close to the differences in the TME of HCC patients. Given the importance of the interaction between immune and metabolism, it is reasonable to expect that the model would have a good performance in predicting prognosis based on the immune- and metabolism-related genes. To our knowledge, a systematic and comprehensive integrative analysis of immune- and metabolism-associated genes characteristic remains poorly understood in HCC. In this study, an immune- and metabolism-related genes signature was constructed, and the prognostic value was verified. Besides, a nomogram was constructed based on five immune- and metabolism-related genes and clinical features. The clinical significance of the IMRGs prognostic signature was assessed by comparing the immune checkpoint expressions between the high-risk group and low-risk groups and exploring the predictive role in response to immunotherapy.

The entire TCGA-LIHC cohort was categorized into two subtypes using NMF algorithm based on 546 DEGs. Compared with cluster 2, cluster 1 exhibited a poor prognosis, which might be

related to the immunosuppressive microenvironment formed by a higher degree of immune infiltration identified by ESTIMATE (25) and MCP counter (26) algorithm. Based on univariate Cox regression and LASSO Cox regression analysis, a prognostic signature of IMRGs consisting of GHR, ACYP1, ADH4, and PPAT was constructed in the TCGA training cohort. Based on the median of RS, the prognostic model was categorized into high- and low-risk groups. Further analysis found that the high-risk group showed more advanced pathological stage, T stage, and tumor grade. Subgroup analysis showed that the prognostic model exhibited good prognostic prediction performance regardless of clinical factors. Besides, the model was validated in internal and external cohorts. The C-index of IMRGs prognostic signature was superior to the four previously reported signatures. All the findings suggested that the immune- and metabolism-related prognostic signature had better prognostic ability.

Growth hormone receptor (GHR), a member of the class I cytokine receptor superfamily, was down-regulation in the high-risk group and was related to chemoresistance, tumor metastasis, and poor prognosis (27–29). Acylphosphatase 1 (ACYP1) involved in the formation of acetic acid from acetyl phosphate, was reported to be related to drug resistance such as imatinib. ACYP1, which was highly expressed in HCC, also was associated with decreased survival time (30). High ACYP1 expression promoted cell survival and apoptosis through the JAK/STAT and PI3K/AKT pathways (31). ADH4, an alcohol dehydrogenase, played critical roles in ethanol metabolism (32). The expression of ADH4 was mediated by miR-148a *via* an AGO1-dependent manner (33) and could be considered as a prognostic biomarker or molecular target for patients with HCC (34, 35). POLR3G, one form of RNA polymerase III, was mainly expressed in stem and cancer cells. Increased gene expression of POLR3G was involved in the proliferation and differentiation of cancer cells and characterized by poor prognosis (34). However, the roles of immune and metabolism-related genes such as GHR, ACYP1, ADH4, POLR3G, and PPAT in the immune environment of HCC were unclear, and further experimental verification was required.

The advent of immunotherapy has provided new ideas for the treatment of HCC, of which immune checkpoint inhibitors (ICIs) have become a potentially effective therapeutic strategy (36–38). The response to ICIs was evaluated by the four scores of IPS, all of which have been shown good performance in predicting the response to immunotherapy efficacy (39). To probe the predictive value of IMRGs prognosticsignature on predicting the response to ICIs, the correlation of RS and IPS was assessed. All the four scores related to a single ICI or a combination of ICIs were higher in the low-risk group, indicating that the IMRGs prognostic signature might have the potential power to predict the immunotherapy efficacy and help personalize immunotherapy for HCC patients. A nomogram is used as a new prognostic tool to improve the accuracy of prognostic prediction (40, 41). A nomogram was constructed by integrating the IMRGs prognostic signature and the clinical parameters identified by univariate and multivariate Cox regression analysis. The results showed that the AUCs of nomogram at 1-, 3-, and 5-year (AUC = 0.829, 0.749, 0.749) were slightly better than that of IMRGs signature (AUC = 0.809, 0.734, 0.711), which further verified that IMRGs prognostic signature established could better predict the risk of prognosis and survival for HCC patients.

There are several strengths in this research as follows: First, the robustness and reliability of IMRGs prognostic signature were evaluated and validated using multiple datasets, including internal and external cohorts. Second, the associations of RS with immune checkpoint expressions, four IPS scores, as well as MSI were comprehensively and deeply explored. Third, a nomogram for quantitative calculation was developed in order to assist with clinical application. Nevertheless, there are still several limitations in this study. For example, The IMRGs prognostic signature and the nomogram were established based on a retrospective study, which needs to be further verified in large multicenter prospective cohorts.

CONCLUSION

The IMRGs prognostic signature was constructed based on the integrated analysis of immune- and metabolism-related genes, which could better predict prognostic risk and the response to immunotherapy. We also developed a nomogram for patients with HCC, providing an effective quantitative analysis tool to realize the clinical application of personalized precision therapy.

DATA AVAILABILITY STATEMENT

The datasets presented in this study can be found in online repositories. The names of the repository/repositories and accession number(s) can be found in the article/**Supplementary Material**.

AUTHOR CONTRIBUTIONS

XT, XZ, and QK conceived and directed the completion of the study. HG collected and downloaded the data. YG conducted the data analysis and drafted the manuscript. JY modified the language and revised the manuscript. All authors contributed to the manuscript and approved the submitted version.

FUNDING

This study was funded by the Medical Science and Technology Research Plan Joint Construction Project of Henan Province, China (No. LHGJ20210282) and the National Key Research and Development Program of China (No. 2020YFC2008304).

ACKNOWLEDGMENTS

We would like to express our utmost appreciation to all the participants in the TCGA-LIHC and ICGC-LIRI-JP cohorts.

SUPPLEMENTARY MATERIAL

The Supplementary Material for this article can be found online at: https://www.frontiersin.org/articles/10.3389/fimmu.2022.927635/full#supplementary-material

REFERENCES

1. Bray F, Ferlay J, Soerjomataram I, Siegel RL, Torre LA, Jemal A. Global Cancer Statistics 2018: GLOBOCAN Estimates of Incidence and Mortality Worldwide for 36 Cancers in 185 Countries. *CA Cancer J Clin* (2018) 68:394–424. doi: 10.3322/caac.21492
2. Allemani C, Matsuda T, Di Carlo V, Harewood R, Matz M, Niksic M, et al. Global Surveillance of Trends in Cancer Survival 2000-14 (CONCORD-3): Analysis of Individual Records for 37 513 025 Patients Diagnosed With One of 18 Cancers From 322 Population-Based Registries in 71 Countries. *Lancet* (2018) 391:1023–75. doi: 10.1016/S0140-6736(17)33326-3
3. Hilmi M, Neuzillet C, Calderaro J, Lafdil F, Pawlotsky JM, Rousseau B. Angiogenesis and Immune Checkpoint Inhibitors as Therapies for Hepatocellular Carcinoma: Current Knowledge and Future Research Directions. *J Immunother Cancer* (2019) 7:333. doi: 10.1186/s40425-019-0824-5
4. Sangro B, Sarobe P, Hervas-Stubbs S, Melero I. Advances in Immunotherapy for Hepatocellular Carcinoma. *Nat Rev Gastroenterol Hepatol* (2021) 18:525–43. doi: 10.1038/s41575-021-00438-0
5. Llovet JM, Castet F, Heikenwalder M, Maini MK, Mazzaferro V, Pinato DJ, et al. Immunotherapies for Hepatocellular Carcinoma. *Nat Rev Clin Oncol* (2022) 19:151–72. doi: 10.1038/s41571-021-00573-2
6. Wu M, Huang Q, Xie Y, Wu X, Ma H, Zhang Y, et al. Improvement of the Anticancer Efficacy of PD-1/PD-L1 Blockade *via* Combination Therapy and PD-L1 Regulation. *J Hematol Oncol* (2022) 15:24. doi: 10.1186/s13045-022-01242-2
7. Osipov A, Lim SJ, Popovic A, Azad NS, Laheru DA, Zheng L, et al. Tumor Mutational Burden, Toxicity, and Response of Immune Checkpoint Inhibitors Targeting PD(L)1, CTLA-4, and Combination: A Meta-Regression Analysis. *Clin Cancer Res* (2020) 26:4842–51. doi: 10.1158/1078-0432.CCR-20-0458
8. Jeng KS, Chang CF, Jeng WJ, Sheen IS, Jeng CJ. Heterogeneity of Hepatocellular Carcinoma Contributes to Cancer Progression. *Crit Rev Oncol Hematol* (2015) 94:337–47. doi: 10.1016/j.critrevonc.2015.01.009
9. Guo Y, Yang J, Ren K, Tian X, Gao H, Tian X, et al. The Heterogeneity of Immune Cell Infiltration Landscape and Its Immunotherapeutic Implications in Hepatocellular Carcinoma. *Front Immunol* (2022) 13:861525. doi: 10.3389/fimmu.2022.861525
10. Makarova-Rusher OV, Medina-Echeverz J, Duffy AG, Greten TF. The Yin and Yang of Evasion and Immune Activation in HCC. *J Hepatol* (2015) 62:1420–9. doi: 10.1016/j.jhep.2015.02.038
11. Martinez-Reyes I, Chandel NS. Cancer Metabolism: Looking Forward. *Nat Rev Cancer* (2021) 21:669–80. doi: 10.1038/s41568-021-00378-6
12. Wolowczuk I, Verwaerde C, Viltart O, Delanoye A, Delacre M, Pot B, et al. Feeding Our Immune System: Impact on Metabolism. *Clin Dev Immunol* (2008) 2008:639803. doi: 10.1155/2008/639803
13. Parks SK, Chiche J, Pouyssegur J. Disrupting Proton Dynamics and Energy Metabolism for Cancer Therapy. *Nat Rev Cancer* (2013) 13:611–23. doi: 10.1038/nrc3579
14. Dai Y, Qiang W, Lin K, Gui Y, Lan X, Wang D. An Immune-Related Gene Signature for Predicting Survival and Immunotherapy Efficacy in Hepatocellular Carcinoma. *Cancer Immunol Immunother* (2021) 70:967–79. doi: 10.1007/s00262-020-02743-0
15. Yang C, Huang X, Liu Z, Qin W, Wang C. Metabolism-Associated Molecular Classification of Hepatocellular Carcinoma. *Mol Oncol* (2020) 14:896–913. doi: 10.1002/1878-0261.12639
16. He L, Chen J, Xu F, Li J, Li J. Prognostic Implication of a Metabolism-Associated Gene Signature in Lung Adenocarcinoma. *Mol Ther Oncolyt* (2020) 19:265–77. doi: 10.1016/j.omto.2020.09.011
17. Bhattacharya S, Andorf S, Gomes L, Dunn P, Schaefer H, Pontius J, et al. ImmPort: Disseminating Data to the Public for the Future of Immunology. *Immunol Res* (2014) 58:234–9. doi: 10.1007/s12026-014-8516-1
18. Ritchie ME, Phipson B, Wu D, Hu Y, Law CW, Shi W, et al. Limma Powers Differential Expression Analyses for RNA-Sequencing and Microarray Studies. *Nucleic Acids Res* (2015) 43:e47. doi: 10.1093/nar/gkv007
19. Charoentong P, Finotello F, Angelova M, Mayer C, Efremova M, Rieder D, et al. Pan-Cancer Immunogenomic Analyses Reveal Genotype-Immunophenotype Relationships and Predictors of Response to Checkpoint Blockade. *Cell Rep* (2017) 18:248–62. doi: 10.1016/j.celrep.2016.12.019
20. Tian D, Yu Y, Zhang L, Sun J, Jiang W. A Five-Gene-Based Prognostic Signature for Hepatocellular Carcinoma. *Front Med (Lausanne)* (2021) 8:681388. doi: 10.3389/fmed.2021.681388
21. Fu XW, Song CQ. Identification and Validation of Pyroptosis-Related Gene Signature to Predict Prognosis and Reveal Immune Infiltration in Hepatocellular Carcinoma. *Front Cell Dev Biol* (2021) 9:748039. doi: 10.3389/fcell.2021.748039
22. Lin Z, Xu Q, Miao D, Yu F. An Inflammatory Response-Related Gene Signature Can Impact the Immune Status and Predict the Prognosis of Hepatocellular Carcinoma. *Front Oncol* (2021) 11:644416. doi: 10.3389/fonc.2021.644416
23. Fang Q, Chen H. Development of a Novel Autophagy-Related Prognostic Signature and Nomogram for Hepatocellular Carcinoma. *Front Oncol* (2020) 10:591356. doi: 10.3389/fonc.2020.591356
24. Vilar E, Gruber SB. Microsatellite Instability in Colorectal Cancer-the Stable Evidence. *Nat Rev Clin Oncol* (2010) 7:153–62. doi: 10.1038/nrclinonc.2009.237
25. Yoshihara K, Shahmoradgoli M, Martinez E, Vegesna R, Kim H, Torres-Garcia W, et al. Inferring Tumour Purity and Stromal and Immune Cell Admixture From Expression Data. *Nat Commun* (2013) 4:2612. doi: 10.1038/ncomms3612
26. Becht E, Giraldo NA, Lacroix L, Buttard B, Elarouci N, Petitprez F, et al. Estimating the Population Abundance of Tissue-Infiltrating Immune and Stromal Cell Populations Using Gene Expression. *Genome Biol* (2016) 17:218. doi: 10.1186/s13059-016-1070-5
27. Lin CC, Liu TW, Yeh ML, Tsai YS, Tsai PC, Huang CF, et al. Significant Down-Regulation of Growth Hormone Receptor Expression Revealed as a New Unfavorable Prognostic Factor in Hepatitis C Virus-Related Hepatocellular Carcinoma. *Clin Mol Hepatol* (2021) 27:313–28. doi: 10.3350/cmh.2020.0247
28. Lin T, Diao YF, Choi HS, Oqani RK, Kang JW, Lee JE, et al. Procedure Used for Denuding Pig Oocytes Influences Oocyte Damage, and Development of *In Vitro* and Nuclear Transfer Embryos. *Anim Reprod Sci* (2015) 152:65–76. doi: 10.1016/j.anireprosci.2014.11.009
29. Gao S, Ni Q, Wu X, Cao T. GHR Knockdown Enhances the Sensitivity of HCC Cells to Sorafenib. *Aging (Albany NY)* (2020) 12:18127–36. doi: 10.18632/aging.103625
30. Sakano Y, Noda T, Kobayashi S, Kitagawa A, Iwagami Y, Yamada D, et al. Clinical Significance of Acylphosphatase 1 Expression in Combined HCC-iCCA, HCC, and iCCA. *Dig Dis Sci* (2021). doi: 10.1007/s10620-021-07266-x
31. Delic D, Wunderlich F, Al-Quraishy S, Abdel-Baki AS, Dkhil MA, Arauzo-Bravo MJ. Vaccination Accelerates Hepatic Erythroblastosis Induced by Blood-Stage Malaria. *Malar J* (2020) 19:49. doi: 10.1186/s12936-020-3130-2
32. Chowdhury NP, Moon J, Muller V. Adh4, an Alcohol Dehydrogenase Controls Alcohol Formation Within Bacterial Microcompartments in the Acetogenic Bacterium Acetobacterium Woodii. *Environ Microbiol* (2021) 23:499–511. doi: 10.1111/1462-2920.15340
33. Luo J, Hou Y, Ma W, Xie M, Jin Y, Xu L, et al. A Novel Mechanism Underlying Alcohol Dehydrogenase Expression: hsa-miR-148a-3p Promotes ADH4 Expression *via* an AGO1-Dependent Manner in Control and Ethanol-Exposed Hepatic Cells. *Biochem Pharmacol* (2021) 189:114458. doi: 10.1016/j.bcp.2021.114458
34. Petrie JL, Swan C, Ingram RM, Frame FM, Collins AT, Dumay-Odelot H, et al. Effects on Prostate Cancer Cells of Targeting RNA Polymerase III. *Nucleic Acids Res* (2019) 47:3937–56. doi: 10.1093/nar/gkz128
35. Wei RR, Zhang MY, Rao HL, Pu HY, Zhang HZ, Wang HY. Identification of ADH4 as a Novel and Potential Prognostic Marker in Hepatocellular Carcinoma. *Med Oncol* (2012) 29:2737–43. doi: 10.1007/s12032-011-0126-3
36. Llovet JM, Montal R, Sia D, Finn RS. Molecular Therapies and Precision Medicine for Hepatocellular Carcinoma. *Nat Rev Clin Oncol* (2018) 15:599–616. doi: 10.1038/s41571-018-0073-4
37. Pinter M, Jain RK, Duda DG. The Current Landscape of Immune Checkpoint Blockade in Hepatocellular Carcinoma: A Review. *JAMA Oncol* (2021) 7:113–23. doi: 10.1001/jamaoncol.2020.3381
38. Pinato DJ, Guerra N, Fessas P, Murphy R, Mineo T, Mauri FA, et al. Immune-Based Therapies for Hepatocellular Carcinoma. *Oncogene* (2020) 39:3620–37. doi: 10.1038/s41388-020-1249-9
39. Yang S, Wu Y, Deng Y, Zhou L, Yang P, Zheng Y, et al. Identification of a Prognostic Immune Signature for Cervical Cancer to Predict Survival and Response to Immune Checkpoint Inhibitors. *Oncoimmunology* (2019) 8:e1659094. doi: 10.1080/2162402X.2019.1659094

40. Gafita A, Calais J, Grogan TR, Hadaschik B, Wang H, Weber M, et al. Nomograms to Predict Outcomes After (177)Lu-PSMA Therapy in Men With Metastatic Castration-Resistant Prostate Cancer: An International, Multicentre, Retrospective Study. *Lancet Oncol* (2021) 22:1115–25. doi: 10.1016/S1470-2045(21)00274-6
41. El Sharouni MA, Ahmed T, Varey AHR, Elias SG, Witkamp AJ, Sigurdsson V, et al. Development and Validation of Nomograms to Predict Local, Regional, and Distant Recurrence in Patients With Thin (T1) Melanomas. *J Clin Oncol* (2021) 39:1243–52. doi: 10.1200/JCO.20.02446

Conflict of Interest: The authors declare that the research was conducted in the absence of any commercial or financial relationships that could be construed as a potential conflict of interest.

Publisher's Note: All claims expressed in this article are solely those of the authors and do not necessarily represent those of their affiliated organizations, or those of the publisher, the editors and the reviewers. Any product that may be evaluated in this article, or claim that may be made by its manufacturer, is not guaranteed or endorsed by the publisher.

frontiers | Frontiers in Immunology

REVIEW
published: 14 July 2022
doi: 10.3389/fimmu.2022.927265

Combination Approaches to Target PD-1 Signaling in Cancer

Emily K. Moore[1,2]*, *Marianne Strazza*[1,2] *and Adam Mor*[1,2,3]*

[1] Division of Rheumatology, Department of Medicine, Columbia University Medical Center, New York, NY, United States, [2] Columbia Center for Translational Immunology, Columbia University Medical Center, New York, NY, United States, [3] Herbert Irving Comprehensive Cancer Center, Columbia University Medical Center, New York, NY, United States

Cancer remains the second leading cause of death in the US, accounting for 25% of all deaths nationwide. Immunotherapy techniques bolster the immune cells' ability to target malignant cancer cells and have brought immense improvements in the field of cancer treatments. One important inhibitory protein in T cells, programmed cell death protein 1 (PD-1), has become an invaluable target for cancer immunotherapy. While anti-PD-1 antibody therapy is extremely successful in some patients, in others it fails or even causes further complications, including cancer hyper-progression and immune-related adverse events. Along with countless translational studies of the PD-1 signaling pathway, there are currently close to 5,000 clinical trials for antibodies against PD-1 and its ligand, PD-L1, around 80% of which investigate combinations with other therapies. Nevertheless, more work is needed to better understand the PD-1 signaling pathway and to facilitate new and improved evidence-based combination strategies. In this work, we consolidate recent discoveries of PD-1 signaling mediators and their therapeutic potential in combination with anti-PD-1/PD-L1 agents. We focus on the phosphatases SHP2 and PTPN2; the kinases ITK, VRK2, GSK-3, and CDK4/6; and the signaling adaptor protein PAG. We discuss their biology both in cancer cells and T cells, with a focus on their role in relation to PD-1 to determine their potential in therapeutic combinations. The literature discussed here was obtained from a search of the published literature and ClinicalTrials.gov with the following key terms: checkpoint inhibition, cancer immunotherapy, PD-1, PD-L1, SHP2, PTPN2, ITK, VRK2, CDK4/6, GSK-3, and PAG. Together, we find that all of these proteins are logical and promising targets for combination therapy, and that with a deeper mechanistic understanding they have potential to improve the response rate and decrease adverse events when thoughtfully used in combination with checkpoint inhibitors.

Keywords: T cell, PD-1, SHP2, ITK, PD-L1

OPEN ACCESS

Edited by:
Xuyao Zhang,
Fudan University, China

Reviewed by:
Avery August,
Cornell University, United States
Lele Zhu,
University of Texas MD Anderson Cancer Center, United States

***Correspondence:**
Emily K. Moore
ekm2150@cumc.columbia.edu
Adam Mor
am5121@columbia.edu

Specialty section:
This article was submitted to Cancer Immunity and Immunotherapy, a section of the journal Frontiers in Immunology

Received: *24 April 2022*
Accepted: *23 June 2022*
Published: *14 July 2022*

Citation:
Moore EK, Strazza M and Mor A (2022) Combination Approaches to Target PD-1 Signaling in Cancer. Front. Immunol. 13:927265. doi: 10.3389/fimmu.2022.927265

INTRODUCTION

Cancer immunotherapies represent an emergent yet powerful therapeutic paradigm, due to both their durable clinical responses and their applicability to a wide variety of tumors. Immune checkpoint therapies block inhibitory receptors on T cells, augmenting anti-tumor immune responses. Programmed cell death protein 1 (PD-1) is a critical inhibitory checkpoint for T cells, and antibodies that block ligand binding free the T cells to identify and clear malignant tumor cells. As

such, PD-1 is the subject of significant testing, with 786 completed and 4,897 ongoing clinical trials targeting it (1). Despite the striking success of these antibodies, most patients do not respond to PD-1 blockade, and many experience immune-related adverse events (irAEs) (2). Moreover, new studies indicate that 5-10% of patients demonstrate accelerated cancer progression after anti-PD-1 treatment, contrary to predicted responses based on current mechanistic models (3). Given such significant successes and failures, a better understanding of how to target the PD-1 signaling pathway is needed. Understanding the underlying mechanisms of clinical responses will promote development of more nuanced pathway-based therapeutics.

A recent publication summarized that 4,062 out of 4,897 ongoing immunotherapy trials are testing PD-1 inhibition in combination regimens with other immunotherapies, targeted therapies, chemotherapies, and radiotherapies (1). Of these combination approaches, immunotherapies lead the space with 1,058 trials, and targeted therapies closely follow with 1,008 trials. The number of monotherapy trials continues to decrease, with less than 20% of active trials using monotherapies against PD-1 or PD-L1, a trend consistent with previous updates (4).

As anti-PD-1 clinical trials continue to move towards combination strategies, we describe in this work effector proteins that are associated with PD-1 downstream signaling and function in T cells: SHP2, ITK, VRK2, PTPN2, GSK-3, CDK4/6, and PAG (**Figure 1**). Through exploring their complex mechanistic involvement in T cell anti-tumor responses, we analyze their promise as therapeutic targets in combination with PD-1 blockade. As many of the potential targets are also expressed in tumor cells, we also consider the therapeutic impact within the tumor cell, but mainly focus on the promise of logically designed T cell intrinsic combination approaches.

PD-1 SIGNALING

To become fully activated, T cells require at least two signals: engagement of the T cell receptor (TCR) by peptide-loaded

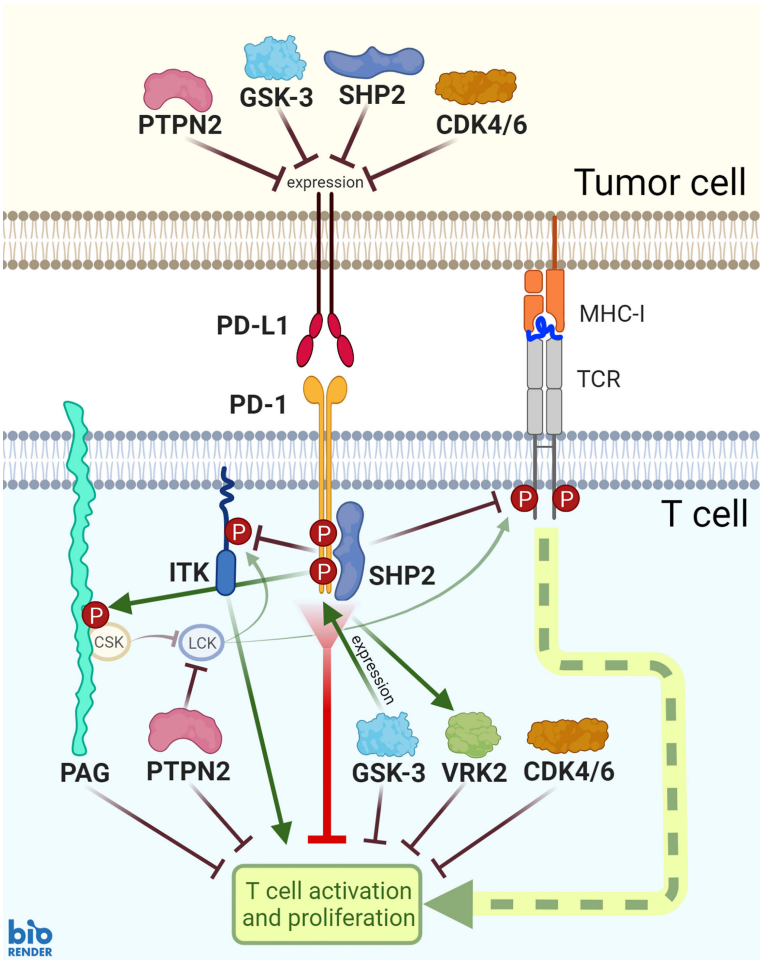

FIGURE 1 | PD-1 functions and PD-L1 expression are mediated by SHP2, PTPN2, PAG, ITK, GSK-3, VRK2, and CDK4/6 signaling. SHP2 is recruited downstream of PD-1 ligation and mediates a number of subsequent signaling events. Additionally, PD-1 ligation is associated with enhanced activity of inhibitory proteins PAG and VRK2 and inhibition of ITK. GSK-3 activates transcription factors to induce PD-1 expression; while GSK-3, PTPN2, SHP2, and CDK4/6 inhibit PD-L1 expression.

major histocompatibility complex (MHC), and co-receptor interactions with ligands on antigen-presenting cells (APC) (5). T cells display a dynamic and complex network of stimulatory and inhibitory co-receptors. Among these, inhibitory receptors provide signals that terminate immune responses and restore homeostasis (6). We discovered that the mechanism by which the co-receptors CTLA-4 and CD28 modulate T cell adhesion is through recruitment of calcium-promoted Ras inactivator (CAPRI) (7). We also reported that engagement of the inhibitory receptor PD-1 by its ligands inhibits Rap1 activation and LFA-1-mediated adhesion (8).

PD-1 is a monomeric transmembrane protein consisting of 288 amino acids, with a single extracellular IgV domain, followed by a transmembrane region and a cytoplasmic tail (9). Despite extensive use of anti-PD-1 antibodies in the clinic, available data on the signaling pathways downstream of this receptor are limited. Because PD-1 does not have direct enzymatic function, it instead serves as a scaffold for other proteins that mediate downstream inhibitory functions (10). Following T cell antigen recognition, PD-1 surface expression is increased, allowing it to bind to its ligands, programmed death ligand 1 (PD-L1) and programmed death ligand 2 (PD-L2) (11). PD-1 then recruits SH2-containing tyrosine phosphatase SHP2. Through mutational analysis of the PD-1 cytoplasmic tail, it has been shown that phosphorylation of the tyrosine within the immunoreceptor tyrosine-based switch motif (ITSM; TXpYXXV/I) following ligand binding recruits SHP2 (12–14); however, for full enzymatic activity, SHP2 must unfold into its active conformation. This is enhanced by phosphorylation of PD-1's immunoreceptor tyrosine-based inhibitory motif (ITIM; V/L/I/XpYXX/L/V) (13).

After PD-1 binds PD-L1 or PD-L2 and recruits and activates SHP2, this phosphatase then dephosphorylates proteins critical for TCR signaling, such as CD3, ZAP70, and C3G (15). Despite the structural similarity between SHP1 and SHP2, only the latter is recruited to the tail of PD-1 (13). Further, the full mechanism connecting PD-1 engagement with SHP2 enzymatic activation remains largely unknown, and is an important area of ongoing research, as is identification of the PD-1 associated substrates of SHP2 (16, 17).

SHP2

Src homology domain-2 (SH2)-containing protein tyrosine phosphatase 2 (SHP2; PTPN11) is a non-receptor tyrosine phosphatase that is expressed in the cytoplasm of cells throughout the body (18). The SHP2 protein is composed of two tandem SH2 domains, a protein tyrosine phosphatase (PTP) domain, and a hydrophobic tail with two tyrosine phosphorylation sites (19). In the inactive state, the proximal SH2 domain is folded onto the PTP site in a closed, autoinhibitory conformation. SHP2 binds to its targets with its SH2 domains, and engagement of both SH2 domains results in highest enzymatic function (20).

SHP2 is recruited to many signaling cascades and plays a role in diverse functions, from proliferation to migration (21). It also plays a role in many diseases, with mutations associated with Noonan syndrome, LEOPARD syndrome, and childhood leukemia (22, 23). Beyond this, SHP2 is implicated in many essential pathways of cancer cells, including proliferation, metastasis, and drug resistance. As such, it has been linked to many gastrointestinal, respiratory, blood, and other cancers, and has drawn attention as a potential therapeutic target (24).

T Cells

SHP2 is recruited to many important signaling cascades, including those downstream of TCR and PD-1 ligation. The signaling pathways downstream of PD-1 that result in the inhibition of T cell functions remain poorly understood (25), but the need for SHP2 in mediating PD-1 function is perhaps the most well-known aspect of PD-1 biology. SHP2 is thought to mediate PD-1 inhibition of T cell function by dephosphorylating tyrosines within the TCR complex to inhibit downstream cascades, including the co-stimulatory receptor CD28 (26). However, SHP2 also plays a critical – and possibly opposing – role in supporting TCR-mediated T cell activation. In this context, SHP2 is considered a positive regulator of T cell activation, using dephosphorylation to turn on positive T-cell regulators (e.g. AKT, ERK) and turn off negative T cell regulators (e.g. CSK, CRK and PAG) (27–30). This paradigm identifies the same SHP2 enzyme serving as a key mediator of two pathways that have opposing functions. There are multiple proposed models explaining how this is executed within the cell. The temporal segregation model proposes that because PD-1 expression is induced only after activation of the TCR, SHP2 first acts downstream of the TCR during the early phase of T cell activation, and transitions to the PD-1 pathway at a later stage of T cell activation after PD-1 expression is increased (31). An alternative model is differential substrate targeting. This model explains that SHP2 has different targets downstream of the TCR and PD-1, and in this way mediates different cellular functions (28, 32). To better resolve the complexity between TCR and PD-1 signalosomes, we need to continue efforts to determine both shared and unique molecular partners and signaling mechanisms involving SHP2, and to identify SHP2 substrates within each of these pathways. The answers to these questions have the potential for significant clinical impact as they may explain the confounding results coming out of clinical trials with SHP2 inhibitors.

Therapeutic Targeting

New promise for therapeutic targeting of SHP2 may lie in combined inhibition of SHP2 and PD-1. A study of methylene blue, a chemical with FDA approval for the treatment of methemoglobinemia, found that it inhibits PD-1 signaling by interfering with SHP2 binding, and interferes with tumor allograft growth (33). Importantly, this work demonstrates that interfering with the mediators of PD-1 signaling can have a favorable impact on tumor progression, and is a valid therapeutic strategy.

Interestingly, it is the activity of SHP2, rather than its expression level, that contributes to the expression of PD-L1 on tumor cells (34). In turn, the expression of PD-L1 correlates with tumor response to immune checkpoint inhibitors in non-

small cell lung cancer (NSCLC) (34). This suggests that current allosteric inhibitors of SHP2 activity may enhance anti-PD-1 efficacy. The fact that a majority of patients with NSCLC do not respond to immune checkpoint inhibitor monotherapy makes it an attractive model for the study of these combinations (35). In a mouse model of anti-PD-1-resistant NSCLC, the triple therapy of anti-PD-1, the oral SHP2 inhibitor SHP099, and radiotherapy had strong anti-tumor effects (36). Similarly, the combined administration of anti-PD-1 antibody and SHP099 had a greater anti-tumor effect than either therapy individually in two murine colon cancer xenograft models (37).

The contribution of SHP2 to PD-1 signaling in T cells was most directly studied in a T cell confined SHP2 knockout (KO) mouse study that found no effect on controlling tumor growth or on the efficacy of PD-1 antibodies, likely due to the impact on SHP2's role in both T cell activating and inhibitory pathways. The T cell SHP2 KO also did not impact the efficacy of PD-1 antibodies, implying that alternative phosphatases may be recruited to PD-1 in the absence of SHP2 (38). Importantly, this leaves open the potential for an additive effect of SHP2- and PD-1- targeting combination therapy strategies.

There are currently 30 trials on ClinicalTrials.gov testing SHP2 inhibitors in cancer patients. Within these trials, there are 11 SHP2 inhibitors being tested, most commonly TNO155, and sodium stibogluconate (a drug primarily used for Leishmaniasis). Five trials are testing SHP2 inhibitors in combination with anti-PD-1 biologics, all of which are still recruiting and have no available results.

SHP2 is an exciting therapeutic target for combination strategies in cancer. SHP2 is known to be pro-oncogenic in many cancers and simultaneously involved in the inhibitory PD-1 pathway in T cells. Thus, intervention with SHP2 inhibitors might concomitantly inhibit cancer cells and activate the anti-tumor immune response. Combination with anti-PD-1/PD-L1 biologic agents is a particularly intriguing area of work since they have overlapping but non-redundant functions. Better yet, SHP2 inhibitors *in vivo* enhance response to anti-PD-1 therapy through PD-L1 upregulation. This would expand the percentage of patients that may respond to anti-PD-1 therapeutic mechanisms. Further, since SHP2 also plays a role in T cell activation, SHP2 inhibitors might help avoid immune related adverse events seen with anti-PD-1 antibody therapy.

ITK

IL-2 inducible T cell kinase (ITK) is a member of the TEC family of kinases with particular importance in T cells. The other members of the protein family are Tec, BTK, BMX, and RLK (39). All TEC kinases include a Tec homology (TH) domain with a zinc binding region and proline rich regions. From N to C termini, ITK includes an N-terminal PH domain, a TH domain, and three SH catalytic domains (39). Unlike other family members, ITK is expressed only in T cells, NK cells, NKT cells, and mast cells (40, 41). ITK deficiency results in susceptibility to severe infections with Epstein Barr virus (EBV) (42).

Tumor Cells

ITK is highly expressed not just in normal T cells, but also in T cell associated malignancies (43). Genetic and pharmacological inhibition of ITK compromises the proliferation, adhesion, invasion, and migration of malignant T cells, which position this kinase as a target for the treatment of primary T cell tumors (43). The promise of targeting ITK in cancer is bolstered by the growing success of targeting protein family member BTK, which plays a similar role in B cells and B cell tumors. BTK has been found to regulate cell proliferation, survival, and migration in various B cell malignancies. Targeting BTK with recently developed BTK inhibitors has been approved by the FDA to treat several B cell malignancies (44). Recent studies have established also that BTK is expressed and plays pro-tumorigenic roles in several epithelial cancers (45).

T Cells

ITK plays a modulatory role in TCR signaling. Unlike ZAP70 and LCK, ITK is not an obligate component of the TCR cascade. Instead, ITK functions as a fine-tuning dial, to translate variations in TCR signal strength into differential programs of gene expression (46). Upon T cell activation, a series of signaling events lead to the recruitment of ITK to the cell membrane in the vicinity of the primed TCR, where it is phosphorylated by LCK on Tyr 512. This leads to ITK autophosphorylation of Tyr 180 and to subsequent downstream phosphorylation of PLCγ1 and LAT, and NFAT translocation into the nucleus (47). Consequently, it was shown *in vivo* that ITK is not required for TCR signaling (48). In the absence of ITK, some aspects of T cell activation appear normal, whereas other T cell functions are impaired. Further, studies in ITK knockout mice show that T cell function is impaired but not entirely blocked (49, 50), a finding that is consistent with a modulating role for ITK, rather than an all-or-nothing molecular switch.

In addition to its role in TCR signaling, ITK is also an important kinase in the PD-1 pathway. Through a phosphoproteomic study, we found ITK mediates many phosphorylation events downstream of PD-1 ligation (10). Using genetic and pharmacological approaches, we then discovered that SHP2 dephosphorylates ITK specifically downstream of PD-1 and that this event is associated with PD-1 function (17). Notably, SHP2 only dephosphorylates ITK in its role downstream of PD-1 signaling. Since ITK is a SHP2-dependent specific mediator of PD-1 signaling, the combination of ITK inhibitors with PD-1 blockade may improve upon PD-1 monotherapy in the treatment of cancer.

Therapeutic Targeting

Ibrutinib is an approved therapy for B cell malignancies that covalently inhibits both BTK and ITK (51). In a recent study, blood samples collected from leukemia patients treated with ibrutinib monotherapy showed downregulated PD-L1 expression on the leukemic cells. Further, the same analysis showed that this was mediated through inhibition of STAT3. Similarly, downregulation of PD-1 expression was observed in the CD4 and CD8 T cells. Taken together, these findings provide

the mechanistic basis for immunomodulation by ibrutinib through inhibition of the STAT3 pathway, a critical pathway in inducing and sustaining tumor immune tolerance. This data also merits testing of combination treatments combining ibrutinib with immune checkpoint inhibitors (52).

Indeed, a published study reported that the combination of anti-PD-L1 antibody and ibrutinib suppressed tumor growth in mouse models of lymphoma that were intrinsically insensitive to ibrutinib (53). The combined effect of these two agents was also documented in mice models of triple negative breast cancer and colon cancer. The enhanced therapeutic activity of PD-L1 blockade by ibrutinib was accompanied by enhanced anti-tumor T cell immune responses. This study suggested that the combination of PD-1 or PD-L1 blockade and ibrutinib should be tested in the clinic for the therapy not only of lymphoma but also in solid tumors that do not even express BTK or ITK (53). Similarly, a study using the Eμ-TCL1 adoptive transfer mouse model of chronic lymphocytic leukemia (CLL), observed that combination of ibrutinib with blocking antibodies targeting the PD-1 or PD-L1 axis *in vivo* improved CD8 T cell effector function and control of lymphocyte proliferation (54). This study suggested that the strong immunomodulatory effects of ibrutinib and its combination with immune checkpoint blockade was a promising approach to treat CLL (54).

Regulatory T cells (Tregs) play an important role in controlling autoimmunity and limiting tissue damage and inflammation. It was shown that either genetic ablation of ITK or inhibition of ITK pharmacologically results in increased number of Tregs (55, 56). This was shown to avert the formation of acute graft-versus-host disease *in vivo*, in part by reducing T cell proliferation and cytokine production. More interestingly, disrupting the SLP76—ITK interaction using a specific peptide inhibitor led to enhanced Treg development in both mouse and primary human cells. Thus, it was suggested that targeting ITK could be a therapeutic strategy to treat not just autoimmunity, but also immune related toxicity of PD-1 blockade (57). Altogether, while additional studies are needed to clarify the impact of treating cancer with a combination of PD-1 blockade and ITK/BTK inhibitors, this possibility is mechanistically promising and clinically feasible with current approved drugs.

VRK2

Vaccinia-related kinase 2 (VRK2) is a serine/threonine kinase that in humans is encoded by the VRK2 gene (58). It is a member of the VRK family, which includes VRK1, VRK2, and VRK3 (59). VRK2 is widely expressed in human tissues and has increased expression in actively dividing cells, such as leukocytes and carcinomas (60). VRK2 has two splice forms, VRK2A and VRK2B. The VRK2A isoform is much more common, and includes a C-terminal hydrophobic tail that tethers it to organelles like the endoplasmic reticulum and mitochondria (61). The rarer isoform, VRK2B, lacks a hydrophobic tail and is found in the nucleus and cytoplasm (61). Among other targets, VRK2 modulates several MAPK signaling pathways through target phosphorylation and impacting the composition of signaling complexes (62).

Tumor Cells

VRK2 is most highly expressed in cells undergoing division, and is therefore present in notable amounts in some cancer cells (63). High VRK2 expression levels are associated with unfavorable prognosis in renal, liver, and pancreatic cancers (63, 64). In pancreatic cancer, VRK2 phosphorylates and stabilizes cell cycle kinase Plk1, resulting in Plk1 overexpression to facilitate pancreatic cancer proliferation and chemotherapy resistance (65). Similarly, pediatric and adult gliomas and neuroblastomas require either VRK1 or VRK2, which have overlapping but essential pro-survival function in these cancers (66). In breast cancer, VRK2 has been found to facilitate tumor cell invasion through phosphorylating transcription factor NFAT1 to increased COX2 expression (60). COX2 is associated with invasive breast cancer, metastasis, and poor prognosis (67, 68). VRK2 is also thought to be protective against apoptosis (69). In contrast, another study found that low VRK2 levels are associated with the abnormal MEK/ERK signaling seen in breast cancer; thus, VRK2 has a complex signaling role in cancer (70).

T Cells

VRK2 has only recently become the subject of study in T cells. Downstream of both TCR and PD-1 ligation, PAK2, a mediator cytoskeleton reorganization, is phosphorylated by VRK2 (71). Thus, VRK2 and PAK2 have conflicting roles downstream of TCR activating signals versus PD-1 inactivating signals; this is analogous to what is known about SHP2 (71). Within the PD-1 pathway, VRK2 mediates one quarter of all the phosphorylation events downstream of PD-1 ligation. In fact, lack of VRK2 activity inhibits PD-1 function, both *in vitro* and *in vivo* (71). The phenotype of VRK2 KO mice is similar to PD-1 KO mice, both presenting with lymphoproliferation and activated T cell subsets. Additionally, in an MC38 murine tumor model, a VRK2 inhibitor AZD-7762 decreased tumor growth in a VRK2-dependent and T cell-dependent manner. When AZD-7762 was used in combination with anti-PD-1 therapy, the mice showed an additive therapeutic impact in terms of tumor growth and final tumor volume (71). Thus, VRK2 acts as an inhibitory kinase that mediates the functions of PD-1 *in vivo*. The fact that a kinase, and not just the phosphatase SHP2, mediates PD-1 function is not just exciting, but also offers opportunities to develop novel kinase inhibitors as an alternative to checkpoint blockades. Though expression of VRK2 is required for PD-1 function, VRK2 has two domains, a kinase domain and a protein-protein docking region, and the contribution of each of the domains to its functions downstream of PD-1 is not completely understood. This knowledge is much needed for better understanding PD-1 signaling and to allow design of optimal VRK2 inhibitors.

Therapeutic Targeting

Because VRK family kinases have a different ATP binding domain structure than other kinases, they are resistant to most current kinase inhibitors. However, studies have noted which inhibitors VRK family proteins are most sensitive to, which is

useful in preclinical studies since high drug concentrations are necessary (58). More importantly, work in 2019 began the development of aminopyridine-based compounds to specifically inhibit VRK1 and VRK2 (72). Fortunately, the unique structure of these kinases means future inhibitors will be specific to VRK family proteins, with little unintended binding to other kinases, making VRK2 a very attractive drug target.

Since VRK2 plays both a pro-tumor role in malignant cells and an inhibitory role in T cells, it has poignant therapeutic potential in cancer. Further, since VRK2 mediates only a subset of PD-1 signaling and also participates in TCR signaling, it has the potential to improve response rates and/or decrease immune related adverse events when used in combination with anti-PD-1 agents, compared to immune checkpoint inhibitor therapy alone.

PTPN2

Protein tyrosine phosphatase non-receptor type 2 (PTPN2, or TCPTP) is a ubiquitously expressed regulator of inflammation. PTPN2 is known to dephosphorylate tyrosine kinases, including JAK1/2/3, SRC family kinases, and STAT1/3/5/6. PTPN2 inhibits pro-inflammatory pathways, including IFN-γ signaling, and mutations in PTPN2 are associated with chronic inflammatory and autoimmune diseases, including type I diabetes and Crohn's disease (73). In contrast, high PTPN2 function is associated with several cancers. PTPN2 levels are high in some gliomas, laryngocarcinoma, and thyroid cancer, with high PTPN2 levels in cancer cells under oxidative stress and inflammatory conditions (74–77). PTPN2 also plays the role of an oncogene in colon cancer by inhibiting the inflammasome (78, 79). In contrast, PTPN2 is likely a tumor suppressor in acute lymphoblastic leukemia (ALL) because it inhibits JAK1, which is oncogenic in ALL, though PTPN2 levels are often low in ALL (80, 81).

T Cells

PTPN2 plays an important role in the development and activation of T cells. PTPN2 knockout mice all died by five weeks of age but showed apparently normal development of CD4 and CD8 T cells (82). However, it is known that PTPN2 dephosphorylates STAT5 in the nucleus to facilitate the transition of precursor cells through the DN2 and DN3 thymocyte differentiation steps to become mature T cells (83). PTPN2 also negatively regulates LCK which, along with STAT5, helps control T cell commitment to alpha/beta versus gamma/delta TCR expression (83). PTPN2 also helps control the T cell activation threshold by dephosphorylating SRC family kinases necessary for functions downstream of TCR ligation (73, 84). Studies *in vitro* and *in vivo* in mice have shown that deletion of PTPN2 in T cells results in enhanced CD8 T cell proliferation and survival, with decreased dependency on pro-survival cytokines like IL-2 and IL-15 (85).

Additionally, PTPN2 is critical for maintaining peripheral tolerance to self-antigens cross-presented on dendritic cells (86). PTPN2 loss of function (LOF) results in systemic autoinflammation in mice, with high systemic cytokines and anti-nuclear antibody levels, supporting the association between PTPN2 LOF and several autoimmune conditions including type I diabetes, Crohn's disease, and Celiac disease (73, 86, 87). PTPN2 has also been shown to play an important role in T cell exhaustion, a state in which chronically stimulated T cells lose their ability to target cancer cells or chronic infections. PTPN2 also reduces type I interferon signaling, leading to a terminally exhausted T cell state. Loss of PTPN2 allows T cells to expand in response to re-stimulation (85). Along with increased proliferation, PTPN2 deficient mice also have enhanced cytotoxicity among Tim-3^+ cells (a marker of the terminally exhausted state), and augmented anti-tumor function, tumor control, and anti-PD-1 responses (88).

Tumor Cells

A CRISPR-Cas9 screen identified PTPN2 deletion to enhance response to anti-PD-1 immunotherapy in a murine tumor model with B16 melanoma cells (89). The PTPN2-null B16 cells had enhanced antigen presentation and increased susceptibility to cytotoxic CD8 T cells (89). PTPN2-null tumors had enhanced CD8 infiltration, and impaired growth in response to IFN-γ (89). An intact JAK/STAT pathway downstream of the IFN-γ receptor on tumor cells induces PD-L1 expression and is critical for response to anti-PD-1 therapy. Since PTPN2 is a negative regulator of JAK/STAT signaling, inhibiting PTPN2 predictably increases responses to anti-PD-L1 therapy in murine melanoma YUMM1.1 cells *in vitro* and *in vivo* (90).

Therapeutic Targeting

Though targeting a phosphatase will include the challenge of developing an inhibitor with appropriate specificity, PTPN2 has proven a promising target. In one study, PTPN2 was targeted by a compound composed of copper-sulfate nano-photothermal materials carrying Cas9 and oligonucleotides to generate a mutation in PTPN2. Its use in mice caused tumor hyperthermia, PTPN2 depletion, increased T cell infiltration into the tumor, and higher intratumoral IFN-γ and TNF-α levels (91). Controlled enhancement of PTPN2 function may be beneficial in autoimmune disease, while targeted inhibition of PTPN2 may help enhance the immune response to cancer. Based on studies with B16 melanoma cells, which typically show resistance to PD-1 therapy, adding a PTPN2 inhibitor to anti-PD-1 regimens may help expand the pool of cancer patients responsive to checkpoint inhibition (88). Yet, because of PTPN2's role in maintaining peripheral tolerance, future therapeutic efforts should consider tumor microenvironment specific targeting and be cognizant of immune related adverse events.

GSK-3

Glycogen synthase kinase 3 (GSK-3) is a ubiquitously expressed serine/threonine kinase and protooncogene (92, 93). GSK-3 has two isoforms, GSK-3α and GSK-3β, which have homologous

kinase domains but divergent C-terminal domains, as well as non-redundant functionality (94). GSK-3 activity is controlled by phosphorylation: phosphorylation at Ser 9 inactivates GSK-3β (Ser 21 in GSK-3α), while phosphorylation at Tyr 216 increases GSK-3β activity (Tyr 279 in GSK-3α) (94). With over 100 downstream phosphorylation targets including transcription factors β-catenin, NFκB, NFAT, CREB, c-Jun, and AP1 (92, 95), GSK-3 has been shown to play a role in many cell functions including glycogen and protein metabolism, tumor growth, metastasis, and various immune functions (92, 96–98).

Tumor Cells

GSK-3 has clear pro-tumor actions in many cancers, notably including KRAS-mutant tumors (92). For example, in non-small cell lung cancer (NSCLC), GSK-3β expression is associated with cervical lymph node metastases, poor differentiation, advanced stage, late diagnosis, and worse survival, while inhibiting GSK-3 can result in cancer cell apoptosis and cell cycle arrest (99, 100). *In vivo* models of pancreatic cancer demonstrate an inverse relationship between survival and the nuclear amount of aberrant GSK-3 (93). GSK-3 inhibition in mice by knockout or small molecule inhibitors increases cytotoxicity against viral infections and tumor cell models of gastric cancer (MFC), melanoma (B16), lymphoma (EL-4), colon cancer (MC38), colorectal cancer (CT26), pancreatic cancer (KPC), and lung cancer (LLC) (94, 101–104).

T Cells

Uniquely, GSK-3 is found in the active state in resting T cells. When active, GSK-3 inhibits T cell proliferation and IL-2 production (105, 106). T cell activation through TCR and CD28 ligation results in PI3K/AKT signaling. This pathway phosphorylates and inactivates GSK-3, which increases T-bet expression levels (92). Inactivation of GSK-3 has been shown to be crucial for T cell activation. In fact, GSK-3 inhibition can substitute for CD28 signaling to induce co-stimulation of T cell proliferation (107, 108). Additionally, GSK-3 inhibition with small molecule inhibitor TWS119 has been shown to induce the Wnt/β-catenin pathway to revert CD8 memory T cells into cytotoxic progenitor memory stem cells that can undergo self-renewal (109).

Notably, GSK-3 was also identified as a major regulator of checkpoint protein expression (110). Cells with GSK-3 inhibition through siRNA or small molecule inhibitors show increased T-bet expression in response to TCR stimulation, which inhibits transcription of both PD-1 in CD8 T cells and Tregs, and LAG3 in CD4 and CD8 T cells (101, 111, 112). Consistently, GSK-3β knockout or *in vivo* inhibition in mice results in decreased PD-1 expression in CD8 T cells; increased expression of T-bet, granzyme B, and IFN-γ; enhanced CTL function ex vivo; increased tumor infiltration; and reverted T cell exhaustion in an LCMV model (94, 101, 113). Treatment of CAR-T cells with GSK-3 inhibitors during T cell activation resulted in lower PD-1 levels. These cells showed increased proliferation, decreased exhaustion, and full tumor elimination in a GBM mouse tumor model (114). GSK-3 inhibition also decreases T cell motility and number of cell-cell contacts, but this is overpowered by greatly enhanced cytotoxicity (115).

Therapeutic Targeting

Given its important role in immune function, GSK-3 inhibitors have been tested for their impact on anti-tumor immunity. Preclinical studies found that GSK-3 inhibitors are as effective as anti-PD-1 or anti-PD-L1 antibodies to inhibit tumor growth in mice (101, 103). More importantly, anti-PD-1 and GSK-3 inhibitor combinations may be effective to treat solid tumors that are otherwise unresponsive to immune checkpoint blockade. This is likely because, GSK-3β phosphorylates PD-L1 in tumor cells to induce its degradation, and GSK-3β inactivation can be seen in some cancers to stabilize PD-L1 expression (116, 117). Similarly, inhibiting GSK-3β with the chemotherapy-sensitization combination disulfiram and copper stabilizes PD-L1 expression in a hepatocellular carcinoma model (118). Compared to anti-PD-1 alone, combination therapy with anti-PD-1 plus GSK-3 inhibitors increased the ratio of CD8 effector memory cells to CD4 Tregs within the tumor (119). Additionally, tumor growth is further inhibited when anti-LAG3 antibodies and GSK-3 inhibitors are used in combination in mice. More specifically, anti-LAG3 and GSK-3 inhibitor SB415286 decreased tumor growth and prevented lung metastasis in a murine melanoma model (112). Anti-PD-1 and anti-LAG3 are a promising combination therapy (120), yet in this study, the combination of a GSK-3 inhibitor and anti-LAG3 showed even stronger therapeutic efficacy (112).

GSK-3 inhibitors are particularly promising for their potential ability to both directly inhibit malignant cells and also enhance the immune response (92). Following a number of promising pre-clinical results, there are eighteen clinical trials completed or ongoing using GSK-3 inhibitors as therapy against a wide range of cancers. Several clinical trials do not give a GSK-3 inhibitor directly to the patients, but rather pre-treat NK cells or CAR-T cells with GSK-3 inhibitors to enhance the anti-tumor activity of these lymphocytes for cellular immunotherapy. During generation of anti-CD19-CAR-T cells, culture conditions include IL-21, IL-7, and GSK-3 inhibitor TWS119. Three of the ten patients in this phase I clinical trial showed regression of their B-cell malignancy, and toxicities were mild and did not include graft-versus-host disease (121). NK studies began with ex vivo experiments showing that peripheral NK cells cultured with IL-15 + GSK-3 inhibitor CHIR99021 upregulate CD57 and undergo late-stage maturation into a maximally cytotoxic form (122, 123). CHIR99021-treated NK cells have increased production of TNF-α and IFN-γ and enhanced antibody dependent cellular cytotoxicity (ADCC) *in vitro*. Adoptive cell transfer of these cells into mice resulted in stronger/prolonged control against acute myeloid leukemia and ovarian cancer models (122, 124). From these results, three Phase I clinical trials are underway that use CHIR99021-treated NK cells with IL-2 or chemotherapy for patients with lymphoma or a number of solid organ tumors.

These results suggest that GSK-3 inhibitors may serve as a promising addition to cancer therapeutic strategies. GSK-3 inhibition lacks harmful effects on normal cell and organ

function in rodent studies and has long history of safe use in bipolar disorder (lithium carbonate inhibits GSK-3β activity) (92, 96). Preclinical studies also suggest that GSK-3 inhibitors may help protect against chemotherapy-induced thrombosis and neurotoxicity, and also decrease the development of tolerance to morphine (96). Should GSK-3 combination therapy allow lower dosing of anti-PD-1 agents, there is potential to assuage some anti-PD-1 side effects. With therapeutic mechanisms acting both directly on cancer cells and enhancing immune responses, GSK-3 inhibitors may be an important part of future checkpoint-focused drug combinations.

CDK4 AND CDK6

Cyclin dependent kinase (CDK) 4 and CDK6 are important kinases in the cell cycle. CDK4/6 activity is regulated by tightly controlled levels of cyclin D (125, 126). Cyclin D binds and activates CDK4/6 during G1 of the cell cycle, and together they phosphorylate retinoblastoma protein (RB1) to promote cell cycle progression into S phase through transcription of genes controlled by transcription factor E2F (127). Cyclin D1 and CDK4/6 promote cell cycle progression and prevent cell senescence through activation of transcription factor FOXM1, inactivation of TGFβ-mediator SMAD3, and indirect activation of p53 (128–130). Constitutive activation of the complex of cyclin D and CDK4/6 results in uncontrolled cell proliferation, and has a strong link to many cancers (127).

Tumor Cells

Cyclin D1 is often genetically upregulated *via* chromosomal translocation in mantle-cell lymphoma, multiple myeloma, and plasma cell leukemia, as well as a significant fraction of breast cancers, head and neck, and esophageal squamous cell carcinomas (131, 132). Other cancers overexpress cyclin D1/2/3, CDK4/6, or have lower levels of CDK4/6 inhibitors (127). Mouse studies have shown that overexpression of cyclin D or CDK4/6 increases susceptibility to breast cancer, while ablation induces tumor shrinkage in HER2+ and NSCLC tumor models (133–135). Due to its evident role in proliferation and cancer, several CDK4/6 inhibitors have been generated, including palbociclib and ribociclib, which specifically target CDK4/6, and abemaciclib which targets CDK4/6 and other similar kinases (127). These agents likely directly inhibit CDK4/6, perhaps by preventing the formation of cyclin D-CDK4/6 complexes or potentially decreasing their stability, though lower complex levels are not seen with inhibitor use (136, 137). Abemaciclib most efficiently crosses the blood brain barrier, and effectiveness of these drugs is best predicted by intact RB1 expression in the tumor cells (138, 139). These and other CDK4/6 inhibitors are currently being used in hundreds of clinical trials across a variety of cancer types. Due to results showing increased progression-free and overall survival, palbociclib, ribociclib, and abemaciclib have all been approved for treatment of advanced or metastatic hormone receptor positive breast cancers (127).

T Cells

In addition to impacting the cancer cell, CDK4/6 inhibitors also impact the immune response. CDK4/6 inhibitors help turn "cold" tumors into "hot" tumors. Treatment in mice induced tumor cell release of type III interferons and increased MHC antigen presentation (140). Increased levels of chemokines such as CXCL9 and CXCL10 from CDK4/6 inhibition also drive T cell tumor infiltration (141). Inhibiting CDK4/6 also reduces Treg proliferation to decrease the intra-tumoral Treg/CTL ratio (140). Additionally, CDK4/6 inhibition enhances transcription of genes under control of the transcription factor NFAT. Without CDK4/6 phosphorylation of NFAT, nuclear NFAT levels increase to promote transcription of T cell activating proteins (141). Abemaciclib treatment was specifically found to increase expression of immune checkpoint proteins on T cells, including CD137, PD-L1 and TIM3 (142). Interestingly, regardless of RB1 status, CDK4/6 inhibitors increase PD-L1 expression on tumor cells by decreasing its rate of degradation (143). Consequently, the combination of CDK4/6 inhibitors with anti-PD-1/PD-L1 therapy showed an additive effect in animal tumor models (142). Different studies showed greater benefit with a varied schedule of drug administration, for example delaying the start of anti-PD-L1 drugs until after the start of abemaciclib or vice versa (142, 144). This treatment regimen resulted in enhanced T cell tumor infiltration, increased MHC-I/II expression on tumor cells and APCs, and improved memory formation (142). Further, a combination of a CDK4/6 inhibitor and a PI3K inhibitor significantly improved response to anti-PD-1 or anti-CTLA-4 therapy (145). Uniquely, CDK4/6 inhibitor trilaciclib has been shown to protect normal cells from chemo-related cytotoxicity, including preserving hematopoietic stem cells to decrease myelosuppression, and thus may also be an important contribution to combination therapy (146, 147).

Therapeutic Targeting

Notably, preclinical trials so far have shown an additive effect of combining CDK4/6 inhibitor with checkpoint blockade agents, including anti-PD-1 and anti-PD-L1 (144). Since many tumors may harbor intrinsic resistance to immune checkpoint inhibitors or to CDK4/6 inhibitors, these pre-clinical results are quite promising. The use of CDK4/6 inhibitors could have several benefits to clinical response to immune checkpoint therapy (144). These inhibitors likely decrease intrinsic and acquired resistance, and amongst responders, may show an additive response compared to either therapy alone. Further, this effect may be seen even in tumors intrinsically resistant to CDK4/6 inhibitors, as their effect on PD-L1 expression is independent of RB-status in tumor cells. Accordingly, there are nine trials covering many cancer types that combine immune checkpoint agents with CDK4/6 inhibitors; results from these trials may have immense implications on the future of combination therapy.

PAG

Phosphoprotein associated with glycosphingolipid rich microdomains 1 (PAG) is an inhibitory transmembrane

protein that is highly expressed on leukocytes, monocytes, and lymphocytes. PAG has a 16 amino acid extracellular domain and a 397 amino acid cytoplasmic tail with ten tyrosine phosphorylation sites (148). Despite being transmembrane, PAG has no known binding partners (149). PAG is palmitoylated to induce localization within the lipid-rich regions of the membrane, along with many important signaling proteins involved in TCR signal transduction and modification (148, 150–152). Consistently, PAG is recruited to the synapse upon immune synapse formation (153). PAG is a member of the family of transmembrane adaptor proteins (TRAPs) and helps organize signaling through the recruitment of cytosolic kinases and phosphatases (150, 154). PAG also has a C-terminal PDZ domain that binds to EBP50, a protein which connects to actin *via* Ezrin (150, 155–157). PDZ domain proteins are important in immune synapse formation and function (158). Actin is a major cytoskeletal protein essential for many cellular functions, including synapse formation (159). Therefore, PAG likely serves as a link between actin and other lipid-raft proteins important for immune synapse signaling.

T Cells

In resting T cells, SRC-phosphorylated PAG recruits the inhibitory tyrosine-protein kinase CSK to lipid rich signaling complexes, which results in inactivation of lymphocyte-specific protein tyrosine kinase (LCK) to prevent signaling through the TCR (148, 154, 160, 161). Upon TCR signaling, PAG is dephosphorylated by PTP1B and releases inhibitory CSK for successful TCR signaling (160). CSK is also a negative regulator of c-SRC, a membrane-anchored tyrosine kinase and proto-oncogene (162). PAG also regulates localization of SRC family kinases FYN and LYN, impacting their signaling (163). Thus, PAG is important in regulating the clustering of synapse-related signaling molecules. Multiple studies showed that overexpression of PAG leads to T cell inhibition, while deleting PAG leads to T cell activation. We confirmed these findings and also showed that reduced tumor size in PAG KO mice was associated with increased T cell activity (153). Similarly, Veillette et al. reported recently that T cells from PAG KO mice had increased resistance to T cell anergy (164). PAG KO mice also demonstrate augmented T cell autoimmunity after challenge (such as MOG in EAE model), suggesting that the importance of PAG-mediated negative regulation is apparent under particular types of immune responses (165).

PAG is a mediator of PD-1 signaling. Phosphorylation of PAG is required for the full strength of PD-1 on many T cell effector functions, including cytokine production, adhesion, activation, and TCR signaling. Further, the phosphorylation status of PAG's many tyrosine phosphorylation sites mediate various PD-1 functions. In the murine MC38 colon adenocarcinoma and B16 melanoma tumor models, our lab showed that PAG KO mice have limited tumor growth and enhanced response to anti-PD-1 treatment (153). This correlated with increased infiltration of both CD4 and CD8 T cells into MC38 tumors in PAG KO mice and enhanced cytotoxicity of PAG KO murine T cells *in vitro* (153). Consistently, patient data shows that high PAG levels are more common among patients who do not respond to anti-PD-1 therapy (153).

Tumor Cells

Patient data shows that higher expression of wild-type PAG is associated with worse outcomes in many cancers, including breast cancer, cervical squamous cell carcinoma, head and neck squamous cell carcinoma, liver hepatocellular carcinoma, uterine corpus endometrial carcinoma, and lung adenocarcinoma (153, 166). High PAG expression also induces resistance to radiotherapy in laryngeal carcinoma (167, 168).

Therapeutic Targeting

Therapeutic intervention targeting PAG could take the form of an inhibitory antibody or a compound to change expression level. The anti-inflammatory/vasodilatory drug pentoxifylline has been shown to decrease PAG expression levels in T cells (169). Because PAG is a transmembrane protein, it can be targeted by the same approach used in traditional immunotherapy – development of an antibody to bind and inhibit signaling. While all other antibodies in therapeutic use inhibit ligand binding, PAG has no known ligand. Instead, binding PAG with a bulky antibody may displace PAG outside of the narrow immune synapse away from sites of TCR and PD-1 signaling. Because of the importance of the subcellular localization of signaling complexes and the complexity of healthy synapse formation in T cell responses, PAG is a strong candidate for therapeutic targeting. We have generated and begun testing an anti-PAG antibody in murine MC38 and B16 tumor models, with promising results.

As a mediator of PD-1 signaling, PAG serves as a new, perhaps more nuanced target for cancer immunotherapy. Combining anti-PD-1 therapy with antibodies or other compounds targeting PAG will likely further impede inhibitory signaling in T cells, *via* PD-1-related and unrelated mechanisms. Together, this combination therapy might better release T cells to continue targeting chronic antigens, such as in cancer, to improve response rates and avoid PD-1 associated adverse events.

CONCLUSIONS

With the remarkable success of anti-PD-1 therapy limited to a fraction of patients, the field is actively working to identify and test new T cell targets to extend the benefits of immunotherapy to a larger group of cancer patients while reducing chances of immune related adverse events. In response, an increasing number of cancer clinical trials include combinations of checkpoint inhibitors and other immunotherapies, targeted therapies, or other therapeutic techniques (4). Ongoing trials show promise for many cancers that have historically not responded to anti-PD-1/PD-L1 monotherapy. However, the number of current PD-1 combination clinical trials is so staggering that trials are competing for patients (1). One way to thin out the number of unsuccessful future trials is to strive for stronger pre-clinical evidence of a new target's promise before bringing a new combination strategy to patient trials. This might

begin with additional mechanistic and translational studies that elucidate signaling pathways to understand the interplay between two proteins of interest. If we understand the signaling relationship between two proteins within immune cells and target cells, researchers can more logically select target combinations with the most promise to enhance responses and/or decrease side effects. In this review, we highlighted a number of promising kinases, phosphatases, and adaptor

TABLE 1 | SHP2, ITK, VRK2, PTPN2, GSK-3, CDK4/6, and PAG all have evidence supporting their relationship to the PD-1 pathway in T cells and pro-tumorigenic role in cancer cells.

	Protein class	Role in PD-1 pathway in T cells ^	Cancer cell intrinsic tumorigenic function ^	Cancer types discussed here	Number of Cancer clinical trials*	Cancer types in clinical trials *	Inhibitors approved or in clinical trial *	Clinical trials with anti-PD-1/PD-L1 *
SHP2	Phosphatase	Chemnitz et al., 2004 (27) Sheppard et al., 2004 (32) Fan et al., 2020 (33)	Niihori et al., 2005 (23) Zhang et al., 2015 [review] (24)	Childhood leukemia, GI and respiratory tumors, NSCLC	30	For trials with ICB: NSCLC, head/neck and esophageal SCC, GI stromal cancer, CRC, KRAS mutant solid tumors	TNO155, sodium stibogluconate, RMC-4630, JAB-3312, JAB-3068, RLY-1971, BBP-398, HBI-2376, ERAS-601, SH3809, GDC-1971, ET0038, HS-10381, BPI-442096	NCT04720976, NCT04418661, NCT04721223, NCT04699188, NCT04000529
ITK	Kinase	Strazza et al., 2021 (17)	Lechner et al., 2020 [review] (43)	Leukemias, lymphomas, breast cancer (model), colon cancer (model)	> 300	Lymphomas, leukemias, MDS, multiple myeloma, aplastic anemia, RAEB-T, SCLC, CRC, melanoma, head/neck SCC, glioblastoma;, kidney, breast, prostate, gastro-esophageal, lung, and pediatric brain cancers	Ibrutinib, CPI-818	N/A
VRK2	Kinase	Peled et al., 2021 (71)	Vazquez-Cedeira et al., 2012 (60, 64–68)	Renal cancer, liver cancer, pancreatic cancer, glioma, neuroblastoma, breast cancer, colon cancer (model)	0	N/A	N/A	N/A
PTPN2	Phosphatase	Manguso et al., 2017 (89)	(74–79) TS (80, 81):	Glioma, laryngocarcinoma, thyroid cancer; ALL (TS), melanoma (model)	0	N/A	N/A	N/A
GSK-3	Kinase	Steele et al., 2021 (94) Taylor et al., 2016 (101) Taylor et al., 2018 (103) Pokhrel et al., 2021 (111)	Domoto et al., 2020 [review] (96) Alves et al., 2021 (99) Zeng et al., 2014 (100)	KRAS mutant cancers, NSCLC, GBM (model), HCC (model), CRC (model), pancreatic cancer (model), lymphoma (model), melanoma (model), gastric cancer (model)	18	Lymphomas, leukemias, sarcoma, glioma, neuroblastoma, adenoid cystic carcinoma, meningioma, SCLC, CRC, neuroendocrine tumor; pancreatic, renal, bone, breast, lung, salivary gland, esophageal, prostate, thyroid, and stomach cancers	TWS119, lithium carbonate, CHIR99021, 9-ING-41, LY2090314	N/A
CDK4 CDK6	Kinase	Schaer et al., 2018 (142) Jerby-Arnon et al., 2018 (144)	Wang et al., 1994 (133) Landis et al., 2006 (134) Puyol et al., 2010 (135)	Mantle-cell lymphoma, multiple myeloma, plasma cell leukemia, breast cancer, head/neck and esophageal SCC	> 300	For trials with ICB: melanoma, pancreatic cancer, breast cancer, head/neck SCC, NSCLC, mesothelioma, liposarcoma, GI cancers	Ribociclib, palbociclib, abemaciclib, Trilaciclib, lerociclib, SHR6390, PF-06873600, FNC-437, Birociclib, HS-10342, CS3002	NCT02791334, NCT03292250, NCT03386929, NCT03654833, NCT03805399, NCT04213404, NCT04360941, NCT04438824, NCT05139082
PAG	Trans-membrane adaptor	Strazza et al., 2021 (153)	Lu et al., 2017 (166) Dong et al.,	Breast cancer, head/neck and cervical SCC, HCC, lung	0	N/A	N/A	N/A

(Continued)

TABLE 1 | Continued

Protein class	Role in PD-1 pathway in T cells ^	Cancer cell intrinsic tumorigenic function ^	Cancer types discussed here	Number of Cancer clinical trials*	Cancer types in clinical trials *	Inhibitors approved or in clinical trial *	Clinical trials with anti-PD-1/PD-L1 *
		2018 (167) Shen et al., 2018 (168)	adenocarcinoma, uterine corpus endometrial carcinoma, CRC and melanoma (model)				

Four of these proteins are already targeted in cancer clinical trials, two of which are also being studied in combination with immune checkpoint blockade.
^Papers establishing these findings.
**Trials on clinical trials.gov at the time of publication.*
GI, gastrointestinal; NSCLC, non-small cell lung cancer; ALL, acute lymphocytic leukemia; HCC, hepatocellular carcinoma; CRC, colorectal carcinoma; SCC, squamous cell carcinoma; MDS, myelodysplastic syndrome; RAEB-T, Refractory Anemia With Excess Blasts in Transformation; TS, tumor suppressor. N/A is not available.

proteins with strong mechanistic evidence supporting their use in combination with anti-PD-1/PD-L1 agents.

Combinational approaches could take many forms. A target downstream of PD-1 ligation has the potential to maintain or improve therapeutic effects, or to assuage negative side effects of anti-PD-1 therapy. A new drug along this pathway may amplify or substitute anti-PD-1 in combinational approaches (**Figure 1**). Substitute PD-1-pathway targets would allow pairing with drugs that target alternative complementary pathways. Combination therapy could also be used to increase the PD-L1 expression on tumor cells. Inducing PD-L1 expression increases tumor responsiveness to concurrent or subsequent anti-PD-1/PD-L1 therapy. The signaling of GSK-3, PTPN2, SHP2, and CDK4/6 all decrease PD-L1 expression on tumor cells (**Figure 1**). Thus, if a therapeutic strategy includes an inhibitor against one of these four kinases or phosphatases, it may best be used in combination with an anti-PD-1 agent.

Preclinical trials have already shown an enhanced response to anti-PD-1 agents when used alongside therapeutic inhibition or genetic deletion of all targets discussed here: SHP2, ITK, VRK2, PTPN2, GSK-3, CDK4/6, and PAG (**Table 1**). Yet, additional mechanistic understanding of new targets is essential to avoid unintended side effects including maladaptive impact on the tumor microenvironment. This includes considering the impact on various cell subsets, such as Tregs, tumor immunogenicity, and tumor immune infiltration.

To address the currently limited response to checkpoint inhibitor therapy, combinational approaches already show great promise. With continued translational studies to further analyze PD-1 signaling, combinational strategies can improve response rates while mitigating adverse effects in cancer immunotherapies.

AUTHOR CONTRIBUTIONS

EM, MS, and AM designed, wrote, and edited the manuscript. All authors contributed to the article and approved the submitted version.

FUNDING

This work was supported by grants from the NIH (AI125640, CA231277, AI150597).

REFERENCES

1. Upadhaya S, Neftelinov ST, Hodge J, Campbell J. Challenges and Opportunities in the PD1/PDL1 Inhibitor Clinical Trial Landscape. *Nat Rev Drug Discov* (2022). doi: 10.1038/d41573-022-00030-4
2. Sandigursky S, Mor A. Immune-Related Adverse Events in Cancer Patients Treated With Immune Checkpoint Inhibitors. *Curr Rheumatol Rep* (2018) 20(10):65. doi: 10.1007/s11926-018-0770-0
3. Liu X, Qiao L. Hyperprogressive Disease in Malignant Carcinoma With Immune Checkpoint Inhibitor Use: A Review. *Front Nutr* (2022) 9:810472. doi: 10.3389/fnut.2022.810472
4. Upadhaya S, Neftelino ST, Hodge JP, Oliva C, Campbell JR, Yu JX. Combinations Take Centre Stage in PD1/PDL1 Inhibitor Clinical Trials. *Nat Rev Drug Discov* (2021) 20(3):168–9. doi: 10.1038/d41573-020-00204-y
5. Bretscher PA. A Two-Step, Two-Signal Model for the Primary Activation of Precursor Helper T Cells. *Proc Natl Acad Sci USA* (1999) 96(1):185–90. doi: 10.1073/pnas.96.1.185
6. Schnell A, Bod L, Madi A, Kuchroo VK. The Yin and Yang of Co-Inhibitory Receptors: Toward Anti-Tumor Immunity Without Autoimmunity. *Cell Res* (2020) 30(4):285–99. doi: 10.1038/s41422-020-0277-x
7. Strazza M, Azoulay-Alfaguter I, Dun B, Baquero-Buitrago J, Mor A. CD28 Inhibits T Cell Adhesion by Recruiting CAPRI to the Plasma Membrane. *J Immunol* (2015) 194(6):2871–7. doi: 10.4049/jimmunol.1401492
8. Azoulay-Alfaguter I, Strazza M, Pedoeem A, Mor A. The Coreceptor Programmed Death 1 Inhibits T-Cell Adhesion by Regulating Rap1. *J Allergy Clin Immunol* (2015) 135(2):564–7. doi: 10.1016/j.jaci.2014.07.055
9. Riley JL. PD-1 Signaling in Primary T Cells. *Immunol Rev* (2009) 229 (1):114–25. doi: 10.1111/j.1600-065X.2009.00767.x
10. Tocheva AS, Peled M, Strazza M, Adam KR, Lerrer S, Nayak S, et al. Quantitative Phosphoproteomic Analysis Reveals Involvement of PD-1 in Multiple T Cell Functions. *J Biol Chem* (2020) 295(52):18036–50. doi: 10.1074/jbc.RA120.014745
11. Boussiotis VA. Molecular and Biochemical Aspects of the PD-1 Checkpoint Pathway. *N Engl J Med* (2016) 375(18):1767–78. doi: 10.1056/NEJMra1514296

12. Patsoukis N, Duke-Cohan JS, Chaudhri A, Aksoylar HI, Wang Q, Council A, et al. Interaction of SHP-2 SH2 Domains With PD-1 ITSM Induces PD-1 Dimerization and SHP-2 Activation. *Commun Biol* (2020) 3(1):128. doi: 10.1038/s42003-020-0845-0
13. Peled M, Tocheva AS, Sandigursky S, Nayak S, Philips EA, Nichols KE, et al. Affinity Purification Mass Spectrometry Analysis of PD-1 Uncovers SAP as a New Checkpoint Inhibitor. *Proc Natl Acad Sci USA* (2018) 115(3):E468–E77. doi: 10.1073/pnas.1710437115
14. Wang Q, Bardhan K, Boussiotis VA, Patsoukis N. The PD-1 Interactome. *Adv Biol (Weinh)* (2021) 5(9):e2100758. doi: 10.1002/adbi.202100758
15. Azoulay-Alfaguter I, Strazza M, Peled M, Novak HK, Muller J, Dustin ML, et al. The Tyrosine Phosphatase SHP-1 Promotes T Cell Adhesion by Activating the Adaptor Protein CrkII in the Immunological Synapse. *Sci Signaling* (2017) 10(491):eaal2880. doi: 10.1126/scisignal.aal2880
16. Pedoeem A, Azoulay-Alfaguter I, Strazza M, Silverman GJ, Mor A. Programmed Death-1 Pathway in Cancer and Autoimmunity. *Clin Immunol* (2014) 153(1):145–52. doi: 10.1016/j.clim.2014.04.010
17. Strazza M, Adam K, Lerrer S, Straube J, Sandigursky S, Ueberheide B, et al. SHP2 Targets ITK Downstream of PD-1 to Inhibit T Cell Function. *Inflammation* (2021) 44(4):1529–39. doi: 10.1007/s10753-021-01437-8
18. Yuan X, Bu H, Zhou J, Yang C-Y, Zhang H. Recent Advances of SHP2 Inhibitors in Cancer Therapy: Current Development and Clinical Application. *J Med Chem* (2020) 63(20):11368–96. doi: 10.1021/acs.jmedchem.0c00249
19. Wang W, Liu L, Song X, Mo Y, Komma C, Bellamy HD, et al. Crystal Structure of Human Protein Tyrosine Phosphatase SHP-1 in the Open Conformation. *J Cell Biochem* (2011) 112(8):2062–71. doi: 10.1002/jcb.23125
20. Lu W, Gong D, Bar-Sagi D, Cole PA. Site-Specific Incorporation of a Phosphotyrosine Mimetic Reveals a Role for Tyrosine Phosphorylation of SHP-2 in Cell Signaling. *Mol Cell* (2001) 8(4):759–69. doi: 10.1016/s1097-2765(01)00369-0
21. Qu CK. The SHP-2 Tyrosine Phosphatase: Signaling Mechanisms and Biological Functions. *Cell Res* (2000) 10(4):279–88. doi: 10.1038/sj.cr.7290055
22. Yu Z-H, Zhang R-Y, Walls CD, Chen L, Zhang S, Wu L, et al. Molecular Basis of Gain-Of-Function LEOPARD Syndrome-Associated SHP2 Mutations. *Biochemistry* (2014) 53(25):4136–51. doi: 10.1021/bi5002695
23. Niihori T, Aoki Y, Ohashi H, Kurosawa K, Kondoh T, Ishikiriyama S, et al. Functional Analysis of PTPN11/SHP-2 Mutants Identified in Noonan Syndrome and Childhood Leukemia. *J Hum Genet* (2005) 50(4):192–202. doi: 10.1007/s10038-005-0239-7
24. Zhang J, Zhang F, Niu R. Functions of Shp2 in Cancer. *J Cell Mol Med* (2015) 19(9):2075–83. doi: 10.1111/jcmm.12618
25. Patsoukis N, Wang Q, Strauss L, Boussiotis VA. Revisiting the PD-1 Pathway. *Sci Adv* (2020) 6(38):1–13. doi: 10.1126/sciadv.abd2712
26. Hui E, Cheung J, Zhu J, Su X, Taylor MJ, Wallweber HA, et al. T Cell Costimulatory Receptor CD28 Is a Primary Target for PD-1-Mediated Inhibition. *Science* (2017) 355(6332):1428–33. doi: 10.1126/science.aaf1292
27. Chemnitz JM, Parry RV, Nichols KE, June CH, Riley JL. SHP-1 and SHP-2 Associate With Immunoreceptor Tyrosine-Based Switch Motif of Programmed Death 1 Upon Primary Human T Cell Stimulation, But Only Receptor Ligation Prevents T Cell Activation. *J Immunol* (2004) 173(2):945–54. doi: 10.4049/jimmunol.173.2.945
28. Celis-Gutierrez J, Blattmann P, Zhai Y, Jarmuzynski N, Ruminski K, Gregoire C, et al. Quantitative Interactomics in Primary T Cells Provides a Rationale for Concomitant PD-1 and BTLA Coinhibitor Blockade in Cancer Immunotherapy. *Cell Rep* (2019) 27(11):3315–30.e7. doi: 10.1016/j.celrep.2019.05.041
29. Frearson JA, Alexander DR. The Phosphotyrosine Phosphatase SHP-2 Participates in a Multimeric Signaling Complex and Regulates T Cell Receptor (TCR) Coupling to the Ras/mitogen-Activated Protein Kinase (MAPK) Pathway in Jurkat T Cells. *J Exp Med* (1998) 187(9):1417–26. doi: 10.1084/jem.187.9.1417
30. Bardhan K, Aksoylar HI, Le Bourgeois T, Strauss L, Weaver JD, Delcuze B, et al. Phosphorylation of PD-1-Y248 Is a Marker of PD-1-Mediated Inhibitory Function in Human T Cells. *Sci Rep* (2019) 9(1):17252. doi: 10.1038/s41598-019-53463-0
31. Valitutti S, Coombs D, Dupre L. The Space and Time Frames of T Cell Activation at the Immunological Synapse. *FEBS Lett* (2010) 584(24):4851–7. doi: 10.1016/j.febslet.2010.10.010
32. Sheppard KA, Fitz LJ, Lee JM, Benander C, George JA, Wooters J, et al. PD-1 Inhibits T-Cell Receptor Induced Phosphorylation of the ZAP70/CD3zeta Signalosome and Downstream Signaling to PKCtheta. *FEBS Lett* (2004) 574(1-3):37–41. doi: 10.1016/j.febslet.2004.07.083
33. Fan Z, Tian Y, Chen Z, Liu L, Zhou Q, He J, et al. Blocking Interaction Between SHP2 and PD-1 Denotes a Novel Opportunity for Developing PD-1 Inhibitors. *EMBO Mol Med* (2020) 12(6):e11571. doi: 10.15252/emmm.201911571
34. Toral KJ, Wuenschel MA, Black EP. Genomic Data From NSCLC Tumors Reveals Correlation Between SHP-2 Activity and PD-L1 Expression and Suggests Synergy in Combining SHP-2 and PD-1/PD-L1 Inhibitors. *PloS One* (2021) 16(8):e0256416. doi: 10.1371/journal.pone.0256416
35. Walsh RJ, Soo RA. Resistance to Immune Checkpoint Inhibitors in non-Small Cell Lung Cancer: Biomarkers and Therapeutic Strategies. *Ther Adv Med Oncol* (2020) 12:1758835920937902. doi: 10.1177/1758835920937902
36. Chen D, Barsoumian HB, Yang L, Younes AI, Verma V, Hu Y, et al. SHP-2 and PD-L1 Inhibition Combined With Radiotherapy Enhances Systemic Antitumor Effects in an Anti-PD-1-Resistant Model of Non-Small Cell Lung Cancer. *Cancer Immunol Res* (2020) 8(7):883–94. doi: 10.1158/2326-6066.CIR-19-0744
37. Zhao M, Guo W, Wu Y, Yang C, Zhong L, Deng G, et al. SHP2 Inhibition Triggers Anti-Tumor Immunity and Synergizes With PD-1 Blockade. *Acta Pharm Sin B* (2019) 9(2):304–15. doi: 10.1016/j.apsb.2018.08.009
38. Rota G, Niogret C, Dang AT, Barros CR, Fonta NP, Alfei F, et al. Shp-2 Is Dispensable for Establishing T Cell Exhaustion and for PD-1 Signaling In Vivo. *Cell Rep* (2018) 23(1):39–49. doi: 10.1016/j.celrep.2018.03.026
39. Mano H. Tec Family of Protein-Tyrosine Kinases: An Overview of Their Structure and Function. *Cytokine Growth Factor Rev* (1999) 10(3-4):267–80. doi: 10.1016/s1359-6101(99)00019-2
40. Pal Singh S, Dammeijer F, Hendriks RW. Role of Bruton's Tyrosine Kinase in B Cells and Malignancies. *Mol Cancer* (2018) 17(1):57. doi: 10.1186/s12943-018-0779-z
41. Sahu N, August A. ITK Inhibitors in Inflammation and Immune-Mediated Disorders. *Curr Top Med Chem* (2009) 9(8):690–703. doi: 10.2174/156802609789044443
42. Lino CNR, Ghosh S. Epstein-Barr Virus in Inborn Immunodeficiency-More Than Infection. *Cancers (Basel)* (2021) 13(19):1–16. doi: 10.3390/cancers13194752
43. Lechner KS, Neurath MF, Weigmann B. Role of the IL-2 Inducible Tyrosine Kinase ITK and its Inhibitors in Disease Pathogenesis. *J Mol Med (Berl)* (2020) 98(10):1385–95. doi: 10.1007/s00109-020-01958-z
44. Lucas F, Woyach JA. Inhibiting Bruton's Tyrosine Kinase in CLL and Other B-Cell Malignancies. *Target Oncol* (2019) 14(2):125–38. doi: 10.1007/s11523-019-00635-7
45. Wang X, Kokabee L, Kokabee M, Conklin DS. Bruton's Tyrosine Kinase and Its Isoforms in Cancer. *Front Cell Dev Biol* (2021) 9:668996. doi: 10.3389/fcell.2021.668996
46. Gallagher MP, Conley JM, Vangala P, Garber M, Reboldi A, Berg LJ. Hierarchy of Signaling Thresholds Downstream of the T Cell Receptor and the Tec Kinase ITK. *Proc Natl Acad Sci USA* (2021) 118(35):1–12. doi: 10.1073/pnas.2025825118
47. Joseph RE, Severin A, Min L, Fulton DB, Andreotti AH. SH2-Dependent Autophosphorylation Within the Tec Family Kinase Itk. *J Mol Biol* (2009) 391(1):164–77. doi: 10.1016/j.jmb.2009.06.023
48. Thelen F, Wissmann S, Ruef N, Stein JV. The Tec Kinase Itk Integrates Naïve T Cell Migration and *In Vivo* Homeostasis. *Front Immunol* (2021) 12:716405. doi: 10.3389/fimmu.2021.716405
49. Grasis JA, Tsoukas CD. Itk: The Rheostat of the T Cell Response. *J Signal Transd* (2011) 2011:297868. doi: 10.1155/2011/297868
50. Zhong Y, Johnson AJ, Byrd JC, Dubovsky JA. Targeting Interleukin-2-Inducible T-Cell Kinase (ITK) in T-Cell Related Diseases. *Postdoc J* (2014) 2(6):1–11. doi: 10.14304/surya.jpr.v2n6.1
51. Zhang J, Lu X, Li J, Miao Y. Combining BTK Inhibitors With BCL2 Inhibitors for Treating Chronic Lymphocytic Leukemia and Mantle Cell Lymphoma. *biomark Res* (2022) 10(1):17. doi: 10.1186/s40364-022-00357-5

52. Kondo K, Shaim H, Thompson PA, Burger JA, Keating M, Estrov Z, et al. Ibrutinib Modulates the Immunosuppressive CLL Microenvironment Through STAT3-Mediated Suppression of Regulatory B-Cell Function and Inhibition of the PD-1/PD-L1 Pathway. *Leukemia* (2018) 32(4):960–70. doi: 10.1038/leu.2017.304
53. Sagiv-Barfi I, Kohrt HE, Czerwinski DK, Ng PP, Chang BY, Levy R. Therapeutic Antitumor Immunity by Checkpoint Blockade is Enhanced by Ibrutinib, an Inhibitor of Both BTK and ITK. *Proc Natl Acad Sci U S A* (2015) 112(9):E966–72. doi: 10.1073/pnas.1500712112
54. Hanna BS, Yazdanparast H, Demerdash Y, Roessner PM, Schulz R, Lichter P, et al. Combining Ibrutinib and Checkpoint Blockade Improves CD8+ T-Cell Function and Control of Chronic Lymphocytic Leukemia in Em-TCL1 Mice. *Haematologica* (2021) 106(4):968–77. doi: 10.3324/haematol.2019.238154
55. Huang W, Jeong AR, Kannan AK, Huang L, August A. IL-2-Inducible T Cell Kinase Tunes T Regulatory Cell Development and is Required for Suppressive Function. *J Immunol* (2014) 193(5):2267–72. doi: 10.4049/jimmunol.1400968
56. Gomez-Rodriguez J, Wohlfert EA, Handon R, Meylan F, Wu JZ, Anderson SM, et al. Itk-Mediated Integration of T Cell Receptor and Cytokine Signaling Regulates the Balance Between Th17 and Regulatory T Cells. *J Exp Med* (2014) 211(3):529–43. doi: 10.1084/jem.20131459
57. Mammadli M, Harris R, Suo L, May A, Gentile T, Waickman AT, et al. Interleukin-2-Inducible T-Cell Kinase (Itk) Signaling Regulates Potent Noncanonical Regulatory T Cells. *Clin Transl Med* (2021) 11(12):e625. doi: 10.1002/ctm2.625
58. Vazquez-Cedeira M, Barcia-Sanjurjo I, Sanz-Garcia M, Barcia R, Lazo PA. Differential Inhibitor Sensitivity Between Human Kinases VRK1 and VRK2. *PloS One* (2011) 6(8):e23235. doi: 10.1371/journal.pone.0023235
59. Nichols RJ, Traktman P. Characterization of Three Paralogous Members of the Mammalian Vaccinia Related Kinase Family. *J Biol Chem* (2004) 279 (9):7934–46. doi: 10.1074/jbc.M310813200
60. Vazquez-Cedeira M, Lazo PA. Human VRK2 (Vaccinia-Related Kinase 2) Modulates Tumor Cell Invasion by Hyperactivation of NFAT1 and Expression of Cyclooxygenase-2. *J Biol Chem* (2012) 287(51):42739–50. doi: 10.1074/jbc.M112.404285
61. Blanco S, Klimcakova L, Vega FM, Lazo PA. The Subcellular Localization of Vaccinia-Related Kinase-2 (VRK2) Isoforms Determines Their Different Effect on P53 Stability in Tumour Cell Lines. *FEBS J* (2006) 273(11):2487–504. doi: 10.1111/j.1742-4658.2006.05256.x
62. Blanco S, Sanz-Garcia M, Santos CR, Lazo PA. Modulation of Interleukin-1 Transcriptional Response by the Interaction Between VRK2 and the JIP1 Scaffold Protein. *PloS One* (2008) 3(2):e1660. doi: 10.1371/journal.pone.0001660
63. *VRK2 The Human Protein Atlas*. Available at: https://www.proteinatlas.org/ENSG00000028116-VRK2.
64. Singh B, Berry JA, Shoher A, Lucci A. COX-2 Induces IL-11 Production in Human Breast Cancer Cells. *J Surg Res* (2006) 131(2):267–75. doi: 10.1016/j.jss.2005.11.582
65. Zhu H, Li Q, Zhao Y, Peng H, Guo L, Zhu J, et al. Vaccinia-Related Kinase 2 Drives Pancreatic Cancer Progression by Protecting Plk1 From Chfr-Mediated Degradation. *Oncogene* (2021) 40(28):4663–74. doi: 10.1038/s41388-021-01893-4
66. So J, Mabe NW, Englinger B, Moyer SM, Trissal MC, Marques JG, et al. VRK1 is Required in VRK2-Methylated Cancers of the Nervous System. *bioRxiv* (2021) 1–66. doi: 10.1101/2021.12.28.474386
67. Kim HS, Moon HG, Han W, Yom CK, Kim WH, Kim JH, et al. COX2 Overexpression Is a Prognostic Marker for Stage III Breast Cancer. *Breast Cancer Res Treat* (2012) 132(1):51–9. doi: 10.1007/s10549-011-1521-3
68. Yiu GK, Toker A. NFAT Induces Breast Cancer Cell Invasion by Promoting the Induction of Cyclooxygenase-2. *J Biol Chem* (2006) 281(18):12210–7. doi: 10.1074/jbc.M600184200
69. Monsalve DM, Merced T, Fernández IF, Blanco S, Vázquez-Cedeira M, Lazo PA. Human VRK2 Modulates Apoptosis by Interaction With Bcl-xL and Regulation of BAX Gene Expression. *Cell Death Dis* (2013) 4(2):e513. doi: 10.1038/cddis.2013.40
70. Fernandez IF, Blanco S, Lozano J, Lazo PA. VRK2 Inhibits Mitogen-Activated Protein Kinase Signaling and Inversely Correlates With ErbB2 in Human Breast Cancer. *Mol Cell Biol* (2010) 30(19):4687–97. doi: 10.1128/MCB.01581-09
71. Peled M, Tocheva AS, Adam K, Mor A. VRK2 Inhibition Synergizes With PD-1 Blockade to Improve T Cell Responses. *Immunol Lett* (2021) 233:42–7. doi: 10.1016/j.imlet.2021.03.007
72. Serafim RAM, de Souza Gama FH, Dutra LA, dos Reis CV, Vasconcelos SNS, da Silva Santiago A, et al. Development of Pyridine-Based Inhibitors for the Human Vaccinia-Related Kinases 1 and 2. *ACS Med Chem Lett* (2019) 10 (9):1266–71. doi: 10.1021/acsmedchemlett.9b00082
73. Smyth DJ, Plagnol V, Walker NM, Cooper JD, Downes K, Yang JH, et al. Shared and Distinct Genetic Variants in Type 1 Diabetes and Celiac Disease. *N Engl J Med* (2008) 359(26):2767–77. doi: 10.1056/NEJMoa0807917
74. Wang PF, Cai HQ, Zhang CB, Li YM, Liu X, Wan JH, et al. Molecular and Clinical Characterization of PTPN2 Expression From RNA-Seq Data of 996 Brain Gliomas. *J Neuroinflammation* (2018) 15(1):145. doi: 10.1186/s12974-018-1187-4
75. Wu L, Wang F, Xu J, Chen Z. PTPN2 Induced by Inflammatory Response and Oxidative Stress Contributed to Glioma Progression. *J Cell Biochem* (2019) 120(11):19044–51. doi: 10.1002/jcb.29227
76. Yang HJ, Yu G, Wang Y, Guo X. Inflammatory Response or Oxidative Stress Induces Upregulation of PTPN2 and Thus Promotes the Progression of Laryngocarcinoma. *Eur Rev Med Pharmacol Sci* (2020) 24(8):4314–9. doi: 10.26355/eurrev_202004_21012
77. Zhang Z, Xu T, Qin W, Huang B, Chen W, Li S, et al. Upregulated PTPN2 Induced by Inflammatory Response or Oxidative Stress Stimulates the Progression of Thyroid Cancer. *Biochem Biophys Res Commun* (2020) 522 (1):21–5. doi: 10.1016/j.bbrc.2019.11.047
78. Spalinger MR, Scharl M. PTPN2 as a Promoter of Colon Carcinoma *via* Reduction of Inflammasome Activation. *Mol Cell Oncol* (2018) 5(4): e1465013. doi: 10.1080/23723556.2018.1465013
79. Spalinger MR, Manzini R, Hering L, Riggs JB, Gottier C, Lang S, et al. PTPN2 Regulates Inflammasome Activation and Controls Onset of Intestinal Inflammation and Colon Cancer. *Cell Rep* (2018) 22(7):1835–48. doi: 10.1016/j.celrep.2018.01.052
80. Kleppe M, Lahortiga I, El Chaar T, De Keersmaecker K, Mentens N, Graux C, et al. Deletion of the Protein Tyrosine Phosphatase Gene PTPN2 in T-Cell Acute Lymphoblastic Leukemia. *Nat Genet* (2010) 42(6):530–5. doi: 10.1038/ng.587
81. Kleppe M, Soulier J, Asnafi V, Mentens N, Hornakova T, Knoops L, et al. PTPN2 Negatively Regulates Oncogenic JAK1 in T-Cell Acute Lymphoblastic Leukemia. *Blood* (2011) 117(26):7090–8. doi: 10.1182/blood-2010-10-314286
82. You-Ten KE, Muise ES, Itié A, Michaliszyn E, Wagner J, Jothy S, et al. Impaired Bone Marrow Microenvironment and Immune Function in T Cell Protein Tyrosine Phosphatase-Deficient Mice. *J Exp Med* (1997) 186(5):683–93. doi: 10.1084/jem.186.5.683
83. Wiede F, Dudakov JA, Lu K-H, Dodd GT, Butt T, Godfrey DI, et al. PTPN2 Regulates T Cell Lineage Commitment and αβ Versus γδ Specification. *J Exp Med* (2017) 214(9):2733–58. doi: 10.1084/jem.20161903
84. Castro-Sanchez P, Teagle AR, Prade S, Zamoyska R. Modulation of TCR Signaling by Tyrosine Phosphatases: From Autoimmunity to Immunotherapy. *Front Cell Dev Biol* (2020) 8:608747. doi: 10.3389/fcell.2020.608747
85. Flosbach M, Oberle SG, Scherer S, Zecha J, von Hoesslin M, Wiede F, et al. PTPN2 Deficiency Enhances Programmed T Cell Expansion and Survival Capacity of Activated T Cells. *Cell Rep* (2020) 32(4):107957. doi: 10.1016/j.celrep.2020.107957
86. Wiede F, Ziegler A, Zehn D, Tiganis T. PTPN2 Restrains CD8+ T Cell Responses After Antigen Cross-Presentation for the Maintenance of Peripheral Tolerance in Mice. *J Autoimmun* (2014) 53:105–14. doi: 10.1016/j.jaut.2014.05.008
87. Spalinger MR, Kasper S, Chassard C, Raselli T, Frey-Wagner I, Gottier C, et al. PTPN2 Controls Differentiation of $CD4^+$ T Cells and Limits Intestinal Inflammation and Intestinal Dysbiosis. *Mucosal Immunol* (2015) 8(4):918–29. doi: 10.1038/mi.2014.122
88. LaFleur MW, Nguyen TH, Coxe MA, Miller BC, Yates KB, Gillis JE, et al. PTPN2 Regulates the Generation of Exhausted CD8+ T Cell Subpopulations

and Restrains Tumor Immunity. *Nat Immunol* (2019) 20(10):1335–47. doi: 10.1038/s41590-019-0480-4
89. Manguso RT, Pope HW, Zimmer MD, Brown FD, Yates KB, Miller BC, et al. *In Vivo* CRISPR Screening Identifies Ptpn2 as a Cancer Immunotherapy Target. *Nature* (2017) 547(7664):413–8. doi: 10.1038/nature23270
90. Luo N, Formisano L, Gonzalez-Ericsson PI, Sanchez V, Dean PT, Opalenik SR, et al. Melanoma Response to Anti-PD-L1 Immunotherapy Requires JAK1 Signaling, But Not JAK2. *OncoImmunology* (2018) 7(6):e1438106. doi: 10.1080/2162402X.2018.1438106
91. Yan T, Yang K, Chen C, Zhou Z, Shen P, Jia Y, et al. Synergistic Photothermal Cancer Immunotherapy by Cas9 Ribonucleoprotein-Based Copper Sulfide Nanotherapeutic Platform Targeting PTPN2. *Biomaterials* (2021) 279:121233. doi: 10.1016/j.biomaterials.2021.121233
92. Augello G, Emma MR, Cusimano A, Azzolina A, Montalto G, McCubrey JA, et al. The Role of GSK-3 in Cancer Immunotherapy: GSK-3 Inhibitors as a New Frontier in Cancer Treatment. *Cells* (2020) 9(6):1–17. doi: 10.3390/cells9061427
93. Park R, Coveler AL, Cavalcante L, Saeed A. GSK-3β in Pancreatic Cancer: Spotlight on 9-ING-41, Its Therapeutic Potential and Immune Modulatory Properties. *Biol (Basel)* (2021) 10(7):1–14. doi: 10.3390/biology10070610
94. Steele L, Mannion AJ, Shaw G, Maclennan KA, Cook GP, Rudd CE, et al. Non-Redundant Activity of GSK-3alpha and GSK-3beta in T Cell-Mediated Tumor Rejection. *iScience* (2021) 24(6):102555. doi: 10.1016/j.isci.2021.102555
95. Beurel E, Grieco SF, Jope RS. Glycogen Synthase Kinase-3 (GSK3): Regulation, Actions, and Diseases. *Pharmacol Ther* (2015) 148:114–31. doi: 10.1016/j.pharmthera.2014.11.016
96. Domoto T, Uehara M, Bolidong D, Minamoto T. Glycogen Synthase Kinase 3β in Cancer Biology and Treatment. *Cells* (2020) 9(6):1388. doi: 10.3390/cells9061388
97. Cohen P, Frame S. The Renaissance of GSK3. *Nat Rev Mol Cell Biol* (2001) 2 (10):769–76. doi: 10.1038/35096075
98. Embi N, Rylatt DB, Cohen P. Glycogen Synthase Kinase-3 From Rabbit Skeletal Muscle. *Eur J Biochem* (1980) 107(2):519–27. doi: 10.1111/j.1432-1033.1980.tb06059.x
99. Alves M, Borges DP, Kimberly A, Martins Neto F, Oliveira AC, de Sousa JC, et al. Glycogen Synthase Kinase-3 Beta Expression Correlates With Worse Overall Survival in Non-Small Cell Lung Cancer-A Clinicopathological Series. *Front Oncol* (2021) 11:621050. doi: 10.3389/fonc.2021.621050
100. Zeng J, Liu D, Qiu Z, Huang Y, Chen B, Wang L, et al. Gsk3β Overexpression Indicates Poor Prognosis and its Inhibition Reduces Cell Proliferation and Survival of non-Small Cell Lung Cancer Cells. *PloS One* (2014) 9(3):e91231. doi: 10.1371/journal.pone.0091231
101. Taylor A, Harker JA, Chanthong K, Stevenson PG, Zuniga EI, Rudd CE. Glycogen Synthase Kinase 3 Inactivation Drives T-Bet-Mediated Downregulation of Co-Receptor PD-1 to Enhance CD8(+) Cytolytic T Cell Responses. *Immunity* (2016) 44(2):274–86. doi: 10.1016/j.immuni.2016.01.018
102. Zhang JY, Zhao YL, Lv YP, Cheng P, Chen W, Duan M, et al. Modulation of CD8+ Memory Stem T Cell Activity and Glycogen Synthase Kinase 3β Inhibition Enhances Anti-Tumoral Immunity in Gastric Cancer. *OncoImmunology* (2018) 7(4):e1412900. doi: 10.1080/2162402X.2017.1412900
103. Taylor A, Rothstein D, Rudd CE. Small-Molecule Inhibition of PD-1 Transcription Is an Effective Alternative to Antibody Blockade in Cancer Therapy. *Cancer Res* (2018) 78(3):706–17. doi: 10.1158/0008-5472.Can-17-0491
104. Allen SD, Liu X, Jiang J, Liao YP, Chang CH, Nel AE, et al. Immune Checkpoint Inhibition in Syngeneic Mouse Cancer Models by a Silicasome Nanocarrier Delivering a GSK3 Inhibitor. *Biomaterials* (2021) 269:120635. doi: 10.1016/j.biomaterials.2020.120635
105. Ohteki T, Parsons M, Zakarian A, Jones RG, Nguyen LT, Woodgett JR, et al. Negative Regulation of T Cell Proliferation and Interleukin 2 Production by the Serine Threonine Kinase Gsk-3. *J Exp Med* (2000) 192(1):99–104. doi: 10.1084/jem.192.1.99
106. Dimou A, Syrigos KN. The Role of GSK3beta in T Lymphocytes in the Tumor Microenvironment. *Front Oncol* (2020) 10:1221. doi: 10.3389/fonc.2020.01221
107. Appleman LJ, van Puijenbroek AA, Shu KM, Nadler LM, Boussiotis VA. CD28 Costimulation Mediates Down-Regulation of P27kip1 and Cell Cycle Progression by Activation of the PI3K/PKB Signaling Pathway in Primary Human T Cells. *J Immunol* (2002) 168(6):2729–36. doi: 10.4049/jimmunol.168.6.2729
108. Taylor A, Rudd CE. Glycogen Synthase Kinase 3 Inactivation Compensates for the Lack of CD28 in the Priming of CD8(+) Cytotoxic T-Cells: Implications for Anti-PD-1 Immunotherapy. *Front Immunol* (2017) 8:1653. doi: 10.3389/fimmu.2017.01653
109. Gattinoni L, Zhong X-S, Palmer DC, Ji Y, Hinrichs CS, Yu Z, et al. Wnt Signaling Arrests Effector T Cell Differentiation and Generates CD8+ Memory Stem Cells. *Nat Med* (2009) 15(7):808–13. doi: 10.1038/nm.1982
110. Krueger J, Rudd CE, Taylor A. Glycogen Synthase 3 (GSK-3) Regulation of PD-1 Expression and and its Therapeutic Implications. *Semin Immunol* (2019) 42:101295. doi: 10.1016/j.smim.2019.101295
111. Pokhrel RH, Acharya S, Ahn J-H, Gu Y, Pandit M, Kim J-O, et al. AMPK Promotes Antitumor Immunity by Downregulating PD-1 in Regulatory T Cells *via* the HMGCR/p38 Signaling Pathway. *Mol Cancer* (2021) 20(1):133. doi: 10.1186/s12943-021-01420-9
112. Rudd CE, Chanthong K, Taylor A. Small Molecule Inhibition of GSK-3 Specifically Inhibits the Transcription of Inhibitory Co-Receptor LAG-3 for Enhanced Anti-Tumor Immunity. *Cell Rep* (2020) 30(7):2075–82.e4. doi: 10.1016/j.celrep.2020.01.076
113. Kazanova A, Krueger J, Rudd CE. CD28 and Glycogen Synthase Kinase-3 (GSK-3) Inhibitor Combination Therapy Generates Tumor Infiltrating T-Cells (TILs) With a Reversal of Markers for T-Cell Exhaustion. *J Immunol* (2020) 204(1 Supplement):165.35.
114. Sengupta S, Katz SC, Sengupta S, Sampath P. Glycogen Synthase Kinase 3 Inhibition Lowers PD-1 Expression, Promotes Long-Term Survival and Memory Generation in Antigen-Specific CAR-T Cells. *Cancer Lett* (2018) 433:131–9. doi: 10.1016/j.canlet.2018.06.035
115. Taylor A, Rudd CE. Glycogen Synthase Kinase 3 (GSK-3) Controls T-Cell Motility and Interactions With Antigen Presenting Cells. *BMC Res Notes* (2020) 13(1):163. doi: 10.1186/s13104-020-04971-0
116. Li CW, Lim SO, Xia W, Lee HH, Chan LC, Kuo CW, et al. Glycosylation and Stabilization of Programmed Death Ligand-1 Suppresses T-Cell Activity. *Nat Commun* (2016) 7:12632. doi: 10.1038/ncomms12632
117. Chen X, Wang K, Jiang S, Sun H, Che X, Zhang M, et al. Eef2k Promotes PD-L1 Stabilization Through Inactivating GSK3β in Melanoma. *J Immunother Cancer* (2022) 10(3):1–15. doi: 10.1136/jitc-2021-004026
118. Zhou B, Guo L, Zhang B, Liu S, Zhang K, Yan J, et al. Disulfiram Combined With Copper Induces Immunosuppression *via* PD-L1 Stabilization in Hepatocellular Carcinoma. *Am J Cancer Res* (2019) 9(11):2442–55.
119. Krueger J, Taylor A, Motta V, Stagg J, Watson I, Rudd CE. Glycogen Synthase Kinase 3 (GSK-3) Synergizes With Immune-Checkpoint Blockade (ICB) to Overcome Tumor Resistance Due to Unique Tumor Infiltrating T-Cell Subsets as Revealed by Mass Cytometry (CyTOF). *J Immunol* (2019) 202(1 Supplement):136.24.
120. Tawbi HA, Schadendorf D, Lipson EJ, Ascierto PA, Matamala L, Castillo Gutierrez E, et al. Relatlimab and Nivolumab Versus Nivolumab in Untreated Advanced Melanoma. *N Engl J Med* (2022) 386(1):24–34. doi: 10.1056/NEJMoa2109970
121. Kochenderfer JN, Dudley ME, Carpenter RO, Kassim SH, Rose JJ, Telford WG, et al. Donor-Derived CD19-Targeted T Cells Cause Regression of Malignancy Persisting After Allogeneic Hematopoietic Stem Cell Transplantation. *Blood* (2013) 122(25):4129–39. doi: 10.1182/blood-2013-08-519413
122. Cichocki F, Valamehr B, Bjordahl R, Zhang B, Rezner B, Rogers P, et al. GSK3 Inhibition Drives Maturation of NK Cells and Enhances Their Antitumor Activity. *Cancer Res* (2017) 77(20):5664–75. doi: 10.1158/0008-5472.CAN-17-0799
123. Björkström NK, Riese P, Heuts F, Andersson S, Fauriat C, Ivarsson MA, et al. Expression Patterns of NKG2A, KIR, and CD57 Define a Process of CD56dim NK-Cell Differentiation Uncoupled From NK-Cell Education. *Blood* (2010) 116(19):3853–64. doi: 10.1182/blood-2010-04-281675

124. Parameswaran R, Ramakrishnan P, Moreton SA, Xia Z, Hou Y, Lee DA, et al. Repression of GSK3 Restores NK Cell Cytotoxicity in AML Patients. *Nat Commun* (2016) 7(1):11154. doi: 10.1038/ncomms11154
125. Sherr CJ, Roberts JM. CDK Inhibitors: Positive and Negative Regulators of G1-Phase Progression. *Genes Dev* (1999) 13(12):1501–12. doi: 10.1101/gad.13.12.1501
126. Patel P, Asbach B, Shteyn E, Gomez C, Coltoff A, Bhuyan S, et al. Brk/Protein Tyrosine Kinase 6 Phosphorylates P27kip1, Regulating the Activity of Cyclin D-Cyclin-Dependent Kinase 4. *Mol Cell Biol* (2015) 35(9):1506–22. doi: 10.1128/mcb.01206-14
127. Fassl A, Geng Y, Sicinski P. CDK4 and CDK6 Kinases: From Basic Science to Cancer Therapy. *Science* (2022) 375(6577):eabc1495. doi: 10.1126/science.abc1495
128. Anders L, Ke N, Hydbring P, Choi YJ, Widlund HR, Chick JM, et al. A Systematic Screen for CDK4/6 Substrates Links FOXM1 Phosphorylation to Senescence Suppression in Cancer Cells. *Cancer Cell* (2011) 20(5):620–34. doi: 10.1016/j.ccr.2011.10.001
129. Matsuura I, Denissova NG, Wang G, He D, Long J, Liu F. Cyclin-Dependent Kinases Regulate the Antiproliferative Function of Smads. *Nature* (2004) 430 (6996):226–31. doi: 10.1038/nature02650
130. Li Y, Chitnis N, Nakagawa H, Kita Y, Natsugoe S, Yang Y, et al. PRMT5 is Required for Lymphomagenesis Triggered by Multiple Oncogenic Drivers. *Cancer Discovery* (2015) 5(3):288–303. doi: 10.1158/2159-8290.Cd-14-0625
131. Hall M, Peters G. Genetic Alterations of Cyclins, Cyclin-Dependent Kinases, and Cdk Inhibitors in Human Cancer. *Adv Cancer Res* (1996) 68:67–108. doi: 10.1016/s0065-230x(08)60352-8
132. Arnold A, Papanikolaou A. Cyclin D1 in Breast Cancer Pathogenesis. *J Clin Oncol* (2005) 23(18):4215–24. doi: 10.1200/jco.2005.05.064
133. Wang TC, Cardiff RD, Zukerberg L, Lees E, Arnold A, Schmidt EV. Mammary Hyperplasia and Carcinoma in MMTV-Cyclin D1 Transgenic Mice. *Nature* (1994) 369(6482):669–71. doi: 10.1038/369669a0
134. Landis MW, Pawlyk BS, Li T, Sicinski P, Hinds PW. Cyclin D1-Dependent Kinase Activity in Murine Development and Mammary Tumorigenesis. *Cancer Cell* (2006) 9(1):13–22. doi: 10.1016/j.ccr.2005.12.019
135. Puyol M, Martín A, Dubus P, Mulero F, Pizcueta P, Khan G, et al. A Synthetic Lethal Interaction Between K-Ras Oncogenes and Cdk4 Unveils a Therapeutic Strategy for Non-Small Cell Lung Carcinoma. *Cancer Cell* (2010) 18(1):63–73. doi: 10.1016/j.ccr.2010.05.025
136. Otto T, Sicinski P. Cell Cycle Proteins as Promising Targets in Cancer Therapy. *Nat Rev Cancer* (2017) 17(2):93–115. doi: 10.1038/nrc.2016.138
137. Polier S, Samant RS, Clarke PA, Workman P, Prodromou C, Pearl LH. ATP-Competitive Inhibitors Block Protein Kinase Recruitment to the Hsp90-Cdc37 System. *Nat Chem Biol* (2013) 9(5):307–12. doi: 10.1038/nchembio.1212
138. Michaud K, Solomon DA, Oermann E, Kim JS, Zhong WZ, Prados MD, et al. Pharmacologic Inhibition of Cyclin-Dependent Kinases 4 and 6 Arrests the Growth of Glioblastoma Multiforme Intracranial Xenografts. *Cancer Res* (2010) 70(8):3228–38. doi: 10.1158/0008-5472.Can-09-4559
139. Raub TJ, Wishart GN, Kulanthaivel P, Staton BA, Ajamie RT, Sawada GA, et al. Brain Exposure of Two Selective Dual CDK4 and CDK6 Inhibitors and the Antitumor Activity of CDK4 and CDK6 Inhibition in Combination With Temozolomide in an Intracranial Glioblastoma Xenograft. *Drug Metab Dispos* (2015) 43(9):1360–71. doi: 10.1124/dmd.114.062745
140. Goel S, DeCristo MJ, Watt AC, BrinJones H, Sceneay J, Li BB, et al. CDK4/6 Inhibition Triggers Anti-Tumour Immunity. *Nature* (2017) 548(7668):471–5. doi: 10.1038/nature23465
141. Deng J, Wang ES, Jenkins RW, Li S, Dries R, Yates K, et al. CDK4/6 Inhibition Augments Antitumor Immunity by Enhancing T-Cell Activation. *Cancer Discovery* (2018) 8(2):216–33. doi: 10.1158/2159-8290.Cd-17-0915
142. Schaer DA, Beckmann RP, Dempsey JA, Huber L, Forest A, Amaladas N, et al. The CDK4/6 Inhibitor Abemaciclib Induces a T Cell Inflamed Tumor Microenvironment and Enhances the Efficacy of PD-L1 Checkpoint Blockade. *Cell Rep* (2018) 22(11):2978–94. doi: 10.1016/j.celrep.2018.02.053
143. Zhang J, Bu X, Wang H, Zhu Y, Geng Y, Nihira NT, et al. Cyclin D-CDK4 Kinase Destabilizes PD-L1 *via* Cullin 3-SPOP to Control Cancer Immune Surveillance. *Nature* (2018) 553(7686):91–5. doi: 10.1038/nature25015
144. Jerby-Arnon L, Shah P, Cuoco MS, Rodman C, Su MJ, Melms JC, et al. A Cancer Cell Program Promotes T Cell Exclusion and Resistance to Checkpoint Blockade. *Cell* (2018) 175(4):984–97.e24. doi: 10.1016/j.cell.2018.09.006
145. Teo ZL, Versaci S, Dushyanthen S, Caramia F, Savas P, Mintoff CP, et al. Combined CDK4/6 and PI3Kα Inhibition Is Synergistic and Immunogenic in Triple-Negative Breast Cancer. *Cancer Res* (2017) 77(22):6340–52. doi: 10.1158/0008-5472.Can-17-2210
146. Bisi JE, Sorrentino JA, Roberts PJ, Tavares FX, Strum JC. Preclinical Characterization of G1T28: A Novel CDK4/6 Inhibitor for Reduction of Chemotherapy-Induced Myelosuppression. *Mol Cancer Ther* (2016) 15 (5):783–93. doi: 10.1158/1535-7163.Mct-15-0775
147. He S, Roberts PJ, Sorrentino JA, Bisi JE, Storrie-White H, Tiessen RG, et al. Transient CDK4/6 Inhibition Protects Hematopoietic Stem Cells From Chemotherapy-Induced Exhaustion. *Sci Transl Med* (2017) 9(387):1–47. doi: 10.1126/scitranslmed.aal3986
148. Brdicka T, Pavlistova D, Leo A, Bruyns E, Korinek V, Angelisova P, et al. Phosphoprotein Associated With Glycosphingolipid-Enriched Microdomains (PAG), a Novel Ubiquitously Expressed Transmembrane Adaptor Protein, Binds the Protein Tyrosine Kinase Csk and is Involved in Regulation of T Cell Activation. *J Exp Med* (2000) 191(9):1591–604. doi: 10.1084/jem.191.9.1591
149. Svec A. Phosphoprotein Associated With Glycosphingolipid-Enriched Microdomains/Csk-Binding Protein: A Protein That Matters. *Pathol Res Pract* (2008) 204(11):785–92. doi: 10.1016/j.prp.2008.06.006
150. Hrdinka M, Horejsi V. PAG - A Multipurpose Transmembrane Adaptor Protein. *Oncogene* (2014) 33(41):4881–92. doi: 10.1038/onc.2013.485
151. Yashiro-Ohtani Y, Zhou XY, Toyo-Oka K, Tai XG, Park CS, Hamaoka T, et al. Non-CD28 Costimulatory Molecules Present in T Cell Rafts Induce T Cell Costimulation by Enhancing the Association of TCR With Rafts. *J Immunol* (2000) 164(3):1251–9. doi: 10.4049/jimmunol.164.3.1251
152. Head BP, Patel HH, Insel PA. Interaction of Membrane/Lipid Rafts With the Cytoskeleton: Impact on Signaling and Function: Membrane/Lipid Rafts, Mediators of Cytoskeletal Arrangement and Cell Signaling. *Biochim Biophys Acta* (2014) 1838(2):532–45. doi: 10.1016/j.bbamem.2013.07.018
153. Strazza M, Azoulay-Alfaguter I, Peled M, Adam K, Mor A. Transmembrane Adaptor Protein PAG is a Mediator of PD-1 Inhibitory Signaling in Human T Cells. *Commun Biol* (2021) 4(1):1–10. doi: 10.1038/s42003-021-02225-8
154. Horejsi V. Transmembrane Adaptor Proteins in Membrane Microdomains: Important Regulators of Immunoreceptor Signaling. *Immunol Lett* (2004) 92 (1-2):43–9. doi: 10.1016/j.imlet.2003.10.013
155. Itoh K, Sakakibara M, Yamasaki S, Takeuchi A, Arase H, Miyazaki M, et al. Cutting Edge: Negative Regulation of Immune Synapse Formation by Anchoring Lipid Raft to Cytoskeleton Through Cbp-EBP50-ERM Assembly. *J Immunol* (2002) 168(2):541–4. doi: 10.4049/jimmunol.168.2.541
156. Brdicková N, Brdicka T, Andera L, Spicka J, Angelisová P, Milgram SL, et al. Interaction Between Two Adapter Proteins, PAG and EBP50: A Possible Link Between Membrane Rafts and Actin Cytoskeleton. *FEBS Lett* (2001) 507(2):133–6. doi: 10.1016/s0014-5793(01)02955-6
157. Lee H-J, Zheng JJ. PDZ Domains and Their Binding Partners: Structure, Specificity, and Modification. *Cell Commun Signaling* (2010) 8(1):8. doi: 10.1186/1478-811X-8-8
158. Barreda D, Gutiérrez-González LH, Martínez-Cordero E, Cabello-Gutiérrez C, Chacón-Salinas R, Santos-Mendoza T. The Scribble Complex PDZ Proteins in Immune Cell Polarities. *J Immunol Res* (2020) 2020:5649790. doi: 10.1155/2020/5649790
159. Mastrogiovanni M, Juzans M, Alcover A, Di Bartolo V. Coordinating Cytoskeleton and Molecular Traffic in T Cell Migration, Activation, and Effector Functions. *Front Cell Dev Biol* (2020) 8:591348(1138). doi: 10.3389/fcell.2020.591348
160. Fan G, Aleem S, Yang M, Miller WT, Tonks NK. Protein-Tyrosine Phosphatase and Kinase Specificity in Regulation of SRC and Breast Tumor Kinase. *J Biol Chem* (2015) 290(26):15934–47. doi: 10.1074/jbc.M115.651703
161. Wange RL, Samelson LE. Complex Complexes: Signaling at the TCR. *Immunity* (1996) 5(3):197–205. doi: 10.1016/s1074-7613(00)80315-5
162. Saitou T, Kajiwara K, Oneyama C, Suzuki T, Okada M. Roles of Raft-Anchored Adaptor Cbp/PAG1 in Spatial Regulation of C-Src Kinase. *PloS One* (2014) 9(3):e93470. doi: 10.1371/journal.pone.0093470

163. Foltz L, Palacios-Moreno J, Mayfield M, Kinch S, Dillon J, Syrenne J, et al. PAG1 Directs SRC-Family Kinase Intracellular Localization to Mediate Receptor Tyrosine Kinase-Induced Differentiation. *Mol Biol Cell* (2020) 31 (20):2269–82. doi: 10.1091/mbc.E20-02-0135
164. Davidson D, Bakinowski M, Thomas ML, Horejsi V, Veillette A. Phosphorylation-Dependent Regulation of T-Cell Activation by PAG/Cbp, a Lipid Raft-Associated Transmembrane Adaptor. *Mol Cell Biol* (2003) 23 (6):2017–28. doi: 10.1128/MCB.23.6.2017-2028.2003
165. Davidson D, Zhong MC, Pandolfi PP, Bolland S, Xavier RJ, Seed B, et al. The Csk-Associated Adaptor PAG Inhibits Effector T Cell Activation in Cooperation With Phosphatase PTPN22 and Dok Adaptors. *Cell Rep* (2016) 17(10):2776–88. doi: 10.1016/j.celrep.2016.11.035
166. Lu Y, Yang Y, Liu Y, Hao Y, Zhang Y, Hu Y, et al. Upregulation of PAG1/Cbp Contributes to Adipose-Derived Mesenchymal Stem Cells Promoted Tumor Progression and Chemoresistance in Breast Cancer. *Biochem Biophys Res Commun* (2017) 494(3-4):719–27. doi: 10.1016/j.bbrc.2017.10.118
167. Dong X, Luo Z, Liu T, Chai J, Ke Q, Shen L. Identification of Integrin β1 as a Novel PAG1-Interacting Protein Involved in the Inherent Radioresistance of Human Laryngeal Carcinoma. *J Cancer* (2018) 9(22):4128–38. doi: 10.7150/jca.26885
168. Shen L, Ke Q, Chai J, Zhang C, Qiu L, Peng F, et al. PAG1 Promotes the Inherent Radioresistance of Laryngeal Cancer Cells *via* Activation of STAT3. *Exp Cell Res* (2018) 370(1):127–36. doi: 10.1016/j.yexcr.2018.06.014
169. Abd el-Aziz A, El-Desouky MA, Shafei A, Elnakib M, Abdelmoniem AM. Influence of Pentoxifylline on Gene Expression of PAG1/miR-1206/SNHG14 in Ischemic Heart Disease. *Biochem Biophysics Rep* (2021) 25:100911. doi: 10.1016/j.bbrep.2021.100911

Conflict of Interest: The authors declare that the research was conducted in the absence of any commercial or financial relationships that could be construed as a potential conflict of interest.

Publisher's Note: All claims expressed in this article are solely those of the authors and do not necessarily represent those of their affiliated organizations, or those of the publisher, the editors and the reviewers. Any product that may be evaluated in this article, or claim that may be made by its manufacturer, is not guaranteed or endorsed by the publisher.

frontiers | Frontiers in Immunology

TYPE Original Research
PUBLISHED 22 July 2022
DOI 10.3389/fimmu.2022.933165

OPEN ACCESS

EDITED BY
Yubin Li,
University of Pennsylvania,
United States

REVIEWED BY
Chongming Jiang,
Baylor College of Medicine,
United States
Xuefeng Li,
Guangzhou Medical University, China

*CORRESPONDENCE
Li Ye
yelil@fudan.edu.cn

†These authors have contributed equally to this work

SPECIALTY SECTION
This article was submitted to Cancer Immunity and Immunotherapy, a section of the journal Frontiers in Immunology

RECEIVED 30 April 2022
ACCEPTED 27 June 2022
PUBLISHED 22 July 2022

CITATION
Wang S, Fu Y, Kuerban K, Liu J, Huang X, Pan D, Chen H, Zhu Y and Ye L (2022) Discoidin domain receptor 1 is a potential target correlated with tumor invasion and immune infiltration in gastric cancer.
Front. Immunol. 13:933165.
doi: 10.3389/fimmu.2022.933165

Discoidin domain receptor 1 is a potential target correlated with tumor invasion and immune infiltration in gastric cancer

Songna Wang[1,2†], Yuan Fu[1†], Kudelaidi Kuerban[1,2], Jiayang Liu[1,2], Xuan Huang[1,2], Danjie Pan[1,2], Huaning Chen[1,2], Yizhun Zhu[3] and Li Ye[1,2,3*]

[1]Minhang Hospital and Department of Biological Medicines at School of Pharmacy, Fudan University, Shanghai, China, [2]Shanghai Engineering Research Center of Immunotherapeutics, School of Pharmacy, Fudan University, Shanghai, China, [3]School of Pharmacy, Macau University of Science and Technology, Macao, Macao SAR, China

Discoidin domain receptor 1 (DDR1) has been demonstrated to be able to promote tumor invasion and metastasis and being closely related to tumor immune infiltration. However, DDR1 has rarely been studied in gastric cancer. Here, we primarily evaluated DDR1 expression in gastric cancer and its cell lines using multiple databases. Subsequently, the cancer prognosis was investigated in relation to DDR1 expression. After analysis, we discovered that DDR1 was highly expressed and significantly connected with poor prognosis in gastric cancer. To comprehensively understand the molecular mechanism of DDR1, we explored genes and proteins interacting with DDR1 in gastric cancer using databases. Additionally, we found that the expression level of DDR1 was inversely correlated with immune infiltration and significantly relative to various immune cell markers. Overall, DDR1 was implicated in invasion, metastasis, and immune infiltration of gastric cancer. Inhibition of DDR1 may have the potential to alleviate the strong invasiveness and metastasis of advanced gastric cancer. Meanwhile, immune exclusion by DDR1 may also provide a new strategy for improving the efficacy of immune checkpoints inhibitors (ICIs), such as programmed cell death protein 1 (PD-1) antibody.

KEYWORDS

DDR1, gastric cancer, invasion, prognosis, immune infiltration

Introduction

Globally, gastric cancer, also called stomach cancer, is the third leading cause of death from cancer (1). One of the most important reasons for its poor prognosis is that it is usually diagnosed at an advanced stage (2), which is characterized by strong invasion and metastasis (3). Although gastric cancer is treated primarily by surgery, the efficacy of surgery is low for patients in advanced stage (4). During the past few years, immune checkpoints inhibitors (ICIs) have been shown to be effective against several solid tumors, but have had limited approval in gastrointestinal cancers (5). Clinical data showed that patients treated with programmed cell death protein 1 (PD-1) antibodies had low response rate in advanced gastric cancer (6). It has been found that ICIs' effectiveness requires the presence of a strong immune infiltration and the ability to produce an effective antitumor response (7). Moreover, infiltration of immune cells is particularly associated with patient prognosis (8). Therefore, there is an urgent need to improve patient sensitivity to ICIs through exploring potential regulatory mechanisms of immune cell infiltration.

DDR1 is a type of collagen receptor with tyrosine kinase activity, which has five isoforms through alternative splicing (9). Cell adhesion, migration, proliferation, and extracellular matrix (ECM) remodeling are regulated by its interactions with ECM components (10, 11). Mounting evidence shows that DDR1 expression is significantly upregulated in a variety of cancers, including ovary, breast, colon, and lung cancers (12–14). It is also associated with malignant behaviors of tumors, such as tumor cells proliferation, invasion, and metastasis (15). Research indicated that the cross-talk between DDR1 and signal transducer and activator of transcription 3 (STAT3) promoted the progression of hepatocellular carcinoma (HCC) *via* epithelial–mesenchymal transition (EMT) and glutamine metabolism (16). In pancreatic cancer, collagen stimulated CXC chemokine ligand-5 (CXCL5) production through the DDR1/PKCθ/spleen tyrosine kinase (SYK)/nuclear factor κB (NF-κB) pathway, which induced neutrophil extracellular traps (NETs) to drive tumor metastasis (17). Other studies also reported that DDR1 could increase invasion and metastatic spread of gastric cancer *via* EMT (18). Research indicated that increased apoptosis and decreased migration in breast cancer were observed when patients were treated with DDR1 inhibitor nilotinib (19). These suggests that inhibition of DDR1 may be beneficial for the treatment of advanced gastric cancer.

Notably, recent studies have found that DDR1 can control certain properties of immune cells. The molecular structure of DDR1 consists of three major domains, including a transmembrane domain, an intracellular kinase domain, and an extracellular domain (ECD) (20). One study proposed that the ECD of DDR1, rather than its intracellular kinase domain, enhanced the alignment of collagen fibers and blocked immune infiltration by binding to collagen (21). Similarly, it was reported that DDR1 expression exhibited inverse correlation with intratumoral T-cell abundance in triple-negative breast cancer (22). Anti-DDR1-ECD monoclonal antibody resulted in fewer and shorter arrangements of collagen fibers at the tumor edge, which enhanced immune cell infiltration, increased the total number of infiltrating $CD8^+$ and $CD4^+$ T cells, and promoted interferon gamma (IFN-γ) production (21). This mechanism of immune exclusion provides a new strategy for improving the effectiveness of ICIs such as PD-1 antibody. Drugs targeting DDR1-ECD will help to reduce immune exclusion in gastric cancer, enhance T-cell infiltration, and reduce NETs, thereby improving the tumor immune microenvironment and slowing tumor progression (23).

Herein, we used a variety of databases including Tumor Immunoassay Resource (TIMER), UCSC Xena, Gene Expression Display Server (GEDS), UALCAN, Gene Expression Profiling Interactive Analysis (GEPIA), Kaplan–Meier plotter, and PrognoScan to study DDR1 gene expression and its impact on prognosis in multiple cancers. We found that DDR1 expression levels were highly upregulated in many cancers, and highly expressed DDR1 significantly affected the prognosis of gastric cancer. Subsequently, genes and proteins interacting with DDR1 were analyzed through STRING, PINA, and Metascape databases. Finally, the effect of DDR1 expression in gastric cancer on immune cell infiltration was investigated through TIMER database. Results indicated that DDR1 expression was negatively related to the infiltration of various immune cells, especially macrophages. Thus, as described in our study, DDR1 might be a potential target for gastric cancer. In addition, it provides a new approach for improving ICI therapy efficacy by enhancing immune infiltration.

Materials and methods

Expression analysis of DDR1

Through TIMER database (https://cistrome.shinyapps.io/timer/), DDR1 expression levels in various cancers were analyzed (24, 25). Test of Wilcoxon significance was performed for differential expression. Subsequently, we used the UCSC Xena online platform (https://xena.ucsc.edu) to assess differences of DDR1 expression between stomach adenocarcinoma (STAD) and normal tissues (26). We obtained gene expression data of 544 STAD patients. Differential expression analysis was performed using Welch's test. By using GEDS (http://bioinfo.life.hust.edu.cn/web/GEDS/), we examined DDR1 expressions in 37 gastric cancer cell lines (27).

UALCAN

UALCAN database (http://ualcan.path.uab.edu/index.html) performed the multifaceted analysis about DDR1 expression in STAD using data from The Cancer Genome Atlas (TCGA) (28). The contents of the analysis include sample types, patient's gender, TP53 mutation status, individual cancer stages, nodal metastasis status, tumor grades, patient's age, and histological subtypes. p-value < 0.05 was considered statistically significant.

PrognoScan database analysis

By searching vast cancer microarray datasets that are publicly available, PrognoScan database (http://dna00.bio.kyutech.ac.jp/PrognoScan/) can effectively help to explore the influences of various gene expression on patients' prognosis, thus evaluating potential markers and targets in oncotherapy (29). We first explored the relationship between DDR1 levels and survival situation in different cancers *via* PrognoScan database. When the p-value was <0.05, it indicated that there was a significant correlation between DDR1 levels and the prognosis of each tumor type and subtype.

Kaplan–Meier plotter

Based on gene chips and RNA-seq data from public databases such as Gene Expression Omnibus (GEO), European Genome–Phenome Archive (EGA), and TCGA, the Kaplan–Meier plotter (http://kmplot.com/analysis/) provides the correlation analysis between a variety of gene expressions and prognosis in 21 cancer types (30). To investigate the prognostic impact of DDR1 expression level, we first used the Kaplan–Meier plotter in breast, ovarian, lung, and gastric cancers because their cohorts possess relatively large sample sizes. It is worth noting that those patient samples were grouped by an automatically selected best cutoff for optimal performance. Moreover, it was further employed to investigate the influences of various clinicopathological characteristics in gastric cancers.

GEPIA

Based on a mass of RNA-sequencing expression data, GEPIA (http://gepia.cancer-pku.cn/index.html) offers a powerful platform to conduct genetic analysis (31). In the "single gene analysis" module of GEPIA, we first generated prognosis curves in 33 divergent types and subtypes of cancers, with DDR1 expressing differently. Additionally, GEPIA was also employed to analyze the links between DDR1 and the specific markers of divergent tumor-infiltrating immune cells (TIICs). The analysis was performed using tumor and normal tissue datasets.

Analysis of genes and proteins that interact with DDR1

Using STRING (https://string-db.org/) (version 11.5), we constructed a protein–protein interaction (PPI) network for DDR1 and related proteins (32–34). The statistical significance of an interaction was established when the combined score was > 0.4. Subsequently, the interaction network was further analyzed and visualized using Cytoscape (version 3.8.2). We also further analyzed genes and proteins interacting with DDR1 in STAD using the PINA database (https://omics.bjcancer.org/pina/) (version 3.0) (35–37).

Tumor-infiltrating immune cells analysis

We further investigated the influences of DDR1 expression level on the infiltration levels of specific immune cell subsets in STAD and lymphoid neoplasm diffuse large B-cell lymphoma (DLBC) using TIMER database. Then, we visualized the survival differences for immune infiltration correlated to DDR1 in STAD and DLBC. Simultaneously, the correlation between DDR1 expression and different immunomarker sets was explored *via* TIMER database. Partial Spearman's correlation adjusted by purity was applied to assess their relationships.

Datasets

All datasets used in this study are publicly available, but there are certain differences in different databases. Among them, datasets used by TIMER, UCSC Xena, UALCAN,and GEPIA are mainly based on STAD-TCGA and DLBC-TCGA. In addition, datasets used by GEDS come from Cancer Cell Line Encyclopedia (CCLE); datasets used in PrognoScan analysis have been marked in the figures, including GSE12417-GPL96, GSE7696, GSE26712, jacob-00182-HLM, GSE16560, GSE2658, E-TABM-158, and GSE17536; and datasets used by Kaplan–Meier plotter are the expression data of six mRNA chips in GEO, including GSE14210, GSE15459, GSE22377, GSE29272, GSE51105, and GSE62254.pt?>

Results

DDR1 is highly expressed in gastric cancer

We first assessed DDR1 expression in multiple tumors and normal tissues by the TIMER database. In comparison with normal tissues, the expression levels of DDR1 were significantly higher in bladder urothelial carcinoma (BLCA), breast invasive

carcinoma (BRCA), cholangiocarcinoma (CHOL), esophageal carcinoma (ESCA), head and neck squamous cell carcinoma (HNSC), kidney chromophobe (KICH), kidney renal clear cell carcinoma (KIRC), kidney renal papillary cell carcinoma (KIRP), liver hepatocellular carcinoma (LIHC), lung adenocarcinoma (LUAD), lung squamous cell carcinoma (LUSC), prostate adenocarcinoma (PRAD), rectum adenocarcinoma (READ), STAD, thyroid carcinoma (THCA), and uterine corpus endometrial carcinoma (UCEC) (Figure 1A). Consistently, the analysis result of UCSC Xena also confirmed that the expression of DDR1 was markedly elevated in STAD (Figure 1B). Furthermore, we interrogated DDR1 expression in 37 gastric cancer cell lines using the GEDS platform (Figure 1C; Supplementary Table S1). Of these, NCC-StC-K140 cells show the highest DDR1 expression, while SNU-1 cells show the lowest. They can be used to study the effect of DDR1 expression on gastric cancer.

DDR1 expression levels in the context of different clinical parameters of gastric cancer

Based on samples from TCGA-STAD in the UALCAN database, DDR1 expression levels in the context of various clinical parameters of gastric cancer were examined. Gastric cancer exhibited significantly increased DDR1 expression compared to normal tissues (Figure 2A). In a similar vein, this trend was observed in both male and female patients (Figure 2B). In contrast with mutant TP53, the non-mutant TP53 showed significantly lower DDR1 expression (Figure 2C). On the basis of individual cancer stages, DDR1 expressions of STAD were markedly higher in stages 1–4 (Figure 2D). Similarly, this increase was observed in N0, N1, and N2 stages (Figure 2E). Considering the tumor grades, DDR1 was more expressed in tumor grades 1–3 than in normal control

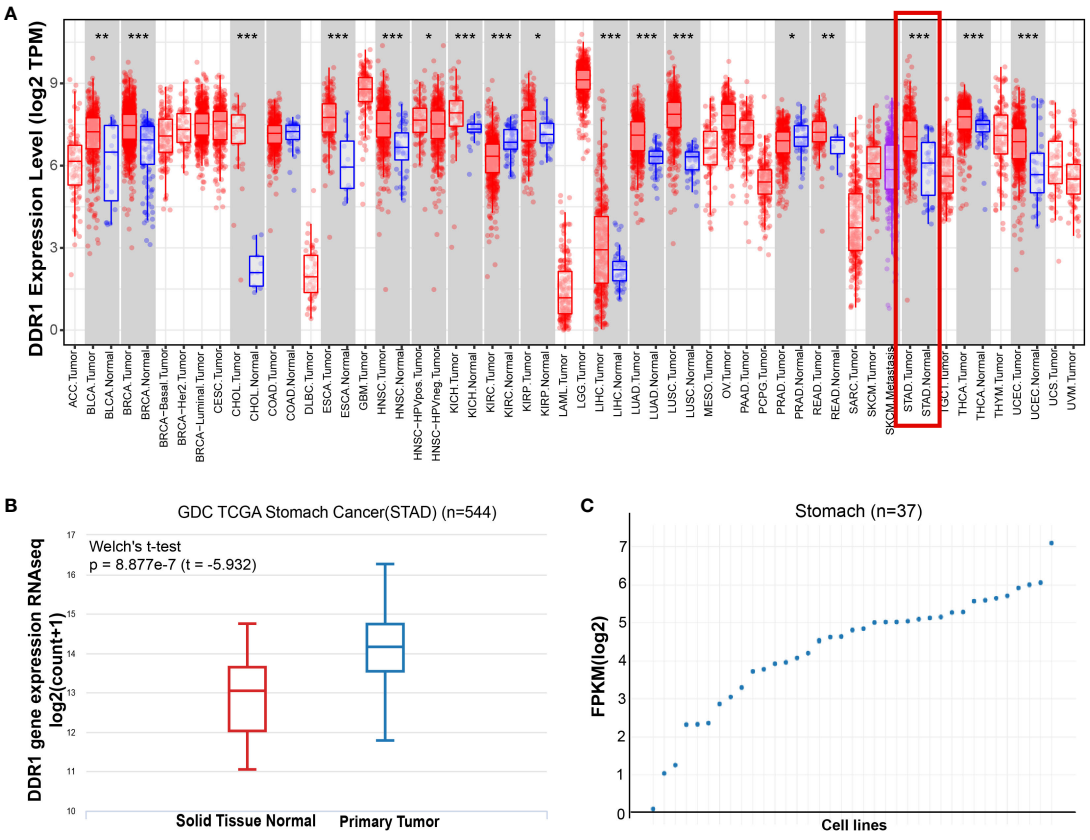

FIGURE 1
The expression level of DDR1 in gastric cancer. **(A)** DDR1 expression levels in multiple tumors and normal tissues were analyzed using the TIMER database (*p < 0.05, **p < 0.01, ***p < 0.001). **(B)** The mRNA level of DDR1 was examined in STAD using UCSC Xena database. Welch's t-test was used for statistical difference. **(C)** A scatter plot of DDR1 expressions in 37 gastric cancer cell lines using the GEDS platform.

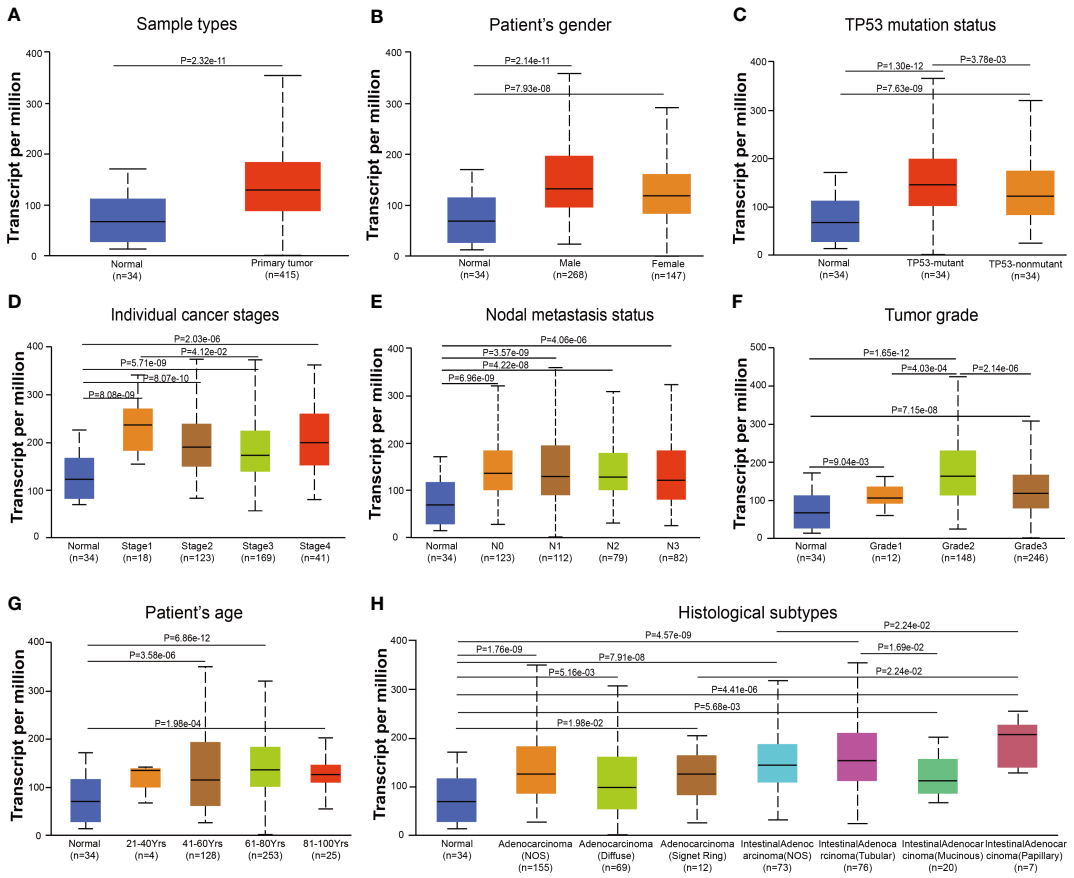

FIGURE 2
DDR1 expression is evaluated in diverse stages based on clinical characteristics by UALCAN database. Analysis of DDR1 expression based on sample types **(A)**, gender **(B)**, TP53 mutation status **(C)**, individual cancer stages **(D)**, nodal metastasis status **(E)**, tumor grades **(F)**, age **(G)**, and histological subtypes **(H)**. Marking the central point is the median. [N0, no regional lymph node metastasis; N1, metastases in one to three axillary lymph nodes; N2, metastases in four to nine axillary lymph nodes; N3, metastases in 10 or more axillary lymph nodes; Grade 1, well differentiated (low grade); Grade 2, moderately differentiated (intermediate grade); Grade 3, poorly differentiated (high grade); Grade 4, undifferentiated (high grade)].

(Figure 2F). Moreover, DDR1 expression of grade 2 was significantly higher than those of grades 1 and 3. With respect to age, DDR1 expression increased significantly in patients over 40 years of age (Figure 2G). Additionally, high DDR1 expressions were observed in various histological subtypes of STAD (Figure 2H).

DDR1 expression correlates with prognosis of cancer patients

To investigate the prognostic value of DDR1 as a target for cancer patients, the PrognoScan database was first employed to evaluate the effect of different DDR1 expression levels on survival situation in patients with multiple cancer types. Preliminary results indicated that the expression of DDR1 was significantly related to the prognosis of patients with various cancer types, including blood, brain, ovarian, lung, prostate, breast and colorectal cancers (Figures 3A–H). Interestingly, with regard to different cancer types and even subtypes, DDR1 expression may be inversely correlated to prognosis. For example, elevated DDR1 expression was significantly correlated with poorer prognosis in acute myelogenous leukemia (AML) but better prognosis in multiple myeloma (MM) (Figures 3A, F).

In addition, the Kaplan–Meier plotter database was also applied to evaluate the prognostic relevance of DDR1 expression levels in various cancers. The elevation of DDR1 expression was observed to be significantly correlated to poor prognosis in patients with lung cancer (OS HR = 1.26,

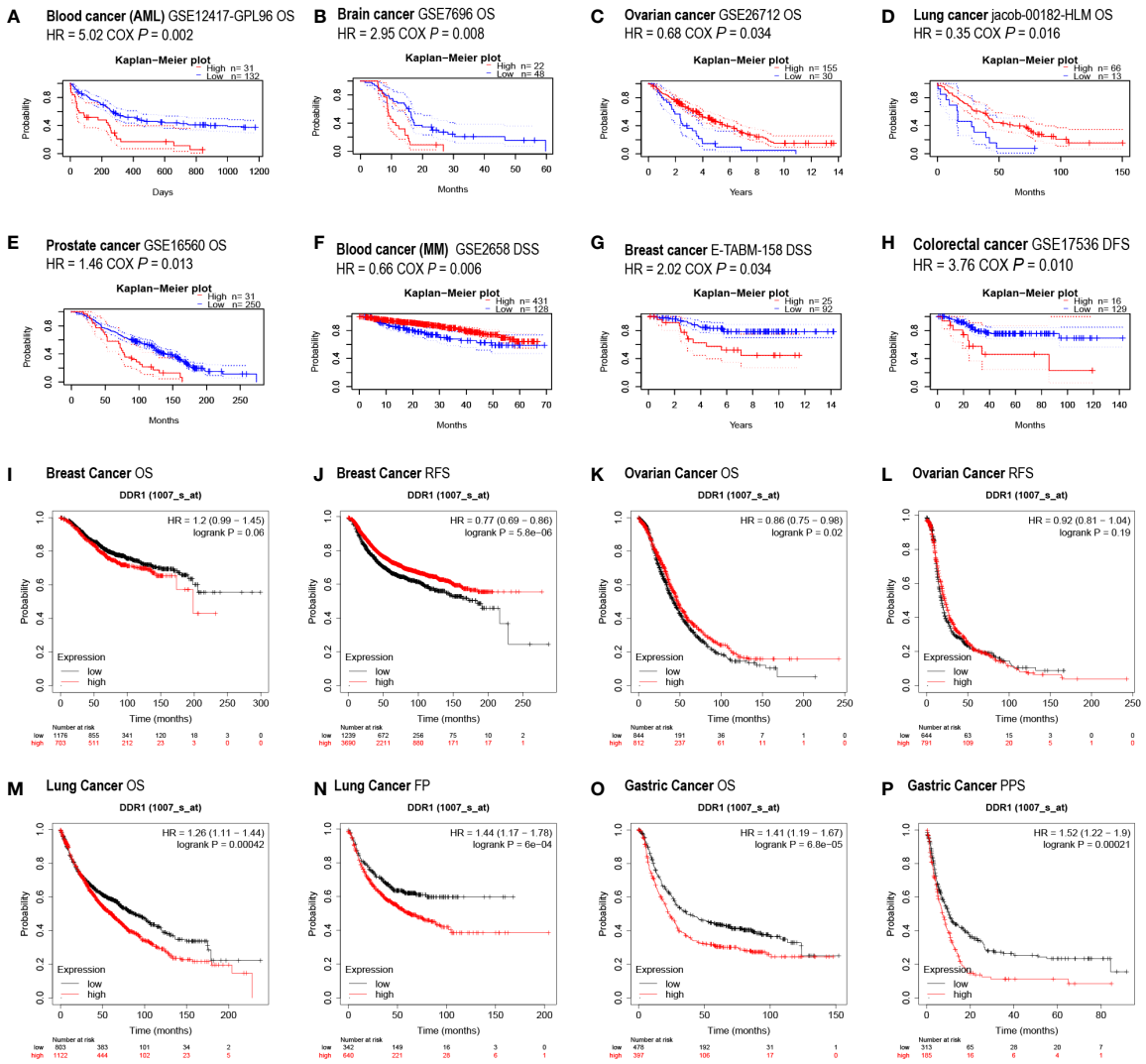

FIGURE 3
Effect of DDR1 expression on different cancers prognosis using PrognoScan and Kaplan–Meier plotter databases. **(A–H)** Survival curves were assessed using PrognoScan database. Survival curves of OS in blood cancer (AML) **(A)**, brain cancer **(B)**, ovarian cancer **(C)**, lung cancer **(D)**, and prostate cancer **(E)** are shown. Survival curves of DSS in blood cancer (MM) **(F)** and breast cancer **(G)** are showed. Survival curve of DFS in the colorectal cancer **(H)** is shown. **(I–P)** Survival curves were analyzed using Kaplan–Meier plotter database. Survival curves of OS **(I)** and RFS **(J)** in breast cancer, OS **(K)** and RFS **(L)** in ovarian cancer, OS **(M)** and FP **(N)** in lung cancer, and OS **(O)** and PPS **(P)** in gastric cancer. AML, acute myelogenous leukemia; MM, multiple myeloma; OS, overall survival; DSS, disease-specific survival; DFS, disease-free survival; RFS, relapse-free survival; FP, first progression; PPS, post-progression survival.

p= 0.00042; FP HR = 1.44, p = 6e–04) and gastric cancer (OS HR = 1.41, p = 6.8e–05; PPS HR = 1.52, p = 0.00021) (Figures 3M–P). However, there was not such a concordant and significant association between the DDR1 expression and the prognosis in breast and ovarian cancer patients (Figures 3I–L).

Eventually, we went the extra mile to investigate the survival curves of 33 TCGA cancer types using GEPIA database, revealing DDR1 expression to be significantly correlated with DFS in CHOL and KICH, OS in mesothelioma (MESO), and both OS and DFS in KIRC (Supplementary Figures S1–3). According to the above analysis, DDR1 expression is clearly demonstrated to be significantly correlated to poorer prognosis across diverse cancer types.

Confirmation of the prognostic value of DDR1 with various clinicopathological characteristics of gastric cancer

Since we have noticed the significant impact of DDR1 expression on the prognosis of gastric cancer patients, the

prognostic value of DDR1 was further evaluated according to various clinicopathological characteristics of gastric cancer by virtue of the Kaplan–Meier plotter database (Table 1). It turned out that the high expression of DDR1 closely related to poor prognosis of both female (OS HR = 1.74, p = 0.002) and male (OS HR = 1.29, p = 0.021; PPS HR = 1.49, p = 0.0026) gastric cancer patients. Specifically, overexpression of DDR1 was significantly correlated with worse OS and PPS in stage 1 (OS HR = 3.21, p = 0.022; PPS HR = 10.27, p = 0.0077) and stage 3 (OS HR = 1.7, p = 0.00026; PPS HR = 2.07, p = 0.00096). In the four N categories and two M categories, stage N2 (OS HR = 2.12, p = 0.0011; PPS HR = 2.28, p = 0.00085) and stage M1 (OS HR = 2.43, p = 0.005; PPS HR = 3.27, p = 0.0025) had the highest HR values of both OS and PPS. Taken together, these results suggest that the high expression of DDR1 affects the prognosis of different gastric cancer classifications to varying degrees.

Genes and proteins that interact with DDR1 in gastric cancer

First, we analyzed DDR1 mutations in gastric cancer using the cBioPortal database. Out of 777 samples, DDR1 gene was altered in 39 (5%) samples (Figure 4A). Most of these mutation types were amplification and deep deletion. There were also a small number of missense mutation, splice mutation, and truncating mutation that might result in unfunctional DDR1. To learn more about the molecular mechanisms involved in DDR1, we used STRING website to search the relationship between DDR1 and its related proteins, while the Cytospace software was applied to generate the network map (Figure 4B). DDR1 was closely related to SHC1 (combined score, 0.949), PTPN11 (combined score, 0.941), TM4SF1 (combined score, 0.904), and WWC1 (combined score, 0.846). Whereafter, we

TABLE 1 Correlation between DDR1 expression and different clinicopathological characteristics in gastric cancer *via* Kaplan–Meier plotter.

Clinicopathological characteristics	OS (n = 881)			PPS (n = 503)		
	N	HR (95%CI)	p-value	N	HR (95%CI)	p-value
Sex						
Female	236	1.74 (1.22–2.48)	**0.0020**	149	1.53 (0.98–2.38)	0.060
Male	544	1.29 (1.04–1.60)	**0.021**	348	1.49 (1.15–1.93)	**0.0026**
Stage						
1	67	3.21 (1.11–9.28)	**0.022**	31	10.27 (1.23–85.58)	**0.0077**
2	140	0.76 (0.36–1.58)	0.45	105	0.63 (0.32–1.22)	0.17
3	305	1.70 (1.28–2.27)	**0.00026**	142	2.07 (1.33–3.22)	**0.00096**
4	148	0.71 (0.47–1.08)	0.11	104	0.73 (0.44–1.20)	0.21
Stage T						
2	241	0.61 (0.40–0.93)	**0.020**	196	0.66 (0.42–1.04)	0.069
3	204	1.77 (1.25–2.52)	**0.0013**	150	1.98 (1.32–2.95)	**0.00071**
4	38	0.29 (0.12–0.70)	**0.0037**	29	0.38 (0.12–1.15)	0.077
Stage N						
0	74	0.59 (0.25–1.40)	0.23	41	0.24 (0.06–1.02)	**0.037**
1	225	1.31 (0.86–2.00)	0.21	169	1.55 (0.95–2.54)	0.079
2	121	2.12 (1.33–3.35)	**0.0011**	105	2.28 (1.39–3.75)	**0.00085**
3	76	0.51 (0.29–0.90)	**0.019**	63	0.57 (0.31–1.03)	0.061
1 + 2 + 3	422	0.83 (0.64–1.09)	0.18	337	1.3 0(0.97–1.76)	0.081
Stage M						
0	444	0.85 (0.64–1.13)	0.25	342	1.38 (1.01–1.88)	**0.04**
1	56	2.43 (1.28–4.61)	**0.0050**	36	3.27 (1.46–7.32)	**0.0025**
Lauren classification						
Intestinal	320	1.86 (1.34–2.59)	**0.00018**	192	2.51 (1.65–3.83)	**0.0000098**
Diffuse	241	0.78 (0.55–1.11)	0.17	176	0.81 (0.55–1.20)	0.29
Differentiation						
Poor	165	1.44 (0.89–2.31)	0.13	49	0.60 (0.31–1.18)	0.13
Moderate	67	1.64 (0.81–3.31)	0.16	24	1.8 0(0.59–5.49)	0.29

p-value of log-rank test compares survival curves between patients with high DDR1 expression and those with low DDR1 expression. Bold values indicate p-value <0.05. OS, overall survival; PPS, post-progression survival; HR, hazard ratio.

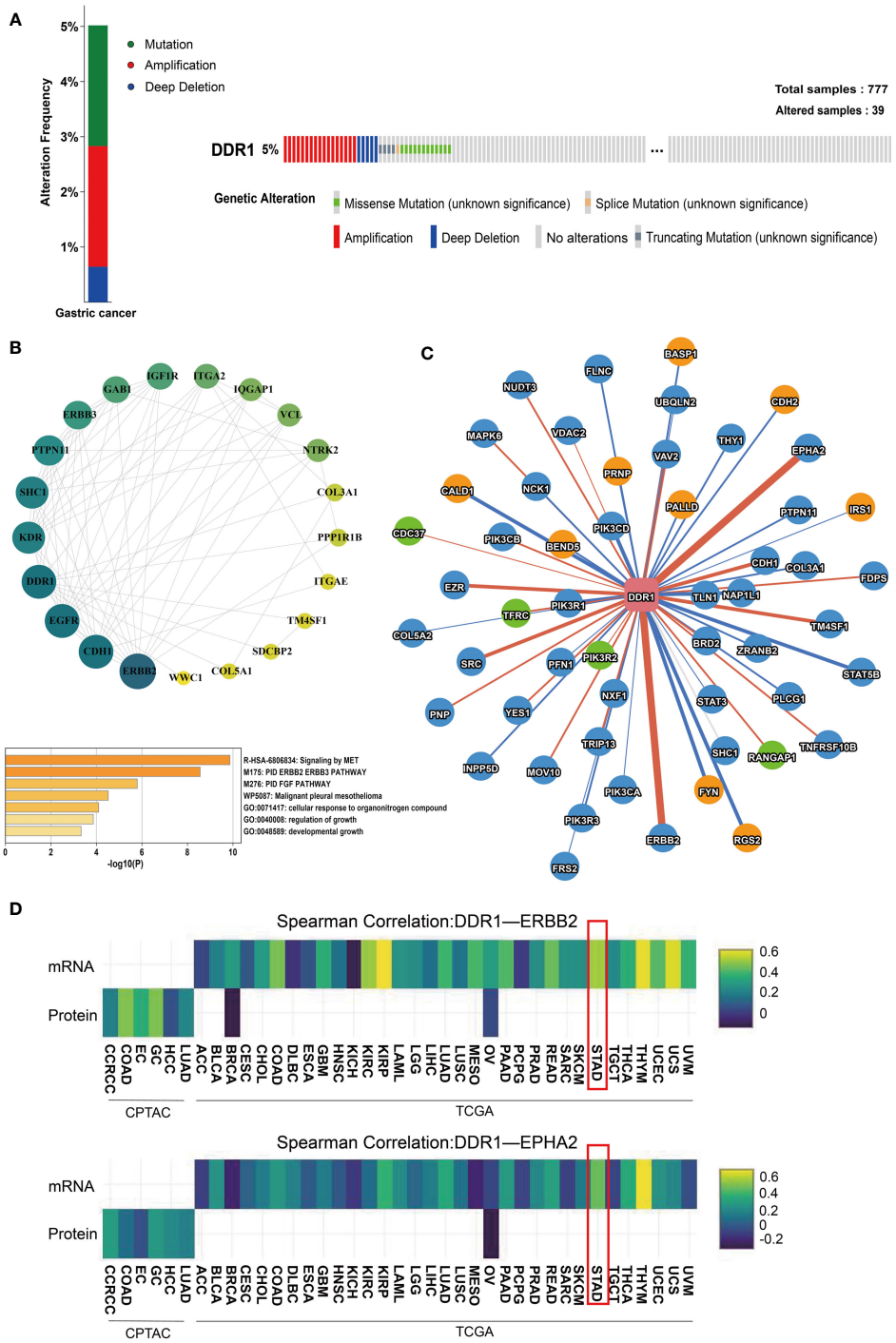

FIGURE 4
Analysis of genes and proteins that interact with DDR1. **(A)** The OncoPrint of DDR1 gene alterations in queried 777 samples of gastric cancer using cBioPortal database. Colors are used to highlight the various genetic alterations. **(B)** A PPI network of DDR1 and its related proteins using the Cytospace software and heatmaps of pathway enrichment using the Metascape. The p-value cutoff is 0.01. **(C)** The interaction network of genes and proteins that interact with DDR1 using PINA database. The yellow nodes represent genes related to poor prognosis ($p < 0.05$, HR>1). The green nodes represent genes connected with good prognosis ($p < 0.05$, HR<1). The red edges represent a positive correlation (FDR <0.05), while the blue edges represent a negative correlation (FDR <0.05). Edge width is relative to correlation coefficients. **(D)** Heatmap shows the correlation coefficients of mRNA expression (top row) and protein abundance (bottom row) among interacting proteins (DDR1-ERBB2 and DDR1-EPHA2) in each tumor type.

used Metascape database for pathway enrichment analysis for the genes above. Pathways were mainly enriched in MET signaling and PID ERBB2 ERBB3 pathway. Considering that the mechanisms of action inside genes differ in different diseases, we used the PINA database to further analyze genes and proteins that interact with DDR1 in STAD. The interaction network diagram of the interacting genes with DDR1 in STAD is shown in Figure 4C. Edge width is relative to correlation coefficients. We noted that ERBB3 and EPHA2 were most strongly associated with DDR1. Therefore, the correlation coefficients of mRNA expression and protein abundance between two genes and DDR1 in tumors were analyzed using heat maps (Figure 4D). ERBB2 is associated with angiogenesis, tumors metastasis, and drug resistance (38). There is also evidence that EPHA2 is linked to increased metastatic potential, poor prognosis, and lower survival rate (39). Considering the role of DDR1, we speculate that DDR1 may be involved in their regulatory mechanism.

DDR1 expression correlates with immune cell infiltration in gastric cancer

Immune cell infiltration has an irreplaceable role in independently predicting prognosis and lymph node metastasis status (40). Therefore, TIMER database was further applied to investigate the effect of DDR1 on the infiltration status of various TIICs in 39 cancer types and subtypes (Supplementary Table S2; Supplementary Figures S4–6). Subsequently, we counted that DDR1 was significantly associated with the tumor purity in 22 types and subtypes of cancer in total and correlated with B-cell infiltration in 12 types and subtypes of cancer, $CD8^+$ T-cell infiltration in 13 types and subtypes of cancer, $CD4^+$ T-cell infiltration in 17 types and subtypes of cancer, macrophage infiltration in 18 types and subtypes of cancer, neutrophil infiltration in 17 types and subtypes of cancer, and dendritic cell (DC) infiltration in 15 types and subtypes of cancer, respectively ($p < 0.05$) (Supplementary Table S2). Concretely, high DDR1 level was significantly and negatively linked to the infiltration of all the above TIICs in STAD, especially $CD8^+$ T cells ($r = -0.257$, $p = 5.32e{-}07$), macrophages ($r = -0.355$, $p = 1.93e{-}12$), and DCs ($r = -0.291$, $p = 1.08e{-}08$) (Figure 5A). However, in DLBC, no significant association between DDR1 and any TIICs was observed. Moreover, we drew Kaplan–Meier plots for different TIICs to visualize the survival differences in STAD using TIMER database, with DLBC serving as a control group. It was only observed that macrophage infiltration was significantly associated to STAD prognosis ($p = 0.004$), while no significant association was noted in DLBC (Figure 5B). Generally, DDR1 level is significantly and negatively associated with immune infiltration in STAD, revealing that DDR1 plays a specific role in gastric cancer through immune cell infiltration, especially $CD8^+$ T cells, macrophages, and DCs.

Correlation between DDR1 expression and various immune markers

To better understand the role of DDR1 in the immune response, the relationships between DDR1 and various markers of diverse TIICs in STAD were further investigated *via* TIMER database (**Table 2**). Among 39 types of cancer analyzed by TIMER database, we found that DDR1 had no significant correlation ($p<0.005$) with six types of TIIC in DLBC, SKCM, and PAAD, which could be better used as the control. In the subsequent correlation analysis of immune markers, DLBC also showed a more significant difference from STAD. Here, we chose DLBC as the control group in order to better highlight the relationship between DDR1 and immune infiltration in STAD. With the adjustment based on purity, the correlation analysis in STAD revealed that DDR1 was closely linked to most of immune markers in various TIICs, such as CD3E of general T cells, CD86 of monocytes, CCL2 of tumor-associated macrophages (TAMs), and CCR7 of neutrophils. However, there were just four immune markers correlated to the DDR1 expression in DLBC ($p < 0.01$) (Table 2).

Interestingly, we noted the significant correlation between DDR1 level and Treg and T cell exhaustion markers like CCR8, PD-1, CTLA-4, and TIM-3 (Table 2), revealing that DDR1 might play a potential role in immune escape in STAD, but further studies are needed about its mechanisms. Furthermore, the DDR1 level was significantly correlated to the majority of monocyte, TAM, and M2 macrophage immune markers in STAD, such as CD86, CCL2, and MS4A4A. To show the relationship between them visually, we thus generated the expression scatterplots in STAD using TIMER database, with DLBC serving as a control group in like manner (Figures 6A, B). Subsequently, the GEPIA database was used to confirm the relationships between DDR1 level and the above monocyte, and TAM, M1, and M2 macrophage markers (Table 3). Just as expected, the correlations in GEPIA corroborated with the previous results. In addition, we directly used 407 STAD samples from TCGA database to calculate the Spearman correlation coefficient of DDR1 and various immune markers (Figure 6C). It also turned out that DDR1 had a significant negative correlation with most immune markers of monocytes, TAMs, M2 macrophages, and DCs, while there was no significant correlation with M1 macrophage markers like PTGS2, or a significantly positive association like IRF5. Therefore, DDR1 may be correlated to regulating the polarization of macrophages in STAD. Simultaneously, its significant correlations with DC markers revealed the significant correlation between DDR1 and DC infiltration.

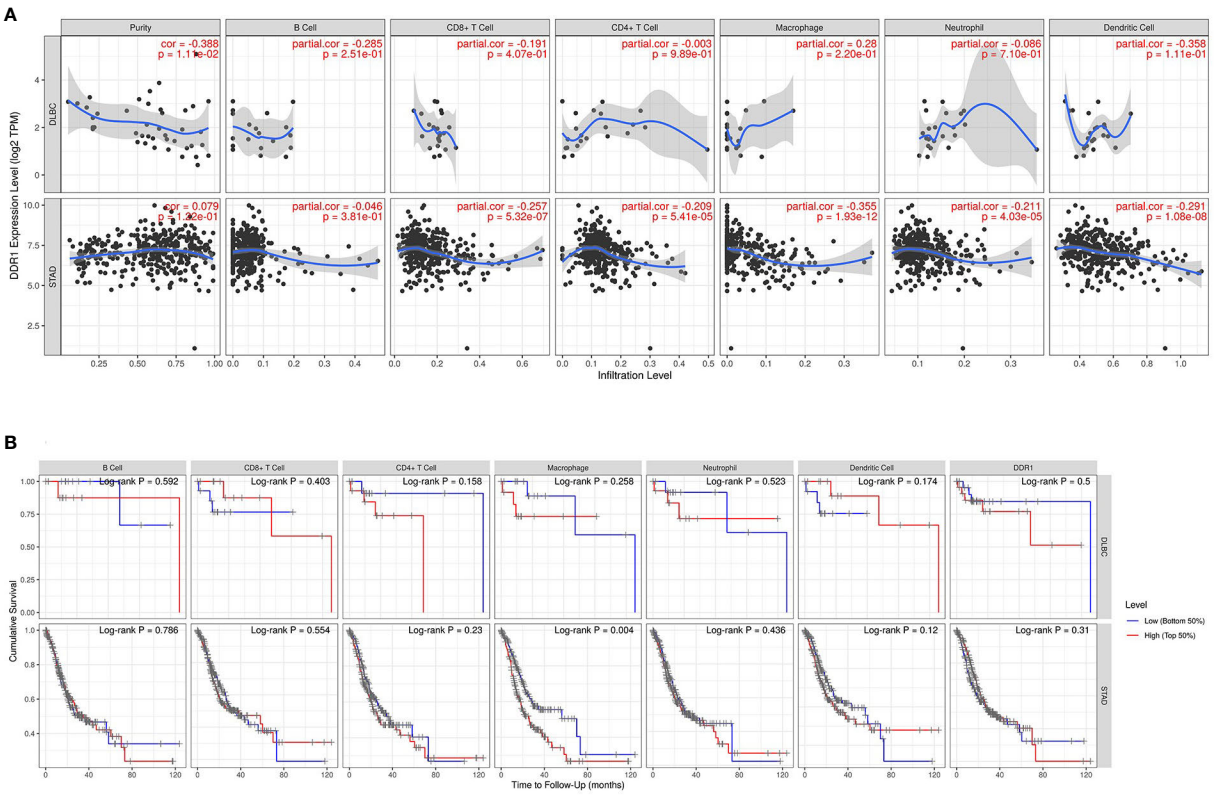

FIGURE 5
DDR1 expression is correlated with immune infiltration in STAD. **(A)** Correlation of DDR1 expression with immune infiltration levels in DLBC and STAD *via* TIMER database. DLBC serves as a control group. **(B)** Kaplan–Meier plots of the relationship between patients' prognosis and immune cells infiltration in DLBC and STAD *via* TIMER database [blue line, low (bottom 50%); red line, high (top 50%)].

Therefore, these findings validate that DDR1 is involved in immune infiltration and immune escape in gastric cancer.

Discussion

Gastric cancer is one of the common malignant tumors worldwide. Due to the difficulty of its early diagnosis and the high late recurrence rate, gastric cancer has poor prognosis and high mortality (41). With the deepening of research, it has been found that gastric cancer, especially in advanced stage, has a strong ability of metastasis and invasion. Inhibition of metastasis thus becomes an essential step in treating gastric cancer. In recent years, more and more researchers have turned their attention to cancer immunotherapy. At present, immunotherapy, such as ICIs, has become a first-line treatment for many advanced cancers. In spite of the fact that ICIs have good efficacy in treating malignant tumors, their application is limited in gastric cancer. A limitation of the application of antibodies is the low or non-response rate in some patients. Promoting intratumoral T-cell infiltration is known to significantly increase the efficacy of PD-1 antibody (42, 43). Therefore, investigating the mechanisms underlying immune cell infiltration is essential to improve the efficacy of ICIs for gastric cancer.

On the basis of previous screening studies, our study selected DDR1 as a target to investigate its role in gastric cancer. As a receptor for collagen tyrosine kinase, DDR1 is a major component of the ECM (44). Previous studies demonstrated that DDR1 was overexpressed and linked to invasion and metastasis in a variety of cancers, such as gastric, bladder, and other cancers (18, 45, 46). A recent study also showed that ECD of DDR1 was associated with immune infiltration of tumors (21). Consequently, we studied data from multiple databases to understand the effect of DDR1 in gastric cancer. Our analysis revealed that the expression of DDR1 was upregulated in gastric cancer (Figure 1). Prognostic analysis conducted by PrognoScan, Kaplan–Meier plotter, and GEPIA databases also suggested that DDR1 affected the prognosis of patients with various types of cancer to varying degrees (Figure 3). These data from multiple sources reflected that the high expression of DDR1 led to a significantly poorer prognosis in gastric cancer patients. Moreover, studies based on gender, tumor–node–metastasis (TNM) stages, Lauren classification, and other clinicopathological characteristics also proved the clinical prognostic value of DDR1 in the treatment of gastric

TABLE 2 Correlation between DDR1 level and markers of immune cells in STAD and DLBC *via* TIMER database.

Description	Gene markers	STAD				DLBC			
		None		Purity		None		Purity	
		Cor	P	Cor	P	Cor	P	Cor	P
CD8$^+$ T cell	CD8A	−0.209	***	−0.220	***	−0.544	**	0.196	0.213
	CD8B	−0.225	***	−0.121	0.018	−0.411	*	0.183	0.246
T cell (general)	CD3D	−0.302	***	−0.315	***	−0.709	***	0.135	0.394
	CD3E	−0.241	***	−0.335	***	−0.750	***	0.145	0.358
	CD2	−0.257	***	−0.303	***	−0.737	***	0.135	0.394
B cell	CD19	−0.232	***	−0.218	***	0.145	0.361	−0.045	0.778
	CD79A	−0.252	***	−0.268	***	0.032	0.841	−0.080	0.612
Monocyte	CD86	−0.202	***	−0.286	***	−0.385	0.012	0.177	0.261
	CD115 (CSF1R)	−0.154	*	−0.208	***	−0.514	**	0.173	0.272
TAM	CCL2	−0.253	***	−0.205	***	−0.252	0.107	0.326	0.036
	CD68	0.072	0.146	−0.159	*	−0.410	*	0.035	0.827
	IL10	−0.165	**	−0.254	***	−0.211	0.180	0.113	0.476
M1 Macrophage	INOS (ISYNA1)	0.156	*	−0.009	0.863	−0.056	0.725	−0.090	0.570
	IRF5	0.178	**	−0.111	0.030	−0.257	0.100	0.020	0.901
	COX2 (PTGS2)	0.010	0.837	−0.126	0.014	−0.324	0.036	0.629	***
M2 Macrophage	CD163	−0.059	0.234	−0.190	**	−0.084	0.597	0.154	0.328
	VSIG4	−0.141	*	−0.166	*	−0.157	0.319	0.114	0.470
	MS4A4A	−0.242	***	−0.191	**	−0.202	0.200	0.189	0.230
Neutrophils	CD66b (CEACAM8)	−0.052	0.293	0.021	0.689	−0.273	0.080	0.199	0.207
	CD11b (ITGAM)	−0.035	0.475	−0.164	*	−0.309	0.046	0.210	0.182
	CCR7	−0.251	***	−0.292	***	−0.498	**	0.367	0.017
NK cell	KIR2DL1	−0.183	**	−0.077	0.137	−0.352	0.022	0.305	0.050
	KIR2DL3	−0.140	*	−0.132	0.010	−0.424	*	0.411	*
	KIR2DL4	−0.024	0.622	−0.165	*	−0.206	0.191	0.242	0.122
	KIR3DL1	−0.156	*	−0.124	0.016	−0.285	0.067	0.108	0.496
	KIR3DL2	−0.175	**	−0.161	*	−0.612	***	0.348	0.024
	KIR3DL3	0.044	0.369	−0.020	0.703	−0.117	0.461	0.122	0.440
	KIR2DS4	−0.131	*	−0.122	0.018	−0.239	0.127	0.092	0.560
DC	HLA-DPB1	−0.206	***	−0.293	***	−0.207	0.188	−0.185	0.240
	HLA-DQB1	−0.078	0.113	−0.282	***	−0.160	0.311	0.111	0.482
	HLA-DRA	−0.132	*	−0.276	***	−0.195	0.215	0.079	0.619
	HLA-DPA1	−0.135	*	−0.276	***	−0.303	0.051	−0.064	0.686
	BDCA-1 (CD1C)	−−0.274	***	−0.285	***	−0.026	0.872	−0.199	0.205
	BDCA-4 (NRP1)	−−0.142	*	−0.173	**	−0.263	0.092	0.337	0.030
	CD11c (ITGAX)	−0.063	0.204	−0.224	***	−0.533	**	0.127	0.422
Th1	T-bet (TBX21)	−0.190	***	−0.254	***	−−0.706	***	0.371	0.016
	STAT4	−0.263	***	−0.245	***	−0.732	***	0.144	0.360
	STAT1	0.156	*	−0.104	0.042	−0.451	*	0.206	0.190
	IFN-γ (IFNG)	−0.054	0.274	−0.190	**	−0.537	**	0.166	0.292
	TNF-α (TNF)	0.101	0.041	−0.281	***	−0.326	0.035	0.150	0.343
Th2	GATA3	−0.201	***	−0.174	**	−0.688	***	0.134	0.395
	BCL6	−0.026	0.599	−0.071	0.049	−0.277	0.011	0.301	*
	IL21	−0.105	0.032	0.011	0.836	0.065	0.684	0.181	0.250
	STAT6	0.201	***	−0.132	0.010	−0.418	*	0.259	0.098
	STAT5A	0.029	0.557	−0.002	0.971	−0.298	0.055	0.377	0.014

(Continued)

10.3389/fimmu.2022.933165

TABLE 2 Continued

Description	Gene markers	STAD				DLBC			
		None		Purity		None		Purity	
		Cor	P	Cor	P	Cor	P	Cor	P
	IL13	−0.042	0.393	−0.135	*	0.181	0.251	−0.097	0.541
Th17	STAT3	0.152	***	−0.136	*	−0.410	*	0.198	0.209
	IL17A	−0.007	0.894	−0.122	0.017	−0.508	**	0.293	0.060
Treg	FOXP3	−0.024	0.630	−0.241	***	−0.633	***	0.337	0.030
	CCR8	−0.028	0.563	−0.168	*	−0.477	*	0.285	0.068
	STAT5B	−0.034	0.489	−0.023	0.661	−0.323	0.037	0.307	0.049
	TGFβ (TGFB1)	−0.061	0.217	−0.169	**	−0.517	**	0.409	*
T cell exhaustion	PD-1 (PDCD1)	−0.084	0.087	−0.175	**	−0.533	**	−0.060	0.704
	CTLA4	−0.087	0.077	−0.197	**	−0.702	***	0.133	0.401
	LAG3	−0.076	0.122	−0.227	***	−0.560	**	0.160	0.312
	TIM-3 (HAVCR2)	−0.127	*	−0.245	***	−0.387	0.011	0.097	0.542
	GZMB	−0.053	0.280	−0.254	***	−0.242	0.122	0.075	0.637

*p < 0.01; **p < 0.001; ***p < 0.0001. TAM, tumor-associated macrophage.

TABLE 3 Correlation between DDR1 level and immune markers of monocyte, TAM, and macrophages of STAD *via* GEPIA database.

Description	Gene markers	STAD			
		Tumor		Normal	
		R	p	R	p
Monocyte	CD86	−0.19	**	0.22	0.20
	CD115 (CSF1R)	−0.11	0.029	0.13	0.46
TAM	CCL2	−0.21	***	−0.52	*
	CD68	0.094	0.058	0.53	*
	IL10	−0.13	*	0.038	0.82
M1 Macrophage	INOS (ISYNA1)	0.16	*	−0.21	0.21
	IRF5	0.24	***	0.69	***
	COX2 (PTGS2)	0.034	0.49	−0.45	*
M2 Macrophage	CD163	−0.12	0.016	−0.42	0.012
	VSIG4	−0.11	0.027	−0.31	0.069
	MS4A4A	−0.20	***	−0.54	**

*p < 0.01; **p < 0.001; ***p < 0.0001.

cancer. The results showed that DDR1 was significantly correlated with a variety of clinicopathological characteristics in STAD (Table 1). Notably, high expression of DDR1 in N2 and M1 stages of gastric cancer had comparatively high HR values in the prognostic analysis, revealing the crucial role of DDR1 in local lymph node metastasis and distant metastasis of gastric cancer. Therefore, we suggest that DDR1 has good prognostic value as a potential tumor therapeutic target in patients with gastric cancer, thereby effectively promoting the development of precision therapy for gastric cancer. Specially, targeting DDR1 is suggested to have a good therapeutic potential for metastatic advanced gastric cancer.

Subsequently, this study further investigated the underlying molecular mechanism of DDR1. We found that DDR1 was closely related to SHC1, PTPN11, TM4SF1, and so on by using STRING. In particular, we found that DDR1 interacted with PPP1R1B. PPP1R1B can modulate downstream signaling of various kinases in pancreatic cancer by regulating proteins phosphatase 1 activity, which in turn regulates the activity of many phosphorylated proteins (47). Among them, the regulation of PPP1R1B induces phosphorylation of Mdm2 Ser166 and promotes the degradation of p53. In addition, DDR1 can regulate p53 *via* the positive feedback of DDR1-RAS/MAPK-p53-P21 module (48). Therefore, we proposed a

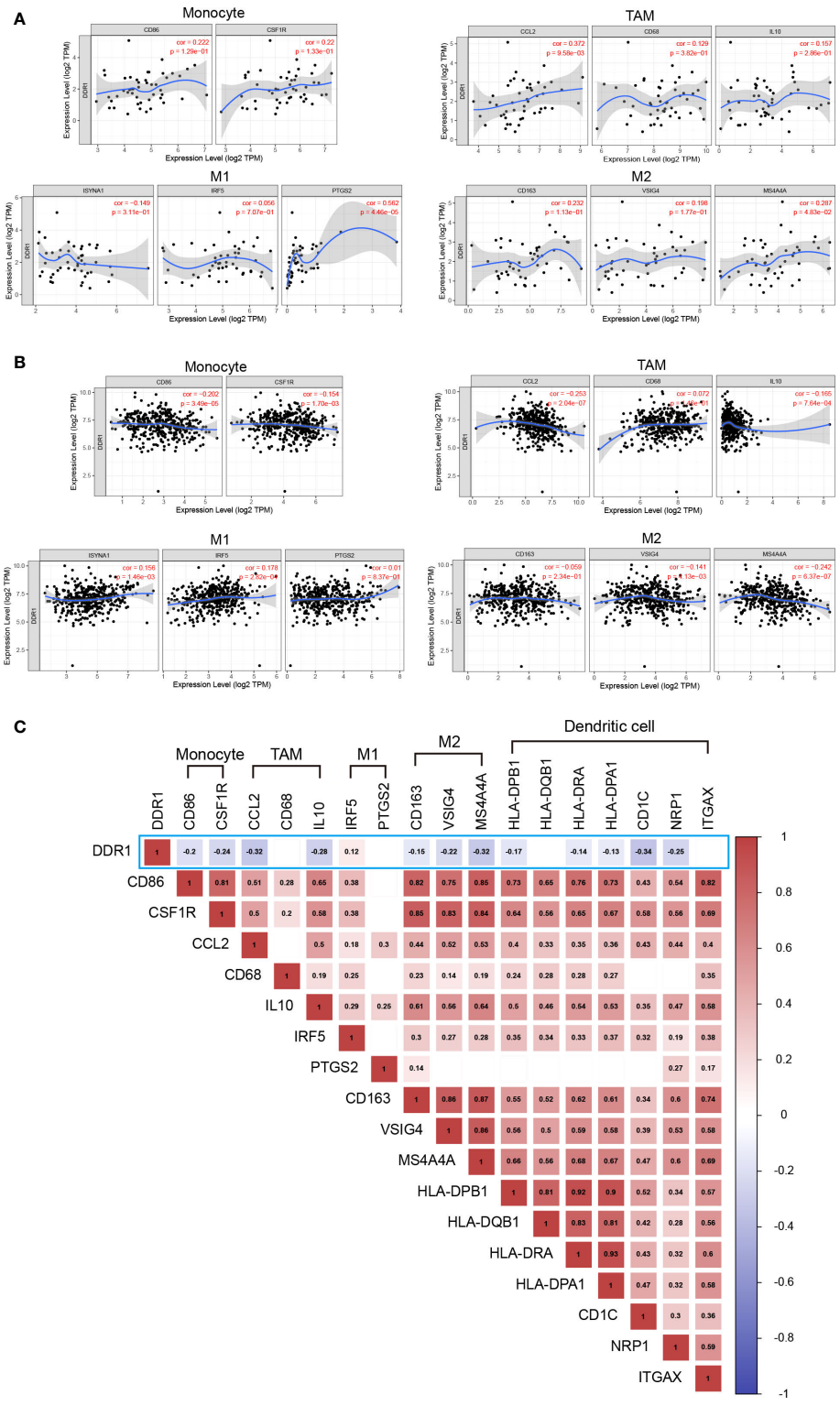

FIGURE 6
Correlation between DDR1 expression level and immune markers in STAD and DLBC. **(A)** Scatterplots of correlation between DDR1 expression level and immunological marker sets of monocytes, TAMs, and M1 and M2 macrophages in DLBC *via* TIMER database. **(B)** Scatterplots of correlation between DDR1 expression level and immunological marker sets of monocytes, TAMs, and M1 and M2 macrophages in STAD *via* TIMER database. **(C)** Correlation heatmap of DDR1 expression level and immunological marker sets of monocytes, TAMs, M1 macrophages, M2 macrophages, and dendritic cells based on 407 STAD samples from TCGA. (Blank indicates the correlation is not significant. The p-value cutoff is 0.05.).

hypothesis that DDR1 interacts with PPP1R1B through the regulation of p53. It would be worthwhile to explore this further. Then, DDR1-interacting genes and proteins were also investigated using the PINA database. The majority of these genes are associated with metastasis and invasion of cancer. The obvious correlation between DDR1 and EBRR2 and the mechanism of action also deserves our further study. In addition, after referring to the analysis of DDR1-related genes in many references and databases, we performed the pathway enrichment analysis of DDR1 and its related genes (9, 16). Pathways were mainly enriched in MET signaling and PID ERBB2 ERBB3 pathway. Here, we also consider that the number of genes that we screened is not large, so the analysis of related pathways also needs further validation.

Previous studies have revealed some key mechanisms of DDR1 in immune infiltration (21, 22). In the present study, we investigated the infiltration situation based on DDR1 in gastric cancer. The results showed that DDR1 expression significantly affected the infiltration of various TIICs in gastric cancer, especially $CD8^+$ cells, macrophages, and DCs (Figure 5A). Thus, DDR1 is reasonably supposed to be involved in macrophage polarization and T-cell activation regulated by DCs and therefore affects immune infiltration. In addition, the prognostic analysis of different TIICs showed that macrophage infiltration significantly correlated with the survival of gastric cancer patients (Figure 5B). Following the assessment of overall infiltration in gastric cancer, we further explored the correlation between DDR1 and various immune cell markers (Figure 6; Table 2). The significant correlation between DDR1 and regulatory T cells and T-cell exhaustion markers such as TGFβ1, PD-1, and CTLA-4 indicated that DDR1 was involved in immune escape and tumor invasion. Moreover, obvious associations between immune markers of T-helper cells and DDR1 were observed as well, such as tumor necrosis factor alpha (TNF-α) of Th1, GATA3 of Th2, and STAT3 of Th17. These results imply the crucial role that DDR1 played in the recruitment, effect, and regulation of various TIICs in gastric cancer.

In summary, this study deepens our understanding of the various roles of DDR1 in the progression of gastric cancer and also demonstrates the potential clinical value of DDR1 as a therapeutic target for gastric cancer. However, there are still limitations in our study. In general, our study principally focused on mRNA levels, and there was not enough data based on protein level to analyze. In addition, we mainly focalize the infiltration study on STAD but lacked the study on other rare subtypes of gastric cancer, such as squamous cell carcinoma of the stomach. In addition, even though there is a significant and negative correlation between DDR1 and many immune markers of various TIICs in gastric cancer, the correlation is not very strong, which also reflects the complexity of the mechanism of immune infiltration. Therefore, the molecular mechanisms and signaling pathways of DDR1 affecting immune infiltration and escape, tumor invasion, and metastasis also remain to be further studied. Overall, our study demonstrates the multiple potentials of DDR1 in the immunotherapy of gastric cancer, including immune infiltration and tumor invasion, and also expands the direction of DDR1 signaling mechanism research. Moreover, all new discoveries of DDR1 may provide a new strategy for improving the efficacy of ICI therapy.

Data availability statement

The datasets presented in this study can be found in online repositories. The names of the repository/repositories and accession number(s) can be found in the article/**Supplementary Material**.

Author contributions

LY, SW, and YF contributed to the conception of the study. DP, HC, and KK contributed the data collection. SW, YF, and KK performed the data analysis. SW and YF wrote the manuscript. YZ, XH, and LY helped perform the analysis with constructive discussions. All authors contributed to article and approved the submitted version.

Funding

This work was supported by Scientific and Innovative Action Plan of Shanghai (no. 20S11901600 and 18431902800) and National Natural Science Foundation of China (no. 81572979).

Conflict of interest

The authors declare that the research was conducted in the absence of any commercial or financial relationships that could be construed as a potential conflict of interest.

Publisher's note

Supplementary material

The Supplementary Material for this article can be found online at: https://www.frontiersin.org/articles/10.3389/fimmu.2022.933165/full#supplementary-material

References

1. Smyth EC, Nilsson M, Grabsch HI, van Grieken NC, Lordick F. Gastric cancer. *Lancet (London England)* (2020) 396(10251):635–48. doi: 10.1016/s0140-6736(20)31288-5

2. Pasechnikov V, Chukov S, Fedorov E, Kikuste I, Leja M. Gastric cancer: Prevention, screening and early diagnosis. *World J Gastroenterol* (2014) 20 (38):13842–62. doi: 10.3748/wjg.v20.i38.13842

3. Li S, Zhang T, Zhou X, Du Z, Chen F, Luo J, et al. The tumor suppressor role of mir-155-5p in gastric cancer. *Oncol Lett* (2018) 16(2):2709–14. doi: 10.3892/ol.2018.8932

4. Tan Z. Recent advances in the surgical treatment of advanced gastric cancer: A review. *Med Sci Monitor Int Med J Exp Clin Res* (2019) 25:3537–41. doi: 10.12659/msm.916475

5. Zayac A, Almhanna K. Esophageal, gastric cancer and immunotherapy: Small steps in the right direction? *Trans Gastroenterol Hepatol* (2020) 5:9. doi: 10.21037/tgh.2019.09.05

6. Muro K, Chung HC, Shankaran V, Geva R, Catenacci D, Gupta S, et al. Pembrolizumab for patients with pd-L1-Positive advanced gastric cancer (Keynote-012): A multicentre, open-label, phase 1b trial. *Lancet Oncol* (2016) 17 (6):717–26. doi: 10.1016/s1470-2045(16)00175-3

7. Angell HK, Bruni D, Barrett JC, Herbst R, Galon J. The immunoscore: Colon cancer and beyond. *Clin Cancer Res Off J Am Assoc Cancer Res* (2020) 26(2):332–9. doi: 10.1158/1078-0432.Ccr-18-1851

8. Waniczek D, Lorenc Z, Śnietura M, Wesecki M, Kopec A, Muc-Wierzgoń M. Tumor-associated macrophages and regulatory T cells infiltration and the clinical outcome in colorectal cancer. *Archivum Immunol Ther Exp* (2017) 65(5):445–54. doi: 10.1007/s00005-017-0463-9

9. Valiathan RR, Marco M, Leitinger B, Kleer CG, Fridman R. Discoidin domain receptor tyrosine kinases: New players in cancer progression. *Cancer Metastasis Rev* (2012) 31(1-2):295–321. doi: 10.1007/s10555-012-9346-z

10. Vogel W, Gish GD, Alves F, Pawson T. The discoidin domain receptor tyrosine kinases are activated by collagen. *Mol Cell* (1997) 1(1):13–23. doi: 10.1016/s1097-2765(00)80003-9

11. Leitinger B. Discoidin domain receptor functions in physiological and pathological conditions. *Int Rev Cell Mol Biol* (2014) 310:39–87. doi: 10.1016/b978-0-12-800180-6.00002-5

12. Quan J, Yahata T, Adachi S, Yoshihara K, Tanaka K. Identification of receptor tyrosine kinase, discoidin domain receptor 1 (Ddr1), as a potential biomarker for serous ovarian cancer. *Int J Mol Sci* (2011) 12(2):971–82. doi: 10.3390/ijms12020971

13. Ambrogio C, Gómez-López G, Falcone M, Vidal A, Nadal E, Crosetto N, et al. Combined inhibition of Ddr1 and notch signaling is a therapeutic strategy for kras-driven lung adenocarcinoma. *Nat Med* (2016) 22(3):270–7. doi: 10.1038/nm.4041

14. Weiner HL, Huang H, Zagzag D, Boyce H, Lichtenbaum R, Ziff EB. Consistent and selective expression of the discoidin domain receptor-1 tyrosine kinase in human brain tumors. *Neurosurgery* (2000) 47(6):1400–9. doi: 10.1097/00006123-200012000-00028

15. Chou ST, Peng HY, Mo KC, Hsu YM, Wu GH, Hsiao JR, et al. Microrna-486-3p functions as a tumor suppressor in oral cancer by targeting Ddr1. *J Exp Clin Cancer Res CR* (2019) 38(1):281. doi: 10.1186/s13046-019-1283-z

16. Lin Y, Jin H, Wu X, Jian Z, Zou X, Huang J, et al. The cross-talk between Ddr1 and Stat3 promotes the development of hepatocellular carcinoma. *Aging* (2020) 12(14):14391–405. doi: 10.18632/aging.103482

17. Deng J, Kang Y, Cheng CC, Li X, Dai B, Katz MH, et al. Ddr1-induced neutrophil extracellular traps drive pancreatic cancer metastasis. *JCI Insight* (2021) 6(17):e146133. doi: 10.1172/jci.insight.146133

18. Xie R, Wang X, Qi G, Wu Z, Wei R, Li P, et al. Ddr1 enhances invasion and metastasis of gastric cancer *Via* epithelial-mesenchymal transition. *Tumour Biol J Int Soc Oncodevelopmental Biol Med* (2016) 37(9):12049–59. doi: 10.1007/s13277-016-5070-6

19. Wang S, Xie Y, Bao A, Li J, Ye T, Yang C, et al. Nilotinib, a discoidin domain receptor 1 (Ddr1) inhibitor, induces apoptosis and inhibits migration in breast cancer. *Neoplasma* (2021) 68(5):975–82. doi: 10.4149/neo_2021_201126N1282

20. Gao Y, Zhou J, Li J. Discoidin domain receptors orchestrate cancer progression: A focus on cancer therapies. *Cancer Sci* (2021) 112(3):962–9. doi: 10.1111/cas.14789

21. Sun X, Wu B, Chiang HC, Deng H, Zhang X, Xiong W, et al. Tumour Ddr1 promotes collagen fibre alignment to instigate immune exclusion. *Nature* (2021) 599(7886):673–8. doi: 10.1038/s41586-021-04057-2

22. Zhong X, Zhang W, Sun T. Ddr1 promotes breast tumor growth by suppressing antitumor immunity. *Oncol Rep* (2019) 42(6):2844–54. doi: 10.3892/or.2019.7338

23. Zhavoronkov A, Ivanenkov YA, Aliper A, Veselov MS, Aladinskiy VA, Aladinskaya AV, et al. Deep learning enables rapid identification of potent Ddr1 kinase inhibitors. *Nat Biotechnol* (2019) 37(9):1038–40. doi: 10.1038/s41587-019-0224-x

24. Li T, Fan J, Wang B, Traugh N, Chen Q, Liu JS, et al. Timer: A web server for comprehensive analysis of tumor-infiltrating immune cells. *Cancer Res* (2017) 77 (21):e108–e10. doi: 10.1158/0008-5472.Can-17-0307

25. Li B, Severson E, Pignon JC, Zhao H, Li T, Novak J, et al. Comprehensive analyses of tumor immunity: Implications for cancer immunotherapy. *Genome Biol* (2016) 17(1):174. doi: 10.1186/s13059-016-1028-7

26. Jeanquartier F, Jean-Quartier C, Holzinger A. Use case driven evaluation of open databases for pediatric cancer research. *BioData Min* (2019) 12:2. doi: 10.1186/s13040-018-0190-8

27. Xia M, Liu CJ, Zhang Q, Guo AY. Geds: A gene expression display server for mrnas, mirnas and proteins. *Cells* (2019) 8(7):675. doi: 10.3390/cells8070675

28. Chandrashekar DS, Bashel B, Balasubramanya SAH, Creighton CJ, Ponce-Rodriguez I, Chakravarthi B, et al. Ualcan: A portal for facilitating tumor subgroup gene expression and survival analyses. *Neoplasia (New York NY)* (2017) 19(8):649–58. doi: 10.1016/j.neo.2017.05.002

29. Mizuno H, Kitada K, Nakai K, Sarai A. Prognoscan: A new database for meta-analysis of the prognostic value of genes. *BMC Med Genomics* (2009) 2:18. doi: 10.1186/1755-8794-2-18

30. Lánczky A, Győrffy B. Web-based survival analysis tool tailored for medical research (Kmplot): Development and implementation. *J Med Internet Res* (2021) 23(7):e27633. doi: 10.2196/27633

31. Tang Z, Li C, Kang B, Gao G, Li C, Zhang Z. Gepia: A web server for cancer and normal gene expression profiling and interactive analyses. *Nucleic Acids Res* (2017) 45(W1):W98–w102. doi: 10.1093/nar/gkx247

32. Szklarczyk D, Gable AL, Nastou KC, Lyon D, Kirsch R, Pyysalo S, et al. The string database in 2021: Customizable protein-protein networks, and functional characterization of user-uploaded Gene/Measurement sets. *Nucleic Acids Res* (2021) 49(D1):D605–d12. doi: 10.1093/nar/gkaa1074

33. Szklarczyk D, Gable AL, Lyon D, Junge A, Wyder S, Huerta-Cepas J, et al. String V11: Protein-protein association networks with increased coverage, supporting functional discovery in genome-wide experimental datasets. *Nucleic Acids Res* (2019) 47(D1):D607–d13. doi: 10.1093/nar/gky1131

34. Szklarczyk D, Morris JH, Cook H, Kuhn M, Wyder S, Simonovic M, et al. The string database in 2017: Quality-controlled protein-protein association networks, made broadly accessible. *Nucleic Acids Res* (2017) 45(D1):D362–d8. doi: 10.1093/nar/gkw937

35. Du Y, Cai M, Xing X, Ji J, Yang E, Wu J. Pina 3.0: Mining cancer interactome. *Nucleic Acids Res* (2021) 49(D1):D1351–d7. doi: 10.1093/nar/gkaa1075

36. Cowley MJ, Pinese M, Kassahn KS, Waddell N, Pearson JV, Grimmond SM, et al. Pina V2.0: Mining interactome modules. *Nucleic Acids Res* (2012) 40 (Database issue):D862–5. doi: 10.1093/nar/gkr967

37. Wu J, Vallenius T, Ovaska K, Westermarck J, Mäkelä TP, Hautaniemi S. Integrated network analysis platform for protein-protein interactions. *Nat Methods* (2009) 6(1):75–7. doi: 10.1038/nmeth.1282

38. Moasser MM. The oncogene Her2: Its signaling and transforming functions and its role in human cancer pathogenesis. *Oncogene* (2007) 26(45):6469–87. doi: 10.1038/sj.onc.1210477

39. Xiao T, Xiao Y, Wang W, Tang YY, Xiao Z, Su M. Targeting Epha2 in cancer. *J Hematol Oncol* (2020) 13(1):114. doi: 10.1186/s13045-020-00944-9

40. Ravelli A, Roviello G, Cretella D, Cavazzoni A, Biondi A, Cappelletti MR, et al. Tumor-infiltrating lymphocytes and breast cancer: Beyond the prognostic and predictive utility. *Tumour Biol J Int Soc Oncodevelopmental Biol Med* (2017) 39 (4):1010428317695023. doi: 10.1177/1010428317695023

41. Zhou L, Li SH, Wu Y, Xin L. Establishment of a prognostic model of four genes in gastric cancer based on multiple data sets. *Cancer Med* (2021) 10 (10):3309–22. doi: 10.1002/cam4.3654

42. Zhang H, Bi Y, Wei Y, Liu J, Kuerban K, Ye L. Blocking Wnt/β-catenin signal amplifies anti-Pd-1 therapeutic efficacy by inhibiting tumor growth, migration, and promoting immune infiltration in glioblastomas. *Mol Cancer Ther* (2021) 20(7):1305–15. doi: 10.1158/1535-7163.Mct-20-0825

43. Li J, Zhang H, Bei S, Zhang X, Li H, Ye L, et al. Disruption of Wnt/β-catenin pathway elevates the sensitivity of gastric cancer cells to pd-1 antibody. *Curr Mol Pharmacol* (2021) 15(3):557-69. doi: 10.2174/1874467214666210617163821

44. Vanharanta S, Massagué J. Origins of metastatic traits. *Cancer Cell* (2013) 24 (4):410–21. doi: 10.1016/j.ccr.2013.09.007

45. Shen Q, Cicinnati VR, Zhang X, Iacob S, Weber F, Sotiropoulos GC, et al. Role of microrna-199a-5p and discoidin domain receptor 1 in human hepatocellular carcinoma invasion. *Mol Cancer* (2010) 9:227. doi: 10.1186/1476-4598-9-227

46. Xie X, Rui W, He W, Shao Y, Sun F, Zhou W, et al. Discoidin domain receptor 1 activity drives an aggressive phenotype in bladder cancer. *Am J Trans Res* (2017) 9(5):2500–7.

47. Tiwari A, Tashiro K, Dixit A, Soni A, Vogel K, Hall B, et al. Loss of Hif1a from pancreatic cancer cells increases expression of Ppp1r1b and degradation of P53 to promote invasion and metastasis. *Gastroenterology* (2020) 159(5):1882–97.e5. doi: 10.1053/j.gastro.2020.07.046

48. Ongusaha PP, Kim JI, Fang L, Wong TW, Yancopoulos GD, Aaronson SA, et al. P53 induction and activation of Ddr1 kinase counteract P53-mediated apoptosis and influence P53 regulation through a positive feedback loop. *EMBO J* (2003) 22(6):1289–301. doi: 10.1093/emboj/cdg129

frontiers | Frontiers in Immunology

ORIGINAL RESEARCH
published: 22 July 2022
doi: 10.3389/fimmu.2022.923194

Single-Cell RNA-Sequencing Atlas Reveals the Tumor Microenvironment of Metastatic High-Grade Serous Ovarian Carcinoma

Yingqing Deng[1,2†], Yuan Tan[1†], Dongmei Zhou[3†], Youhuang Bai[2†], Ting Cao[3], Caizhou Zhong[1,2], Weilai Huang[4,5], Yuhua Ou[6], Linlang Guo[7], Qianqian Liu[8], Deling Yin[2], Lipai Chen[8], Xiping Luo[6], Deqiang Sun[1,2,5] and Xiujie Sheng[3*]*

[1] Key Laboratory of Biological Targeting Diagnosis, Therapy and Rehabilitation of Guangdong Higher Education Institutes, The Fifth Affiliated Hospital of Guangzhou Medical University, Guangzhou, China, [2] Department of Cardiology of The Second Affiliated Hospital, Cardiovascular Key Laboratory of Zhejiang Province, School of Medicine, Zhejiang University, Hangzhou, China, [3] Department of Obstetrics and Gynecology, Center for Reproductive Medicine/Department of Fetal Medicine and Prenatal Diagnosis/BioResource Research Center, Key Laboratory for Major Obstetric Disease of Guangdong Province, The Third Affiliated Hospital of Guangzhou Medical University, Guangzhou, China, [4] School of Life Science and Technology, Tongji University, Shanghai, China, [5] Department of Research and Development, Zhejiang Gaomei Genomics, Hangzhou, China, [6] Department of Obstetrics and Gynecology, Guangdong Women and Children Hospital, Guangzhou, China, [7] Department of Pathology, Zhujiang Hospital, Southern Medical University, Guangzhou, China, [8] Affiliated Cancer Hospital and Institute of Guangzhou Medical University, Guangzhou, China

OPEN ACCESS

Edited by:
Xian Zeng,
Fudan University, China

Reviewed by:
Chen Wang,
Mayo Clinic, United States
Juliette Roels,
Ghent University, Belgium

***Correspondence:**
Deqiang Sun
deqiang@zju.edu.cn
Xiujie Sheng
2008691150@gzhmu.edu.cn

†These authors have contributed equally to this work

Specialty section:
This article was submitted to Cancer Immunity and Immunotherapy, a section of the journal Frontiers in Immunology

Received: *19 April 2022*
Accepted: *20 June 2022*
Published: *22 July 2022*

Citation:
Deng Y, Tan Y, Zhou D, Bai Y, Cao T, Zhong C, Huang W, Ou Y, Guo L, Liu Q, Yin D, Chen L, Luo X, Sun D and Sheng X (2022) Single-Cell RNA-Sequencing Atlas Reveals the Tumor Microenvironment of Metastatic High-Grade Serous Ovarian Carcinoma. Front. Immunol. 13:923194. doi: 10.3389/fimmu.2022.923194

Ovarian cancer is the most common and lethal gynecological tumor in women worldwide. High-grade serous ovarian carcinoma (HGSOC) is one of the histological subtypes of epithelial ovarian cancer, accounting for 70%. It often occurs at later stages associated with a more fatal prognosis than endometrioid carcinomas (EC), another subtype of epithelial ovarian cancer. However, the molecular mechanism and biology underlying the metastatic HGSOC (HG_M) immunophenotype remain poorly elusive. Here, we performed single-cell RNA sequencing analyses of primary HGSOC (HG_P) samples, metastatic HGSOC (HG_M) samples, and endometrioid carcinomas (EC) samples. We found that ERBB2 and HOXB-AS3 genes were more amplified in metastasis tumors than in primary tumors. Notably, high-grade serous ovarian cancer metastases are accompanied by dysregulation of multiple pathways. Malignant cells with features of epithelial-mesenchymal transition (EMT) affiliated with poor overall survival were identified. In addition, cancer-associated fibroblasts with EMT-program were enriched in HG_M, participating in angiogenesis and immune regulation, such as IL6/STAT3 pathway activity. Compared with ECs, HGSOCs exhibited higher T cell infiltration. PRDM1 regulators may be involved in T cell exhaustion in ovarian cancer. The CX3CR1_macro subpopulation may play a role in promoting tumor progression in ovarian cancer with high expression of

BAG3, IL1B, and VEGFA. The new targets we discovered in this study will be useful in the future, providing guidance on the treatment of ovarian cancer.

Keywords: scRNA-seq, tumor microenvironment, T cells, myeloid cells, high-grade serous ovarian carcinoma

INTRODUCTION

Epithelial ovarian cancer usually occurs at an advanced stage and is the most common cause of death from gynecological cancer (1). High-grade serous ovarian carcinoma (HGSOC) is a common histological subtype of epithelial ovarian carcinoma, for 70 to 80%, while the endometrioid carcinoma (EC) subtype accounts for 10% (2). HGSOC is associated with a more fatal prognosis and frequent recurrences, with more than 85% of women with this type having a 10-year mortality rate of 70%, whereas endometrioid carcinoma is thought to originate in endometriosis, a histologic type that tends to have a better prognosis. Our knowledge of the molecular etiology and clinical pathology of HGSOC has greatly improved, and recent therapy has advanced (3–6). However, most patients are diagnosed at a late stage, when cancer has already metastasized, and the diagnosis results in 5-year survival of 30%. Accordingly, the development of effective therapies for metastatic ovarian cancer is urgently needed. To do so, we need to comprehensively characterize the cellular heterogeneity and define transcriptional features within the tumor microenvironment.

Genomic analysis of HGSOC revealed a mutation in the tumor suppressor gene TP53, which is also seen in endometrioid carcinoma (3), promoting ovarian cancer metastasis and chemoresistance, and defecting in homologous recombination (HR) DNA repair, which contributes to the somatic BRCA mutation (7). The Cancer Genome Atlas (TCGA) project has classified HGSOC into four transcriptional subtypes: 'differentiated', 'immunoreactive', 'proliferative', and 'mesenchymal' (8, 9).

Recently, a scRNA-seq study of six metastatic omental tumors that derived from primary HGSOCs unraveled the genetic signatures of immune cell subsets within the tumor microenvironment and identified $NR1H2^+$ $IRF8^+$ and $CD274^+$ macrophage clusters, which were suggested with an anti-tumor response (10). Another scRNA-seq study revealed that the inhibition of the JAK/STAT pathway has potential anti-tumor activity (11). The heterogeneity of tumor cells and different immune cell types within the TME play a paramount role in shaping tumor behavior (12–14). Therefore, characterizing the complex interplay between tumor cells and immune cell phenotype within HGSOC will be beneficial to find the critical factors of ovarian carcinogenesis, metastasis, and targeted treatment.

In this study, we conducted single-cell RNA sequencing of five primary high-grade serous carcinomas samples (HG_P), three metastases from HGSOC to the peritoneum (HG_M), one normal ovarian sample, and two primary Endometrioid (EC_P) samples. By comparing HG_M with HG_P and EC_P, we comprehensively characterized the heterogeneity of tumor cells and immune cells in ovarian cancer lesions, as well as the dynamic changes in cell-type composition and intercellular interactions, providing new insights into the biological basis of the development of HGSOCs and ECs.

RESULTS

Single-Cell Transcriptomic Profiling of the Cellular Heterogeneity of the HGSOCs

Droplet-based single RNA-seq (10X Genomic) was performed on a total of eight samples from five treatment-naive patients. For parallel analyses, the public scRNA-data of 1 HG_P and 2 HG_M samples (15) from the same patient were downloaded (**Figure 1A**, **Tables S1, S2**). After quality filtering, approximately 0.68 billion unique molecular identifiers (UMIs) were collected from 55802 cells with >250 genes detected. Of these cells, 28,571(51.2%) cells were from HG_P, 8925 (16%) cells were from HG_M, and 12751(22.9%) cells were from EC_P. All high-quality cells were used to perform canonical correlation analysis (CCA) and identify anchors or mutual nearest neighbors (MNNs). Then, we integrated all cells, conducting unsupervised graph-based clustering (16).

By Uniform Manifold Approximation and Projection (UMAP) with the resolution of 1.1, we identified 10 major lineages (epithelial cells, B cells, NK cells, T cells, plasma cells, fibroblasts, mesenchymal stem cells (MSCs), endothelial cells, neutrophils, and myeloid cells) (**Figures 1B, C**, **S1A**). The cell types were mainly assigned based on canonical cell markers and functional categories according to significantly differential genes expressed from different clusters (17, 18). One remaining cluster was labeled as "N" because we could not confidently recognize this cell type (10). The respective proportion of each cell type was varied and significantly differed between tumors (**Figure 1D**, proportion test, df=10, p-value < 2.2e-16). Interestingly, the boxplot exhibited that the medians in B cells, NK/T cells, and myeloid cells were higher in HG_P than HG_M and EC_P, whereas plasma cells were more enriched in EC_P (**Figure S1B**).

Previously, The Cancer Genome Atlas (TCGA) had stratified HGSOC into four molecular subtypes. We wondered if the inter-patient variability among tumors were consistent with these subtypes. To this end, we assigned molecular subtypes to our samples with the consensusOV (9) classifier (Version 1.14.0) (**Figure 1D**, **S2A**). We found that all four subtypes were well presented in each ovarian lesion. EC_P expressed the DIF signature slightly over HG_P and HG_M, while HG_P was comparable with HG_M, and EC_P presented the lowest IMR signature, supporting low immune-cell infiltration (**Figure 1E**). What's more, certain subtypes tended to be consistent with specific cell types (**Figure S2B**). Epithelial cells highly expressed the differential (DIF) signature and lesser expressed proliferative (PRO) signature. The mesenchymal (MES) signature was strongly expressed by the fibroblasts and MSCs cells, while the immunoreactive (IMR) signature mainly consisted of myeloid, T cells, and NK cells. Notably, more fibroblasts were classified as proliferative subtypes in our data, suggesting that there are more fibroblasts with relatively high tumor purity. Based on this result, we wanted to know which genes made the most contribution to this

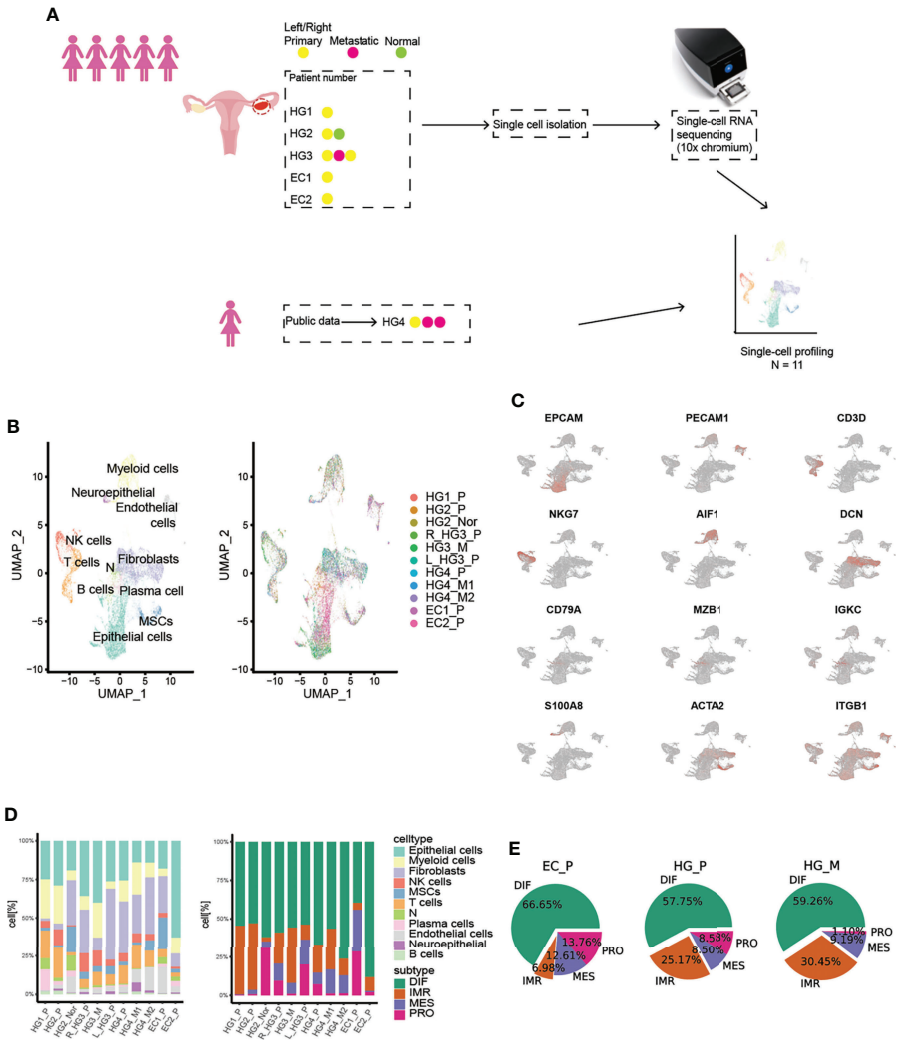

FIGURE 1 | Overview of TME in primary HGSOCs, metastatic HGSOCs, and ECs. **(A)** Workflow of the samples collected and the data analysis strategy. **(B)** Cell populations identified. The UMAP projection of 55802 single cells from HG_P (n=5), HG_M (N=3), EC_P (n=2), HG_Nor (n=1) samples shows the 10 main clusters with annotation. Each dot corresponds to a single cell, colored according to cell type. **(C)** Canonical cell markers are used to identify the clusters. **(D)** Barplots of the cell type and cancer subtypes for all 11 tumors. **(E)** The cancer subtypes proportion for each pathological group.

classification. Thus, we extracted markers that were used for classification and calculated their average expression in each cell type (**Figure S3A**). As expected, proliferative markers such as MARCKSL1, STMN1, UCHL1, MFAP2, TRO, etc. are indeed expressed at higher levels in fibroblasts than others. Likewise, we plotted these markers in the heatmap in each cell of fibroblasts (**Figure S3B**) and we found PRO-markers like MARCKSL1 and STMN1, especially for MARCKSL1, which are highly expressed in most cells. And these markers contribute the most to the classifications of proliferative-subtype, while other PRO-related markers, UCHL1 and MFAP2, are not expressed significantly per cell in fibroblasts though their average expression is higher than other cell types. These results illustrated the importance of fibroblasts in cancer progression and indicated that a subset of fibroblasts in our data is cancer-associated fibroblasts (CAFs).

In addition, we can assess TCGA-subtypes at the patient level from our single-cell data by calculating the average of each gene per sample. Validated with the dataset from a previous study (19) (**Figure S4A-4C**), we had a high degree of confidence to infer the subtypes of HG1_P, HG2_P, HG4_M2, and EC2_P (**Figure S4D, 4E**). Their subtypes are likely to be IMR, IMR, MES, and DIF. Overall, our findings fully illustrated the difference in subtype classification between bulk samples and single-cell data, where single cells can more accurately describe the TCGA-subtype and characterize the heterogeneity of ovarian cancer.

Distinguish Worse Survival Cells from Cancer Epithelial Cells of HGSOCs

Based on the expression of PAX8 and CD24 (20, 21), we found that they were mainly expressed in epithelial cells as well as the subtype

DIF (**Figures S2A, S5A**), which we termed "cancer epithelial cells". In addition, we used T cells and myeloid cells from the normal sample (HG2_nor) as controls by inferring chromosomal copy number alterations (InferCNV, Version 1.2.1) (11) to confirm this (**Figure S6**). As shown below, we found that CNV trends in the same chromosomal region of different primary patients were distinct, whereas they were approximately consistent in the same patient (**Figures 2A, B**, **S5B**). Obviously, the genes generally mutated in ovarian cancer were more amplified in chr17 in HG3_M than in the primary tumors on both sides, such as the ERBB2 and HOXB-AS3 genes, which are generally mutated in ovarian cancer (8). These results demonstrated both intertumoral heterogeneity between patients and consistency within the same patient lesion.

Re-running UMAP analysis on these cells, a total of eight subclusters were identified, of which revealed interpatient tumor-specific clusters (22, 23) (**Figure 2C**). Conversely, re-clustering the subsets like T cells and fibroblast cells without integration, we found that ovarian lesions from the same batch clustered together (**Figure S5C**). Differentially expressed genes in each cluster, interpatient GSVA, and cell cycle analysis were also shown (**Figures 2D** and **S5D, 5E**). We then used a Scissor algorithm (Version 2.0.0) to classify cells associated with worse

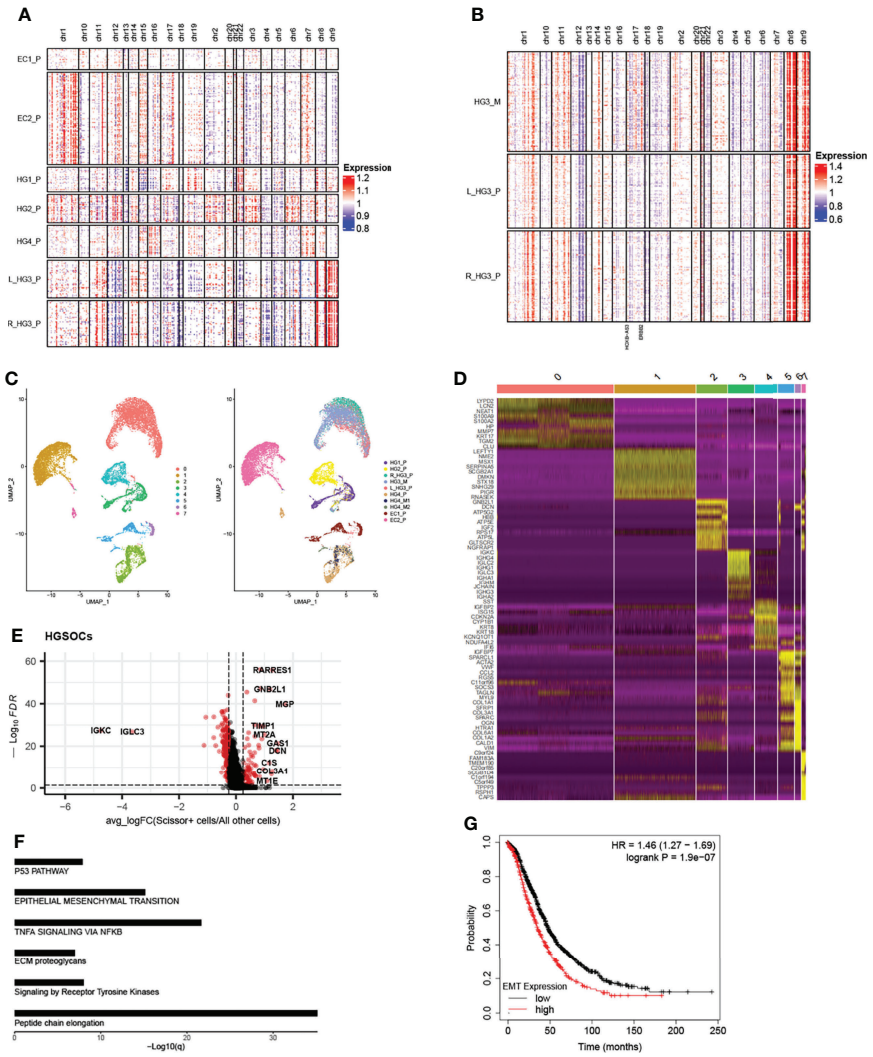

FIGURE 2 | Copy number profiles, intertumoral heterogeneity, and EMT signature subpopulations are identified. **(A)** The chromosomal landscape of copy number for 13,634 epithelial cells of seven primary tumors; amplification (red) and deletions (blue). **(B)** The chromosomal landscape of copy number for 2849 epithelial cells of metastatic tumors and primary tumors of the HG3 patient (L_HG3_P means the primary tumor from the left ovary in the HG3 patient; R_HG3_P means the primary tumor from the right ovary in HG3 patient). **(C)** The UMAP projection of 17,551 epithelial cells from 10 tumors of six patients (indicated by labels and colors) reveals tumor-specific clusters. **(D)** Differentially expressed genes of the top 10 genes (rows) that are differentially expressed in each cluster (columns). **(E)** Differentially expressed genes between Scissor^{+} cells and all other cells in HGSOCs, each point represents a gene. Red: significant genes; Black: NS genes. avg_logFC: log 2 fold-change of the average expression between the two groups. ((log-FC > 0.25, FDR <0.05) **(F)** Enrichment of significant genes related to Reactome and Hallmark pathways. **(G)** Kaplan-Meier plot shows that high expression of EMT signature has shorter overall survival in ovarian cancer. The high and low patients are split by the mean expression of the EMT-related gene set.

survival (Scissor$^+$ cells) from cancer epithelial cells, based on GDC TCGA bulk RNA-seq expression and clinical phenotype (24). As described previously, Scissor can quantify the similarity between single-cell data and bulk data through measurements, for example, Pearson correlations, and then it optimizes a regression model on the correlation matrix with the sample clinical phenotype. After that, it will provide feedback on three cell types, such as cells associated with worse prognosis (Scissor$^+$ cells), cells related to better prognosis (Scissor$^-$ cells), and cells that have no relationship with prognosis (Background cells).

In HGSOCs, we found that Scissor$^+$ epithelial cells mainly accumulated in patients with metastasis (**Figure S7A**). To distinguish Scissor$^+$ cells from Scissor$^-$ cells and Background cells (All other cells), we compared their gene expression (**Figure 2E**, **S7C**, cut off: avg_log-FC > 0.25, FDR <0.05). Interestingly, high expression of EMT-related genes like GAS1, DCN, COL1A1, MGP, etc. in HGSOCs Scissor$^+$ cells derived predominantly from patients with tumors metastasized (**Figures 2E**, **S7B**). Genes such as STMN1, CCND1, TUBA1B, and TUBB significantly expressed in Scissor$^+$ cells of ECs were associated with the cell cycle (**Figure S7E**), which is a barometer of epithelial tumor cells proliferation (25). Furthermore, functional enrichment analysis of significantly expressed genes in Scissor$^+$ cells also confirmed these (**Table 1**, **Figures 2F**, **S7D**), and survival analyses revealed that high levels of EMT and cell cycle signature were significantly related to poor overall survival in the Ovarian Cohort (**Figures 2G**, **S7F**). The observation of HGSOCs was consistent with the previous report that EMT is involved in increasing the invasion and metastasis of epithelial tumors (26–29). Therefore, targeting epigenetic regulation of EMT is a potentially powerful approach to inhibit the migration and invasiveness of HGSOCs.

Dynamic Trajectory Analysis During the Progression of HGSOCs

In the recent past, omentum metastasis has been reported (10). But in general, there are still few studies on the genetic dynamics of high-grade serous ovarian cancer metastasis, especially on the transcription factors involved in tumor progression. Based on the Monocle2 method (Version 2.21.1), pseudo-time reconstruction of epithelial cells was performed to infer the progression path of HGSOC (**Figure 3A**, and **S8A**). Macroscopically, the number of metastatic epithelial cells increased along the trajectory at the later stage. Besides, we also estimated the RNA velocities of every single cell by distinguishing un-spliced and spliced mRNAs, a function provided by velocyto (30) package. According to the direction of movement of each cell, the process of metastasis of HGSOCs can be clearly detected (**Figure S8D**).

In particular, the dynamic gene expression profiles during the development of tumors were extracted. (**Figures 3C, D**). Interestingly, we found that the molecular mechanisms involved in metastatic HGSOCs were consistent whether the primary HGSOC was on the left or right side (**Figures 3C**, **S8E**). Genes related to the immune response were significantly decreased, whereas the genes related to DNA replication, cell cycle, epithelial cell proliferation, oxidative phosphorylation, and TCA cycle were significantly increased (**Figures 3C, D**). These results also suggested that inhibitors based on poly (ADP-ribose) polymerase (PARP), which aids in stopping the regeneration of cancer cells, such as Olaparib and Rucaparib, may be helpful for the treatment of metastatic HGSOCs (31–33). Meanwhile, the transcriptional factors (TFs) related to immune regulation, such as ARID5A, NFKB1, RORA, and ZNF683, were gradually downregulated along with the trajectory differentiation process (**Figure 3E**). And these immune-related TFs were scattered in the clusters of epithelial cells as well as other cell types (**Figure S8B**). Conversely, some well-known factors related to tumor growth promotion, such as HMGA1, GTF3A, PHF19, CENPX, and MBD2, were upregulated. Zingg emphasized that loss of cilia accelerates melanoma metastasis in benign cells by enhancing Wnt/β-Catenin Signaling (34). In our data, the expression of epithelial cilium movement markers, including FOXJ1, PRG, RFX2, and TMF1, although increased during the process, were mainly overexpressed in primary tumor cells (**Figures 3A, F**). This may indicate that disruption of cilia assembly leads to primary ovarian cancer that metastasizes to the peritoneum.

We also utilized GeneSwitches (35) (Version 0.1.0) to predict the genes that act as on/off switches between cell states in order during the tumor's metastasis process (**Figures 3B**, **S8C**). Accordingly, overexpression of some acting on genes like FOSL2, NFIB, NFIC,

TABLE 1 | Functional enrichment analysis based on the upregulated genes in HGSOCs Scissor$^+$ cells versus All other cells (Scissor$^-$ and Background cells).

Pathological subtype	Category	Description	Log10 (q)	Genes
HGSOC	Reactome Gene Sets	Peptide chain elongation	-35.94	COL3A1, MT1E, MT2A, ZFP36, FOS, HBB, RPS17, NNMT, RPL13A, COL6A2, COL6A1, RPS9, JUN, RPL31, SLC25A6, RPL34, SAT1, RPS4X, ZFP36L1, RPS6, EEF2, RPS5, RPL11, RPL13, RPL23, CEBPB, RPL10A, RPS12, RPS20, RPL19, RPL10, RPS16, RPLP2, ID1, ACTB, RPL18, RPS14, RPS3, RPL7
HGSOC	Reactome Gene Sets	Signaling by Receptor Tyrosine Kinases	-8.00	COL3A1, COL1A1, FOS, JUNB, ID3, COL6A2, EGR1, FOSB, LAMA4, NR4A1, COL6A1, MYC, FN1, ID1, ACTB
HGSOC	Reactome Gene Sets	ECM proteoglycans	-6.99	DCN, COL3A1, COL1A1, C3, TIMP1, HBB, COL6A2, HP, HTRA1, LAMA4, COL6A1, FN1, FTL
HGSOC	Hallmark Gene Sets	HALLMARK_TNFA_SIGNALING_VIA NFKB	-21.61	DCN, MT1E, MT2A, ZFP36, FOS, JUNB, EGR1, DUSP1, FOSB, CYR61, NR4A1, PNRC1, MYC, IER2, JUN, KLF4, SAT1, NR4A2, IER3, CEBPB, KLF6, EIF1, UGP2
HGSOC	Hallmark Gene Sets	HALLMARK_EPITHELIAL_MESENCHYMAL TRANSITION	-15.12	MGP, GAS1, DCN, COL3A1, COL1A1, TIMP1, VIM, NNMT, COL6A2, CYR61, HTRA1, JUN, FN1, SAT1, IGFBP4
HGSOC	Hallmark Gene Sets	HALLMARK_P53_PATHWAY	-7.88	GNB2L1, FOS, JUN, KLF4, SAT1, ZFP36L1, IER3, RPS12, RPL18, ISCU

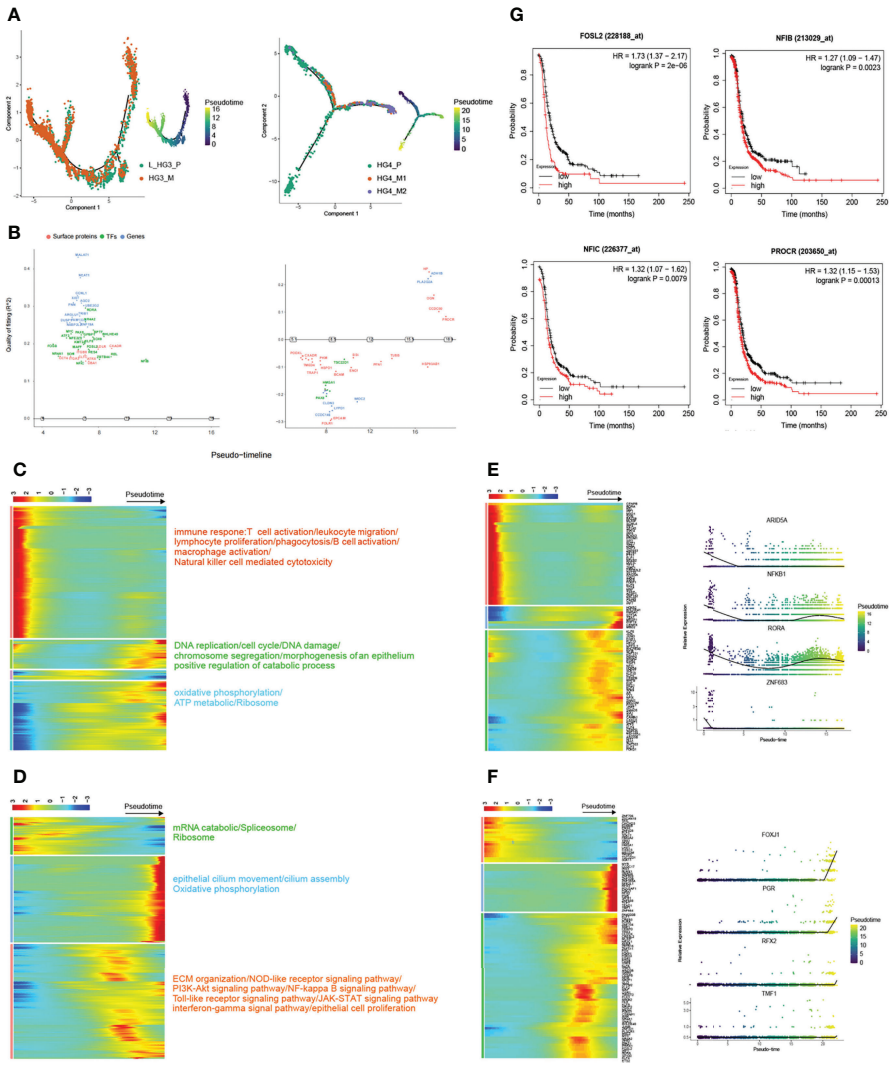

FIGURE 3 | Trajectory reconstruction during metastatic HGSOCs. **(A)** Monocle2 infers the development of epithelial cells along with pseudo-time (from patients HG3 and HG4 respectively, L_HG3_P means the primary tumor from the left ovary). Pseudo-time legend from dark to bright indicates cancer progression from the early to late stage. **(B)** Genswitches deduces the genes switch between cell states (left: L_HG3; right: HG4). **(C**, **D)** The heatmap displays the dynamic gene expression profiles during metastasis of ovarian cancer (from patients HG3 and HG4 respectively). The color key from blue to red indicates relative expression levels from low to light. The top annotated GO and KEGG terms in each cluster are shown. **(E**, **F)** Top 100 differentially expressed transcription factor genes (TFs; left) and the expression of specific TFs are on view along with the pseudo-time curve in (right). **(G)** Overexpression of proliferation and metastasis-related genes predicts poor prognosis in HGSOCs.

and PROCR, which are associated with proliferation and metastasis, predicts poor prognosis in high-grade serous ovarian cancer (**Figure 3G**). Taken together, these results reveal dynamic gene expression profiles, highlighting several quintessential TFs and surface proteins that are dysregulated during ovarian cancer progression.

Cancer-Associated Fibroblasts with the EMT Program Enriched in Metastatic HGSOCs

Fibroblast is another vital biological cell type that synthesizes the extracellular matrix and collagen to maintain the structural integrity of connective tissue. In this study, 12,236 fibroblast cells were categorized into five distinct sub-clusters (**Figures 4A**, **S9B, 9C**). Fibro_1 cells were marked by STAR, an exclusive marker for ovarian stromal cells as previously reported (15). Fibro_2 cells were characterized by collagen (COL1A1, COL3A1) and cancer-associated fibroblast genes (CTHRC1, FAP). Fibro_3 cells expressed immunomodulatory (CFD, OGN) and tumor suppressor genes (CCDC80, PLA2G2A). Fibro_4 cells expressed growth factors (EGFR, IER2M KLF2). Fibro_5 cells were characterized by conserved and nuclear-enriched lncRNA (MALAT1, NEAT1), and MALAT1 modulates the expression of cell cycle-related genes in lung fibroblast and EMT-related genes in breast cancer (36, 37)

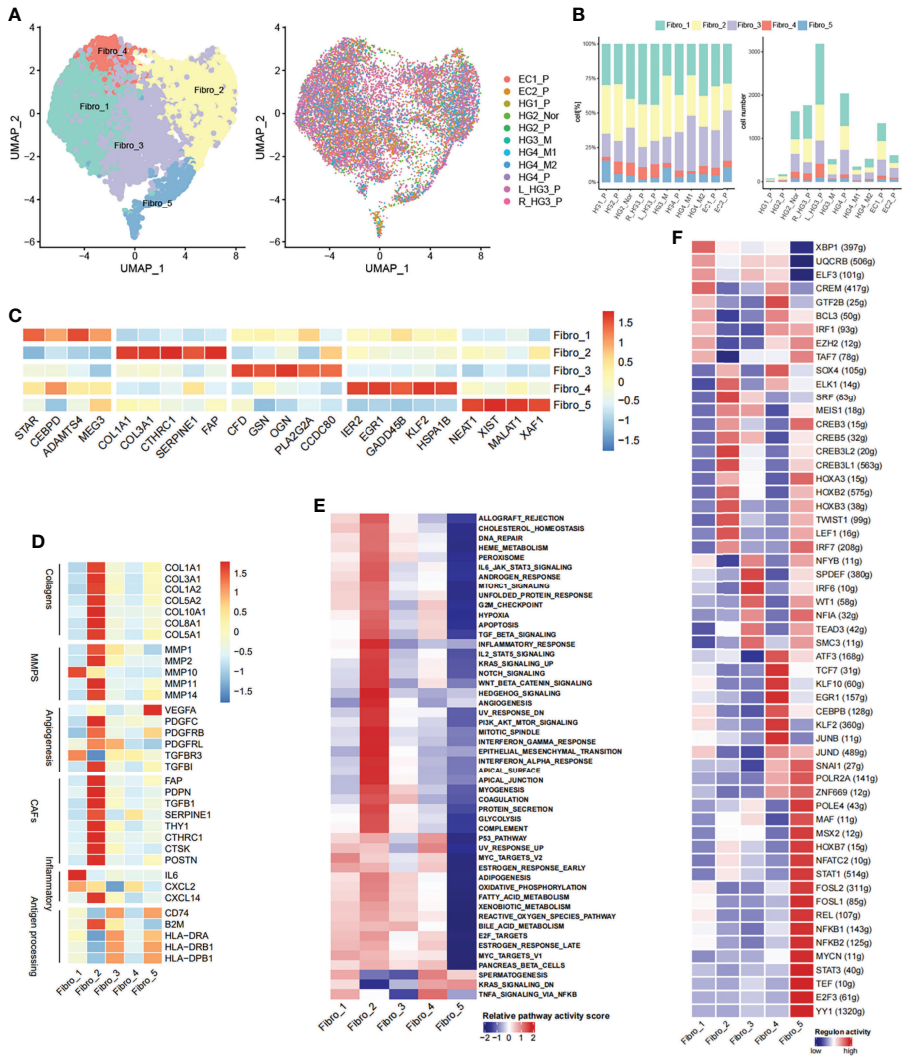

FIGURE 4 | Diversity of fibroblasts in HG_M. **(A)** The UMAP projection of 12,236 fibroblast cells of 11 samples from six patients (indicated by labels and colors). **(B)** Proportion and cell number of each fibroblast subtype in 11 samples. **(C)** Heatmap of marker genes expression. **(D)** Heatmap of functional gene sets. **(E)** GSVA analysis of differential pathways is scored per cell among five fibroblast subsets. **(F)** Active regulons in each fibroblast subsets.

(**Figure 4C**). The distribution of fibroblast sub-clusters in each tumor was varied (**Figure 4B**). In addition, comparisons based on hallmark gene sets of fibroblasts had been conducted. Fibroblasts from HG_M were more abundant in supporting tumor progress than HG_P, including angiogenesis, coagulation system, and EMT (**Figure S9D**). Fibroblasts from EC_P were more enriched in the structure formation of tissue than HG_P, such as myogenesis and adipogenesis, whereas inflammatory pathways including TNFA signaling *via* NFκB and inflammatory response more enriched in HG_P than EC_P (**Figure S9E**). Combined with the analysis of normal fallopian tubes (nFT) from previous studies (38, 39), we found that fibroblasts from HG_P were more abundant in supporting interferon-alpha/gamma response than HG_nor/nFT while estrogen responses early activity was more active in HG_nor/nFT than HG_P (**Figure S9F**).

Notably, Fibro_2 cells, the most enriched subtype in HG_M, accounting for 32%, expressed genes of cancer-associated fibroblasts (CAFs), angiogenesis, and collagen at a high level (**Figures 4D**, **S9A**). CAFs have been verified to promote tumor metastasis through upregulating genes like HSF1, which was involved in the pro-tumorigenic pathway (40). Furthermore, Hallmark pathway analysis also confirmed that Fibro_2 cells had more relevance with the pathways that sustain tumor growth, including angiogenesis, epithelial-mesenchymal transition (EMT), hypoxia, and PI3K/AKT/mTOR signaling (**Figure 4E**). Compared with HG_M and EC_P, Fibro_3 cells (19%) and Fibro_5 cells (3%) accounted for less proportion in HG_P. Intriguingly, Fibro_3 cells and Fibro_5 cells were both consistent with the characteristic of "antigen-presenting CAFs" as previously discerned (41), owning to express genes like CD74 and human leukocyte antigen (**Figure 4D**).

With the help of the SCENIC tool, we identified regulons unique to each fibroblast sub-clusters (**Figure 4F**). For instance, the transcription factors of SOX4 and SRF underpinned Fibro_2, while Fibro_5 cells were characterized by STAT1/STAT3 and NFKB1/NFKB2. Strikingly, SOX4 has been proven as an important co-factor of SMAD3, controlling pro-metastatic gene transcription and shaping the cell response to TGF-β in different scenarios, thereby promoting tumorigenesis (42). While STAT3 and NF-κB are pro-inflammatory regulators and they form transcriptional complexes that positively regulate gene expression in oncogenic pathways (43).

Heterogeneity of Tumor-Infiltrating Lymphocytes in HGSOCs

Infiltration of T cells into tumors modifies the natural course of the disease and plays a critical role in cancer immunotherapy (44, 45). From the ovarian cancer lesion, we classified a total of 7967 T and NK cells into eight subtypes: $CD4^+$ T cells (CD4 IL7R; $CD3D^+$ $CD4^+$), regulatory $CD4^+$ T cells (Tregs FOXP3; CD4, FOXP3), $CD8^+$ T cells (CD8 GZMK, CD8 GZMH; $CD3D^+$ $CD8^+$), NK cells (NK CD56, NK IL7R; NCAM1, GNLY, TYROBP, NKG7), NKT cells (CD3D, CD8A, FCGR3A, GNLY), and Innate Lymphoid Cells (ILCs; CD3D) (**Figures 5A, C** and **S10A**). The number of cells and the proportion of each subtype in each tumor were shown (**Figure 5B**). Notably, 1665 T/NK cells were obtained from HG_M, while 5394 T/NK cells were from HG_P. Using a dendrogram to group the tumors based on the average expression of T cell markers, we found that HG_M showed a similar pattern to HG_P, whereas EC_P emerged with low expression in $CD4^+$ T and $CD8^+$ T cells (**Figure 5D**). This observation was consistent with the boxplot shown, the lower proportion of $CD4^+$ T cells and $CD8^+$ T cells was detected in EC_P than in HG_P and HG_M (**Figure S10B**). The low tumor-suppressive status in EC_P suggested that T cell-based immunotherapy may be inefficient in EC_P.

Among $CD4^+$ T cells, we identified naive (CD4 IL7R; TCF7, CCR7, SELL, LEF1) and regulatory (Tregs FOXP3; IL2RA, FOXP3, IKZF2). The Tregs FOXP3 cells highly expressed inhibitory genes, including TIGIT, CTLA4, and ENTPD1, and they also relatively expressed high levels of costimulatory molecules CD28, TNFRSF14, ICOS, TNFRSF9, which stimulate the inhibitory activities (**Figure 5F**). The tumor-suppressive microenvironment mediated by Tregs is a significant obstacle to successful immunotherapy, suggesting that depletion of Treg cells, like immune checkpoint blockade of CTLA-4 or PD1/PDL1, could be a potentially effective immunotherapy for ovarian cancer (46).

Among $CD8^+$ T cells, CD8 GZMK and CD8 GZMH T cells were characterized by relatively high cytotoxic genes granzyme K (GZMK) and granzyme H (GZMH), respectively. Meanwhile, these cells also positively expressed T cell exhaustion markers, including LAG3 and PDCD1, indicating that the $CD8^+$ T cells are exhausted after initial activation in ovarian cancer (**Figure 5F**). In addition, we inferred the gene regulatory networks across the TILs subtypes by SCENIC method (**Figure 5G**). The regulon of PRDM1 was upregulated in CD8 GZMK and CD8 GZMH T cells, which is connected with terminal T cell differentiation and contributes to the maintenance of an early memory phenotype and cytokine poly-functionality in TILs after knockout (47). Consequently, we concluded that PRDM1 might be one of the factors contributing to the exhaustion of CD8 GZMK and CD8 GZMH T cells. Indeed, verified by bulk RNA-seq from the TCGA dataset, it was a slightly significant Spearman correlation between PRDM1 expression and immune exhausted infiltrate in ovarian cancer (Cor:0.41, FDR: $2e^{-12}$, **Figure S10C**). Beyond that, higher expression of PRDM1 predicted a worse prognosis in ovarian cancer (**Figure 5H**).

Next, we performed pseudo-time trajectory analysis to explore the dynamic states and cell transitions of $CD4^+$ IL7R to $CD8^+$ T cells *via* Monocle2. In the developmental trajectory, $CD4^+$ IL7R started as a root, and gradually evolved into CD8 GZMK and CD8 GZMH, presenting a binary branched structure in which one side was the end of exhausted T cells, and the other side was the end of cytotoxic T cells (**Figure 5E**). In HG_M, the proportion of $CD8^+$ cytotoxic T cells was higher than in HG_P (**Figure 5I**). On the contrary, the percentage of exhausted $CD8^+$ T cells in HG_P was more than that in HG_M (**Figure S10D**).

We noticed three sub-clusters expressing the NK cells marker: TYROBP, GNLY, and NKG7. NK CD56 cells were characterized by NCAM1 (CD56), NK IL7R cells were characterized by IL7R, and NKT cells were identified by the specific T-cell markers including CD3D and CD8A (**Figures 5C, D**). NKT cells strongly expressed the GZMB, GZMA, GZMH, and PRF1 genes, indicating that they promoted tumor cytotoxicity in ovarian cancer (**Figure 5F**). Generally speaking, NK CD56 and NKT cells were more enriched in HG_P and HG_M than EC_P (**Figure S10E**).

Trajectory Reconstruction of HGSOCs Revealed Monocyte-to-Macrophage Differentiation

Tumor-infiltrating myeloid cells (TIMs) are critical regulators in tumor progression, playing essential roles in modulating tumor inflammation and angiogenesis (48, 49). Altogether, 7265 myeloid cells were collected, revealing 23 subsets through the ROGUE statistic (Version 1.0) (50) purified the cell population (**Figures S11A, 11B**). Then, we identified four common linages (cDCs, monocytes, or macrophage and monocytes derived DC) based on canonical cell markers and they were well presented in each sample (**Figures 6A, B, D**, **S11D, 11E**). Moreover, a subset of myeloid cells expressed myeloid/T-cells markers simultaneously (CD3D_undefined), which was not discussed below.

Monocytes are the progenitors of monocytes-derived macrophages and contribute to the overall coordination of immunity (51). Correspondingly, Monocytes can be separated from macrophages based on phylogenetic reconstruction (**Figure S11F**). CD14_mono cells were characterized by CD14, SELL, and S100A8/9, representing classical monocytes and being recruited during inflammation (**Figure 6I**). They also highly expressed FCN1, a complement system protein that defends against infectious agents (52). CD16_mono cells were less abundant and represented non-classical monocytes with high expression of FCGR3A (CD16), CDKN1C, LST1, and low expression of CD14. Similarly, CD16_mono cells expressed FCN1 at high levels but were more enriched in HG_M (**Figure S11C**).

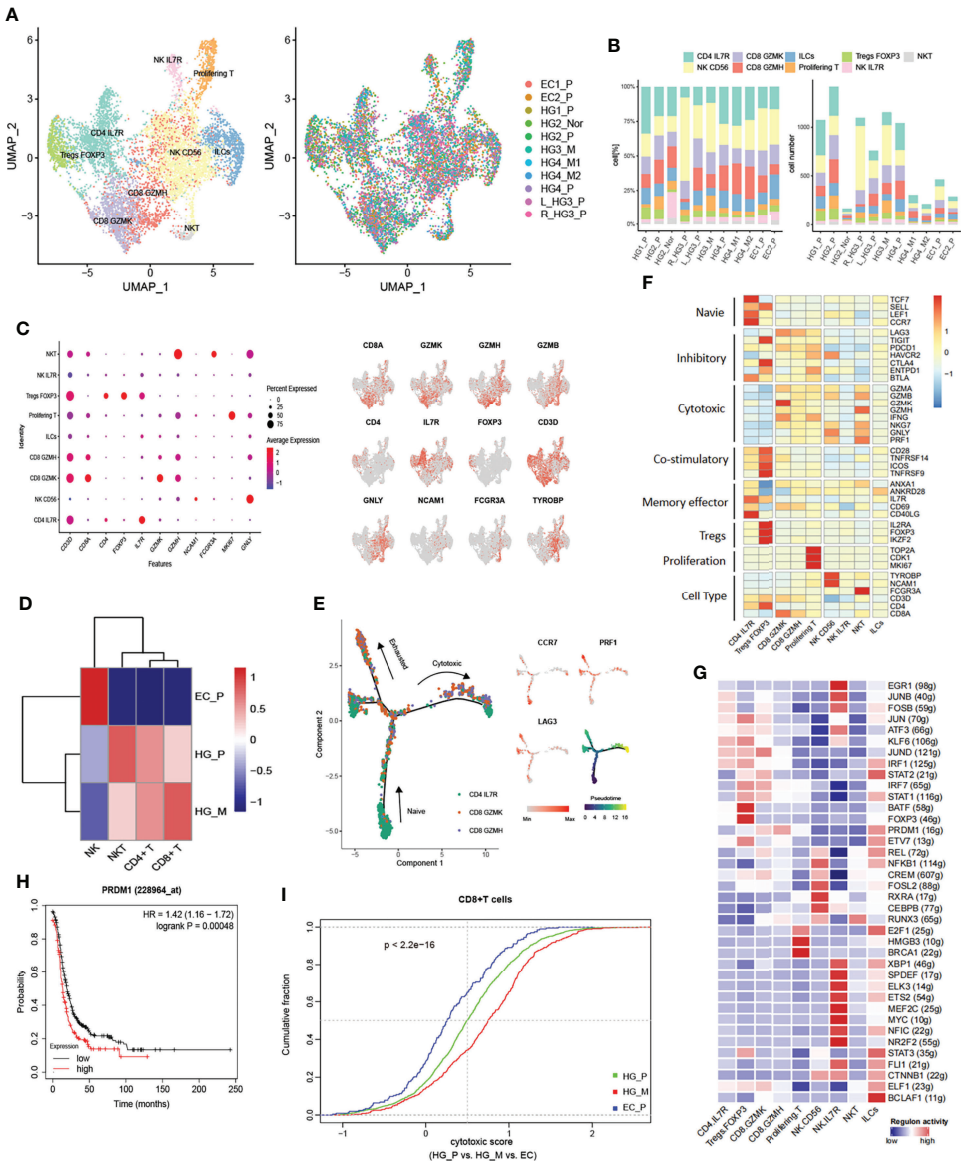

FIGURE 5 | Subpopulations of tumor-infiltrating lymphocytes (TILs) in HG_M. **(A)** The UMAP projection of 7967 TILs of 11 samples from six patients (indicated by labels and colors). **(B)** Proportion and cell number of each subtype in 11 samples. **(C)** Dot plot (left) and UMAP-plot (right) display canonical cell markers. **(D)** Hierarchical clustering heatmap groups the tumors between HG_P, HG_M, and EC_P. **(E)** Reconstruction trajectory of $CD8^+$ T cells inferred by Monocle2 (color by subtypes, expression of signature genes, and pseudotime). **(F)** Heatmap of the functional gene sets in TILs. **(G)** Active Regulons in each TILs. **(H)** Overexpression of the PRDM1 gene predicts a worse prognosis in ovarian cancer. **(I)** Cumulative distribution of cytotoxic $CD8^+$ T cells between HG_P, HG_M, and EC_P. The cytotoxic score is calculated based on the average expression of cytotoxic markers. P-value was calculated by a two-sided unpaired Kruskal-Wallis rank-sum test.

DC cells were classified according to their origin and typical genes. CLEC10A_mono-DC with lower abundance was characterized by CLEC10A and CD14 representing monocyte-derived dendritic cells. CD1C_DC cells represented a classic cDCs subset, with high expression of CD1C, CD1E, and CLEC10A.

Macrophage cells were characterized by tissue-resident and their pro-inflammatory or anti-inflammatory function. CCL2_macro represented early-stage macrophage with the expression of CCL2. CX3CR1_macro expressed genes involved in immune modulation of chemokines, such as CCL3, CCL4, and CXCL8. What's more, CX3CR1_macro significantly secreted BAG3 (**Figure 6I**), a multifunctional protein, which can combine with a specific receptor IFITM2 to induce the release of factors that sustain the growth and metastasis of tumor (53). MMP9_macro expressed genes related to inflammatory chemokines (CXCL2, CXCL3, CXCL8) and genes like MMPs (MMP19, MMP9), which play an important role in tumor tissue remodeling. CCL18_macro expressed both M1 marker (CD68) and M2 markers (CCL18, GPNMB). By the way, CCL18 played a

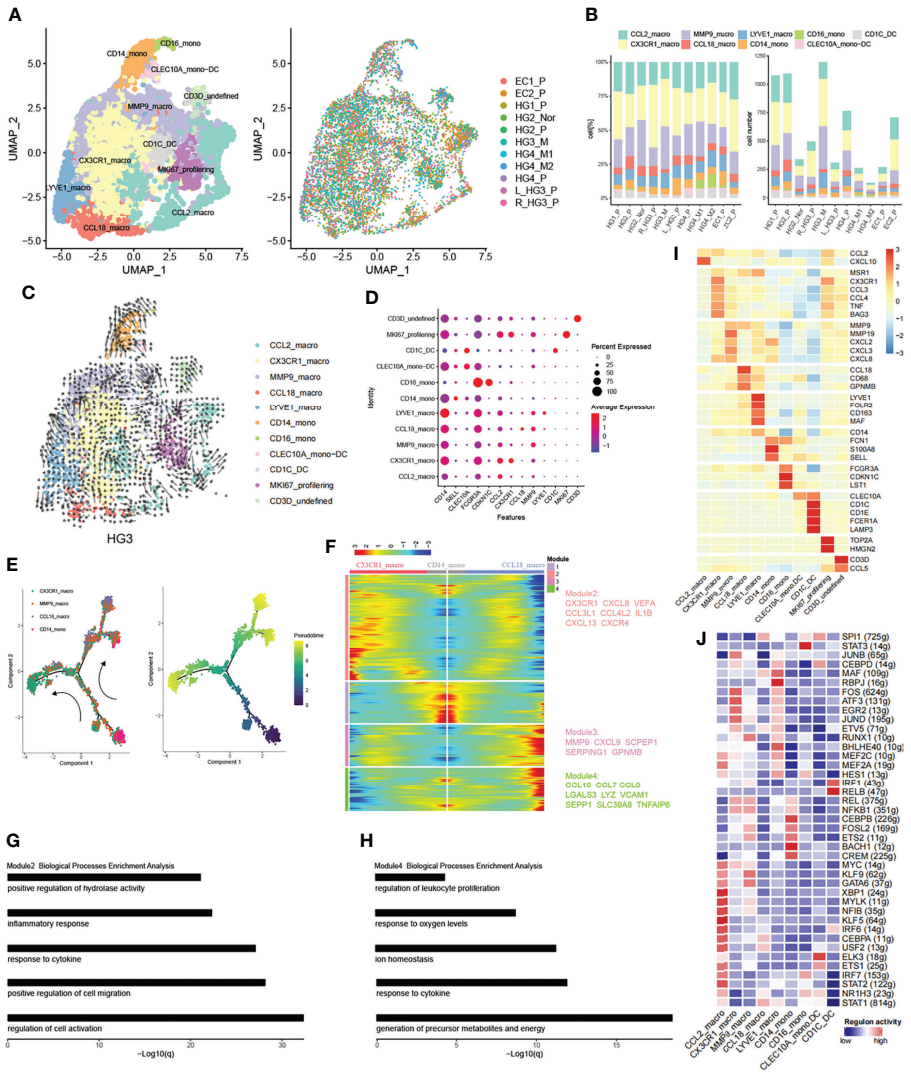

FIGURE 6 | Subpopulations of myeloid cells in HG_M. **(A)** The UMAP projection of 7265 myeloid cells of 11 samples from six patients (indicated by labels and colors). **(B)** Proportion and cell number of each myeloid subtype in 11 samples. **(C)** RNA velocity of each myeloid subtype. **(D)** The dot plot displays canonical cell markers. **(E)** Trajectory reconstruction of monocyte evolved into macrophages. **(F)** Dynamics gene expression profile during monocyte-to-macrophage terminal differentiation. **(G, H)** Biological processes enrichment analysis of module 2 and module 4. **(I)** Heatmap of significant genes in each subtype. **(J)** Activate regulons in each myeloid subtype.

key role in recruiting immunosuppressive myeloid cells (54). Finally, LYVE1_macro represented resident macrophages with a high level of LYVE1 and FOLR2.

Early works have supported that macrophages can either originate from monocyte cells or tissue-resident macrophages (55–57). Accordingly, we employed the RNA velocity to explore the ovarian cancer lineage trajectories and we found that a small number of CD14_mono evolved toward MMP9_macro, while LYVE1_macro evolved toward CCL18_macro as well as toward MMP9_macro (**Figure 6C**). To further investigate the dynamic change of genes during the differentiation of CD14_mono into macrophages in the ovarian lesions, we extracted classical monocytes (CD14_mono) and related macrophages (MMP9_macro, CCL18_macro, CX3CR1_macro) to delineate monocyte-to-macrophage differentiation by trajectory development analysis (**Figure 6E**). During the trajectory, CD14_mono were progenitor cells for MMP9_macrophage and then further separated into CX3CR1_macro and CCL18_macro. Profiling of gene expression dynamics along the trajectory had been divided into four modules (**Figure 6F**). Genes like CX3CR1, CXCL8, CXCR4, CCL3L1, VEGFA, and IL1B in Module 2 increased during the evolution of the branch of CX3CR1, whereas, they decreased during the evolution of the branch of CCL18_macro. Vice versa, Genes in Module 4 like CCL18, CCL7, and CCL8 were increased in the branch of CCL18_macro and reduced in the branch of CX3CR1. To reveal the biological characteristics of these two branches, we performed gene functional enrichment analysis. In the branch of

CX3CR1_macro, the corresponding high expressed genes tend to be associated with inflammatory response and positive regulation of cell migration (**Figure 6G**), which is consistent with the suggestion that the high VEGF, $CXCL8^+$ $IL1\beta^+$ TAMs with the features of inflammatory could promote tumor progression in ovarian cancer (54, 58). Parallel results, in the branch which evolved into CCL18_macro, their corresponding high expressed genes were associated with metabolic precursor and energy production (**Figure 6H**).

We further characterized the functions of nine subtypes explained above by comparing pathway activities (**Figure S11G**). Pathways involved in angiogenesis, EMT, TNFA signaling *via* NFKB, and hypoxia were upregulated in CX3CR1_macro, MMP9_macro, and CD14_mono. These results indicate the potential tumor-promoting feature of CX3CR1_macro derived from CD14_mono. Finally, we applied SCENIC to identify TFs underlying each phenotype (**Figure 6J**). Interestingly, some recruited macrophage phenotypes shared similar TFs expression patterns with monocytes and tissue-resident macrophages.

Intercellular Communication Networks

As mentioned above, we have obtained cancer epithelial cells with poor prognosis ($Scissor^+$ Epithelial cells), and we wondered what function they are involved in with the crosstalk of the tumor microenvironment in ovarian lesions. To this end, the CellphoneDB repository (Version 2.1.4) (59) was used to predict putative intercellular interactions between $Scissor^+$ Epithelial cells and other cell types based on ligand-receptor signaling. Interestingly, many significantly overexpressed molecular pairs were associated with immunosuppression and HG_M showed a similar pattern to HG_P (**Figures 7B, C**). Compared with EC_P, $Scissor^+$ Epithelial cells in HG_M and HG_P had more outgoing interactions with other cell types. Of note, macrophage and fibroblasts connected with $Scissor^+$ Epithelial more frequently in HG_M (**Figure 7A**). When $Scissor^+$ Epithelial cells expressed a relatively high level of EGFR as receptors, their corresponding ligands, such as AREG, COPA, GRN, MIF, and TGFB1, were widely expressed in other cells. When $Scissor^+$ Epithelial cells expressed genes related to angiogenesis (VEGFA), the interactions (VEGFA_FLT1, VEGFA_KDR) were slightly abundant in HG_M. In addition, when $Scissor^+$ Epithelial expressed ACKR2 acting as a receptor for chemokines including CCL3/CCL4/CCL5, their interactions were more abundant in HG_P than that of the other two groups (**Figure 7B**). It has been reported that ACKR2 is a scavenger receptor for chemokines and its deficiency against metastasis (60). And, CCL5 is important for the recruitment and activation of lymphocytes (61), so we proposed that ACKR2_CCL5 may weaken the recruitment and activation of lymphocytes, contributing to the metastasis of primary high-grade serous carcinoma. Among the three groups, the MDK_LRP1 molecule pair between $Scissor^+$ Epithelial cells and myeloid cells expressed significantly, while their mean expression level in EC_P was higher than HG_P and HG_M (**Figure 7B**). MDK can combine with its receptor LRP1, which is beneficial to tumor-infiltrating macrophages, promoting myeloid inhibitory cell differentiation (MDSCs) (62, 63). Thus, MDK targeted therapy should suggest an effective treatment for ovarian cancer.

In general, these results revealed that the crosstalk between $Scissor^+$ Epithelial cell and other cell types *via* diverse receptor-ligand signals may profoundly affect ovarian cancer development and metastasis.

DISCUSSION

Our current study has comprehensively characterized the dynamic variation of gene profiles during tumor progression in HGSOCs, as well as the heterogeneity of tumor cells, fibroblast cells, and immunophenotype, and the intricate intercellular interactions across HG_P, HG_M, and EC_P. We have identified unique subpopulations such as $Scissor^+$ Epithelial cells, CAFs–Fibro_2, CX3CR1/CCL18 macrophages, and GZMK/GZMH $CD8^+$ T cells. Those results provide a new perspective on the tumor microenvironment of ovarian cancer.

Epithelial cells were the largest cluster of cells, composing ~31% of the cells analyzed. However, current single-cell studies of ovarian cancer cannot explicitly distinguish cells with specific clinical phenotypes (24). To this end, $Scissor^+$ cells with poor prognosis were identified by the Scissor algorithm. Consistent with the previous conclusion that the EMT signature is a potential factor for tumor invasion and metastasis (26, 27), the genes related to the EMT signature, including MGP, GAS1, and JUN, were found in $Scissor^+$ cells of metastatic HGSOCs lesions. Moreover, during HGSOCs progression, several signaling pathways such as the cell cycle, tumor cell proliferation, oxidative phosphorylation, and TCA cycle, which needed energy metabolism, were markedly enhanced, suggesting that poly (ADP-ribose) polymerase (PARP) inhibition may be a targeted strategy for the treatment of metastatic HGSOCs (31–33). Strikingly, in our data, regardless of whether the primary tumor was from the left ovary or the right, the pathway activities generated by the tumor progression were basically consistent, as well as their copy number alterations in one segment of chromosomes.

Since the fibroblasts were the second-largest cluster cells analyzed, we observed Fibro_2, a subtype of CAF expressing the EMT program was specifically enriched in HG_M. This result supports that CAFs contribute to the EMT in HG_M and subsequently promote metastasis (64). Beyond that, the IL6_JAK_STAT3 signal pathway was also more enriched in Fibro_2. Consistently, JAK/STAT inhibitor JSI-124 has been proven to have an anti-tumor property in HGSOC cell lines (11). Combination therapies with the EMT or JAK/STAT inhibitor may help in the treatment of HGSOCs.

T cells are the crucial players in cancer immunotherapy (44, 45). Olalekan has revealed that ovarian cancer with high infiltration of $CD8^+$ TOX^+ and $CD4^+$ GNLY T cells may be a good indication for patients (10). In our data, we found low T cell infiltration in EC_P compared with HG_P and HG_M. Furthermore, GZMH CD8 cells and GZMK CD8 cells simultaneously presented cytotoxicity and cell exhaustion. Notably, HG_M showed the highest cytotoxic of $CD8^+$ T cells while the highest exhaustion of $CD8^+$ T cells was in HG_P.

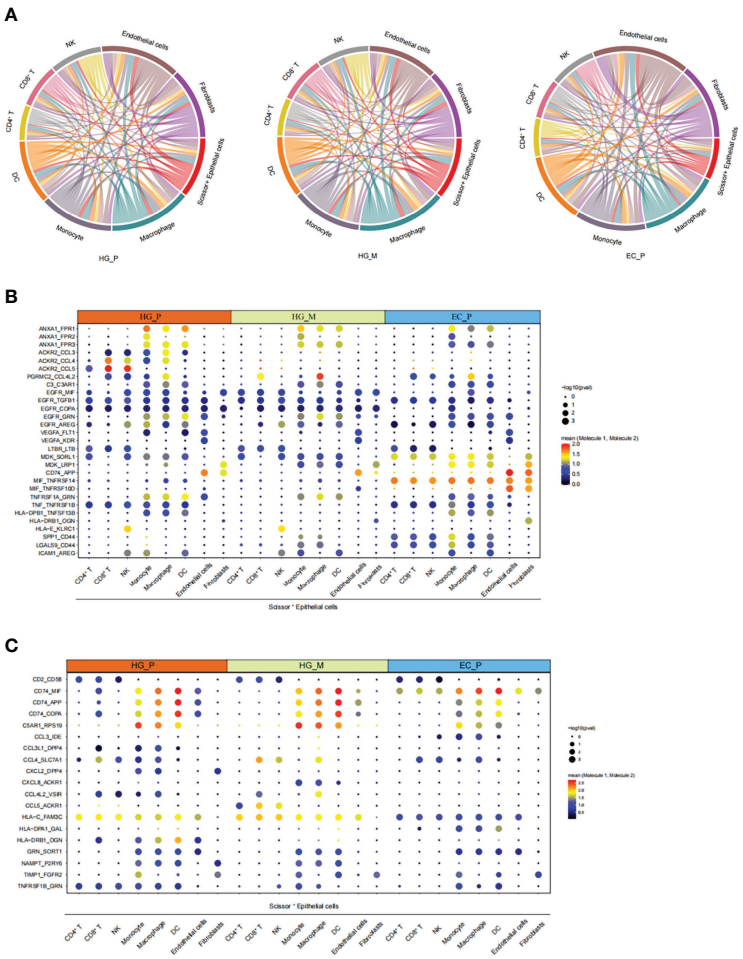

FIGURE 7 | The intricate intercellular interplay in HG_P, HG_M, and EC_P. **(A)** Circos plot shows the intercellular interactions in HG_P, HG_M, and EC_P. Each line represents an interaction where one end represents a ligand that is expressed in one cell type and the other end represents a receptor that is expressed in another cell type. The thickness of each line corresponds to the number of distinct interacting pairs. **(B, C)** Dot plot shows the means of the average expression levels and the possibility of occurrence in selective interaction pairs.

Through the gene regulatory networks analysis, we speculated that PRDM1 may be involved in $CD8^+$ T cells exhaustion and predicted that its high expression in ovarian cancer was associated with poor prognosis.

It has been manifested that TAM can promote the formation of niches before metastasis by secreting specific cytokines (65). They also can regulate the Tregs and Th17 cells to create immunosuppression, thereby promoting invasion and metastasis of ovarian cancer (66). On the basis of these theories, we have identified a subtype of TAM (CX3CR1_macro) with abundant production of BAG3, which can combine with IFITM2, leading to tumor metastasis (53). This TAM subtype also owns a high level of VEGFA, CXCL8, and IL1β, similar to previously reported TAM induced from monocyte with factor-1a stabilization in solid ovarian cancer that promoted tumor inflammation and metastasis (54).

By investigating the signaling network of $Scissor^+$ Epithelial cells - other cells communication, we detected several receptor-ligand complexes that should be paramount for ovarian cancer development. Compared with HG_P and EC_P, stronger angiogenesis and tumor cell proliferation of intercellular interactions in HG_M. Metastasis of high-grade serous carcinoma may be related to the interaction between high expression of ACKR2 chemokine receptor and cytokines such as CCL5. The apparent pair of MDK_LRP1 among the three groups suggested that inhibition of the MDK_LRP1 pair might be an effective therapeutic target for ovarian cancer to reduce myeloid inhibitory cell differentiation (MDSCs).

We note that there are several limitations to our study. First, the number of patients with metastatic HGSOCs is small. Second, the clonal relationship of T cells was not investigated while T cell receptor therapy is an alternate therapy with great potential for ovarian cancer treatment (67). Hence, enlarging the cohort of metastatic HGSOCs and conducting immune profiling of T cell receptors and spatial transcriptomic may help unravel molecular mechanisms and elucidate the roles of different immune cells in HG_M.

In conclusion, our data have shed light on the tumor microenvironment of metastatic high-grade serous ovarian cancer at the single-cell level. Several novel markers and the potential therapeutic target detected in this study could provide valuable guidance for future clinical treatment.

MATERIALS AND METHODS

Patients and Samples Collection

In this study, a total of eight samples, including one metastatic HGSOC matched two primary HGSOCs, one pair of matched primary HGSOC and normal ovary, one primary HGSOC and two ECs were collected from The Third Affiliated Hospital of Guangzhou Medical University, which have been subjected to pathological diagnosis. The clinical information of these patients is summarized in **Table S1**.

Preparation of Single-Cell Suspension

Specimens collected from patients with ovarian cancer were minced into fragments (< 1 mm3) and digested with 0.25% trypsin-EDTA (GIBCO) and DNase I (Roche Diagnostics) for 30 min at 37°C with agitation. The dissociated cell suspension was filtered through 70 μm strainer (BD Falcon), washed with cold PBS, and centrifuged at 4°C, x400g for 5 min. The cell pellet was resuspended in serum-free DMEM for further use.

Droplet-Based scRNA-Seq Data Preprocessing

The Cell Ranger (Version 6.0.2) pipeline generated raw gene expression matrices with human reference genome GRCh38. After removing doublets with DoubletFinder (Version 2.0.3) in each sample individually, the remaining cells were imported into R software (Version 4.1.0) for subsequent analysis by the Seurat package (Version 3.2.3). Cells with > 200 genes detected, genes expressed >5 cells, and genes expression >0 in all cells were selected for further analysis. Low-quality cells were removed according to the following criteria: unique molecular identifiers (UMIs) <500; genes <250 or genes >11000; UMIs derived from the mitochondrial genome >25%. After quality control, the gene expression was normalized by NormalizeData function, and cellular sequencing depth was adjusted by the SCTransform method.

Multiple Datasets Integration

To integrate multiple datasets across three conditions, we used the integration methods described at https://satijalab.org/seurat/v3.0/integration.html and https://hbctraining.github.io/scRNA-seq/lessons/06_SC_SCT_and_integration.html. The Seurat package (version 3.0.0) was used to assemble multiple distinct scRNA-seq datasets into an integrated and unbatched dataset. In brief, we used Sctransform to regress out confounding factors: number of UMIs, percentage of mitochondrial RNA, estimating the variance of the raw filtered data, and identifying the 3000 most variable genes. After that, we performed canonical correlation analysis (CCA) and then "integrated" the conditions to overlay cells that were similar or had a "common set of biological features" between groups.

Identification of Major Cell Types and Their Phenotype

Differential gene expression analysis was performed for clusters generated at various resolutions by both the Wilcoxon rank-sum test of Single-cell Transcriptomics (MAST) using the FindMarkers function. Annotation of the resulting clusters to cell types was based on the expression of marker genes along with the cell types assigned by SingleR packages (version '1.6.1').

TCGA Subtype Classification

Single cell subtypes were classified by the consensusOV (version 1.14.0) package, with get.consensus.subtypes function, which also returns random forest probabilities for each subtype. The core principle of consensusOV is that it: 1. standardizes genes in each dataset to the same mean and variance, 2. computes binary gene pairs based on the standardized expression values.

CNV Estimation and Identification of Malignant Cells

We used an approach described previously to infer CNVs from the scRNA-seq data. Its R code was provided online. (https://github.com/broadinstitute/inferCNV) We set the cut off=0.1, denoise=TRUE, HSMM=TRUE, and hclust_method='ward.D2'. Immune cells from normal samples were considered as putative nonmalignant cells as control, and their CNV estimates were used to define a baseline. All epithelial cells from the ovarian tumor sample were used as input.

Distinguish Phenotype-Associated Cells

To link cells with specific phenotypes, we used the Scissor algorithm, a novel R package (Version 2.0.0) to identify the populations of the single-cell data associated with given phenotypes. (https://github.com/sunduanchen/Scissor)

Scissor integrates phenotype-associated bulk expression data and single-cell data by quantifying the similarity between every single cell and bulk sample. To identify relevant subpopulations, it then optimizes a regression model on the correlation matrix with the sample phenotype. The core formula of Scissor is as follows:

$$\min_{\beta} -\frac{1}{n} l(\beta) + \lambda \left\{ \alpha \| \beta \|_1 + \frac{1-\alpha}{2} \beta^T L \beta \right\}$$

where L is a symmetric normalized Laplacian matrix; the tuning parameter λ controls the overall strength of the penalty, and α balances the amount of regularization between smoothing and sparsity. The phenotype-related cell subsets of interest are selected using the non-zero coefficient β solved for by the optimization model described above.

Statistical test: The scissors algorithm incorporates a reliability test to rule out false associations between identified cell subsets and bulk phenotypes. This statistical test can determine whether the inferred phenotype-cell association is reliable (P<0.05) or a false positive. First, it performs k-fold cross-validation (CV) on the correlation matrix S and estimates the cell coefficients in Scissor using only the training set. The predictive performance of the trained Scissor model is evaluated on the test set, and an averaged evaluation metric is obtained as the actual test statistic. Second, the bulk sample labels are randomized

multiple times to break the original bulk phenotype-genotype relationship. Predictive performance at the random level was quantified by performing the same Scissor analysis and CV assessment using each permuted batch of data, obtaining the background distribution of the corresponding assessment measures. Finally, the actual test statistic calculated in the raw data is compared to the background distribution value. The reliability significance test p-value is the number of permutations-based test statistics above (or below) the actual test statistic divided by the number of permutations. In this study, the evaluation measures used in reliability significance tests were mean squared error (MSE) for linear regression (smaller is better), area under the ROC curve (AUC) for classification (higher is better), and agreement Sex index (C-index) for Cox regression (higher is better).

In actual operation, we set the family=" cox", alpha=0.077 for the HG group, and alpha=0.0265 for the EC group to select the phenotype-associated cell subpopulations by a Cox regression model. The number of the Scissor selected cells should not exceed 20% of the total cells in the single-cell data.

SCENIC Analysis

The regulons and TF activity (AUC) for each cell were calculated with the SCENIC (version 1.2.4) pipeline with motif collection version mc9nr, using per cell type with raw count matrices as input. We used GRNBoost (in Python) instead of GENIE3 to detect positive and negative associations for a bigger dataset. The function of exportsForGRNBoost was used to generate a gene expression matrix and TF list in special formats for GRNBoost to load.

Trajectory Inference Analysis

Trajectory analysis was performed using Monocle 2 (version 2.20.0), We assessed the significant gene by the differential gene expression analysis, and DEGs between the clusters were applied for dimension reduction using the reduceDimension function. Genes that changed along with the pseudotime were calculated and visualized with the plot_pseudotime_heatmap and the genes were clustered into subgroups according to the gene expression patterns. To identify the genes that separate cells into branches, the branch expression analysis modeling (BEAM) analysis was performed and genes resulting from the BEAM analysis with a q-value < 10−4 were separated into groups and visualized with the plot_genes_branched_heatmap function.

Estimations of RNA Velocities by Velocyto Package

In order to smoothly assess spliced and un-spliced mRNAs, we needed to convert the bam file to loom file by the function of run10x, provided by velocyto.py. Next, we merged multiple loom files by the function of loompy.combinem and then loaded the merged loom file into R software to combine analysis with the Seurat package.

Ordering the Gene Expression During Cell State Transitions

The genes, including the human surface proteins and transcription factors (TFs), act as on/off switches between cell states and are discovered by GenSwitches R packages (Version 0.1.0). The workflow of GeneSwitches is as follows:

1. Binarize gene expression data into 1(on) or 0(off).
2. Fit logistic regression on the binary states of gene expression and estimate switching time.
3. According to the default Settings, the poorly fitting genes are filtered and specific genes are extracted for plotting.

Gene Set Variation Analysis (GSVA)

Pathway analyses were performed on the 50 hallmark pathways described in the molecular signature database. We also evaluated the activity of 65 specific KEGG pathway activities from the Canonical pathway KEGG subset. To assign pathway activity estimates to individual cells, we applied GSVA (Version '1.34.0') with standard settings.

Enrichment Analysis of Marker Genes

Gene Ontology (GO) enrichment and Kyoto Encyclopedia of Genes and Genomes (KEGG) pathway analysis of differential genes was implemented by the clusterProfiler (version 4.0.2) package. Reactome and Hallmark pathways analysis on differential genes was implemented by Metascape web-based portal (68).

Cell Cycle Scoring Assign

Each cell in the epithelial subpopulation was assigned a cell cycle-related score based on the gene expression of the G2/M and S phases. The "CellCycleScoring" function of the Seurat package was used to calculate the cell cycle score and store G2/M and S phase scores into data objects to predict the cell state.

TCGA Database

The cohort of TCGA ovarian cancer data was downloaded from https://xenabrowser.net/datapages/. The gene expression matrix and clinical phenotypes of HGSOCs and ECs were assessed using different datasets (GDC TCGA Ovarian Cancer (OV) & TCGA Endometrioid Cancer (UCEC)).

Survival Analysis

The Kaplan-Meier method evaluated ovarian cancer survival utilizing the KM plotter database (https://kmplot.com/analysis/).

We set split patients by 'Auto select best cutoff', which chooses the best performing threshold as cut-off among all possibilities between the lower and upper quartiles. All datasets provided by the KM plotter were taken into consideration for analysis.

Definition of Cytotoxicity and Exhaustion Scores

Cytotoxicity and exhaustion scores were calculated by the average expression of the genes from the predefined gene sets in $CD8^+$ T cells of each group. To implement this method, the AddModuleScore function of the Seurat package was applied as previously described. We used eight cytotoxicity associated genes (GZMA, GZMB, GZMH, GZMH, IFNG, NKG7, PRF1, GNLY) and seven exhaustion associated genes (LAG3, TIGIT, PDCD1, HAVCR2, CTLA4, ENTPD1, BTLA) to define cytotoxicity and exhaustion scores

Correlation Analysis Between Immune Infiltration and Single Gene Expression

Spearman correlation between mRNA expression and exhausted infiltrate in ovarian cancer was performed by immune cell abundance pattern of Gene Set Cancer Analysis (GSCA) (69).(http://bioinfo.life.hust.edu.cn/GSCA/#/).

Statistics

Statistical analysis was carried out using R and Bioconductor.

Cell-Cell Communication Network

To investigate potential interactions between different cell types in the ovarian cancer tumor microenvironment, cell-cell communication analysis was performed as described previously by the CellPhoneDB Python package (Version 2.1.4), a publicly available repository of curated receptors and ligands and their interactions. Prediction of enriched receptor-ligand pairs between two cell types was derived from the expression of a receptor by one cell type and the expression of the corresponding ligand by another cell type. By default, only ligands and receptors expressed in at least 10% of cells in a given cell cluster were taken into consideration.

Pairwise comparisons between selective cell types were performed. We randomly permuted the cluster labels of all cells 1000 times to determine the mean of average ligand and receptor expression levels of the interactions, generating a null distribution for each receptor-ligand pair. A p-value for the likelihood of cell-type specificity of the corresponding receptor-ligand complex was obtained by calculating the proportion of the means as high as or above the actual mean. Then, we can select biologically relevant interactions.

DATA AVAILABILITY STATEMENT

Single-cell RNA data reported in this paper have been deposited (PRJCA009148) in the Genome Sequence Archive in the BIG Data Center under accession number HRA002345 that are publicly accessible at https://ngdc.cncb.ac.cn/gsa-human/. All relevant data are available from the corresponding author upon reasonable request.

ETHICS STATEMENT

The studies involving human participants were reviewed and approved by The Third Affiliated Hospital of Guangzhou Medical University (No: 2017-075). The patients/participants provided their written informed consent to participate in this study.

AUTHOR CONTRIBUTIONS

XS and DS directed and oversaw the project. YT, DZ, and TC collected ovarian tissue samples. YD performed comprehensive bioinformatics analyses. YD, YB, and DS wrote the manuscript with all the other authors participating in the discussion, data interpretation, and manuscript editing. All authors contributed to the article and approved the submitted version.

FUNDING

This research was supported by the Natural Science Foundation of Guangdong Province (no. 2020A1515010082), National Natural Science Foundation of China (NSFC, Project 81773012), National Science Foundation of China (grant 82170242 and 81570454), Science and Technology Planning Project of Guangzhou (202102010003), The Project for Key Medicine Discipline Construction of Guangzhou Municipality (no.2021-2023-17), and China Postdoctoral Science Foundation (2019M662858).

ACKNOWLEDGMENTS

We thank all the participants and their families for supporting this study. We thank The Third Affiliated Hospital of Guangzhou Medical University in China for providing samples.

SUPPLEMENTARY MATERIAL

The Supplementary Material for this article can be found online at: https://www.frontiersin.org/articles/10.3389/fimmu.2022.923194/full#supplementary-material

REFERENCES

1. Lheureux S, Gourley C, Vergote I, Oza AM. Epithelial Ovarian Cancer. *Lancet* (2019) 393(10177):1240–53. doi: 10.1016/s0140-6736(18)32552-2
2. Stewart C, Ralyea C, Lockwood S. Ovarian Cancer: An Integrated Review. *Semin Oncol Nurs* (2019) 35(2):151–6. doi: 10.1016/j.soncn.2019.02.001
3. Jayson GC, Kohn EC, Kitchener HC, Ledermann JA. Ovarian Cancer. *Lancet* (2014) 384(9951):1376–88. doi: 10.1016/s0140-6736(13)62146-7
4. Bowtell DD, Bohm S, Ahmed AA, Aspuria PJ, Bast RC Jr., Beral V, et al.? Rethinking Ovarian Cancer Ii: Reducing Mortality From High-Grade Serous Ovarian Cancer. *Nat Rev Cancer* (2015) 15(11):668–79. doi: 10.1038/nrc4019
5. Lheureux S, Cristea MC, Bruce JP, Garg S, Cabanero M, Mantia-Smaldone G, et al. Adavosertib Plus Gemcitabine for Platinum-Resistant or Platinum-Refractory Recurrent Ovarian Cancer: A Double-Blind, Randomised, Placebo-Controlled, Phase 2 Trial. *Lancet* (2021) 397(10271):281–92. doi: 10.1016/S0140-6736(20)32554-X
6. Shih AJ, Menzin A, Whyte J, Lovecchio J, Liew A, Khalili H, et al. Identification of Grade and Origin Specific Cell Populations in Serous Epithelial Ovarian Cancer by Single Cell Rna-Seq. *PloS One* (2018) 13(11): e0206785. doi: 10.1371/journal.pone.0206785
7. Hao Q, Li J, Zhang Q, Xu F, Xie B, Lu H, et al. Single-Cell Transcriptomes Reveal Heterogeneity of High-Grade Serous Ovarian Carcinoma. *Clin Transl Med* (2021) 11(8):e500. doi: 10.1002/ctm2.500
8. Cancer Genome Atlas Research N. Integrated Genomic Analyses of Ovarian Carcinoma. *Nature* (2011) 474(7353):609–15. doi: 10.1038/nature10166
9. Chen GM, Kannan L, Geistlinger L, Kofia V, Safikhani Z, Gendoo DMA, et al. Consensus on Molecular Subtypes of High-Grade Serous Ovarian Carcinoma. *Clin Cancer Res* (2018) 24(20):5037–47. doi: 10.1158/1078-0432.CCR-18-0784
10. Olalekan S, Xie B, Back R, Eckart H, Basu A. Characterizing the Tumor Microenvironment of Metastatic Ovarian Cancer by Single-Cell Transcriptomics. *Cell Rep* (2021) 35(8):109165. doi: 10.1016/j.celrep.2021.109165

11. Izar B, Tirosh I, Stover EH, Wakiro I, Cuoco MS, Alter I, et al. A Single-Cell Landscape of High-Grade Serous Ovarian Cancer. *Nat Med* (2020) 26 (8):1271–9. doi: 10.1038/s41591-020-0926-0
12. Sun Y, Wu L, Zhong Y, Zhou K, Hou Y, Wang Z, et al. Single-Cell Landscape of the Ecosystem in Early-Relapse Hepatocellular Carcinoma. *Cell* (2021) 184 (2):404–21 e16. doi: 10.1016/j.cell.2020.11.041
13. Zhou Y, Yang D, Yang Q, Lv X, Huang W, Zhou Z, et al. Single-Cell RNA Landscape of Intratumoral Heterogeneity and Immunosuppressive Microenvironment in Advanced Osteosarcoma. *Nat Commun* (2020) 11 (1):6322. doi: 10.1038/s41467-020-20059-6
14. Ahmed N, Escalona R, Leung D, Chan E, Kannourakis G. Tumour Microenvironment and Metabolic Plasticity in Cancer and Cancer Stem Cells: Perspectives on Metabolic and Immune Regulatory Signatures in Chemoresistant Ovarian Cancer Stem Cells. *Semin Cancer Biol* (2018) 53:265–81. doi: 10.1016/j.semcancer.2018.10.002
15. Qian J, Olbrecht S, Boeckx B, Vos H, Laoui D, Etlioglu E, et al. A Pan-Cancer Blueprint of the Heterogeneous Tumor Microenvironment Revealed by Single-Cell Profiling. *Cell Res* (2020) 30(9):745–62. doi: 10.1038/s41422-020-0355-0
16. Stuart T, Butler A, Hoffman P, Hafemeister C, Papalexi E, Mauck WM 3rd, et al. Comprehensive Integration of Single-Cell Data. *Cell* (2019) 177(7):1888–902 e21. doi: 10.1016/j.cell.2019.05.031
17. Aran D, Looney AP, Liu L, Wu E, Fong V, Hsu A, et al. Reference-Based Analysis of Lung Single-Cell Sequencing Reveals a Transitional Profibrotic Macrophage. *Nat Immunol* (2019) 20(2):163–72. doi: 10.1038/s41590-018-0276-y
18. Wu T, Hu E, Xu S, Chen M, Guo P, Dai Z, et al. Clusterprofiler 4.0: A Universal Enrichment Tool for Interpreting Omics Data. *Innovation* (2021) 2 (3):100141. doi: 10.1016/j.xinn.2021.100141
19. Geistlinger L, Oh S, Ramos M, Schiffer L, LaRue RS, Henzler CM, et al. Multiomic Analysis of Subtype Evolution and Heterogeneity in High-Grade Serous Ovarian Carcinoma. *Cancer Res* (2020) 80(20):4335–45. doi: 10.1158/0008-5472.CAN-20-0521
20. Winterhoff BJ, Maile M, Mitra AK, Sebe A, Bazzaro M, Geller MA, et al. Single Cell Sequencing Reveals Heterogeneity Within Ovarian Cancer Epithelium and Cancer Associated Stromal Cells. *Gynecol Oncol* (2017) 144(3):598–606. doi: 10.1016/j.ygyno.2017.01.015
21. Kristiansen G, Denkert C, Schlüns K, Dahl E, Pilarsky C, Hauptmann S. CD24 is Expressed in Ovarian Cancer and is a New Independent Prognostic Marker of Patient Survival. *Am J Pathol* (2002) 161(4):1215–21. doi: 10.1016/s0002-9440(10)64398-2
22. Chen YP, Yin JH, Li WF, Li HJ, Chen DP, Zhang CJ, et al. Single-Cell Transcriptomics Reveals Regulators Underlying Immune Cell Diversity and Immune Subtypes Associated With Prognosis in Nasopharyngeal Carcinoma. *Cell Res* (2020) 30(11):1024–42. doi: 10.1038/s41422-020-0374-x
23. Hornburg M, Desbois M, Lu S, Guan Y, Lo AA, Kaufman S, et al. Single-Cell Dissection of Cellular Components and Interactions Shaping the Tumor Immune Phenotypes in Ovarian Cancer. *Cancer Cell* (2021) 39(7):928–44 e6. doi: 10.1016/j.ccell.2021.04.004
24. Sun D, Guan X, Moran AE, Wu LY, Qian DZ, Schedin P, et al. Identifying Phenotype-Associated Subpopulations by Integrating Bulk and Single-Cell Sequencing Data. *Nat Biotechnol* (2021) 40(4):527–538. doi: 10.1038/s41587-021-01091-3
25. Tian T, Guo T, Zhen W, Zou J, Li F. Bet Degrader Inhibits Tumor Progression and Stem-Like Cell Growth *via* Wnt/B-Catenin Signaling Repression in Glioma Cells. *Cell Death Dis* (2020) 11(10):1–13. doi: 10.1038/s41419-020-03117-1
26. Nieto MA, Huang RY, Jackson RA, Thiery JP. Emt: 2016. *Cell* (2016) 166 (1):21–45. doi: 10.1016/j.cell.2016.06.028
27. Bakir B, Chiarella AM, Pitarresi JR, Rustgi AK. EMT, MET, Plasticity, and Tumor Metastasis. *Trends Cell Biol* (2020) 30(10):764–76. doi: 10.1016/j.tcb.2020.07.003
28. Xing X, Yang F, Huang Q, Guo H, Li J, Qiu M, et al. Decoding the Multicellular Ecosystem of Lung Adenocarcinoma Manifested as Pulmonary Subsolid Nodules by Single-Cell RNA Sequencing. *Sci Adv* (2021) 7(5):eabd9738. doi: 10.1126/sciadv.abd9738
29. Majc B, Sever T, Zarić M, Breznik B, Turk B, Lah TT. Epithelial-To-Mesenchymal Transition as the Driver of Changing Carcinoma and Glioblastoma Microenvironment. *Biochim Biophys Acta -Molecul Cell Res* (2020) 1867(10):118782. doi: 10.1016/j.bbamcr.2020.118782
30. La Manno G, Soldatov R, Zeisel A, Braun E, Hochgerner H, Petukhov V, et al. RNA Velocity of Single Cells. *Nature* (2018) 560(7719):494–8. doi: 10.1038/s41586-018-0414-6
31. Ledermann J, Harter P, Gourley C, Friedlander M, Vergote I, Rustin G, et al. Olaparib Maintenance Therapy in Platinum-Sensitive Relapsed Ovarian Cancer. *New Engl J Med* (2012) 366(15):1382–92. doi: 10.1056/NEJMoa1105535
32. Moore K, Colombo N, Scambia G, Kim B-G, Oaknin A, Friedlander M, et al. Maintenance Olaparib in Patients With Newly Diagnosed Advanced Ovarian Cancer. *New Engl J Med* (2018) 379(26):2495–505. doi: 10.1056/NEJMoa1810858
33. Kristeleit R, Shapiro GI, Burris HA, Oza AM, LoRusso P, Patel MR, et al. A Phase I–II Study of the Oral PARP Inhibitor Rucaparib in Patients With Germline BRCA1/2-Mutated Ovarian Carcinoma or Other Solid Tumors. *Clin Cancer Res* (2017) 23(15):4095–106. doi: 10.1158/1078-0432.CCR-16-2796
34. Zingg D, Debbache J, Pena-Hernandez R, Antunes AT, Schaefer SM, Cheng PF, et al. Ezh2-Mediated Primary Cilium Deconstruction Drives Metastatic Melanoma Formation. *Cancer Cell* (2018) 34(1):69–84 e14. doi: 10.1016/j.ccell.2018.06.001
35. Cao EY, Ouyang JF, Rackham OJJB. Geneswitches: Ordering Gene Expression and Functional Events in Single-Cell Experiments. *Bioinformatics* (2020) 36 (10):3273–5. doi: 10.1093/bioinformatics/btaa099
36. Tripathi V, Shen Z, Chakraborty A, Giri S, Freier SM, Wu X, et al. Long Noncoding RNA MALAT1 Controls Cell Cycle Progression by Regulating the Expression of Oncogenic Transcription Factor B-MYB. *PloS Genet* (2013) 9 (3):e1003368. doi: 10.1371/journal.pgen.1003368
37. Jadaliha M, Zong X, Malakar P, Ray T, Singh DK, Freier SM, et al. Functional and Prognostic Significance of Long non-Coding RNA MALAT1 as a Metastasis Driver in ER Negative Lymph Node Negative Breast Cancer. *Oncotarget* (2016) 7(26):40418. doi: 10.18632/oncotarget.9622
38. Hu Z, Artibani M, Alsaadi A, Wietek N, Morotti M, Shi T, et al. The Repertoire of Serous Ovarian Cancer Non-Genetic Heterogeneity Revealed by Single-Cell Sequencing of Normal Fallopian Tube Epithelial Cells. *Cancer Cell* (2020) 37(2):226–42 e7. doi: 10.1016/j.ccell.2020.01.003
39. Ulrich ND, Shen YC, Ma Q, Yang K, Hannum DF, Jones A, et al. Cellular Heterogeneity of Human Fallopian Tubes in Normal and Hydrosalpinx Disease States Identified Using scRNA-Seq. *Dev Cell* (2022) 57(7):914–29 e7. doi: 10.1016/j.devcel.2022.02.017
40. Kalluri R. The Biology and Function of Fibroblasts in Cancer. *Nat Rev Cancer* (2016) 16(9):582–98. doi: 10.1038/nrc.2016.73
41. Elyada E, Bolisetty M, Laise P, Flynn WF, Courtois ET, Burkhart RA, et al. Cross-Species Single-Cell Analysis of Pancreatic Ductal Adenocarcinoma Reveals Antigen-Presenting Cancer-Associated Fibroblasts. *Cancer Discov* (2019) 9(8):1102–23. doi: 10.1158/2159-8290.CD-19-0094
42. Vervoort SJ, Lourenço AR, Tufegdzic Vidakovic A, Mocholi E, Sandoval JL, Rueda OM, et al. Sox4 can Redirect TGF-β-Mediated SMAD3-Transcriptional Output in a Context-Dependent Manner to Promote Tumorigenesis. *Nucleic Acids Res* (2018) 46(18):9578–90. doi: 10.1093/nar/gky755
43. Ji Z, He L, Regev A, Struhl K. Inflammatory Regulatory Network Mediated by the Joint Action of NF-KB, STAT3, and AP-1 Factors is Involved in Many Human Cancers. *Proc Natl Acad Sci* (2019) 116(19):9453–62. doi: 10.1073/pnas.1821068116
44. van der Leun AM, Thommen DS, Schumacher TN. CD8(+) T Cell States in Human Cancer: Insights From Single-Cell Analysis. *Nat Rev Cancer* (2020) 20 (4):218–32. doi: 10.1038/s41568-019-0235-4
45. Duong CP, Yong CS, Kershaw MH, Slaney CY, Darcy PK. Cancer Immunotherapy Utilizing Gene-Modified T Cells: From the Bench to the Clinic. *Mol Immunol* (2015) 67(2):46–57. doi: 10.1016/j.molimm.2014.12.009
46. Liu X, Mo W, Ye J, Li L, Zhang Y, Hsueh EC, et al. Regulatory T Cells Trigger Effector T Cell DNA Damage and Senescence Caused by Metabolic Competition. *Nat Commun* (2018) 9(1):249. doi: 10.1038/s41467-017-02689-5
47. Yoshikawa T, Wu Z, Inoue S, Kasuya H, Matsushita H, Takahashi Y, et al. Genetic Ablation of PRDM1 in Antitumor T Cells Enhances Therapeutic Efficacy of Adoptive Immunotherapy. *Blood* (2021). doi: 10.1182/blood.2021012714

48. Cheng S, Li Z, Gao R, Xing B, Gao Y, Yang Y, et al. A Pan-Cancer Single-Cell Transcriptional Atlas of Tumor Infiltrating Myeloid Cells. *Cell* (2021) 184 (3):792–809 e23. doi: 10.1016/j.cell.2021.01.010
49. Engblom C, Pfirschke C, Pittet MJ. The Role of Myeloid Cells in Cancer Therapies. *Nat Rev Cancer* (2016) 16(7):447–62. doi: 10.1038/nrc.2016.54
50. Liu B, Li C, Li Z, Wang D, Ren X, Zhang Z. An Entropy-Based Metric for Assessing the Purity of Single Cell Populations. *Nat Commun* (2020) 11 (1):3155. doi: 10.1038/s41467-020-16904-3
51. Murray PJ. Immune Regulation by Monocytes. *Semin Immunol* (2018) 35:12–8. doi: 10.1016/j.smim.2017.12.005
52. Okuzaki D, Ota K, Takatsuki S-I, Akiyoshi Y, Naoi K, Yabuta N, et al. FCN1 (M-Ficolin), Which Directly Associates With Immunoglobulin G1, is a Molecular Target of Intravenous Immunoglobulin Therapy for Kawasaki Disease. *Sci Rep* (2017) 7(1):1–12. doi: 10.1038/s41598-017-11108-0
53. De Marco M, Basile A, Iorio V, Festa M, Falco A, Ranieri B, et al. Role of BAG3 in Cancer Progression: A Therapeutic Opportunity. *Semin Cell Dev Biol* (2018) 78:85–92. doi: 10.1016/j.semcdb.2017.08.049
54. Paolini L, Adam C, Beauvillain C, Preisser L, Blanchard S, Pignon P, et al. Lactic Acidosis Together With GM-CSF and M-CSF Induces Human Macrophages Toward an Inflammatory Protumor Phenotype. *Cancer Immunol Res* (2020) 8(3):383–95. doi: 10.1158/2326-6066.CIR-18-0749
55. Ramachandran P, Dobie R, Wilson-Kanamori JR, Dora EF, Henderson BEP, Luu NT, et al. Resolving the Fibrotic Niche of Human Liver Cirrhosis at Single-Cell Level. *Nature* (2019) 575(7783):512–8. doi: 10.1038/s41586-019-1631-3
56. Italiani P, Boraschi D. From Monocytes to M1/M2 Macrophages: Phenotypical vs. Functional Differentiation. *Front Immunol* (2014) 5:514. doi: 10.3389/fimmu.2014.00514
57. Sharma A, Seow JJW, Dutertre CA, Pai R, Bleriot C, Mishra A, et al. Onco-Fetal Reprogramming of Endothelial Cells Drives Immunosuppressive Macrophages in Hepatocellular Carcinoma. *Cell* (2020) 183(2):377–94.e21. doi: 10.1016/j.cell.2020.08.040
58. Wang N, Wang S, Wang X, Zheng Y, Yang B, Zhang J, et al. Research Trends in Pharmacological Modulation of Tumor-Associated Macrophages. *Clin Transl Med* (2021) 11(1):e288. doi: 10.1002/ctm2.288
59. Efremova M, Vento-Tormo M, Teichmann SA, Vento-Tormo R. CellPhonedDB: Inferring Cell-Cell Communication From Combined Expression of Multi-Subunit Ligand-Receptor Complexes. *Nat Protoc* (2020) 15(4):1484–506. doi: 10.1038/s41596-020-0292-x
60. Massara M, Bonavita O, Savino B, Caronni N, Mollica Poeta V, Sironi M, et al. ACKR2 in Hematopoietic Precursors as a Checkpoint of Neutrophil Release and Anti-Metastatic Activity. *Nat Commun* (2018) 9(1):676. doi: 10.1038/s41467-018-03080-8
61. Tavares LP, Garcia CC, Goncalves APF, Kraemer LR, Melo EM, Oliveira FMS, et al. ACKR2 Contributes to Pulmonary Dysfunction by Shaping CCL5: CCR5-Dependent Recruitment of Lymphocytes During Influenza A Infection in Mice. *Am J Physiol Lung Cell Mol Physiol* (2020) 318(4):L655–L70. doi: 10.1152/ajplung.00134.2019
62. Filippou PS, Karagiannis GS, Constantinidou AJO. Midkine (MDK) Growth Factor: A Key Player in Cancer Progression and a Promising Therapeutic Target. *Oncogene* (2020) 39(10):2040–54. doi: 10.1038/s41388-019-1124-8
63. Zhang Y, Zuo C, Liu L, Hu Y, Yang B, Qiu S, et al. Single-Cell RNA-Sequencing Atlas Reveals an MDK-Dependent Immunosuppressive Environment in ErbB Pathway-Mutated Gallbladder Cancer. *J Hepatol* (2021) 75(5):1128–41. doi: 10.1016/j.jhep.2021.06.023
64. Erin N, Grahovac J, Brozovic A, Efferth TJDRU. Tumor Microenvironment and Epithelial Mesenchymal Transition as Targets to Overcome Tumor Multidrug Resistance. *Drug Resist Update* (2020) 53:100715. doi: 10.1016/j.drup.2020.100715
65. Larionova I, Tuguzbaeva G, Ponomaryova A, Stakheyeva M, Cherdyntseva N, Pavlov V, et al. Tumor-Associated Macrophages in Human Breast, Colorectal, Lung, Ovarian and Prostate Cancers. *Front Oncol* (2020) 10:566511. doi: 10.3389/fonc.2020.566511
66. Zhou J, Li X, Wu X, Zhang T, Zhu Q, Wang X, et al. Exosomes Released From Tumor-Associated Macrophages Transfer miRNAs That Induce a Treg/Th17 Cell Imbalance in Epithelial Ovarian Cancer. *Cancer Immunol Res* (2018) 6 (12):1578–92. doi: 10.1158/2326-6066.CIR-17-0479
67. Wu JW, Dand S, Doig L, Papenfuss AT, Scott CL, Ho G, et al. T-Cell Receptor Therapy in the Treatment of Ovarian Cancer: A Mini Review. *Front Immunol* (2021) 12:1141. doi: 10.3389/fimmu.2021.672502
68. Zhou Y, Zhou B, Pache L, Chang M, Khodabakhshi AH, Tanaseichuk O, et al. Metascape Provides a Biologist-Oriented Resource for the Analysis of Systems-Level Datasets. *Nat Commun* (2019) 10(1):1523. doi: 10.1038/s41467-019-09234-6
69. Liu C-J, Hu F-F, Xia M-X, Han L, Zhang Q, Guo A-YJB. GSCALite: A Web Server for Gene Set Cancer Analysis. *Bioinformatics* (2018) 34(21):3771–2. doi: 10.1093/bioinformatics/bty411

Conflict of Interest: The authors declare that the research was conducted in the absence of any commercial or financial relationships that could be construed as a potential conflict of interest.

frontiers | Frontiers in Immunology

TYPE Review
PUBLISHED 25 July 2022
DOI 10.3389/fimmu.2022.920059

OPEN ACCESS

EDITED BY
Yubin Li,
University of Pennsylvania,
United States

REVIEWED BY
Sanjima Pal,
McGill University, Canada
Kai Yu,
Sun Yat-sen University Cancer Center (SYSUCC), China

*CORRESPONDENCE
Ning Liu
ningliu@cmu.edu.cn

SPECIALTY SECTION
This article was submitted to Cancer Immunity and Immunotherapy, a section of the journal Frontiers in Immunology

RECEIVED 14 April 2022
ACCEPTED 27 June 2022
PUBLISHED 25 July 2022

CITATION
Zhang C and Liu N (2022) Ferroptosis, necroptosis, and pyroptosis in the occurrence and development of ovarian cancer.
Front. Immunol. 13:920059.
doi: 10.3389/fimmu.2022.920059

Ferroptosis, necroptosis, and pyroptosis in the occurrence and development of ovarian cancer

Chunmei Zhang and Ning Liu*

Department of Obstetrics and Gynecology, Shengjing Hospital of China Medical University, Shenyang, China

Ovarian cancer (OC) is one of the most common malignancies that causes death in women and is a heterogeneous disease with complex molecular and genetic changes. Because of the relatively high recurrence rate of OC, it is crucial to understand the associated mechanisms of drug resistance and to discover potential target for rational targeted therapy. Cell death is a genetically determined process. Active and orderly cell death is prevalent during the development of living organisms and plays a critical role in regulating life homeostasis. Ferroptosis, a novel type of cell death discovered in recent years, is distinct from apoptosis and necrosis and is mainly caused by the imbalance between the production and degradation of intracellular lipid reactive oxygen species triggered by increased iron content. Necroptosis is a regulated non-cysteine protease–dependent programmed cell necrosis, morphologically exhibiting the same features as necrosis and occurring *via* a unique mechanism of programmed cell death different from the apoptotic signaling pathway. Pyroptosis is a form of programmed cell death that is characterized by the formation of membrane pores and subsequent cell lysis as well as release of pro-inflammatory cell contents mediated by the abscisin family. Studies have shown that ferroptosis, necroptosis, and pyroptosis are involved in the development and progression of a variety of diseases, including tumors. In this review, we summarized the recent advances in ferroptosis, necroptosis, and pyroptosis in the occurrence, development, and therapeutic potential of OC.

KEYWORDS

ovarian cancer, ferroptosis, necroptosis, pyroptosis, malignant progression

Introduction

Ovarian cancer (OC) is one kind of gynecologic malignancies with high mortality (1) and annually increased incidence (2, 3), which seriously threatens women's life and

health. OC is prevalent in middle-aged and elderly women. There is often no obvious clinical manifestation in the early stage. About 70% of patients first present with abdominal distention, ascites, and abdominal pain (4). Therefore, more than 75% of patients with OC present with advanced stages at the time of first or confirmed diagnosis (5, 6). In clinical settings, OC is featured with insidious onset, lack of early diagnostic markers, high malignancy, easy metastasis, and poor prognosis (7, 8). Currently, surgery combined with platinum and paclitaxel-based chemotherapy is the mainstream treatment for OC (7, 9). Although surgery and chemotherapy have significantly improved the prognosis of patients with OC in recent years, the 5-year survival rate of patients with advanced OC remains low (10, 11) because most patients with OC are advanced at the time of diagnosis and some patients with OC develop chemoresistance later following treatment (12, 13). Therefore, the search for potential biomarkers and therapeutic targets is of great clinical importance for early screening of patients with OC and improving the prognosis of patients with OC.

Cell death is a life phenomenon and an irreversible life process of cells. Cell death plays an indispensable role in the biological process of maintaining the normative homeostasis of the body and inhibiting the rapid proliferation of tumor cells (14, 15). Cell death includes regulated cell death (RCD) and accidental cell death (ACD) (16–18). RCD is a genetically determined form of active and ordered cell death that plays an important role in the maintenance of homeostasis (19, 20). Currently, the common types of RCD include apoptosis, necroptosis, ferroptosis, autophagy, and pyroptosis (21). Ferroptosis, a newly discovered non-apoptotic form of cell death, is essentially iron ion–dependent RCD. Necroptosis is mainly mediated by cytokines (TNF-α, IFN-α, and IFN-γ), Toll-like receptors (TLR3, TLR4, and TLR9), and nucleic acid (DNA and RNA) receptors. RIPK1/3 and MLKL are involved in the development of necroptosis, with MLKL being the key molecule (22, 23). Pyroptosis, which is a pathological form of suicide of cells distinct from apoptosis, is mainly mediated by Caspase-1 and Caspase-4/5/11. Pyroptotic signaling pathway mainly includes classical pyroptosis pathway and non-classical pyroptosis pathway, with inflammatory vesicle production and Gasdermin D (GSDMD) activation as the hallmarks of pyroptosis pathway (24, 25). Gasdermin B (GSDMB) is highly expressed in inflammatory bowel disease and contributes to the progression of inflammation by disrupting epithelial barrier function and promoting the development of ferroptosis (26). Necroptosis is mainly mediated by cytokines (TNF-α, IFN-α, and IFN-γ), Toll-like receptors (TLR3, TLR4, and TLR9), and nucleic acid (DNA and RNA) receptors. RIPK1/3 and MLKL are involved in the development of necroptosis, with MLKL being the key molecule (22, 23). Necroptosis is induced by cigarette smoke exposure and is increased in the lungs of patients with chronic obstructive pulmonary disease (COPD) and patients with experimental COPD. Inhibition of necroptosis attenuated cigarette smoke-induced airway inflammation, airway remodeling, and emphysema (27). Recently, accumulating evidence has showed that ferroptosis, necroptosis, and pyroptosis play an important role in tumor development. Expression levels of ZBP1 are significantly increased in necrotic tumors. In addition, ZBP1 deficiency blocked necroptosis and significantly inhibited tumor metastasis during breast cancer development (28). In breast cancer, DRD2 promotes M1 polarization of macrophages and triggers GSDME-executed pyroptosis that regulates the tumor microenvironment and inhibits tumor malignant progression (29). All these pieces of evidence highlight the important roles of ferroptosis, necroptosis, and pyroptosis in the progression and metastasis of human malignancies.

RCD in malignancies has been extensively studied and more and more pieces of evidence reveals that ferroptosis, necroptosis, and pyroptosis are highly involved the development, progression, and regression of OC (30, 31). In this paper, we reviewed the molecular mechanisms of ferroptosis, necroptosis, and pyroptosis and their regulatory roles in OC, providing a new perspective on the pathogenesis and targeted therapy of OC and exploring their potential as potential therapeutic targets for death.

Abbreviations: OC, ovarian cancer; RCD, regulated cell death; ACD, accidental cell death; TLRs, Toll-like receptors; GSDMB, Gasdermin B; ACSL4, acyl-coa synthetase long-chain family member 4; LPCAT3, lysophosphatidylcholine acyltransferase 3; LOX, lipoxygenase; NFS1, nitrogen fixation 1; TFRC, transferrin receptor; FTH1, ferritin heavy chain 1; NCOA4, nuclear receptor coactivator 4; NADH, nicotinamide adenine dinucleotide; RIPK1, serine/threonine protein kinase 1; MLKL, mixed lineage kinase domain–like pseudokinase; caspase-1, cysteine-aspartic proteases 1; FADD, Fas-associating protein with a novel death domain; TNF-α, tumor necrosis factor α; TRADD, TNFR1-associated death domain protein; LUBAC, linear ubiquitin chain assembly complex; NF-κB, nuclear factor κB; MAPK, mitogen-activated protein kinase; RHIM, RIP homotypic interaction motif; PRRs, pattern recognition receptors; ASC, apoptosis-associated speck-like protein; NLRP1, nucleotide-binding oligomerization domain–like receptor protein 1; PYD, pyrin domain; CARD, caspase activation and recruitment domain; TAMs, tumor-associated macrophages; GPX4, glutathione peroxide 4; PAMP, pathogen-associated molecular pattern; LUAD, lung adenocarcinoma; FAC, ferrous ammonium citrate; FZD7, Frizzled 7; IAP, inhibitor of apoptosis protein; LGSCs, low-grade serous carcinomas; CNL, ceramide nanoliposomes; BBR, berberine.

Ferroptosis

The overview of ferroptosis

Programmed cell death plays an important biological effect in maintaining the homeostasis of the organism. As a novel

mode of cell death, ferroptosis was first described in 2012. The small-molecule inhibitor erastin was found to induce a unique mode of cell death in ras mutant cells that could not be rescued by apoptosis inhibitors and necrosis inhibitors but was reversed by the iron ion chelator deferoxamine. Later, this novel mode of cell death was named ferroptosis (32). Ferroptosis is an iron- and ROS-dependent mode of cell death, which is characterized by major cytological changes including reduction or loss of mitochondrial cristae, rupture of the outer mitochondrial membrane, and mitochondrial membrane ruffling (33, 34). All these above changes are caused to loss of selective permeability of the cell membrane due to the occurrence of peroxidation of lipid components of the cell membrane and oxidative stress (35, 36). In addition, different physiological conditions and pathological stresses have been found to induce tissue ferroptosis (37, 38). Ferroptosis is gradually recognized as an adaptive process by which the body eliminates malignant cells by removing cells damaged by nutritional deficiency, infection, or stress (39–41). Thus, ferroptosis has an inhibitory effect on tumorigenesis under normal conditions, and abnormalities in the oxidative stress pathway are an important cause of ferroptosis. Although tumor cells are in a constant state of excessive oxidative stress, they are less likely to develop ferroptosis, which is mainly dependent on their own antioxidant system (42, 43). In-depth studies based on the mechanisms of ferroptosis occurrence and regulation in tumor cells are of great clinical importance for the formation of new strategies for tumor therapy.

Regulatory mechanisms of ferroptosis

Phospholipid hyperoxidation of polyunsaturated fatty acids in the cytoplasmic membrane has been shown to be the most important driver of ferroptosis (44). The proportion of polyunsaturated fatty acids in lipids determines the ease with which lipid peroxidation occurs in cells. Acyl-coa synthetase long-chain family member 4 (ACSL4) and lysophosphatidylcholine acyltransferase 3 (LPCAT3) are key enzymes that regulate polyunsaturated fatty acid synthesis in phospholipid membranes, whereas the inhibition of both ACSL4 and LPCAT3 promotes ferroptosis resistance (45). There are two types of intracellular lipid peroxidation, namely, non-enzymatic and enzymatic lipid peroxidation. Non-enzymatic lipid peroxidation, also known as lipid autoxidation, is mainly a free radical-mediated chain reaction in which hydroxyl radicals generated by the Fenton reaction oxidize polyunsaturated fatty acids to lipid hydroperoxides (46). In contrast, enzymatic lipid peroxidation is mainly a process of direct oxidation of free polyunsaturated fatty acids to various types of lipid hydroperoxides catalyzed by lipoxygenase (LOX) (47, 48). Lipid hydroperoxides are catalyzed by iron ions to generate alkoxy radicals, which participate in the next lipid peroxidation chain reaction, ultimately leading to cell death (49). The exact mechanism by which lipid peroxidation leads to cellular ferroptosis is still not well understood. It could be due to the formation of structural lipid gaps, similar to protein gaps in necrosis and focal death. It is also possible that the depletion of polyunsaturated fatty acids causes structural changes in the fluidity of the cell membrane as well as an increase in membrane permeability, ultimately leading to loss of membrane integrity (50). In addition, lipid peroxides can be broken down into toxic aldehydes, which can further enhance the lipid peroxidation of ferroptosis by promoting protein inactivation through cross-linking reactions (51, 52). The mechanisms of amino acids and lipid metabolism in ferroptosis were displayed in **Figure 1**. Iron ions are important catalysts for lipid peroxidation reactions. Intracellular uptake, release, and storage of iron ions are all important regulators of ferroptosis. Inhibition of nitrogen fixation 1 (NFS1), which provides sulfur from cysteine for the synthesis of iron-sulfur clusters, activates the iron starvation response by simultaneously increasing transferrin receptor (TFRC) expression and degrading ferritin heavy chain 1 (FTH1), causing an increase in free iron ions, thereby making cells sensitive to ferroptosis activator (53–55). Overactivated heme oxygenase 1 increases intracellular free iron content and enhances ferroptosis effect by degrading hemoglobin into free iron, biliverdin, and carbon monoxide (56–58). Nuclear receptor coactivator 4 (NCOA4) recognizes intracellular after ferritin recognition, and ferritin transfers stored ferric ions to the autophagosome for degradation, which, in turn, releases ferric ions into the cytoplasm to become free iron, a process also known as iron autophagy (59, 60). In addition, genes such as nuclear receptor coactivator (NRF2) and heat shock protein B1 have been found to affect the sensitivity of cells to ferroptosis inducers by regulating intracellular iron ion metabolism (61, 62). This shows that iron ion metabolism is a potential regulatory point for the induction of cellular ferroptosis. The mechanisms of iron metabolism in ferroptosis were displayed in **Figure 2**. In addition to iron metabolism and lipid peroxidation responses, a wide range of intracellular antioxidant mechanisms also plays an important role in regulating ferroptosis sensitivity (63, 64). Glutathione (GSH), the most important intracellular antioxidant metabolite, requires cysteine as a raw material for its synthesis, and cells can endogenously synthesize cysteine *via* the transsulfuration pathway to resist ferroptosis (65, 66). In addition, myristoylation modification of ferroptosis inhibitory protein 1 leads to a nicotinamide adenine dinucleotide (NADH)–dependent decrease in coenzyme Q, which acts as a radical-trapping antioxidant to inhibit lipid peroxide proliferation (67, 68).

Necroptosis

The overview of necroptosis

Necroptosis, also known as programmed necrosis, is a necrosis-like form of cell death that relies on receptor

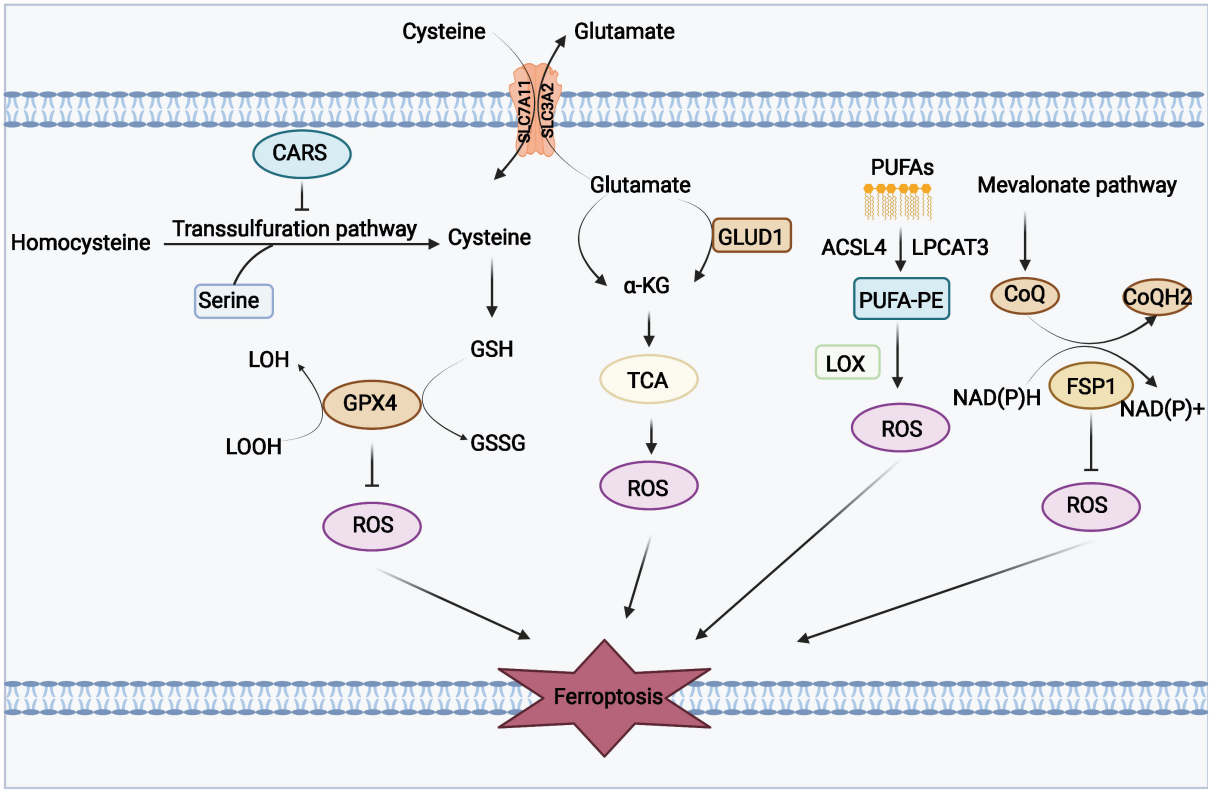

FIGURE 1
Mechanisms of amino acids and lipid metabolism in ferroptosis. Cysteine can be transported into the cell, whereas glutamate can be transported out of the cell by the Xc-system. Cysteine can be used to synthesize glutathione to maintain the balance of the redox state, and it can also be synthesized through the transsulfurization pathway blocked by CARS. Glutamate can be converted to a-KG by transaminase or GLUD1 pathway and participate in TCA, thereby generating ROS. PUFAs derived from cell membranes can be catalyzed by ACSL4 and LPCAT to PUFA-PE, and PUFA-PE can be peroxidized by the LOX family. FSP1 and coenzyme Q also play an important role in the antioxidant system of coenzyme Q.

interacting serine/threonine protein kinase 1 (RIPK1), RIPK3, and mixed lineage kinase domain–like pseudokinase (MLKL) and does not depend on cysteine-aspartic proteases 1 (caspase-1) (23, 69, 70). Necrosis was once thought to be passive and non-programmed, but recent studies have revealed that cell necrosis is an active and modifiable process (71). In the absence or inhibition of caspase-8 or Fas-associating protein with a novel death domain (FADD), cells induced by tumor necrosis factor α (TNF-α) still die, and the cell death morphology resembles that of necrotic cells (72–74), gradually revealing a caspase-independent cell death similar to necrosis. Degterev et al. first described the role of the small-molecule Nec-1 in regulating cell necrosis, updating, for the first time, the concept of unregulated necrosis to cells that can be regulated by Nec-1 necroptosis (16, 75). Since then, necroptosis has been defined as programmed necrosis, whereby cells undergoing necroptosis have their cell membranes ruptured, releasing intracellular material that can stimulate a variety of cells (including macrophages, fibroblasts, and endothelial cells) to participate in the intrinsic immune response and exacerbate the inflammatory response by releasing inflammatory cytokines, leading to a dual role for necroptosis in different physiological or pathological processes (22, 23).

Regulatory mechanisms of necroptosis

The potential mechanism of necroptosis is shown in **Figure 3**. The programmed cell death pattern is driven by RIPK1 through its kinase function, including through the formation of complex iia leading to apoptosis and complex iib leading to necroptosis (18, 76, 77). After TNF-α interacts with TNFR, TNFR1 starts to recruit the downstream protein molecules TNFR1- associated death domain protein (TRADD), RIPK1, TRAF2/5, and linear ubiquitin chain assembly complex (LU-BAC) proteins to form complex I, in which RIPK1 is polyubiquitinated and activates nuclear RIPK1 polyubiquitinates and activates the nuclear factor κB (NF-κB)

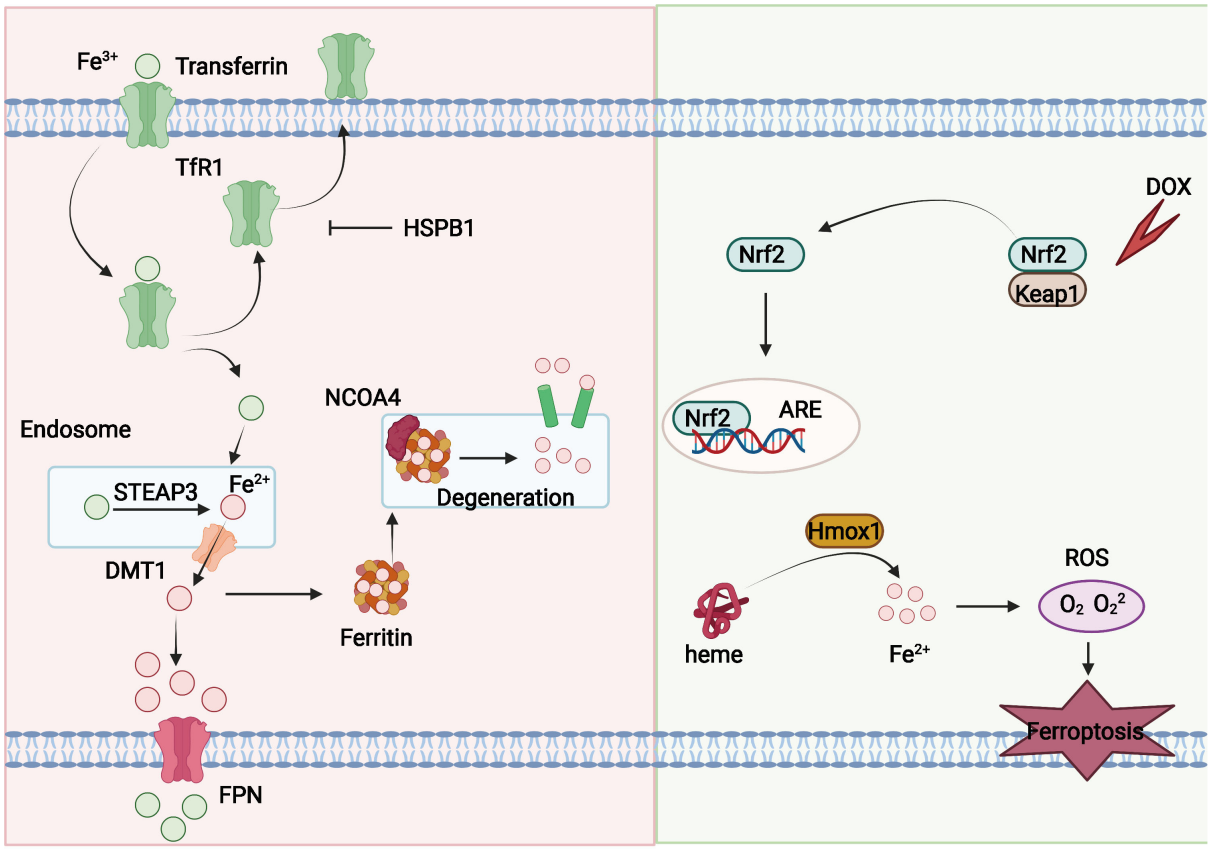

FIGURE 2
Mechanisms of iron metabolism in ferroptosis. Fe^{3+} can couple to transferrin and enter the intercellular milieu mediated by TfR1. Transferrin can be recycled and exported extracellularly and blocked by HSPB1. Fe^{3+} is reduced to Fe^{2+} by DMT1 in endosomes, and Fe^{2+} can be transported into the cytoplasm. Fe^{2+} can be released from ferritin through NCOA4-mediated ferritin phagocytosis, and part of Fe^{2+} can be exported outside the cell and oxidized by FPN. In addition, DOX can also induce ferroptosis. Cardiac output of DOX activates the Keap1/Nrf2 pathway, and Nrf2 further activates the downstream protein Hmox1 and prompts it to oxidize heme and release iron, leading to ferroptosis.

and mitogen-activated protein kinase (MAPK) signaling pathways, inhibiting caspase-8 activation and promoting cell survival (72, 78–80). If TNF-α recruits TRADD, FADD, pro–caspase-8, and RIPK1 to form complex iia, then complex iia promotes activation of caspase-8, and activated caspase-8 undergoes apoptosis by activating caspase-3 (73, 81, 82). When caspase-8 is inhibited or its activity level is relatively low, RIPK1 recruits RIPK3 and both recruit MLKL through the RIP homotypic interaction motif (RHIM) to form complex iib, also known as necrosome (83, 84). MLKL phosphorylation causes oligomerization and membrane localization. Oligomerized MLKL has the ability to bind directly to lipids, allowing polymerized MLKL to form membrane permeable pores, disrupt cell membrane integrity, and undergo necroptosis (71, 85). However, it inhibits the formation of complex iib to inhibit necroptosis, so the role of RIPK1 in cells can be determined by targeting the drug to determine whether the cells survive or undergo necroptosis (74, 86, 87).

Pyroptosis

The overview of pyroptosis

Pyroptosis is a caspase-1–mediated mode of programmed cell death (88, 89) characterized by rapid plasma membrane rupture followed by the release of cellular contents and pro-inflammatory substances such as IL, which triggers an inflammatory cascade response that results in cellular damage (24, 90). As early as 1992, Zychlinsky et al. observed experimentally that Shigella fowleri could induce lytic death in infected host macrophages (91). In 2001, Cookson et al. showed that this form of death was caspase-1 activity–dependent, unlike caspase-3 activity–dependent apoptosis (92). They first defined focal cell death as a caspase-1–dependent form of cell death. Furthermore, Shao et al. showed that cell scorch death can also be induced by the activation of caspase-4/5/11 by intracytoplasmic LPS and that activated caspase-4/5/11

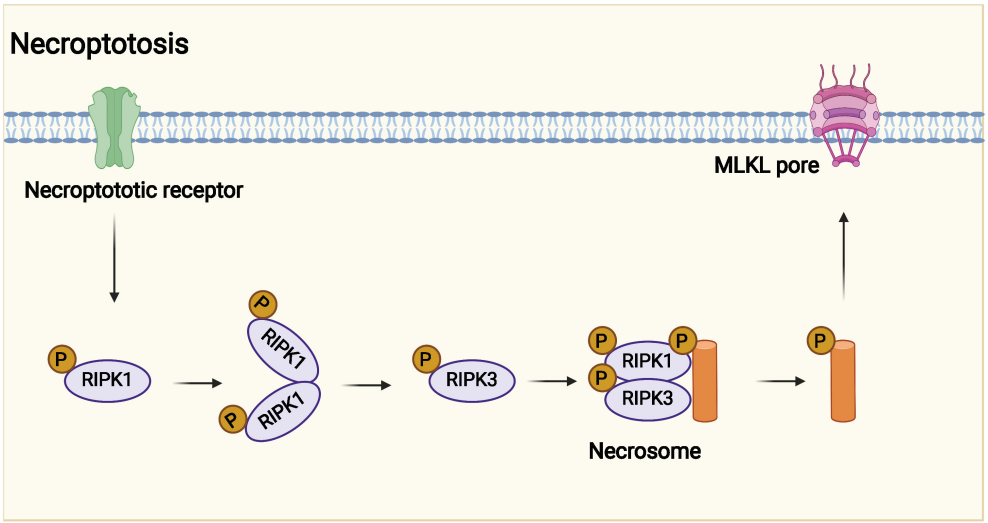

FIGURE 3
Potential mechanism of necroptosis. Necroptotic death may have evolved into the innate immune mechanism that complements apoptosis to eliminate pathogens. Necroptosis is affected by receptor interacting protein kinase 3 (RIPK3) and mixed lineage kinase domain-like protein (MLKL).

ultimately induces cell scorch death through cleavage of Gasdermin family proteins. Therefore, they defined cell scorch death as programmed cell necrosis mediated by the Gasdermin family (93, 94). When cell death occurs, the nucleus is condensed, chromatin DNA is randomly broken and degraded, numerous pores appear in the cell membrane, the cell membrane loses its ability to regulate the entry and exit of substances, the cell loses internal and external ionic balance, osmotic swelling occurs, and the membrane ruptures, releasing cell contents and other active substances, stimulating the body's immune response, and recruiting more inflammatory cells. This stimulates the body's immune response, recruits more inflammatory cells, and amplifies the inflammatory response.

Regulatory mechanisms of pyroptosis

The potential mechanism of pyroptosis is shown in **Figure 4**. The assembly of the inflammasome is the initiating step of the classical pathway of pyroptosis, a complex of intracellular macromolecular proteins necessary for inflammation to occur and capable of recognizing dangerous signaling molecules such as bacteria and viruses. The inflammasome is mainly composed of pattern recognition receptors (prrs), apoptosis-associated speck-like protein (ASC), and pro–caspase-1 (95–98). Among them, prrs are receptor proteins responsible for the recognition of different intracellular signaling stimuli, which are mainly composed of nucleotide-binding oligomerization domain–like receptor protein 1 (NLRP1) and NLRP3; nucleotide ASC is an articulated protein that consists mainly of the N-terminal pyrin domain (PYD), caspase activation, and recruitment domain (CARD) (95, 99). Pro–caspase-1 is an effector molecule that is activated to specifically cleave GSDMD. Danger-signaling sensors after the recognition of the danger signaling molecule by NLRP1, NLRP3, or AIM2 bind to the PYD structural domain at the N-terminal end of the bridging protein through its N-terminal PYD structural domain, and ASC then recruits caspase-1 through the interaction of the CARDCARD structural domain to complete the assembly of the inflammasome (100, 101). The inflammasome acts by activating the effector molecule pro–caspase-1 to form active caspase-1. Activated caspase-1 is able to specifically cleave the GSDMD to generate the N-terminal and C-terminal ends, and the N-terminal end of the GSDMD binds to cell membrane phospholipids, causing many small pores to form in the cell membrane (102, 103). The integrity of the cell is disrupted, and the water flows inward, leading to cell swelling and rupture, releasing intracellular inflammatory substances, and inducing pyroptosis (104). In addition, caspase-1 also promotes the maturation of IL-18 and IL-1β precursors, which are cleaved into active IL-18 and IL-1β (90, 105, 106) and secreted through the cell membrane pores to the outside of the cell, recruiting more inflammatory cells and causing an inflammatory waterfall response. This caspase-1–mediated cell death is called the classical pathway of pyroptosis. The non-classical pathway of pyroptosis is mainly mediated by caspase-4, caspase-5, and caspase-11. Upon stimulation of cells by bacterial LPS, caspase-4, caspase-5, and caspase-11 bind directly to and are activated by bacterial LPS (40, 107). Activated caspase-4,

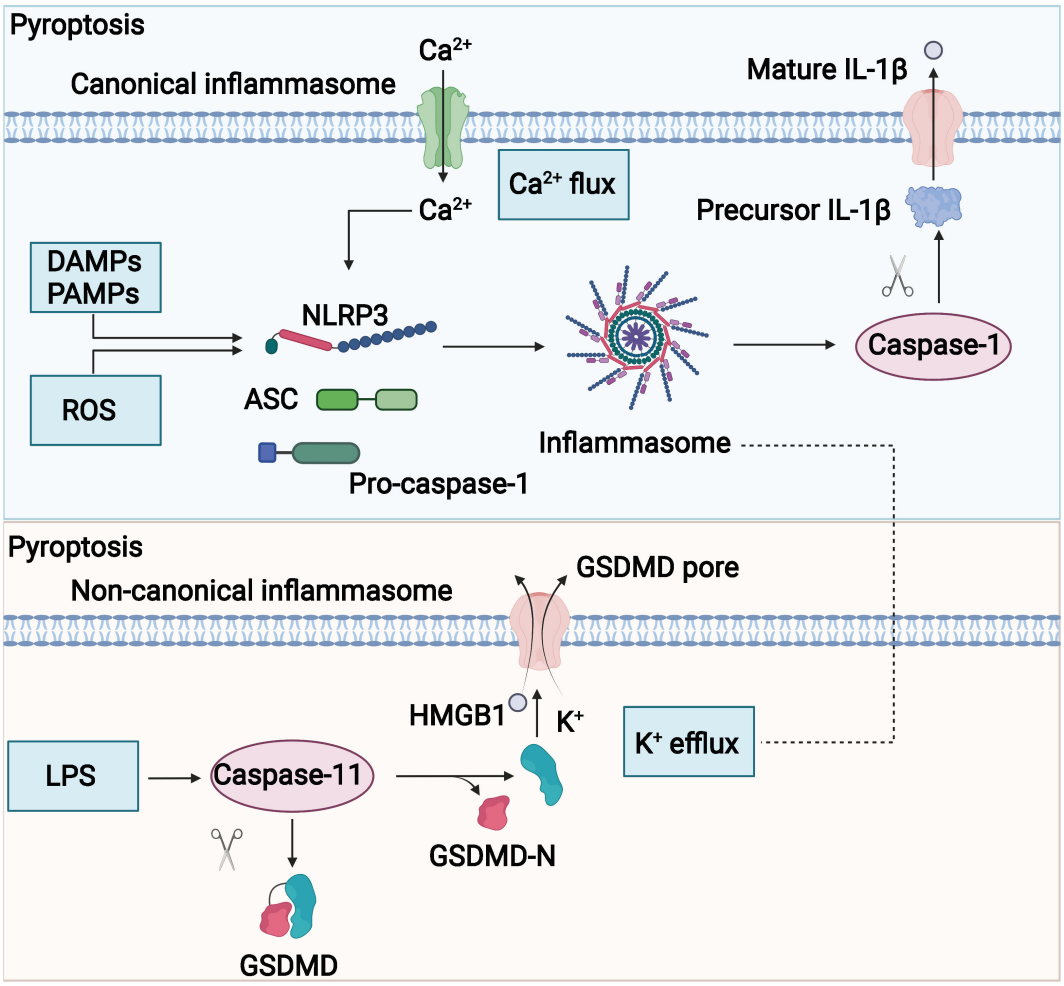

FIGURE 4
Potential mechanism of pyroptosis. The molecular mechanisms of pyrolysis mainly include canonical and noncanonical signaling.

caspase-5, and caspase-11 specifically cleave the GSDMD, relieving intramolecular inhibition of the GSDMD N structural domain (108), and the GSDMD N terminus binds to cell membrane phospholipids, causing cell membrane pore formation, cell swelling, rupture, and induction of pyroptosis (108). The GSDMD N terminus also amplifies the inflammatory response by activating the NLRP3 inflammasome, which, in turn, activates caspase-1 (109), which stimulates the maturation of IL-18 and IL-1β precursors and secretes IL-18 and IL-1β extracellularly (110).

Role of ferroptosis, necroptosis, and pyroptosis in tumors

Ferroptosis is a novel form of RCD induced by iron-dependent lipid peroxidation damage, which is morphologically, genetically, and molecularly different from other cell death modalities such as apoptosis, autophagy, and necrosis. The relationship between ferroptosis and tumors is extremely close, and there are numerous studies to design and develop ferroptosis-based anticancer drugs, and ferroptosis is expected to be a novel therapeutic approach for tumors. The interactive dialogue between triple-negative breast cancer (TNBC) cells and tumor-associated macrophages (tams) promotes the sustained activation of HLF in tumor cells through the IL-6–TGF-β1 axis. Subsequently, hepatic leukemia factor (HLF) promotes resistance to ferroptosis in TNBC cells *via* GGT1, ultimately promoting malignant tumor progression (1). The current design of corresponding compounds targeting key molecules in ferroptosis can effectively inhibit tumor progression with significant clinical translational implications. Mimetic drugs composed of small-molecule inducers of ferroptosis, erastin, and RSL3 with BH3 were effective in synergistically killing U251 cells and inhibiting malignant

progression of glioblastoma (111). Nanocatalytic activity leads to simultaneous inhibition of GPX4/GSH and FSP1/coq10h2 pathways and synergizes with the GPX4 inactivation function of RSL3 to cause significant ferroptosis damage and thus inhibit malignant progression of triple-negative breast cancer (112). Depletion of PSTK leads to inactivation of GSH peroxide 4 (GPX4) and inhibition of selenocysteine and cysteine synthesis. GSH metabolism is disrupted due to inhibition of selenocysteine and cysteine synthesis, which enhances the induction of ferroptosis after targeted chemotherapy, leading to malignant progression of hepatocellular liver cancer (113). The use of PSTK inhibitor-punicalin together with sorafenib for the treatment of HCC *in vitro* and *in vivo* exhibits synergistic effects.

Research on targeted tumor therapy based on necroptosis is currently underway, suggesting that necroptosis will provide a new strategy for tumor treatment. Disintegrin and Metalloprotease 17 (ADAM17) was identified as a novel important regulator of necroptosis whose activity could significantly affect the role of TNFR1-dependent tumor cell induction of endothelial cell death, tumor cell extravasation, and subsequent metastatic seeding (114). Furthermore, mediated TNFR1 extracellular domain shedding and subsequent processing by the γ-secretase complex are key enzymatic steps in the induction of TNF-induced necrotic apoptosis.ADAM17 may serve as an important target as an anti-metastatic and advanced cancer therapy. RIPK3 may act as a tumor suppressor to inhibit malignant progression of malignant mesothelioma through induction of necrotic apoptosis, whereas RIPK3 DNA epigenetic silencing of methylation impairs necroptosis and leads to chemoresistance as well as poorer prognosis in malignant mesothelioma (115). Tsc1/mTOR has a critical role in suppressing RIPK3 expression and activation in intestinal epithelial cells through TRIM11-mediated ubiquitination and autophagy-dependent degradation. mTOR can act on RIPK3 to enhance the expression and activation of RIPK3 by TNF and microbial pathogen-associated molecular pattern (PAMP)–induced necroptosis. mTOR/RIPK3/necroptosis axis is a driver of intestinal inflammation and cancer (116).

Various components of the scorch pathway are associated with tumorigenesis, invasion, and metastasis, and studies on scorch death have opened up new frontiers in tumor therapy. maternal embryonic leucine zipper kinase (MELK) expression is elevated in lung adenocarcinoma (LUAD) and promotes the malignant progression of LUAD cells by regulating the PLK1-CDC25C-CDK1 signaling pathway to promote proliferation and inhibit apoptosis-mediated cell scorch (16, 117). GSDME-mediated cell scorch death promotes colorectal cancer progression by releasing HMGB1, which induces tumor cell proliferation and PCNA expression through the extracellular regulated protein kinases 1/2 (ERK1/2) pathway (118). Circneil3, a circulating RNA, can act as a sponge by directly binding to mir-1184 and thereby releasing the inhibitory effect of miR-1184. The inhibition of PIF1 by mir-1184 ultimately induces DNA damage and triggers AIM2 inflammasome activation-mediated cell scorching (119). Mediating the cell scorch-induced circneil3/mir-1184/PIF1 regulatory axis may be a promising clinical therapeutic strategy for lung cancer.

Accumulating evidence has identified the crosstalk between ferroptosis, necroptosis, and pyroptosis. A number of factors including NEK7, Tom20, and caspase-1 have been found to mediate the crosstalk between these programmed cell death pathways. For instance, necroptosis and pyroptosis are both able to promote cell lysis. Z-DNA binding protein 1 (ZBP1) has been found to promote pyroptosis and necroptosis upon sensing infection with fungus (120). A well-established cell marker for apoptosis, Bcl-2, is found to regulate pyroptosis and necroptosis by targeting BH3-like domains in GSDMD and MLKL (121). Moreover, caspase-8 plays a key role in switching from necroptosis topyroptosis (122). Moreover, the key molecular regulator for ferroptosis, iron, could promote excessive reactive oxygen species (ROS) production and mediate crosstalk between ferroptosis and necroptosis (123). In the model of myocardial fibrosis, it has been reported that mixed-lineage kinase 3 (MLK3) modulates pyroptosis and ferroptosis *via* distant signaling pathways (124). Interestingly, non-coding RNAs have also been reported to play a key role in the crosstalk between necroptosis, ferroptosis, and pyroptosis (125). All these pieces of evidence highlight the correlation between necroptosis, pyroptosis, and ferroptosis.

Roles of cell deaths: ferroptosis, necroptosis, and pyroptosis in OC

Apoptosis used to be considered the predominant means of programmed cell death in tumor cells that decide the proliferation rate of cells. Lately, mounting evidence has showed that other types of programmed cell death including ferroptosis, necroptosis, and pyroptosis are highly involved in a variety of cell processes of OC cells, such as chemoresistance and immune response.

Role of ferroptosis in OC

In brief, the regulatory role of ferroptosis related genes in OC progression was displayed in **Table 1**. Studies have shown that elevated intracellular iron levels are closely associated with OC. FPN was decreased, TFR1 and TF were increased, and iron levels were elevated in high-grade plasma cytotic OC tissues compared with normal ovarian tissues (141). Genetic models of OC initiating cells also exhibit reduced iron efflux pumps and upregulated expression of iron transport–related proteins. This

TABLE 1 The regulatory role of ferroptosis related genes in ovarian cancer progression.

Target	Mechanism	Function	Reference
FAC	Target $Fe2^+$ and GPX4	Induce ferroptosis and inhibit ovarian cancer	(126)
SCD1	Target unsaturated fatty acyl chain	Induce ferroptosis and inhibit ovarian cancer	(127)
miR-424-5p	Target ACSL4/erastin/RSL3	Induce ferroptosis and inhibit ovarian cancer	(128)
SPIO-serum	Target GPX4/xCT	Induce ferroptosis and inhibit ovarian cancer	(129)
PARP	Target SLC7A11	Induce ferroptosis and inhibit ovarian cancer	(130)
SNAI2	Target SLC7A11	Induce ferroptosis and inhibit ovarian cancer	(131)
ADAMTS9-AS1	Target miR-587/SLC7A11	Inhibit ferroptosis and promote ovarian cancer	(132)
Sodium molybdate	Target NO/GSH	Induce ferroptosis and inhibit ovarian cancer	(133)
TAZ	Target ANGPTL4/NOX2	Induce ferroptosis and reduce drug resistance	(134)
CBS	/	Inhibit ferroptosis and promote ovarian cancer	(135)
FZD7	Target Tp63	Induce ferroptosis and reduce platinum resistance	(136)
Erastin	Target ROS	Induce ferroptosis and inhibit ovarian cancer	(137)
GALNT14	Target EGFR/mTOR	Induce ferroptosis and reduce platinum resistance	(138)
MAP30	Target Ca2+	Induce ferroptosis and reduce platinum resistance	(139)
Lidocaine	Target miR-382-5p/SLC7A11	Induce ferroptosis and inhibit ovarian cancer	(140)

suggests that intracellular iron levels are elevated in OC cells early in the development of OC. Li et al. (126) found that ferrous ammonium citrate (FAC) promoted intracellular iron expression levels in OC cells and inhibited OC cell proliferation, induced apoptosis, promoted inflammatory responses, and inhibited the reduction of lipid peroxides. Inhibition of GPX4 modulated intracellular iron homeostasis and lipid peroxide reduction, induced ferroptosis, and exerted anti-cancer effects.

In ferroptosis, lipid peroxidation driven by ROS plays an important role in the ferroptosis pathway. Tesfay et al. (127) found that steroyl coa desaturase (SCD1) was highly expressed in OC tissues, cell lines, and genetic models of OC stem cells. Inhibition of SCD1 significantly reduced unsaturated fatty acyl chains and increased long-chain saturated ceramides in membrane phospholipids and enhanced the anti-tumor effects of ferroptosis inducers in OC cell lines and *in situ* xenograft models in mice.

OC is associated with abnormal expression of many genes. Ma et al. (128) demonstrated that upregulation of mir-424-5p inhibited ACSL4 expression by directly binding to the 3′-untranslated region (UTR) of ACSL4, thereby reducing erastin- and RSL3-induced ferroptosis and ultimately inhibiting the malignant progression of OC. Mutation of the p53 gene alone caused migration of mouse oviductal epithelial cells; when p53 mutation combined with K-ras activation occurred, mouse oviductal epithelial cells were transformed into tumor cells (142). Zhang et al. (129) found that superparamagnetic iron oxide (SPIO)-serum effectively induced lipid peroxidation and produced large amounts of toxic ROS and promoted the down-regulation of GPX4 and xct, leading to iron-dependent oxidative death. These effects could be reversed using the iron chelator DFO and the lipid peroxidation inhibitor Fer-1. In addition, p53 contributed to promote SPIO-serum–induced ferroptosis in OC cells. Inhibition of PARP downregulates the expression of the cystine transporter protein SLC7A11 in a p53-dependent manner, which, in turn, leads to reduced GSH biosynthesis and promotes lipid peroxidation and ferroptosis (130). SNAI2 inhibits the malignant progression of OC by binding to the promoter region of SLC7A11 and thereby inducing the onset of ferroptosis in OC cells (131). Cai et al. (132) found that ADAMTS9-AS1 can inhibit the malignant progression of OC by regulating the mir-587/SLC7A11 axis to attenuate ferroptosis process in OC and promote proliferation, migration, and invasion of OC cells, leading to malignant progression of OC.

Numerous studies have confirmed that elevated intracellular GSH levels and high expression of related metabolic enzymes are closely associated with drug resistance in OC. Mao et al. (133) found that sodium molybdate induced elevated pools of unstable iron in OC cells and induced GSH depletion by mediating nitric oxide (NO) production and further promoted ferroptosis in OC cells. In addition, NO induces mitochondrial damage through inhibition of mitochondrial aconitase activity, ATP production, and mitochondrial membrane potential, leading to apoptosis in OC cells. Yang et al. (134) found that transcriptional coactivator with PDZ-binding motif (TAZ) removed conferred ferroptosis resistance, whereas overexpression of TAZS89A promoted cellular susceptibility to ferroptosis, and lower TAZ levels were an important reason for reduced ferroptosis susceptibility in chemotherapy-resistant relapsed OC TAZ that can promote OC cell sensitivity to ferroptosis by regulating ANGPTL4 and activating NOX2 entry and exit. Liu et al. (143) established erastin-tolerant cell lines and found that the cell lines could still maintain GSH levels, suggesting the existence of other intracellular pathways for cystine synthesis. The assay revealed

high expression of CBS, a key enzyme of the transsulfuration pathway, suggesting that the erastin-tolerant cell line provides cystine to the cells through the upregulated transsulfuration pathway. Verschoor et al. (144) treated an OC cell model using an Xc-system inhibitor and a transsulfuration pathway inhibitor and found that intracellular GSH levels were significantly reduced after transsulfuration pathway inhibition, suggesting that the transsulfuration. Chakraborty et al. (135) found that the expression level of CBS in the transsulfuration pathway was elevated in a few OC cell lines and that CBS gene silencing inhibited cell migration and invasion of OC cells.

The mechanism of action of platinum drug is based on the generation of intracellular ROS, eventually leading to cellular damage and death. Wang et al. (136) found that platinum-resistant cells and tumors exhibited Frizzled 7 (FZD7) expression and that knockdown of FZD7 increased platinum sensitivity and delayed tumorigenesis. In contrast, overexpression of FZD7 activated the oncogenic factor Tp63, which promoted upregulation of the metabolic pathway, leading to platinum resistance in OC cells. Chen et al. (137) found that erastin induced ferroptosis and increased ROS levels, thereby enhancing the cytotoxic effects of cisplatin. Erastin synergistically with cisplatin significantly inhibited OC cell growth. polypeptide N-acetylgalactosaminyltransferase (GALNT14) promoted mtor by modifying EGFR. The combination of mtor inhibitor and cisplatin resulted in a cumulative effect on cell death (138). Santos et al. (145) speculated that reversal of drug resistance by interfering with cysteine metabolism was suggested by the results of a study suggesting that selenium-containing salicin could contribute to a reduction in GSH levels and that an inhibitory effect on CBS was inhibited. Designing a nanodrug could be a new strategy to improve OC treatment.

The mechanism of ferroptosis-related drugs remained to be investigated, but they may be a new pathway to improve OC treatment through the ferroptosis pathway. Chan et al. (139) reported that MAP30 induces an increase in intracellular Ca^{2+} ion concentration, which triggers ROS-mediated cancer cell death through apoptosis and ferroptosis. Natural MAP30 may be used as a non-toxic supplement to enhance chemotherapy in patients with OC with peritoneal metastases. Sun et al. (140) found that lidocaine could inhibit the ferroptosis process in OC cells by enhancing the expression of mir-382-5p in cells, which, in turn, inhibited the ferroptosis process in OC cells by targeting SLC7A11. Lidocaine treatment inhibited tumor growth of OC *in vivo*.

In addition, many other authors have explored the expression levels of ferroptosis-related genes and proteins in patients with OC and the correlation with patient prognosis by bioinformatics analysis. The results of all analyses are presented in **Table 2**.

Role of necroptosis in OC

In brief, the regulatory role of necroptosis related genes in OC progression was displayed in **Table 3**. Hahne et al. (156) explored the ability of the PI3K/AKT inhibitor AEZS-126 alone and in combination with rapamycin to selectively target OC cell proliferation and survival *in vitro*. They found by validation that AEZS-126 exhibited anti-cytotoxicity in an *in vitro* model of OC and that the primary mechanism was the regulation of the necroptotic apoptotic process in OC cells. Mccabe et al. (157) found that inhibitor of apoptosis protein (IAP) plus cystein inhibitor (IZ) treatment selectively induced TNFα-dependent death in several anti-apoptotic cell lines and patient xenografts.

TABLE 2 Ferroptosis related genes in patients with ovarian cancer.

Related Genes	Diagnostic Potential	Prognostic Potential	Reference
LPCAT3, ACSL3, CRYAB, PTGS2, ALOX12, HSBP1, SLC1A5, SLC7A11, and ZEB1	√	√	(146)
CDKN1B, FAS, FOS, FOXO1, GABARAPL1, HDAC1, NFKB1, PEX3, PPP1R15A, SIRT2, IFNG, IL24, MTMR14, and RB1	×	√	(147)
ALOX12, ACACA, SLC7A11, FTH1, and CD44	×	√	(148)
DNAJB6, RB1, VIMP/SELENOS, STEAP3, BACH1, and ALOX12	√	√	(149)
Staurosporine, epothilone B, DMOG, and HG6-64-1	×	√	(150)
SLC7A11, RB1, GCH1, LPCAT3, PCBP2, ZFP36, STEAP3, MAPK8, GABARAPL1, IFNG, PHKG2, HSPA5, MAP1LC3C, and ALOX5	√	√	(151)
AC138904.1, AP005205.2, AC007114.1, LINC00665, UBXN10-AS1 AC083880.1, LINC01558, and AL023583.1	×	√	(152)
HIC1, LPCAT3, and DUOX1	√	√	(153)
AC007848.1, AC011445.1, AC093895.1, AC010336.5, AL157871.2, AP001033.1, AC009403.1, AC068792.1, LINC01857, LINC00239, and AL513550.1	×	√	(154)
FMR1, HNRNPC, METTL16, METTL3, and METTL5	×	√	(155)

TABLE 3 The regulatory role of necroptosis related genes in ovarian cancer progression.

Target	Mechanism	Function	Reference
AEZS-126	Target PI3K/AKT	Induce necroptosis and reduce platinum resistance	(156)
IAPs	Target TNF-α	Induce necroptosis and promote ovarian cancer	(157)
CD40L	Target caspase-3	Induce necroptosis and promote ovarian cancer	(158)
BMI1	Target PINK1-PARK2	Induce necroptosis and promote ovarian cancer	(159)
Caspase8	Target NF-κB and RIPK1	Suppress necroptosis and inhibit ovarian cancer	(160)
Luteal-phase progesterone	Target TNF-a/RIPK1/RIPK3/MLKL	Suppress necroptosis and inhibit ovarian cancer	(161)
CNL	Target MLKL	Induce necroptosis and promote ovarian cancer	(162)
DEBIO 1143	Target cIAP1, XIAP, and caspase-9	Induce necroptosis and promote ovarian cancer	(163)
ALDH1Ai	/	Induce necroptosis and promote ovarian cancer	(164)
CuS–MnS2	/	Suppress necroptosis and inhibit ovarian cancer	(165)
Berberine	Target Caspase-3, Caspase-8, RIPK3, and MLKL	Induce necroptosis and promote ovarian cancer	(166)
RIP1	Target ROS	Induce necroptosis and promote ovarian cancer	(167)

Qiu et al. (158) found that upregulation of CD40 may be relatively common in low-grade serous carcinomas (lgscs) and that CD40 activation induced RIP1-dependent, necrosis-like cell death in LGSC cells. Dey et al. (159)found that BMI1 in OC was able to participate in the PINK1-PARK2–dependent mitochondrial pathway and induce a novel non-apoptotic, necroptosis-mediated cell death pattern. Necroptosis enhances the phosphorylation of the downstream substrate MLKL by activating the RIPK1-RIPK3 complex. In addition, inhibition of caspase-8 was found to significantly inhibit NF-κB signaling and lead to necrotic cell death by stabilizing RIPK1 expression (160). Blocking NF-κB signaling and depleting cIAP using SMAC mimics could further render these cells susceptible to necroptosis killing. Increasing caspase-8 expression *in vivo* may be an important tool to improve the prognosis of patients with OC.

In addition, studies have shown that targeting necroptosis may also promote prognosis in patients with OC. Wu et al. found that luteal-phase progesterone (P4) binds to P4 receptors (prs) and *via* the TNF-a/RIPK1/RIPK3/MLKL pathway in the oviductal epithelium of Trp53M$^{-/-}$ mice, and immortalized human p53-deficient bacterial hair epithelium induces necrotic apoptosis (161), which may be a potential mechanism for progesterone to prevent OC onset. MLKL may be a novel pro-necrotic apoptotic target of ceramide in OC models, and knockdown of MLKL with small interfering RNA (siRNA) significantly abrogated ceramide nanoliposomes (CNL)–induced cell death (162). As a SMAC (second mitochondria-derived activator of caspase) mimetic, DEBIO 1143 was able to reverse resistance to carboplatin by targeting cIAP1, XIAP, and caspase-9 and inducing apoptosis or necroptosis depending on the cell line. Chefetz et al. (164) identified two selective inhibitors of the ALDH1A family (ALDH1Ai) and found that they preferentially killed CD133^{+} OC stem cell-like cells (CSC). ALDH1Ai induced mitochondrial uncoupling proteins and reduced oxidative phosphorylation to induce necrotizing CSC death. In addition, they found that ALDH1Ai was highly synergistic with chemotherapy, significantly reducing tumor initiation capacity and increasing tumor eradication *in vivo*. Chen et al. (165) found that excellent tumor ablation could be achieved by combining treatment with cus-mns2 nanoflowers and 808-nm NIR laser. Cusmns2 nanoflowers could be used as a promising multifunctional nanotheranostic agent for MRI and as a photothermal/photodynamic cancer therapy agent through necroptosis. Liu et al. (166) found that berberine (BBR) could significantly inhibit the proliferative capacity of OC cells in a dose- and time-dependent manner. Combined treatment with BBR and DDP significantly promoted the proportion of necrotic apoptosis in OC cells and had a significant effect on OC cell proliferation and induction of G0/G1 cell cycle arrest. Combined treatment with BBR and DDP significantly increased OC cell death through induction of apoptosis and necroptosis, thereby enhancing the anticancer effects of chemotherapeutic agents. In addition, both ROS-mediated apoptosis and necroptosis could be involved in cisplatin-induced cell death. Therefore, RIP1 can act as a tumor suppressor that promotes the anticancer effects of chemotherapeutic agents such as cisplatin.

Role of pyroptosis in OC

In brief, the regulatory role of pyroptosis-related genes in OC progression was displayed in **Table 4**. The mechanisms of inflammatory cells in the tumor microenvironment are gradually being understood with the advancement of research. Recent studies have shown that the occurrence and development of OC are closely associated with elevated levels of various inflammatory factors. Qiao et al. (169) found that knockdown of caspase-4 or GSDMD in OC cells significantly inhibited the killing activity of a-NETA cells, suggesting that a-NETA may play a biological role by regulating the cell scorching pathway. Zhang et al. (170) found that nobiletin, a prospective food-derived

TABLE 4 The regulatory role of pyroptosis-related targets in ovarian cancer progression.

Target	Mechanism	Function	Reference
Caspase-4/GSDMD	Target a-NETA	Inhibit pyroptosis and suppress ovarian cancer	(156)
Nobiletin	Target ROS	Induce pyroptosis and suppress ovarian cancer	(157)
Osthole	/	Induce pyroptosis and suppress ovarian cancer	(168)
HOTTIP	Target miR-148a-3/AKT2-ASK1/JNK	Induce pyroptosis and promote ovarian cancer	(159)

phytochemical derived from citrus fruits, could induce apoptosis and trigger ROS-mediated cell scorch death by regulating autophagy in OC cells, thereby inhibiting the malignant progression of OC. Liang et al. (168) found that serpentine, a derivative of coumarin, significantly inhibited OC cell growth and induced OC cell death by regulating OC cell apoptosis, cell scorching, and autophagic processes, with good therapeutic promise. HOXA transcript at the distal tip (HOTTIP) was able to increase AKT2 expression and inhibit ASK1/JNK signaling through negative regulation of mir-148a-3p, which, in turn, led to OC cell proliferation and NLRP1 inflammasome-mediated cell scorching process, resulting in OC malignant progression (171).

In addition, many other authors have explored the expression levels offerroptosis-related genes and proteins in patients with OC and the correlation with patient prognosis by bioinformatics analysis. The results of all analyses are presented in **Table 5**.

Conclusion and prospects

Programmed cell death is a hot issue in biological and medical research, and targeting the cell death process is a common approach in tumor therapy. However, current compounds that induce programmed death are only effective against certain tumor cells, and different types of cancers seem to have different sensitivities to programmed death (177–179). Efforts to understand the sensitivity of different tissue tumors to programmed death are important for the practice of clinical application of programmed death in tumor therapy. Regarding how programmed death is precisely induced *in vivo*, the key regulators of programmed death that have been identified provide important therapeutic targets. Currently, the commonly used anti-tumor drugs in clinical practice have disadvantages such as poor selectivity, toxic side effects, and the tendency to develop drug resistance, which seriously limit their efficacy. According to the characteristics of TCM, studying the effect of TCM and its specific components on programmed tumor death, discovering effective anti-tumor components, and combining multi-disciplinary and multi-disciplinary approaches to target tumor sites by loading programmed death inducers, reactants of programmed death process, or TCM preparations through nanotechnology, so that drug concentrations accumulate at tumor sites, may bring new options for cancer treatment based on programmed death (178, 180, 181). The exploration of Chinese medicine to intervene in programmed death is still in its infancy, but there are already studies, showing extraordinary research prospects by loading Chinese medicine with nanotechnology for tumor treatment (182).

Ferroptosis has become a hot research topic in tumor; the pathway network between iron metabolism, Fenton reaction, Xc-system, and GPX4 has been initially established (183, 184); and other important related pathways (including transsulfur pathway) and ferroptosis-related drugs need to be further investigated. Current chemotherapy regimens for OC are still dominated by platinum and paclitaxel drugs, but the prognosis of patients with advanced OC remains bleak. An in-depth investigation of the link between ferroptosis pathway and OC will facilitate the search for a new chemotherapeutic regimen. Ferroptosis inducers and inhibitors are expected to be used effectively and rationally in the future, thus improving the precision of treatment for OC and other tumors. As a newly discovered mode of programmed cell death, necroptosis is closely related to a variety of case-physiological processes (185, 186), and most of the studies related to necroptosis are at the stage of basic experiments. Necroptosis plays an opposing role in anti-tumor; on the one hand, it can inhibit the proliferation and

TABLE 5 Pyroptosis-related genes in patients with ovarian cancer.

Related genes	Diagnostic potential	Prognostic potential	Reference
CASP3, CASP6, AIM2, PLCG1, ELANE, PJVK and GSDMA	×	√	(172)
GSDMD, GSDMC, GSDME, and PJVK	×	×	(173)
SLC31A2, LYN, CD44, EPB41L3, VSIG4, FCN1, IRF4, and ISG20	×	√	(174)
AC006001.2, LINC02585, AL136162.1, AC005041.3, AL023583.1, and LINC02881	×	√	(175)
DICER1-AS1, MIR600HG, AC083880.1, AC109322.1, AC007991.4, IL6RAS1, AL365361.1, and AC022098.2	√	√	(176)

migration of tumor cells; on the other hand, it can play a pro-tumor growth role and participate in early tumor formation. Further in-depth study on the molecular mechanism of necroptosis pathway and the relationship between upstream and downstream signaling molecules of related signaling pathways, to explore its role in OC in different modes and to find corresponding target drugs, is one of the future directions to improve the therapeutic effect of OC. Cell scorch is a programmed cell death mediated mainly by inflammatory caspases (177). NLRP3 inflammatory vesicles activate caspase-1, which, in turn, causes pro–IL-1β and pro–IL-18 to form mature IL-1β and IL-18 and trigger cellular inflammation (187, 188). At the same time, caspase-1 cleaves the downstream factor abscisicin D. These actions create active pores in the cell membrane and lead to the onset of cellular scorching. The occurrence and development of OC are closely related to the inflammatory response, so the cell scorching caused by inflammatory vesicles/factors may play an important role in OC. A variety of Chinese herbal components and formulations have regulatory effects on cell scorch, and with further research, Chinese medicine may be used to regulate cell scorch in the prevention and treatment of OC.

In conclusion, this article reviews the progress of research on ferroptosis, necroptosis, or pyroptosis in the development of OC and after prognosis and treatment. Nevertheless, the exact roles of ferroptosis, necroptosis, and pyroptosis in OC remain to be fully elucidated. It is important to investigate the molecular mechanisms and physiopathological roles of ferroptosis, necroptosis, and pyroptosis and to specifically design the corresponding drug therapy for OC.

Author contributions

Original draft preparation, allocation, supplementation, and editing: CZ. Revision: NL and CZ. All authors have read and agreed to the published version of the manuscript.

Funding

This work was supported by the internal fund of Shenjing Hospital of China Medical University (Grant No. M0797).

Conflict of interest

The authors declare that the research was conducted in the absence of any commercial or financial relationships that could be construed as a potential conflict of interest.

Publisher's note

References

1. Li H, Yang P, Wang J, Zhang J, Ma Q, Jiang Y, et al. HLF regulates ferroptosis, development and chemoresistance of triple-negative breast cancer by activating tumor cell-macrophage crosstalk. *J Hematol Oncol* (2022) 15:2. doi: 10.1186/s13045-021-01223-x

2. Fillon M. Opportunistic salpingectomy may reduce ovarian cancer risk. *CA Cancer J Clin* (2022) 72:97–9. doi: 10.3322/caac.21716

3. Torre LA, Trabert B, DeSantis CE, Miller KD, Samimi G, Runowicz CD, et al. Ovarian cancer statistics, 2018. *CA Cancer J Clin* (2018) 68:284–96. doi: 10.3322/caac.21456

4. Gardner GJ, Chi DS. Recurrent ovarian cancer - sculpting a promising future with surgery. *N Engl J Med* (2021) 385:2187–8. doi: 10.1056/NEJMe2116353

5. Kosaka M, Mizutani T, Ishiki H. What is the optimal treatment for vulnerable older women with ovarian cancer? *JAMA Oncol* (2021) 7:1725–6. doi: 10.1001/jamaoncol.2021.4125

6. Kurian AW, Abrahamse P, Bondarenko I, Hamilton AS, Deapen D, Gomez SL, et al. Association of genetic testing results with mortality among women with breast cancer or ovarian cancer. *J Natl Cancer Inst* (2022) 114:245–53. doi: 10.1093/jnci/djab151

7. Kuroki L, Guntupalli SR. Treatment of epithelial ovarian cancer. *BMJ* (2020) 371:m3773. doi: 10.1136/bmj.m3773

8. Nameki R, Chang H, Reddy J, Corona RI, Lawrenson K. Transcription factors in epithelial ovarian cancer: histotype-specific drivers and novel therapeutic targets. *Pharmacol Ther* (2021) 220:107722. doi: 10.1016/j.pharmthera.2020.107722

9. Wang Z, Meng F, Zhong Z. Emerging targeted drug delivery strategies toward ovarian cancer. *Adv Drug Delivery Rev* (2021) 178:113969. doi: 10.1016/j.addr.2021.113969

10. Baert T, Ferrero A, Sehouli J, O'Donnell DM, Gonzalez-Martin A, Joly F, et al. The systemic treatment of recurrent ovarian cancer revisited. *Ann Oncol* (2021) 32:710–25. doi: 10.1016/j.annonc.2021.02.015

11. Ledermann JA. Front-line therapy of advanced ovarian cancer: new approaches. *Ann Oncol* (2017) 28:viii46–50. doi: 10.1093/annonc/mdx452

12. Chiappa M, Guffanti F, Bertoni F, Colombo I, Damia G. Overcoming PARPi resistance: Preclinical and clinical evidence in ovarian cancer. *Drug Resist Update* (2021) 55:100744. doi: 10.1016/j.drup.2021.100744

13. Mirza MR, Coleman RL, Gonzalez-Martin A, Moore KN, Colombo N, Ray-Coquard I, et al. The forefront of ovarian cancer therapy: update on PARP inhibitors. *Ann Oncol* (2020) 31:1148–59. doi: 10.1016/j.annonc.2020.06.004

14. Zeng Q, Ma X, Song Y, Chen Q, Jiao Q, Zhou L. Targeting regulated cell death in tumor nanomedicines. *Theranostics* (2022) 12:817–41. doi: 10.7150/thno.67932

15. Tummers B, Green DR. The evolution of regulated cell death pathways in animals and their evasion by pathogens. *Physiol Rev* (2022) 102:411–54. doi: 10.1152/physrev.00002.2021

16. Zamzami N, Hirsch T, Dallaporta B, Petit PX, Kroemer G. Mitochondrial implication in and programmed cell death: apoptosis and necrosis. *J Bioenerg Biomembr* (1997) 29(2):185–93. doi: 10.1023/A:1022694131572

17. Christgen S, Tweedell RE, Kanneganti TD. Programming inflammatory cell death for therapy. *Pharmacol Ther* (2022) 232:108010. doi: 10.1016/j.pharmthera.2021.108010

18. Moujalled D, Strasser A, Liddell JR. Molecular mechanisms of cell death in neurological diseases. *Cell Death Differ* (2021) 28:2029–44. doi: 10.1038/s41418-021-00814-y

19. Dionisio PA, Amaral JD, Rodrigues CMP. Oxidative stress and regulated cell death in parkinson's disease. *Ageing Res Rev* (2021) 67:101263. doi: 10.1016/j.arr.2021.101263

20. Koren E, Fuchs Y. Modes of regulated cell death in cancer. *Cancer Discov* (2021) 11:245–65. doi: 10.1158/2159-8290.CD-20-0789

21. Bertheloot D, Latz E, Franklin BS. Necroptosis, pyroptosis and apoptosis: an intricate game of cell death. *Cell Mol Immunol* (2021) 18:1106–21. doi: 10.1038/s41423-020-00630-3

22. Verdonck S, Nemegeer J, Vandenabeele P, Maelfait J. Viral manipulation of host cell necroptosis and pyroptosis. *Trends Microbiol* (2021) 30:593–605. doi: 10.1016/j.tim.2021.11.011

23. Roberts JZ, Crawford N, Longley DB. The role of ubiquitination in apoptosis and necroptosis. *Cell Death Differ* (2022) 29:272–84. doi: 10.1038/s41418-021-00922-9

24. Yu P, Zhang X, Liu N, Tang L, Peng C, Chen X. Pyroptosis: mechanisms and diseases. *Signal Transduct Target Ther* (2021) 6:128. doi: 10.1038/s41392-021-00507-5

25. Wu D, Wang S, Yu G, Chen X. Cell death mediated by the pyroptosis pathway with the aid of nanotechnology: Prospects for cancer therapy. *Angew Chem Int Ed Engl* (2021) 60:8018–34. doi: 10.1002/anie.202010281

26. Rana N, Privitera G, Kondolf HC, Bulek K, Lechuga S, De Salvo C, et al. GSDMB is increased in IBD and regulates epithelial restitution/repair independent of pyroptosis. *Cell* (2022) 185:283–298.e217. doi: 10.1016/j.cell.2021.12.024

27. Lu Z, Van Eeckhoutte HP, Liu G, Nair PM, Jones B, Gillis CM, et al. Necroptosis signaling promotes inflammation, airway remodeling, and emphysema in chronic obstructive pulmonary disease. *Am J Respir Crit Care Med* (2021) 204:667–81. doi: 10.1164/rccm.202009-3442OC

28. Baik JY, Liu Z, Jiao D, Kwon HJ, Yan J, Kadigamuwa C, et al. ZBP1 not RIPK1 mediates tumor necroptosis in breast cancer. *Nat Commun* (2021) 12:2666. doi: 10.1038/s41467-021-23004-3

29. Tan Y, Sun R, Liu L, Yang D, Xiang Q, Li L, et al. Tumor suppressor DRD2 facilitates M1 macrophages and restricts NF-kappaB signaling to trigger pyroptosis in breast cancer. *Theranostics* (2021) 11:5214–31. doi: 10.7150/thno.58322

30. Chen J, Wei Z, Fu K, Duan Y, Zhang M, Li K, et al. Non-apoptotic cell death in ovarian cancer: Treatment, resistance and prognosis. *BioMed Pharmacother* (2022) 150:112929. doi: 10.1016/j.biopha.2022.112929

31. Liu T, Hou M, Li M, Qiu C, Cheng L, Zhu T, et al. Pyroptosis: A developing foreland of ovarian cancer treatment. *Front Oncol* (2022) 12:828303. doi: 10.3389/fonc.2022.828303

32. Dixon SJ, Lemberg KM, Lamprecht MR, Skouta R, Zaitsev EM, Gleason CE, et al. Ferroptosis: an iron-dependent form of nonapoptotic cell death. *Cell* (2012) 149:1060–72. doi: 10.1016/j.cell.2012.03.042

33. Rodriguez R, Schreiber SL, Conrad M. Persister cancer cells: Iron addiction and vulnerability to ferroptosis. *Mol Cell* (2022) 82:728–40. doi: 10.1016/j.molcel.2021.12.001

34. Yao X, Li W, Fang, Xiao C, Wu X, Li M, et al. Emerging roles of energy metabolism in ferroptosis regulation of tumor cells. *Adv Sci (Weinh)* (2021) 8:e2100997. doi: 10.1002/advs.202100997

35. Ajoolabady A, Aslkhodapasandhokmabad H, Libby P, Tuomilehto J, Lip GYH, Penninger JM, et al. Ferritinophagy and ferroptosis in the management of metabolic diseases. *Trends Endocrinol Metab* (2021) 32:444–62. doi: 10.1016/j.tem.2021.04.010

36. Chen X, Kang R, Kroemer G, Tang D. Ferroptosis in infection, inflammation, and immunity. *J Exp Med* (2021) 218(6):e2021051. doi: 10.1084/jem.20210518

37. Wang ZL, Yuan L, Li W, Li JY. Ferroptosis in parkinson's disease: glia-neuron crosstalk. *Trends Mol Med* (2022) 28:258–69. doi: 10.1016/j.molmed.2022.02.003

38. Chen X, Kang R, Kroemer G, Tang D. Organelle-specific regulation of ferroptosis. *Cell Death Differ* (2021) 28:2843–56. doi: 10.1038/s41418-021-00859-z

39. Ebrahimi N, Adelian S, Shakerian S, Afshinpour M, Chaleshtori SR, Rostami N, et al. Crosstalk between ferroptosis and the epithelial-mesenchymal transition: Implications for inflammation and cancer therapy. *Cytokine Growth Factor Rev* (2022) 64:33–45. doi: 10.1016/j.cytogfr.2022.01.006

40. Yang Z, Shi J, Chen L, Fu C, Shi D, Qu H. Role of pyroptosis and ferroptosis in the progression of atherosclerotic plaques. *Front Cell Dev Biol* (2022) 10:811196. doi: 10.3389/fcell.2022.811196

41. Chen J, Li X, Ge C, Min J, Wang F. The multifaceted role of ferroptosis in liver disease. *Cell Death Differ* (2022) 29:467–80. doi: 10.1038/s41418-022-00941-0

42. Lei G, Zhuang L, Gan B. Targeting ferroptosis as a vulnerability in cancer. *Nat Rev Cancer* (2022) 22:381–96. doi: 10.1038/s41568-022-00459-0

43. Zhang C, Liu X, Jin S, Chen Y, Guo R. Ferroptosis in cancer therapy: a novel approach to reversing drug resistance. *Mol Cancer* (2022) 21:47. doi: 10.1186/s12943-022-01530-y

44. Friedmann Angeli JP, Xavier da Silva TN, Schilling B. CD8(+) T cells PUF(A)ing the flames of cancer ferroptotic cell death. *Cancer Cell* (2022) 40:346–8. doi: 10.1016/j.ccell.2022.03.003

45. Shui S, Zhao Z, Wang H, Conrad M, Liu G. Non-enzymatic lipid peroxidation initiated by photodynamic therapy drives a distinct ferroptosis-like cell death pathway. *Redox Biol* (2021) 45:102056. doi: 10.1016/j.redox.2021.102056

46. Saito Y. Lipid peroxidation products as a mediator of toxicity and adaptive response - the regulatory role of selenoprotein and vitamin e. *Arch Biochem Biophys* (2021) 703:108840. doi: 10.1016/j.abb.2021.108840

47. Foret MK, Lincoln R, Do Carmo S, Cuello AC, Cosa G. Connecting the "Dots": From free radical lipid autoxidation to cell pathology and disease. *Chem Rev* (2020) 120:12757–87. doi: 10.1021/acs.chemrev.0c00761

48. Stoyanovsky DA, Tyurina YY, Shrivastava I, Bahar I, Tyurin VA, Protchenko O, et al. Iron catalysis of lipid peroxidation in ferroptosis: Regulated enzymatic or random free radical reaction? *Free Radic Biol Med* (2019) 133:153–61. doi: 10.1016/j.freeradbiomed.2018.09.008

49. Li Y, Yang J, Gu G, Guo X, He C, Sun J, et al. Pulmonary delivery of theranostic nanoclusters for lung cancer ferroptosis with enhanced Chemodynamic/Radiation synergistic therapy. *Nano Lett* (2022) 22:963–72. doi: 10.1021/acs.nanolett.1c03786

50. Lu S, Wang XZ, He C, Wang L, Liang SP, Wang CC, et al. ATF3 contributes to brucine-triggered glioma cell ferroptosis *via* promotion of hydrogen peroxide and iron. *Acta Pharmacol Sin* (2021) 42:1690–702. doi: 10.1038/s41401-021-00700-w

51. Feng Z, Qin Y, Huo F, Jian Z, Li X, Geng J, et al. NMN recruits GSH to enhance GPX4-mediated ferroptosis defense in UV irradiation induced skin injury. *Biochim Biophys Acta Mol Basis Dis* (2022) 1868:166287. doi: 10.1016/j.bbadis.2021.166287

52. Zhu ZY, Liu YD, Gong Y, Jin W, Topchiy E, Turdi S, et al. Mitochondrial aldehyde dehydrogenase (ALDH2) rescues cardiac contractile dysfunction in an APP/PS1 murine model of alzheimer's disease *via* inhibition of ACSL4-dependent ferroptosis. *Acta Pharmacol Sin* (2022) 43:39–49. doi: 10.1038/s41401-021-00635-2

53. Alvarez SW, Sviderskiy VO, Terzi EM, Papagiannakopoulos T, Moreira AL, Adams S, et al. NFS1 undergoes positive selection in lung tumours and protects cells from ferroptosis. *Nature* (2017) 551:639–43. doi: 10.1038/nature24637

54. Wei XB, Jiang WQ, Zeng JH, Huang LQ, Ding HG, Jing YW, et al. Exosome-derived lncRNA NEAT1 exacerbates sepsis-associated encephalopathy by promoting ferroptosis through regulating miR-9-5p/TFRC and GOT1 axis. *Mol Neurobiol* (2022) 59:1954–69. doi: 10.1007/s12035-022-02738-1

55. Zhang R, Pan T, Xiang Y, Zhang M, Xie H, Liang Z, et al. Curcumenol triggered ferroptosis in lung cancer cells *via* lncRNA H19/miR-19b-3p/FTH1 axis. *Bioact Mater* (2022) 13:23–36. doi: 10.1016/j.bioactmat.2021.11.013

56. Shi H, Hou B, Li H, Zhou H, Du B. Cyclophosphamide induces the ferroptosis of tumor cells through heme oxygenase-1. *Front Pharmacol* (2022) 13:839464. doi: 10.3389/fphar.2022.839464

57. Yang S, Ouyang J, Lu Y, Harypursat V, Chen Y. A dual role of heme oxygenase-1 in tuberculosis. *Front Immunol* (2022) 13:842858. doi: 10.3389/fimmu.2022.842858

58. Yang Y, Lin Y, Wang M, Yuan K, Wang Q, Mu P, et al. Targeting ferroptosis suppresses osteocyte glucolipotoxicity and alleviates diabetic osteoporosis. *Bone Res* (2022) 10:26. doi: 10.1038/s41413-022-00198-w

59. He J, Li Z, Xia P, Shi A, FuChen X, Zhang J, et al. Ferroptosis and ferritinophagy in diabetes complications. *Mol Metab* (2022) 60:101470. doi: 10.1016/j.molmet.2022.101470

60. Santana-Codina N, Gikandi A, Mancias JD. The role of NCOA4-mediated ferritinophagy in ferroptosis. *Adv Exp Med Biol* (2021) 1301:41–57. doi: 10.1007/978-3-030-62026-4_4

61. Liu B, Li X, Wang D, Yu Y, Lu D, Chen L, et al. CEMIP promotes extracellular matrix-detached prostate cancer cells survival by inhibiting ferroptosis. *Cancer Sci* (2022) 113:2056–70. doi: 10.1111/cas.15356

62. Wu X, Qin K, Iroegbu CD, Xiang K, Peng J, Guo J, et al. Genetic analysis of potential biomarkers and therapeutic targets in ferroptosis from coronary artery disease. *J Cell Mol Med* (2022) 26:2177–90. doi: 10.1111/jcmm.17239

63. Zhou Y, Lin W, Rao T, Zheng J, Zhang T, Zhang M, et al. Ferroptosis and its potential role in the nervous system diseases. *J Inflammation Res* (2022) 15:1555–74. doi: 10.2147/JIR.S351799

64. Homma T, Kobayashi S, Conrad M, Konno H, Yokoyama C, Fujii J. Nitric oxide protects against ferroptosis by aborting the lipid peroxidation chain reaction. *Nitric Oxide* (2021) 115:34–43. doi: 10.1016/j.niox.2021.07.003

65. Huang C, Zhan L. Network pharmacology identifies therapeutic targets and the mechanisms of glutathione action in ferroptosis occurring in oral cancer. *Front Pharmacol* (2022) 13:851540. doi: 10.3389/fphar.2022.851540

66. Li Q, Su R, Bao X, Cao K, Du Y, Wang N, et al. Glycyrrhetinic acid nanoparticles combined with ferrotherapy for improved cancer immunotherapy. *Acta Biomater* (2022) 144:109–20. doi: 10.1016/j.actbio.2022.03.030

67. Pallotti F, Bergamini C, Lamperti C, Fato R. The roles of coenzyme q in disease: Direct and indirect involvement in cellular functions. *Int J Mol Sci* (2021) 23:128. doi: 10.3390/ijms23010128

68. Gan B. Mitochondrial regulation of ferroptosis. *J Cell Biol* (2021) 220(9): e202105043. doi: 10.1083/jcb.202105043

69. Yan J, Wan P, Choksi S, Liu ZG. Necroptosis and tumor progression. *Trends Cancer* (2022) 8:21–7. doi: 10.1016/j.trecan.2021.09.003

70. Wang B, Cui Y, Zhang Q, Wang S, Xu S. Selenomethionine alleviates LPS-induced JNK/NLRP3 inflammasome-dependent necroptosis by modulating miR-15a and oxidative stress in chicken lungs. *Metallomics* (2021) 13(8):mfab048. doi: 10.1093/mtomcs/mfab048

71. Wang Y, Kanneganti TD. From pyroptosis, apoptosis and necroptosis to PANoptosis: A mechanistic compendium of programmed cell death pathways. *Comput Struct Biotechnol J* (2021) 19:4641–57. doi: 10.1016/j.csbj.2021.07.038

72. Teh CE, Preston SP, Robbins AK, Stutz MD, Cooney J, Clark MP, et al. Caspase-8 has dual roles in regulatory T cell homeostasis balancing immunity to infection and collateral inflammatory damage. *Sci Immunol* (2022) 7:eabn8041. doi: 10.1126/sciimmunol.abn8041

73. Li X, Li F, Zhang X, Zhang H, Zhao Q, Li M, et al. Caspase-8 auto-cleavage regulates programmed cell death and collaborates with RIPK3/MLKL to prevent lymphopenia. *Cell Death Differ* (2022). doi: 10.1038/s41418-022-00938-9

74. Yin H, Guo X, Chen Y, Zeng Y, Mo X, Hong S, et al. TAB2 deficiency induces dilated cardiomyopathy by promoting RIPK1-dependent apoptosis and necroptosis. *J Clin Invest* (2022) 132(4):e152297. doi: 10.1172/JCI152297

75. Rosenbaum DM, Degterev A, David J, Rosenbaum PS, Roth S, Grotta JC, et al. Necroptosis, a novel form of caspase-independent cell death, contributes to neuronal damage in a retinal ischemia-reperfusion injury model. *J Neurosci Res* (2010) 88:1569–76. doi: 10.1002/jnr.22314

76. Zhang R, Kang R, Tang D. The STING1 network regulates autophagy and cell death. *Signal Transduct Target Ther* (2021) 6:208. doi: 10.1038/s41392-021-00613-4

77. Meng Y, Sandow JJ, Czabotar PE, Murphy JM. The regulation of necroptosis by post-translational modifications. *Cell Death Differ* (2021) 28:861–83. doi: 10.1038/s41418-020-00722-7

78. Nicole L, Sanavia T, Cappellesso R, Maffeis V, Akiba J, Kawahara A, et al. Necroptosis-driving genes RIPK1, RIPK3 and MLKL-p are associated with intratumoral CD3(+) and CD8(+) T cell density and predict prognosis in hepatocellular carcinoma. *J Immunother Cancer* (2022) 10(3):e004031. doi: 10.1136/jitc-2021-004031

79. Mohanty S, Yadav P, Lakshminarayanan H, Sharma P, Vivekanandhan A, Karunagaran D. RETRA induces necroptosis in cervical cancer cells through RIPK1, RIPK3, MLKL and increased ROS production. *Eur J Pharmacol* (2022) 920:174840. doi: 10.1016/j.ejphar.2022.174840

80. Xu D, Zou C, Yuan J. Genetic regulation of RIPK1 and necroptosis. *Annu Rev Genet* (2021) 55:235–63. doi: 10.1146/annurev-genet-071719-022748

81. Peng T, Tao X, Xia Z, Hu S, Xue J, Zhu Q, et al. Pathogen hijacks programmed cell death signaling by arginine ADPR-deacylization of caspases. *Mol Cell* (2022) 82:1806–20.e8. doi: 10.1016/j.molcel.2022.03.010

82. Woznicki JA, Saini N, Flood P, Rajaram S, Lee CM, Stamou P, et al. TNF-alpha synergises with IFN-gamma to induce caspase-8-JAK1/2-STAT1-dependent death of intestinal epithelial cells. *Cell Death Dis* (2021) 12:864. doi: 10.1038/s41419-021-04151-3

83. Karlowitz R, van Wijk SJL. Surviving death: emerging concepts of RIPK3 and MLKL ubiquitination in the regulation of necroptosis. *FEBS J* (2021). doi: 10.1111/febs.16255

84. Sethi A, Horne CR, Fitzgibbon C, Wilde K, Davies KA, Garnish SE, et al. Membrane permeabilization is mediated by distinct epitopes in mouse and human orthologs of the necroptosis effector, MLKL. *Cell Death Differ* (2022). doi: 10.1038/s41418-022-00965-6

85. Martens S, Bridelance J, Roelandt R, Vandenabeele P, Takahashi N. MLKL in cancer: more than a necroptosis regulator. *Cell Death Differ* (2021) 28:1757–72. doi: 10.1038/s41418-021-00785-0

86. Shlomovitz I, Erlich Z, Arad G, Edry-Botzer L, Zargarian S, Cohen H, et al. Proteomic analysis of necroptotic extracellular vesicles. *Cell Death Dis* (2021) 12:1059. doi: 10.1038/s41419-021-04317-z

87. Yu Z, Jiang N, Su W, Zhuo Y. Necroptosis: A novel pathway in neuroinflammation. *Front Pharmacol* (2021) 12:701564. doi: 10.3389/fphar.2021.701564

88. Liu L, Li H, Hu D, Wang Y, Shao W, Zhong J, et al. Insights into N6-methyladenosine and programmed cell death in cancer. *Mol Cancer* (2022) 21:32. doi: 10.1186/s12943-022-01508-w

89. Bauernfried S, Hornung V. Human NLRP1: From the shadows to center stage. *J Exp Med* (2022) 219(1):e20211405. doi: 10.1084/jem.20211405

90. Hou J, Hsu JM, Hung MC. Molecular mechanisms and functions of pyroptosis in inflammation and antitumor immunity. *Mol Cell* (2021) 81:4579–90. doi: 10.1016/j.molcel.2021.09.003

91. Zychlinsky A, Prevost MC, Sansonetti PJ. Shigella flexneri induces apoptosis in infected macrophages. *Nature* (1992) 358:167–9. doi: 10.1038/358167a0

92. Cookson BT, Brennan MA. Pro-inflammatory programmed cell death. *Trends Microbiol* (2001) 9:113–4. doi: 10.1016/S0966-842X(00)01936-3

93. Shi J, Zhao Y, Wang Y, Gao W, Ding J, Li P, et al. Inflammatory caspases are innate immune receptors for intracellular LPS. *Nature* (2014) 514:187–92. doi: 10.1038/nature13683

94. Shi J, Zhao Y, Wang K, Shi X, Wang Y, Huang H, et al. Cleavage of GSDMD by inflammatory caspases determines pyroptotic cell death. *Nature* (2015) 526:660–5. doi: 10.1038/nature15514

95. Diaz-Garcia E, Garcia-Tovar S, Alfaro E, Jaureguizar A, Casitas R, Sanchez-Sanchez B, et al. Inflammasome activation: A keystone of proinflammatory response in obstructive sleep apnea. *Am J Respir Crit Care Med* (2022) 205:1337–48. doi: 10.1164/rccm.202106-1445OC

96. Hsu CG, Chavez CL, Zhang C, Sowden M, Yan C, Berk BC. The lipid peroxidation product 4-hydroxynonenal inhibits NLRP3 inflammasome activation and macrophage pyroptosis. *Cell Death Differ* (2022). doi: 10.1038/s41418-022-00966-5

97. Xu T, Yu W, Fang H, Wang Z, Chi Z, Guo X, et al. Ubiquitination of NLRP3 by gp78/Insig-1 restrains NLRP3 inflammasome activation. *Cell Death Differ* (2022). doi: 10.1038/s41418-022-00947-8

98. Ross C, Chan AH, Pein JBv, Maddugoda MP, Boucher D, Schroder K. Inflammatory caspases: Toward a unified model for caspase activation by inflammasomes. *Annu Rev Immunol* (2022) 40:249–69. doi: 10.1146/annurev-immunol-101220-030653

99. Camilli G, Bohm M, Piffer AC, Lavenir R, Williams DL, Neven B, et al. Beta-glucan-induced reprogramming of human macrophages inhibits NLRP3 inflammasome activation in cryopyrinopathies. *J Clin Invest* (2020) 130:4561–73. doi: 10.1172/JCI134778

100. Lee S, Ishitsuka A, Noguchi M, Hirohama M, Fujiyasu Y, Petric PP, et al. Influenza restriction factor MxA functions as inflammasome sensor in the respiratory epithelium. *Sci Immunol* (2019) 4(40):eaau4643. doi: 10.1126/sciimmunol.aau4643

101. Stancu IC, Cremers N, Vanrusselt H, Couturier J, Vanoosthuyse A, Kessels S, et al. Aggregated tau activates NLRP3-ASC inflammasome exacerbating exogenously seeded and non-exogenously seeded tau pathology *in vivo*. *Acta Neuropathol* (2019) 137:599–617. doi: 10.1007/s00401-018-01957-y

102. Zhang P, Liu Y, Hu L, Huang K, Hong M, Wang Y, et al. NLRC4 inflammasome-dependent cell death occurs by a complementary series of three death pathways and determines lethality in mice. *Sci Adv* (2021) 7:eabi9471. doi: 10.1126/sciadv.abi9471

103. Wu J, Raman A, Coffey NJ, Sheng X, Wahba J, Seasock MJ, et al. The key role of NLRP3 and STING in APOL1-associated podocytopathy. *J Clin Invest* (2021) 131(20):e136329. doi: 10.1172/JCI136329

104. Ding B, Sheng J, Zheng P, Li C, Li D, Cheng Z, et al. Biodegradable upconversion nanoparticles induce pyroptosis for cancer immunotherapy. *Nano Lett* (2021) 21:8281–9. doi: 10.1021/acs.nanolett.1c02790

105. de Carvalho Ribeiro M, Szabo G. Role of the inflammasome in liver disease. *Annu Rev Pathol* (2022) 17:345–65. doi: 10.1146/annurev-pathmechdis-032521-102529

106. Shao S, Chen C, Shi G, Zhou Y, Wei Y, Fan N, et al. Therapeutic potential of the target on NLRP3 inflammasome in multiple sclerosis. *Pharmacol Ther* (2021) 227:107880. doi: 10.1016/j.pharmthera.2021.107880

107. Liu J, Du S, Kong Q, Zhang X, Jiang S, Cao X, et al. HSPA12A attenuates lipopolysaccharide-induced liver injury through inhibiting caspase-11-mediated hepatocyte pyroptosis *via* PGC-1alpha-dependent acyloxyacyl hydrolase expression. *Cell Death Differ* (2020) 27:2651–67. doi: 10.1038/s41418-020-0536-x

108. Lee BL, Stowe IB, Gupta A, Kornfeld OS, Roose-Girma M, Anderson K, et al. Caspase-11 auto-proteolysis is crucial for noncanonical inflammasome activation. *J Exp Med* (2018) 215:2279–88. doi: 10.1084/jem.20180589

109. Gao W, Li Y, Liu X, Wang S, Mei P, Chen Z, et al. TRIM21 regulates pyroptotic cell death by promoting gasdermin d oligomerization. *Cell Death Differ* (2022) 29:439–50. doi: 10.1038/s41418-021-00867-z

110. Petrovski G, Ayna G, Majai G, Hodrea J, Benko S, Madi A, et al. Phagocytosis of cells dying through autophagy induces inflammasome activation

and IL-1beta release in human macrophages. *Autophagy* (2011) 7:321–30. doi: 10.4161/auto.7.3.14583

111. Moujalled D, Southon AG, Saleh E, Brinkmann K, Ke F, Iliopoulos M, et al. BH3 mimetic drugs cooperate with temozolomide, JQ1 and inducers of ferroptosis in killing glioblastoma multiforme cells. *Cell Death Differ* (2022). doi: 10.1038/s41418-022-00977-2

112. Li K, Lin C, Li M, Xu K, He Y, Mao Y, et al. Multienzyme-like reactivity cooperatively impairs glutathione peroxidase 4 and ferroptosis suppressor protein 1 pathways in triple-negative breast cancer for sensitized ferroptosis therapy. *ACS Nano* (2022) 16:2381–98. doi: 10.1021/acsnano.1c08664

113. Chen Y, Li L, Lan J, Cui Y, Rao X, Zhao J, et al. CRISPR screens uncover protective effect of PSTK as a regulator of chemotherapy-induced ferroptosis in hepatocellular carcinoma. *Mol Cancer* (2022) 21:11. doi: 10.1186/s12943-021-01466-9

114. Bolik J, Krause F, Stevanovic M, Gandrass M, Thomsen I, Schacht SS, et al. Inhibition of ADAM17 impairs endothelial cell necroptosis and blocks metastasis. *J Exp Med* (2022) 219(1):e20201039. doi: 10.1084/jem.20201039

115. Tan Y, Sementino E, Cheung M, Peri S, Menges CW, Kukuyan AM, et al. Somatic epigenetic silencing of RIPK3 inactivates necroptosis and contributes to chemoresistance in malignant mesothelioma. *Clin Cancer Res* (2021) 27:1200–13. doi: 10.1158/1078-0432.CCR-18-3683

116. Xie Y, Zhao Y, Shi L, Li W, Chen K, Li M, et al. Gut epithelial TSC1/mTOR controls RIPK3-dependent necroptosis in intestinal inflammation and cancer. *J Clin Invest* (2020) 130:2111–28. doi: 10.1172/JCI133264

117. Tang Q, Li W, Zheng X, Ren L, Liu J, Li S, et al. MELK is an oncogenic kinase essential for metastasis, mitotic progression, and programmed death in lung carcinoma. *Signal Transduct Target Ther* (2020) 5:279. doi: 10.1038/s41392-020-00288-3

118. Tan G, Huang C, Chen J, Zhi F. HMGB1 released from GSDME-mediated pyroptotic epithelial cells participates in the tumorigenesis of colitis-associated colorectal cancer through the ERK1/2 pathway. *J Hematol Oncol* (2020) 13:149. doi: 10.1186/s13045-020-00985-0

119. Zhang T, Wu DM, Luo PW, Liu T, Han R, Deng SH, et al. CircNEIL3 mediates pyroptosis to influence lung adenocarcinoma radiotherapy by upregulating PIF1 through miR-1184 inhibition. *Cell Death Dis* (2022) 13:167. doi: 10.1038/s41419-022-04561-x

120. Banoth B, Tuladhar S, Karki R, Sharma BR, Briard B, Kesavardhana S, et al. ZBP1 promotes fungi-induced inflammasome activation and pyroptosis, apoptosis, and necroptosis (PANoptosis). *J Biol Chem* (2020) 295:18276–83. doi: 10.1074/jbc.RA120.015924

121. Shi CS, Kehrl JH. Bcl-2 regulates pyroptosis and necroptosis by targeting BH3-like domains in GSDMD and MLKL. *Cell Death Discovery* (2019) 5:151. doi: 10.1038/s41420-019-0230-2

122. Fritsch M, Gunther SD, Schwarzer R, Albert MC, Schorn F, Werthenbach JP, et al. Caspase-8 is the molecular switch for apoptosis, necroptosis and pyroptosis. *Nature* (2019) 575:683–7. doi: 10.1038/s41586-019-1770-6

123. Zhou B, Zhang JY, Liu XS, Chen HZ, Ai YL, Cheng K, et al. Tom20 senses iron-activated ROS signaling to promote melanoma cell pyroptosis. *Cell Res* (2018) 28:1171–85. doi: 10.1038/s41422-018-0090-y

124. Wang J, Deng B, Liu Q, Huang Y, Chen W, Li J, et al. Pyroptosis and ferroptosis induced by mixed lineage kinase 3 (MLK3) signaling in cardiomyocytes are essential for myocardial fibrosis in response to pressure overload. *Cell Death Dis* (2020) 11:574. doi: 10.1038/s41419-020-02777-3

125. Liu Y, Chen Q, Zhu Y, Wang T, Ye L, Han L, et al. Non-coding RNAs in necroptosis, pyroptosis and ferroptosis in cancer metastasis. *Cell Death Discovery* (2021) 7(1):210. doi: 10.1038/s41420-021-00596-9

126. Li D, Zhang M, Chao H. Significance of glutathione peroxidase 4 and intracellular iron level in ovarian cancer cells-"utilization" of ferroptosis mechanism. *Inflammation Res* (2021) 70:1177–89. doi: 10.1007/s00011-021-01495-6

127. Tesfay L, Paul BT, Konstorum A, Deng Z, Cox AO, Lee J, et al. Stearoyl-CoA desaturase 1 protects ovarian cancer cells from ferroptotic cell death. *Cancer Res* (2019) 79:5355–66. doi: 10.1158/0008-5472.CAN-19-0369

128. Ma LL, Liang L, Zhou D, Wang SW. Tumor suppressor miR-424-5p abrogates ferroptosis in ovarian cancer through targeting ACSL4. *Neoplasma* (2021) 68:165–73. doi: 10.4149/neo_2020_200707N705

129. Zhang Y, Xia M, Zhou Z, Hu X, Wang J, Zhang M, et al. p53 promoted ferroptosis in ovarian cancer cells treated with human serum incubated-superparamagnetic iron oxides. *Int J Nanomed* (2021) 16:283–96. doi: 10.2147/IJN.S282489

130. Hong T, Lei G, Chen X, Li H, Zhang X, Wu N, et al. PARP inhibition promotes ferroptosis *via* repressing SLC7A11 and synergizes with ferroptosis inducers in BRCA-proficient ovarian cancer. *Redox Biol* (2021) 42:101928. doi: 10.1016/j.redox.2021.101928

131. Jin Y, Chen L, Li L, Huang G, Huang H, Tang C. SNAI2 promotes the development of ovarian cancer through regulating ferroptosis. *Bioengineered* (2022) 13:6451–63. doi: 10.1080/21655979.2021.2024319

132. Cai L, Hu X, Ye L, Bai P, Jie Y, Shu K. Long non-coding RNA ADAMTS9-AS1 attenuates ferroptosis by targeting microRNA-587/solute carrier family 7 member 11 axis in epithelial ovarian cancer. *Bioengineered* (2022) 13:8226–39. doi: 10.1080/21655979.2022.2049470

133. Mao G, Xin D, Wang Q, Lai D. Sodium molybdate inhibits the growth of ovarian cancer cells *via* inducing both ferroptosis and apoptosis. *Free Radic Biol Med* (2022) 182:79–92. doi: 10.1016/j.freeradbiomed.2022.02.023

134. Yang WH, Huang Z, Wu J, Ding CC, Murphy SK, Chi JT. A TAZ-ANGPTL4-NOX2 axis regulates ferroptotic cell death and chemoresistance in epithelial ovarian cancer. *Mol Cancer Res* (2020) 18:79–90. doi: 10.1158/1541-7786.MCR-19-0691

135. Chakraborty PK, Xiong X, Mustafi SB, Saha S, Dhanasekaran D, Mandal NA, et al. Role of cystathionine beta synthase in lipid metabolism in ovarian cancer. *Oncotarget* (2015) 6:37367–84. doi: 10.18632/oncotarget.5424

136. Wang Y, Zhao G, Condello S, Huang H, Cardenas H, Tanner EJ, et al. Frizzled-7 identifies platinum-tolerant ovarian cancer cells susceptible to ferroptosis. *Cancer Res* (2021) 81:384–99. doi: 10.1158/0008-5472.CAN-20-1488

137. Cheng Q, Bao L, Li M, Chang K, Yi X. Erastin synergizes with cisplatin *via* ferroptosis to inhibit ovarian cancer growth *in vitro* and in vivo. *J Obstet Gynaecol Res* (2021) 47:2481–91. doi: 10.1111/jog.14779

138. Li HW, Liu MB, Jiang X, Song T, Feng SX, Wu JY, et al. GALNT14 regulates ferroptosis and apoptosis of ovarian cancer through the EGFR/mTOR pathway. *Future Oncol* (2022) 18:149–61. doi: 10.2217/fon-2021-0883

139. Chan DW, Yung MM, Chan YS, Xuan Y, Yang H, Xu D, et al. MAP30 protein from momordica charantia is therapeutic and has synergic activity with cisplatin against ovarian cancer *in vivo* by altering metabolism and inducing ferroptosis. *Pharmacol Res* (2020) 161:105157. doi: 10.1016/j.phrs.2020.105157

140. Sun D, Li YC, Zhang XY. Lidocaine promoted ferroptosis by targeting miR-382-5p /SLC7A11 axis in ovarian and breast cancer. *Front Pharmacol* (2021) 12:681223. doi: 10.3389/fphar.2021.681223

141. Basuli D, Tesfay L, Deng Z, Paul B, Yamamoto Y, Ning G, et al. Iron addiction: a novel therapeutic target in ovarian cancer. *Oncogene* (2017) 36:4089–99. doi: 10.1038/onc.2017.11

142. Quartuccio SM, Karthikeyan S, Eddie SL, Lantvit DD , Ó hAinmhire E, Modi DA, et al. Mutant p53 expression in fallopian tube epithelium drives cell migration. *Int J Cancer* (2015) 137:1528–38. doi: 10.1002/ijc.29528

143. Liu N, Lin X, Huang C. Activation of the reverse transsulfuration pathway through NRF2/CBS confers erastin-induced ferroptosis resistance. *Br J Cancer* (2020) 122:279–92. doi: 10.1038/s41416-019-0660-x

144. Verschoor ML, Singh G. Ets-1 regulates intracellular glutathione levels: key target for resistant ovarian cancer. *Mol Cancer* (2013) 12:138. doi: 10.1186/1476-4598-12-138

145. Santos I, Ramos C, Mendes C, Sequeira CO, Tome CS, Fernandes DGH, et al. Targeting glutathione and cystathionine beta-synthase in ovarian cancer treatment by selenium-chrysin polyurea dendrimer nanoformulation. *Nutrients* (2019) 11:2523. doi: 10.3390/11102523.

146. Yang L, Tian S, Chen Y, Miao C, Zhao Y , Wang R, et al. Ferroptosis-related gene model to predict overall survival of ovarian carcinoma. *J Oncol* (2021) 2021:6687391. doi: 10.1155/2021/6687391

147. Zhang J, Xi J, Huang P, Zeng S. Comprehensive analysis identifies potential ferroptosis-associated mRNA therapeutic targets in ovarian cancer. *Front Med (Lausanne)* (2021) 8:644053. doi: 10.3389/fmed.2021.644053

148. Ye Y, Dai Q, Li S, He J, Qi H. A novel defined risk signature of the ferroptosis-related genes for predicting the prognosis of ovarian cancer. *Front Mol Biosci* (2021) 8:645845. doi: 10.3389/fmolb.2021.645845

149. Yu Z, He H, Chen Y, Ji Q, Sun M. A novel ferroptosis related gene signature is associated with prognosis in patients with ovarian serous cystadenocarcinoma. *Sci Rep* (2021) 11:11486. doi: 10.1038/s41598-021-90126-5

150. You Y, Fan Q, Huang J, Wu Y, Lin H, Zhang Q. Ferroptosis-related gene signature promotes ovarian cancer by influencing immune infiltration and invasion. *J Oncol* (2021) 2021:9915312. doi: 10.1155/2021/9915312

151. Li XX, Xiong L, Wen Y, Zhang ZJ. Comprehensive analysis of the tumor microenvironment and ferroptosis-related genes predict prognosis with ovarian cancer. *Front Genet* (2021) 12:774400. doi: 10.3389/fgene.2021.774400

152. Feng S, Yin H, Zhang K, Shan M, Ji X, Luo S, et al. Integrated clinical characteristics and omics analysis identifies a ferroptosis and iron-metabolism-related lncRNA signature for predicting prognosis and therapeutic responses in ovarian cancer. *J Ovarian Res* (2022) 15:10. doi: 10.1186/s13048-022-00944-y

153. Wang H, Cheng Q, Chang K, Bao L, Yi X. Integrated analysis of ferroptosis-related biomarker signatures to improve the diagnosis and prognosis prediction of ovarian cancer. *Front Cell Dev Biol* (2021) 9:807862. doi: 10.3389/fcell.2021.807862

154. Peng J, Hao Y, Rao B, Zhang Z. A ferroptosis-related lncRNA signature predicts prognosis in ovarian cancer patients. *Transl Cancer Res* (2021) 10:4802–16. doi: 10.21037/tcr-21-1152

155. Zheng J, Guo J, Wang Y, Zheng Y, Zhang K, Tong J. Bioinformatic analyses of the ferroptosis-related lncRNAs signature for ovarian cancer. *Front Mol Biosci* (2021) 8:735871. doi: 10.3389/fmolb.2021.735871

156. Hahne JC, Kurz A, Meyer SR, Dietl J, Engel JB, Honig A. Anti-tumour activity of phosphoinositide-3-kinase antagonist AEZS-126 in models of ovarian cancer. *Arch Gynecol Obstet* (2015) 291:131–41. doi: 10.1007/s00404-014-3389-z

157. McCabe KE, Bacos K, Lu D, Delaney JR, Axelrod J, Potter MD, et al. Triggering necroptosis in cisplatin and IAP antagonist-resistant ovarian carcinoma. *Cell Death Dis* (2014) 5:e1496. doi: 10.1038/cddis.2014.448

158. Qiu X, Klausen C, Cheng JC, Leung PC. CD40 ligand induces RIP1-dependent, necroptosis-like cell death in low-grade serous but not serous borderline ovarian tumor cells. *Cell Death Dis* (2015) 6:e1864. doi: 10.1038/cddis.2015.229

159. Dey A, Mustafi SB, Saha S, Kumar Dhar Dwivedi S, Mukherjee P, Bhattacharya R. Inhibition of BMI1 induces autophagy-mediated necroptosis. *Autophagy* (2016) 12:659–70. doi: 10.1080/15548627.2016.1147670

160. Hernandez L, Kim MK, Noonan AM, Sagher E, Kohlhammer H, Wright G, et al. A dual role for Caspase8 and NF-kappaB interactions in regulating apoptosis and necroptosis of ovarian cancer, with correlation to patient survival. *Cell Death Discov* (2015) 1:15053. doi: 10.1038/cddiscovery.2015.53

161. Wu NY, Huang HS, Chao TH, Chou HM, Fang C, Qin CZ, et al. Progesterone prevents high-grade serous ovarian cancer by inducing necroptosis of p53-defective fallopian tube epithelial cells. *Cell Rep* (2017) 18:2557–65. doi: 10.1016/j.celrep.2017.02.049

162. Zhang X, Kitatani K, Toyoshima M, Ishibashi M, Usui T, Minato J, et al. Ceramide nanoliposomes as a MLKL-dependent, necroptosis-inducing, chemotherapeutic reagent in ovarian cancer. *Mol Cancer Ther* (2018) 17:50–9. doi: 10.1158/1535-7163.MCT-17-0173

163. Thibault B, Genre L, Le Naour A, Broca C, Mery E, Vuagniaux G, et al. DEBIO 1143, an IAP inhibitor, reverses carboplatin resistance in ovarian cancer cells and triggers apoptotic or necroptotic cell death. *Sci Rep* (2018) 8:17862. doi: 10.1038/s41598-018-35860-z

164. Chefetz I, Grimley E, Yang K, Hong L, Vinogradova EV, Suciu R, et al. A pan-ALDH1A inhibitor induces necroptosis in ovarian cancer stem-like cells. *Cell Rep* (2019) 26:3061–3075.e3066. doi: 10.1016/j.celrep.2019.02.032

165. Chen W, Wang X, Zhao B, Zhang R, Xie Z, He Y, et al. CuS-MnS2 nanoflowers for magnetic resonance imaging guided photothermal/photodynamic therapy of ovarian cancer through necroptosis. *Nanoscale* (2019) 11:12983–9. doi: 10.1039/C9NR03114F

166. Liu L, Fan J, Ai G, Liu J, Luo N, Li C, et al. Berberine in combination with cisplatin induces necroptosis and apoptosis in ovarian cancer cells. *Biol Res* (2019) 52:37. doi: 10.1186/s40659-019-0243-6

167. Zheng XL, Yang JJ, Wang YY, Li Q, Song YP, Su M, et al. RIP1 promotes proliferation through G2/M checkpoint progression and mediates cisplatin-induced apoptosis and necroptosis in human ovarian cancer cells. *Acta Pharmacol Sin* (2020) 41:1223–33. doi: 10.1038/s41401-019-0340-7

168. Liang J, Zhou J, Xu Y, Huang X, Wang X, Huang W, et al. Osthole inhibits ovarian carcinoma cells through LC3-mediated autophagy and GSDME-dependent pyroptosis except for apoptosis. *Eur J Pharmacol* (2020) 874:172990. doi: 10.1016/j.ejphar.2020.172990

169. Qiao L, Wu X, Zhang J, Liu L, Sui X, Zhang R, et al. Alpha-NETA induces pyroptosis of epithelial ovarian cancer cells through the GSDMD/caspase-4 pathway. *FASEB J* (2019) 33:12760–7. doi: 10.1096/fj.201900483RR

170. Zhang R, Chen J, Mao L, Guo Y, Hao Y, Deng Y, et al. Nobiletin triggers reactive oxygen species-mediated pyroptosis through regulating autophagy in ovarian cancer cells. *J Agric Food Chem* (2020) 68:1326–36. doi: 10.1021/acs.jafc.9b07908

171. Tan C, Liu W, Zheng ZH, Wan XG. LncRNA HOTTIP inhibits cell pyroptosis by targeting miR-148a-3p/AKT2 axis in ovarian cancer. *Cell Biol Int* (2021) 45:1487–97. doi: 10.1002/cbin.11588

172. Ye Y, Dai Q, Qi H. A novel defined pyroptosis-related gene signature for predicting the prognosis of ovarian cancer. *Cell Death Discovery* (2021) 7:71. doi: 10.1038/s41420-021-00451-x

173. Berkel C, Cacan E. Differential expression and copy number variation of gasdermin (GSDM) family members, pore-forming proteins in pyroptosis, in normal and malignant serous ovarian tissue. *Inflammation* (2021) 44:2203–16. doi: 10.1007/s10753-021-01493-0

174. Zhou M, Li B, Liu J, Hong L. Genomic, immunological, and clinical characterization of pyroptosis in ovarian cancer. *J Inflammation Res* (2021) 14:7341–58. doi: 10.2147/JIR.S344554

175. Zhang Z, Xu Z, Yan Y. Role of a pyroptosis-related lncRNA signature in risk stratification and immunotherapy of ovarian cancer. *Front Med (Lausanne)* (2021) 8:793515. doi: 10.3389/fmed.2021.793515

176. Cao X, Zhang Q, Zhu Y, Huo X, Bao J, Su M. Derivation, comprehensive analysis, and assay validation of a pyroptosis-related lncRNA prognostic signature in patients with ovarian cancer. *Front Oncol* (2022) 12:780950. doi: 10.3389/fonc.2022.780950

177. Cai Z, Yuan S, Luan X, Feng J, Deng L, Zuo Y, et al. Pyroptosis-related inflammasome pathway: A new therapeutic target for diabetic cardiomyopathy. *Front Pharmacol* (2022) 13:842313. doi: 10.3389/fphar.2022.842313

178. Qi X, Li Q, Che X, Wang Q, Wu G. Application of regulatory cell death in cancer: Based on targeted therapy and immunotherapy. *Front Immunol* (2022) 13:837293. doi: 10.3389/fimmu.2022.837293

179. Zhao J, Jiang P, Guo S, Schrodi SJ, He D. Apoptosis, autophagy, NETosis, necroptosis, and pyroptosis mediated programmed cell death as targets for innovative therapy in rheumatoid arthritis. *Front Immunol* (2021) 12:809806. doi: 10.3389/fimmu.2021.809806

180. Park Y, Kim MJ, Choi Y, Kim NH, Kim L, Hong SPD, et al. Role of mass spectrometry-based serum proteomics signatures in predicting clinical outcomes and toxicity in patients with cancer treated with immunotherapy. *J Immunother Cancer* (2022) 10(3):e00356. doi: 10.1136/jitc-2021-003566

181. Huang J, Chang Z, Lu Q, Chen X, Najafi M. Nobiletin as an inducer of programmed cell death in cancer: a review. *Apoptosis* (2022) 27:297–310. doi: 10.1007/s10495-022-01721-4

182. Zhang S, Wang J, Kong Z, Sun X, He Z, Sun B, et al. Emerging photodynamic nanotherapeutics for inducing immunogenic cell death and potentiating cancer immunotherapy. *Biomaterials* (2022) 282:121433. doi: 10.1016/j.biomaterials.2022.121433

183. Zuo YB, Zhang YF, Zhang R, Tian JW, Lv XB, Li R, et al. Ferroptosis in cancer progression: Role of noncoding RNAs. *Int J Biol Sci* (2022) 18:1829–43. doi: 10.7150/ijbs.66917

184. Yang J, Hu S, Bian Y, Yao J, Wang D, Liu X, et al. Targeting cell death: Pyroptosis, ferroptosis, apoptosis and necroptosis in osteoarthritis. *Front Cell Dev Biol* (2021) 9:789948. doi: 10.3389/fcell.2021.789948

185. Xu W, Huang Y. Regulation of inflammatory cell death by phosphorylation. *Front Immunol* (2022) 13:851169. doi: 10.3389/fimmu.2022.851169

186. Zhuang J, Xie L, Zheng L. A glimpse of programmed cell death among bacteria, animals, and plants. *Front Cell Dev Biol* (2021) 9:790117. doi: 10.3389/fcell.2021.790117

187. Liu X, Wan L. Molecular insights into the biochemical functions and signalling mechanisms of plant NLRs. *Mol Plant Pathol* (2022) 23:772–80. doi: 10.1111/mpp.13195

188. Ryan TAJ, Preston RJS, O'Neill LAJ. Immunothrombosis and the molecular control of tissue factor by pyroptosis: prospects for new anticoagulants. *Biochem J* (2022) 479:731–50. doi: 10.1042/BCJ20210522

frontiers | Frontiers in Immunology

TYPE Review
PUBLISHED 26 July 2022
DOI 10.3389/fimmu.2022.956090

OPEN ACCESS

EDITED BY
Xuyao Zhang,
Fudan University, China

REVIEWED BY
Lijie Zhao,
University of Michigan, United States
Qiuju Han,
Shanghai Jiao Tong University, China

*CORRESPONDENCE
Nan Lu
nan.lu@ntu.edu.sg
Zhang-Suo Liu
zhangsuoliu@zzu.edu.cn

SPECIALTY SECTION
This article was submitted to Cancer Immunity and Immunotherapy, a section of the journal Frontiers in Immunology

RECEIVED 29 May 2022
ACCEPTED 07 July 2022
PUBLISHED 26 July 2022

CITATION
Huo J-L, Wang Y-T, Fu W-J, Lu N and Liu Z-S (2022) The promising immune checkpoint LAG-3 in cancer immunotherapy: from basic research to clinical application. *Front. Immunol.* 13:956090. doi: 10.3389/fimmu.2022.956090

The promising immune checkpoint LAG-3 in cancer immunotherapy: from basic research to clinical application

Jin-Ling Huo[1], Ya-Tao Wang[2], Wen-Jia Fu[1], Nan Lu[3]* and Zhang-Suo Liu[1]*

[1]Traditional Chinese Medicine Integrated Department of Nephrology, the First Affiliated Hospital of Zhengzhou University, Research Institute of Nephrology, Zhengzhou University, Henan Province Research Center For Kidney Disease, Key Laboratory of Precision Diagnosis and Treatment for Chronic Kidney Disease in Henan Province, Zhengzhou, China, [2]Department of Orthopedics, First People's Hospital of Shangqiu, Shangqiu, China, [3]School of Mechanical and Aerospace Engineering, Nanyang Technological University, Singapore, Singapore

LAG-3, a type of immune checkpoint receptor protein belonging to the immunoglobulin superfamily, is confirmed to be expressed on activated immune cells, mainly including activated T cells. LAG-3 can negatively regulate the function of T cells, exerting important effects on maintaining the homeostasis of the immune system under normal physiological conditions and promoting tumor cells immune escape in the tumor microenvironment. Given its important biological roles, LAG-3 has been regarded as a promising target for cancer immunotherapy. To date, many LAG-3 inhibitors have been reported, which can be divided into monoclonal antibody, double antibody, and small molecule drug, some of which have entered the clinical research stage. LAG-3 inhibitors can negatively regulate and suppress T cell proliferation and activation through combination with MHC II ligand. Besides, LAG-3 inhibitors can also affect T cell function *via* binding to Galectin-3 and LSECtin. In addition, LAG-3 inhibitors can prevent the FGL1-LAG-3 interaction, thereby enhancing the human body's antitumor immune effect. In this review, we will describe the function of LAG-3 and summarize the latest LAG-3 inhibitors in the clinic for cancer therapy.

KEYWORDS

LAG-3, immune checkpoint, cancer immunotherapy, tumor microenvironment, T cell

Introduction

A large amount of evidence from literature has manifested that tumor cells can effectively avoid being recognized and killed by the immune system through immune checkpoint receptor proteins, suggesting that blocking immune checkpoint receptors is a new immunotherapy for human cancers (1, 2). The most well-studied immune checkpoint receptors mainly include programmed cell death 1/programmed cell death 1 ligand (PD-1/PD-L1) and cytotoxic T lymphocyte-associated antigen-4 (CTLA-4) (3–6). However, due to the treatment tolerance, low response, or significant increase in toxicity of previously discovered antibody drugs targeting PD-1/PD-L1 or CTLA-4 (7–9), it is very necessary to investigate new targets against immune checkpoint receptor proteins.

Lymphocyte activation gene-3 (LAG-3, also named CD223 or FDC protein), is a new class of immune checkpoint receptors, which was first isolated and reported by French immunologist Frédéric Triebel and colleagues in 1990 (10). LAG-3, as a key member of the immunoglobulin superfamily (IgSF) locating on human chromosome 12, is a type I transmembrane protein containing 498 amino acids, consisting of transmembrane region, the extracellular region, and cytoplasmic region (11). The expression level of LAG-3 is closely related to the prognosis of human tumors. High level of LAG-3 in kidney renal clear cell carcinoma, non-small cell lung cancer (NSCLC), primary central nervous system lymphoma (PCNSL), hepatocellular carcinoma (HCC) and muscle invasive bladder cancer (MIBC) indicates a poor prognosis, whereas in gastric carcinoma and melanoma predicts a better prognosis (12). LAG-3 is detected to be expressed on the surface of effector T cells and regulatory T cells (Tregs) that participate in the regulation of T lymphocytes and antigen-presenting cells (APCs) signaling pathways and play a crucial part in the adaptive immune response (13). Consistent with CTLA-4 and PD-1/PD-L1, LAG-3 is induced on CD8+ and CD4+ T cells upon persistent antigenic stimulation, rather than expressed on naive T cells (14). Since the inhibitory function of LAG-3 is closely associated with its expression level on the activated immune cells, the blockage and inhibition of LAG-3 expression through antibody drugs or small molecule inhibitors are critical. Prolonged infection with viruses, fungus, and bacteria results in sustained exposure to antigens, leading to high levels of persistent expression of LAG-3 and other inhibitory co-receptors on CD8+ and CD4+ T cells (15). These T cells lose powerful effector functions, known as exhausted T cells, resulting in decreased tumor lethality and response rate, and upregulation of Treg immunosuppressive function (15). Studies have shown that blockage or inhibition of LAG-3 can allow T cells to regain cytotoxic activity and reduce the function of regulating T cells to suppress immune responses, thereby enhancing the killing effect on tumors (16, 17). It was observed that simultaneous blockage of LAG-3 activity and anti-PD-1 or PD-L1 in tumor cells has dual inhibitory effects, including inhibiting Treg activity, promoting dendritic cells (DCs) maturation, and rescuing dysfunctional CD4+/CD8+ T cells (18–20). LAG-3 has been regarded as an indicator of tumor prognosis and become a novel tumor immunotherapy target beyond PD-1/PD-L1 and CTLA-4. Herein, we aim to describe the structure and the known ligands of LAG-3 and summarize the immune-regulatory effects on active T cells in tumor microenvironment, as well as the LAG-3 inhibitors which have been evaluated in the clinic.

LAG-3 structure and ligands

LAG3 co-localizates with CD4, CD8, and CD3 molecules within lipid rafts. The structure of LAG-3 is essentially different from that of CD3 and CD8, whereas it is highly homologous to CD4. LAG-3 consists of three parts: transmembrane region, extracellular region, and cytoplasmic region. In the transmembrane-cytoplasmic part, LAG-3 breaks away from the cell membrane under the action of metalloproteinases ADAM10/17, which can regulate the function of LAG-3. The extracellular domain is responsible for binding to the ligands and consists of four IgSF domains, namely D1, D2, D3, and D4. The D1 domain contains a loop domain rich in proline (~30) and an in-chain disulfide bond, which is species-specific and is known as the V immunoglobulin superfamily. However, D2, D3, and D4 belong to the C2 family. The cytoplasmic region of LAG-3 consists of three parts: the serine phosphorylation site S454 (substrates for protein kinase C, PKC), the highly conserved "KIEELE" motif, and the glutamate-proline dipeptide repeat motif (EP sequence) (Figure 1) (21, 22). Importantly, KIEELE mutant resulted in complete loss of LAG-3 function, which proved that the "KIEELE" motif was crucial to the function of LAG-3 (23).

LAG-3 was detected to be mainly expressed on the surface of activated T cells (CD8+ T cells and CD4+ T cells), naturalkiller cells (NK cells), B cells, and DCs under physiological conditions, and negatively regulate T cell function. Researchers also found a small number of LAG-3+ lymphocytes in inflammatory lymphoid tissues, such as tonsils or lymph nodes (24). In pathological state, LAG-3 was reported to be highly expressed on the surface of tumor-infiltrating lymphocytes (TILs), the expression level of which was positively correlated with the occurrence and development of human tumors, such as non-small cell lung cancer (NSCLC) and hepatocellular carcinoma (HCC) (25–27). LAG-3 negatively regulates the function of T cells and plays significant roles in maintaining the homeostasis of immune system under normal physiological conditions and promoting tumor cells immune escape in the tumor microenvironment, indicating a promising target for tumor immunotherapy.

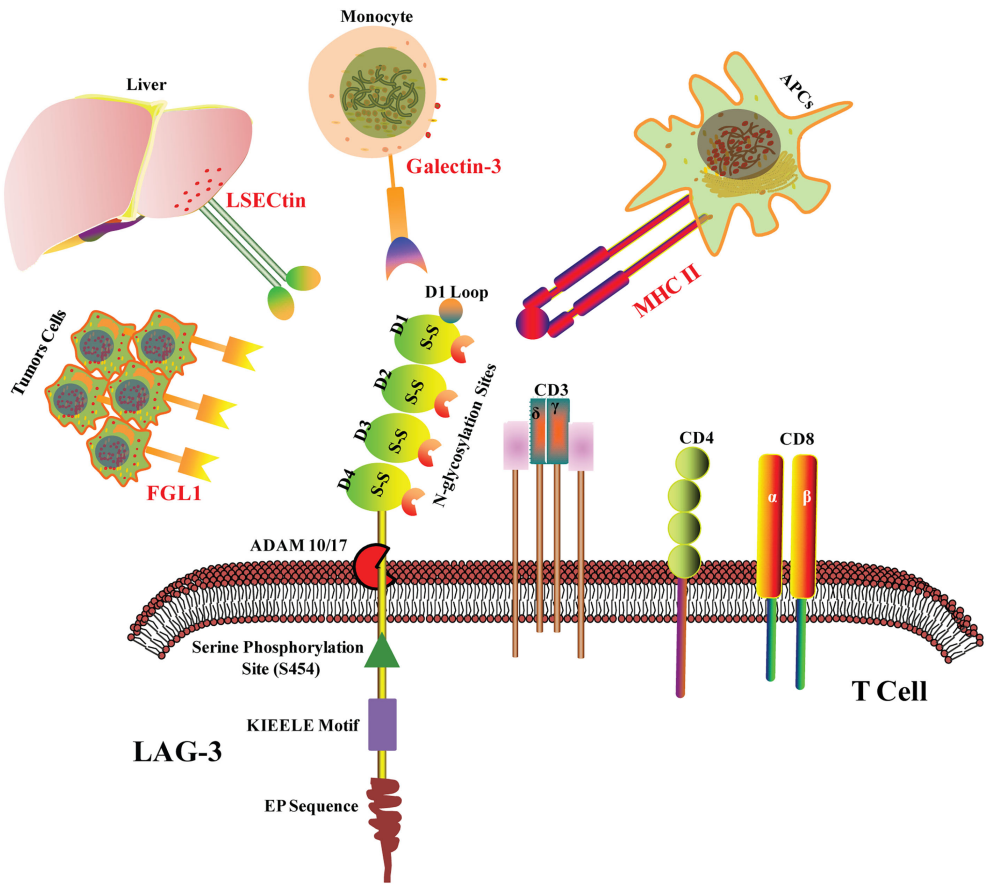

FIGURE 1
LAG-3 structure and ligands. LAG-3 consists of extracellular region, transmembrane region and cytoplasmic region. The extracellular domain is composed of four IgSF domains, namely D1, D2, D3 and D4. The D1 domain contains a loop domain rich in proline and an in-chain disulfide bond. In the transmembrane- cytoplasmic part, LAG-3 breaks away from the cell membrane under the action of metalloproteinases ADAM10/17. The cytoplasmic region of LAG-3 consists of three parts: the serine phosphorylation site S454, the highly conserved "KIEELE" motif and the glutamate-proline dipeptide repeat motif (EP sequence). MHC II, Galectin-3, LSECtin and FGL1 are the confirmed ligands of LAG-3 in tumor microenvironment.

It has been reported four ligands of LAG-3 in tumor microenvironment mainly including galactose lectin-3 (Galectin-3), major histocompatibility complex II (MHC II), fibrinogen-like protein 1 (FGL1), and hepatic sinusoid endothelial cell lectin (LSECtin) (Figure 1). MHC II is the main ligand of LAG-3 (28). Due to the high homology of LAG3 and CD4, MHC II is the common ligand of LAG3 and CD4. However, LGA3 and MHC II shows 100 times higher in binding affinity than CD4, suggesting that CD4 and LAG3 may competitively bind to MHC II, thereby negatively regulating the function of CD4 (29, 30). Studies have shown that although LAG3 mutants unable to bind MHC II exhibit reduced inhibitory function (21), tail mutations in the intracellular domain of LAG3 lead to loss of inhibitory effect, further suggesting that the intracellular domain is critical for inhibiting signal transduction (23). It is possible that LAG3 acts not primarily by interfering with the interaction of MHC II and CD4, but rather by transmitting inhibitory signals *via* the cytoplasmic domain (23), although the exact character of this signal is unclear.

Galectin-3, another ligand of LAG-3, is a 31-kDa soluble lectin (Figure 1). Studies have shown that LAG3 is highly glycosylated and can interact with Galectin-3, which regulates T cell responses *via* several mechanisms (28). *In vitro* experiments showed that LAG3 played important roles in Galectin-3-mediated inhibition of IFN-γ secretion by CD8+ T cells (31). Furthermore, Galectin-3 expressed by a variety of cells in the tumor microenvironment instead of the tumor itself may interact with LAG3 on tumor-specific CD8+ T cells, thus resulting in the modulation of anti-tumor immune responses (32). LSECtin, a potential ligand of LAG-3, belongs to the C-type lectin receptor superfamily and is mainly expressed in liver (33). LSECtin has also been found in human melanoma tissues. The interaction between LSECtin and LAG-3 promotes tumor

growth through suppression of anti-tumor T cell response in melanoma cells (34).

Jun Wang et al. found that FGL1 is an immune inhibitory ligand of LAG-3 independent of MHC II (Figure 1). LAG-3 binds with FGL1 through the domains of D1 and D2. The interaction between FGL1 and LAG-3 mutually promotes tumor immune escape through inhibiting the activation of antigen-specific T cell (35). Notably, a recent study has revealed that the binding of LAG-3 to MHC II but not to FGL1 mediated the suppression of T cells (36). Of course, other LAG3 ligands have not yet been discovered. In addition, a study has shown that LAG3 binds preformed fibrils of α-synuclein in the central nervous system, thereby promoting the pathogenesis of Parkinson's disease in a mouse model (37), suggesting that LAG3 may also have functions outside the immune system.

LAG-3 immunological functions

LAG-3 interacts with its ligands to regulate the function of T cells. The interaction between MHC II and LAG-3 can down-regulate the cytokine secretion level and proliferation ability of CD4+ T cells (Figure 2). The anti-LAG-3 antibody can restore CD4+ T cells activity. Nevertheless, the specific regulatory

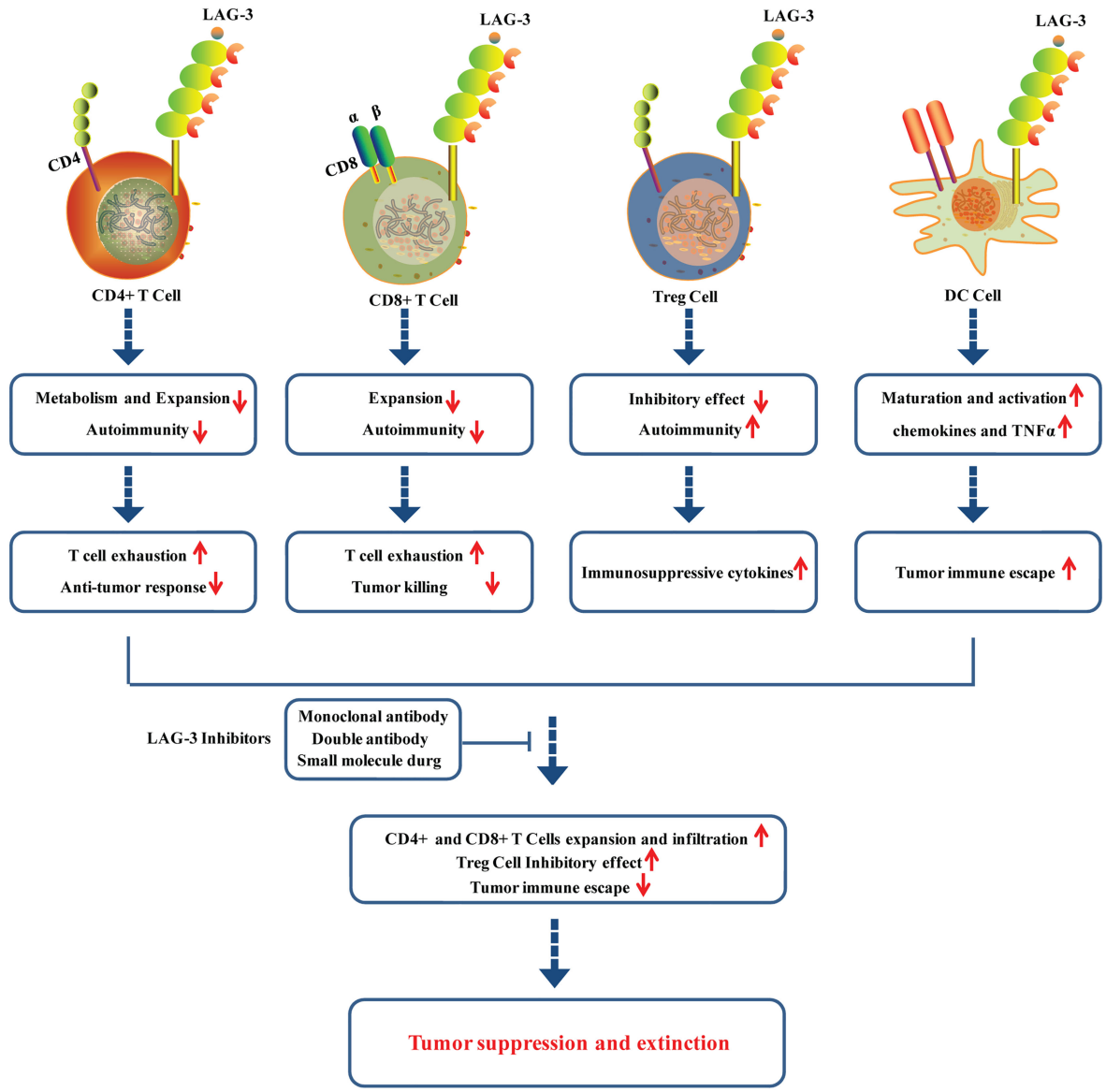

FIGURE 2
Roles of LAG-3 in CD+4 cells, CD8+ cells, Treg cells and DC cells in tumor microenvironment.

mechanism remains unknown (38, 39). It is worth noting that LAG-3 selectively binds to antigen peptide-MHC II (pMHC II), thus inhibiting pMHC II-responsive CD4+ T cells (40, 41). LAG-3 was found to negatively regulate the mitochondrial activity in naive CD4+ T cells, restricting the normal metabolism and expansion of naive CD4+ T cells and leading to T cell exhaustion and anti-tumor response (42). In addition, LAG-3 was also observed to be upregulated in CD8+ T cells stimulated with tumor antigens (Figure 2) (43). CD8+ T cells in LAG-3-deficient mice exhibited significantly higher activity than that in normal mice, suggesting that LAG-3 has an inhibitory effect on CD8+ T cells. LAG-3 has been demonstrated to directly inhibit CD8+ T cells *via* signal transduction, independent of the role of MHC II and CD4+ T cells (44, 45). LAG-3 can also enhance the function of regulatory T cells (Treg cells) (Figure 2). Treg cells play a negative role in immune regulation and can down-regulate T cell activity. Common types of Treg cells include natural regulatory T cells (nTreg cells) and inducible regulatory T cells (iTreg cells). LAG-3 can positively induce Treg cells activation and stimulate their immunosuppressive function (46–48). LAG-3 may synergize with other inhibitory molecules (PD-1, CTLA-4) to improve the inhibitory activity of Treg cells, leading to APC-induced immune tolerance (49).

LAG-3 also plays immune adjuvant roles and participates in the tumor immune escape. LAG-3 can induce the maturation and activation of DC cells through regulation of intracellular protein phosphorylation and promotion of the chemokines and tumor necrosis factor α (TNFα) production (Figure 2) (50). LAG-3 highly expressed on the TILs interacts with ligands located on the surface of tumor cells to cause T cell dysfunction or even exhaustion, promoting tumor immune escape, the phenomenon of which is particularly evident in CD8+ T cells (25, 51, 52). Moreover, it is confirmed that LAG-3 displayed potential roles in activation of NK cells, although its underling mechanisms remains to be further studied.

Roles of blocking LAG-3 in the tumor microenvironment

LAG-3 is confirmed to be highly expressed on TILs of various solid tumors, including colon cancer, NSCLC, head and neck cell cancer, and pancreatic cancer (18, 53–55). LAG-3 has been revealed to play a vital role in regulating T cell activation, proliferation, homeostasis, and T cell-depleted immune microenvironments. LAG-3 was also found to be co-expressed with PD-1 in the tumor microenvironment. LAG-3 and PD-1 induced T cell function inhibition through different signaling pathways, which may synergistically lead to exhaustion of T cells. Studies have shown that co-blockade of PD1 and LAG3 expressed on CD8+ and CD4+ TILs exhibited enhanced antitumor responses in some preclinical mouse models of ovarian cancer, colon adenocarcinoma, and melanoma (52, 56, 57). LAG3 expressed on iTreg cells induces the production of TGF-β1 and IL-10, which contributes to tumor immune escape. The blocking LAG3 antibodies can reduce the inhibitory effect of Tregs, resulting in the restoration of CD8+ TIL activity (57, 58) (Figure 2).

Studies have shown that inhibition of LAG-3 can allow T cells to regain cytotoxic activity and reduce the function of regulating T cells to suppress immune responses, enhancing the killing effect on tumors (59) (Figure 2). Blocking LAG-3 activity and anti-PD-1 or PD-L1 in tumor cells has dual inhibitory effects, including inhibiting Treg activity, promoting DC maturation, and rescuing dysfunctional CD4+/CD8+ T cells (60). LAG-3 has become a novel tumor immunotherapy target beyond CTLA-4 and PD-1/PD-L1. The overall drug types of LAG-3 inhibitors can be divided into monoclonal antibody, double antibody, and small molecule drug, some of which have entered the clinical research stage. More than 80 clinical trials are underway globally to evaluate the drug candidates targeting LAG-3.

LAG-3 inhibitors can directly bind LAG-3 molecules or their ligands, blocking the interaction between ligands and LAG-3, and downregulating the inhibitory efficacy of LAG-3 toward the immune system. LAG-3 antibodies not only restore T cell function, but also inhibit Treg cells activity. In previous studies, antibodies against PD-1 can only activate T cells, but cannot inhibit the activity of Treg cells (61–63). Taken together, LAG-3 inhibitors may have a better therapeutic effect, further demonstrating a novel tumor immunotherapy target of LAG-3 beyond PD-1/PD-L1 and CTLA-4.

Clinical development of LAG-3 targeted cancer immunotherapy

As a promising target for cancer immunotherapy, LAG3 has been hotly pursued by academia and pharmaceutical companies. In the past, significant progress has been made in the discovery of many LAG3 modulators and some of them are currently in the clinic as anticancer drugs, which are summarized in Table 1, involving LAG3-targeted cancer immunotherapy that are either completed, ongoing, or recruiting participants (ClinicalTrials.gov). Eftilagimod alpha, developed by Immutep S.A.S. as the initial first-in-class LAG3 modulator, could activate APCs *via* interacting with canonical ligand (MHC class II), which has been also found to enhance Treg immunosuppression, stimulate the proliferation of DCs, and ameliorate antigen crosspresentation to CD8+ T cells (64). Three clinical trials for Eftilagimod alpha have been completed, and three others are recruiting participants as shown in Table 1. In addition, 10 different LAG3-specific monoclonal antibodies and six bispecific antibodies are currently under

TABLE 1 LAG3-modulating candidates[a].

Drug	Phase	ClinicalTrials.gov ID	Indications	Status
Nivolumab/Relatlimab	Phase 1	NCT04658147	Hepatocellular Carcinoma	Recruiting
	Phase 1	NCT02966548	Cancer	Active, not recruiting
	Phase 1	NCT03335540	Advanced Cancer	Active, not recruiting
	Phase 1	NCT03044613	Gastric Cancer	Active, not recruiting
	Phase 1/2	NCT03459222	Advanced Cancer	Recruiting
	Phase 1/2	NCT02061761	Hematologic Neoplasms	Recruiting
	Phase 1/2	NCT03310619	Lymphoma	Recruiting
	Phase 1/2	NCT02488759	Various Advanced Cancer	Active, not recruiting
	Phase 1/2	NCT03610711	Gastroesophageal Cancer Immune Checkpoint Inhibition	Recruiting
	Phase 1/2	NCT04611126	Metastatic Ovarian Cancer	Recruiting
	Phase 1/2	NCT05134948	Advanced Solid Tumors	Recruiting
	Phase 1/2	NCT03978611	Melanoma	Recruiting
	Phase 1/2	NCT05337137	Carcinoma, Hepatocellular	Recruiting
	Phase 1/2	NCT05255601	Lymphoma, Non-Hodgkin Hodgkin Disease	Not yet recruiting
	Phase 1/2	NCT04150965	Multiple Myeloma	Recruiting
	Phase 2	NCT04552223	Metastatic Uveal Melanoma	Recruiting
	Phase 2	NCT04095208	Soft Tissue Sarcoma Adult Advanced Cancer	Recruiting
	Phase 2	NCT03623854	Chordoma	Recruiting
	Phase 2	NCT03743766	Melanoma	Recruiting
	Phase 2	NCT04080804	Head and Neck Squamous Cell Carcinoma	Recruiting
	Phase 2	NCT04913922	Acute Myeloid Leukemia	Recruiting
	Phase 2	NCT05002569	Melanoma	Recruiting
	Phase 2	NCT04112498	Cancer	Active, not recruiting
	Phase 2	NCT03607890	Refractory MSI-H Solid Tumors Prior of PD-(L) 1 Therapy MSI-H Tumors	Recruiting
	Phase 2	NCT03642067	Microsatellite Stable (MSS) Colorectal Adenocarcinomas Colorectal Adenocarcinoma	Recruiting
	Phase 2	NCT03724968	Melanoma	Terminated
	Phase 2	NCT03704077	Gastric Cancer	Withdrawn
	Phase 2	NCT02750514	Advanced Cancer	Terminated
	Phase 2	NCT04567615	Hepatocellular Carcinoma	Recruiting
	Phase 2	NCT03521830	Basal Cell Carcinoma	Recruiting
	Phase 2	NCT04326257	Squamous Cell Carcinoma of the Head and Neck	Recruiting
	Phase 2	NCT04623775	Non-small Cell Lunch Cancer	Recruiting
	Phase 2	NCT05347212	Carcinomas	Not yet recruiting
	Phase 2	NCT04205552	NSCLC Stage I/II/IIIA	Recruiting
	Phase 2	NCT03867799	Metastatic Colorectal Cancer	Active, not recruiting
	Phase 2	NCT05148546	Renal Cell Carcinoma	Recruiting
	Phase 2	NCT01968109	Neoplasms by Site	Active, not recruiting
	Phase 2	NCT03662659	Gastric Cancer	Active, not recruiting
	Phase 2	NCT02519322	Stage IIIB-IV melanoma	Active, not recruiting
	Phase 2	NCT04062656	Gastric Cancer	Recruiting
	Phase 2	NCT02996110	Advanced Cancer	Active, not recruiting
	Phase 2	NCT02935634	Advanced Gastric Cancer	Active, not recruiting
	Phase 2	NCT02465060	solid tumors or lymphomas	Recruiting
	Phase 2/3	NCT03470922	Melanoma	Active, not recruiting

(Continued)

TABLE 1 Continued

Drug	Phase	ClinicalTrials.gov ID	Indications	Status
	Phase 3	NCT05328908	Colorectal Neoplasms	Recruiting
	Not Applicable	NCT04866810	Melanoma	Recruiting
Tebotelimab	Phase 1	NCT03219268	HER2-positive Advanced Solid Tumors	Active, not recruiting
	Phase 2	NCT04634825	Head and Neck Cancer, Neoplasms, Squamous Cell Carcinoma	Recruiting
	Phase 2/3	NCT04082364	Gastric Cancer	Active, not recruiting
Chlorogenic acid	Phase 1	NCT02728349	Glioblastoma	Completed
	Phase 1	NCT02245204	Advanced Cancer	Completed
	Phase 1	NCT02136342	Advanced Cancer	Terminated
	Phase 1/2	NCT03751592	Advanced Lung Cancer	Unknown
RO-7247669	Phase 1	NCT04140500	Solid Tumors	Recruiting
	Phase 1/2	NCT04524871	Advanced Liver Cancers	Recruiting
	Phase 1/2	NCT05116202	Melanoma	Recruiting
	Phase 2	NCT04785820	Advanced or Metastatic Esophageal Squamous Cell Carcinoma	Recruiting
Favezelimab	Phase 1	NCT02720068	Neoplasms	Active, not recruiting
	Phase 1/2	NCT04938817	Small Cell Lung Carcinoma	Recruiting
	Phase 1/2	NCT04626479	Carcinoma, Renal Cell	Recruiting
	Phase 1/2	NCT05342636	Esophageal Squamous Cell Carcinoma (ESCC)	Not yet recruiting
	Phase 1/2	NCT03598608	Hodgkin Disease Lymphoma	Recruiting
	Phase 1/2	NCT04626518	Carcinoma, Renal Cell	Recruiting
	Phase 2	NCT04895722	Colorectal Cancer	Recruiting
	Phase 2	NCT03516981	Advanced Non-Small Cell Lung Cancer	Active, not recruiting
	Phase 3	NCT05064059	Colorectal Cancer	Recruiting
INCAGN-2385	Phase 1	NCT03538028	Advanced Malignancies	Completed
	Phase 1/2	NCT04370704	Melanoma	Recruiting
	Phase 2	NCT05287113	Head and Neck Cancer	Not yet recruiting
	Phase 2	NCT04586244	Urothelial Carcinoma	Recruiting
IBI-110	Phase 1	NCT04085185	Advanced Malignancies	Recruiting
	Phase 1	NCT05039658	DLBCL	Not yet recruiting
	Phase 2	NCT05026593	SCLC	Recruiting
	Phase 2	NCT05088967	Non-small Cell Lung Cancer	Recruiting
Eftilagimod alpha	Phase 1	NCT02676869	Stage III/IV Melanoma	Completed
	Phase 1	NCT04252768	Metastatic Breast Cancer	Not yet recruiting
	Phase 1	NCT03600090	Solid Tumor, Adult	Completed
	Phase 2	NCT03625323	Non-small cell lung carcinoma, head and neck carcinoma	Active, not recruiting
	Phase 2	NCT04811027	HNSCC	Recruiting
	Phase 2	NCT02614833	Adenocarcinoma Breast Stage IV	Completed
Sym-022	Phase I	NCT03489369	Metastatic Cancer, Solid Tumor Lymphoma	Completed
	Phase I	NCT04641871	Metastatic Cancer Solid Tumor	Recruiting
	Phase 1	NCT03311412	Metastatic Cancer, Solid Tumor Lymphoma	Completed
	Phase I	NCT04414150	Malignant Tumors	Unknown
	Phase 2	NCT05208177	Advanced Solid Tumor	Not yet recruiting
LBL-007	Phase 1	NCT04640545	Advanced Melanoma	Recruiting

(Continued)

TABLE 1 Continued

Drug	Phase	ClinicalTrials.gov ID	Indications	Status
	Phase 1/2	NCT05102006	Advanced Solid Tumor	Recruiting
ABL-501	Phase I	NCT05101109	Advanced Solid Tumor	Recruiting
Anti-LAG3 antibody	Phase 1	NCT02658981	Glioblastoma	Active, not recruiting
HLX 26	Phase I	NCT05078593	Solid Tumor	Recruiting
IBI-323	Phase I	NCT04916119	Advanced Malignancies	Recruiting
Ieramilimab	Phase 1/2	NCT02460224	Advanced Solid Tumors	Completed
FS 118	Phase 1/2	NCT03440437	Advanced Cancer	Recruiting
EMB-02	Phase 1/2	NCT04618393	Advanced Solid Tumors	Recruiting
Fianlimab	Phase 3	NCT05352672	Melanoma	Not yet recruiting

[a]The data were from https://www.clinicaltrials.gov/#opennewwindow.

investigation at various clinical stages for the treatment of cancer (Table 1). As the first anti-LAG3 human IgG4 monoclonal antibody and novel immune checkpoint inhibitor, relatlimab, discovered by Bristol-Myers Squibb, is currently undergoing 46 different clinical trials for cancer therapy (65). As the first commercially developed anti-LAG-3 antibody, relatlimab entered the clinical trials in 2013 (66). However, due to the limited efficacy of relatlimab alone, it is generally used in combination with other checkpoint inhibitors, including CTLA-4 inhibitors (ipilimumab) or PD-1 inhibitors (nivolumab), to synergistically improve the efficacy (39). Encouragingly, relatlimab in combination with the PD-1 inhibitor nivolumab received FDA approval in March 2022 as the first approved monoclonal antibody to treat unresectable or metastatic melanoma (67).

Discussion

Since its discovery in 1990, LAG3 has gained widespread interest and been regarded as a promising target for cancer immunotherapy. LAG-3 plays an important immunoregulatory role in a variety of human tumors, and blocking LAG-3 can enhance the proliferation of TILs and the secretion of cytokines, and enhance anti-tumor immunity. Many LAG3 inhibitors have been discovered and are currently in the clinic. Single anti-LAG3 therapy was demonstrated to be modest benefit, supporting a potential combination approach with other inhibitory receptors. LAG-3 inhibitors, together with CTLA-4 or PD-1/PD-L1 inhibitors, have been extensively explored in the different clinical trials for cancer therapy, which can not only avoid drug tolerance but also improve the clinical efficacy of LAG-3 inhibitors. No evidence reveals the feasibility of the combination between LAG-3 inhibitors and other immune checkpoint inhibitors. So far, the regulatory mechanism of LAG-3 has not been fully explored and the clinical efficacy of its inhibitors is uncertain. Based on the current clinical data, the early therapeutic effect of LAG-3 monoclonal antibody is not satisfactory. According to the phase I clinical data of LAG-3 monoclonal antibody MK-4280 published by Merck, the objective response rate (ORR) among 18 patients with solid tumors that failed other treatments was only 6%, and the disease control rate is only 17%. Therefore, it is mainly to explore the combination strategy, especially the combination of LAG-3 and PD-1. The bi-functional monoclonal antibody is worthy of attention and exploration. There are only a few interim reports of the combination therapies targeting LAG-3 and PD-1. Evidence revealed that the combination exerted better tolerance and higher ORR, extended progression-free survival, as well as a lower risk of death (13). The exact efficacy of anti-LAG-3 antibodies as monotherapy and the additive effects of anti-LAG-3 antibodies in the combination therapy targeting PD-1 and LAG-3 need to be further explored.

Inevitably, there are still many questions that remain to be resolved regarding the understanding of LAG3 biology, the exact signaling pathway and the potential ligands, as well as the mechanism underlying synergistic effect with other immune checkpoint molecules, although the development of LAG-3 inhibitors is in full swing. If these problems could be solved, the research on LAG-3 and its related drugs will make significant progress for cancer therapy.

Author contributions

J-LH and NL conceptualized the ideas. Y-TW, W-JF, J-LH, and NL drafted the original manuscript. Z-SL revised the manuscript. All the authors approved the final version of the manuscript.

Funding

This work was financially supported by the General Program of the National Natural Science Foundation of China General

Project (No. 81970633) and National Natural Science Foundation of China Joint project (NO. U21A20348).

Conflict of interest

The authors declare that the research was conducted in the absence of any commercial or financial relationships that could be construed as a potential conflict of interest.

Publisher's note

References

1. Villadolid J, Amin A. Immune checkpoint inhibitors in clinical practice: update on management of immune-related toxicities. *Transl Lung Cancer Res* (2015) 4(5):560–75. doi: 10.3978/j.issn.2218-6751.2015.06.06

2. Darvin P, Toor SM, Sasidharan NV, Elkord E. Immune checkpoint inhibitors: recent progress and potential biomarkers. *Exp Mol Med* (2018) 50 (12):1–11. doi: 10.1038/s12276-018-0191-1

3. Blank C, Gajewski TF, Mackensen A. Interaction of PD-L1 on tumor cells with PD-1 on tumor-specific T cells as a mechanism of immune evasion: implications for tumor immunotherapy. *Cancer Immunol Immunother* (2005) 54 (4):307–14. doi: 10.1007/s00262-004-0593-x

4. Lin C, Chen X, Liu J, Huang Y, Ou-Yang X. Advances of PD-1/PD-L1 signaling pathway in immune escape and treatment for non-small cell lung cancer. *Zhongguo Fei Ai Za Zhi* (2014) 17(10):734–40. doi: 10.3779/j.issn.1009-3419.2014.10.05

5. Yi M, Jiao D, Xu H, Liu Q, Zhao W, Han X, et al. Biomarkers for predicting efficacy of PD-1/PD-L1 inhibitors. *Mol Cancer* (2018) 17(1):129. doi: 10.1186/s12943-018-0864-3

6. Rowshanravan B, Halliday N, Sansom DM. CTLA-4: a moving target in immunotherapy. *Blood* (2018) 131(1):58–67. doi: 10.1182/blood-2017-06-741033

7. Hodi FS, O'Day SJ, McDermott DF, Weber RW, Sosman JA, Haanen JB, et al. Improved survival with ipilimumab in patients with metastatic melanoma. *N Engl J Med* (2010) 363(8):711–23. doi: 10.1056/NEJMoa1003466

8. Topalian SL, Hodi FS, Brahmer JR, Gettinger SN, Smith DC, McDermott DF, et al. Safety, activity, and immune correlates of anti-PD-1 antibody in cancer. *N Engl J Med* (2012) 366(26):2443–54. doi: 10.1056/NEJMoa1200690

9. Postow MA, Chesney J, Pavlick AC, Robert C, Grossmann K, McDermott D, et al. Nivolumab and ipilimumab versus ipilimumab in untreated melanoma. *N Engl J Med* (2015) 372(21):2006–17. doi: 10.1056/NEJMoa1414428

10. Triebel F, Jitsukawa S, Baixeras E, Roman-Roman S, Genevee C, Viegas-Pequignot E, et al. LAG-3, a novel lymphocyte activation gene closely related to CD4. *J Exp Med* (1990) 171(5):1393–405. doi: 10.1084/jem.171.5.1393

11. Triebel F. LAG-3: a regulator of T-cell and DC responses and its use in therapeutic vaccination. *Trends Immunol* (2003) 24(12):619–22. doi: 10.1016/j.it.2003.10.001

12. Shi AP, Tang XY, Xiong YL, Zheng KF, Liu YJ, Shi XG, et al. Immune checkpoint LAG3 and its ligand FGL1 in cancer. *Front Immunol* (2021) 12:785091. doi: 10.3389/fimmu.2021.785091

13. Maruhashi T, Sugiura D, Okazaki IM, Okazaki T. LAG-3: from molecular functions to clinical applications. *J Immunother Cancer* (2020) 8(2):e001014. doi: 10.1136/jitc-2020-001014

14. Qin S, Xu L, Yi M, Yu S, Wu K, Luo S. Novel immune checkpoint targets: moving beyond PD-1 and CTLA-4. *Mol Cancer* (2019) 18(1):155. doi: 10.1186/s12943-019-1091-2

15. Anderson AC, Joller N, Kuchroo VK. Lag-3, Tim-3, and TIGIT: Co-inhibitory receptors with specialized functions in immune regulation. *Immunity* (2016) 44(5):989–1004. doi: 10.1016/j.immuni.2016.05.001

16. Puhr HC, Ilhan-Mutlu A. New emerging targets in cancer immunotherapy: the role of LAG3. *ESMO Open* (2019) 4(2):e482. doi: 10.1136/esmoopen-2018-000482

17. Ruffo E, Wu RC, Bruno TC, Workman CJ, Vignali D. Lymphocyte-activation gene 3 (LAG3): The next immune checkpoint receptor. *Semin Immunol* (2019) 42:101305. doi: 10.1016/j.smim.2019.101305

18. Andrews LP, Marciscano AE, Drake CG, Vignali DA. LAG3 (CD223) as a cancer immunotherapy target. *Immunol Rev* (2017) 276(1):80–96. doi: 10.1111/imr.12519

19. Sato H, Okonogi N, Nakano T. Rationale of combination of anti-PD-1/PD-L1 antibody therapy and radiotherapy for cancer treatment. *Int J Clin Oncol* (2020) 25(5):801–9. doi: 10.1007/s10147-020-01666-1

20. Yi M, Zheng X, Niu M, Zhu S, Ge H, Wu K. Combination strategies with PD-1/PD-L1 blockade: current advances and future directions. *Mol Cancer* (2022) 21(1):28. doi: 10.1186/s12943-021-01489-2

21. Huard B, Mastrangeli R, Prigent P, Bruniquel D, Donini S, El-Tayar N, et al. Characterization of the major histocompatibility complex class II binding site on LAG-3 protein. *Proc Natl Acad Sci U.S.A.* (1997) 94(11):5744–9. doi: 10.1073/pnas.94.11.5744

22. Wang JH, Meijers R, Xiong Y, Liu JH, Sakihama T, Zhang R, et al. Crystal structure of the human CD4 n-terminal two-domain fragment complexed to a class II MHC molecule. *Proc Natl Acad Sci U.S.A.* (2001) 98(19):10799–804. doi: 10.1073/pnas.191124098

23. Workman CJ, Dugger KJ, Vignali DA. Cutting edge: molecular analysis of the negative regulatory function of lymphocyte activation gene-3. *J Immunol* (2002) 169(10):5392–5. doi: 10.4049/jimmunol.169.10.5392

24. Huard B, Tournier M, Hercend T, Triebel F, Faure F. Lymphocyte-activation gene 3/major histocompatibility complex class II interaction modulates the antigenic response of CD4+ T lymphocytes. *Eur J Immunol* (1994) 24(12):3216–21. doi: 10.1002/eji.1830241246

25. Baitsch L, Baumgaertner P, Devevre E, Raghav SK, Legat A, Barba L, et al. Exhaustion of tumor-specific CD8(+) T cells in metastases from melanoma patients. *J Clin Invest* (2011) 121(6):2350–60. doi: 10.1172/JCI46102

26. Ma QY, Huang DY, Zhang HJ, Wang S, Chen XF. Function and regulation of LAG3 on CD4(+)CD25(-) T cells in non-small cell lung cancer. *Exp Cell Res* (2017) 360(2):358–64. doi: 10.1016/j.yexcr.2017.09.026

27. Hald SM, Rakaee M, Martinez I, Richardsen E, Al-Saad S, Paulsen EE, et al. LAG-3 in non-small-cell lung cancer: Expression in primary tumors and metastatic lymph nodes is associated with improved survival. *Clin Lung Cancer* (2018) 19 (3):249–59. doi: 10.1016/j.cllc.2017.12.001

28. Baixeras E, Huard B, Miossec C, Jitsukawa S, Martin M, Hercend T, et al. Characterization of the lymphocyte activation gene 3-encoded protein. a new ligand for human leukocyte antigen class II antigens. *J Exp Med* (1992) 176(2):327–37. doi: 10.1084/jem.176.2.327

29. Huard B, Prigent P, Tournier M, Bruniquel D, Triebel F. CD4/major histocompatibility complex class II interaction analyzed with CD4- and lymphocyte activation gene-3 (LAG-3)-Ig fusion proteins. *Eur J Immunol* (1995) 25(9):2718–21. doi: 10.1002/eji.1830250949

30. Weber S, Karjalainen K. Mouse CD4 binds MHC class II with extremely low affinity. *Int Immunol* (1993) 5(6):695–8. doi: 10.1093/intimm/5.6.695

31. Kouo T, Huang L, Pucsek AB, Cao M, Solt S, Armstrong T, et al. Galectin-3 shapes antitumor immune responses by suppressing CD8+ T cells *via* LAG-3 and inhibiting expansion of plasmacytoid dendritic cells. *Cancer Immunol Res* (2015) 3 (4):412–23. doi: 10.1158/2326-6066

32. Dumic J, Dabelic S, Flogel M. Galectin-3: an open-ended story. *Biochim Biophys Acta* (2006) 1760(4):616–35. doi: 10.1016/j.bbagen.2005.12.020

33. Liu W, Tang L, Zhang G, Wei H, Cui Y, Guo L, et al. Characterization of a novel c-type lectin-like gene, LSECtin: demonstration of carbohydrate binding and expression in sinusoidal endothelial cells of liver and lymph node. *J Biol Chem* (2004) 279(18):18748–58. doi: 10.1074/jbc.M311227200

34. Xu F, Liu J, Liu D, Liu B, Wang M, Hu Z, et al. LSECtin expressed on melanoma cells promotes tumor progression by inhibiting antitumor T-cell responses. *Cancer Res* (2014) 74(13):3418–28. doi: 10.1158/0008-5472.CAN-13-2690

35. Wang J, Sanmamed MF, Datar I, Su TT, Ji L, Sun J, et al. Fibrinogen-like protein 1 is a major immune inhibitory ligand of LAG-3. *Cell* (2019) 176(1-2):334–47. doi: 10.1016/j.cell.2018.11.010

36. Maruhashi T, Sugiura D, Okazaki IM, Shimizu K, Maeda TK, Ikubo J, et al. Binding of LAG-3 to stable peptide-MHC class II limits T cell function and suppresses autoimmunity and anti-cancer immunity. *Immunity* (2022) 55(5):912–24. doi: 10.1016/j.immuni.2022.03.013

37. Mao X, Ou MT, Karuppagounder SS, Kam TI, Yin X, Xiong Y, et al. Pathological alpha-synuclein transmission initiated by binding lymphocyte-activation gene 3. *Science* (2016) 353(6307):aah3374. doi: 10.1126/science.aah3374

38. Zhang J, Liu W, Xie T, Huang L, Hu Y, Wen B, et al. Elevated LAG-3 on CD4(+) T cells negatively correlates with neutralizing antibody response during HCV infection. *Immunol Lett* (2019) 212:46–52. doi: 10.1016/j.imlet.2019.06.003

39. Yu X, Huang X, Chen X, Liu J, Wu C, Pu Q, et al. Characterization of a novel anti-human lymphocyte activation gene 3 (LAG-3) antibody for cancer immunotherapy. *Mabs-Austin* (2019) 11(6):1139–48. doi: 10.1080/19420862.2019.1629239

40. Maruhashi T, Okazaki IM, Sugiura D, Takahashi S, Maeda TK, Shimizu K, et al. LAG-3 inhibits the activation of CD4(+) T cells that recognize stable pMHCII through its conformation-dependent recognition of pMHCII. *Nat Immunol* (2018) 19(12):1415–26. doi: 10.1038/s41590-018-0217-9

41. Hoffmann MM, Slansky JE. T-Cell receptor affinity in the age of cancer immunotherapy. *Mol Carcinog* (2020) 59(7):862–70. doi: 10.1002/mc.23212

42. Previte DM, Martins CP, O'Connor EC, Marre ML, Coudriet GM, Beck NW, et al. Lymphocyte activation gene-3 maintains mitochondrial and metabolic quiescence in naive CD4(+) T cells. *Cell Rep* (2019) 27(1):129–41. doi: 10.1016/j.celrep.2019.03.004

43. Ascione A, Arenaccio C, Mallano A, Flego M, Gellini M, Andreotti M, et al. Development of a novel human phage display-derived anti-LAG3 scFv antibody targeting CD8(+) T lymphocyte exhaustion. *BMC Biotechnol* (2019) 19(1):67. doi: 10.1186/s12896-019-0559-x

44. Grosso JF, Kelleher CC, Harris TJ, Maris CH, Hipkiss EL, De Marzo A, et al. LAG-3 regulates CD8+ T cell accumulation and effector function in murine self- and tumor-tolerance systems. *J Clin Invest* (2007) 117(11):3383–92. doi: 10.1172/JCI31184

45. Mei Z, Huang J, Qiao B, Lam AK. Immune checkpoint pathways in immunotherapy for head and neck squamous cell carcinoma. *Int J Oral Sci* (2020) 12(1):16. doi: 10.1038/s41368-020-0084-8

46. Huang CT, Workman CJ, Flies D, Pan X, Marson AL, Zhou G, et al. Role of LAG-3 in regulatory T cells. *Immunity* (2004) 21(4):503–13. doi: 10.1016/j.immuni.2004.08.010

47. Okamura T, Yamamoto K, Fujio K. Early growth response gene 2-expressing CD4(+)LAG3(+) regulatory T cells: The therapeutic potential for treating autoimmune diseases. *Front Immunol* (2018) 9:340. doi: 10.3389/fimmu.2018.00340

48. Camisaschi C, Casati C, Rini F, Perego M, De Filippo A, Triebel F, et al. LAG-3 expression defines a subset of CD4(+)CD25(high)Foxp3(+) regulatory T cells that are expanded at tumor sites. *J Immunol* (2010) 184(11):6545–51. doi: 10.4049/jimmunol.0903879

49. Liang B, Workman C, Lee J, Chew C, Dale BM, Colonna L, et al. Regulatory T cells inhibit dendritic cells by lymphocyte activation gene-3 engagement of MHC class II. *J Immunol* (2008) 180(9):5916–26. doi: 10.4049/jimmunol.180.9.5916

50. Avice MN, Sarfati M, Triebel F, Delespesse G, Demeure CE. Lymphocyte activation gene-3, a MHC class II ligand expressed on activated T cells, stimulates TNF-alpha and IL-12 production by monocytes and dendritic cells. *J Immunol* (1999) 16:10072520. doi: 10.1084/jem.171.5.1393

51. Gandhi MK, Lambley E, Duraiswamy J, Dua U, Smith C, Elliott S, et al. Expression of LAG-3 by tumor-infiltrating lymphocytes is coincident with the suppression of latent membrane antigen-specific CD8+ T-cell function in Hodgkin lymphoma patients. *Blood* (2006) 108(7):2280–9. doi: 10.1182/blood-2006-04-015164

52. Matsuzaki J, Gnjatic S, Mhawech-Fauceglia P, Beck A, Miller A, Tsuji T, et al. Tumor-infiltrating NY-ESO-1-specific CD8+ T cells are negatively regulated by LAG-3 and PD-1 in human ovarian cancer. *Proc Natl Acad Sci U.S.A.* (2010) 107(17):7875–80. doi: 10.1073/pnas.1003345107

53. Andrews LP, Yano H, Vignali D. Inhibitory receptors and ligands beyond PD-1, PD-L1 and CTLA-4: breakthroughs or backups. *Nat Immunol* (2019) 20(11):1425–34. doi: 10.1038/s41590-019-0512-0

54. McLane LM, Abdel-Hakeem MS, Wherry EJ. CD8 T cell exhaustion during chronic viral infection and cancer. *Annu Rev Immunol* (2019) 37:457–95. doi: 10.1146/annurev-immunol-041015-055318

55. Turnis ME, Andrews LP, Vignali DA. Inhibitory receptors as targets for cancer immunotherapy. *Eur J Immunol* (2015) 45(7):1892–905. doi: 10.1002/eji.201344413

56. Woo SR, Turnis ME, Goldberg MV, Bankoti J, Selby M, Nirschl CJ, et al. Immune inhibitory molecules LAG-3 and PD-1 synergistically regulate T-cell function to promote tumoral immune escape. *Cancer Res* (2012) 72(4):917–27. doi: 10.1158/0008-5472.CAN-11-1620

57. Chen J, Chen Z. The effect of immune microenvironment on the progression and prognosis of colorectal cancer. *Med Oncol* (2014) 31(8):82. doi: 10.1007/s12032-014-0082-9

58. Workman CJ, Vignali DA. The CD4-related molecule, LAG-3 (CD223), regulates the expansion of activated T cells. *Eur J Immunol* (2003) 33(4):970–9. doi: 10.1002/eji.200323382

59. Melaiu O, Lucarini V, Giovannoni R, Fruci D, Gemignani F. News on immune checkpoint inhibitors as immunotherapy strategies in adult and pediatric solid tumors. *Semin Cancer Biol* (2022) 79:18–43. doi: 10.1016/j.semcancer.2020.07.001

60. Jiang H, Ni H, Zhang P, Guo X, Wu M, Shen H, et al. PD-L1/LAG-3 bispecific antibody enhances tumor-specific immunity. *Oncoimmunology* (2021) 10(1):1943180. doi: 10.1080/2162402X.2021.1943180

61. Wang X, Bao Z, Zhang X, Li F, Lai T, Cao C, et al. Effectiveness and safety of PD-1/PD-L1 inhibitors in the treatment of solid tumors: a systematic review and meta-analysis. *Oncotarget* (2017) 8(35):59901–14. doi: 10.18632/oncotarget.18316

62. Jiang Z, Pan Z, Ren X. Progress of PD-1/PD-L1 inhibitors in non-small cell lung cancer. *Zhongguo Fei Ai Za Zhi* (2017) 20(2):138–42. doi: 10.3779/j.issn.1009-3419.2017.02.09

63. Bagchi S, Yuan R, Engleman EG. Immune checkpoint inhibitors for the treatment of cancer: Clinical impact and mechanisms of response and resistance. *Annu Rev Pathol* (2021) 16:223–49. doi: 10.1146/annurev-pathol-042020-042741

64. Legat A, Maby-El HH, Baumgaertner P, Cagnon L, Abed MS, Geldhof C, et al. Vaccination with LAG-3Ig (IMP321) and peptides induces specific CD4 and CD8 T-cell responses in metastatic melanoma patients–report of a phase I/IIa clinical trial. *Clin Cancer Res* (2016) 22(6):1330–40. doi: 10.1158/1078-0432.CCR-15-1212

65. Available at: https://www.fda.gov/drugs/resources-information-approved-drugs/fda-approves-opdualag-unresectable-or-metastatic-melanoma (Accessed Mar 21, 2022).

66. Sordo-Bahamonde C, Lorenzo-Herrero S, Gonzalez-Rodriguez AP, Payer AR, Gonzalez-Garcia E, Lopez-Soto A, et al. LAG-3 blockade with relatlimab (BMS-986016) restores anti-leukemic responses in chronic lymphocytic leukemia. *Cancers (Basel)* (2021) 13(9):2112. doi: 10.3390/cancers13092112

67. Available at: https://www.biospace.com/article/releases/u-s-food-and-drug-administration-approves-first-lag-3-blocking-antibody-combination-opdualag-nivolumab-and-relatlimab-rmbw-as-treatment-for-patients-with-unresectable-or-metastatic-melanoma/?s=74 (Accessed Mar 18, 2022).

frontiers | Frontiers in Immunology

TYPE Original Research
PUBLISHED 27 July 2022
DOI 10.3389/fimmu.2022.931612

OPEN ACCESS

EDITED BY
Yubin Li,
University of Pennsylvania,
United States

REVIEWED BY
Xi Lou,
University of Alabama at Birmingham,
United States
Qiaosi Tang,
University of Pennsylvania,
United States

*CORRESPONDENCE
Chongming Jiang
chongming.jiang@bcm.edu
Cheng-Chi Chao
Chengchi@biomap.com

SPECIALTY SECTION
This article was submitted to Cancer Immunity and Immunotherapy, a section of the journal Frontiers in Immunology

RECEIVED 29 April 2022
ACCEPTED 29 June 2022
PUBLISHED 27 July 2022

CITATION
Jiang C, Li J, Zhang W, Zhuang Z, Liu G, Hong W, Li B, Zhang X and Chao C-C (2022) Potential association factors for developing effective peptide-based cancer vaccines. *Front. Immunol.* 13:931612. doi: 10.3389/fimmu.2022.931612

Potential association factors for developing effective peptide-based cancer vaccines

Chongming Jiang[1,2,3]*, Jianrong Li[1,2,3], Wei Zhang[4], Zhenkun Zhuang[4], Geng Liu[4], Wei Hong[1,2,3], Bo Li[4], Xiuqing Zhang[4] and Cheng-Chi Chao[5]*

[1]Department of Medicine, Baylor College of Medicine, Houston TX, United States, [2]Dan L Duncan Comprehensive Cancer Center, Baylor College of Medicine, Houston, TX, United States, [3]Institute for Clinical and Translational Research, Baylor College of Medicine, Houston, TX, United States, [4]Institute of Super Cell, BGI-Shenzhen, Shenzhen, China, [5]Department of Pipeline Development, Biomap, Inc, San Francisco, CA, United States

Peptide-based cancer vaccines have been shown to boost immune systems to kill tumor cells in cancer patients. However, designing an effective T cell epitope peptide-based cancer vaccine still remains a challenge and is a major hurdle for the application of cancer vaccines. In this study, we constructed for the first time a library of peptide-based cancer vaccines and their clinical attributes, named CancerVaccine (https://peptidecancervaccine.weebly.com/). To investigate the association factors that influence the effectiveness of cancer vaccines, these peptide-based cancer vaccines were classified into high (HCR) and low (LCR) clinical responses based on their clinical efficacy. Our study highlights that modified peptides derived from artificially modified proteins are suitable as cancer vaccines, especially for melanoma. It may be possible to advance cancer vaccines by screening for HLA class II affinity peptides may be an effective therapeutic strategy. In addition, the treatment regimen has the potential to influence the clinical response of a cancer vaccine, and Montanide ISA-51 might be an effective adjuvant. Finally, we constructed a high sensitivity and specificity machine learning model to assist in designing peptide-based cancer vaccines capable of providing high clinical responses. Together, our findings illustrate that a high clinical response following peptide-based cancer vaccination is correlated with the right type of peptide, the appropriate adjuvant, and a matched HLA allele, as well as an appropriate treatment regimen. This study would allow for enhanced development of cancer vaccines.

KEYWORDS

cancer vaccine, peptide, clinical response, machine learning, potential factors

Introduction

Cancer is a heterogeneous disease with mixed clinical outcomes (1). Conventional cancer treatments tend to non-specifically kill tumor cells. Some of these tumor cells survive due to resistance to therapy and drug toxicity, eventually leading to tumor relapse and metastasis (2, 3). Cancer immunotherapy is a treatment strategy that uses a patient's own immune system to fight the cancerous cells (4, 5). Immunotherapy has become a promising alternative cancer treatment after surgery, radiotherapy, and chemotherapy in recent years because of its mild side effects and significant therapeutic benefits (6–8). T cell epitope peptide-based cancer vaccine is one of the representative strategies of cancer immunotherapy, relying on short peptide fragments to engineer the induction of highly targeted immune responses (9–11).

Previous studies (12–17) have demonstrated the effectiveness of peptide-based cancer vaccines in treating several common types of cancer, such as breast cancer, melanoma, colorectal and lung cancer. This strategy exploits the fact that the surfaces of cancer cells have various peptide epitopes (i.e., peptides of usually 8-17 residues in length), which bind to major histocompatibility complex (MHC) proteins. T cells can attack these cancer cells after recognizing the peptide/MHC complex (18). T cells aimed to induce immune recognition of tumor cells are then able to eradicate them by generating a sustained and potent anti-tumor immune response. Therefore, a key determinant for an anti-tumor immune response to lead to the effective killing of cancer cells is the selection of immunogenic peptide epitopes as the target (19). Many peptide epitopes have been identified and molecularly characterized in experiments (12–17). While there are many options in selecting immunogenic antigens, it is not clear which selected epitopes can induce the dominant immune system mediated by T cells. Many clinical studies in cancer vaccines have been initiated to assess the therapeutic potential of active immunization or vaccination with peptide epitopes in cancer patients. However, it is still unclear what the ideal characteristics of selected peptide epitopes should be and which could induce stronger anti-tumor responses. Therefore, it remains highly challenging to design an effective cancer vaccine that can achieve a meaningful clinical benefit in patients.

There have been many breakthroughs in prior studies that investigated the optimal conditions for designing a peptide-based cancer vaccine (20–25). Thomas et al, Zhang et al, and Liu et al found differences in the therapeutic efficacy of peptide-based cancer vaccines prepared from different sources of peptides (26–28). Furthermore, patients with certain HLA alleles might be more sensitive to respond to cancer vaccines (29, 30). The same cancer vaccine with different adjuvants might also have an impact on the outcome of treatment (28, 31). In addition, different treatment strategies could also affect the efficacy and side effects of cancer vaccines, such as the dose of vaccine used, injection interval, number of injections, and injection methods (28, 32). However, due to the limited number of clinical trials available, combined with the difference in cancer types and patient conditions, it is difficult to improve a cancer vaccine design by directly referring to the design of other cancer vaccines. Machine learning (ML) options such as Random forest (RF) (33)could improve cancer vaccine design by utilizing large data repositories to identify novel features and more complex interactions among these features.

In this study, a library of peptide-based cancer vaccines used in clinical studies from public and private sources was established from multiple sources, such as PubMed, ClinicalTrials.gov, and Web of Science, using databases up to January 1, 2022. The statistical analysis of types of peptides, adjuvants, treatment regimen, human leukocyte antigen (HLA) alleles of peptides, and other features in vaccine therapy was obtained from the results in high clinical response (HCR) and low clinical response (LCR) in the database to find the associations which influence the treatment effect of cancer immunotherapy. Finally, we built a random forest model to help distinguish which kinds of cancer vaccines in patients are most likely to achieve a high clinical response.

Material and methods

Data utilized in this study screening and extraction

We screen and extracted all the peptide-based cancer vaccine relevant studies, retrieved from the PubMed, ClinicalTrials.gov, and Web of Science, using databases up to January 1, 2022. All studies were browsed, searched, prioritized, and filtered by the investigators based on the keywords: peptide*, vaccine*, cancer/tumor*, human, HLA, clinical. These extracted studies were then reviewed according to the inclusion and exclusion criteria. In cases in which the results obtained were different, the case was discussed further to obtain consensus. Further details are provided in the following sections. Finally, A total of 705 peptides resulting from 152 clinical studies containing peptide-based cancer vaccine features and clinical treatment information were registered in our library, which has been posted to our web-accessible library, CancerVaccine (https://peptidecancervaccine.weebly.com/).

Inclusion criteria

The inclusion criteria were as follows: 1. The study focused on human cancer research. 2. The study used the peptide as the vaccine to treat cancer patients. 3. They are not review reports; there are cancer detail descriptions and treatment information about the clinical trials.

Exclusion criteria

The exclusion criteria were as follows: 1. The peptide-based cancer vaccine was not associated with humans. 2. There was no associated peptide information. 3. There was no treatment information for the peptide-based cancer vaccine.

Feature selection procedure

Exploratory data analysis: First, we checked the types of variables. There were no missing values in the data (Figure S3A). Next, we created a bar graph for the categorical variables; if the levels of all categorical variables looked correct, we kept the original levels for these variables (Figure S3B). Finally, four features were recommended for the model: injection interval and injection time, adjuvants, and HLA alleles; the blue dot represents the optimal solution, as shown in Figure S3C.

Classifier

We use a random forest model (random Forest package in R) (34) to construct a feature-based classifier. The prediction performance (estimated by 10-fold cross-validation) is best when the top 4 features with the most differentiation are included (injection interval, injection times, adjuvant types, and HLA alleles), indicating that these 4 features have the greatest differentiation power. Using these 4 features as predictors, the area under the receiver operating characteristic (ROC) curve (AUC) was 0.97. The ROC curves were plotted using the pROC R package.

The area under the precision-recall curve

For computing the AUPRC, we used the function metrics.precision_recall_curve and metrics.auc from the R package, ROCR 1.0-11 version (35). We first randomly divided the library cohort with known high or low clinical response into a training set (50% randomly selected samples) and a test set (50% randomly selected samples) based on cancer type. Then, the merged training set was used as the training set and the merged test set was used as the test set. Finally, we logit-transformed AUPRC values before testing (using two-tailed Welch's t-test). We carried out 1,000 replications of 5-fold cross-validation; within each replication, across the 5-folds, we obtained prediction scores for each cancer type from the fold in which the cancer type was in the test set, enabling us to compute an overall AUPRC within each replication.

Statistical analysis

The R statistical package was used for all data processing and statistical analysis (R package: stats v3.6.2). All details of the statistical tests are specified in the associated text or figure legends. For the statistical analyses, P-values were calculated by using the "Wilcox_test" function from the R package: stats v3.6.2, which applies the two-sided Wilcoxon rank-sum test and corrected multiple testing using the Holm–Bonferroni method. A statistically significant difference was assumed when $P \leq 0.05$.

Results

Data filtering and features of selected trials

To investigate what classes of peptide-based cancer vaccine can help achieve satisfactory results from clinical treatment, we reviewed a total of 302 relevant studies, retrieved from the PubMed, ClinicalTrials.gov, and Web of Science, using databases up to January 1, 2022. PubMed.gov is a free search engine that accesses the MEDLINE database on life sciences and biomedical topics primarily at the U.S. National Institutes of Health's National Library of Medicine. The database of ClinicalTrials.gov is a service of the U.S. National Institute of Health. After removing duplicates, we screened 206 potentially relevant articles by scanning the titles and abstracts. We reviewed the full text and screened the candidate studies according to the inclusion criteria, and 43 studies were excluded. Of the remaining 163 studies, 11 were excluded due to describing the same repeated clinical trials. A total of 705 peptides resulting from 152 clinical studies containing peptide-based cancer vaccine features and clinical treatment information were registered in our library (12–14, 36–163). Details of the study identification process can be found in Figure 1A. The final study population included 6,713 participants. All studies were retrospective studies published between January 1, 1997 and January 1, 2022, and involved various tumor types. The details of the library in this study have been posted to our web-accessible library, CancerVaccine (https://peptidecancervaccine.weebly.com/).

In order to analyze this library in a comprehensive and in-depth manner, we mapped the types of cancer and peptide, adjuvant, HLA allele, and treatment regimen (injection interval and injection times) landscapes of the library, as shown in Figures 1B-G, respectively. We found that melanoma, colorectal cancer, and breast cancer are the most common cancer types investigated in cancer vaccine therapy (Figure 1B). The peptides were divided into five categories based on the origin of peptides: tumor expressed peptides, tumor overexpressed peptides, fusion peptides, modified peptides, and single-nucleotide variant (SNV) peptides. For tumor expressed peptides, the genes in which the peptides were co-expressed are found in both cancer and normal tissues (144, 164–166). For tumor overexpressed peptides, the genes in which the peptides were located are found overexpressed in the tumor tissue only (129, 167, 168). For fusion peptides, the peptides were derived from gene fusion (57, 122, 130, 136, 155). For modified peptides, the amino acids (AA) had been artificially modified (15, 65, 67, 89, 99, 107, 110, 118, 134, 138, 147, 169–171).

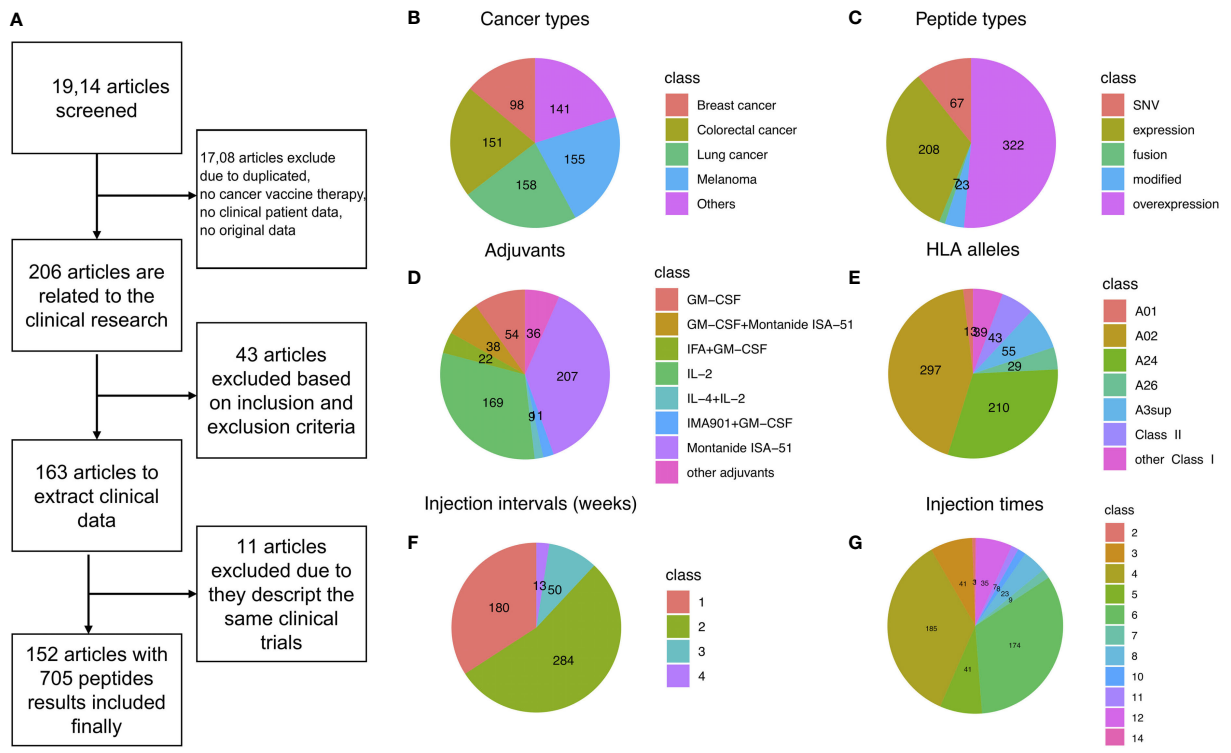

FIGURE 1
Data filtering summary landscape of the library, CancerVaccine (https://peptidecancervaccine.weebly.com/). **(A)** Data filtering process. **(B)** The landscape of cancer types. **(C)** The landscape of peptide types. **(D)** The landscape of adjuvants. **(E)** The landscape of HLA alleles. **(F)** The landscape of treatment regimen (injection interval). **(G)** The landscape of treatment regimen (injection times).

The SNV derived peptides were neoantigen, or a new AA sequence that forms on cancer cells when somatic mutations occur in tumor DNA sequences (40, 44, 58, 62, 67, 70, 80, 83, 84, 106, 114, 117, 123, 131, 143, 152, 156, 159, 161, 163, 165).

We found that more than half the peptides (51.4%) used in cancer vaccine preparation were overexpressed in the targeted tumor cells (Figure 1C). We also found that Montanide ISA-51 was the most widely used adjuvant in cancer vaccines. IL-2 was the most widely used cytokine as a vaccine adjuvant in cancer vaccines (Figure 1D). Interestingly, most clinical phase peptides are focused on the HLA class I alleles, especially the A02 and A24, as shown in Figure 1E. In addition, we noted that more than half of peptide-based cancer vaccines were injected weekly (53.9%, Figure 1F) and more than half of the patients had greater than four vaccine injections (Figure 1G).

The prognostic evaluation of anti-tumor effect in clinical trials

After building this library, we wanted to further explore the causes which influence the effectiveness of peptide-based cancer vaccine results. We divided these peptide-based cancer vaccine results into high clinical response (HCR) and low clinical response (LCR) results based on their clinical efficacy and safety (172).

The specific classification criteria and basis of a high clinical response were presented in the form of an evolutionary tree, as shown in Figure 2. The prerequisite criteria was whether there have been any vaccine-related deaths; if there were vaccine-related deaths, it was excluded from this study. A total of 78 peptides which involved 673 patients were excluded from this study. We next examined whether patients in the best objective response (complete or partial response, according to modified World Health Organization criteria) had been reported (172–174). Due to the complex tumor microenvironment and vaccine technology limitations, it is difficult to achieve a complete response with vaccine therapy; therefore, the best objective response indicates that the clinical response of the vaccine therapy is high (175). We also looked at cases where there were no best objective response patients, investigating whether more than 50% of patients achieved stable disease (SD) or progression-free survival (PFS) if the previous conditions were not met. If more than half of the patients achieved SD or PFS, we took this as an indication that the cancer vaccine was effective (174, 176). Finally, we compared whether the overall survival time was significantly longer in the

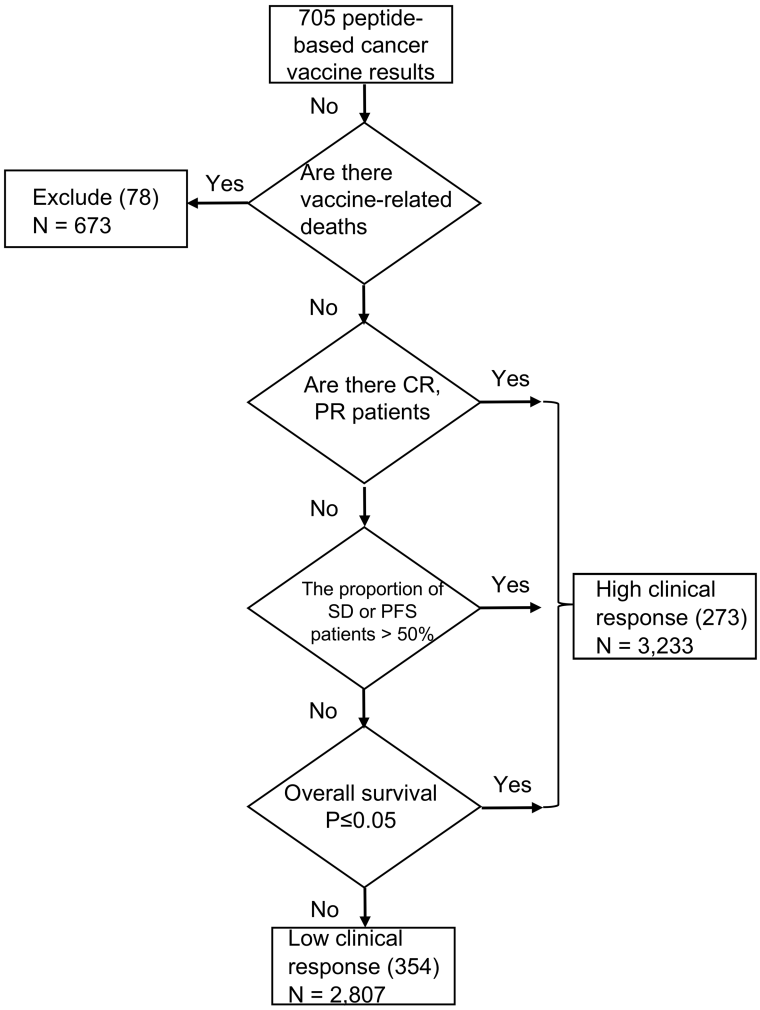

FIGURE 2
Cancer vaccine criteria and feature comparison. The specific criteria of a clinical treatment response. A total of 78 peptides resulting which involved 673 patients were excluded. 273 high clinical response results (3,233 patients involved) and 354 low clinical response results (2,807 patients involved) were finally included in this study.

vaccine group than in the control group; a significantly longer overall survival time in the vaccine group could also indicate that the vaccine worked well (177, 178). If none of these progressive conditions were met, then the clinical result was classified as a low clinical response result. The clinical efficacy evaluation was performed using the immune-related response criteria (irRC) (179) and response evaluation criteria in solid tumors (RECIST 1.1) standard criteria (180). Toxicities were reported using the World Health Organization grading system (181). In total, 273 high clinical response results (3,233 patients involved) and 354 low clinical response results (2,807 patients involved) were included in this study (Figure 2).

To further investigate which factors influence the efficacy of cancer vaccines, we specifically explored the types of peptides, HLA alleles, adjuvants, and treatment regimens (injection interval and injection times) in the high and low clinical response groups. Further details are provided in the following sections.

Modified and tumor overexpressed peptides could be suitably selected for cancer vaccines

Cancer vaccines face a number of challenges, including finding suitable sources of peptides that work best *in vivo*. The peptides were divided into five categories based on the origin of peptides (182, 183): the tumor expressed peptides, tumor overexpressed peptides, fusion peptides, modified peptides, and single-nucleotide variant (SNV) peptides. We summarized their

distribution in the results from high and low clinical responses (Figure 3). As shown in Figure 3A, most of the peptides in the library are expressed or overexpressed in cancer. The overexpressed peptides achieved many of the high clinical response results (41.3%), especially in colorectal cancer (59.6% *vs.* 40.4% in high *vs.* low clinical response results, Figures 3A, C). The fusion cancer vaccines were not as efficacious in clinical trials, as they did not lead to any high clinical responses (Figure 3A). However, modified peptides, in which the amino acids (AA) were artificially modified, appeared to be the most suitable method for cancer vaccine (69.6% of modified peptides achieved high clinical response results), especially for melanoma immunotherapy (84.2%, Figures 3B, C). In this study, we also listed the top 8 most frequent peptide gene names and the top 18 most commonly used peptides, as shown in Figure S1.

HLA class II peptide-based cancer vaccines could achieve high clinical response results

The cytotoxic T cell (CTL) epitope peptides were restricted with HLA alleles when they were prepared as cancer vaccines (102, 184–186). Previous studies have reported that an accurate HLA allele is a key factor in successful cancer vaccinations (186, 187). More than 90% of cancer vaccines in our library are typed for HLA Class I alleles (Figure 4A), with the most common being HLA- A02, A24, A3sup, A26, and A01. This is generally consistent with the proportional rank of these alleles in the population (188, 189). We noticed that patients with melanoma achieved more high clinical response results when using peptides typed for HLA-A01 and HLA Class II. For example, all peptides with HLA-A01 alleles achieved high clinical response results in melanoma (13 *vs.* 0, Figures 4B, C), although this is limited by the sample size and we may need more data to verify whether a similar trend exists in other cancer types (Figure S4). The peptides with HLA Class II alleles also achieved more high clinical response results (28 *vs.* 15, P = 0.0049, Figures 4A, B), especially for melanoma and lung cancer patients (Figure 4C). HLA Class II alleles are highly associated with the CD4+ T cells; CD4+ T cells primarily mediate anti-tumor immunity by providing help for CD8+ CTL and antibody responses, as well as *via* secretion of effector cytokines such as interferon-γ (IFNγ) and tumor necrosis factor-α (TNFα). Under specific contexts, they can also mediate anti-tumor immunity *via* direct cytotoxicity against tumor cells (190–193). Therefore, peptide epitopes targeting HLA Class II could be more likely to achieve high clinical response results.

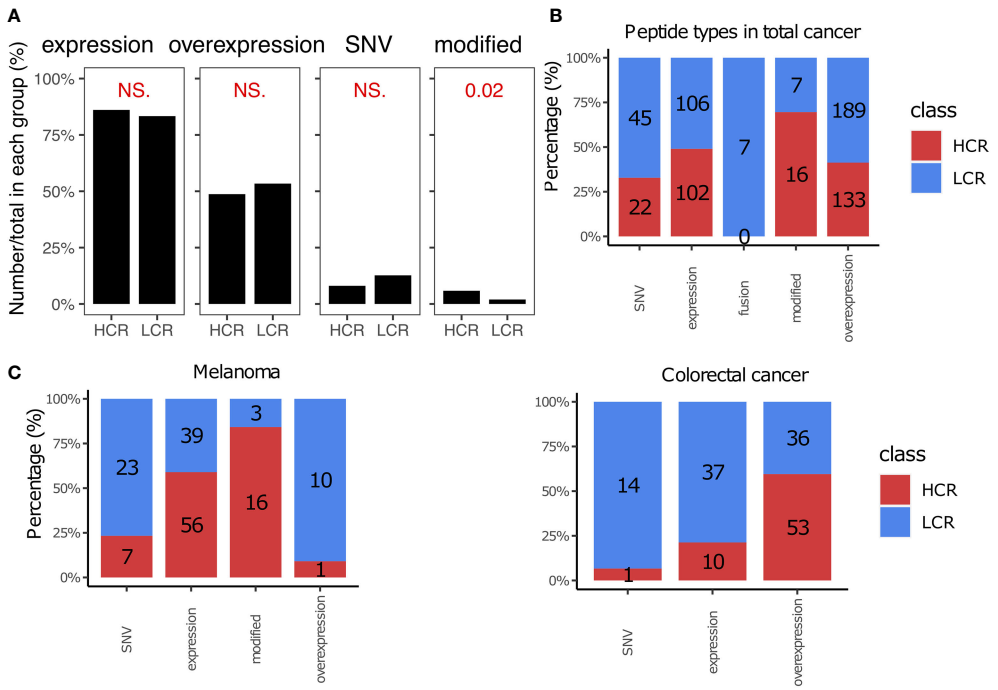

FIGURE 3
Peptide types in high and low clinical response results. **(A)** Comparison of peptide types between high clinical response (HCR) results and low clinical response (LCR) results. The distribution of peptide types in HCR and LCR results. **(B)** The distribution of peptide types in HCR and LCR results. **(C)** The distribution of peptide types in HCR and LCR results in melanoma and colorectal cancer, respectively. P-values were calculated using two-sided Wilcoxon rank-sum tests. NS., not significant.

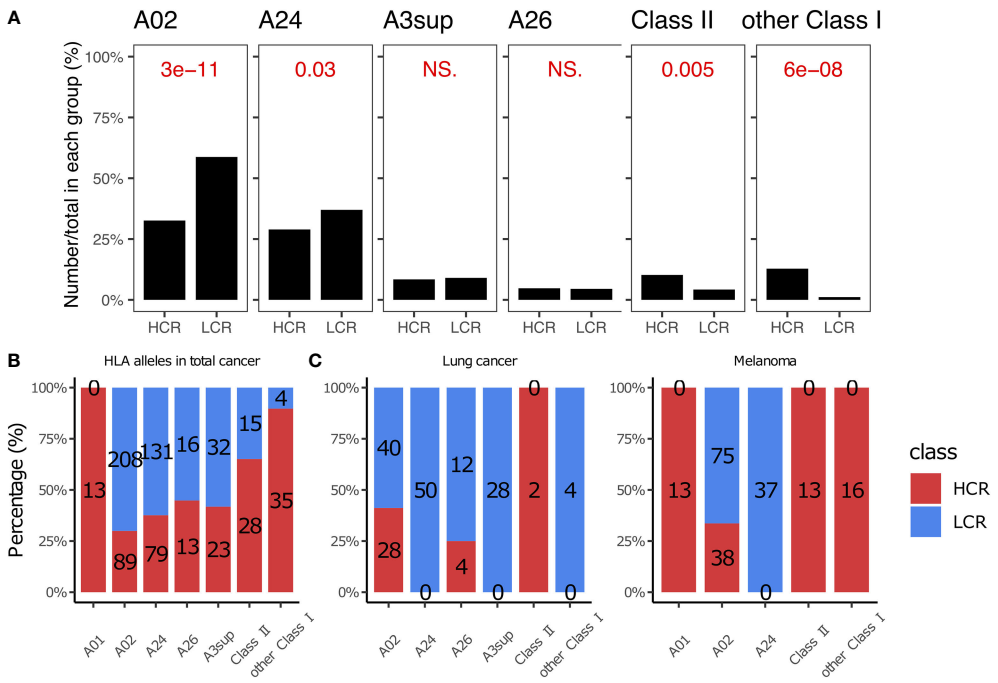

FIGURE 4
HLA alleles in high and low clinical response results. **(A)** Comparison of HLA alleles between HCR and LCR results. **(B)** The distribution of HLA alleles in HCR and LCR results. **(C)** The distribution of HLA alleles in HCR and LCR results in melanoma and lung cancer, respectively. P-values were calculated using two-sided Wilcoxon rank-sum tests. NS, not significant.

Montanide ISA-51 was identified as an effective adjuvant in the treatment of cancer vaccines, especially for breast and colorectal cancers

An adjuvant is an ingredient that can help create a stronger immune response in patients receiving the vaccine (194, 195). Many cancer vaccines use adjuvants to enhance therapeutic efficacy.

We found that Montanide ISA-51 and Granulocyte-macrophage colony-stimulating factor (GM-CSF) were the two most widely used adjuvants in cancer vaccines (Figure 5A), and they also appeared most frequently in high clinical response results (P = 6.83e-19 and 0.045, respectively, Figures 5A, B). Montanide ISA-51, in particular, was the most frequently used adjuvant with high clinical response results (59.4%, Figure 5B), especially in breast cancer and colorectal cancer (92.1% and 95.6%, respectively, Figure 5C). Cytokines in cancer immunity and immunotherapy, cytokine modulation is necessary for efficacious treatment of experimental neuropathic pain (196). IL-2, IL-4, and IL-12 were the most widely used cytokines as vaccine adjuvants, especially IL-2, which was used as an immune adjuvant in many kinds of cancer types, such as lung cancer, colorectal cancer, and melanoma (Figure 5C). However, IL-2, IL-4, and IL-12 are not very effective when used alone in peptide-based cancer vaccines (Figures 5B, C).

Treatment regimens with weekly intervals and greater than four injections could be more likely to achieve a better clinical response

The type of treatment regimen is also one of the major challenges affecting the effectiveness of cancer vaccine therapy (32, 197, 198). We evaluated the influences of treatment regimens on cancer vaccine efficacy.

Our study found a significant difference in the vaccine injection intervals between the HCR and LCR results (Figure 6A, left). Treatment regimens with shorter vaccine injection intervals yielded more high clinical response results. The number of high clinical response results decreases from 141 to 4 with the increase in vaccine injection intervals, implying that shorter vaccine injection intervals (weeks) may be more favorable for patients to achieve high clinical response results, as shown in Figure 6A. We also found that the number of vaccine injections associated with high clinical response results was significantly higher than that of the low clinical response results (Figure 6A, right). Patients with greater than four vaccination injections achieved more high clinical response results (Figure 6C). We also found similar results in main cancer types, such as breast cancer, melanoma, colorectal cancer, and lung cancer. The details are shown in the

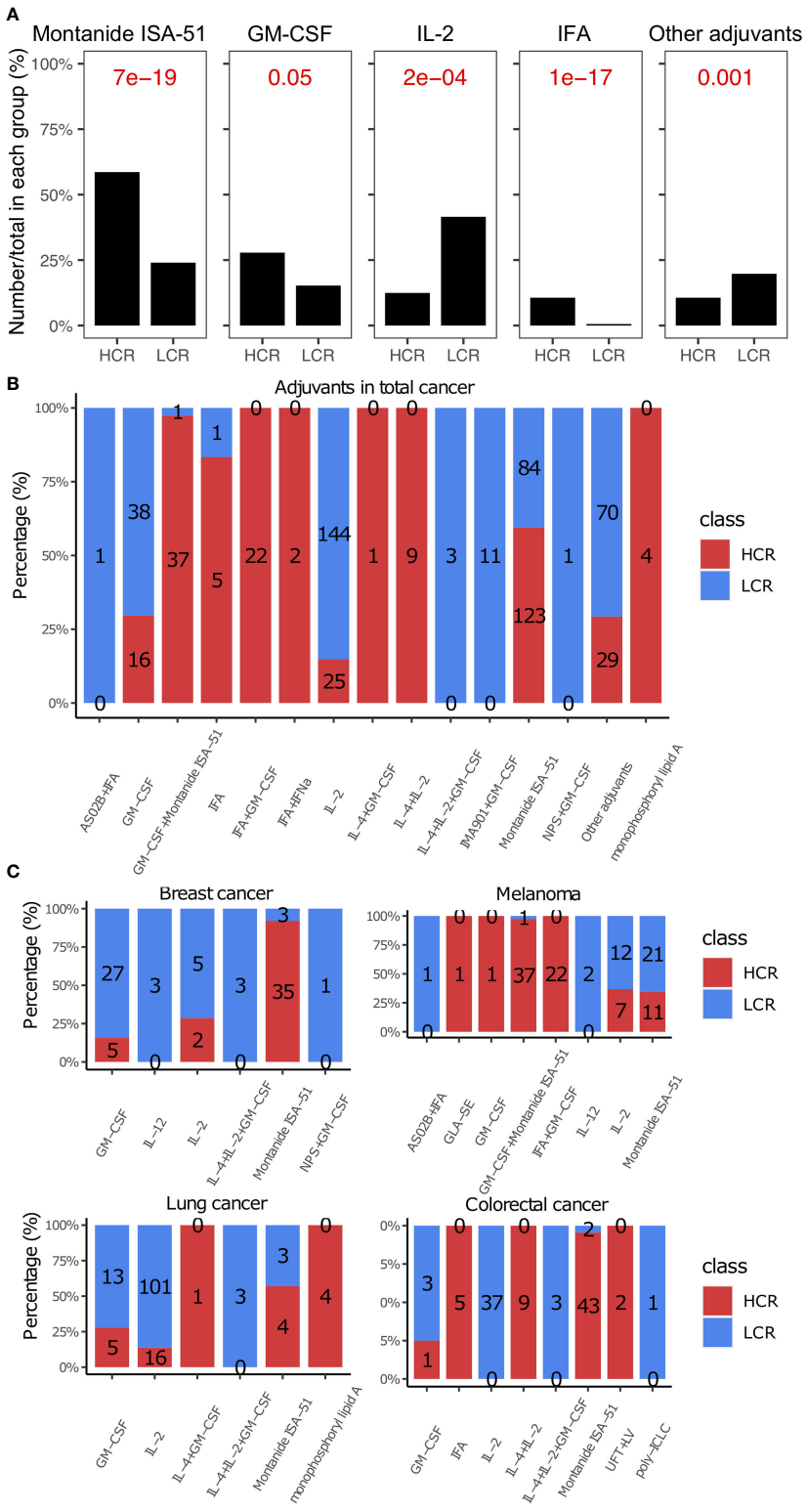

FIGURE 5
Adjuvants in high and low clinical response results. **(A)** Comparison of adjuvants between HCR and LCR results. **(B)** The distribution of adjuvants in HCR and LCR results. **(C)** The distribution of adjuvants in HCR and LCR results in four main cancer types (breast cancer, melanoma, lung cancer, and colorectal cancer). P-values were calculated using two-sided Wilcoxon rank-sum tests.

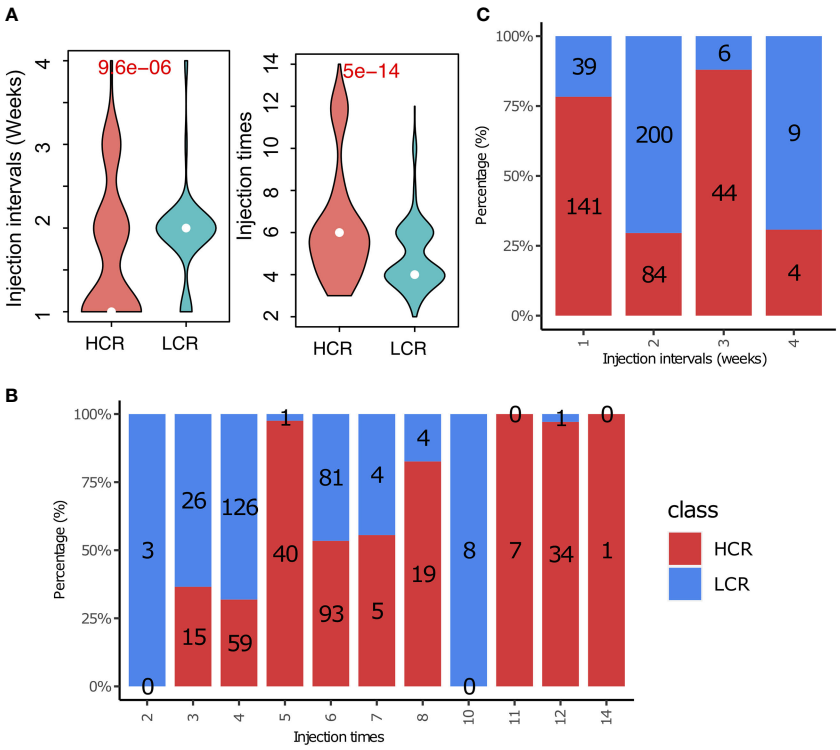

FIGURE 6
Treatment regimens play an important role in cancer immunotherapy. **(A)** The distribution of treatment regimens (injection interval) in HCR and LCR results. **(B)** The distribution of treatment regimens (injection times) in HCR and LCR results. **(C)** Comparison of treatment regimens (injection interval and injection times) between HCR and LCR results. P-values were calculated using two-sided Wilcoxon rank-sum tests.

supplement materials [injection interval (Figure S2A) and injection times (Figure S2B), respectively].

Generation of a random forest model from clinical responses for cancer vaccines

Given that some redundant or irrelevant features in the new data set may exert an influence on the classifying effects of a machine learning model, the importance value of cancer vaccine features was first calculated by means of a Random Forest algorithm, followed by the selection of the optimal features based on each feature's importance (Figure 7A and Supplemental Figure S3). From the methodological perspective of feature selection, the random forest is a kind of embedded feature selector that can automatically produce the relative importance of features during the model training process. We investigated the relative importance of multiple features, such as the peptide types, adjuvant, HLA alleles, tumor stages, chemotherapy, and treatment regimens, in cancer vaccines. Four features were chosen for the random forest-based modeling in this study: injection interval, injection times, adjuvant types, and HLA alleles (Figure 7A).

For the random forest-based modeling, the library cohort with known high or low clinical response was randomly split into a training set (50% randomly selected samples) and a test set (50% randomly selected samples) according to the cancer types. The merged training set was used as the training set and the merged test set as the test set. The model was trained on the training set and tested on the test set, with 1,000 repeated nested 5-fold cross-validation. The model achieved a high area under the curve (AUC) of 0.97 sensitivity on the test set (Figure 7B, black curve). The prediction model's performance was first assessed in four independent cancer type cohorts (breast cancer, melanoma, lung cancer, and colorectal cancer) with the equilibrium of class distribution and balanced data. Our model also achieved AUCs of 0.87, 0.99, 0.99, and 0.98 for independent breast cancer, melanoma, lung cancer, and colorectal cancer datasets, respectively, demonstrating that our model could predict their vaccine responses from the features we selected (Figure 7B). In addition, the prediction model was also evaluated from the perspectives of the average precision score and precision-recall (AUPRC) (Figure S3D).

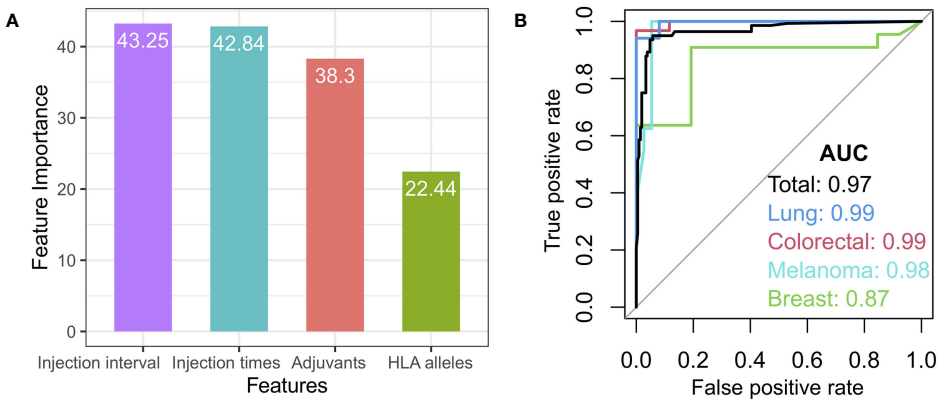

FIGURE 7
Features selection and model. **(A)** The variable importance for the selected features, such as injection interval, injection times, adjuvant types, and HLA alleles. **(B)** Receiver Operating Characteristic (ROC) curve for the total test set (black) and independent breast cancer (green), melanoma (light blue), lung cancer (blue), and colorectal cancer datasets (red).

Random forest yields high discriminative performance in cancer vaccine clinical response prediction. Thus, the model could be helpful in identifying cancer vaccines with high clinical responses.

Discussion

Immunotherapies such as peptide-based cancer vaccines have proven to be effective in enhancing the immune response in cancer patients to fight cancer cells. Cancer vaccines that specifically target high expression of gp100 in melanoma have already been approved (199). However, one of the key factors limiting the application of immunotherapy is how to rationally design a peptide-based cancer vaccine that generates an anti-tumor immune response leading to the effective killing of tumor cells (200–202). The goal of our study is to determine the key criteria for cancer vaccines that may lead to better clinical outcomes.

We collected T cell epitopes from several databases that had been applied to clinical studies to construct *in silico* a library of peptide-based cancer vaccines. These candidate T cell epitopes could activate CD8+ or CD4+ T cells to induce cytotoxicity for tumor cells. The selected peptide epitopes could be used as cancer vaccines or as target antigens for adoptive cell therapy of DC, CTL, TCR-T, and CAR-T cells. To find the associations which influence treatment effectiveness of cancer vaccines, several critical factors, including types of peptides, HLA alleles, adjuvants, and treatment regimens, were analyzed in patients with high and low clinical responses.

We found that studies often chose tumor expressed or overexpressed peptides to prepare cancer vaccines (Figures 1, 3). However, modified peptides in which the amino acids (AAs) always were artificially modified, could be more suitable for cancer vaccines, especially for melanoma immunotherapy (65, 67, 79, 99, 110, 118, 147) (Figure 3). The reason modified peptides are more effective may be because the AAs of modified peptides are altered and these modified peptides will be treated as exogenous peptides, which are more easily recognized by T cells and therefore more immunogenic (12, 203–205). Alternatively, the genes of these modified peptides are always expressed or overexpressed in tumor cells (Figure S1), and their comparative wild-type peptides are usually known to have binding affinities for certain HLA alleles (206–208). Based on this information, we could make targeted modifications to the modified peptides, further enhancing the affinity of modified peptides for pMHC, potentially making modified peptides more immunogenic and therapeutically effective. However, it is possible that modified peptides are also expressed in normal cells, which could lead to uncertain side effects (205, 208).

Based on our study, Montanide ISA-51, in particular, was the most frequently used adjuvant with high clinical response results (59.4%, P = 1.3e-17, Figure 5), especially in breast cancer and colorectal cancer (92.1% and 95.6%, respectively, as shown in Figure 5A, C). Montanide ISA-51 can enhance antigen-specific antibody titers and cytotoxic T-lymphocyte responses. Doorn et al. reported that a proper mixture of peptide epitopes and Montanide ISA-51 could help effectively avoid or mitigate adverse events (209, 210). Because cytokine modulation is necessary for efficacious treatment of experimental neuropathic pain (196). Many cytokines, such as IL-2, IL-4, and IL-12, were widely used cytokines as vaccine adjuvants. IL-2 in particular was used as an immune adjuvant in many cancer types, such as lung cancer, colorectal cancer, and melanoma. However, as vaccination

adjuvants, these cytokines are less efficient than Montanide ISA-51 or GM-CSF (Figure 5). There are several possible explanations for this. One explanation is that cytokines are susceptible to degradation due to their short half-life (211, 212). Another explanation could be that the main role of adjuvants is to activate the immune system and activate effector T cells (194). If we use IL-2, IL-4, and IL-12 as the adjuvant in cancer vaccine therapy, we need them to activate effector T cells. However, IL-2 has a higher affinity and stimulatory effect on regulatory T cells (Tregs). Therefore, IL-2 will activate Treg cells along with effector T cells. Tregs are a specialized subpopulation of T cells that act to suppress the immune response. Thus, it is difficult to achieve a high clinical response with IL-2 alone. IL-4 is a cytokine that induces the differentiation of naive helper T cells (Th0 cells) to Th2 cells, thereby inducing immunosuppression (213). Therefore, IL-4 generally does not have a good antitumor effect in cancer vaccines as an adjuvant alone. IL-12 is an interleukin that is naturally produced by dendritic cells (214). It has a strong anti-tumor therapeutic effect, but IL-12 is difficult to use in molecular therapy alone (215). Thus, IL-2, IL-4, and IL-12 are not very effective when used alone in peptide-based cancer vaccines. Antigen-specific specificity is important in cancer vaccinations. However, antigen-specific cytokines do not exist; cytokines can activate many non-specific or tumor growth promoting pathways, which is ineffective and unhelpful for the specificity of a cancer vaccine (216, 217). IL-2, IL-4, and IL-12 may need to be modified or combined with other adjuvants, such as Montanide ISA-51 or GM-CSF in peptide-based cancer vaccine therapies to increase effectiveness.

In addition to these cancer vaccines that utilized various adjuvants, we also observed that many cases did not use any adjuvants in cancer vaccine preparation, which could be a factor leading to the poor clinical outcomes of many peptide vaccinations in clinical trials (38, 41, 49, 53, 68, 72, 74, 81, 82, 86, 95, 98, 110, 117, 127, 131, 143, 151, 160, 218–221)

The treatment regimen also plays an important role in the therapeutic efficacy of cancer vaccines. The treatment regimens with weekly injection intervals and greater than four vaccination injections were more likely to achieve a high clinical response (Figure 6). Short vaccine injection intervals and multiple vaccinations could continually activate the immune system, ensuring that there are enough cytotoxic T cells to kill tumor cells, enhancing the tumor-killing effect and making it easier to get a high clinical response (222). However, many of the available treatment regimens did not use shorter vaccine intervals and more frequent injections. This could be because many of the patients who participated in the cancer vaccine clinical trials had gone through various conventional treatments, and many of them also had stage III or stage IV tumors. As a result, they were already in a weakened condition. Shortened vaccination intervals and an increased frequency could lead to stronger side effects that would be difficult for these weaker patients to tolerate. Therefore, shorter intervals and more frequent injections may be more appropriate for patients with early-stage tumors, while relatively frail patients could have longer injection intervals, but no less than four injections are recommended.

Finally, we investigated the correlation between multiple features, such as the peptide types, adjuvant, HLA alleles, and treatment regimens, in cancer vaccines, and we built a random forest model to distinguish the peptide-based cancer vaccines with high clinical responses (Figures 7, S3). In addition, we also investigated the effect of the tumor stages and chemotherapy, which could reflect the patient's health condition and medical treatment prior to vaccination on the model prediction. We summarized their distribution in the results from the high and low clinical responses (Figures S4A, B). The relative importance of the tumor stages and chemotherapy are weaker than the peptide types, adjuvant, HLA alleles, and treatment regimens in this study (Figure S4C). The prediction accuracy of our model was also not improved by introducing them (Figure S4D). Possible causes for this are that many clinical trials included patients with different tumor stages, and some others omitted patients' tumor stages information. There is no significant difference between the chemotherapy group and the no or unknown chemotherapy group (Figure S4B). The cause could be that many of the cancer vaccine trials included patients who had undergone conventional medical treatments, which included but are not limited to chemotherapy. Moreover, some clinical trials excluded patients who had received chemotherapy (41, 45) or required patients to wait a period of time after chemotherapy before participating in cancer vaccine therapy to eliminate and minimize the impact of chemotherapy on vaccine therapy (49, 64, 74, 133, 220). Therefore, we think that the tumor stage and chemotherapy may have less impact on the improvement of prediction accuracy (Figure S4D).

We found a combination of the modified peptides, Montanide ISA-51, a short interval between vaccine injections, and multiple vaccinations could be helpful in effectively activating the immune system to kill tumors, enhancing the tumor-killing effect, and resulting in high clinical responses.

The severe acute respiratory syndrome coronavirus 2 (SARS-CoV-2) virus is prone to specific mutations that alter viral surface peptide epitopes, making the virus more susceptible to immune escape (223). Peptide-based tumor vaccine research has also contributed to the development of COVID-19 vaccines targeting COVID-19-specific peptide epitopes (224, 225).

There are several limitations noted in this study. First, there are no prior studies that quantitatively distinguish between high or low results in cancer vaccine clinical trials; it is possible that we missed information in classifying a high or low response result. Next, due to lack of sufficient data for a single tumor type, we could not directly explore the difference in each cancer type between the high- and low- clinical response groups.

In addition, the effect of the tumor mutation burden, the dose of the cancer vaccine, and the specific method of injection, such as subcutaneous, intranasal, intravenous, and transdermal, may also need to be further explored in the future studies. Lastly, the effect of coupling multiple features on cancer vaccine efficacy is complex and was not investigated in depth in this study. Thus, future studies can explore further the effects of coupling multiple features on cancer vaccine efficacy based on a larger cohort.

Altogether, we presented CancerVaccine, a peptide-based cancer vaccine library that stored and aggregated the results of peptide-based cancer vaccines and their clinical attributes. CancerVaccine can be accessed at https://peptidecancervaccine.weebly.com/. We demonstrated that CancerVaccine is a versatile resource that can be used to screen for useful peptides epitopes and aid in the design of new cancer vaccines. Our study describes a design strategy in peptide vaccination treatment relating to the appropriate types of peptides, suitable adjuvants, matched HLA alleles, and suitable treatment regimens. Furthermore, we developed a high AUC machine learning model, which could be helpful in identifying peptide-based cancer vaccines with high clinical responses. The results of this study could impact future exploration of vaccine designs, taking into consideration identifying suitable peptide antigens and treatment conditions for cancer and personalized immunotherapy.

Data availability statement

The original contributions presented in the study are included in the article/**Supplementary Material**. Further inquiries can be directed to the corresponding author/s.

Author contributions

C-CC and CJ conceived the project. CJ, JL, WZ, ZZ, and GL prepared and analyzed the database. CJ and C-CC, evaluated the conclusions, wrote the manuscript. CJ, C-CC, WH, BL, and XZ reviewed and revised the content. All authors read and approved the final manuscript. All authors contributed to the article and approved the submitted version.

Funding

This work is supported by the Cancer Prevention Research Institute of Texas (CPRIT) (RR180061).

Acknowledgments

We would like to give special thanks to Chao Cheng and other members of the Chao Cheng lab for their valuable discussions and critical feedback. We especially thank Aude Angelini, Xiaoshi Zhang, Si Qiu, Wenhui Li, and Xiuying Li for their valuable suggestions.

Conflict of interest

Author C-CC was employed by the company Biomap, Inc. Authors WZ, ZZ, GL, XZ and BL are employed by the company BGI-Shenzhen.

The remaining authors declare that the research was conducted in the absence of any commercial or financial relationships that could be construed as a potential conflict of interest.

Publisher's note

Supplementary material

The Supplementary Material for this article can be found online at: https://www.frontiersin.org/articles/10.3389/fimmu.2022.931612/full#supplementary-material

References

1. Arora A, Olshen AB, Seshan VE, Shen R. Pan-cancer identification of clinically relevant genomic subtypes using outcome-weighted integrative clustering. *Genome Med* (2020) 12:1–13. doi: 10.1186/s13073-020-00804-8

2. Chang L, Graham P, Hao J, Ni J, Deng J, Bucci J, et al. Cancer stem cells and signaling pathways in radioresistance. *Oncotarget* (2016) 7:11002–17. doi: 10.18632/oncotarget.6760

3. Lyakhovich A, Lleonart ME. Bypassing mechanisms of mitochondria-mediated cancer stem cells resistance to chemo- and radiotherapy. *Oxid Med Cell Longev* (2016) 2016:10. doi: 10.1155/2016/1716341

4. Wang R-F, Wang HY. Immune targets and neoantigens for cancer immunotherapy and precision medicine. *Cell Res* (2017) 27:11–37. doi: 10.1038/cr.2016.155

5. Fischbach MA, Bluestone JA, Lim WA. Cell-based therapeutics: the next pillar of medicine. *Sci Transl Med* (2013) 5:179ps7. doi: 10.1126/scitranslmed.3005568

6. Rosenberg SA. Progress in human tumour immunology and immunotherapy. *Nature* (2001) 411:380–4. doi: 10.1038/35077246

7. Rosenberg SA, Yang JC, Restifo NP. Cancer immunotherapy: moving beyond current vaccines. *Nat Med* (2004) 10:909–15. doi: 10.1038/nm1100

8. Rook AH, Raphael BA. Progress in immunotherapy of cancer. *N Engl J Med* (2012) 367:1168. doi: 10.1056/NEJMc1208946

9. Li W, Joshi MD, Singhania S, Ramsey KH, Murthy AK. Peptide vaccine: Progress and challenges. *Vaccines* (2014) 2:515–36. doi: 10.3390/vaccines2030515

10. Stephens AJ, Burgess-Brown NA, Jiang S. Beyond just peptide antigens: The complex world of peptide-based cancer vaccines. *Front Immunol* (2021) 12:696791. doi: 10.3389/fimmu.2021.696791

11. Chukwudozie OS, Gray CM, Fagbayi TA, Chukwuanukwu RC, Oyebanji VO, Bankole TT, et al. Immuno-informatics design of a multimeric epitope peptide based vaccine targeting SARS-CoV-2 spike glycoprotein. *PloS One* (2021) 16:1–25. doi: 10.1371/journal.pone.0248061

12. Carreno BM, Magrini V, Becker-Hapak M, Kaabinejadian S, Hundal J, Petti AA, et al. Cancer immunotherapy. a dendritic cell vaccine increases the breadth and diversity of melanoma neoantigen-specific T cells. *Science* (2015) 348:803–8. doi: 10.1126/science.aaa3828

13. Peoples GE, Holmes JP, Hueman MT, Mittendorf EA, Amin A, Khoo S, et al. Combined clinical trial results of a HER2/neu (E75) vaccine for the prevention of recurrence in high-risk breast cancer patients: U.S. military cancer institute clinical trials group study I-01 and I-02. *Clin Cancer Res* (2008) 14:797–803. doi: 10.1158/1078-0432.CCR-07-1448

14. Walter S, Weinschenk T, Stenzl A, Zdrojowy R, Pluzanska A, Szczylik C, et al. Multipeptide immune response to cancer vaccine IMA901 after single-dose cyclophosphamide associates with longer patient survival. *Nat Med* (2012) 18:1254–61. doi: 10.1038/nm.2883

15. Weber JS, Dummer R, de Pril V, Lebbé C, Hodi FS. Patterns of onset and resolution of immune-related adverse events of special interest with ipilimumab: detailed safety analysis from a phase 3 trial in patients with advanced melanoma. *Cancer* (2013) 119:1675–82. doi: 10.1002/cncr.27969

16. Wu YL, Park K, Soo RA, Sun Y, Tyroller K, Wages D, et al. INSPIRE: A phase III study of the BLP25 liposome vaccine (L-BLP25) in Asian patients with unresectable stage III non-small cell lung cancer. *BMC Cancer* (2011) 11:430. doi: 10.1186/1471-2407-11-430

17. Yadav M, Jhunjhunwala S, Phung QT, Lupardus P, Tanguay J, Bumbaca S, et al. Predicting immunogenic tumour mutations by combining mass spectrometry and exome sequencing. *Nature* (2014) 515:572–6. doi: 10.1038/nature14001

18. Hundal J, Carreno BM, Petti AA, Linette GP, Griffith OL, Mardis ER, et al. pVAC-seq: A genome-guided in silico approach to identifying tumor neoantigens. *Genome Med* (2016) 8:11. doi: 10.1186/s13073-016-0264-5

19. Chen DS, Mellman I. Oncology meets immunology: The cancer-immunity cycle. *Immunity* (2013) 39:1–10. doi: 10.1016/j.immuni.2013.07.012

20. Sultan H, Fesenkova VI, Addis D, Fan AE, Kumai T, Wu J, et al. Designing therapeutic cancer vaccines by mimicking viral infections. *Cancer Immunol Immunother* (2017) 66:203–13. doi: 10.1007/s00262-016-1834-5

21. Sultan H, Kumai T, Nagato T, Wu J, Salazar AM, Celis E. The route of administration dictates the immunogenicity of peptide-based cancer vaccines in mice. *Cancer Immunol Immunother* (2019) 68:455–66. doi: 10.1007/s00262-018-02294-5

22. Kumai T, Lee S, Cho H-I, Sultan H, Kobayashi H, Harabuchi Y, et al. Optimization of peptide vaccines to induce robust antitumor CD4 T-cell responses. *Cancer Immunol Res* (2017) 5:72–83. doi: 10.1158/2326-6066.CIR-16-0194

23. Noguchi M, Matsumoto K, Uemura H, Arai G, Eto M, Naito S, et al. An open-label, randomized phase II trial of personalized peptide vaccination in patients with bladder cancer that progressed after platinum-based chemotherapy. *Clin Cancer Res* (2016) 22:54–60. doi: 10.1158/1078-0432.CCR-15-1265

24. Jiang C, Chao C, Cheng C. Abstract 6618: A database of potential T cell epitopes for cancer immunotherapy. *Immunology* (2020) 80:6618–8. doi: 10.1158/1538-7445.AM2020-6618

25. Jiang C, Liu G, Zhang W, Zhuang Z, Li W, Qiu S, et al. Abstract LB051: The landscape of peptide vaccinein clinical trials for cancer. *Cancer Res* (2021) 81: LB051–1. doi: 10.1158/1538-7445.AM2021-LB051

26. Zhang L, Huang Y, Lindstrom AR, Lin TY, Lam KS, Li Y. Peptide-based materials for cancer immunotherapy. *Theranostics* (2019) 9:7807–25. doi: 10.7150/thno.37194

27. Liu J, Fu M, Wang M, Wan D, Wei Y, Wei X. Cancer vaccines as promising immuno-therapeutics: platforms and current progress. *J Hematol Oncol* (2022) 15:1–26. doi: 10.1186/s13045-022-01247-x

28. Thomas S, Prendergast GC. Cancer vaccines: A brief overview. *Methods Mol Biol* (2016) 1403:755–61. doi: 10.1007/978-1-4939-3387-7_43

29. Sakamoto S, Matsueda S, Takamori S, Toh U, Noguchi M, Yutani S, et al. Immunological evaluation of peptide vaccination for cancer patients with the HLA -A11+ or -A33+ allele. *Cancer Sci* (2017) 108:598–603. doi: 10.1111/cas.13189

30. Sayad A, Akbari MT, Mehdizadeh M, Taheri M, Hajifathali A. HLA-A*26 and susceptility of iranian patients with non-Hodgkin lymphoma. *Iran J Immunol* (2014) 11:269–74. doi: IJIv11i4A5

31. Malonis RJ, Lai JR, Vergnolle O. Peptide-based vaccines: Current progress and future challenges. *Chem Rev* (2020) 120:3210–29. doi: 10.1021/acs.chemrev.9b00472

32. Liu W, Tang H, Li L, Wang X, Yu Z, Li J. Peptide-based therapeutic cancer vaccine: Current trends in clinical application. *Cell Prolif* (2021) 54:1–16. doi: 10.1111/cpr.13025

33. Fernández-Delgado M, Sirsat MS, Cernadas E, Alawadi S, Barro S, Febrero-Bande M. An extensive experimental survey of regression methods. *Neural Netw* (2019) 111:11–34. doi: 10.1016/j.neunet.2018.12.010

34. Liaw A, Wiener M. Classification and regression by randomForest. *R News* (2002) 2:18–22. doi: 10.1177/154405910408300516

35. Sing T, Sander O, Beerenwinkel N, Lengauer T. ROCR: Visualizing classifier performance in r. *Bioinformatics* (2005) 21:3940–1. doi: 10.1093/bioinformatics/bti623

36. Salazar LG, Fikes J, Southwood S, Ishioka G, Knutson KL, Gooley TA, et al. Immunization of cancer patients with HER-2/neu-derived peptides demonstrating high-affinity binding to multiple class II alleles. *Clin Cancer Res* (2003) 9:5559–65.

37. Mittendorf EA, Clifton GT, Holmes JP, Schneble E, van Echo D, Ponniah S, et al. Final report of the phase I/II clinical trial of the E75 (nelipepimut-s) vaccine with booster inoculations to prevent disease recurrence in high-risk breast cancer patients. *Ann Oncol* (2014) 25:1735–42. doi: 10.1093/annonc/mdu211

38. Wada S, Tsunoda T, Baba T, Primus FJ, Kuwano H, Shibuya M, et al. Rationale for antiangiogenic cancer therapy with vaccination using epitope peptides derived from human vascular endothelial growth factor receptor 2. *Cancer Res* (2005) 65:4939–46. doi: 10.1158/0008-5472.CAN-04-3759

39. Yajima N, Yamanaka R, Mine T, Tsuchiya N, Homma J, Sano M, et al. Immunologic evaluation of personalized peptide vaccination for patients with advanced malignant glioma. *Clin Cancer Res* (2005) 11:5900–11. doi: 10.1158/1078-0432.CCR-05-0559

40. Nishida S, Koido S, Takeda Y, Homma S, Komita H, Takahara A, et al. Wilms tumor gene (WT1) peptide-based cancer vaccine combined with gemcitabine for patients with advanced pancreatic cancer. *J Immunother* (2014) 37:105–14. doi: 10.1097/CJI.0000000000000020

41. Sadanaga N, Nagashima H, Mashino K, Tahara K, Yamaguchi H, Ohta M, et al. Dendritic cell vaccination with MAGE peptide is a novel therapeutic approach for gastrointestinal carcinomas. *Clin Cancer Res* (2001) 7:2277–84.

42. Okuno K, Sugiura F, Inoue K, Sukegawa Y. Clinical trial of a 7-peptide cocktail vaccine with oral chemotherapy for patients with metastatic colorectal cancer. *Anticancer Res* (2014) 34:3045–52.

43. Liénard D, Rimoldi D, Marchand M, Dietrich P-Y, van Baren N, Geldhof C, et al. Ex vivo detectable activation of melan-a-specific T cells correlating with inflammatory skin reactions in melanoma patients vaccinated with peptides in IFA. *Cancer Immun* (2004) 4:4.

44. Babatz J, Rollig C, Lobel B, Folprecht G, Haack M, Gunther H, et al. Induction of cellular immune responses against carcinoembryonic antigen in patients with metastatic tumors after vaccination with altered peptide ligand-loaded dendritic cells. *Cancer Immunol Immunother* (2006) 55:268–76. doi: 10.1007/s00262-005-0021-x

45. Creelan BC, Antonia S, Noyes D, Hunter TB, Simon GR, Bepler G, et al. Phase II trial of a GM-CSF-producing and CD40L-expressing bystander cell line combined with an allogeneic tumor cell-based vaccine for refractory lung adenocarcinoma. *J Immunother* (2013) 36:442–50. doi: 10.1097/CJI.0b013e3182a80237

46. Yoshiyama K, Terazaki Y, Matsueda S, Shichijo S, Noguchi M, Yamada A, et al. Personalized peptide vaccination in patients with refractory non-small cell lung cancer. *Int J Oncol* (2012) 40:1492–500. doi: 10.3892/ijo.2012.1351

47. Baxevanis CN, Voutsas IF, Gritzapis AD, Perez SA, Papamichail M. HER-2/neu as a target for cancer vaccines. *Immunotherapy* (2010) 2:213–26. doi: 10.2217/imt.09.89

48. Imai N, Harashima N, Ito M, Miyagi Y, Harada M, Yamada A, et al. Identification of lck-derived peptides capable of inducing HLA-A2-restricted and tumor-specific CTLs in cancer patients with distant metastases. *Int J Cancer* (2001) 94:237–42. doi: 10.1002/ijc.1461

49. Fay JW, Palucka AK, Paczesny S, Dhodapkar M, Johnston DA, Burkeholder S, et al. Long-term outcomes in patients with metastatic melanoma vaccinated with melanoma peptide-pulsed CD34+ progenitor-derived dendritic cells. *Cancer Immunol Immunother* (2006) 55:1209–18. doi: 10.1007/s00262-005-0106-6

50. Takahashi R, Ishibashi Y, Hiraoka K, Matsueda S, Kawano K, Kawahara A, et al. Phase II study of personalized peptide vaccination for refractory bone and soft tissue sarcoma patients. *Cancer Sci* (2013) 104:1285–94. doi: 10.1111/cas.12226

51. Sangha R, Butts C. L-BLP25: a peptide vaccine strategy in non small cell lung cancer. *Clin Cancer Res* (2007) 13:s4652–4. doi: 10.1158/1078-0432.CCR-07-0213

52. Yoshikawa T, Nakatsugawa M, Suzuki S, Shirakawa H, Nobuoka D, Sakemura N, et al. HLA-A2-restricted glypican-3 peptide-specific CTL clones induced by peptide vaccine show high avidity and antigen-specific killing activity against tumor cells. *Cancer Sci* (2011) 102:918–25. doi: 10.1111/j.1349-7006.2011.01896.x

53. Disis ML, Wallace DR, Gooley TA, Dang Y, Slota M, Lu H, et al. Concurrent trastuzumab and HER2/neu-specific vaccination in patients with metastatic breast cancer. *J Clin Oncol* (2009) 27:4685–92. doi: 10.1200/JCO.2008.20.6789

54. Miyatake T, Ueda Y, Morimoto A, Enomoto T, Nishida S, Shirakata T, et al. WT1 peptide immunotherapy for gynecologic malignancies resistant to conventional therapies: a phase II trial. *J Cancer Res Clin Oncol* (2013) 139:457–63. doi: 10.1007/s00432-012-1348-2

55. Hazama S, Nakamura Y, Takenouchi H, Suzuki N, Tsunedomi R, Inoue Y, et al. A phase I study of combination vaccine treatment of five therapeutic epitope-peptides for metastatic colorectal cancer; safety, immunological response, and clinical outcome. *J Transl Med* (2014) 12:63. doi: 10.1186/1479-5876-12-63

56. Harashima N, Tanaka K, Sasatomi T, Shimizu K, Miyagi Y, Yamada A, et al. Recognition of the lck tyrosine kinase as a tumor antigen by cytotoxic T lymphocytes of cancer patients with distant metastases. *Eur J Immunol* (2001) 31:323–32. doi: 10.1002/1521-4141(200102)31:2<323::AID-IMMU323>3.0.CO;2-0

57. Tada F, Abe M, Hirooka M, Ikeda Y, Hiasa Y, Lee Y, et al. Phase I/II study of immunotherapy using tumor antigen-pulsed dendritic cells in patients with hepatocellular carcinoma. *Int J Oncol* (2012) 41:1601–9. doi: 10.3892/ijo.2012.1626

58. Khleif SN, Abrams SI, Hamilton JM, Bergmann-Leitner E, Chen A, Bastian A, et al. A phase I vaccine trial with peptides reflecting ras oncogene mutations of solid tumors. *J Immunother* (1999) 22:155–65. doi: 10.1097/00002371-199903000-00007

59. Tanaka F, Haraguchi N, Isikawa K, Inoue H, Mori M. Potential role of dendritic cell vaccination with MAGE peptides in gastrointestinal carcinomas. *Oncol Rep* (2008) 20:1111–6.

60. Miyagi Y, Imai N, Sasatomi T, Yamada A, Mine T, Katagiri K, et al. Induction of cellular immune responses to tumor cells and peptides in colorectal cancer patients by vaccination with SART3 peptides. *Clin Cancer Res* (2001) 7:3950–62.

61. Ogata R, Matsueda S, Yao A, Noguchi M, Itoh K, Harada M. Identification of polycomb group protein enhancer of zeste homolog 2 (EZH2)-derived peptides immunogenic in HLA-A24+ prostate cancer patients. *Prostate* (2004) 60:273–81. doi: 10.1002/pros.20078

62. Hamid O, Solomon JC, Scotland R, Garcia M, Sian S, Ye W, et al. Alum with interleukin-12 augments immunity to a melanoma peptide vaccine: Correlation with time to relapse in patients with resected high-risk disease. *Clin Cancer Res* (2007) 13:215–22. doi: 10.1158/1078-0432.CCR-06-1450

63. Butterfield LH, Ribas A, Meng WS, Dissette VB, Amarnani S, Vu HT, et al. T-Cell responses to HLA-A*0201 immunodominant peptides derived from alpha-fetoprotein in patients with hepatocellular cancer. *Clin Cancer Res* (2003) 9:5902–8.

64. Brunsvig PF, Aamdal S, Gjertsen MK, Kvalheim G, Markowski-Grimsrud CJ, Sve I, et al. Telomerase peptide vaccination: a phase I/II study in patients with non-small cell lung cancer. *Cancer Immunol Immunother* (2006) 55:1553–64. doi: 10.1007/s00262-006-0145-7

65. Becker JC, Andersen MH, Hofmeister-Muller V, Wobser M, Frey L, Sandig C, et al. Survivin-specific T-cell reactivity correlates with tumor response and patient survival: a phase-II peptide vaccination trial in metastatic melanoma. *Cancer Immunol Immunother* (2012) 61:2091–103. doi: 10.1007/s00262-012-1266-9

66. Scardino A, Alves P, Gross DA, Tourdot S, Graff-Dubois S, Angevin E, et al. Identification of HER-2/neu immunogenic epitopes presented by renal cell carcinoma and other human epithelial tumors. *Eur J Immunol* (2001) 31:3261–70. doi: 10.1002/1521-4141(200111)31:11<3261::AID-IMMU3261>3.0.CO;2-4

67. Slingluff CL, Petroni GR, Chianese-Bullock KA, Smolkin ME, Hibbitts S, Murphy C, et al. Immunologic and clinical outcomes of a randomized phase II trial of two multipeptide vaccines for melanoma in the adjuvant setting. *Clin Cancer Res* (2007) 13:6386–95. doi: 10.1158/1078-0432.CCR-07-0486

68. Liu KJ, Wang CC, Chen LT, Cheng AL, Lin DT, Wu YC, et al. Generation of carcinoembryonic antigen (CEA)-specific T-cell responses in HLA-A*0201 and HLA-A*2402 late-stage colorectal cancer patients after vaccination with dendritic cells loaded with CEA peptides. *Clin Cancer Res* (2004) 10:2645–51. doi: 10.1158/1078-0432.CCR-03-0430

69. Shomura H, Shichijo S, Komatsu N, Matsueda S, Mine T, Rikimaru T, et al. Identification of epidermal growth factor receptor-derived peptides recognised by both cellular and humoral immune responses in HLA-A24+ non-small cell lung cancer patients. *Eur J Cancer* (2004) 40:1776–86. doi: 10.1016/j.ejca.2004.04.003

70. Kabaker K, Shell K, Kaufman HL. Vaccines for colorectal cancer and renal cell carcinoma. *Cancer J* (2011) 17:283–93. doi: 10.1097/PPO.0b013e318232ff44

71. Rapoport AP, Aqui NA, Stadtmauer EA, Vogl DT, Fang HB, Cai L, et al. Combination immunotherapy using adoptive T-cell transfer and tumor antigen vaccination on the basis of hTERT and survivin after ASCT for myeloma. *Blood* (2011) 117:788–97. doi: 10.1182/blood-2010-08-299396

72. Morse MA, Deng Y, Coleman D, Hull S, Kitrell-Fisher E, Nair S, et al. A phase I study of active immunotherapy with carcinoembryonic antigen peptide (CAP-1)-pulsed, autologous human cultured dendritic cells in patients with metastatic malignancies expressing carcinoembryonic antigen. *Clin Cancer Res* (1999) 5:1331–8.

73. Cormier JN, Salgaller ML, Prevette T, Barracchini KC, Rivoltini L, Restifo NP, et al. Enhancement of cellular immunity in melanoma patients immunized with a peptide from MART-1/Melan a. *Cancer J Sci Am* (1997) 3:37–44.

74. Butts C, Murray N, Maksymiuk A, Goss G, Marshall E, Soulières D, et al. Randomized phase IIB trial of BLP25 liposome vaccine in stage IIIB and IV non-small-cell lung cancer. *J Clin Oncol* (2005) 23:6674–81. doi: 10.1200/JCO.2005.13.011

75. Nakao M, Shichijo S, Imaizumi T, Inoue Y, Matsunaga K, Yamada A, et al. Identification of a gene coding for a new squamous cell carcinoma antigen recognized by the CTL. *J Immunol* (2000) 164:2565–74. doi: 10.4049/jimmunol.164.5.2565

76. Ito M, Shichijo S, Miyagi Y, Kobayashi T, Tsuda N, Yamada A, et al. Identification of SART3-derived peptides capable of inducing HLA-A2-restricted and tumor-specific CTLs in cancer patients with different HLA-A2 subtypes. *Int J Cancer* (2000) 88:633–9. doi: 10.1002/1097-0215(20001115)88:4<633::AID-IJC18>3.0.CO;2-N

77. Kobayashi K, Noguchi M, Itoh K, Harada M. Identification of a prostate-specific membrane antigen-derived peptide capable of eliciting both cellular and humoral immune responses in HLA-A24+ prostate cancer patients. *Cancer Sci* (2003) 94:622–7. doi: 10.1111/j.1349-7006.2003.tb01493.x

78. Choi C, Witzens M, Bucur M, Feuerer M, Sommerfeldt N, Trojan A, et al. Enrichment of functional CD8 memory T cells specific for MUC1 in bone marrow of patients with multiple myeloma. *Blood* (2005) 105:2132–4. doi: 10.1182/blood-2004-01-0366

79. Sarnaik AA, Yu B, Yu D, Morelli D, Hall M, Bogle D, et al. Extended dose ipilimumab with a peptide vaccine: immune correlates associated with clinical benefit in patients with resected high-risk stage IIIc/IV melanoma. *Clin Cancer Res* (2011) 17:896–906. doi: 10.1158/1078-0432.CCR-10-2463

80. Bolonaki I, Kotsakis A, Papadimitraki E, Aggouraki D, Konsolakis G, Vagia A, et al. Vaccination of patients with advanced non – small-cell lung cancer with an optimized cryptic human telomerase reverse transcriptase peptide. *J Clin Oncol* (2007) 25:2727–34. doi: 10.1200/JCO.2006.10.3465

81. Barnea E, Beer I, Patoka R, Ziv T, Kessler O, Tzehoval E, et al. Analysis of endogenous peptides bound by soluble MHC class I molecules: A novel approach for identifying tumor-specific antigens. *Eur J Immunol* (2002) 32:213–22. doi: 10.1002/1521-4141(200201)32:1<213::AID-IMMU213>3.0.CO;2-8

82. Yang D, Nakao M, Shichijo S, Sasatomi T, Takasu H, Matsumoto H, et al. Identification of a gene coding for a protein possessing shared tumor epitopes capable of inducing HLA-A24-restricted cytotoxic T lymphocytes in cancer patients. *Cancer Res* (1999) 59:4056–63. doi: 10.1002/1521-4141(200201)32:1<213::AID-IMMU213>3.0.CO;2-8

83. Butler MO, Lee JS, Ansén S, Neuberg D, Hodi FS, Murray AP, et al. Long-lived antitumor CD8+ lymphocytes for adoptive therapy generated using an artificial antigen-presenting cell. *Clin Cancer Res* (2007) 13:1857–67. doi: 10.1158/1078-0432.CCR-06-1905

84. Lee P, Wang F, Kuniyoshi J, Rubio V, Stuges T, Groshen S, et al. Effects of interleukin-12 on the immune response to a multipeptide vaccine for resected metastatic melanoma. *J Clin Oncol* (2001) 19:3836–47. doi: 10.1200/JCO.2001.19.18.3836

85. Matsushita N, Aruga A, Inoue Y, Kotera Y, Takeda K, Yamamoto M. Phase I clinical trial of a peptide vaccine combined with tegafur-uracil plus leucovorin for treatment of advanced or recurrent colorectal cancer. *Oncol Rep* (2013) 29:951–9. doi: 10.3892/or.2013.2231

86. Yamada A, Kawano K, Koga M, Matsumoto T, Itoh K. Multidrug resistance-associated protein 3 is a tumor rejection antigen recognized by HLA-A2402-restricted cytotoxic T lymphocytes. *Cancer Res* (2001) 61:6459–66.

87. Kibe S, Yutani S, Motoyama S, Nomura T, Tanaka N, Kawahara A, et al. Phase II study of personalized peptide vaccination for previously treated advanced colorectal cancer. *Cancer Immunol Res* (2014) 2:1154–62. doi: 10.1158/2326-6066.CIR-14-0035

88. Tanaka T, Kitamura H, Inoue R, Nishida S, Takahashi-Takaya A, Kawami S, et al. Potential survival benefit of anti-apoptosis protein: survivin-derived peptide vaccine with and without interferon alpha therapy for patients with advanced or

recurrent urothelial cancer–results from phase I clinical trials. *Clin Dev Immunol* (2013) 2013:262967. doi: 10.1155/2013/262967

89. Svane IM, Pedersen AE, Johansen JS, Johnsen HE, Nielsen D, Kamby C, et al. Vaccination with p53 peptide-pulsed dendritic cells is associated with disease stabilization in patients with p53 expressing advanced breast cancer; monitoring of serum YKL-40 and IL-6 as response biomarkers. *Cancer Immunol Immunother* (2007) 56:1485–99. doi: 10.1007/s00262-007-0293-4

90. Zeestraten ECM, Speetjens FM, Welters MJP, Saadatmand S, Stynenbosch LFM, Jongen R, et al. Addition of interferon-α to the p53-SLP® vaccine results in increased production of interferon-γ in vaccinated colorectal cancer patients: a phase I/II clinical trial. *Int J Cancer* (2013) 132:1581–91. doi: 10.1002/ijc.27819

91. Dai S, Zhou X, Wang B, Wang Q, Fu Y, Chen T, et al. Enhanced induction of dendritic cell maturation and HLA-A*0201-restricted CEA-specific CD8+ CTL response by exosomes derived from IL-18 gene-modified CEA-positive tumor cells. *J Mol Med* (2006) 84:1067–76. doi: 10.1007/s00109-006-0102-0

92. Noguchi M, Sasada T, Itoh K. Personalized peptide vaccination: A new approach for advanced cancer as therapeutic cancer vaccine. *Cancer Immunol Immunother* (2013) 62:919–29. doi: 10.1007/s00262-012-1379-1

93. Sato Y, Maeda Y, Shomura H, Sasatomi T, Takahashi M, Une Y, et al. A phase I trial of cytotoxic T-lymphocyte precursor-oriented peptide vaccines for colorectal carcinoma patients. *Br J Cancer* (2004) 90:1334–42. doi: 10.1038/sj.bjc.6601711

94. Lekka E, Gritzapis AD, Perez SA, Tsavaris N, Missitzis I, Mamalaki A, et al. Identification and characterization of a HER-2/neu epitope as a potential target for cancer immunotherapy. *Cancer Immunol Immunother* (2010) 59:715–27. doi: 10.1007/s00262-009-0791-7

95. Thorn M, Wang M, Kloverpris H, Schmidt EG, Fomsgaard A, Wenandy L, et al. Identification of a new hTERT-derived HLA-A*0201 restricted, naturally processed CTL epitope. *Cancer Immunol Immunother* (2007) 56:1755–63. doi: 10.1007/s00262-007-0319-y

96. Harada M, Kobayashi K, Matsueda S, Nakagawa M, Noguchi M, Itoh K. Prostate-specific antigen-derived epitopes capable of inducing cellular and humoral responses in HLA-A24+ prostate cancer patients. *Prostate* (2003) 57:152–9. doi: 10.1002/pros.10280

97. Karanikas V, Hwang LA, Pearson J, Ong CS, Apostolopoulos V, Vaughan H, et al. Antibody and T cell responses of patients with adenocarcinoma immunized with mannan-MUC1 fusion protein. *J Clin Invest* (1997) 100:2783–92. doi: 10.1172/JCI119825

98. Wobser M, Keikavoussi P, Kunzmann V, Weininger M, Andersen MH, Becker JC. Complete remission of liver metastasis of pancreatic cancer under vaccination with a HLA-A2 restricted peptide derived from the universal tumor antigen survivin. *Cancer Immunol Immunother* (2006) 55:1294–8. doi: 10.1007/s00262-005-0102-x

99. Filipazzi P, Pilla L, Mariani L, Patuzzo R, Castelli C, Camisaschi C, et al. Limited induction of tumor cross-reactive T cells without a measurable clinical benefit in early melanoma patients vaccinated with human leukocyte antigen class I-modified peptides. *Clin Cancer Res* (2012) 18:6485–96. doi: 10.1158/1078-0432.CCR-12-1516

100. Matsueda S, Takedatsu H, Yao A, Tanaka M, Noguchi M, Itoh K, et al. Identification of peptide vaccine candidates for prostate cancer patients with HLA-A3 supertype alleles. *Clin Cancer Res* (2005) 11:6933–43. doi: 10.1158/1078-0432.CCR-05-0682

101. Holmes JP, Gates JD, Benavides LC, Hueman MT, Carmichael MG, Patil R, et al. Optimal dose and schedule of an HER-2/neu (E75) peptide vaccine to prevent breast cancer recurrence: from US military cancer institute clinical trials group study I-01 and I-02. *Cancer* (2008) 113:1666–75. doi: 10.1002/cncr.23772

102. Sakamoto S, Matsueda S, Takamori S, Toh U, Noguchi M, Yutani S, et al. Immunological evaluation of peptide vaccination for cancer patients with the HLA-A26 allele. *Cancer Sci* (2015) 106:1257–63. doi: 10.1111/cas.12757

103. Kimura T, McKolanis JR, Dzubinski LA, Islam K, Potter DM, Salazar AM, et al. MUC1 vaccine for individuals with advanced adenoma of the colon: A cancer immunoprevention feasibility study. *Cancer Prev Res* (2013) 6:18–26. doi: 10.1158/1940-6207.CAPR-12-0275

104. Naito M, Komohara Y, Ishihara Y, Noguchi M, Yamashita Y, Shirakusa T, et al. Identification of lck-derived peptides applicable to anti-cancer vaccine for patients with human leukocyte antigen-A3 supertype alleles. *Br J Cancer* (2007) 97:1648–54. doi: 10.1038/sj.bjc.6604071

105. Staff C, Mozaffari F, Frödin J-E, Mellstedt H, Liljefors M. Telomerase (GV1001) vaccination together with gemcitabine in advanced pancreatic cancer patients. *Int J Oncol* (2014) 45:1293–303. doi: 10.3892/ijo.2014.2496

106. Gjertsen MK, Buanes T, Rosseland AR, Bakka A, Gladhaug I, Søreide O, et al. Intradermal ras peptide vaccination with granulocyte-macrophage colony-stimulating factor as adjuvant: Clinical and immunological responses in patients with pancreatic adenocarcinoma. *Int J Cancer* (2001) 92:441–50. doi: 10.1002/ijc.1205

107. Morita S, Oka Y, Tsuboi A, Kawakami M, Maruno M, Izumoto S, et al. A phase I/II trial of a WT1 (Wilms' tumor gene) peptide vaccine in patients with solid malignancy: safety assessment based on the phase I data. *Jpn J Clin Oncol* (2006) 36:231–6. doi: 10.1093/jjco/hyl005

108. Speiser DE, Schwarz K, Baumgaertner P, Manolova V, Devevre E, Sterry W, et al. Memory and effector CD8 T-cell responses after nanoparticle vaccination of melanoma patients. *J Immunother* (2010) 33:848–58. doi: 10.1097/CJI.0b013e3181f1d614

109. Suzuki N, Hazama S, Ueno T, Matsui H, Shindo Y, Iida M, et al. A phase I clinical trial of vaccination with KIF20A-derived peptide in combination with gemcitabine for patients with advanced pancreatic cancer. *J Immunother* (2014) 37:36–42. doi: 10.1097/CJI.0000000000000012

110. McDermott D, Haanen J, Chen T-T, Lorigan P, O'Day S. Efficacy and safety of ipilimumab in metastatic melanoma patients surviving more than 2 years following treatment in a phase III trial (MDX010-20). *Ann Oncol* (2013) 24:2694–8. doi: 10.1093/annonc/mdt291

111. Karbach J, Gnjatic S, Bender A, Neumann A, Weidmann E, Yuan J, et al. Tumor-reactive CD8+ T-cell responses after vaccination with NY-ESO-1 peptide, CpG 7909 and montanide® ISA-51: Association with survival. *Int J Cancer* (2010) 126:909–18. doi: 10.1002/ijc.24850

112. Tsuruma T, Hata F, Torigoe T, Furuhata T, Idenoue S, Kurotaki T, et al. Phase I clinical study of anti-apoptosis protein, survivin-derived peptide vaccine therapy for patients with advanced or recurrent colorectal cancer. *J Transl Med* (2004) 2:19. doi: 10.1186/1479-5876-2-19

113. Benavides LC, Gates JD, Carmichael MG, Patil R, Patel R, Holmes JP, et al. The impact of HER2/neu expression level on response to the E75 vaccine: from U.S. military cancer institute clinical trials group study I-01 and I-02. *Clin Cancer Res* (2009) 15:2895–904. doi: 10.1158/1078-0432.CCR-08-1126

114. Barve M, Bender J, Senzer N, Cunningham C, Greco FA, McCune D, et al. Induction of immune responses and clinical efficacy in a phase II trial of IDM-2101, a 10-epitope cytotoxic T-lymphocyte vaccine, in metastatic non-small-cell lung cancer. *J Clin Oncol* (2008) 26:4418–25. doi: 10.1200/JCO.2008.16.6462

115. Asahara S, Takeda K, Yamao K, Maguchi H, Yamaue H. Phase I/II clinical trial using HLA-A24-restricted peptide vaccine derived from KIF20A for patients with advanced pancreatic cancer. *J Transl Med* (2013) 11:291. doi: 10.1186/1479-5876-11-291

116. Takahashi R, Toh U, Iwakuma N, Takenaka M, Otsuka H, Furukawa M, et al. Feasibility study of personalized peptide vaccination for metastatic recurrent triple-negative breast cancer patients. *Breast Cancer Res* (2014) 16:R70. doi: 10.1186/bcr3685

117. Fong L, Hou Y, Rivas A, Benike C, Yuen A, Fisher GA, et al. Altered peptide ligand vaccination with Flt3 ligand expanded dendritic cells for tumor immunotherapy. *Proc Natl Acad Sci U S A* (2001) 98:8809–14. doi: 10.1073/pnas.141226398

118. Slingluff CL, Lee S, Zhao F, Chianese-Bullock KA, Olson WC, Butterfield LH, et al. A randomized phase II trial of multiepitope vaccination with melanoma peptides for cytotoxic T cells and helper T cells for patients with metastatic melanoma (E1602). *Clin Cancer Res* (2013) 19:4228–38. doi: 10.1158/1078-0432.CCR-13-0002

119. Terazaki Y, Yoshiyama K, Matsueda S, Watanabe N, Kawahara A, Naito Y, et al. Immunological evaluation of personalized peptide vaccination in refractory small cell lung cancer. *Cancer Sci* (2012) 103:638–44. doi: 10.1111/j.1349-7006.2012.02202.x

120. Inoue Y, Takaue Y, Takei M, Kato K, Kanai S, Harada Y, et al. Induction of tumor specific cytotoxic T lymphocytes in prostate cancer using prostatic acid phosphatase derived HLA-A2402 binding peptide. *J Urol* (2001) 166:1508–13. doi: 10.1016/S0022-5347(05)65821-1

121. Morse MA, Niedzwiecki D, Marshall JL, Garrett C, Chang DZ, Aklilu M, et al. A randomized phase II study of immunization with dendritic cells modified with poxvectors encoding CEA and MUC1 compared with the same poxvectors plus GM-CSF for resected metastatic colorectal cancer. *Ann Surg* (2013) 258:879–86. doi: 10.1097/SLA.0b013e318292919e

122. Holmes JP, Benavides LC, Gates JD, Carmichael MG, Hueman MT, Mittendorf EA, et al. Results of the first phase I clinical trial of the novel II-key hybrid preventive HER-2/neu peptide (AE37) vaccine. *J Clin Oncol* (2008) 26:3426–33. doi: 10.1200/JCO.2007.15.7842

123. Toubaji A, Achtar M, Provenzano M, Herrin VE, Behrens R, Hamilton M, et al. Pilot study of mutant ras peptide-based vaccine as an adjuvant treatment in pancreatic and colorectal cancers. *Cancer Immunol Immunother* (2008) 57:1413–20. doi: 10.1007/s00262-008-0477-6

124. Mittendorf EA, Holmes JP, Murray JL, von Hofe E, Peoples GE. CD4+ T cells in antitumor immunity: utility of an li-key HER2/neu hybrid peptide vaccine (AE37). *Expert Opin Biol Ther* (2009) 9:71–8. doi: 10.1517/14712590802614538

125. Domchek SM, Recio A, Mick R, Clark CE, Carpenter EL, Fox KR, et al. Telomerase-specific T-cell immunity in breast cancer: effect of vaccination on tumor immunosurveillance. *Cancer Res* (2007) 67:10546–55. doi: 10.1158/0008-5472.CAN-07-2765

126. Mittendorf EA, Clifton GT, Holmes JP, Clive KS, Patil R, Benavides LC, et al. Clinical trial results of the HER-2/neu (E75) vaccine to prevent breast cancer recurrence in high-risk patients: From US military cancer institute clinical trials group study I-01 and I-02. *Cancer* (2012) 118:2594–602. doi: 10.1002/cncr.26574

127. Harrop R, Drury N, Shingler W, Chikoti P, Redchenko I, Carroll MW, et al. Vaccination of colorectal cancer patients with TroVax given alongside chemotherapy (5-fluorouracil, leukovorin and irinotecan) is safe and induces potent immune responses. *Cancer Immunol Immunother* (2008) 57:977–86. doi: 10.1007/s00262-007-0428-7

128. Kameshima H, Tsuruma T, Kutomi G, Shima H, Iwayama Y, Kimura Y, et al. Immunotherapeutic benefit of α-interferon (IFNα) in survivin2B-derived peptide vaccination for advanced pancreatic cancer patients. *Cancer Sci* (2013) 104:124–9. doi: 10.1111/cas.12046

129. Czerniecki BJ, Koski GK, Koldovsky U, Xu S, Cohen PA, Mick R, et al. Targeting HER-2/neu in early breast cancer development using dendritic cells with staged interleukin-12 burst secretion. *Cancer Res* (2007) 67:1842–52. doi: 10.1158/0008-5472.CAN-06-4038

130. Sato N, Hirohashi Y, Tsukahara T, Kikuchi T, Sahara H, Kamiguchi K, et al. Molecular pathological approaches to human tumor immunology. *Pathol Int* (2009) 59:205–17. doi: 10.1111/j.1440-1827.2009.02353.x

131. Bernhardt SL, Gjertsen MK, Trachsel S, Moller M, Eriksen JA, Meo M, et al. Telomerase peptide vaccination of patients with non-resectable pancreatic cancer: A dose escalating phase I/II study. *Br J Cancer* (2006) 95:1474–82. doi: 10.1038/sj.bjc.6603437

132. Slingluff CL, Petroni GR, Olson W, Czarkowski A, Grosh WW, Smolkin M, et al. Helper T-cell responses and clinical activity of a melanoma vaccine with multiple peptides from MAGE and melanocytic differentiation antigens. *J Clin Oncol* (2008) 26:4973–80. doi: 10.1200/JCO.2008.17.3161

133. Masuzawa T, Fujiwara Y, Okada K, Nakamura A, Takiguchi S, Nakajima K, et al. Phase I/II study of s-1 plus cisplatin combined with peptide vaccines for human vascular endothelial growth factor receptor 1 and 2 in patients with advanced gastric cancer. *Int J Oncol* (2012) 41:1297–304. doi: 10.3892/ijo.2012.1573

134. Svane IM, Pedersen AE, Nikolajsen K, Zocca M-B. Alterations in p53-specific T cells and other lymphocyte subsets in breast cancer patients during vaccination with p53-peptide loaded dendritic cells and low-dose interleukin-2. *Vaccine* (2008) 26:4716–24. doi: 10.1016/j.vaccine.2008.06.085

135. Gritzapis AD, Voutsas IF, Lekka E, Tsavaris N, Missitzis I, Sotiropoulou P, et al. Identification of a novel immunogenic HLA-A*0201-binding epitope of HER-2/neu with potent antitumor properties. *J Immunol* (2008) 181:146–54. doi: 10.4049/jimmunol.181.1.146

136. Dakappagari NK, Pyles J, Parihar R, Carson WE, Young DC, Kaumaya PTP. A chimeric multi-human epidermal growth factor receptor-2 b cell epitope peptide vaccine mediates superior antitumor responses. *J Immunol* (2003) 170:4242–53. doi: 10.4049/jimmunol.170.8.4242

137. Slingluff CLJ, Petroni GR, Yamshchikov GV, Barnd DL, Eastham S, Galavotti H, et al. Clinical and immunologic results of a randomized phase II trial of vaccination using four melanoma peptides either administered in granulocyte-macrophage colony-stimulating factor in adjuvant or pulsed on dendritic cells. *J Clin Oncol* (2003) 21:4016–26. doi: 10.1200/JCO.2003.10.005

138. Iiyama T, Udaka K, Takeda S, Takeuchi T, Adachi YC, Ohtsuki Y, et al. WT1 (Wilms' tumor 1) peptide immunotherapy for renal cell carcinoma. *Microbiol Immunol* (2007) 51:519–30. doi: 10.1111/j.1348-0421.2007.tb03940.x

139. Slingluff CLJ, Petroni GR, Yamshchikov GV, Hibbitts S, Grosh WW, Chianese-Bullock KA, et al. Immunologic and clinical outcomes of vaccination with a multiepitope melanoma peptide vaccine plus low-dose interleukin-2 administered either concurrently or on a delayed schedule. *J Clin Oncol* (2004) 22:4474–85. doi: 10.1200/JCO.2004.10.212

140. Ito M, Shichijo S, Tsuda N, Ochi M, Harashima N, Saito N, et al. Molecular basis of T cell-mediated recognition of pancreatic cancer cells. *Cancer Res* (2001) 61:2038–46.

141. Speetjens FM, Kuppen PJK, Welters MJP, Essahsah F, Van Den Brink AMEGV, Lantrua MGK, et al. Induction of p53-specific immunity by a p53 synthetic long peptide vaccine in patients treated for metastatic colorectal cancer. *Clin Cancer Res* (2009) 15:1086–95. doi: 10.1158/1078-0432.CCR-08-2227

142. Miles D, Papazisis K. Rationale for the clinical development of STn-KLH (Theratope) and anti-MUC-1 vaccines in breast cancer. *Clin Breast Cancer* (2003) 3 Suppl 4:S134–8. doi: 10.3816/CBC.2003.s.002

143. Kotsakis A, Papadimitraki E, Vetsika EK, Aggouraki D, Dermitzaki EK, Hatzidaki D, et al. A phase II trial evaluating the clinical and immunologic response of HLA-A2(+) non-small cell lung cancer patients vaccinated with an hTERT cryptic peptide. *Lung Cancer* (2014) 86:59–66. doi: 10.1016/j.lungcan.2014.07.018

144. Sawada Y, Yoshikawa T, Nobuoka D, Shirakawa H, Kuronuma T, Motomura Y, et al. Phase I trial of a glypican-3-derived peptide vaccine for advanced hepatocellular carcinoma: Immunologic evidence and potential for improving overall survival. *Clin Cancer Res* (2012) 18:3686–96. doi: 10.1158/1078-0432.CCR-11-3044

145. Brunsvig PF, Kyte JA, Kersten C, Sundstrøm S, Møller M, Nyakas M, et al. Telomerase peptide vaccination in NSCLC: a phase II trial in stage III patients vaccinated after chemoradiotherapy and an 8-year update on a phase I/II trial. *Clin Cancer Res* (2011) 17:6847–57. doi: 10.1158/1078-0432.CCR-11-1385

146. Yao A, Harada M, Matsueda S, Ishihara Y, Shomura H, Noguchi M, et al. Identification of parathyroid hormone-related protein-derived peptides immunogenic in human histocompatibility leukocyte antigen-A24+ prostate cancer patients. *Br J Cancer* (2004) 91:287–96. doi: 10.1038/sj.bjc.6601960

147. Schaefer C, Butterfield LH, Lee S, Kim GG, Visus C, Albers A, et al. Function but not phenotype of melanoma peptide-specific CD8(+) T cells correlate with survival in a multiepitope peptide vaccine trial (ECOG 1696). *Int J Cancer* (2012) 131:874–84. doi: 10.1002/ijc.26481

148. Rongcun Y, Salazar-Onfray F, Charo J, Malmberg KJ, Evrin K, Maes H, et al. Identification of new HER2/neu-derived peptide epitopes that can elicit specific CTL against autologous and allogeneic carcinomas and melanomas. *J Immunol* (1999) 163:1037–44.

149. Ishikawa H, Imano M, Shiraishi O, Yasuda A, Peng YF, Shinkai M, et al. Phase i clinical trial of vaccination with LY6K-derived peptide in patients with advanced gastric cancer. *Gastric Cancer* (2014) 17:173–80. doi: 10.1007/s10120-013-0258-6

150. Markovic SN, Suman VJ, Ingle JN, Kaur JS, Pitot HC, Loprinzi CL, et al. Peptide vaccination of patients with metastatic melanoma: improved clinical outcome in patients demonstrating effective immunization. *Am J Clin Oncol* (2006) 29:352–60. doi: 10.1097/01.coc.0000217877.78473.a4

151. Neumann F, Sturm C, Hülsmeyer M, Dauth N, Guillaume P, Luescher IF, et al. Fab antibodies capable of blocking T cells by competitive binding have the identical specificity but a higher affinity to the MHC-peptide-complex than the T cell receptor. *Immunol Lett* (2009) 125:86–92. doi: 10.1016/j.imlet.2009.06.002

152. Alves PM, Viatte S, Fagerberg T, Michielin O, Bricard G, Bouzourene H, et al. Immunogenicity of the carcinoembryonic antigen derived peptide 694 in HLA-A2 healthy donors and colorectal carcinoma patients. *Cancer Immunol Immunother* (2007) 56:1795–805. doi: 10.1007/s00262-007-0323-2

153. Tamura M, Nishizaka S, Maeda Y, Ito M, Harashima N, Harada M, et al. Identification of cyclophilin b-derived peptides capable of inducing histocompatibility leukocyte antigen-A2-restricted and tumor-specific cytotoxic T lymphocytes. *Jpn J Cancer Res* (2001) 92:762–7. doi: 10.1111/j.1349-7006.2001.tb01159.x

154. Amin A, Benavides LC, Holmes JP, Gates JD, Carmichael MG, Hueman MT, et al. Assessment of immunologic response and recurrence patterns among patients with clinical recurrence after vaccination with a preventive HER2/neu peptide vaccine: from US military cancer institute clinical trials group study I-01 and I-02. *Cancer Immunol Immunother* (2008) 57:1817–25. doi: 10.1007/s00262-008-0509-2

155. Kawaguchi S, Wada T, Ida K, Sato Y, Nagoya S, Tsukahara T, et al. Phase I vaccination trial of SYT-SSX junction peptide in patients with disseminated synovial sarcoma. *J Transl Med* (2005) 3:1. doi: 10.1186/1479-5876-3-1

156. de Vries IJM, Bernsen MR, Lesterhuis WJ, Scharenborg NM, Strijk SP, Gerritsen M-JP, et al. Immunomonitoring tumor-specific T cells in delayed-type hypersensitivity skin biopsies after dendritic cell vaccination correlates with clinical outcome. *J Clin Oncol* (2005) 23:5779–87. doi: 10.1200/JCO.2005.06.478

157. Clive KS, Tyler JA, Clifton GT, Holmes JP, Ponniah S, Peoples GE, et al. The GP2 peptide: a HER2/neu-based breast cancer vaccine. *J Surg Oncol* (2012) 105:452–8. doi: 10.1002/jso.21723

158. Ullenhag GJ, Frödin J-E, Mosolits S, Kiaii S, Hassan M, Bonnet MC, et al. Immunization of colorectal carcinoma patients with a recombinant canarypox virus expressing the tumor antigen ep-CAM/KSA (ALVAC-KSA) and granulocyte macrophage colony- stimulating factor induced a tumor-specific cellular immune response. *Clin Cancer Res* (2003) 9:2447–56.

159. Oka Y, Tsuboi A, Taguchi T, Osaki T, Kyo T, Nakajima H, et al. Induction of WT1 (Wilms' tumor gene)-specific cytotoxic T lymphocytes by WT1 peptide vaccine and the resultant cancer regression. *Proc Natl Acad Sci U S A* (2004) 101:13885–90. doi: 10.1073/pnas.0405884101

160. Svane IM, Pedersen AE, Johnsen HE, Nielsen D, Kamby C, Gaarsdal E, et al. Vaccination with p53-peptide-pulsed dendritic cells, of patients with advanced breast cancer: report from a phase I study. *Cancer Immunol Immunother* (2004) 53:633–41. doi: 10.1007/s00262-003-0493-5

161. Schwartzentruber DJ, Lawson DH, Richards JM, Conry RM, Miller DM, Treisman J, et al. Gp100 peptide vaccine and interleukin-2 in patients with

advanced melanoma. *N Engl J Med* (2011) 364:2119–27. doi: 10.1056/NEJMoa1012863

162. Hazama S, Nakamura Y, Tanaka H, Hirakawa K, Tahara K, Shimizu R, et al. A phase II study of five peptides combination with oxaliplatin-based chemotherapy as a first-line therapy for advanced colorectal cancer (FXV study). *J Transl Med* (2014) 12:108. doi: 10.1186/1479-5876-12-108

163. Meyer RG, Korn S, Micke P, Becker K, Huber C, Wölfel T, et al. An open-label, prospective phase I/II study evaluating the immunogenicity and safety of a ras peptide vaccine plus GM-CSF in patients with non-small cell lung cancer. *Lung Cancer* (2007) 58:88–94. doi: 10.1016/j.lungcan.2007.05.003

164. Bolhassani A, Safaiyan S, Rafati S. Improvement of different vaccine delivery systems for cancer therapy. *Mol Cancer* (2011) 10:3. doi: 10.1186/1476-4598-10-3

165. Carreno BM, Magrini V, Becker-Hapak M, Kaabinejadian S, Hundal J, Petti AA, et al. A dendritic cell vaccine increases the breadth and diversity of melanoma neoantigen-specific T cells. *Science* (2015) 348:1–9. doi: 10.1126/science.aaa3828

166. Brichard VG, Lejeune D. Cancer immunotherapy targeting tumour-specific antigens: Towards a new therapy for minimal residual disease. *Expert Opin Biol Ther* (2008) 8:951–68. doi: 10.1517/14712598.8.7.951

167. Zaremba S, Barzaga E, Zhu M, Soares N, Tsang KY, Schlom J. Identification of an enhancer agonist cytotoxic T lymphocyte peptide from human carcinoembryonic antigen. *Cancer Res* (1997) 57:4570–7.

168. Goldman B, DeFrancesco L. The cancer vaccine roller coaster. *Nat Biotechnol* (2009) 27:129–39. doi: 10.1038/nbt0209-129

169. Robert C, Schadendorf D, Messina M, Hodi FS, O'Day S. Efficacy and safety of retreatment with ipilimumab in patients with pretreated advanced melanoma who progressed after initially achieving disease control. *Clin Cancer Res* (2013) 19:2232–9. doi: 10.1158/1078-0432.CCR-12-3080

170. Hodi FS, O'Day SJS, McDermott DF, Weber RW, Sosman JA, Haanen JB, et al. Improved survival with ipilimumab in patients with metastatic melanoma. *N Engl J Med* (2010) 363:711–23. doi: 10.1056/NEJMoa1003466

171. Revicki DA, van den Eertwegh AJM, Lorigan P, Lebbe C, Linette G, Ottensmeier CH, et al. Health related quality of life outcomes for unresectable stage III or IV melanoma patients receiving ipilimumab treatment. *Health Qual Life Outcomes* (2012) 10:66. doi: 10.1186/1477-7525-10-66

172. Weissman JP, Samlowski W, Meoz R. Hedgehog inhibitor induction with addition of concurrent superficial radiotherapy in patients with locally advanced basal cell carcinoma: A case series. *Oncologist* (2021) 26:e2247–53. doi: 10.1002/onco.13959

173. Raphael BA, Shin DB, Suchin KR, Morrissey KA, Vittorio CC, Kim EJ, et al. High clinical response rate of sézary syndrome to immunomodulatory therapies: Prognostic markers of response. *Arch Dermatol* (2011) 147:1410–5. doi: 10.1001/archdermatol.2011.232

174. Mamounas EP, Fisher B. Preoperative chemotherapy for operable breast cancer. *Cancer Treat Res* (2000) 103:137–55. doi: 10.1007/978-1-4757-3147-7_7

175. Boussios S, Sheriff M, Rassy E, Moschetta M, Samartzis EP, Hallit R, et al. Immuno-oncology: a narrative review of gastrointestinal and hepatic toxicities. *Ann Transl Med* (2021) 9:423. doi: 10.21037/atm-20-7361

176. Dimopoulos MA, Terpos E. Lenalidomide: An update on evidence from clinical trials. *Blood Rev* (2010) 24:S21–6. doi: 10.1016/S0268-960X(10)70005-9

177. Moore DH. Treatment of stage IB2 (bulky) cervical carcinoma. *Cancer Treat Rev* (2003) 29:401–6. doi: 10.1016/S0305-7372(03)00075-6

178. Wistuba-Hamprecht K, Martens A, Heubach F, Romano E, Geukes Foppen M, Yuan J, et al. Peripheral CD8 effector-memory type 1 T-cells correlate with outcome in ipilimumab-treated stage IV melanoma patients. *Eur J Cancer* (2017) 73:61–70. doi: 10.1016/j.ejca.2016.12.011

179. Wolchok JD, Hoos A, O'Day S, Weber JS, Hamid O, Lebbé C, et al. Guidelines for the evaluation of immune therapy activity in solid tumors: Immune-related response criteria. *Clin Cancer Res* (2009) 15:7412–20. doi: 10.1158/1078-0432.CCR-09-1624

180. Duffaud F, Therasse P. [New guidelines to evaluate the response to treatment in solid tumors]. *Bull Cancer* (2000) 87:881–6.

181. Louis DN, Ohgaki H, Wiestler OD, Cavenee WK, Burger PC, Jouvet A, et al. The 2007 WHO classification of tumours of the central nervous system. *Acta Neuropathol* (2007) 114:97–109. doi: 10.1007/s00401-007-0243-4

182. Löwik DWPM, van Hest JCM. Peptide based amphiphiles. *Chem Soc Rev* (2004) 33:234–45. doi: 10.1039/B212638A

183. Yamada A, Sasada T, Noguchi M, Itoh K. Next-generation peptide vaccines for advanced cancer. *Cancer Sci* (2013) 104:15–21. doi: 10.1111/cas.12050

184. Takedatsu H, Shichijo S, Katagiri K, Sawamizu H, Sata M, Itoh K. Identification of peptide vaccine candidates sharing among HLA-A3 +, -A11+, -A31+, and -A33+ cancer patients. *Clin Cancer Res* (2004) 10:1112–20. doi: 10.1158/1078-0432.CCR-0797-3

185. Abelin JG, Harjanto D, Malloy M, Suri P, Colson T, Goulding SP, et al. Defining HLA-II ligand processing and binding rules with mass spectrometry enhances cancer epitope prediction. *Immunity* (2019) 51:1–14. doi: 10.1016/j.immuni.2019.08.012

186. Hu Z, Ott PA, Wu CJ. Towards personalized, tumour-specific, therapeutic vaccines for cancer. *Nat Rev Immunol* (2018) 18:168–82. doi: 10.1038/nri.2017.131

187. Nagorsen D, Thiel E. HLA typing demands for peptide-based anti-cancer vaccine. *Cancer Immunol Immunother* (2008) 57:1903–10. doi: 10.1007/s00262-008-0493-6

188. González-Galarza FF, Takeshita LYC, Santos EJM, Kempson F, Maia MHT, Da Silva ALS, et al. Allele frequency net 2015 update: New features for HLA epitopes, KIR and disease and HLA adverse drug reaction associations. *Nucleic Acids Res* (2015) 43:D784–8. doi: 10.1093/nar/gku1166

189. Jiang C, Schaafsma E, Hong W, Zhao Y, Zhu K, Chao CC, et al. Influence of T cell-mediated immune surveillance on somatic mutation occurrences in melanoma. *Front Immunol* (2022) 12:703821. doi: 10.3389/fimmu.2021.703821

190. Matsuzaki J, Qian F, Luescher I, Lele S, Ritter G, Shrikant PA, et al. Recognition of naturally processed and ovarian cancer reactive CD8 + T cell epitopes within a promiscuous HLA class II T-helper region of NY-ESO-1. *Cancer Immunol Immunother* (2008) 57:1185–95. doi: 10.1007/s00262-008-0450-4

191. Baxevanis CN, Voutsas IF, Tsitsilonis OE, Gritzapis AD, Sotiriadou R, Papamichail M. Tumor-specific CD4 + T lymphocytes from cancer patients are required for optimal induction of cytotoxic T cells against the autologous tumor. *J Immunol* (2000) 164:3902–12. doi: 10.4049/jimmunol.164.7.3902

192. Tay RE, Richardson EK, Toh HC. Revisiting the role of CD4+ T cells in cancer immunotherapy–new insights into old paradigms. *Cancer Gene Ther* (2021) 28:5–17. doi: 10.1038/s41417-020-0183-x

193. Borst J, Ahrends T, Bąbała N, Melief CJM, Kastenmüller W. CD4+ T cell help in cancer immunology and immunotherapy. *Nat Rev Immunol* (2018) 18:635–47. doi: 10.1038/s41577-018-0044-0

194. Coffman RL, Sher A, Seder RA. Vaccine adjuvants: Putting innate immunity to work. *Immunity* (2010) 33:492–503. doi: 10.1016/j.immuni.2010.10.002

195. De Gregorio E, Caproni E, Ulmer JB. Vaccine adjuvants: mode of action. *Front Immunol* (2013) 4:214. doi: 10.3389/fimmu.2013.00214

196. Sacerdote P, Franchi S, Moretti S, Castelli M, Procacci P, Magnaghi V, et al. Cytokine modulation is necessary for efficacious treatment of experimental neuropathic pain. *J Neuroimmune Pharmacol* (2013) 8:202–11. doi: 10.1007/s11481-012-9428-2

197. Hollingsworth RE, Jansen K. Turning the corner on therapeutic cancer vaccines. *NPJ Vaccines* (2019) 4:7. doi: 10.1038/s41541-019-0103-y

198. Carretero-Iglesia L, Couturaud B, Baumgaertner P, Schmidt J, Maby-El Hajjami H, Speiser DE, et al. High peptide dose vaccination promotes the early selection of tumor antigen-specific CD8 T-cells of enhanced functional competence. *Front Immunol* (2020) 10:3016. doi: 10.3389/fimmu.2019.03016

199. Nathan P, Hassel JC, Rutkowski P, Baurain J-F, Butler MO, Schlaak M, et al. Overall survival benefit with tebentafusp in metastatic uveal melanoma. *N Engl J Med* (2021) 385:1196–206. doi: 10.1056/NEJMoa2103485

200. Purcell AW, McCluskey J, Rossjohn J. More than one reason to rethink the use of peptides in vaccine design. *Nat Rev Drug Discov* (2007) 6:404–14. doi: 10.1038/nrd2224

201. Yu Z, Restifo NP. Cancer vaccines: Progress reveals new complexities. *J Clin Invest* (2002) 110:289–94. doi: 10.1172/JCI0216216

202. Cuzzubbo S, Mangsbo S, Nagarajan D, Habra K, Pockley AG, McArdle SEB. Cancer vaccines: Adjuvant potency, importance of age, lifestyle, and treatments. *Front Immunol* (2021) 11. doi: 10.3389/fimmu.2020.615240

203. McGranahan N, Furness AJS, Rosenthal R, Ramskov S, Lyngaa R, Saini SK, et al. Clonal neoantigens elicit T cell immunoreactivity and sensitivity to immune checkpoint blockade. *Science (80-)* (2016) 354:1–11. doi: 10.1126/science.aaf1490

204. Iero M, Filipazzi P, Castelli C, Belli F, Valdagni R, Parmiani G, et al. Modified peptides in anti-cancer vaccines: Are we eventually improving anti-tumour immunity? *Cancer Immunol Immunother* (2009) 58:1159–67. doi: 10.1007/s00262-008-0610-6

205. Xu M, Liu X, Li P, Yang Y, Zhang W, Zhao S, et al. Modified natriuretic peptides and their potential role in cancer treatment. *BioMed J* (2021) 45:1–14. doi: 10.1016/j.bj.2021.06.007

206. Sun W, Shi J, Wu J, Zhang J, Chen H, Li Y, et al. A modified HLA-A*0201-restricted CTL epitope from human oncoprotein (hPEBP4) induces more efficient antitumor responses. *Cell Mol Immunol* (2018) 15:768–81. doi: 10.1038/cmi.2017.155

207. Chiangjong W, Chutipongtanate S, Hongeng S. Anticancer peptide: Physicochemical property, functional aspect and trend in clinical application (Review). *Int J Oncol* (2020) 57:678–96. doi: 10.3892/ijo.2020.5099

208. Xie M, Liu D, Yang Y. Anti-cancer peptides: Classification, mechanism of action, reconstruction and modification: Anticancer peptides. *Open Biol* (2020) 10::200004.

209. Van Doorn E, Liu H, Huckriede A, Hak E. Safety and tolerability evaluation of the use of montanide ISATM51 as vaccine adjuvant: A systematic review. *Hum Vaccines Immunother* (2016) 12:159–69. doi: 10.1080/21645515.2015.1071455

210. Aucouturier J, Dupuis L, Deville S, Ascarateil S, Ganne V. Montanide ISA 720 and 51: A new generation of water in oil emulsions as adjuvants for human vaccines. *Expert Rev Vaccines* (2002) 1:111–8. doi: 10.1586/14760584.1.1.111

211. Donnelly RP, Young HA, Rosenberg AS. An overview of cytokines and cytokine antagonists as therapeutic agents. *Ann N Y Acad Sci* (2009) 1182:1–13. doi: 10.1111/j.1749-6632.2009.05382.x

212. Liu C, Chu D, Kalantar-Zadeh K, George J, Young HA, Liu G. Cytokines: From clinical significance to quantification. *Adv Sci* (2021) 8:e2004433. doi: 10.1002/advs.202004433

213. Gadani SP, Cronk JC, Norris GT, Kipnis J. IL-4 in the brain: A cytokine to remember. *J Immunol* (2012) 189:4213–9. doi: 10.4049/jimmunol.1202246

214. Tatsumi T, Takehara T, Kanto T, Hori M, Miyagi T, Kuzushita N, et al. Administration of interleukin-12 enhances the therapeutic efficacy of dendritic cell-based tumor vaccines in mouse hepatocellular carcinoma. *Cancer Res* (2001) 61:7563–7.

215. Chmielewski M, Kopecky C, Hombach AA, Abken H. IL-12 release by engineered T cells expressing chimeric antigen receptors can effectively muster an antigen-independent macrophage response on tumor cells that have shut down tumor antigen expression. *Cancer Res* (2011) 71:5697–706. doi: 10.1158/0008-5472.CAN-11-0103

216. Setrerrahmane S, Xu H. Tumor-related interleukins: Old validated targets for new anti-cancer drug development. *Mol Cancer* (2017) 16:1–17. doi: 10.1186/s12943-017-0721-9

217. Zhao H, Wu L, Yan G, Chen Y, Zhou M, Wu Y, et al. Inflammation and tumor progression: signaling pathways and targeted intervention. *Signal Transduct Target Ther* (2021) 6:263. doi: 10.1038/s41392-021-00658-5

218. Bolonaki I, Kotsakis A, Papadimitraki E, Aggouraki D, Konsolakis G, Vagia A, et al. Vaccination of patients with advanced non-small-cell lung cancer with an optimized cryptic human telomerase reverse transcriptase peptide. *J Clin Oncol* (2007) 25:2727–34. doi: 10.1200/JCO.2006.10.3465

219. Zhang W, Lu X, Cui P, Piao C, Xiao M, Liu X, et al. Phase I/II clinical trial of a wilms' tumor 1-targeted dendritic cell vaccination-based immunotherapy in patients with advanced cancer. *Cancer Immunol Immunother* (2019) 68:121–30. doi: 10.1007/s00262-018-2257-2

220. Wen PY, Reardon DA, Armstrong TS, Phuphanich S, Aiken RD, Landolfi JC, et al. A randomized double-blind placebo-controlled phase II trial of dendritic cell vaccine ICT-107 in newly diagnosed patients with glioblastoma. *Clin Cancer Res* (2019) 25:5799–807. doi: 10.1158/1078-0432.CCR-19-0261

221. Rosenbaum P, Artaud C, Bay S, Ganneau C, Campone M, Delaloge S, et al. The fully synthetic glycopeptide MAG-Tn3 therapeutic vaccine induces tumor-specific cytotoxic antibodies in breast cancer patients. *Cancer Immunol Immunother* (2020) 69:703–16. doi: 10.1007/s00262-020-02503-0

222. Pollard AJ, Bijker EM. A guide to vaccinology: from basic principles to new developments. *Nat Rev Immunol* (2021) 21:83–100. doi: 10.1038/s41577-020-00479-7

223. Harvey WT, Carabelli AM, Jackson B, Gupta RK, Thomson EC, Harrison EM, et al. SARS-CoV-2 variants, spike mutations and immune escape. *Nat Rev Microbiol* (2021) 19:409–24. doi: 10.1038/s41579-021-00573-0

224. Garrett ME, Galloway JG, Wolf C, Logue JK, Franko N, Chu HY, et al. Comprehensive characterization of the antibody responses to SARS-CoV-2 spike protein finds additional vaccine-induced epitopes beyond those for mild infection. *Elife* (2022) 11:1–20. doi: 10.7554/eLife.73490

225. Long Y, Sun J, Song T-Z, Liu T, Tang F, Zhang X, et al. CoVac501, a self-adjuvanting peptide vaccine conjugated with TLR7 agonists, against SARS-CoV-2 induces protective immunity. *Cell Discov* (2022) 8:9. doi: 10.1038/s41421-021-00370-2

frontiers | Frontiers in Immunology

ORIGINAL RESEARCH
published: 27 July 2022
doi: 10.3389/fimmu.2022.946861

Lenvatinib Plus Programmed Cell Death Protein-1 Inhibitor Beyond First-Line Systemic Therapy in Refractory Advanced Biliary Tract Cancer: A Real-World Retrospective Study in China

Changying Shi[1†], Yulong Li[2†], Cheng Yang[3†], Liang Qiao[1], Liukang Tang[2], Yuting Zheng[2], Xue Chen[4], Youwen Qian[5], Jiamei Yang[3], Dong Wu[1*] and Feng Xie[2*]*

[1] Department of Liver Surgery I, Eastern Hepatobiliary Surgery Hospital, Affiliated to Naval Medical University, Shanghai, China, [2] Department of Biliary Tract Surgery III, Eastern Hepatobiliary Surgery Hospital, Affiliated to Naval Medical University, Shanghai, China, [3] Department of Special Treatment, Eastern Hepatobiliary Surgery Hospital, Affiliated to Naval Medical University, Shanghai, China, [4] Department of Radiology, Eastern Hepatobiliary Surgery Hospital, Affiliated to Naval Medical University, Shanghai, China, [5] Department of Pathology, Eastern Hepatobiliary Surgery Hospital, Affiliated to Naval Medical University, Shanghai, China

OPEN ACCESS

Edited by:
Xian Zeng,
Fudan University, China

Reviewed by:
Tao Zheng,
BenQ Medical Center, China
Guang Zhi Wang,
Weifang Medical University, China

***Correspondence:**
Feng Xie
xiefeng@smmu.edu.cn
Dong Wu
wudong1005@sina.com.cn
Changying Shi
mmmscy@smmu.edu.cn

[†]These authors have contributed equally to this work

Specialty section:
This article was submitted to Cancer Immunity and Immunotherapy, a section of the journal Frontiers in Immunology

Received: *18 May 2022*
Accepted: *20 June 2022*
Published: *27 July 2022*

Citation:
Shi C, Li Y, Yang C, Qiao L, Tang L, Zheng Y, Chen X, Qian Y, Yang J, Wu D and Xie F (2022) Lenvatinib Plus Programmed Cell Death Protein-1 Inhibitor Beyond First-Line Systemic Therapy in Refractory Advanced Biliary Tract Cancer: A Real-World Retrospective Study in China. Front. Immunol. 13:946861. doi: 10.3389/fimmu.2022.946861

Background: Currently, no second-line systemic treatment regimen has been recommended in advanced biliary tract cancer (BTC). Cumulative clinical evidence showed that systemic treatment with tyrosine kinase inhibitors (TKIs) in combination with immunotherapy may shed light on the dim clinical outcome in advanced BTC.

Objective: The aim of this study is to evaluate the anticancer efficacy of lenvatinib plus programmed cell death protein-1 (PD-1) antibody in patients with BTC who progressed after first-line cisplatin/gemcitabine (CisGem) chemotherapy.

Methods: Patients with advanced BTCs who progressed after CisGem were recruited. A combination regimen of lenvatinib (8/12 mg daily) plus PD-1 antibody (200/240 mg injection every 3 weeks) was prescribed. Clinicopathological information and therapeutic outcome, including tumor subtypes, biomarkers, treatment duration, adverse events (AE), progression-free survival (PFS), and overall survival (OS), were recorded and estimated.

Results: A total of 351 patients with BTCs were reviewed and 74 were recruited eventually: 35 had intrahepatic cholangiocarcinoma (47.3%), 4 had extrahepatic cholangiocarcinoma (5.4%), and 35 had gallbladder cancer (47.3%). The median administered cycles of PD-1 antibody were 6.43 (95% CI: 5.83–7.04) cycles, and the median duration of lenvatinib medication was 21.0 weeks (95% CI: 18.04–23.93). Twenty-eight patients (37.83%) experienced detectable objective response per RECIST1.1 within a median follow-up duration of 15.0 months. The objective response rate (ORR) was 20.27% (95% CI: 10.89%–29.65%), and the disease control rate (DCR) was 71.62% (95% CI: 61.11%–82.14%). The median PFS and OS were 4.0 months (95% CI: 3.5–5.0) and 9.50 months (95% CI: 9.0–11.0), respectively. Seventy-three patients

(98.64%) reported AEs and 39 (52.70%) experienced ≥grade 3 AEs. In subgroup analyses, tumoral PD-L1 expression ≥50% and tumor mutation burden (TMB) ≥2.5 Muts/Mb were associated with prolonged PFS.

Conclusion: Lenvatinib plus PD-1 antibody treatment shows an active trend towards improving survival in patients with advanced BTCs after failure with CisGem chemotherapy. The treatment-related AEs are worthy of attention and are manageable.

Keywords: lenvatinib, PD-1 inhibitor, immunotherapy, target therapy, biliary tract cancer, second-line agents

INTRODUCTION

The incidence of biliary tract cancer (BTC), formerly considered rare, increased significantly in the last two decades globally (1). Although increasing types of biological agents and immune-oncology regimens emerged in hepatocellular carcinoma, there are limited therapies available in advanced BTC. Cisplatin/gemcitabine (CisGem)-based chemotherapy is currently recommended as the standard first-line therapy in advanced BTCs, although both its efficacy and tolerance are suboptimal (2). In the recent ABC-06 study, FOLFOX (folinic acid, fluoroutacil, and oxaliplatin) was evaluated as a second-line treatment after progression with CisGem (3). It demonstrated only a modest 1-month survival benefit against best supportive care. This frustrating result prompts novel effective therapeutic strategies to be tested so as to qualify as a second- or above-line therapy.

Although immunotherapy has revolutionized the treatment standard of several hematological and solid malignancies, its role in advanced BTC is still unclear. Monotherapy with immune checkpoint inhibitors (ICIs) in advanced BTC has presented conflicting results, suggesting further investigation in agent combination and deeper insight into subgroup selection.

Lenvatinib is an inhibitor of receptor tyrosine kinases, targeting vascular endothelial growth factor receptors (VEGFR1–3), fibroblast growth factor receptors (FGFR1–4), KIT, and RET (4). Owing to its capability of inhibiting multiple kinases in nanomole concentration, lenvatinib is now broadly used in the treatment of a variety of solid cancers, including differentiated thyroid cancer, hepatocellular carcinoma, and renal cell carcinoma, as a single agent or in combination with another drug (5). Several preliminary assessments of lenvatinib monotherapy or combination therapy with ICIs as first- or non-first-line therapy were reported, but the results were suboptimal and need further validation (6–9). Hereby, we reported a single arm of patients with refractory advanced BTCs, treated with lenvatinib plus programmed cell death protein-1 (PD-1) antibody as a second- or above-line systemic therapy.

MATERIALS AND METHODS

Study Design and Patients

This was a single-center retrospective study assessing the efficacy and safety of TKI lenvatinib associated with PD-1 antibody as a systemic therapy beyond 1st-line after the failure of CisGem chemotherapy at a hepatobiliary specific referral center (Eastern Hepatobiliary Surgery Hospital). BTC patients who received lenvatinib plus PD-1 antibody synchronously or successively as a second- or above-line systemic therapy from January 1, 2019 to March 31, 2021 were reviewed. This study was approved by the Institutional Ethics Committee of Shanghai Eastern Hepatobiliary Surgery Hospital. The study protocol conformed to the principles of the Declaration of Helsinki. The statistical analysis was conducted according to the intention-to-treat principle. All the data were updated and censored on February 28, 2022.

The patients with advanced BTCs who experienced progression after CisGem in first-line therapy were permitted to enroll. Advanced BTC was defined as initially diagnosed unresectable BTC (pathologically proved by biopsy or surgical specimen, multiple lesions, extrahepatic metastasis, and less future remnant liver) or relapses after surgery. Other eligibility criteria included good physical status with an Eastern Co-operative Oncology Group (ECOG) performance status score of 0–2, a Child–Pugh score of 5–6, and no severe comorbidities. The patients previously treated with other chemotherapy regimens or immunotherapies were excluded. Detailed information of the clinical protocol was explained to each patient, and the written informed consent forms were collected.

Treatment Protocol

Patients were prescribed to orally take lenvatinib mesilate capsules (Patheon Inc.) 12 mg/day for body weight ≥ 60 kg or 8 mg/day for body weight < 60 kg as standard. To avoid acute intolerable side effects caused by lenvatinib from the start, a stepwise manner was undertaken. Patients were encouraged to take a reduced dose from 8 mg/day (≥60 kg) or 4 mg/day (<60 kg) for a week before reverting to the standard dose on day 8. Those who developed adverse events (AEs) related to lenvatinib had their dose reduced, or had their medication interrupted or discontinued depending on the severity. The PD-1 antibody was intravenously administered (200 mg of sintilimab or tislelizumab or 240 mg of nivolumab or toripalimab) in a 3-week cycle. The medication would not be halted unless disease progression (PD) or ≥grade 3 treatment-related adverse event (TRAE) occurred.

Response Assessment

Clinical information and laboratory data prior to initial medication from eligible patients were collected. Tumor evaluation was conducted based on computed tomography (CT) or magnetic resonance imaging (MRI). Response evaluation criteria in solid

tumor (RECIST1.1) and immunotherapy-related RECIST (irRECIST) were utilized to evaluate tumor response (10–12). The investigators and a panel of independent radiologists evaluated the images separately. Any discrepancy, mainly regarding lymph node enlargement-triggered PD and irRECIST-related partial response (PR)/stable disease (SD), was discussed and combined. The objective response rate (ORR) was defined as the proportion of patients with complete response (CR) or PR of total evaluated. The disease control rate (DCR) was defined as the proportion of patients with CR, PR, and SD. Overall survival was calculated from the date of medication initiation until the date of death. Progression-free survival (PFS) was measured from the date of medication initiation until the date of disease progression or death.

Safety Evaluation and Quality of Life

Safety was continuously evaluated every 4 weeks by manifestation and laboratory tests, including hemogram, liver function, thyroid function, and myocardial enzyme. TRAEs were recorded according to National Cancer Institute Common Terminology Criteria for Adverse Events version 5.0 (CTCAE 5.0) (13). The quality of life (QOL) was assessed with ECOG score (14). A rising score from baseline to 3 or higher was regarded as a significant disturbance to QOL.

Histological Biomarker Assessment

PD-L1 expression and tumor mutation burden (TMB) were investigated as potential biomarkers in this study. Immunohistochemistry was performed to determine the expression of PD-L1 using E1L3N (PD-L1 XP Rabbit mAb, Cell Signaling Technology, Danvers, USA) on tumor biopsy samples. Samples with 50% or more tumor cells for PD-L1 exhibiting linear cell membranous staining were considered positive (15, 16). The TMB was determined using next-generation sequencing (NGS, Illumina nova seq) (17). Genomic alterations including base substitutions, insertions, deletions, gene rearrangement, and fusions were analyzed to form mutation load according to the megabase (Mb) (Integrated DNA Technologies, USA).

Statistical Analysis

The continuous and categorical variables were calculated with the appropriate method including the Student's *t*-test, the Mann–Whitney *U*-test, the Chi-square test, or Fisher's exact test. The Kaplan–Meier method was employed to estimate the PFS and OS, and to accomplish the survival comparison in subgroups. The statistical analyses were performed with SPSS 21.0 for Windows (SPSS, Chicago, IL, USA) and R software 4.0.2 (R Foundation for Statistical Computing, Vienna, Austria). A p-value < 0.05 was considered statistically significant.

RESULTS

Patients' Baseline Characteristics

A total of 351 patients diagnosed with BTC were reviewed and 74 patients were recruited. All the patients were willing to attend the systemic therapy. The flowchart of the study and the treatment protocol is shown in **Figure 1**. The cohort included 35 (47.3%) with intrahepatic cholangiocarcinoma (iCCA), 4 (5.4%) with extrahepatic cholangiocarcinoma (eCCA), and 35 (47.3%) with gallbladder cancer (GBC), with a male/female ratio of 1.55 (45/29). The median age was 62.5 years (range: 43–78). In etiology surveillance, 24 patients (32.43%) had background liver diseases, which included 23 (31.08%) hepatitis B virus infections. Most patients had good physical performance except for two patients who got an ECOG PS score of 2. Twenty-five patients had received local regional therapy previously, including surgery (11, 14.86%), radiotherapy (11, 14.86%), and TACE (3, 4.05%). Forty-four patients (59.46%) had extrahepatic metastases. The baseline patient demographics and clinical characteristics are summarized in **Table 1**.

Treatment

The lenvatinib+PD-1 antibody regimen was administered as the 2nd-line systemic therapy in 54 patients (73.0%), the 3rd-line therapy in 17 (23.0%), and the 4th-line therapy in 3 (4.1%). The usage of PD-1 antibody injection included nivolumab (6.8%), sintilimab (51.4%), toripalimab (24.3%), and tislelizumab (17.6%). The median administered cycles of PD-1 antibody were 6.43 cycles (95% CI: 5.83–7.04), and all patients received at least 2 shots. The median duration of lenvatinib intake was 21.0 weeks (95% CI: 18.04–23.93), and all patients took lenvatinib for at least 4 weeks. Twenty-two patients were given reduced lenvatinib dosage in case of intolerable AEs. Sixty-three patients discontinued treatment owing to tumor progression, 5

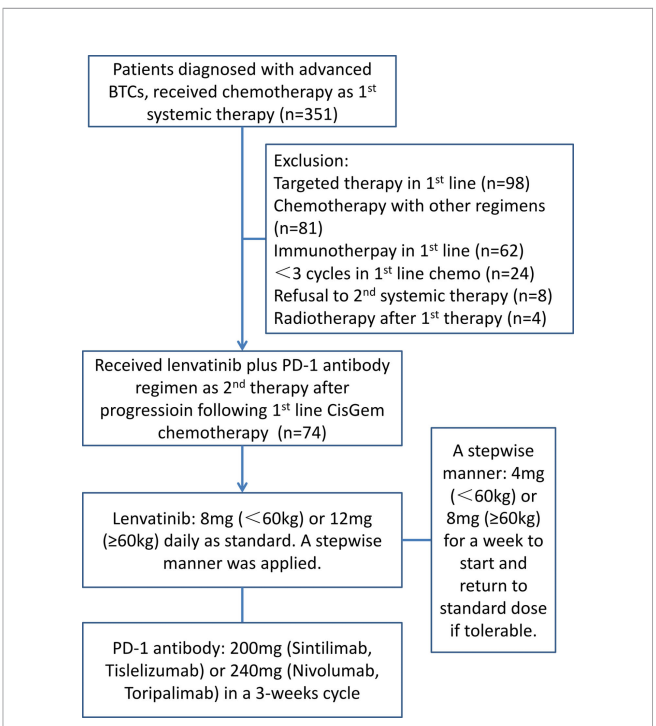

FIGURE 1 | The flowchart of the study illustrates the enrollment procedure and the treatment protocol.

TABLE 1 | Baseline demographics.

Parameters	Subjects (N=74)
Gender, *n* (%)	
Male	45 (60.8%)
Female	29 (39.2%)
Age years, (median, range)	62.5 (43–78)
Age group	
<60 years	26 (35.1%)
≥60	48 (46.9%)
ECOG performance, *n* (%)	
0	33 (44.6%)
1	39 (52.7%)
2	2 (2.7%)
Tumor subtype, *n* (%)	
Intrahepatic cholangiocarcinoma	35 (47.3%)
Extrahepatic cholangiocarcinoma	4 (5.4%)
Gallbladder cancer	35 (47.3%)
Background liver diseases, *n* (%)	24 (32.4%)
Hepatitis B virus infection, *n* (%)	23 (31.1%)
Previous local regional therapy, *n* (%)	
Surgery	11 (14.9%)
Radiation	11 (14.9%)
Transarterial chemo-emblization	3 (4.1%)
Child–Pugh score, *n* (%)	
5	62 (83.8%)
6	20 (13.5%)
7	2 (2.7%)
CA19-9, *n* (%)	
<500 μg/L	27 (36.5%)
≥500 μg/L	47 (63.5%)
Extrahepatic metastasis, *n* (%)	
Yes	30 (40.5%)
Measurable lesions burden, *n* (%)	
<3	54 (73.0%)
≥3	20 (27.0%)
TNM stage	
$T_3N_0M_0$	22 (29.7%)
$T_{1\text{-}3}N_1M_0$	27 (36.4%)
$T_4N_{0\text{-}1}M_0$	6 (8.1%)
$T_{any}N_{2\ or\ any}M_{0\ or\ 1}$	19 (25.6%)
White cell counts, (median×10^9/L, Range)	7.10 (4.09–9.93)
Platelet counts, (median×10^9/L, Range)	174.5 (57–299)
Prior chemotherapy cycles, *n* (%)	
<6 cycles	43 (58.1%)
≥6 cycles	31 (41.9%)
Line	
2nd line, *n* (%)	54 (73.0%)
3rd line, *n* (%)	17 (23.0%)
4th line, *n* (%)	3 (4.1%)

Data were presented as n (%) or median with range as appropriate.

discontinued due to intolerable AEs, and 6 patients remained under medication before the cutoff date.

Efficacy

Within a median follow-up duration of 15.0 months (95% CI: 12.874–17.126), 66 (89.19%) patients were available for efficacy assessment. Twenty-eight patients (37.83%) experienced detectable objective response per irRECIST, while 38 patients showed augmentation of measurable tumors. **Figure 2** shows the maximum change of the sum of measurable lesions and the best overall response.

The ORR following lenvatinib+PD-1 antibody treatment as the 2nd- and above-line systemic therapy in advanced BTCs was 20.27% (95% CI: 10.89%–29.65%), with 0 CR (0%) and 15 (20.27%) PRs. Thirty-eight patients achieved stable disease, and DCR was 71.62% (95% CI: 61.11%–82.14%) (**Table 2**). The median PFS was 4.0 months (95% CI: 3.5–5.0), and the PFS rate at 12 weeks was 70.0% (**Figure 3A**). The median OS was 9.50 months (95% CI: 9.0–11.0) and 1-year OS rate was 23% (**Figure 3B**). **Table 2** displays the detailed information of the therapeutic responses. Five patients experienced a deep regression in tumor size and did not progress until the censored follow-up date (**Figures 4A, B**). The ORR in iCCA, eCCA, and GBC was 20.69% (95% CI: 5.01%–36.4%), 33.33% (95% CI: −110%–177%), and 23.53% (95% CI: 8.51%–38.6%), respectively. The DCR in iCCA, eCCA, and GBC was 75.86% (95% CI: 59.3%–92.4%), 100%, and 82.35% (95% CI: 68.9%–95.9%), respectively (**Table 3**).

Tolerability and Safety

In total, 73 patients (98.64%) reported AEs and 39 (52.70%) experienced ≥grade 3 AEs. The most common AEs were decreased appetite (81.08%), fatigue (31.08%), elevated aspartate aminotransferase (27.03%), hypertension (21.62%), and diarrhea (20.27%). Detailed information of AEs is shown in **Table 4**. Most patients were advised to continue taking the medication through reduced dosage or to have medical support. Five patients (6.76%) withdrew from treatment due to intolerable AEs, which included 1 grade 3 diarrhea, 1 grade 3 increased aspartate aminotransferase, 1 grade 4 immune-associated pneumonitis (**Figures 5A, B**), 1 grade 3 immune-related erythema (**Figures 5C, D**) and 1 grade 2 immune-associated myocarditis. Patients with immune related AEs (irAE) were treated with low-dose corticosteroids and recovered. The ECOG score increased from 0/1 to 2 in 42 (56.75%) patients after at least 4 weeks of treatment and caused a disturbance to QOL.

Biomarkers

The spider diagram illustrated the serum CA19-9 concentration change in treatment duration (**Supplementary Figure 1A**). The change flow was well correlated to the tumor regression and progression accordingly with an area under the curve of 0.554 (**Supplementary Figure 1B**).

The genomic profile of PD-L1 expression and TMB was available in 22 patients. Tumoral PD-L1 staining (**Figures 4C, D**) was positive (≥50% cells as cutoff) in 8 patients (36.36%), 6 of whom (75.0%) achieved objective response and all patients had their disease controlled. Compared with negative expression, patients with tumoral PD-L1 expression presented prolonged PFS (5.50 months, 95% CI: 2.035–8.965 vs. 4.00 months, 95% CI: 3.414–4.586; $p = 0.004$), but not OS (13.00 months, 95% CI: 9.741–16.259 vs. 8.50 months, 95% CI: 5.778–11.222; $p = 0.064$) (**Figure 6A**).

The cutoff value of TMB was set at 2.5 Muts/Mb according to the average value released on The Cancer Genome Atlas (TCGA) website. Ten patients had higher TMB (≥2.5 Muts/Mb), and subgroup survival analysis revealed a prolonged PFS (5.00 months, 95% CI: 2.934–7.066, $p = 0.036$) in the higher TMB group, but not OS (12.0 months, 95% CI: 8.964–15.036, $p = 0.092$) (**Figure 6B**).

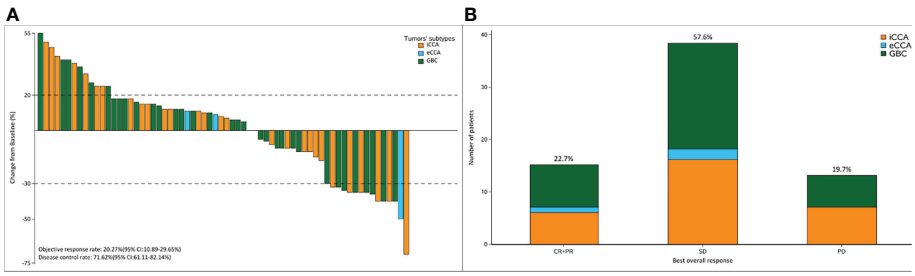

FIGURE 2 | **(A)** The maximum of change of the sum of the target lesions; **(B)** best overall response per RECIST1.1 according to the tumor subtypes. The ORR and DCR were 22.7% and 71.62%, respectively.

TABLE 2 | Treatment summary and therapeutic responds.

Category	Outcome
Lenvatinib regimen duration (weeks, median, range)	18.5 (6–69)
PD-1 cycles (*n*, median, range)	6 (2–14)
Complete response (CR, *n*, %)	0 (0%)
Partial response (PR, *n*, %)	15 (20.3%)
Stable disease (SD, *n*, %)	38 (51.4%)
Progression disease (PD, *n*, %)	13 (17.6%)
ORR	20.27% (95% CI: 10.89%–29.65%)
DCR	71.62% (95% CI: 61.11%–82.14%)

PD-1, programmed cell death protein-1; ORR, objective response rate; DCR, disease control rate.

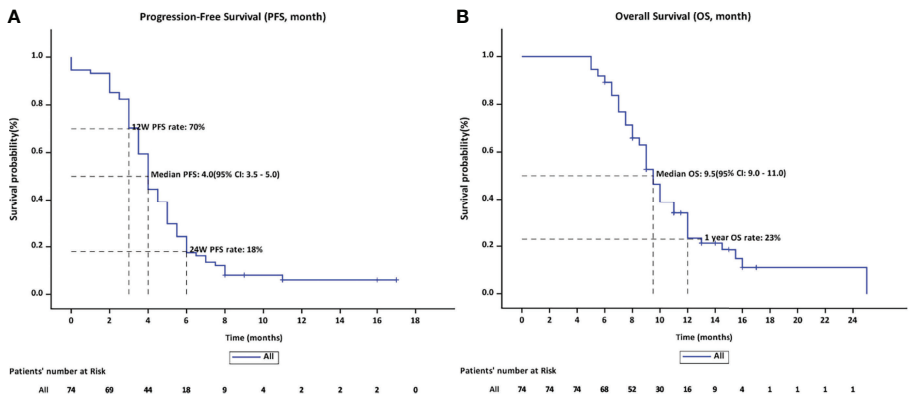

FIGURE 3 | **(A)** The PFS rate on 12 weeks and 24 weeks were 70% and 18%, respectively, with a median PFS of 4.0 months. **(B)** The median OS was 9.5 months (95% CI: 9.0–11.0) and the OS rate of 1 year was 23%.

DISCUSSION

This study evaluated the efficacy and safety of the two-drug regimen, lenvatinib plus PD-1 inhibitor, as a second- or above-line systemic therapy in refractory advanced BTCs. The results showed an ORR of 20.27% (95% CI: 10.89%–29.65%) and a DCR of 71.62% (95% CI: 61.11%–82.14%), with a median OS of 9.5 months. A total of 98.64% patients developed any-grade AEs and 52.70% developed grade 3/4 AEs. The results were similar to those of recent studies involving a single agent and combined regimens treating refractory advanced BTCs (7, 15, 18–21). This combination regimen prolonged the survival duration in both second- and above-line systemic therapies, without significant difference ($p = 0.809$). Additionally, this study found that 56.75% of the population got a worse ECOG physical score, which partly played a negative role in ensuring patients' compliance.

The long-term survival of patients with BTCs was dismal, with 5-year survival rates of 10%–50% (1, 21). ABC-01 and ABC-02 clinical trials established the standard of CisGem as a first-line systemic therapy in local advanced and metastatic BTCs (2, 22). The

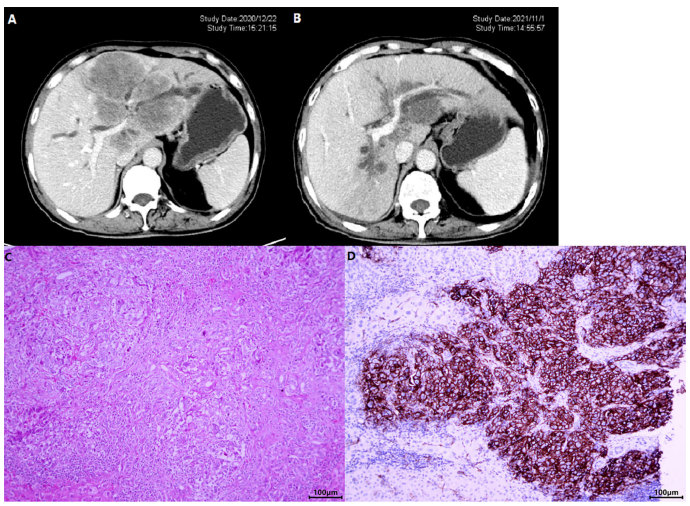

FIGURE 4 | A patient with iCCA received lenvatinib+sintilimab as 2nd-line systemic therapy. The CT images before **(A)** and after **(B)** nearly 1-year therapy showed a significant shrinkage of the target lesion, which was mainly located in the left hemi-liver and invaded the left branch of portal vein. **(C)** Shows the HE staining of the tumor and **(D)** displays the photomicrographs of immunohistochemistry staining of PD-L1 expression.

TABLE 3 | Objective response rate/Disease control rate.

Tumor subtype	ORR	DCR
iCCA	20.69% (95% CI: 5.01%–36.4%)	75.86% (95% CI: 59.3%–92.4%)
eCCA	33.33% (95% CI: –110%–177%)	100%
GBC	23.53% (95% CI: 8.51%–38.6%)	82.35% (95% CI: 68.9%–95.9%)

ORR, objective response rate; DCR, disease control rate; iCCA, intrahepatic cholangiocarcinoma; eCCA, extrahepatic cholangiocarcinoma; GBC, gallbladder cancer.

TABLE 4 | Adverse events ranking.

Events	Any AE (*n*, %)	Grade 1–2 AEs (*n*, %)	≥Grade 3 AEs (*n*, %)
Total	73 (98.64%)	60 (81.08%)	39 (52.70%)
Decreased appetite	60 (81.08%)	56 (75.68%)	13 (17.57%)
Fatigue	23 (31.08%)	23 (31.08%)	7 (9.46%)
Elevated aspartate aminotransferase	20 (27.03%)	16 (21.62%)	4 (5.41%)
Hypertension	16 (21.62%)	14 (18.92%)	8 (10.81%)
Diarrhea	15 (20.27%)	10 (13.51%)	5 (6.76%)
Abdominal pain	11 (14.86%)	10 (13.51%)	1 (1.35%)
Nausea	10 (13.51%)	10 (13.51%)	-
Palmar plantar erythrodysesthesia syndrome	9 (12.16%)	9 (12.16%)	-
Thrombocytopenia	9 (12.16%)	9 (12.16%)	-
Anemia	9 (12.16%)	8 (10.81%)	1 (1.35%)
Headache	8 (10.81%)	8 (10.81%)	-
Erythema	7 (9.46%)	7 (9.46%)	2 (2.70%)
Proteinuria	6 (8.11%)	6 (8.11%)	-
Hypothyroidism	5 (6.76%)	5 (6.76%)	-
Myalgia	4 (5.41%)	4 (5.41%)	-
Alopecia	3 (4.05%)	3 (4.05%)	-
Immune-associated pneumonitis	2 (2.70%)	1 (1.35%)	1 (1.35%)
Immune-associated myocarditis	1 (1.35%)	1 (1.35%)	-

AE, adverse event.

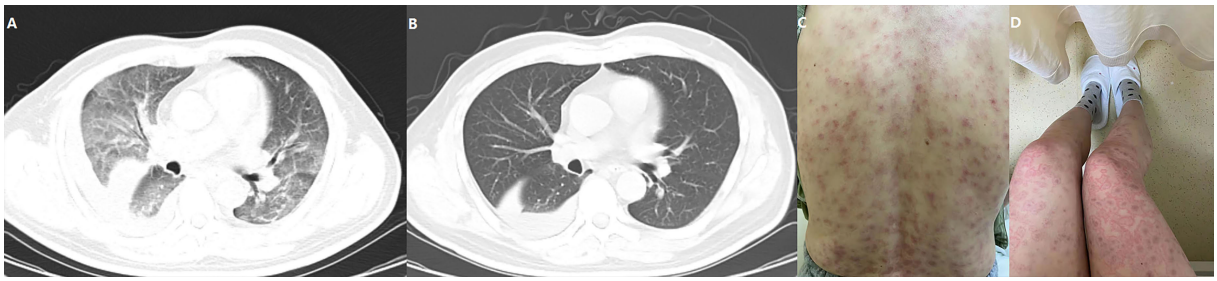

FIGURE 5 | One patient experienced a grade 4 immune-related pneumonitis **(A)** and recovered following corticosteroid injection **(B)**. Another patient developed severe erythema that affected more than 80% of the skin area (**C**: back; **D**: thigh and legs), but the inner environment was not bothered.

ABC-06 trial explored the effectiveness of the FOLFOX regimen as a second-line chemotherapy after progression (3). This study reported a median OS, 6-month survival rate, and 12-month survival of 6.2 months, 50.6%, and 25.9%, respectively, in the FOLFOX plus active symptom control population, which showed a significant improvement in survival compared with the active symptom control group. However, it also reported relatively high AE rates, with a 52% incidence rate of grade 3–5 AEs. Three patients died due to chemotherapy-related adverse effects. Considering its limited survival benefit and high adverse effects, the FOLFOX regimen might not be an ideal second-line therapy in refractory advanced BTCs.

Efforts were made to find potential targeted strategies in treating BTCs, including multiple pathways like angiogenesis, human epidermal growth factor receptor family, and other actionable targets (23, 24). Several existing and emerging molecular targeted agents were tested as second-line therapy. In the REACHIN study, 66 patients diagnosed with BTC who had already progressed to CisGem chemotherapy were randomized in a phase II study to receive regorafenib or placebo (25). Although the regorafenib group

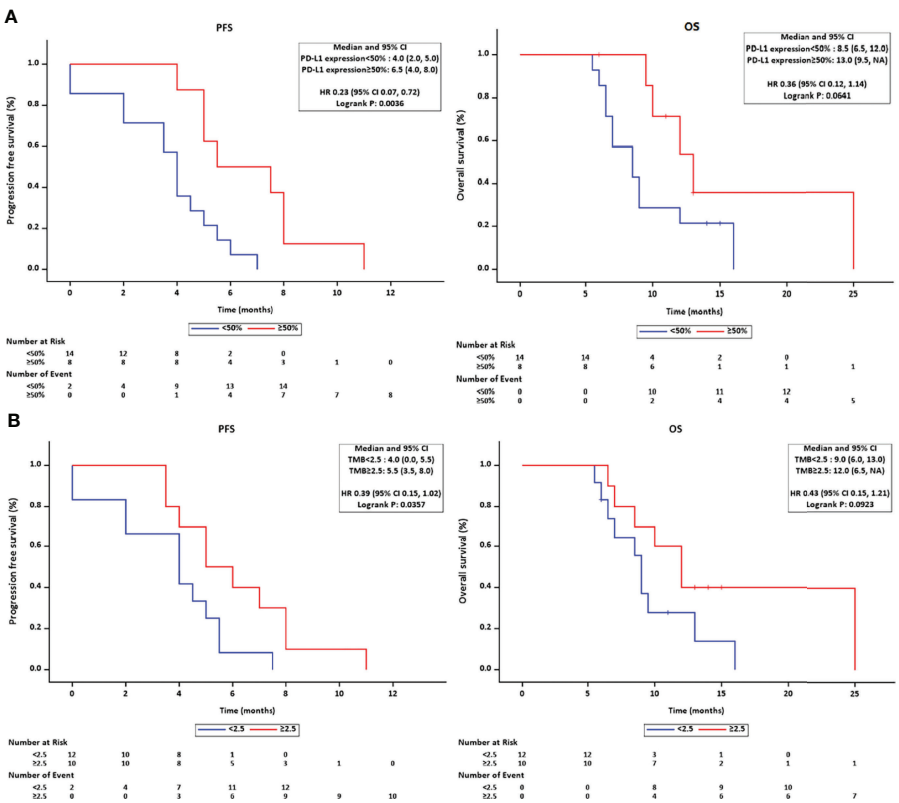

FIGURE 6 | **(A)** The Kaplan–Meier method estimated the survival length in PD-L1-positive/-negative subgroups and found a marginal superiority for RFS in the PD-L1 positive group. **(B)** A significant longer PFS was observed in the higher TMB subgroup.

showed an improved PFS versus the placebo group (3.0 months, 95% CI: 2.3–4.9 vs. 1.5 months, 95% CI: 1.2–2.0, $p = 0.004$), no patients reached objective response and no survival benefit was found regarding OS. The result showed that the addition of sorafenib to gemcitabine did not demonstrate improved efficacy in advanced BTC patients. Recently, the efficacy and safety of lenvatinib in treating advanced BTC were evaluated in a single-arm study (18). Forty-one patients with histologically confirmed BTCs received 8 mg (weight < 60 kg) or 12 mg (weight ≥ 60 kg) of lenvatinib orally per day. The ORR was 12%, with a median PFS of 3.8 months and an OS of 11.4 months. Up to 95.1% patients in total experienced TRAEs. In a phase II study of lenvatinib monotherapy as a 2nd-line treatment, the ORR was 11.5% and the ≥grade 3 AEs occurred in 80.8% of total patients (20). The median PFS and median OS were 3.19 months per investigator assessment and 7.35 months, respectively. In another study in China, with pembrolizumab combined with lenvatinib as a non-first-line therapy, the ORR and the DCR were 25% and 78.1%, respectively. The median PFS and median OS were 4.9 months and 11.0 months, respectively (7). Our results on lenvatinib plus PD-1 antibody showed a close survival benefit with an mPFS of 4.0 months and an mOS of 9.5 months. This indicated that accumulated clinical practices would probably pave the way to expand the usage of targeted agents combined with ICIs in advanced BTCs. There are several ongoing clinical trials regarding the lenvatinib plus ICIs combination regimen. **Supplementary Table 1** summarizes the ongoing trials registered on clinicaltrials.gov.

Among patients who progressed from the first-line CisGem regimen, their AE experiences in chemotherapy may probably be an obstacle to achieve good compliance in subsequent treatments, especially in a TKI/PD-1 antibody combination regimen. The two-drug pembrolizumab plus lenvatinib regimen reportedly obtained a 100% and 59.3% rate of any-grade AEs and ≥grade 3 AEs, respectively (7). In a systematic review evaluating the safety and efficacy of pembrolizumab plus lenvatinib in cancers, ≥grade 3 AEs occurred in 68.0% of all patients (26). Our result showed a 98.64% occurrence rate of any-grade AEs and a 48.65% occurrence rate of ≥grade 3 AEs, even under a stepwise manner. The treatment was called off in five patients due to intolerable AEs. More than half of the patients (56.75%) reported a decline in QOL related to the treatment, which should not be neglected.

The prognostic value of the tumoral expression of PD-L1 and a higher TMB in molecular targeted therapy and immunotherapy were not validated. Korean researchers reported a 71% positive (defined as ≥1% cells stained) rate of PD-L1 in BTCs, and the ORR with pembrolizumab treatment was improved in the PD-L1 expression ≥ 50% subgroup (16). In another study, KRAS alteration and chromosomal instability tumors were associated with resistance to immunotherapy, and the majority of patients (95.0%) with these resistance factors showed no clinical benefit to PD-1/PD-L1 blockade and harbored low TMB (27). Germline or somatic mutations in DNA damage repair (DDR) genes were found in 63.5% of patients with BTC and were significantly associated with longer survival while receiving first-line platinum-containing chemotherapies (28). Our study, with a limited sample size, showed a probability of survival benefit regarding PFS in tumoral PD-L1 expression ≥50% or in TMB ≥2.5 Muts/Mb. Cumulative research indicated that BTCs held scores of mutational varieties in genomic profiling. It is still a long way to go in finding genomic prognostic biomarkers in BTC.

This study has its share of limitations. Firstly, this study was retrospectively designed with a relatively small sample size, which might contribute to the sample bias. Secondly, the contribution of the three different anatomical locations derived from BTCs was not balanced, and a subtype analysis was not available due to the limited sample size. A relatively small proportion of patients with advanced eCCAs received systemic therapy owing to a constantly uncompensated liver function caused by biliary tract obstruction. This might be the reason why only three patients with eCCA were enrolled in this study. Lastly, a marginal survival benefit was detected in the PD-L1-positive or high TMB profile subgroup. Further investigation is necessary due to the limited sample size.

CONCLUSION

Lenvatinib plus PD-1 blockade played an active role in the treatment of patients with advanced refractory BTCs who progressed following CisGem chemotherapy. A moderate proportion of treatment-related AEs could not be neglected in practice, though they could be treated with further observation and care.

DATA AVAILABILITY STATEMENT

The data presented in the study are deposited in the Sequence Read Archive (SRA), https://www.ncbi.nlm.nih.gov/sra. The accession number is PRJNA857805.

ETHICS STATEMENT

The studies involving human participants were reviewed and approved by the Institutional Ethics Committee of Shanghai Eastern Hepatobiliary Surgery Hospital. The patients/participants provided their written informed consent to participate in this study.

AUTHOR CONTRIBUTIONS

SC, XF, WD and YJ designed this study. LY, YC, QL, TL,XC, YQ and ZY collected the data and perform the follow-up. SC, LY, and YC performed or supervised analyses. SC, WD, and XF interpreted the results. SC, LY and YC wrote the

original manuscript. WD and XF revised the manuscript. All authors reviewed the manuscript and approved the final version submitted.

FUNDING

This research has received funding from the Shanghai Municipal Health Commission Program (202140362), the Natural Science Foundation of Shanghai (Grant No. 16ZR1449200), and the Shanghai Shen Kang Hospital Development Center Planning (Grant No. SHDC12017X14).

ACKNOWLEDGMENTS

We thank all the patients and their families for their participation and thank Ms. Wang Yalin from MSD medical affairs for her contribution in terms of material support.

SUPPLEMENTARY MATERIAL

The Supplementary Material for this article can be found online at: https://www.frontiersin.org/articles/10.3389/fimmu.2022.946861/full#supplementary-material

REFERENCES

1. Brindley PJ, Bachini M, Ilyas SI, Khan SA, Loukas A, Sirica AE, et al. Cholangiocarcinoma. *Nat Rev Dis Primers* (2021) 7(1):65. doi: 10.1038/s41572-021-00300-2
2. Valle JW, Wasan H, Johnson P, Jones E, Dixon L, Swindell R, et al. Gemcitabine Alone or in Combination With Cisplatin in Patients With Advanced or Metastatic Cholangiocarcinomas or Other Biliary Tract Tumours: A Multicentre Randomised Phase II Study - The UK ABC-01 Study. *Br J Can* (2009) 101(4):621–7. doi: 10.1038/sj.bjc.6605211
3. Lamarca A, Palmer DH, Wasan HS, Ross PJ, Ma YT, Arora A, et al. Advanced Biliary Cancer Working GroupSecond-Line FOLFOX Chemotherapy Versus Active Symptom Control for Advanced Biliary Tract Cancer (ABC-06): A Phase 3, Open-Label, Randomised, Controlled Trial. *Lancet Oncol* (2021) 22 (5):690–701. doi: 10.1016/S1470-2045(21)00027-9
4. Ogasawara S, Mihara Y, Kondo R, Kusano H, Akiba J, Yano H. Antiproliferative Effect of Lenvatinib on Human Liver Cancer Cell Lines *In Vitro* and *In Vivo*. *Anticancer Res* (2019) 39(11):5973–82. doi: 10.21873/anticanres.13802
5. Hao Z, Wang P. Lenvatinib in Management of Solid Tumors. *Oncologist.* (2020) 25(2):e302–10. doi: 10.1634/theoncologist.2019-0407
6. Zhang Q, Liu X, Wei S, Zhang L, Tian Y, Gao Z, et al. Lenvatinib Plus PD-1 Inhibitors as First-Line Treatment in Patients With Unresectable Biliary Tract Cancer: A Single-Arm, Open-Label, Phase II Study. *Front Oncol* (2021) 11:751391. doi: 10.3389/fonc.2021.751391
7. Lin J, Yang X, Long J, Zhao S, Mao J, Wang D, et al. Pembrolizumab Combined With Lenvatinib as Non-First-Line Therapy in Patients With Refractory Biliary Tract Carcinoma. *Hepatobiliary Surg Nutr* (2020) 9(4):414–24. doi: 10.21037/hbsn-20-338
8. Dreikhausen L, Kusnik A, Schulte N, Eckardt M, Teufel A, Gaiser T, et al. Durable Response With Lenvatinib and Pembrolizumab Combination Therapy in a Patient With Pre-Treated Metastatic Cholangiocarcinoma. *J Gastrointestin Liver Dis* (2021) 30(3):409–10. doi: 10.15403/jgld-3730
9. Chen WX, Li GX, Hu ZN, Zhu P, Zhang BX, Ding ZY. Significant Response to Anti-PD-1 Based Immunotherapy Plus Lenvatinib for Recurrent Intrahepatic Cholangiocarcinoma With Bone Metastasis: A Case Report and Literature Review. *Med (Baltimore)* (2019) 98(45):e17832. doi: 10.1097/MD.0000000000017832
10. Eisenhauer EA, Therasse P, Bogaerts J, Schwartz LH, Sargent D, Ford R, et al. New Response Evaluation Criteria in Solid Tumours: Revised RECIST Guideline (Version 1.1). *Eur J Can* (2009) 45(2):228–47. doi: 10.1016/j.ejca.2008.10.026
11. Seymour L, Bogaerts J, Perrone A, Ford R, Schwartz LH, Mandrekar S, et al. RECIST Working Group. iRECIST: Guidelines for Response Criteria for Use in Trials Testing Immunotherapeutics. *Lancet Oncol* (2017) 18(3):e143–52. doi: 10.1016/S1470-2045(17)30074-8
12. Hodi FS, Ballinger M, Lyons B, Soria JC, Nishino M, Tabernero J, et al. Immune-Modified Response Evaluation Criteria In Solid Tumors (imRECIST): Refining Guidelines to Assess the Clinical Benefit of Cancer Immunotherapy. *J Clin Oncol* (2018) 36(9):850–8. doi: 10.1200/JCO.2017.75.1644
13. Freites-Martinez A, Santana N, Arias-Santiago S, Viera A. Using the Common Terminology Criteria for Adverse Events (CTCAE - Version 5.0) to Evaluate the Severity of Adverse Events of Anticancer Therapies. *Actas Dermosifiliogr (Engl Ed)* (2021) 112(1):90–2. doi: 10.1016/j.ad.2019.05.009
14. Ma C, Bandukwala S, Burman D, Bryson J, Seccareccia D, Banerjee S, et al. Interconversion of Three Measures of Performance Status: An Empirical Analysis. *Eur J Can* (2010) 46(18):3175–83. doi: 10.1016/j.ejca.2010.06.126
15. Kang J, Jeong JH, Hwang HS, Lee SS, Park DH, Oh DW, et al. Efficacy and Safety of Pembrolizumab in Patients With Refractory Advanced Biliary Tract Cancer: Tumor Proportion Score as a Potential Biomarker for Response. *Cancer Res Treat* (2020) 52(2):594–603. doi: 10.4143/crt.2019.493
16. Ahn S, Lee JC, Shin DW, Kim J, Hwang JH. High PD-L1 Expression is Associated With Therapeutic Response to Pembrolizumab in Patients With Advanced Biliary Tract Cancer. *Sci Rep* (2020) 10(1):12348. doi: 10.1038/s41598-020-69366-4
17. Antoniotti C, Korn WM, Marmorino F, Rossini D, Lonardi S, Masi G, et al. Tumour Mutational Burden, Microsatellite Instability, and Actionable Alterations in Metastatic Colorectal Cancer: Next-Generation Sequencing Results of TRIBE2 Study. *Eur J Can* (2021), 155:73–84. doi: 10.1016/j.ejca.2021.06.037
18. Wang Y, Yang X, Wang D, Yang X, Wang Y, Long J, et al. Lenvatinib Beyond First-Line Therapy in Patients With Advanced Biliary Tract Carcinoma. *Front Oncol* (2022) 12:785535. doi: 10.3389/fonc.2022.785535
19. Kim RD, Chung V, Alese OB, El-Rayes BF, Li D, Al-Toubah TE, et al. A Phase 2 Multi-Institutional Study of Nivolumab for Patients With Advanced Refractory Biliary Tract Cancer. *JAMA Oncol* (2020) 6(6):888–94. doi: 10.1001/jamaoncol.2020.0930
20. Ueno M, Ikeda M, Sasaki T, Nagashima F, Mizuno N, Shimizu S, et al. Phase 2 Study of Lenvatinib Monotherapy as Second-Line Treatment in Unresectable Biliary Tract Cancer: Primary Analysis Results. *BMC Can* (2020) 20(1):1105. doi: 10.1186/s12885-020-07365-4
21. Pavicevic S, Reichelt S, Uluk D, Lurje I, Engelmann C, Modest DP, et al. Prognostic and Predictive Molecular Markers in Cholangiocarcinoma. *Cancers (Basel)* (2022) 14(4):1026. doi: 10.3390/cancers14041026
22. Valle J, Wasan H, Palmer DH, Cunningham D, Anthoney A, Maraveyas A, et al. ABC-02 Trial Investigators. Cisplatin Plus Gemcitabine Versus Gemcitabine for Biliary Tract Cancer. *N Engl J Med* (2010) 362(14):1273–81. doi: 10.1056/NEJMoa0908721
23. Valle JW, Lamarca A, Goyal L, Barriuso J, Zhu AX. New Horizons for Precision Medicine in Biliary Tract Cancers. *Cancer Discovery* (2017) 7 (9):943–62. doi: 10.1158/2159-8290.CD-17-0245
24. Lamarca A, Barriuso J, McNamara MG, Valle JW. Molecular Targeted Therapies: Ready for "Prime Time" in Biliary Tract Cancer. *J Hepatol* (2020) 73(1):170–85. doi: 10.1016/j.jhep.2020.03.007
25. Demols A, Borbath I, Van den Eynde M, Houbiers G, Peeters M, Marechal R, et al. Regorafenib After Failure of Gemcitabine and Platinum-Based Chemotherapy for Locally Advanced/Metastatic Biliary Tumors: REACHIN, a Randomized, Double-Blind, Phase II Trial. *Ann Oncol* (2020) 31(9):1169–77. doi: 10.1016/j.annonc.2020.05.018
26. Mo DC, Luo PH, Huang SX, Wang HL, Huang JF. Safety and Efficacy of Pembrolizumab Plus Lenvatinib Versus Pembrolizumab and Lenvatinib Monotherapies in Cancers: A Systematic Review. *Int Immunopharmacol* (2021) 91:107281. doi: 10.1016/j.intimp.2020.107281

27. Yoon JG, Kim MH, Jang M, Kim H, Hwang HK, Kang CM, et al. Molecular Characterization of Biliary Tract Cancer Predicts Chemotherapy and Programmed Death 1/Programmed Death-Ligand 1 Blockade Responses. *Hepatology*. (2021) 74(4):1914–31. doi: 10.1002/hep.31862
28. Chae H, Kim D, Yoo C, Kim KP, Jeong JH, Chang HM, et al. Therapeutic Relevance of Targeted Sequencing in Management of Patients With Advanced Biliary Tract Cancer: DNA Damage Repair Gene Mutations as a Predictive Biomarker. *Eur J Can* (2019) 120:31–9. doi: 10.1016/j.ejca.2019.07.022

Conflict of Interest: The authors declare that the research was conducted in the absence of any commercial or financial relationships that could be construed as a potential conflict of interest.

Publisher's Note: All claims expressed in this article are solely those of the authors and do not necessarily represent those of their affiliated organizations, or those of the publisher, the editors and the reviewers. Any product that may be evaluated in this article, or claim that may be made by its manufacturer, is not guaranteed or endorsed by the publisher.

frontiers | Frontiers in Immunology

TYPE Original Research
PUBLISHED 08 August 2022
DOI 10.3389/fimmu.2022.947756

OPEN ACCESS

EDITED BY
Yubin Li,
University of Pennsylvania,
United States

REVIEWED BY
Xin He,
Zhongshan School of Medicine, Sun Yat-sen University, China
Dongxiao Yang,
University of St Andrews,
United Kingdom

*CORRESPONDENCE
Xuyao Zhang
xuyaozhang15@fudan.edu.cn
Meiqing Feng
fmq@fudan.edu.cn

SPECIALTY SECTION
This article was submitted to Cancer Immunity and Immunotherapy, a section of the journal Frontiers in Immunology

RECEIVED 19 May 2022
ACCEPTED 15 July 2022
PUBLISHED 08 August 2022

CITATION
Wang R, Liu H, He P, An D, Guo X, Zhang X and Feng M (2022) Inhibition of PCSK9 enhances the antitumor effect of PD-1 inhibitor in colorectal cancer by promoting the infiltration of $CD8^+$ T cells and the exclusion of Treg cells.
Front. Immunol. 13:947756.
doi: 10.3389/fimmu.2022.947756

Inhibition of PCSK9 enhances the antitumor effect of PD-1 inhibitor in colorectal cancer by promoting the infiltration of $CD8^+$ T cells and the exclusion of Treg cells

Rui Wang, Hongchuan Liu, Peng He, Duopeng An, Xiaohan Guo, Xuyao Zhang* and Meiqing Feng*

Department of Biological Medicines & Shanghai Engineering Research Center of Immunotherapeutics, Fudan University School of Pharmacy, Shanghai, China

Immunotherapy especially immune checkpoint inhibitors (ICIs) has brought favorable clinical results for numerous cancer patients. However, the efficacy of ICIs in colorectal cancer (CRC) is still unsatisfactory due to the poor median progression-free survival and overall survival. Here, based on the CRC models, we tried to elucidate novel relapse mechanisms during anti-PD-1 therapy. We found that PD-1 blockade elicited a mild antitumor effect in these tumor models with both increased $CD8^+$ T cells and Treg cells. Gene mapping analysis indicated that proprotein convertase subtilisin/kexin type 9 (PCSK9), low-density lipoprotein receptor, transforming growth factor-β (TGF-β), and CD36 were unexpectedly upregulated during PD-1 blockade. To investigate the critical role of these proteins especially PCSK9 in tumor growth, anti-PCSK9 antibody in combination with anti-PD-1 antibody was employed to block PCSK9 and PD-1 simultaneously in CRC. Data showed that neutralizing PCSK9 during anti-PD-1 therapy elicited a synergetic antitumor effect with increased $CD8^+$ T-cell infiltration and inflammatory cytokine releases. Moreover, the proportion of Treg cells was significantly reduced by co-inhibiting PCSK9 and PD-1. Overall, inhibiting PCSK9 can further enhance the antitumor effect of anti-PD-1 therapy in CRC, indicating that targeting PCSK9 could be a promising approach to potentiate ICI efficacy.

KEYWORDS

PD-1, $CD8^+$ T cells, regulatory T cells, tumor microenvironment, PCSK9

Introduction

Colorectal cancer (CRC) is the second leading cause of cancer-related death with an incidence of 10.2% and a mortality of 9.2% (1, 2). As a promising treatment to modulate the host's immune system, immunotherapy such as immune checkpoint inhibitors (ICIs) shows durable antitumor effects and revolutionizes the management of various cancers including melanoma and non-small cell lung cancer (NSCLC) (3, 4). However, the low response rate and emerging resistance mechanism still pose limitations to the application of ICIs in CRC (5). Therefore, studies dedicated to overcoming CRC resistance to ICIs are in urgent need.

Studies have uncovered that tumor microenvironment (TME) consisting of various components plays a critical role during antitumor immunity induced by ICIs. Infiltration of immune cells and the interaction between immune cells and tumor cells posed a significant impact on the outcomes of ICI therapy (6). Furthermore, the nutrient-deficient and hypoxic microenvironment also force immune cells to undergo metabolic transformation to immune-tolerant phenotypes. Metabolic regulation of glucose, lactate, and especially lipid can refuel immune cells to favor antitumor immunity in TME (7, 8). Glycolysis induced by autophagy was indispensable for oncogenic transformation (9). Our previous research also demonstrated that inhibiting autophagy could enhance phagocytosis and cytotoxicity of macrophages and further potentiate the antitumor effect of ICIs (10, 11). Cholesterol accumulation in TME facilitates the polarization and activity of tumor-associated macrophages (TAMs) and further impairs cytokine release of $CD8^+$ T cells (12, 13). These studies indicate that targeting metabolism in TME could be a potential modality to potentiate the efficacy of ICIs.

Recently, proprotein convertase subtilisin/kexin type 9 (PCSK9), a lipid metabolism-related protein, has been reported to be critical for tumorigenesis and progression (14). PCSK9 is an indispensable element in regulating lipid metabolism by inducing the degradation of low-density lipoprotein receptor (LDLR) in lysosome. Inhibitors of PCSK9 have been approved for the treatment of atherosclerotic cardiovascular diseases associated with hypercholesterolemia (15, 16). More importantly, PCSK9 has been proven to disrupt the recycling of MHC I to the cell surface by promoting MHC I degradation. Inhibiting PCSK9 by small molecular compounds or monoclonal antibodies increases the expression of MHC I on the tumor cell surface, promoting intratumoral infiltration of cytotoxic lymphocytes (17, 18). These data reveal that PCSK9 may be a crucial regulator for cancer immunotherapy. However, the effects of PCSK9 in CRC under anti-PD-1 therapy are still unclear. Hence, in this study, two syngeneic CRC models were constructed to elucidate the crucial role and mechanism of PCSK9 during anti-PD-1 therapy.

Results

PD-1 blockade presented a mild antitumor effect with increased $CD8^+$ T cells and Treg cells

To examine the effect of PD-1 blockade in CRC, MC38 and CT26 tumor models were well-constructed and anti-PD-1 antibody was administered at a dose of 5 mg/kg twice a week. In the MC38 tumor model, results showed that PD-1 blockade exerted a mild antitumor effect as the tumor growth was delayed 14 days after the first administration (Figure 1A). However, no antitumor effect of the anti-PD-1 antibody was observed in the CT26 tumor model (Figure 1B). In view of the mild efficacy of anti-PD-1 therapy in CRC, we detected the infiltration of $CD8^+$ T cells in the tumors. Flow cytometry analysis showed that $CD45^+CD3^+$ T lymphocytes and $CD8^+$ T cells were significantly increased in both CRC models (Figures 1C, D). However, regulatory T (Treg) cells were also elevated by PD-1 blockade in these models (Figure 1C). Furthermore, IHC staining confirmed that PD-1 blockade increased both $CD8^+$ T lymphocytes and $Foxp3^+$ cells in the tumors (Figures 1E, F). These results indicated that anti-PD-1 antibody elicited a mild antitumor effect in CRC with increased infiltration of Tregs and $CD8^+$ T cells.

PD-1 blockade enhanced PCSK9 expression

To further explore the underlying mechanism leading to the mild antitumor effect of anti-PD-1 ICI in CRC, several landmark cytokines of immune cell cytotoxicity including IFN-γ, granzyme B, and TNF-α were evaluated. As shown in Figure 2, IFN-γ and granzyme B in CRC models were upregulated after blocking PD-1 while the level of TNF-α was barely affected (Figures 2A, B). Except for these inflammation-related cytokines, we found that anti-PD-1 therapy also engaged in the regulation of lipid metabolism-related proteins including PCSK9 and LDLR (Figures 2C, D). LDLR is a pivotal receptor in cholesterol regulation, which is targeted by PCSK9. When binding to LDLR, PCSK9 can promote its degradation in lysosome (19). Interestingly, the mRNA level of CD36 was upregulated in CT26 tumors but not in MC38 tumors. In summary, PD-1 blockade showed a significant influence on the gene expression of lipid metabolism-related proteins including PCSK9 in colorectal tumors.

Co-targeting PD-1 and PCSK9 elicited an enhanced antitumor effect

Considering the enhanced PCSK9 expression during anti-PD-1 therapy, anti-PCSK9 antibody was employed to detect the

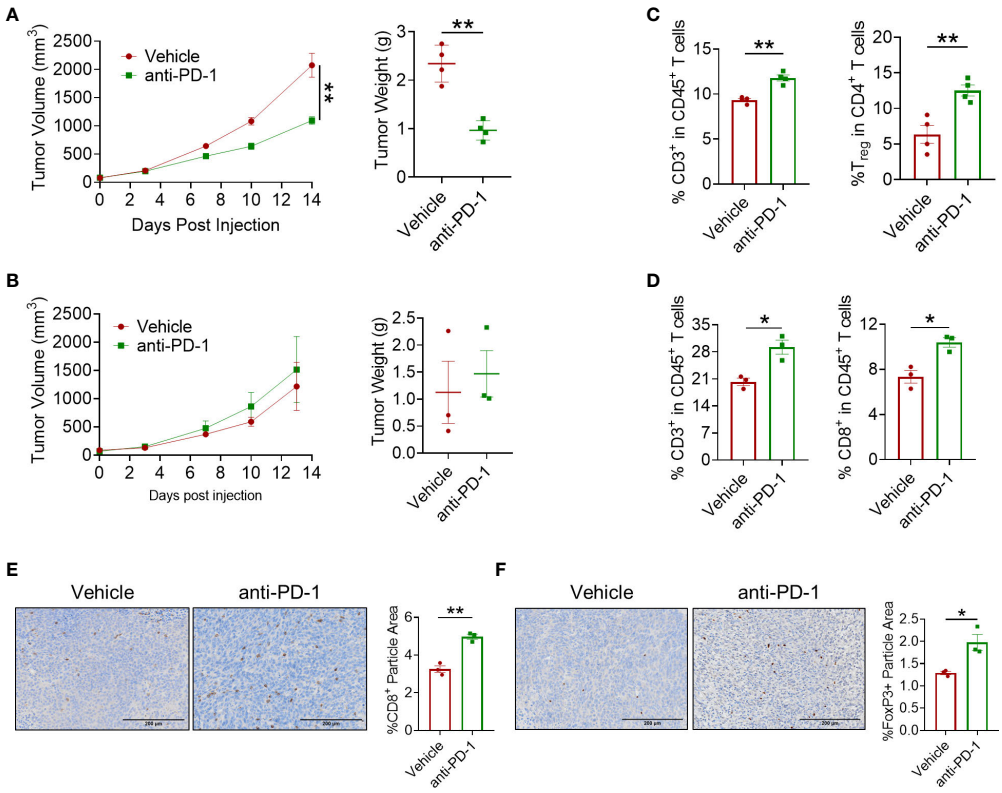

FIGURE 1
In vivo antitumor effect of anti-PD-1 antibody. **(A)** Tumor volume and tumor weight in the MC38 tumor model. Anti-PD-1 mAb administration was 5 mg/kg, n = 4 mice/group. **(B)** Tumor volume and tumor weight of CT26 tumor model. Anti-PD-1 mAb administration was 5 mg/kg, n = 3 mice/group. **(C, D)** Flow cytometry analysis of tumor-infiltrating T cells for mice treated with PBS or anti-PD-1 antibody in MC38 tumor model **(C)** and in CT26 tumor model **(D)**. **(E, F)** IHC staining of CD8a and Foxp3 in CT26 tumors. "*" means p-value < 0.05 and "**" means p-value < 0.01.

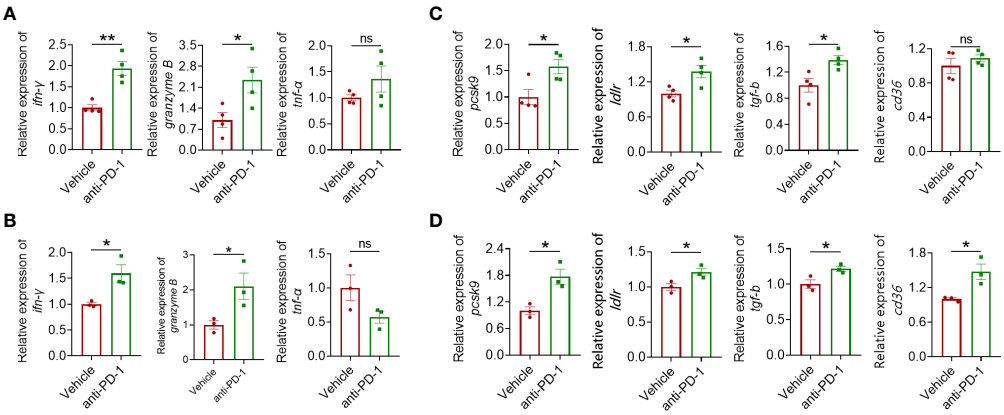

FIGURE 2
Quantitative real-time PCR (qRT-PCR) analysis of IFN-γ, granzyme B, and TNF-α gene expression in MC38 tumors **(A)** and CT26 tumors **(B)**. RT-qPCR analysis of PCSK9, LDLR, TGF-β, and CD36 gene expression in tumor of the MC38 tumor model **(C)** and the CT26 tumor model **(D)**. "*" means p-value < 0.05 and "**" means p-value < 0.01 while "ns" means not statistically significant.

critical role of PCSK9 in CRC. Figure 3A shows that anti-PCSK9 antibody further potentiated the antitumor effect of PD-1 inhibitor in the MC38 tumor model. In the CT26 tumor model, PD-1 inhibitor in combination with anti-PCSK9 antibody elicited synergetic antitumor effects while PD-1 blockade or anti-PCSK9 alone displayed indiscernible effects on the tumor growth (Figure 3B). PD-1 ICI in combination with anti-PCSK9 antibody showed enhanced antitumor effects in CRC models (Figures 3A, B), but a similar effect was not observed in a breast cancer model (data not shown). On D10 after administration, tumors were excised to detect the level of IFN-γ, TNF-α, and granzyme B. In MC38 tumors, anti-PD-1 antibody and anti-PCSK9 antibody co-treatment led to significant increases in granzyme B and IFN-γ (Figure 3C, Supplementary Figure 1A). Then, we analyzed the level of PCSK9, LDLR, TGF-β, and CD36. Compared to PD-1 inhibitor alone, anti-PCSK9 antibody diminished the increased expression of PCSK9, LDLR, TGF-β, and CD36 (Figures 3C–H, Supplementary Figures 1B–E). These data indicated that targeting PD-1 and PCSK9 elicited a synergetic antitumor effect in CRC.

Anti-PCSK9 promoted $CD8^+$ T-cell infiltration induced by PD-1 inhibitor

To explore the synergetic antitumor effect of anti-PD-1 and anti-PCSK9 antibodies in CRC, tumor-infiltrating $CD8^+$ T cells were detected. IHC staining showed that PD-1 inhibition led to the increased tumor-infiltrating $CD8^+$ T cells in MC38 and CT26 tumor models. Despite no significant elevation of $CD8^+$ T cells induced by PCSK9 blockade alone, PD-1 inhibitor combined with anti-PCSK9 antibody indeed potentiated the infiltration of $CD8^+$ T cells (Figures 4A, B). In addition, flow cytometry analysis showed that the proportion of tumor-infiltrating $CD8^+$ T cells in the combination therapy was obviously higher than either monotherapy group (Figure 4C). These data demonstrated that targeting PCSK9 potentiated the antitumor effect of PD-1 blockade *via* promoting the infiltration of cytotoxic $CD8^+$ T cells.

PCSK9 blockade eliminated the increased Treg cells induced by PD-1 inhibitor

Treg cell is a typical suppressive immune cell, promoting tumor cells to escape from immune surveillance. We next detected whether anti-PCSK9 antibody affected PD-1 blockade-induced Treg cells *via* IHC analysis. Compared with PD-1 blockade, anti-PCSK9 antibody alone has no obvious effect on Treg cells, while anti-PCSK9 antibody combined with anti-PD-1 antibody eliminated the increased Treg cells (Figures 5A, B). Furthermore, flow cytometry further confirmed that the PD-1 inhibitor-increased percentage of Treg cell proportion was decreased by anti-PCSK9 antibody (Figure 5C). Except for $CD8^+$ T cells and Treg cells, we did not observe significant influence on innate immune cells including macrophages, natural killer cells, and dendritic cells by simultaneous inhibition of PD-1 and PCSK9 (Supplementary Figures 2A, B).

Finally, to verify which lymphocyte subpopulation contributed to the synergistic antitumor effect of targeting PD-1 and PCSK9 in CRC, anti-CD4, anti-CD8, anti-NK1.1, and anti-CSF1R antibody were applied to deplete the corresponding subset of immune cells, respectively. These antibodies have been proved to block the cells with relevant marker in mouse spleen (Supplementary Figure 2C). As shown in Figures 5D, E, $CD8^+$ T depletion totally eliminated the antitumor effect of targeting PD-1 and PCSK9. Depletion of NK cells or macrophages barely affected the tumor burden. Importantly, $CD4^+$ T cell-depleting antibody presented an unexpected enhancement on the antitumor effect of anti-PD-1 and anti-PCSK9 cotreatment. Overall, our results indicated that PCSK9 blockade enhanced the antitumor effect of PD-1 inhibitor through eliminating the increased Treg cells.

Discussion

Since the discovery of ICIs, the therapeutic paradigm of cancer has been changed remarkably. However, the antitumor efficacy of ICIs in solid tumor is still unsatisfied although it has achieved tumor remission in some patients. Compared with melanoma or NSCLC, the objective response rate of ICI therapy in CRC patients is much lower (20). Currently, because of the extensive application of ICIs in clinic, many strategies attempt to overcome resistance to ICIs. The combination of different ICIs or ICIs with proinflammatory cytokines has been proposed to further enhance antitumor immune response. Simultaneous administration of immune-enhancing agents can indeed improve antitumor immunity but is accompanied by a higher risk of immune-related adverse effects (21). Triple combination therapy, such as anti-PD-L1 antibody, poly-(ADP-ribose) polymerase inhibitor, and MEK inhibitor, was also applied to overcome resistance to anti-PD-L1 therapies in KRAS mutant cancer (22). Agonists targeting STING in combination with CTLA-4 or PD-1 inhibitor also exerted refreshing efficacy in the CRC model with complete tumor regression and long-lasting immune memory (23). In this study, we investigated PCSK9 during anti-PD-1 therapy in CRC models, and PD-1 inhibitor and anti-PCSK9 antibody were administered to confirm the synergetic antitumor effect of targeting PD-1 and PCSK9 in CRC.

In syngeneic CRC models, PD-1 inhibitor only has a limited antitumor effect with the infiltration of $CD8^+$ T cells and Tregs. As a type of immunosuppressive T cell, Treg is indispensable in

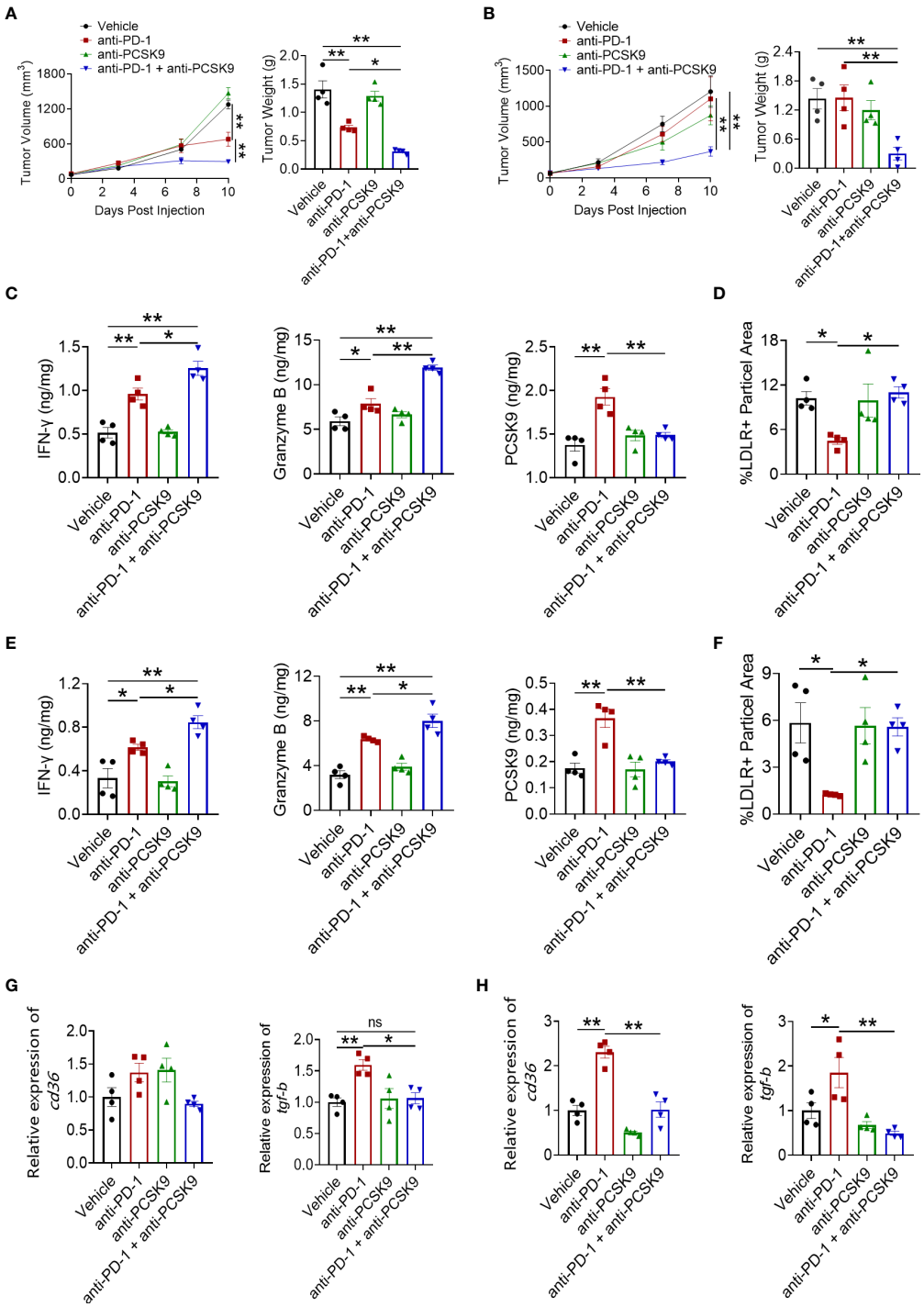

FIGURE 3
Tumor volume and tumor weight in MC38 tumor model **(A)** and CT26 tumor model **(B)** treated with anti-PD-1 or anti-PCSK9 antibody. Analysis of IFN-γ, granzyme B and PCSK9 protein level in tumor of MC38 tumor model **(C)** and CT26 tumor model **(E)** by ELISA. Quantitative analysis of LDLR expression on cell membrane in MC38 tumors **(D)** and CT26 tumors **(F)** by immunofluorescence. Quantitative RT-PCR analysis of CD36 and TGF-β gene expression in MC38 tumors **(G)** and in CT26 tumors **(H)**. "*" means p-value < 0.05 and "**" means p-value < 0.01 while "ns" means not statistically significant.

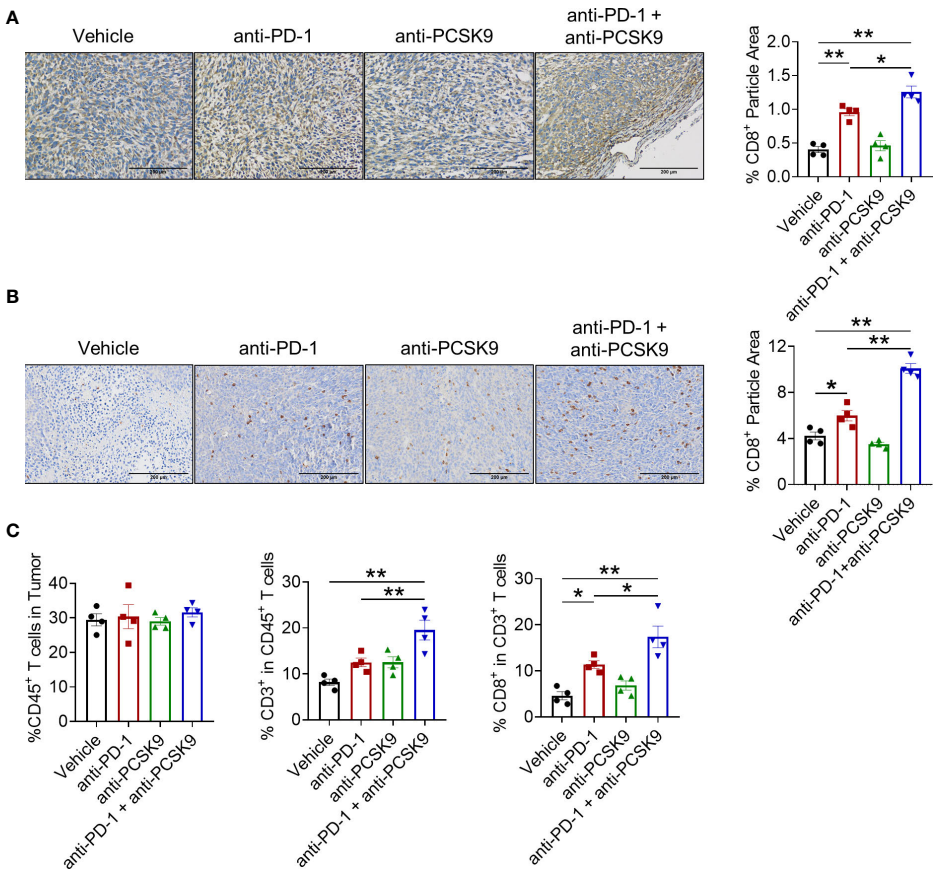

FIGURE 4
(A) IHC staining of CD8a in tumor of the MC38 tumor model treated with anti-PD-1 or anti-PCSK9 antibody and quantitative analysis of positive particles and **(B)** for the CT26 tumor model. **(C)** Flow cytometry analysis of $CD45^+$, $CD3^+$, and $CD8^+$ T-cell infiltration in MC38 tumors. "*" means p-value < 0.05 and "**" means p-value < 0.01.

maintaining normal tissue homeostasis by restraining excessive immune responses. However, the immunosuppressive effect of Tregs also facilitates tumor cells to avoid immune surveillance (24). Studies have indicated that Tregs performed immunosuppressive function through multifaceted ways including repressing the production of $CD8^+$ T cell-derived IFN-γ and converting ATP to adenosine (25, 26). In our research, we found that PCSK9 blockade could eliminate increased tumor-infiltrating Tregs induced by PD-1 inhibitor. As a result, the antitumor effect of PD-1 blockade was significantly potentiated after Treg exclusion.

TGF-β signaling potentiates the immunosuppressive activity of Tregs, leading to a poor outcome of PD-L1 blockade, and TGF-β neutralization could help overcome the resistance to ICIs (27–29). A previous study uncovered that PCSK9 deficiency could reduce SMAD2 phosphorylation and further promote TGFβR1 degradation in lysosome (30), indicating the internal relation between PCSK9 and TGF-β in TME. Consistent with these concepts, we observed the upregulation of TGF-β expression during anti-PD-1 therapy, which could be diminished by the administration of anti-PCSK9 antibody. Furthermore, studies indicated that expression of CD36, a type of scavenger receptor, was elevated on tumor-infiltrating Tregs and $CD8^+$ T cells (31). In Tregs, CD36 could facilitate lipid uptake and stimulate mitochondrial fitness to maintain cell survival and proliferation, while CD36 enhanced oxidized low-density lipoprotein uptake and induced an unfavorable metabolic reprogramming in $CD8^+$ T cells (32, 33). In this work, we confirmed that PD-1 blockade induced CD36 expression in CRC tumors and PSCK9 deficiency could eliminate the increased CD36.

In summary, the efficacy of PD-1 inhibitor was related to the expression level of PCSK9 in CRC. PCSK9-neutralizing antibody could enhance the antitumor effect of PD-1 inhibitor with increased $CD8^+$ T-cell infiltration and Treg exclusion. Moreover, inhibiting PCSK9 could regulate lipid metabolism in CRC tumors *via* the downregulated expression of LDLR and CD36 to remodel TME to pro-inflammatory circumstance.

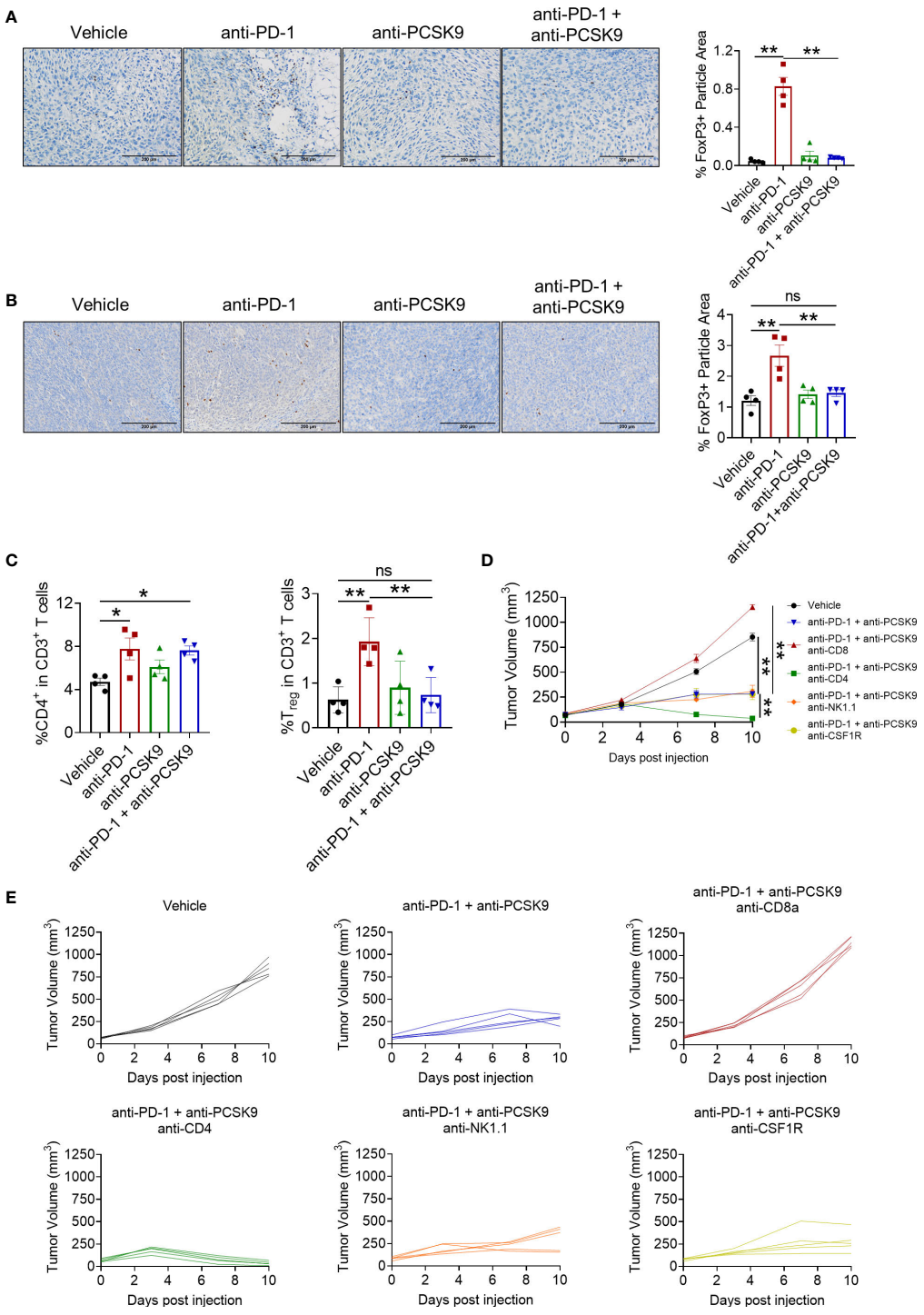

FIGURE 5
(A) IHC staining of Foxp3 in MC38 tumors treated with anti-PD-1 or anti-PCSK9 antibody and quantitative analysis of positive particles and **(B)** for CT26 tumors. **(C)** Flow cytometry analysis of $CD4^+$ and $Foxp3^+$ T-cell infiltration in MC38 tumors. **(D, E)** Tumor volume in the mice under the treatment of anti-PD-1 and anti-PCSK9 antibody with/without anti-CD8, anti-CD4, anti-NK1.1, and anti-CSF1R antibody. "*" means p-value < 0.05 and "**" means p-value < 0.01 while "ns" means not statistically significant.

Overall, our research proposed a novel idea to overcome ICI resistance in CRC by simultaneous inhibition of PD-1 and PCSK9.

Materials and methods

CRC cells and tumor models

Murine CRC cell lines MC38 and CT26 were cultured as described in previous articles (34, 35). Mice were provided by Shanghai Slack Laboratory Animal Co., Ltd. (Shanghai, China) and the animal experiments were approved by the Animal Ethical Committee of School of Pharmacy Fudan University. CRC tumor models were also well established according to the methods in the articles (34, 35). In brief, mice were randomly divided into the indicated groups. The formula for tumor volume was ½ × length × width^2. Anti-PD-1 antibody monotherapy for MC38 and CT26 CRC models was injected (i.p.) twice a week at a dose of 5 mg/kg. Anti-PCSK9 antibody was injected (i.p.) twice a week at a dose of 10 mg/kg. Anti-CD8a, anti-CD4, antiNK1.1, and anti-CSF1R antibody was injected (i.p.) 1 day before antibody treatment at doses of 200 μg, 200 μg, 400 μg, and 300 μg per mouse, respectively.

IHC staining

Tumor was fixed in formalin and then embedded with paraffin for section preparation. After the sections were dewaxed and hydrated, tissue antigen was repaired with citrate buffer. Endogenous peroxidase was deactivated using H_2O_2 and then blocked with BSA. The sections were incubated with primary antibody and HRP-labeled secondary antibodies, respectively. Then, these sections were counterstained with hematoxylin. Images were obtained by a microscope for analysis. The following were the antibodies used: rabbit anti-mouse CD8a antibody (Servicebio, GB11068), rabbit anti-mouse Foxp3 antibody (Servicebio, GB112325), rabbit anti-mouse CSF1R antibody (Servicebio, GB11581), rabbit anti-mouse NK1.1 antibody (abcam, ab289542), rabbit anti-mouse CD11b antibody (Servicebio, GB11581), and rabbit anti-mouse CD4 antibody (Servicebio, GB13064-2). Proportions of the positive area were counted by ImageJ software.

IF staining

All operations were performed referring to a previous article (36). Materials used were as follows: DAPI (Servicebio, G1012) and rabbit anti-mouse LDLR antibody (Servicebio, GB11369). Proportions of the positive area were counted by ImageJ software.

Flow cytometry analysis

Tumors were obtained to prepare single-cell suspension and then incubated with red blood cells lysis buffer. Cell density was adjusted to 1×10^6 per milliliter. Cells were incubated with anti-CD16/32 antibody to block Fc receptors. After incubating with antibody targeted cell surface antigen including anti-45, anti-CD3, anti-CD8, anti-CD4, and anti-CD25 antibodies, cells were fixed with 1× Foxp3 Fix/Perm buffer and next incubated with 1× Foxp3 Perm buffer for the detection of intracellular antigen Foxp^3. Finally, cells were incubated with anti-Foxp3 antibody in the dark at room temperature and analyzed with CytoFlex S (Beckman). The antibodies used were as follows: anti-CD45 antibody (MultiSciences, Violetflour 450, cat.70-AM04512-100; BioLegend, APC/Cyanine7, cat.103116), anti-CD3ϵ antibody (BioLegend, PE/Cyanine7, cat.100320; BioLegend, PerCP/Cyanine5.5, cat.100328), anti-CD4 antibody (BioLegend, APC, cat.100412), anti-CD8a antibody (BioLegend, PerCP, cat.100732; BioLegend, FITC, cat.100706), and anti-Foxp3 antibody (BioLegend, PE, cat.320008).

ELISA

All the operations were carried out according to the manufacturer' s instructions. ELISA kits used are as follows: IFN-γ ELISA kit (MultiSciences, cat. EK280/3-96), granzyme B ELISA kit (MultiSciences, cat. EK2173-96), and PCSK9 ELISA kit (Solarbio, cat. SEKM-0243).

RT-PCR analysis

All the operations were carried out according to the manufacturer' s instructions. Gene expression was normalized to β-actin and calculated with the formula $2^{-\Delta\Delta Ct}$. Reagent kits used are as follows: TRIzol (Vazyme, cat. R401-01), HiScript II Q RT SuperMix for qPCR kit (Vazyme, cat. R223-01), and ChamQ Universal SYBR qPCR Master Mix kit (Vazyme, cat. Q711-02/03). Primers are shown as follows: β-actin (F: AGCCTTCCT TCTTGGGTATGG; R: CAACGTCACACTTCATGATGG AAT), pcsk9 (F: GAGACCCAGAGGCTACAGATT; R: AAT GTACTCCACATGGGGCAA), ifn-γ (F: CAACAGCAAG GCGAAAAAGG; R: CCTGTGGGTTGTTGACCTCAA), gzmb (F: ATCAAGGATCAGCAGCCTGA; R: TGATGT CATTGGAGAATGTCT), tnf-α (F: GCCACCACGCTCTT CTGTCT; R: GGTCTGGGCCATAGAACTGATG), perforin (F: AGCACAAGTTCGTGCCAGG; R: GCGTCTCTCATTAG GGAGTTTTT), ldlr (F: CCTCAAGTACCTTGGTATGACGC; R: GAGGCTGTCGGTCAGGATG), cd36 (F: TCGGAACTGTG GGCTCATTG; R: CCTCGGGGTCCTGAGTTATATTTTC), cd8a (F: CCGTTGACCCGCTTTCTGT; R: CGGCGTCCATTT

TCTTTGGAA), and tgf-β (F: CCGCAACAACGCCATCTATG; R: CTCTGCACGGGACAGCAAT).

Statistical analysis

Unpaired *t*-test, one-way ANOVA, or two-way ANOVA was performed for the comparison between groups. Data are presented as mean ± standard error. p-value < 0.05 was considered to be significant ("*" means p-value < 0.05 and "**" means p-value < 0.01 while "ns" means not statistically significant).

Data availability statement

The original contributions presented in the study are included in the article/Supplementary material. Further inquiries can be directed to the corresponding authors.

Ethics statement

The animal study was reviewed and approved by Animal Ethical Committee of School of Pharmacy Fudan University.

Author contributions

RW, PH, and HL completed the biological and analysis experiment, and drafted the manuscript. XZ and MF conceived and proofread the manuscript. All authors approved the submitted version.

Funding

This work was supported by the Science and Technology Supporting Project by Shanghai Municipal Science and Technology Committee (19431903000) and Shanghai Sailing Program (21YF1401900).

Conflict of interest

The authors declare that the research was conducted in the absence of any commercial or financial relationships that could be construed as a potential conflict of interest.

Publisher's note

All claims expressed in this article are solely those of the authors and do not necessarily represent those of their affiliated organizations, or those of the publisher, the editors and the reviewers. Any product that may be evaluated in this article, or claim that may be made by its manufacturer, is not guaranteed or endorsed by the publisher.

Supplementary material

The Supplementary Material for this article can be found online at: https://www.frontiersin.org/articles/10.3389/fimmu.2022.947756/full#supplementary-material

References

1. Bray F, Ferlay J, Soerjomataram I, Siegel RL, Torre LA, Jemal A. Global cancer statistics 2018: GLOBOCAN estimates of incidence and mortality worldwide for 36 cancers in 185 countries. *CA Cancer J Clin* (2018) 68(6):394–424. doi: 10.3322/caac.21492

2. Lombardi L, Morelli F, Cinieri S, Santini D, Silvestris N, Fazio N, et al. Adjuvant colon cancer chemotherapy: where we are and where we'll go. *Cancer Treat Rev* (2010) 36 Suppl 3:S34–41. doi: 10.1016/s0305-7372(10)70018-9

3. Carlino MS, Larkin J, Long GV. Immune checkpoint inhibitors in melanoma. *Lancet* (2021) 398(10304):1002–14. doi: 10.1016/s0140-6736(21)01206-x

4. Zhou F, Qiao M, Zhou C. The cutting-edge progress of immune-checkpoint blockade in lung cancer. *Cell Mol Immunol* (2021) 18(2):279–93. doi: 10.1038/s41423-020-00577-5

5. He M, Yang T, Wang Y, Wang M, Chen X, Ding D, et al. Immune checkpoint inhibitor-based strategies for synergistic cancer therapy. *Adv Healthc Mater* (2021) 10(9):e2002104. doi: 10.1002/adhm.202002104

6. Petitprez F, Meylan M, de Reyniès A, Sautès-Fridman C, Fridman WH. The tumor microenvironment in the response to immune checkpoint blockade therapies. *Front Immunol* (2020) 11:784. doi: 10.3389/fimmu.2020.00784

7. Ringel AE, Drijvers JM, Baker GJ, Catozzi A, García-Cañaveras JC, Gassaway BM, et al. Obesity shapes metabolism in the tumor microenvironment to suppress anti-tumor immunity. *Cell* (2020) 183(7):1848–66.e26. doi: 10.1016/j.cell.2020.11.009

8. Bader JE, Voss K, Rathmell JC. Targeting metabolism to improve the tumor microenvironment for cancer immunotherapy. *Mol Cell* (2020) 78(6):1019–33. doi: 10.1016/j.molcel.2020.05.034

9. Lock R, Roy S, Kenific CM, Su JS, Salas E, Ronen SM, et al. Autophagy facilitates glycolysis during ras-mediated oncogenic transformation. *Mol Biol Cell* (2011) 22(2):165–78. doi: 10.1091/mbc.E10-06-0500

10. Zhang X, Wang S, Nan Y, Fan J, Chen W, Luan J, et al. Inhibition of autophagy potentiated the anti-tumor effects of VEGF and CD47 bispecific therapy in glioblastoma. *Appl Microbiol Biotechnol* (2018) 102(15):6503–13. doi: 10.1007/s00253-018-9069-3

11. Zhang X, Fan J, Wang S, Li Y, Wang Y, Li S, et al. Targeting CD47 and autophagy elicited enhanced antitumor effects in non-small cell lung cancer. *Cancer Immunol Res* (2017) 5(5):363–75. doi: 10.1158/2326-6066.Cir-16-0398

12. Ma X, Xiao L, Liu L, Ye L, Su P, Bi E, et al. CD36-mediated ferroptosis dampens intratumoral CD8(+) T cell effector function and impairs their antitumor ability. *Cell Metab* (2021) 33(5):1001–12.e5. doi: 10.1016/j.cmet.2021.02.015

13. Su P, Wang Q, Bi E, Ma X, Liu L, Yang M, et al. Enhanced lipid accumulation and metabolism are required for the differentiation and activation of tumor-associated macrophages. *Cancer Res* (2020) 80(7):1438–50. doi: 10.1158/0008-5472.Can-19-2994

14. Zhang SZ, Zhu XD, Feng LH, Li XL, Liu XF, Sun HC, et al. PCSK9 promotes tumor growth by inhibiting tumor cell apoptosis in hepatocellular carcinoma. *Exp Hematol Oncol* (2021) 10(1):25. doi: 10.1186/s40164-021-00218-1

15. Barale C, Melchionda E, Morotti A, Russo I. PCSK9 biology and its role in atherothrombosis. *Int J Mol Sci* (2021) 22(11):5880. doi: 10.3390/ijms22115880

16. Qi Z, Hu L, Zhang J, Yang W, Liu X, Jia D, et al. PCSK9 (Proprotein convertase Subtilisin/Kexin 9) enhances platelet activation, thrombosis, and myocardial infarct expansion by binding to platelet CD36. *Circulation* (2021) 143(1):45–61. doi: 10.1161/circulationaha.120.046290

17. Liu X, Bao X, Hu M, Chang H, Jiao M, Cheng J, et al. Inhibition of PCSK9 potentiates immune checkpoint therapy for cancer. *Nature* (2020) 588(7839):693–8. doi: 10.1038/s41586-020-2911-7

18. Yuan J, Cai T, Zheng X, Ren Y, Qi J, Lu X, et al. Potentiating CD8(+) T cell antitumor activity by inhibiting PCSK9 to promote LDLR-mediated TCR recycling and signaling. *Protein Cell* (2021) 12(4):240–60. doi: 10.1007/s13238-021-00821-2

19. Lagace TA. PCSK9 and LDLR degradation: regulatory mechanisms in circulation and in cells. *Curr Opin Lipidol* (2014) 25(5):387–93. doi: 10.1097/mol.0000000000000114

20. Brahmer JR, Tykodi SS, Chow LQ, Hwu WJ, Topalian SL, Hwu P, et al. Safety and activity of anti-PD-L1 antibody in patients with advanced cancer. *N Engl J Med* (2012) 366(26):2455–65. doi: 10.1056/NEJMoa1200694

21. Marin-Acevedo JA, Chirila RM, Dronca RS. Immune checkpoint inhibitor toxicities. *Mayo Clin Proc* (2019) 94(7):1321–9. doi: 10.1016/j.mayocp.2019.03.012

22. Yang B, Li X, Fu Y, Guo E, Ye Y, Li F, et al. MEK inhibition remodels the immune landscape of mutant KRAS tumors to overcome resistance to PARP and immune checkpoint inhibitors. *Cancer Res* (2021) 81(10):2714–29. doi: 10.1158/0008-5472.Can-20-2370

23. Yang H, Lee WS, Kong SJ, Kim CG, Kim JH, Chang SK, et al. STING activation reprograms tumor vasculatures and synergizes with VEGFR2 blockade. *J Clin Invest* (2019) 129(10):4350–64. doi: 10.1172/jci125413

24. Saleh R, Elkord E. Treg-mediated acquired resistance to immune checkpoint inhibitors. *Cancer Lett* (2019) 457:168–79. doi: 10.1016/j.canlet.2019.05.003

25. Liu C, Chikina M, Deshpande R, Menk AV, Wang T, Tabib T, et al. Treg cells promote the SREBP1-dependent metabolic fitness of tumor-promoting macrophages *via* repression of CD8(+) T cell-derived interferon-γ. *Immunity* (2019) 51(2):381–97.e6. doi: 10.1016/j.immuni.2019.06.017

26. Maj T, Wang W, Crespo J, Zhang H, Wang W, Wei S, et al. Oxidative stress controls regulatory T cell apoptosis and suppressor activity and PD-L1-blockade resistance in tumor. *Nat Immunol* (2017) 18(12):1332–41. doi: 10.1038/ni.3868

27. Dodagatta-Marri E, Meyer DS, Reeves MQ, Paniagua R, To MD, Binnewies M, et al. α-PD-1 therapy elevates Treg/Th balance and increases tumor cell pSmad3 that are both targeted by α-TGFβ antibody to promote durable rejection and immunity in squamous cell carcinomas. *J Immunother Cancer* (2019) 7(1):62. doi: 10.1186/s40425-018-0493-9

28. de Streel G, Bertrand C, Chalon N, Liénart S, Bricard O, Lecomte S, et al. Selective inhibition of TGF-β1 produced by GARP-expressing tregs overcomes resistance to PD-1/PD-L1 blockade in cancer. *Nat Commun* (2020) 11(1):4545. doi: 10.1038/s41467-020-17811-3

29. Canè S, Van Snick J, Uyttenhove C, Pilotte L, Van den Eynde BJ. TGFβ1 neutralization displays therapeutic efficacy through both an immunomodulatory and a non-immune tumor-intrinsic mechanism. *J Immunother Cancer* (2021) 9(2):e001798. doi: 10.1136/jitc-2020-001798

30. Roudaut M, Idriss S, Caillaud A, Girardeau A, Rimbert A, Champon B, et al. PCSK9 regulates the NODAL signaling pathway and cellular proliferation in hiPSCs. *Stem Cell Rep* (2021) 16(12):2958–72. doi: 10.1016/j.stemcr.2021.10.004

31. Wang J, Li Y. CD36 tango in cancer: signaling pathways and functions. *Theranostics* (2019) 9(17):4893–908. doi: 10.7150/thno.36037

32. Wang H, Franco F, Tsui YC, Xie X, Trefny MP, Zappasodi R, et al. CD36-mediated metabolic adaptation supports regulatory T cell survival and function in tumors. *Nat Immunol* (2020) 21(3):298–308. doi: 10.1038/s41590-019-0589-5

33. Xu S, Chaudhary O, Rodríguez-Morales P, Sun X, Chen D, Zappasodi R, et al. Uptake of oxidized lipids by the scavenger receptor CD36 promotes lipid peroxidation and dysfunction in CD8(+) T cells in tumors. *Immunity* (2021) 54(7):1561–77.e7. doi: 10.1016/j.immuni.2021.05.003

34. Liu H, Zhao Z, Zhang L, Li Y, Jain A, Barve A, et al. Discovery of low-molecular weight anti-PD-L1 peptides for cancer immunotherapy. *J Immunother Cancer* (2019) 7(1):270. doi: 10.1186/s40425-019-0705-y

35. Liu H, Wang R, An D, Liu H, Ye F, Li B, et al. An engineered IL-21 with half-life extension enhances anti-tumor immunity as a monotherapy or in combination with PD-1 or TIGIT blockade. *Int Immunopharmacol* (2021) 101(Pt A):108307. doi: 10.1016/j.intimp.2021.108307

36. Liu J, Meng Z, Xu T, Kuerban K, Wang S, Zhang X, et al. A SIRPαFc fusion protein conjugated with the collagen-binding domain for targeted immunotherapy of non-small cell lung cancer. *Front Immunol* (2022) 13:845217. doi: 10.3389/fimmu.2022.845217

frontiers | Frontiers in Immunology

TYPE Case Report
PUBLISHED 08 August 2022
DOI 10.3389/fimmu.2022.943916

OPEN ACCESS

EDITED BY
Xian Zeng,
Fudan University, China

REVIEWED BY
Chae Moon Hong,
Kyungpook National University, South Korea
Zhongling Qiu,
Shanghai Jiao Tong University, China

*CORRESPONDENCE
Yansong Lin
linyansong1968@163.com

†These authors have contributed equally to this work and share first authorship

SPECIALTY SECTION
This article was submitted to Cancer Immunity and Immunotherapy, a section of the journal Frontiers in Immunology

RECEIVED 14 May 2022
ACCEPTED 27 June 2022
PUBLISHED 08 August 2022

CITATION
Li J, Zhang X, Mu Z, Sun D, Sun Y and Lin Y (2022) Response to apatinib and camrelizumab combined treatment in a radioiodine refractory differentiated thyroid cancer patient resistant to prior anti-angiogenic therapy: A case report and literature review. *Front. Immunol.* 13:943916. doi: 10.3389/fimmu.2022.943916

Response to apatinib and camrelizumab combined treatment in a radioiodine refractory differentiated thyroid cancer patient resistant to prior anti-angiogenic therapy: A case report and literature review

Jiayi Li[1,2,3†], Xin Zhang[1,2,3,4†], Zhuanzhuan Mu[1,2,3,4], Di Sun[1,2,3,4], Yuqing Sun[1,2,3,4] and Yansong Lin[1,2,3*]

[1]Department of Nuclear Medicine, Peking Union Medical College Hospital, Beijing, China, [2]Beijing Key Laboratory of Molecular Targeted Diagnosis and Therapy in Nuclear Medicine, Beijing, China, [3]State Key Laboratory of Complex Severe and Rare Diseases, Peking Union Medical College Hospital, Chinese Academy of Medical Science and Peking Union Medical College, Beijing, China, [4]Chinese Academy of Medical Sciences & Peking Union Medical College, Beijing, China

Background: Patients with radioactive iodine refractory progressive (RAIR) differentiated thyroid cancer (DTC) often developed resistance after first-line therapy. Apatinib plus camrelizumab is a therapy with promising efficacy in patients with other malignant cancers. Herein, we presented a case of progressive RAIR DTC treated with apatinib plus camrelizumab.

Case presentation: We reported a 43-year-old man diagnosed as DTC with metastases in the lungs, the 7th cervical vertebra, and malignant lymph nodes mainly in the mediastinum. While initially showing disease stabilization after giving the first-line multitargeted kinase inhibitor (MKI) therapy, the patient developed progressive disease and was enrolled into a combined therapy with both apatinib and camrelizumab on November 10, 2020. Upon the first 6 months, the combination therapy showed disease control in terms of both stable structural lesions and biochemical thyroglobulin (Tg) level. Six months later, a decrease over the targeted lesions was observed and a partial response (PR) according to RECIST 1.1 criteria was finally achieved upon 12 months' assessment, followed by the decline in serum Tg level. The main adverse event was occasional diarrhea without treatment interruption.

Conclusion: We reported a case with RAIR DTC that benefited from combination immunotherapy, apatinib plus camrelizumab, after resistance from donafenib. We observed a gradually getting better efficacy and a mild and long duration of this combination therapy and hoped to provide a therapeutic choice for these patients.

KEYWORDS

radioactive iodine refractory, differentiated thyroid cancer, combination immunotherapy, multitargeted kinase inhibitors plus PD-1/PD-L1 inhibitors therapy, apatinib plus camrelizumab treatment

Introduction

The progression in differentiated thyroid cancer (DTC) can occur in up to approximately 20% after standard therapeutic approaches in the 10-year follow-up (1). After radioactive iodine (RAI) therapy, loss of the ability of iodine uptake can occur in two-thirds of these patients, which are called RAI-refractory, progressive differentiated thyroid cancer (RAIR-DTC) (2). Those with RAIR-DTC have a 10-year survival rate less than 10% survival, which greatly reduce clinical dilemma.

Currently, two multitargeted kinase inhibitors (MKI) sorafenib and lenvatinib have been approved for use in patients with progressive RAIR DTC by the National Medical Products Administration (NMPA) as the first-line systemic therapy based upon their promising antitumor activity (3). However, most RAIR-DTC patients developed resistance to MKIs over the following 1 to 2 years (4). In addition, drug-induced adverse effects were commonly seen with MKI treatment under standard doses, which may downgrade the patients' quality of life and even lead to termination of MKI therapy (5). Cabozantinib is a recently approved therapy after first-line resistance (6). However, it is still a MKI therapy and could not be available in Chinese patients.

Immunotherapy PD-1/PD-L1 inhibitors have also achieved promising results in many tumor types such as melanoma and non-small cell lung cancer (7). A non-randomized, phase Ib trial KEYNOTE-028 estimated response of patients with RAIR-DTC to PD-1 and observed objective responses in a minority of patients (8). The influence of PD-1 treatment to RAIR-DTC must be substantiated in subsequent clinical trials. The combination of immunotherapy and MKIs is a topic of high interest in the treatment of advanced malignant tumors. Lenvatinib plus pembrolizumab showed more potent antitumor activity compared with either agent alone in mouse xenograft (9) and human studies (10), showing promising benefit in RAIR-DTC (11). Apatinib is a domestic MKI which showed rapid and significant efficacy in its phase II and phase III studies conducted in progressive RAIR-DTC (12), and apatinib plus camrelizumab is a combined therapy which has shown promising efficacy recently in patients with hepatocellular carcinoma or neuroendocrine carcinoma (13).

To our knowledge, apatinib combined with camrelizumab therapy has not been systematically reported in thyroid cancers. We presented here a case of progressive RAIR-DTC treated with apatinib plus camrelizumab (ClinicalTrials.gov Identifier: NCT04560127).

Case presentation

A 43-year-old man diagnosed with follicular thyroid cancer (FTC) with metastases in the lungs, the 7th cervical vertebra, and malignant lymph nodes mainly in the mediastinum and resistance to first-line MKI was given a combined therapy of antiangiogenic MKI apatinib and anti-PD-1 antibody camrelizumab in October 2020.

In 2015, the patient was diagnosed with DTC (Figures 1A, B) and received radical thyroidectomy and subsequent RAI therapy. Mutation analysis was performed, and results were positive for TERT, BRAF p.L597Q, and VEGF, while negative for RAS and BRAF p.VAL600. During the regular follow-up including cervical ultrasound and chest computed tomography (CT) scanning accompanied by TSH suppression therapy, recurrences were found in cervical lymph nodes, mediastinal lymph nodes, lungs, and the 7th cervical vertebra in 2017. Therefore, he received cervical lymph node dissection and several subsequent RAI therapies. However, his pulmonary lesions did not take iodine revealed by whole-body iodine scan after last RAI therapy in October 2019 (Figure 1C). Thus, he was identified as RAIR after receiving several surgeries and RAI therapies with a cumulative dose of 670 mCi. He was then given a first-line MKI in October 2019. While initially showing disease stabilization after giving the first-line MKI, the patient developed

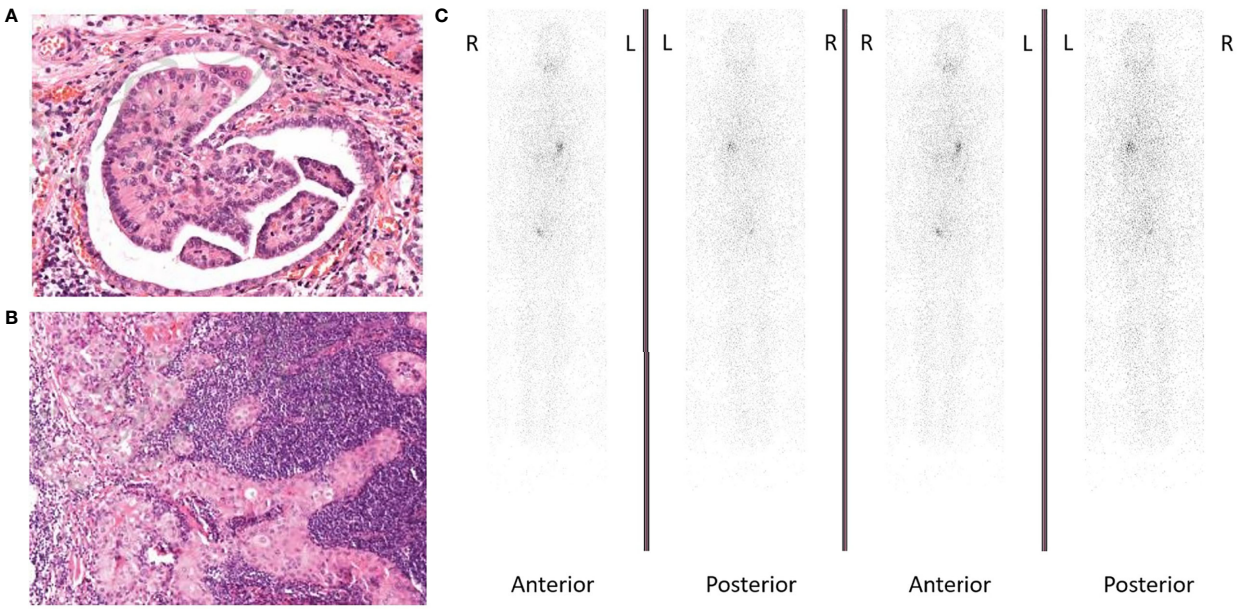

FIGURE 1
(A) Hematoxylin and eosin (H&E) staining showing follicular thyroid cancer cells (magnification ×100). **(B)** Hematoxylin and eosin (H&E) staining showing lymph node metastasis from follicular thyroid cancer (magnification ×100). **(C)** Whole-body iodine scan showed radioactive iodine refractory.

progressive disease (PD) and terminated the first-line MKI therapy on September 10, 2020.

Followed by a 4-week discontinuation, the patient was enrolled into an exploratory phase II clinical trial combining antiangiogenic MKI apatinib and anti-PD-1 antibody camrelizumab in November 2020. The therapeutic schedule was given by 250 mg apatinib orally once daily and 200 mg camrelizumab intravenously once every 2 weeks in a 4-week cycle. The patient was evaluated every cycle in the first 2 cycles and every 2 cycles thereafter. During the first 6 months' assessment, the combination therapy initially showed disease control in terms of both stable structural lesions and biochemical thyroglobulin (Tg) level (Figure 2). Six months later from April 2021, the targeted and non-targeted lesions began to shrink rapidly followed by a rapid decrease in serum Tg, and a partial response (PR) according to RECIST 1.1 criteria was finally achieved upon 12 months' assessment in October 2021 (targeted lesions: 4.7 to 2.9 cm) (Figures 2B, C). Along with this process, the biochemical Tg level also decreased from 22,481 ng/ml (October 2020) to 5,351 ng/ml (October 2021) (Figure 2D).

During this process, the main adverse event was occasional diarrhea without treatment interruption. The patient was in the state of PR at the last assessment and will be followed up in the future.

Discussion

We presented here a case of RAIR DTC with disease progression that responded to apatinib plus camrelizumab after resistance to an antiangiogenic drug. To our knowledge, we believed this was the first case of RAIR DTC with disease progression treated with apatinib plus camrelizumab. The patient showed a durable and safe response of nearly 1 year.

In our case, the patient with RAIR DTC got resistant to the first MKI donafenib. There were no public-approved treatments for RAIR DTC patients who became resistant to MKI in China. A number of previous clinical studies have explored the use of camrelizumab combined with apatinib for hepatocellular carcinoma, NSCLC, SCLC, cervical cancer, breast cancer, osteosarcoma, esophageal squamous cell carcinoma, colorectal carcinoma, gestational trophoblastic neoplasia, biliary tract cancer, and gastric and esophagogastric junction cancer and showed promising results (14–25) (Table 1). Another combination therapy of immunotherapy PD-1 inhibitors and MKIs, lenvatinib plus pembrolizumab, showed disease control in thyroid cancer. Luongo et al. (26) showed that patients with paucicellular variant anaplastic thyroid cancer reached PR 5 months after giving lenvatinib plus pembrolizumab and PR persisted over 18 months. Dierks et al. (27) and Iyer et al. (28) showed that disease control happened in over half of patients with thyroid cancer after lenvatinib plus pembrolizumab therapy (Table 2). The efficacy of these studies was consistent with our research. The mechanism may be related to that use of MKI could normalize the abnormal tumor vasculature, thus increasing the infiltration of immune effector cells like CD4+ and CD8+ T cells into tumors (30–32). Preclinical experiments also found that apatinib could enhance the efficacy of PD-1/PD-L1 blockade through alleviating hypoxia, increasing

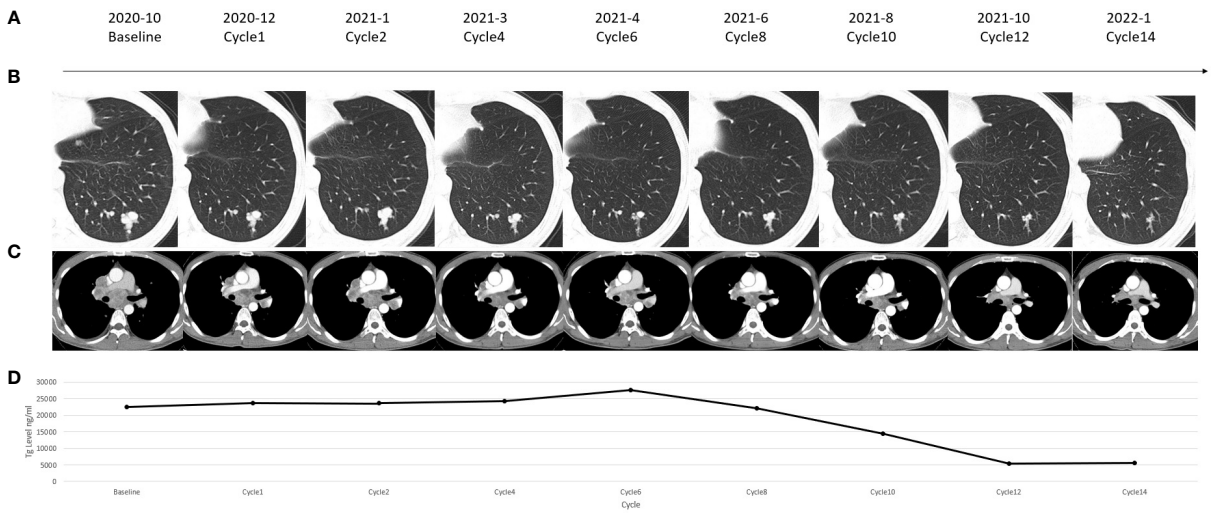

FIGURE 2
(A) Timeline of the reported case. **(B)** Chest computed tomography (CT) scanning showed change of a pulmonary lesion which was located in the left lower lobe of the lung. **(C)** Chest CT scanning showed change of a subcarinal lymph node lesion. **(D)** Change in the serum thyroglobulin (Tg) level in each assessment.

the infiltration of CD8+ T cells, and reducing tumor-associated macrophage recruitment and TGFβ amounts in both tumor and serum (33). The selection of dosing is also a question needed to be resolved. Previous fundamental studies observed a more favorable microenvironment for immunotherapy in low-dose apatinib instead of high-dose treatment (33). Therefore, the dose of our case is 250 mg apatinib in combination with 200 mg camrelizumab, which was consistent with previous studies (Table 1).

The response pattern of this combined therapy featured as initial stabilization and delayed tumor reduction was quite different from the current effect of mono-MKI therapy, which may suggest the difference between our combined effect and monotherapy. As we previously mentioned, patients always showed rapid response to antiangiogenic drugs but progressed eventually. Previous studies found that in apatinib monotherapy, the serum Tg level decreased as early as 2 weeks (34), the median time to objective response was 1.9 months (29), and an expected time to progression was between 11 and 18 months (33, 35). Meanwhile, the response to immunotherapy seems to be more durable. A study found that time to response for patients with DTC after PD-1 inhibitor therapy who reached PR was 4 to 5 months (11). For our patient, time to PR was much longer than previous research of apatinib monotherapy. In addition, we did not find the patient who showed the same response pattern in apatinib monotherapy. Therefore, the first 6-month response in this patient may suggest the effect of a low-dose MKI to some extent, while the subsequent response may suggest the effect of immunotherapy. The long duration indicated a mild and lasting therapeutic effect of low-dose apatinib combined with camrelizumab in thyroid cancer.

During this process, the main adverse event was occasional diarrhea without treatment interruption. Adverse events including hand–foot syndrome, hypertension, and proteinuria are commonly observed in apatinib therapy but did not appear in this patient (36), which may suggest the safety of a low-dose schedule. The reactive cutaneous capillary endothelial proliferation was a common adverse event in camrelizumab therapy (37). There is a hypothesis that apatinib, a kind of antiangiogenic drug, would inhibit the proliferation of endothelial cells and thus would present a counteracting effect against adverse effects of camrelizumab. Compared with camrelizumab monotherapy, the skin capillary hyperplasia symptoms in combined therapy were lower than before (Table 1).

The change in serum Tg level in our case also suggested the potential prediction value of serum Tg on target and immunotherapy. The correlation between ps-Tg and therapeutic response was proposed in 2015 American Thyroid Association guidelines, and the relationship between Tg and apatinib plus camrelizumab therapy needed to be confirmed (2). Therefore, our results indicated the value of Tg in observing response to target therapy.

TABLE 1 Clinical trials for camrelizumab combined with apatinib for the treatment of other diseases.

Author	Disease	Interventions	Efficacy	Adverse event
Jianming Xu et al. (15)	Advanced hepatocellular carcinoma	Camrelizumab 200 mg (for bodyweight ≥50 kg) or 3 mg/kg (for bodyweight <50 kg) every 2 weeks plus apatinib 250 mg daily	First-line ORR 34.3%, median PFS 5.7 months, 12-month survival rate 74.7%; second-line ORR 22.5%, median PFS 5.5 months, 12-month survival rate 68.2%	Grade ≥3 AEs 77.4%, most hypertension 34.2%; serious AEs 28.9%, treatment-related deaths 1.1%
Kuimin Mei et al. (14)	Advanced primary liver cancer	Camrelizumab (3 mg/kg, once every 2 weeks) plus apatinib (125, 250, 375, or 500 mg; once per day)	ORR 10.7%, median PFS 3.7 months, median OS 13.2 months	grade ≥3 AEs 92.9%
Shengxiang Ren et al. (16)	Advanced non-squamous NSCLC	Camrelizumab 200 mg every 2 weeks plus apatinib 250 mg once daily	ORR 40.0%, disease control rate 92.0%, median PFS 9.6 months	Grade ≥3 AEs 80%
Yun Fan et al. (17)	Extensive-stage SCLC	Camrelizumab 200 mg every 2 weeks plus apatinib 375 mg once daily	ORR 34.0%, median PFS 3.6 months, median OS 8.4 months	Grade ≥3 AEs 72.9%; discontinued 8.5%
Chunyan Lan et al. (18)	Advanced cervical cancer	Camrelizumab 200 mg every 2 weeks and apatinib 250 mg once per day	ORR 55.6%, median PFS 8.8 months	Grade ≥3 AEs 71.1%, hypertension 24.4%, anemia 20.0%, fatigue 15.6%
Jieqiong Liu et al. (19)	Advanced triple-negative breast cancer	Camrelizumab every 2 weeks with apatinib 250 mg at either continuous dosing (d1–d14) or intermittent dosing (d1–d7)	Continuous cohort: ORR 43.3%, median PFS 3.7 months; intermittent cohort ORR 0, median PFS 1.9 months	Grade ≥3 AEs 46.7%
Lu Xie et al. (20)	Advanced osteosarcoma	Apatinib 500 mg once daily plus camrelizumab 200 mg by every 2 weeks	ORR 20.9%, Median PFS 6.2 months, median OS 11.3 months	Grade ≥3 AEs 69.8%
Xiangrui Meng et al. (21)	Advanced esophageal squamous cell carcinoma	Camrelizumab 200 mg once every 2 weeks plus apatinib 250 mg once daily	ORR 34.6%, disease control 78.8%, median PFS 6.8 months, median OS 15·8 months	Grade ≥3 AEs 44%; most increased aspartate aminotransferase 19%, increased gamma-glutamyl transferase 19%, increased alanine aminotransferase 10%
Chao Ren et al. (22)	Metastatic colorectal cancer	Camrelizumab 200 mg every 2 weeks and apatinib 250–375 mg once daily	ORR 0%, disease control rate 22.2%, median PFS 1.83 months, median OS 7.80 months	Grade 3 AEs 90%, most hypertension 30%
Hongyan Cheng et al. (23)	Chemorefractory or relapsed gestational trophoblastic neoplasia	Camrelizumab 200 mg every 2 weeks plus apatinib 250 mg once per day	ORR 55%, complete response 50%	Grade 3 AEs 60%
Dongxu Wang et al. (24)	Advanced biliary tract cancer	Apatinib at 250 mg per a day and camrelizumab intravenously at 200 mg every three weeks	PR 19%, disease control rate 71.4%, median PFS 4.4 months, median OS 13.1 months	Grade ≥3 AEs 63.6%
Jianming Xu et al. (25)	Advanced hepatocellular carcinoma, gastric, or esophagogastric junction cancer	Camrelizumab 200 mg every 2 weeks and apatinib 125–500 mg once daily	PR 50.0%, ORR 30.8%	Grade ≥3 AEs 60.6%

ORR, objective response rate; PFS, progression-free survival; OS, overall survival; AEs, adverse effects; PR, partial response. SD, stable disease; PD, progressive disease.

TABLE 2 Clinical studies for lenvatinib combined with pembrolizumab for the treatment of thyroid cancer.

Author	Disease	Interventions	Efficacy	Adverse event
Christine Dierks et al. (27)	6 patients with metastatic ATC and 2 patients with PDTC	Lenvatinib 14–24 mg daily combined with pembrolizumab 200 mg every 3 weeks	Overall PR 6/8, ATCs ORR 66%, median PFS 17.75 months, median OS 18.5 months	Grade ≥3 AEs 50%
Cristina Luongo et al. (26)	One patient with paucicellular variant ATC	Lenvatinib (24 mg daily) in combination with pembrolizumab (200 mg every 21 days)	PR achieved after 5 months, PR of lung metastasis persisted over 18 months	Grade 3 diarrhea, vomiting, and weight loss
Priyanka C Iyer et al. (28)	12 patients with ATC	6 patients: pembrolizumab plus dabrafenib and trametinib; 5 patients: pembrolizumab plus lenvatinib; 1 patient: pembrolizumab plus trametinib	PR 5/12 (42%), SD 4/12 (33%), PD 3/12 (25%), median OS 6.93 months, median PFS 2.96 months	Fatigue, anemia, hypertension

ATC, anaplastic thyroid carcinoma; PDTC, poorly differentiated thyroid carcinoma; ORR, objective response rate; PFS, progression-free survival; OS, overall survival; AEs, adverse effects; PR, partial response; SD, stable disease; PD, progressive disease.

Data availability statement

The original contributions presented in the study are included in the article/supplementary material. Further inquiries can be directed to the corresponding author.

Ethics statement

The study was approved by the Ethics Committee of Peking Union Medical College Hospital. The patients/participants provided their written informed consent to participate in this study.

Author contributions

JL and XZ: conceptualization; data curation; formal analysis; investigation; methodology; software; visualization; writing—original draft. ZM, DS, and YS: supervision; validation; visualization; writing—review and editing. YL: conceptualization; funding acquisition; methodology; project administration; resources; software; supervision; validation; visualization; writing—review and editing. All authors contributed to the article and approved the submitted version.

Funding

This study was funded by the CAMS Innovation Fund for Medical Sciences (CIFMS) (No. 2020-I2M-2-003), the CSCO-Hengrui Research Foundation (No. Y-HR2018-143, Y-HR2018-144), the National Natural Science Foundation of China (grant 81771875), and the Project on Inter-Governmental International Scientific and Technological Innovation Cooperation in the National Key Projects of Research and Development Plan (grant 2019YFE0106400). In addition, apatinib and camrelizumab were provided by Jiangsu Hengrui Pharmaceuticals Co Ltd.

Conflict of interest

The authors declare that this study was funded by the CAMS Innovation Fund for Medical Sciences (CIFMS) (No. 2020-I2M-2-003), the CSCO-Hengrui Research Foundation (No. Y-HR2018-143, Y-HR2018-144), the National Natural Science Foundation of China (grant 81771875), the Project on Inter-Governmental International Scientific and Technological Innovation Cooperation in the National Key Projects of Research and Development Plan (grant 2019YFE0106400). In addition, apatinib and camrelizumab were provided by Jiangsu Hengrui Pharmaceuticals Co Ltd. The funder was not involved in the study design, collection, analysis, interpretation of data, the writing of this article or the decision to submit it for publication.

Publisher's note

References

1. Schlumberger M, Brose M, Elisei R, Leboulleux S, Luster M, Pitoia F, et al. Definition and management of radioactive iodine-refractory differentiated thyroid cancer. *Lancet Diabetes Endocrinol* (2014) 2:356–8. doi: 10.1016/s2213-8587(13)70215-8

2. Haugen BR, Alexander EK, Bible KC, Doherty GM, Mandel SJ, Nikiforov YE, et al. 2015 American Thyroid association management guidelines for adult patients with thyroid nodules and differentiated thyroid cancer: The American thyroid association guidelines task force on thyroid nodules and differentiated thyroid cancer. *Thyroid* (2016) 26:1–133. doi: 10.1089/thy.2015.0020

3. Brose MS, Nutting CM, Jarzab B, Elisei R, Siena S, Bastholt L, et al. Sorafenib in radioactive iodine-refractory, locally advanced or metastatic differentiated thyroid cancer: a randomised, double-blind, phase 3 trial. *Lancet* (2014) 384:319–28. doi: 10.1016/s0140-6736(14)60421-9

4. Schlumberger M, Tahara M, Wirth LJ, Robinson B, Brose MS, Elisei R, et al. Lenvatinib versus placebo in radioiodine-refractory thyroid cancer. *N Engl J Med* (2015) 372:621–30. doi: 10.1056/NEJMoa1406470

5. Pitoia F, Jerkovich F. Selective use of sorafenib in the treatment of thyroid cancer. *Drug Des Devel Ther* (2016) 10:1119–31. doi: 10.2147/dddt.s82972

6. Wang E, Karedan T, Perez CA. New insights in the treatment of radioiodine refractory differentiated thyroid carcinomas: to lenvatinib and beyond. *Anticancer Drugs* (2015) 26:689–97. doi: 10.1097/cad.0000000000000247

7. Ancker OV, Krüger M, Wehland M, Infanger M, Grimm D. Multikinase inhibitor treatment in thyroid cancer. *Int J Mol Sci* (2019) 21. doi: 10.3390/ijms21010010

8. Laursen R, Wehland M, Kopp S, Pietsch J, Infanger M, Grosse J, et al. Effects and role of multikinase inhibitors in thyroid cancer. *Curr Pharm Des* (2016) 22:5915–26. doi: 10.2174/1381612822666160614084943

9. Brose MS, Robinson B, Sherman SI, Krajewska J, Lin CC, Vaisman F, et al. Cabozantinib for radioiodine-refractory differentiated thyroid cancer (COSMIC-311): a randomised, double-blind, placebo-controlled, phase 3 trial. *Lancet Oncol* (2021) 22:1126–38. doi: 10.1016/s1470-2045(21)00332-6

10. Alsaab HO, Sau S, Alzhrani R, Tatiparti K, Bhise K, Kashaw SK, et al. PD-1 and PD-L1 checkpoint signaling inhibition for cancer immunotherapy: Mechanism, combinations, and clinical outcome. *Front Pharmacol* (2017) 8:561. doi: 10.3389/fphar.2017.00561

11. Mehnert JM, Varga A, Brose MS, Aggarwal RR, Lin CC, Prawira A, et al. Safety and antitumor activity of the anti-PD-1 antibody pembrolizumab in patients with advanced, PD-L1-positive papillary or follicular thyroid cancer. *BMC Cancer* (2019) 19:196. doi: 10.1186/s12885-019-5380-3

12. Kimura T, Kato Y, Ozawa Y, Kodama K, Ito J, Ichikawa K, et al. Immunomodulatory activity of lenvatinib contributes to antitumor activity in the Hepa1-6 hepatocellular carcinoma model. *Cancer Sci* (2018) 109:3993–4002. doi: 10.1111/cas.13806

13. Mo DC, Luo PH, Huang SX, Wang HL, Huang JF. Safety and efficacy of pembrolizumab plus lenvatinib versus pembrolizumab and lenvatinib monotherapies in cancers: A systematic review. *Int Immunopharmacol* (2021) 91:107281. doi: 10.1016/j.intimp.2020.107281

14. Mei K, Qin S, Chen Z, Liu Y, Wang L, Zou J. Camrelizumab in combination with apatinib in second-line or above therapy for advanced primary liver cancer: cohort a report in a multicenter phase Ib/II trial. *J Immunother Cancer* (2021) 9. doi: 10.1136/jitc-2020-002191

15. Xu J, Shen J, Gu S, Zhang Y, Wu L, Wu J, et al. Camrelizumab in combination with apatinib in patients with advanced hepatocellular carcinoma (RESCUE): A nonrandomized, open-label, phase II trial. *Clin Cancer Res* (2021) 27:1003–11. doi: 10.1158/1078-0432.ccr-20-2571

16. Ren S, He J, Fang Y, Chen G, Ma Z, Chen J, et al. Camrelizumab plus apatinib in treatment-naive patients with advanced nonsquamous NSCLC: A multicenter, open-label, single-arm, phase 2 trial. *JTO Clin Res Rep* (2022) 3:100312. doi: 10.1016/j.jtocrr.2022.100312

17. Fan Y, Zhao J, Wang Q, Huang D, Li X, Chen J, et al. Camrelizumab plus apatinib in extensive-stage SCLC (PASSION): A multicenter, two-stage, phase 2 trial. *J Thorac Oncol* (2021) 16:299–309. doi: 10.1016/j.jtho.2020.10.002

18. Lan C, Shen J, Wang Y, Li J, Liu Z, He M, et al. Camrelizumab plus apatinib in patients with advanced cervical cancer (CLAP): A multicenter, open-label, single-arm, phase II trial. *J Clin Oncol* (2020) 38:4095–106. doi: 10.1200/jco.20.01920

19. Liu J, Liu Q, Li Y, Li Q, Su F, Yao H, et al. Efficacy and safety of camrelizumab combined with apatinib in advanced triple-negative breast cancer: an open-label phase II trial. *J Immunother Cancer* (2020) 8. doi: 10.1136/jitc-2020-000696

20. Xie L, Xu J, Sun X, Guo W, Gu J, Liu K, et al. Apatinib plus camrelizumab (anti-PD1 therapy, SHR-1210) for advanced osteosarcoma (APFAO) progressing after chemotherapy: a single-arm, open-label, phase 2 trial. *J Immunother Cancer* (2020) 8. doi: 10.1136/jitc-2020-000798

21. Meng X, Wu T, Hong Y, Fan Q, Ren Z, Guo Y, et al. Camrelizumab plus apatinib as second-line treatment for advanced oesophageal squamous cell carcinoma (CAP 02): a single-arm, open-label, phase 2 trial. *Lancet Gastroenterol Hepatol* (2022) 7:245–53. doi: 10.1016/s2468-1253(21)00378-2

22. Ren C, Mai ZJ, Jin Y, He MM, Wang ZQ, Luo HY, et al. Anti-PD-1 antibody SHR-1210 plus apatinib for metastatic colorectal cancer: a prospective, single-arm, open-label, phase II trial. *Am J Cancer Res* (2020) . 10:2946–54.

23. Cheng H, Zong L, Kong Y, Wang X, Gu Y, Cang W, et al. Camrelizumab plus apatinib in patients with high-risk chemorefractory or relapsed gestational trophoblastic neoplasia (CAP 01): a single-arm, open-label, phase 2 trial. *Lancet Oncol* (2021) 22:1609–17. doi: 10.1016/s1470-2045(21)00460-5

24. Wang D, Yang X, Long J, Lin J, Mao J, Xie F, et al. The efficacy and safety of apatinib plus camrelizumab in patients with previously treated advanced biliary tract cancer: A prospective clinical study. *Front Oncol* (2021) 11:646979. doi: 10.3389/fonc.2021.646979

25. Xu J, Zhang Y, Jia R, Yue C, Chang L, Liu R, et al. Anti-PD-1 antibody SHR-1210 combined with apatinib for advanced hepatocellular carcinoma, gastric, or esophagogastric junction cancer: An open-label, dose escalation and expansion study. *Clin Cancer Res* (2019) 25:515–23. doi: 10.1158/1078-0432.ccr-18-2484

26. Luongo C, Porcelli T, Sessa F, De Stefano MA, Scavuzzo F, Damiano V, et al. Combination of lenvatinib and pembrolizumab as salvage treatment for paucicellular variant of anaplastic thyroid cancer: A case report. *Curr Oncol* (2021) 28:5401–7. doi: 10.3390/curroncol28060450

27. Dierks C, Seufert J, Aumann K, Ruf J, Klein C, Kiefer S, et al. Combination of lenvatinib and pembrolizumab is an effective treatment option for anaplastic and poorly differentiated thyroid carcinoma. *Thyroid* (2021) 31:1076–85. doi: 10.1089/thy.2020.0322

28. Iyer PC, Dadu R, Gule-Monroe M, Busaidy NL, Ferrarotto R, Habra MA, et al. Salvage pembrolizumab added to kinase inhibitor therapy for the treatment of anaplastic thyroid carcinoma. *J Immunother Cancer* (2018) 6:68. doi: 10.1186/s40425-018-0378-y

29. Lin Y, Qin S, Li Z, Yang H, Fu W, Li S, et al. Apatinib vs placebo in patients with locally advanced or metastatic, radioactive iodine-refractory differentiated thyroid cancer: The REALITY randomized clinical trial. *JAMA Oncol* (2022) 8:242–50. doi: 10.1001/jamaoncol.2021.6268

30. Fukumura D, Kloepper J, Amoozgar Z, Duda DG, Jain RK. Enhancing cancer immunotherapy using antiangiogenics: opportunities and challenges. *Nat Rev Clin Oncol* (2018) 15:325–40. doi: 10.1038/nrclinonc.2018.29

31. Huang Y, Yuan J, Righi E, Kamoun WS, Ancukiewicz M, Nezivar J, et al. Vascular normalizing doses of antiangiogenic treatment reprogram the immunosuppressive tumor microenvironment and enhance immunotherapy. *Proc Natl Acad Sci U.S.A.* (2012) 109:17561–6. doi: 10.1073/pnas.1215397109

32. Schmittnaegel M, Rigamonti N, Kadioglu E, Cassará A, Wyser Rmili C, Kiialainen A, et al. Dual angiopoietin-2 and VEGFA inhibition elicits antitumor immunity that is enhanced by PD-1 checkpoint blockade. *Sci Transl Med* (2017) 9. doi: 10.1126/scitranslmed.aak9670

33. Zhao S, Ren S, Jiang T, Zhu B, Li X, Zhao C, et al. Low-dose apatinib optimizes tumor microenvironment and potentiates antitumor effect of PD-1/PD-L1 blockade in lung cancer. *Cancer Immunol Res* (2019) 7:630–43. doi: 10.1158/2326-6066.cir-17-0640

34. Lin Y, Wang C, Gao W, Cui R, Liang J. Overwhelming rapid metabolic and structural response to apatinib in radioiodine refractory differentiated thyroid cancer. *Oncotarget* (2017) 8:42252–61. doi: 10.18632/oncotarget.15036

35. Brose MS, Schlumbeger M, Jeffers M, Kappeler C, Meinhardt G, Peña CEA. Analysis of biomarkers and association with clinical outcomes in patients with differentiated thyroid cancer: Subanalysis of the sorafenib phase III DECISION trial. *Clin Cancer Res* (2019) 25:7370–80. doi: 10.1158/1078-0432.ccr-18-3439

36. Shao F, Zhang H, Yang X, Luo X, Liu J. Adverse events and management of apatinib in patients with advanced or metastatic cancers: A review. *Neoplasma* (2020) 67:715–23. doi: 10.4149/neo_2020_190801N701

37. Wang F, Qin S, Sun X, Ren Z, Meng Z, Chen Z, et al. Reactive cutaneous capillary endothelial proliferation in advanced hepatocellular carcinoma patients treated with camrelizumab: data derived from a multicenter phase 2 trial. *J Hematol Oncol* (2020) 13:47. doi: 10.1186/s13045-020-00886-2

frontiers | Frontiers in Immunology

TYPE Perspective
PUBLISHED 09 August 2022
DOI 10.3389/fimmu.2022.963533

OPEN ACCESS

EDITED BY
Xuyao Zhang,
Fudan University, China

REVIEWED BY
Xiaotian Sun,
Fudan University, China
Graham Robert Leggatt,
The University of Queensland,
Australia

*CORRESPONDENCE
Xinye Qian
qianxy21@mails.tsinghua.edu.cn

†These authors have contributed equally to this work

SPECIALTY SECTION
This article was submitted to Cancer Immunity and Immunotherapy, a section of the journal Frontiers in Immunology

RECEIVED 07 June 2022
ACCEPTED 18 July 2022
PUBLISHED 09 August 2022

CITATION
Qian X, Hu W and Yan J (2022) Nano-Chemotherapy synergize with immune checkpoint inhibitor- A better option? *Front. Immunol.* 13:963533. doi: 10.3389/fimmu.2022.963533

Nano-Chemotherapy synergize with immune checkpoint inhibitor- A better option?

Xinye Qian[1,2*†], Wang Hu[1,2†] and Jun Yan[1,2†]

[1]Center of Hepatobiliary Pancreatic Disease, Beijing Tsinghua Changgung Hospital, School of Clinical Medicine, Tsinghua University, Beijing, China, [2]School of Clinical Medicine, Tsinghua University, Beijing, China

Immune checkpoint inhibitor (ICI) is one of the most important tumor treatment methods. Although the therapeutic efficiency of immune checkpoint inhibitor mono-therapy is limited, the combination of chemotherapy plus immune checkpoint inhibitors has shown great advantages in cancer treatment. This is mainly due to the fact that tumor reactive T cells could fully provide their anti-tumor function as chemotherapy could not only cause immunogenic cell death to increase antigen presentation, but also improve the immunosuppressive tumor micro-environment to synergize with immune checkpoint inhibitors. However, traditional chemotherapy still has shortcomings such as insufficient drug concentration in tumor region, short drug duration, drug resistance, major adverse events, etc, which might lead to the failure of the therapy. Nano chemotherapeutic drugs, which refer to chemotherapeutic drugs loaded in nano-based drug delivery system, could overcome the above shortcomings of traditional chemotherapeutic drugs to further improve the therapeutic effect of immune checkpoint inhibitors on tumors. Therefore, the scheme of nano chemotherapeutic drugs combined with immune checkpoint inhibitors might lead to improved outcome of cancer patients compared with the scheme of traditional chemotherapy combined with immune checkpoint inhibitors.

KEYWORDS

nano-chemotherapy, immune checkpoint inhibitor, treatment efficiency, tumor, toxicity

Introduction

The development of immune checkpoint inhibitors (ICI) has brought new opportunities for tumor patients (1). Mainly two kinds of immune checkpoint inhibitors are currently applied in clinic, including CTLA-4 inhibitors (2) and PD-1/PD-L1 inhibitors (3). Moreover, novel immune checkpoint inhibitors, like TIGIT inhibitor (4), are under clinical trials. Its main principle is to restore the anti-tumor

function of tumor-reactive T cells by blocking immune regulation (inhibition) pathways (5). However, the theoretically perfect immune checkpoint inhibitor monotherapy has not exceeded traditional cancer treatment in many tumors like pancreatic cancer, breast cancer, etc (6). To Improve treatment effect, the combination of immune checkpoint inhibitors and chemotherapy has been invented. The combination has already shown improved therapeutic effects on a number of tumors, including esophageal cancer, lung cancer, triple-negative breast cancer and so on (7). In this paper, nano chemotherapeutic drugs are suggested as a better option for combined immune checkpoint inhibitor therapy to achieve better therapeutic effect in tumor patients by analyzing the therapeutic principle behind this combination of immune checkpoint inhibitor plus chemotherapy, and by comparing the differences between Nano chemotherapeutic drugs and traditional chemotherapeutic drugs.

Mechanism to improve the therapeutic effect of immune checkpoint inhibitor

The rationale of immune checkpoint inhibitor therapy is based on the anti-tumor function of tumor reactive T cells (CD8+ cytotoxic T lymphocytes) (8), which depend not only on the inhibition of immunosuppressive pathways, but also on other mechanisms.

First, the immune system must recognize tumor cells, which depends on presentation of tumour antigens by antigen-presenting cells (APC) (9). Apoptosis of tumor cells with new antigens might not start the antigen presentation process (10), which would lead to the failure of the immune system recognizing tumor cells. Only when immunogenic cell death (ICD, a type of cancer cell death involves the activation of the immune system against cancer in immunocompetent hosts) were triggered, APC cells would be activated and present the specific antigens of tumor cells to tumor reactive T cells so that these T cells could recognize tumor cells and produce anti-tumor effect (11).

Second, tumor reactive T cells that could recognize tumor antigens need to contact with tumor cells to provide their anti-tumor effect. However, tumors develop multiple mechanisms to escape the "hunt" from tumor reactive T cells. One way is to exhaust tumor reactive T cells to impair their anti-tumor function, like expressing immune checkpoint molecules (such as PD-L1) to induce tumor reactive T cells apoptosis or exhaustion by activating immunosuppressive pathways (12), or recruiting immunosuppressive cells such as tumor associated macrophages (TAM), tumor associated fibroblasts (CAF), regulatory T cells (Tregs) and myelogenous suppressor cells (MDSCs) to suppress the activity of cytotoxic T lymphocytes (CTLs) (13, 14).

Another way is to reduce the number of tumor reactive T cells at the tumor site. The failure to attract tumour-reactive T cells to the tumour could be caused by the lack of appropriate chemokine secretion from the tumor (e.g. the down regulation of CXCL9 prevents CD8+ T cell tumor-infiltration. Thus, impairing anti-PD1 therapy) (15). The activity of immunosuppressive cells is also important for suppressing the infiltration of CTLs into the tumor area; for example, CAF could release chemokine CXCL12, which could inhibit T cell infiltration in tumors (16). Also, this immunosuppressive micro-environment could reduce the recruitment of DC cells so that tumor antigens cannot be presented, resulting in the failure of the adaptive immune system to recognize tumor cells (16). Moreover, CTLs are not generally able to reach the edge area of some tumors due to trapping within the stroma of tumor or in the peri-tumoral tissue because of a unique architecture of tumor immunosuppressive environment (16).

Therefore, if tumor antigen presentation and tumor reactive T cells infiltration could be ensured, the therapeutic efficiency of immune checkpoint inhibitors on tumors could be improved as tumor reactive T cells could fully act its anti-tumor effect.

Mechanism and therapeutic effect of chemotherapy plus immune checkpoint inhibitor

Immune checkpoint inhibitor combined with chemotherapy has been proved to increase the efficiency of tumor treatment in a variety of clinical studies. For example, nivolumab (PD-1 antibody) plus first-line chemotherapy resulted in significantly longer overall survival than chemotherapy alone in patients with advanced esophageal squamous-cell carcinomaincluding esophageal cancer (13.2 months vs 10.7 month) (17); the combination of pembrolizumab (PD-1 antibody) with standard chemotherapy of pemetrexed and a platinum-based drug resulted in significantly longer overall survival and progression-free survival than chemotherapy alone in metastatic non-small cell Lung Cancer (18); Pembrolizumab plus chemotherapy showed a significant and clinically meaningful improvement in progression-free survival versus placebo-chemotherapy among patients with metastatic triple-negative breast cancer with CPS (combined positive score) of 10 or more (19); etc. The underlying mechanism is that while immune checkpoint inhibitors block the immunosuppressive pathways, chemotherapy might improve the presentation of tumor antigen and the infiltration of tumor reactive T cells.

On the one hand, traditional chemotherapy could lead to immunogenic cell death (ICD) of tumor cell (20), which could promote the presentation of tumor antigens so that the adaptive immune system could recognize tumor cells. Importantly, the molecular mechanism by which chemotherapeutic drugs activate the immune activation pathway does not necessarily overlap with its cytotoxic mechanism. It is reported that the DNA-intercalating agents adriamycin and oxaliplatin, mainly inhibit topoisomerase II at clinically relevant doses, could also induce eIF2α phosphorylation in enucleated cancer cells. This means that these chemotherapeutic drugs could act on cytoplasmic (extra-nuclear) structures to stimulate ICD related stress pathways (21), suggesting that the traditional chemotherapy drugs could still promote antigen presentation of tumor cells even if they fail to cause tumor cell death directly. Recent studies found that a variety of chemotherapy drugs, including carboplatin (22) and gemcitabine (23), could promote the recruitment of DC cells in tumor micro-environment, further indicating that they could facilitate the adaptive immune system to recognize tumor cells. The mechanism might be as follows: the activation of ICD-linked danger signaling; the elevation of cytokine secretion, such as type I IFNs; the reversal of immunosuppressive micro-environment, such as the depletion of TAMs, the decreased secretion of TGFβ, etc.

On the other hand, traditional chemotherapy could reverse the immunosuppressive tumor micro-environment, including the depletion of immunosuppressive cells, like CD4+CD25+FOXP3+ regulatory T (Treg) cells, myelogenous suppressor cells (MDSCs) and M2 like tumor associated macrophages (TAMs) (24, 25), and the activation of immune effector cells, including M1 like TAMs (26), DCs (27) and CTLs (28). Meanwhile, chemotherapy could also increase reactive T cell infiltration in tumor areas, which further ensures the anti-tumor effect of tumor reactive T cells. A systematic review including 110 studies confirmed that chemotherapy could regulate the tumor immune microenvironment, including increasing infiltration of CD8+ cytotoxic T cells, reduction of FOXP3+ Treg and higher PD-L1 expression (29), proving that traditional chemotherapy could cooperate with immune checkpoint inhibitors to improve the anti-tumor ability of tumor reactive T cells by altering tumor immune micro-environment (Figure 1A). The mechanism of

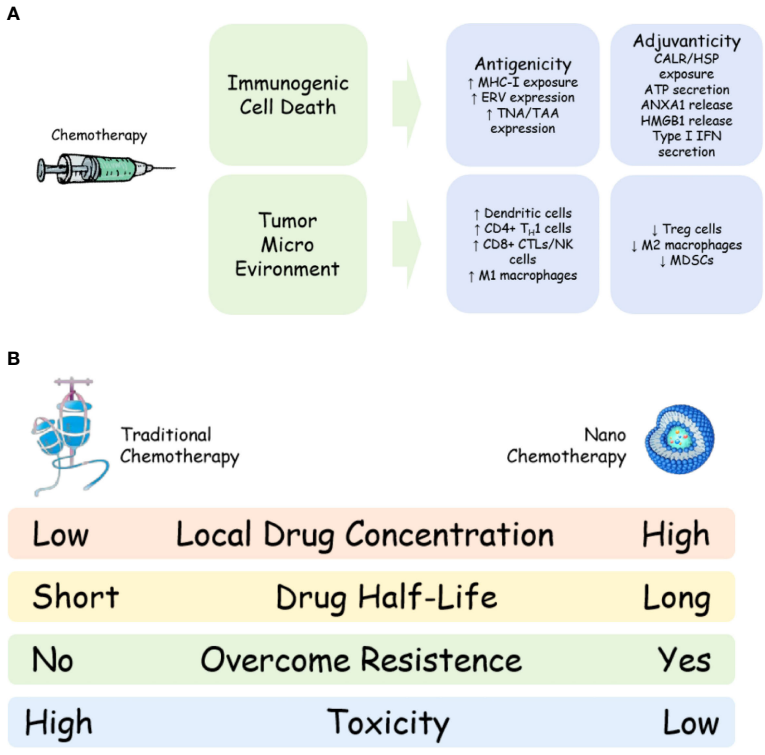

FIGURE 1
Mechanism and advantage of nano-chemotherapy. **(A)** Mechanism of chemotherapy to synergize with immune checkpoint inhibitor; **(B)** Advantages of nano-chemotherapy compared with traditional chemotherapy. MHC-I, major histocompatibility complex class I;ERV, endogenous retrovirus; TAA, tumour associated antigen; TNA, tumour neoantigen; CALR, calreticulin; HSP, heat shock protein;ANXA1, annexin A1; HMGB1, high mobility group box 1; IFN, interferon; TH1, T helper 1; CTL, cytotoxic T lymphocyte; NK, natural killer cells; MDSC, myeloid-derived suppressor cell; Treg, regulatory T cells.

increasing infiltration of CD8+ cytotoxic T cells after chemotherapy might be that chemotherapy like gemcitabine, 5-Fluorouracil, etc, might decrease Treg and MDSC numbers and increase pro-inflammatory cytokines (such as IFN-γ, IL-2, IL-6, etc) in the tumor region, leading to T cell infiltration to the tumor (24, 25), though further validation is needed.

Based on the above analysis, the combination of chemotherapy and immune checkpoint inhibitors could be called a "Golden Combination" as tumor reactive T cells to fully exert their anti-tumor effects. This is because chemotherapy could promote tumor antigen presentation and tumor reactive T cells infiltration while the immune checkpoint inhibitor could block the immunosuppressive pathway.

However, the disadvantages of traditional chemotherapy might affect this "Golden Combination". First of all, traditional chemotherapy is usually administrated by a single dose at a regular interval (the interval of chemotherapy is usually over 3 weeks because of its side effects on patients). Drug concentration at tumor region would rapid decrease after chemotherapy (within 3 days after chemotherapy), which might reduce the tumor's response to chemotherapy (30). Such a drug delivery method might also produce a drug resistance mechanism in tumor cells by over-expression of membrane transporters, like P-glycoproteins on the membrane surface that could expel chemotherapeutic drugs from cells, causing a decrease in the total amount of drugs in cells and failure of chemotherapy (31). These would result in the failure of combination therapy (immune checkpoint inhibitor plus traditional chemotherapy) because tumor antigen could not be present and tumor immune micro-environment could not be improved.

Second, traditional chemotherapy often causes serious side effects in cancer patients (32). Traditional chemotherapy might suppress the immune system by causing lymphocyte depletion (33, 34), which might be detrimental to cancer treatment basing on normal quantity and function of T cells, such as immune checkpoint inhibitor. Although the depletion of lymphocytes might restart the immune system so that the immune system can better fight against tumors (35), this theory has not been confirmed. In addition, doxorubicin and gemcitabine have been found to increase circulating MDSC cells in patients (36), which might worsen the tumor immune micro-environment. Moreover, traditional chemotherapy would cause multiple side effects, including gastrointestinal toxicity (loss of appetite, nausea, vomiting, diarrhea, malabsorption and disorders), myelosuppression, liver and kidney function damage, etc (37). Immune checkpoint inhibitor would also cause side effects, including cardiotoxicity, abnormal liver function, kidney failure, etc (38). Side effects from both chemotherapy and immune checkpoint inhibitor would decrease patient's tolerability, leading to increased drop out rate or prolonged treatment interval among cancer patients receiving this combination therapy. As a result, these patients might not get better treatment results. In addition, many chemotherapeutic drugs, such as paclitaxel (39), have to be administrated with steroids to reduce their side effects because of their strong toxic effects; but steroids have immunosuppressive effect in mechanism, which would harm the anti-tumor function of T cells (40).

Nano chemotherapy

Nano chemotherapeutic drugs, which refer to chemotherapeutic drugs loaded in nano-based drug delivery system, are developed to overcome the shortcomings of traditional chemotherapy, including low bio-availability, low local concentration, short duration, major systemic side effects, etc. There are mainly two kinds of nano chemotherapeutic drugs in clinic currently, including Nab-paclitaxel and liposomal chemotherapeutic drugs (Table 1).

Table 1 Nano-chemotherapeutic Drugs approved in clinic.

Nab-paclitaxel is a 130 nm particle formulation comprising albumin nanoparticles and paclitaxel with non-covalent bonds, which could largely reduce the adverse effect of solvent-based paclitaxel, including bone marrow suppression, allergic reactions, neurotoxicity and systemic toxicity (52). Food and Drug Administration (FDA) lists nab-paclitaxel as a vital drug for the treatment of non-small cell lung cancers, pancreatic cancers and breast cancers. Patients with relapsed small cell lung cancer who received nab-paclitaxel had a response rate of 29.4%, prolonged progression-free survival (48 days), and prolonged overall survival (134 days) (53). A systematic review including 63 studies has shown that nab-Paclitaxel continues to demonstrate promising efficacy in breast cancer, including high pathological complete response rates in early-stage breast cancer, particularly in triple-negative breast cancer, and encouraging overall survival in metastatic breast cancer across doses and schedules (54). Furthermore, nab-paclitaxel plus gemcitabine significantly improved overall survival, progression-free survival, and response rate in patients with advanced pancreatic cancer with acceptable adverse events (55), suggesting nab-paclitaxel could combine with other chemotherapy or anti-tumor therapy.

Liposomal chemotherapeutic drugs are chemotherapeutic drugs loaded in liposomes (a revolutionizing nano carrier). Their success is attributed to stable drug loading, extended pharmacokinetics, reduced off-target side effects, and enhanced delivery efficiency to disease targets (56). There are more kinds of liposomal chemotherapeutic drugs than albumin nanoparticle based chemotherapeutic drugs as various chemotherapeutic drugs could be loaded in liposomes (57). Pegylated liposomal doxorubicin provides comparable efficacy to doxorubicin, with significantly reduced cardiotoxicity, myelosuppression, vomiting and alopecia as first-line therapy for patients with metastatic breast cancer (58). Phase III NAPOLI-1 trial showed that intravenous administration of liposomal irinotecan + 5-FU/LV

TABLE 1 Nano-chemotherapeutic Drugs approved in clinic.

Product name	Drug	Targeted tumor	Main cytokines	Immune infiltrate	Reference
Doxil/Caelyx	Liposomal Doxorubicin	Breast cancer; Kaposi's sarcoma; Ovarian cancer	↑IL-1β, IL-12, IFNγ	↑DCs, CD8+ CTLs, CD4+ T cells; ↓MDSCs, Treg cells	(41)
Myocet	Liposomal Doxorubicin	Breast cancer			(42)
DaunoXome	Liposomal Daunorubicin	Kaposi's sarcoma	↑Type I IFNs, IFNγ, IL-17	↑DCs, CD8+ CTLs, NK cells; ↓Treg cells	(43)
Lipusu	Liposomal Paclitaxel	Gastric cancer	↑IL-1β, IL-12, TNF	↑DCs, M1 macrophages; ↓Treg cells	(44)
Abraxane	Nab-paclitaxel	Breast Cancer; pancreatic cancer; Non-small cell lung cancer			(45)
Endo-Tag-1	Cationic liposomal paclitaxel	Solid tumors			(46)
Marqibo	LiposomalVincristine	Solid Tumors; Acute lymphoblastic leukemia	ND	↑DCs	(47)
Onivyde	LiposomalIrinotecan	Pancreatic cancer	ND	↑DCs, CD8+ CTLs	(48)
CPX-1	LiposomalIrinotecan	Colorectal cancer			(49)
SPI-077	Liposomal Cis-platin	Solid tumors	↑Type I IFNs, IFNγ	↑DCs, CD8+ CTLs, NK cells	(50)
Lipoplatin	Liposomal Cis-platin	Ovarian cancer; Metastatic non-small cell lung cancer; breast cancer			(51)

IL, interleukin; IFN, interferon; CTL, cytotoxic T lymphocyte; DC, dendritic cell; MDSC, myeloid-derived suppressor cell; NK, natural killer; NKT, natural killer T; ND, not determined; Treg, regulatory T cell.

to gemcitabine-pretreated patients with metastatic pancreatic adenocarcinoma was associated with a prolonged overall survival compared with 5-FU/LV alone (2 months) (59). All these founding demonstrated that nano chemotherapeutic drugs play a vital role in cancer treatment.

Potential combination of nano-chemotherapy plus immune checkpoint inhibitor

In the combination therapy of chemotherapy plus immune checkpoint inhibitor, only local therapeutic effect of chemotherapy in the tumor region is needed. Jie Mei et al. has confirmed this concept in patients with hecepocellular carcinoma (HCC), which is normally considered chemotherapy insensitive (59). Researchers combined hepatic arterial infusion chemotherapy (HAIC), a local chemotherapy technique, with immune checkpoint inhibitor (PD-1 Inhibitor) and tyrosine kinase inhibitor (Lenvatinib) to treat hepatocellular carcinoma; This treatment scheme showed higher treatment efficiency in hepatocellular carcinoma as the objective response rate (ORR) was 40% with acceptable complications as every patient in the HAIC group finished the treatment with less major adverse events (60). This provides a theoretical basis for the combination of local chemotherapy plus immune checkpoint inhibitor to treat cancers. Based on the above facts, nano chemotherapeutic drugs might have great potential in combination therapy with immune checkpoint inhibitors for cancer patients.

Firstly, concentration of nano chemotherapeutic drugs in tumor region would be higher than traditional chemotherapeutic drugs, improving the therapeutic effect. Compared with the traditional doxorubicin, Doxil (liposomal doxorubicin) showed 4 to 16 times the doxorubicin concentration in the tumor regions of patients using the drug (61). Other studies on the tissue distribution of Doxil using mice models also showed that drug concentration of Doxil in tumor regions was significantly higher than that of free doxorubicin (62). Similarly, animal studies have confirmed that nab-paclitaxel would aggregate in the tumor regions; it also presents a higher bio-availability than its traditional counterpart (63). Jiao-Ren Huang et al. have confirmed that liposomal irinotecan not only increased local drug concentration, but also lasted significantly longer than conventional drugs in the tumor region (64). These evidences showed that nano chemotherapeutic drugs could indeed achieve higher drug concentration and longer existence in tumor area than traditional chemotherapeutic drugs, allowing nano chemotherapy drugs to achieve better clinical therapeutic effect. The combination therapy of liposome irinotecan and 5-fu/lv has improve the overall survival of patients with advanced pancreatic cancer (59); Thus, the treatment schedule is recommended as the second-line treatment for advanced pancreatic cancer. Liposomal doxorubicin has also been recommended by NCCN guidelines for the treatment of ovarian cancer, non Hodgkin's lymphoma, multiple myeloma,

breast cancer, uterine tumor, soft tissue sarcoma and other malignant tumors (65). Nab-paclitaxel has also been approved for the first-line treatment of non-small cell lung cancer and the treatment of advanced pancreatic cancer (53). These evidences further illustrate the advantages of nano chemotherapeutic drugs over traditional chemotherapeutic drugs.

Secondly, nano chemotherapy drugs could reduce systemic toxicity. Almost all the clinical trials of nano chemotherapeutic drugs have proved this point. In a study comparing traditional paclitaxel with nab-paclitaxel, although there was no significant difference in the incidence and degree of side effects between the two drugs, almost every patient in the traditional paclitaxel group received steroid treatment; moreover, patients in the traditional paclitaxel group were more likely to have granulocytopenia above grade 4 (66). A meta-analysis showed that liposomal doxorubicin has less cardio- and other- toxicity than traditional doxorubicin (67). A real-world study found that liposomal doxorubicin could significantly reduce bone marrow suppression, nausea, anorexia and cardiotoxicity caused by traditional chemotherapy (68). These facts not only indicate that patients' compliance might be improved using nano chemotherapeutic drugs, but also indicate that nano chemotherapeutic drugs could allow more combination treatments for cancer patients. For example, a combination of three drugs is used for advanved pancreatic cancer, including liposomal doxorubicin, PD-1 inhibitor and CXC4 inhibitor; The low toxicity of nano chemotherapeutic drugs greatly enhanced the tolerance of the scheme (69). If the study use traditional doxorubicin instead of liposomal doxorubicin, increasing drop out rate of patients would be observed. Furthermore, due to the decrease of systemic drug concentration, the inhibitory effect of nano chemotherapy drugs on patients' systemic immune system is also significantly reduced, which might protect the number and the function of T cells, which play an important role in cancer immunotherapy (Figure 1B).

In 2019, nab-paclitaxel combined with PD-L1 inhibitor was written into the treatment guidelines for metastatic triple negative breast cancer due to its good therapeutic effect with an ORR rate of 56%, much higher than historical ORR of nab-paclitaxel or PD-L1 inhibitor alone (70). In a phase 2 clinical trial, the authors found the combination of pembrolizumab and liposomal doxorubicin was manageable, without unexpected toxicities, and showed preliminary evidence of clinical benefit in the treatment of platinum resistant ovarian cancer (71). The ORR (26.1%) of combination therapy in this study was higher than that of liposomal doxorubicin (ORR 8.3%) or anti-PD-1/PD-L1 agents (ORR 7.4%) alone in advanced ovarian cancer. Another study focusing on relapsed/refractory classical Hodgkin lymphomaon found that the GVD (gemcitabine, vinorelbine, liposomal doxorubicin)+PD-1 group tended to have a higher CR rate than GVD group (85.2% vs. 65.8%), and had a better event-free survival (the toxicity of the GVD+PD-1 regimen was comparable to the GVD regimen) (72). In addition, in the study of using liposomal irinotecan combined with pembrolizumab (a PD1 monoclonal antibody) and CXCR4 inhibitor to treat pancreatic cancer, the ORR reached 13.2% while the DCR reached 63.2% (60 53). More studies focusing on the combination of nano chemotherapy plus immune checkpoint inhibitor is going on. The ALICE study is planning to compare the therapeutic effect between atezolizumab (PD-L1 inhibitor) plus immunogenic chemotherapy (liposomal doxorubicin + cyclophosphamide) and immunogenic chemotherapy alone on metastatic triple-negative breast cancer (73). Although few clinical studies have been completed so far, these clinical results have already shown that nano chemotherapy drugs combined with immune checkpoint inhibitors might be a potential treatment scheme better than the current traditional chemotherapy plus immune checkpoint inhibitor.

Although clinical evidence is rare, the effectiveness and advantages of therapeutic scheme of nano chemotherapeutic drugs combined with immune checkpoint inhibitors have been confirmed many times *in vivo* experiments. Kuai et al. constructed liposomes loaded with doxorubicin to stimulate the immune system and enhance the efficiency of immunotherapy (74). Results showed that the liposomal doxorubicin ccould trigger a strong CD8+ T cell response without other off-target side effects. When the drug delivery system was further combined with anti-PD-1 antibody, more than 80% of the tumors in mice (both breast and colon cancer models) were completely resolved (74). Moreover, Na Shen et al. constructed P-cis, a kind of cisplatin nanoparticles. Vivo study using tumor mice model showed that P-Cis plus PD1/PD-L1 inhibitors had synergistic and therapeutic advantages compared with traditional cisplatin plus PD1/PD-L1 inhibitors (75).

These *in vivo* studies also confirmed that nano chemotherapeutic drugs could have better local effects, including causing antigen exposure, promoting antigen presentation, and improving the tumor immune micro-environment (76), which would further enhance the anti-tumor function of T cells whose immunosuppressive pathway could be blocked by immune checkpoint inhibitors. With these pre-clinical evidence, it could be expected that more clinical data in the future would be able to confirm the superiority of this scheme over the existing schemes.

Nano chemotherapy drugs could gather in the tumor region and increase the local concentration of drugs. The enhanced permeability and retention (EPR) effect might be the mechanism for the local aggregation (77). There is a hypothesis that the EPR effect is caused by the existence of vascular leakage and damage to the lymphatic system in the tumor. Based on the EPR effect at the tumor site, nano drugs could "passively" accumulate at the site where the vascular permeability increases. In addition, liposomes are not easy to leak into normal tissues with tight endothelial connections so that the side effects of liposomes are significantly reduced compared with free drugs. Active targeting is another way to gather nano chemotherapeutic drugs in the

tumor region. In order to achieve the active targeting of cancer sites, a variety of ligands are utilized to exploit any specific antigens expressed by cancer cells, which exhibited increased drug delivery to prostate tumor tissue compared to non-targeting nanoparticles (77). However, there is no active-targeting nano chemotherapeutic drugs applied in clinic currently. Because of their better tumor targeting effect, nano chemotherapeutic drugs with active targeting might be even better than the current nano chemotherapeutic drugs, with more local therapeutic effects and less side effects.

At present, there are few choices of nano chemotherapeutic drugs, which might be due to the limited therapeutic effect of mono-chemotherapy in many advanced tumors, resulting in the slow development of new nano chemotherapeutic drugs. The current treatment scheme of chemotherapy combined with immune checkpoint inhibitors has given new value to nano chemotherapeutic drugs. It does not necessarily lie in the direct anti-tumor effect, but in improving the tumor local immune micro-environment to enhance cancer treatment. Many nano chemotherapeutic drugs use nano vehicles that have already been proved by the FDA, such as liposomes (78). If the treatment scheme could improve the clinical treatment effect for advanced tumors, novel nano chemotherapeutic drugs might soon be developed and put into clinical practice.

Summary and future perspective

Nano chemotherapy drugs combined with immune checkpoint inhibitors might be a better combination to improve the efficiency of the current scheme of traditional chemotherapy plus immune checkpoint inhibitors in the treatment of tumors. This combination could not only increase the local therapeutic effect of chemotherapy, including increasing antigen presentation and improving the immune micro-environment, thus increasing the therapeutic effect of immune checkpoint inhibitors, but also reduce T cells depletion and systemic toxicity of chemotherapy drugs so that patients would better tolerate this treatment regimen, which would benefit cancer patients ultimately. Current evidence from clinical trials are limited; further validation for its safety and efficiency is needed. Also, novel kinds of nano-chemotherapeutic drugs with better tumor targetability could be expected to improve the therapeutic effect of nano-chemotherapy plus immune checkpoint inhibitors.

Data availability statement

The original contributions presented in the study are included in the article/supplementary material. Further inquiries can be directed to the corresponding author.

Author contributions

XQ, WH and JY conceptualized, wrote, and reviewed the manuscript. All authors approved the submitted version.

Funding

Start up Fund for Talent Researchers of Tsinghua University (No. 10001020507).

Acknowledgments

We thank Dr. Qian Lu for many fruitful discussions.

Conflict of interest

The authors declare that the research was conducted in the absence of any commercial or financial relationships that could be construed as a potential conflict of interest.

Publisher's note

References

1. Bagchi S, Yuan R, Engleman EG. Immune checkpoint inhibitors for the treatment of cancer: Clinical impact and mechanisms of response and resistance. *Annu Rev Pathol* (2021) 16:223–49. doi: 10.1146/annurev-pathol-042020-042741

2. Smith KM, Desai J. Nivolumab for the treatment of colorectal cancer. *Expert Rev Anticancer Ther* (2018) 18(7):611–8. doi: 10.1080/14737140.2018.1480942

3. Stenehjem DD, Tran D, Nkrumah MA, Gupta S. PD1/PDL1 inhibitors for the treatment of advanced urothelial bladder cancer. *Onco Targets Ther* (2018) 11:5973–89. doi: 10.2147/OTT.S135157

4. Niu J, Maurice-Dror C, Lee DH, Kim DW, Nagrial A, Voskoboynik M, et al. First-in-human phase 1 study of the anti-TIGIT antibody vibostolimab as monotherapy or with pembrolizumab for advanced solid tumors, including non-

small-cell lung cancer(). *Ann Oncol* (2022) 33(2):169–80. doi: 10.1016/j.annonc.2021.11.002

5. Carlino MS, Larkin J, Long GV. Immune checkpoint inhibitors in melanoma. *Lancet* (2021) 398(10304):1002–14. doi: 10.1016/S0140-6736(21)01206-X

6. Bonaventura P, Shekarian T, Alcazer V, Valladeau-Guilemond J, Valsesia-Wittmann S, Amigorena S, et al. Cold tumors: A therapeutic challenge for immunotherapy. *Front Immunol* (2019) 10:168. doi: 10.3389/fimmu.2019.00168

7. Galluzzi L, Humeau J, Buque A, Zitvogel L, Kroemer G. Immunostimulation with chemotherapy in the era of immune checkpoint inhibitors. *Nat Rev Clin Oncol* (2020) 17(12):725–41. doi: 10.1038/s41571-020-0413-z

8. Farhood B, Najafi M, Mortezaee K. CD8(+) cytotoxic T lymphocytes in cancer immunotherapy: A review. *J Cell Physiol* (2019) 234(6):8509–21. doi: 10.1002/jcp.27782

9. Chen DS, Mellman I. Oncology meets immunology: the cancer-immunity cycle. *Immunity* (2013) 39:1–10. doi: 10.1016/j.immuni.2013.07.012

10. Blass E, Ott PA. Advances in the development of personalized neoantigen-based therapeutic cancer vaccines. *Nat Rev Clin Oncol* (2021) 18(4):215–29. doi: 10.1038/s41571-020-00460-2

11. Galluzzi L, Buque A, Kepp O, Zitvogel L, Kroemer G. Immunogenic cell death in cancer and infectious disease. *Nat Rev Immunol* (2017) 17(2):97–111. doi: 10.1038/nri.2016.107

12. Sharpe AH, Pauken KE. The diverse functions of the PD1 inhibitory pathway. *Nat Rev Immunol* (2018) 18(3):153–67. doi: 10.1038/nri.2017.108

13. Mortezaee K. Hypoxia induces core-to-edge transition of progressive tumoral cells: A critical review on differential yet corroborative roles for HIF-1alpha and HIF-2alpha. *Life Sci* (2020) 242:117145. doi: 10.1016/j.lfs.2019.117145

14. Najafi M, Mortezaee K, Majidpoor J. Stromal reprogramming: A target for tumor therapy. *Life Sci* (2019) 239:117049. doi: 10.1016/j.lfs.2019.117049

15. Zhang J, Endres S, Kobold S. Enhancing tumor T cell infiltration to enable cancer immunotherapy. *Immunotherapy* (2019) 11(3):201–13. doi: 10.2217/imt-2018-0111

16. Bassani-Sternberg M, Digklia A, Huber F, Wagner D, Sempoux C, Stevenson BJ, et al. A phase ib study of the combination of personalized autologous dendritic cell vaccine, aspirin, and standard of care adjuvant chemotherapy followed by nivolumab for resected pancreatic adenocarcinoma-a proof of antigen discovery feasibility in three patients. *Front Immunol* (2019) 10:1832. doi: 10.3389/fimmu.2019.01832

17. Doki Y, Ajani JA, Kato K, Xu J, Wyrwicz L, Motoyama S, et al. Nivolumab combination therapy in advanced esophageal squamous-cell carcinoma. *N Engl J Med* (2022) 386(5):449–62. doi: 10.1056/NEJMoa2111380

18. Gandhi L, Rodriguez-Abreu D, Gadgeel S, Esteban E, Felip E, De Angelis F, et al. Pembrolizumab plus chemotherapy in metastatic non-Small-Cell lung cancer. *N Engl J Med* (2018) 378(22):2078–92. doi: 10.1056/NEJMoa1801005

19. Cortes J, Cescon DW, Rugo HS, Nowecki Z, Im SA, Yusof MM, et al. Pembrolizumab plus chemotherapy versus placebo plus chemotherapy for previously untreated locally recurrent inoperable or metastatic triple-negative breast cancer (KEYNOTE-355): a randomised, placebo-controlled, double-blind, phase 3 clinical trial. *Lancet* (2020) 396(10265):1817–28. doi: 10.1016/S0140-6736(20)32531-9

20. Vanmeerbeek I, Sprooten J, De Ruysscher D, Tejpar S, Vandenberghe P, Fucikova J, et al. Trial watch: chemotherapy-induced immunogenic cell death in immuno-oncology. *Oncoimmunology* (2020) 9(1):1703449. doi: 10.1080/2162402X.2019.1703449

21. Panaretakis T, Kepp O, Brockmeier U, Tesniere A, Bjorklund AC, Chapman DC, et al. Mechanisms of pre-apoptotic calreticulin exposure in immunogenic cell death. *EMBO J* (2009) 28(5):578–90. doi: 10.1038/emboj.2009.1

22. Yamazaki T, Buque A, Ames TD, Galluzzi L. PT-112 induces immunogenic cell death and synergizes with immune checkpoint blockers in mouse tumor models. *Oncoimmunology* (2020) 9(1):1721810. doi: 10.1080/2162402X.2020.1721810

23. Yamamura Y, Tsuchikawa T, Miyauchi K, Takeuchi S, Wada M, Kuwatani T, et al. The key role of calreticulin in immunomodulation induced by chemotherapeutic agents. *Int J Clin Oncol* (2015) 20(2):386–94. doi: 10.1007/s10147-014-0719-x

24. Gabrilovich DI. Myeloid-Derived Suppressor Cells. *Cancer Immunol Res* (2017) 5(1):3–8. doi: 10.1158/2326-6066.CIR-16-0297

25. Dimeloe S, Frick C, Fischer M, Gubser PM, Razik L, Bantug GR, et al. Human regulatory T cells lack the cyclophosphamide-extruding transporter ABCB1 and are more susceptible to cyclophosphamide-induced apoptosis. *Eur J Immunol* (2014) 44(12):3614–20. doi: 10.1002/eji.201444879

26. Wanderley CW, Colon DF, Luiz JPM, Oliveira FF, Viacava PR, Leite CA, et al. Paclitaxel reduces tumor growth by reprogramming tumor-associated macrophages to an M1 profile in a TLR4-dependent manner. *Cancer Res* (2018) 78(20):5891–900. doi: 10.1158/0008-5472.CAN-17-3480

27. Ma Y, Mattarollo SR, Adjemian S, Yang H, Aymeric L, Hannani D, et al. CCL2/CCR2-dependent recruitment of functional antigen-presenting cells into tumors upon chemotherapy. *Cancer Res* (2014) 74(2):436–45. doi: 10.1158/0008-5472.CAN-13-1265

28. Schaer DA, Geeganage S, Amaladas N, Lu ZH, Rasmussen ER, Sonyi A, et al. The folate pathway inhibitor pemetrexed pleiotropically enhances effects of cancer immunotherapy. *Clin Cancer Res* (2019) 25(23):7175–88. doi: 10.1158/1078-0432.CCR-19-0433

29. van den Ende T, van den Boorn HG, Hoonhout NM, van Etten-Jamaludin FS, Meijer SL, Derks S, et al. Priming the tumor immune microenvironment with chemo(radio)therapy: A systematic review across tumor types. *Biochim Biophys Acta Rev Cancer* (2020) 1874(1):188386. doi: 10.1016/j.bbcan.2020.188386

30. De Souza R, Zahedi P, Allen CJ, Piquette-Miller M. Polymeric drug delivery systems for localized cancer chemotherapy. *Drug Deliv* (2010) 17(6):365–75. doi: 10.3109/10717541003762854

31. Galletti G, Leach BI, Lam L, Tagawa ST. Mechanisms of resistance to systemic therapy in metastatic castration-resistant prostate cancer. *Cancer Treat Rev* (2017) 57:16–27. doi: 10.1016/j.ctrv.2017.04.008

32. Zraik IM, Hess-Busch Y. Management of chemotherapy side effects and their long-term sequelae. *Urologe A.* (2021) 60(7):862–71. doi: 10.1007/s00120-021-01569-7

33. Mackall CL, Fleisher TA, Brown MR, Magrath IT, Shad AT, Horowitz ME, et al. Lymphocyte depletion during treatment with intensive chemotherapy for cancer. *Blood* (1994) 84(7):2221–8. doi: 10.1182/blood.V84.7.2221.2221

34. Verma R, Foster RE, Horgan K, Mounsey K, Nixon H, Smalle N, et al. Lymphocyte depletion and repopulation after chemotherapy for primary breast cancer. *Breast Cancer Res* (2016) 18(1):10. doi: 10.1186/s13058-015-0669-x

35. Ghosh A, Politikos I, Perales MA. Stop and go: hematopoietic cell transplantation in the era of chimeric antigen receptor T cells and checkpoint inhibitors. *Curr Opin Oncol* (2017) 29(6):474–83. doi: 10.1097/CCO.0000000000000408

36. Wesolowski R, Duggan MC, Stiff A, Markowitz J, Trikha P, Levine KM, et al. Circulating myeloid-derived suppressor cells increase in patients undergoing neo-adjuvant chemotherapy for breast cancer. *Cancer Immunol Immunother* (2017) 66(11):1437–47. doi: 10.1007/s00262-017-2038-3

37. Livshits Z, Rao RB, Smith SW. An approach to chemotherapy-associated toxicity. *Emerg Med Clin North Am* (2014) 32(1):167–203. doi: 10.1016/j.emc.2013.09.002

38. Schierz JH, Sarikaya I, Wollina U, Unger L, Sarikaya A. Immune checkpoint inhibitor-related adverse effects and (18)F-FDG PET/CT findings. *J Nucl Med Technol* (2021) 49(4):324–9. doi: 10.2967/jnmt.121.262151

39. Yenilmez A, Hood AP, Nguyen LH, Merl MY. Paclitaxel pre-medication: A comparison of two steroid pre-medication protocols. *J Oncol Pharm Pract* (2017) 23(7):491–5. doi: 10.1177/1078155216664203

40. Di Maira T, Little EC, Berenguer M. Immunosuppression in liver transplant. *Best Pract Res Clin Gastroenterol* (2020) 46-47:101681. doi: 10.1016/j.bpg.2020.101681

41. Barenholz Y. Doxil(R)–the first FDA-approved nano-drug: lessons learned. *J Control Release* (2012) 160(2):117–34. doi: 10.1016/j.jconrel.2012.03.020

42. Dalu D, Fasola C, Ammoni L, De Francesco D, Cona MS, Rota S, et al. egylated liposomal doxorubicin as first line treatment in aids-related Kaposi's sarcoma: a real-life study. *J Chemother* (2021) 33(5):342–47. doi: 10.1080/1120009X.2021.1920248

43. Batist G, Ramakrishnan G, Rao CS, Chandrasekharan A, Gutheil J, Guthrie T, et al. Reduced cardiotoxicity and preserved antitumor efficacy of liposome-encapsulated doxorubicin and cyclophosphamide compared with conventional doxorubicin and cyclophosphamide in a randomized, multicenter trial of metastatic breast cancer. *J Clin Oncol* (2001) 19(5):1444–54. doi: 10.1200/JCO.2001.19.5.1444

44. Xu X, Wang L, Xu HQ, Huang XE, Qian YD, Xiang J. Clinical comparison between paclitaxel liposome (Lipusu(R)) and paclitaxel for treatment of patients with metastatic gastric cancer. *Asian Pac J Cancer Prev* (2013) 14(4):2591–4. doi: 10.7314/apjcp.2013.14.4.2591

45. Abu Samaan TM, Samec M, Liskova A, Kubatka P, Busselberg D. Paclitaxel's mechanistic and clinical effects on breast cancer. *Biomolecules* (2019) 9(12):789–811. doi: 10.3390/biom9120789

46. Fasol U, Frost A, Buchert M, Arends J, Fiedler U, Scharr D, et al. Vascular and pharmacokinetic effects of EndoTAG-1 in patients with advanced cancer and liver metastasis. *Ann Oncol* (2012) 23(4):1030–6. doi: 10.1093/annonc/mdr300

47. Rodriguez MA, Pytlik R, Kozak T, Chhanabhai M, Gascoyne R, Lu B, et al. Vincristine sulfate liposomes injection (Marqibo) in heavily pretreated patients

with refractory aggressive non-Hodgkin lymphoma: report of the pivotal phase 2 study. *Cancer* (2009) 115(15):3475–82. doi: 10.1002/cncr.24359

48. Bulbake U, Doppalapudi S, Kommineni N, Khan W. Liposomal formulations in clinical use: An updated review. *Pharmaceutics* (2017) 9(2):12–45. doi: 10.3390/pharmaceutics9020012

49. Dicko A, Mayer LD, Tardi PG. Use of nanoscale delivery systems to maintain synergistic drug ratios *in vivo*. *Expert Opin Drug Delivery* (2010) 7 (12):1329–41. doi: 10.1517/17425247.2010.538678

50. Raj H, Keerthi MSS, Palaniappan R, Prakash U, Dhanushkodi M, Ganesan TS. Phase 2 non-randomised trial of secondary cytoreduction and hyperthermic intraperitoneal chemotherapy in recurrent platinum-sensitive ovarian cancer. *Ecancermedicalscience* (2021) 15:1260–70. doi: 10.3332/ecancer.2021

51. Stathopoulos GP, Antoniou D, Dimitroulis J, Stathopoulos J, Marosis K, Michalopoulou P. Comparison of liposomal cisplatin versus cisplatin in non-squamous cell non-small-cell lung cancer. *Cancer Chemother Pharmacol* (2011) 68 (4):945–50. doi: 10.1007/s00280-011-1572-5

52. Kim G. nab-Paclitaxel for the treatment of pancreatic cancer. *Cancer Manag Res* (2017) 9:85–96. doi: 10.2147/CMAR.S127840

53. Nakao M, Fujita K, Suzuki Y, Arakawa S, Sakai Y, Sato H, et al. Nab-paclitaxel monotherapy for relapsed small cell lung cancer: Retrospective analysis and review. *Anticancer Res* (2020) 40(3):1579–85. doi: 10.21873/anticanres.14105

54. Brufsky A. Nab-paclitaxel for the treatment of breast cancer: an update across treatment settings. *Exp Hematol Oncol* (2017) 6:7. doi: 10.1186/s40164-017-0066-5

55. Von Hoff DD, Ervin T, Arena FP, Chiorean EG, Infante J, Moore M, et al. Increased survival in pancreatic cancer with nab-paclitaxel plus gemcitabine. *N Engl J Med* (2013) 369(18):1691–703. doi: 10.1056/NEJMoa1304369

56. Fan Y, Marioli M, Zhang K. Analytical characterization of liposomes and other lipid nanoparticles for drug delivery. *J Pharm BioMed Anal* (2021) 192:113642. doi: 10.1016/j.jpba.2020.113642

57. Allen TM, Cullis PR. Liposomal drug delivery systems: from concept to clinical applications. *Adv Drug Delivery Rev* (2013) 65(1):36–48. doi: 10.1016/j.addr.2012.09.037

58. O'Brien ME, Wigler N, Inbar M, Rosso R, Grischke E, Santoro A, et al. Reduced cardiotoxicity and comparable efficacy in a phase III trial of pegylated liposomal doxorubicin HCl (CAELYX/Doxil) versus conventional doxorubicin for first-line treatment of metastatic breast cancer. *Ann Oncol* (2004) 15(3):440–9. doi: 10.1093/annonc/mdh097

59. Frampton JE. Liposomal irinotecan: A review in metastatic pancreatic adenocarcinoma. *Drugs* (2020) 80(10):1007–18. doi: 10.1007/s40265-020-01336-6

60. Mei J, Tang YH, Wei W, Shi M, Zheng L, Li SH, et al. Hepatic arterial infusion chemotherapy combined with PD-1 inhibitors plus lenvatinib versus PD-1 inhibitors plus lenvatinib for advanced hepatocellular carcinoma. *Front Oncol* (2021) 11:618206. doi: 10.3389/fonc.2021.618206

61. Gabizon A, Catane R, Uziely B, Kaufman B, Safra T, Cohen R, et al. Prolonged circulation time and enhanced accumulation in malignant exudates of doxorubicin encapsulated in polyethylene-glycol coated liposomes. *Cancer Res* (1994) 54(4):987–92.

62. Ouyang B, Poon W, Zhang YN, Lin ZP, Kingston BR, Tavares AJ, et al. The dose threshold for nanoparticle tumour delivery. *Nat Mater* (2020) 19(12):1362–71. doi: 10.1038/s41563-020-0755-z

63. Li R, Ng TSC, Wang SJ, Prytyskach M, Rodell CB, Mikula H, et al. Therapeutically reprogrammed nutrient signalling enhances nanoparticulate albumin bound drug uptake and efficacy in KRAS-mutant cancer. *Nat Nanotechnol* (2021) 16(7):830–9. doi: 10.1038/s41565-021-00897-1

64. Huang JR, Lee MH, Li WS, Wu HC. Liposomal irinotecan for treatment of colorectal cancer in a preclinical model. *Cancers (Basel)* (2019) 11(3):281–300. doi: 10.3390/cancers11030281

65. Makwana V, Karanjia J, Haselhorst T, Anoopkumar-Dukie S, Rudrawar S. Liposomal doxorubicin as targeted delivery platform: Current trends in surface functionalization. *Int J Pharm* (2021) 593:120117. doi: 10.1016/j.ijpharm.2020.120117

66. Yamamoto Y, Kawano I, Iwase H. Nab-paclitaxel for the treatment of breast cancer: efficacy, safety, and approval. *Onco Targets Ther* (2011) 4:123–36. doi: 10.2147/OTT.S13836

67. Xing M, Yan F, Yu S, Shen P. Efficacy and cardiotoxicity of liposomal doxorubicin-based chemotherapy in advanced breast cancer: A meta-analysis of ten randomized controlled trials. *PloS One* (2015) 10(7):e0133569. doi: 10.1371/journal.pone.0133569

68. Zhang J, Jiang H, Zhang J, Bao G, Zhang G, Wang H, et al. Effectiveness and safety of pegylated liposomal doxorubicin versus epirubicin as neoadjuvant or adjuvant chemotherapy for breast cancer: A real-world study. *BMC Cancer* (2021) 21(1):1301. doi: 10.1186/s12885-021-09050-6

69. Bockorny B, Macarulla T, Semenisty V, Borazanci E, Feliu J, Ponz-Sarvise M, et al. Motixafortide and pembrolizumab combined to nanoliposomal irinotecan, fluorouracil, and folinic acid in metastatic pancreatic cancer: The COMBAT/KEYNOTE-202 trial. *Clin Cancer Res* (2021) 27(18):5020–7. doi: 10.1158/1078-0432.CCR-21-0929

70. Schmid P, Adams S, Rugo HS, Schneeweiss A, Barrios CH, Iwata H, et al. Atezolizumab and nab-paclitaxel in advanced triple-negative breast cancer. *N Engl J Med* (2018) 379(22):2108–21. doi: 10.1056/NEJMoa1809615

71. Lee EK, Xiong N, Cheng SC, Barry WT, Penson RT, Konstantinopoulos PA, et al. Combined pembrolizumab and pegylated liposomal doxorubicin in platinum resistant ovarian cancer: A phase 2 clinical trial. *Gynecol Oncol* (2020) 159(1):72–8. doi: 10.1016/j.ygyno.2020.07.028

72. Zhang YC, Wang JN, Ma SY, Cai J, Su N, Huang HQ, et al. Combination of PD-1 inhibitor with GVD (gemcitabine, vinorelbine, liposomal doxorubicin) versus GVD regimen as second-line therapy for relapsed/refractory classical Hodgkin lymphoma. *Br J Haematol* (2022) 196(1):127–35. doi: 10.1111/bjh.17849

73. Kyte JA, Rossevold A, Falk RS, Naume B. ALICE: a randomized placebo-controlled phase II study evaluating atezolizumab combined with immunogenic chemotherapy in patients with metastatic triple-negative breast cancer. *J Transl Med* (2020) 18(1):252. doi: 10.1186/s12967-020-02424-7

74. Kuai R, Yuan W, Son S, Nam J, Xu Y, Fan Y, et al. Elimination of established tumors with nanodisc-based combination chemoimmunotherapy. *Sci Adv* (2018) 4 (4):eaao1736. doi: 10.1126/sciadv.aao1736

75. Shen N, Yang C, Zhang X, Tang Z, Chen X. Cisplatin nanoparticles possess stronger anti-tumor synergy with PD1/PD-L1 inhibitors than the parental drug. *Acta Biomater* (2021) 135:543–55. doi: 10.1016/j.actbio.2021.08.013

76. Yang M, Li J, Gu P, Fan X. The application of nanoparticles in cancer immunotherapy: Targeting tumor microenvironment. *Bioact Mater* (2021) 6 (7):1973–87. doi: 10.1016/j.bioactmat.2020.12.010

77. Alavi M, Hamidi M. Passive and active targeting in cancer therapy by liposomes and lipid nanoparticles. *Drug Metab Pers Ther* (2019) 34(1):509–17. doi: 10.1515/dmpt-2018-0032

78. Almeida B, Nag OK, Rogers KE, Delehanty JB. Recent progress in bioconjugation strategies for liposome-mediated drug delivery. *Molecules* (2020) 25(23):5672–700. doi: 10.3390/molecules25235672

frontiers | Frontiers in Immunology

TYPE Original Research
PUBLISHED 10 August 2022
DOI 10.3389/fimmu.2022.958161

OPEN ACCESS

EDITED BY
Claude Lambert,
Centre Hospitalier Universitaire (CHU) de Saint-Étienne, France

REVIEWED BY
Quan Zou,
University of Electronic Science and Technology of China, China
Yanzhang Luo,
South China University of Technology, China

*CORRESPONDENCE
Yongqiang Zhang
zyq1014zyq1014@163.com
Gen Li
superleegen@hotmail.com

†These authors have contributed equally to this work

SPECIALTY SECTION
This article was submitted to Cancer Immunity and Immunotherapy, a section of the journal Frontiers in Immunology

RECEIVED 31 May 2022
ACCEPTED 18 July 2022
PUBLISHED 10 August 2022

CITATION
Guo C, Tang Y, Yang Z, Li G and Zhang Y (2022) Hallmark-guided subtypes of hepatocellular carcinoma for the identification of immune-related gene classifiers in the prediction of prognosis, treatment efficacy, and drug candidates. *Front. Immunol.* 13:958161. doi: 10.3389/fimmu.2022.958161

Hallmark-guided subtypes of hepatocellular carcinoma for the identification of immune-related gene classifiers in the prediction of prognosis, treatment efficacy, and drug candidates

Chengbin Guo[1†], Yuqin Tang[2†], Zhao Yang[3], Gen Li[1*] and Yongqiang Zhang[4*]

[1]Guangzhou Institute of Pediatrics, Guangzhou Women and Children's Medical Center, Guangzhou Medical University, Guangzhou, China, [2]State Key Laboratory of Southwestern Chinese Medicine Resources, School of Basic Medical Sciences, Chengdu University of Traditional Chinese Medicine, Chengdu, China, [3]West China School of Medicine, West China Hospital, Sichuan University, Chengdu, China, [4]Wuhan Institute of Virology, Center for Biosafety Mega-Science, Chinese Academy of Sciences, Wuhan, China

Hepatocellular carcinoma (HCC), accounting for ~90% of all primary liver cancer, is a prevalent malignancy worldwide. The intratumor heterogeneity of its causative etiology, histology, molecular landscape, and immune phenotype makes it difficult to precisely recognize individuals with high mortality risk or tumor-intrinsic treatment resistance, especially immunotherapy. Herein, we comprehensively evaluated the activities of cancer hallmark gene sets and their correlations with the prognosis of HCC patients using gene set variation analysis (GSVA) and identified two HCC subtypes with distinct prognostic outcomes. Based on these subtypes, seven immune-related genes (TMPRSS6, SPP1, S100A9, EPO, BIRC5, PLXNA1, and CDK4) were used to construct a novel prognostic gene signature [hallmark-guided subtypes-based immunologic signature (HGSIS)] *via* multiple statistical approaches. The HGSIS-integrated nomogram suggested an enhanced predictive performance. Interestingly, oncogenic hallmark pathways were significantly enriched in the high-risk group and positively associated with the risk score. Distinct mutational landscapes and immune profiles were observed between different risk groups. Moreover, immunophenoscore (IPS) and tumor immune dysfunction and exclusion (TIDE) analysis showed different sensitivities of HGSIS risk groups for immune therapy efficacy, and the pRRophetic algorithm indicated distinguishable responses for targeted/chemotherapies in different groups. KIF2C was picked out as the key target concerning HGSIS, and the top 10 small molecules were predicted to bind to the active site of KIF2C *via* molecular docking, which might be further used for candidate drug discovery of HCC. Taken together, our study

offers novel insights for clinically significant subtype recognition, and the proposed signature may be a helpful guide for clinicians to improve the treatment regimens.

KEYWORDS

hepatocellular carcinoma, hallmark gene sets and molecule subtypes, immunotherapy efficacy, immune infiltration, prognosis, molecular docking

Introduction

Liver cancer is the fourth leading cause of cancer-related death and hepatocellular carcinoma (HCC) is the most prevalent type of liver cancer (1). The infection of hepatitis B virus (HBV) and hepatitis C virus (HCV) is the main etiological risk factors for HCC, although non-alcoholic steatohepatitis (NASH) associated with metabolic syndrome or diabetes mellitus is the fastest-growing cause of HCC, especially in the West (2). HCC is a highly heterogeneous disease, which arises in a background of long-time chronic liver diseases in most cases (3). HCC heterogeneity is constituted by multiple features including genomic instability, molecular and signal transduction network disorders, and microenvironment discrepancies, contributing to the main reason for the ineffectiveness of traditional treatment (4–6). Likewise, the intralesional, interlesional, and intertumoral heterogeneity of HCC is challenging the prognostic prediction and personalized therapy development for HCC patients (7). Thus, identification of HCC subtypes with clinical significance and novel prognostic biomarkers or signatures are urgently needed for improved risk stratification and personalized treatment in HCC patients.

Exploring molecular alterations and signaling pathways related to cancer hallmarks is critical for classifying HCC subtypes to devise personalized treatments. While traditional experimental approaches that focus on one signaling pathway or a molecule could provide insight into the understanding of cancer initiation or progression, they are not suitable to develop a valid standard of HCC classification for further risk assessment. Meanwhile, gene set-based approaches have attracted considerable attention for HCC risk stratification recently; for example, ferroptosis-related genes, hypoxia-related genes, and lipid metabolism-related genes have been investigated to develop prognostic gene signatures in HCC (8–10). However, systematic exploration of cancer hallmark-related multiple gene sets to define HCC subtypes with appealing implications for the prediction of prognosis, treatment responses, and candidate drugs is still limited.

Recent studies have found that the tumor immune microenvironment (TIME) has a significant impact on the occurrence and development of tumors (11, 12). In HCC, cancer immunotherapy is developing rapidly since encouraging clinical outcomes have been obtained with monoclonal antibodies (mAbs), which target immune checkpoints to reverse the inactivation of T cells to eliminate tumor cells. Hopefully, for patients with advanced HCC, nivolumab, the PD1 inhibitor, was approved in the United States (13). Tremelimumab, an anti-CTLA4 immune checkpoint inhibitor (ICI), made exciting progress in a clinical trial (14). The combination of the anti-PD1 antibody atezolizumab and the VEGF-neutralizing antibody bevacizumab is exceedingly promising as a first-line drug for the treatment of HCC (15). However, immune cells constitute the trickiest component of the tumor microenvironment (TME) in HCC, of which the heterogeneity poses a significant challenge for the classification of HCC, leading to the uncertainty of prognosis (16).

Gene set variation analysis (GSVA) is a state-of-the-art framework to generate sample-level pathway scores in an unsupervised manner from gene expression profiles, which represents the starting point to develop pathway-centric models of biology and provides increased power than other sample-wise enrichment approaches to evaluate the variation of pathway activity. Compared with the popular gene set enrichment analysis (GSEA) method, GSVA is a more convenient algorithm without having to pre-define the classes of a given sample population, and it provides greater biological interpretability (17). In the present study, the GSVA scores of 50 hallmark gene sets from the molecular signature database (MSigdb) (18, 19) were computed using the TCGA-LIHC dataset, and robust prognostic hallmark gene sets were comprehensively screened and used to generate two HCC subtypes with divergent survival outcomes. Based on the two subtypes, a seven-gene immunologic signature that was named HGSIS for predicting the prognosis of HCC was established and validated with multiple statistical approaches. Distinct TIME profiles and mutational landscapes regarding HGSIS were characterized, and the significant association between HGSIS and immunotherapy efficacy was unraveled. Notably, we predicted candidate drugs that might bind to the crucial target

of HGSIS with molecular docking. The flowchart of the study is shown in Figure 1.

Materials and methods

Patient information and data collection

Gene expression data of HCC patients were downloaded from The Cancer Genome Atlas (TCGA) and International Cancer Genome Consortium (ICGC) databases. Those patients with incomplete overall survival (OS) information and with an OS time of <30 days were excluded as reported before (20, 21). The clinicopathological features and other types of survival outcomes including progression-free survival (PFS), disease-free survival (DFS), and disease-specific survival (DSS) were also collected. The transcriptomic stemness index mRNAsi evaluating the degree of cancer stemness for each of all the HCC patients from the TCGA dataset was computed with the OCLR-based algorithm (22). Consequently, 336 samples from TCGA (the whole TCGA cohort) and 238 samples from the ICGC (ICGC-LIHC-JP) were included in the study. The whole TCGA cohort was randomly divided into the training dataset (n = 222) and validation dataset (n = 114) with an approximate ratio of 2:1. Moreover, the whole TCGA cohort and the ICGC-LIHC-JP cohort further served as the internal and external validation sets. The patient population and the clinicopathological characteristics are summarized in Supplementary Table 1. The normalized RNA sequencing profiles were retrieved and preprocessed as previously reported (20, 23, 24). For the analysis of somatic mutation information, we gathered the available mutation annotation format (MAF) file from the TCGA data portal (http://tcga-data.nci.nih.gov/tcga/) using the "maftools" package (25). Additionally, 1,118 unique immune-related genes (IRGs) were achieved from the Immunology Database and Analysis Portal (ImmPort) database (https://www.immport.org/home) (26).

Gene set variation analysis and consensus clustering

The relative enrichment scores of the 50 cancer hallmark gene sets from Msidb (h.all.v7.1.symbols) (19) for the whole TCGA cohort, which were used to estimate the activities of these cancer hallmark pathways, were computed by the GSVA algorithm using the "GSVA" package (17). Kaplan–Meier analysis with log-rank test was utilized to examine the associations between each gene set and the OS. To increase the robustness of the prognostic gene sets, we adopted the "multi-split" strategy with 100 randomized subsamples as we reported before (24), and only those that repeatedly showed significance in all 100 times were considered as prognostic gene sets (Supplementary Figure 1). Based on the prognostic gene sets, unsupervised clustering was applied for all the HCC patients from TCGA with the "ConsensusClusterPlus" package (27) to distinguish different molecular patterns with divergent OS outcomes. This process was performed with 1,000 iterations by sampling 80% of all the data for each iteration to ensure clustering stability. The optimal clustering number was comprehensively determined by the item-consensus plots, the consensus heatmap, and the change in the area under the cumulative distribution function (CDF) curves, which was further confirmed by the proportion of ambiguous clustering

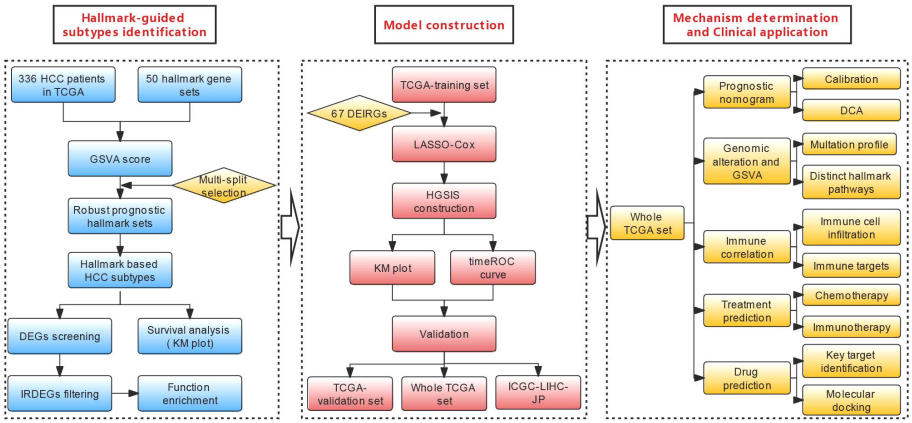

FIGURE 1
Flowchart of the current study.

(PAC) algorithm (28, 29). Two hallmark-guided subtypes with distinct OS outcomes were recognized and visualized with principal component analysis (PCA) plots. Additionally, Kaplan–Meier plots were depicted to evaluate the prognosis of patients in different Hallmark-guided subtype groups.

Screening of the immune-related DEGs (IRDEGs) between HCC subtypes

Differentially expressed genes (DEGs) between the two hallmark-guided subtypes were screened by the "limma" package with the criteria of adjusted p-values <0.01 and |logFC| >1 (30, 31). A volcano plot was drawn to show these DEGs using the "ggplot2" package (https://cran.r-project.org/web/packages/ggplot2), followed by the identification of IRDEGs with a Venn plot. The "pheatmap" package was utilized to show the IRDEGs' expression patterns between the two HCC subtypes. As previously described, Gene Ontology (GO) enrichment and Kyoto Encyclopedia of Genes and Genomes (KEGG) analysis for these IRDEGs were conducted *via* the "clusterProfiler" package with an adjusted $p < 0.05$ (20, 23, 32).

Signature establishment and evaluation

The aforementioned IRDEGs were next subjected to the comprehensive feature selection, followed by the construction of the HGSIS signature on the training set, whose effectiveness and performance were evaluated on the training and validation datasets. Specifically, Univariate Cox (UniCox) proportional hazards regression analysis was used to pick out candidate IRDEGs with prognostic significance according to the criteria of $p < 0.05$. The least absolute shrinkage and selection operator (LASSO) regression algorithm was then applied by the "glmnet" package to find out the best subset of prognostic genes (33). We chose the significant IRDEGs that repeatedly appeared more than 50 times from 100 models to develop the scoring system HGSIS: Risk score = $\Sigma(\text{coef}(\beta)^*\text{EXP}_\beta)$, where β stands for each selected IRDEG. All patients were classified into the high- and low-risk groups using the median risk score of the training set.

To assess the reliability of HGSIS, Kaplan–Meier curves were depicted for the TCGA training set, the TCGA validation set, the whole TCGA cohort, and the external validation set to compare the OS of different risk groups *via* the "survival" package. Time-dependent receiver operating characteristic (tROC) curves were also drawn to evaluate the predictive performance of HGSIS. In addition, we compared the area under the curve (AUC) values of the 3-year and 5-year tROC curves between HGSIS and other published HCC signatures as well as popular biomarkers for immunotherapy, i.e., a TP53-associated gene signature by Long et al. ("Long signature") (34) and two immune-related gene signatures ("Dai signature" and "Wang signature") (35, 36), TMB, and PD1.

Correlation of HGSIS with clinicopathological features

The relationship between HGSIS and clinicopathological parameters was examined using nonparametric tests and visualized by the "ggplot2" package. The correlation between HGSIS and mRNAsi was measured using the Pearson correlation test *via* the "ggstatsplot" package. Stratified survival analysis was carried out for selected clinicopathological factors such as age, gender, and BMI to further validate the additional prognostic value of the HGSIS model. Then, univariate and multivariate regression analyses were conducted to verify the independent prognostic value of HGSIS in HCC. Based on the univariate analysis, an HGSIS-integrated nomogram was created by the "rms" package to quantitatively predict the OS probability, whose predictive accuracy was evaluated by calibration plots. The concordance index was further used to assess its performance. Moreover, decision curve analysis (DCA) was used to explore the potential clinical benefit of HGSIS as described (20). Additionally, Kaplan–Meier analysis with a log-rank test was applied to the output of the nomogram-based classifier for the whole TCGA cohort to further compare the differences in OS, DFS, PFS, and DSS between different risk classes.

Genomic alterations and hallmark pathway analysis

Genomic mutations have been reported to be relevant to immunity and immunotherapy (20, 37–39); thus, we explored the somatic mutation analysis for the HGSIS high- and low-risk groups. The "maftools" R package was used to depict the waterfall plots showing the mutation landscapes of different risk groups of the whole TCGA cohort. Mutation types and frequencies of the most commonly mutated genes in each risk group were manifested. TMB values were computed with non-synonymous mutations as described previously to reveal the total mutation numbers of HCC patients (40, 41). Meanwhile, a linear model was employed to compare the GSVA scores of the 50 cancer hallmark gene sets between HGSIS risk groups to uncover the relative activities of these pathways in terms of HGSIS (42). Those with an adjusted p-value of < 0.01 were defined as significant gene sets and Kaplan–Meier analysis was then used to verify the prognostic value of typical oncogenic hallmark pathways.

TIME patterns and immunological targets of HGSIS

For the estimation of TIME patterns regarding HGSIS, ssGSEA, a deconvolution algorithm implemented in the GSVA package (17, 43), was utilized to quantify the compositions of 30 types of TME cells, namely, 28 adaptive and innate immune cell types (44) and 2 stromal components (fibroblasts and endothelial cells) (45) based on the transcriptional data of the whole TCGA cohort. The ssGSEA scores representing the abundance of these TIME cells were next compared between different HGSIS risk groups, and the Spearman correlation analysis was performed to investigate the relationship between the HGSIS risk score and each TIME cell type. The prognostic values of these TIME cells were examined by Kaplan–Meier survival analysis. Furthermore, we contrasted the expression levels of 50 immunological targets that were classified into several groups such as receptors, ligands, and co-inhibitors (20, 46–48) to determine the intrinsic immune escape regarding HGSIS groups.

Prediction of therapeutic responses

Based on the HCC patients' data from TCGA, we predicted the putative sensitivities of HGSIS in immunotherapy and targeted/chemotherapies. For immunotherapy responses, we used the immunophenoscore (IPS) (44), which is calculated *via* machine learning and could be derived from The Cancer Immunome Atlas (TCIA) (https://tcia.at/home) to represent tumor immunogenicity of HCC patients. Moreover, the tumor immune dysfunction and exclusion (TIDE) score is a framework that was developed to infer the possible influences on survival and responses to immunotherapy. Two primary mechanisms (T-cell exclusion and T-cell dysfunction) of tumor immune evasion were integrated by the TIDE algorithm (http://tide.dfci.harvard.edu/) (49) with gene expression profiles of large cohorts to determine the clinical response to immunotherapy of HCC patients. The differences of IPS and TIDE scores between different groups were compared by the Wilcoxon test, and a lower TIDE score and a higher IPS indicate better sensitivities to immunotherapy. Furthermore, the half-maximal inhibitory concentration (IC_{50}) values of 138 drugs were estimated by the "pRRophetic package" (50) and further normally transformed to evaluate the predictive capacity of HGSIS for the responses to targeted/chemotherapies.

PPI network construction and key target identification

The limma package (31) was adopted to screen the DEGs between the HGSIS high- and low-risk groups using the whole TCGA cohort, and an adjusted p-value <0.01 and $|\log FC| \geq 1.5$ was set as the cutoff. The DEGs were then uploaded to the STRING database (version 11.5), an online database for the investigation of interactive relationships among proteins, to build a PPI network with a combined confidence score of ≥0.7. The STRING-based PPI network was next imported into Cytoscape (51) (version 3.8.2) for visualization. Furthermore, the MCODE plugin (52) was applied for cluster analysis and seed nodes identification, which were considered the key targets.

Molecular docking

The process of molecular docking was completed with Glide of Schrodinger as previously reported (20). Specifically, the crystal structure of the key target of HGSIS was derived from the RCSB PDB database (www.rcsb.org/), followed by the recognition of its active site using the DeepSite tool (53) from the PlayMolecule platform (https://www.playmolecule.com/). The protein docking structure was prepared by the Protein Preparation Wizard in the Maestro 11.6 version of the Schrödinger suite. Additionally, 111,178 compounds' structures involved in the in-man subset were downloaded from the ZINC 15 database (https://zinc15.docking.org). The virtual screening was conducted with the Glide Virtual Screening Workflow module integrated in the Schrödinger suite, the three main steps of which were applied to screen the candidates of KIF2C active affinity ligands. The first step was the high-throughput virtual screening (HTVS) mode starting with the 111,178 compounds, and subsequently, compounds with the top 10% of HTVS score were measured by the SP (Standard Precision) docking method. The third step was XP (Extra Precision) for the calculation of the top 10% SP docking score ranked compounds. OPLS-2005 force field was used during ligand–protein docking analysis to estimate the binding affinity.

Statistical analysis

The R package "survival" was utilized to pick out the significant hallmark gene sets, IRDEGs, and clinicopathological factors for OS, together with the hazard ratios (HRs) and 95% confidence intervals (CIs). Kaplan–Meier analysis with a log-rank test was used to analyze the differences between two subgroups of categorical variables for the OS, DFS, PFS, and DSS of HCC patients. The best cutoff for Kaplan–Meier survival analysis was determined by using the "survminer" package. Multivariate analysis was used to identify independent prognostic indicators. The package "timeROC" was used to depict the tROC curves to assess the predictive ability of HGSIS for OS. The comparison of survival rates between different risk groups was completed using the Pearson Chi-square test. Wilcoxon test was used to compare the distribution of continuous data for three or more groups and

Kruskal–Wallis test was used to determine the statistical difference of that for two groups. Correlations between two quantitative variables were explored by Pearson's correlation test. All the above statistical analyses were conducted by the R software (version 3.6.1). Unless otherwise noted, $p < 0.05$ was considered statistically significant.

Results

Hallmark-guided recognition of HCC subtypes with prognostic significance

Hallmark gene sets from MSigDB are coherently expressed signatures representing well-defined biological states or processes; thus, it is reasonable to identify specific hallmark-based HCC subtypes with distinct prognoses. Motivated by this rationale, we obtained 336 HCC patients' mRNA expression matrix with corresponding clinical information from the TCGA database, followed by the computation of the enrichment scores for all 50 hallmark gene sets of each sample by GSVA. Next, we screened the robust hallmark gene sets significantly correlated to the prognosis of HCC patients with the "multi-split" strategy (Supplementary Figure 1). As a result, 15 hallmark gene sets were consistently significant 100 times in 100 subsamples, which were considered as prognostic hallmark gene sets. Based on the 15 hallmark gene sets, we performed the unsupervised clustering analysis for subtype classification. Our results showed that the optimal number of clusters was 2, which generated the greatest increase in the area under the CDF curves, and it was further validated by the PAC algorithm (Figures 2A–C and Supplementary Figure 2). Thus, we further classified all HCC patients into two distinct subtypes (Figures 2D, E). Notably, Kaplan–Meier analysis found that the patients in subtype 2 had a shorter survival time than the patients in subtype 1 (Figures 2F–I).

Construction of HGSIS

The significant difference in OS outcomes between the two subtypes prompted us to pick out the DEGs between them. Using the package "limma", we detected 881 DEGs between subtype 1 and subtype 2, which intersected with 1,811 immune-related genes from the ImmPort database, and 67 overlapping immune-related DEGs (IRDEGs) were identified (Figures 3A, B and Supplementary Table 2). The expression heatmap of IRDEGs in the two subtypes is shown in Figure 3C. GO enrichment analysis revealed that the most significant terms enriched by these IRDEGs were the biological process (BP) of antimicrobial humoral response, cellular component (CC) of collagen-containing extracellular matrix, and molecular function (MF) of receptor-ligand activity and signaling receptor activator activity (Figure 3D). For the KEGG analysis, IRDEGs mostly participated in the pathway of cytokine–cytokine receptor interaction (Figure 3E). Subsequently, we inputted the IRDEGs into UniCox regression analysis and found 28 significant prognostic IRDEGs with a p-value lower than 0.05 (Supplementary Table 3). Next, we conducted LASSO Cox regression with the 28 genes and acquired seven robust genes (TMPRSS6, SPP1, S100A9, EPO, BIRC5, PLXNA1, and CDK4) that were significantly correlated with the OS of HCC patients, and the selection of the tuning parameter in the LASSO model is shown in Figure 3F. The seven genes were subsequently incorporated into an HGSIS model for predicting the prognosis of HCC. Figures 3G, H showed the UniCox and MultiCox results of the selected seven genes with the corresponding hazard ratio (HR) and statistical significance.

Evaluation and validation of HGSIS

Based on the median risk score of HGSIS, HCC patients from different datasets were classified as high- or low-risk groups (Figure 4A). According to the corresponding prognostic data, the high-risk groups of the TCGA training set, TCGA validation set, whole TCGA cohort, and ICGC-LIRI-JP cohort all had higher mortality (Figure 4B). Kaplan–Meier analysis showed that high-risk patients had exceedingly lower OS rates relative to low-risk patients in different datasets (Figure 4C). Additionally, the time-dependent receiver operating characteristic (tROC) curve analysis was applied to evaluate the accuracy of the HGSIS model. As shown in Figure 4D, the area under the ROC curve (AUC) was 0.797, 0.710, and 0.721 in 1-year, 3-year, and 5-year survival, respectively, for the TCGA training set. Interestingly, the AUC values for all the three validation datasets were even higher than the training set, suggesting that HGSIS had excellent performance in predicting the OS of HCC. In comparison with other published immune-related signatures and widely used biomarkers of cancer immunotherapy, HGSIS achieved higher predictive accuracy (Figure 4E). Moreover, to explore the potential relationship between HGSIS and multiple clinicopathological traits, correlation analysis was conducted and it revealed that HCC subtype, tumor grade, stage, and mRNAsi were significantly correlated with HGSIS (Figure 4F and Supplementary Figure 3). Stratification analysis for clinicopathological traits demonstrated the extra predictive value of HGSIS (Supplementary Figure 4). Additionally, we examined the potential of HGSIS in predicting the DFS, PFS, and DSS of HCC patients, and it revealed similar results to that of OS analysis (Supplementary Figure 5). Taken together, all these data presented above convincingly indicated the strong prognostic-prediction capability of HGSIS.

10.3389/fimmu.2022.958161

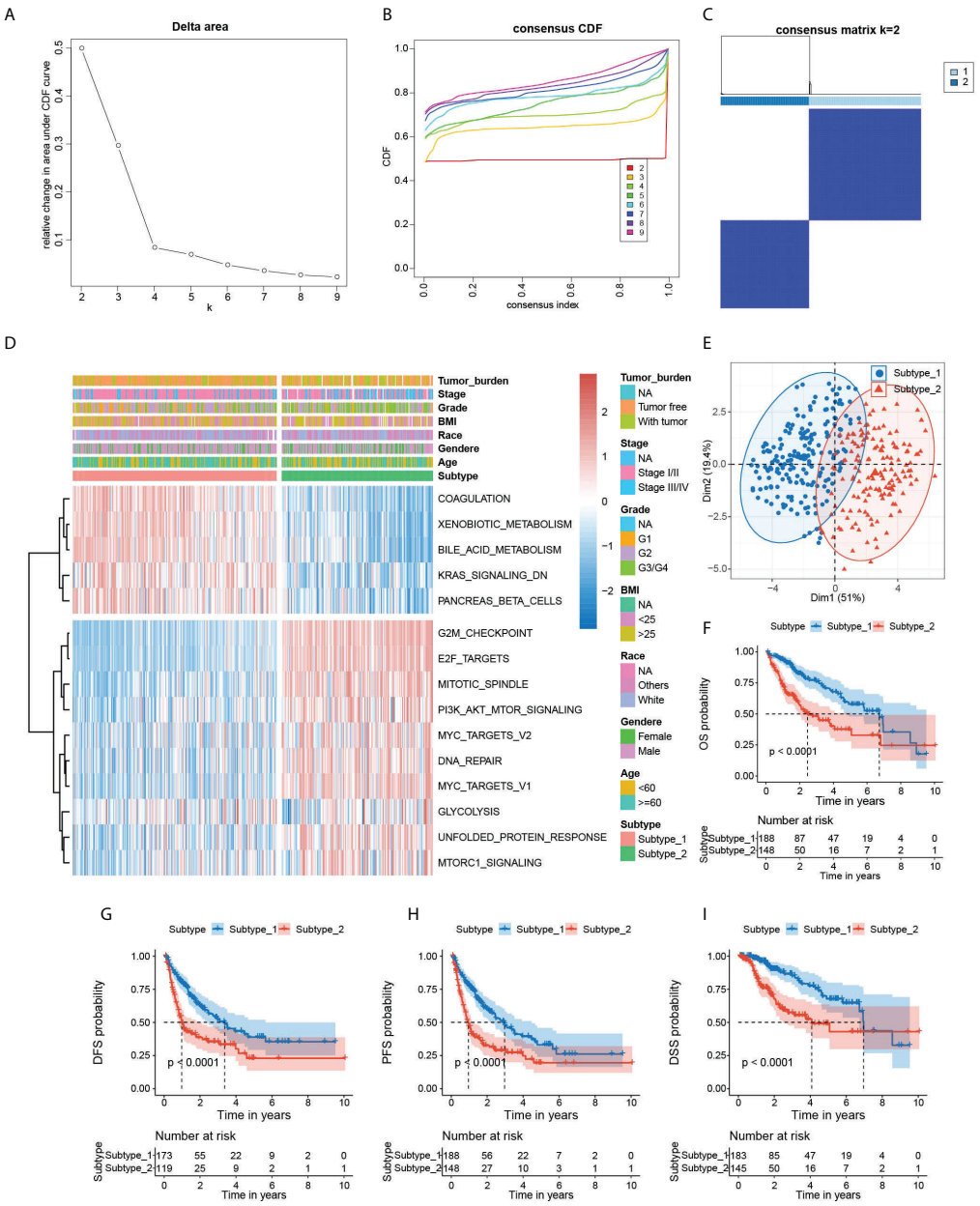

FIGURE 2
Identification of hallmark-based HCC subtypes. **(A)** The corresponding relative change in area under the cumulative distribution function **(C, D, F)** curves and the optimal number of cluster(*k*) was 2. **(B)** Consensus clustering CDF for *k* = 2 to 9. **(C)** Heatmap of sample clustering at consensus *k* = 2. **(D)** Heatmap showing the GSVA score of 15 hallmark gene sets, tumor burden, stage, grade BMI, race, gender, and age in two subtypes of HCC. **(E)** PCA plot visualizing the two HCC subtypes with 15 hallmark gene sets. **(F–I)** Kaplan–Meier survival plots of subtype 1 and subtype 2 for OS, DFS, PFS, and DSS. OS, overall survival. DFS, disease-free survival. PFS, progression-free survival. DSS, disease-specific survival. PCA, principal component analysis. GSVA, Gene set variation analysis.

Establishment of the HGSIS-integrated nomogram

Accurate and individualized prediction of the postoperative mortality risk of HCC patients has been a tough challenge in clinical decision-making. In this case, we considered constructing a novel nomogram combining HGSIS and multiple clinicopathological traits to provide an accurate and quantitative prognosis-predictive tool for HCC patients. Univariate and multivariate Cox analyses on HCC prognosis with HGSIS and clinicopathological factors were at first carried out using the whole TCGA cohort. As shown in Figure 5A, the

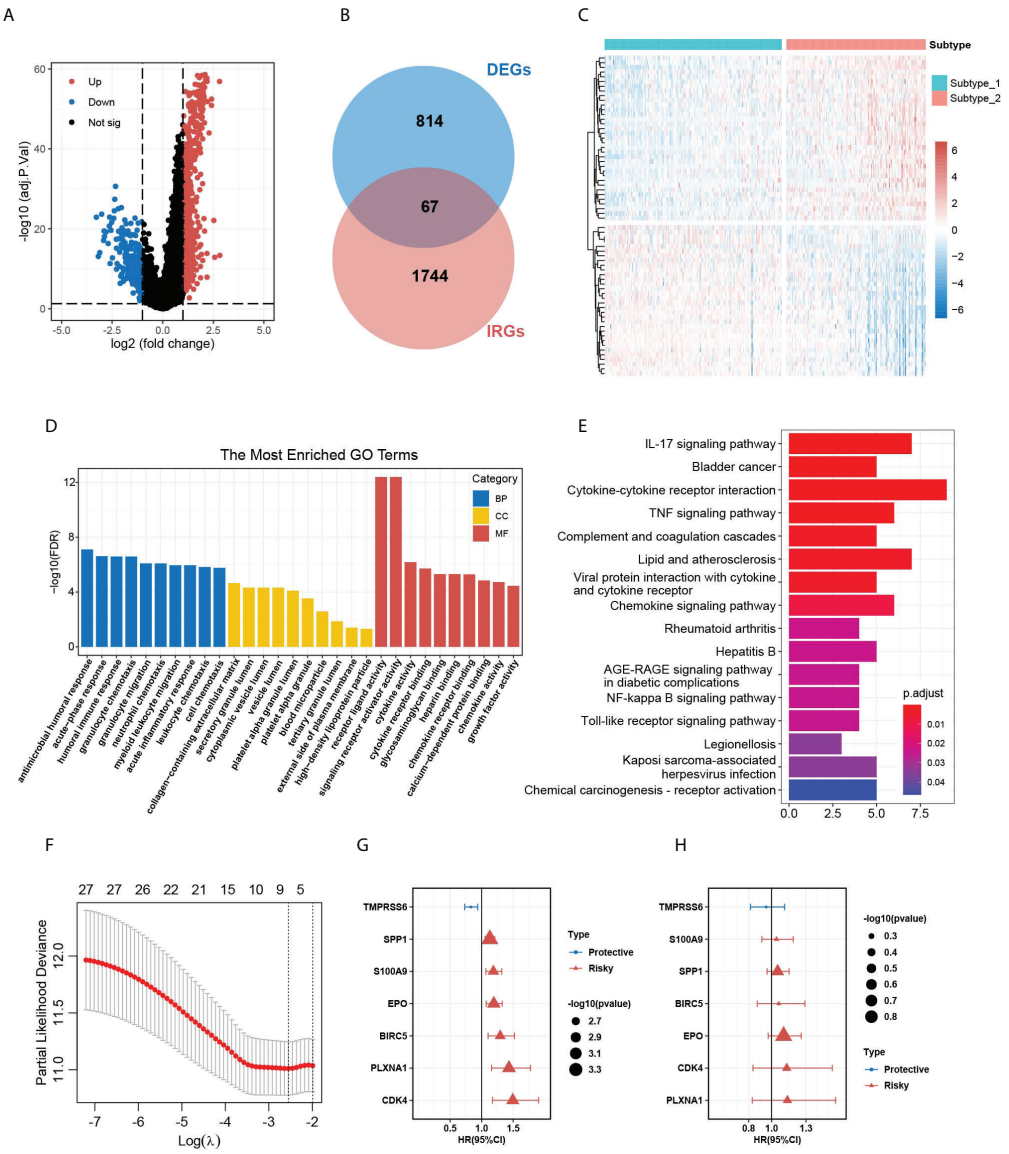

FIGURE 3
DEG analysis in the two HCC subtypes and the construction of HGSIS. **(A)** Volcano plot of 881 DEGs between the two HCC subtypes. **(B)** Venn plot showing 67 immune-related DEGs. **(C)** Heatmap of the IRDEGs in the two subtypes. **(D, E)** GO and KEGG enrichment analysis for the 67 IRDEGs. **(F)** Selection of the tuning parameter (lambda) in the LASSO model by 10-fold cross-validation. **(G, H)** Hazard ratio with 95% CI of the seven genes in the HGSIS signature computed by UniCox and MultiCox, respectively. HCC, hepatocellular carcinoma. GO, gene oncology; KEGG, Kyoto Encyclopedia of Genes and Genomes. HGSIS, hallmark-guided subtypes-based immunologic signature. IRDEGs, immune-related DEGs.

HGSIS risk model, stage, and tumor burden were significantly high-risk factors for HCC in both univariate and multivariate Cox analysis, indicating that HGSIS was an independent prognostic indicator [HR (95% CI) = 2.478 (1.619–3.793), $p < 0.001$]. By integrating the three parameters, we constructed a prognostic nomogram to predict the 1-, 3-, and 5-year survival in HCC patients (Figure 5B). Calibration curves of the nomogram for the predicted and observed 3- and 5-year OS are shown in Figure 5C, suggesting the good consistency of the nomogram. Meanwhile, comparing with stage, tumor burden, and the combination of both, the HGSIS-integrated nomogram had the highest C-index, representing its best predictive accuracy (Figure 5D). In 3- and 5-year OS prediction for HCC patients, the nomogram showed the highest net benefit over most of the risk thresholds (Figures 5E, F). Furthermore, we divided HCC patients into high- and low-risk groups based on

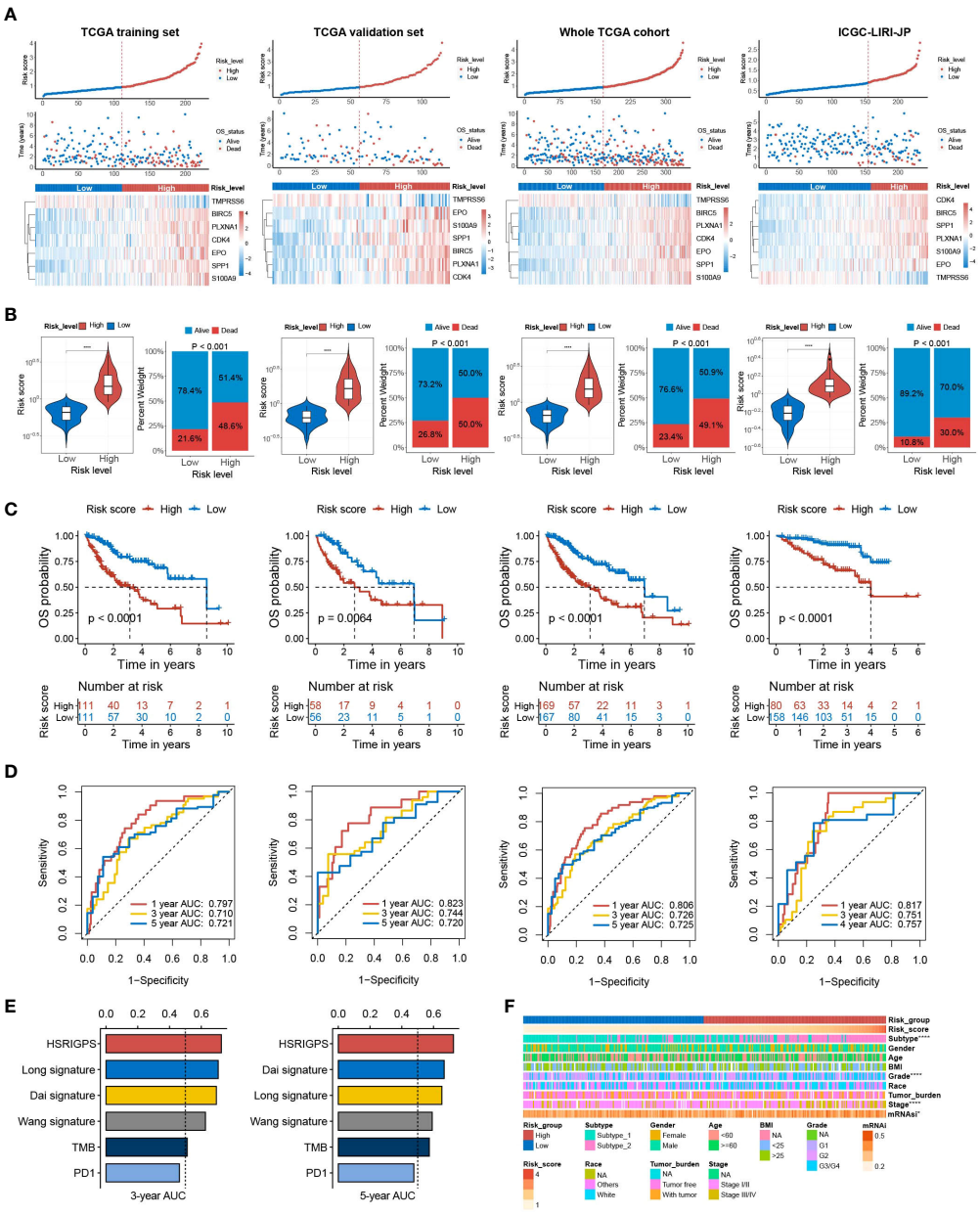

FIGURE 4
Prognostic value of HGSIS for OS in HCC patients. **(A)** Risk score distribution, survival status, and the expression of seven HGSIS signature genes for patients in the low- and high-risk groups from four datasets (TCGA training set, TCGA validation set, whole TCGA cohort, and ICGC-LIRI-JP cohort). **(B)** Risk score and mortality rates of patients in the low- and high-risk groups from four datasets. **(C)** Kaplan–Meier survival plots of the low- and high-risk groups from four datasets for OS. **(D)** tROC curves of HGSIS in the four datasets. **(E)** The comparison of AUC values for the 3-year and 5-year survival between HGSIS and other published signatures or common immunotherapeutic biomarkers. **(F)** Correlation analysis between HGSIS and multiple clinicopathological traits. **** means $p < 0.0001$.

the median score of the HGSIS-integrated nomogram, and remarkably elevated OS, DFS, PFS, and DSS rates were observed in the low-risk group (Figure 5G). All these findings indicate that the HGSIS-integrated nomogram can serve as a powerful and valuable tool for individualized OS survival prediction in HCC patients.

Genomic characteristics and regulatory mechanisms of the HGSIS-defined subgroups in HCC

We further analyzed the underlying molecular mechanisms of HGSIS on the landscape of somatic mutation and hallmark

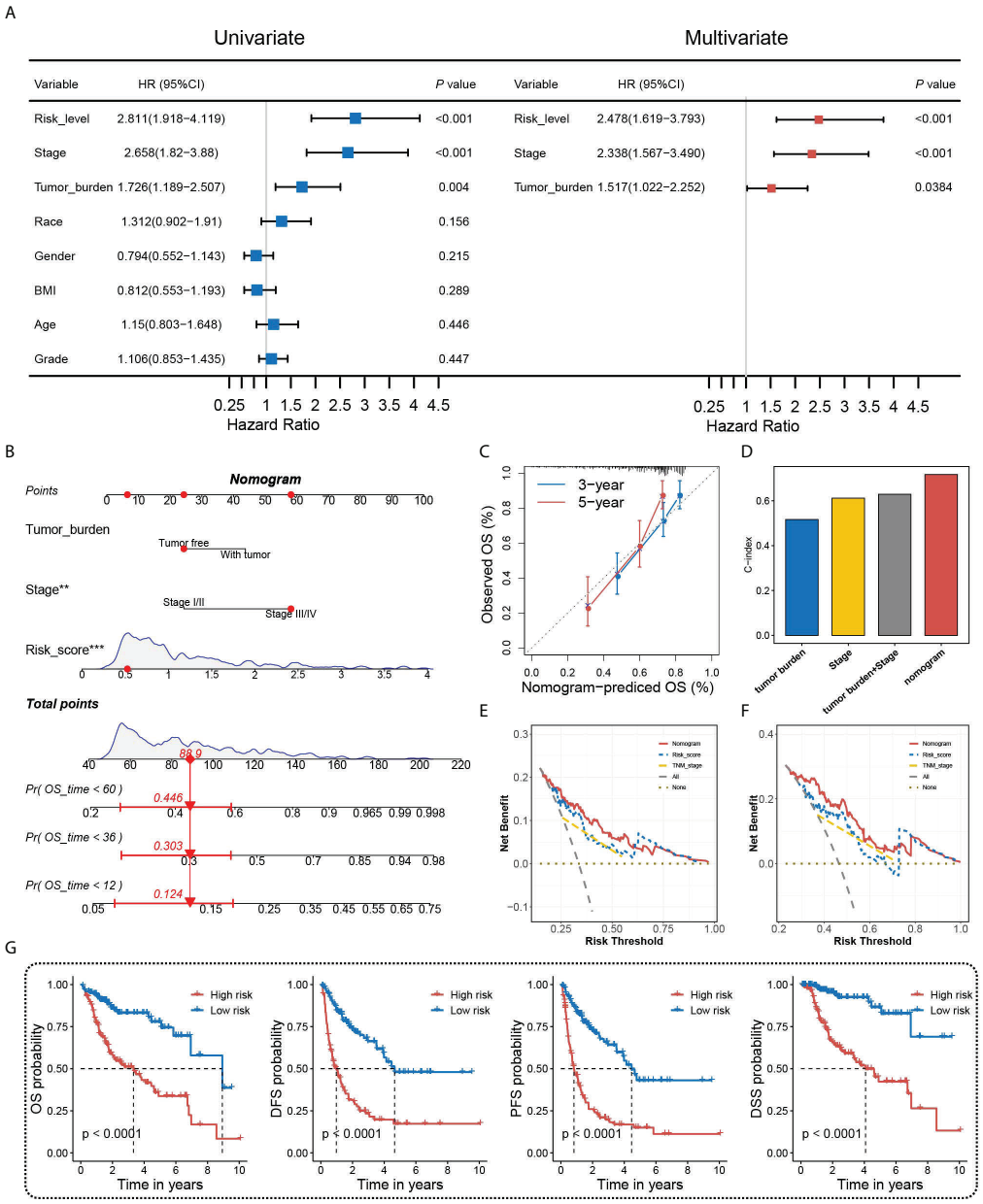

FIGURE 5
Nomogram construction and assessment. **(A)** Univariate and multivariate Cox regression analyses of HGSIS and other clinicopathological traits for OS in HCC patients. **(B)** Nomogram built by HGSIS, stage, and tumor burden to predict 1-,3- and 5-year OS in HCC patients. **(C)** Calibration plot of the nomogram. **(D)** C-index values of the nomogram and clinicopathological traits. **(E, F)** Comparison of net benefits of each model for 3-year **(E)** and 5-year **(F)** OS. **(G)** Kaplan–Meier survival analysis of the integrated nomogram for OS, DFS, PFS, and DSS in HCC patients.

pathway enrichment. We firstly examined the 20 genes with the highest mutation frequency in the low- and high-risk groups and the oncoplots showed that the most mutated genes were TP53 (43%) and CTNNB1 (27%) in the two different risk groups, respectively. Meanwhile, four genes (TP53, TTN, CTNNB1, and MUC16) simultaneously had high mutation frequencies in both two groups (Figures 6A, B). The summary of the mutation information is shown in Supplementary Figure 6. Fisher's exact test was applied to extract the distinct mutation status between two groups and the forest plot showed that TP53 mutated more frequently while HERC2 mutation occurred less in the high-risk group significantly (Figure 6C). Moreover, considering that TP53 was the most notable mutated gene, a lollipop chart was established to reveal the detailed mutation sites of TP53, and

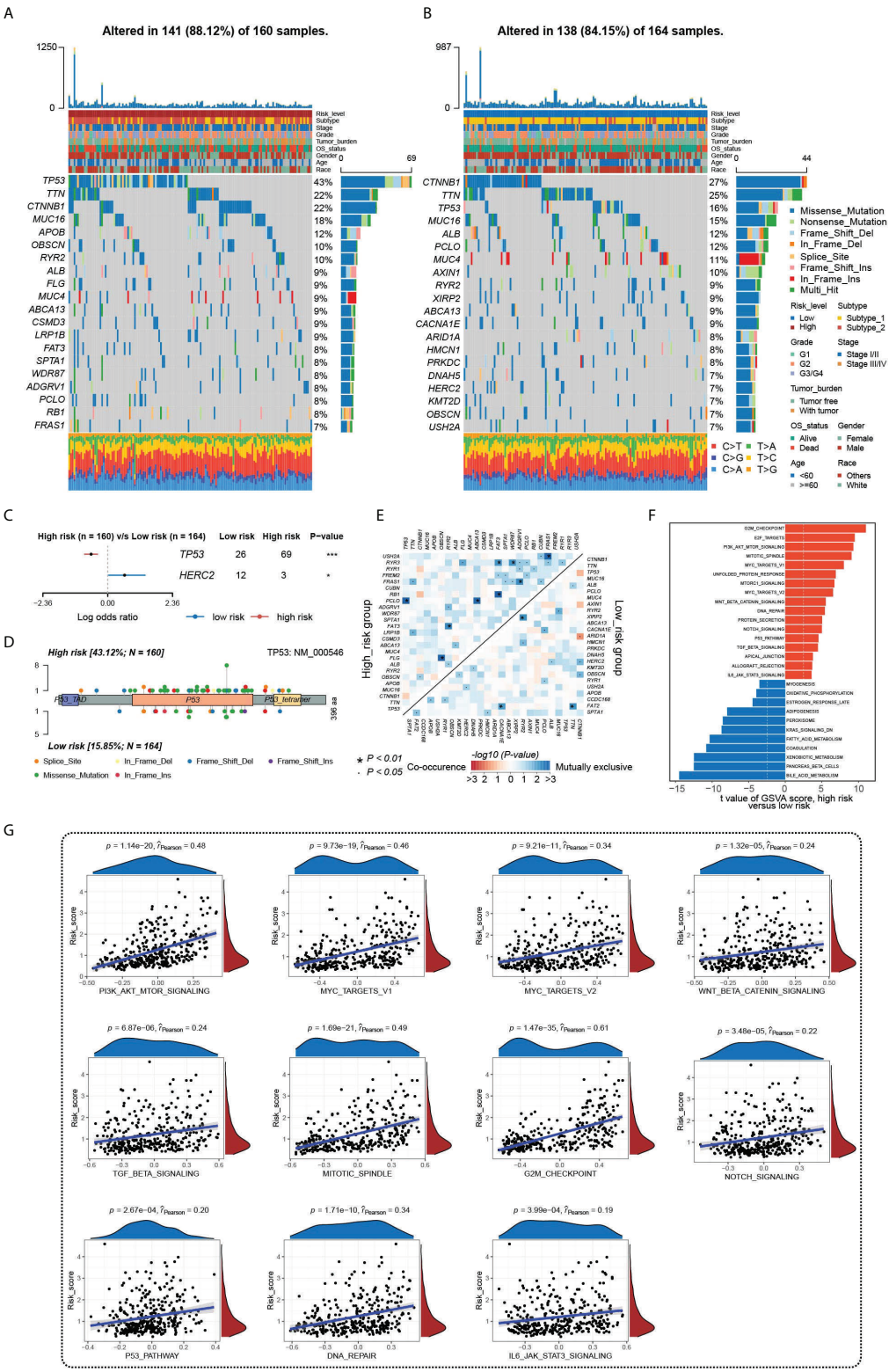

FIGURE 6
Underlying molecular mechanisms of HGSIS. **(A, B)** Oncoprint analysis of the high-risk **(A)** and low-risk groups **(B)**. **(C)** Forest plot showing genes mutated differentially in patients of the low- and high-risk groups. **(D)** Lollipop plot of mutation sites of TP53. **(E)** Interaction effect of 25 mutated genes in the low- and high-risk groups. **(F)** Distinct hallmark pathways between the two HGSIS risk groups. **(G)** Correlation analysis between 11 oncogenic hallmark pathways and HGSIS-based risk score, respectively. * means $p < 0.05$; *** means $p < 0.001$.

more missense mutation was observed in the high-risk group (Figure 6D). The co-occurrences and mutual exclusions of the top 25 mutated genes in two risk groups were also shown in Figure 6E. To unravel the underlying transcriptomic mechanisms of HGSIS, we calculated the GSVA scores of 50 hallmark pathways in the low- and high-risk groups, respectively, to identify the key hallmark pathways associated with HGSIS, the integral landscape of which is shown in Supplementary Figure 7. Of the 50 hallmark pathways, 28 were found to be of significant difference between two risk groups, of which 17 hallmark pathways were upregulated while 11 hallmark pathways were downregulated in the high-risk group (Figure 6F). Notably, all the 11 oncogenic hallmark pathways that were upregulated in the HGSIS high-risk group were positively correlated to the HGSIS model-based risk score significantly (Figure 6G), indicating the tight linkage between HGSIS and those well-known oncogenic pathways.

HGSIS was associated with the immune status in the HCC tumor microenvironment

To further examine the potential clinical value of HGSIS, we outlined the immune cells' infiltration profile of the whole TCGA cohort by ssGSEA, a reliable and popular algorithm computing the relative proportion of 28 types of immune cells and two types of stromal cells in TME. As Figure 7A shows, the HGSIS risk group was significantly correlated with most infiltrating immune cell types including activated CD4 T cell, central memory CD8 T cell, regulatory T cell, effector memory CD4 T cell, immature B cell, T follicular helper cell, type 2 T helper cell, central memory CD4 T cell, macrophage, natural killer T cell, eosinophil, mast cell, activated dendritic cell, immature dendritic cell, MDSC, and plasmacytoid dendritic cell. Moreover, we performed correlation analysis on HGSIS risk score and TME cells, and as the result shows, 19 cell types were isolated in association with HGSIS (Figure 7B). Additionally, UniCox analysis found that nine types of TME cells were significantly associated with the prognosis of HCC (Supplementary Table 4). Combining the results of differential analysis, correlation analysis, and survival analysis of the 30 TME cell types, we plotted the Venn diagram exhibiting the four overlapping cell types (natural killer T cell, eosinophil, endothelial cells, and immature dendritic cell) (Figure 7C). Figure 7D exhibits the Kaplan–Meier curves indicating the significant implications of the four cell types for the OS of HCC patients. Meanwhile, with great anticipation, we found that the expression of the vast majority of immune checkpoints in HCC patients was significantly correlated with HGSIS, suggesting that HGSIS had the potential to predict the immune checkpoints' expression level broadly in HCC (Figure 7E).

Evaluation of HGSIS in predicting therapy response potential

The significant correlation between HGSIS and multiple immune checkpoints was of great interest to us, especially as immune checkpoint therapy held promise for the clinical treatment of cancer nowadays. We first explored the relationship between HGSIS and immunophenoscore (IPS) in HCC patients. IPS was well-known to be capable of predicting immune checkpoint therapy response, based on the evaluation of the pivotal immune-related gene expression. As shown in Figure 8A, the IPS score was significantly elevated in the low-risk group, representing higher sensitivity to immunotherapy. Although the scores of IPS-CTLA4 and PD1/PD-L1/PD-L2 blocker, IPS-CTLA4 blocker, and IPS-PD1/PD-L1/PD-L2 blocker were not statistically associated with HGSIS, the low-risk group tended to have increased scores than the high-risk group. We further measured the TIDE scores in HCC patients of the TCGA training set, the TCGA validation set, the whole TCGA cohort, and the ICGC-LIRI-JP dataset, and the low-risk groups all had significantly lower TIDE scores than the high-risk groups, suggesting that the patients in the low-risk groups were predicted to have better responses to immunotherapy (Figure 8B). In addition, we used the "pRRophetic" algorithm to estimate the IC_{50} values of 138 drugs for not only immunotherapy but also chemotherapy and targeted therapy for HCC patients (Figure 8C). Interestingly, we found that high-risk patients might be sensitive to more drugs than low-risk patients (Figure 8C and Supplementary Figure 8).

KIF2C is a key target of HGSIS

To identify the key targets relating to HGSIS, we utilized the limma package to screen the DEGs between the high- and low-risk groups of the whole TCGA cohort. Consequently, 85 genes were significantly downregulated while another 85 genes were upregulated in the high-risk group (Supplementary Table 5). With the strict criterion of a combined score of >0.7, we constructed a PPI network of 95 nodes and 212 edges (Supplementary Figure 9). Furthermore, the MCODE app identified five clusters (default parameters) of the network. As shown in Figure 9A, KIF2C, HP, PKM, MMP9, and CYP2C8 were recognized as the "seed" nodes of these clusters (red ovals represent "seed" nodes, and blue ovals represent "clustered" nodes). Interestingly, four clusters were highly connected by driver oncogenes of HCC or immunologic genes such as CXCL8, UBE2C, and MMP9. Notably, we observed the most conspicuous cluster that consisted of several hub genes of HCC (CCNB1, CDC20, TOP2A, and UBE2C) (23, 24). Thus, the "seed" node of this cluster, KIF2C, was considered as the key target of HGSIS, and its crucial role in the discovery of putative drugs is worth looking into.

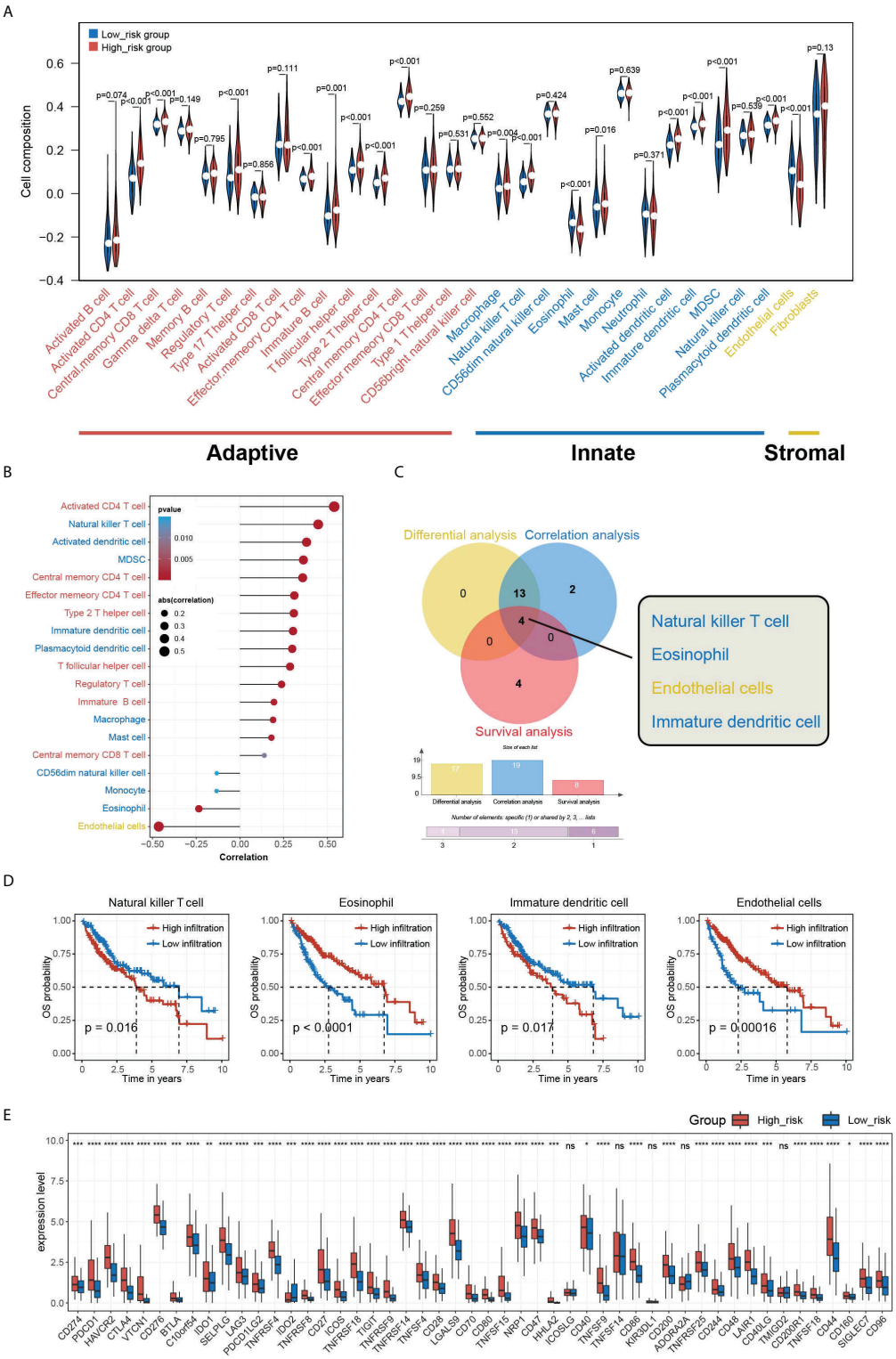

FIGURE 7
Overview of HGSIS-related immune infiltration. **(A)** Violin plot presenting the relative composition of multiple cell types in the low- and high-risk groups. **(B)** Correlation analysis of immune infiltration and HGSIS risk score. **(C)** Venn diagram revealing the four intersected cell types among differential analysis (yellow), correlation analysis (blue), and survival analysis (red). **(D)** Kaplan–Meier survival analysis of the four TME cell types. **(E)** Expression levels of common immune checkpoints in two HGSIS risk groups. TME, tumor microenvironment. * means $p < 0.05$; ** means $p < 0.01$; *** means $p < 0.001$; **** means $p < 0.0001$; ns, no significance.

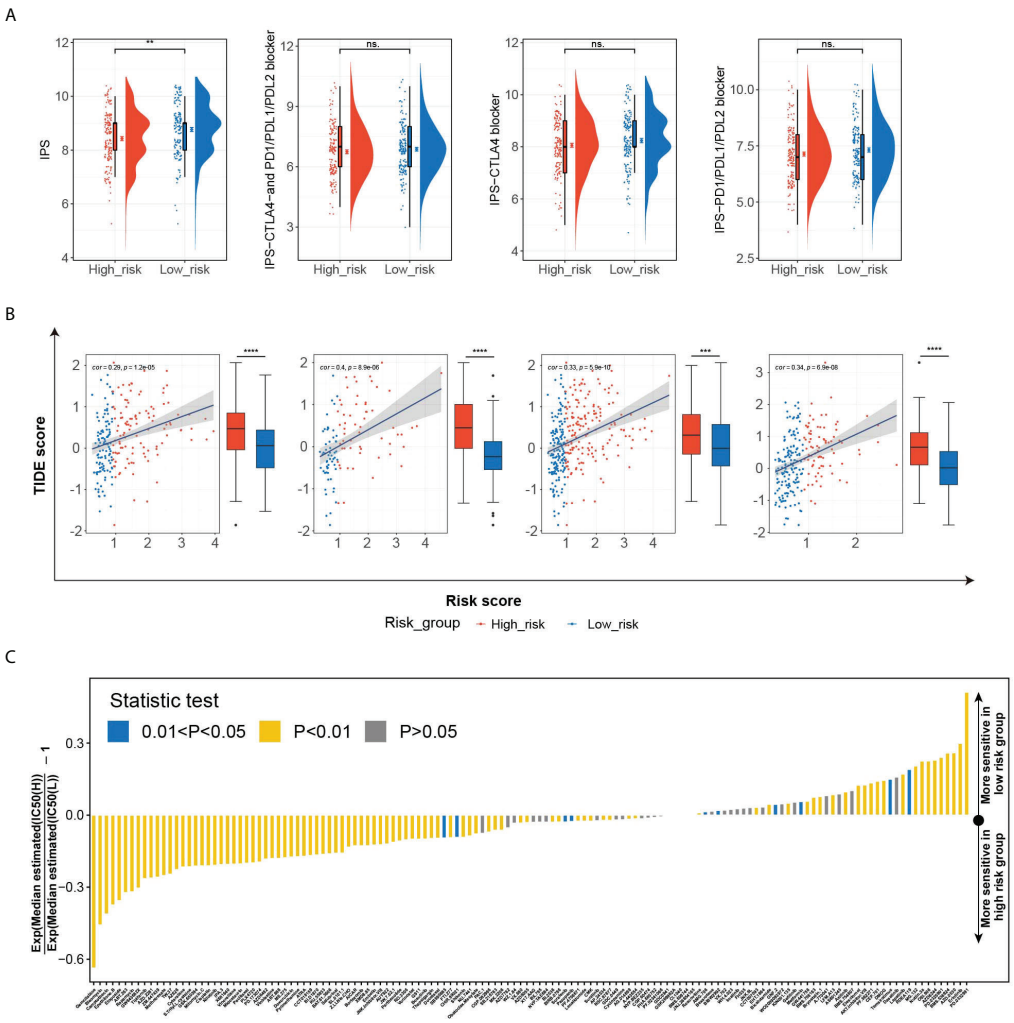

FIGURE 8
The potential role of HGSIS in predicting therapeutic sensitivity. **(A)** The correlation between HGSIS and IPS based on the whole TCGA cohort. **(B)** Distribution of TIDE scores in the TCGA training set, TCGA validation set, whole TCGA cohort, and ICGC-LIRI-JP dataset. **(C)** Estimation of 138 drugs' normalized IC_{50} values. $^{**}p < 0.01$, $^{***}p < 0.001$, $^{****}p < 0.0001$, ns, not significant.

Candidate small molecule prediction

Molecular docking is an effective computational method that provides insights into molecular interactions between candidate drugs and proteins. In the present study, we further predicted possible small molecules that may bind to the key target of HGSIS, KIF2C, *via in silico* molecular docking. As shown in Figure 9B, 24 small compounds were successfully filtered out from a public library that contains a large number of small molecules from the ZINC 15 database, which includes 10 commercially available molecules that were considered as potential affinity ligands of KIF2C protein (Supplementary Table 6). The 3D interaction diagrams of the 10 docking models showing the detailed binding energy are displayed in Figure 9C and Supplementary Figure 10. The interaction diagram of lactoyl-ph4 at the binding pocket of KIF2C suggested the formation of hydrogen bonds with key residues GLN-475, VAL-547, and ASP-550. Similarly, dihydrobiopterin also relied on hydrogen bonds between the active site and several amino acid residues to remain its high affinity with KIF2C.

Discussions

Like most malignancies (54–57), the classification of distinct subtypes of HCC has been widely recognized in

10.3389/fimmu.2022.958161

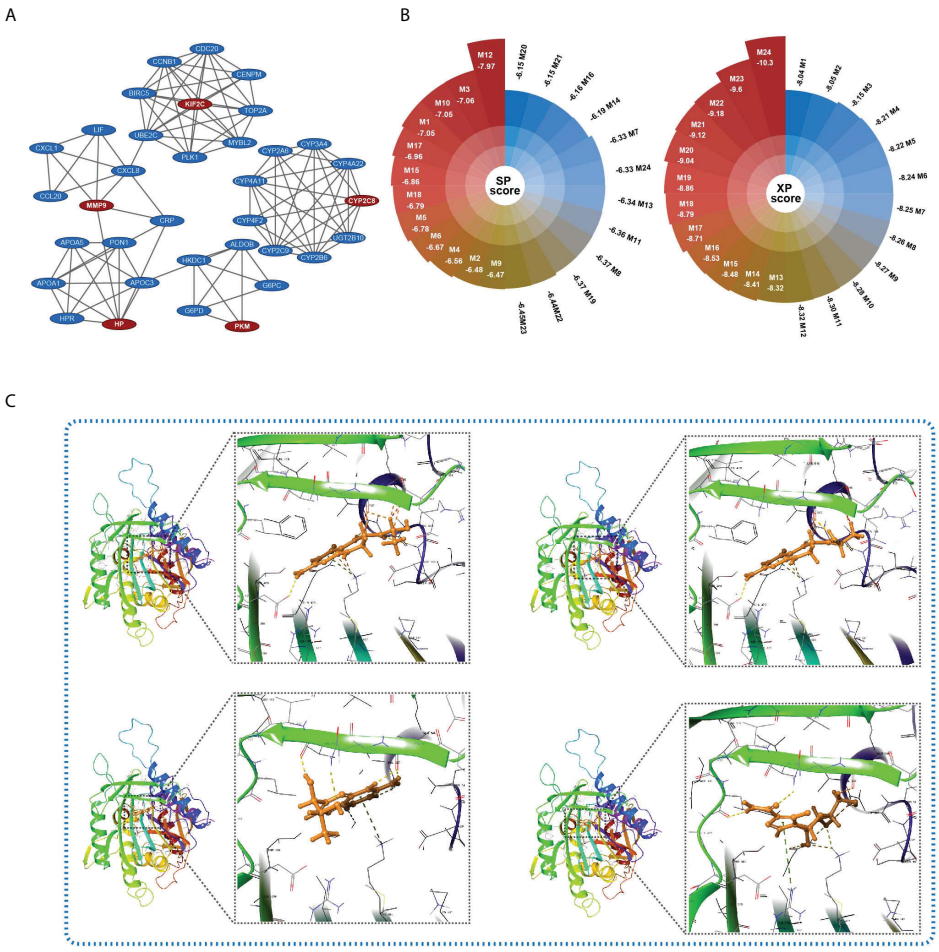

FIGURE 9
Key target identification and candidate small molecule prediction. **(A)** Five clusters identified by the MCODE app of Cytoscape 3.8.2. Red ovals represent "seed" nodes and blue ovals represent "clustered" nodes. **(B)** The docking score (XP and SP score) of the top 24 small compounds that bind to KIF2C with the lowest total energy score. **(C)** Structures and docking models of the top four small compounds (lactoyl-ph4, dihydrobiopterin, 7-biopterin, and mizoribine) and the active site of KIF2C.

clinical practice (58–60). To date, with the increasing knowledge of the HCC TME, the exploration of the intratumoral immune ecosystem has been extensively involved in the study of HCC heterogeneity (61–63). Therefore, the new classification of biologically meaningful HCC subtypes gained widespread interest from either researchers or pathologists, contributing to the development of clinically useful biomarkers or signatures to predict the prognosis of HCC more precisely and individually.

In this study, we firstly employed GSVA to compute the GSVA scores of 50 hallmark gene sets that represent predefined specific gene signatures with biological significance. Robust prognostic hallmark gene sets were comprehensively identified and used to pick out distinct HCC subtypes *via* consensus clustering. Based on the hallmark-guided subtypes, we successfully developed and validated a prognostic gene signature of HCC, i.e., HGSIS. Multivariate analysis confirmed that HGSIS was an independent factor for the prediction of HCC patients' OS survival, and the established nomogram showed increased accuracy and great potential in clinical practice.

As an advanced computational method, GSVA is one of the best and most up-to-date algorithms throwing light on the discovery of subtle pathway activity changes in a given population by condensing gene expression profiles into pathways. Herein, we defined two distinct HCC subtypes with 15 prognostic hallmark gene sets, most of which were metabolism-related and immune-related. For example, glycolysis gene sets included genes encoding proteins involved in glycolysis and gluconeogenesis, defined as biological processes responsible for the regulation of proliferation, immune evasion, invasion, metastasis, angiogenesis, and drug resistance in HCC (64). The PI3K/AKT/mTOR pathway was linked to drug

resistance and the occurrence of HCC in a recent clinical study (65). Based on the hallmark-guided subtypes of HCC, we focused on the immune-related genes expressed differently between two subtypes, and 67 IRDEGs were extracted from 881 DEGs. HGSIS construction was carried out with UniCox and LASSO Cox analysis on 67 IRDEGs, leading to a seven-gene prognostic signature (TMPRSS6, SPP1, S100A9, EPO, BIRC5, PLXNA1, and CDK4). TMPRSS6 was reported to express much lower in HCC cell lines when compared to normal liver samples, which was consistent with our HGSIS model, presenting a protective role of TMPRSS6 in HCC (66). Ma et al. found that SPP1 expression was tightly linked to the TME reprogramming and tumor progression in response to therapy by single-cell transcriptomic analysis (67). S100A9, PLXNA1, and EPO were also reported as candidates for HCC prognostic signatures, implying their subtle effects on the disease progression of HCC patients (68–70). Moreover, BIRC5 was also found to be highly expressed in liver cancer (71). CDK4 was a well-recognized oncogene, and it was encouraging that Palbociclib, a CDK4 inhibitor, showed significant benefit in preclinical models of HCC (72). In summary, HGSIS was a model that fitted well with HCC. After being validated internally and externally, HGSIS showed outstanding prediction accuracy for HCC patients, and the HGSIS high-risk group obviously presented a worse prognosis.

A growing number of prognostic gene classifiers have been developed to evaluate the mortality risks of HCC patients, most of which were based on limited gene sets or DEGs between tumor and adjacent normal samples. For instance, Liu et al. discovered a six-gene signature presenting a strong ability for differentiating HCC tumors and normal tissues (73). Li et al. constructed an lncRNA signature for estimating OS of HCC patients (74). However, few previous studies combined multi-gene sets to recognize HCC subtypes with distinct survival outcomes, and here, we, for the first time, adopted the hallmark-guided subtype-based identification of immunologic gene signatures to predict the OS of HCC patients. Importantly, the comparison of AUC values between HGSIS and other reported signatures or immunotherapeutic targets demonstrated the reliability of our novel strategy in building a prognostic classifier. Thus, our study provided a novel perspective for the first time, that hallmark-gene set-based cancer subtypes could make a firm basis for clinical classifiers construction. Another strength of the present study was the integrative and combined strategy that included GSVA, unsupervised clustering, UniCox, and LASSO-Cox, which was more effective and reliable than that where only one or two algorithms were applied. Thirdly, unlike most studies that did not assess the feasibility of prognostic signatures for drug prediction, we employed PPI construction, key genes identification, and molecular docking to select the most probable small compounds from a large number of potential drugs, some of which had been reported to have an anti-cancer effect in several cancers. Furthermore, it cannot be denied that, at all levels from molecular alterations to histopathologic diversity, more comprehensive research would provide better references for understanding the mechanisms of drug resistance or treatment inefficiencies in HCC patients (75).

Tumor mutational burden (TMB) has been confirmed to be related to the immunotherapy effectiveness and prognosis in various malignancies; however, its underlying mechanism in HCC remained unclear (76). Therefore, we used maftools to evaluate the mutation status in HGSIS low- and high-risk groups. TP53 showed the highest mutation frequency (43%) in the high-risk group while CTNNB1 mutated most frequently in the low-risk group. Consistent with previous reports, TP53 and CTNNB1 are the most common genetic alterations in HCC (77, 78). Interestingly, by exome sequencing analysis, a remarkable study found that alcohol-related HCC was significantly associated with CTNNB1 mutation, and TP53 mutation frequently occurred in HBV-related HCC (79). Logically, more alcoholics might be classified into the low-risk group and more patients infected with HBV might be related to the high-risk group. Several well-recognized oncogenic signaling pathways were transcriptionally activated in the high-risk group including the most researched TP53 pathway, MYC pathway, Wnt/β-Catenin pathway, PI3K/AKT/mTOR pathway, and Notch pathway (64, 80–82). Thus, HGSIS was capable of separating groups of different mutation statuses in HCC.

Given that tumor-infiltrating immune cells constituting the major component of TME are associated with the prognosis and immunotherapy efficacy of HCC (83), ssGSEA algorithm was used to estimate the relative proportion of TME cell types in the HGSIS low- and high-risk groups. The relative abundance of 17 TME cell types differed significantly between the two subgroups. A large body of studies has illustrated that regulatory T cells (Tregs) played an immunosuppressive role in TME and were associated with a poor prognosis of HCC (84–86). Unsurprisingly, our study found that more Tregs infiltrated in TME of patients from the high-risk group. In the past decade, immunotherapy, especially ICIs, has become a highlight research direction for the treatment of broad-spectrum malignancies. Moreover, as HCC usually arises in the context of virus-related chronic inflammation, immunotherapy is likely to be an ideal therapeutic option for HCC. In our study, differential analysis revealed relatively higher levels of immune checkpoint expression in the HGSIS high-risk group, indicating that patients in the high-risk group were accompanied by a worse anti-TIME. For the results of IPS and TIDE analysis, we found that the low-risk group had higher IPS scores while having a lower TIDE score, and higher IPS and lower TIDE corresponded to a better prognosis. On the other hand, we estimated the sensitivity of 138 drugs included in

immunotherapy, chemotherapy, and targeted therapy and found that the high-risk group was sensitive to more drugs. Taken together, the HGSIS model could potentially serve as a reference for individualized immunotherapy design.

To screen small molecules used as potential drugs to reverse the high risk of HCC patients, we analyzed the DEGs between the two HGSIS risk groups, which were utilized to build an interactive PPI network. From the network, KIF2C was identified to be the key node that connected to several hub oncogenes of HCC. Notably, KIF2C has been revealed as a prognostic biomarker in endometrial cancer and correlated with the infiltration level of CD8+ T cells (87). In HCC, Wei et al. disclosed that KIF2C is associated with a poor prognosis of HCC and interacts with TBC1D7 to enhance the mTORC1 signal transduction (88). In the present study, using the structure-based approach, we identified 10 purchasable small compounds that may bind well to KIF2C from a large number of small compounds. Among them, mizoribine is a novel and effective immunosuppressant that inhibits the activity of HCV RNA replication, and it is also a selective inhibitor of inosine-5'-monophosphate dehydrogenase (IMPDH) that has been clinically used throughout Asia. Importantly, mizoribine exhibits far superior antitumor activity compared with several FDA-approved IMPDH inhibitors, and mizoribine treatment shows a more durable antitumor response than the mTOR inhibitor rapamycin (89). In addition, mitoxantrone, a firmly established inhibitor of type II topoisomerase and protein kinase C (PKC), is reported to exert its anti-cancer effect in lymphomas, leukemias, and breast, colorectal, and prostate cancers (90–97). Although more preclinical investigations need to be completed to validate their anti-cancer activities, the selected small molecules hold great potential in the future application of clinical treatment of HCC.

The study's limitations should be noted. First, real-world evidence from large clinical cohorts is required to test the utility and significance of HGSIS for further clinical practice. Second, more *in vitro* and *in vivo* experiments were needed to unveil the molecular underpinnings in terms of HGSIS, as well as the effectiveness of the putative drugs for treating HCC.

Conclusion

In conclusion, two hallmark-guided subtypes of HCC were extensively identified. Based on the HCC subtypes, an immunological prognostic signature, HGSIS, was developed and validated, which was associated with tumor immune phenotypes, distinct genomic landscapes, and therapeutic responses. Combining HGSIS, PPI network construction, and structure-based *in silico* docking, we also predicted candidate small drugs that may bind to the key target of HGSIS, which act as potential drugs for HCC. Therefore, our study provides a novel perspective to recognizing cancer subtypes with clinical implications, which serves as an entry point for the construction of better risk classifiers to design personalized treatment to prolong patients' survival.

Data availability statement

Publicly available datasets were analyzed in this study. This data can be found here: https://portal.gdc.cancer.gov/and https://icgc.org/.

Author contributions

YZ, and GL conceived the study. YZ, CG, and YT contributed to data collection, analysis, and interpretation. YZ and CG completed the drafting of the manuscript. ZY contributed to the revision of the manuscript. All authors contributed to the article and approved the submitted version.

Acknowledgments

We acknowledge The Cancer Genome Atlas (TCGA) and International Cancer Genome Consortium (ICGC) for data sharing.

Conflict of interest

The authors declare that the research was conducted in the absence of any commercial or financial relationships that could be construed as a potential conflict of interest.

Publisher's note

Supplementary material

The Supplementary Material for this article can be found online at: https://www.frontiersin.org/articles/10.3389/fimmu.2022.958161/full#supplementary-material

References

1. Gong J, Li R, Chen Y, Zhuo Z, Chen S, Cao J, et al. Hcc subtypes based on the activity changes of immunologic and hallmark gene sets in tumor and nontumor tissues. *Brief Bioinform* (2021) 22(5):bbaa427. doi: 10.1093/bib/bbaa427

2. Llovet JM, Kelley RK, Villanueva A, Singal AG, Pikarsky E, Roayaie S, et al. Hepatocellular carcinoma. *Nat Rev Dis Primers* (2021) 7(1):6. doi: 10.1038/s41572-020-00240-3

3. El Jabbour T, Lagana SM, Lee H. Update on hepatocellular carcinoma: Pathologists' review. *World J Gastroenterol* (2019) 25(14):1653–65. doi: 10.3748/wjg.v25.i14.1653

4. Zhang Q, Lou Y, Yang J, Wang J, Feng J, Zhao Y, et al. Integrated multiomic analysis reveals comprehensive tumour heterogeneity and novel immunophenotypic classification in hepatocellular carcinomas. *Gut* (2019) 68 (11):2019–31. doi: 10.1136/gutjnl-2019-318912

5. Ho DW, Tsui YM, Sze KM, Chan LK, Cheung TT, Lee E, et al. Single-cell transcriptomics reveals the landscape of intra-tumoral heterogeneity and stemness-related subpopulations in liver cancer. *Cancer Lett* (2019) 459:176–85. doi: 10.1016/j.canlet.2019.06.002

6. Li L, Wang H. Heterogeneity of liver cancer and personalized therapy. *Cancer Lett* (2016) 379(2):191–7. doi: 10.1016/j.canlet.2015.07.018

7. Farmer DG, Rosove MH, Shaked A, Busuttil RW. Current treatment modalities for hepatocellular carcinoma. *Ann Surg* (1994) 219(3):236–47. doi: 10.1097/00000658-199403000-00003

8. Liang JY, Wang DS, Lin HC, Chen XX, Yang H, Zheng Y, et al. A novel ferroptosis-related gene signature for overall survival prediction in patients with hepatocellular carcinoma. *Int J Biol Sci* (2020) 16(13):2430–41. doi: 10.7150/ijbs.45050

9. Zhang B, Tang B, Gao J, Li J, Kong L, Qin L. A hypoxia-related signature for clinically predicting diagnosis, prognosis and immune microenvironment of hepatocellular carcinoma patients. *J Transl Med* (2020) 18(1):342. doi: 10.1186/s12967-020-02492-9

10. Hu B, Yang XB, Sang XT. Construction of a lipid metabolism-related and immune-associated prognostic signature for hepatocellular carcinoma. *Cancer Med* (2020) 9(20):7646–62. doi: 10.1002/cam4.3353

11. Kurebayashi Y, Ojima H, Tsujikawa H, Kubota N, Maehara J, Abe Y, et al. Landscape of immune microenvironment in hepatocellular carcinoma and its additional impact on histological and molecular classification. *Hepatology* (2018) 68(3):1025–41. doi: 10.1002/hep.29904

12. Hanahan D, Coussens LM. Accessories to the crime: Functions of cells recruited to the tumor microenvironment. *Cancer Cell* (2012) 21(3):309–22. doi: 10.1016/j.ccr.2012.02.022

13. Sangro B, Sarobe P, Hervas-Stubbs S, Melero I. Advances in immunotherapy for hepatocellular carcinoma. *Nat Rev Gastroenterol Hepatol* (2021) 18(8):525–43. doi: 10.1038/s41575-021-00438-0

14. Sangro B, Gomez-Martin C, de la Mata M, Inarrairaegui M, Garralda E, Barrera P, et al. A clinical trial of ctla-4 blockade with tremelimumab in patients with hepatocellular carcinoma and chronic hepatitis c. *J Hepatol* (2013) 59(1):81–8. doi: 10.1016/j.jhep.2013.02.022

15. Finn RS, Qin S, Ikeda M, Galle PR, Ducreux M, Kim T-Y, et al. Imbrave150: Updated overall survival (Os) data from a global, randomized, open-label phase iii study of atezolizumab (Atezo) plus bevacizumab (Bev) versus sorafenib (Sor) in patients (Pts) with unresectable hepatocellular carcinoma (Hcc). *J Clin Oncol* (2021) 39(3):267. doi: 10.1200/JCO.2021.39.3_suppl.267

16. Palucka AK, Coussens LM. The basis of oncoimmunology. *Cell* (2016) 164 (6):1233–47. doi: 10.1016/j.cell.2016.01.049

17. Hanzelmann S, Castelo R, Guinney J. Gsva: Gene set variation analysis for microarray and rna-seq data. *BMC Bioinf* (2013) 14:7. doi: 10.1186/1471-2105-14-7

18. Subramanian A, Tamayo P, Mootha VK, Mukherjee S, Ebert BL, Gillette MA, et al. Gene set enrichment analysis: A knowledge-based approach for interpreting genome-wide expression profiles. *Proc Natl Acad Sci USA* (2005) 102(43):15545–50. doi: 10.1073/pnas.0506580102

19. Liberzon A, Birger C, Thorvaldsdottir H, Ghandi M, Mesirov JP, Tamayo P. The molecular signatures database (Msigdb) hallmark gene set collection. *Cell Syst* (2015) 1(6):417–25. doi: 10.1016/j.cels.2015.12.004

20. Tang Y, Guo C, Yang Z, Wang Y, Zhang Y, Wang D. Identification of a tumor immunological phenotype-related gene signature for predicting prognosis, immunotherapy efficacy, and drug candidates in hepatocellular carcinoma. *Front Immunol* (2022) 13:862527. doi: 10.3389/fimmu.2022.862527

21. Cai WY, Dong ZN, Fu XT, Lin LY, Wang L, Ye GD, et al. Identification of a tumor microenvironment-relevant gene set-based prognostic signature and related therapy targets in gastric cancer. *Theranostics* (2020) 10(19):8633–47. doi: 10.7150/thno.47938

22. Malta TM, Sokolov A, Gentles AJ, Burzykowski T, Poisson L, Weinstein JN, et al. Machine learning identifies stemness features associated with oncogenic dedifferentiation. *Cell* (2018) 173(2):338–54 e15. doi: 10.1016/j.cell.2018.03.034

23. Zhang Y, Tang Y, Guo C, Li G. Integrative analysis identifies key mrna biomarkers for diagnosis, prognosis, and therapeutic targets of hcv-associated hepatocellular carcinoma. *Aging (Albany NY)* (2021) 13:12865–95. doi: 10.18632/aging.202957

24. Tang Y, Zhang Y, Hu X. Identification of potential hub genes related to diagnosis and prognosis of hepatitis b virus-related hepatocellular carcinoma *Via* integrated bioinformatics analysis. *BioMed Res Int* (2020) 2020:4251761. doi: 10.1155/2020/4251761

25. Mayakonda A, Lin DC, Assenov Y, Plass C, Koeffler HP. Maftools: Efficient and comprehensive analysis of somatic variants in cancer. *Genome Res* (2018) 28 (11):1747–56. doi: 10.1101/gr.239244.118

26. Bhattacharya S, Andorf S, Gomes L, Dunn P, Schaefer H, Pontius J, et al. Immport: Disseminating data to the public for the future of immunology. *Immunol Res* (2014) 58(2-3):234–9. doi: 10.1007/s12026-014-8516-1

27. Wilkerson MD, Hayes DN. Consensusclusterplus: A class discovery tool with confidence assessments and item tracking. *Bioinformatics* (2010) 26 (12):1572–3. doi: 10.1093/bioinformatics/btq170

28. Chen D, Huang H, Zang L, Gao W, Zhu H, Yu X. Development and verification of the hypoxia- and immune-associated prognostic signature for pancreatic ductal adenocarcinoma. *Front Immunol* (2021) 12:728062. doi: 10.3389/fimmu.2021.728062

29. Wang Z, Wang Y, Yang T, Xing H, Wang Y, Gao L, et al. Machine learning revealed stemness features and a novel stemness-based classification with appealing implications in discriminating the prognosis, immunotherapy and temozolomide responses of 906 glioblastoma patients. *Brief Bioinform* (2021) 22(5):bbab032. doi: 10.1093/bib/bbab032

30. Guo C, Tang Y, Zhang Y, Li G. Mining tcga data for key biomarkers related to immune microenvironment in endometrial cancer by immune score and weighted correlation network analysis. *Front Mol Biosci* (2021) 8:645388. doi: 10.3389/fmolb.2021.645388

31. Ritchie ME, Phipson B, Wu D, Hu Y, Law CW, Shi W, et al. Limma powers differential expression analyses for rna-sequencing and microarray studies. *Nucleic Acids Res* (2015) 43(7):e47. doi: 10.1093/nar/gkv007

32. Yu G, Wang LG, Han Y, He QY. Clusterprofiler: An r package for comparing biological themes among gene clusters. *OMICS* (2012) 16(5):284–7. doi: 10.1089/omi.2011.0118

33. Friedman J, Hastie T, Tibshirani R. Regularization paths for generalized linear models *Via* coordinate descent. *J Stat Softw* (2010) 33(1):1–22. doi: 10.18637/jss.v033.i01

34. Long J, Wang A, Bai Y, Lin J, Yang X, Wang D, et al. Development and validation of a Tp53-associated immune prognostic model for hepatocellular carcinoma. *EBioMedicine* (2019) 42:363–74. doi: 10.1016/j.ebiom.2019.03.022

35. Wang Z, Zhu J, Liu Y, Liu C, Wang W, Chen F, et al. Development and validation of a novel immune-related prognostic model in hepatocellular carcinoma. *J Transl Med* (2020) 18(1):67. doi: 10.1186/s12967-020-02255-6

36. Dai Y, Qiang W, Lin K, Gui Y, Lan X, Wang D. An immune-related gene signature for predicting survival and immunotherapy efficacy in hepatocellular carcinoma. *Cancer Immunol Immunother* (2021) 70(4):967–79. doi: 10.1007/s00262-020-02743-0

37. Sayaman RW, Saad M, Thorsson V, Hu D, Hendrickx W, Roelands J, et al. Germline genetic contribution to the immune landscape of cancer. *Immunity* (2021) 54(2):367–86 e8. doi: 10.1016/j.immuni.2021.01.011

38. Thorsson V, Gibbs DL, Brown SD, Wolf D, Bortone DS, Ou Yang TH, et al. The immune landscape of cancer. *Immunity* (2018) 48(4):812–30 e14. doi: 10.1016/j.immuni.2018.03.023

39. Rooney MS, Shukla SA, Wu CJ, Getz G, Hacohen N. Molecular and genetic properties of tumors associated with local immune cytolytic activity. *Cell* (2015) 160(1-2):48–61. doi: 10.1016/j.cell.2014.12.033

40. Chalmers ZR, Connelly CF, Fabrizio D, Gay L, Ali SM, Ennis R, et al. Analysis of 100,000 human cancer genomes reveals the landscape of tumor mutational burden. *Genome Med* (2017) 9(1):34. doi: 10.1186/s13073-017-0424-2

41. Sun J, Shi R, Zhang X, Fang D, Rauch J, Lu S, et al. Characterization of immune landscape in papillary thyroid cancer reveals distinct tumor immunogenicity and implications for immunotherapy. *Oncoimmunology* (2021) 10(1):e1964189. doi: 10.1080/2162402X.2021.1964189

42. Lambrechts D, Wauters E, Boeckx B, Aibar S, Nittner D, Burton O, et al. Phenotype molding of stromal cells in the lung tumor microenvironment. *Nat Med* (2018) 24(8):1277–89. doi: 10.1038/s41591-018-0096-5

43. Wang S, Zhang Q, Yu C, Cao Y, Zuo Y, Yang L. Immune cell infiltration-based signature for prognosis and immunogenomic analysis in breast cancer. *Brief Bioinform* (2020) 22(2):2020–31. doi: 10.1093/bib/bbaa026

44. Charoentong P, Finotello F, Angelova M, Mayer C, Efremova M, Rieder D, et al. Pan-cancer immunogenomic analyses reveal genotype-immunophenotype relationships and predictors of response to checkpoint blockade. *Cell Rep* (2017) 18 (1):248–62. doi: 10.1016/j.celrep.2016.12.019

45. Becht E, Giraldo NA, Lacroix L, Buttard B, Elarouci N, Petitprez F, et al. Estimating the population abundance of tissue-infiltrating immune and stromal cell populations using gene expression. *Genome Biol* (2016) 17(1):218. doi: 10.1186/s13059-016-1070-5

46. Wu XN, Su D, Mei YD, Xu MQ, Zhang H, Wang ZY, et al. Identified lung adenocarcinoma metabolic phenotypes and their association with tumor immune microenvironment. *Cancer Immunol Immunother* (2021) 70(10):2835–50. doi: 10.1007/s00262-021-02896-6

47. Wu J, Li L, Zhang H, Zhao Y, Zhang H, Wu S, et al. A risk model developed based on tumor microenvironment predicts overall survival and associates with tumor immunity of patients with lung adenocarcinoma. *Oncogene* (2021) 40 (26):4413–24. doi: 10.1038/s41388-021-01853-y

48. Liu Z, Lu T, Wang L, Liu L, Li L, Han X. Comprehensive molecular analyses of a novel mutational signature classification system with regard to prognosis, genomic alterations, and immune landscape in glioma. *Front Mol Biosci* (2021) 8:682084. doi: 10.3389/fmolb.2021.682084

49. Jiang P, Gu S, Pan D, Fu J, Sahu A, Hu X, et al. Signatures of T cell dysfunction and exclusion predict cancer immunotherapy response. *Nat Med* (2018) 24(10):1550–8. doi: 10.1038/s41591-018-0136-1

50. Geeleher P, Cox N, Huang RS. Prrophetic: An r package for prediction of clinical chemotherapeutic response from tumor gene expression levels. *PloS One* (2014) 9(9):e107468. doi: 10.1371/journal.pone.0107468

51. Shannon P, Markiel A, Ozier O, Baliga NS, Wang JT, Ramage D, et al. Cytoscape: A software environment for integrated models of biomolecular interaction networks. *Genome Res* (2003) 13(11):2498–504. doi: 10.1101/gr.1239303

52. Bader GD, Hogue CW. An automated method for finding molecular complexes in Large protein interaction networks. *BMC Bioinf* (2003) 4:2. doi: 10.1186/1471-2105-4-2

53. Jimenez J, Doerr S, Martinez-Rosell G, Rose AS, De Fabritiis G. Deepsite: Protein-binding site predictor using 3d-convolutional neural networks. *Bioinformatics* (2017) 33(19):3036–42. doi: 10.1093/bioinformatics/btx350

54. Zhang YQ, Wang WY, Xue JX, Xu Y, Fan P, Caughey BA, et al. Microrna expression profile on solid subtype of invasive lung adenocarcinoma reveals a panel of four mirnas to be associated with poor prognosis in Chinese patients. *J Cancer* (2016) 7(12):1610–20. doi: 10.7150/jca.14923

55. Zhu B, Tse LA, Wang D, Koka H, Zhang T, Abubakar M, et al. Immune gene expression profiling reveals heterogeneity in luminal breast tumors. *Breast Cancer Res* (2019) 21(1):147. doi: 10.1186/s13058-019-1218-9

56. Marusyk A, Janiszewska M, Polyak K. Intratumor heterogeneity: The Rosetta stone of therapy resistance. *Cancer Cell* (2020) 37(4):471–84. doi: 10.1016/j.ccell.2020.03.007

57. Bruun J, Kryeziu K, Eide PW, Moosavi SH, Eilertsen IA, Langerud J, et al. Patient-derived organoids from multiple colorectal cancer liver metastases reveal moderate intra-patient pharmacotranscriptomic heterogeneity. *Clin Cancer Res* (2020) 26(15):4107–19. doi: 10.1158/1078-0432.CCR-19-3637

58. Yasui K, Hashimoto E, Komorizono Y, Koike K, Arii S, Imai Y, et al. Characteristics of patients with nonalcoholic steatohepatitis who develop hepatocellular carcinoma. *Clin Gastroenterol Hepatol* (2011) 9(5):428–33. doi: 10.1016/j.cgh.2011.01.023

59. Cheuk W, Chan JK. Clear cell variant of fibrolamellar carcinoma of the liver. *Arch Pathol Lab Med* (2001) 125(9):1235–8. doi: 10.5858/2001-125-1235-CCVOFC

60. Lee JH, Choi MS, Gwak GY, Lee JH, Koh KC, Paik SW, et al. Clinicopathologic characteristics and long-term prognosis of scirrhous hepatocellular carcinoma. *Dig Dis Sci* (2012) 57(6):1698–707. doi: 10.1007/s10620-012-2075-x

61. Zhang Q, He Y, Luo N, Patel SJ, Han Y, Gao R, et al. Landscape and dynamics of single immune cells in hepatocellular carcinoma. *Cell* (2019) 179 (4):829–45 e20. doi: 10.1016/j.cell.2019.10.003

62. Santhakumar C, Gane EJ, Liu K, McCaughan GW. Current perspectives on the tumor microenvironment in hepatocellular carcinoma. *Hepatol Int* (2020) 14 (6):947–57. doi: 10.1007/s12072-020-10104-3

63. Ringelhan M, Pfister D, O'Connor T, Pikarsky E, Heikenwalder M. The immunology of hepatocellular carcinoma. *Nat Immunol* (2018) 19(3):222–32. doi: 10.1038/s41590-018-0044-z

64. Feng J, Li J, Wu L, Yu Q, Ji J, Wu J, et al. Emerging roles and the regulation of aerobic glycolysis in hepatocellular carcinoma. *J Exp Clin Cancer Res* (2020) 39 (1):126. doi: 10.1186/s13046-020-01629-4

65. Harding JJ, Nandakumar S, Armenia J, Khalil DN, Albano M, Ly M, et al. Prospective genotyping of hepatocellular carcinoma: Clinical implications of next-generation sequencing for matching patients to targeted and immune therapies. *Clin Cancer Res* (2019) 25(7):2116–26. doi: 10.1158/1078-0432.CCR-18-2293

66. Dion SP, Beliveau F, Morency LP, Desilets A, Najmanovich R, Leduc R. Functional diversity of Tmprss6 isoforms and variants expressed in hepatocellular carcinoma cell lines. *Sci Rep* (2018) 8(1):12562. doi: 10.1038/s41598-018-30618-z

67. Ma L, Wang L, Khatib SA, Chang CW, Heinrich S, Dominguez DA, et al. Single-cell atlas of tumor cell evolution in response to therapy in hepatocellular carcinoma and intrahepatic cholangiocarcinoma. *J Hepatol* (2021) 75(6):1397–408. doi: 10.1016/j.jhep.2021.06.028

68. Wang Y, Yang Y, Zhao Z, Sun H, Luo D, Huttad L, et al. A new nomogram model for prognosis of hepatocellular carcinoma based on novel gene signature that regulates cross-talk between immune and tumor cells. *BMC Cancer* (2022) 22 (1):379. doi: 10.1186/s12885-022-09465-9

69. Hu B, Yang XB, Sang XT. Development and verification of the hypoxia-related and immune-associated prognosis signature for hepatocellular carcinoma. *J Hepatocell Carcinoma* (2020) 7:315–30. doi: 10.2147/JHC.S272109

70. Hu B, Yang XB, Sang XT. Molecular subtypes based on immune-related genes predict the prognosis for hepatocellular carcinoma patients. *Int Immunopharmacol* (2021) 90:107164. doi: 10.1016/j.intimp.2020.107164

71. Chaudhary K, Poirion OB, Lu L, Garmire LX. Deep learning-based multi-omics integration robustly predicts survival in liver cancer. *Clin Cancer Res* (2018) 24(6):1248–59. doi: 10.1158/1078-0432.CCR-17-0853

72. Bollard J, Miguela V, Ruiz de Galarreta M, Venkatesh A, Bian CB, Roberto MP, et al. Palbociclib (Pd-0332991), a selective Cdk4/6 inhibitor, restricts tumour growth in preclinical models of hepatocellular carcinoma. *Gut* (2017) 66(7):1286–96. doi: 10.1136/gutjnl-2016-312268

73. Liu GM, Zeng HD, Zhang CY, Xu JW. Identification of a six-gene signature predicting overall survival for hepatocellular carcinoma. *Cancer Cell Int* (2019) 19:138. doi: 10.1186/s12935-019-0858-2

74. Li W, Chen QF, Huang T, Wu P, Shen L, Huang ZL. Identification and validation of a prognostic lncrna signature for hepatocellular carcinoma. *Front Oncol* (2020) 10:780. doi: 10.3389/fonc.2020.00780

75. Cancer Genome Atlas Research Network. Electronic address wbe, cancer genome atlas research n. comprehensive and integrative genomic characterization of hepatocellular carcinoma. *Cell* (2017) 169(7):1327–41 e23. doi: 10.1016/j.cell.2017.05.046

76. Tang B, Zhu J, Zhao Z, Lu C, Liu S, Fang S, et al. Diagnosis and prognosis models for hepatocellular carcinoma patient's management based on tumor mutation burden. *J Adv Res* (2021) 33:153–65. doi: 10.1016/j.jare.2021.01.018

77. Calderaro J, Ziol M, Paradis V, Zucman-Rossi J. Molecular and histological correlations in liver cancer. *J Hepatol* (2019) 71(3):616–30. doi: 10.1016/j.jhep.2019.06.001

78. Candia J, Bayarsaikhan E, Tandon M, Budhu A, Forgues M, Tovuu LO, et al. The genomic landscape of Mongolian hepatocellular carcinoma. *Nat Commun* (2020) 11(1):4383. doi: 10.1038/s41467-020-18186-1

79. Schulze K, Imbeaud S, Letouze E, Alexandrov LB, Calderaro J, Rebouissou S, et al. Exome sequencing of hepatocellular carcinomas identifies new mutational signatures and potential therapeutic targets. *Nat Genet* (2015) 47(5):505–11. doi: 10.1038/ng.3252

80. Levrero M, Zucman-Rossi J. Mechanisms of hbv-induced hepatocellular carcinoma. *J Hepatol* (2016) 64(1 Suppl):S84–S101. doi: 10.1016/j.jhep.2016.02.021

81. Perugorria MJ, Olaizola P, Labiano I, Esparza-Baquer A, Marzioni M, Marin JJG, et al. Wnt-Beta-Catenin signalling in liver development, health and disease. *Nat Rev Gastroenterol Hepatol* (2019) 16(2):121–36. doi: 10.1038/s41575-018-0075-9

82. Khemlina G, Ikeda S, Kurzrock R. The biology of hepatocellular carcinoma: Implications for genomic and immune therapies. *Mol Cancer* (2017) 16(1):149. doi: 10.1186/s12943-017-0712-x

83. Lu C, Rong D, Zhang B, Zheng W, Wang X, Chen Z, et al. Current perspectives on the immunosuppressive tumor microenvironment in hepatocellular carcinoma: Challenges and opportunities. *Mol Cancer* (2019) 18 (1):130. doi: 10.1186/s12943-019-1047-6

84. Bozward AG, Warricker F, Oo YH, Khakoo SI. Natural killer cells and regulatory T cells cross talk in hepatocellular carcinoma: Exploring therapeutic options for the next decade. *Front Immunol* (2021) 12:643310. doi: 10.3389/fimmu.2021.643310

85. Singh V, Khurana A, Allawadhi P, Banothu AK, Bharani KK, Weiskirchen R. Emerging role of pd-1/Pd-L1 inhibitors in chronic liver diseases. *Front Pharmacol* (2021) 12:790963. doi: 10.3389/fphar.2021.790963

86. Chen J, Gingold JA, Su X. Immunomodulatory tgf-beta signaling in hepatocellular carcinoma. *Trends Mol Med* (2019) 25(11):1010–23. doi: 10.1016/j.molmed.2019.06.007

87. An L, Zhang J, Feng D, Zhao Y, Ouyang W, Shi R, et al. Kif2c is a novel prognostic biomarker and correlated with immune infiltration in endometrial cancer. *Stem Cells Int* (2021) 2021:1434856. doi: 10.1155/2021/1434856

88. Wei S, Dai M, Zhang C, Teng K, Wang F, Li H, et al. Kif2c: A novel link between Wnt/Beta-catenin and Mtorc1 signaling in the pathogenesis of hepatocellular carcinoma. *Protein Cell* (2021) 12(10):788–809. doi: 10.1007/s13238-020-00766-y

89. Valvezan AJ, McNamara MC, Miller SK, Torrence ME, Asara JM, Henske EP, et al. Impdh inhibitors for antitumor therapy in tuberous sclerosis complex. *JCI Insight* (2020) 5(7):e135071. doi: 10.1172/jci.insight.135071

90. Evison BJ, Sleebs BE, Watson KG, Phillips DR, Cutts SM. Mitoxantrone, more than just another topoisomerase ii poison. *Med Res Rev* (2016) 36(2):248–99. doi: 10.1002/med.21364

91. Basch EM, Scholz M, de Bono JS, Vogelzang N, de Souza P, Marx G, et al. Cabozantinib versus mitoxantrone-prednisone in symptomatic metastatic castration-resistant prostate cancer: A randomized phase 3 trial with a primary pain endpoint. *Eur Urol* (2019) 75(6):929–37. doi: 10.1016/j.eururo.2018.11.033

92. Guan Y, Jiang S, Ye W, Ren X, Wang X, Zhang Y, et al. Combined treatment of mitoxantrone sensitizes breast cancer cells to rapalogs through blocking eef-2k-Mediated activation of akt and autophagy. *Cell Death Dis* (2020) 11(11):948. doi: 10.1038/s41419-020-03153-x

93. Zeidner JF, Lin TL, Vigil CE, Fine G, Yair Levy M, Nazha A, et al. A prospective biomarker analysis of alvocidib followed by cytarabine and mitoxantrone in mcl-1-Dependent Relapsed/Refractory acute myeloid leukemia. *Blood Cancer J* (2021) 11(10):175. doi: 10.1038/s41408-021-00568-3

94. Ge C, Wang Y, Feng Y, Wang S, Zhang K, Xu X, et al. Suppression of oxidative phosphorylation and Idh2 sensitizes colorectal cancer to a naphthalimide derivative and mitoxantrone. *Cancer Lett* (2021) 519:30–45. doi: 10.1016/j.canlet.2021.06.015

95. Orlando BJ, Liao M. Abcg2 transports anticancer drugs *via* a closed-to-Open switch. *Nat Commun* (2020) 11(1):2264. doi: 10.1038/s41467-020-16155-2

96. Advani AS, Cooper B, Visconte V, Elson P, Chan R, Carew J, et al. A phase I/Ii trial of mec (Mitoxantrone, etoposide, cytarabine) in combination with ixazomib for relapsed refractory acute myeloid leukemia. *Clin Cancer Res* (2019) 25(14):4231–7. doi: 10.1158/1078-0432.CCR-18-3886

97. Kreft D, Wang Y, Rattay M, Toensing K, Anselmetti D. Binding mechanism of anti-cancer chemotherapeutic drug mitoxantrone to DNA characterized by magnetic tweezers. *J Nanobiotechnol* (2018) 16(1):56. doi: 10.1186/s12951-018-0381-y

frontiers | Frontiers in Immunology

TYPE Review
PUBLISHED 12 August 2022
DOI 10.3389/fimmu.2022.969447

OPEN ACCESS

EDITED BY
Xian Zeng,
Fudan University, China

REVIEWED BY
Islam M. Saadeldin,
Chungnam National University, South Korea
Paola Saccomandi,
Politecnico di Milano, Italy
Manuel Bañobre-López,
International Iberian Nanotechnology Laboratory (INL), Portugal

*CORRESPONDENCE
Yingchun He
heyingchun@hnucm.edu.cn

SPECIALTY SECTION
This article was submitted to Cancer Immunity and Immunotherapy, a section of the journal Frontiers in Immunology

RECEIVED 15 June 2022
ACCEPTED 27 July 2022
PUBLISHED 12 August 2022

CITATION
Yang X, Gao M, Xu R, Tao Y, Luo W, Wang B, Zhong W, He L and He Y (2022) Hyperthermia combined with immune checkpoint inhibitor therapy in the treatment of primary and metastatic tumors.
Front. Immunol. 13:969447.
doi: 10.3389/fimmu.2022.969447

Hyperthermia combined with immune checkpoint inhibitor therapy in the treatment of primary and metastatic tumors

Ximing Yang[1], Miaozhi Gao[1], Runshi Xu[1], Yangyang Tao[1], Wang Luo[1], Binya Wang[1], Wenliang Zhong[1,2], Lan He[3,4] and Yingchun He[1,2,3]*

[1]Medical School, Hunan University of Chinese Medicine, Changsha, China, [2]Hunan Provincial Ophthalmology and Otolaryngology Diseases Prevention and Treatment with Traditional Chinese Medicine and Visual Function Protection Engineering and Technological Research Center, Changsha, China, [3]Hunan Provincial Key Laboratory for the Prevention and Treatment of Ophthalmology and Otolaryngology Diseases with Traditional Chinese Medicine, Changsha, China, [4]The First Hospital of Hunan University of Chinese Medicine, Changsha, China

According to the difference in temperature, thermotherapy can be divided into thermal ablation and mild hyperthermia. The main advantage of thermal ablation is that it can efficiently target tumors in situ, while mild hyperthermia has a good inhibitory effect on distant metastasis. There are some similarities and differences between the two therapies with respect to inducing anti-tumor immune responses, but neither of them results in sustained systemic immunity. Malignant tumors (such as breast cancer, pancreatic cancer, nasopharyngeal carcinoma, and brain cancer) are recurrent, highly metastatic, and highly invasive even after treatment, hence a single therapy rarely resolves the clinical issues. A more effective and comprehensive treatment strategy using a combination of hyperthermia and immune checkpoint inhibitor (ICI) therapies has gained attention. This paper summarizes the relevant preclinical and clinical studies on hyperthermia combined with ICI therapies and compares the efficacy of two types of hyperthermia combined with ICIs, in order to provide a better treatment for the recurrence and metastasis of clinically malignant tumors.

KEYWORDS

thermal ablation, mild hyperthermia, immune checkpoint inhibitor, malignant tumor, combined therapy

Introduction

Hyperthermia (HT) appears more and more in the clinical comprehensive treatment strategy of tumor. There are many clinical benefits of hyperthermia, especially its ability to regulate immune responses. Immunotherapy has shed light on a new form of tumor therapy. New immune checkpoint inhibitors (ICIs) have been developed as treatment strategies to

target the immune evasion characteristics of tumors (1). Immunotherapy, especially PD-1 and anti-PD-L1 antagonists, has shown therapeutic effects on many malignant tumors. However, the response rate of immunotherapy is still not high, and the most lasting immune response is only observed in a small number of patients. The activation and maintenance of anti-tumor immune response depends on immune cells, such as dendritic cell (DC), natural killer cell (NK), T lymphocytes, B lymphocytes. First, tumor-associated antigens are recognized by DCs, with the latter becoming mature and activated; then, mature DCs present antigens to the initial T cells, which are activated into effector T cells, especially cytotoxic CD8+T cells, infiltrating distant tumors and kill the remaining tumor cells (2–4). NK cells are activated in a manner similar to that of CD8+T cells by releasing cytotoxic particles containing perforin and granzyme to directly lyse tumor cells. At the same time, NK cells are important in regulating adaptive immune response because of their ability to release interferon-γ (IFN–γ) and tumor necrosis factor-α (TNF–α) (5–7). In addition, some studies have shown that the expression of B cell-related genes, such as MZB1, JCHAIN and IGLL5, is significantly increased in patients who respond to ICI therapy, suggesting the potential of B cells in improving anti-tumor immune response (8). However, Tumor cells evade immunity through the expression of programmed cell death ligand (pdl-1) and similar inhibitory gene products, such as indoleamine 2 and 3 dioxygenase (Ido), transforming growth factor-β (TGF-β) and interleukin-10 (IL-10) (9). One of the important mechanisms of tumor immune escape is the inactivation or silencing of effector T cells. the depletion of T cells is closely related to inhibitory receptors, such as programmedcelldeathprotein-1 (PD-1), TIM-3 (mucin3) and LAG-3 (Lymphocyteactivationgeneprotein-3) (10, 11). Therefore, these receptors and their corresponding ligands form new immune checkpoints. At present, the treatment strategy of ICIs is mainly targeted at T cells, but the response rate of patients to ICIs is often not high. Based on the low response rate of immunotherapy, combination therapy has been proposed to provide a lasting systemic anti-tumor immune response. Among these combined strategies, it is surprising to find that the combination of HT and ICIs may enhance the anti-tumor immune response (2). Therefore, at present, the research on the combination of them in the treatment of malignant tumors is a hot spot.

In 1927, Wagner-Jauregg won the Nobel Prize in Physiology and Medicine for the use of hyperthermia. He found that the high fever associated with malaria hindered the infectious factor and, through this study, he was able to identify the preliminary role of hyperthermia. Previously, hyperthermia was defined as a core body temperature greater than 41 °C for more than 60 minutes (12). Currently, according to the temperature, hyperthermia therapy can be further divided into two sub treatments: thermal ablation and mild hyperthermia (13).

Thermal ablation causes direct necrosis in the central area of the tumor by increasing the temperature in the tumor to more than 55 °C. However, the temperature during mild hyperthermia is relatively low, and tumor cell damage is often induced in the range of 41 to 45 °C (14). The temperature difference between the two types of hyperthermia and their different effects often lead to different therapeutic outcomes. At the same time, thermal ablation is similar to surgical treatment, mostly disposable treatment; mild hyperthermia, due to the low energy input, usually requires repeated, longer heating time (> 30 min) to achieve any effect (15). Mild hyperthermia presents a more tedious regimen, and the killing effect on tumor needs to be studied. However, like thermal ablation, mild hyperthermia also can elicit immune responses, and several studies demonstrate that the immune responses to thermal ablation may have been induced by mild hyperthermia. The connection between the immune responses to thermal ablation and mild hyperthermia have garnered interest and further investigation is warranted. Current literature lacks studies on the intersection and comparison of the two therapies in anti-tumor treatment; hence, this paper provides a reference for the better use of the combination of hyperthermia and ICI therapy by comparing the different immune responses brought by various hyperthermia methods.

Effects of thermal ablation and mild hyperthermia on the immune response

Both thermal ablation and mild hyperthermia use heat to destroy tumor tissue, but the effects of the two treatments on the immune response may vary. After thermal ablation, the tumor tissue can be divided into the central area (> 55 °C), transitional zone (41 °C-45 °C), and normal tissue area (16). Coagulative necrosis often occurs in the central area, leading to the release of new antigens in tumor cells, which is called tumor *in situ* vaccination, while the transition zone is easily affected by residual temperature, resulting in secondary effects such as immune activation (17). However, the latest research shows that thermal ablation not only irreversibly denatures the newly released antigens in the central area of tumor tissues but may also upregulate some carcinogenic factors (such as interleukin-6(IL-6) and vascular endothelial growth factor(VEGF)), aggravating the progression of tumor metastasis (18, 19). However, thermal ablation still has some positive immunomodulatory effects, such as the release of positive immunomodulatory factors, initiation of a local inflammatory response, and recruitment of immune cells (18, 20). Compared with thermal ablation, the main effect of mild hyperthermia is not necrosis, but apoptosis, vascular permeability, and immune effect. Among them, the effect of mild hyperthermia on tumor immune response is mainly seen *via* an increase in immunogenicity, promotion of innate immune cell infiltration, and improvement in the tumor microenvironment (TME) (21–23).

The above processes involve all aspects of an immune response. Thermal ablation and mild hyperthermia can

respectively induce a series of immune-related factors to enhance the immunogenicity and immunoreactivity of ICIs in the TME (24–26). Next, we will explore the complementary effects of hyperthermia on ICIs from several angles, namely, the effects on immunogenicity, on immune cell activation, and on the immunosuppressive TME.

Effect on immunogenicity

Immunogenicity is the basis of an anti-tumor immune response, which requires two aspects in order to be initiated: the existence of antigen library and the occurrence of an immunogenic reaction (27). According to the consensus guidelines for immunogenic cell death (ICD), the presence of antigens alone is not sufficient to initiate an anti-tumor immune response, which requires the presence of ICD (28).

On the one hand, in many preclinical studies, thermal ablation has been proved to have the ability to release tumor associated antigens (TAAs). Ghanamah et al. and Leibovici et al. observed transient increases in carcinoembryonic antigen (CEA) and prostate specific antigen (PSA) levels in colorectal cancer and pancreatic cancer, respectively (29, 30). Among them, 59% of colorectal cancer patients (10/17) had a rapid increase in CEA levels 1 day after thermal ablation, suggesting that thermal ablation accelerated the tumor immune cycle. However, too high of a temperature during thermal ablation often leads to degeneration of new tumor antigens. Mild hyperthermia has an advantage in this respect, because a temperature range of 41 to 45 °C is insufficient to cause antigenic degeneration. Ruoping et al. reported a method of inducing mild hyperthermia based on copper sulfide nanoparticles (CuSNPs), which enhanced the capture of tumor antigens released during hyperthermia and induced the tumor immunogenic microenvironment, suggesting the potential of mild hyperthermia in improving immunogenicity (31).

On the other hand, thermal ablation mainly caused cell necrosis, while mild hyperthermia mainly caused apoptosis (32, 33). The advantage of inducing apoptosis over direct necrosis is that more damage-related molecules (DAMPs) are released during apoptosis to induce ICD (34). Studies have shown that mild hyperthermia induces ICD in a ROS-dependent manner, which is evidenced by the occurrence of a key ICD event: phosphorylation of eIF2 α (35, 36). Currently, there is no direct evidence of ICD induction by thermal ablation, but the effects on immune cell activation are clear.

Effect on the activation and action of immune cells

Previously, it was believed that the efficacy of thermal ablation primarily depended on its ability to ablate the tumor *in situ* (37). In fact, thermal ablation has been increasingly used in the treatment of metastatic tumors depending on its secondary effects, such as activating anti-tumor immune responses. Mature dendritic cells (DCs) play a key role before T cells are recruited, recognize tumor cells, and infiltrate the tumor site. After thermoablation, DC and natural killer (NK) cells are recruited to the tumor site, while regulatory T cells (Tregs) are significantly downregulated (38). Muxin et al. confirmed that hyperthermia inhibits the progression of primary and pulmonary metastasis of breast cancer by activating the macrophage/IL-15/NK cell axis (39). However, Muxin et al. and other researchers have not observed significant T cell immune response (40, 41), suggesting that Tregs may play a key role in the efficacy of thermal ablation, but the role of other T cells in it is still worthy of attention.

It is well known that mild hyperthermia can improve vascular permeability, which provides a good platform for the passage of innate immune cells and lays a foundation for inhibiting distant metastasis of tumors (42, 43). Yuefei et al. found that mild hyperthermia not only activated macrophages and DCs in tumors but also improved the structure of tumor vessels by reducing the levels of transforming growth factor-β (TGF-β) and hypoxia-inducible factor-1 α (HIF-1α) and significantly increased the proportion of CD8+IFN- γ + T cells (44). In breast cancer, Wan et al. found a significant increase and infiltration of DC, NK, B and CD8+T cells after mild hyperthermia (45), while Muxin et al. did not observe a significant T cell response induced by hyperthermia (39). Thus, at least in breast cancer, mild hyperthermia may lead to more effective immune stimulation and longer-lasting immune memory than thermal ablation.

Influence on the immunosuppressive TME

The efficacy of ICIs in the treatment of malignant tumors depends, to a large extent, on the immune status of the TME (46, 47). According to the immune status of the TME, tumors can be divided into “cold” and “hot” tumors. The characteristics of “cold” tumors include less tumor infiltrating T cells (TIL), low expression of PD-L1, enrichment of immunosuppressive cells, and decrease in tumor mutation, so the response rate to PD-1/PD-L1mAb is usually low (48). In other words, if thermal ablation or mild hyperthermia changed some of the characteristics of “cold” tumors, it could increase the sensitivity of ICIs, which would help improve the efficacy of this therapy in conjunction with ICIs.

The infiltration of TILs and the reduction of immunosuppressive cells (such as Tregs) are often considered to be a temperature-sensitive event. Liping et al. designed a mild hyperthermia method combined with PD-L1 inhibitors for the “cold” TME of breast cancer mouse models (4T1 and B16F10). The results showed that the CD8+T and CD4+T cell populations in the treatment group

were 11.8 and 8.2 times higher than those in the PBS group, respectively, promoting the differentiation of immature T cells (49). More importantly, the infiltration of CD8+T cells was also significantly increased, and the number of Tregs and the level of Treg surface markers such as CD4, CD25, and Foxp3 were significantly decreased. Interestingly, they found that the expression of PD-L1 on the surface of tumor cells increased with the increase in temperature in the range of 37–45°C, suggesting the sensitizing effect of mild hyperthermia on ICIs. In addition to these, Changdong et al. also found that whole body hyperthermia (WBH) has a good effect on α4β1 or α4β7 integrin-mediated T cell adhesion and migration (50), which may be one of the mechanisms by which hyperthermia inhibits distant tumor metastasis.

Magnetic nanoparticles as thermal effectors and drug carriers

Modified nanoparticles play a key role in the combined treatment strategy of cancer based on magnetic hyperthermia (MHT) and immunotherapy. Superparamagnetic iron oxide nanoparticles (SPIONs) smaller than 20-25 nm have attracted much attention because of their good superparamagnetism, chemical stability, high saturation magnetization and proper biocompatibility (51). Based on the above characteristics, the coupling of SPION with drugs can better maintain the retention time of drugs in the blood, control the degradation rate of drugs and reduce toxicity, suggesting that this coupling is helpful for better targeted delivery of drugs to tumor sites, and provides the possibility for the combination of magnetic hyperthermia and immunotherapy (52). However, it is worth noting that this targeted transport often depends on monoclonal antibodies to recognize the receptors overexpressed on the cell surface, in which SPION mainly plays the role of a carrier, in other words, it is difficult to target nanoparticles at low-specific tumor locations.

The combination of magnetic nanoparticles (MNPs) and alternating magnetic field (AMF) is called MHT, which is essentially a kind of thermotherapy with magnetic induction characteristics (53). SPIONs belongs to a kind of MNP, Tetsuya. After coupling SPION with anti-HER2 antibody trastuzumab, it was found that anti-HER2SPIONS selectively targeted HER2-expressing cancer cells and induced apoptosis only in cancer cells expressing HER2, suggesting the specificity of this coupling against cancer (53). Not only that, SPION also performs well in high intensity focused ultrasound (HIFU). Compared with HIFU therapy alone, Haiyan et al. invented a kind of nanoparticles with superparamagnetic iron oxide (SPIO,Fe3O4NPs) as shell and poly (lactide-glycolide) nanoparticles (Fe3O4@PLGA/LANPs) as core, which showed synergistic inhibitory effect on breast cancer, which was related to the accumulation and long-term retention of SPION in tumor site (54). Many MNP are evolved on the basis of SPION, other MNP including CoFe2O4@MnFe2O4, PEGylatedFeNP, etc., can also provide magnetic targeting efficacy, but compared with SPION, some nanoparticles that are too large or too small cannot avoid liver uptake (55).

However, some questions about the efficacy of hyperthermia are also emerging. For example, tumor cells often produce heat resistance during or after hyperthermia, which is characterized by resistance and regenerative response to high temperature (51). The reason behind this phenomenon is closely related to the enhancement of heat shock protein synthesis (56). Although HSP70 and many other HSPs have immunostimulatory effects, there is considerable evidence that some HSPs inhibit the anti-tumor immune response (57, 58). The targets of SPIONs include hsp70 and hsp90, which may help to prevent the production of heat tolerance and restore the anti-tumor immune response.

Role of exosomes as mediators in the hyperthermia-induced immune response

Exosome, a small membrane vesicle derived from endocytosis, mediates cellular communication between tumor cells and immune cells by wrapping and transmitting signal molecules such as mRNA, miRNA and other non-coding RNA and proteins. Among them, HSP has attracted much attention because of its diverse mechanisms of expression and regulation of tumorigenesis and development. During hyperthermia, cells under heat stress enhance immune response by promoting the release of more exosomes rich in tumor antigens, chemokines (including CCL2, CCL3, CCL4, CCL5 and CCL20, etc.) and HSP to APC to identify and destroy tumor cells (59). The contents of TEX (HS-TEX) under heat stress play an important role in its function in TME. Compared with apoptotic fragments and HSP-70 knockout exosomes, HSP-70-rich exosomes recruit more NK cells and promote the killing of NK cells (60). In addition, recent studies have found that exosomes extracted from heat-stressed tumor cells (HS-TEX) can reverse immunosuppressive TME from the following four aspects, including: ① activation of DCs;② as a cancer vaccine promotes IL-6;③ secretion by cells to reduce the proportion of Treg and MDSCs, while increasing the proportion of Th1 and Th17;④ promote the differentiation of CD8+T cells (60–62).

However, exosomes can also produce immunosuppressive activity. Some TEX have been shown to contain ligands such as FasL and TRAIL, which can induce apoptosis of activated T cells. Exosomes can also contain NKG2D ligands, which can block NKG2D receptors and inhibit the cytotoxicity of NK cells and CD8+T cells. One study also showed that HS-TEX can induce a bystander effect (BE) in tumor cells and promote the survival of stress-free cells (63). In addition, PD-L1 can be expressed in TEX to evade immunity (64).

It is worth noting that recently, it has been found that exosomes not only participate in the regulation of immune response, but also promote the survival of thermostable cells. The survival of thermostable cells is inseparable from a mechanism called "Anastasis", through which cells can recover from apoptotic lesions and have their previous functional state, which is closely related to the role of HSP released by TEX in the fight against apoptosis and lethal stimuli. The increase of Hsp70 and Hsp90, a common feature of thermostable cells, also confirms this point. A recent study also reported that HSP70, HSP90 and HSP60 are secreted by cancer cells through exocytosis and may play a key role in inhibiting the host's anti-tumor immune response (65). Moreover, this heat tolerance mediated by TEX may be achieved by inhibiting apoptosis by HSP, including inhibition of cascade activation of caspase and splicing of t-BID fragments, which is antagonistic to apoptosis induced by mild hyperthermia. However, TEX rich in HSPs can also induce anti-tumor immunity. For example, studies have suggested that exosome from heat-treated malignant ascites from gastric cancer patients are rich in HSP70 and HSP60, which promote DC maturation and induce tumor-specific CTL response (62). Generally speaking, the key to find a breakthrough between immune stimulation and immunosuppression and the emergence or disappearance of heat tolerance may lie in the role of exosome contents, especially the complex role of HSPs remains to be further studied. In summary, the above data suggest that hyperthermia can be used as an adjuvant therapy for ICIs to temporarily activate the anti-tumor immune response (66). Therefore, several studies propose a therapeutic strategy of TILs infiltration in tumor microenvironment (60), up-regulated expression of PD-L1 and combined with ICIs after thermal ablation or mild hyperthermia, to investigate whether these therapies could elicit stronger and more lasting systemic immunity in tumor patients to resolve recurrence and distant metastasis after hyperthermia (Figure 1).

Thermal ablation or mild hyperthermia combined with ICIs: A preclinical study

The earlier section was only meant to be a general introduction to the immune effects of hyperthermia. Here, we compared the combined effects of each hyperthermia technique in more detail, in order to investigate which one was more efficacious. Thermal ablation mainly included microwave ablation (MWA), radiofrequency ablation (RFA), cryoablation (CA),high intensity focused ultrasound (HIFU) and laser ablation (67, 68). Mild hyperthermia therapies were mainly photothermal therapy (PTT) and magnetothermotherapy (MHT) (69). PTT uses near infrared (NIR) light in the range between 700nm and 900nm to generate thermal energy, including gold, copper, graphene, polymer nanoparticles and carbon nanotubes under study (70–74). This characteristic of near-infrared light determines that PTT can maintain a penetration depth of approximately 1 cm, therefore PTT is more suitable for subcutaneous tumors, surgical exposures, or catheters. MHT uses magnetic nanoparticles (mainly iron oxide (Fe2O3) nanoparticles and its derivatives) to create alternating magnetic fields to generate heat. Compared with PTT, MHT is advantageous because it has excellent tissue penetration for deep tumors using hyperthermia induced by alternating magnetic fields. However, this may also lead to nanoparticles not being located in tumors to unnecessarily heat healthy tissue (75, 76).

Currently, the commonly used immune checkpoint inhibitors approved by FDA included anti-PD-1/PD-L1 inhibitors and anti-CTLA-4 inhibitors (77). Malignant tumors often use the inhibitory PD-1/PD-L1 or CTLA-4 pathway to escape the immune system. The principle of this biological behavior is that the PD-L1 molecule located on the surface of tumor cells binds to the transmembrane protein PD-1 expressed on T cells, B cells and natural killer cells (NK cells), which depletes T cells and promotes immune escape (78). On the other hand, CTLA-4 molecules block the binding of B7 ligands to T cell costimulatory molecules by binding to CD80 and CD86, thus blocking intracellular signal transmission and ultimately specifically preventing T cell activation and proliferation. Therefore, PD-1/PD-L1 blockers and CTLA-4 inhibitors play different roles by blocking parallel but different pathways on tumor cells (9). Common PD-1 antagonists include nivolumab and pembrolizumab, PD-L1 antagonists include atezolizumab and durvalumab, and CTLA-4 antagonists include ipilimumab, temlimumab (79, 80). A single antagonist is not frequently used because of the low patients' response rate. The combination of two checkpoint inhibitors, such as CTLA and PD-1, has shown some efficacy in melanoma, renal cell carcinoma, non-small cell lung cancer and other malignant tumors. However, treatment of metastatic tumors, which is the real cause of death in most clinical tumor patients, is still not effective, so researchers have shifted their attention from the sequential treatment of single or multiple ICIs to the combination of ICIs and other treatments (11). The combination of ICIs and hyperthermia has performed well in some preclinical studies and may be used as a potential combination therapy to improve the response rate and survival rate in the clinical setting. Next, combined with the characteristics of each tumor, this paper will specifically describe the combined effect of thermal ablation or mild hyperthermia and ICIs, especially in the treatment of metastatic tumors.

Breast cancer

Triple negative breast cancer (TNBC) is a special subtype of breast cancer, accounting for 15%-20% of all breast cancers. It

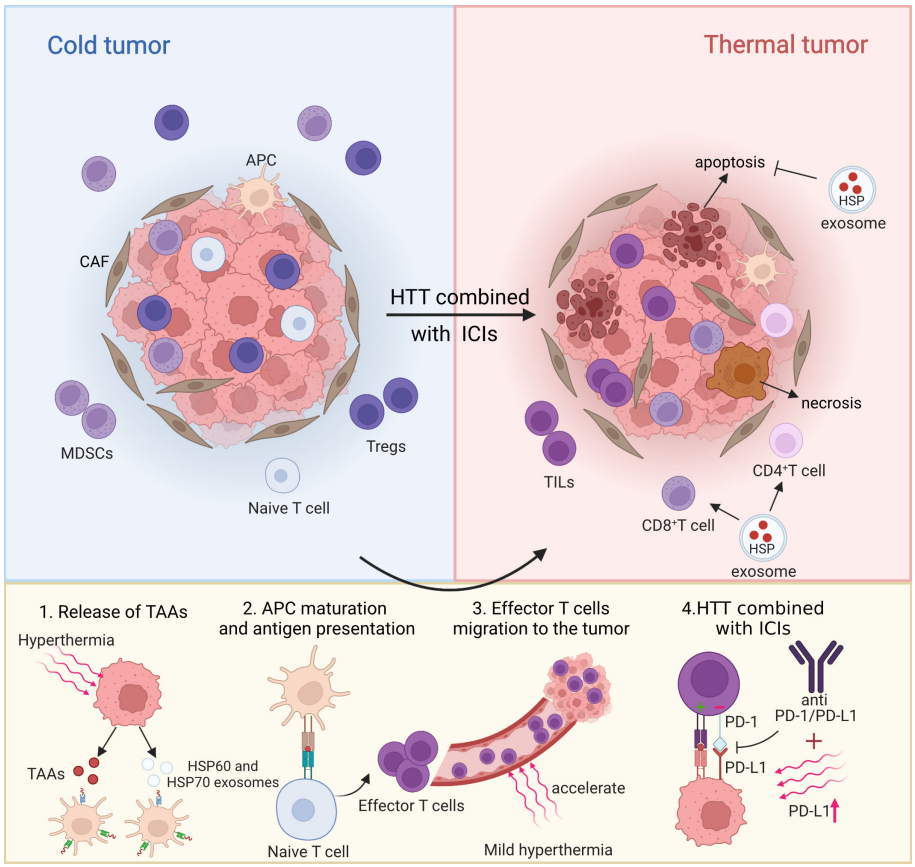

FIGURE 1
Partial mechanism diagram of hyperthermia combined with ICIs on tumor microenvironment. Created with BioRender.com.

has strong invasive clinical characteristics and an early high recurrence rate (81). Chemotherapy is the standard treatment for TNBC, but the overall prognosis is poor, with a median overall survival time (OS) of only 12-18 months, while hyperthermia combined with immunotherapy seems to provide better prognosis in the preclinical model of TNBC (82). The tumor formed by 4T1 cells in BALB/c mice is highly similar to the one found in human breast cancer in terms of growth and metastasis, so it is often used as an animal model for the study of human stage IV breast cancer. At the same time, it is also a highly invasive and metastatic model, often with lung, liver, and lymph node metastasis, in line with the characteristics of TNBC (83).

The main advantage of thermal ablation is that it has a strong *in situ* tumor ablation ability. When HIFU is combined with anti-PD-1, tumor proliferation-related genes such as Wnt7b,S100a14 and Erbb2 are significantly downregulated, and newly released tumor-specific antigens, cytokines, and cell fragments act as agonists of innate immunity (84). However, the disadvantage of thermal ablation is that it may enhance the immunosuppressive effect of distant Tregs (84).

Compared with thermal ablation, mild hyperthermia showed a better inhibitory effect on distant metastasis (49, 85). A study by Hongwei et al. reported that PTT combined with anti-CTLA-4 therapy can effectively inhibit the growth and lung metastasis of invasive 4T1 tumors, which could not be achieved by using PTT or anti-CTLA-4 inhibitors alone (86). Interestingly, only one combination of PTT and sequential PTT alone did not cause significant inhibitory effect, or even immune rejection, while the inhibitory effect of sequential PTT combined with anti-CTLA-4 therapy was significant. The reason behind this phenomenon may be explained by a short treatment window after the second dose of PTT treatment. Most of the Treg cells were eliminated and the activated cytotoxic T lymphocytes (CTL) had not infiltrated the tumor tissue. Combined anti-CTLA-4 therapy could accelerate this process and produce stronger TAA-specific CD8+T cells and immune memory than sequential PTT alone. However, when MHT was added to the combination of radiotherapy and anti-PD-1 or anti-CTLA-4, only CD3+T lymphocyte infiltration was observed, which helped reduce the lung metastasis of 4T1 breast cancer but did not improve the overall survival time. Moreover, the combination of

MHT and anti-PD-1 or anti-CTLA-4 even showed the possibility of increasing lung metastasis (83). In summary, PTT could be the first to show more potent inhibitory effect than MHT in distant metastasis of breast cancer, suggesting the possibility of a photothermal vaccine (55).

Pancreatic cancer

Pancreatic cancer is generally considered to be a "cold" malignant tumor of the digestive tract, mainly due to its immunosuppressive "cold" TME (87). At the same time, it is highly metastatic in the early stage because of its incomplete capsule, rich lymphatic and blood circulation, and highly invasive capability (88, 89).

The combination of thermal ablation and mild hyperthermia with ICIs seems to make this "cold" tumor "hot". PetrosX et al. developed a pulsed high-intensity focused ultrasound (pHIFU) technique based on HIFU. Mechanical damage induced by pHIFU leads to a sustained increase in the level of CD8+ tumor-infiltrating T cells (TILs) in tumors (90). When pHIFU was used in combination with anti-PD-1, the immunosuppression of the PD-1/PD-L1 axis of pancreatic cancer KPC cells was relieved, and the survival rate of the treatment group was significantly increased. In addition, one of the key findings of PetrosX et al., who investigated the combination of thermal ablation and ICIs, was that this combination of therapies induces a local tumor pro-inflammatory microenvironment, which is evidenced by the increased infiltration and proportion of several types of inflammatory cells (CD8+TIL, CD8+ IFN γ + TIL, and CD4+T cells) 48 hours after treatment.

From a cellular structural point of view, the "cold" tumors in pancreatic cancers comprised of dense connective tissue stroma and extracellular matrix, which set up barriers that prevented immune cells from infiltrating to the tumor site (91). Recently, mild hyperthermia has been shown to alter the dense structure of tumor tissue (92). Qianwen et al. designed a PTT therapy based on nanoparticles BMS-202 (a small molecular inhibitor of PD-1/PD-L1). It was found that PTT can dilate tumor vascular morphology and enhance tumor vascular permeability compared to the untreated group, suggesting that this PTT therapy could be beneficial in reshaping the immunosuppressive microenvironment in pancreatic cancer (93). Unsurprisingly, this PTT therapy not only decreased the expression of HIF-1 α and effectively reduced the hypoxia of TME but also promoted the maturation of DC in the spleen of tumor-bearing mice and reactivated the immunosuppressive microenvironment. When combined with nanoparticles BMS-202, the lung and liver metastatic nodules of pancreatic cancer were significantly reduced.

In short, when combined with ICIs, thermal ablation and mild hyperthermia could enhance the therapeutic effect of ICIs and make pancreatic cancer "hot" again by inducing local tumor pro-inflammatory microenvironment and activating tumor immunosuppressive microenvironment, respectively. It is worth mentioning that PTT therapy based on nanoparticles BMS-202 could also inhibit the metastasis of cancer cells through blood vessels to distant organs.

Nasopharyngeal carcinoma

Nasopharyngeal carcinoma (NPC) is a malignant tumor that often occurs at the top of the nasopharynx. Although it is sensitive to radiotherapy, and simultaneous radiotherapy and chemotherapy are often used in clinics, 30% to 40% of patients die of local recurrence and metastasis, which may be related to radiation resistance (94, 95). At the same time, patients often suffer from many adverse reactions (such as radionecrosis, dysphagia, and vomiting) (96, 97). Hyperthermia can solve the problem of radiation resistance and adverse reactions to some extent, which may be helpful to inhibit the recurrence and metastasis of nasopharyngeal carcinoma.

Recent studies have found that PTT had a good effect in the treatment of nasopharyngeal carcinoma. Qinmin et al. invented a USPIO-PEG-sLex nanoparticle as a photothermal agent for PTT, which proved that it could effectively inhibit the growth and promote apoptosis of nasopharyngeal carcinoma *in vivo* and *in vitro*, and there was no metastasis or invasion in the xenotransplantation model (98). This has also been well established by Naveen et al., and the role of PTT in inducing apoptosis could be related to the surge in ROS level (99). However, after objectively evaluating this method, it might not be possible to use PTT alone for antineoplastic therapy. Hence, to address the question of whether a combination of hyperthermia and other treatments might benefit NPC patients, a retrospective analysis found that the 5-year overall survival rate (OS) of patients treated with whole body hyperthermia (WBH) combined with CRT increased from 65.2% to 80.3% (100) compared with advanced NPC patients who received only radiotherapy and chemotherapy (CRT). More importantly, there was no significant toxicity in these patients, suggesting that WBH helps to improve radiation resistance and reduce therapeutic toxicity in patients with NPC. The effect of the combination of WBH and CRT is gratifying, therefore there are studies on the combination of mild hyperthermia and CRT plus cetuximab to test the efficacy of this triple therapy. The results showed that the apoptosis rate of nasopharyngeal carcinoma CNE induced by triple therapy was further increased on the basis of mild hyperthermia and CRT, and the curative effect was stronger than that of other groups. The mechanism may be related to the synergistic effect of blocking the binding of EGFR and its ligands and the increase of the Bax/Bcl-2 ratio (101). At the same time, this triple therapy has been implemented in pancreatic cancer, and its feasibility has been confirmed, but its safety has yet to be evaluated.

Brain cancer

Glioblastoma (GBM) is a highly invasive and destructive brain tumor characterized by poor prognosis and high recurrence rate (102). As a result of the tumor microenvironment of restricted blood-brain barrier (BBB) and GBM immunosuppression, immunotherapy, such as ICIs, is ineffective in the treatment of intracranial malignant tumors (103). On the one hand, the lack of TILs and the formation of immunosuppressive mechanism make GBM become a kind of "cold" tumor. On the other hand, monoclonal antibodies are difficult to enter the brain through BBB because of their large molecular size and low BBB permeability.

Laser interstitial thermotherapy (LITT) is a common method for the treatment of recurrent or deep brain tumors. The combination of LITT and ICIs may hopefully change the "cold" state of GBM immunosuppression into a "hot" state that is more sensitive to ICIs. Some studies have generated gold nanoparticles that have a therapeutic action similar to LITT, amplifying the effect of light-based photothermal ablation. When combined with anti-PD-L1, the tumor of GBM model mice reduces in size and the survival rate increases, showing long-lasting anti-tumor immunity (104). At the same time, solving effectively the problem of monoclonal antibody penetrating BBB is the key to improve the efficacy of monoclonal antibody in the treatment of GBM. Recently, MHT has shown good potential, with its mechanism potentially being related to the nanoparticle-encapsulated monoclonal antibodies passing through BBB. The combination of FeNP-based MHT with local injection of nano-adjuvants and systemic injection of anti-CTLA4 can lead to systemic therapeutic responses to inhibit tumor metastasis (75). In addition, nano-drugs, especially NPs combined with hyperthermia, are being studied as potential ways to enhance tumor drug delivery in patients with GBM (105).

In addition to GBM, studies have shown that a common, refractory pediatric cancer called neuroblastoma is sensitive to a combination of Prussian blue nanoparticles (PBNP) photothermotherapy (PTT) and anti-CTLA-4 checkpoint inhibitors. Compared with the group treated with PTT or anti-CTLA-4 checkpoint inhibitor alone, mice treated with this photothermal immunotherapy not only increased the survival rate by 43% or 55.5%, respectively, but also showed protection against neuroblastoma re-attack, suggesting the potential of PTT and ICIs in the treatment of brain tumors (106).

Thermal ablation or mild hyperthermia combined with ICIs: A clinical study

It has been established that the immune response mediated by T cells released by ICIs is non-specific (107), and thermal ablation may be able to correct this. In a clinical trial to evaluate the efficacy of RFA, patients with liver metastasis from colorectal cancer developed a tumor antigen-specific T cell response after RFA (108). Although RFA does not ablate tumor cells, it offers the possibility of therapy involving a combination of hyperthermia and ICIs. RFA may also make up for the deficiency of nonspecific T cell response induced by ICI (109). Secondly, ICIs therapy often causes adverse reactions. For instance, in patients with advanced melanoma, 96.8% of patients treated with ipilimumab and nivolumab had immune-related adverse events (irAE), and 59% of patients developed grade 3 or 4 irAE. A retrospective study of 131 patients with stage IV melanoma found that when combined with systemic or local hyperthermia, the incidence of grade 3 and grade 4 irAE in these patients decreased to 6.11% and 2.29% respectively, suggesting that mild hyperthermia combined with ICIs is safer (110). This has also been confirmed by a prospective phase I clinical trial. Guoliang et al. found that HT combined with adoptive cell therapy (ACT) and anti-PD-1 therapy was safe and feasible, but this combination of therapies also enriched the TCR library of clinical immune responders and promoted favorable changes in serum IL-2, IL-4, TNF- α and IFN- γ levels (111).

In short, combined with the current evidence, hyperthermia has an advantage in providing a tumor antigen-specific T cell response, while mild hyperthermia combined with ICIs can ensure safety while having anticancer efficacy, and the safety is easy to be ignored (Table 1).

Conclusions and future perspectives

Previous studies have mostly focused on the immune effect of hyperthermia, and the combination therapy of hyperthermia and ICIs has been a new field of investigation. This paper first compares the different effects of thermal ablation and mild hyperthermia on immune response, then summarizes the recent examples of preclinical and clinical studies of hyperthermia combined with ICIs, and analyzes the underlying reasons combined with the mechanism of hyperthermia, in order to provide theoretical and experimental basis for research on hyperthermia and ICI combined therapy.

This paper presents some limitations, such as a limited description of the methods and materials used in hyperthermia, whereby there is regular, rapid development of this technique. At the same time, due to the lack of clinical research on the combination of hyperthermia and ICIs, some key questions remain unanswered, such as: how can we better induce anti-tumor immune response with ICIs combined with thermal ablation or mild hyperthermia; at which temperature range does the body have the strongest immunity; what the immune-related factors that affect the efficacy of both are; how safe both techniques are; and how the combined therapy affects the survival rate of patients. These issues need to be addressed in order to greatly improve the outcome of combined therapy with HT and ICIs.

However, combined with the existing evidence, we can still draw some new key conclusions (1): CD8+T cell group is one of

the important mechanisms of antitumor immunity in mild hyperthermia, but it may not be as crucial in thermal ablation (2); both thermal ablation and mild hyperthermia can partially improve the immunosuppressive TME and increase the sensitivity of tumor cells to ICIs (112) (3); mild hyperthermia showed a better inhibitory effect on the high metastasis of some tumors, which may be related to the improvement of distant vascular permeability and the promotion of immune cell infiltration (113); and (4) thermal ablationcan provide tumor antigen specific T cell response to ICIs, while mild hyperthermia combined with ICIs can provide safety. However, there are some limitations in thermal ablation, mild hyperthermia or ICIs. The main issue of using thermal ablation or mild hyperthermia itself is the unnecessary heating of healthy tissue and heat tolerance of cells. ICIs has the ability to specifically target cancer cells, which can help some nanoparticles reach the tumor site during hyperthermia, accurately identify and kill cancer cells while protecting normal cells as much as possible. In the clinical treatment of ICIs, treatment-related irAE events often occur, including nausea, diarrhea, loss of appetite, weakness, metabolic abnormalities. Mild hyperthermia reduces the incidence of irAE events, especially for grade 3-4 irAE reaction, which ensures safety while enhances their therapeutic effect. For example, in the clinical application of HIFU, coagulation necrosis caused by excessive ultrasound energy destroys the structure and blood vessels of the tumor to a great extent, thus limiting the ability of immune cells to reach and interact with the tumor. Therefore, some researchers invented p-HIFU technology to reduce

TABLE 1 Examples of ongoing clinical studies combining ICIs with hyperthermia therapy.

Trail	Status	Phase	Hyperthermia specifications	Type of neoplasm	Involving metastatic tumors	Treatment	Endpoints
NCT02833233	Active	Pilot	CA	Breast cancer	No	anti-PD-1+anti-CTLA-4+CA	Safety
NCT03237572	Recruiting	I	HIFU, target 50% of the tumor, up to 3 cubic centimeters	Breast cancer	Yes	anti-PD-1+HIFU	Immune response, Safety
NCT04116320	Recruiting	I	Focused ultrasound ablation (FUSA)	Advanced tumor	No	anti-PD-1+HIFU	Immune response, Safety
NCT04156087	Recruiting	II	Minimally Invasive Surgical Microwave Ablation (MIS-MWA)	PC	No	anti-PD-1+MWA +Gemcitabine	PFS
NCT04220944	Recruiting	I	MWA(covered at least two thirds the size of the nodules)	HCC	No	anti-PD-1+MWA/ TACE	PFS, ORR, TTP, OS, Safety
NCT03864211	Active	I/II	MWA/RFA under CT or ultrasound guidance	HCC	No	anti-PD-1+MWA/ RFA	PFS, OS, Safety
NCT01853618	Completed	I/II	RFA/TACE/CA	HCC	No	anti-CTLA-4 +RFA/TACE/CA	Safety, feasibility, RR, TTP, OS
NCT03939975	Completed	II	MWA/RFA	HCC	No	anti-PD-1+MWA/ RFA	Safety, RR, PFS, OS
NCT03753659	Recruiting	II	MWA/RFA under CT or ultrasound guidance	HCC	No	anti-PD-1+MWA/ RFA	ORR, OS, Safety
NCT04150744	Recruiting	II	RFA	HCC	No	anti-PD-1+RFA	PFS, ORR, OS, TTP
NCT03337841	Unknown	II	RFA	HCC	No	anti-CTLA-4 +RFA/Surgery	PFS, OS, ORR, Safety
NCT02821754	Active	II	RFA/CA	HCC、BTC	No	anti-PD-L1+RFA/ TACE/CA	PFS, Safety
NCT02469701	Completed	II	CA	NSCLC	Yes	anti-PD-1+CA	RR
NCT02437071	Active	II	RFA	CRC	Yes	anti-PD-1+RFA	Safety, RR
NCT03101475	Completed	II	RFA	CRLM	Yes	anti-PD-L1+RFA +SBRT	Immune response, OS, Safety
NCT03393858	Unknown	I/II	Thermotron RF-8EX, Hyperthermia for 40 minutes on 42°C ± 0.5°C	MM	No	anti-PD-1+MH +DC-CIK	PFS, OS, Safety
NCT03757858	Unknown	I/II	Thermotron RF-8, Hyperthermia for 40 minutes on 42°C ± 0.5°C	Abdominal and pelvic malignant tumor	Yes	anti-PD-1+MH +CAR-T	Safety, ORR, PFS

CA, Cryoablation; HIFU, High intensity focused ultrasound; MWA, Microwave ablation; TACE, Transcatheter arterial chemoembolization; RFA, Radiofrequency ablation; SBRT, Systems Biology Research Tool; MH, Mild hyperthermia; PC, Pancreatic cancer; HCC, Hepatocellular carcinoma; BTC, Biliary Tract Carcinomas; NSCLC, non-small cell lung cancer; CRC, colorectal cancer; CRLM, colorectal cancer liver metastases; MM,Malignant mesothelioma; PFS, Progression-Free-Survival; ORR, Overall Response Rate; TTP, Time to Progression; OS, Overall Survival; RR,response rate.
Note: the data in this table is quoted from clinicaltrials.gov.

ultrasound energy and found that the combination of p-HIFU and anti-PD-1 can promote immune cells to reach the tumor site and induce a local tumor pro-inflammatory microenvironment more effectively. Compared with RFA, MWA and laser, the release of TAA, cytokines and cell fragments caused by HIFU combined with anti-PD-1 acts as an agonist of innate immunity and takes the lead in showing advantages in thermal ablation. At the same time, more research on the combination of CA and ICIs is also needed. The opposite extreme temperature of CA can also cause a stronger immunostimulatory response, which is characterized by a significant increase in the levels of serum IL-1, IL-6, nuclear factor-kappa β and tumor necrosis factor-α after ablation. A preliminary study of patients with breast cancer receiving CA and anti-CTLA-4mAb has shown promising efficacy and good tolerance (114).

Therefore, in the future, hyperthermia and ICIs should be combined as a method to enhance local immune response and avoid systemic immunotoxicity. The goal of the combination of hyperthermia and ICIs will not simply transform the patient's immunosuppressive state into an activated state but can induce the body's own immunity. This is beneficial to the low-dose use of ICIs to reduce the occurrence of irAE events, as expected by Edward Jenner (110). In addition, whether hyperthermia and ICIs can make up for each other's shortcomings and exert synergistic effect also depends on a key question-whether a TME characterized by PD-L1 overexpression and TIL enrichment can be produced (60). The enrichment of TILs by hyperthermia has been confirmed (115, 116), but there are limited studies on the expression of PD-L1 or other immune checkpoints during hyperthermia. If hyperthermia can upregulate the expression of PD-1, PD-L1 or CTLA-4, it could be used as an ICIs sensitizer to bring improved efficacy to clinical malignant tumor patients while explaining the mechanism behind it, which is very important.

Author contributions

XY performed the manuscript preparation and drafted the manuscript. MG, RX, YT helped draft the manuscript. WL, WZ, LH, BW revised the manuscript and approved the final version. YCH contributed to the conception and design of the current study, revised the manuscript, and approved the final version. All authors contributed to the article and approved the submitted version.

Funding

This work was supported by the National Natural Science Foundation of China (grant nos. 81874408), the Project of the Hunan Provincial Department of Education (grant nos. 21B0359), the Project of Hunan Provincial Health Commission (grant no. 202207015643), and the Domestic First-Class Discipline Construction Project of Chinese Medicine of Hunan University of Chinese Medicine (grant nos. 2022ZYX03).

Acknowledgments

We would like to thank Editage (www.editage.cn) for English language editing.

Conflict of interest

The authors declare that the research was conducted in the absence of any commercial or financial relationships that could be construed as a potential conflict of interest.

Publisher's note

References

1. Lentz RW, Colton MD, Mitra SS, Messersmith WA. Innate immune checkpoint inhibitors: The next breakthrough in medical oncology? *Mol Cancer Ther* (2021) 20(6):961–74. doi: 10.1158/1535-7163.MCT-21-0041

2. Petitprez F, Meylan M, de Reynies A, Sautes-Fridman C, Fridman WH. The tumor microenvironment in the response to immune checkpoint blockade therapies. *Front Immunol* (2020) 11:784. doi: 10.3389/fimmu.2020.00784

3. Dolina JS, Van Braeckel-Budimir N, Thomas GD, Salek-Ardakani S. CD8(+) T cell exhaustion in cancer. *Front Immunol* (2021) 12:715234. doi: 10.3389/fimmu.2021.715234

4. Zhang Z, Lu M, Qin Y, Gao W, Tao L, Su W, et al. Neoantigen: A new breakthrough in tumor immunotherapy. *Front Immunol* (2021) 12:672356. doi: 10.3389/fimmu.2021.672356

5. Liu S, Galat V, Galat Y, Lee YKA, Wainwright D, Wu J. NK cell-based cancer immunotherapy: from basic biology to clinical development. *J Hematol Oncol* (2021) 14(1):7. doi: 10.1186/s13045-020-01014-w

6. Khan M, Arooj S, Wang H. NK cell-based immune checkpoint inhibition. *Front Immunol* (2020) 11:167. doi: 10.3389/fimmu.2020.00167

7. Abel AM, Yang C, Thakar MS, Malarkannan S. Natural killer cells: Development, maturation, and clinical utilization. *Front Immunol* (2018) 9:1869. doi: 10.3389/fimmu.2018.01869

8. Helmink BA, Reddy SM, Gao J, Zhang S, Basar R, Thakur R, et al. B cells and tertiary lymphoid structures promote immunotherapy response. *Nature* (2020) 577 (7791):549–55. doi: 10.1038/s41586-019-1922-8

9. Esin E. Clinical applications of immunotherapy combination methods and new opportunities for the future. *BioMed Res Int* (2017) 2017:1623679. doi: 10.1155/2017/1623679

10. Joshi S, Durden DL. Combinatorial approach to improve cancer immunotherapy: Rational drug design strategy to simultaneously hit multiple targets to kill tumor cells and to activate the immune system. *J Oncol* (2019) 2019:5245034. doi: 10.1155/2019/5245034

11. Kruger S, Ilmer M, Kobold S, Cadilha BL, Endres S, Ormanns S, et al. Advances in cancer immunotherapy 2019 - latest trends. *J Exp Clin Cancer Res* (2019) 38(1):268. doi: 10.1186/s13046-019-1266-0

12. Alpard SK, Vertrees RA, Tao W, Deyo DJ, Brunston RLJr., Zwischenberger JB. Therapeutic hyperthermia. *Perfusion* (1996) 11(6):425–35. doi: 10.1177/026765919601100602

13. Payne M, Bossmann SH, Basel MT. Direct treatment versus indirect: Thermo-ablative and mild hyperthermia effects. *Wiley Interdiscip Rev Nanomed Nanobiotechnol* (2020) 12(5):e1638. doi: 10.1002/wnan.1638

14. Habash RWY. Therapeutic hyperthermia. *Handb Clin Neurol* (2018) 157:853–68. doi: 10.1016/B978-0-444-64074-1.00053-7

15. Dunne M, Regenold M, Allen C. Hyperthermia can alter tumor physiology and improve chemo- and radio-therapy efficacy. *Adv Drug Deliv Rev* (2020) 163-164:98–124. doi: 10.1016/j.addr.2020.07.007

16. Gou Q, Zhou Z, Zhao M, Chen X, Zhou Q. Advances and challenges of local thermal ablation in non-small cell lung cancer. *Zhongguo Fei Ai Za Zhi* (2020) 23 (2):111–7. doi: 10.3779/j.issn.1009-3419.2020.02.06

17. Cho SJ, Baek JH, Chung SR, Choi YJ, Lee JH. Thermal ablation for small papillary thyroid cancer: A systematic review. *Thyroid* (2019) 29(12):1774–83. doi: 10.1089/thy.2019.0377

18. Lu C, Li X, Chu X, Li R, Li J, Wang J, et al. Clinical effects of microwave ablation in the treatment of low-risk papillary thyroid microcarcinomas and related histopathological changes. *Front Endocrinol (Lausanne)* (2021) 12:751213. doi: 10.3389/fendo.2021.751213

19. Markezana A, Goldberg SN, Kumar G, Zorde-Khvalevsky E, Gourevtich S, Rozenblum N, et al. Incomplete thermal ablation of tumors promotes increased tumorigenesis. *Int J Hyperthermia* (2021) 38(1):263–72. doi: 10.1080/02656736.2021.1887942

20. Qu S, Worlikar T, Felsted AE, Ganguly A, Beems MV, Hubbard R, et al. Non-thermal histotripsy tumor ablation promotes abscopal immune responses that enhance cancer immunotherapy. *J Immunother Cancer* (2020) 8(1):e000200. doi: 10.1136/jitc-2019-000200

21. Dumolard L, Ghelfi J, Roth G, Decaens T, Macek Jilkova Z. Percutaneous ablation-induced immunomodulation in hepatocellular carcinoma. *Int J Mol Sci* (2020) 21(12):4398. doi: 10.3390/ijms21124398

22. Pan J, Xu Y, Wu Q, Hu P, Shi J. Mild magnetic hyperthermia-activated innate immunity for liver cancer therapy. *J Am Chem Soc* (2021) 143(21):8116–28. doi: 10.1021/jacs.1c02537

23. Maimaitiyiming Y, Wang QQ, Yang C, Ogra Y, Lou Y, Smith CA, et al. Hyperthermia selectively destabilizes oncogenic fusion proteins. *Blood Cancer Discovery* (2021) 2(4):388–401. doi: 10.1158/2643-3230.BCD-20-0188

24. Nicolas-Boluda A, Laurent G, Bazzi R, Roux S, Donnadieu E, Gazeau F. Two step promotion of a hot tumor immune environment by gold decorated iron oxide nanoflowers and light-triggered mild hyperthermia. *Nanoscale* (2021) 13 (44):18483–97. doi: 10.1039/D1NR03201A

25. Sen K, Sheppe AEF, Singh I, Hui WW, Edelmann MJ, Rinaldi C. Exosomes released by breast cancer cells under mild hyperthermic stress possess immunogenic potential and modulate polarization *in vitro* in macrophages. *Int J Hyperthermia* (2020) 37(1):696–710. doi: 10.1080/02656736.2020.1778800

26. Huang PY, Zhu YY, Zhong H, Chen PL, Shi QY, Chen JY, et al. Autophagy-inhibiting biomimetic nanodrugs enhance photothermal therapy and boost antitumor immunity. *Biomater Sci* (2022) 10(5):1267–80. doi: 10.1039/D1BM01888D

27. van den Bijgaart RJE, Schuurmans F, Futterer JJ, Verheij M, Cornelissen LAM, Adema GJ. Immune modulation plus tumor ablation: Adjuvants and antibodies to prime and boost anti-tumor immunity in situ. *Front Immunol* (2021) 12:617365. doi: 10.3389/fimmu.2021.617365

28. Galluzzi L, Vitale I, Warren S, Adjemian S, Agostinis P, Martinez AB, et al. Consensus guidelines for the definition, detection and interpretation of immunogenic cell death. *J Immunother Cancer* (2020) 8(1):e000337. doi: 10.1136/jitc-2019-000337corr1

29. Ghanamah M, Berber E, Siperstein A. Pattern of carcinoembryonic antigen drop after laparoscopic radiofrequency ablation of liver metastasis from colorectal carcinoma. *Cancer* (2006) 107(1):149–53. doi: 10.1002/cncr.21959

30. Leibovici D, Zisman A, Lindner A, Stav K, Siegel YI. PSA elevation during prostate cryosurgery and subsequent decline. *Urol Oncol* (2005) 23(1):8–11. doi: 10.1016/j.urolonc.2004.06.005

31. Wang R, He Z, Cai P, Zhao Y, Gao L, Yang W, et al. Surface-functionalized modified copper sulfide nanoparticles enhance checkpoint blockade tumor immunotherapy by photothermal therapy and antigen capturing. *ACS Appl Mater Interfaces* (2019) 11(15):13964–72. doi: 10.1021/acsami.9b01107

32. Cheng Y, Weng S, Yu L, Zhu N, Yang M, Yuan Y. The role of hyperthermia in the multidisciplinary treatment of malignant tumors. *Integr Cancer Ther* (2019) 18:1534735419876345. doi: 10.1177/1534735419876345

33. Ahmed K, Zaidi SF, Mati Ur R, Rehman R, Kondo T. Hyperthermia and protein homeostasis: Cytoprotection and cell death. *J Therm Biol* (2020) 91:102615. doi: 10.1016/j.jtherbio.2020.102615

34. Zhou J, Wang G, Chen Y, Wang H, Hua Y, Cai Z. Immunogenic cell death in cancer therapy: Present and emerging inducers. *J Cell Mol Med* (2019) 23 (8):4854–65. doi: 10.1111/jcmm.14356

35. Hou CH, Lin FL, Hou SM, Liu JF. Hyperthermia induces apoptosis through endoplasmic reticulum and reactive oxygen species in human osteosarcoma cells. *Int J Mol Sci* (2014) 15(10):17380–95. doi: 10.3390/ijms151017380

36. Bezu L, Sauvat A, Humeau J, Gomes-da-Silva LC, Iribarren K, Forveille S, et al. eIF2alpha phosphorylation is pathognomonic for immunogenic cell death. *Cell Death Differ* (2018) 25(8):1375–93. doi: 10.1038/s41418-017-0044-9

37. Takaki H, Cornelis F, Kako Y, Kobayashi K, Kamikonya N, Yamakado K. Thermal ablation and immunomodulation: From preclinical experiments to clinical trials. *Diagn Interv Imaging* (2017) 98(9):651–9. doi: 10.1016/j.diii.2017.04.008

38. Yang W, Wang W, Liu B, Zhu B, Li J, Xu D, et al. Immunomodulation characteristics by thermal ablation therapy in cancer patients. *Asia Pac J Clin Oncol* (2018) 14(5):e490–e7. doi: 10.1111/ajco.12836

39. Yu M, Pan H, Che N, Li L, Wang C, Wang Y, et al. Microwave ablation of primary breast cancer inhibits metastatic progression in model mice *via* activation of natural killer cells. *Cell Mol Immunol* (2021) 18(9):2153–64. doi: 10.1038/s41423-020-0449-0

40. Li L, Wang W, Pan H, Ma G, Shi X, Xie H, et al. Microwave ablation combined with OK-432 induces Th1-type response and specific antitumor immunity in a murine model of breast cancer. *J Transl Med* (2017) 15(1):23. doi: 10.1186/s12967-017-1124-9

41. Zhu J, Yu M, Chen L, Kong P, Li L, Ma G, et al. Enhanced antitumor efficacy through microwave ablation in combination with immune checkpoints blockade in breast cancer: A pre-clinical study in a murine model. *Diagn Interv Imaging* (2018) 99(3):135–42. doi: 10.1016/j.diii.2017.12.011

42. Oei AL, Kok HP, Oei SB, Horsman MR, Stalpers LJA, Franken NAP, et al. Molecular and biological rationale of hyperthermia as radio- and chemosensitizer. *Adv Drug Delivery Rev* (2020) 163–164:84–97. doi: 10.1016/j.addr.2020.01.003

43. Tydings C, Sharma KV, Kim A, Yarmolenko PS. Emerging hyperthermia applications for pediatric oncology. *Adv Drug Deliv Rev* (2020) 163-164:157–67. doi: 10.1016/j.addr.2020.10.016

44. Fang Y, He Y, Wu C, Zhang M, Gu Z, Zhang J, et al. Magnetism-mediated targeting hyperthermia-immunotherapy in "cold" tumor with CSF1R inhibitor. *Theranostics* (2021) 11(14):6860–72. doi: 10.7150/thno.57511

45. Wan Mohd Zawawi WFA, Hibma MH, Salim MI, Jemon K. Hyperthermia by near infrared radiation induced immune cells activation and infiltration in breast tumor. *Sci Rep* (2021) 11(1):10278. doi: 10.1038/s41598-021-89740-0

46. Chen Q, Sun T, Jiang C. Recent advancements in nanomedicine for 'Cold' tumor immunotherapy. *Nanomicro Lett* (2021) 13(1):92. doi: 10.1007/s40820-021-00622-6

47. Wang M, Wang S, Desai J, Trapani JA, Neeson PJ. Therapeutic strategies to remodel immunologically cold tumors. *Clin Transl Immunol* (2020) 9(12):e1226. doi: 10.1002/cti2.1226

48. Teng MW, Ngiow SF, Ribas A, Smyth MJ. Classifying cancers based on T-cell infiltration and PD-L1. *Cancer Res* (2015) 75(11):2139–45. doi: 10.1158/0008-5472.CAN-15-0255

49. Huang L, Li Y, Du Y, Zhang Y, Wang X, Ding Y, et al. Mild photothermal therapy potentiates anti-PD-L1 treatment for immunologically cold tumors *via* an all-in-one and all-in-control strategy. *Nat Commun* (2019) 10(1):4871. doi: 10.1038/s41467-019-12771-9

50. Lin C, Liu Z, Li Y, Chen J. Protocol for fever-range whole-body hyperthermia (WBH) in mice to study febrile effect on T-cell adhesion and migration. *STAR Protoc* (2021) 2(3):100720. doi: 10.1016/j.xpro.2021.100720

51. Hoter A, Alsantely AO, Alsharaeh E, Kulik G, Saadeldin IM. Combined thermotherapy and heat shock protein modulation for tumor treatment. In: AAA Asea and P Kaur, editors. *Heat shock proteins in human diseases*, vol. p . Cham: Springer International Publishing; (2021). p. 53–78.

52. Khaledian M, Nourbakhsh MS, Saber R, Hashemzadeh H, Darvishi MH. Preparation and evaluation of doxorubicin-loaded PLA-PEG-FA copolymer containing superparamagnetic iron oxide nanoparticles (SPIONs) for cancer

treatment: Combination therapy with hyperthermia and chemotherapy. *Int J Nanomed* (2020) 15:6167–82. doi: 10.2147/IJN.S261638

53. Kagawa T, Matsumi Y, Aono H, Ohara T, Tazawa H, Shigeyasu K, et al. Immuno-hyperthermia effected by antibody-conjugated nanoparticles selectively targets and eradicates individual cancer cells. *Cell Cycle* (2021) 20(13):1221–30. doi: 10.1080/15384101.2021.1915604

54. Yang H, Jiang F, Zhang L, Wang L, Luo Y, Li N, et al. Multifunctional l-arginine-based magnetic nanoparticles for multiple-synergistic tumor therapy. *Biomater Sci* (2021) 9(6):2230–43. doi: 10.1039/D0BM01932A

55. Chang M, Hou Z, Wang M, Li C, Lin J. Recent advances in hyperthermia therapy-based synergistic immunotherapy. *Adv Mater* (2021) 33(4):e2004788. doi: 10.1002/adma.202004788

56. van den Tempel N, Horsman MR, Kanaar R. Improving efficacy of hyperthermia in oncology by exploiting biological mechanisms. *Int J Hyperthermia* (2016) 32(4):446–54. doi: 10.3109/02656736.2016.1157216

57. Stephen ZR, Zhang M. Recent progress in the synergistic combination of nanoparticle-mediated hyperthermia and immunotherapy for treatment of cancer. *Adv Healthc Mater* (2021) 10(2):e2001415. doi: 10.1002/adhm.202001415

58. Lin K, Rockliffe N, Johnson GG, Sherrington PD, Pettitt AR. Hsp90 inhibition has opposing effects on wild-type and mutant p53 and induces p21 expression and cytotoxicity irrespective of p53/ATM status in chronic lymphocytic leukaemia cells. *Oncogene* (2008) 27(17):2445–55. doi: 10.1038/sj.onc.1210893

59. Saadeldin IM, Hussein MA, Magdeldin S. Heat shock proteins mediate anastasis and plasticity of thermotolerant cells. In: AAA Asea and P Kaur, editors. *Heat shock proteins in human diseases*. Cham: Springer International Publishing; (2021). p. 281–94.

60. Li Z, Deng J, Sun J, Ma Y. Hyperthermia targeting the tumor microenvironment facilitates immune checkpoint inhibitors. *Front Immunol* (2020) 11:595207. doi: 10.3389/fimmu.2020.595207

61. Guo D, Chen Y, Wang S, Yu L, Shen Y, Zhong H, et al. Exosomes from heat-stressed tumour cells inhibit tumour growth by converting regulatory T cells to Th17 cells *via* IL-6. *Immunology* (2018) 154(1):132–43. doi: 10.1111/imm.12874

62. Zhong H, Yang Y, Ma S, Xiu F, Cai Z, Zhao H, et al. Induction of a tumour-specific CTL response by exosomes isolated from heat-treated malignant ascites of gastric cancer patients. *Int J Hyperthermia* (2011) 27(6):604–11. doi: 10.3109/02656736.2011.564598

63. Alharbi MG, Lee SH, Abdelazim AM, Saadeldin IM, Abomughaid MM. Role of extracellular vesicles in compromising cellular resilience to environmental stressors. *BioMed Res Int* (2021) 2021:9912281. doi: 10.1155/2021/9912281

64. Poggio M, Hu T, Pai CC, Chu B, Belair CD, Chang A, et al. Suppression of exosomal PD-L1 induces systemic anti-tumor immunity and memory. *Cell* (2019) 177(2):414–27.e13. doi: 10.1016/j.cell.2019.02.016

65. Cordonnier M, Chanteloup G, Isambert N, Seigneuric R, Fumoleau P, Garrido C, et al. Exosomes in cancer theranostic: Diamonds in the rough. *Cell Adh Migr* (2017) 11(2):151–63. doi: 10.1080/19336918.2016.1250999

66. Sivori S, Pende D, Quatrini L, Pietra G, Della Chiesa M, Vacca P, et al. NK cells and ILCs in tumor immunotherapy. *Mol Aspects Med* (2021) 80:100870. doi: 10.1016/j.mam.2020.100870

67. Min Y, Wang X, Chen H, Chen J, Xiang K, Yin G. Thermal ablation for papillary thyroid microcarcinoma: How far we have come? *Cancer Manag Res* (2020) 12:13369–79. doi: 10.2147/CMAR.S287473

68. Xu D, Ge M, Yang A, Cheng R, Sun H, Wang H, et al. Expert consensus workshop report: Guidelines for thermal ablation of thyroid tumors (2019 edition). *J Cancer Res Ther* (2020) 16(5):960–6. doi: 10.4103/jcrt.JCRT_558_19

69. Zhang Y, Gao X, Yan B, Wen N, Lee WSV, Liang XJ, et al. Enhancement of CD8(+) T-Cell-Mediated tumor immunotherapy *via* magnetic hyperthermia. *ChemMedChem* (2022) 17(2):e202100656. doi: 10.1002/cmdc.202100656

70. Liu Y, Crawford BM, Vo-Dinh T. Gold nanoparticles-mediated photothermal therapy and immunotherapy. *Immunotherapy* (2018) 10(13):1175–88. doi: 10.2217/imt-2018-0029

71. Cantu T, Walsh K, Pattani VP, Moy AJ, Tunnell JW, Irvin JA, et al. Conductive polymer-based nanoparticles for laser-mediated photothermal ablation of cancer: synthesis, characterization, and *in vitro* evaluation. *Int J Nanomed* (2017) 12:615–32. doi: 10.2147/IJN.S116583

72. Huang N, Wang H, Zhao J, Lui H, Korbelik M, Zeng H. Single-wall carbon nanotubes assisted photothermal cancer therapy: animal study with a murine model of squamous cell carcinoma. *Lasers Surg Med* (2010) 42(9):638–48. doi: 10.1149/MA2010-01/19/1044

73. Liu X, Wang Q, Li C, Zou R, Li B, Song G, et al. Cu(2)-xSe@mSiO(2)-PEG core-shell nanoparticles: a low-toxic and efficient difunctional nanoplatform for chemo-photothermal therapy under near infrared light radiation with a safe power density. *Nanoscale* (2014) 6(8):4361–70. doi: 10.1039/C3NR06160D

74. Yang K, Zhang S, Zhang G, Sun X, Lee ST, Liu Z. Graphene in mice: ultrahigh *in vivo* tumor uptake and efficient photothermal therapy. *Nano Lett* (2010) 10(9):3318–23. doi: 10.1021/nl100996u

75. Chao Y, Chen G, Liang C, Xu J, Dong Z, Han X, et al. Iron nanoparticles for low-power local magnetic hyperthermia in combination with immune checkpoint blockade for systemic antitumor therapy. *Nano Lett* (2019) 19(7):4287–96. doi: 10.1021/acs.nanolett.9b00579

76. Pan J, Hu P, Guo Y, Hao J, Ni D, Xu Y, et al. Combined magnetic hyperthermia and immune therapy for primary and metastatic tumor treatments. *ACS Nano* (2020) 14(1):1033–44. doi: 10.1021/acsnano.9b08550

77. Bagchi S, Yuan R, Engleman EG. Immune checkpoint inhibitors for the treatment of cancer: Clinical impact and mechanisms of response and resistance. *Annu Rev Pathol* (2021) 16:223–49. doi: 10.1146/annurev-pathol-042020-042741

78. O'Donnell JS, Long GV, Scolyer RA, Teng MW, Smyth MJ. Resistance to PD1/PDL1 checkpoint inhibition. *Cancer Treat Rev* (2017) 52:71–81. doi: 10.1016/j.ctrv.2016.11.007

79. Owonikoko TK, Park K, Govindan R, Ready N, Reck M, Peters S, et al. Nivolumab and ipilimumab as maintenance therapy in extensive-disease small-cell lung cancer: CheckMate 451. *J Clin Oncol* (2021) 39(12):1349–59. doi: 10.1200/JCO.20.02212

80. Al-Salama ZT. Durvalumab: A review in extensive-stage SCLC. *Target Oncol* (2021) 16(6):857–64. doi: 10.1007/s11523-021-00843-0

81. Loibl S, Poortmans P, Morrow M, Denkert C, Curigliano G. Breast cancer. *Lancet* (2021) 397(10286):1750–69. doi: 10.1016/S0140-6736(20)32381-3

82. Zhao W, Hu X, Li W, Li R, Chen J, Zhou L, et al. M2-like TAMs function reversal contributes to breast cancer eradication by combination dual immune checkpoint blockade and photothermal therapy. *Small* (2021) 17(13):e2007051. doi: 10.1002/smll.202007051

83. Oei AL, Korangath P, Mulka K, Helenius M, Coulter JB, Stewart J, et al. Enhancing the abscopal effect of radiation and immune checkpoint inhibitor therapies with magnetic nanoparticle hyperthermia in a model of metastatic breast cancer. *Int J Hyperthermia* (2019) 36(sup1):47–63. doi: 10.1080/02656736.2019.1685686

84. Fite BZ, Wang J, Kare AJ, Ilovitsh A, Chavez M, Ilovitsh T, et al. Immune modulation resulting from MR-guided high intensity focused ultrasound in a model of murine breast cancer. *Sci Rep* (2021) 11(1):927. doi: 10.1038/s41598-020-80135-1

85. Granja A, Pinheiro M, Sousa CT, Reis S. Gold nanostructures as mediators of hyperthermia therapies in breast cancer. *Biochem Pharmacol* (2021) 190:114639. doi: 10.1016/j.bcp.2021.114639

86. Chen H, Luan X, Paholak HJ, Burnett JP, Stevers NO, Sansanaphongpricha K, et al. Depleting tumor-associated tregs *via* nanoparticle-mediated hyperthermia to enhance anti-CTLA-4 immunotherapy. *Nanomed (Lond)* (2020) 15(1):77–92. doi: 10.2217/nnm-2019-0190

87. Tao J, Yang G, Zhou W, Qiu J, Chen G, Luo W, et al. Targeting hypoxic tumor microenvironment in pancreatic cancer. *J Hematol Oncol* (2021) 14(1):14. doi: 10.1186/s13045-020-01030-w

88. Karniadakis I, Garoufalia Z, Kouskos E, Mantas D. Pancreatic adenocarcinoma presenting with cushing's syndrome. *Lancet* (2021) 398(10294):e1. doi: 10.1016/S0140-6736(21)01114-4

89. Park W, Chawla A, O'Reilly EM. Pancreatic cancer: A review. *JAMA* (2021) 326(9):851–62. doi: 10.1001/jama.2021.13027

90. Mouratidis PXE, Costa M, Rivens I, Repasky EE, Ter Haar G. Pulsed focused ultrasound can improve the anti-cancer effects of immune checkpoint inhibitors in murine pancreatic cancer. *J R Soc Interface* (2021) 18(180):20210266. doi: 10.1098/rsif.2021.0266

91. Lucas AT, Price LS, Schorzman A, Zamboni WC. Complex effects of tumor microenvironment on the tumor disposition of carrier-mediated agents. *Nanomed (Lond)* (2017) 12(16):2021–42. doi: 10.2217/nnm-2017-0101

92. Chen Q, Xu L, Liang C, Wang C, Peng R, Liu Z. Photothermal therapy with immune-adjuvant nanoparticles together with checkpoint blockade for effective cancer immunotherapy. *Nat Commun* (2016) 7:13193. doi: 10.1038/ncomms13193

93. Yu Q, Tang X, Zhao W, Qiu Y, He J, Wan D, et al. Mild hyperthermia promotes immune checkpoint blockade-based immunotherapy against metastatic pancreatic cancer using size-adjustable nanoparticles. *Acta Biomater* (2021) 133:244–56. doi: 10.1016/j.actbio.2021.05.002

94. Chen YP, Liu X, Zhou Q, Yang KY, Jin F, Zhu XD, et al. Metronomic capecitabine as adjuvant therapy in locoregionally advanced nasopharyngeal carcinoma: a multicentre, open-label, parallel-group, randomised, controlled, phase 3 trial. *Lancet* (2021) 398(10297):303–13. doi: 10.1016/S0140-6736(21)01123-5

95. Kerbel RS, Andre N. Adjuvant metronomic chemotherapy for locoregionally advanced nasopharyngeal carcinoma. *Lancet* (2021) 398(10297):278–9. doi: 10.1016/S0140-6736(21)01240-X

96. Jackson RK, Liew LP, Hay MP. Overcoming radioresistance: Small molecule radiosensitisers and hypoxia-activated prodrugs. *Clin Oncol (R Coll Radiol)* (2019) 31(5):290–302. doi: 10.1016/j.clon.2019.02.004

97. Chen W, Wang F, Yang Z, Zhang T, Shen M, Wang R, et al. Long-term efficacy and adverse reactions of IMRT combined with endostar versus IMRT combined with chemotherapy for locally advanced nasopharyngeal carcinoma: a retrospective study. *Ann Palliat Med* (2021) 10(11):11891–900. doi: 10.21037/apm-21-3018

98. Liu Q, Liu L, Mo C, Zhou X, Chen D, He Y, et al. Polyethylene glycol-coated ultrasmall superparamagnetic iron oxide nanoparticles-coupled sialyl Lewis X nanotheranostic platform for nasopharyngeal carcinoma imaging and photothermal therapy. *J Nanobiotechnol* (2021) 19(1):171. doi: 10.1186/s12951-021-00918-0

99. Bejjanki NK, Zhong Y, Liu J, Li Q, Xu H, Shen H, et al. Surface charge transition nano-theranostics based on ultra-small Fe3O4 nanoparticles for enhanced photodynamic and photothermal therapy against nasopharyngeal carcinoma. *Biochem Biophys Res Commun* (2021) 557:240–6. doi: 10.1016/j.bbrc.2021.03.168

100. Zheng N, Xu A, Lin X, Mo Z, Xie X, Huang Z, et al. Whole-body hyperthermia combined with chemotherapy and intensity-modulated radiotherapy for treatment of advanced nasopharyngeal carcinoma: a retrospective study with propensity score matching. *Int J Hyperthermia* (2021) 38(1):1304–12. doi: 10.1080/02656736.2021.1971778

101. Liu W, Kang M, Qin Y, Wei Z, Wang R. Apoptosis-inducing effects of cetuximab combined with radiotherapy and hypothermia on human nasopharyngeal carcinoma CNE cells. *Int J Clin Exp Med* (2015) 8(2):2182–9.

102. Yang J, Shi Z, Liu R, Wu Y, Zhang X. Combined-therapeutic strategies synergistically potentiate glioblastoma multiforme treatment *via* nanotechnology. *Theranostics* (2020) 10(7):3223–39. doi: 10.7150/thno.40298

103. Persano S, Vicini F, Poggi A, Fernandez JLC, Rizzo GMR, Gavilan H, et al. Elucidating the innate immunological effects of mild magnetic hyperthermia on U87 human glioblastoma cells: An in vitro study. *Pharmaceutics* (2021) 13(10):1668. doi: 10.3390/pharmaceutics13101668

104. Liu Y, Chongsathidkiet P, Crawford BM, Odion R, Dechant CA, Kemeny HR, et al. Plasmonic gold nanostar-mediated photothermal immunotherapy for brain tumor ablation and immunologic memory. *Immunotherapy* (2019) 11(15):1293–302. doi: 10.2217/imt-2019-0023

105. Wiwatchaitawee K, Quarterman JC, Geary SM, Salem AK. Enhancement of therapies for glioblastoma (GBM) using nanoparticle-based delivery systems. *AAPS PharmSciTech* (2021) 22(2):71. doi: 10.1208/s12249-021-01928-9

106. Cano-Mejia J, Burga RA, Sweeney EE, Fisher JP, Bollard CM, Sandler AD, et al. Prussian Blue nanoparticle-based photothermal therapy combined with checkpoint inhibition for photothermal immunotherapy of neuroblastoma. *Nanomedicine* (2017) 13(2):771–81. doi: 10.1016/j.nano.2016.10.015

107. Das S, Johnson DB. Immune-related adverse events and anti-tumor efficacy of immune checkpoint inhibitors. *J Immunother Cancer* (2019) 7(1):306. doi: 10.1186/s40425-019-0805-8

108. Loffler MW, Nussbaum B, Jager G, Jurmeister PS, Budczies J, Pereira PL, et al. A non-interventional clinical trial assessing immune responses after radiofrequency ablation of liver metastases from colorectal cancer. *Front Immunol* (2019) 10:2526. doi: 10.3389/fimmu.2019.02526

109. Wang S, Song Y, Cao K, Zhang L, Fang X, Chen F, et al. Photothermal therapy mediated by gold nanocages composed of anti-PDL1 and galunisertib for improved synergistic immunotherapy in colorectal cancer. *Acta Biomater* (2021) 134:621–32. doi: 10.1016/j.actbio.2021.07.051

110. Kleef R, Nagy R, Baierl A, Bacher V, Bojar H, McKee DL, et al. Low-dose ipilimumab plus nivolumab combined with IL-2 and hyperthermia in cancer patients with advanced disease: exploratory findings of a case series of 131 stage IV cancers - a retrospective study of a single institution. *Cancer Immunol Immunother* (2021) 70(5):1393–403. doi: 10.1007/s00262-020-02751-0

111. Qiao G, Wang X, Zhou X, Morse MA, Wu J, Wang S, et al. Immune correlates of clinical benefit in a phase I study of hyperthermia with adoptive T cell immunotherapy in patients with solid tumors. *Int J Hyperthermia* (2019) 36(sup1):74–82. doi: 10.1080/02656736.2019.1647350

112. Wen Y, Chen X, Zhu X, Gong Y, Yuan G, Qin X, et al. Photothermal-chemotherapy integrated nanoparticles with tumor microenvironment response enhanced the induction of immunogenic cell death for colorectal cancer efficient treatment. *ACS Appl Mater Interfaces* (2019) 11(46):43393–408. doi: 10.1021/acsami.9b17137

113. Adkins I, Sadilkova L, Hradilova N, Tomala J, Kovar M, Spisek R. Severe, but not mild heat-shock treatment induces immunogenic cell death in cancer cells. *Oncoimmunology* (2017) 6(5):e1311433. doi: 10.1080/2162402X.2017.1311433

114. McArthur HL, Diab A, Page DB, Yuan J, Solomon SB, Sacchini V, et al. A pilot study of preoperative single-dose ipilimumab and/or cryoablation in women with early-stage breast cancer with comprehensive immune profiling. *Clin Cancer Res* (2016) 22(23):5729–37. doi: 10.1158/1078-0432.CCR-16-0190

115. He K, Liu P, Xu LX. The cryo-thermal therapy eradicated melanoma in mice by eliciting CD4(+) T-cell-mediated antitumor memory immune response. *Cell Death Dis* (2017) 8(3):e2703. doi: 10.1038/cddis.2017.125

116. Mace TA, Zhong L, Kokolus KM, Repasky EA. Effector CD8+ T cell IFN-gamma production and cytotoxicity are enhanced by mild hyperthermia. *Int J Hyperthermia* (2012) 28(1):9–18. doi: 10.3109/02656736.2011.616182

frontiers | Frontiers in Oncology

TYPE Review
PUBLISHED 17 August 2022
DOI 10.3389/fonc.2022.948405

OPEN ACCESS

EDITED BY
Xian Zeng,
Fudan University, China

REVIEWED BY
Ewa Kalinka,
Polish Mother's Memorial Hospital Research Institute, Poland
Ilaria Attili,
European Institute of Oncology (IEO), Italy

*CORRESPONDENCE
Yuan Wan
ywan@binghamton.edu
Wenjun Mao
maowenjun1@njmu.edu.cn

†These authors have contributed equally to this work

SPECIALTY SECTION
This article was submitted to Cancer Immunity and Immunotherapy, a section of the journal Frontiers in Oncology

RECEIVED 19 May 2022
ACCEPTED 22 July 2022
PUBLISHED 17 August 2022

CITATION
Mussafi O, Mei J, Mao W and Wan Y (2022) Immune checkpoint inhibitors for PD-1/PD-L1 axis in combination with other immunotherapies and targeted therapies for non-small cell lung cancer.
Front. Oncol. 12:948405.
doi: 10.3389/fonc.2022.948405

Immune checkpoint inhibitors for PD-1/PD-L1 axis in combination with other immunotherapies and targeted therapies for non-small cell lung cancer

Ofek Mussafi[1,2†], Jie Mei[3†], Wenjun Mao[1*] and Yuan Wan[2*]

[1]Department of Cardiothoracic Surgery, The Affiliated Wuxi People's Hospital of Nanjing Medical University, Wuxi, China, [2]The Pq Laboratory of BiomeDx/Rx, Department of Biomedical Engineering, Binghamton University-SUNY, Binghamton, NY, United States, [3]Department of Oncology, The Affiliated Wuxi People's Hospital of Nanjing Medical University, Wuxi, China

It has been widely acknowledged that the use of immune checkpoint inhibitors (ICI) is an effective therapeutic treatment in many late-stage cancers. However, not all patients could benefit from ICI therapy. Several biomarkers, such as high expression of PD-L1, high mutational burden, and higher number of tumor infiltration lymphocytes have shown to predict clinical benefit from immune checkpoint therapies. One approach using ICI in combination with other immunotherapies and targeted therapies is now being investigated to enhance the efficacy of ICI alone. In this review, we summarized the use of other promising immunotherapies and targeted therapies in combination with ICI in treatment of lung cancers. The results from multiple animals and clinical trials were reviewed. We also briefly discussed the possible outlooks for future treatment.

KEYWORDS

immunotherapy, PD-1, PD-L1, immune checkpoint inhibitor, lung cancer

Introduction

One mechanism in which cancer weakens the body is through binding of the programmed death-ligand 1 (PD-L1) expressed on the surface of cancer cells with the programmed death 1 (PD-1) expressed on the surface of T cells. Over time this affinity leads to exhaustion of T cells and a weakened immune system through various signaling pathways due to the inhibitory nature of the PD-L1. So far, several mechanisms have been elucidated. PD-1/PD-L1 binding complex triggers the immunoreceptor tyrosine-

based switch motif (ITSM) found in the intracellular head of the PD-1 receptor to undergo phosphorylation. Next binding occurs between the high affinity T cell SHP2 molecule and the phosphorylated ITSM. This induces proximal T-cell receptor molecules such as zeta-chain (TCR)-associated protein kinase (ZAP70) to undergo dephosphorylation (1). ZAP70 binds directly with the major histocompatibility complex (MHC) receptor and plays a role in T-cell signaling. Dephosphorylation of ZAP70 leads to inhibition in downstream PI3K-AKT and RAS-ERK signaling, further reduces T-cell receptor (TCR)-mediated interleukin-2 (IL-2) and T cell proliferation, and thus promotes T-cell immunosuppression (2). Moreover, PD-1/PD-L1 interaction also leads to downregulation of LCK proto-oncogene (Lck) activity (3). Downregulation of Lck activity leads to a reduction of phosphorylated ZAP70 and ultimately to a downstream inhibition of the PI3K/Akt/mTOR pathway and the Ras/MEK/ERK pathway. Low Lck levels also leads to a reduction in phosphorylated CD3ζ, decreasing intracellular signaling and TCR surface expression. PKCθ is an enzyme found in the T cell that plays a role in intracellular signaling and is essential for T cell activation and IL-2 production. A reduction in Lck activity means less activated PKCθ availability and, therefore, a reduction in essential T-cell functions. Altogether, these pathways combine to exhaust T cells' post PD-1/PD-L1 activation complex. Furthermore, PD-1 activation complex leads to downregulation of the CK2 molecule which phosphorylates the PTEN cytoplasmic domain. Higher levels of dephosphorylated PTEN lead to continued phosphatase activity and ultimately, inhibition of TCR activation signals. Together, these responses in T cells are linked to decrease function, proliferation, and overall, an exhausted phenotype.

PD-1/PD-L1 monoclonal antibodies (mAbs) trigger an antitumor response by blocking this binding complex between T cells and tumor cells. These mAbs bind directly to the PD-1 on T-cell membranes or the PD-L1 on tumor-cell membranes. Once binding occurs, these mAbs will stop the inhibition of the T-cell immune surveillance response. Moreover, they can increase the production of interferon-gamma (IFN-γ), IL-2, and interleukin-7 (IL-7) (4). IFN-γ is a cytokine found in T cells that plays a role in inducing and modulating several immune responses. IL-2 is another cytokine that has been shown to be induced *via* three different signaling pathways, i.e., JAK-STAT, PI3K/Akt/mTOR, and MAPK/ERK pathways, all of which are suppressed by PD-1/PD-L1 binding (5). IL-2 plays a role in T-cell immune regulation by converting T cells into Treg cells to prevent strong autoimmune response and enhance activation-induced cell death (AICD). It is also involved in increasing T-cell differentiation into effector T cells and memory B cells to fight off pathogens and tumor-associated antigens. IL-7 is an important cytokine involved in the development and growth of B cells and T cells. During early T-cell development, IL-7 plays a role as an important cofactor for V(D)J rearrangement of the T-cell receptor beta (TCRB) (6). Through the inhibition of the PD-1/PD-L1 binding complex and the up-regulation of these cytokines patients can achieve profound survival benefits including higher overall survival (OS) and objective response rate (ORR). Briefly, mAbs targeting the PD-1/PD-L1 axis has shown tremendous benefit in clinical trials and have been approved as second-line or first-line therapies for an increasing number of carcinomas, including lung cancer, melanoma, lymphoma, among others (7). Currently, FDA-approved drugs for use in PD-1 blockade include pembrolizumab, nivolumab, avelumab, and in PD-L1 blockade include atezolizumab and durvalumab. These drugs fall into a class of therapeutics known as checkpoint inhibitor blockade (ICB). ICB fall into a bigger class known as immunotherapies, which are considered one of the most important advancements in cancer treatment.

Since FDA approval of nivolumab and pembrolizumab, two mAbs targeting PD-1, for the treatment of advanced melanoma in 2014, countless studies on PD-1/PD-L1 have flooded the scientific community (8). This review will focus on lung cancers, specifically non-small cell lung cancer (NSCLC). It has been revealed that only 30% of NSCLC patients are diagnosed at stage I, for which the 5-year survival rate is 65%. In contrast, the 5-year survival rate for stage IV is only 5% (9).. Around 85% of all lung cancer cases are NSCLC (10). PD-1/PD-L1 drugs have shown promising benefits and low treatment-related adverse events (AE) for NSCLC in many clinical trials. A study of 495 NSCLC patients treated with pembrolizumab monotherapy achieved an ORR of 19.4%, and a median duration of response of 12.5 months, leading to pembrolizumab was approved as a single agent for the first-line treatment for NSCLC patient with PD-L1 TPS ≥1% and without driver gene mutations (11). Another randomized NSCLC study testing nivolumab in comparison to docetaxel demonstrated that progression-free survival (PFS), OS, and ORR were considerably improved with nivolumab irrespective of PD-L1 expression (12). Based on the findings, nivolumab was approved as second-line treatment of non-squamous advanced NSCLC after failure of prior platinum-based chemotherapy. When the PD-L1 inhibitor durvalumab was given to NSCLC patients after concurrent chemoradiotherapy, investigators saw an increased OS rate (66.3% in the durvalumab group *vs.* 55.6% in the control group), increased PFS (17.2 months for durvalumab group *vs.* 5.6 months in the control group), and increased median time to death or distant metastasis (28.3 months in the durvalumab group *vs.* 16.2 months in the control group) (13). Based on the findings, FDA approved durvalumab as the first maintenance therapy for stage III unresectable NSCLC.

Despite promising clinical benefits, a large percentage (>50%) of cancer patients still do not respond to the ICB. Mainly, the reasons for this can be attributed to a decreased number of tumor-infiltrating lymphocytes (TILs) and a lack of highly expressed PD-1/PD-L1 axis on all cancer cells. Therefore, colleagues speculate that patients with PD-L1 overexpressing

tumor may have optimal treatment outcomes (14–16). Another major concern in ICB is the toxic AE, which are commonly experienced alongside a new growing list of immune-related adverse effects. In some instances, these AEs prove more harm than benefits, and, thus, the treatment must be discontinued. With these challenges being the major setbacks in ICB, modern therapeutic approaches are now looking to expand upon PD-1/PD-L1 inhibition in ways to minimize adverse events, while increasing treatment efficacy. Accordingly, researchers have been exploring combination strategies with other types of cancer therapy, such as chemotherapy, targeted therapy, radiotherapy, and immunotherapy (17, 18). Unlike chemotherapy and radiotherapy that damage tumors indiscriminately, immunotherapy and targeted therapy use specific protein-targeted approaches that reduce cytotoxicity to normal cells. This allows for lower rate of AEs in comparison. For instance, one study compared immunotherapy with the combination of immunotherapy and chemotherapy. The investigators found the combinational therapy demonstrated higher ORR (15.2% *vs*. 43.5%) and significantly longer PFS (4.6 *vs*. 15.5 months) in NSCLC patients (19). In another study, in comparison with chemotherapy alone, combinational therapy demonstrated a higher ORR (19.9% and 48.3%) and longer 2-year PFS (3.4% *vs*. 22%) in advanced NSCLC (20). Given immunotherapy is very promising, we particularly reviewed ICB in combination with other immunotherapy and targeted therapies in NSCLC, which includes cancer vaccine, mAb, oncolytic viruses, protein targeted compounds, immunomodulators, and adoptive cell transfer therapy. Going forward, we acknowledge that the scope of this research is vast with far too many significant treatments to cover in one review. Therefore, we dedicated our focus to combinations of immunotherapy with high potential for lung cancers.

Combination with cancer vaccine

Neoantigen-based vaccines

Modern vaccinations typically work by introducing a foreign substance or antigen in small or weakened doses into the body, which allows the immune system to develop antibodies specifically programmed to eliminate the antigen. Vaccines are now also being tested in cancer therapy. In cancer treatment, vaccinations use the antigens found in tumor cell membranes as therapeutic targets, which can be recognized and targeted by immune cells, thus triggering specific immune response against tumor cells (21, 22). Neoantigen vaccines work by identifying and targeting antigens found exclusively on the surface of cancer cells known as tumor-specific antigens (TSA). Every patient has a unique set of TSA, which requires personalized treatment typically targeting up to 20 unique neoantigens. Neoantigen-based vaccines promote neoantigen-specific CD4+ T cells and CD8+ T cells against neoantigen expressing cells. Subsequently, T cells can search, recognize, and kill cells harboring these antigens, achieving a powerful and specific anti-tumor response. This boost in the immune system in combination with ICB can potentially increase treatment efficacy. Indeed, T cell targeting neoantigens has been associated with anti-tumor activity and has long been believed to be effective targets for anti-tumor response (23, 24). In a recent study, neoantigens were successfully identified as targets through RNA sequencing of NSCLC tumor and blood samples harvested from patients. The RNA sequencing data were analyzed to identify mutations, genetic expression information, and human leukocyte antigen (HLA) typing in order for several mutated neoantigens characterized by strong HLA affinity to be chosen and tested (25). Through *in vitro* experiments and neoantigen reactive T cells (NRT)-induced cytotoxicity *in vivo* evaluation, they demonstrated NRT had responses against neoantigens with high HLA affinity. In mice models bearing the NSCLC tumors, they were able to show that targeted therapy against ACAD8-T105I, BCAR1-G23V, and PLCG1-M245L led to improved immune cell response, demonstrating the feasibility of treatment *in vivo*. In a stage III/IV NSCLC study with 24 patients, neoantigens-based personalized vaccination was developed based on predictions using a panel of 508 tumor-associated genes from tumor biopsies, with peptides also demonstrating high affinity to HLA class I and II, determined through HLA typing (26). Researchers were able to demonstrate OS and median PFS of 8.9 and 6 months, respectively. Five patients demonstrated vaccine induced CD8+ T cell responses against epidermal growth factor receptor (EGFR) neoantigen peptides, showing that personalized neoantigen vaccination is a feasible and safe method to increase immune response against tumor cells harboring EGFR mutations. Another study tested the efficacy of PD-1 inhibitor nivolumab in combination with personal neoantigen vaccine, NEO-PV-01 (27). This was the first time ICI was tested in combination with neoantigen vaccine in NSCLC patients. It was determined that the approach provided minimal toxic AEs, while specifically activating CD4+ and CD8+, MHC class I, and MHC class II against restricted neoantigen epitopes. It is noteworthy that only three patients with NSCLC were treated, and, therefore, further clinical data are needed to confirm the findings of this study and to demonstrate the feasibility of this combination approach.

CIMAvax

EGFR and epidermal growth factor (EGF) play critical roles in healthy cell tissue development and homeostasis (28). EGFR falls into a receptor class that is heavily involved in a multimodal signaling cascade responsible for cellular migration, differentiation, and proliferation (29). Overexpression of EGFR occurs in ~60% of NSCLC patients and is associated with poor

differentiation, increased tumor proliferation, higher incidence of metastases, and lower efficacy (30, 31). The EGFR/EGF complex has long been viewed as therapeutic targets in NSCLC. The mode of action behind these treatments involves inhibition of EGFR, cutting off tumors' main mechanism to proliferate and undergo angiogenesis. Another form of treatment involves binding to the EGF directly to create a conformational change, decreasing the amount of available EGF in the bloodstream for cancer cell binding. CIMAvax-EGF vaccine is a recombinant Neisseria Meningitis B bacterium-derived outer membrane protein P64K, conjugated onto human recombinant EGF and using Montanide ISA51 as an adjuvant, leads to an upregulation of anti-EGF antibodies (32). Ultimately, the decrease in EGF in the bloodstream starves cancer cells, directly deregulating critical pathways involved in tumor growth, signaling, and differentiation. In phase III randomized study testing CIMAvax-EGF in advanced NSCLC patients that were previously treated with frontline chemotherapy, results showed that median OS in vaccinated and nonvaccinated patients was 12.43 and 9.43 months. Moreover, long-term survival in vaccinated and nonvaccinated after 2 years was 37% and 20%, and after 5 years was 23% and 0%, respectively (33). The researchers hypothesized that high level of EGF (>870 pg/ml) could be used as a predictive biomarker of CIMAvax efficacy. Interim results from a phase I/II study using nivolumab in combination with CIMAvax in advanced NSCLC showed ORR 44% (four out of nine) of patients with no AE of 3+, except in one patient due to nivolumab alone (34). Compared to nivolumab monotherapy, where ORR was reported as 23% (12 out 52). These findings indicate an improvement in efficacy for this combinational approach (35). Importantly, three out of the four patients had PD-L1 expression <1%, demonstrating success in cancer patients that normally exhibit poor prognosis with anti-PD-L1 treatments. It was determined that four doses of the GIMAvax-EGF vaccine were optimal, and the only dosing scheme where >50% of patients achieved sufficient antibody responders. Results from nivolumab/pembrolizumab in combination therapy with CIMAvax are awaited as the trial is still recruiting at the time of this publication (NCT02955290). Despite promising results, it is important to acknowledge that there exists a lack of data regarding the possibility of vaccine neutralization from the patient's immune system, which should be further explored. Additionally, it would be interesting to see how anti-EGFR antibodies compared with CIMAvax-EGF.

TG4010

MU1 is an antigen from a family of mucin. This glycoprotein plays a role in keeping pathogens out of the body through binding oligosaccharides to its extracellular domain (36). Overexpression of MU1 has been associated with lung, colon, breast, and pancreatic cancers (37). Additionally, biochemical differences exist between healthy MU1 expression and tumor associated MU1 expression. For example, MU1 transcriptional genes, such as STAT3, NF-kB, p53, and β-catenin are associated with tumor invasion, proliferation, and angiogenesis (38). TG4010 vaccine is a modified virus designed to express coding genes for MU1 and IL-2. This vaccine therapy deregulates critical pathways for NSCLC cell survival and, therefore, could prove effective in combination with ICB. In a phase II/III randomized, double-blind study testing stage IV NSCLC patients lacking an EGFR mutation while also expressing ≥ 50% of MUC1 on tumor cell surface, 222 patients received standard first-line chemotherapy in combination and without combination of TG4010 vaccine (39). Results showed that median PFS was 5.1 months in the group without TG4010 and 5.9 months in the group with TG4010. The adverse event was 4% in the combinational therapy group and 10% in the control group. Following up on the promising findings, two ongoing clinical trials are testing the feasibility of nivolumab in combination with TG4010 (NCT02823990) and triple arm nivolumab in combination with TG4010 and chemotherapy II with PD-L1 <50% (NCT03353675).

Cell-based vaccines

Antigen-presenting cells (APC) such as mature dendritic cells (mDC) are now being utilized in cancer vaccine therapies. Normally, APCs function as a surveillance system in the body continuously monitoring the extracellular environment for antigens. Once an antigen is identified, they return to the lymph nodes and bind to T cells through MHC I and MHC II, which cause activation against the antigen. In cancer therapy, one approach requires the use of neoantigens or TSA found in the patients to transfect mDC *in vitro* creating APCs that promote targeting to specific neoantigens or TSA. Subsequently, once educated mDCs are transplanted into the patient, these mDCs can simulate CD4+ and CD8+ T cells against tumor cells. However, this approach has proven to be impractical and time-consuming. A new approach is using the patient's intratumor as the neoantigen and creating vaccine response *in vivo*. This approach creates antitumor-specific CD8+ T cells by acting more of a primer releasing pro-inflammatory chemokines including CCL4, CCL5, CXCL10, and cytokines at the time of intra-tumoral administration, rather than an antigen-presenting platform helping induce the recruitment of immune cells, including T cells to the injection site (40, 41). T-cell activation can potentially demonstrate a key agonist that can help improve PD-1/PD-L1 treatments. Current ongoing clinical trials of combination mDC vaccine and PD-1/PD-L1 inhibitors include pembrolizumab in NSCLC (NCT03546361), pembrolizumab in solid tumors

(NCT03735290), and Pembrolizumab in plasmacytoid dendritic cells (PDC) derived from NY-ESO-1 antigens (NCT03970746). The ongoing clinical trials testing vaccine-based therapeutics with ICI were listed in Table 1.

Combination with mAb

Anti-EGFR antibody

Overexpression of EGFR is commonly found in a variety of cancers including NSCLC. Gene mutations at the EGFR are responsible for continuous autophosphorylation and a continuous activated state, which, ultimately, leads to carcinogenesis. Currently, there are two common approaches by which targeted treatment to this complex occurs. One is through an anti-EGFR mAb binding directly to the extracellular domain of EGFR, which will be primarily covered here. The other is *via* small-molecule EGFR tyrosine kinase inhibitors (TKI), binding competitively with adenosine 5′ triphosphate to the intracellular catalytic head of EGFR, covered more in depth in the next section (42). The binding of both therapeutics downregulates continuous phosphorylation and activation pathways involved in oncogenic mutations. Additionally, one anti-EGFR mAb known as cetuximab suggests that inhibition of this receptor-ligand axis also leads to immune stimulation and is associated with counterregulatory mechanisms. Cetuximab is also thought to be linked in immune suppression feedback loops that include an increase in the expression level of immune checkpoint receptors like PD-L1 in cancer cells (43). These results suggest an additive effect that is ideal for increasing treatment efficacy for ICB by increasing levels of PD-1/PD-L1. A stage IV NSCLC phase Ib dose-escalating trial of necitumumab, an anti-EGFR mAb, combined with pembrolizumab demonstrated ORR of 23.4%, PFS of 4.1 months regardless of PD-L1 status (44). The OS of patients at 6 months was 74.7%. It is noteworthy that patients with PD-L1 expression of ≥1% had improved ORR and medium PFS when compared to PD-L1 negative patients. It was concluded that the approach was tolerable with no dose-limiting toxicities reported and provided better efficacy than treatment in monotherapy, particularly in tumors of <50% PD-L1 expression. In a phase II trial for NSCLC testing avelumab in combination with cetuximab and chemotherapy results from 43 patients demonstrated ORR of 30.2%, OS of 10 months, and medium PFS of 6.1 months (45). No significant toxic AEs occurred compared either Avelumab or Cetuximab alone. However, anti-EGFR mAb and anti-PD-1/PD-L1 combination approach is still in the early stage of testing, and, therefore, due to lack of data, these findings are hard to validate.

TABLE 1 Ongoing clinical trials testing vaccine-based therapeutics with PD-1/PD-L1 checkpoint inhibitors.

Clinical Trial	Cancer Type	Setting	Phase	VaccineAgent	Anti-PD-1/ PD-L1	Primary Outcomes	N. Patients
NCT03639714	Advanced Solid Tumors	Personalize Neoantigen cancer vaccine	I/II	GRT-C901/GRT-R902	nivolumab/ ipilimumab	AE, SAE, DLT, ORR, RP2D	214
NCT04266730	Squamous NSCLC	Personalized and Adaptive Neoantigen, Dose-Adjusted vaccine	I	PANDA-VAC	pembrolizumab	AE	6
NCT03953235	NSCLC	Personalized Vaccine targeting shared Neoantigens	I/II	GRT-C903/ GRT-R904	nivolumab/ ipilimumab	AE, SAE, DLT, ORR, RP2D	144
NCT04998474	NSCLC	Personalized Vaccine	II	FRAME-001	pembrolizumab	Antigen-specific immune response	15
NCT03380871	Advanced or Metastatic non-squamous NSCLC.	Neo-PV-01 plus pembrolizumab Plus Chemotherapy	I	NEO-PV-01	pembrolizumab	AE	38
NCT02897765	NSCLC	NEO-PV-01 + Adjuvant With nivolumab	I	NEO-PV-01	nivolumab	SAE, AE,	34
NCT02955290	NSCLC, Metastatic and Unresectable NSCLC	CIMAvax + pembrolizumab/nivolumab	I/II	CIMAvax	pembrolizumab, nivolumab	DLT, AE, OS	42
NCT02823990	NSCLC	TG4010 + nivolumab	II	TG4010	nivolumab	ORR	13
NCT03353675	NSCLC	TG4010 + chemotherapy + nivolumab	II	TG4010	nivolumab	ORR	39
NCT03970746	NSCLC	PDC*Lung01 + injectable pembrolizumab/ pemetrexed	I/II	PDC*lung01	pembrolizumab	DLT	64
NCT03546361	NSCLC	Autologous Dendritic Cell-Adenovirus CCL21 Vaccine + pembrolizumab	I	CCL21 Vaccine	pembrolizumab	MTD/MAD, ORR	24
NCT03735290	NSCLC	ilixadencel + pembrolizumab	I/II	ilixadencel	pembrolizumab	AE, SAE, DLT, ORR	150
NCT03847519	NSCLC	ADXS-503 + pembrolizumab	I/II	ADXS-503	pembrolizumab	AE, DLT, anti-tumor activity	74

Anti-VEGF/VEGFR mAb

Vascular endothelial growth factor (VEGF) is a protein that promotes angiogenesis. In the cases of malignant cells, VEGF/VEGFR is commonly overexpressed leading to rapid proliferation and expansion of tumor tissue. Inhibition of this receptor-protein complex acts as an angiogenesis antagonist, leading to a decrease in cancer metastases and proliferation. Results from Bevacizumab, an anti-VEGFA mAb, in combination with atezolizumab demonstrated ORR of 64% and medium duration of response of 10.4 months as a first-line chemo-free therapy in NSCLC with PD-L1 expression >50% (46). However, despite promising results, prolonged exposure to VEGF/VEGFR mAb can lead to adaptive resistance by tumors and create a path for new expansion mechanisms. Ongoing clinical trials with anti-VEGF/VEGFR mAb are summarized in Table 2 with more results awaited to provide relevant information on the combination approach.

Combination with targeted therapies

Targeting tyrosine kinase

In addition to anti-EGFR mAb, a different approach exists targeting the EGF/EGFR complex, using TKIs instead. Activation of the oncogenic EGFR pathway in preclinical studies has shown enhancements in the susceptibility of lung tumors to anti PD-1 inhibitors in mice models, suggesting that EGRF TKIs in combination ICI may be a promising therapeutic approach, especially in EGFR mutated NSCLC (47). However, clinical trial data have been inconclusive with some reports finding AEs outweighing efficacy. In an EGFR mutation-positive NSCLC clinical trial, nivolumab in combination with Erlotinib (EGFR TKI) resulted in tolerable safety profile with an ORR of 19%, and durable response was observed in four out of 20 patients (48). A previously untreated stage IIIb/IV EGFR-mutant NSCLC study combining pembrolizumab and erlotinib reached an ORR rate of 41.7% with similar toxicities as pembrolizumab monotherapy (49). When comparing to a pembrolizumab monotherapy, where ORR was reported as 44.8%, no improvement in ORR was present for pembrolizumab alone (50). However, when compared to erlotinib monotherapy, which showed ORR of 22.7%, results do show a significant increase in ORR (51). This suggests that the combination approach has an increase in ORR when compared to EGF inhibitor alone, but no noticeable increase when compared to pembrolizumab alone. Importantly, different EGFR mutations can lead to different treatment outcomes. EGFR exon 18 G719, exon 19 K757R, exon 20 S768I, exon 21 G836S, and E746G mutations have been correlated to successful treatment outcomes in NSCLC patients, whereas tumors exhibiting exon 18 S720I mutation demonstrated poor clinical outcomes to erlotinib (52). It's worth mentioning most anti-EGFR treated patients build an adaptive resistance to treatment, raising speculation on the viability of this combination approach. Nonetheless, further data are awaited with Table 3 capturing the ongoing clinical trials of combination ICI with anti-EGF/EGFR therapeutics. In addition, anlotinib is a small molecule that acts as a receptor tyrosine kinase (RTK) inhibitor with multi-RTKs inhibition pathways including VEGFR-2 and VEGFR-3, fibroblast growth factor receptor (FGFR), stem cell-factor receptor (c-Kit), and platelet-derived growth factor receptor (PDGFR) (53). This agent may both inhibit angiogenesis and downregulate tumor expansion. Clinical trials have indicated that anlotinib significantly prolonged OS (9.3 *vs.* 6.3 months) and PFS (4.8 *vs.* 1.2 months) of patients with advanced NSCLC (54). Evidence shows that a combination approach can reverse PD-1/PD-L1 resistance when combined with nivolumab. In a phase Ib study of sintilimab in combination with anlotinib as first-line therapy, out of the 22 NSCLC patients enrolled in the study, 16 demonstrated an ORR of 72.7% and the 12-month PFS was 71.4% (55).

TABLE 2 Ongoing clinical trials testing VEGF targeted antibodies in combination with PD-1/PD-L1 checkpoint inhibitors.

Clinical Trial	Cancer Type	Intervention	Phase	VEGFAgent	Anti-PD-1/ PD-L1	Primary Outcomes	N. Patients
NCT03786692	Stage IV NSCLC	carboplatin, + pemetrexed, + bevacizumab, +/- atezolizumab	II	bevacizumab	atezolizumab	PFS	117
NCT04124731	Advanced NSCLC	sintilimab plus anlotinib	II	anlotinib	sintilimab	ORR	98
NCT04471428	Metastatic NSCLC	cabozantinib + atezolizumab	III	cabozantinib	atezolizumab	OS	366
NCT03386929	Metastatic/Stage III NSCLC	avelumab + axitinib + palbociclib	I/II	axitinib	avelumab	DLT, AE, RR, DR, PFS, OS, SIM	130
NCT05078931	NSCLC	pembrolizumab + lenvatinib	II	lenvatinib	pembrolizumab	PFS	35
NCT04147351	NSCLC Stage III-IV	atezolizumab; bevacizumab	II	bevacizumab	atezolizumab	ORR	22
NCT04459663	NSCLC	toripalimab injection combined with axitinib	II	axitinib	toripalimab	Antitumor activity, ORR	50
NCT03971474	Recurrent NSCLC	ramucirumab + pembrolizumab	II	ramucirumab	pembrolizumab	OS	166

TABLE 3 Ongoing clinical trials testing EGF/EGFR TKI and targeted antibodies in combination with PD-1/PD-L1 checkpoint inhibitors.

Clinical Trial	Cancer Type	Intervention	Phase	EGF/ EGFRAgent	Anti-PD-1/ PD-L1	Primary Outcomes	N. Patients
NCT02924233	NSCLC	Sym004 + nivolumab	I/II	Sym004	nivolumab	DLT, RP2D	0
NCT04042701	NSCLC	DS-8201a + pembrolizumab	I	DS-8201a	pembrolizumab	DLT, ORR	115
NCT04976647	Squamous NSCLC	HLX07 + HLX10	II	HLX07	HLX10	ORR, PFS	156
NCT04646330	NSCLC	AK104+anlotinib	I/II	anlotinib	AK104	ORR	120
NCT02013219	NSCLC	erlotinib + atezolizumab	I	erlotinib	atezolizumab	DLT, RP2D,	52
NCT02947386	Recurrent NSCLC, Stage III-IV NSCLC	nimotuzumab + nivolumab	I/II	nimotuzumab	nnivolumab	DLT, ORR	48

Targeting KRAS

KRAS mutant genes, the most frequent altered gene in NSCLC for years has been sought after as a therapeutic target with little success partly due to its high affinity for GTP and complex down streaming pathways (56). Recent FDA approval of KRAS G12C inhibitor, sotorasib has opened light on this treatment approach. Current dose exploration and dose expansion clinical trial combining sotorasib with pembrolizumab (NCT04185883) is undergoing, which included participants with KRAS p.G12C advanced non-small cell lung cancer. Upon completing the dose exploration, dose expansion may also proceed consisting of participants with KRAS p.G12C mutant advanced NSCLC. In addition, another trial on sotorasib in combination with pembrolizumab (NCT03785249) is also undergoing, which is a phase 1 evaluation of the safety, tolerability, and clinical activity in patients with KRAS G12C mutant unresectable or metastatic NSCLC.

Targeting IDO1

Indoleamine 2,3-Dioxygenase 1 (IDO1) is an enzyme expressed by the IDO1 gene, which is responsible for catalyzing tryptophan into kynurenine *via* the tryptophan-kynurenine-aryl hydrocarbon receptor (Trp-Kyn-AhR) pathway. Tryptophan is associated with healthy T-cell function (57). Depletion of tryptophan inhibits mTORC1 signaling pathway, which leads to T-cell autophagy and the release of GCN2-mediated phosphorylation of eIF-2. Finally, the ripple effects induce cell-cycle arrest and death in T cells (58). Therefore, upregulation of the IDO1 gene is associated with increased immunosuppression due to T-cell apoptosis and increased metabolites of IDO1 in the tumor microenvironment (TME) (59). Furthermore, IDO1 overexpression has been observed after ICB in NSCLC patients, suggesting a possible role in the process of acquired resistance and has been hypothesized to negatively affect post-treatment prognosis (60). Clinical studies indicated that IDO1 inhibition combined with ICB may have added antitumor effects and heightened immune response. In a phase I/II trial, IDO-1 inhibitor epacadostat, in combination with pembrolizumab for pretreated advanced NSCLC, demonstrated ORR of 35% with generally good tolerability. Signs of toxicity were present as 11% of patients had to discontinue treatment due to AEs (61). However, a phase III trial of the same treatment demonstrated no advantage from the combination approach in comparison with pembrolizumab alone (median PFS of 4.7 *vs.* 4.9 months; ORR of 34% *vs.* 32%) (62). In a phase I study to explore the combination of navoximod (another IDO1 inhibitor) with atezolizumab for the first time as treatment for patients with advanced cancer, navoximod combined with atezolizumab demonstrated good tolerability and acceptable safety (63). In the dose escalation stage, six of 66 (9%) patients achieved PR, and 11 (17%) patients achieved SD, and the rate of treatment-related Grade ≥ 3 adverse event increases with increasing doses of navoximod (63). However, there was no clear evidence of benefit from the combination approach in comparison with atezolizumab alone. The mixed results from these trials indicated that IDO1 inhibition alone might not sufficiently induce T-cell activation. More clinical trials are underway to better understand IDO1 inhibition and its potential in combination with ICI (Table 4).

Combination with oncolytic virus

Oncolytic virus and TME

Oncolytic viruses (OV) are typically engineered from existing virus models and repurposed to target cancer cells. A promising therapeutic PD-1/PD-L1 combination approach involves the use of OV. To promote immunogenic cell death (ICD), the virus first must replicate exclusively in cancer cells and then promote antitumor responses *via* activation of mDC and T cells. Secretion of damage-associated molecular patterns such as adenosine triphosphate (ATP) and high-mobility group box protein 1 (HMGB1) are usually a characteristics of such responses (64, 65). Many virus models have been explored as potential therapies. Some of the more studied models include

TABLE 4 Ongoing clinical trials testing IDO1 targeted antibodies in combination with PD-1/PD-L1 checkpoint inhibitors.

Clinical Trial	Cancer Type	Intervention	Phase	IDO1Agent	Anti-PD-1/ PD-L1	Primary Outcomes	N. Patients
NCT03322540	Metastatic NSCLC	epacadostat + pembrolizumab, epacadostat + placebo	II	epacadostat	pembrolizumab	ORR	154
NCT03322566	Metastatic NSCLC	epacadostat + pembrolizumab, +/- chemotherapy	II	epacadostat	pembrolizumab	ORR	23
NCT03347123	Advanced or Metastatic solid tumors	epacadostat + nivolumab, + ipilimumab /lirilumab	I/II	epacadostat	nivolumab	TEAE, ORR	11
NCT05077709	Metastatic NSCLC	IO102-IO103 + pembrolizumab	II	IO102-IO103	pembrolizumab	ORR, PFS	90
NCT03343613	Solid tumors	LY3381916 + LY3300054	I	LY3381916	LY3300054	DLT	60
NCT03562871	NSCLC	IO102 + pembrolizumab	I/II	IO102	pembrolizumab	DLT, ORR	108

measles virus, retroviruses, herpes simplex viruses, adenovirus, bovine papillomavirus, among others. As stated, a major limitation of PD-1/PD-L1 inhibitors is the lack of patients responding to treatment. To effectively increase the rate of successful treatment outcomes, better understanding of the TME is needed. Benefits of ICI appear most successful with tumors categorized by high PD-L1 expression, increased mutational burden, and high level of TILs. These tumor types are classified as treatment-receptive tumors otherwise known as immunologically "hot" (66, 67). On the other hand, tumors classified as immunologically "cold" tumors demonstrate reduced therapeutic benefit. These tumors, express low or no TSAs, have decreased TILs density, and a low rate of suppressive immune-cell subtypes infiltrating deep tumor regions including myeloid-derived suppressor cells, regulatory T cells, NK cells, neutrophils, or macrophages. Additionally, they demonstrate low expression of immune-suppressive molecules such as (including IL-10, IDO, CD73, PD-L1, and prostaglandin E2) (68–72). A promising approach for combination ICB would ideally alter these "cold" tumors into "hot" tumors. OV therapy can heat up immunologically "cold" tumors by enabling ICB and converting immunosuppressive cells to a pro-inflammatory phenotype to effectively break the immune tolerance of the TME (73). Recently, breakthroughs and discoveries have allowed for better understanding of the mechanism behind OV therapy. It is now understood that the clinical efficacy of OVs is highly dependent on the vaccine's ability to transform tumors into biological "vaccine factories". OVs can promote the recruitment and activation of lymphocytes, upregulate the expression of PD-1/PD-L1 effectively increasing efficacy and downregulating resistance of ICI, as well as alter components of the antitumor immune response including small, e.g., uric acid) (74), ATP, protein mediators such as HMGB1 and IFN signaling (75, 76). The mechanisms inducing these benefits involve tumor lysis, TME alteration, TIL activation, and recruitment, triggering of immune responses mediated by innate immune cells and CB8 + T cells through antigen binding, as well as inhibition of tumor angiogenesis, neovascularization, and other such vascular modifications (77, 78). Through these responses, OV treatment can lead to increased neoantigen spreading and tumor antigen presentation, infiltration of NK cells and T cells into the TME, and increase T-cell effector function leading to a phenomenon known as the "bystander effect" both at proximal and distal sites of tumors (79). The results from one study of intra-tumoral mJX-594 treatment targeting granulocyte-macrophage colony-stimulating factor (GM-CSF) gene showed a highly altered TME, while promoting suppressed growth of tumors treated with ICB (80). These promising results led to an increase response to immunotherapy treatment. Furthermore, the combination of anti-PD-1 mAb and mJX-594 reduced tumor growth by 70%, whereas anti-PD-1 and mJX-594 monotherapy delayed tumor growth by 23% and 44%. The combination of TME alteration with PD-1 therapy is a promising approach to increasing PD-L1 expression and tumor-associated antigens, therefore, improving efficacy and the percentage of patients affected by anti-PD-1 inhibitors alone.

Coxsackievirus A21

Coxsackievirus A21 is another OV targeting ICAM-1 on tumor cells. A phase Ib KEYNOTE-200 trial of coxsackievirus A21 in combination with Pembrolizumab demonstrated good tolerability with no dose-limiting toxicities and no grade 4/5 AEs (81). Currently, the available data show medium OS of 9.5 months, ORR of 23%, and 33% for patients with ALK-negative and EGFR-negative NSCLC. The final results of the study are awaited. Notable increases in PD-L1 tumor levels were observed indicating combination OV with ICI could have additive effects. Current findings indicate that a combination of anit-PD-1 mAb with an optimal dose of OV does not significantly increase toxicity and, in most cases, is tolerated with grade ≥3 AEs. However, a major setback is acquired resistance that arises after multiple therapies, and, generally, therapy becomes ineffective after the third dose of treatment. Nonetheless, the ongoing clinical trials testing OV in combination with ICB in NSCLC are highly anticipated and summarized in Table 5.

Combination with immune modulators

CTLA4

Cytotoxic T-lymphocyte–associated protein 4 (CTLA-4) a member of the immunoglobulin superfamily and encodes a protein, which transmits an inhibitory signal to T cells (82). Ipilimumab is an immune-checkpoint inhibitor targeting CTLA-4, which is first approved for use as monotherapy in metastatic melanoma (83). Previous research revealed that the combination of ipilimumab with nivolumab has demonstrated superior efficacy compared with nivolumab alone in patients with advanced melanoma (84, 85). Similarly, phase 1 and 2 studies in patients with untreated advanced NSCLC showed promising early results with nivolumab plus ipilimumab, and recent phase 3 trials in this population demonstrated superiority of the combination either alone or with chemotherapy compared with chemotherapy alone (86–89). Nivolumab plus ipilimumab combined with chemotherapy (2 cycles) have been approved as first-line treatment for patients with metastatic or recurrent NSCLC, with no EGFR, or ALK genomic tumor aberrations in many countries (90). However, in this phase 3 randomized clinical trial, ipilimumab plus nivolumab did not improve outcomes in patients with advanced, pretreated, immune-checkpoint inhibitor-naive lung squamous cancer (91). Several studies suggested ipilimumab plus pembrolizumab do not improve efficacy and are associated with greater toxicity as first-line and second-line or later therapy treatment for NSCLC, suggesting ipilimumab plus pembrolizumab may not be a well choice (92, 93). In a phase 1b trial, preliminary efficacy of atezolizumab, a PD-L1 inhibitor, plus ipilimumab were observed in metastatic NSCLC, and the combination had manageable toxicity, with a safety profile consistent with those of the individual agents (94). Overall, anti-PD-1/PD-L1 therapy plus anti-CTLA-4 therapy could be promising for advanced NSCLC, but the proper combination strategy is still needed to be explored. The ongoing clinical trials testing the combination of anti-PD-1/PD-L1 and anti-CTLA-4 therapy in NSCLC are summarized in Table 6.

LAG-3

Lymphocyte activation gene-3 (LAG-3) is a cell surface receptor expressed on activated NK cells, B cells, and T cells. Its high binding affinity to the MHC-II triggers important T-cell

TABLE 5 Ongoing clinical trials testing oncolytic virus in combination with PD-1/PD-L1 checkpoint inhibitors.

Clinical Trial	Cancer Type	Intervention	Phase	Oncolytic Virus Vector	Anti-PD-1/ PD-L1	Primary Outcomes	N. Patients
NCT02879760	NSCLC	Ad-MAGEA3 injection + MG1-MAGEA3 infusion + pembrolizumab infusion	I/II	MG1-MAGEA3	pembrolizumab	AE, ORR	16
NCT03004183	Metastatic NSCLC	ADV/HSV-tk + valacyclovir + radiation + pembrolizumab	II	ADV/HSV-tk	pembrolizumab	ORR	57
NCT02824965	Advanced NSCLC	CVA21 + pembrolizumab	I	CVA21	pembrolizumab	TEAE	11
NCT03767348	NSCLC	RP1 + nivolumab	II	RP1	nivolumab	AE, SAE, DLT, ORR, MTD	300
NCT04725331	NSCLC	BT-001 + pembrolizumab	I/II	BT-001	pembrolizumab	AE, RDPB, ORR, DCR	48
NCT04355806	NSCLC	Inactivated trivalent influenza vaccine + nivoluamb /pembrozliumab /atezolizumab, durvalumab	I	Inactivated trivalent influenza vaccine	Inactivated trivalent influenza vaccine	ADCC, irAE, PFS, OS	160

TABLE 6 Ongoing clinical trials testing anti-CTLA-4 inhibitors in combination with PD-1/PD-L1 checkpoint inhibitors.

Clinical Trial	Cancer Type	Intervention	Phase	CTLA-4 Agent	Anti-PD-1/PD-L1	Primary Outcomes	N. Patients
NCT04140526	NSCLC, Solid Tumors	ONC-392, +/- pembrolizumab	IA/IB/ II	ONC-392	pembrolizumab	DLT, MTD, AE, RP2D	468
NCT04043195	NSCLC	nivolumab + oxaliplatin + ipilimumab	I/II	ipilimumab	nivolumab	ORR	30
NCT05187338	NSCLC, Solid Tumors	ipilimumab + pembrolizumab + durvalumab	I/II	ipilimumab	pembrolizumab + durvalumab	AE, PFS, DCR, DOR	100
NCT04606472	NSCLC, Solid Tumors	SI-B003	I	SI-B003	SI-B003	DLT, MTD, MAD, AE, RP2D	159
NCT03377023	NSCLC	ipilimumab + nivolumab +nintedanib	I/II	iipilimumab	nivolumab	MTD, ORR	68

functions including T-cell proliferation, activation, cytolytic activity, cytokine production, and other functions (95). In cancer therapy binding between LAG-3/MCH-II triggers anti-immune response including tumor escape, decreased production of cytokines, and a reduction in CD8+ T cells response (96). However, the exact mechanism at which this immune escape occurs is unclear. Overexpression of LAG-3 has been associated with exhaustion of the immune system and is emerging as a new checkpoint inhibitor target. Furthermore, targeting LAG-3 alongside PD-1 has been shown to strengthen immune response (97). A recent study tested 20 NSCLC tumor tissue samples for identification of potential biomarkers. They found that TILs in the tumor region had increased levels of both LAG-3 and PD-1 suggesting the apparent synergy and benefit of dual checkpoint blockade therapy in NSCLC (98). In a phase I/II trial testing LAG525, an anti-LAG-3 agent, in combination with PDR001, an experimental anti-PD-1 agent showed conversion of immune cold to immune-activated TME and durable response in 12 patients (11 partial response and one complete response). It was noted that LAG525 alone and LAG525 in combination with PDR001 demonstrated high progressive disease of 79% and 67%, respectively (99). A follow up study was recently completed (NCT02460224). However, statistic data were not fully disclosed. In a phase I/II testing relatlimab, an experimental anti-LAG-3 agent in combination with nivolumab showed ORR 11.5% and disease control rate (DCR) of 49% with acceptable AEs (grade ≥ 3 in 10% of patients) (100). Additionally, FDA approval of Opdualag for melanoma, a fixed-dose combination of relatlimab and nivolumab demonstrated increased PFS of 10.1 months for Opdualag compared to 4.6 months for the nivolumab monotherapy (NCT03470922). Although not approved for NSCLC, this first ever phase III trial of a LAG-3 antibodies demonstrates the validity of the methodology behind treatment. Promising combination approaches for NSCLC are now being tested in several ongoing clinical trials including phase I/II studies of neoadjuvant nivolumab in combination with relatlimab, eftilagimod alpha in combination with pembrolizumab (NCT03625323) (101), BMS-986,016 in combination with nivolumab (NCT01968109), and more which are summarized in Table 7.

OX-40

OX-40 is a type 1 transmembrane glycoprotein found on the surface of activated CD8+ and CD4+ T cell and part of the tumor necrosis factor receptor family. Activation of the OX-40/OX-40L axis acts as a costimulatory signal triggering T cell survival and division for both effector and memory cell populations against target antigens (102). Additionally, OX-40 activation suppresses proliferation and functionality of Tregs, preventing the TGF-β–mediated conversion of CD4+ T cells into Tregs, further increasing immune activity (103). Therefore, activation of OX-40 has been sought out as a therapeutic target for cancer immunotherapy. OX-40 inhibitors have shown to be effective in immunogenic tumors on some cancer cells lines including MCA303 (sarcoma tumors), SM1 (breast cancer), and CT26 (colon carcinoma tumors) (104). However, in immunogenic cold tumors, data were less promising. Considering the variability of immunogenicity in tumors from patient to patient and cancer type to cancer type (105), enhancing OX-40 efficacy *via* combination approaches has been explored. Some studies have demonstrated that the combination of anti-PD-1 ICI in combination with OX-40 inhibitors is feasible. Evidence from an OX-40 antagonist trial demonstrated synergic effects on different types of murine models with sequential combination of anti-PD-1 ICI showing 40% survival rate at day 100, compared to 0% survival rate with no treatment (106). A recent biomarker analysis study with 139 NSCLC patients showed that high PD-1 expression is negatively correlated with TILs OX-40 and OX-40L expression (0.250 and 0.386), according to linear regression models (107). This indicates that some patients with low PD-1 expression may have higher OX-40 and OX-40L expressions, suggesting OX-40 inhibitors have potential to be effective in patients at lower chances of benefiting from anti-PD-1 inhibitors monotherapy. In a phase I trial of anti-OX-40 mAb, GSK3174998 administered

TABLE 7 Ongoing clinical trials testing anti-LAG-3 inhibitors in combination with PD-1/PD-L1 checkpoint inhibitors.

Clinical Trial	Cancer Type	Intervention	Phase	LAG-3 Agent	Anti-PD-1/ PD-L1	Primary Outcomes	N. Patients
NCT03625323	NSCLCHNSCC	eftilagimod alpha + pembrolizumab	II	eftilagimod alpha	pembrolizumab	ORR	189
NCT01968109	NSCLC	BMS-986213, +/- nivolumab	I/IIa	BMS-986016	nivolumab	AE, SAE, ORR, DCR, DOR	1499
NCT02460224	Advanced Solid Tumors	LAG525, +/- PDR001	I/II	LAG525	PDR001	DLT, ORR	490
NCT04140500	NSCLC, Solid Tumors	RO7247669	I	RO7247669	RO7247669	DLT, AE, ORR, DOR, PFS	320
NCT03849469	NSCLC	XmAb®22841, + pembrolizumab	I	XmAb®22841	pembrolizumab	AE	242

as monotherapy or combined with pembrolizumab demonstrated no dose-limiting toxicities, indicating feasibility in solid and NSCLC cancer models (108). A phase I trial results testing MEDI0562, a humanized IgG1k OX-40 mAb in combination with durvalumab or tremelimumab, an anti-CLTA-4 inhibitor, for patients with late-stage solid tumors demonstrated OS of 17.4 and 11.9 months, respectively (109). A different triple combination approach testing BMS-986178, an OX-40 agonist, with ipilimumab with/without nivolumab in phase I/II demonstrated grade 3–4 AEs in six out 79 patients (8%) in anti-OX-40 with nivolumab. However, no clear efficacy benefit was observed when compared to nivolumab monotherapy (110). Further ongoing clinical trials are awaited to get a better understanding of the mechanism behind this novel combination approach and are summarized in Table 8.

TIGIT

A target for immunotherapy in NK-cells that has been grabbing a lot of attention is the poliovirus receptor (CD155). The binding of this protein in the body can lead to either improve immune response or increased immune suppression in cancer patients (111, 112). CD155 acts as a ligand and binds three ways in cancer patients triggering three distinct responses (113, 114). One of its binding domains is a glycoprotein called DNAM-1. DNAM-1 is commonly expressed on NK and CD8+ T cells and binding with CD155 leads to an increased anti-tumor response by activation of immune cells. The second binding domain is the TIGIT immunoreceptor for which CD155 has a higher affinity than DNAM-1. However, binding leads to an immunosuppressive response. TIGIT is quickly becoming a new immune checkpoint target in combination with PD-1/PD-L1. One study showed that high TIGIT/DNAM-1 ratio in Treg cells found in tumor tissue demonstrated a correlation to poor clinical outcomes after treatment with anti–PD-1 ICB (115). Furthermore, combination of anti-TIGIT with other therapies, mainly PD-1/PD-L1 ICB, have shown to overcome the limited efficacy of anti-TIGIT mAb alone in subcutaneous mouse tumors (116, 117). In a randomized phase II study of advanced NSCLC patients treated with tiragolumab, an anti-TIGIT antibody, combined with atezolizumab results showed that compared to a control group there was significant increase in PFS (5.6 *vs*. 3.9 months) and ORR (37.3% *vs*. 20.6%) and after 10.9 months follow up (118). Following these results, the FDA granted approval of tiragolumab in combination with atezolizumab for first line treatment in metastatic NSCLC categorized with high PD-L1 expression. Currently, ongoing clinical trials are testing anti-TIGIT mAb in combination with PD-1/PD-L1 therapy, including locally advanced or metastatic NSCLC (NCT03563716), advanced or metastatic solid cancers (NCT02913313), untreated locally advanced unresectable or metastatic NSCLC (NCT04294810), and more with a full list summarized in Table 9. The third type of binding occurs with CD96, and while less data are available regarding its interaction with CD155 in humans, mice models suggest that the binding promotes tumor escape from the immune system (119, 120). These mechanisms, however, are more complex and have more than one ligand/receptor combination. Recently, TIGIT and DNAM-1 have been found to bind to a ligand called CD112, which also binds to the immune-cell receptor CD112R (PVRIG) causing DNAM-1 and TIGIT to compete for the binding of CD112 (121–123). The DNAM-1/TIGIT/CD96 pathways offer new ways to improve immune-cell anti-tumor response.

TABLE 8 Ongoing clinical trials testing anti-OX-40 inhibitors in combination with PD-1/PD-L1 checkpoint inhibitors.

Clinical Trial	Cancer Type	Intervention	Phase	OX40 Agent	Anti-PD-1/ PD-L1	Primary Outcomes	N. Patients
NCT02528357	Neoplasms	GSK3174998, +/- pembrolizumab	I	GSK3174998	pembrolizumab	SAE, DLT,	141
NCT02410512	Neoplasms	MOXR0916 + atezolizumab	I	MOXR0916	atezolizumab	DLT, AE	610
NCT02554812	Advanced Cancer	avelumab, + PF-04518600, +/- utomilumab	II	avelumab	utomilumab	DLT, ORR	398
NCT02221960	Recurrent or Metastatic Solid Tumors	MEDI6383, +/- durvalumab	I	MEDI6383	durvalumab	AE, SAE	39
NCT03241173	Advanced or metastatic NSCLC	INCAGN01949 + nivolumab	I/II	INCAGN01949	nivolumab	TEAE, ORR	52
NCT04198766	Advanced or Metastatic NSCLC	INBRX-106, +/- pembrolizumab	I	INBRX-106	pembrolizumab	AE, SAE, MTD, RP2D	150
NCT03758001	Advanced Solid Tumors	IBI101, +/- sintilimab	I	IBI101	sintilimab	AE	38
NCT04215978	Advanced Soldi Tumors	BGB-A445, +/- tislelizumab	I	BGB-A445	tislelizumab	AE, SAE, MTD, RP2D, ORR	68
NCT02705482	Advanced Solid Tumors	MEDI0562	I	MEDI0562	durvalumab	AE	58
NCT02737475	Advanced Cancer	BMS-986178, +/- nivolumab, +/ipilimumab	I/II	BMS-986178	nivolumab	AE, SAE,	171

TABLE 9 Ongoing clinical trials testing anti-TIGIT inhibitors in combination with PD-1/PD-L1 checkpoint inhibitors.

Clinical Trial	Cancer Type	Intervention	Phase	Anti-TIGIT Agent	Anti-PD-1/ PD-L1	Primary Outcomes	N. Patients
NCT05014815	NSCLC	ociperlimab, +/- tislelizumab, + chemotherapy/placebo	II	ociperlimab	tislelizumab	PFS	200
NCT04294810	NSCLC	tiragolumab, + atezolizumab/placebo	III	tiragolumab	atezolizumab	PFS, OS	635
NCT03563716	NSCLC	tiragolumab, + atezolizumab/placebo	II	tiragolumab	atezolizumab	ORR, PFS	135
NCT04513925	NSCLC	tiragolumab, +/- atezolizumab	III	tiragolumab	atezolizumab	PFS,	800
NCT03628677	Solid Tumors	domvanalimab, +/- zimberelimab	I	domvanalimab	zimberelimab	TEAE	74
NCT04262856	NSCLC	zimberelimab, +/- domvanalimab, +/- etrumadenant	II	domvanalimab	zimberelimab	ORR, PFS	150
NCT02964013	Neoplasms	vibostolimab, +/pembrolizumab, +/- chemotherapy	I	vibostolimab	pembrolizumab	DLT, AE	492
NCT04165070	NSCLC	vibostolimab, +/- pembrolizumab, +/- chemotherapy	II	vibostolimab	pembrolizumab	ORR	270
NCT02913313	Solid Tumor	BMS-986207, +/- nivolumab, +/- ipilimumab	I/II	BMS-986207	nivolumab	AE, SAE, ORR, mDOR, PFS	130
NCT03260322	Solid Tumors	ASP8374, +/- pembrolizumab	I	ASP8374	pembrolizumab	DLT, AE, irAE	169
NCT03119428	Advanced or Metastatic Solid Tumors	OMP-313M32, +/- nivolumab	I	OMP-313M32	nivolumab	DLT, AE	33

However, their mechanism in cancer therapy is not fully understood yet.

IL-2

IL-2 is a cytokine that plays multiple roles in the activation and stimulation of the immune system. Binding occurs between the IL-2 ligand and IL-2 receptor (IL-2R) which is widely expressed on the surface of many immune cells types, including Foxp3+ regulatory T cells, CD4+ and CD8+ T cells, B cells, and NK cells (124). Upon activation, CD8+ and CD4+ T cells secrete large amounts of IL-2 in autocrine and paracrine pathways to recruit neighboring IL-2R+ cells. These circulating IL-2 molecules also bind to interleukin 2 receptor α-chain (IL-2Rα; CD25) expressed on Treg cells, which restrain immune responses to self and foreign antigens. There exist varying binding affinities of the IL-2/IL-2R pathway. IL-2R is composed of different subunits, IL-2Rα, IL-2Rβ (CD122), and IL-2Rγ (CD132), which are found at varying concentrations on the surface of different species of immune cells (125–127). In the body, low concentrations of IL-2 bind to the high-affinity receptors found on Treg cells leading to an immunosuppressive response. Only in higher concentrations can IL-2 bind to the lower affinity IL-2R found on CD8+ T-cells and NK-cells. These mechanisms are believed to help regulate immune response and prevent T-cell overstimulation from IL-2 signals and consistent TCR stimulation from tumor and self-antigens, which have shown to lead to T cell exhaustion or Fas (CD95)-mediated apoptosis (5). To overcome these regulatory mechanisms in cancer therapy, one approach is utilizing a combination strategy with PD-1/PD-L1 ICI. A study using TCB2, a newly engineered IL-2 antibody to specifically target the receptor of T cells and NK cells has been tested on mice models. Noticeably, it was shown that when a suboptimal dosage of anti-PD-1 mAb was used in combination with hIL-2/TCB2c, all seven mice models were tumor free after 19 days of treatment (128). A single-arm, phase I-dose escalation trial testing nivolumab combined with NKTR-214, a CD122-preferential IL2 pathway agonist, demonstrated ORR at 59.5% (22/37) and complete response at 18.9% (seven out of 37) for solid tumors patients including NSCLC. Additionally, analysis of tumor biopsies on a genetic and cellular level showed increased numbers of activated CD8+ T cells, without Treg cell activation (129). An ongoing dose-expansion phase II trial with optimal doses of 0.006 mg/kg and 360 mg every 3 weeks of NKTR-214 with nivolumab, respectively, demonstrated acceptable toxicity, while also promoting treatment efficacy regardless of PD-L1 levels (NCT02983045). It was reported that eight patients (21%) had grade 3/4 AEs with no cases of deaths from treatment. Total ORR for the various tumor types (melanoma, renal cell carcinoma, and NCSLC) and dose cohorts were 59.5% (22 out of 37), with complete response in seven patients (18.9%). Gene and cellular expression analysis of tumor samples demonstrated increased cytotoxicity, activation, and infiltration of CD8+ T cells without triggering Treg cell activation. Another ongoing clinical trial including NKT-214 with pembrolizumab in solid tumors (NCT03138889), IL-2 in combination with nivolumab for advanced NSCLC (NCT03215810). On a final note, high IL-2 circulating levels have been correlated with improved OS and response to PD-1/PD-L1 blockade in NSCLC demonstrating a potential for improved treatment outcomes in patient groups with higher risk of poor prognosis to anti-PD-1/PD-L1 inhibitors (130).

Combination adoptive cell transfer

CAR T cell

In recent years, T cell therapy has been gaining momentum as a new immunotherapy approach. Perhaps, the most popular model, chimeric antigen receptors (CAR) T cell treatment utilizes the patient's own T cells and genetically modifies them to target cancer cells. Briefly, CAR were expressed on the patient's T cells surface typically using an unarmed virus. Finally, they are injected back into the patient with hopes of giving a lasting antitumor response. In 2017, CD19 CAR T cell became the first FDA approve adoptive T cell transfer therapy after remarkable therapeutic effects in large B cell lymphoma or acute lymphoblastic leukemia (131, 132). Recently, reports have shown that the potential of CAR T cell immunotherapy in NSCLC (133). For NSCLC the most common TSA targets include EGFR, mesothelin, MUC1, CD80/CD86, PD-L1, inactive tyrosine-protein kinase transmembrane receptor (ROR1), carcinoembryonic antigen (CEA), among others (134). One CAR T cell study targeting EGFR in advanced NSCLC (NCT01869166) had reported preliminary results showing 45.5% (five out of 11) of patients achieved stable disease, and 18.2% (2/11) achieved partial response (135). CAR T cells targeting these antigens have been promising. However, some key challenges relating to CAR T cells include manufacturing concerns, restricted trafficking, infiltration and activation within tumors, severe toxicities, insufficient persistence *in vivo*, heterogeneity, and antigen escape (136).. In efforts to increase efficacy, some studies have attempted combining anti-PD-1 inhibitors with CAR T cell therapy. In a study testing CAR T cell combined with anti-PD-1 mAb, results showed significantly increased growth and survival inhibition of two different HER2+ transgenic mouse tumor models when compared to either treatment in monotherapy (137). A study for anti-MUC1 CAR T cells in combination with engineered PD-1 deficient T cells in NSCLC patients demonstrated 33% (two out of six) patients had significant shrunken tumors after 4 weeks of treatment (138). A clinical trial testing PD-1 knockout (KO) CAR T cells in NSCLC proved to be safe and well-tolerated by all patients, demonstrating stable disease in 55% (11 out of 20) patients (139). It is important to note that the combination of PD-1/PD-L1 targeted pathways and the CAR T cell treatment in clinical trials are still in early development, and there is a lack of necessary data to draw valid conclusions (140). Nonetheless, new promising methodologies are being awaited with CAR T cell therapy including CRISPER CAS-9 PD-1-knockout–modified CAR T cells and engineered CAR T cells with the capabilities of secreting PD-1-blocking single-chain variable fragments (scFv) (141, 142). With new innovations in genetic engineering, CAR T cell therapy may utilize PD-1/PD-L1 ICI or genetic alterations to improve efficacy in combination treatment.

NK cell

NK cells are another rising form of immunotherapy found in combination with PD-1– based inhibitor drugs. They are natural cytotoxic cells found in the body and require no stimulation to activate. They work by binding to receptors or antibodies present on abnormal cells such as cancer cells or TME. Cancer therapy has explored the use of autologous or allogeneic NK cell-based therapy, transplanting different subsets of NK cell populations into a cancer patient to achieve an anti-tumor response. Moreover, some studies demonstrate the benefit of combining NK cell therapy with ICI. One study suggests that PD-L1 mAb can directly upregulate and activate the cytotoxic effector functions of NK cells without any correlation to PD-L1 tumor status (143). Furthermore, *via* the AKT signaling pathway, PD-L1 mAbs were found to enhance NK cell function and prevent cell exhaustion, through upregulation of PD-L1 expression on NK cell surface. Recent study demonstrated that the combination of mHsp-70 targeting autologous NK cells therapy with nivolumab and radiochemotherapy was well tolerated with tumor progression or metastases not detectable 33 months post-diagnosis for one NSCLC patient (144). A study testing pembrolizumab in combination with allogeneic NK cells in comparison with pembrolizumab monotherapy in advanced NSCLC results demonstrated higher PFS (6.5 months *vs*. 4.3 months) and higher median OS (5.5 months *vs*. 13.3 months) (145). Several courses of NK cell injection demonstrated better OS (18.5 months) compared to single-course infusion (13.5 months), notably with the combination approach having much higher median OS and PFS in PD-L1 tumor portion score (TPS) ≥50%. One purpose mechanism for this increased efficacy involves the mechanism at which expanded NK cells engage with the TME. Through a contact-independent mechanism, NK cells promote endogenous TILs and upregulation of PD-L1 TPS (146). The difference between expanded NK cells and NK cells, which found naturally in the body, is that they are less susceptible to tumor suppression, therefore allowing them to upregulate immune response through binding with PD-L1 tumors. NK cells therapy can potentially turn nonresponding tumors into more susceptible to PD-1/PD-L1 treatment. Currently, an ongoing phase I clinical trial is testing the combination of PD-1/PD-L1, chemotherapy, and FT538 allogeneic NK cell therapy in advanced solid cancer (NCT05069935). These studies demonstrate a correlation between NK cell function and PD-1/PD-L1 inhibition; however, there lacks a mechanistic *in vivo* studies explaining these responses (147). Another issue with the use of autologous NK cell transfer is that the procedure is often expensive as each treatment is personalized and based on cells from the patient or donor. Lastly, the personalized process is time-consuming and due to the nature of the disease might prove inapplicable in some cases. NKG2A is an inhibitory signaling receptor found on the surface of NK cells.

Similar to the NKG2D ligand, efforts have been focused on increasing the efficacy of NK cell transfer treatment by targeting this axis. A popular anti-NKG2A antibody, known as monalizumab, is now being tested with anti-PD-1 blockade. One clinical trial testing these agents demonstrated the feasibility of combination treatment with ORR of 8% and a DCR at 16 weeks of 31% (148). *In vitro* and *in vivo* blocking on mice models demonstrated that when NKG2A and PD-1 blockers were combined, results showed a significant increase in the rate of tumor regression and anti-tumor immunity (149, 150). The NKG2A/NKG2D axis offers a viable way to increase the efficacy of PD-1 treatment by improving NK cell function and homeostasis in the body. In addition, combination immunotherapy with anti-PD-1/anti-PD-L1 and anti-NKG2 to improve efficacy of previously less effective anti-PD-1 treatments characterized by high levels of circulating sMIC should be explored.

Modified NK cell

To get around these issues, new forms of genetically engineered NK cells are now being brought into the market and sold as "off-the-shelf" universal treatment. A common type uses CAR NK cells, which are engineered to present antibodies on their surface and bind to antigens on the surface of cancer cells. CAR NK cell therapy does not require matching HLA donors unlike allogeneic NK cells or CAR T cell transplants and has a higher safety profile in this sense. This allows for large-scale commercial treatments to be manufactured. NK cells prove more challenging to extract and isolate than T cells. However, a line of NK-92 cells has been found to expand easily *in vitro* and engineered to present CAR on their surface. In theory, this CAR-NK cell line would be comparable to a universal CAR T cell treatment but, simply adding CAR receptors to NK cells is proving to be insufficient. Most CAR models are engineered based on T-cell structure and functionality. For example, CAR models containing co-stimulatory CD28 domains intended for T cells are commonly used in NK cells despite having no effect or activating NK cells (151). Currently, the latest advances in NK cell therapy are working to increase the efficacy of treatment through a better understanding of the NK cell activation mechanism and newly modified NK cell treatments. One clinical trial underway is testing the use of iPSC-derived NK cells combined with pembrolizumab, nivolumab, and atezolizumab in late-stage solid tumors, including NSCLC (NCT03841110). Another approach, derived from several studies, utilizes the NKG2D ligand, which plays a critical role in NK cell activation. The most common molecules released from the NKG2D ligand family in tumors are MICA and MICB, otherwise, referred to as sMIC. In a study targeting tumor-derived soluble NKG2D MIC molecules, simultaneously targeting sMIC with a PD-1/PD-L1 inhibitor resulted in enhanced infiltration, intrinsic function, and proliferation of CD8+ T cells with a TILs score recorded at 32.5% compared to 21% TILs of anti-PD-L1 monotherapy (152).. This study suggests through these antibodies targeting sMIC can increase the efficacy of T cell therapy in combination with ICB. Furthermore, the NKG2D ligand is either not induced or induced in low levels under normal conditions and that it is overexpressed only on the oncogenic cell surface or in the TME (153–159). This allows specific ligand to act not only as a target receptor for elimination of cancer cells but also as an indicator of such abnormalities [133]. However, this approach is not fully proven. Elevated levels of circulating NKG2D are correlated with poor outcomes in anti-PD-1/PD-L1 clinical trials (160). This is, in part, due to a process of proteolytic shedding (161–164), in which the tumor releases the ligands from its cell surface leading to powerful immune-suppressive responses and disturbing NK cells homeostatic maintenance and function (165, 166). A new strategy for the creation of universal super NK cell therapy has been proposed. This new strategy involves the use of aptamer-equipped NK cells engineered *via* metabolic glycan biosynthesis and, thus, avoids the use of genetic alteration (167). This approach allows for specific tumor targeting therapies *via* modified receptors on the NK cell surface. Furthermore, to enhance immunotherapy, PD-L1 targeting aptamers were also modified on the NK cell surface to regulate PD-1/PD-L1 signaling. This lead substantial upregulation of PD-L1 expression in HepG2 cells improving ICB. Although the mechanism remains unclear, it is known that increased levels of PD-L1 expression have been correlated with higher success from immunotherapies (168). Additionally, imaging of intravital tumor sites showed high levels of modified NK cells in deep tumor regions, indicating better infiltration and therapeutic efficacy for solid tumors. This approach of increasing infiltration in solid tumors *via* chemical engineering and has several benefits. First, the engineering strategy is simple and efficient and does not require genetic modification that reduces the risk for side effects in clinical applications. Secondly, the NK cells are biodegradable biocompatible, and no signs of toxicity was detected on mice models in the study. Third, the strategy is universal and by simply changing the target aptamer, different types of solid tumors can be targeted. This is made possible by systematically increasing ligands through exponential enrichment technology, while screening for aptamers from various cancer cell types giving a dataset of aptamers/cancer compatible combinations (169–173). Fourth and perhaps the most remarkable benefit, the study found aptamer-equipped NK cells to upregulate PD-L1 expression. This directly targets one of the major issues lying in targeting this axis, which was the lack of PD-L1 expression on cancer cells. For these reasons and, in particular, the upregulation of PD-L1, this new strategy of chemically modified NK cells needs further testing and to test the feasibility of combination with PD-1/PD-L1 inhibitors. Aptamer-equipped glycan biosynthesis NK cells may

potentially be the first step in providing successful universal NK cell transplants. CAR NK cells and iPSC NK cells also provide a pathway to universal treatment, however, face issues with functionally. Additionally, autologous NK cells have shown promising clinical trial data when combined with pembrolizumab and nivolumab. These promising results, notably, are preliminary mechanistic studies that show potential for NK cells in combination with PD-1/PD-L1 inhibitors. More clinical trial data are highly anticipated with these ongoing combination approaches summarized in Table 10.

Probody therapeutics

Finally, a new approach to improve PD-1/PD-L1 inhibitors efficacy is using a masked peptide linker to inhibit the binding of therapeutics to normal cells, while becoming unmasked and activated in the TME exclusively. Probody therapeutics are a next generation antibody using a masked peptide to cover the fab region. Once in the TME, the fab region gets cleaved off by tumor-associated proteases exposing the PD-L1 substrate domain. One study using extracted tumor samples from cancer patients demonstrated over 90% of cancer patients had sufficient protease activity to activate treatment *in vivo* (174). Initial *in vitro* results showed that the masked Pb-TCB reduced cytotoxicity by 100,000-fold, whereas the unmasked molecule proved potent in tumor killing at proper dosing schemes (175). From the concluded preclinical and preliminary clinical studies, one Probody PD-L1 targeting compound called CX-072 has demonstrated potential to optimize cancer treatment, while minimizing toxicity (176). CX-072 is a next generation of cancer immunotherapy that offers a new way to increase the percentage of patients affected by PD-L1 targeted treatments, while potentially reducing the rate of AEs associated with PD-1/PD-L1 blockade by overlooking normal tissue (176). In a dosing-finding clinical trial (NCT03013491), CX-072 was tolerated with indications of antitumor activity in patients without high levels of PD-L1 (177). As to our current knowledge, this treatment has not been tested in NSCLC. However, it offers a new approach to increase the percentage of NSCLC patients benefiting from PD-1/PD-L1 by increasing the precision of targeted treatment consequently decreasing required minimum dose and, therefore, rates of toxic adverse effects.

Discussion

For the past decade, ICI inhibitors and particularly PD-1/PDL-1 ICB have revolutionized NSCLC therapy. However, over 50% of patients do not respond to PD-1/PDL-1 inhibitor-based monotherapy due to low expression of PD-L1 in lung cancer patients, low numbers of TILs, and low mutational burden (178–180). Targeting specific characteristics of cancer patients alongside incorporating combination approaches based on tumor genomics and immunology data is the future of treatment. Ideally, a successful combination approach would stimulate one of the abovementioned factors associated with poor prognosis of PD-1 therapy alone. Vaccine therapy offers the potential to do just do that based on the biological mechanisms of how vaccines work. Alteration of the immune system to express certain receptors, activation of T cells against those receptors, and release of antibodies all pose the capability of producing additive antitumor response when used in combination with PD-1/PD-L1 ICI for patients who are prone to poor prognosis. However, neutralization is currently a key setback, especially with multiple doses and future emphasis should focus on exploring the immune mechanisms leading to this.

Another issue that lies with PD-1 therapies arises from NSCLC resistance to ICB. Treatment outcomes are not yet universal, but one theory shows that this might be mediated through carcinoma-associated fibroblasts (CAF), which also influence the CXCR4/CXCL12 axis (181). While the mechanism is not yet fully understood, it is hypothesized that

TABLE 10 Ongoing clinical trials testing cell-based therapies in combination with PD-1/PD-L1 checkpoint inhibitors.

Clinical Trial	Cancer Type	Intervention	Phase	Cell Therapy	Anti-PD-1/PD-L1	Primary Outcomes	N. Patients
NCT03525782	NSCLC	CAR-T Cell, +/- PD-1 knockout T-cell	I/II	CAR-T Cell, PD-1 knockout T-cell	pembrolizumab	AE, DLT	60
NCT04556669	Solid Tumor, NSCLC	Autologous aPD-L1 armored CD22-targeting CAR T cells	I	Autologous aPD-L1 armored CD22-targeting CAR T cells	Autologous aPD-L1	irAE	30
NCT05069935	Solid Tumor	FT538, +/- avelumab, +/- atezolizumab, +/- nivolumab, +/-pembrolizumab	I	FT538 allogeneic NK-Cell immunotherapy	avelumab, atezolizumab, nivolumab, pembrolizumab,	RP2D, AE	189
NCT03841110	NSCLC, Advanced Solid Tumors	FT500, +/- nivolumab, +/- pembrolizumab, +/- atezolizumab, +/- chemotherapy	I	FT500, an allogeneic, iPSC-derived Natural Killer (NK)	nivolumab, pembrolizumab, atezolizumab	DLT	37

CXCR4/CXCL12 axis and CAF may be responsible for resistance to ICB (182). For example, one ovarian mouse model with dual blockade CXCR4/CXL12 using AMD3100 and PD-1/PDL-1 showed increased effector T cell infiltration, function, and memory in tumors (183). Future advances on therapeutics targeting this axis should focus on optimal dosing and minimizing toxicity. VEGFR is another commonly overexpressed receptor found on NSCLC that can be used to overcome immune resistance to PD-1/PD-L1 drugs. A combination approach using anlotinib showed promising results in NSCLC clinical trials with significant improvements in OS and PFS. A targeted EGF TKI Erlotinib demonstrated additive effects with PD-1 drugs with a 19% ORR (48). However, a follow-up phase I/II study concluded no significant improvements in ORR between pembrolizumab monotherapy and the combination approach using Erlotinib (49). The early nature of these studies makes it difficult to conclude any solid findings. Furthermore, VEGF and EGF TKIs are prone to adaptive resistance to treatment by NSCLC, which could prove treatment in multiple doses to be ineffective or even create a more difficult disease to treat. These treatments may prove only beneficial in early-stage NSCLC since the larger the tumor gets, the harder it would be to clear it completely. If the tumor is harder to clear, more treatment dosages would be needed and, therefore, a higher likelihood for adaptive resistance to occur is present. Further data from phase I/II clinical trials found in Table 2 are waited for better understanding of this combination approach.

A universal challenge in cancer treatment lies in tumor evasion from immune detection. ICB has the potential to down regulate immune escape mechanism as they can directly suppress or stimulate the immune system. LAG-3/MHC-II binding complex has shown to play key roles in cancer immune escape. Anti-PD-1 combined with anti-LAG-3, therefore, poses promising synergy benefits and data from various clinical trials showed promising effects from dual block therapy in NSCLC (99–101). OX-40 has been shown to downregulate Treg function, while acting as a costimulatory cytokine for CD4+ and CD8+ T cells, with both functionalities corresponding to improve immune function. This combination approach demonstrates potential to increase immune response and infiltration of T cell into tumor region, a key setback of PD-1/PD-L1 monotherapy. However, in a phase I/II of BMS-986178, an OX-40 inhibitor combined with nivolumab/ipilimumab showed no clear benefit (110). It is unclear how exactly these two therapeutic agents work together; however, due to the boost in immune response, OX-40 does have the potential to improve NSCLC treatment efficacy and should be explored further. Another approach covered used an anti-TIGIT in combination with PD-1/PD-L1. CD155 is an upcoming immunotherapy with three distinct methods of binding that could lead to three different outcomes. The highest affinity TIGIT molecule showed promising result when combined with anti-PD-L1 in a phase II study testing tiragolumab in combination with atezolizumab. IL-2 is a circulating cytokine with multiple mechanisms of action in immune response *via* the JAK-STAT, PI3K/Akt/mTOR, and MAPK/ERK pathways. Low concentration of IL-2 led to increased immune suppression by binding to Treg, while increased levels led to immune activation by binding/activating NK and CD8+ T cells and were correlated with improved OS and better response to PD-1/PD-L1 blockade in NSCLC. Therefore, this cytokine can be used in combination approach as both as a therapeutic target and biomarker. However, it also important to note that combination of immunomodulators and PD-1/PD-L1 inhibitors led to a high number of AEs in some clinical trials. Additionally, BMS-986178 and OX-40 phase I/II clinical studies showed no increased benefits. It is possible that these combination regimes might only be effective for a specific patient group, categorizes by tumor receptor expression level, TME antigen concentration and stage of disease. Nonetheless, immunomodulators combined with PD-1/PD-L1 are promising and require further review for a better understanding of the complex immune activation mechanisms.

NK cells have been gaining a lot of momentum in recent years. Many variations of the NK cell type have been tested. NK cells have showed promising results *via* autologous transplantation. However, the procedure is expensive and time-consuming. Modified CAR-NK cells conceptually seemed like a promising approach. However, CAR models designed for T cells did not activate NK cells as they would in T cells. A promising approach used a metabolic glycan biosynthesis and click reaction to chemically bind dual aptamers to target cancers and regulate PD-1/PD-L1 signaling (167). Its interchangeable aptamers pose a way to effectively target a wide variety of NSCLC mutations and regulation of the PD-1/PD-L1 axis may increase the efficacy of PD-1 inhibitor drugs. It is important to note that this therapy is in very early stages and more studies are needed to validate these findings to begin entering this combination approach into clinical trials.

Another combination approach that led to increased immune activation was OV therapy. OV therapy can be used to activate TILs, suppress tumor growth, and alter the TME. These responses pose synergy effects to patients who do not respond to PD-1/PD-L1 inhibitors well and making this combination promising. Currently, six clinical trials are ongoing of PD-1/PD-L1 combined with OV therapy, and we await the data from these trials to gain a better understanding of an optimal combination approaches. A downside of the treatment is that extensive use of OV therapy arising from repeat administrations can lead to progressively weakened response and spread of viral infection due to rapid neutralization by the immune system (184). Hosts with normal immunity have shown decreased reduced anti-tumor activity, viral clearance, and oncolytic viral replication in various pre-clinical and phase I clinical studies (185–192). OV therapy,

which attempts to overcome these challenges, lies brought on by neutralization of the immune system through cell encapsulation (193), immunomodulators (194), and DNA aptamers (195, 196). The future of OV therapy needs to focus on optimal combination approaches, while minimizing neutralization and toxicity.

It is important to note that these combination strategies are the latest advances in the field of NSCLC treatment. Our current understanding of immunotherapy suggests that these treatments are promising. However, they might not be ideal for everyone. As these trials are still in early stages, results should still be treated with caution. Additionally, although not primarily focused on in this paper, chemotherapy and radiotherapy are effective cancer treatments with over 60% of patient's diagnosis at stage III/IV receiving a dose of one or other (197). The future of ICI therapy involves understanding of tumor immunology. Tumors continuously evolve throughout the disease causing a high level of spatial and temporal heterogeneity. In addition, intra- and inter-tumor regions also express heterogeneity throughout the different stages. This heterogeneity is a key hurdle in the way of predicting treatment outcomes accurately. To mainstream cancer treatment, it now understood that analyzing tumor genomics and immunomodulating activities are critical for increasing success rates. This "new-revolution" of cancer therapy directly relies on the use of the TME and tumor immunology as predictive biomarkers for the development of optimal combination approaches. These approaches can be achieved to directly target overexpression and suppressed immune pathways. It is known that each tumor demonstrates different levels of biologic expressions, and this varies greatly from person to person. The near future of the field will orientate more towards a personalized approach to first screen tumors for key antigens in the TME and expression levels of important receptors on NSCLC, such as PD-L1 and CT-L4. Ideally, a biopsy of the tumor will also be used to perform DNA assays and determine tumor mutations. Finally, early diagnosis has proven to be a key factor in lowering the mortality rate. Awareness needs to be spread to encourage periodic testing to those higher risk groups such as those exposed to cigarette smoke. As more data will be released, it will be necessary to create a system to gather, manipulate, and utilize the findings from combination PD-1/PD-L1 in clinical trials. Using data and machine learning models to diagnosis, creating treatment combinations and dosage regimes is the future of cancer therapy and, ultimately, is a feasible method to universally treat NSCLC, while bypassing the need for a universal treatment.

Author contributions

YW and WM designed the study and participated in coordination and project control. OM and JM wrote the manuscript. JM and OM prepared Tables. YW and WM revised the manuscript. All authors contributed to the article and approved the submitted version.

Funding

This work was supported by National Cancer Institute (1R01CA230339) subaward and 1R37CA255948), Natural Science Foundation of Jiangsu Province (BK20210068), and the High-end Medical Expert Team of the 2019 Taihu Talent Plan (2019-THRCTD-1).

Conflict of interest

The authors declare that the research was conducted in the absence of any commercial or financial relationships that could be construed as a potential conflict of interest.

Publisher's note

References

1. Yokosuka T, Takamatsu M, Kobayashi-Imanishi W, Hashimoto-Tane A, Azuma M, Saito T. Programmed cell death 1 forms negative costimulatory microclusters that directly inhibit T cell receptor signaling by recruiting phosphatase Shp2. *J Exp Med* (2012) 209 (6):1201–17. doi: 10.1084/jem.20112741

2. Liu Q, Qu J, Zhao M, Xu Q, Sun Y. Targeting Shp2 as a promising strategy for cancer immunotherapy. *Pharmacol Res* (2020) 152:104595. doi: 10.1016/j.phrs.2019.104595

3. Salmaninejad A, Valilou SF, Shabgah AG, Aslani S, Alimardani M, Pasdar A, et al. Pd-1/Pd-L1 pathway: Basic biology and role in cancer immunotherapy. *J Cell Physiol* (2019) 234(10):16824–37. doi: 10.1002/jcp.28358

4. Faghfuri E, Faramarzi MA, Nikfar S, Abdollahi M. Nivolumab and pembrolizumab as immune-modulating monoclonal antibodies targeting the pd-1 receptor to treat melanoma. *Expert Rev Anticancer Ther* (2015) 15(9):981–93. doi: 10.1586/14737140.2015.1074862

5. Arenas-Ramirez N, Woytschak J, Boyman O. Interleukin-2: Biology, design and application. *Trends Immunol* (2015) 36(12):763–77. doi: 10.1016/j.it.2015.10.003

6. Nguyen V, Mendelsohn A, Larrick JW. Interleukin-7 and immunosenescence. *J Immunol Res* (2017) 2017:4807853. doi: 10.1155/2017/4807853

7. Havel JJ, Chowell D, Chan TA. The evolving landscape of biomarkers for checkpoint inhibitor immunotherapy. *Nat Rev Cancer* (2019) 19(3):133–50. doi: 10.1038/s41568-019-0116-x

8. Khoja L, Butler MO, Kang SP, Ebbinghaus S, Joshua AM. Pembrolizumab. *J Immunother Cancer* (2015) 3:36. doi: 10.1186/s40425-015-0078-9

9. Miller KD, Nogueira L, Devasia T, Mariotto AB, Yabroff KR, Jemal A, et al. Cancer treatment and survivorship statistics, 2022. *CA Cancer J Clin* (2022) 0:1–28. Epub 2022/06/24. doi: 10.3322/caac.21731

10. Zappa C, Mousa SA. Non-small cell lung cancer: Current treatment and future advances. *Transl Lung Cancer Res* (2016) 5(3):288–300. doi: 10.21037/tlcr.2016.06.07

11. Garon EB, Rizvi NA, Hui R, Leighl N, Balmanoukian AS, Eder JP, et al. Pembrolizumab for the treatment of non-Small-Cell lung cancer. *N Engl J Med* (2015) 372(21):2018–28. doi: 10.1056/NEJMoa1501824

12. Borghaei H, Paz-Ares L, Horn L, Spigel DR, Steins M, Ready NE, et al. Nivolumab versus docetaxel in advanced nonsquamous non-Small-Cell lung cancer. *N Engl J Med* (2015) 373(17):1627–39. doi: 10.1056/NEJMoa1507643

13. Antonia SJ, Villegas A, Daniel D, Vicente D, Murakami S, Hui R, et al. Overall survival with durvalumab after chemoradiotherapy in stage iii nsclc. *N Engl J Med* (2018) 379(24):2342–50. doi: 10.1056/NEJMoa1809697

14. Casey SC, Tong L, Li Y, Do R, Walz S, Fitzgerald KN, et al. Myc regulates the antitumor immune response through Cd47 and pd-L1. *Science* (2016) 352 (6282):227–31. doi: 10.1126/science.aac9935

15. Horton BL, Williams JB, Cabanov A, Spranger S, Gajewski TF. Intratumoral Cd8(+) T-cell apoptosis is a major component of T-cell dysfunction and impedes antitumor immunity. *Cancer Immunol Res* (2018) 6(1):14–24. doi: 10.1158/2326-6066.Cir-17-0249

16. Gorbet MJ, Ranjan A. Cancer immunotherapy with immunoadjuvants, nanoparticles, and checkpoint inhibitors: Recent progress and challenges in treatment and tracking response to immunotherapy. *Pharmacol Ther* (2020) 207:107456. doi: 10.1016/j.pharmthera.2019.107456

17. Upadhaya S, Neftelinov ST, Hodge J, Campbell J. Challenges and opportunities in the Pd1/Pdl1 inhibitor clinical trial landscape. *Nat Rev Drug Discovery* (2022) 21:482–43. doi: 10.1038/d41573-022-00030-4

18. Attili I, Tarantino P, Passaro A, Stati V, Curigliano G, de Marinis F. Strategies to overcome resistance to immune checkpoint blockade in lung cancer. *Lung Cancer* (2021) 154:151–60. doi: 10.1016/j.lungcan.2021.02.035

19. Wang X, Niu X, An N, Sun Y, Chen Z. Comparative efficacy and safety of immunotherapy alone and in combination with chemotherapy for advanced non-small cell lung cancer. *Front Oncol* (2021) 11:611012. doi: 10.3389/fonc.2021.611012

20. Rodríguez-Abreu D, Powell SF, Hochmair MJ, Gadgeel S, Esteban E, Felip E, et al. Pemetrexed plus platinum with or without pembrolizumab in patients with previously untreated metastatic nonsquamous nsclc: Protocol-specified final analysis from keynote-189. *Ann Oncol* (2021) 32(7):881–95. doi: 10.1016/j.annonc.2021.04.008

21. Hammerich L, Binder A, Brody JD. *In situ* vaccination: Cancer immunotherapy both personalized and off-the-Shelf. *Mol Oncol* (2015) 9 (10):1966–81. doi: 10.1016/j.molonc.2015.10.016

22. Lizotte PH, Wen AM, Sheen MR, Fields J, Rojanasopondist P, Steinmetz NF, et al. *In situ* vaccination with cowpea mosaic virus nanoparticles suppresses metastatic cancer. *Nat Nanotechnol* (2016) 11(3):295–303. doi: 10.1038/nnano.2015.292

23. Schumacher TN, Schreiber RD. Neoantigens in cancer immunotherapy. *Science* (2015) 348(6230):69–74. doi: 10.1126/science.aaa4971

24. Hacohen N, Fritsch EF, Carter TA, Lander ES, Wu CJ. Getting personal with neoantigen-based therapeutic cancer vaccines. *Cancer Immunol Res* (2013) 1 (1):11–5. doi: 10.1158/2326-6066.Cir-13-0022

25. Zhang W, Yin Q, Huang H, Lu J, Qin H, Chen S, et al. Personal neoantigens from patients with nsclc induce efficient antitumor responses. *Front Oncol* (2021) 11:628456. doi: 10.3389/fonc.2021.628456

26. Li F, Deng L, Jackson KR, Talukder AH, Katailiha AS, Bradley SD, et al. Neoantigen vaccination induces clinical and immunologic responses in non-small cell lung cancer patients harboring egfr mutations. *J Immunother Cancer* (2021) 9 (7):e002531. doi: jitc-2020/jitc-2021-002531

27. Ott PA, Govindan R, Naing A, Friedlander TW, Margolin K, Lin JJ, et al. Abstract Ct125: A personal neoantigen vaccine, neo-Pv-01, with anti-Pd1 induces broad *De novo* anti-tumor immunity in patients with metastatic melanoma, nsclc, and bladder cancer. *Cancer Res* (2018) 78(13_Supplement):CT125–CT. doi: 10.1158/1538-7445.Am2018-ct125

28. Sigismund S, Avanzato D, Lanzetti L. Emerging functions of the egfr in cancer. *Mol Oncol* (2018) 12(1):3–20. doi: 10.1002/1878-0261.12155

29. Seshacharyulu P, Ponnusamy MP, Haridas D, Jain M, Ganti AK, Batra SK. Targeting the egfr signaling pathway in cancer therapy. *Expert Opin Ther Targets* (2012) 16(1):15–31. doi: 10.1517/14728222.2011.648617

30. Toyooka S, Mitsudomi T, Soh J, Aokage K, Yamane M, Oto T, et al. Molecular oncology of lung cancer. *Gen Thorac Cardiovasc Surg* (2011) 59(8):527–37. doi: 10.1007/s11748-010-0743-3

31. Volm M, Drings P, Wodrich W. Prognostic significance of the expression of c-fos, c-jun and c-Erbb-1 oncogene products in human squamous cell lung carcinomas. *J Cancer Res Clin Oncol* (1993) 119(9):507–10. doi: 10.1007/bf01686458

32. González G, Crombet T, Catalá M, Mirabal V, Hernández JC, González Y, et al. A novel cancer vaccine composed of human-recombinant epidermal growth factor linked to a carrier protein: Report of a pilot clinical trial. *Ann Oncol* (1998) 9 (4):431–5. doi: 10.1023/a:1008261031034

33. Rodriguez PC, Popa X, Martínez O, Mendoza S, Santiesteban E, Crespo T, et al. A phase iii clinical trial of the epidermal growth factor vaccine cimavax-egf as switch maintenance therapy in advanced non-small cell lung cancer patients. *Clin Cancer Res* (2016) 22(15):3782–90. doi: 10.1158/1078-0432.Ccr-15-0855

34. Dy G, Dozier A, Reid M, Lee K, Miller A, Wallace P, et al. P2.04-26 interim results from a phase I/Ii trial of nivolumab in combination with cimavax-egf as second-line therapy in advanced nsclc. *J Thorac Oncol* (2018) 13(10):S740. doi: 10.1016/j.jtho.2018.08.1250

35. Gettinger S, Rizvi NA, Chow LQ, Borghaei H, Brahmer J, Ready N, et al. Nivolumab monotherapy for first-line treatment of advanced non-Small-Cell lung cancer. *J Clin Oncol* (2016) 34(25):2980–7. doi: 10.1200/jco.2016.66.9929

36. Moncada DM, Kammanadiminti SJ, Chadee K. Mucin and toll-like receptors in host defense against intestinal parasites. *Trends Parasitol* (2003) 19 (7):305–11. doi: 10.1016/s1471-4922(03)00122-3

37. Gendler SJ. Muc1, the renaissance molecule. *J Mammary Gland Biol Neoplasia* (2001) 6(3):339–53. doi: 10.1023/a:1011379725811

38. Nath S, Mukherjee P. Muc1: A multifaceted oncoprotein with a key role in cancer progression. *Trends Mol Med* (2014) 20(6):332–42. doi: 10.1016/j.molmed.2014.02.007

39. Quoix E, Lena H, Losonczy G, Forget F, Chouaid C, Papai Z, et al. Tg4010 immunotherapy and first-line chemotherapy for advanced non-Small-Cell lung cancer (Time): Results from the phase 2b part of a randomised, double-blind, placebo-controlled, phase 2b/3 trial. *Lancet Oncol* (2016) 17(2):212–23. doi: 10.1016/s1470-2045(15)00483-0

40. Ock CY, Keam B, Kim S, Lee JS, Kim M, Kim TM, et al. Pan-cancer immunogenomic perspective on the tumor microenvironment based on pd-L1 and Cd8 T-cell infiltration. *Clin Cancer Res* (2016) 22(9):2261–70. doi: 10.1158/1078-0432.Ccr-15-2834

41. Karlsson-Parra A, Kovacka J, Heimann E, Jorvid M, Zeilemaker S, Longhurst S, et al. Ilixadencel - an allogeneic cell-based anticancer immune primer for intratumoral administration. *Pharm Res* (2018) 35(8):156. doi: 10.1007/s11095-018-2438-x

42. Martinelli E, De Palma R, Orditura M, De Vita F, Ciardiello F. Anti-epidermal growth factor receptor monoclonal antibodies in cancer therapy. *Clin Exp Immunol* (2009) 158(1):1–9. doi: 10.1111/j.1365-2249.2009.03992.x

43. Ferris RL, Lenz HJ, Trotta AM, García-Foncillas J, Schulten J, Audhuy F, et al. Rationale for combination of therapeutic antibodies targeting tumor cells and immune checkpoint receptors: Harnessing innate and adaptive immunity through Igg1 isotype immune effector stimulation. *Cancer Treat Rev* (2018) 63:48–60. doi: 10.1016/j.ctrv.2017.11.008

44. Besse B, Garrido P, Cortot AB, Johnson M, Murakami H, Gazzah A, et al. Efficacy and safety of necitumumab and pembrolizumab combination therapy in patients with stage iv non-small cell lung cancer. *Lung Cancer* (2020) 142:63–9. doi: 10.1016/j.lungcan.2020.02.003

45. Andric ZG, Gálffy G, Dols MC, Szima B, Stojanovic G, Petrovic MD, et al. 103p first-line avelumab in combination with cetuximab and chemotherapy in patients with advanced squamous non-small cell lung cancer (Nsclc). *J Thorac Oncol* (2021) 16(4):S753–S4. doi: 10.1016/S1556-0864(21)01945-6

46. Seto T, Nosaki K, Shimokawa M, Toyozawa R, Sugawara S, Hayashi H, et al. Lba55 wjog @Be study: A phase ii study of atezolizumab (Atez) with bevacizumab (Bev) for non-squamous (Sq) non-small cell lung cancer (Nsclc) with high pd-L1 expression. *Ann Oncol* (2020) 31:S1185–S6. doi: 10.1016/j.annonc.2020.08.2288

47. Ahn MJ, Sun JM, Lee SH, Ahn JS, Park K. Egfr tki combination with immunotherapy in non-small cell lung cancer. *Expert Opin Drug Saf* (2017) 16 (4):465–9. doi: 10.1080/14740338.2017.1300656

48. Gettinger S, Hellmann MD, Chow LQM, Borghaei H, Antonia S, Brahmer JR, et al. Nivolumab plus erlotinib in patients with egfr-mutant advanced nsclc. *J Thorac Oncol* (2018) 13(9):1363–72. doi: 10.1016/j.jtho.2018.05.015

49. Yang JC, Gadgeel SM, Sequist LV, Wu CL, Papadimitrakopoulou VA, Su WC, et al. Pembrolizumab in combination with erlotinib or gefitinib as first-line therapy for advanced nsclc with sensitizing egfr mutation. *J Thorac Oncol* (2019) 14 (3):553–9. doi: 10.1016/j.jtho.2018.11.028

50. Reck M, Rodríguez-Abreu D, Robinson AG, Hui R, Csőszi T, Fülöp A, et al. Pembrolizumab versus chemotherapy for pd-L1-Positive non-Small-Cell lung cancer. *N Engl J Med* (2016) 375(19):1823–33. doi: 10.1056/NEJMoa1606774

51. Giaccone G, Gallegos Ruiz M, Le Chevalier T, Thatcher N, Smit E, Rodriguez JA, et al. Erlotinib for frontline treatment of advanced non-small cell lung cancer: A phase ii study. *Clin Cancer Res* (2006) 12(20 Pt 1):6049–55. doi: 10.1158/1078-0432.Ccr-06-0260

52. Klughammer B, Brugger W, Cappuzzo F, Ciuleanu T, Mok T, Reck M, et al. Examining treatment outcomes with erlotinib in patients with advanced non-small cell lung cancer whose tumors harbor uncommon egfr mutations. *J Thorac Oncol* (2016) 11(4):545–55. doi: 10.1016/j.jtho.2015.12.107

53. Shen G, Zheng F, Ren D, Du F, Dong Q, Wang Z, et al. Anlotinib: A novel multi-targeting tyrosine kinase inhibitor in clinical development. *J Hematol Oncol* (2018) 11(1):120. doi: 10.1186/s13045-018-0664-7

54. Han B, Li K, Zhao Y, Li B, Cheng Y, Zhou J, et al. Anlotinib as a third-line therapy in patients with refractory advanced non-Small-Cell lung cancer: A multicentre, randomised phase ii trial (Alter0302). *Br J Cancer* (2018) 118 (5):654–61. doi: 10.1038/bjc.2017.478

55. Chu T, Zhong R, Zhong H, Zhang B, Zhang W, Shi C, et al. Phase 1b study of sintilimab plus anlotinib as first-line therapy in patients with advanced nsclc. *J Thorac Oncol* (2021) 16(4):643–52. doi: 10.1016/j.jtho.2020.11.026

56. Liu P, Wang Y, Li X. Targeting the untargetable kras in cancer therapy. *Acta Pharm Sin B* (2019) 9(5):871–9. doi: 10.1016/j.apsb.2019.03.002

57. Fallarino F, Grohmann U, Vacca C, Bianchi R, Orabona C, Spreca A, et al. T Cell apoptosis by tryptophan catabolism. *Cell Death Differ* (2002) 9(10):1069–77. doi: 10.1038/sj.cdd.4401073

58. Labadie BW, Bao R, Luke JJ. Reimagining ido pathway inhibition in cancer immunotherapy *Via* downstream focus on the tryptophan-Kynurenine-Aryl hydrocarbon axis. *Clin Cancer Res* (2019) 25(5):1462–71. doi: 10.1158/1078-0432.Ccr-18-2882

59. Munn DH. Indoleamine 2,3-dioxygenase, tumor-induced tolerance and counter-regulation. *Curr Opin Immunol* (2006) 18(2):220–5. doi: 10.1016/j.coi.2006.01.002

60. Botticelli A, Cerbelli B, Lionetto L, Zizzari I, Salati M, Pisano A, et al. Can ido activity predict primary resistance to anti-Pd-1 treatment in nsclc? *J Transl Med* (2018) 16(1):219. doi: 10.1186/s12967-018-1595-3

61. Mitchell TC, Hamid O, Smith DC, Bauer TM, Wasser JS, Olszanski AJ, et al. Epacadostat plus pembrolizumab in patients with advanced solid tumors: Phase I results from a multicenter, open-label phase I/Ii trial (Echo-202/Keynote-037). *J Clin Oncol* (2018) 36(32):3223–30. doi: 10.1200/jco.2018.78.9602

62. Long GV, Dummer R, Hamid O, Gajewski TF, Caglevic C, Dalle S, et al. Epacadostat plus pembrolizumab versus placebo plus pembrolizumab in patients with unresectable or metastatic melanoma (Echo-301/Keynote-252): A phase 3, randomised, double-blind study. *Lancet Oncol* (2019) 20(8):1083–97. doi: 10.1016/s1470-2045(19)30274-8

63. Jung KH, LoRusso P, Burris H, Gordon M, Bang YJ, Hellmann MD, et al. Phase I study of the indoleamine 2,3-dioxygenase 1 (Ido1) inhibitor navoximod (Gdc-0919) administered with pd-L1 inhibitor (Atezolizumab) in advanced solid tumors. *Clin Cancer Res* (2019) 25(11):3220–8. doi: 10.1158/1078-0432.Ccr-18-2740

64. Kroemer G, Galluzzi L, Kepp O, Zitvogel L. Immunogenic cell death in cancer therapy. *Annu Rev Immunol* (2013) 31:51–72. doi: 10.1146/annurev-immunol-032712-100008

65. Kepp O, Senovilla L, Vitale I, Vacchelli E, Adjemian S, Agostinis P, et al. Consensus guidelines for the detection of immunogenic cell death. *Oncoimmunology* (2014) 3(9):e955691. doi: 10.4161/21624011.2014.955691

66. Gujar S, Pol JG, Kroemer G. Heating it up: Oncolytic viruses make tumors 'Hot' and suitable for checkpoint blockade immunotherapies. *Oncoimmunology* (2018) 7(8):e1442169. doi: 10.1080/2162402x.2018.1442169

67. Galon J, Costes A, Sanchez-Cabo F, Kirilovsky A, Mlecnik B, Lagorce-Pagès C, et al. Type, density, and location of immune cells within human colorectal tumors predict clinical outcome. *Science* (2006) 313(5795):1960–4. doi: 10.1126/science.1129139

68. Gajewski TF, Schreiber H, Fu YX. Innate and adaptive immune cells in the tumor microenvironment. *Nat Immunol* (2013) 14(10):1014–22. doi: 10.1038/ni.2703

69. Tran Janco JM, Lamichhane P, Karyampudi L, Knutson KL. Tumor-infiltrating dendritic cells in cancer pathogenesis. *J Immunol* (2015) 194 (7):2985–91. doi: 10.4049/jimmunol.1403134

70. Lanitis E, Dangaj D, Irving M, Coukos G. Mechanisms regulating T-cell infiltration and activity in solid tumors. *Ann Oncol* (2017) 28(suppl_12):xii18–32. doi: 10.1093/annonc/mdx238

71. Bilir C, Sarisozen C. Indoleamine 2,3-dioxygenase (Ido): Only an enzyme or a checkpoint controller? *J Oncol Sci* (2017) 3(2):52–6. doi: 10.1016/j.jons.2017.04.001

72. Antonioli L, Yegutkin GG, Pacher P, Blandizzi C, Haskó G. Anti-Cd73 in cancer immunotherapy: Awakening new opportunities. *Trends Cancer* (2016) 2 (2):95–109. doi: 10.1016/j.trecan.2016.01.003

73. Ribas A, Dummer R, Puzanov I, VanderWalde A, Andtbacka RHI, Michielin O, et al. Oncolytic virotherapy promotes intratumoral T cell infiltration and improves anti-Pd-1 immunotherapy. *Cell* (2017) 170(6):1109–19.e10. doi: 10.1016/j.cell.2017.08.027

74. Endo Y, Sakai R, Ouchi M, Onimatsu H, Hioki M, Kagawa S, et al. Virus-mediated oncolysis induces danger signal and stimulates cytotoxic T-lymphocyte activity *Via* proteasome activator upregulation. *Oncogene* (2008) 27(17):2375–81. doi: 10.1038/sj.onc.1210884

75. Achard C, Boisgerault N, Delaunay T, Tangy F, Grégoire M, Fonteneau J-F. Induction of immunogenic tumor cell death by attenuated oncolytic measles virus. *J Clin Cell Immunol* (2015) 6(1):291. doi: 10.4172/2155-9899.1000291

76. Kaufman HL, Kohlhapp FJ, Zloza A. Oncolytic viruses: A new class of immunotherapy drugs. *Nat Rev Drug Discovery* (2015) 14(9):642–62. doi: 10.1038/nrd4663

77. Lin CZ, Xiang GL, Zhu XH, Xiu LL, Sun JX, Zhang XY. Advances in the mechanisms of action of cancer-targeting oncolytic viruses. *Oncol Lett* (2018) 15 (4):4053–60. doi: 10.3892/ol.2018.7829

78. Senior M. Checkpoint inhibitors go viral. *Nat Biotechnol* (2019) 37(1):12–7. doi: 10.1038/nbt.4327

79. Ajina A, Maher J. Prospects for combined use of oncolytic viruses and car T-cells. *J Immunother Cancer* (2017) 5(1):90. doi: 10.1186/s40425-017-0294-6

80. Chon HJ, Lee WS, Yang H, Kong SJ, Lee NK, Moon ES, et al. Tumor microenvironment remodeling by intratumoral oncolytic vaccinia virus enhances the efficacy of immune-checkpoint blockade. *Clin Cancer Res* (2019) 25(5):1612–23. doi: 10.1158/1078-0432.Ccr-18-1932

81. Pandha HS, Ralph C, Harrington K, Curti BD, Sanborn RE, Akerley WL, et al. Keynote-200 phase 1b: A novel combination study of intravenously delivered coxsackievirus A21 and pembrolizumab in advanced cancer patients. *J Clin Oncol* (2017) 35(15_suppl):TPS3108–TPS. doi: 10.1200/JCO.2017.35.15_suppl.TPS3108

82. Walker LS, Sansom DM. The emerging role of Ctla4 as a cell-extrinsic regulator of T cell responses. *Nat Rev Immunol* (2011) 11(12):852–63. doi: 10.1038/nri3108

83. Lipson EJ, Drake CG. Ipilimumab: An anti-Ctla-4 antibody for metastatic melanoma. *Clin Cancer Res* (2011) 17(22):6958–62. doi: 10.1158/1078-0432.CCR-11-1595

84. Larkin J, Chiarion-Sileni V, Gonzalez R, Grob JJ, Cowey CL, Lao CD, et al. Combined nivolumab and ipilimumab or monotherapy in untreated melanoma. *N Engl J Med* (2015) 373(1):23–34. doi: 10.1056/NEJMoa1504030

85. Wolchok JD, Chiarion-Sileni V, Gonzalez R, Rutkowski P, Grob JJ, Cowey CL, et al. Overall survival with combined nivolumab and ipilimumab in advanced melanoma. *N Engl J Med* (2017) 377(14):1345–56. doi: 10.1056/NEJMoa1709684

86. Hellmann MD, Rizvi NA, Goldman JW, Gettinger SN, Borghaei H, Brahmer JR, et al. Nivolumab plus ipilimumab as first-line treatment for advanced non-Small-Cell lung cancer (Checkmate 012): Results of an open-label, phase 1, multicohort study. *Lancet Oncol* (2017) 18(1):31–41. doi: 10.1016/S1470-2045(16)30624-6

87. Ready N, Hellmann MD, Awad MM, Otterson GA, Gutierrez M, Gainor JF, et al. First-line nivolumab plus ipilimumab in advanced non-Small-Cell lung cancer (Checkmate 568): Outcomes by programmed death ligand 1 and tumor mutational burden as biomarkers. *J Clin Oncol* (2019) 37(12):992–1000. doi: 10.1200/JCO.18.01042

88. Hellmann MD, Paz-Ares L, Bernabe Caro R, Zurawski B, Kim SW, Carcereny Costa E, et al. Nivolumab plus ipilimumab in advanced non-Small-Cell lung cancer. *N Engl J Med* (2019) 381(21):2020–31. doi: 10.1056/NEJMoa1910231

89. Paz-Ares L, Ciuleanu TE, Cobo M, Schenker M, Zurawski B, Menezes J, et al. First-line nivolumab plus ipilimumab combined with two cycles of chemotherapy in patients with non-Small-Cell lung cancer (Checkmate 9la): An international, randomised, open-label, phase 3 trial. *Lancet Oncol* (2021) 22 (2):198–211. doi: 10.1016/S1470-2045(20)30641-0

90. John T, Sakai H, Ikeda S, Cheng Y, Kasahara K, Sato Y, et al. First-line nivolumab plus ipilimumab combined with two cycles of chemotherapy in advanced non-small cell lung cancer: A subanalysis of Asian patients in checkmate 9la. *Int J Clin Oncol* (2022) 27(4):695–706. doi: 10.1007/s10147-022-02120-0

91. Gettinger SN, Redman MW, Bazhenova L, Hirsch FR, Mack PC, Schwartz LH, et al. Nivolumab plus ipilimumab vs nivolumab for previously treated patients with stage iv squamous cell lung cancer: The lung-map S1400i phase 3 randomized clinical trial. *JAMA Oncol* (2021) 7(9):1368–77. doi: 10.1001/jamaoncol.2021.2209

92. Boyer M, Sendur MAN, Rodriguez-Abreu D, Park K, Lee DH, Cicin I, et al. Pembrolizumab plus ipilimumab or placebo for metastatic non-Small-Cell lung cancer with pd-L1 tumor proportion score >/= 50%: Randomized, double-blind phase iii keynote-598 study. *J Clin Oncol* (2021) 39(21):2327–38. doi: 10.1200/JCO.20.03579

93. Gubens MA, Sequist LV, Stevenson JP, Powell SF, Villaruz LC, Gadgeel SM, et al. Pembrolizumab in combination with ipilimumab as second-line or later therapy for advanced non-Small-Cell lung cancer: Keynote-021 cohorts d and h. *Lung Cancer* (2019) 130:59–66. doi: 10.1016/j.lungcan.2018.12.015

94. Wong DJ, Bauer TM, Gordon MS, Bene-Tchaleu F, Zhu J, Zhang X, et al. Safety and clinical activity of atezolizumab plus ipilimumab in locally advanced or metastatic non-small cell lung cancer: Results from a phase 1b trial. *Clin Lung Cancer* (2022) 23(3):273–81. doi: 10.1016/j.cllc.2021.07.002

95. Goldberg MV, Drake CG. Lag-3 in cancer immunotherapy. *Curr Top Microbiol Immunol* (2011) 344:269–78. doi: 10.1007/82_2010_114

96. Donia M, Andersen R, Kjeldsen JW, Fagone P, Munir S, Nicoletti F, et al. Aberrant expression of mhc class ii in melanoma attracts inflammatory tumor-specific Cd4+ T- cells, which dampen Cd8+ T-cell antitumor reactivity. *Cancer Res* (2015) 75(18):3747–59. doi: 10.1158/0008-5472.Can-14-2956

97. Ruffo E, Wu RC, Bruno TC, Workman CJ, Vignali DAA. Lymphocyte-activation gene 3 (Lag3): The next immune checkpoint receptor. *Semin Immunol* (2019) 42:101305. doi: 10.1016/j.smim.2019.101305

98. Juncker-Jensen A, Nagy M, Kuo J, Leones E, Sahafi F, Pham K, et al. Pd-1 and lag-3 synergize to drive tumour-infiltration of T cytotoxic cells in nsclc tumours. *Ann Oncol* (2019) 30:xi48–xi9. doi: 10.1093/annonc/mdz452.002

99. Uboha NV, Milhem MM, Kovacs C, Amin A, Magley A, Purkayastha DD, et al. Phase ii study of spartalizumab (Pdr001) and Lag525 in advanced solid tumors and hematologic malignancies. *J Clin Oncol* (2019) 37(15_suppl):2553. doi: 10.1200/JCO.2019.37.15_suppl.2553

100. Ascierto PA, Bono P, Bhatia S, Melero I, Nyakas MS, Svane IM, et al. Efficacy of bms-986016, a monoclonal antibody that targets lymphocyte activation gene-3 (Lag-3), in combination with nivolumab in pts with melanoma who progressed during prior anti-Pd-1/Pd-L1 therapy (Mel prior io) in all-comer and biomarker-enriched populations. *Ann Oncol* (2017) 28:v611–v2. doi: 10.1093/annonc/mdx440.011

101. Peguero JA, Bajaj P, Carcereny E, Clay TD, Doger B, Felip E, et al. A multicenter, phase ii study of soluble lag-3 (Eftilagimod alpha) in combination with pembrolizumab (Tacti-002) in patients with advanced non-small cell lung cancer (Nsclc) or head and neck squamous cell carcinoma (Hnscc). *J Clin Oncol* (2019) 37 (15_suppl):TPS2667–TPS. doi: 10.1200/JCO.2019.37.15_suppl.TPS2667

102. Croft M, So T, Duan W, Soroosh P. The significance of Ox40 and Ox40l to T-cell biology and immune disease. *Immunol Rev* (2009) 229(1):173–91. doi: 10.1111/j.1600-065X.2009.00766.x

103. Vu MD, Xiao X, Gao W, Degauque N, Chen M, Kroemer A, et al. Ox40 costimulation turns off Foxp3+ tregs. *Blood* (2007) 110(7):2501–10. doi: 10.1182/blood-2007-01-070748

104. Weinberg AD, Rivera MM, Prell R, Morris A, Ramstad T, Vetto JT, et al. Engagement of the ox-40 receptor in vivo enhances antitumor immunity. *J Immunol* (2000) 164(4):2160–9. doi: 10.4049/jimmunol.164.4.2160

105. Blankenstein T, Coulie PG, Gilboa E, Jaffee EM. The determinants of tumour immunogenicity. *Nat Rev Cancer* (2012) 12(4):307–13. doi: 10.1038/nrc3246

106. Messenheimer DJ, Jensen SM, Afentoulis ME, Wegmann KW, Feng Z, Friedman DJ, et al. Timing of pd-1 blockade is critical to effective combination immunotherapy with anti-Ox40. *Clin Cancer Res* (2017) 23(20):6165–77. doi: 10.1158/1078-0432.Ccr-16-2677

107. Kunert A, Basak EA, Hurkmans DP, Balcioglu HE, Klaver Y, van Brakel M, et al. Cd45ra≪Sup<+≪/Sup<Ccr7≪Sup<-≪/Sup< Cd8 T cells lacking Co-stimulatory receptors demonstrate enhanced frequency in peripheral blood of nsclc patients responding to nivolumab. *J Immunother Cancer* (2019) 7(1):149. doi: 10.1186/s40425-019-0608-y

108. Infante JR, Ahlers CM, Hodi FS, Postel-Vinay S, Schellens JHM, Heymach J, et al. Engage-1: A first in human study of the Ox40 agonist Gsk3174998 alone and in combination with pembrolizumab in patients with advanced solid tumors. *J Clin Oncol* (2016) 34(15_suppl):TPS3107–TPS. doi: 10.1200/JCO.2016.34.15_suppl.TPS3107

109. Goldman JW, Piha-Paul SA, Curti BD, Pedersen K, Bauer TM, Groenland SL, et al. Safety and tolerability of Medi0562 in combination with durvalumab or tremelimumab in patients with advanced solid tumors. *J Clin Oncol* (2020) 38 (15_suppl):3003. doi: 10.1200/JCO.2020.38.15_suppl.3003

110. Gutierrez M, Moreno V, Heinhuis KM, Olszanski AJ, Spreafico A, Ong M, et al. Ox40 agonist bms-986178 alone or in combination with nivolumab and/or ipilimumab in patients with advanced solid tumors. *Clin Cancer Res* (2021) 27 (2):460–72. doi: 10.1158/1078-0432.Ccr-20-1830

111. Kučan Brlić P, Lenac Roviš T, Cinamon G, Tsukerman P, Mandelboim O, Jonjić S. Targeting pvr (Cd155) and its receptors in anti-tumor therapy. *Cell Mol Immunol* (2019) 16(1):40–52. doi: 10.1038/s41423-018-0168-y

112. Molfetta R, Zitti B, Lecce M, Milito ND, Stabile H, Fionda C, et al. Cd155: A multi-functional molecule in tumor progression. *Int J Mol Sci* (2020) 21(3):922. doi: 10.3390/ijms21030922

113. Gilfillan S, Chan CJ, Cella M, Haynes NM, Rapaport AS, Boles KS, et al. Dnam-1 promotes activation of cytotoxic lymphocytes by nonprofessional antigen-presenting cells and tumors. *J Exp Med* (2008) 205(13):2965–73. doi: 10.1084/jem.20081752

114. Pende D, Spaggiari GM, Marcenaro S, Martini S, Rivera P, Capobianco A, et al. Analysis of the receptor-ligand interactions in the natural killer-mediated lysis of freshly isolated myeloid or lymphoblastic leukemias: Evidence for the involvement of the poliovirus receptor (Cd155) and nectin-2 (Cd112). *Blood* (2005) 105(5):2066–73. doi: 10.1182/blood-2004-09-3548

115. Fourcade J, Sun Z, Chauvin JM, Ka M, Davar D, Pagliano O, et al. Cd226 opposes tigit to disrupt tregs in melanoma. *JCI Insight* (2018) 3(14):e121157. doi: 10.1172/jci.insight.121157

116. Johnston RJ, Comps-Agrar L, Hackney J, Yu X, Huseni M, Yang Y, et al. The immunoreceptor tigit regulates antitumor and antiviral Cd8(+) T cell effector function. *Cancer Cell* (2014) 26(6):923–37. doi: 10.1016/j.ccell.2014.10.018

117. Dixon KO, Schorer M, Nevin J, Etminan Y, Amoozgar Z, Kondo T, et al. Functional anti-tigit antibodies regulate development of autoimmunity and antitumor immunity. *J Immunol* (2018) 200(8):3000–7. doi: 10.4049/jimmunol.1700407

118. Rodriguez-Abreu D, Johnson ML, Hussein MA, Cobo M, Patel AJ, Secen NM, et al. Primary analysis of a randomized, double-blind, phase ii study of the anti-tigit antibody tiragolumab (Tira) plus atezolizumab (Atezo) versus placebo plus atezo as first-line (1l) treatment in patients with pd-L1-Selected nsclc (Cityscape). *J Clin Oncol* (2020) 38(15_suppl):9503–. doi: 10.1200/JCO.2020.38.15_suppl.9503

119. Chan CJ, Martinet L, Gilfillan S, Souza-Fonseca-Guimaraes F, Chow MT, Town L, et al. The receptors Cd96 and Cd226 oppose each other in the regulation of natural killer cell functions. *Nat Immunol* (2014) 15(5):431–8. doi: 10.1038/ni.2850

120. Blake SJ, Stannard K, Liu J, Allen S, Yong MC, Mittal D, et al. Suppression of metastases using a new lymphocyte checkpoint target for cancer immunotherapy. *Cancer Discovery* (2016) 6(4):446–59. doi: 10.1158/2159-8290.Cd-15-0944

121. Tahara-Hanaoka S, Shibuya K, Onoda Y, Zhang H, Yamazaki S, Miyamoto A, et al. Functional characterization of dnam-1 (Cd226) interaction with its ligands pvr (Cd155) and nectin-2 (Prr-2/Cd112). *Int Immunol* (2004) 16(4):533–8. doi: 10.1093/intimm/dxh059

122. Zhu Y, Paniccia A, Schulick AC, Chen W, Koenig MR, Byers JT, et al. Identification of Cd112r as a novel checkpoint for human T cells. *J Exp Med* (2016) 213(2):167–76. doi: 10.1084/jem.20150785

123. Levy O, Christopher C, Cojocaru G, Liang SC, Ophir E, Ganguly S, et al. Abstract 581: Discovery and development of Com701, a therapeutic antibody targeting the novel immune checkpoint pvrig. *Cancer Res* (2017) 77:581–. doi: 10.1158/1538-7445.AM2017-581

124. Boyman O, Sprent J. The role of interleukin-2 during homeostasis and activation of the immune system. *Nat Rev Immunol* (2012) 12(3):180–90. doi: 10.1038/nri3156

125. Boyman O, Kovar M, Rubinstein MP, Surh CD, Sprent J. Selective stimulation of T cell subsets with antibody-cytokine immune complexes. *Science* (2006) 311(5769):1924–7. doi: 10.1126/science.1122927

126. Wang X, Rickert M, Garcia KC. Structure of the quaternary complex of interleukin-2 with its alpha, beta, and gammac receptors. *Science* (2005) 310 (5751):1159–63. doi: 10.1126/science.1117893

127. Rickert M, Wang X, Boulanger MJ, Goriatcheva N, Garcia KC. The structure of interleukin-2 complexed with its alpha receptor. *Science* (2005) 308 (5727):1477–80. doi: 10.1126/science.1109745

128. Lee JY, Lee E, Hong SW, Kim D, Eunju O, Sprent J, et al. Tcb2, a new anti-human interleukin-2 antibody, facilitates heterodimeric il-2 receptor signaling and improves anti-tumor immunity. *Oncoimmunology* (2020) 9(1):1681869. doi: 10.1080/2162402x.2019.1681869

129. Diab A, Tannir NM, Bentebibel SE, Hwu P, Papadimitrakopoulou V, Haymaker C, et al. Bempegaldesleukin (Nktr-214) plus nivolumab in patients with advanced solid tumors: Phase I dose-escalation study of safety, efficacy, and immune activation (Pivot-02). *Cancer Discovery* (2020) 10(8):1158–73. doi: 10.1158/2159-8290.Cd-19-1510

130. Boutsikou E, Domvri K, Hardavella G, Tsiouda D, Zarogoulidis K, Kontakiotis T. Tumour necrosis factor, interferon-gamma and interleukins as predictive markers of antiprogrammed cell-death protein-1 treatment in advanced non-small cell lung cancer: A pragmatic approach in clinical practice. *Ther Adv Med Oncol* (2018) 10:1758835918768238. doi: 10.1177/1758835918768238

131. O'Leary MC, Lu X, Huang Y, Lin X, Mahmood I, Przepiorka D, et al. Fda approval summary: Tisagenlecleucel for treatment of patients with relapsed or refractory b-cell precursor acute lymphoblastic leukemia. *Clin Cancer Res* (2019) 25 (4):1142–6. doi: 10.1158/1078-0432.Ccr-18-2035

132. Bouchkouj N, Kasamon YL, de Claro RA, George B, Lin X, Lee S, et al. Fda approval summary: Axicabtagene ciloleucel for relapsed or refractory Large b-cell lymphoma. *Clin Cancer Res* (2019) 25(6):1702–8. doi: 10.1158/1078-0432.Ccr-18-2743

133. Doroshow DB, Sanmamed MF, Hastings K, Politi K, Rimm DL, Chen L, et al. Immunotherapy in non-small cell lung cancer: Facts and hopes. *Clin Cancer Res* (2019) 25(15):4592–602. doi: 10.1158/1078-0432.Ccr-18-1538

134. Qu J, Mei Q, Chen L, Zhou J. Chimeric antigen receptor (Car)-T-Cell therapy in non-Small-Cell lung cancer (Nsclc): Current status and future perspectives. *Cancer Immunol Immunother* (2021) 70(3):619–31. doi: 10.1007/s00262-020-02735-0

135. Zhang C, Leighl NB, Wu Y-L, Zhong W-Z. Emerging therapies for non-small cell lung cancer. *J Hematol Oncol* (2019) 12(1):45. doi: 10.1186/s13045-019-0731-8

136. Locke FL, Ghobadi A, Jacobson CA, Miklos DB, Lekakis LJ, Oluwole OO, et al. Long-term safety and activity of axicabtagene ciloleucel in refractory Large b-cell lymphoma (Zuma-1): A single-arm, multicentre, phase 1-2 trial. *Lancet Oncol* (2019) 20(1):31–42. doi: 10.1016/s1470-2045(18)30864-7

137. John LB, Devaud C, Duong CP, Yong CS, Beavis PA, Haynes NM, et al. Anti-Pd-1 antibody therapy potently enhances the eradication of established tumors by gene-modified T cells. *Clin Cancer Res* (2013) 19(20):5636–46. doi: 10.1158/1078-0432.Ccr-13-0458

138. Chen S, Lin Y, Zhong S, An H, Lu Y, Yin M, et al. Anti-Muc1 car-T cells combined with pd-1 knockout engineered T cells for patients with non-small cell lung cancer (Nsclc): A pilot study. *Ann Oncol* (2018) 29:x11. doi: 10.1093/annonc/mdy485.002

139. Lin Y, Chen S, Zhong S, An H, Yin H, McGowan E. 35o - phase I clinical trial of pd-1 knockout anti-Muc1 car-T cells in the treatment of patients with non-small cell lung cancer. *Ann Oncol* (2019) 30:xi12. doi: 10.1093/annonc/mdz448

140. Enblad G, Karlsson H, Gammelgård G, Wenthe J, Lövgren T, Amini RM, et al. A phase I/Iia trial using Cd19-targeted third-generation car T cells for lymphoma and leukemia. *Clin Cancer Res* (2018) 24(24):6185–94. doi: 10.1158/1078-0432.Ccr-18-0426

141. Shah NN, Highfill SL, Shalabi H, Yates B, Jin J, Wolters PL, et al. Cd4/Cd8 T-cell selection affects chimeric antigen receptor (Car) T-cell potency and toxicity: Updated results from a phase I anti-Cd22 car T-cell trial. *J Clin Oncol* (2020) 38 (17):1938–50. doi: 10.1200/jco.19.03279

142. Baumeister SH, Murad J, Werner L, Daley H, Trebeden-Negre H, Gicobi JK, et al. Phase I trial of autologous car T cells targeting Nkg2d ligands in patients with Aml/Mds and multiple myeloma. *Cancer Immunol Res* (2019) 7(1):100–12. doi: 10.1158/2326-6066.Cir-18-0307

143. Dong W, Wu X, Ma S, Wang Y, Nalin AP, Zhu Z, et al. The mechanism of anti-Pd-L1 antibody efficacy against pd-L1-Negative tumors identifies nk cells expressing pd-L1 as a cytolytic effector. *Cancer Discovery* (2019) 9(10):1422–37. doi: 10.1158/2159-8290.Cd-18-1259

144. Kokowski K, Stangl S, Seier S, Hildebrandt M, Vaupel P, Multhoff G. Radiochemotherapy combined with nk cell transfer followed by second-line pd-1 inhibition in a patient with nsclc stage iiib inducing long-term tumor control: A case study. *Strahlenther Onkol* (2019) 195(4):352–61. doi: 10.1007/s00066-019-01434-9

145. Lin M, Luo H, Liang S, Chen J, Liu A, Niu L, et al. Pembrolizumab plus allogeneic nk cells in advanced non-small cell lung cancer patients. *J Clin Invest* (2020) 130(5):2560–9. doi: 10.1172/jci132712

146. Poznanski SM, Ritchie TM, Fan IY, El-Sayes A, Portillo AL, Ben-Avi R, et al. Expanded human nk cells from lung cancer patients sensitize patients' Pdl1-negative tumors to Pd1-blockade therapy. *J Immunother Cancer* (2021) 9(1): e001933. doi: jitc-2020/jitc-2020-001933

147. Hsu J, Hodgins JJ, Marathe M, Nicolai CJ, Bourgeois-Daigneault MC, Trevino TN, et al. Contribution of nk cells to immunotherapy mediated by pd-1/Pd-L1 blockade. *J Clin Invest* (2018) 128(10):4654–68. doi: 10.1172/jci99317

148. Segal NH, Naidoo J, Curigliano G, Patel S, Sahebjam S, Papadopoulos KP, et al. First-in-Human dose escalation of monalizumab plus durvalumab, with expansion in patients with metastatic microsatellite-stable colorectal cancer. *J Clin Oncol* (2018) 36(15_suppl):3540. doi: 10.1200/JCO.2018.36.15_suppl.3540

149. Ager C, Reilley M, Nicholas C, Bartkowiak T, Jaiswal A, Curran M, et al. 31st annual meeting and associated programs of the society for immunotherapy of cancer (Sitc 2016): Part two: National harbor, md, USA. 9-13 November 2016. *J Immunother Cancer* (2016) 4(Suppl 1):107–221. doi: 10.1186/s40425-016-0173-6

150. Soulas C, Remark R, Brezar V, Lopez J, Bonnet E, Caraguel F, et al. Abstract 2714: Combination of monalizumab and durvalumab as a potent immunotherapy treatment for solid human cancers. *Immunology* (2018) 78(13 supplement):2714. doi: 10.1158/1538-7445.AM2018-2714

151. Hermanson DL, Kaufman DS. Utilizing chimeric antigen receptors to direct natural killer cell activity. *Front Immunol* (2015) 6:195. doi: 10.3389/fimmu.2015.00195

152. Zhang J, Larrocha PS, Zhang B, Wainwright D, Dhar P, Wu JD. Antibody targeting tumor-derived soluble Nkg2d ligand smic provides dual Co-stimulation of Cd8 T cells and enables smic(+) tumors respond to Pd1/Pd-L1 blockade therapy. *J Immunother Cancer* (2019) 7(1):223. doi: 10.1186/s40425-019-0693-y

153. Bauer S, Groh V, Wu J, Steinle A, Phillips JH, Lanier LL, et al. Activation of nk cells and T cells by Nkg2d, a receptor for stress-inducible mica. *Science* (1999) 285(5428):727–9. doi: 10.1126/science.285.5428.727

154. Jamieson AM, Diefenbach A, McMahon CW, Xiong N, Carlyle JR, Raulet DH. The role of the Nkg2d immunoreceptor in immune cell activation and natural killing. *Immunity* (2002) 17(1):19–29. doi: 10.1016/s1074-7613(02)00333-3

155. Raulet DH. Roles of the Nkg2d immunoreceptor and its ligands. *Nat Rev Immunol* (2003) 3(10):781–90. doi: 10.1038/nri1199

156. Roberts AI, Lee L, Schwarz E, Groh V, Spies T, Ebert EC, et al. Nkg2d receptors induced by il-15 costimulate Cd28-negative effector ctl in the tissue microenvironment. *J Immunol* (2001) 167(10):5527–30. doi: 10.4049/jimmunol.167.10.5527

157. Zhang J, Basher F, Wu JD. Nkg2d ligands in tumor immunity: Two sides of a coin. *Front Immunol* (2015) 6:97. doi: 10.3389/fimmu.2015.00097

158. Groh V, Rhinehart R, Randolph-Habecker J, Topp MS, Riddell SR, Spies T. Costimulation of Cd8αβ T cells by Nkg2d *Via* engagement by mic induced on virus-infected cells. *Nat Immunol* (2001) 2(3):255–60. doi: 10.1038/85321

159. Rajasekaran K, Xiong V, Fong L, Gorski J, Malarkannan S. Functional dichotomy between Nkg2d and Cd28-mediated Co-stimulation in human Cd8+ T cells. *PloS One* (2010) 5(9):e12635. doi: 10.1371/journal.pone.0012635

160. López-Soto A, Gonzalez S, Galluzzi L. Soluble Nkg2d ligands limit the efficacy of immune checkpoint blockade. *Oncoimmunology* (2017) 6(10):e1346766. doi: 10.1080/2162402x.2017.1346766

161. Maurer S, Kropp KN, Klein G, Steinle A, Haen SP, Walz JS, et al. Platelet-mediated shedding of Nkg2d ligands impairs nk cell immune-surveillance of tumor cells. *Oncoimmunology* (2018) 7(2):e1364827. doi: 10.1080/2162402x.2017.1364827

162. Salih HR, Holdenrieder S, Steinle A. Soluble Nkg2d ligands: Prevalence, release, and functional impact. *Front Biosci* (2008) 13:3448–56. doi: 10.2741/2939

163. Baragaño Raneros A, Suarez-Álvarez B, López-Larrea C. Secretory pathways generating immunosuppressive Nkg2d ligands: New targets for therapeutic intervention. *Oncoimmunology* (2014) 3:e28497. doi: 10.4161/onci.28497

164. Chitadze G, Lettau M, Bhat J, Wesch D, Steinle A, Fürst D, et al. Shedding of endogenous mhc class I-related chain molecules a and b from different human tumor entities: Heterogeneous involvement of the "a disintegrin and metalloproteases" 10 and 17. *Int J Cancer* (2013) 133(7):1557–66. doi: 10.1002/ijc.28174

165. Groh V, Wu J, Yee C, Spies T. Tumour-derived soluble mic ligands impair expression of Nkg2d and T-cell activation. *Nature* (2002) 419(6908):734–8. doi: 10.1038/nature01112

166. Wu JD, Higgins LM, Steinle A, Cosman D, Haugk K, Plymate SR. Prevalent expression of the immunostimulatory mhc class I chain-related molecule is counteracted by shedding in prostate cancer. *J Clin Invest* (2004) 114(4):560–8. doi: 10.1172/jci22206

167. Zhang D, Zheng Y, Lin Z, Liu X, Li J, Yang H, et al. Equipping natural killer cells with specific targeting and checkpoint blocking aptamers for enhanced adoptive immunotherapy in solid tumors. *Angew Chem Int Ed Engl* (2020) 59 (29):12022–8. doi: 10.1002/anie.202002145

168. Wang X, Zhang D, Wang G, Duan A, Ruan X, Zhao T. Association between pd-L1 variants and pd-L1 expression: A pan-cancer analysis. *J Clin Oncol* (2020) 38(15_suppl):e13661–e. doi: 10.1200/JCO.2020.38.15_suppl.e13661

169. Sefah K, Shangguan D, Xiong X, O'Donoghue MB, Tan W. Development of DNA aptamers using cell-selex. *Nat Protoc* (2010) 5(6):1169–85. doi: 10.1038/nprot.2010.66

170. Fang X, Tan W. Aptamers generated from cell-selex for molecular medicine: A chemical biology approach. *Accounts Chem Res* (2010) 43(1):48–57. doi: 10.1021/ar900101s

171. Li J, Mo L, Lu CH, Fu T, Yang HH, Tan W. Functional nucleic acid-based hydrogels for bioanalytical and biomedical applications. *Chem Soc Rev* (2016) 45 (5):1410–31. doi: 10.1039/c5cs00586h

172. Xu F, Yang S, Chen X, Liu Q, Li H, Wang H, et al. Energy-storage covalent organic frameworks: Improving performance *Via* engineering polysulfide chains on walls. *Chem Sci* (2019) 10(23):6001–6. doi: 10.1039/c8sc04518f

173. Liang H, Chen S, Li P, Wang L, Li J, Li J, et al. Nongenetic approach for imaging protein dimerization by aptamer recognition and proximity-induced DNA assembly. *J Am Chem Soc* (2018) 140(12):4186–90. doi: 10.1021/jacs.7b11311

174. Desnoyers LR, Vasiljeva O, Richardson JH, Yang A, Menendez EE, Liang TW, et al. Tumor-specific activation of an egfr-targeting probody enhances therapeutic index. *Sci Transl Med* (2013) 5(207):207ra144. doi: 10.1126/scitranslmed.3006682

175. Autio KA, Boni V, Humphrey RW, Naing A. Probody therapeutics: An emerging class of therapies designed to enhance on-target effects with reduced off-tumor toxicity for use in immuno-oncology. *Clin Cancer Res* (2020) 26(5):984–9. doi: 10.1158/1078-0432.Ccr-19-1457

176. Wong C, Mei L, Wong KR, Menendez EEM, Vasiljeva O, Richardson JH, et al. Abstract A081: A pd-L1-Targeted probody provides antitumor efficacy while minimizing induction of systemic autoimmunity. *Cancer Immunol Res* (2016) 4 (1_Supplement):A081–A. doi: 10.1158/2326-6074.CRICIMTEATIAACR15-A081

177. Naing A, Thistlethwaite F, De Vries EGE, Eskens FALM, Uboha N, Ott PA, et al. Cx-072 (Pacmilimab), a Probody≪Strong<≪Sup<®≪/Sup<≪/Strong< pd-L1 inhibitor, in advanced or recurrent solid tumors (Proclaim-Cx-072): An open-label dose-finding and first-in-Human study. *J ImmunoTher Cancer* (2021) 9(7):e002447. doi: jitc-2020/jitc-2021-002447

178. Brahmer J, Reckamp KL, Baas P, Crinò L, Eberhardt WE, Poddubskaya E, et al. Nivolumab versus docetaxel in advanced squamous-cell non-Small-Cell lung cancer. *N Engl J Med* (2015) 373(2):123–35. doi: 10.1056/NEJMoa1504627

179. Kang YK, Boku N, Satoh T, Ryu MH, Chao Y, Kato K, et al. Nivolumab in patients with advanced gastric or gastro-oesophageal junction cancer refractory to, or intolerant of, at least two previous chemotherapy regimens (Ono-4538-12, attraction-2): A randomised, double-blind, placebo-controlled, phase 3 trial. *Lancet* (2017) 390(10111):2461–71. doi: 10.1016/s0140-6736(17)31827-5

180. Haanen J. Converting cold into hot tumors by combining immunotherapies. *Cell* (2017) 170(6):1055–6. doi: 10.1016/j.cell.2017.08.031

181. Fearon DT. The carcinoma-associated fibroblast expressing fibroblast activation protein and escape from immune surveillance. *Cancer Immunol Res* (2014) 2(3):187–93. doi: 10.1158/2326-6066.Cir-14-0002

182. Scala S. Molecular pathways: Targeting the Cxcr4-Cxcl12 axis–untapped potential in the tumor microenvironment. *Clin Cancer Res* (2015) 21(19):4278–85. doi: 10.1158/1078-0432.Ccr-14-0914

183. Zeng Y, Li B, Liang Y, Reeves PM, Qu X, Ran C, et al. Dual blockade of Cxcl12-Cxcr4 and pd-1-Pd-L1 pathways prolongs survival of ovarian tumor-bearing mice by prevention of immunosuppression in the tumor microenvironment. *FASEB J* (2019) 33(5):6596–608. doi: 10.1096/fj.201802067RR

184. Filley AC, Dey M. Immune system, friend or foe of oncolytic virotherapy? *Front Oncol* (2017) 7:106. doi: 10.3389/fonc.2017.00106

185. Nemunaitis J, Cunningham C, Senzer N, Kuhn J, Cramm J, Litz C, et al. Pilot trial of genetically modified, attenuated salmonella expressing the e. coli cytosine deaminase gene in refractory cancer patients. *Cancer Gene Ther* (2003) 10 (10):737–44. doi: 10.1038/sj.cgt.7700634

186. Parato KA, Senger D, Forsyth PA, Bell JC. Recent progress in the battle between oncolytic viruses and tumours. *Nat Rev Cancer* (2005) 5(12):965–76. doi: 10.1038/nrc1750

187. Thorne SH, Negrin RS, Contag CH. Synergistic antitumor effects of immune cell-viral biotherapy. *Science* (2006) 311(5768):1780–4. doi: 10.1126/science.1121411

188. Chen Y, Yu DC, Charlton D, Henderson DR. Pre-existent adenovirus antibody inhibits systemic toxicity and antitumor activity of Cn706 in the nude mouse lncap xenograft model: Implications and proposals for human therapy. *Hum Gene Ther* (2000) 11(11):1553–67. doi: 10.1089/10430340050083289

189. White CL, Twigger KR, Vidal L, De Bono JS, Coffey M, Heinemann L, et al. Characterization of the adaptive and innate immune response to intravenous oncolytic reovirus (Dearing type 3) during a phase I clinical trial. *Gene Ther* (2008) 15(12):911–20. doi: 10.1038/gt.2008.21

190. Rudin CM, Poirier JT, Senzer NN, Stephenson JJr., Loesch D, Burroughs KD, et al. Phase I clinical study of Seneca valley virus (Svv-001), a replication-competent picornavirus, in advanced solid tumors with neuroendocrine features. *Clin Cancer Res* (2011) 17(4):888–95. doi: 10.1158/1078-0432.Ccr-10-1706

191. Tsai V, Johnson DE, Rahman A, Wen SF, LaFace D, Philopena J, et al. Impact of human neutralizing antibodies on antitumor efficacy of an oncolytic adenovirus in a murine model. *Clin Cancer Res* (2004) 10(21):7199–206. doi: 10.1158/1078-0432.Ccr-04-0765

192. Sumida SM, Truitt DM, Lemckert AA, Vogels R, Custers JH, Addo MM, et al. Neutralizing antibodies to adenovirus serotype 5 vaccine vectors are directed primarily against the adenovirus hexon protein. *J Immunol* (2005) 174(11):7179–85. doi: 10.4049/jimmunol.174.11.7179

193. Berkeley RA, Steele LP, Mulder AA, van den Wollenberg DJM, Kottke TJ, Thompson J, et al. Antibody-neutralized reovirus is effective in oncolytic virotherapy. *Cancer Immunol Res* (2018) 6(10):1161–73. doi: 10.1158/2326-6066.Cir-18-0309

194. Jayawardena N, Poirier JT, Burga LN, Bostina M. Virus-receptor interactions and virus neutralization: Insights for oncolytic virus development. *Oncolytic Virother* (2020) 9:1–15. doi: 10.2147/ov.S186337

195. Niemann J, Woller N, Brooks J, Fleischmann-Mundt B, Martin NT, Kloos A, et al. Molecular retargeting of antibodies converts immune defense against oncolytic viruses into cancer immunotherapy. *Nat Commun* (2019) 10(1):3236. doi: 10.1038/s41467-019-11137-5

196. Zhang Z, Krimmel J, Zhang Z, Hu Z, Seth P. Systemic delivery of a novel liver-detargeted oncolytic adenovirus causes reduced liver toxicity but maintains the antitumor response in a breast cancer bone metastasis model. *Hum Gene Ther* (2011) 22(9):1137–42. doi: 10.1089/hum.2011.003

197. Miller KD, Siegel RL, Lin CC, Mariotto AB, Kramer JL, Rowland JH, et al. Cancer treatment and survivorship statistics, 2016. *CA Cancer J Clin* (2016) 66 (4):271–89. doi: 10.3322/caac.21349

frontiers | Frontiers in Immunology

TYPE Original Research
PUBLISHED 19 August 2022
DOI 10.3389/fimmu.2022.954440

OPEN ACCESS

EDITED BY
Xian Zeng,
Fudan University, China

REVIEWED BY
Yuqi Xia,
Renmin Hospital of Wuhan University, China
Jindong Xie,
Sun Yat-sen University Cancer Center (SYSUCC), China

*CORRESPONDENCE
Ke Cao
csucaoke@163.com;
csucaoke@csu.edu.cn

†These authors have contributed equally to this work and share first authorship

SPECIALTY SECTION
This article was submitted to Cancer Immunity and Immunotherapy, a section of the journal Frontiers in Immunology

RECEIVED 27 May 2022
ACCEPTED 05 August 2022
PUBLISHED 19 August 2022

CITATION
Zhang G, Chen X, Fang J, Tai P, Chen A and Cao K (2022) Cuproptosis status affects treatment options about immunotherapy and targeted therapy for patients with kidney renal clear cell carcinoma. *Front. Immunol.* 13:954440. doi: 10.3389/fimmu.2022.954440

Cuproptosis status affects treatment options about immunotherapy and targeted therapy for patients with kidney renal clear cell carcinoma

Ganghua Zhang†, Xinyu Chen†, Jianing Fang, Panpan Tai, Aiyan Chen and Ke Cao*

Department of Oncology, Third Xiangya Hospital, Central South University, Changsha, China

The development of immunotherapy has changed the treatment landscape of advanced kidney renal clear cell carcinoma (KIRC), offering patients more treatment options. Cuproptosis, a novel cell death mode dependent on copper ions and mitochondrial respiration has not yet been studied in KIRC. We assembled a comprehensive cohort of The Cancer Genome Atlas (TCGA)-KIRC and GSE29609, performed cluster analysis for typing twice using seven cuproptosis-promoting genes (CPGs) as a starting point, and assessed the differences in biological and clinicopathological characteristics between different subtypes. Furthermore, we explored the tumor immune infiltration landscape in KIRC using ESTIMATE and single-sample gene set enrichment analysis (ssGSEA) and the potential molecular mechanisms of cuproptosis in KIRC using enrichment analysis. We constructed a cuproptosis score (CUS) using the Boruta algorithm combined with principal component analysis. We evaluated the impact of CUS on prognosis, targeted therapy, and immunotherapy in patients with KIRC using survival analysis, the predictions from the Cancer Immunome Atlas database, and targeted drug susceptibility analysis. We found that patients with high CUS levels show poor prognosis and efficacy against all four immune checkpoint inhibitors, and their immunosuppression may depend on *TGFB1*. However, the high-CUS group showed higher sensitivity to sunitinib, axitinib, and elesclomol. Sunitinib monotherapy may reverse the poor prognosis and result in higher progression free survival. Then, we identified two potential CPGs and verified their differential expression between the KIRC and the normal samples. Finally, we explored the effect of the key gene *FDX1* on the proliferation of KIRC cells and confirmed the presence of cuproptosis in KIRC cells. We developed a targeted therapy and immunotherapy strategy for advanced KIRC based on CUS. Our findings provide new insights into the relationship among cuproptosis, metabolism, and immunity in KIRC.

KEYWORDS

kidney renal clear cell carcinoma, cuproptosis, immune cell infiltration, immunotherapy, targeted therapy, prognosis

Introduction

Renal cell carcinoma (RCC) is one of the most common malignancies of the urinary system, and its most common subtype is kidney renal clear cell carcinoma (KIRC), which accounts for approximately 75% of all RCC cases (1). Currently, early resection is considered the basic treatment for patients with KIRC (2); however, up to 40% of patients develop metastases after primary surgical treatment for local RCC, resulting in poor prognosis (3). Furthermore, randomized controlled clinical studies have shown that postoperative adjuvant cytokine therapy, radiotherapy and chemotherapy have little impact on reducing recurrence and metastasis rates (4, 5). Therefore, once KIRC is metastatic or unresectable, the treatment options become very limited.

The rapid development of targeted therapy and immunotherapy has been a turning point in treating patients with metastatic or unresectable KIRC. These two treatments and their combinations have become the required options for these patients. Initially, targeted therapy was shown to substantially prolong survival in advanced KIRC (6, 7). Multitarget drugs, such as sunitinib and sorafenib, have become the first choice for patients with metastatic or unresectable KIRC (8). In recent years, researchers have found that targeted therapy combined with immunotherapy has beneficial treatment effects and good prospects in patients with advanced KIRC, and has shown a trend of gradually replacing targeted therapy alone (9). However, many patients do not benefit from the combined therapy because of the overlapping drug toxicity that affects their quality of life (10). Therefore, new molecular phenotypes should be established to divide the population more finely for the individualized selection of effective immunotherapy drugs or targeted drugs for patients with advanced or unresectable KIRC.

Copper (Cu) ion is a double-edged sword in the life activities of cells: on the one hand, Cu ions are key co-factors for many enzymes, such as cytochrome c oxidase, which relies on Cu ions to complete cellular respiration (11). On the other hand, excess Cu ions induce cuproptosis in cells (12). Cuproptosis is an emerging form of programmed cell death, dependent on intracellular copper accumulation, which is distinct from the known forms of cell death, such as ferroptosis, pyroptosis, and apoptosis. Human mitochondrial ferredoxin 1 (*FDX1*) positively regulates lipoylated enzymes, and Cu ions directly bind to lipoylated components in the tricarboxylic acid cycle (TCA) pathway, resulting in abnormal aggregation of lipoylated proteins and loss of iron-sulfur cluster proteins and proteotoxic stress response. This eventually leads to cuproptosis of cells (13). Cu ions, protein lipoylation, and mitochondrial respiration are important determinants of cuproptosis. Therefore, in cancers that express a large number of lipoylated mitochondrial proteins and have a high degree of respiration, the use of metal carriers to transport Cu ions and activate cuproptosis can kill cancer cells with this metabolic feature. This approach could potentially become a new cancer treatment (14). KIRC cells show the classic Warburg effect as the main metabolic feature (15). Since they do not participate in the mitochondrial respiratory pathway, we hypothesized that cuproptosis would be inhibited in KIRC; thus, it is important to promote cuproptosis in KIRC. In addition, intratumoral copper levels affect the expression of programmed death ligand 1 (PD-L1) in cancer cells, and Cu regulates a key signaling pathway that mediates PD-L1-driven cancer immune evasion (16). However, no reports have suggested a correlation between cuproptosis and immunotherapy, and no studies are available on the effect of cuproptosis on KIRC.

In this study, we selected seven genes that promote cuproptosis as starting points for typing. We comprehensively used the KIRC cohort of The Cancer Genome Atlas (TCGA) and Gene Expression Omnibus (GEO) databases to establish novel molecular typing and explored the intratumoral immune infiltration landscape of KIRC using ESTIMATE and single-sample gene set enrichment analysis (ssGSEA) algorithms. We used a novel scoring model, the cuproptosis score (CUS), to predict the prognosis and the efficacy of targeted therapy and immunotherapy in patients with KIRC and explored specific targets and drugs. Our results provide a new and detailed strategy for individualized targeted therapy and immunotherapy in patients with advanced or unresectable KIRC.

Abbreviations: CNV, copy number variation; CPG, cuproptosis-promoting gene; CSRG, cuproptosis subtypes related gene; CUS, cuproptosis score; Cu, Copper; CCK8, Cell Counting Kit-8; DEG, differentially expressed gene; EdU, Ethynyl-2'-deoxyuridine; GEO, Gene Expression Omnibus; GEPIA, Gene Expression Profiling Interactive Analysis; GSCA, Gene Set Cancer Analysis; HPA, Human Protein Atlas; IC50, half maximal inhibitory concentration; ICI, immune checkpoint inhibitor; IPS, Immunophenoscore; KEGG, Kyoto Encyclopedia of Genes and Genomes; KIRC, kidney renal clear cell carcinoma; OS, overall survival; PCA, principal component analysis; qRT-PCR, quantitative reverse transcription polymerase chain reaction; SNV, single nucleotide variation; ssGSEA, single sample gene set enrichment analysis; TCA, tricarboxylic acid cycle; TCGA, The Cancer Genome Atlas; TCIA, The Cancer Immunome Atlas.

Materials and methods

Exploration of the genetics and biological significance of cuproptosis-promoting genes in KIRC

P. Tsvetkov et al. identified seven cuproptosis-promoting genes (CPGs): *FDX1*, *LIAS*, *LIPT1*, *DLD*, *DLAT*, *PDHA1* and *PDHB* (13). The Gene Set Cancer Analysis (GSCA) database (http://bioinfo.life.hust.edu.cn/GSCA/#/) was used to analyze differential mRNA expression, single nucleotide variation (SNV), copy number variation (CNV), and methylation of

seven CPGs (17). A network of seven CPGs was drawn using the "igraph" R package. Attributes in the network were determined using intergene correlations and univariate Cox regression analysis.

Data collection and processing of KIRC comprehensive cohort

The TCGA-KIRC cohort containing 534 KIRC samples from the TCGA database (https://tcga-data.nci.nih.gov/tcga/) and the GSE29609 cohort (platform GPL1708) containing 39 KIRC samples from the GEO database (http://www.ncbi.nlm.nih.gov/geo/) were used for data merging. Normalized matrix files and clinical data were downloaded from the GEO database; RNA sequencing data (fragments per kilobase million, FPKM values) of gene expression and clinical data were obtained from TCGA. The FPKM values were then converted to transcripts per kilobase million (TPM) values for further analysis, "ComBat" from the "SVA" R package was used to eliminate the batch effects (18), and principal component analysis (PCA) was used to eliminate the batch effects. Samples without complete survival data were excluded. Finally, we obtained a comprehensive KIRC cohort containing 537 samples and 14074 genes.

First unsupervised clustering based on seven CPGs

We used the "ConsensusClusterPlus" R package for unsupervised clustering and classification based on seven CPGs (19), using agglomerative pam clustering with the Euclidean distance and resampling 80% of the samples for 50 repetitions. We then used survival analysis to compare the differences in overall survival (OS) between different subtypes, box plots to compare the expression of seven CPGs between different subtypes, and used the "pheatmap" R package to draw a cluster heatmap to show the relationship between the expression of seven CPGs, clinicopathological features, and classification.

Gene set variation analysis

We downloaded the data of the HALLMARK pathway, the Kyoto Encyclopedia of Genes and Genomes (KEGG) pathway, and the Reactome pathway from the Molecular Signatures Database (MsigDB, http://software.broadinstitute.org/gsea/msigdb/), and acquired "h.all.v7.5.1. symbols.gmt," "c2.cp.kegg.v7.5.1. symbols.gmt," and "c2.cp.reactome.v7.5.1. symbols.gmt" as reference gene sets (20). Then, we used the "GSVA" R package to perform Gene Set Variation Analysis (GSVA) for different subtypes and drew a heatmap to display the analysis results.

Construction of KIRC immune infiltration landscape

The "ESTIMATE" R package was used to calculate StromalScore, ImmuneScore, and ESTIMATEScore. StromalScore and ImmuneScore represent the abundance of stromal and immune components, respectively, whereas ESTIMATEScore is the sum of StromalScore and ImmuneScore, which is negatively correlated with tumor purity (21). The "GSVA" R package was then used for ssGSEA to calculate the enrichment score that represents the relative infiltrating abundance of each immune cell (22).

Screening of differentially expressed genes (DEGs) and enrichment analysis

The "limma" R package (23) was used to screen for differentially expressed genes (DEGs) between different subtypes with |logFoldChange| >1 and $p < 0.05$. KEGG and Gene Ontology (GO) functional enrichment analyses were implemented using the "clusterProfiler" R package (24), and adjusted p-value <0.05 represented statistically significant results.

Secondary unsupervised clustering based on cuproptosis subtypes related genes

We screened the DEGs with $p < 0.05$ using univariate Cox regression analysis and named them cuproptosis subtype-related genes (CSRGs). The "forestplot" R package was used to draw a forest plot of the results. Then, secondary unsupervised clustering classification was performed based on CSRGs, with the same specific clustering parameters. Subsequently, we used survival analysis to compare the differences in OS between different subtypes, used box plots to compare CSRGs expressions between different subtypes, and drew a cluster heatmap to show the relationship among CSRGs expression, clinicopathological features, and classification.

Calculation of cuproptosis score (CUS)

According to the positive and negative relationships between the CSRGs and the cluster signature, the CSRGs were divided into two groups, namely sigC1 and sigC2. Then, the "clusterProfiler" R package was used for gene annotation. We then used the Boruta algorithm (25)combined with PCA to reduce the dimensionality of the CSRGs subgroups and calculated the CUS for each sample. The KIRC comprehensive cohort was divided into the high- and low-CUS groups based on

the optimal cutoff value. The CUS of each KIRC sample was calculated using the following formula:

$$CUS = \sum PsigC1 - \sum PsigC2$$

Prognosis and immune exploration based on CUS grouping

We used the "survival" and "survminer" R packages to perform survival analysis to compare the differences in OS between the high- and low-CUS groups, and used the "ggalluvial" R package to draw Sankey diagrams to visualize the correspondence among CUS groups, different subtypes, and prognosis. Box plots were used to compare the differences in the CUS of different subtypes. ssGSEA was used to quantify the infiltration abundance of immune cells, and the relationship between CUS and immune cell infiltration levels was displayed using a correlation heat map.

Clinical subgroup analysis based on CUS grouping

We selected "survival status," "histological grade," "T stage," "N stage," "M stage" and "clinical stage" as clinical subgroup characteristics, and drew box plots to show the differences in the CUS between different clinical characteristics. A stacked histogram was drawn to show the proportion of each clinical characteristic in the high- and low-CUS groups.

Comparison of immune targets and prediction of immunotherapy efficacy

We used the "limma" R package to compare the differences in the gene expression of several common immune targets. Next, we downloaded the immunophenoscore (IPS) data of the TCGA-KIRC cohort from The Cancer Immunome Atlas (TCIA) database to explore the differences in the efficacy of the four immune checkpoint inhibitors (ICIs) between the high- and low-CUS groups (26), including ctla4_pos_pd1_pos, ctla4_neg_pd1_pos, ctla4_pos_pd1_neg, and ctla4_neg_pd1_neg.

Analysis of targeted therapy based on CUS grouping

We estimated the half maximal inhibitory concentration (IC50) using the "pRRophetic" R package to predict the sensitivity of the high- and low-CUS groups to 138 targeted drugs. We selected eight commonly used targeted drugs for advanced KIRC (sunitinib, axitinib, sorafenib, erlotinib, lapatinib, gefitinib, pazopanib, and temsirolimus) and a cuproptosis-targeting drug (elesclomol) for key observation (27). Subsequently, we downloaded the gene expression profile and clinical data of the sunitinib monotherapy cohort in the NCT02684006 clinical trial from the supplementary material of PMID:32895571 (28). We used differential analysis to explore the relationship between CUS groups and progression and compared the differences in progression-free survival (PFS) between the high- and low-CUS groups *via* survival analysis. The significance of the difference in comparing the progression rates of different CUS groups was achieved by the chi-square test.

Mining seven CPGs-related targeted drugs

We calculated the correlation between the mRNA expression of seven CPGs and drug IC50 values *via* Pearson's correlation analysis of the "GDSC drug" and "CTRP drug" modules in the GSCA database. The p-value was adjusted using the false discovery rates (FDR).

Screening and validation of potential CPGs and *FDX1*

Hazard ratio (HR) and p values of univariate COX regression analysis were used to identify potential CPGs. Potential CPGs were screened using $p < 0.001$ and 1-HR > 0.4 as the inclusion criteria. Then, a comprehensive analysis was performed integrating TCGA and the Genotype Tissue Expression (GTEx) (https://commonfund.nih.gov/GTEx/) databases (29) through the "Expression DIY" module of the Gene Expression Profiling Interactive Analysis (GEPIA, http://gepia.cancer-pku.cn/) website (30). $|Log2FC| > 1$ and $p < 0.01$ were set as the cutoff values. Additionally, immunohistochemical (IHC) staining results of the three genes between normal renal tubular epithelial and KIRC tissues at the protein level were obtained from Human Protein Atlas (HPA, https://www.proteinatlas.org/) database.

Cell culture and transfection

Human renal tubular epithelial cells (HK-2) and KIRC cells (Caki-1 and 786-O) were obtained from the American Type Culture Collection (ATCC, Manassas, VA, USA). All cells were cultured in RPMI 1640 medium (Hyclone, Logan, UT, USA) supplemented with 15% fetal bovine serum (Gibco, Grand Island, NY, USA) and 1% penicillin-streptomycin (Hyclone). Small interfering RNAs (siRNAs) targeting FDX1 were synthesized by GenePharma (Shanghai, China). siRNA-FDX1

and siRNA-control were cotransfected into Caki-1 cells using Lipofectamine 2000 (Invitrogen, Carlsbad, CA, USA). The primer sequences of siRNAs are listed in Supplementary Table 2.

Quantitative reverse transcription polymerase chain reaction

Total RNA from the cultured cells was extracted using a Faster reagent (Invitrogen). The PrimeScript RT Reagent Kit (TaKaRa, Shiga, Japan) was used to reverse transcribe 1μg total RNA into cDNA, and the SYBR Green PCR Master Mix was used for quantitative reverse transcription polymerase chain reaction (qRT-PCR). Relative gene expression was calculated using equation $2^{-\Delta\Delta CT}$, with GAPDH as an internal loading control. Visualization of qRT-PCR results and two samples unpaired t-test was performed using GraphPad Prism version 9.0.1 (GraphPad Software, San Diego, California USA, www.graphpad.com). All the primers used for qRT–PCR were synthesized by Tsingke Biotech (Tsingke, China). The primer sequences used are listed in Supplementary Table 2.

Western blotting

The total protein in human renal tubular epithelial cells (HK-2) and KIRC cells (Caki-1 and 786-O) were extracted using radioimmunoprecipitation assay (RIPA) buffer (Beyotime, Shanghai, China), Protease Inhibitor Cocktail (Cwbio, CW2200) and Phosphatase Inhibitor Cocktail (Cwbio, CW2383) for 20 min at 4°C. Protein concentration was determined using a BCA protein assay kit (Beyotime, Shanghai, China). The protein samples were separated on an SDS-PAGE Loading Buffer (Cwbio, CW0027), and transferred onto polyvinylidene difluoride (PVDF) membranes (Millipore, IPVH00010). Subsequently, the membrane was blocked in Tris-buffered saline plus tween-20 (TBST; Servicebio, G0001) containing 5% nonfat powdered milk (Sangon Biotech, A600669) for 1 h. Anti-FDX1 (1:1000, A20895; Abclonal), anti-ACAT1 (1:1000; 16215-1-AP, Proteintech), Beta Tubulin (1:1000; 10094-1-AP, Proteintech) and GAPDH (1:1000; R24404, Zen-Bioscience) were used as primary antibodies, and the membrane was submerged in primary antibodies overnight at 4°C. Then, the membrane was washed with TBST 3 times and incubated with Goat Anti-Rabbit IgG-Horseradish Peroxidase (1:5000; Elabscience, E-AB-1003) for 1 h at room temperature. Immunoassay was performed by an enhanced chemiluminescence detection system (ECL; Biosharp, BL520A) combined with a Western blot system (Auragene). The expression of the target band relative to the loading control was quantified with integrated density by ImageJ software.

Cell Counting Kit-8 (CCK-8) assay

The transfected Caki-1 cells were adjusted to 2000 cells/well (100 μL medium) in 96-well plates and cultured for the indicated days. Then, 10 μL of CCK-8 (BS350A, Biosharp Life Sciences) was added to the cells, and the cells were cultured at 37°C for 1.5 hours. Optical density was measured at 450 nm (OD_{450nm}) using a microplate reader.

Caki-1 cells were transferred into 96-well plates at a density of 2500 cells/well (100 μL medium). After 24 h the cells were divided into 8 groups (n=3 per group), incubated with 100μL of fresh medium containing $CuCl_2$ (100nM; RHAWN, R019783), Elesclomol (100nM; MedChemExpress, HY-12040), $CuCl_2$ (100nM)& Elesclomol (100nM), $CuCl_2$ (200nM), Elesclomol (200nM), $CuCl_2$ (200nM)& Elesclomol (200nM) or control agents for indicated days. Briefly, 10 μL of CCK-8 was added and OD_{450nm} was measured.

Ethynyl-2′-deoxyuridine (EdU) assay

Caki-1 cells were stained using BeyoClick™ EdU-555 Cell Proliferation Kit (Beyotime, Shanghai, China). To be specific, Caki-1 cells (1.0×10^5 cells/well) were seeded in a 6-well plate, transfected with NC or si-FDX1, and cultured in an incubator at 37°C for 72 h. Then, Caki-1 cells were incubated with EdU for 2 h, fixed with 1 mL paraformaldehyde (4%) for 15 min, and permeabilized with 0.3% Triton X-100 (Beyotime) for 15 min. After that, the Caki-1 cells were incubated with 500μL of the click reaction mixture for 30 min in the dark, washed three times with PBS containing 3% BSA, and incubated with Hoechst 33342 for another 10 min. Finally, fluorescence microscopy was used for detection.

Colony formation assay

The transfected cells were cultured up to the logarithmic growth phase and then counted and adjusted to 500 cells/well in 6-well plates. Cells were incubated for 2 weeks at 37°C, 5% CO_2. After being washed with PBS twice, the cells were fixed with paraformaldehyde (4%) for 15 min and stained with crystal violet buffer (Solarbio, Beijing, China) for 30 min. The clone was counted if the number of cells in the clone was at least 50 under a microscope.

Statistical analysis

All analyses were performed using R version 4.1.1. Unless otherwise specified, Pearson's correlation coefficient was used for

correlation analysis in this study. For comparison between the two groups in the bioinformatics analysis section, the Wilcoxon test was used for difference analysis. For comparison between the two groups in the experimental section, the Students' t-test was used for difference analysis. Two-way ANOVA was used for difference comparison in CCK8 assay. For comparisons between more than two groups, the Kruskal-Wallis test was used for the difference analysis. Kaplan-Meier survival analysis and log-rank tests were used to compare the survival of the different groups of patients. For all statistical analyses, a two-tailed $p < 0.05$ was considered statistically significant.

Results

Genetic, transcriptional and post-transcriptional alterations of CPGs in KIRC

The workflow of this study is illustrated in Figure 1. We performed different levels of analysis of the seven CPGs using the GSCA database. At the mRNA level, *DLAT*, *DLD*, *FDX1*, *PDHB*, and *PDHA1* showed low expression in KIRC compared to the normal samples (FDR <0.05, Supplementary Figure 1A). The SNV frequencies of the six CPGs are shown in the form of a heat map (no data are available for *FDX1*), with DLD having the highest SNV frequency (Supplementary Figure 1B). Seven CPGs showed large differences in CNV types (including heterozygous amplification, homozygous amplification, heterozygous deletion, and homozygous deletion) and proportions, and *PDHB* had a very large proportion of heterozygous deletions, whereas *DLD* had only heterozygous amplification (Supplementary Figure 1C). The CNV of CPGs was positively correlated with their mRNA expression, especially that of *PDHB* (Supplementary Figure 1D). Conversely, methylation levels of CPGs were negatively correlated with mRNA expression (Supplementary Figure 1E). However, the methylation of CPGs was not significantly different between KIRC and normal samples (no data available for *FDX1*, Supplementary Figure 1F).

Construction of comprehensive KIRC cohort and CPGs network

We merged the TCGA-KIRC and GSE29609 datasets and removed the batch effects to obtain a comprehensive cohort of 537 samples and 14,074 genes. PCA showed that batch effects were effectively eliminated (Figure 2A). The baseline data on the clinical characteristics of the comprehensive cohort are presented in Table 1. The network of seven CPGs showed the results of the correlation analysis and Cox regression analysis; seven CPGs had significant positive correlations ($p < 0.0001$) and were protective factors for KIRC (HR < 1, Figure 2B). Finally, the Kaplan-Meier survival analysis suggested that six CPGs significantly affected the prognosis of patients with KIRC ($p < 0.05$, Figure 2C).

Identification and evaluation of subtypes based on seven CPGs

We performed unsupervised clustering and classification based on seven CPGs. The best classification effect could be obtained when the patients were divided into Clusters A and B (Figure 3A). The clustering results are shown in Supplementary Figures 2A–C. There was a significant difference in OS between the two subtypes,

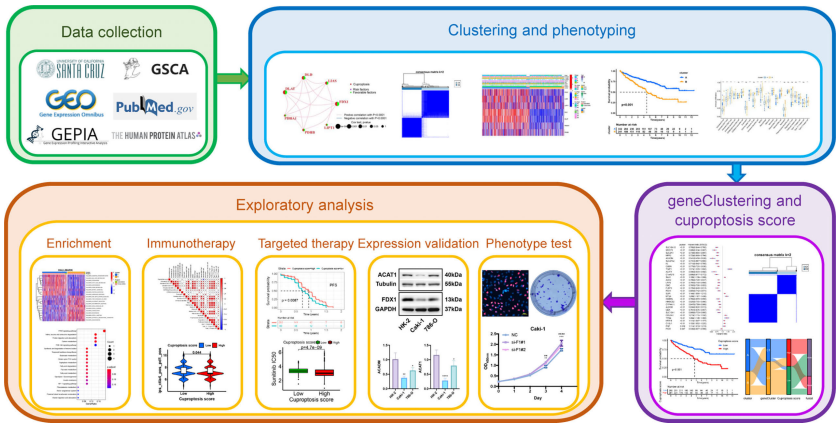

FIGURE 1
The flowchat of this study.

with cluster A having a better prognosis than cluster B (p <0.001, Figure 3B). Seven CPGs showed higher expression levels in cluster A (p <0.001, Figure 3C). We showed the clinicopathological features of the two subtypes and the expression distribution of the seven CPGs using a heat map (Figure 3D). We used GSVA to compare the enrichment pathways of the two subtypes from the three sets of the HALLMARK pathway (Supplementary Figure 3A), KEGG pathway (Supplementary Figure 3B), and Reactome pathway (Supplementary Figure 3C), and detected significant differences between the two subtypes, mainly in multiple metabolic pathways.

Patients in different clusters showed feature distinguishability based on PCA (Figure 4A). Next, we used ESTIMATE to quantify the infiltration characteristics of the tumor microenvironment in patients with KIRC and observed that Cluster B had higher StromalScore, ImmuneScore, and ESTIMATEScore than Cluster A (p <0.001, Figure 4B). We used ssGSEA to quantify the infiltrating abundance of 23 immune cells and explored the differential patterns of the immune-infiltrating landscape of the two subtypes. The infiltration levels of activated B cells, CD4 T cells, CD8 T cells, dendritic cells, CD56^{dim} structural killer cells, gamma delta T cells, myeloid-derived suppressor cells (MDSC), macrophages, mast cells, monocytes, natural killer T cells, natural killer cells, type 1 T helper cells, and type 2 T helper cells were significantly higher in cluster B than in cluster A (p <0.05, Figure 4C). These results suggest that Cluster B has a higher level of stromal and immune cell infiltration than Cluster A.

Identification of CSRGs and the secondary clustering

To further explore the potential biological behavior of each cuproptosis subtype, we performed a differential analysis of the two cuproptosis subtypes. The DEGs are shown using volcano plots (p <0.05, Figure 5A). We then screened DEGs with | logFoldChange| >1 and p <0.05, and identified 31 cuproptosis-related DEGs. KEGG (Figure 5C) and GO (Figure 5D) enrichment analyses were performed on these DEGs, and the top five pathways based on the adjusted p-value in KEGG analysis and their relationship networks with related genes were displayed (p <0.05, Figure 5B). Several pathways were related to mitochondrial metabolism, including the peroxisome proliferator-activated receptor (PPAR) signaling pathway, carbon metabolism, citrate cycle (TCA cycle), fatty acid degradation, and the PI3K-Akt signaling pathway.

To identify cuproptosis-related genes with prognostic significance for KIRC, we performed a univariate Cox regression analysis on 31 cuproptosis-related DEGs; the results are shown in Supplementary Table 1. All 31 DEGs had prognostic significance and were identified as CSRGs (p <0.05, Figure 6A). Based on 31 CSRGs, we performed secondary clustering and identified two subtypes: gene clusters C1 and C2 (Figure 6C). The clustering results are shown in Supplementary Figures 2D–F. The plots of the Kaplan-Meier

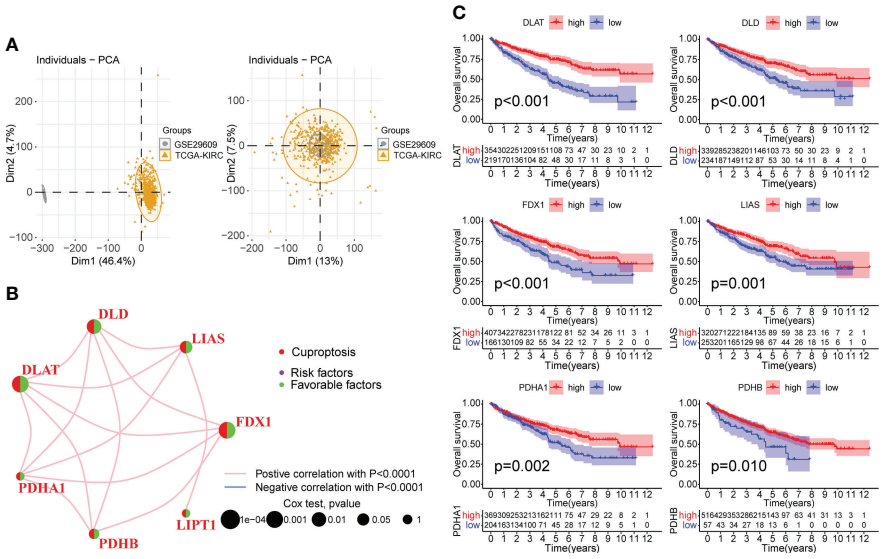

FIGURE 2
Correlation analysis and survival analysis of CPGs in KIRC. **(A)** Fusion of TCGA-KIRC and GSE29609 cohort data and removal of batch effects. The left plot shows PCA before removing batch effects, and the right plot shows PCA post removing batch effects. **(B)** Correlation network of seven CPGs. The line represents a correlation between genes, the sphere represents the COX test of each gene. **(C)** Kaplan-Meier survival analysis of CPGs in KIRC (OS, Log-rank test, p < 0.05). CPG, cuproptosis-promoting gene.

TABLE 1 Baseline Data Sheet for the Comprehensive Cohort of TCGA-KIRC and GSE29609.

Characteristic	levels	N (%)
Age	>60 years old	291 (50.8%)
	≤60 years old	282 (49.2%)
Grade	G1	15 (2.7%)
	G2	243 (43%)
	G3	217 (38.4%)
	G4	90 (15.9%)
T_stage	T1	285 (49.7%)
	T2	75 (13.1%)
	T3	201 (35.1%)
	T4	12 (2.1%)
N_stage	N0	271 (91.9%)
	N1	21 (7.1%)
	N2	3 (1%)
M_stage	M0	449 (83%)
	M1	92 (17%)
Stage	I	268 (50.5%)
	II	58 (10.9%)
	III	123 (23.2%)
	IV	82 (15.4%)

survival curves of C1 and C2 showed that C2 had a better prognosis than C1 (p <0.001, Figure 6B). The 31 CSRGs were significantly differentially expressed between C1 and C2 (p <0.001, Supplementary Figure 4A). We used a heatmap to show the clinicopathological characteristics of the two subtypes and the expression distribution of the 31 CSRGs (Supplementary Figure 4B). According to the positive and negative relationships between DEGs and cluster features, CSRGs were divided into two groups: sigC1 and sigC2. The genes in the sigC1 group were highly expressed in C2 and lowly expressed in C1, whereas the opposite was true for the genes in the sigC2 group.

Calculation of CUS and classification of patients with KIRC

To quantify the cuproptosis status to predict the clinical characteristics and treatment outcomes of the patients, we calculated the CUS for each sample using the Boruta algorithm combined with PCA based on two gene sets, sigC1 and sigC2. According to the best cutoff value "-0.4318927," the samples of the comprehensive cohort were divided into the high- and low-CUS groups. The results of the Kaplan-Meier survival analysis revealed that patients in the high-CUS group had a poorer prognosis (Figure 7A). The Sankey diagram shows the corresponding relationship among the CUS, classification, and prognosis (Figure 7B). Patients with KIRC in cluster B had a higher probability of corresponding to genecluster C1, with a higher CUS and poorer prognosis. The different box plots also verify this conclusion (p <2.22e-16, Figures 7D, E). We created a correlation heatmap to explore the relationship between the CUS and immune cell infiltration (Figure 7C) and observed a negative but weak correlation between the CUS and most immune cells (p <0.05, except natural killer cells).

CUS-related clinical subgroup analysis

To further explore the correlation between the CUS, prognosis, and clinical characteristics, we used box plots to show the differences in the CUS between different clinical characteristics and stacked histograms to show the proportion of each clinical characteristic in the high- and low-CUS groups. Patients who died had a higher CUS than those alive (p =2.4e-09, Supplementary Figure 5A); patients with histological grade G4 had a higher CUS than those with histological grade G1, G2 and G3 (p <0.1, Supplementary Figure 5B); patients with T4 had a higher CUS, while patients with T1 had a lower CUS (p <0.05, Supplementary Figure 5C); CUS did not show a significant difference in lymph node metastasis (Supplementary Figure 5D); patients with distant metastasis had a higher CUS than those without distant metastasis (p =0.009, Supplementary Figure 5E), and patients with clinical stage I had a lower CUS than those with clinical stage II, III and IV (p <0.05, Supplementary Figure 5F).

Exploration of immunotherapy targets and efficacy based on CUS

To explore the potential relationship between CUS and immunotherapy, we compared the expression levels of several common immune-related targets in the high- and low-CUS groups. In the high-CUS group, the *TGFB1* expression level was higher (p =4.8e-05, Figure 8D), whereas CD274 expression was lower (p =0.012, Figure 8C) than that in the low-CUS group. There were no significant differences in PDCD1 (Figure 8A) and CTLA4 (Figure 8B) expression levels between the high- and low-CUS groups. In addition, we downloaded the IPS of the TCGA-KIRC cohort from the TCIA database to explore differences in the efficacy of immunotherapy between the high- and low-CUS groups. The IPS of ctla4_pos_pd1_pos (Figure 8E), ctla4_neg_pd1_pos (Figure 8F), ctla4_pos_pd1_neg (Figure 8G), and ctla4_neg_pd1_neg (Figure 8H) was lower in the high-CUS group (p <0.05) than in the low-CUS group.

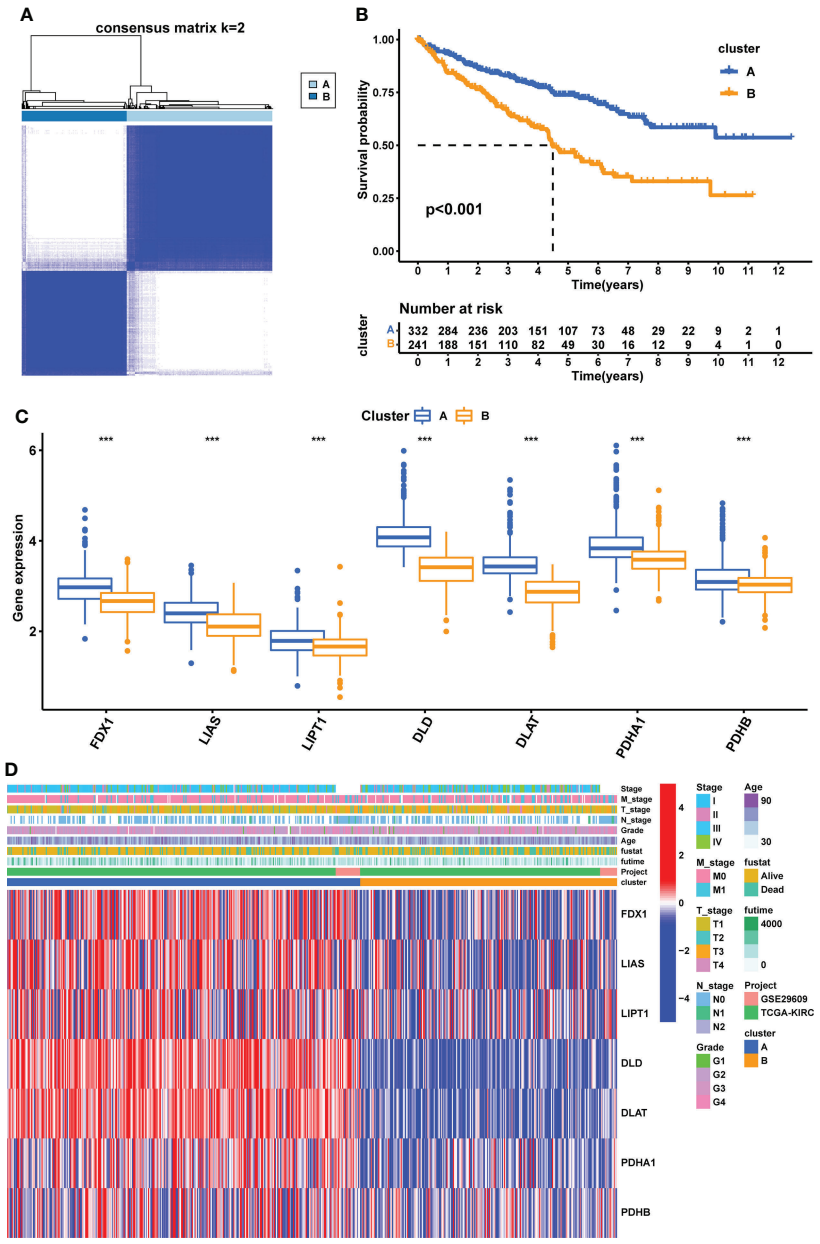

FIGURE 3
Construction of CPG subtypes and exploration about clinical and biological features of subtypes. **(A)** consensus matrix that divides all KIRC samples into two clusters (k=2). **(B)** Kaplan–Meier curves for the two subtypes of KIRC patients (OS, Log-rank test, p < 0.001). **(C)** Expression differences of seven CPGs between the two subtypes. **(D)** Heatmap of the distribution of clinicopathological features and CPG expression between two different subtypes. CPG, cuproptosis-promoting gene; ***p < 0.001.

Sensitivity analysis and efficacy prediction of targeted drugs

To explore the impact of the CUS on targeted therapy, we first calculated the IC50 values of a variety of commonly used targeted drugs for advanced KIRC using the pRRophetic package and then predicted the sensitivity of targeted drugs. For sunitinib, axitinib, and elesclomol, the IC50 values of the high-CUS group were lower and showed higher sensitivity ($p < 0.05$, Figures 9D–F). For sorafenib, erlotinib, and lapatinib, the high-CUS group had higher IC50 values and lower sensitivity ($p < 0.0001$, Figures 9A–C). However, the IC50 values of gefitinib, pazopanib, and temsirolimus were not significantly different between the high- and low-CUS groups (Figures 9G–I).

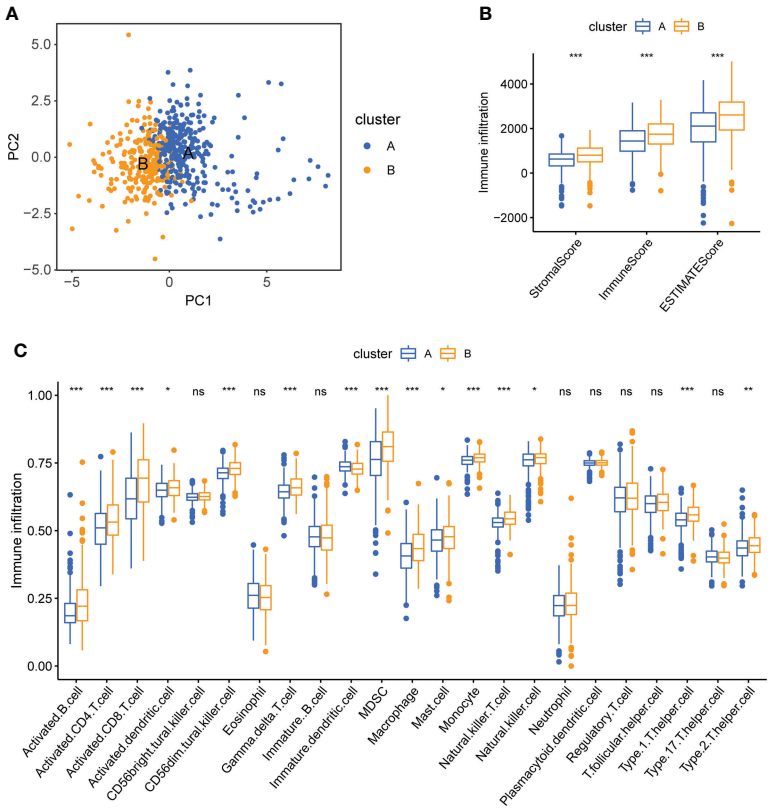

FIGURE 4
Tumor immune microenvironment analysis of two CPG subtypes. **(A)** PCA shows a significant difference in transcriptomes between the two subtypes. **(B)** Correlations between the two CPG subtypes and TME score. **(C)** The abundance of 23 kinds of infiltrating immune cells was evaluated by ssGSEA in the two CPG subtypes. CPG, cuproptosis-promoting gene; ns, no significant difference, *p < 0.05; **p < 0.01; and ***p < 0.001.

Furthermore, we downloaded the cohort data from NCT02684006 using sunitinib-targeted therapy for prognostic analysis. The proportion of patients with progression in the high-CUS group was lower than that in the low-CUS group (42% vs. 59%, Figure 9J), and the patients who progressed had lower CUS than those who did not (p <0.05, Figure 9K). The results of the Kaplan-Meier survival analysis showed that the high-CUS group had a longer PFS than the low-CUS group (p =0.0087, Figure 9L).

Additionally, we systematically mined the targeted drugs associated with the seven CPGs using the GSCA database. Using the GDSC (Supplementary Figure 6A) and CTRP data sources (Supplementary Figure 6B), the top 30 targeted drugs whose sensitivity was most strongly correlated with the mRNA expression of the seven CPGs were determined.

Identification and multi-level expression validation of potential CPGs

We identified two potential CPGs, *ACADM* and *ACAT1*, based on 31 CSRGs. We then performed differential expression validation of these two potential CPGs and seven identified CPGs (*FDX1*, *LIAS*, *LIPT1*, *DLD*, *DLAT*, *PDHA1* and *PDHB*). The GEPIA database showed that the expression of *FDX1* (Figure 10A), *ACADM* (Figure 10D) and *ACAT1* (Figure 10G) in KIRC was lower than that in the normal kidney tissue (p <0.05). The immunohistochemical results of *FDX1* (Figure 10B), *ACADM* (Figure 10E) and *ACAT1* (Figure 10H) in the HPA database showed that the protein expression of these genes significantly decreased in KIRC tissues compared to that in normal renal tubular epithelial tissues. In addition, we

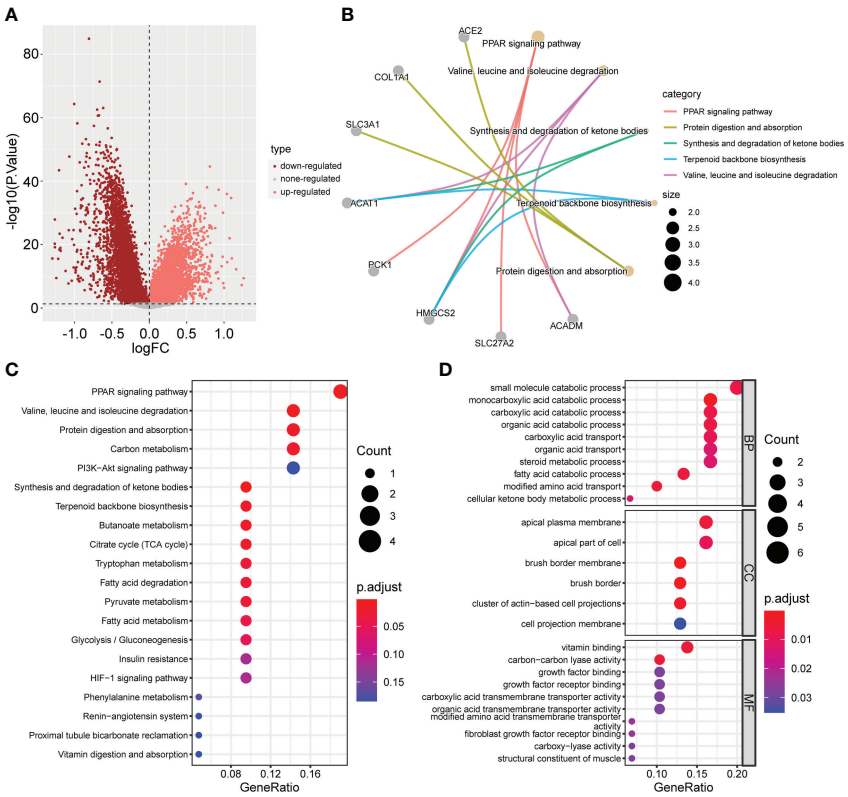

FIGURE 5
Screening and enrichment analysis of DEGs between the two CPG subtypes. **(A)** Volcano plot about Difference analysis between the two CPG subtypes. **(B)** The network diagram shows the correspondence between the KEGG top five pathways and related genes. **(C)** KEGG enrichment analysis of DEGs among two CPG subtypes. **(D)** GO enrichment analysis of DEGs among two CPG subtypes. DEG, differentially expressed gene; CPG, cuproptosis-promoting gene.

detected the expression differences of *FDX1* (Figure 10C), *ACADM* (Figure 10F), *ACAT1* (Figure 10I), *PDHA1* (Figure 10K), *PDHB* (Figure 10L), *DLAT* (Figure 10M), *DLD* (Figure 10N), *LIAS* (Figure 10O) and *LIPT1* (Figure 10P) between renal tubular epithelial cells (HK-2) and KIRC cells (Caki-1 and 786-O) using qRT-PCR. The expression of these genes was significantly down-regulated in Caki-1 cells compared to that in HK-2 cells ($p < 0.05$). Finally, western blot results indicated that *FDX1* and *ACAT1* expression was higher in HK-2 cells than in Caki-1 cells, but there was no significant difference between 786-O and HK-2 cells (Figure 10J).

Proliferation functional validation of *FDX1* and validation of cuproptosis in KIRC cells

To further investigate the function of *FDX1*, a key cuproptosis gene, in KIRC, we silenced *FDX1* to detect its effect on Caki-1 cells' proliferation. Subsequently, si-FDX1#1 and si-FDX1#2 were determined for further study because they showed higher silencing efficacy compared to NC-transfected cells (Figure 11A). CCK8 and EdU assays showed that FDX1 depletion promoted KIRC cell growth (Figures 11B, C), and the clone formation assay demonstrated that FDX1 improves the proliferative capacity of KIRC cells (Figure 11D). To figure out the relationship between FDX1 and two potential CPGs, we detected the expression of ACADM and ACAT1 in transfected Caki-1 cells. However, no significant expression difference was found (Figure 11E).

Elesclomol has recently been found to be a potent copper ionophore. We performed the CCK8 assay of elesclomol and $CuCl_2$ to test whether there is cuproptosis in Caki-1 cells. Compared with the negative control group, the $CuCl_2$ group showed slight cytotoxicity, but was not very significant, the elesclomol group showed certain cytotoxicity, while $CuCl_2$& elesclomol group had a significantly enhanced cytotoxicity on Caki-1 cells (Figure 11F).

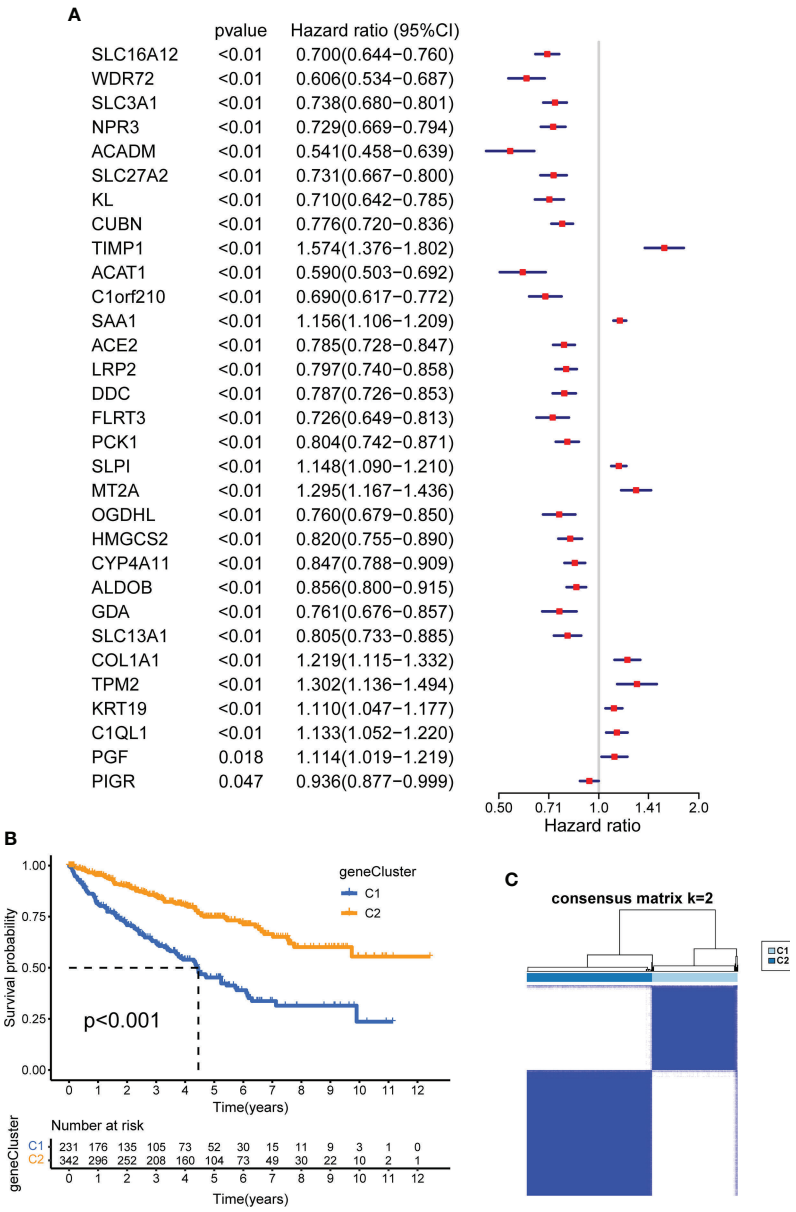

FIGURE 6
Construction of CSRG gene subtypes and prognostic analysis. **(A)** Univariate COX regression analysis of 31 DEGs to screen CSRGs. **(B)** Kaplan–Meier curves for the two gene subtypes (OS, Log-rank test, $p < 0.001$). **(C)** consensus matrix that divides all samples into two geneclusters (k=2). CSRG, cuproptosis subtypes related gene; DEG, differentially expressed gene.

Discussion

KIRC is insensitive to both radiotherapy and chemotherapy (5), and targeted therapy has been the mainstay of treatment of advanced KIRC. In recent years, the development of ICIs has changed the treatment landscape of advanced KIRC and ICIs have become the first-line treatment option (31). Single-agent pembrolizumab has shown antitumor activity in the first-line treatment of patients with advanced KIRC according to the phase II KEYNOTE-427 study (32). In the phase III CheckMate 214 clinical trial, nivolumab combined with ipilimumab improved OS in patients with intermediate- or low-risk previously untreated advanced KIRC (33). Targeted therapy combined with immunotherapy has become the first-line treatment for metastatic or unresectable KIRC and tends to gradually replace targeted therapy alone (9). However, there is

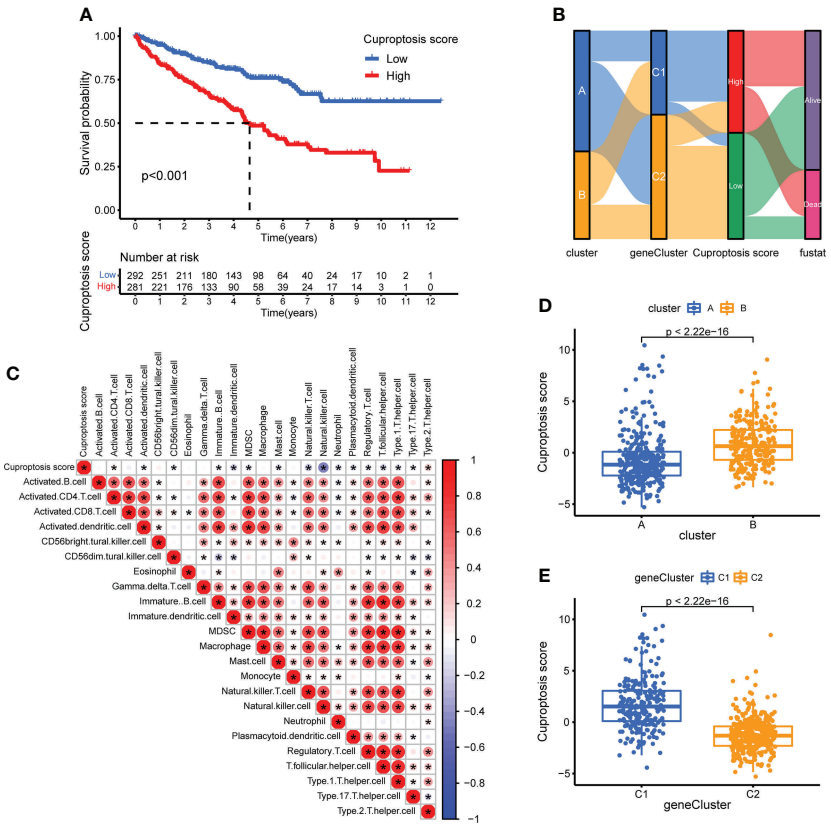

FIGURE 7
Construction of CUS and grouping based on score. **(A)** Kaplan–Meier survival analysis between the high- and low-CUS groups (OS, Log-rank test, $p < 0.001$). **(B)** Sankey diagram of subtype distributions in groups with different CUSs and survival outcomes. **(C)** The correlation matrix of cuproptosis and all 22 infiltrating immune cells. Red means positive correlation, whereas blue means negative correlation. $p < 0.05$ was the cut-off. **(D)** Differences in CUS levels between the two CPG subtypes. **(E)** Differences in CUS levels between the two CSRG gene subtypes. CUS, cuproptosis score; CPG, cuproptosis-promoting gene; CSRG, cuproptosis subtypes related gene; *$p < 0.05$.

still a lack of effective targets to help patients with metastatic or unresectable KIRC more precisely and to individually select therapeutic drugs.

Cuproptosis is an emerging cell death mechanism, which is closely related to mitochondrial metabolism and the TCA cycle, which is different from other death modes such as ferroptosis, necroptosis, and pyroptosis. It is precise because of the unique metabolic characteristics of cuproptosis that KIRC is considered to be more closely related to cuproptosis than to several other cell death modes. These previously discovered cell death modes have been found to have many predictive models and molecular typing constructed in KIRC (34–36), and cuproptosis still has great research prospects for KIRC typing. *FDX1*, a key gene that promotes cuproptosis, functions as an upstream regulator of protein lipoylation. The lipoylated component of the TCA cycle directly binds to Cu ions to activate cuproptosis (13). Therefore, both Cu ions and mitochondrial respiration are key factors in cuproptosis. KIRC has a unique metabolic profile that exhibits the classic Warburg effect *in vivo* (37). This means that KIRC exhibits marked inhibition of glucose oxidation and activation of aerobic glycolysis (38). Based on the correlation between worsening prognosis and metabolic shifts in patients with KIRC, including decreased TCA cycle activity, increased dependence on pentose phosphate shunt, decreased AMP-activated protein kinase, increased glutamine transport, and fatty acid production (39), we hypothesized that cuproptosis may be suppressed in KIRC. Differential analysis verified our conjecture, and seven CPGs displayed varying degrees of low expression in KIRC. This result suggests an association between cuproptosis and the gene map of KIRC.

First, we selected seven CPGs with similar functions and strong correlations and identified two clusters with different biological and clinical characteristics in the comprehensive cohort of TCGA-KIRC and GSE29609. Cluster B showed a poorer prognosis and a higher level of immune infiltration than cluster A, which includes immune-promoting cells, such as CD4+ T cells, CD8+ T cells, and immune-suppressing cells, such as MDSCs and macrophages. Next, we performed a

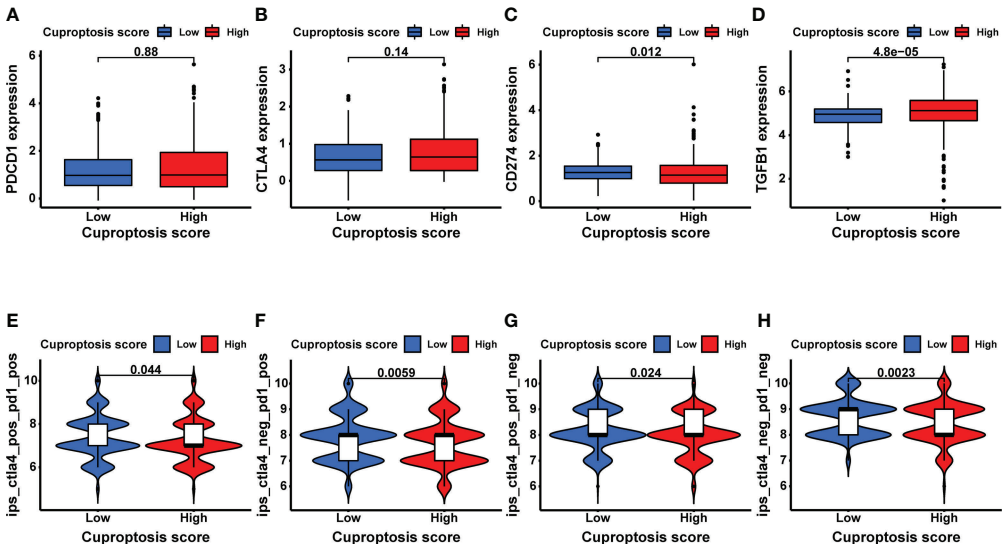

FIGURE 8
Exploratory analysis of immunotherapy based on CUS grouping. **(A–D)** The expression levels of immune target genes in different CUS groups: *PDCD1* **(A)**, *CTLA4* **(B)**, *CD274* **(C)** and *TGFB1* **(D)**. **(E–H)** The efficacy of 4 ICIs was predicted by IPS scores from the TCGA-KIRC cohort in TCIA database: ctla4_pos_pd1_pos **(E)**, ctla4_neg_pd1_pos **(F)**, ctla4_pos_pd1_neg **(G)** and ctla4_neg_pd1_neg **(H)**. CUS, cuproptosis score; ICI: immune checkpoint inhibitor; IPS, immune cell proportion score; pos, positive; neg, negative.

differential analysis of the two subtypes and identified 31 DEGs. Enrichment analysis revealed that DEGs were associated with various metabolic pathways, including the PPAR signaling pathway, carbon metabolism, TCA cycle, fatty acid degradation, and the PI3K-Akt signaling pathway. The PPAR signaling pathway is related to mitochondrial metabolism, fatty acylation of proteins involves the attachment of fatty acids to peptide chains in the form of fatty acyl groups, and lipoylation of key proteins in the mitochondrial TCA cycle is the core mechanism of cuproptosis. The downstream target of PI3K/Akt is a mammalian target of rapamycin (mTOR), which is key to the treatment of advanced KIRC. This finding also provided us with more potential molecular mechanisms of cuproptosis in KIRC.

Using univariate Cox regression analysis, we selected all 31 DEGs for CSRGs. We further constructed two new clusters based on the 31 CSRGs. Among them, geneclusterC1 had the poorest prognosis. To quantify the status of cuproptosis, predict the prognosis of KIRC more accurately, and guide clinical decision-making, we constructed the CUS using the Boruta algorithm combined with PCA. The patients in the high-CUS group had a poorer prognosis. The expression of immune-related targets showed that patients in the high-CUS group had significantly higher expression of *TGFB1*, which is one of the ligands of the TGFB pathway and is the most prevalent isoform expressed in many human tumors. Regulatory T cells (Tregs) exert a contact-dependent inhibitory effect on immune cells by producing TGFB1. On the surface of Tregs, TGFB1 binds to the membrane protein GARP in its inactive form. Monoclonal antibodies against the GARP/TGFB1 complex alone or in combination with antibodies targeting the CTLA4 or PD1/PD-L1 pathways can improve the efficacy of immunotherapy (40). In addition, selective inhibition of *TGFB1* may alter resistance to anti-PD-1 therapy by altering the tumor immune environment (41). Galunisertib is a novel inhibitor of TGF-β receptor 1. Phase 1 studies have demonstrated the safety of galunisertib and its antitumor activity in patients with glioma (42). In addition, combination therapy with *TGFB* and ICIs is in the clinical drug development stage for hepatocellular carcinoma, non-small cell lung cancer, and pancreatic cancer (NCT02423343; NCT02734160) (43). We then used TCIA data to predict the efficacy of immunotherapy and observed that the patients in the high-CUS group showed poorer results for all four ICIs. This finding suggests that the effect of different CUS values on the efficacy of immunotherapy is not dependent on *PD1* and *CTLA4*, but may be dependent on *TGFB1*. This finding is consistent with the results of our study. Therefore, our findings suggest that the combination of *TGFB1* inhibitors and immunotherapy may improve the efficacy of immunotherapy for patients in the high-CUS group.

Next, we explored targeted therapy. The results of the IC50 drug susceptibility analysis suggested that the patients in the high-CUS group were more likely to develop resistance to sorafenib, erlotinib, and lapatinib, but they were more sensitive to sunitinib and axitinib. Thus, although patients in the high-CUS group have poorer prognosis and immunotherapy

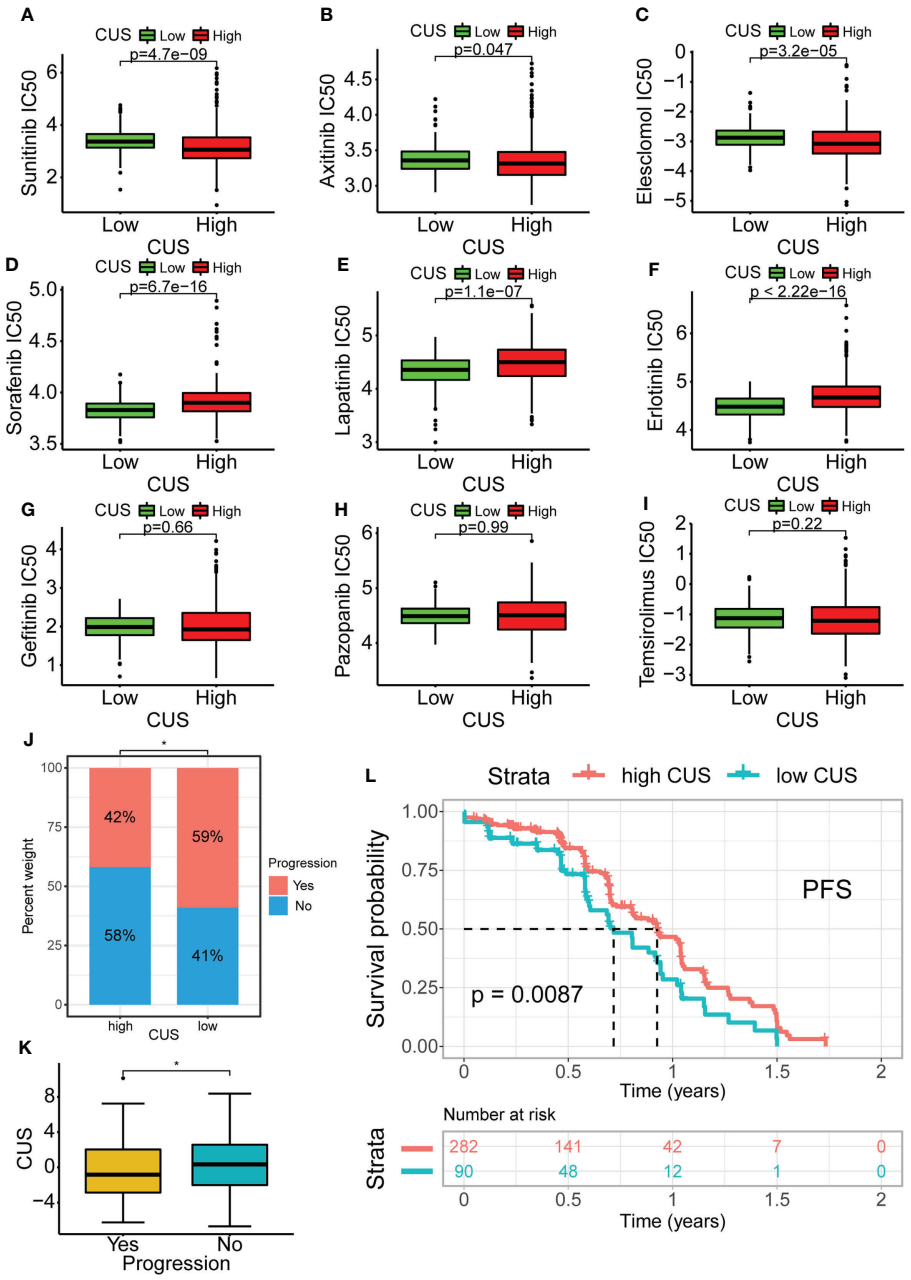

FIGURE 9
Drug susceptibility analysis of common targeted drugs and validation of targeted therapy cohort in KIRC. Based on cuproptosis grouping, drug sensitivity of Sunitinib**(A)**, Axitinib **(B)**, Elesclomol **(C)**, Sorafenib **(D)**, Lapatinib **(E)**, Erlotinib **(F)**, Gefitinib **(G)**, Pazopanib **(H)** and Temsirolimus **(I)** is conducted. **(J)** Obtaining data from the KIRC cohort using Sunitinib in NCT02684006. Proportional distribution of progression status in the high- and low-CUS groups. **(K)** Comparison of CUS levels between progression group and non-progression group. **(L)** Kaplan–Meier survival analysis between the high- and low-CUS groups (PFS, Log-rank test, p < 0.001). CUS, cuproptosis score; PFS: progression free survival; *p < 0.05.

efficacy, sunitinib and axitinib may bring clinical benefits. Sunitinib monotherapy is the classic first-line therapy for advanced KIRC (7, 44). We further performed prognostic validation in a cohort of patients with sunitinib-treated advanced KIRC in NCT02684006. After sunitinib treatment, the high-CUS group showed slower progression and even reversed the original poor prognosis in the PFS curve. This suggests that sunitinib may be one of the few treatment options for patients with high CUS.

Drug susceptibility analysis also revealed that the patients in the high-CUS group were more sensitive to elesclomol. Cancer cells with high mitochondrial respiration are more prone to

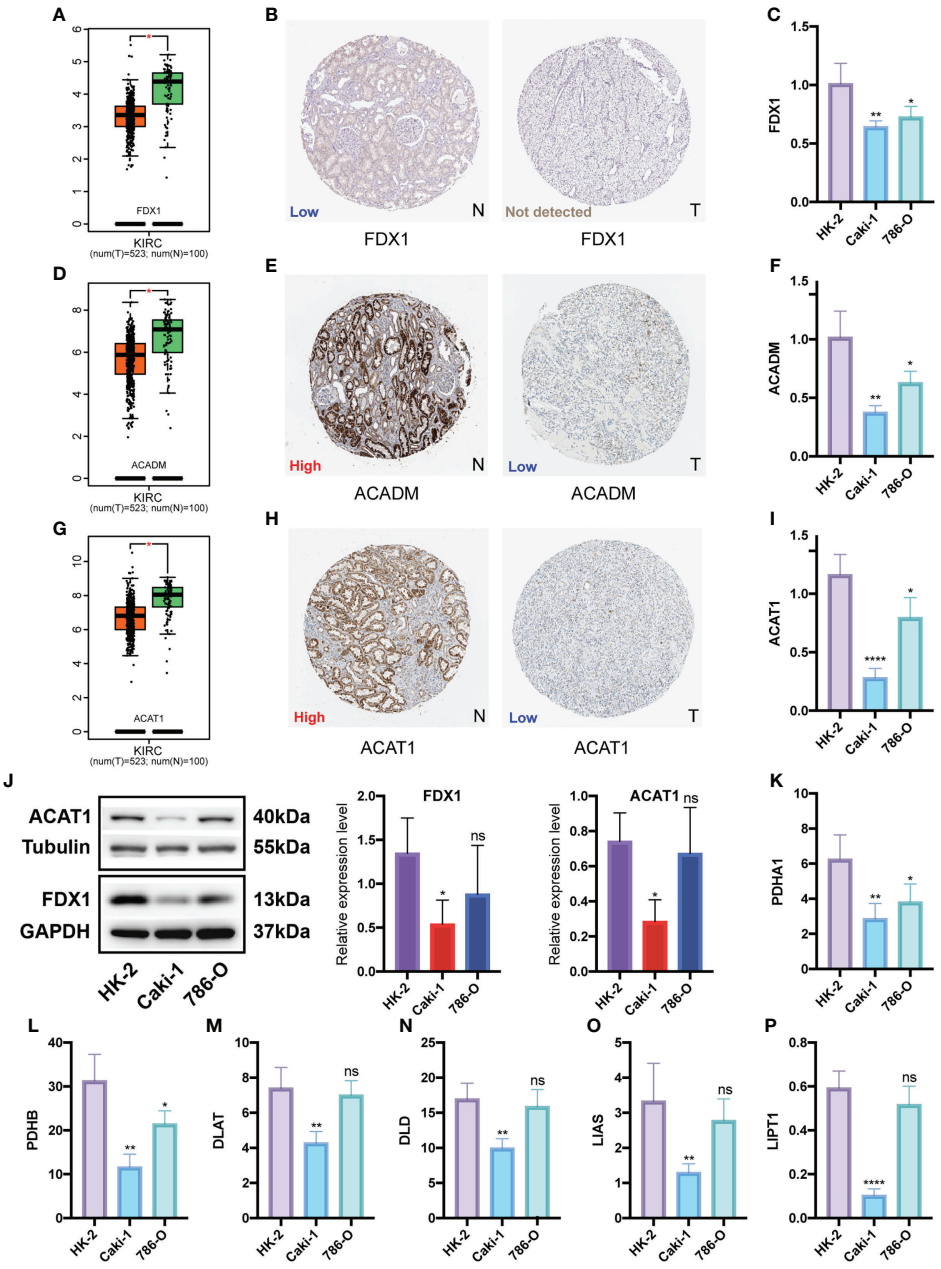

FIGURE 10
Differential expression validation of 7 CPGs and 2 potential CPGs between KIRC and normal samples. GEPIA database was used to compare the expression differences of *FDX1* **(A)**, *ACADM* **(D)** and *ACAT1* **(G)** between KIRC and normal kidney tissues. The HPA database showed the expression of *FDX1* **(B)**, *ACADM* **(E)** and *ACAT1***(H)** at the tissue protein level by immunohistochemistry. Western Blot was used to compare the protein levels of *FDX1* and *ACAT1* in KIRC cells (Caki-1 and 786-0) and normal renal tubular epithelial cells (HK-2), and the results were semi-quantified by integrated density **(J)**. qRT-PCR was used to compare mRNA levels of *FDX1* **(C)**, *ACADM* **(F)**, *ACAT1* **(I)**, *PDHA1* **(K)**, *PDHB* **(L)**, *DLAT* **(M)**, *DLD* **(N)**, *LIAS* **(O)** and *LIPT1* **(P)** in KIRC cells (Caki-1, 786-0) and normal renal tubular epithelial cells (HK-2). CPG, cuproptosis-promoting gene; N, normal; T,tumor; ns, no significant difference, *p < 0.05, **p < 0.01, and ****p < 0.0001. Western Blot data are means ± SD, with n = 3; qRT-PCR data are means ± SD, with n = 4.

cuproptosis, and copper ionophores represented by elesclomol may present a new cancer therapy (13). Current clinical trials of elesclomol have not achieved satisfactory results (14, 45), however, we expect to discover new ways to activate cuproptosis. The distinct metabolic profile of KIRC suggests that activation of cuproptosis may require a combination of elesclomol and aerobic glycolysis inhibitors. Studies have shown a relationship between metabolic and immune activity in KIRC (46), whereas *TGFB* was

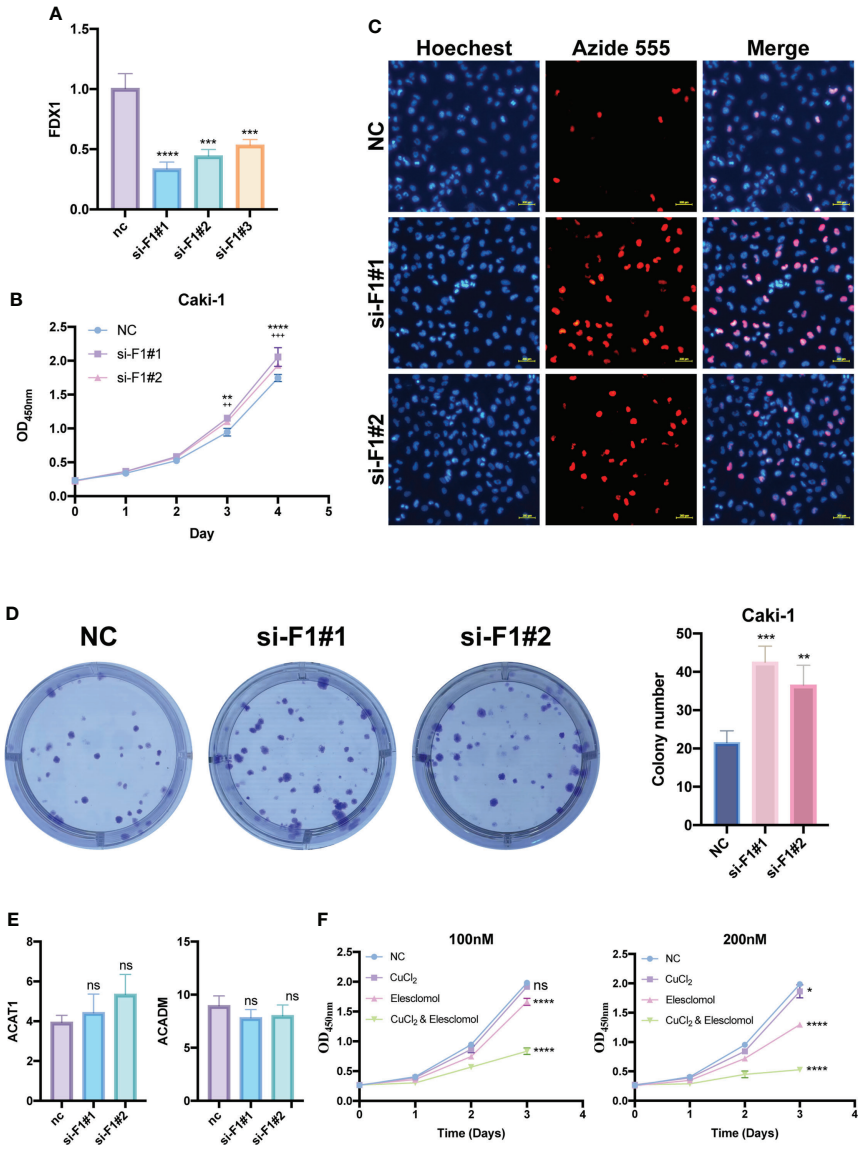

FIGURE 11
Proliferation functional validation of *FDX1* and validation of cuproptosis in KIRC cells. **(A)** Silencing efficiency of *FDX1* by qRT-PCR. CCK8 assay **(B)**, EDU assay **(C)** and Colony formation assay **(D)** show the effect of *FDX1* knockdown on the proliferation of Caki-1 cells. * is for si-F1#1, $^{+}$ is for si-F1#2. **(E)** Changes in *ACADM* and *ACAT1* mRNA expression levels after knockdown of *FDX1* by qRT-PCR. **(F)** The effects of elesclomol and $CuCl_2$ on Caki-1 cell death were explored by CCK8 assay. si-F1#1, si-FDX1#1; si-F1#2, si-FDX1#2; ns, no significant difference, *p < 0.05, **p < 0.01, ***p < 0.001 and ****p < 0.0001; $^{++}$p < 0.01 and $^{+++}$ p < 0.001; CCK8 assay and Colony formation assay data are means ± SD, with n = 3; qRT-PCR data are means ± SD, with n = 4.

found to promote aerobic glycolysis in renal fibroblasts (47). *TGFB1* may play a role in this relation; therefore, combination therapy may benefit from *TGFB1* inhibitors.

Finally, we identified two potential CPGs from 31 CSRGs: *ACADM* and *ACAT1*. We verified that these two genes were weakly expressed in KIRC compared to the normal samples through three levels of validation in the GEPIA database, HPA database, and qRT-PCR results. The main function of *ACADM* is to catalyze the initial step of the mitochondrial fatty acid β-oxidation pathway. Inhibition of *ACADM* can promote dysregulation of fatty acid oxidation, leading to hepatocellular carcinoma progression (48). *ACAT1* is a key enzyme that catalyzes the production of mitochondrial ketone bodies. Combination therapy with an *ACAT1* inhibitor and anti-PD-1 antibody showed better efficacy than immunotherapy alone in controlling tumor progression (49). Previous studies show that *ACADM* and *ACAT1* are protective tumor suppressors of KIRC, which is consistent with our findings (50, 51).

In summary, we performed cluster analysis for typing based on CPGs and constructed a score that quantifies the cuproptosis status. The CUS can effectively predict the prognosis and efficacy of targeted therapy and immunotherapy. In conjunction with the 2021 National Comprehensive Cancer Network (NCCN) guidelines (52), we developed a detailed treatment strategy for treatment options for patients with metastatic or unresectable KIRC. For patients in the low-CUS group, conventional targeted therapy combined with immunotherapy strategies recommended by the guidelines can be used as the first-line treatment. Note that among the targeted therapy drugs, axitinib and sunitinib can be avoided if possible. For the first-line treatment of patients in the high-CUS group, we recommend a triple-drug combination of axitinib, pembrolizumab, and a *TGFB1* inhibitor. Sunitinib monotherapy is also a feasible treatment option. Axitinib monotherapy can be used as a second-line therapy.

To further explore the relationship between the cuproptosis gene and KIRC, we first verified the differential expression of the CPGs at mRNA and protein levels. Next, we silenced *FDX1* in Caki-1 cells and found that the proliferation of Caki-1 cells was significantly promoted. Finally, to provide preliminary evidence that Cuproptosis may be present in KIRC, we designed CCK8 assays with reference to the research of Tsvetkov P et al. (53). We found that when copper was added to elesclomol at a molar ratio of 1:1, it significantly reduced the activity of KIRC cells. These results suggest that the delivery of large amounts of copper ions into cells by elesclomol may trigger cuproptosis in KIRC.

The study has some limitations. First, more cohorts of immunotherapy and targeted therapy are needed to validate and optimize the conclusions and improve the predictive power of the scoring system. Second, *TGFB1* inhibitors, elesclomol, and aerobic glycolysis inhibitors are new therapeutic agents based on cuproptosis. Further basic clinical trials are required to explore the efficacy of these agents.

Conclusion

In this study, a scoring system for cuproptosis—CUS was constructed, which developed a novel and precise strategy for the selection of targeted therapy and immunotherapy in patients with advanced KIRC, and also provided new insights into the relationship among cuproptosis, metabolism and immunity in KIRC.

Data availability statement

The datasets presented in this study can be found in online repositories. The names of the repository/repositories and accession number(s) can be found in the article/Supplementary Material. Due to the large size of the original data and code files, the complete original data and code can be downloaded from https://www.jianguoyun.com/p/DVP0rksQ3rToChjO1M4EIAA. If the link does not work, please contact our corresponding author's email address and we will provide it.

Author contributions

KC designed the study, GZ and XC conducted the data analysis, and wrote the manuscript. GZ, XC, and JF participated in and contributed to the experiments of this study. JF, PT, and AC participated in manuscript revision. All authors read and approved the final manuscript.

Funding

This work was supported by the National Natural Science Foundation of China (81874137), Funds for International Cooperation and Exchange of the National Natural Science Foundation of China (GZ1699), key research and development projects in Hunan Province (2022SK2022), the science and technology innovation Program of Hunan Province (2020RC4011), the Hunan Province Science and Technology Talent Promotion Project (2019TJ-Q10), Scientific research project of Hunan Provincial Health Commission (202209034683), Young Scholars of "Furong Scholar Program" in Hunan Province, and the Wisdom Accumulation and Talent Cultivation Project of the Third Xiangya Hospital of Central South University (BJ202001).

Acknowledgments

We sincerely thank the public databases, including GEPIA2, GSCA, HPA, UCSC Xena and GEO for providing open access.

Conflict of interest

The authors declare that the research was conducted in the absence of any commercial or financial relationships that could be construed as a potential conflict of interest.

Publisher's note

Supplementary material

The Supplementary Material for this article can be found online at: https://www.frontiersin.org/articles/10.3389/fimmu.2022.954440/full#supplementary-material.

SUPPLEMENTARY FIGURE 1
Genetic, transcriptional and post-transcriptional alterations of CPGs in KIRC in GSCA database. **(A)** Expression level of seven CPGs. **(B)** Frequencies of SNV among CPGs. **(C)** Percentage of various types of CNV in CPGs. **(D)** Spearman correlation between mRNA expression and CNV levels of CPGs. **(E)** Spearman correlation between mRNA expression and methylation levels of CPGs. **(F)** Differences in methylation levels of CPGs. CPG: cuproptosis-promoting gene.

SUPPLEMENTARY FIGURE 2
Detailed results of consensus clustering. **(A–C)** Detailed Results of consensus clustering to construct CPGs subtypes: cumulative distribution curve **(A)**, area under the cumulative distribution curve **(B)** and tracking plot **(C)**. **(D–F)** Detailed Results of consensus clustering to construct CSRGs gene subtypes: cumulative distribution curve **(D)**, area under the cumulative distribution curve **(E)** and tracking plot **(F)**. CPG, cuproptosis-promoting gene; CSRG, cuproptosis subtypes related gene.

SUPPLEMENTARY FIGURE 3
Difference comparison of enriched pathways of two different CPG subtypes by GSVA. **(A–C)** Heatmaps comparing GSVA pathway scores for two CPG subtypes from three items: HALLMARK **(A)**, KEGG **(B)**, and Reactome **(C)**. CPG, cuproptosis-promoting gene.

SUPPLEMENTARY FIGURE 4
Differences in clinicopathological and biological features between two gene subtypes. **(A)** Expression differences of 31 CSRGs between the two gene subtypes. **(B)** Heatmap of the distribution of clinicopathological features and CSRG expression between two different gene subtypes. CSRG, cuproptosis subtypes related gene; ***p < 0.001.

SUPPLEMENTARY FIGURE 5
Clinical subgroup analysis of CUS in KIRC. **(A–G)** Finding the relationship between six clinical features and CUS by difference comparison and ratio distribution: fustat **(A)**, Grade **(B)**, T_stage **(C)**, N_stage **(D)**, M_stage **(E)** and Stage **(F)**. CUS, cuproptosis score.

SUPPLEMENTARY FIGURE 6
Observation of the sensitivity of CPGs to targeted drugs using the GSCA database. **(A)** Correlation between GDSC drug sensitivity and CPGs mRNA expression. **(B)** Correlation between CTRP drug sensitivity and CPGs mRNA expression. CPG, cuproptosis-promoting gene.

References

1. Linehan WM, Ricketts CJ. The cancer genome atlas of renal cell carcinoma: findings and clinical implications. *Nat Rev Urol* (2019) 16(9):539–52. doi: 10.1038/s41585-019-0211-5

2. Rini BI, Campbell SC, Escudier B. Renal cell carcinoma. *Lancet* (2009) 373 (9669):1119–32. doi: 10.1016/s0140-6736(09)60229-4

3. Fisher R, Gore M, Larkin J. Current and future systemic treatments for renal cell carcinoma. *Semin Cancer Biol* (2013) 23(1):38–45. doi: 10.1016/j.semcancer.2012.06.004

4. Master VA, Gottschalk AR, Kane C, Carroll PR. Management of isolated renal fossa recurrence following radical nephrectomy. *J Urol* (2005) 174(2):473–7. doi: 10.1097/01.ju.0000165574.62188.d0

5. Jacobsohn KM, Wood CG. Adjuvant therapy for renal cell carcinoma. *Semin Oncol* (2006) 33(5):576–82. doi: 10.1053/j.seminoncol.2006.06.005

6. Bagcchi S. Sunitinib still fi rst-line therapy for metastatic renal cancer. *Lancet Oncol* (2014) 15(10):e420. doi: 10.1016/s1470-2045(14)70366-3

7. Ravaud A, Motzer RJ, Pandha HS, George DJ, Pantuck AJ, Patel A, et al. Adjuvant sunitinib in high-risk renal-cell carcinoma after nephrectomy. *N Engl J Med* (2016) 375(23):2246–54. doi: 10.1056/NEJMoa1611406

8. Hsieh JJ, Purdue MP, Signoretti S, Swanton C, Albiges L, Schmidinger M, et al. Renal cell carcinoma. *Nat Rev Dis Primers* (2017) 3:17009. doi: 10.1038/nrdp.2017.9

9. Rini BI, Plimack ER, Stus V, Gafanov R, Hawkins R, Nosov D, et al. Pembrolizumab plus axitinib versus sunitinib for advanced renal-cell carcinoma. *N Engl J Med* (2019) 380(12):1116–27. doi: 10.1056/NEJMoa1816714

10. Yu EM, Linville L, Rosenthal M, Aragon-Ching JB. A contemporary review of immune checkpoint inhibitors in advanced clear cell renal cell carcinoma. *Vaccines (Basel)* (2021) 9(8):919. doi: 10.3390/vaccines9080919

11. Tsang T, Davis CI, Brady DC. Copper biology. *Curr Biol* (2021) 31(9):R421–r427. doi: 10.1016/j.cub.2021.03.054

12. Saporito-Magriñá CM, Musacco-Sebio RN, Andrieux G, Kook L, Orrego MT, Tuttolomondo MV, et al. Copper-induced cell death and the protective role of glutathione: the implication of impaired protein folding rather than oxidative stress. *Metallomics* (2018) 10(12):1743–54. doi: 10.1039/c8mt00182k

13. Tsvetkov P, Coy S, Petrova B, Dreishpoon M, Verma A, Abdusamad M, et al. Copper induces cell death by targeting lipoylated TCA cycle proteins. *Science* (2022) 375(6586):1254–61. doi: 10.1126/science.abf0529

14. O'Day SJ, Eggermont AM, Chiarion-Sileni V, Kefford R, Grob JJ, Mortier L, et al. Final results of phase III SYMMETRY study: randomized, double-blind trial of elesclomol plus paclitaxel versus paclitaxel alone as treatment for chemotherapy-naive patients with advanced melanoma. *J Clin Oncol* (2013) 31(9):1211–8. doi: 10.1200/jco.2012.44.5585

15. Teng R, Liu Z, Tang H, Zhang W, Chen Y, Xu R, et al. HSP60 silencing promotes warburg-like phenotypes and switches the mitochondrial function from ATP production to biosynthesis in ccRCC cells. *Redox Biol* (2019), 24:101218. doi: 10.1016/j.redox.2019.101218

16. Voli F, Valli E, Lerra L, Kimpton K, Saletta F, Giorgi FM, et al. Intratumoral copper modulates PD-L1 expression and influences tumor immune evasion. *Cancer Res* (2020) 80(19):4129–44. doi: 10.1158/0008-5472.Can-20-0471

17. Liu CJ, Hu FF, Xia MX, Han L, Zhang Q, Guo AY. GSCALite: a web server for gene set cancer analysis. *Bioinformatics* (2018) 34(21):3771–2. doi: 10.1093/bioinformatics/bty411

18. Johnson WE, Li C, Rabinovic A. Adjusting batch effects in microarray expression data using empirical bayes methods. *Biostatistics* (2007) 8(1):118–27. doi: 10.1093/biostatistics/kxj037

19. Wilkerson MD, Hayes DN. ConsensusClusterPlus: a class discovery tool with confidence assessments and item tracking. *Bioinformatics* (2010) 26 (12):1572–3. doi: 10.1093/bioinformatics/btq170

20. Hänzelmann S, Castelo R, Guinney J. GSVA: gene set variation analysis for microarray and RNA-seq data. *BMC Bioinf* (2013) 14:7. doi: 10.1186/1471-2105-14-7

21. Yoshihara K, Shahmoradgoli M, Martínez E, Vegesna R, Kim H, Torres-Garcia W, et al. Inferring tumour purity and stromal and immune cell admixture from expression data. *Nat Commun* (2013), 4:2612. doi: 10.1038/ncomms3612

22. Subramanian A, Tamayo P, Mootha VK, Mukherjee S, Ebert BL, Gillette MA, et al. Gene set enrichment analysis: a knowledge-based approach for interpreting genome-wide expression profiles. *Proc Natl Acad Sci U.S.A.* (2005) 102(43):15545–50. doi: 10.1073/pnas.0506580102

23. Ritchie ME, Phipson B, Wu D, Hu Y, Law CW, Shi W, et al. Limma powers differential expression analyses for RNA-sequencing and microarray studies. *Nucleic Acids Res* (2015) 43(7):e47. doi: 10.1093/nar/gkv007

24. Yu G, Wang LG, Han Y, He QY. clusterProfiler: an r package for comparing biological themes among gene clusters. *Omics* (2012) 16(5):284–7. doi: 10.1089/omi.2011.0118

25. Degenhardt F, Seifert S, Szymczak S. Evaluation of variable selection methods for random forests and omics data sets. *Brief Bioinform* (2019) 20 (2):492–503. doi: 10.1093/bib/bbx124

26. Charoentong P, Finotello F, Angelova M, Mayer C, Efremova M, Rieder D, et al. Pan-cancer immunogenomic analyses reveal genotype-immunophenotype

relationships and predictors of response to checkpoint blockade. *Cell Rep* (2017) 18 (1):248–62. doi: 10.1016/j.celrep.2016.12.019

27. Geeleher P, Cox N, Huang RS. pRRophetic: an r package for prediction of clinical chemotherapeutic response from tumor gene expression levels. *PloS One* (2014) 9(9):e107468. doi: 10.1371/journal.pone.0107468

28. Motzer RJ, Robbins PB, Powles T, Albiges L, Haanen JB, Larkin J, et al. Avelumab plus axitinib versus sunitinib in advanced renal cell carcinoma: biomarker analysis of the phase 3 JAVELIN renal 101 trial. *Nat Med* (2020) 26 (11):1733–41. doi: 10.1038/s41591-020-1044-8

29. GTEx Consortium. The genotype-tissue expression (GTEx) project. *Nat Genet* (2013) 45(6):580–5. doi: 10.1038/ng.2653

30. Tang Z, Kang B, Li C, Chen T, Zhang Z. GEPIA2: an enhanced web server for large-scale expression profiling and interactive analysis. *Nucleic Acids Res* (2019) 47(W1):W556–w560. doi: 10.1093/nar/gkz430

31. Lin E, Liu X, Liu Y, Zhang Z, Xie L, Tian K, et al. Roles of the dynamic tumor immune microenvironment in the individualized treatment of advanced clear cell renal cell carcinoma. *Front Immunol* (2021) 12:653358. doi: 10.3389/fimmu.2021.653358

32. McDermott DF, Lee JL, Bjarnason GA, Larkin JMG, Gafanov RA, Kochenderfer MD, et al. Open-label, single-arm phase II study of pembrolizumab monotherapy as first-line therapy in patients with advanced clear cell renal cell carcinoma. *J Clin Oncol* (2021) 39(9):1020–8. doi: 10.1200/jco.20.02363

33. Cella D, Grünwald V, Escudier B, Hammers HJ, George S, Nathan P, et al. Patient-reported outcomes of patients with advanced renal cell carcinoma treated with nivolumab plus ipilimumab versus sunitinib (CheckMate 214): a randomised, phase 3 trial. *Lancet Oncol* (2019) 20(2):297–310. doi: 10.1016/s1470-2045(18)30778-2

34. Xing XL, Liu Y, Liu J, Zhou H, Zhang H, Zuo Q, et al. Comprehensive analysis of ferroptosis- and immune-related signatures to improve the prognosis and diagnosis of kidney renal clear cell carcinoma. *Front Immunol* (2022) 13:851312. doi: 10.3389/fimmu.2022.851312

35. Xin S, Mao J, Duan C, Wang J, Lu Y, Yang J, et al. Identification and quantification of necroptosis landscape on therapy and prognosis in kidney renal clear cell carcinoma. *Front Genet* (2022) 13:832046. doi: 10.3389/fgene.2022.832046

36. Sun Z, Jing C, Guo X, Zhang M, Kong F, Wang Z, et al. Comprehensive analysis of the immune infiltrates of pyroptosis in kidney renal clear cell carcinoma. *Front Oncol* (2021), 11:716854. doi: 10.3389/fonc.2021.716854

37. Linehan WM, Srinivasan R, Schmidt LS. The genetic basis of kidney cancer: a metabolic disease. *Nat Rev Urol* (2010) 7(5):277–85. doi: 10.1038/nrurol.2010.47

38. Courtney KD, Bezwada D, Mashimo T, Pichumani K, Vemireddy V, Funk AM, et al. Isotope tracing of human clear cell renal cell carcinomas demonstrates suppressed glucose oxidation in vivo. *Cell Metab* (2018) 28(5):793–800.e2. doi: 10.1016/j.cmet.2018.07.020

39. Cancer Genome Atlas Research Network. Comprehensive molecular characterization of clear cell renal cell carcinoma. *Nature* (2013) 499(7456):43–9. doi: 10.1038/nature12222

40. Cuende J, Liénart S, Dedobbeleer O, van der Woning B, De Boeck G, Stockis J, et al. Monoclonal antibodies against GARP/TGF-β1 complexes inhibit the immunosuppressive activity of human regulatory T cells in vivo. *Sci Transl Med* (2015) 7(284):284ra56. doi: 10.1126/scitranslmed.aaa1983

41. Martin CJ, Datta A, Littlefield C, Kalra A, Chapron C, Wawersik S, et al. Selective inhibition of TGFβ1 activation overcomes primary resistance to checkpoint blockade therapy by altering tumor immune landscape. *Sci Transl Med* (2020) 12(536): eaay8456. doi: 10.1126/scitranslmed.aay8456

42. Rodon J, Carducci MA, Sepulveda-Sánchez JM, Azaro A, Calvo E, Seoane J, et al. First-in-human dose study of the novel transforming growth factor-β receptor I kinase inhibitor LY2157299 monohydrate in patients with advanced cancer and glioma. *Clin Cancer Res* (2015) 21(3):553–60. doi: 10.1158/1078-0432.Ccr-14-1380

43. Holmgaard RB, Schaer DA, Li Y, Castaneda SP, Murphy MY, Xu X, et al. Targeting the TGFβ pathway with galunisertib, a TGFβRI small molecule inhibitor, promotes anti-tumor immunity leading to durable, complete responses, as monotherapy and in combination with checkpoint blockade. *J Immunother Cancer* (2018) 6(1):47. doi: 10.1186/s40425-018-0356-4

44. Staehler M, Motzer RJ, George DJ, Pandha HS, Donskov F, Escudier B, et al. Adjuvant sunitinib in patients with high-risk renal cell carcinoma: safety, therapy management, and patient-reported outcomes in the s-TRAC trial. *Ann Oncol* (2018) 29(10):2098–104. doi: 10.1093/annonc/mdy329

45. Monk BJ, Kauderer JT, Moxley KM, Bonebrake AJ, Dewdney SB, Secord AA, et al. A phase II evaluation of elesclomol sodium and weekly paclitaxel in the treatment of recurrent or persistent platinum-resistant ovarian, fallopian tube or primary peritoneal cancer: An NRG oncology/gynecologic oncology group study. *Gynecol Oncol* (2018) 151(3):422–7. doi: 10.1016/j.ygyno.2018.10.001

46. Wang Y, Zheng XD, Zhu GQ, Li N, Zhou CW, Yang C, et al. Crosstalk between metabolism and immune activity reveals four subtypes with therapeutic implications in clear cell renal cell carcinoma. *Front Immunol* (2022) 13:861328. doi: 10.3389/fimmu.2022.861328

47. Ding H, Jiang L, Xu J, Bai F, Zhou Y, Yuan Q, et al. Inhibiting aerobic glycolysis suppresses renal interstitial fibroblast activation and renal fibrosis. *Am J Physiol Renal Physiol* (2017) 313(3):F561–f575. doi: 10.1152/ajprenal.00036.2017

48. Ma APY, Yeung CLS, Tey SK, Mao X, Wong SWK, Ng TH, et al. Suppression of ACADM-mediated fatty acid oxidation promotes hepatocellular carcinoma *via* aberrant CAV1/SREBP1 signaling. *Cancer Res* (2021) 81(13):3679–92. doi: 10.1158/0008-5472.Can-20-3944

49. Yang W, Bai Y, Xiong Y, Zhang J, Chen S, Zheng X, et al. Potentiating the antitumour response of CD8(+) T cells by modulating cholesterol metabolism. *Nature* (2016) 531(7596):651–5. doi: 10.1038/nature17412

50. Xiao H, Chen P, Zeng G, Xu D, Wang X, Zhang X. Three novel hub genes and their clinical significance in clear cell renal cell carcinoma. *J Cancer* (2019) 10 (27):6779–91. doi: 10.7150/jca.35223

51. Chen L, Peng T, Luo Y, Zhou F, Wang G, Qian K, et al. ACAT1 and metabolism-related pathways are essential for the progression of clear cell renal cell carcinoma (ccRCC), as determined by Co-expression network analysis. *Front Oncol* (2019) 9:957. doi: 10.3389/fonc.2019.00957

52. Motzer RJ, Jonasch E, Boyle S, Carlo MI, Manley B, Agarwal N, et al. NCCN guidelines insights: Kidney cancer, version 1.2021. *J Natl Compr Canc Netw* (2020) 18(9):1160–70. doi: 10.6004/jnccn.2020.0043

53. Tsvetkov P, Detappe A, Cai K, Keys HR, Brune Z, Ying W, et al. Mitochondrial metabolism promotes adaptation to proteotoxic stress. *Nat Chem Biol* (2019) 15(7):681–9. doi: 10.1038/s41589-019-0291-9

frontiers | Frontiers in Oncology

TYPE Original Research
PUBLISHED 22 August 2022
DOI 10.3389/fonc.2022.905212

OPEN ACCESS

EDITED BY
Xian Zeng,
Fudan University, China

REVIEWED BY
Lian Xiang Luo,
Guangdong Medical University, China
Ming Jun Zheng,
Ludwig Maximilian University of Munich, Germany

*CORRESPONDENCE
Wentian Zhang
dr_zhangwentian@163.com

SPECIALTY SECTION
This article was submitted to Cancer Immunity and Immunotherapy, a section of the journal Frontiers in Oncology

RECEIVED 26 March 2022
ACCEPTED 22 July 2022
PUBLISHED 22 August 2022

CITATION
Wei S, Gu X and Zhang W (2022) Development and validation of a novel fibroblast scoring model for lung adenocarcinoma.
Front. Oncol. 12:905212.
doi: 10.3389/fonc.2022.905212

Development and validation of a novel fibroblast scoring model for lung adenocarcinoma

Shiyou Wei[1], Xuyu Gu[2] and Wentian Zhang[3]*

[1]Department of Anesthesiology, Shanghai Pulmonary Hospital, School of Medicine, Tongji University, Shanghai, China, [2]School of Medicine, Southeast University, Nanjing, China, [3]Department of Thoracic Surgery, Shanghai Pulmonary Hospital, School of Medicine, Tongji University, Shanghai, China

The interaction between cancer-associated fibroblasts (CAFs) and the tumor microenvironment (TME) is a key factor for promoting tumor progression. In lung cancer, the crosstalk between CAFs and malignant and immune cells is expected to provide new directions for the development of immunotherapy. In this study, we have systematically analyzed a single-cell dataset and identified interacting genes between CAFs and other cells. Subsequently, a robust fibroblast-related score (FRS) was developed. Kaplan-Meier (KM) and ROC analyses showed its good predictive power for patient prognoses in the training set comprising of specimens from the cancer genome atlas (TCGA) and in three external validation sets from the Gene Expression Omnibus (GEO). Univariate and multivariate Cox regression analyses suggested that FRS was a significant prognostic factor independent of multiple clinical characteristics. Functional enrichment and ssGSEA analyses indicated that patients with a high FRS developed "cold" tumors with active tumor proliferation and immunosuppression capacities. In contrast, those with a low FRS developed "hot" tumors with active immune function and cell killing abilities. Genomic variation analysis showed that the patients with a high FRS possessed a higher somatic mutation burden and copy number alterations and were more sensitive to chemotherapy; patients with a low FRS were more sensitive to immunotherapy, particularly anti-PD1 therapy. Overall, these findings advance the understanding of CAFs in tumor progression and we generated a reliable FRS-based model to assess patient prognoses and guide clinical decision-making.

KEYWORDS

lung adenocarcinoma, cancer-associated fibroblasts, tumor microenvironment, scoring model, prognosis

Introduction

Lung cancer has the highest incidence among all cancer types and is the leading cause of cancer-related deaths (1); lung adenocarcinoma (LUAD) is its most common histological type. Several epidemiological investigations and experimental studies have attributed the onset and progression of LUAD primarily to environmental factors and genetic alterations (2–4). Given a large number of non-smokers with LUAD, previous theories based solely on environmental factors have been disproven and research attention has been re-focused on profound alterations in the genetic content. To date, there are two main genetic factor-related treatment strategies, namely, targeted therapy and immunotherapy (5). However, most patients who receive targeted therapy are prone to resistance, and only a minority of them may benefit from immunotherapy. Therefore, it is crucial to develop robust tools for prognostic prediction and assessment of treatment responses to further facilitate accurate diagnoses and devise individualized treatment strategies.

Tumor microenvironment (TME) is defined as the environment surrounding the tumor, including the extracellular matrix, immune cells, and stromal cells, all of which are closely associated with tumor progression and treatment outcomes (6). Accumulating evidence elucidate the role of TME infiltration in immune therapeutic responses and resistance against different cancer types; these studies have also investigated their impact on patient prognoses (7, 8). Previous studies have focused more on immune cells. However, several findings have now highlighted the importance of stromal cells in tumor progression (9, 10). Cancer-associated fibroblasts (CAFs), a representative component of stromal cells, play crucial roles in cancer genesis, progression, and invasion (11, 12). Recently, the interaction between CAFs and the tumor immune microenvironment (TIME) has been identified as a key factor in promoting tumor progression (13, 14). CAFs interact with immune cells and other immune components within the TIME through various secreted cytokines, growth factors, and chemokines, resulting in an immunosuppressive TME that allows cancer cells to evade the surveillance mechanisms of the immune system (14, 15). Therefore, further investigation into the crosstalk between CAFs and TME is expected to provide new strategies for LUAD treatment, in particular for immunotherapy.

In this study, we used the single-cell dataset, GSE131907, to evaluate the crosstalk between CAFs and other cells. In addition, receptor-ligand pairs were systematically identified for interactions of CAFs with other cells. Based on these receptor-ligand genes, we generated the fibroblast-associated score (FRS) using the LASSO algorithm in the TCGA-LUAD cohort and the GEO meta-cohort to predict patient prognoses and estimate their sensitivity to chemotherapy and immunotherapy. Additionally, the associations among FRS, biological functions, TIME, and genomic alterations were systematically assessed. In summary, our findings are expected to advance the understanding of CAF functions in cancer as we have constructed and described here a robust scoring system to accurately predict patient prognoses and guide clinical decision-making.

Material and methods

Data extraction from online databases

The single-cell transcriptome dataset, GSE131907, was extracted from the GEO database (https://www.ncbi.nlm.nih.gov/geo/), consisting of data of 58 sequences from 44 patients. Next, these data were processed using the 10x Genomics method. Of these, we selected 29 normal lung tissues and early, advanced, and brain-metastasized lung tissues for further analyses. Detailed data processing procedures and ethical approval have been described previously (16).

The data of transcriptome RNA sequencing, Mutect2 mutation, HumanMethylation450 array, copy number variations (CNVs), and the corresponding clinical information were downloaded from TCGA database (https://cancergenome.nih.gov/) using the GDC API. A total of 492 LUAD samples were collected after the exclusion of patients with missed visits and incomplete clinical information. The raw FPKM sequencing data were normalized by TPM and used as the training cohort. Three mature LUAD cohorts were collected from GEO, including dataset GSE30219 from the Affymetrix HG-U133 Plus 2.0 Array platform, dataset GSE72094 from the Rosetta/Merck Human RSTA Custom Affymetrix 2.0 platform, and dataset GSE42127 from the Illumina HumanWG-6 v3.0 expression bead chip. To prevent batch effects on these chips, we merged the three GEO datasets and normalized the data by the log2 transformation using the combat function of the "sva" package (17). Subsequently, LUAD meta-data containing the complete clinical information of 615 individuals were used as the validation cohort. Additionally, we collected the publicly available immunotherapy cohorts with complete clinical information and transcriptomic data. Finally, the information of a cohort of advanced uroepithelial carcinoma treated with anti-PD-L1 immunotherapy (Imvigor210) consisting of 298 patients (8) and a cohort of non-small cell lung cancer (NSCLC) of 27 patients treated with PD1 (GSE135222) was collected.

Single-cell data analysis

The R package, "Seurat", was used to process the scRNA-seq data. In addition, cells with "min.cells < 3" and "min.features < 200" were excluded. After filtering out the cells with > 60% mitochondrial sequencing count and nFeature_RNA > 7000, a

total of 47822 cells were retained for subsequent analyses. The dataset was then normalized using the NormalizeData and ScaleData functions in Seurat. Cell types were identified according to the cell annotations provided in the original article.

To unravel the changes in the cell clusters during tumor progression, we used the R package, 'monocle', for the analysis of the single-cell trajectory. Subsequently, single-cell developmental trajectories were identified using the top 1500 variable genes (18). The Python package, "CellphoneDB", was used to identify receptor-ligand exchanges between cell clusters; the receptor-ligand interactions between eight-cell clusters were thus identified at the molecular level (19). Receptor-ligand pairs with p-values < 0.05 were screened to assess the molecular interaction network among CAFs and other cells. Corresponding interacting genes were identified as fibroblast-related genes (FRGs). Finally, the GGplot2 package was used to visualize these results.

Construction and validation of the FRS model

LUAD-TCGA cohort was used to train the model. Specifically, independent prognostic factors among FRGs were first screened by univariate Cox regression, and genes with P < 0.05 were included for further analysis. Subsequently, a Cox proportional risk model with LASSO penalties was used to identify the best prognostic model. To prevent overfitting, a five-fold cross-validation process was set up. Considering random sampling for cross-validation, 300 iterations were performed to identify the most stable prognostic model. The model with the highest frequency of occurrence in the 300 iterations served as the final prognostic model. Finally, FRS was calculated according to the following equation:

$$FRS = \sum i \quad Coefficient(mRNA_i) \times Expression(mRNA_i)$$

To assess the predictive power of the risk scores in the training and validation sets, the consistency index (C-index) was calculated using the "survcomp" R package, with a larger C-index indicating a more accurate predictive power of model (20). Patients were classified into high- and low-risk groups based on the median FRS. Furthermore, the prognostic value of the risk model was systematically assessed using the Kaplan Meir (KM) survival curves, univariate and multivariate Cox regression analyses, and time-dependent ROC curves.

Functional enrichment and immune infiltration analyses

We performed a single-sample gene set enrichment analysis (ssGSEA) based on the previously published molecular markers using the R package, "gsva", to assess the activities of the biological pathways for the samples, including angiogenesis, epithelial-mesenchymal transition (EMT), myeloid inflammation, and molecular markers for other immune-related pathways (21–24). Molecular markers for hypoxia were collected from Msigdb (25). Detailed pathway-related gene markers are shown in Table S1. Additionally, GSEA was performed between high- and low-FRS groups, and the significant KEGG pathways were screened using the set threshold of P < 0.05. Moreover, functional enrichment of genes was obtained using the Metascape (www.metascape.org/) database.

The abundances of immune cell infiltrate in tumor samples were estimated using the R package, "CIBERSORT", to evaluate the degree of infiltration of 22 immune cell types (26). The immune activity and tumor purity of the samples were assessed using the Estimate algorithm (27). The immunophenoscores (IPS) of the samples were calculated based on a previous study, with a higher IPS indicating a stronger immune activity of the sample (28). In short, IPS is calculated on a scale of 0-10 based on the transcriptome of the representative genes of the immunophenotype. Samplewise Z scores were positively weighted according to effective immune cells, negatively weighted according to inhibitive immune cells, and then averaged. Z score ≥ 3 is defined as IPS10, and Z score ≤ 0 is defined as IPS0.

Finally, homologous recombination deficiency (HRD) scores, indel neoantigens, and SNV neoantigens of the samples were obtained from Thorsson et al. (29).

Comparison of genomic variation landscapes between two groups

To compare the differences in mutation burdens between the two groups, the mutation data were processed using the 'maftools' package in R. The total number of mutations in the samples was first calculated, and genes with a minimum number of mutations > 30 were identified. The differences in mutation frequencies between the high- and low-FRS groups were then compared using a chi-square test and visualized using maftools (30). CNV data were processed using the GISTIC 2.0 webtool in Genepattern. Subsequently, significantly amplified and missing chromosomal segments were identified and differences in CNVs on the chromosomal arms were assessed. Finally, these CNV results were visualized using the R package, "ggplot2".

Clinical significance of the risk model

The five most commonly used first-line drugs, including cisplatin, docetaxel, gemcitabine, paclitaxel, and vinorelbine, were selected for the treatment of LUAD. Ridge regression was used to calculate the half-maximal inhibitory concentration (IC50) for each sample, which was then used to assess the

sensitivities of patients to chemotherapy in the high- and low-risk groups. Moreover, the accuracy of these predictions was assessed by a 10-fold cross-validation process (31). Furthermore, differentially expressed genes between the two groups were considered as potential therapeutic targets. The CMap database (https://clue.io/) was used to obtain the potential compounds targeting these genes. This database can not only predict drugs based on the gene expression profiles but also elucidate the mode of action (MoA) of these compounds targeting the corresponding molecular pathways. To assess the patient responses to immunotherapy, the TIDE online tool (http://tide.dfci.harvard.edu) was used (32). In addition, the unsupervised subclass mapping algorithm (https://cloud.genepattern.org/gp/) was used to assess the patient responses to anti-PD1 and anti-CTLA-4 immunotherapeutic regimens. Finally, we validated the predictive efficacy of FRS in the immunotherapy cohorts, Imvigor210 and GSE135222.

Clinical specimens

We obtained 50 tissue specimens from patients who received surgical resection of primary LUAD in Shanghai Pulmonary Hospital from September 2015 to April 2016, including 27 males and 23 females, with a mean age of (66.24 ± 7.3) years. And all patients were followed up every three months for five years. Inclusion criteria: 1, all were diagnosed as lung adenocarcinoma by postoperative pathological examination; 2, all did not receive radiotherapy or chemotherapy before surgery; 3, clinical data were complete. Exclusion criteria: 1, combined with chronic systemic diseases; 2, combined with other malignant tumors. Written informed consents of all patients were obtained before the study. The study was approved by Shanghai Pulmonary Hospital Ethics Committee (ethical lot number: K21-111Y).

Immunohistochemistry staining

After obtaining the tumor tissue, the tissue was routinely paraffin-embedded and preserved. In the experiment, tissue sections were dewaxed and rehydrated, and antigen repair was performed by incubating the slides in 10 mmol/L sodium citrate buffer and microwave treating the samples for 20 min. After being closed with 3% H2O2 and 10% normal goat serum (NGS), the slides were incubated with primary antibody at 4°C overnight. The paraffin-embedded LUAD sections were incubated with anti-TNFSF14 (ab115544, ABCAM), anti-JAM2 (ab156586, ABCAM), anti- LIFR (ab202847, ABCAM)、anti-SPN(ab101533, ABCAM)、anti- HGF (ab118871, ABCAM). The slides were then incubated with biotin-coupled anti-rabbit secondary antibody (1:1000, ab205718, Abcam, UK) for 2h at 37°C using the ABC kit from Vector Laboratories (Burlingame, CA, USA).

The sections were then incubated with polymeric HRP reagent and peroxidase activity was observed with diaminobenzidine tetrahydroxyl chloride solution (Vector Laboratories), and the sections were re-stained with hematoxylin. Ouant center is the analysis software of Pannoramic viewer. When the images of the tissue microarrays are scanned, the TMA software in Ouant center sets the numbers that correspond to the arrangement of the tissue sections. Thereafter, the densito quantification software in Quant center automatically identifies all dark brown dots in the microarray tissue as strongly positive, tan dots as moderately positive, light yellow dots as weakly positive, and blue cell nuclei only as negative, and analyzes the percentage of each stained (strong, moderate, weak, and negative) area in pixels, and finally performs an H-Score score.

Bioinformatic and statistical analyses

All statistical analyses and graph plotting were performed using the R software (version: 4.04). Comparisons between the two groups were made using the Wilcoxon test and differences in proportions were compared using the chi-square test. The KM plotter was used to generate the survival curves and statistically significant differences were assessed using the log-rank test. Time-dependent ROC curves (tROC) were plotted using the R package 'survivalROC'. Univariate and multivariate COX regression analyses were performed using the R package, "survival". Additionally, 'rms' was used to plot nomograms and calibration curves, and decision curve analysis (DCA) was performed using the "DCA" package (33). Unless specified otherwise, two-tailed $P < 0.05$ denoted statistical significance.

Results

CAF clustering and identification of FRGs

In order to explore the cross-talk between CAF and other cells and identifying the FRGs. We first analyzed the dataset, GSE131907, at single-cell resolution and identified a total of eight-cell clusters according to their original annotation (Figure 1A). The pseudo-time analysis suggested that CAFs were mainly aligned at the beginning of the trajectory (Figure 1B). Subsequently, the communication network between the eight-cell clusters was analyzed (Figure 1C). Specifically, CAFs were found to communicate the most with endothelial cells, followed by myeloid cells (Figure 1D). Significant receptor-ligand pairs were obtained as FRGs for subsequent analysis based on a set threshold of $P < 0.05$. The Dot plot was used to visualize the top five receptor-ligand pairs between CAFs and other cells (Figure 1E). Detailed results were shown in Table S2.

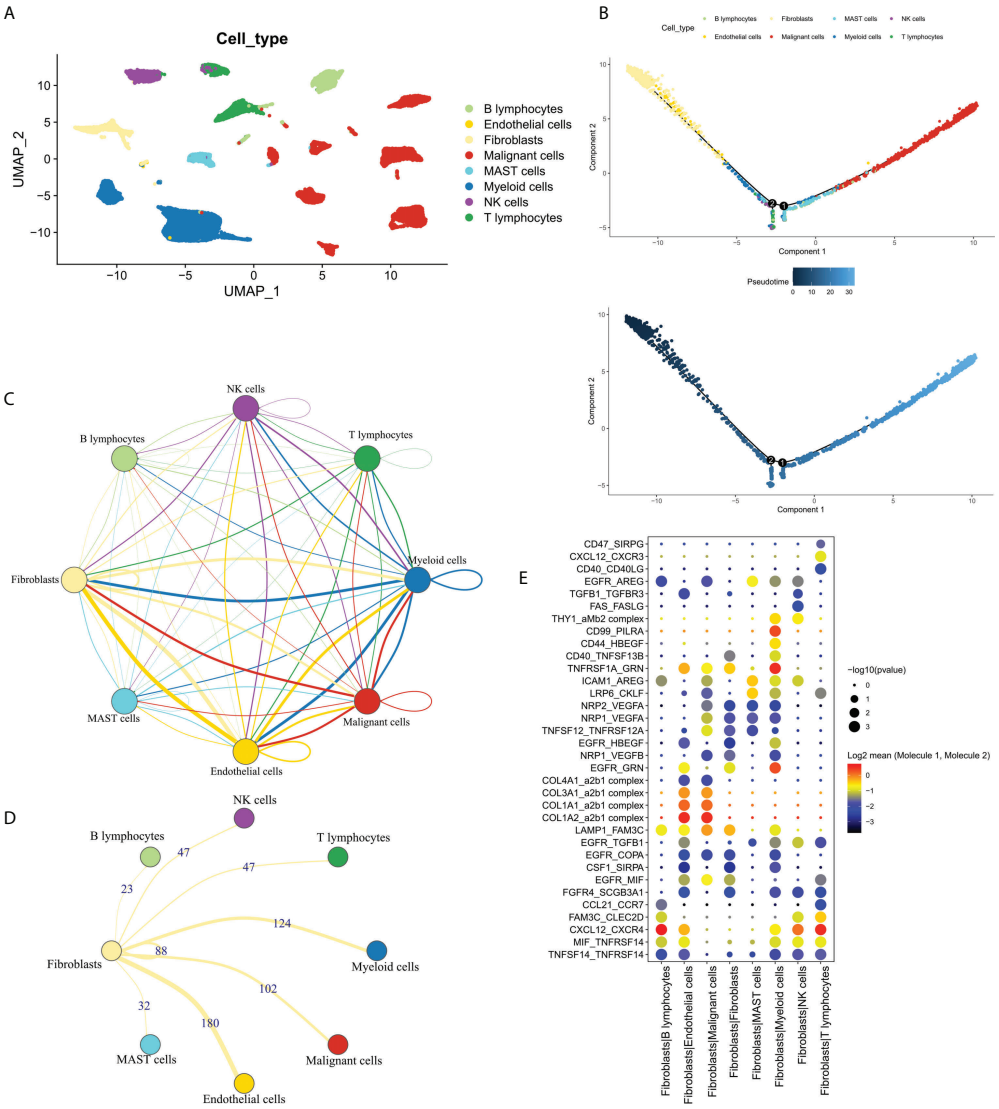

FIGURE 1
The single-cell profile of CAFs. **(A)** Eight cell clusters identified by cell clustering; **(B)** Pseudo-time analysis of the eight-cell clusters. Upper panel: cell cluster distribution, lower panel: pseudo-time distribution; **(C)** Communication network of the eight-cell clusters; **(D)** Communication network of CAFs with other cells, wherein the numbers represent the number of receptor-ligand pairs; **(E)** The top 5 receptor-ligand pairs of CAFs communicating with other cell types.

We then focused on FRGs with independent prognostic values. Univariate Cox analysis showed 33 independent prognostic factors in 127 FRGs. The loop graph in Figure 2A shows the correlation network and hazard ratios (HRs) for these 33 FRGs. Figure 2B displays the mutational landscape of the 37 FRGs. EGFR and COL5A2 were the top two genes with the highest mutation frequencies. The most common mutation was the missense mutation, whereas single nucleotide point mutation was the most common type of mutation, with the most frequently occurring change being from cytosine to adenine. The waterfall plot in Figure 2C shows the mutational landscape of 16 FRGs in patients. The bar chart displays the CNV profile of the 37 FRGs in TCGA-LUAD. Furthermore, FRGs underwent extensive CNV events. LAMC1 and TNFSF14 were the genes that experienced the most amplification and deletion events, respectively (Figure 2D). The loop graph was plotted to visualize the overall CNV profile of the 37 FRGs on the chromosomes (Figure 2E).

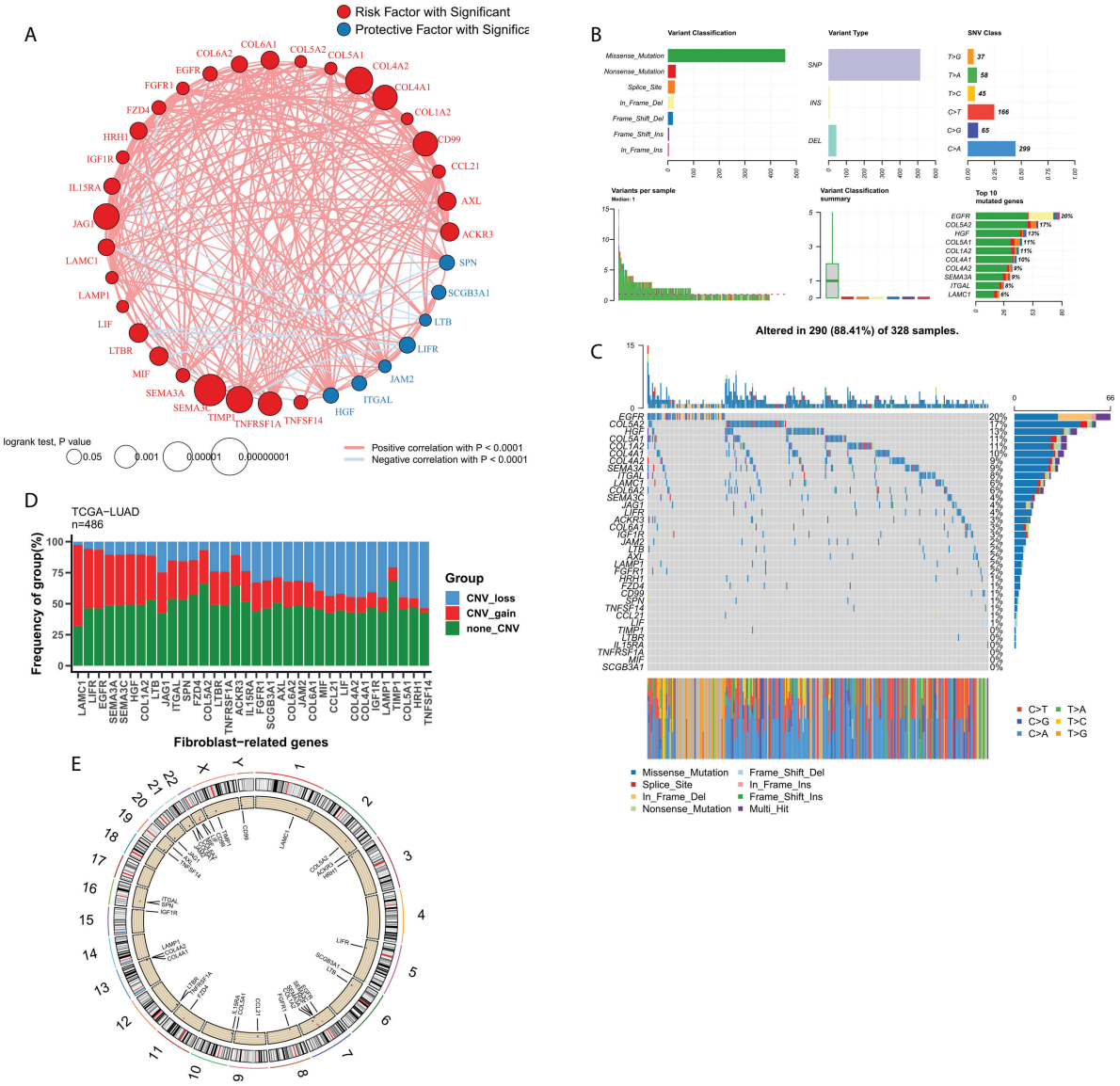

FIGURE 2
Genomic profile of FRGs in LUAD. **(A)** Correlation network of FRGs; **(B)** Summary of mutational events for FRGs in TCGA-LUAD; **(C)** Oncoplot showing the mutational mapping of FRGs; **(D)** Summary of CNV events for FRGs in TCGA-LUAD; **(E)** A loop graph showing CNV events for FRGs on chromosomes.

Construction of an FRG-related risk model

An FRG-related risk model was constructed using the 37 FRGs with a prognostic value, on which 300 iterations of LASSO regression were performed. Of all the five combinations, the model containing seven genes was found to be the most stable and showed good accuracy in both the training and validation cohorts (TCGA: 0.715; GEO: 0.667) (Figure 3A). This LASSO model was constructed based on the optimal λ value of 0.01608, and FRS was calculated based on the following equation:

$$FRS = \sum i \quad Coefficient(mRNA_i) \times Expression(mRNA_i)$$

Figure 3B shows the LASSO coefficients for the model genes, detailed coefficients of 27 FRGs can be found in Table S3. Patients at high- and low-risk were distinguished based on the median FRS. Survival analysis suggested that patients in the high-risk group had significantly lower survival rates relative to those in the low-risk group (Figure 3C; P < 0.0001). Figure 3D shows the distribution of FRS in TCGA cohort and the transcriptional profiles of the model genes. 1, 3, 5, and 8-year AUC values for the model were 0.66, 0.67, 0.68, and 0.70

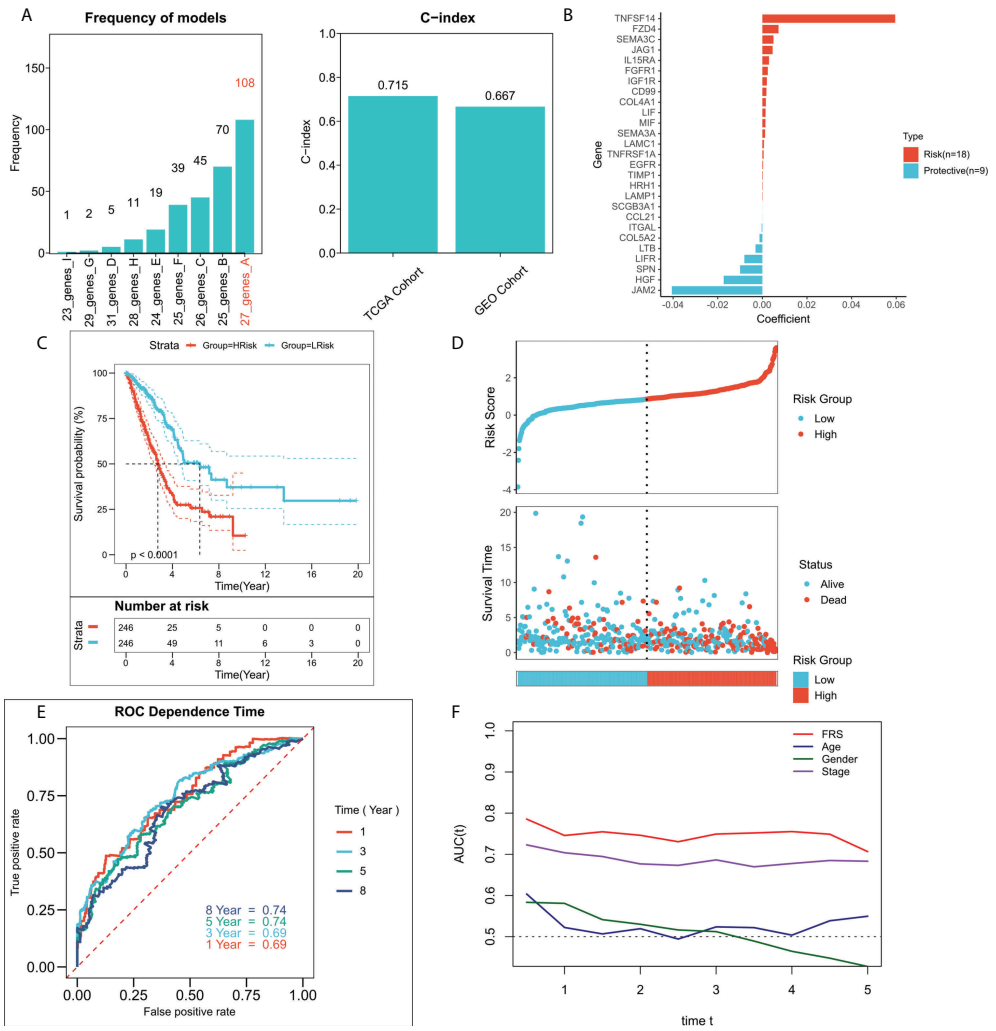

FIGURE 3
Construction of the FRG-related risk model. **(A)** Screening for the best LASSO model. Left panel: frequency of different gene combinations in the LASSO Cox regression model; Right panel: C-index of the best model in both TCGA and GEO cohorts; **(B)** LASSO coefficients for the 27 model genes; **(C)** KM survival curves for the high-FRS and low-FRS groups in the TCGA cohort; **(D)** Survival status and FRS of patients in TCGA cohort; **(E)** 1-, 3-, 5-, and 8-year ROC curves for FRS in TCGA cohort; **(F)** tROC curves for FRS and clinical characteristics in TCGA cohort.

respectively (Figure 3E). The tROC analysis suggested that FRS and TNM staging were the best predictors (Figure 3F). Subsequently, the predictive efficacy of the model was also assessed in the validation set. The survival analysis suggested that patients in the high-FRS group showed significantly worse survival (Figure S1A; $P < 0.0001$). The ROC analysis suggested that the model had satisfactory predictive power in the external validation set, with 1, 3, 5, and 8-year AUC values of 0.68, 0.69, 0.69, and 0.71 respectively (Figure S1B). Figure S1C shows the distribution of FRS and model gene expression in the GEO cohort.

Predictive independence of the risk model

We then validate the prognosis value of the FRS model in the TCGA cohort and GEO meta cohort. The relationship between the risk scores and the clinical characteristics of the patients and their prognoses were analyzed using the univariate and multivariate Cox regression analyses. The results of the univariate Cox regression analysis suggested that FRS was an independent prognostic indicator in both the training and validation cohorts ($P < 0.0001$) (Figure 4A). The results of the

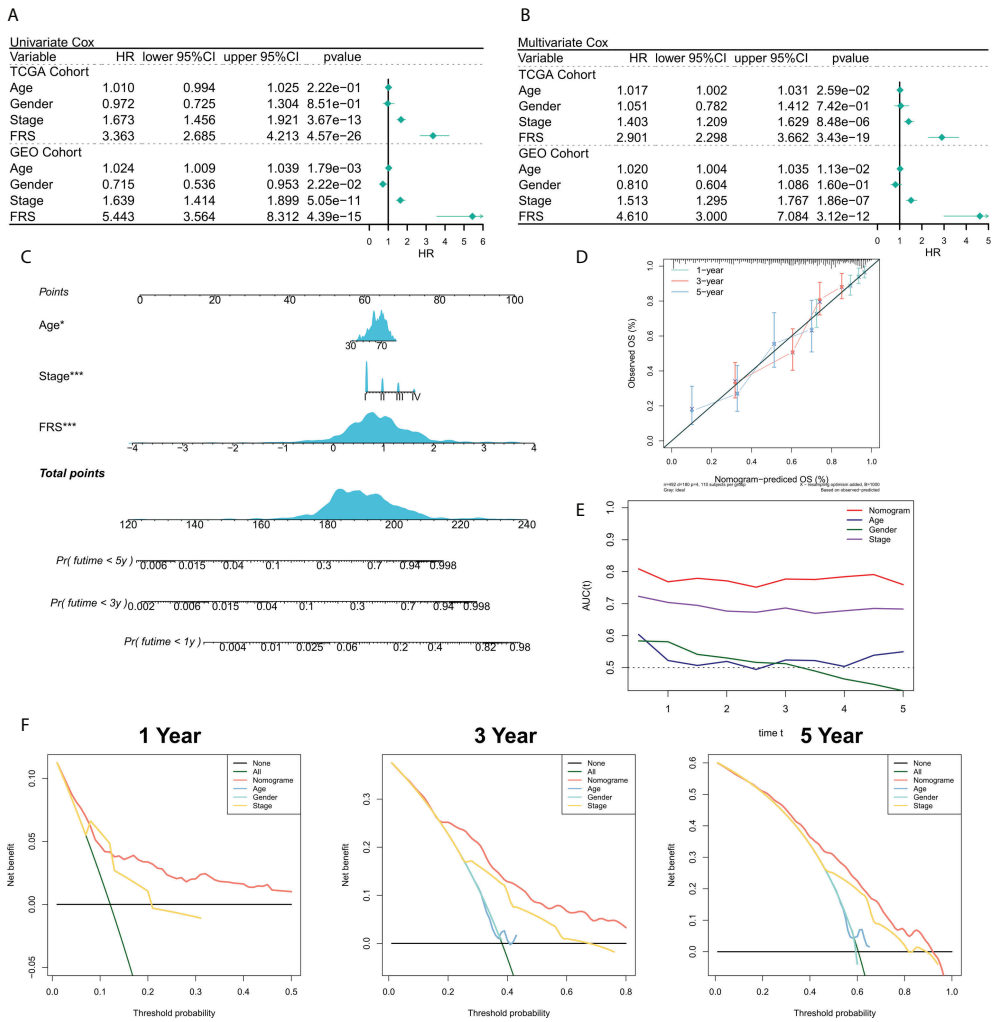

FIGURE 4
Validation of the FRG-related risk model. **(A)** Univariate Cox regression analysis of OS in TCGA and GEO cohorts; **(B)** Multivariate Cox regression analysis of OS in TCGA and GEO cohorts. **(C)** FRS-based nomogram; **(D)** Calibration curves for the nomogram; **(E)** tROC curves for the nomogram and clinical characteristics; **(F)** 1-, 3-, and 5-year DCA curves for the nomogram.

multivariate Cox regression analysis showed that FRS remained an independent prognostic factor for overall survival (OS) in both the training and validation cohorts after correcting for other clinical characteristics ($P < 0.0001$) (Figure 4B). Furthermore, subgroup analysis indicated that FRS remained a reliable prognostic factor in different clinical groups (Figure S2). Therefore, risk scores could serve as a reliable prognostic marker for predicting OS in patients with LUAD. Subsequently, the nomogram was constructed to better assess the risk of patients with LUAD (Figure 4C). The correction curves for the nomogram showed a good 1-, 3-, and 5-year stability and accuracy of the nomogram model (Figure 4D). tROC analysis suggested that the nomogram model was a better predictor relative to the clinical characteristics (Figure 4E). Additionally, a DCA was conducted to assess the decision benefit of the nomogram model. The results showed that this nomogram model was suitable for 1-, 3-, and 5-year risk assessments of patients with LUAD (Figure 4F).

Functional enrichment analysis of FRS

We tried to explain the potential biological logic of the differences in clinical outcomes among high- and low-FRS groups. Therefore, we assessed the correlation between FRS and some typical biological pathways. The heat map was plotted to illustrate the relationship among FRS, biological pathway activities, and clinical characteristics (Figure 5A), and the correlational analysis between FRS and biological pathways is shown on the right panel (Figure 5B). Angiogenesis, myeloid

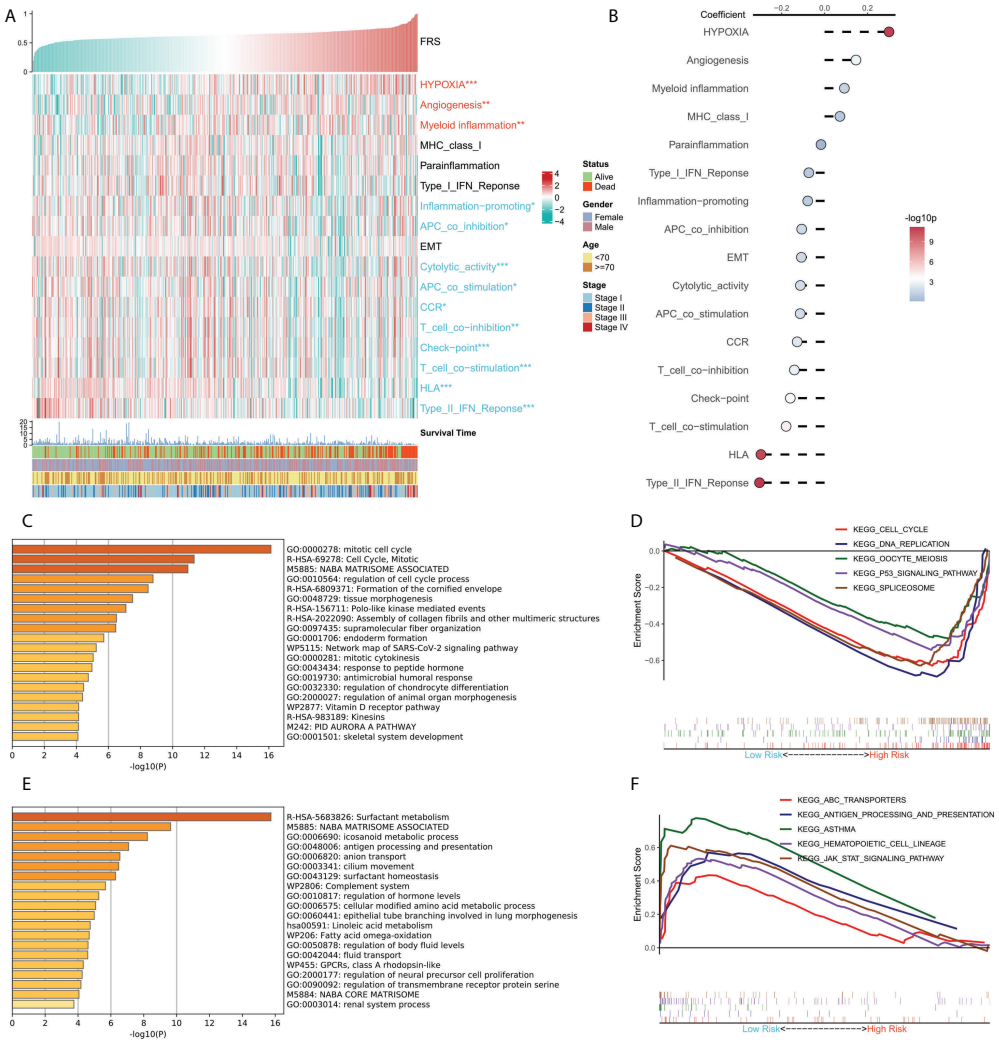

FIGURE 5
Functional analysis for FRS. **(A)** Heat map showing the correlation between FRS, biological pathway activities, and clinical characteristics; **(B)** Correlational analysis of FRS and biological pathways; **(C)** Functional enrichment analysis of the upregulated genes in the high group; **(D)** GSEA enrichment plot showing the five pathways of interest in the high group; **(E)** Functional enrichment analysis of the upregulated genes in the low group; **(F)** GSEA enrichment plot showing the five pathways of interest in the low group.

inflammation, and hypoxia were significantly positively correlated with FRS and their levels were markedly higher in the high-FRS group. GO analysis showed that the upregulated genes in the high-FRS group were mainly associated with the cell cycle, mitosis, and cytoskeleton (Figure 5C), whereas those in the low-FRS group were mainly related to antigen presentation and the complement system (Figure 5E). Further, GSEA showed that the cell cycle-related pathways such as the P53 signaling cascade, spliceosome, and DNA repair were significantly enriched in the high-risk group (Figure 5D), whereas antigen presentation, hematopoietic cell lineage, and the JAK-STAT signaling cascade were significantly enriched in the low-risk group (Figure 5F). Thus, these results suggested that tumor angiogenesis and DNA replication were active in the high-FRS group, whereas immune activity and immune cell differentiation were active in the low-FRS group.

Immune landscape in the risk model

TME plays a dual role in the tumorigenesis and progression of tumor and anti-tumor response. The correlation between FRS and the immune landscape was assessed in further detail. The heat map in Figure 6A demonstrates the relationship of FRS with the Estimate scores, abundances of immune-infiltrating cells, typical immune checkpoints (including CD274, CTLA4,

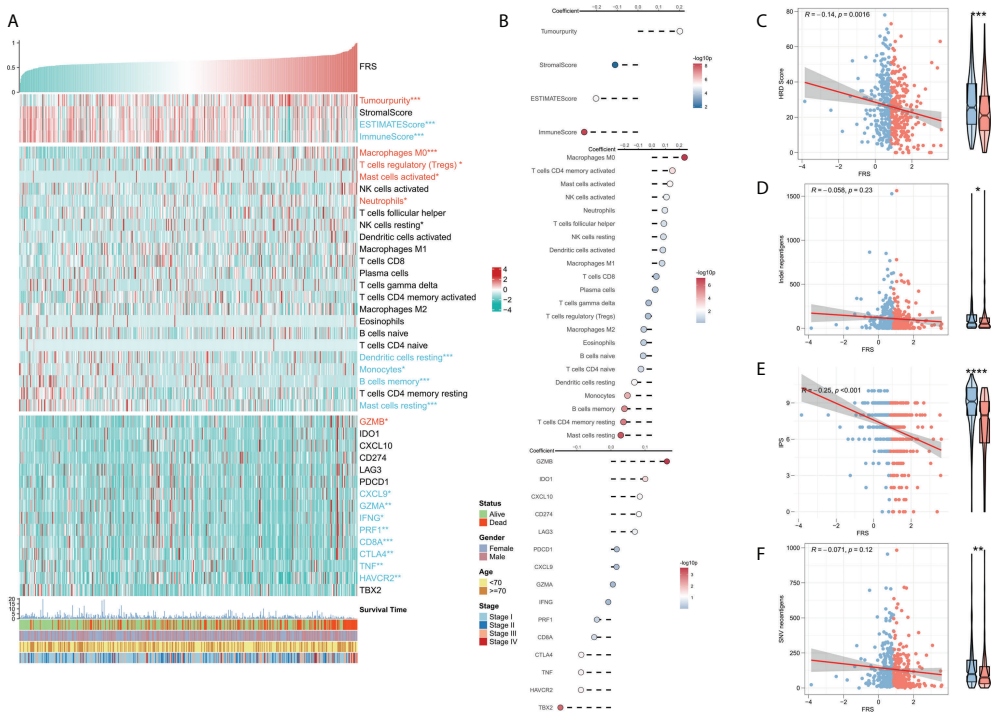

FIGURE 6
Immune infiltration analysis for FRS. **(A)** Heat map showing the correlation of FRS with the Estimate score, immune cell infiltration abundances, immune checkpoint expression, and clinical characteristics; **(B)** From top to bottom: correlational analysis of FRS with the Estimate score, immune cell infiltration abundances, and immune checkpoint expression. Scatter plot and box plot show the correlation of FRS with **(C)** HRD score; **(D)** Indel neoantigens; **(E)** IPS, and **(F)** SNV neoantigens."Red name with * represents upregulated in high-risk score group, and blue name with * represents upregulated in low-risk score group; *p < 0.05; **p < 0.01; ***p < 0.001; ****p < 0.001.

HAVCR2, IDO1, LAG3, and PDCD1), immune active features (including CD8A, CXCL10, CXCL9, GZMA, GZMB, IFNG, PRF1, TBX2, and TNF), and clinical characteristics of the patients. The corresponding correlational analysis is shown on the right side of the heat map (Figure 6B). Tumor purity, M0 macrophages, and T regs were significantly positively correlated with FRS and these levels were significantly elevated in the high-FRS groups. In contrast, the Estimate score, immune score, DC cells, B cells, and monocytes were negatively correlated with FRS and these levels were significantly lowered in the low-FRS groups. Furthermore, the activities of CXCL9, GZMA, IFNG, PRF1, CD8A, CTLA4, TNF, and HAVCR2 were negatively correlated with FRS and enhanced in the low-FRS group. Subsequently, we focused on the four indicators related to tumor-specific antigens, including HRD score (Figure 6C), indel neoantigens (Figure 6D), IP S(Figure 6E), and SNV neoantigens (Figure 6F). The results showed that FRS was negatively correlated with the HRD score, IPS, and SNV neoantigens, and their levels were significantly elevated in the low-FRS group. These results suggested that patients in the low-FRS group experienced more chromosomal instability and had more tumor neoantigens, thereby contributing to a stronger immune system activity. Thus, we inferred that the patients with a low FRS may stand to gain more benefits from immunotherapy (34–36).

Correlation between FRS and somatic variations

Several recent studies indicate that TMB is associated with patient responses to immunotherapy, whereby more somatic mutations may generate more potential mutation-derived antigens that can be recognized by the immune system. Further, the recognition of these antigens with mutant peptides by the immune system can activate immune functions and enhance anti-tumor immunity (37–39). Considering the clinical significance of TMB, we examined the correlation between TMB and FRS. The forest plot showed that the mutational frequencies of ZFHX4, ADAMTS12, TP53, KRAS, TTN, XIRP2, LRP1B, and CSMD3 were significantly greater in the high FRS-group (Figure 7A). The results of the mutation co-occurrence analysis suggested that the mutations in all the eight genes were highly co-occurring (Figure 7B).

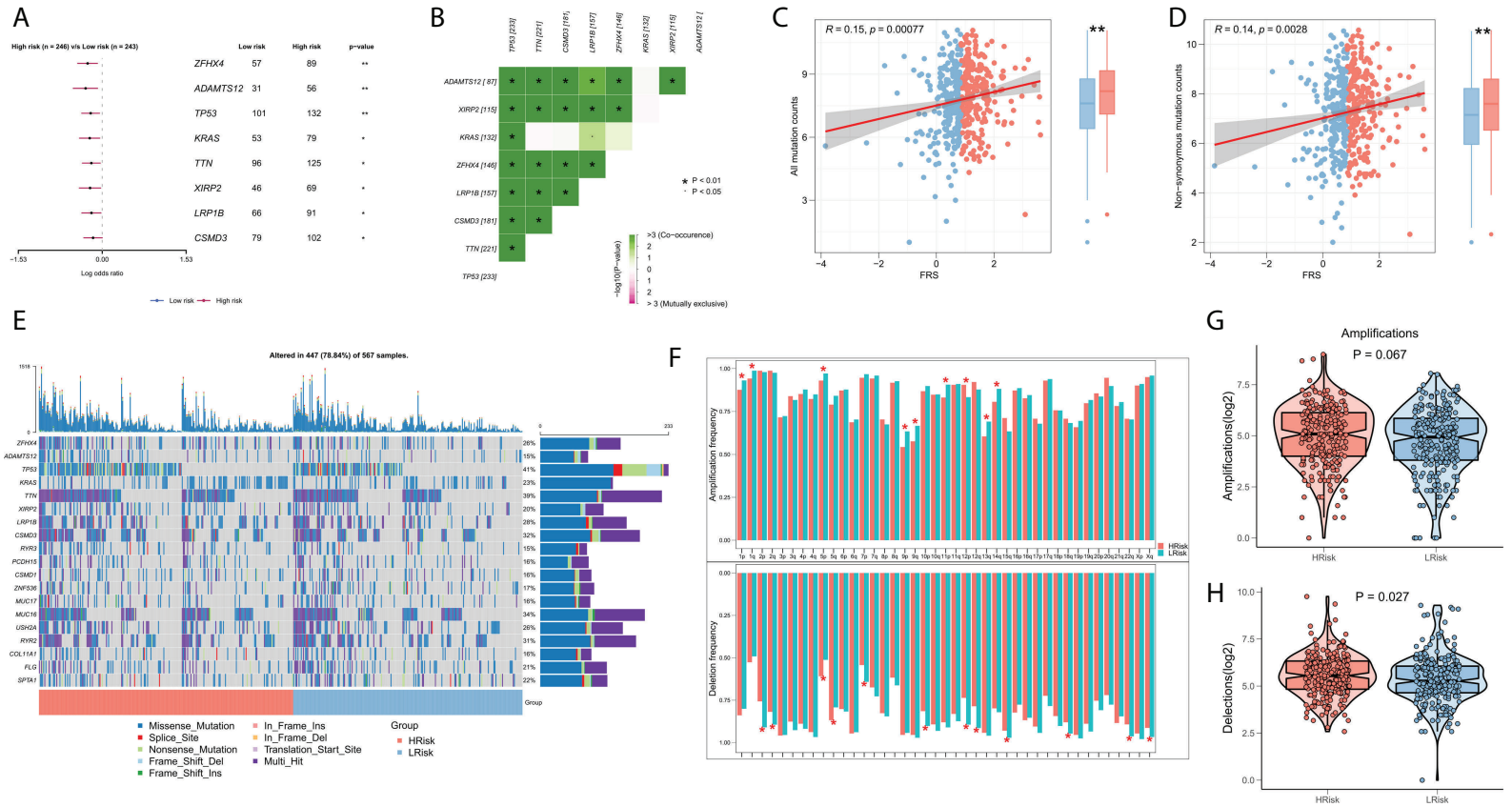

FIGURE 7
Genomic variation landscape of FRS. **(A)** Forest plots showing statistically significant differentially mutated genes between the high- and low-FRS groups; **(B)** Co-occurrence analysis of differentially mutated genes; **(C)** Correlation of FRS and all types of mutation burdens; **(D)** Correlation of FRS with non-synonymous mutation burden; **(E)** Oncoplot of high-frequency mutated genes between the high- and low-FRS groups; **(F)** Bar graph showing the CNV events on different chromosome arms in the high- and low-FRS groups; **(G)** Box plot showing the differences in the number of chromosome amplifications between high- and low-FRS groups; **(H)** Box plots showing the differences in the number of chromosomal deletions high- and low-FRS groups. *p < 0.05; **p < 0.01.

10.3389/fonc.2022.905212

Correlation analysis showed that all mutation burdens and the non-synonymous mutation burden were significantly positively correlated with FRS and markedly increased in the high-FRS group (Figures 7C, D). Figure 7E details the mutational landscape of the high-frequency mutated genes in patients with LUAD. CNVs cause chromosomal variations differently. Thus, we further evaluated the correlation between FRS and CNV and found an increased frequency of amplifications and deletions in the low-FRS group at the level of the chromosome arm (Figure 7F). The box plots in Figures 7G, H show a significant increase in the chromosomal deletion events and an upward trend in amplification events in the high-FRS group.

FRS-related guidance for clinical decision-making

Previous results suggested that patients in different FRS groups have interesting differences in biological function, TME, and genomic variation, which may lead to different responses to chemotherapy and immunotherapy. Differences in patient sensitivities towards chemotherapeutic agents for LUAD were assessed and the results showed that patients in the high-FRS group in TCGA cohort were more sensitive to the commonly used five first-line agents (Figure 8A). The same results were observed in the validation cohort (Figure S1D). Overall, patients in the high-FRS group were more sensitive to chemotherapy. Based on the value of |log2 FC|, the top 300 differential expression genes between the high and low FRS groups were uploaded to the CMap database to search the underlying small molecular drugs. As shown in Figure S3, a total of 47 potential small molecular drugs were identified to target 35 biological process. Differences in the immune landscape and genomic alterations between the two groups suggested that FRS may be associated with immunotherapeutic efficacy. Therefore, we assessed the patient response rates to immunotherapy using the TIDE algorithm. The results showed a higher response rate to immunotherapy in the low-FRS group in TCGA cohort (Figure 8B; P = < 0.001). In the validation cohort, patients in the low-FRS group also responded substantially more to immunotherapy (Figure S1E; P < 0.001). The results of subclass mapping suggested that the patients in the low-FRS group were more sensitive to anti-PD1 therapy in both TCGA and GEO cohorts (TCGA: FDR = 0.011; GEO: FDR = 0.027) (Figure 8C; Figure S1F). Subsequently, we evaluated the prognostic performances of FRS in an immunotherapy cohort of NSCLC. The results showed that patients in the high-FRS group had a worse survival (Figure 8D; P = 0.078). Finally, we evaluated the utility of FRS in a large immunotherapy cohort, which also suggested that the patients in the high-FRS group had a significantly worse survival (Figure 8E; P = 0.00038),. Overall, these results demonstrated that the risk model constructed in this study was a powerful tool to guide decisions related to chemotherapy and immunotherapy for the treatment of LUAD.

Validation of key FRGs in the clinical samples

We extracted the most representative top 5 genes according to lasso coefficient for external validation. The staining intensity of TNFSF14, JAM2, HGF, SPN, and LIFR in the tumors of 50 lung adenocarcinoma patients was first analyzed by immunohistochemistry and quantified according to H-scores. Subsequently, they were defined as the high expression group (H scores > median value) and low expression group (H scores < median value) according to the median value of H-scores, respectively. Subsequently, we performed a prognostic analysis of their Kaplan-Meier according to staining intensity, and we found that patients with higher staining intensity in TNFSF14 had a significantly worse prognosis and had shorter survival cycles (Figure 9A). However, patients with higher staining intensity for JAM2, HGF, and LIFR had significantly higher survival cycles than those with lower staining intensity for lung adenocarcinoma (Figures 9B, D, E), but for SPN, there was no significant correlation between their staining intensity and patients' survival cycles (Figure 9C).

Discussion

Considering the complexity of TME in LUAD patients, previous research attention was focused more on the immune cells, however, the crosstalk between CAFs and other cells remains far less understood. In this study, we used single-cell RNA sequencing data to assess the communication between CAFs and other cells and identified the interacting molecules. Subsequently, FRS was constructed from bulk sequencing data based on interacting genes and its significance in prognostic and therapeutic decision-making was determined. Functional enrichment analysis was employed to understand FRS-related biological functions. Additionally, CIBERSORT, ssGSEA, and ESTIMATE algorithms were used to map the TIME landscape and assess the associations between FRS and TIME by analyzing the LUAD-related genomic information. Finally, the intrinsic associations between FRS and genomic alterations were assessed in terms of tumor mutation burden and CNV effects.

CAF is a pro-tumor stromal cell component in most solid tumors. The interaction between CAFs and various cellular components in TME regulates tumor progression and invasion (13, 14, 40). In this study, we first examined the intercommunication between CAFs and other cells. The pseudotime analysis showed that the distribution of CAFs was mainly at the beginning of cell sorting trajectories, thus suggesting that CAFs were involved in the formation of

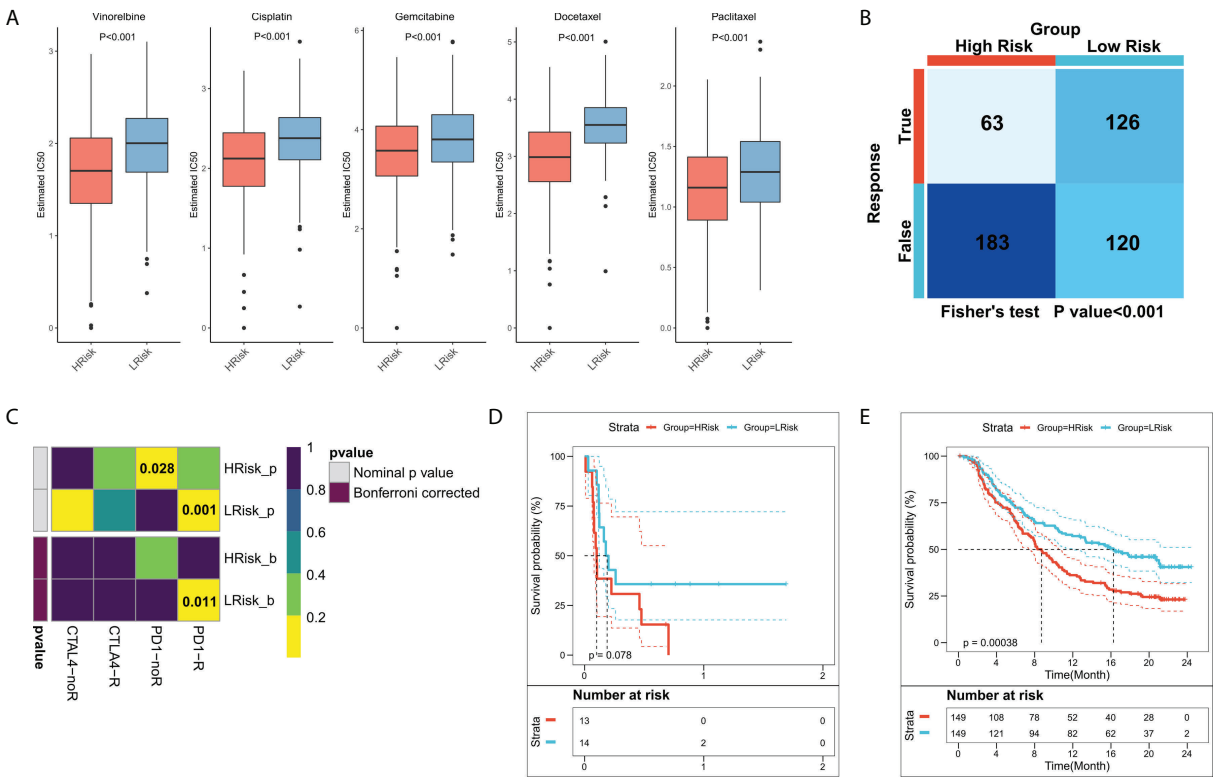

FIGURE 8
Role of the FRS-related risk model in guiding clinical treatment decisions. **(A)** Box plots showing the predicted IC50 values for the five most commonly used drugs in high- and low-FRS groups; **(B)** Predicted responses to immunotherapy for patients in the high- and low-FRS groups using the TIDE algorithm; **(C)** Sensitivity of patients in the high- and low-FRS groups to PD1 and CTLA4 treatment regimens predicted by subclass mapping; **(D)** KM survival curves for patients in the high- and low-FRS groups in GSE135222 cohort; **(E)** KM survival curves for patients in the high- and low-FRS groups in IMvigor210 cohort.

stromal components in the early stages of cancer progression. Cellular communication analysis revealed additional interactions of CAFs with endothelial, malignant, and myeloid cells. These findings demonstrated that CAFs were not only involved in stromal formation and regulation of tumor progression but also interacted extensively with immune cells. Receptor-ligand analysis suggested that the CAFs could regulate immune cells mainly through the TNF signaling pathway. Subsequently, the significant receptor-ligand pairs were identified as FRGs and an FRG-based FRS model was generated using the LASSO algorithm. This model showed excellent predictive performances in both the training and the external validation cohorts and suggested a significant deterioration in survival among the high-risk patients.

Patients with LUAD have a high tumor mutation burden and show strong immunogenicity. Therefore, LUAD is an ideal indication for immunotherapy (41). However, the overall response rate of patients towards immunotherapy is low and only a certain proportion of patients benefit from it (42). Therefore, identifying "hot" tumors in LUAD is expected to enhance the decision and selection of those who would benefit from immunotherapy. In the present study, functional enrichment analysis suggested that a high FRS was associated with hypoxia, angiogenesis, and myeloid immunity; among them, hypoxia is often considered a limiting factor for TME and can lead to treatment resistance (43). Angiogenesis is essential for tumor growth and metastases, and both angiogenesis and myeloid immunity are inhibitors of the immune system functions (44–47). The activities of most anti-tumor immune and antigen-presentation pathways were markedly increased in patients with a low FRS. The interaction between TIME and immune cells is closely related to immunotherapy and patient prognoses (48–50). We further analyzed the abundances of immune infiltrates in TME and the findings suggested that a high FRS was associated with a higher tumor purity and an elevated Treg level, ultimately leading to immunosuppression (51). In contrast, patients in the low FRS group had higher immune scores, an increased proportion of DC cells, and enhanced immune checkpoint activities. Further, the immunophenotype scores were found to be negatively correlated with FRS and were markedly high in the low-FRS group. These results suggested a low FRS-activated

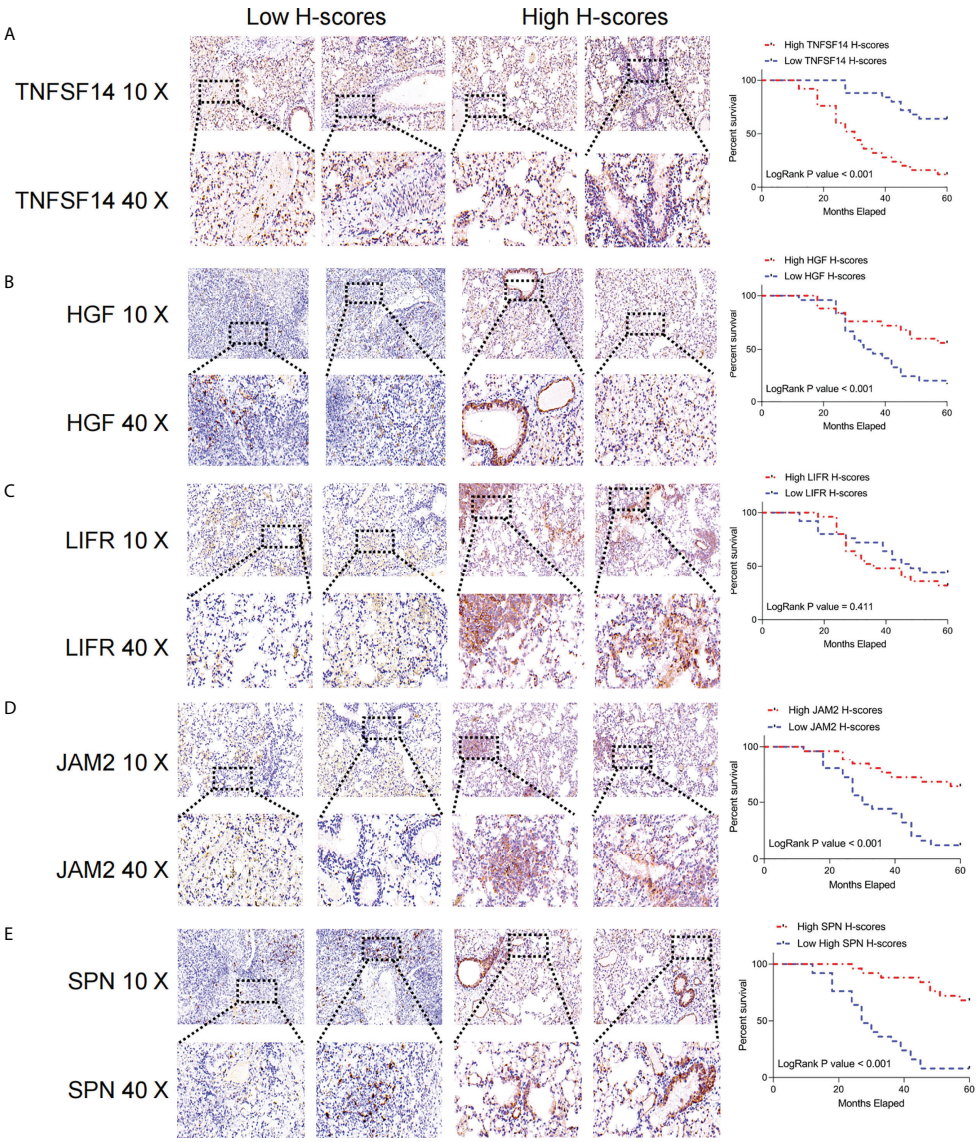

FIGURE 9
Immunohistochemical analysis of the key FRGs in the FRS model. High TNFSF14 expression, low JAM2, HGF, and SPN expression were associated with poor prognosis in patients with LUAD. **(A)** Immunohistochemical analysis of the intensity of TNFSF14 staining in tumors from 50 patients with lung adenocarcinoma and Kaplan-Meier analysis of the correlation between H-scores of immunohistochemistry for TNFSF14 and the survival cycle of patients with LUAD; **(B)** Immunohistochemical analysis of the intensity of HGF staining in tumors from 50 patients with lung adenocarcinoma and Kaplan-Meier analysis of the correlation between H-scores of immunohistochemistry for HGF and the survival cycle of patients with LUAD. **(C)** Immunohistochemical analysis of LFR staining intensity in tumors from 50 lung adenocarcinoma patients, Kaplan-Meier analysis of H-scores of immunohistochemistry for LFR correlated with the survival cycle of LUAD patients; **(D)** Immunohistochemical analysis of JAM2 staining intensity in tumors from 50 lung adenocarcinoma patients, Kaplan-Meier analysis of JAM2 H-scores of immunohistochemistry correlated with the survival cycle of LUAD patients; **(E)** immunohistochemistry analyzed the intensity of SPN staining in the tumors of 50 lung adenocarcinoma patients, and Kaplan-Meier analyzed the correlation of H-scores of immunohistochemistry of SPN with the survival cycle of LUAD patients.

immunophenotype (29, 52), consistent with the better survival of the patients in the low-FRS group and the resultant development of "hot" tumors sensitive towards immunotherapy. Additionally, HRD scores, indel neoantigens, and SNV neoantigens were elevated in the low-FRS group. These findings suggested that more tumor-specific neoantigens may be present in patients in the low-FRS group and they may be more likely to benefit from immunotherapy (53–55).

A recent study shows that genomic alterations are closely related to neoantigen formation and immunotherapeutic

responses (56). However, the results of this study suggest that patients in the low-FRS group experience less TMB and that the high-frequency mutated genes were mutated more frequently in the high-FRS group. To elucidate this phenomenon, the mutational co-occurrence of the high-frequency mutated genes was examined. As these were all highly co-mutated genes, patients in the high-FRS group showed a higher TMB frequency. Furthermore, patients in the low-FRS group experienced a higher frequency of CNVs in the chromosomal arms but fewer CNV events in total. These results suggested that FRS could better reflect the immune status of the tumor and predict the patient responses to immunotherapy relative to TMB and CNV.

In summary, low FRS resulted in "hot" tumors with an immune-activating phenotype and possibly the production of more tumor neoantigenic peptides. We then systematically evaluated the patient responses to chemotherapy and immunotherapy. Patients with a high FRS were more sensitive to chemotherapy. Previous functional enrichment results suggested that the cell cycle-related pathways, as targets for chemotherapy, were active in patients with a high FRS, thereby leading to better chemotherapeutic benefits. Subsequently, the TIDE and subclass mapping algorithms predicted a higher patient sensitivity towards anti-PD1 therapy in those with a low FRS, consistent with our previous findings. Moreover, we observed better survival in patients with a low FRS in both the external NSCLC immunotherapy and the large immunotherapy cohorts. Overall, these results demonstrated that the FRS model is a powerful tool that can guide the treatment-decision making for patients with LUAD. Patients with a high FRS are better suited for chemotherapy, whereas those with a low FRS are more likely to benefit from immunotherapy.

However, the present study has some limitations. First, the similarity of expression profiles of CAFs and vascular cells may confound our analysis due to the lack of finer cell classification. Second, bulk sequencing only reflects inter-patient heterogeneity and not intra-tumoral heterogeneity. Third, although we have employed several algorithms to assess the accuracy of this FRS model for predicting patient sensitivity towards chemotherapy and immunotherapy, further validation of these findings by prospective cohort studies and clinical data is required. Finally, additional *in vivo* and *in vitro* experiments should be performed to confirm the specific mechanisms underlying the crosstalk of FRGs with other cells in CAFs, which are expected to contribute to the further understanding of the functions of these CAFs.

In summary, this study contributed towards the understanding of cellular interactions in CAFs and TME, and we developed a novel, FRS-based model. This model allowed for the systematic quantification of "cold" and "hot" tumor patterns from multiple perspectives, including function, immune infiltration, and genomic alterations. Moreover, it can also facilitate the quantitative estimation of patient prognoses and guide the clinical decision-making for chemotherapy and immunotherapy.

Data availability statement

The original contributions presented in the study are included in the article/Supplementary Material. Further inquiries can be directed to the corresponding author.

Ethics statement

The study was approved by Shanghai Pulmonary Hospital Ethics Committee (K21-111Y). The patients consented to participate.

Author contributions

SW analyzed the data and wrote the manuscript. XG carried out data interpretations and helped data discussion. WZ conceived and designed the whole project and drafted the manuscript. All authors read and approved the final manuscript.

Funding

This work was supported by the Youth Found of National Natural Science Foundation of China (82103309).

Acknowledgments

The authors hereby express their gratitude to all participants who supported the study.

Conflict of interest

The authors declare that the research was conducted in the absence of any commercial or financial relationships that could be construed as a potential conflict of interest.

Publisher's note

Supplementary material

The Supplementary Material for this article can be found online at: https://www.frontiersin.org/articles/10.3389/fonc.2022.905212/full#supplementary-material

SUPPLEMENTARY FIGURE 1
External validation of FRS **(A)** KM survival curves for patients in the high- and low-FRS groups in the GEO cohort; **(B)** 1-, 3-, 5-, and 8-year ROC curves for FRS in the GEO cohort; **(C)** Survival status and FRS of patients in the GEO cohort; **(D)** Box plots showing the predicted IC50 values of the five most commonly used drugs in high- and low- FRS groups in the GEO cohort; **(E)** Immunotherapeutic responses of patients in the high- and low-FRS groups in the GEO cohort predicted using the TIDE algorithm; **(F)** Sensitivity of the patients in the high- and low-FRS groups to PD1 and CTLA4 treatment regimens in the GEO cohort predicted using the subclass mapping algorithm.

SUPPLEMENTARY FIGURE 2
Subgroup Cox analysis of FRS Subgroup Cox regression analysis of FRS in TCGA **(A)** and GEO **(B)** cohorts.

SUPPLEMENTARY FIGURE 3
Prediction of FRS-related small molecule compounds.

References

1. Siegel RL, Miller KD, Fuchs HE, Jemal A. Cancer statistics, 2021. *CA: Cancer J Clin* (2021) 71(1):7–33. doi: 10.3322/caac.21654

2. Ortega-Gómez A, Rangel-Escareño C, Molina-Romero C, Macedo-Pérez EO, Avilés-Salas A, Lara-García A, et al. Gene-expression profiles in lung adenocarcinomas related to chronic wood smoke or tobacco exposure. *Respir Res* (2016) 17:42. doi: 10.1186/s12931-016-0346-3

3. Song MA, Benowitz NL, Berman M, Brasky TM, Cummings KM, Hatsukami DK, et al. Cigarette filter ventilation and its relationship to increasing rates of lung adenocarcinoma. *J Natl Cancer Instit* (2017) 109(12):djx075. doi: 10.1093/jnci/djx075

4. Vaz M, Hwang SY, Kagiampakis I, Phallen J, Patil A, O'Hagan HM, et al. Chronic cigarette smoke-induced epigenomic changes precede sensitization of bronchial epithelial cells to single-step transformation by KRAS mutations. *Cancer Cell* (2017) 32(3):360–76.e6. doi: 10.1016/j.ccell.2017.08.006

5. Herbst RS, Morgensztern D, Boshoff C. The biology and management of non-small cell lung cancer. *Nature* (2018) 553(7689):446–54. doi: 10.1038/nature25183

6. Binnewies M, Roberts EW, Kersten K, Chan V, Fearon DF, Merad M, et al. Understanding the tumor immune microenvironment (TIME) for effective therapy. *Nat Med* (2018) 24(5):541–50. doi: 10.1038/s41591-018-0014-x

7. Gentles AJ, Bratman SV, Lee LJ, Harris JP, Feng W, Nair RV, et al. Integrating tumor and stromal gene expression signatures with clinical indices for survival stratification of early-stage non-small cell lung cancer. *J Natl Cancer Instit* (2015) 107(10):djv211. doi: 10.1093/jnci/djv211

8. Mariathasan S, Turley SJ, Nickles D, Castiglioni A, Yuen K, Wang Y, et al. TGFβ attenuates tumour response to PD-L1 blockade by contributing to exclusion of T cells. *Nature* (2018) 554(7693):544–8. doi: 10.1038/nature25501

9. Lambrechts D, Wauters E, Boeckx B, Aibar S, Nittner D, Burton O, et al. Phenotype molding of stromal cells in the lung tumor microenvironment. *Nat Med* (2018) 24(8):1277–89. doi: 10.1038/s41591-018-0096-5

10. Auciello FR, Bulusu V, Oon C, Tait-Mulder J, Berry M, Bhattacharyya S, et al. A stromal lysolipid-autotaxin signaling axis promotes pancreatic tumor progression. *Cancer Discover* (2019) 9(5):617–27. doi: 10.1158/2159-8290.Cd-18-1212

11. Sahai E, Astsaturov I, Cukierman E, DeNardo DG, Egeblad M, Evans RM, et al. A framework for advancing our understanding of cancer-associated fibroblasts. *Nat Rev Canc* (2020) 20(3):174–86. doi: 10.1038/s41568-019-0238-1

12. Boyle ST, Poltavets V, Kular J, Pyne NT, Sandow JJ, Lewis AC, et al. ROCK-mediated selective activation of PERK signalling causes fibroblast reprogramming and tumour progression through a CRELD2-dependent mechanism. *Nat Cell Biol* (2020) 22(7):882–95. doi: 10.1038/s41556-020-0523-y

13. Barrett RL, Puré E. Cancer-associated fibroblasts and their influence on tumor immunity and immunotherapy. *eLife* (2020) 9:e57243. doi: 10.7554/eLife.57243

14. Mao X, Xu J, Wang W, Liang C, Hua J, Liu J, et al. Crosstalk between cancer-associated fibroblasts and immune cells in the tumor microenvironment: new findings and future perspectives. *Mol Canc* (2021) 20(1):131. doi: 10.1186/s12943-021-01428-1

15. Erez N, Truitt M, Olson P, Arron ST, Hanahan D. Cancer-associated fibroblasts are activated in incipient neoplasia to orchestrate tumor-promoting inflammation in an NF-kappaB-Dependent manner. *Cancer Cell* (2010) 17(2):135–47. doi: 10.1016/j.ccr.2009.12.041

16. Kim N, Kim HK, Lee K, Hong Y, Cho JH, Choi JW, et al. Single-cell RNA sequencing demonstrates the molecular and cellular reprogramming of metastatic lung adenocarcinoma. *Nat Commun* (2020) 11(1):2285. doi: 10.1038/s41467-020-16164-1

17. Leek JT, Johnson WE, Parker HS, Jaffe AE, Storey JD. The sva package for removing batch effects and other unwanted variation in high-throughput experiments. *Bioinf (Oxford England)* (2012) 28(6):882–3. doi: 10.1093/bioinformatics/bts034

18. Qiu X, Mao Q, Tang Y, Wang L, Chawla R, Pliner HA, et al. Reversed graph embedding resolves complex single-cell trajectories. *Nat Methods* (2017) 14 (10):979–82. doi: 10.1038/nmeth.4402

19. Efremova M, Vento-Tormo M, Teichmann SA, Vento-Tormo R. CellPhoneDB: inferring cell-cell communication from combined expression of multi-subunit ligand-receptor complexes. *Nat Protoc* (2020) 15(4):1484–506. doi: 10.1038/s41596-020-0292-x

20. Schröder MS, Culhane AC, Quackenbush J, Haibe-Kains B. Survcomp: an R/Bioconductor package for performance assessment and comparison of survival models. *Bioinf (Oxford England)* (2011) 27(22):3206–8. doi: 10.1093/bioinformatics/btr511

21. McDermott DF, Huseni MA, Atkins MB, Motzer RJ, Rini BI, Escudier B, et al. Clinical activity and molecular correlates of response to atezolizumab alone or in combination with bevacizumab versus sunitinib in renal cell carcinoma. *Nat Med* (2018) 24(6):749–57. doi: 10.1038/s41591-018-0053-3

22. Gibbons DL, Creighton CJ. Pan-cancer survey of epithelial-mesenchymal transition markers across the cancer genome atlas. *Dev Dyn* (2018) 247(3):555–64. doi: 10.1002/dvdy.24485

23. Ayers M, Lunceford J, Nebozhyn M, Murphy E, Loboda A, Kaufman DR, et al. IFN-γ-related mRNA profile predicts clinical response to PD-1 blockade. *J Clin Invest* (2017) 127(8):2930–40. doi: 10.1172/jci91190

24. Liang JY, Wang DS, Lin HC, Chen XX, Yang H, Zheng Y, et al. A novel ferroptosis-related gene signature for overall survival prediction in patients with hepatocellular carcinoma. *Int J Biol Sci* (2020) 16(13):2430–41. doi: 10.7150/ijbs.45050

25. Liberzon A, Subramanian A, Pinchback R, Thorvaldsdóttir H, Tamayo P, Mesirov JP. Molecular signatures database (MSigDB) 3.0. *Bioinf (Oxford England)* (2011) 27(12):1739–40. doi: 10.1093/bioinformatics/btr260

26. Newman AM, Liu CL, Green MR, Gentles AJ, Feng W, Xu Y, et al. Robust enumeration of cell subsets from tissue expression profiles. *Nat Methods* (2015) 12 (5):453–7. doi: 10.1038/nmeth.3337

27. Yoshihara K, Shahmoradgoli M, Martínez E, Vegesna R, Kim H, Torres-Garcia W, et al. Inferring tumour purity and stromal and immune cell admixture from expression data. *Nat Commun* (2013) 4:2612. doi: 10.1038/ncomms3612

28. Charoentong P, Finotello F, Angelova M, Mayer C, Efremova M, Rieder D, et al. Pan-cancer immunogenomic analyses reveal genotype-immunophenotype relationships and predictors of response to checkpoint blockade. *Cell Rep* (2017) 18 (1):248–62. doi: 10.1016/j.celrep.2016.12.019

29. Thorsson V, Gibbs DL, Brown SD, Wolf D, Bortone DS, Ou Yang TH, et al. The immune landscape of cancer. *Immunity* (2018) 48(4):812–30.e14. doi: 10.1016/j.immuni.2018.03.023

30. Mayakonda A, Lin DC, Assenov Y, Plass C, Koeffler HP. Maftools: efficient and comprehensive analysis of somatic variants in cancer. *Genome Res* (2018) 28 (11):1747–56. doi: 10.1101/gr.239244.118

31. Geeleher P, Cox N, Huang RS. pRRophetic: an r package for prediction of clinical chemotherapeutic response from tumor gene expression levels. *PloS One* (2014) 9(9):e107468. doi: 10.1371/journal.pone.0107468

32. Jiang P, Gu S, Pan D, Fu J, Sahu A, Hu X, et al. Signatures of T cell dysfunction and exclusion predict cancer immunotherapy response. *Nat Med* (2018) 24(10):1550–8. doi: 10.1038/s41591-018-0136-1

33. Vickers AJ, Cronin AM, Elkin EB, Gonen M. Extensions to decision curve analysis, a novel method for evaluating diagnostic tests, prediction models and molecular markers. *BMC Med Inf Decis Makin* (2008) 8:53. doi: 10.1186/1472-6947-8-53

34. van Wilpe S, Tolmeijer SH, Koornstra RHT, de Vries IJM, Gerritsen WR, Ligtenberg M, et al. Homologous recombination repair deficiency and implications for tumor immunogenicity. *Cancers* (2021) 13(9):13092249. doi: 10.3390/cancers13092249

35. Desrichard A, Snyder A, Chan TA. Cancer neoantigens and applications for immunotherapy. *Clin Cancer Res* (2016) 22(4):807–12. doi: 10.1158/1078-0432.Ccr-14-3175

36. Hu Z, Ott PA, Wu CJ. Towards personalized, tumour-specific, therapeutic vaccines for cancer. *Nat Rev Immunol* (2018) 18(3):168–82. doi: 10.1038/nri.2017.131

37. Chan TA, Yarchoan M, Jaffee E, Swanton C, Quezada SA, Stenzinger A, et al. Development of tumor mutation burden as an immunotherapy biomarker: utility for the oncology clinic. *Ann Oncol* (2019) 30(1):44–56. doi: 10.1093/annonc/mdy495

38. Matsushita H, Vesely MD, Koboldt DC, Rickert CG, Uppaluri R, Magrini VJ, et al. Cancer exome analysis reveals a T-cell-dependent mechanism of cancer immunoediting. *Nature* (2012) 482(7385):400–4. doi: 10.1038/nature10755

39. Rizvi NA, Hellmann MD, Snyder A, Kvistborg P, Makarov V, Havel JJ, et al. Cancer immunology. mutational landscape determines sensitivity to PD-1 blockade in non-small cell lung cancer. *Sci (New York NY)* (2015) 348 (6230):124–8. doi: 10.1126/science.aaa1348

40. Gagliano T, Shah K, Gargani S, Lao L, Alsaleem M, Chen J, et al. PIK3Cδ expression by fibroblasts promotes triple-negative breast cancer progression. *J Clin Invest* (2020) 130(6):3188–204. doi: 10.1172/jci128313

41. Li X, Shao C, Shi Y, Han W. Lessons learned from the blockade of immune checkpoints in cancer immunotherapy. *J Hematol Oncol* (2018) 11(1):31. doi: 10.1186/s13045-018-0578-4

42. Forde PM, Chaft JE, Smith KN, Anagnostou V, Cottrell TR, Hellmann MD, et al. Neoadjuvant PD-1 blockade in resectable lung cancer. *New Engl J Med* (2018) 378(21):1976–86. doi: 10.1056/NEJMoa1716078

43. Riera-Domingo C, Audigé A, Granja S, Cheng WC, Ho PC, Baltazar F, et al. Immunity, hypoxia, and metabolism-the ménage à trois of cancer: Implications for immunotherapy. *Physiol Rev* (2020) 100(1):1–102. doi: 10.1152/physrev.00018.2019

44. Sharma RA, Harris AL, Dalgleish AG, Steward WP, O'Byrne KJ. Angiogenesis as a biomarker and target in cancer chemoprevention. *Lancet Oncol* (2001) 2(12):726–32. doi: 10.1016/s1470-2045(01)00586-1

45. Motz GT, Coukos G. The parallel lives of angiogenesis and immunosuppression: cancer and other tales. *Nat Rev Immunol* (2011) 11 (10):702–11. doi: 10.1038/nri3064

46. Welti J, Loges S, Dimmeler S, Carmeliet P. Recent molecular discoveries in angiogenesis and antiangiogenic therapies in cancer. *J Clin Invest* (2013) 123 (8):3190–200. doi: 10.1172/jci70212

47. Gabrilovich DI, Nagaraj S. Myeloid-derived suppressor cells as regulators of the immune system. *Nat Rev Immunol* (2009) 9(3):162–74. doi: 10.1038/nri2506

48. Zhang Y, Zhang Z. The history and advances in cancer immunotherapy: understanding the characteristics of tumor-infiltrating immune cells and their therapeutic implications. *Cell Mol Immunol* (2020) 17(8):807–21. doi: 10.1038/s41423-020-0488-6

49. Duan Q, Zhang H, Zheng J, Zhang L. Turning cold into hot: Firing up the tumor microenvironment. *Trends Canc* (2020) 6(7):605–18. doi: 10.1016/j.trecan.2020.02.022

50. Fu T, Dai LJ, Wu SY, Xiao Y, Ma D, Jiang YZ, et al. Spatial architecture of the immune microenvironment orchestrates tumor immunity and therapeutic response. *J Hematol Oncol* (2021) 14(1):98. doi: 10.1186/s13045-021-01103-4

51. Lim SA, Wei J, Nguyen TM, Shi H, Su W, Palacios G, et al. Lipid signalling enforces functional specialization of t(reg) cells in tumours. *Nature* (2021) 591 (7849):306–11. doi: 10.1038/s41586-021-03235-6

52. Hamanishi J, Mandai M, Iwasaki M, Okazaki T, Tanaka Y, Yamaguchi K, et al. Programmed cell death 1 ligand 1 and tumor-infiltrating CD8+ T lymphocytes are prognostic factors of human ovarian cancer. *Proc Natl Acad Sci USA* (2007) 104(9):3360–5. doi: 10.1073/pnas.0611533104

53. Shi Z, Zhao Q, Lv B, Qu X, Han X, Wang H, et al. Identification of biomarkers complementary to homologous recombination deficiency for improving the clinical outcome of ovarian serous cystadenocarcinoma. *Clin Trans Med* (2021) 11(5):e399. doi: 10.1002/ctm2.399

54. Ganesh K, Stadler ZK, Cercek A, Mendelsohn RB, Shia J, Segal NH, et al. Immunotherapy in colorectal cancer: rationale, challenges and potential. *Nat Rev Gastroenterol Hepatol* (2019) 16(6):361–75. doi: 10.1038/s41575-019-0126-x

55. Eso Y, Shimizu T, Takeda H, Takai A, Marusawa H. Microsatellite instability and immune checkpoint inhibitors: toward precision medicine against gastrointestinal and hepatobiliary cancers. *J Gastroenterol* (2020) 55(1):15–26. doi: 10.1007/s00535-019-01620-7

56. Anagnostou V, Smith KN, Forde PM, Niknafs N, Bhattacharya R, White J, et al. Evolution of neoantigen landscape during immune checkpoint blockade in non-small cell lung cancer. *Cancer Discov* (2017) 7(3):264–76. doi: 10.1158/2159-8290.Cd-16-0828

frontiers | Frontiers in Immunology

TYPE Original Research
PUBLISHED 25 August 2022
DOI 10.3389/fimmu.2022.923528

OPEN ACCESS

EDITED BY
Xuyao Zhang,
Fudan University, China

REVIEWED BY
Zhi-Liang Ji,
Xiamen University, China
Yuwei Liu,
Jiangsu University, China

*CORRESPONDENCE
Xin Chen
xinchen@zju.edu.cn

SPECIALTY SECTION
This article was submitted to Cancer Immunity and Immunotherapy, a section of the journal Frontiers in Immunology

RECEIVED 16 May 2022
ACCEPTED 05 August 2022
PUBLISHED 25 August 2022

CITATION
Liang S, Li Y, Dong Q and Chen X (2022) MMKP: a mind mapping knowledgebase prototyping tool for precision medicine.
Front. Immunol. 13:923528.
doi: 10.3389/fimmu.2022.923528

MMKP: A mind mapping knowledgebase prototyping tool for precision medicine

Siliang Liang, Yun Li, Qingling Dong and Xin Chen*

Institute of Pharmaceutical Biotechnology and the First Affiliated Hospital Department of Radiation Oncology, Zhejiang University School of Medicine, Hangzhou, China

Background: With significant advancements in the area of precision medicine, the breadth and complexity of the relevant knowledge in the field has increased significantly. However, the difficulty associated with dynamic modelling and the disorganization of such knowledge hinders its rapid development potential.

Results: To overcome the difficulty in using the relational database model for dynamic modelling, and to aid in the organization of precision medicine knowledge, we developed the Mind Mapping Knowledgebase Prototyping (MMKP) tool. The MMKP implements a novel design that we call a "polymorphic foreign key", which allows the establishment of a logical linkage between a single table field and a record from any table. This design has advantages in supporting dynamic changes to the structural relationships in precision medicine knowledge. Knowledge stored in MMKP is presented as a mind map to facilitate human interaction. When using this tool, medical experts may curate the structure and content of the precision knowledge in a flow that is similar to the human thinking process.

Conclusions: The design of polymorphic foreign keys natively supports knowledge modelling in the form of mind mapping, which avoids the hard-coding of medical logic into a rigid database schema and significantly reduces the workload that is required for adapting a relational data model to future changes to the medical logic. The MMKP tool provides a graphical user interface for both data management and knowledgebase prototyping. It supports the flexible customization of the data field constraints and annotations. MMKP is available as open-source code on GitHub: https://github.com/ZjuLiangsl/mmkp.

KEYWORDS

precision medicine, knowledgebase, polymorphic foreign key, mind map, prototyping tool

Abbreviations: MMKP, Mind Mapping Knowledgebase Prototyping; RDBMS, relational database management system; CPIC, The Clinical Pharmacogenetics Implementation Consortium; CDS, clinical decision support; 6-MP, 6-Mercaptopurine; TPMT, Thiopurine methyltransferase; ITPA, inosine triphosphate pyrophosphatase.

Background

Precision medicine is a domain that was built on the border between medicine, genetics and information technology that led to the development of modern medical sciences and technologies (1). A core objective of precision medicine is to build a comprehensive knowledge network that illustrates the molecular mechanisms of individual diseases through integration and analysis of a large scale of samples and massive amounts of data (2). This allows prevention and treatment to be personalized according to an individual's characteristics, such as their genomic traits (3). Through the years, precision medicine has guided numerous genetic traits as medical indicators into clinical practice. A series of evolving theories on the effective usages of these indicators are associated with these indicators (4–6). The modelling, organization and management of such precision medicine knowledge is a challenge because of its dynamic nature. Existing database solutions presently need to manage large amounts of data with nonvolatile relationships (7–9).

The state-of-the-art knowledgebase management solutions, including knowledgebases that manage precision medicine knowledge, mostly use the relational database management system (RDBMS) model. RDBMS supports recursive query and is able to query the transfer relationship in a general data model (10). While RDBMS is convenient for storing and querying a large amount of data with a stable relational structure, making changes to the data structure in an RDBMS is difficult. It was argued that RDBMS is incompetent for the management of fast-evolving precision medicine knowledge (11). Precision medicine knowledge is typically made of a large number of different categories of information, where the pieces of information in each category are not as abundant as compared to other domains of database applications. The structural complexity of the precision medicine knowledgebase built by RDBMS adds to the complexity when the relational structure of the database needs to be changed to reflect the addition of a new type of knowledge (12, 13). An example is shown in a later section to illustrate this deficiency.

More recently, researchers have also tried non-RDBMS technologies for building precision medicine knowledgebases. Examples include semantic networks (12), distributed file systems (13) and graph databases (14, 15). Semantic networks describe knowledge in the form of triplets, which have a limited expression power (16) and are difficult to use when modelling natural language-based precision medicine knowledge. The distributed file system and graph database, also known as the NoSQL database, are relatively new and still lack a medical expert-friendly integrated development environment and a globally-accepted standard (17). In this regard, RDBMS-based relational modelling and data management are still competitive approaches; it exhibits good semantic capturing abilities and technical stability. RDBMS is still the first choice when a new precision medicine knowledgebase is being developed.

This work presents MMKP, a fast-prototyping tool for precision medicine knowledgebase systems that uses RDBMS as a backend. MMKP supports the modelling of precision medicine knowledge with a new design pattern that we call a polymorphic foreign key, which significantly improves the capability of the resulting knowledgebase to adapt to changes in knowledge structures. This tool also supports the visualized curation of a knowledgebase schema and knowledge content in the form of a mind map, which is a human-friendly way to model and express medical knowledge (18, 19). In addition, users may alternatively revise knowledge structures and knowledge content, which simulates the flow of a human expert learning new knowledge.

Results

The schematic design of the MMKP

In the area of knowledge representation, scientists have discovered that a semantic unit may be abstracted as a category or an entity. A knowledge entity is an object or a phenomenon recognized by an individual, while a knowledge category is the cognition acquired by abstracting a class of entities of which the commonalities are shared. Traditionally, when implementing a relational data model, it is necessary to first go through the domain knowledge and extract all the categories (20). Database tables are then established with fields corresponding to these categories of knowledge. Foreign key relationships are established to constrain a table filed to be associated with the record of another table. This procedure adapts well to the domains of knowledge modelling where the knowledge structure remains stable. However, in the area of precision medicine, new types of principles, theories or mechanisms are frequently proposed and integrated into practice (21, 22). Consequently, there is a frequent need to add new knowledge categories into the existing knowledgebases. It is virtually impossible for a knowledgebase designer to know *a priori* the complete list of categories that modelling certain precision knowledge would require. Instead, additional categories of knowledge must be continuously integrated with the existing system. Therefore, a tool that supports interactive knowledge structures and knowledge content development, i.e., a tool that supports alternative curation and revision of the knowledge structure and knowledge content, would be desirable. Such a tool will require a nontraditional design to enable its capability to model dynamic knowledge structures.

MMKP implements a new design to represent knowledge linkages instead of using the foreign key constraint. This design is called a polymorphic foreign key. A polymorphic foreign key

can be intuitively understood as a pair of identifiers, one of which identifies a table, and the other of which identifies a record that can be connected in this tables. In contrast to the foreign key constraint, a polymorphic foreign key enables one table field to connect with a record that may be stored in multiple potential tables. This design enables efficient revision of the knowledge structure, where new types of knowledge (tables) may be easily wired into the existing knowledge system. For example, the practice of disease diagnosis may be modelled as a flow of action steps. Each step has a "next step". However, it is difficult for us to know *a priori* all possible types of diagnostic actions (e.g., do some tests, prepare a room, etc.) and design their tables accordingly. We expect new types of diagnostics (new tables) to be integrated into the knowledgebase constantly. In MMKP, we create a field called the "next step" with its data type set to a polymorphic foreign key (which is denoted "reference" for short in the MMKP interface). This field may store an identifier to link the current step (the current record) to any type of next step (a record in another table). New types of diagnostic steps can therefore be easily integrated into the knowledge system by adding new tables, and existing knowledge can link with new knowledge through the polymorphic foreign key field. A more detailed discussion is given later in the section with an example.

Knowledge modelling of a precision medicine guide using the polymorphic foreign key

The Clinical Pharmacogenetics Implementation Consortium (CPIC) is a source of well-established pharmacogenetic dosing guidelines. The organizations of precision medicine knowledge in CPIC are generalizable examples for evaluating whether a knowledge modelling tool can effectively process precision medicine knowledge. We illustrate the usage of MMKP modelling a point-of-care clinical decision support (CDS) in the CPIC Guideline for one of the thiopurines, 6-Mercaptopurine (6-MP), with the Thiopurine methyltransferase (TPMT) and *NUDT15* genotypes. Detailed information can be found in Table 1.

This CDS document presents precision medicine knowledge as a decision flow, which connects different diagnostic states to different next steps according to the decision criteria in the flow. Three categories of actions may be taken for a patient in a specific diagnostic state. These categories of actions include judgement, drug order suggestion and test alert suggestion. In the CDS document, judgement is represented by a rhomboid box with a criterion on a patient's measurement. Drug order suggestions and test alert suggestions are represented by rectangular boxes with white and blue backgrounds, respectively (Figure 1A).

In MMKP modelling of the CDS, the judgement table contains a criterion based on which patients in a specific diagnostic state may be directed to the next step. The next step may be a judgement, a drug order suggestion or a test alert suggestion. The linkages between the "next step" field of the judgement table and the actual next step description (stored as records in the judgement table, drug order suggestion table and test alert suggestion table) are implemented by polymorphic foreign keys (Figure 1B). With this approach, the entire CDS is therefore stored in three tables by the MMKP. As in this example, it is expected that more types of actions that are defined by different specifications and require the storing of different tables need to be integrated into the current CDS when knowledge advances. Because the design of polymorphic foreign keys allows the dynamic addition of new types of table records into the possibilities that a field may link to, the addition of new types of actions is natively supported by an MMKP knowledgebase, which, in contrast, would require a complex effort in a traditionally designed knowledgebase. A hypothetical example is given later.

The MMKP tool

The current version of the MMKP tool provides a mind mapping interface for designing table structures and the linkages between tables. An example showing the process of modelling 6-MP usage within patients with the *TPMT* and *NUDT15* genotypes, the CDS, is illustrated in Figure 2. In this example, the table "Judgement" is logically linked to the "Judgement" table

TABLE 1 Web locations of CPIC information.

Description	Location
CPIC Guideline for Thiopurines and TPMT and NUDT15	https://cpicpgx.org/guidelines/guideline-for-thiopurines-and-tpmt/
Most recent guideline publication	https://files.cpicpgx.org/data/guideline/publication/thiopurines/2018/30447069-supplement.pdf
TPMT consult and implementation workflow	https://files.cpicpgx.org/data/report/current/gene_cds/TPMT_CDS.xlsx
Mercaptopurine pre- and post-test alerts	https://files.cpicpgx.org/data/guideline/publication/thiopurines/mercaptopurine_Pre_and_Post_Test_Alerts_and_Flow_Chart.xlsx
Thioguanine pre- and post-test alerts	https://files.cpicpgx.org/data/guideline/publication/thiopurines/thioguanine_Pre_and_Post_Test_Alerts_and_Flow_Chart.xlsx

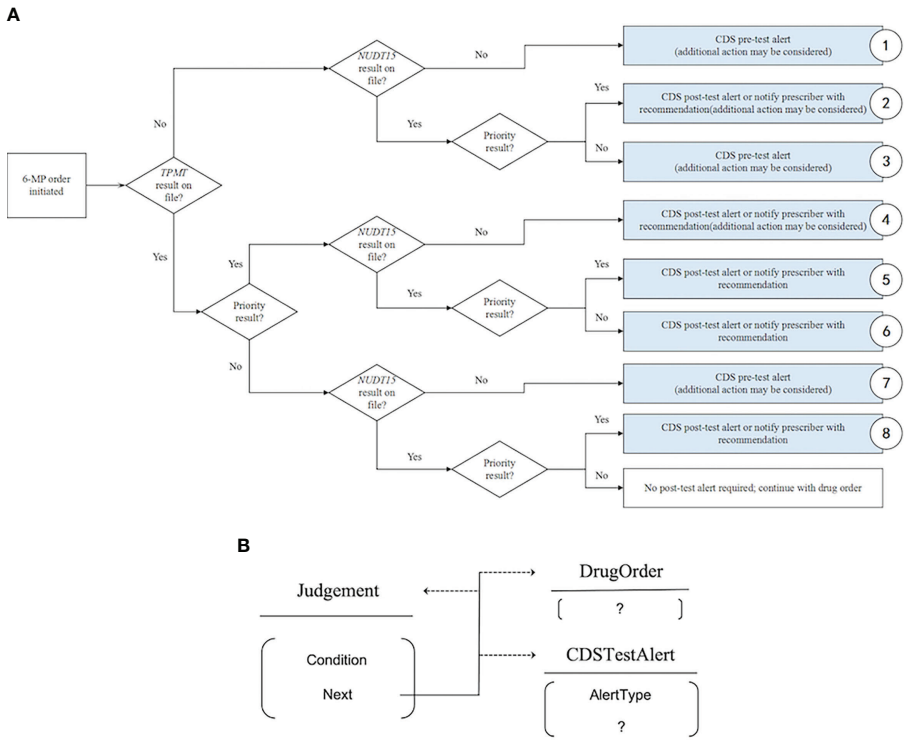

FIGURE 1
Decision flow in the CDS and its modelling. **(A)** The decision flow in dosing guidelines. **(B)** MMKP modelling of the decision flow using a polymorphic foreign key.

itself, to the "DrugOrder" table and to the "CDSTestAlert" table through the field "Next" with the data type "polymorphic foreign key".

After the knowledge structure is modelled, the MMKP provides an interface for knowledge entry. As in a typical clinical decision-making flow, each decision leads to a "next step". When entering one step (table record), the user is allowed to leave the "next step" field blank at first. After the next step description has been recorded in its own table, the user can link this record back to the "next step" field of the record

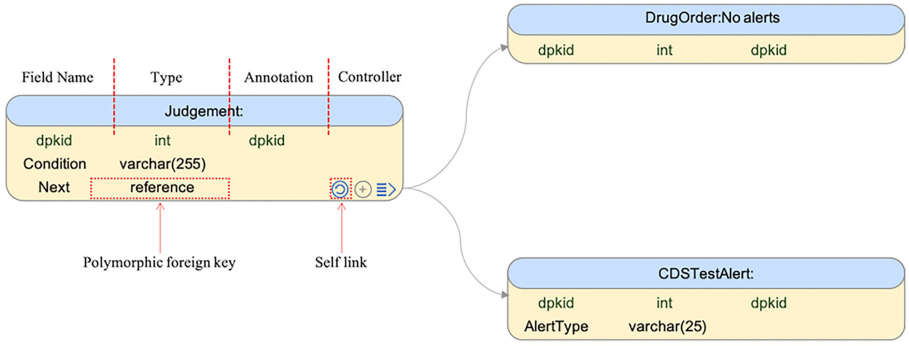

FIGURE 2
Interface of the MMKP schema design. Three knowledge tables abstracted from the decision flow are shown, of which the cells from left to right refer to the field name, field type, manual annotation and polymorphic foreign key controller. The Type 'Reference' indicates that field 'Next' is a polymorphic foreign key. The Controller button from left to right adds the polymorphic foreign key link to its main table, to a new table, or shows the already-linked tables in the working canvas.

representing its previous step. All records are shown on a graphical canvas, and the linkages can be created and modified by drag and drop. This design facilitates knowledge entry by intuitively showing the logical relationship between logically connected records that spread over multiple tables (Figure 3). The MMKP tool ensures the constraint that a polymorphic foreign key field links only to one record in a table. This method of knowledge entry simulates the method of human thinking and is therefore more user-friendly than existing database management tools that rely on the traditional relation data model.

In addition to knowledge modelling, the current version of the MMKP tool supports a range of auxiliary functions, such as metadata management and data dictionaries, as well as a flexible tool to specify table field constraints. The MMKP tool is implemented with Java. It uses an open source Vue-based mind map module as an interface and uses the Springboot framework for project management.

Internally, the MMKP tool uses a meta-database and an entity base for data organization and data buffer management. This design ensures the stability of the data source by making it relatively isolated from user activities. Knowledge structures and knowledge entries created by MMKP may be exported and stored in a variety of backend database management systems for subsequent development. The source code for MMKP is available at https://github.com/ZjuLiangsl/mmkp.

Discussion

A polymorphic foreign key is an efficient design for modelling dynamic knowledge

In the above example, knowledge modelling by the MMKP is achieved by three tables, corresponding to the three types of knowledge that logically require their own table to store. The logical links between these tables are stored in a polymorphic foreign key field, which avoids stereotyping known medical logic into a materialized database schema and allows for future extension. In the MMKP, the polymorphic foreign key field actually models a higher-level concept of the human mind (the "next step" concept in this example). The MMKP approach may therefore be regarded as a higher-level abstraction of a knowledge structure. This higher-level abstraction can remain stable when a lower-level abstraction (data fields that make up a table) changes. This pattern of higher-level abstraction is frequently found in natural human thinking. MMKP is a tool that is capable of such higher-level modelling of knowledge.

This higher-level abstraction of knowledge bestows the advantage of a more stable knowledgebase schema, with new types of knowledge (data tables) easily being incorporated into the existing system. Below, we show an example. Assume that new evidence emerges that new genotype test result of inosine triphosphate pyrophosphatase (ITPA) and its new therapy have

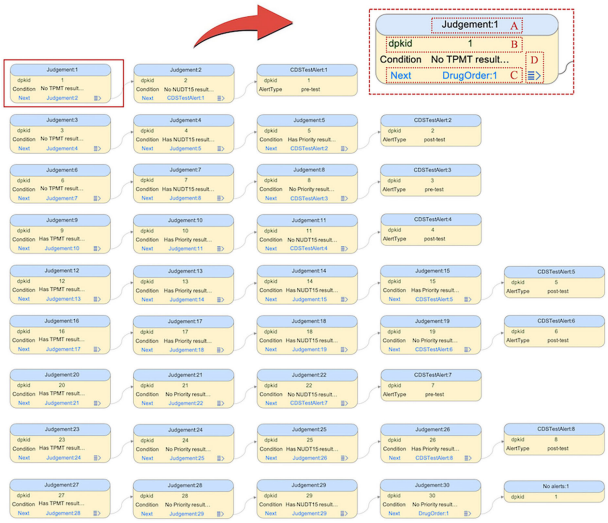

FIGURE 3
Interface of MMKP knowledge entry. Each cell frame represents a judgement or a decision in the decision flow. **(A)** Each frame is identified by its table name and primary key, which is quoted by the polymorphic foreign key. **(B)** Only tables with a single unique key can be linked by polymorphic foreign keys. The MMKP tool will automatically create a unique self-incrementing key for each table record, and this key is marked in green. **(C)** The value of the polymorphic foreign key is definite and unique and is marked blue. Users can drag and drop to make connections between a polymorphic foreign key field and a table record. **(D)** Users can choose to display or hide the downstream tables as necessary by expanding the controller.

become available for patients. Subsequently, the decision flow needs to be modified as shown in Figure 4. In the MMKP, the necessary changes include, first, adding a new table to store the therapy specification and then rewiring the polymorphic foreign key links accordingly. There is no modification of the existing table structure or table constraint needed. This process is intuitive and safe and alleviates the subsequent need to modify knowledgebase application codes to accommodate the new change.

In contrast, the traditional way of designing a relational database follows the database schema design norms (17). A typical design is shown in Figure 5, which includes three tables: "Condition", "Decision", and "Judgement". The "Condition" table stores a patient's measurements for decision-making, which are stored in different fields that correspond to whether the patient has "TPMT_result_on_file", "NUDT15_result_on_file", etc. The "Decision" table stores a collection of outcomes of the decision-making flow, which includes the fields of "alert_type" and "drug_order_description". The "Judgement" table stores the correspondence between the condition table and the decision table. To accommodate the change that new genotype test result and therapy for patients becomes available, a number of changes, including data structure changes, are needed. New fields 'ITPA_result_on_file' and 'priority_result_ITPA' must be added into table "Condition", which leads to the necessary action to modify all existing records in the condition table. In addition, a detailed description of the new therapy needs to be recorded. A new field 'new_therapy_description' needs to be added to table "Decision", which also requires modification of all records in this table. Compared to the MMKP process, implementing this process requires a careful plan, is nonintuitive, and leads to extensive downstream work updating the database access codes for the knowledgebase application.

Outside the domain of database management, the action of linking one object to multiple objects of different types is also needed. For example, when building a web application, one

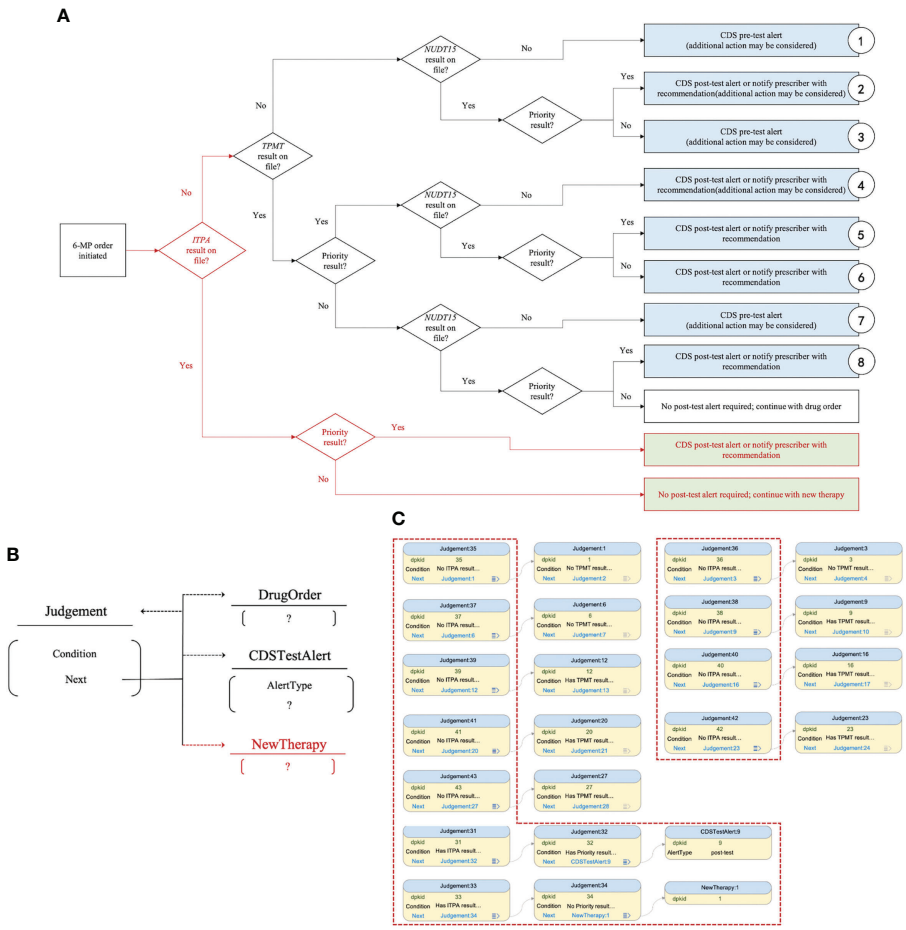

FIGURE 4
Change of decision flow modelled by MMKP. **(A)** Addition of a new genotype test result *ITPA* and its new therapy for patients. **(B)** Knowledge content reflecting the new decision flow in MMKP. **(C)** Knowledge content entry in MMKP, with the updated content in a red dashed box.

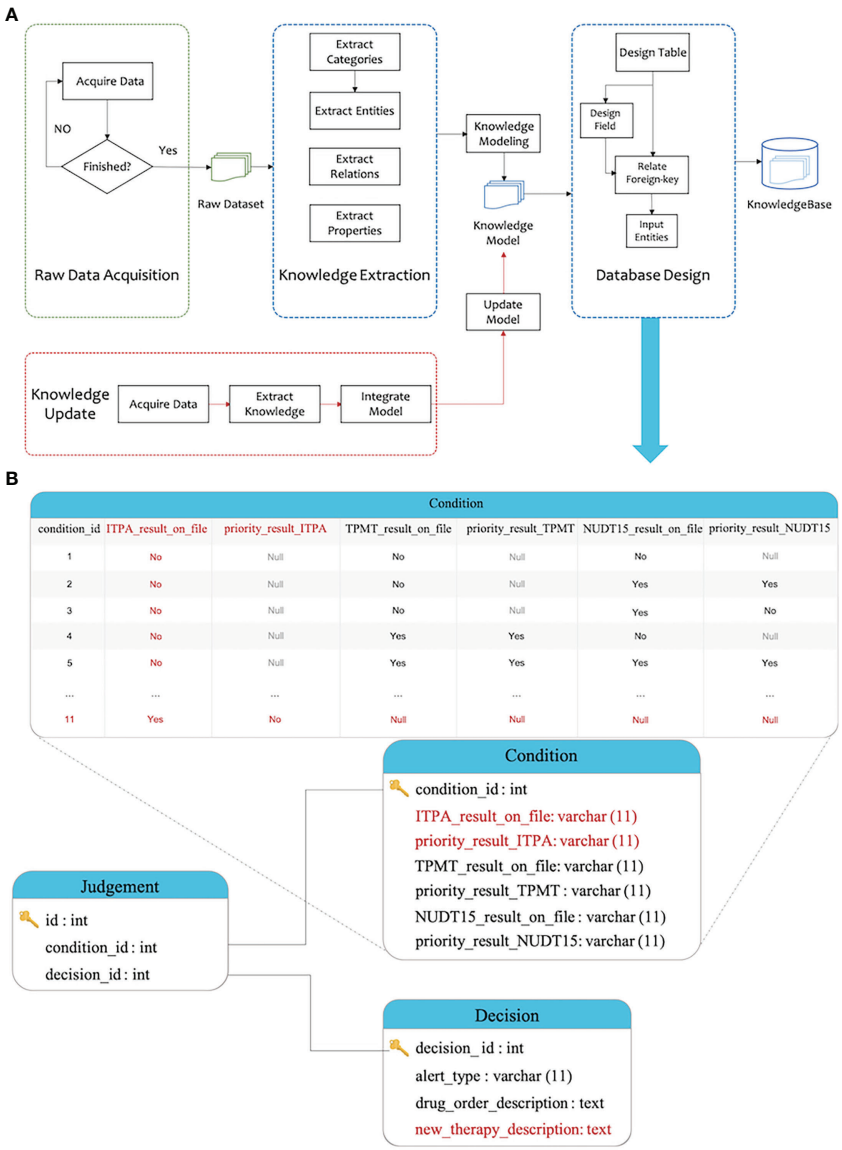

FIGURE 5
Modelling of CDS and its change with the traditional approach. **(A)** The traditional approach requires complex modifications to accommodate a new data table. **(B)** The knowledge content in the traditionally modelled knowledgebase. Table records need to be modified when a new data table is to be integrated into the knowledgebase.

content item is frequently needed to be linked to multiple other content items of different types. The Django web framework provides a Java based programming model to implement such links from one instance of a specific content type class to multiple instances of other content type classes. By this means, the Django web framework supports the development of reusable web applications, web sites and web tools. In the Django web framework, such technology is called "generic foreign keys". Comparing to the generic foreign keys technology, our polymorphic foreign key technology provides a database management system-based solution to the need of complex links, which manages information instead of web components, and provides a method for data curators to model higher-level abstract concepts in scientific information.

Precision medicine knowledge requires a dynamic modelling tool

As discussed previously, the traditional database design norm requires medical researchers to fully collect all categories and entities in a knowledge domain to compose a schema.

Because of the lack of flexibility of the foreign key constraint, connection from a high-level concept (e.g., "next step") to its real meaning (a record in a table) typically requires multiple foreign key fields if this high-level concept can refer to things that belong to different knowledge categories. Each foreign key field links to one category. Later, an addition to the schema would be complex and error prone and requires substantial downstream work. This approach is not sufficient to meets the needs of precision medicine knowledge management that deals with highly complex data and rapidly evolving knowledge categories.

Moreover, it is difficult to train medical experts and computer experts with expertise from each other (23, 24). The traditional model of knowledgebase design requires well-trained computer experts who understand medical knowledge to create a database schema (25). Due to the complexity and dynamic nature of medical knowledge, this process is often of very low efficiency, prone to misunderstanding and lasts for multiple cycles. The MMKP tool facilitates this process by allowing medical experts to express their knowledge using high-level concepts, leading to a more stable schema, as well as allowing for incomplete collection of knowledge categories at the initial stage, and permitting integration of new knowledge categories into the existing system with low costs.

With the efficient polymorphic foreign key design, the MMKP tool supports a data modelling process that simulates human thinking. MMKP allows alternative curation of the data schema and data content, i.e., users may create and modify knowledge structures and knowledge content in any order that is intuitive to the user. The curation of data content in the middle of a process curating a knowledge structure may also serve as a validation step to check whether the knowledge structure is correct and comprehensive (Figure 6).

With these features, MMKP demonstrates advantages over traditional database design tools such as 'Sequel Pro' (26) and 'MySQL Workbench' (27, 28) in modelling precision medicine knowledge, which are more suitable for precision medicine knowledgebase prototyping.

Currently, knowledge management for precision medicine faces multiple challenges including expert training, knowledgebase curation, and maintenance. MMKP provides a user-friendly mind mapping interface for domain experts to curate knowledgebases, which may facilitate the training of curation experts. When adopted widely, MMKP is expected to notably reduce the amount of time and effort that is necessary for domain expects to curate data. In addition, because that the data structure used by MMKP follows the thinking model of domain expects instead of programming specialists, knowledge stored in such structure is easy to understand and extend, which also facilitates the collaboration between different data curation teams to connect their knowledgebases. After a knowledgebase is initially created with MMKP, as illustrated before, extending it to include the latest discoveries is also simpler than knowledgebases created by other tools.

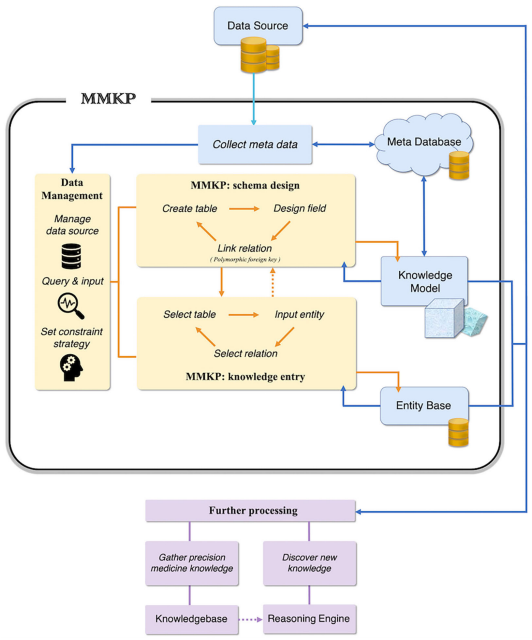

FIGURE 6
The schematic design of MMKP. MMKP applies a cyclic schema to model the precision knowledge and enter content, which supports alternative curation and revision of the knowledge structures and knowledge content. MMKP stores models and entities in the inner meta-database and entity base, keeping user operations independent of the data source before exporting.

Limitations and future of the MMKP

Precision medicine is a rapidly developing area, yet its translation to clinically proven patient benefits is still difficult. One of the bottlenecks is the information management efficiency. There are a greater number of precise indicators that may lead to different optimal decisions than those that a medical practitioner can remember and recall. However, the creation of a knowledgebase with the traditional data modelling approach is hindered by the fast-evolving knowledge structures in this field. The MMKP provides a solution for the efficient modelling and organization of precision medicine knowledge; however, this knowledge is still static. MMKP is not a tool that can help medical practitioners use this knowledge.

Medical artificial intelligence that supports clinical decision-making holds promise in breaking through this bottleneck. However, the development of such medical artificial intelligence is also hindered by the lack of a stable approach to represent medical knowledge, without which efficient reasoning algorithms are impossible to develop. In this regard, MMKP provides a way of representing precision medicine knowledge with higher-level concepts, leading to a more stable table

schema. This advantage may also facilitate the development of efficient medical artificial intelligence applications on top of the MMKP data schema.

Conclusions

In this paper, we introduce a precision medicine knowledgebase fast prototyping tool, MMKP. It uses a polymorphic foreign key to associate a higher-level concept with knowledge pieces from multiple knowledge categories, allowing alternative creation and modification of knowledge structures and knowledge content. It provides a web interface capable of knowledge modelling, knowledge content entry and exportation of curated knowledgebase prototypes to a series of database system backends. It provides a web interface that is graphical and was inspired by the form of a mind map. The MMKP tool is open source and available in GitHub.

Data availability statement

The original contributions presented in the study are publicly available. This data can be found here: https://github.com/ZjuLiangsl/mmkp.

Author contributions

SL and XC designed the MMKP. SL developed the MMKP. QD, YL and XC contributed valuable discussions in regard to the program design of the MMKP. SL and XC wrote substantial parts of the manuscript, and all authors proofread and approved the final version of the manuscript.

Funding

This work was financially supported by the National Key Research and Development Program (2021YFC2100601), the National Natural Science Foundation of China (81830073).

Acknowledgments

We thank Dr. Jin Jie for suggestions on website design.

Conflict of interest

The authors declare that the research was conducted in the absence of any commercial or financial relationships that could be construed as a potential conflict of interest.

Publisher's note

References

1. Twilt M. Precision medicine: The new era in medicine. *EBioMedicine* (2016) 4:24–5. doi: 10.1016/j.ebiom.2016.02.009

2. Collins FS, Varmus H. A new initiative on precision medicine. *New Engl J Med* (2015) 372(9):793–5. doi: 10.1056/NEJMp1500523

3. Compton C. Precision medicine core: Progress in prognostication-populations to patients. *Ann Surg Oncol* (2018) 25(2):349–50. doi: 10.1245/s10434-017-6024-y

4. Ielapi N, Andreucci M, Licastro N, Faga T, Grande R, Buffone G, et al. Precision medicine and precision nursing: The era of biomarkers and precision health. *Int J Gen Med* (2020) 13:1705–11. doi: 10.2147/IJGM.S285262

5. Phillips KA, Deverka PA, Hooker GW, Douglas MR. Genetic test availability and spending: Where are we now? *Where Are We Going? Health Affairs* (2018) 37 (5):710–6. doi: 10.1377/hlthaff.2017.1427

6. Yin T. Application research of precision medical model based on big data in primary health care in China. *Afr Asian Stud* (2020) 19(4):323–35. doi: 10.1163/15692108-12341470

7. Ziegler A. Precision medicine in pediatric neurology exemplified by the new treatment forms. *Nervenarzt* (2022) 93(2):122–34. doi: 10.1007/s00115-021-01251-5

8. Sanz-Garcia E, Zhao E, Bratman SV, Siu LL. Monitoring and adapting cancer treatment using circulating tumor DNA kinetics: Current research, opportunities, and challenges. *Sci Advances* (2022) 8(4). doi: 10.1126/sciadv.abi8618

9. Van den Bossche V, Zaryouh H, Vara-Messler M, Vignau J, Machiels J-P, Wouters A, et al. Microenvironment-driven intratumoral heterogeneity in head and neck cancers: clinical challenges and opportunities for precision medicine. *Drug Resistance Updates Rev Commentaries Antimicrobial Anticancer Chemother* (2022) 60:100806–. doi: 10.1016/j.drup.2022.100806

10. Schadow G, Barnes MR, McDonald CJ. Representing and querying conceptual graphs with relational database management systems is possible. *J Am Med Inf Assoc* (2001), 598–602.

11. Qi M, Liu Y, Lu L, Liu J, Li M. Big data management in digital forensics, in: *IEEE 17th International Conference on Computational Science and Engineering (CSE).* (2014) 238–43. doi: 10.1109/CSE.2014.74

12. Lukovic V, Cukovic S, Milosevic D, Devedzic G. An ontology-based module of the information system ScolioMedIS for 3D digital diagnosis of adolescent scoliosis. *Comput Methods Programs Biomed* (2019) 178:247–63. doi: 10.1016/j.cmpb.2019.06.027

13. Ramos M, Sanchez-de-Madariaga R, Barros J, Carrajo L, Vazquez G, Perez S, et al. An archetype query language interpreter into MongoDB: Managing NoSQL standardized electronic health record extracts systems. *J Biomed Inf* (2020) 101. doi: 10.1016/j.jbi.2019.103339

14. Santos A, Colaco AR, Nielsen AB, Niu L, Strauss M, Geyer PE, et al. A knowledge graph to interpret clinical proteomics data. *Nat Biotechnol* (2022) 40 (5):692–702. doi: 10.1038/s41587-021-01145-6

15. Nguyen T, Lee SC, Quinn TP, Truong B, Li X, Tran T, et al. PAN: Personalized annotation-based networks for the prediction of breast cancer relapse. *Ieee-Acm Trans Comput Biol Bioinf* (2021) 18(6):2841–7. doi: 10.1109/TCBB.2021.3076422

16. Marinov M, Zheliazkova I. An interactive tool based on priority semantic networks. *Knowledge-Based Systems* (2005) 18(2-3):71–7. doi: 10.1016/j.knosys.2004.08.001

17. Contos P, Holubova I, Svoboda M. Multi-model data modeling and representation: State of the art and research challenges, in: *25th International Database Applications and Engineering Symposium (IDAES)* (2021) 242–51.

18. Sarmah P, Hemavathi H, Sharvani R, Shenoy P. EVALUATION OF MIND MAPS AS a LEARNING TOOL IN MICROBIOLOGY FOR MEDICAL STUDENTS. *J Evol Med Dental Sciences-Jemds.* 6(1):27–9. doi: 10.14260/Jemds/2017/8

19. Nair SSK, Al Farei KIeee. A brain friendly tool to facilitate research-teaching nexus: Mind maps, in: *8th International Conference on Information and Communication Systems (ICICS)*, (2017) 82–5.

20. Li K, Zhou C, Luo XR, Benitez J, Liao Q. Impact of information timeliness and richness on public engagement on social media during COVID-19 pandemic: An empirical investigation based on NLP and machine learning. *Decision Support Systems* (2022), 113752–. doi: 10.1016/j.dss.2022.113752

21. Solis RN, Silverman DA, Birkeland AC. Current trends in precision medicine and next-generation sequencing in head and neck cancer. *Curr Treat Options Oncol* (2022), 23(2):254–67. doi: 10.1007/s11864-022-00942-8

22. Salter B, Lacy P, Mukherjee M. Biologics in asthma: A molecular perspective to precision medicine. *Front Pharmacol* (2022) 12. doi: 10.3389/fphar.2021.793409

23. Auffray C, Balling R, Barroso I, Bencze L, Benson M, Bergeron J, et al. Making sense of big data in health research: Towards an EU action plan. *Genome Med* (2016) 8. doi: 10.1186/s13073-016-0323-y

24. Bertier G, Carrot-Zhang J, Ragoussis V, Joly Y. Integrating precision cancer medicine into healthcare-policy, practice, and research challenges. *Genome Med* (2016) 8. doi: 10.1186/s13073-016-0362-4

25. Gomez-Lopez G, Dopazo J, Cigudosa JC, Valencia A, Al-Shahrour F. Precision medicine needs pioneering clinical bioinformaticians. *Briefings Bioinf* (2019) 20(3):752–66. doi: 10.1093/bib/bbx144

26. Krauskopf E. A bibiliometric analysis of the journal of infection and public health: 2008-2016. *J Infect Public Health* (2018) 11(2):224–9. doi: 10.1016/j.jiph.2017.12.011

27. Urbanczyk T, Peter L. Database development for the urgent department of hospital based on tagged entity storage following the IoT concept, in: *14th IFAC Conference on Programmable Devices and Embedded Systems (PDES)*, (2016) 49 (25): 278–83.

28. Bjelic M, Poscic P, Jaksic D. DATABASE MODELING TOOLS REVIEW - MYSQL WORKBENCH, OPEN MODELSPHERE, DIA. *Zbornik Veleucilista U Rijeci-Journal Polytechnics Rijeka* (2018) 6(1):251–60. doi: 10.31784/zvr.6.1.18

frontiers | Frontiers in Immunology

TYPE Original Research
PUBLISHED 31 August 2022
DOI 10.3389/fimmu.2022.930461

OPEN ACCESS

EDITED BY
Xuyao Zhang,
Fudan University, China

REVIEWED BY
Zhijun Liu,
First Affiliated Hospital of Xi'an Jiaotong University, China
Erik Soule,
University of Florida, United States

*CORRESPONDENCE
Weijun Fan
fanwj@sysucc.org.cn
Lujun Shen
shenlj@sysucc.org.cn

†These authors have contributed equally to this work

SPECIALTY SECTION
This article was submitted to Cancer Immunity and Immunotherapy, a section of the journal Frontiers in Immunology

RECEIVED 28 April 2022
ACCEPTED 15 August 2022
PUBLISHED 31 August 2022

CITATION
Wu Y, Cao F, Zhou D, Chen S, Qi H, Huang T, Tan H, Shen L and Fan W (2022) Cryoablation reshapes the immune microenvironment in the distal tumor and enhances the anti-tumor immunity.
Front. Immunol. 13:930461.
doi: 10.3389/fimmu.2022.930461

Cryoablation reshapes the immune microenvironment in the distal tumor and enhances the anti-tumor immunity

Ying Wu[1,2,3†], Fei Cao[1,2†], Danyang Zhou[4†], Shuanggang Chen[5†], Han Qi[1,2], Tao Huang[1,2], Hongtong Tan[1,2], Lujun Shen[1,2*] and Weijun Fan[1,2*]

[1]Department of Minimally Invasive Interventional Therapy, Sun Yat-sen University Cancer Center, Guangzhou, China, [2]State Key Laboratory of Oncology in South China, Collaborative Innovation Center of Cancer Medicine, Sun Yat-sen University, Guangzhou, China, [3]Department of Interventional Therapy, Shenzhen Second People's Hospital, The First Affiliated Hospital of Shenzhen University, Shenzhen, China, [4]Department of Oncology, Peking University Shenzhen Hospital, Shenzhen, China, [5]Department of Oncology, Yuebei People's Hospital, Shantou University Medical College, Shaoguan, China

As one of the local treatments, cryoablation plays an increasingly important role in the comprehensive treatment of malignant tumors with its advantages of less trauma, high reproducibility, and minimally invasive. Activation of anti-tumor immunity, another characteristic of cryoablation, has attracted more and more attention with the extensive application of immunotherapy. Unfortunately, the mechanism by which cryoablation enhances anti-tumor immunity is still unclear. In this study, we applied a multi-omics approach to investigate the effects of local cryoablation in the distal tumor microenvironment. The results revealed that large amounts of tumor antigens were released post-cryoablation, leading to a sterile inflammatory response in distant tumors. During this period, activated lysosome-related pathways result in over-expression of SNAP23 (Synaptosome associated protein 23) and STXBP2 (Syntaxin binding protein 2), activation of immune effector cells, suppression of the release of immunosuppressive factors, and finally enhancement of anti-tumor immunity, which shows a broad prospect in combined immunotherapy.

KEYWORDS

cryoablation, tumor microenvironment, lysosome, SNAP23, STXBP2

Introduction

Cryoablation has a long history and was first used in the 1840s to treat breast and uterine cancers (1). Cryoablation is a local treatment method with minimally invasive and practical, with fewer complications, short hospital stays, and repeatable operations (2). With the development of cryoablation technology, cryoablation has been used to treat various solid tumors, including skin, liver, lung, breast, and bone tumors (3).

With the wide application of cryoablation in clinical practice, its minimally invasive nature has been recognized, and the immune response post cryoablation has attracted more and more attention. Tumor cells are damaged by repeated freeze-thaw cycles, accompanied by the release of cell contents. Therefore, these released cell contents retain their original properties, leading to another anti-tumor mechanism after cryoablation: stimulated immunological targeting of tumor cells (1, 3–8). Previous studies have reported spontaneous resolution of distant metastases during cryoablation of prostate cancer (9, 10). Besides, other studies have shown that cryoablation reduces tumor metastasis and that the T lymphocyte in tumor-draining lymph nodes (TDLN) secrete higher levels of interferon-gamma (IFN-γ) than surgery (5). Moreover, tumors that remain *in situ* after cryoablation could protect against subsequent tumor rechallenge (11, 12).

Unfortunately, the mechanism by which cryoablation enhances anti-tumor immunity is still unclear. Previous studies reported that cell contents released by cryoablation contain "danger signals" such as pro-inflammatory cytokine, heat shock protein, DNA, and RNA recognized by toll-like receptors, which activate the natural immune response (1, 3, 4, 7, 13–15). With the wide application of the new generation of immunotherapy represented by immune-checkpoint inhibitors, cryoablation combined with immunotherapy has shown more and more broad prospects, and several clinical trials are currently exploring combination therapies (16–22). However, the timing and sequence of cryoablation, the extent of cryoablation, and the choice of target tumor are still unclear, which requires further understanding of the mechanism of cryoablation enhancing anti-tumor immunity.

In this study, we applied a multi-omics approach to investigate the effects of local cryoablation on the distal tumor microenvironment, providing a theoretical basis for cryoablation in combination with other immunotherapy regimens.

Methods

Cell culture and primary mouse

Mouse colon cancer MC38 was purchased from Guangzhou Saifei Trading Co., Ltd. (Jennie biological technology). Cells were regularly tested for Mycoplasma contamination by quantitative PCR. All of these cells were cultured in Dulbecco's modified Eagle's medium (DMEM; Gibco) supplemented with 10% fetal bovine serum (FBS; Gibco); and 100 μg/ml Penicillin/Streptomycin (Gibco).

Primary mouse and mouse models

C57BL/6J mice were purchased from Guangdong medical laboratory animal center. Mouse xenografts were generated in 6-8-week-old C57BL/6J mice by subcutaneous implantation of 0.5×10^6 cells (both sides). Animals were randomized into two groups (control VS cryoablation) for collection and analysis. On the 7th day, the subcutaneous tumor of the mice grew to about 5-6 mm in diameter. After anesthesia, one side of the tumor was subjected to cryoablation. The cryoablation was performed using Visual-ICE™ System (Galil Medical, Israel). The cryoprobe was inserted into the targeted lesions, and two 40-sec freezing cycles, separated by a 20-sec freezing and an active 20-sec thawing session, were performed. The subcutaneous tumor achieved complete ablation. On the contralateral tumor, two orthogonal diameters were measured every 2-3 days (control vs. cryoablation). Tumor volume was calculated as $V = \pi/6 \times L \times W \times H$, where L, W, and H represent the length, width, and height, respectively. All experiments with mice were performed by protocols approved by the Sun Yat-sen University Cancer Center (SYSUCC). The experiments were repeated at least two times.

Immune profiling by flow cytometry

Implants of the indicated MC38 cell populations in D1, D3, D5, D7, D9 and were measured for total weight. Biopsies were then minced using scalpels and digested with 500 U/ml Collagenase IV (Sigma–Aldrich) and 0.02 mg/ml DNAse I (Coolaber) and 300 mg/ml-Hyaluronidase (Solarbio) per 0.3 g tumor weight for 30-50 min at 37°C. After digestion, the cell suspension was passed through a 40 μm cell strainer to remove large pieces of undigested tissue. Erythrocytes were lysed using Red Blood Cell Lysis Solution (TIANGEN; RT122-02).

In terms of cell surface stain, 1×10^6 cells were incubated with an anti-Fc receptor blocking antibody and stained with the indicated antibodies in stain buffer (BD) for 30 min on ice. Viability was assessed by staining with Fixable Viability Stain 620 (BD). For intracellular staining of Foxp3, cells were first fixed and permeabilized using a Fixation/Permeabilization Solution Kit (BD). All flow cytometry was performed on a CytoFLEX LX (Beckman Coulter). The flow cytometry data was analyzed using FlowJo V10.6.2 (BD). Flow cytometry antibodies were used as follows (all from BD): Anti-CD45 FITC (Clone 30-f11), Anti- CD8a APC-H7 (Clone 53-6.7), Anti- CD4 BV510 (Clone RM4-5), Anti- CD279 BB700 (Clone

J43), Anti- IFN-Gma PE-Cy7 (Clone XMG 1.2), Anti- Foxp3 Alexa 647 (Clone MF23), Anti- LY-6G BV786 (Clone 1A8), Anti- CD11b BV605 (Clone M1/70), Anti- CD16/CD32 Pure (Clone 2.4G2). The experiments were repeated at least two times.

After gating single cell types and excluding non-viable cells by staining with Fixable Viability Stain 620 and excluding debris with side scatter area and forward scatter area, the cells are identified using the following combination of cell markers: $CD4^+$ T cell: $CD45^+CD4^+$; $CD8^+$ T cell: $CD45^+CD8^+$; Treg cell: $CD45^+CD4^+Foxp3^+$.

Bulk RNA-seq and data analysis

Extract mRNA with a magnetic bead adsorption method and cut it into a small fragment to synthesize cDNA. The RNA samples were sequenced by the Shanghai Personalbio Company. The library preparations were sequenced on a NovaSeq platform after cluster generation. Differential expression analysis was performed using the edgeR R package (3.18.1). The P values were adjusted using the Benjamini & Hochberg method, and the absolute foldchange of 1 and P-value of 0.05 were set as the threshold for identification of differentially expressed genes. STRING database was used for Protein-protein interaction network analysis (PPI) analysis. CIBERSORT was used for calculating immune cell infiltration in the tumor.

Quantitative proteomics and data analysis

Pre- (3 samples) and post-cryoablation (4 samples) samples were obtained from advanced melanoma patients who had progressed after a series of therapies, including chemotherapy, targeted therapy, and immunotherapy. We obtained tumor tissue from the same distal tumor (without cryoablation) by fine-needle aspiration biopsy before and three weeks after cryoablation. The patients and Ethics Committee have approved all procedures. No related complications occurred in all patients. The samples were frozen in liquid nitrogen and ground with a pestle and mortar. The protein samples were sequenced in Shanghai Genechem Co., LTD (4D Label-free). The MS data were analyzed using MaxQuant software version 1.6.14.0. Samples were analyzed on a nanoElute (Bruker, Bremen, Germany) coupled to a timsTOF Pro (Bruker, Bremen, Germany) equipped with a CaptiveSpray source, and the timsTOF Pro (Bruker, Bremen, Germany) was operated in PASEF mode. The global false discovery rate (FDR) cutoff for peptide and protein identification was set to 0.01. Proteins which Fold change>2 or <0.5 and p-value (Student's t-test) <0.05 were considered to be differentially expressed proteins. We applied the SangerBox tool to further bioinformatics analysis of DEGs (sangerbox.com).

Statistical Analysis

For categorical variables versus categorical variables, Fisher's exact test was used; for categorical variables versus continuous variables, the Kruskal-Wallis test was used to test if any of the differences between the subgroups were statistically significant. Tumor growth curves were analyzed by one- and two-way analysis of variance (ANOVA). All statistical tests were two-sided, and statistical significance was considered when p value <0.05 unless otherwise indicated. All the analyses of clinical data were performed in R (version 4.1.1). R software, with limma, ggplot2, dplyr, reshape2, RColorBrewer packages, etc.

Result

Cryoablation could prolong the survival of mice without a significant effect on the distant tumor volume control

On the D7 day, the subcutaneous tumor of the mice grew to about 5-6mm in diameter. After anesthesia, one side of the tumor was subjected to cryoablation (Figure 1A). The cryoprobes were inserted into the targeted lesions, and two 40-sec freezing cycles, separated by a 20-sec freezing and an active 20-sec thawing session, were performed. The histopathology examination at D14 day after cryoablation showed complete ablation of the subcutaneous tumor (Figure 1B). Post-cryoablation, the tumor appeared to have coagulative necrosis with mang inflammatory cell infiltration.

Two orthogonal diameters were measured on the contralateral tumor every 2-3 days. There was no significant difference in tumor volume between the cryoablation group and the control group (Figures 2A–D). However, the survival time of mice in the cryoablation group was significantly prolonged post cryoablation (Figure 2B).

Cryoablation increased the number and infiltration of immune effector cells in distant tumors

To further study the changes in immune microenvironment in distant tumors of mice, the distant tumors and peripheral blood mononuclear cell (PBMC) of mice were detected by flow cytometry on days D1, D3, D5, D7, and D9 post cryoablation. The results indicated that the changes in immune cells, including CD4, CD8, and Treg cells in the PBMC of mice, were not significant post cryoablation (Figures 3A, C).

However, the immune cells isolated from the distant tumor post cryoablation varied significantly over time. In distant tumors, $CD4^+$ T cells in the cryoablation group were

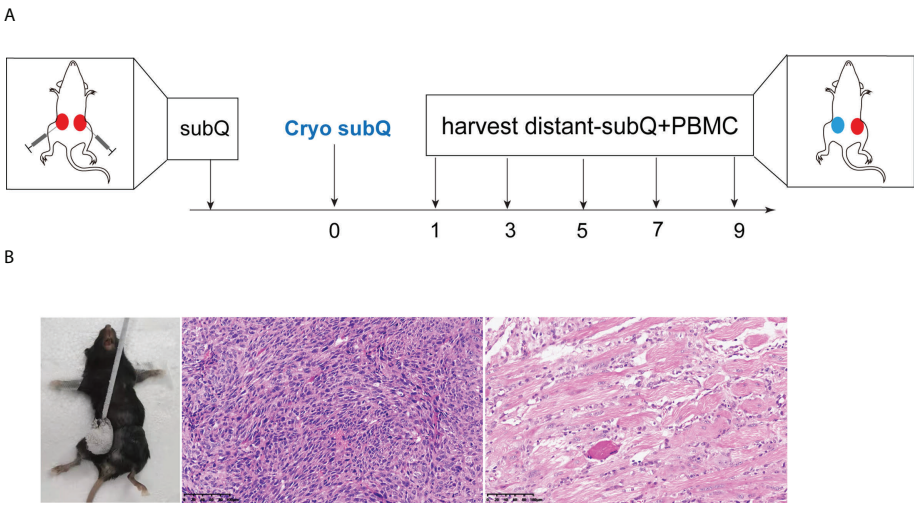

FIGURE 1
Animal model of cryoablation *in vivo*. **(A)** Mouse xenografts were generated in 6-8-week-old C57BL/6J mice by subcutaneous implantation of 0.5×10^6 MC38 cells (both sides). On the 7th day, one side of the tumor was subjected to cryoablation; **(B)** The histopathology examination at D14 days after cryoablation showed complete ablation of the subcutaneous tumor (20x).

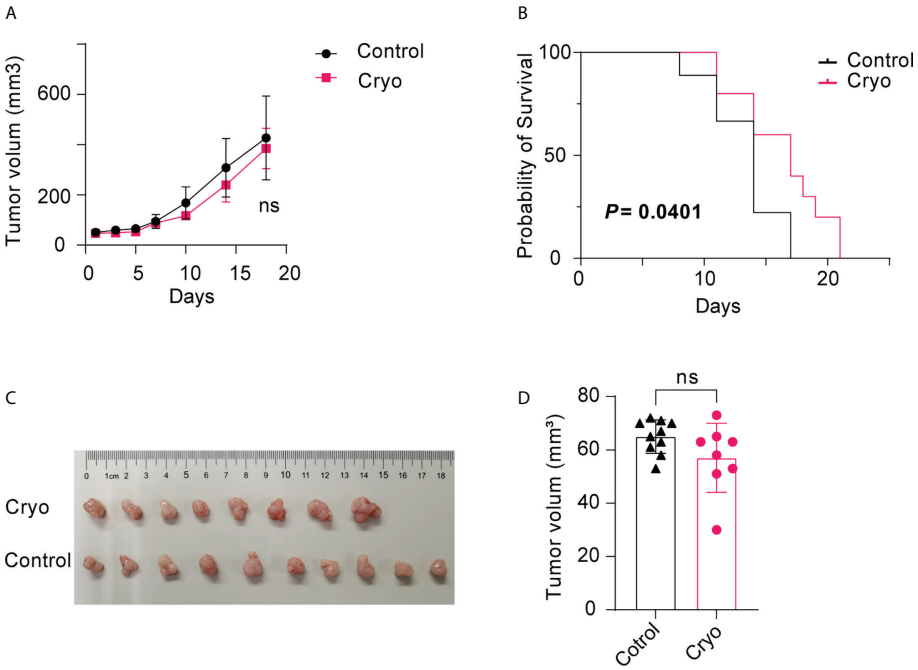

FIGURE 2
(A) There was no significant difference in tumor volume between the cryoablation (5 mice) and the control group (5 mice); **(B)** The survival time of mice in the cryoablation group was significantly prolonged than control group post cryoablation; **(C,D)** There was no significant difference in tumor volume between the control (10 mice) and the cryoablation (8 mice) group on the D5 day after cryoablation. The experiments were repeated at least two times. ns, not statistically significant.

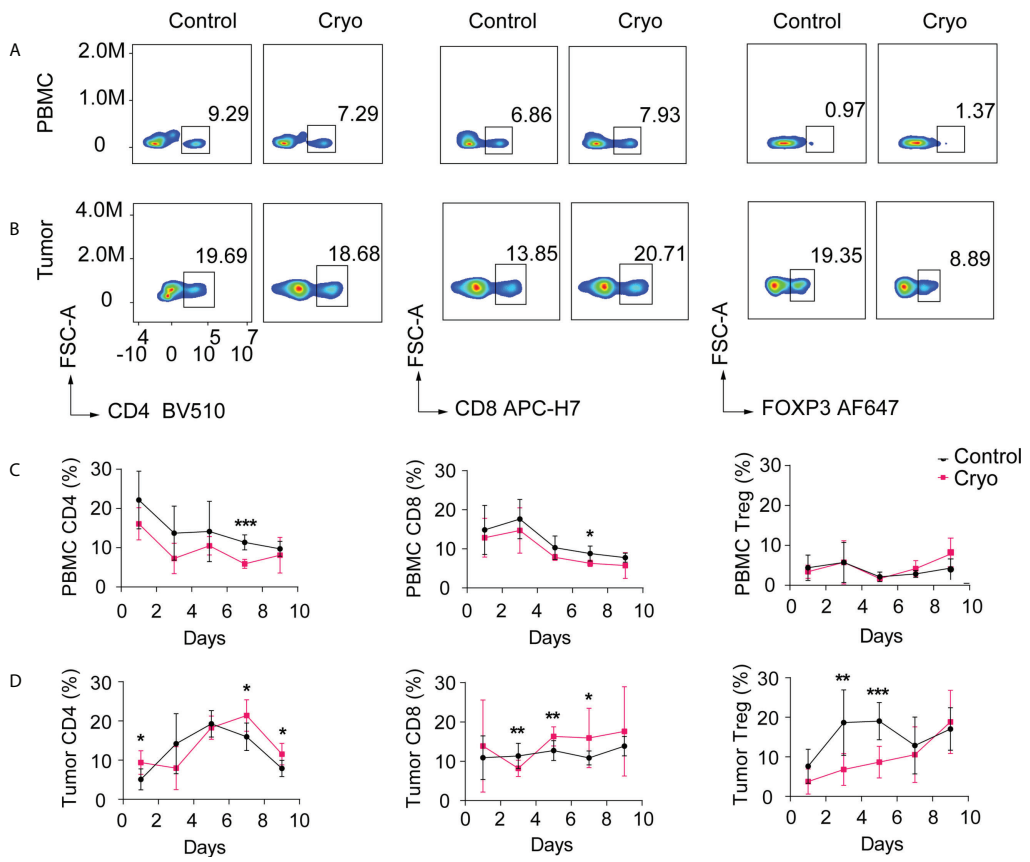

FIGURE 3
(A, B) Flow chart of CD4$^+$ T cells, CD8$^+$ T cells, Treg cells in PBMC, and distal tumor on day 5. The distant tumors and peripheral blood mononuclear cells (PBMC) of mice were detected by flow cytometry on days D1, D3, D5, D7, and D9 post cryoablation. **(C)** Changes in the proportion of CD4$^+$ T cells, CD8$^+$ T cells, and Treg cells in peripheral blood (PBMC); **(D)** Changes in the proportion of CD4$^+$ T cells, CD8$^+$ T cells, and Treg cells in the distant tumor (non-cryoablation tumors). *: p<0.05, **: p<0.01, ***: p<0.001, ns: not statistically significant. The experiments were repeated at least two times.

significantly higher than those in the control group on the first-day post cryoablation. There was no difference between the two groups on D3-D5 days, but there was a significant increase after D5 days in the cryoablation group. CD8$^+$ T cells increased significantly on the D5-D7 days post cryoablation, but there was no significant difference between the two groups on the D9 day. Treg cells decreased substantially on the D3-D6 days post cryoablation, but there was no significant difference between the two groups on the D7 day (Figures 3B, D).

The immunohistochemical results showed that most of the immune cells in the distant tumor were located in the periphery of the tumor, and few could infiltrate into the tumor (Figure S1). The results of immunohistochemical were primarily consistent with those of flow cytometry. CD8$^+$ T cells in the cryoablation group were more than those in the control group on D5-D7 days and infiltrated more into the tumor.

Bulk RNA-seq results indicated that cryoablation could reverse the immunosuppressive environment of distal tumors and enhance the anti-tumor immune

To further study the molecular mechanism of the enhancement of anti-tumor immunity by cryoablation, the mice were sacrificed on the 5th day after cryoablation. Then the contralateral tumors (non-cryoablation tumors) were frozen in liquid nitrogen for 15 min and stored at -80°C, parallel bulk RNA sequencing. D5 day was chosen because there were more CD8$^+$ T cells in the distal tumors and fewer immunosuppressive Treg cells.

Through linear transformation, Principal Components Analysis (PCA) reduces high-dimensional data to two-dimensional or three-dimensional while maintaining the

characteristics of the most significant contribution of variance, reducing data complexity. PCA analysis of the RNA-seq in the cryoablation group (9 samples) and the control group (8 samples) showed no significant clustering between the two groups (Figure 4A). The differentially expressed genes were analyzed by DESeq, and the conditions of the differentially expressed genes were: multiple of expression |log2foldchange| > 1, significant p-value < 0.05 (Table S1). The results revealed that 46 genes were up-regulated, and 42 were down-regulated (Control vs. Cryo) (Figure 4B).

We used topGO for GO enrichment analysis to determine the GO term in which the differentially expressed genes (DEGs) were significantly enriched compared with the whole genome background and to determine the main biological functions of the DEGs (Table S2). Among the DEGs, we found a significant enrichment of biological processes (BP) about the "Oxygen transport," "Response to external stimulus," "Response to stimulus," and the "Neutrophil aggregation"; Cellular component (CC) pertaining to the "Hemoglobin complex related" and the "Extracellular related"; Molecular function pertaining to the "Haptoglobin binding" (Figure 4C). Besides, we use ClusterProfiler for KEGG enrichment analysis (Table S3). Some of the pathways are related to the organismal systems, environmental information processing, and cellular processes, including "IL-17 signaling pathway", "Th1 and Th2 cell differentiation", "Cytokine-cytokine receptor interaction," "TNF signaling pathway," and "Autophagy" so on (Figure 4D).

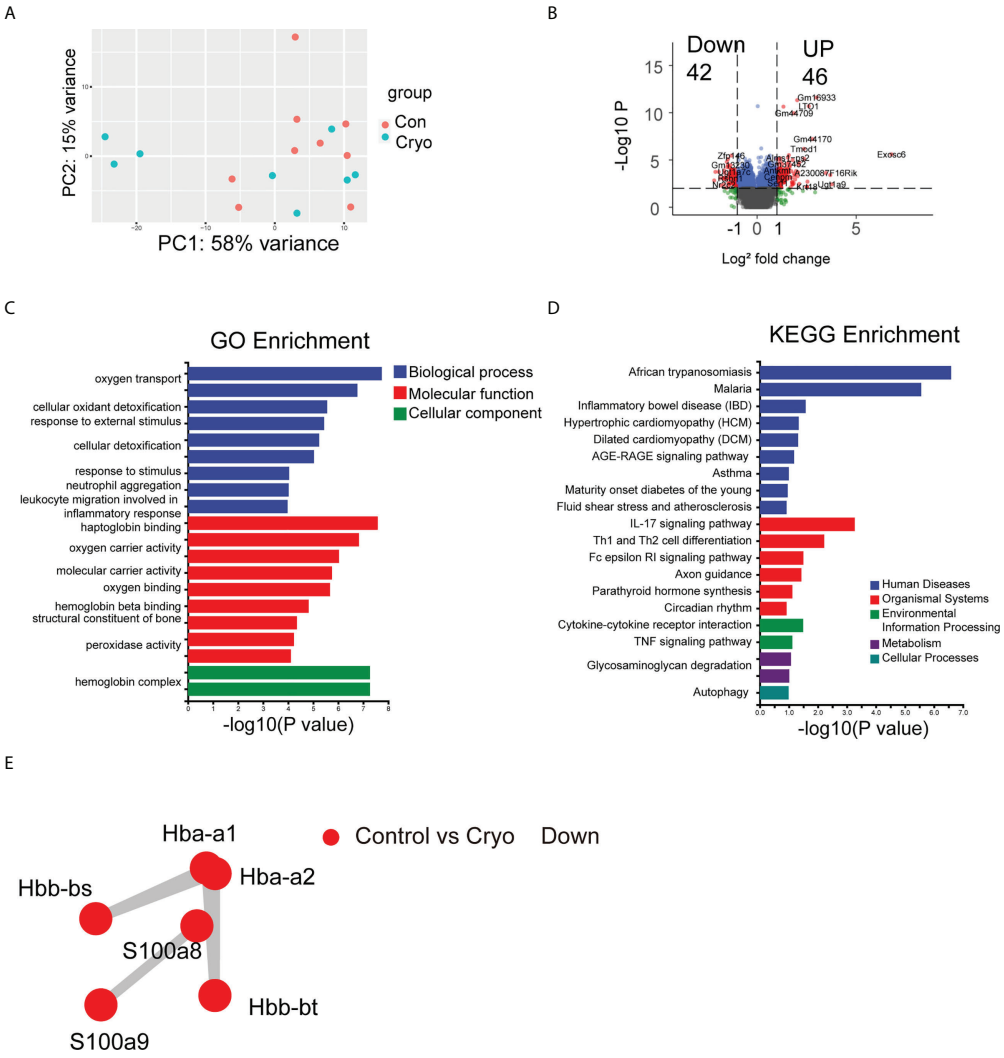

FIGURE 4
The results of bulk RNA-seq. **(A)** PCA analysis of the RNA-seq in the cryoablation group (9 samples) and the control group (8 samples) showed no significant clustering between the two groups; **(B)** The Volcano plot revealed that 42 genes were up-regulated and 42 genes were down-regulated (Control vs Cryo); **(C,D)** GO and KEGG enrichment analysis results; **(E)** The PPI results showed that the major interacting DEGs were Hba-a1, Hba-a2, Hbb-bs, Hbb-bt, S100A8, and S100A9 (Control vs Cryo down-regulated).

Protein-protein interaction network analysis (PPI) is an analysis that reveals the interaction between genes. Analyze the prediction of the interaction relationship of DEGs using the STRING database. The results showed that the significant interacting DEGs were Hba-a1, Hba-a2, Hbb-bs, Hbb-bt, S100A8, and S100A9 (Control vs. Cryo down-regulated) (Figure 4E).

Cryoablation enhanced anti-tumor effect through the lysosome-related pathway

To further analyze the effect of cryoablation on the microenvironment of distant tumors at the protein level, we collected tumor samples from patients with advanced melanoma pre- (3 samples) and post-cryoablation (4 samples).

The cluster analysis results showed significant differences in protein grouping between pre-and post-cryoablation (Figure S2B). The results of differential proteins showed that there were 31 up-regulated proteins and 50 down-regulated proteins (pre- vs. post-cryoablation) (Figure S2A) (Table S4). Further analysis of differential proteins' subcellular localization revealed that 28% were located in the nucleus, 28% in the cytosol, 20% in the plasma membrane, 15% in the mitochondria, and 9% in the extracellular (Figure 5A). The analysis of the domain of differential proteins showed that it was mainly related to "Sorbin and SH3 domain-containing protein," "SoHo domain," "C3HC4 Zinc finger," and "Pleckstrin homology domain," "MHC class II-beta chain-N terminal" and so on (Figure S2C). However, there is no overlap between the differentially expressed proteins of the protein spectrum and the DEGs of the bulk RNA-seq (Figure S2D).

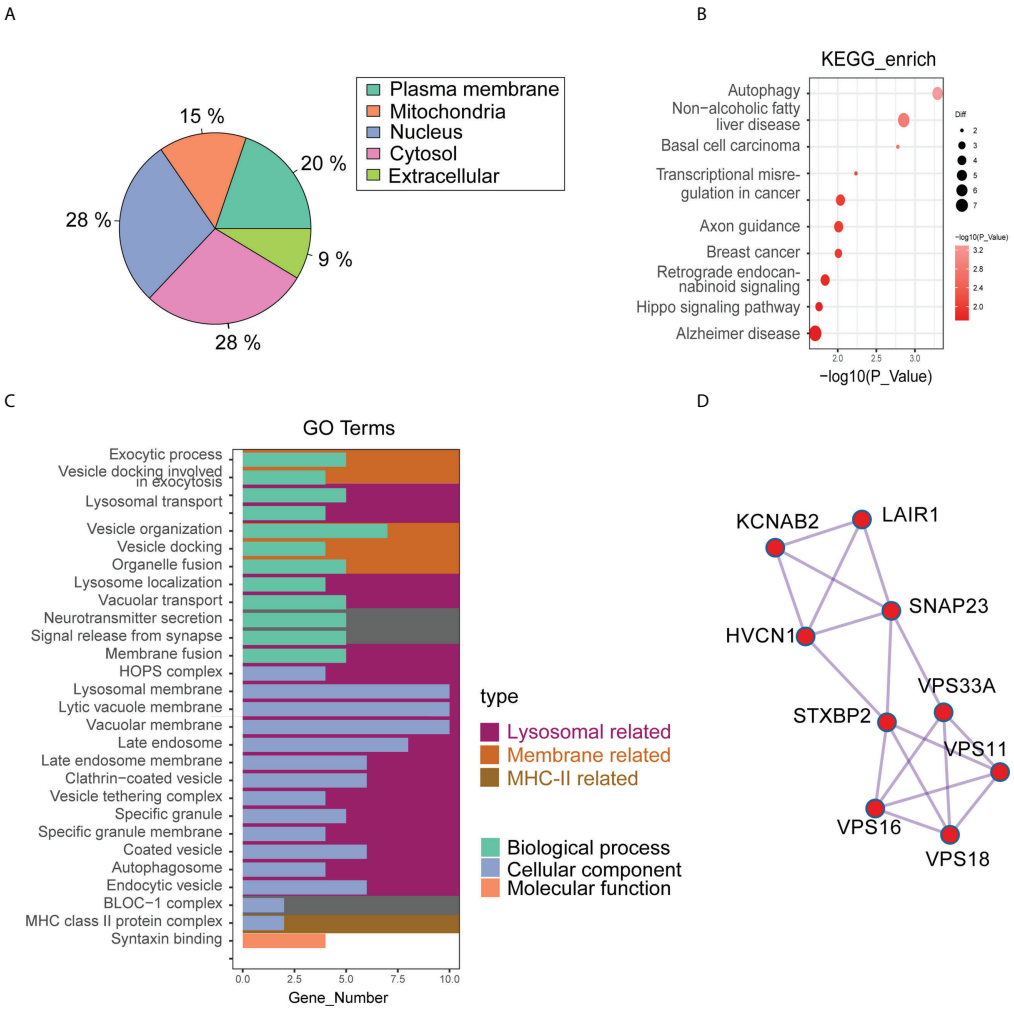

FIGURE 5
The results of quantitative proteomics (4D Label-free) of pre- (3 samples) and post-cryoablation (4 samples). **(A)** The differential proteins' subcellular localization; **(B,C)** GO and KEGG enrichment analysis results; **(D)** The PPI results showed that the major interacting differentially expressed proteins were KCNAB2, LAIR1, HVCN1, SNAP23, STXBP2, VPS33A, VPS11, VPS16, and VPS18.

Among the differential proteins, we found a significant GO enrichment of pathways pertaining to the "lysosomal related," "membrane related," and "MHC-II related" (Figure 5C) (Table S5). Besides, we also found a significant KEGG enrichment of pathways pertaining to autophagy, non-alcoholic fatty liver disease, basal cell carcinoma, Hippo signaling pathway, and so on (Figure 5B) (Table S6). PPI analysis used the STRING database to predict interactions between differential proteins. The results showed that the significant interacting differentially expressed proteins were KCNAB2, LAIR1, HVCN1, SNAP23, STXBP2, VPS33A, VPS11, VPS16, and VPS18 (Figure 5D). Among these proteins, proteins associated with the lysosomal pathway found in GO enrichment analysis were SNAP23, STXBP2, VPS33A, VPS11, and VPS18. Moreover, the expression of SNAP23 and STXBP2 proteins increased significantly in distant tumors post cryoablation (Figures 6A, C).

Further to investigate the relationship between SNAP23 and STXBP2 and patient survival, we further analyzed the pan-cancer data in TCGA. The results showed that high expression of SNAP23 was a protective factor in SKCM (Skin Cutaneous Melanoma) and KIRC (Kidney renal clear cell carcinoma). In contrast, high expression of STXBP2 was a protective factor in BLCA (Bladder Urothelial Carcinoma), SARC (Sarcoma), SKCM, THYM (Thymoma), and CHOL (Cholangiocarcinoma) (Figure S3). High expression of protein SNAP23 (HR: 0.73, 95%CI:0.62-0.85, P=0.00064) (Figure 6B) and STXBP2 (HR: 0.88, 95%CI:0.79-0.99, P=0.016) (Figure 6D) are associated with better prognosis in SKCM.

Moreover, tumor tissue does not simply contain tumor cells. It comprises various types of cells, including stromal cells, fibroblasts cells, immunocytes, etc., which constitute the tumor microenvironment (TME). CIBERSORT is a commonly used method for calculating immune cell infiltration. We analyzed the impact of SNAP23 and STXBP2 genes on the immune microenvironment in SKCM tumors through CIBERSORT (Figure 7C). The results showed that the expression of SNAP23 was positively correlated with the number of M1 cells and negatively correlated with the number of Treg cells (Figure 7A). The expression of STXBP2 was positively correlated with the expression of M1 cells, CD8 cells, and NK-activated cells, but negatively correlated with the expression of M2 cells (Figure 7B).

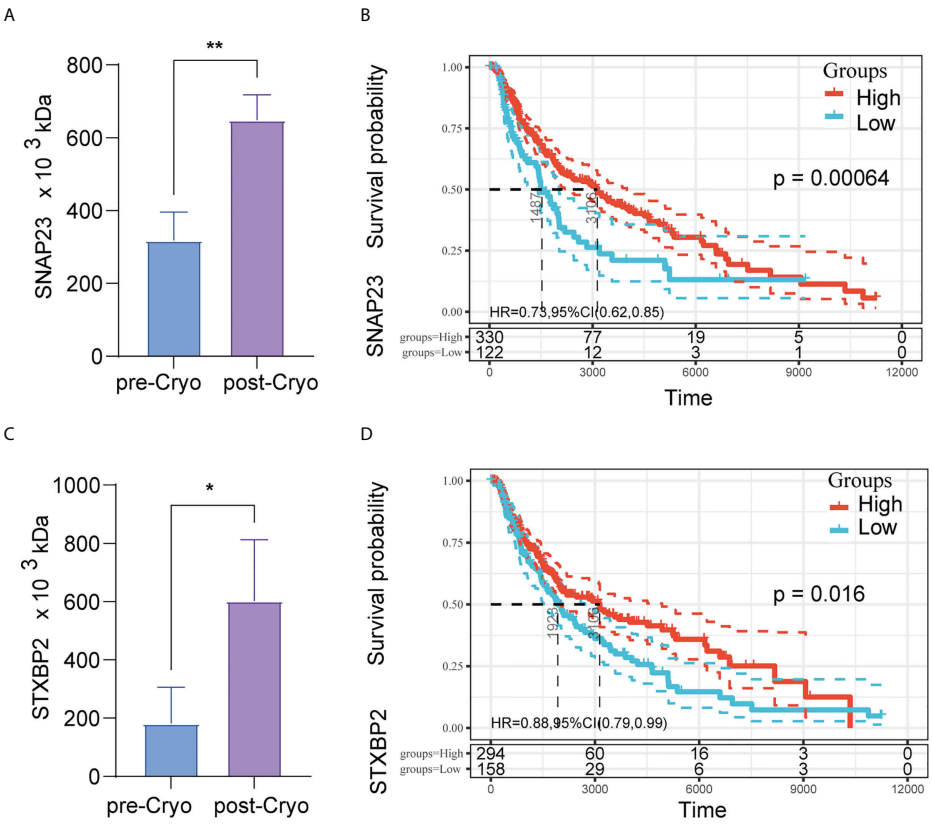

FIGURE 6
The expression of SNAP23 and STXBP2 proteins increased significantly in distant tumors post cryoablation **(A,C)**; High expression of protein SNAP23 (HR: 0.73, 95%CI:0.62-0.85, P=0.00064) **(B)** and STXBP2 (HR: 0.88, 95%CI:0.79-0.99, P=0.016) **(D)** are associated with better prognosis in TCGA-SKCM (N=452).

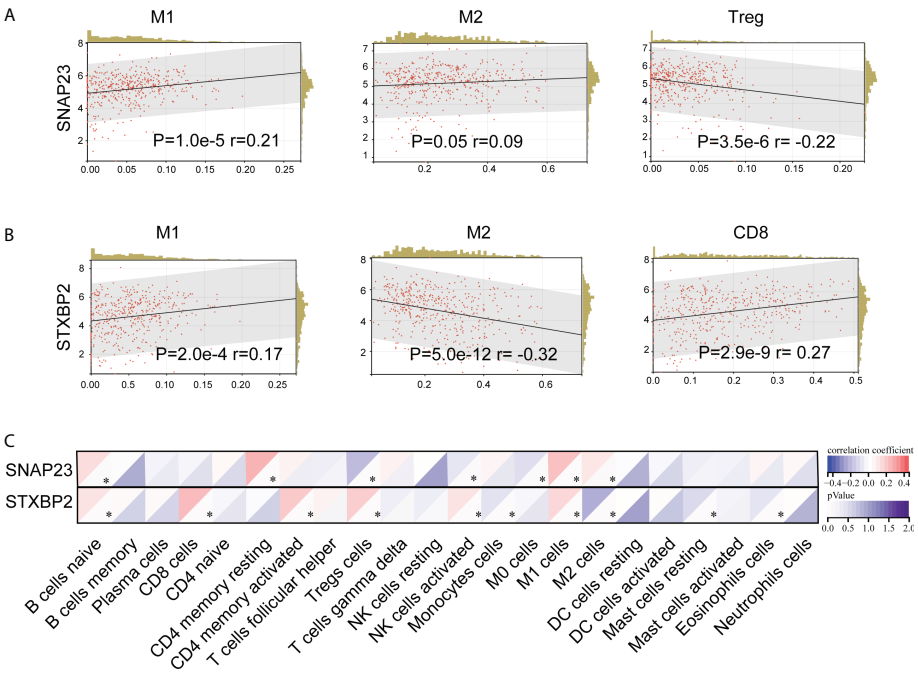

FIGURE 7
CIBERSORT analysis of the effect of SNAP23 **(A)** and STXBP2 **(B)** genes on TCGA-SKCM (N=452) tumor immune microenvironment **(C)**..

Discussion

As one of the local treatments, cryoablation plays an increasingly important role in the comprehensive treatment of malignant tumors with its advantages of less trauma, high reproducibility, and minimally invasive (23). With the development of cryoablation technology, cryoablation has been used to treat various solid tumors, including skin tumors, liver cancer (24), lung cancer (25), breast cancer (26), and other tumors (22, 23, 27, 28).

Since the 1970s, cryoablation has been reported to stimulate humoral immunity and induce the disappearance of metastatic tumors (29, 30). Compared with partial hepatectomy, partial liver cryoablation has been reported to cause a systemic inflammatory response associated with distant organ injury and NF-κb-dependent cytokine overproduction (31–33). Current research suggests that due to the previously shielded tumor antigens being continuously exposed to the immune system, the unique function of ablation provides a therapeutic opportunity for immune stimulation (3). However, the inner mechanism of the enhancement of anti-tumor immunity induced by cryoablation is still unclear. Current studies suggest that tumor antigens, previously blocked, are continuously exposed to the immune system post cryoablation, providing therapeutic opportunities for immune stimulation.

In this study, we applied a multi-omics approach to investigate the effects of local cryoablation on the distal tumor microenvironment. *In vivo*, we demonstrated that cryoablation altered the immune microenvironment of distant tumors, resulting in an increase in immune effector cells and a decrease in immunosuppressive Treg cells, M2 macrophages cells, and thus prolonged mouse survival. A large amount of cell debris and contents were released post cryoablation, so we analyzed the proteomics of the samples pre- and post-cryoablation. The results revealed that the lysosome- and MHC-II-related pathways were activated after cryopreservation, and the expression of SNAP23 and STXBP2 increased significantly after cryopreservation. Further analysis of TCGA pan-cancer data revealed that both SNAP23 and STXBP2 overexpression were associated with a better prognosis of SKCM. Moreover, the analysis of the tumor microenvironment of SKCM in TCGA showed that the expression of SNAP23 was positively correlated with the number of immunes enhancing M1 cells while negatively correlated with the number of immunosuppressive immune Treg cells. The expression of STXBP2 was positively correlated with the number of immune-enhancing M1 and CD8 cells while negatively correlated with the number of immunosuppressive immune M2 cells.

Gazzaniga, S et al. found that extensive edema and proliferation of fibroblasts first appeared in the tumor ablation region post-cryoablation, followed by collagen accumulation.

During this period, a large number of neutrophil cells began to accumulate around the tumor post-cryoablation at 1-3 days, and a large number of macrophages at 3-7 days, and then both gradually decreased (34). The reaction in and around the tumor was intense for about seven days and then gradually reduced to about two weeks. During this period, many tumors interact with immune cells and may affect the microenvironment of distant tumors (34). In this study, we found an increase in immune effector cells and a decrease in immunosuppressive Treg cells in distant tumors post-cryoablation. Since the effect did not last long and only about a week, it did not control the tumor volume immediately, but it significantly prolonged the survival of the mice. In the analysis of the immune microenvironment of Bulk RNA-seq, it was also found that cryoablation could change the immune microenvironment of distant tumors, increase effector cells and decrease immunosuppressive cells. Activation of response to stimulus, neutrophil aggregation, IL-17 signaling, and TNF signaling pathway post-cryoablation may be the reason for changes in the distal tumors' immune microenvironment.

S100A8/A9 protein belongs to the Ca2 + combined with the S100 protein family (35). S100A8/A9 is mainly secreted from activated neutrophils and monocytes. Moreover, S100A8/A9 is important in regulating the inflammatory process by stimulating leukocyte aggregation and inducing cytokine secretion (36–38). In this study, S100A8/A9 was significantly enriched post-cryoablation in PPI analysis. This indicated that cryoablation promotes inflammation in distant tumors, leading to enhanced anti-tumor immunity.

Cryoablation destroys the tumor cell membrane at a low temperature and releases a large number of cell structures and cell contents, which can well maintain the original structure of cell contents and expose to a large number of effective tumor antigens (39). Previous studies reported that cell contents released by cryoablation contain "danger signals" such as pro-inflammatory cytokine, heat shock protein, DNA, and RNA recognized by toll-like receptors, which activate the natural immune response (1, 13, 40). Further analysis of the changes in protein in distant tumors pre- and post-cryoablation revealed that the significant activation pathways were the lysosomal-related, membrane-related, and MHC-II-related pathways. Therefore, it is demonstrated that cryoablation could induce the release of tumor-associated antigens and activate the anti-tumor immune function of distal tumors.

Synaptosome associated protein 23 (SNAP23) is an essential component of membrane insertion machinery (41). Its related pathways are "Class I MHC mediated antigen processing and presentation" and "Vesicle-mediated transport." SNAP23 and its partner SNAREs mediate the fusion of the plasma membrane with intracellular organelles or vesicles to form phagosomes, as well as the fusion of phagosomes with endosomes or lysosomes to induce phagosome maturation, characterized by reactive oxygen species production and acidification (42). Syntaxin binding protein 2 (STXBP2) is involved in intracellular trafficking, control of SNARE (soluble NSF attachment protein receptor) complex assembly, and the release of cytotoxic granules by natural killer cells (43–45). In this study, we found that SNPA23 and STXBP2 expression increased post-cryoablation significantly.

Further analysis of TCGA data showed that both SNAP23 and STXBP2 were positively correlated with the number of SKCM immune effector cells but negatively correlated with the number of immunosuppressive cells. Furthermore, high expression of SNAP23 and STXBP2 was associated with a better prognosis of SKCM. Notch1 (Notch Receptor 1) is critical in modulating melanoma tumor cell growth and survival (46). Besides, Notch1 inhibition improves tumor responses to immune checkpoint inhibitors. Notch1 contributes to an immune-suppressive tumor microenvironment by inhibiting the expression of SNAP23 and overexpression of IL-6, IL-8, and CCL5 downstream of the pathway, thus affecting the efficacy of immune-checkpoint inhibitors (47). This provides a possible internal mechanism for the expression of SNAP23 to increase post-cryoablation, change the immune microenvironment in distant tumors, and improve prognosis.

In summary, this study applied a multi-omics approach to investigate the effects of local cryoablation on the distal tumor microenvironment. Those results proved that large amounts of tumor antigens are released post-cryoablation, leading to a sterile inflammatory response in distant tumors. During this period, lysosome-related pathways are activated, resulting in overexpression of SNAP23 and STXBP2, activation of immune effector cells, suppression of the release of immunosuppressive factors, and finally, enhancement of anti-tumor immunity.

Despite the great potential of immune-checkpoint inhibitors, many cancer patients still do not respond well to treatment (The efficacy of the single drug is only 20-40%), mainly due to the lack of tumor antigens, lymphocytes, and immunosuppressive tumor microenvironment (48). Combined with immune-checkpoint inhibitors, cryoablation can release many original, undenatured tumor-associated antigens, producing a more potent anti-tumor immune effect (3, 8, 49). In our previous studies, it has been demonstrated that cryoablation combined with Pembrolizumab (CATAP) could significantly improve the objective response rate in patients with liver metastases from melanoma with minimal side effects (22). Even one patient with diffuse liver metastasis achieved complete remission (CR). At the same time, cryoablation combined with the immune adjuvant, cell therapy, immune-checkpoint inhibitors, and other treatment methods is also being explored.

Data availability statement

The data presented in the study are deposited in the NCBI, GEO DataSets repository, accession number GSE201590.

Ethics statement

The studies involving human participants were reviewed and approved by Sun Yat-sen University Cancer Center (SYSUCC). The patients/participants provided their written informed consent to participate in this study. The animal study was reviewed and approved by Sun Yat-sen University Cancer Center (SYSUCC).

Author contributions

YW, CF, TH, DZ, HQ, and HT performed experiments. WF and LS planned the study and analyzed the data. YW and SC wrote the manuscript. All authors contributed to, read, and approved the final manuscript.

Funding

This work was funded by the Guangdong Provincial Key R&D Programme. Grant number: 2019B110233001.

Conflict of interest

The authors declare that the research was conducted in the absence of any commercial or financial relationships that could be construed as a potential conflict of interest.

Publisher's note

Supplementary material

The Supplementary Material for this article can be found online at: https://www.frontiersin.org/articles/10.3389/fimmu.2022.930461/full#supplementary-material

SUPPLEMENTARY FIGURE 1
The immunohistochemical results showed that most of the immune cells in the distant tumor were located in the periphery of the tumor and few could infiltrate into the tumor. Red arrow: CD8+ T cells in the cryoablation group were more than those in the control group on D5-D7 days and infiltrated more into the tumor.

SUPPLEMENTARY FIGURE 2
(A) The results of differential proteins showed that there were 31 up-regulated proteins and 50 down-regulated proteins (pre- vs. post-cryoablation); **(B)** The cluster analysis results showed significant differences in protein grouping between pre-and post-cryoablation; **(C)** The analysis results of the domain of differential proteins; **(D)** There is no overlap between the differentially expressed proteins of the protein spectrum and the DEGs of the bulk RNA-seq.

References

1. Sabel MS. Cryo-immunology: a review of the literature and proposed mechanisms for stimulatory versus suppressive immune responses. *Cryobiology* (2009) 58:1–11. doi: 10.1016/j.cryobiol.2008.10.126

2. Liu Y, Huang T, Shen L, Wu Y, Chen S, Fan W. Research progress on anti-tumor immune effect of cryoablation. *Chin J Acad Radiol* (2022) 5:74–81. doi: 10.1007/s42058-022-00092-8

3. Chu KF, Dupuy DE. Thermal ablation of tumours: Biological mechanisms and advances in therapy. *Nat Rev Cancer* (2014) 14:199–208. doi: 10.1038/nrc3672

4. Sidana A. Cancer immunotherapy using tumor cryoablation. *Immunotherapy* (2014) 6:85–93. doi: 10.2217/imt.13.151

5. Sabel MS, Nehs MA, Su G, Lowler KP, Ferrara JLM, Chang AE. Immunologic response to cryoablation of breast cancer. *Breast Cancer Res Treat* (2005) 90:97–104. doi: 10.1007/s10549-004-3289-1

6. Xu H, Wang Q, Lin C, Yin Z, He X, Pan J, et al. Synergism between cryoablation and GM-CSF: enhanced immune function of splenic dendritic cells in mice with glioma. *Neuroreport* (2015) 26:346–53. doi: 10.1097/WNR.0000000000000351

7. Baust JG, Gage AA, Bjerklund Johansen TE, Baust JM. Mechanisms of cryoablation: clinical consequences on malignant tumors. *Cryobiology* (2014) 68:1–11. doi: 10.1016/j.cryobiol.2013.11.001

8. Yakkala C, Denys A, Kandalaft L, Duran R. Cryoablation and immunotherapy of cancer. *Curr Opin Biotechnol* (2020) 65:60–4. doi: 10.1016/j.copbio.2020.01.006

9. Soanes WA, Ablin RJ, Gonder MJ. Remission of metastatic lesions following cryosurgery in prostatic cancer: immunologic considerations. *J Urol* (1970) 104:154–9. doi: 10.1016/s0022-5347(17)61690-2

10. Alblin RJ, Soanes WA, Gonder MJ. Prospects for cryo-immunotherapy in cases of metastasizing carcinoma of the prostate. *Cryobiology* (1971) 8:271–9. doi: 10.1016/0011-2240(71)90050-2

11. den Brok MHMGM, Sutmuller RPM, Nierkens S, Bennink EJ, Toonen LWJ, Figdor CG, et al. Synergy between *in situ* cryoablation and TLR9 stimulation results in a highly effective *in vivo* dendritic cell vaccine. *Cancer Res* (2006) 66:7285–92. doi: 10.1158/0008-5472.CAN-06-0206

12. Peng P, Hu H, Liu P, Xu LX. Neoantigen-specific CD4 T-cell response is critical for the therapeutic efficacy of cryo-thermal therapy. *J Immunother Cancer* (2020) 8:e000421. doi: 10.1136/jitc-2019-000421

13. Škoberne M, Beignon AS, Bhardwaj N. Danger signals: A time and space continuum. *Trends Mol Med* (2004) 10:251–7. doi: 10.1016/j.molmed.2004.04.001

14. Zhu J, Zhang Y, Zhang A, He K, Liu P, Xu LX. Cryo-thermal therapy elicits potent anti-tumor immunity by inducing extracellular Hsp70-dependent MDSC differentiation. *Sci Rep* (2016) 6:27136. doi: 10.1038/srep27136

15. Yakkala C, Chiang CLL, Kandalaft L, Denys A, Duran R. Cryoablation and immunotherapy: An enthralling synergy to confront the tumors. *Front Immunol* (2019) 10:2283. doi: 10.3389/fimmu.2019.02283

16. Campbell MT, Matin SF, Tam AL, Sheth RA, Ahrar K, Tidwell RS, et al. Pilot study of tremelimumab with and without cryoablation in patients with metastatic renal cell carcinoma. *Nat Commun* (2021) 12:6375. doi: 10.1038/s41467-021-26415-4

17. Kwak K, Yu B, Lewandowski RJ, Kim D-H. Recent progress in cryoablation cancer therapy and nanoparticles mediated cryoablation. *Theranostics* (2022) 12:2175–204. doi: 10.7150/thno.67530

18. Wang K, Wang C, Jiang H, Zhang Y, Lin W, Mo J, et al. Combination of ablation and immunotherapy for hepatocellular carcinoma: Where we are and where to go. *Front Immunol* (2021) 12:792781. doi: 10.3389/fimmu.2021.792781

19. Li X, Xu J, Gu X, Chen L, Wu Q, Li H, et al. Case report: Antiangiogenic therapy plus immune checkpoint inhibitors combined with intratumoral cryoablation for hepatocellular carcinoma. *Front Immunol* (2021) 12:740790. doi: 10.3389/fimmu.2021.740790

20. Ho AY, Tabrizi S, Dunn SA, McArthur HL. Current advances in immune checkpoint inhibitor combinations with radiation therapy or cryotherapy for breast cancer. *Breast Cancer Res Treat* (2022) 191:229–41. doi: 10.1007/s10549-021-06408-z

21. Doshi A, Zhou M, Bui N, Wang DS, Ganjoo K, Hwang GL. Safety and feasibility of cryoablation during immunotherapy in patients with metastatic soft tissue sarcoma. *J Vasc Interv Radiol* (2021) 32:1688–94. doi: 10.1016/j.jvir.2021.08.017

22. Shen L, Qi H, Chen S, Cao F, Xie L, Wu Y, et al. Cryoablation combined with transarterial infusion of pembrolizumab (CATAP) for liver metastases of melanoma: an ambispective, proof-of-concept cohort study. *Cancer Immunol Immunother* (2020) 69:1713–24. doi: 10.1007/s00262-020-02566-z

23. Kongnyuy M, Halpern DM, Kosinski KE, Katz AE. Cryosurgery, an alternative treatment option for organ-confined prostate cancer: current beliefs and practice patterns of urologists. *Int Urol Nephrol* (2017) 49:43–8. doi: 10.1007/s11255-016-1440-7

24. Shi J, Li Y, Liang S, Zeng J, Liu G, Mu F, et al. Circulating tumour cells as biomarkers for evaluating cryosurgery on unresectable hepatocellular carcinoma. *Oncol Rep* (2016) 36:1845–51. doi: 10.3892/or.2016.5050

25. Kumar A, Kumar S, Katiyar VK, Telles S. Phase change heat transfer during cryosurgery of lung cancer using hyperbolic heat conduction model. *Comput Biol Med* (2017) 84:20–9. doi: 10.1016/j.compbiomed.2017.03.009

26. Pusceddu C, Paliogiannis P, Nigri G, Fancellu A. Cryoablation in the management of breast cancer: Evidence to date. *Breast Cancer (Dove Med Press* (2019) 11:283–92. doi: 10.2147/BCTT.S197406

27. Breen DJ, King AJ, Patel N, Lockyer R, Hayes M. Image-guided cryoablation for sporadic renal cell carcinoma: Three- and 5-year outcomes in 220 patients with biopsy-proven renal cell carcinoma. *Radiology* (2018) 289:554–61. doi: 10.1148/radiol.2018180249

28. Xing M, Kokabi N, Zhang D, Ludwig JM, Kim HS. Comparative effectiveness of thermal ablation, surgical resection, and active surveillance for T1a renal cell carcinoma: A surveillance, epidemiology, and end results (SEER)-medicare-linked population study. *Radiology* (2018) 288:81–90. doi: 10.1148/radiol.2018171407

29. Gursel E, Roberts M, Veenema RJ. Regression of prostatic cancer following sequential cryotherapy to the prostate. *J Urol* (1972) 108:928–32. doi: 10.1016/s0022-5347(17)60909-1

30. Ablin RJ. Cryoimmunotherapy. *Br Med J* (1972) 3:476. doi: 10.1136/bmj.3.5824.476

31. Chapman WC, Debelak JP, Wright Pinson C, Washington MK, Atkinson JB, Venkatakrishnan A, et al. Hepatic cryoablation, but not radiofrequency ablation, results in lung inflammation. *Ann Surg* (2000) 231:752–61. doi: 10.1097/00000658-200005000-00016

32. Chapman WC, Debelak JP, Blackwell TS, Gainer KA, Christman JW, Pinson CW, et al. Hepatic cryoablation-induced acute lung injury: pulmonary hemodynamic and permeability effects in a sheep model. *Arch Surg* (2000) 135:663–7. doi: 10.1001/archsurg.135.6.667

33. Washington K, Debelak JP, Gobbell C, Sztipanovits DR, Shyr Y, Olson S, et al. Hepatic cryoablation-induced acute lung injury: histopathologic findings. *J Surg Res* (2001) 95:1–7. doi: 10.1006/jsre.2000.5976

34. Gazzaniga S, Bravo A, Goldszmid SR, Maschi F, Martinelli J, Mordoh J, et al. Inflammatory changes after cryosurgery-induced necrosis in human melanoma xenografted in nude mice. *J Invest Dermatol* (2001) 116:664–71. doi: 10.1046/j.0022-202x.2001.01313.x

35. Pruenster M, Vogl T, Roth J, Sperandio M. S100A8/A9: From basic science to clinical application. *Pharmacol Ther* (2016) 167:120–31. doi: 10.1016/j.pharmthera.2016.07.015

36. Raju MS, Jahnavi V, Kamaraju RS, Sritharan V, Rajkumar K, Natarajan S, et al. Continuous evaluation of changes in the serum proteome from early to late stages of sepsis caused by klebsiella pneumoniae. *Mol Med Rep* (2016) 13:4835–44. doi: 10.3892/mmr.2016.5112

37. De Jong HK, Achouiti A, Koh GCKW, Parry CM, Baker S, Faiz MA, et al. Expression and function of S100A8/A9 (calprotectin) in human typhoid fever and the murine salmonella model. *PLoS Negl Trop Dis* (2015) 9:e0003663. doi: 10.1371/journal.pntd.0003663

38. Tsai S-Y, Segovia JA, Chang T-H, Morris IR, Berton MT, Tessier PA, et al. DAMP molecule S100A9 acts as a molecular pattern to enhance inflammation during influenza a virus infection: role of DDX21-TRIF-TLR4-MyD88 pathway. *PLoS Pathog* (2014) 10:e1003848. doi: 10.1371/journal.ppat.1003848

39. Shao Q, O'Flanagan S, Lam T, Roy P, Pelaez F, Burbach BJ, et al. Engineering T cell response to cancer antigens by choice of focal therapeutic conditions. *Int J Hyperth* (2019) 36:130–8. doi: 10.1080/02656736.2018.1539253

40. Matzinger P. Tolerance, danger, and the extended family. *Annu Rev Immunol* (1994) 12:991–1045. doi: 10.1146/annurev.iy.12.040194.005015

41. Asraf H, Bogdanovic M, Gottesman N, Sekler I, Aizenman E, Hershfinkel M. SNAP23 regulates KCC2 membrane insertion and activity following mZnR/GPR39 activation in hippocampalneurons. *iScience* (2022) 25:103751. doi: 10.1016/j.isci.2022.103751

42. Hatsuzawa K, Sakurai C. Regulatory mechanism of SNAP23 in phagosome formation and maturation. *Yonago Acta Med* (2020) 63:135–45. doi: 10.33160/yam.2020.08.001

43. Côte M, Ménager MM, Burgess A, Mahlaoui N, Picard C, Schaffner C, et al. Munc18-2 deficiency causes familial hemophagocytic lymphohistiocytosis type 5 and impairs cytotoxic granule exocytosis in patient NK cells. *J Clin Invest* (2009) 119:3765–73. doi: 10.1172/JCI40732

44. Lopez JA, Noori T, Minson A, Jovanoska LL, Thia K, Hildebrand MS, et al. Bi-allelic mutations in STXBP2 reveal a complementary role for STXBP1 in cytotoxic lymphocyte killing. *Front Immunol* (2018) 9:529. doi: 10.3389/fimmu.2018.00529

45. Spessott WA, Sanmillan ML, McCormick ME, Patel N, Villanueva J, Zhang K, et al. Hemophagocytic lymphohistiocytosis caused by dominant-negative mutations in STXBP2 that inhibit SNARE-mediated membrane fusion. *Blood* (2015) 125:1566–77. doi: 10.1182/blood-2014-11-610816

46. Wieland E, Rodriguez-Vita J, Liebler SS, Mogler C, Moll I, Herberich SE, et al. Endothelial Notch1 activity facilitates metastasis. *Cancer Cell* (2017) 31:355–67. doi: 10.1016/j.ccell.2017.01.007

47. Qiu H, Zmina PM, Huang AY, Askew D, Bedogni B. Inhibiting Notch1 enhances immunotherapy efficacy in melanoma by preventing Notch1 dependent immune suppressive properties. *Cancer Lett* (2018) 434:144–51. doi: 10.1016/j.canlet.2018.07.024

48. Gravante G, Sconocchia G, Ong SL, Dennison AR, Lloyd DM. Immunoregulatory effects of liver ablation therapies for the treatment of primary and metastatic liver malignancies. *Liver Int Off J Int Assoc Study Liver* (2009) 29:18–24. doi: 10.1111/j.1478-3231.2008.01915.x

49. He X-Z, Wang Q-F, Han S, Wang H-Q, Ye Y-Y, Zhu Z-Y, et al. Cryoablation improves anti-tumor immunity through recovering tumor educated dendritic cells in tumor-draining lymph nodes. *Drug Des Devel Ther* (2015) 9:1449–58. doi: 10.2147/DDDT.S76592

frontiers | Frontiers in Immunology

TYPE Review
PUBLISHED 02 September 2022
DOI 10.3389/fimmu.2022.972345

OPEN ACCESS

EDITED BY
Xuyao Zhang,
Fudan University, China

REVIEWED BY
Xin Han,
Zhejiang University, China
Qiuju Han,
Shanghai Jiao Tong University, China

*CORRESPONDENCE
Nan Lu
nan.lu@ntu.edu.sg
Xiang-Qian Jia
2021108@hlju.edu.cn
Zhang-Suo Liu
zhangsuoliu@zzu.edu.cn

SPECIALTY SECTION
This article was submitted to Cancer Immunity and Immunotherapy, a section of the journal Frontiers in Immunology

RECEIVED 18 June 2022
ACCEPTED 18 August 2022
PUBLISHED 02 September 2022

CITATION
Huo J-L, Fu W-J, Liu Z-H, Lu N, Jia X-Q and Liu Z-S (2022) Research Advance of Natural Products in Tumor Immunotherapy.
Front. Immunol. 13:972345.
doi: 10.3389/fimmu.2022.972345

Research advance of natural products in tumor immunotherapy

Jin-Ling Huo[1], Wen-Jia Fu[1], Zheng-Han Liu[2,3], Nan Lu[4]*, Xiang-Qian Jia[2,3]* and Zhang-Suo Liu[1]*

[1]Department of Integrated Traditional and Western Nephrology, the First Affiliated Hospital of Zhengzhou University, Research Institute of Nephrology, Zhengzhou University, Henan Province Research Center For Kidney Disease, Key Laboratory of Precision Diagnosis and Treatment for Chronic Kidney Disease in Henan Province, Zhengzhou, China, [2]Engineering Research Center of Agricultural Microbiology Technology, Ministry of Education, Heilongjiang University, Harbin, China, [3]Heilongjiang Provincial Key Laboratory of Ecological Restoration and Resource Utilization for Cold Region, School of Life Sciences, Heilongjiang University, Harbin, China, [4]School of Mechanical and Aerospace Engineering, Nanyang Technological University, Singapore, Singapore

Cancer immunotherapy has emerged as a novel anti-tumor treatment. Despite significant breakthroughs, cancer immunotherapy remains focused on several types of tumors that are sensitive to the immune system. Therefore, effective strategies to expand its indications and improve its efficacy become key factors for the further development of cancer immunotherapy. In recent decades, the anticancer activities of natural products are reported to have this effect on cancer immunotherapy. And the mechanism is largely attributed to the remodeling of the tumor immunosuppressive microenvironment. The compelling data highlight that natural products offer an alternative method option to improve immune function in the tumor microenvironment (TME). Currently, more attention is being paid to the discovery of new potential modulators of tumor immunotherapy from natural products. In this review, we describe current advances in employing natural products and natural small-molecule drugs targeting immune cells to avoid tumor immune escape, which may bring some insight for guiding tumor treatment.

KEYWORDS

tumor immunotherapy, immune cells, natural products, active chemicals, tumor microenvironment

Introduction

The immune system is a sophisticated integrated network consisted of various immune cells, organs, and soluble mediators that developed to protect the biosome against outside assault which threatens the integrity of biosome (1). The immune system's critical role in host defense is best seen when things go wrong; underactivity

leads to severe infections and tumors, while abnormal activity leads to allergy and autoimmune illnesses, especially tumor escape. Immune cells are an important part of the immune system, including lymphocytes, dendritic cells (DCs), monocytes/macrophages, natural killer (NK) cells, and so on (2). It is now clear that in addition to cancer cells, the tumor microenvironment (TME) contains a repertoire of endothelial cells, stromal cells and immune cells (3). In contrast to traditional chemotherapy, immunotherapy focuses on the specific recognition and attack of cancer cells using immune cells inside and outside of TME (4). Thus, immunotherapy approaches are theoretically shown to have higher specificity and lower side effects.

Cancer immunotherapy is defined that regulates immunological response through activating the organism's immune defense system to suppress and prevent tumor growth (5). Now, a variety of cancer vaccines, immune-checkpoint inhibitors and adoptive immune-cell immunotherapies for anti-cancer treatments are approved by the US Food and Drug Administration (FDA) (6–8). Despite significant breakthroughs, cancer immunotherapy remains focused on several types of tumors that are sensitive to the immune system. The main reason for this limitation is the immunosuppressive microenvironment within the tumor site, which effectively blunts cancer immunotherapy (9). Therefore, effective strategies that can reverse and reshape the complex immunosuppressive microenvironment within tumors are a key factor in expanding the indications for cancer immunotherapy.

Natural products used to treat human diseases can date back over 3000 years and contain several active components found in medicinal plants. Furthermore, mangy natural products were verified and documented in several publications in ancient China. Numerous studies currently have demonstrated that natural products play an important role in the development of new anti-cancer drugs and lead compounds due to their wide range of sources, low cost, structural diversity, diverse biological activities and low adverse effects (10, 11). Several well-known natural products, including polysaccharides (e.g., astragalus polysaccharides, shiitake polysaccharides), alkaloids (e.g., matrine, berberine), saponins (e.g., ginsenoside, total saponin of acanthopanax bark), flavonoids (e.g., baicalin, apigenin), and terpenoids (e.g., artemisinin, paclitaxel) have potential anti-tumor immunomodulatory effects (12) (Table 1). In addition, natural products have achieved great success in effectively expanding the indications and improving the efficacy of various types of cancer immunotherapy, such as immune checkpoint inhibitors, cancer vaccines, and adoptive immune cell transfer therapy (13–15). In this paper, we describe the immunomodulatory effects of natural products, as well as the underlying processes of the immune response activation in TME (16–18).

TABLE 1 Representative natural products with immuno-tumor therapeutic effects.

Category	Natural product	Source	Mechanism
Polysaccharides	Ascophyllan	Ascophyllum nodosum	Increasing MHC I, MHC II and pro-inflammatory levels of cytokines; ultimately inducing activation of DCs and antigen-specific immune responses
	Ganodema polysaccharides	Ganodema	Down-regulate the expression of PD-1 and PD-L1 through STAT3 pathway
	CMPB90-1	Cordyceps militaris	Down-regulate the expression of PD-L1 through NF-kB pathway
	Fucoidan	Ascophyllum nodosum	Promotes the growth of human peripheral blood DC
Alkaloids	Chloroquine	Cinchona bar	Increasing the lysosomal pH of TAM, mediating Ca2+ release and activating TFEB
	Tryptanthrin-5c	Polygonum tinctorium and Isatis tinctoria	nhibits the activity of IDO and treg accumulation
	5-Br-brassinin	Cruciferous sp.	Inhibiting the activity of IDO1 and mediating tumor regression when combined with chemotherapeutic drugs in MMTV-Neu mice
Saponins	QS-21	Quillaja saponaria Molin	Enhance the anti-cancer effect of cancer vaccines
	Sapogenin	Panax ginseng	Down-regulation of PD-1 and PD-L1 expression through the STAT3 pathway
	Diosgenin	Acacia concinna	Enhancing the anti-cancer effects of anti-PD-1 antibodies
Flavonoids	Hesperidin	Orange peel	Downregulation of PD-L1 expression *via* NF-kB pathway
	Baicalein	Scutellaria	Downregulation of PD-L1 expression *via* JAKSTAT pathway
	Procyanidin	Fruits	Enhancing the anti-cancer effects of cancer peptide vaccines
Terpenoids	Artemisinin	Artemisia annua	Inhibiting the proliferation of MDSCs and Tregs, and promoting the proliferation of CD4 + T and CD8 + T cells
	Ginsenoside Rk1	Black ginseng	Downregulation of PD-L1 by inhibiting NF-κB signaling
	Ingenol-3,20-dibenzoate	Euphorbia esula L	Activating PKC, promoting IFN-γ secretion and degranulation, and ultimately increasing NK cell cytotoxicity

Immune modulation of natural products to immune cells

In general, the immune cells that have an effect on tumors can be divided into two types: tumor-promoting and tumor-antagonizing immune cells. These two types of cells play various roles at different stages of tumor progression (3, 19). The tumor-antagonizing immune cells mainly consist of NK cells, effector T cells (including effector CD4+ T cells and CD8+ cytotoxic T cells), M1-polarized macrophages and DCs. Except for the tumor-antagonizing immune cells, there are a plenty of tumor-promoting immune cells mainly consisting of regulatory T cells (Tregs) (4) (Figure 1). Natural products can activate specific intrinsic immune cells to kill tumor cells by enhancing antigen presentation or cellular immune processes. They can also inhibit the formation of blood vessels in the TME and the metastasis of tumors by suppressing certain intrinsic immune cells (Figure 2).

Effects of natural products on monocytes and macrophages

Monocytes/macrophages are derived from bone marrow stem cells, which can enter the bloodstream and be distributed in various organ tissues after developing into monocytes.

In the process of participating in innate immunity, monocytes/macrophages can identify pathogen-associated molecular patterns (PAMP) and play an important role in innate immunity. On the other hand, monocytes/macrophages also can mediate and promote inflammatory responses and implement immunity killing, and antigen presentation (20, 21). Tumor associated macrophages (TAM) are traditionally classified into two kinds, termed as polarization: the immunosuppressive/anabolic M2 phenotype and the classical inflammatory M1 phenotype. M1 macrophages are the main effector cells for host destruction of pathogens and M2 macrophages have anti-inflammatory and angiogenic functions in tumors (22, 23). M1 can produce pro-inflammatory cytokines and reactive oxygen/nitrogen species, which are essential for host defense and tumor cell killing and are therefore considered to be 'good' macrophages (24).

Natural products can inhibit the M2-like polarization of TAM and block tumor growth and migration. Emodin attenuated tumor growth by inhibiting IRF4, STAT6, and C/EBPβ signaling and M2-like polarization (25). Astragalus has been demonstrated to have anti-inflammatory and anti-fibrotic properties. Astragalus can inhibit the aggregation and activation of monocytes/macrophages, and reduce the production of TGF-β1 at the peritoneal site (26). Phenylpropanoid is the main active ingredient in ginger, which can directly inhibit cytoplasmic phospholipase 2 (cPLA2) and IL-1β in macrophage expression (27). Inonotus sanghuang, a medicinal plant rich in quercetin, isorhamnetin, quercitrin, rutin and chlorogenic acid, has been demonstrated to decrease inflammation *via* altering the interaction of macrophages and fat cells. It has been proposed that doing so may improve insulin resistance and the metabolic syndrome (28). Additionally, Garlic water-soluble extract has been shown to elevate intracellular thiol and glutathione concentrations in human primary monocytes. These results suggest that the extract of Garlic can regulate the differentiation of monocytes into macrophages, thereby playing a protective role (29). Macrophages are critical players in the development of nonalcoholic steatohepatitis (NASH) and hepatocarcinoma.

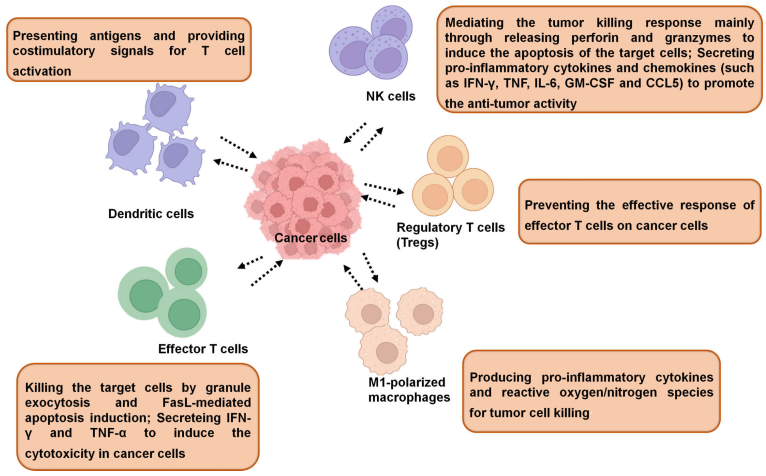

FIGURE 1
The immune cells in TME. The tumor-associated immune cells can be divided into two types: tumor-antagonizing and tumor-promoting immune cells.

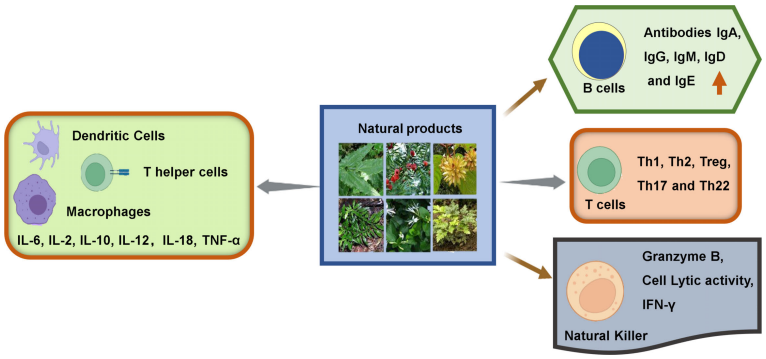

FIGURE 2
Immunomodulatory effects of natural products on immune cells within TME.

Natural products have crucial roles in modulating macrophage activation, recruitment, and polarization, making them promising treatment possibilities for hepatocarcinoma (Figure 3) (30). Angiogenesis in the tumor microenvironment not only nourishes tumor cells and promotes their growth, but is also closely associated with tumor metastasis. Lentinan is a bioactive compound extracted from Lentinus edodes, which promotes the expression of the angiogenesis inhibitory factor IFN-γ, thereby inhibiting tumor angiogenesis (31).

Effects of natural products on dendritic cells

DCs are the most powerful antigen-presenting cells, acting to condition the adaptive immune system to identify foreign antigens and serving as a link between the innate and adaptive immune responses (32). Different subsets of DCs can induce naïve $CD4^+$ T cells to develop into Th1, Th2, Th17 and Treg cells, thereby modulating T cell-mediated immune response types that act as effector cells in the innate immune response (33, 34). DCs can exert their ability to induce, regulate and control T cell responses (35). Infiltration of mature, active DCs into the tumor increases immune activation and recruitment of immune effector cells.

Natural products can enhance anti-tumor immunity by promoting DCs maturation. Ganoderma lucidum polysaccharides, the main biologically active ingredient of Ganoderma lucidum, efficiently stimulate the activation and maturation of human monocyte-derived DCs. Ganoderma lucidum polysaccharides can also increase the expression of CD80, CD86, CD83, CD40, CD54, and human leukocyte antigen DR on the DC surface (36). Lycium barbarum polysaccharide (LBP), the main active ingredient in lycium barbarum, upregulates CD11c expression and induces DCs maturation through the TLR2/TLR4-mediated NF-κB

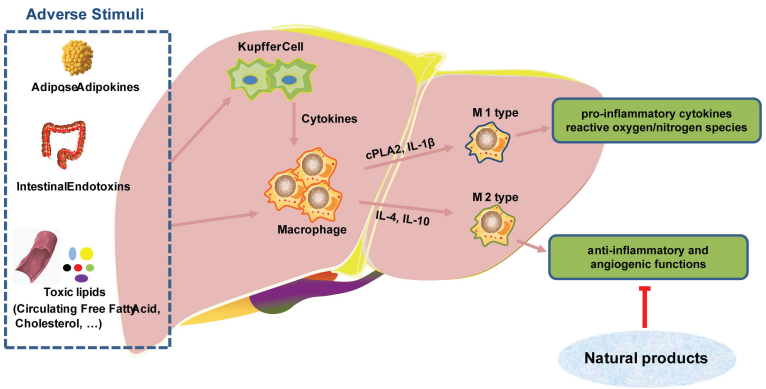

FIGURE 3
Natural products targeting macrophages in the treatment of liver cancer.

pathway. LBP-treated DCs are more effective in promoting lymphocyte activation and proliferation, enhancing the immune response (37). Recently, there is increasing evidence that components of natural products can modulate the immune system by targeting DCs, including flavonoids, polysaccharides, phenolic compounds, saponins, and so on (38).

Effects of natural products on natural killer cells

NK cells are also produced from bone marrow stem cells, which are mostly found in peripheral circulation and serve as the body's first line of defense. At the same time, it can also participate in the cellular immune response and play an important role in tumor diseases *in vivo* (39). NK cells have a powerful cytolytic activity and play an important role in immune control (40). NK cells mediate the tumor killing response mainly by releasing perforin and granzyme to induce apoptosis in target cells (41). In addition, NK cells secrete chemokines and pro-inflammatory cytokines to promote anti-tumor activity (42). Besides, the NK cells may promote the formation and response of tumor-specific CD4+ and CD8+T cells (43).

The production of IL-2 and IFN- by $CD4^+$ T cells can activate NK cells (44). When activated, NK cells release perforin and granzyme B, which cause apoptosis and necrosis in target cells. Numerous studies have revealed that resveratrol can activate and enhance the killing ability of NK cells. The low concentration of resveratrol can increase the expression of NKG2D and IFN-γ in NK cells (45). The resveratrol treatment group can upregulate its anti-tumor and anti-infective abilities by enhancing the activity of NK cells (46). In animal models, green tea catechin metabolitesincrease NK cell cytotoxicity, while quercetin increases NK cell lytic activity (47, 48). Berries high in flavonoids and pro-anthocyanidins not only prevent the progress of cancer but also play a role in the modulation of NK cell (49). After taking garlic extract for 90 days, NKG2D was found to be up-regulated in NK cells. It proves that garlic extract can improve the activity of NK cells and enhance immunity (50). When vitamin A, B, C, D, and E are applied to NK cells, they have stimulatory properties. Although the precise mechanism remains unknown in the majority of cases, components appear to be promising candidates for NK cell-stimulating drugs in tumors (51).

Effects of natural products on regulatory T cells

Regulatory T (Treg) cells are a subtype of T cells with immunomodulatory functions that are closely related to the pathological processes of a variety of human tumors (52). When the suppressive function of Treg cells is compromised, the activity of helper T cells (Th) and killer T cells can induce autoimmune disorders, such as rheumatoid arthritis, multiple sclerosis, and systemic lupus erythematosus (53, 54). On the contrary, the immunosuppressive function of Treg cells is too strong to cause tumor immune escape, such as tumorigenesis (55, 56). Similar to M2 macrophages, Treg cells can inhibit the release of cytokines from Th1 cells and promote angiogenesis in the tumor microenvironment (57).

Kaempferol enhanced Treg cell immunosuppressive activity by inhibiting the activity of proto-oncogene serine/threonine kinase (PIM1) (58). The compound triptolide isolated from Triptolide obviously inhibited the Th2, Th1, and Th17 cell-mediated inflammatory responses and up-regulated the expression of FOXP3 (59). Evidence has demonstrated that lentinan decreased tumor vascular function in a non-T-cell dependent manner by increasing IFNγ production, and showed anti-tumor effect in LAP0297 lung tumor model (31). Lentinan significantly inhibited anti-inflammatory IL-10 and TGF-β 1, and increased the expression of pro-inflammatory chemokines/cytokines (IFN-γ and TNF-α) and IL-12, and decreased immunosuppressive Treg cells. The downregulation of Treg cells is associated with the over-induction of IFN-γ and TNF-α in non-small cell lung cancer (NSCLC), and the inflammatory state of Lentinoglycan treated NSCLC patients can change from Th2 to Th1 (60).

Effects of natural products on effector T cells

Effector T cells include CD8+ cytotoxic T cells (CTLs) and effector CD4+ T cells. In the "activated" state, CTL can induce target cancer cells killing through granule cytokinesis and Fas ligand (FasL)-mediated apoptosis (61). CD4+ T cells are helper T cells that aid in the activation and regulation of immune cells. CD4+ T cells can directly help CD8+ T cell activation and proliferation (62–65). Furthermore, they can also help to shape CD8+ T cells into memory CTLs (66). When the T cell receptor (TCR) is activated, CD4+ T cells differentiate into Th1 or Th2 cells. The balance of Th1 and Th2 plays vital roles in the progress of cancers. With further study of T cells, researchers discovered a new T cell subpopulation called Th17 cells (67, 68). Th17 cells produce IL-17, IL-22, and chemokine ligands 20 (CCL20) (69, 70).

Ginsenosides are the active ingredients of ginseng. Studies have confirmed that ginsenoside Rg1 has a direct effect on the activity of Th and the development of the Th1/Th2 system (71). In addition, ginsenoside Rg1 can selectively enhance the expression of germline transcription products (GLTs), increase the production of IgA antibodies and promote humoral immunity (72). In a mouse model of melanoma, ginsenoside

Rh2 induced a large number of CD4+ and CD8a+T lymphocytes to infiltrate into the tumor tissue, indicating an enhanced immune response and enhanced cytotoxicity of lymphocytes to melanoma cells B16-F10 (73). In mice, polyphenols, such as apigenin and chrysin inhibit ovalbumin immunization-induced serum IgE by downregulating Th2 responses (74). Likewise, tea polyphenols, such as EGCG, diminish Th1 differentiation and the numbers of Th17 and Th9 cells (61), while resveratrol reduces Th17 cell counts (75). Resveratrol dramatically reduced the fraction of CD4+CD25+ cells among CD4+ T cells in both *in vitro* and *in vivo* tests, demonstrating a dose-dependent mechanism (76).

Natural products effectively expanding indications of various types cancer immunotherapy

Recent studies have shown that natural products can enhance the therapeutic effect of cancer vaccines and immune checkpoints inhibitors. Next, we focus on how natural products can improve both treatments through multi-cellular and multi-pathway modulation.

Effects of natural products on the immune checkpoints inhibitors

Immune checkpoint molecules can regulate the immune state by activating or inhibiting immune signaling pathways. Overexpression of some of these molecules in TME leads to T cell dysfunction and ultimately promotes immune escape and tumor survival. Some immune checkpoint antibodies have been used in clinical anti-tumor therapy (77).

The PD-1/PD-L1 pathway, which promotes T cell functional failure, apoptosis and anergy, has stood out among immunological checkpoints due to the outstanding treatment outcomes in many studies (78). However, the presence of an immunosuppressive microenvironment in tumors limits the use of anti-PD-1/PD-L1 antibodies. Natural products have been reported to be key screening targets for PD-1/PD-L1 small molecule inhibitors and reversal of immunosuppression. Besides the ability to regulate the expression of PD-1 and PD-L1, the combination of natural products with anti-PD-1/PD-L1 antibodies has also shown excellent therapeutic efficacy.

The triterpenoid saponin isolated from Anemone flaccida inhibits the growth of hepatocellular carcinoma cells by downregulating the STAT3 signaling pathway to block the activation of PD-1 and PD-L1 (79). Ganoderma lucidum polysaccharide combined with paclitaxel (PTX) preserves the exhausted state of tumor-infiltrating lymphocytes (TILs) by downregulating PD-1 expression (80). Resveratrol can downregulate PD-L1 expression by activating HDAC3/p300/NF-κB signaling pathway in colorectal and breast cancer cells (81). Liu et al. find that combination of andrographolide isolated from Andrographis paniculata and anti-PD-1 antibody is more effective than monotherapy in the treatment of CT26 colon cancer (82). Diosgenin isolated from Acacia concinna in combination with anti-PD-1 antibody can effectively promote necrosis and apoptosis of melanoma cells. Furthermore, their findings suggest that the mechanism of diosgenin sensitivity to anti-PD-1 antibodies mainly contributes to the regulatory function of gut microbiota (83). Therefore, natural products have their unique advantages in immune checkpoints therapy.

Effects of natural products on the cancer vaccines

Cancer vaccines, including cancer treatment vaccines and cancer prevention vaccines, are one of cancer-specific active immunotherapies. The effectiveness of cancer vaccines depends on the optimal combination of adjuvant, antigen, vaccination route and vector. Natural products can improve the immune-stimulate effect of cancer vaccines as adjuvants. QS-21 isolated from Quillaja Saponaria Molina can promote the antigen presentation process and remodel the immunosuppression by regulating Th1 cytokines. Meanwhile a series of Phase I-III clinical trials (leukemia, carcinoma,prostate, ovary, or lung) have investigated the effect of QS-21 as an immune adjuvant in cancer vaccines designed (84). Curcumin has the potential to improve the therapeutic outcome of Bacillus Calmette-Guerin and significantly enhance the efficacy of TRP2 peptide vaccine against melanoma. In addition, curcumin has been reported to inhibit IDO expression by blocking the JAK-STAT1 signaling pathway and to sensitize melanoma FAPαc vaccine by this mechanism (85).

In addition to the effective activation of CD8+ cytotoxic T lymphocytes, cancer vaccines must also face a challenge: poor immunogenicity. It is reported that natural products can enhance tumor immunogenicity by inducing immunogenic cell death (ICD) effects. The pathway of ICD-induced tumour cell death relies on damage-associated molecular patterns (DAMPs) such as heat shock proteins (HSPs), high mobility group box 1 (HMGB1) and calreticulin (CRT), making tumour cells a “therapeutic vaccine” that can induce anti-tumour immunity (86). Capsaicin has been reported to trigger ICD effects in primary effusion lymphoma (PEL) cells by inducing exposure to DAMPs (87). Ginsenoside Rg3 isolated from ginseng can induce ICD and enhance interferon g (IFN-g) secretion to inhibit tumor growth (88). oreover, shikonin can improve the expressions of MHC II and CD86, and enhance tumor-immunogenicity of tumor vaccines *via* ICD (89).

Discussion

Given the multi-pharmacological activity and chemical diversity, natural products have been described as a non-substitutable source of clinical therapeutics for human tumors. Natural products can mediate multiple immune responses and reduce the tumor escape. They enhance the interaction of immune cells while decreasing the expression of pro-inflammatory cytokines. Previous studies have shown that natural products can exert anticancer activity through immune regulation *in vivo* and *in vitro*. Unlike traditional chemoimmunotherapy in tumor, natural products display many advantages, such as wide sources, less toxic and side effects, as well as diverse immunomodulatory activities, suggesting that natural products have an attractive prospect in the research of novel tumor immunotherapy. The combination of natural products and chemotherapeutic drugs may exert stronger therapeutic effect than chemotherapeutic drugs alone in tumors, which has synergistic and reducing toxic and side effects.

Although natural products have made encouraging appear promising and progress in various studies as modulators of tumor immunotherapy. For natural products to be better used in cancer immunotherapy, a number of issues still need to be addressed. First of all, natural products will face the problem of individual patient differences, TME differences, tumor heterogeneity. Secondly, a deeper and more comprehensive exploration of the signalling pathways of the immune system relevant to tumor immunotherapy is needed to help select more effective natural products. Thirdly, most natural products have a wide range of pharmacological effects, but their targets and molecular mechanisms relevant to tumour immunity have not been fully elucidated.

Above all, the emerging role of natural products in tumor immunotherapy still has greater potential and deserves attention. Future research can screen natural products for targeted antitumor immune drugs using advanced technologies, such as metabolomics, single-cell sequencing, novel drug delivery technologies, and computer-aided design techniques.

Author contributions

X-QJ conceptualized the ideas. X-QJ, NL, W-JF, Z-HL, and J-LH performed the literature search, drafted the original manuscript, and drew the figures. Z-SL revised the manuscript. All the authors approved the final version of the manuscript.

Funding

This work was financially supported by General Program of the National Natural Science Foundation of China Joint project (NO. U21A20348), National Natural Science Foundation of China General Project (No.81970633), Heilongjiang Provincial Higher Education Institutions Basic Research Business Expenses (2021KYYWF0046).

Conflict of interest

The authors declare that the research was conducted in the absence of any commercial or financial relationships that could be construed as a potential conflict of interest.

Publisher's note

References

1. Venter C, Eyerich S, Sarin T, Klatt KC. Nutrition and the immune system: A complicated tango. *Nutrients* (2020) 12(3):818. doi: 10.3390/nu12030818

2. Artis D, Spits H. The biology of innate lymphoid cells. *Nature* (2015) 517 (7534):293–301. doi: 10.1038/nature14189

3. Hanahan D, Weinberg RA. Hallmarks of cancer: the next generation. *Cell* (2011) 144(5):646–74. doi: 10.1016/j.cell.2011.02.013

4. Yost KE, Satpathy AT, Wells DK, Qi Y, Wang C, Kageyama R, et al. Clonal replacement of tumor-specific T cells following PD-1 blockade. *Nat Med* (2019) 25 (8):1251–9. doi: 10.1038/s41591-019-0522-3

5. Finck A, Gill SI, June CH. Cancer immunotherapy comes of age and looks for maturity. *Nat Commun* (2020) 11(1):3325. doi: 10.1038/s41467-020-17140-5

6. Hargadon KM, Johnson CE, Williams CJ. Immune checkpoint blockade therapy for cancer: An overview of FDA-approved immune checkpoint inhibitors. *Int Immunopharmacol* (2018) 62:29–39. doi: 10.1016/j.intimp.2018.06.001

7. O'Leary MC, Lu X, Huang Y, Lin X, Mahmood I, Przepiorka D, et al. FDA Approval summary: Tisagenlecleucel for treatment of patients with relapsed or refractory b-cell precursor acute lymphoblastic leukemia. *Clin Cancer Res* (2019) 25 (4):1142–6. doi: 10.1158/1078-0432.CCR-18-2035

8. Bouchkouj N, Kasamon YL, de Claro RA, George B, Lin X, Lee S, et al. FDA Approval summary: Axicabtagene ciloleucel for relapsed or refractory Large b-cell lymphoma. *Clin Cancer Res* (2019) 25(6):1702–8. doi: 10.1158/1078-0432.CCR-18-2743

9. Garner H, de Visser KE. Immune crosstalk in cancer progression and metastatic spread: a complex conversation. *Nat Rev Immunol* (2020) 20(8):483–97. doi: 10.1038/s41577-019-0271-z

10. Farzaei MH, Rahimi R, Abdollahi M. The role of dietary polyphenols in the management of inflammatory bowel disease. *Curr Pharm Biotechnol* (2015) 16 (3):196–210. doi: 10.2174/1389201016666150118131704

11. Andreicut AD, Parvu AE, Mot AC, Parvu M, Fischer FE, Catoi AF, et al. Phytochemical analysis of anti-inflammatory and antioxidant effects of mahonia

aquifolium flower and fruit extracts. *Oxid Med Cell Longev* (2018) 2018:2879793. doi: 10.1155/2018/2879793

12. Liao K, Li J, Wang Z. Dihydroartemisinin inhibits cell proliferation *via* AKT/GSK3beta/cyclinD1 pathway and induces apoptosis in A549 lung cancer cells. *Int J Clin Exp Pathol* (2014) 7(12):8684–91.

13. Wang Y, Zhang Q, Chen Y, Liang CL, Liu H, Qiu F, et al. Antitumor effects of immunity-enhancing traditional Chinese medicine. *BioMed Pharmacother* (2020) 121:109570. doi: 10.1016/j.biopha.2019.109570

14. He J, Yin P, Xu K. Effect and molecular mechanisms of traditional Chinese medicine on tumor targeting tumor-associated macrophages. *Drug Des Devel Ther* (2020) 14:907–19. doi: 10.2147/DDDT.S223646

15. Sudhakaran M, Sardesai S, Doseff AI. Flavonoids: New frontier for immuno-regulation and breast cancer control. *Antioxidants (Basel)* (2019) 8(4):103. doi: 10.3390/antiox8040103

16. Ferreira SS, Passos CP, Madureira P, Vilanova M, Coimbra MA. Structure-function relationships of immunostimulatory polysaccharides: A review. *Carbohydr Polym* (2015) 132:378–96. doi: 10.1016/j.carbpol.2015.05.079

17. Gandhi GR, Neta M, Sathiyabama RG, Quintans J, de Oliveira ESA, Araujo A, et al. Flavonoids as Th1/Th2 cytokines immunomodulators: A systematic review of studies on animal models. *Phytomedicine* (2018) 44:74–84. doi: 10.1016/j.phymed.2018.03.057

18. Boland JW, Foulds GA, Ahmedzai SH, Pockley AG. A preliminary evaluation of the effects of opioids on innate and adaptive human *in vitro* immune function. *BMJ Support Palliat Care* (2014) 4(4):357–67. doi: 10.1136/bmjspcare-2013-000573

19. Lei X, Lei Y, Li JK, Du WX, Li RG, Yang J, et al. Immune cells within the tumor microenvironment: Biological functions and roles in cancer immunotherapy. *Cancer Lett* (2020) 470:126–33. doi: 10.1016/j.canlet.2019.11.009

20. Wynn TA, Chawla A, Pollard JW. Macrophage biology in development, homeostasis and disease. *Nature* (2013) 496(7446):445–55. doi: 10.1038/nature12034

21. Nikitina E, Larionova I, Choinzonov E, Kzhyshkowska J. Monocytes and macrophages as viral targets and reservoirs. *Int J Mol Sci* (2018) 19(9):2821. doi: 10.3390/ijms19092821

22. Sica A, Mantovani A. Macrophage plasticity and polarization: *in vivo* veritas. *J Clin Invest* (2012) 122(3):787–95. doi: 10.1172/JCI59643

23. Locati M, Curtale G, Mantovani A. Diversity, mechanisms, and significance of macrophage plasticity. *Annu Rev Pathol* (2020) 15:123–47. doi: 10.1146/annurev-pathmechdis-012418-012718

24. Aras S, Zaidi MR. TAMeless traitors: macrophages in cancer progression and metastasis. *Br J Cancer* (2017) 117(11):1583–91. doi: 10.1038/bjc.2017.356

25. Iwanowycz S, Wang J, Hodge J, Wang Y, Yu F, Fan D. Emodin inhibits breast cancer growth by blocking the tumor-promoting feedforward loop between cancer cells and macrophages. *Mol Cancer Ther* (2016) 15(8):1931–42. doi: 10.1158/1535-7163.MCT-15-0987

26. Li Z, Zhang L, He W, Zhu C, Yang J, Sheng M. Astragalus membranaceus inhibits peritoneal fibrosis *via* monocyte chemoattractant protein (MCP)-1 and the transforming growth factor-beta1 (TGF-beta1) pathway in rats submitted to peritoneal dialysis. *Int J Mol Sci* (2014) 15(7):12959–71. doi: 10.3390/ijms150712959

27. Nievergelt A, Marazzi J, Schoop R, Altmann KH, Gertsch J. Ginger phenylpropanoids inhibit IL-1beta and prostanoid secretion and disrupt arachidonate-phospholipid remodeling by targeting phospholipases A2. *J Immunol* (2011) 187(8):4140–50. doi: 10.4049/jimmunol.1100880

28. Zhang M, Xie Y, Su X, Liu K, Zhang Y, Pang W, et al. Corrigendum: Inonotus sanghuang polyphenols attenuate inflammatory response *Via* modulating the crosstalk between macrophages and adipocytes. *Front Immunol* (2021) 12:633354. doi: 10.3389/fimmu.2021.633354

29. Morihara N, Ide N, Weiss N. Aged garlic extract inhibits CD36 expression in human macrophages *via* modulation of the PPARgamma pathway. *Phytother Res* (2010) 24(4):602–8. doi: 10.1002/ptr.3008

30. Li CL, Zhou WJ, Ji G, Zhang L. Natural products that target macrophages in treating non-alcoholic steatohepatitis. *World J Gastroenterol* (2020) 26(18):2155–65. doi: 10.3748/wjg.v26.i18.2155

31. Deng S, Zhang G, Kuai J, Fan P, Wang X, Zhou P, et al. Lentinan inhibits tumor angiogenesis *via* interferon gamma and in a T cell independent manner. *J Exp Clin Cancer Res* (2018) 37(1):260. doi: 10.1186/s13046-018-0932-y

32. Buckwalter MR, Albert ML. Orchestration of the immune response by dendritic cells. *Curr Biol* (2009) 19(9):R355–61. doi: 10.1016/j.cub.2009.03.012

33. Peron G, de Lima TL, Camargo DRL, Thome R, Cardoso VL. Modulation of dendritic cell by pathogen antigens: Where do we stand? *Immunol Lett* (2018) 196:91–102. doi: 10.1016/j.imlet.2018.02.001

34. Shortman K, Liu YJ. Mouse and human dendritic cell subtypes. *Nat Rev Immunol* (2002) 2(3):151–61. doi: 10.1038/nri746

35. Schulke S. Induction of interleukin-10 producing dendritic cells as a tool to suppress allergen-specific T helper 2 responses. *Front Immunol* (2018) 9:455. doi: 10.3389/fimmu.2018.00455

36. Lin YL, Liang YC, Lee SS, Chiang BL. Polysaccharide purified from ganoderma lucidum induced activation and maturation of human monocyte-derived dendritic cells by the NF-kappaB and p38 mitogen-activated protein kinase pathways. *J Leukoc Biol* (2005) 78(2):533–43. doi: 10.1189/jlb.0804481

37. Zhu J, Zhang Y, Shen Y, Zhou H, Yu X. Lycium barbarum polysaccharides induce toll-like receptor 2- and 4-mediated phenotypic and functional maturation of murine dendritic cells *via* activation of NF-kappaB. *Mol Med Rep* (2013) 8 (4):1216–20. doi: 10.3892/mmr.2013.1608

38. Li J, Li J, Zhang F. The immunoregulatory effects of Chinese herbal medicine on the maturation and function of dendritic cells. *J Ethnopharmacol* (2015) 171:184–95. doi: 10.1016/j.jep.2015.05.050

39. Mathew A. Defining the role of NK cells during dengue virus infection. *Immunology* (2018) 154(4):557–62. doi: 10.1111/imm.12928

40. Ruggeri L, Capanni M, Urbani E, Perruccio K, Shlomchik WD, Tosti A, et al. Effectiveness of donor natural killer cell alloreactivity in mismatched hematopoietic transplants. *Science* (2002) 295(5562):2097–100. doi: 10.1126/science.1068440

41. Voskoboinik I, Smyth MJ, Trapani JA. Perforin-mediated target-cell death and immune homeostasis. *Nat Rev Immunol* (2006) 6(12):940–52. doi: 10.1038/nri1983

42. Guillerey C, Huntington ND, Smyth MJ. Targeting natural killer cells in cancer immunotherapy. *Nat Immunol* (2016) 17(9):1025–36. doi: 10.1038/ni.3518

43. Pahl J, Cerwenka A. Tricking the balance: NK cells in anti-cancer immunity. *Immunobiology* (2017) 222(1):11–20. doi: 10.1016/j.imbio.2015.07.012

44. Hu JY, Zhang J, Cui JL, Liang XY, Lu R, Du GF, et al. Increasing CCL5/CCR5 on CD4+ T cells in peripheral blood of oral lichen planus. *Cytokine* (2013) 62(1):141–5. doi: 10.1016/j.cyto.2013.01.020

45. Leischner C, Burkard M, Pfeiffer MM, Lauer UM, Busch C, Venturelli S. Nutritional immunology: function of natural killer cells and their modulation by resveratrol for cancer prevention and treatment. *Nutr J* (2016) 15(1):47. doi: 10.1186/s12937-016-0167-8

46. Lu CC, Lai HC, Hsieh SC, Chen JK. Resveratrol ameliorates serratia marcescens-induced acute pneumonia in rats. *J Leukoc Biol* (2008) 83(4):1028–37. doi: 10.1189/jlb.0907647

47. Exon JH, Magnuson BA, South EH, Hendrix K. Dietary quercetin, immune functions and colonic carcinogenesis in rats. *Immunopharmacol Immunotoxicol* (1998) 20(1):173–90. doi: 10.3109/08923979809034816

48. Kim YH, Won YS, Yang X, Kumazoe M, Yamashita S, Hara A, et al. Green tea catechin metabolites exert immunoregulatory effects on CD4(+) T cell and natural killer cell activities. *J Agric Food Chem* (2016) 64(18):3591–7. doi: 10.1021/acs.jafc.6b01115

49. McAnulty LS, Nieman DC, Dumke CL, Shooter LA, Henson DA, Utter AC, et al. Effect of blueberry ingestion on natural killer cell counts, oxidative stress, and inflammation prior to and after 2.5 h of running. *Appl Physiol Nutr Metab* (2011) 36(6):976–84. doi: 10.1139/h11-120

50. Nantz MP, Rowe CA, Muller CE, Creasy RA, Stanilka JM, Percival SS. Supplementation with aged garlic extract improves both NK and gammadelta-T cell function and reduces the severity of cold and flu symptoms: a randomized, double-blind, placebo-controlled nutrition intervention. *Clin Nutr* (2012) 31 (3):337–44. doi: 10.1016/j.clnu.2011.11.019

51. Grudzien M, Rapak A. Effect of natural compounds on NK cell activation. *J Immunol Res* (2018) 2018:4868417. doi: 10.1155/2018/4868417

52. Guo J, Zhou X. Regulatory T cells turn pathogenic. *Cell Mol Immunol* (2015) 12(5):525–32. doi: 10.1038/cmi.2015.12

53. Buckner JH. Mechanisms of impaired regulation by CD4(+)CD25(+) FOXP3(+) regulatory T cells in human autoimmune diseases. *Nat Rev Immunol* (2010) 10(12):849–59. doi: 10.1038/nri2889

54. Miyara M, Ito Y, Sakaguchi S. TREG-cell therapies for autoimmune rheumatic diseases. *Nat Rev Rheumatol* (2014) 10(9):543–51. doi: 10.1038/nrrheum.2014.105

55. Tanaka A, Sakaguchi S. Regulatory T cells in cancer immunotherapy. *Cell Res* (2017) 27(1):109–18. doi: 10.1038/cr.2016.151

56. Shuai Z, Leung MW, He X, Zhang W, Yang G, Leung PS, et al. Adaptive immunity in the liver. *Cell Mol Immunol* (2016) 13(3):354–68. doi: 10.1038/cmi.2016.4

57. Facciabene A, Peng X, Hagemann IS, Balint K, Barchetti A, Wang LP, et al. Tumour hypoxia promotes tolerance and angiogenesis *via* CCL28 and t(reg) cells. *Nature* (2011) 475(7355):226–30. doi: 10.1038/nature10169

58. Lin F, Luo X, Tsun A, Li Z, Li D, Li B. Kaempferol enhances the suppressive function of treg cells by inhibiting FOXP3 phosphorylation. *Int Immunopharmacol* (2015) 28(2):859–65. doi: 10.1016/j.intimp.2015.03.044

59. Li Y, Yu C, Zhu WM, Xie Y, Qi X, Li N, et al. Triptolide ameliorates IL-10-deficient mice colitis by mechanisms involving suppression of IL-6/STAT3

signaling pathway and down-regulation of IL-17. *Mol Immunol* (2010) 47 (15):2467–74. doi: 10.1016/j.molimm.2010.06.007

60. Wang XE, Wang YH, Zhou Q, Peng M, Zhang J, Chen M, et al. Immunomodulatory effect of lentinan on aberrant T subsets and cytokines profile in non-small cell lung cancer patients. *Pathol Oncol Res* (2020) 26 (1):499–505. doi: 10.1007/s12253-018-0545-y

61. Tanaka H, Yoshizawa H, Yamaguchi Y, Ito K, Kagamu H, Suzuki E, et al. Successful adoptive immunotherapy of murine poorly immunogenic tumor with specific effector cells generated from gene-modified tumor-primed lymph node cells. *J Immunol* (1999) 162(6):3574–82.

62. Bourgeois C, Rocha B, Tanchot C. A role for CD40 expression on CD8+ T cells in the generation of CD8+ T cell memory. *Science* (2002) 297(5589):2060–3. doi: 10.1126/science.1072615

63. Mackey MF, Barth RJ, Noelle RJ. The role of CD40/CD154 interactions in the priming, differentiation, and effector function of helper and cytotoxic T cells. *J Leukoc Biol* (1998) 63(4):418–28. doi: 10.1002/jlb.63.4.418

64. Mackey MF, Gunn JR, Ting PP, Kikutani H, Dranoff G, Noelle RJ, et al. Protective immunity induced by tumor vaccines requires interaction between CD40 and its ligand, CD154. *Cancer Res* (1997) 57(13):2569–74.

65. Cheng LE, Ohlen C, Nelson BH, Greenberg PD. Enhanced signaling through the IL-2 receptor in CD8+ T cells regulated by antigen recognition results in preferential proliferation and expansion of responding CD8+ T cells rather than promotion of cell death. *Proc Natl Acad Sci USA* (2002) 99(5):3001–6. doi: 10.1073/pnas.052676899

66. Borst J, Ahrends T, Babala N, Melief C, Kastenmuller W. CD4(+) T cell help in cancer immunology and immunotherapy. *Nat Rev Immunol* (2018) 18(10):635–47. doi: 10.1038/s41577-018-0044-0

67. Park H, Li Z, Yang XO, Chang SH, Nurieva R, Wang YH, et al. A distinct lineage of CD4 T cells regulates tissue inflammation by producing interleukin 17. *Nat Immunol* (2005) 6(11):1133–41. doi: 10.1038/ni1261

68. Harrington LE, Hatton RD, Mangan PR, Turner H, Murphy TL, Murphy KM, et al. Interleukin 17-producing CD4+ effector T cells develop *via* a lineage distinct from the T helper type 1 and 2 lineages. *Nat Immunol* (2005) 6(11):1123–32. doi: 10.1038/ni1254

69. Louten J, Boniface K, de Waal MR. Development and function of TH17 cells in health and disease. *J Allergy Clin Immunol* (2009) 123(5):1004–11. doi: 10.1016/j.jaci.2009.04.003

70. Zheng Y, Danilenko DM, Valdez P, Kasman I, Eastham-Anderson J, Wu J, et al. Interleukin-22, a T(H)17 cytokine, mediates IL-23-induced dermal inflammation and acanthosis. *Nature* (2007) 445(7128):648–51. doi: 10.1038/nature05505

71. Lee EJ, Ko E, Lee J, Rho S, Ko S, Shin MK, et al. Ginsenoside Rg1 enhances CD4(+) T-cell activities and modulates Th1/Th2 differentiation. *Int Immunopharmacol* (2004) 4(2):235–44. doi: 10.1016/j.intimp.2003.12.007

72. Park HY, Lee SH, Lee KS, Yoon HK, Yoo YC, Lee J, et al. Ginsenoside Rg1 and 20(S)-Rg3 induce IgA production by mouse b cells. *Immune Netw* (2015) 15 (6):331–6. doi: 10.4110/in.2015.15.6.331

73. Wang M, Yan SJ, Zhang HT, Li N, Liu T, Zhang YL, et al. Ginsenoside Rh2 enhances the antitumor immunological response of a melanoma mice model. *Oncol Lett* (2017) 13(2):681–5. doi: 10.3892/ol.2016.5490

74. Yano S, Umeda D, Yamashita T, Ninomiya Y, Sumida M, Fujimura Y, et al. Dietary flavones suppresses IgE and Th2 cytokines in OVA-immunized BALB/c mice. *Eur J Nutr* (2007) 46(5):257–63. doi: 10.1007/s00394-007-0658-7

75. Xuzhu G, Komai-Koma M, Leung BP, Howe HS, McSharry C, McInnes IB, et al. Resveratrol modulates murine collagen-induced arthritis by inhibiting Th17 and b-cell function. *Ann Rheum Dis* (2012) 71(1):129–35. doi: 10.1136/ard.2011.149831

76. Bahrami A, Fereidouni M, Pirro M, Bianconi V, Sahebkar A. Modulation of regulatory T cells by natural products in cancer. *Cancer Lett* (2019) 459:72–85. doi: 10.1016/j.canlet.2019.06.001

77. Bagchi S, Yuan R, Engleman EG. Immune checkpoint inhibitors for the treatment of cancer: Clinical impact and mechanisms of response and resistance. *Annu Rev Pathol* (2021) 16:223–49. doi: 10.1146/annurev-pathol-042020-042741

78. Ishida Y, Agata Y, Shibahara K, Honjo T. Induced expression of PD-1, a novel member of the immunoglobulin gene superfamily, upon programmed cell death. *EMBO J* (1992) 11(11):3887–95. doi: 10.1002/j.1460-2075.1992.tb05481.x

79. Han L, Yao S, Cao S, Mo G, Li J, Cao Y, et al. Triterpenoid saponins from anemone flaccida suppress tumor cell proliferation by regulating MAPK, PD1/PDL1, and STAT3 signaling pathways and altering cancer metabolism. *Onco Targets Ther* (2019) 12:10917–30. doi: 10.2147/OTT.S212666

80. Chen Y, Wang Y, Xu L, Zhu W, Xu C, Xu M, et al. Influence of total glucosides of paeony on PD-1/PD-L1 expression in primary sjogren's syndrome. *Int J Rheum Dis* (2019) 22(2):200–6. doi: 10.1111/1756-185X.13391

81. Lucas J, Hsieh TC, Halicka HD, Darzynkiewicz Z, Wu JM. Upregulation of PDL1 expression by resveratrol and piceatannol in breast and colorectal cancer cells occurs *via* HDAC3/p300mediated NFkappaB signaling. *Int J Oncol* (2018) 53 (4):1469–80. doi: 10.3892/ijo.2018.4512

82. Liu W, Fan T, Li M, Zhang G, Guo W, Yang X, et al. Andrographolide potentiates PD-1 blockade immunotherapy by inhibiting COX2-mediated PGE2 release. *Int Immunopharmacol* (2020) 81:106206. doi: 10.1016/j.intimp.2020.106206

83. Kukhetpitakwong R, Hahnvajanawong C, Homchampa P, Leelavatcharamas V, Satra J, Khunkitti W. Immunological adjuvant activities of saponin extracts from the pods of acacia concinna. *Int Immunopharmacol* (2006) 6 (11):1729–35. doi: 10.1016/j.intimp.2006.07.008

84. Gilewski T, Adluri S, Ragupathi G, Zhang S, Yao TJ, Panageas K, et al. Vaccination of high-risk breast cancer patients with mucin-1 (MUC1) keyhole limpet hemocyanin conjugate plus QS-21. *Clin Cancer Res* (2000) 6(5):1693–701.

85. Tharakan ST, Inamoto T, Sung B, Aggarwal BB, Kamat AM. Curcumin potentiates the antitumor effects of gemcitabine in an orthotopic model of human bladder cancer through suppression of proliferative and angiogenic biomarkers. *Biochem Pharmacol* (2010) 79(2):218–28. doi: 10.1016/j.bcp.2009.08.007

86. Kroemer G, Galluzzi L, Kepp O, Zitvogel L. Immunogenic cell death in cancer therapy. *Annu Rev Immunol* (2013) 31:51–72. doi: 10.1146/annurev-immunol-032712-100008

87. Granato M, Gilardini MM, Filardi M, Faggioni A, Cirone M. Capsaicin triggers immunogenic PEL cell death, stimulates DCs and reverts PEL-induced immune suppression. *Oncotarget* (2015) 6(30):29543–54. doi: 10.18632/oncotarget.4911

88. Son KJ, Choi KR, Lee SJ, Lee H. Immunogenic cell death induced by ginsenoside Rg3: Significance in dendritic cell-based anti-tumor immunotherapy. *Immune Netw* (2016) 16(1):75–84. doi: 10.4110/in.2016.16.1.75

89. Lin TJ, Lin HT, Chang WT, Mitapalli SP, Hsiao PW, Yin SY, et al. Shikonin-enhanced cell immunogenicity of tumor vaccine is mediated by the differential effects of DAMP components. *Mol Cancer* (2015) 14:174. doi: 10.1186/s12943-015-0435-9

frontiers | Frontiers in Oncology

TYPE Review
PUBLISHED 05 September 2022
DOI 10.3389/fonc.2022.949193

OPEN ACCESS

EDITED BY
Xian Zeng,
Fudan University, China

REVIEWED BY
Patricia Kunda,
Consejo Nacional de Investigaciones Científicas y Técnicas (CONICET), Argentina
Xuan Xiao,
Renmin Hospital of Wuhan University, China

*CORRESPONDENCE
Lin Ye
yelin0711@126.com

SPECIALTY SECTION
This article was submitted to Cancer Immunity and Immunotherapy, a section of the journal Frontiers in Oncology

RECEIVED 20 May 2022
ACCEPTED 12 August 2022
PUBLISHED 05 September 2022

CITATION
Wang L, Li S, Mei J and Ye L (2022) Immunotherapies of retinoblastoma: Effective methods for preserving vision in the future.
Front. Oncol. 12:949193.
doi: 10.3389/fonc.2022.949193

Immunotherapies of retinoblastoma: Effective methods for preserving vision in the future

Ling Wang, Shixu Li, Jun Mei and Lin Ye*

Shenzhen Eye Hospital, Jinan University, Shenzhen Eye Institute, Shenzhen, China

Retinoblastoma is the most common intraocular tumor in children. Patients can be cured by enucleation, but it can lead to vision loss. Chemotherapy is the main method of treatment for RB currently. Unfortunately, chemoresistant and tumor metastasis often happen, resulting in a relatively poor prognosis. Therefore, immunotherapy becomes one of the optimal choices. Targeting not only tumor cells but also the active tumor microenvironment is a novel strategy for RB treatment. Here, we conclude several potential targets for RB immunotherapy, including gangliosides GD2, PD-1 and PD-L1, B7H3, EpCAM and SYK. We also review the techniques for CART, bispecific antibodies and genetically modified Dendritic cells according to the characteristics of different targets and discuss the feasibility of immunotherapy with different targets.

KEYWORDS

retinoblastoma, immunotherapy, CART, bispecific antibody, monoclonal antibody

Introduction

Retinoblastoma has significant morbidity in young children and is one of the most common ocular tumors in children. Virtually all cases of retinoblastoma occur because of germline cancer susceptibility (1). Patients with this predisposition were also more likely to develop bilateral retinoblastoma. In children with this inherited disorder, retinoblastoma affects both eyes (bilateral) in 80% of cases and intracranial tumors (trilaterally) in 5%. Enucleation can cure children with unilateral intraocular retinoblastoma without any further treatment and subsequent vision loss. In localized tumor cases, and where appropriate, it can also be treated by laser application of cryotherapy or brachytherapy and/or local intra-arterial chemotherapy to save vision and preserve the eye. At present, the most common treatment for retinoblastoma remains systemic, subconjunctival, intraarterial, or intravitreal chemotherapy (2). It is also the current standard of care for managing orbital exenteration cases. The tumor

unresponsiveness and recurrence are the most significant concern after chemo reduction. For larger tumors, systemic chemotherapy can achieve an initial decrease in tumor size, allowing for subsequent local treatment options. For unresponsive extraocular and/or metastatic disease, reserve high-dose systemic chemotherapy with stem cell rescue (3, 4). Despite high overall survival rates (> 95%) in Western countries, long-term survival is reduced in children treated with eye-preserving radiotherapy and/or chemotherapy compared with enucleation alone because of the higher incidence of secondary malignancies (5, 6). Retinoblastoma can be transmitted to the central nervous system *via* the optic nerve and to distant metastatic sites in lymph nodes, bone, bone marrow, and liver *via* the sclera *via* lymphatic or blood circulation to orbital bones. High-dose chemotherapy is often unsuccessful in rescuing in these cases, and because of its very aggressive nature, high-dose may cause lifelong sequelae to the patient (2, 7–9). As a local treatment modality, ophthalmic artery chemosurgery significantly reduced the rate of enucleation in unilateral and bilateral retinoblastoma, saving the majority of affected eyes without compromising survival. Although treatment outcomes are excellent in developed countries because of early diagnosis, patients with both metastatic and recurrent disease are common in developing countries, resulting in relatively poor prognosis. Therefore, it is essential to find new treatment strategies that are more effective and tolerable to effectively control retinoblastoma and protect eyeball and children's vision, especially with minimal short- and long-term side effects.

Paradigm advances in cancer therapy have been made in the past decades, targeting not only tumor cells but also the active tumor microenvironment (TME) (10). The changes in the tumor microenvironment and protein communication between primary retinoblastoma and chemo-reduced retinoblastoma have not been reported. Therefore, it is important to understand the contribution of immune checkpoint markers in the microenvironment of retinoblastoma tumors. The TME comprises malignant and non-malignant cells such as cytokine, growth factors, extracellular proteins, endothelial cells, fibroblasts, and inflammatory cells (7). Targeting the tumor microenvironment has great potential because new immunotherapy strategies may be involved in tumor progression and metastasis (10). Despite the evolving nature of chemotherapeutic agents and the delivery of the agents, the development of novel targeted treatments requires a better understanding of the pathophysiology of retinoblastoma (9). Targeting the tumor microenvironment is less likely to cause adaptive mutations and metastasis because non-malignant cells are genetically more stable than tumor cells (11). Exploring functional changes in TME may provide essential considerations for ongoing studies of primary and chemo-reduced retinoblastoma. The use of immune checkpoint inhibitors has improved overall survival rates in treating many different solid tumors.

In the present review, we described the latest innovations in retinoblastoma immunotherapy targeting GD2, PD-1, B7H3, EpCAM and SYK.

GD2

GD2, a disialoganglioside highly expressed in cancer cells (12), is involved in many signaling cascade pathways, such as MAPK, PI3K/Akt, and FAK/paxillin (13–15), in which cells can accelerate proliferation, migration, and stemness chemoresistance. Previous studies have focused on the diagnostic study of GD2 in some disseminated diseases such as bone marrow and cerebrospinal fluid. Since 1993, researchers have begun to examine the expression of GD2 and GD2 synthase in retinoblastoma (16). The most significant proportion of GD2 staining was studied in non-white populations. GD2 was expressed primarily on the membranes of retinoblastoma cells, and the positive rate of the assay was 37%, which suggests that GD2 has the capacity to be a potential therapeutic target for RB (17, 18). The heterogeneous expression of GD2 in positively stained samples further demonstrates a multifocal origin and distinct cytogenetic clones within a tumor (19). The relationship between GD2 expression and tumor stage and proliferation index suggests that GD2 expression is associated with poor patient prognosis (20). GD2 is widely expressed in retinoblastoma, and MYCN amplification in pretreated chemo-refractory cases, suggesting that for treatment of RB, anti-GD2 monoclonal antibodies may be effective (21, 22). Anti-GD2 mAbs have three proposed mechanisms of action against GD2-expressing tumor cells. First, GD2 mAbs initiate the phagocytosis by macrophages (Figure 1A) destruction of tumor cells by natural killer cells and the cytotoxicity of granulocytes mediated by killing tumor cells. Second, GD2 mAbs mediate the lysis of tumor cells *via* complement-dependent cytotoxicity (Figure 1B). Third, GD2 mAbs direct induction of cell death due to the specific binding of anti-GD2 mAbs to GD2 (Figure 1C) (23). In Michelle's study (24), intending to improve survival in high-risk neuroblastoma, researchers used an anti-GD2-based monoclonal antibody (dinutuximab) in the maintenance phase of treatment. COG-ANBL0032 protocol comparing the ch14.18 antibody (dinutuximab) in combination with isotretinoin and alternating GM-CSF and IL-2 to single-agent isotretinoin in the maintenance phase of treatment. There were 20% and 11% increases in event-free survival (EFS) and 11% and 16% increases in overall survival (OS) after 2 and 5 years, respectively.

Improved early response and outcome of GD2 monoclonal antibody (hu14.18K322A) in children with newly diagnosed high-risk neuroblastoma by six cycles of concurrent induction chemotherapy with hu14.18K322A, GM-CSF, and low-dose IL-2 was evaluated by another group. After the first two cycles of chemoimmunotherapy, 42 of 63 evaluable patients had partial responses (PRs) or better. At the end of induction, partial

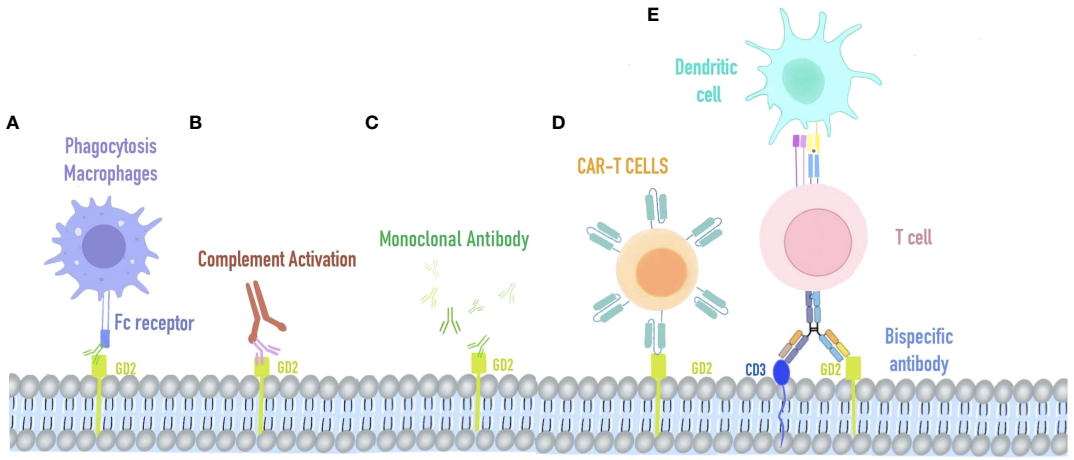

FIGURE 1
Immunotherapy strategy targeting GD2. **(A)** Macrophage phagocytosis combined with retinoblastoma cells mediated by anti-GD2 Fc receptors. **(B)** Complement activation on GD2-expressing retinoblastoma. **(C)** AntiGD2 monoclonal antibody is used for high-risk retinoblastoma. **(D)** CAR-T cells recognize retinoblastoma cells via their specific T cell receptors against GD2. **(E)** Bispecific antibody of GD2 and CD3, redirecting T cells and accessory immune cells (via their functioning Fc-fragment) toward retinoblastoma cells.

responses or better were seen in 60 of 62 patients (97%). No patient developed progressive disease throughout the induction period (25).After being tested in clinical trials, anti-GD2 monoclonal antibodies proved their safety and efficacy suggesting that GD2 could be an essential immune target for the treatment of RB (21).

T lymphocytes isolated from patients were designed to express CD19-specific chimeric antigen receptors (CARs) and showed significant antitumor effects against acute B-cell leukemia and non-Hodgkin's lymphoma. CAR-T has two distinguishing features: substantial toxicity of cytotoxic T lymphocytes and specific antigen-binding of monoclonal antibodies. It led to the creation of a GD2-specific chimeric antigen receptor (CAR)-modified T-cell therapy for retinoblastoma (Figure 1D) Sujjitjoon et al. developed a novel 4SCAR-GD2 T for the treatment of retinoblastoma (26). The intracellular domain of 4SCAR-GD2 T contains CD28, 41BB, and CD3ζ, and its scFv fragment derived from the monoclonal antibody hu3F8, recognizes human GD2 (Figure 1E) *In vitro* studies using Y79RB cells found that this 4SCAR-GD2 T had high cytotoxicity. To mimic the high tumor burden *in vivo*, the investigators increased the number of Y79RB cells by 3-fold after the first round of killing and prolonged the co-culture time of 4SCAR-GD2 with Y79RB. After 6 days of co-culture, some Y79RB cells survived with reduced expression of GD2 on their cell surface compared to before (from 93.2% to 65.5%). Typically, immune checkpoint blockade is the main reason for tumor cell escape. Therefore, further detection was carried out and revealed that there was no PD-L1 expression on the surface of parental Y79RB cells. After co-culture with 4SCAR-GD2 T, the expression of PD-L1 on the surface of Y79RB cells was up-regulated, and the expression of PD-1 on the surface of 4SCAR-GD2 T in the co-culture system was also up-regulated. This result indicates that PD1: PD-L1 is involved in the immune escape of tumor cells and suppresses the function of CAR T cells after repeated antigen exposure.

PD-1

Programmed cell death 1 (PD-1), programmed cell death ligand 1 (PD-L1), and cytotoxic T lymphocyte-associated antigen-4 (CTLA-4), have been the focus of research in immunotherapy fields (Figure 2). Promising results regarding their efficacy in fighting tumors in patients with advanced tumors continue to emerge (27). An indication of cancer, as noted in numerous publications, is the absence of immune control (28). Closely associated with tumorigenesis and progression and playing a key role in tumor immune escape and TME formation is PD-1 and its ligand PD-L1 (29). PD-1 is commonly expressed on the surface of activated immune cells, such as T cells, B cells, and bone marrow cells. These two ligands, PD-L1 (B7-H1) and PD-L2 (B7-DC), expressed mainly in the placenta, tonsil, and retina, both belong to the B7 family of cell surface glycoproteins (30).PD-L1 is expressed in non-hematopoietic cells such as endothelial, epithelial, and tumor cells and appears in dendritic cells, myeloid cells, T and B cells, and other hematopoietic cells (31). A widely accepted method to assess PD-1/PD-L1 expression in cancer biology is immunohistochemistry. The most widely used practice for predictive biomarker detection of anti-PD-1/PD-L1 and CTLA-4 therapies in tumors is IHC for PD-L1 protein expression (32).

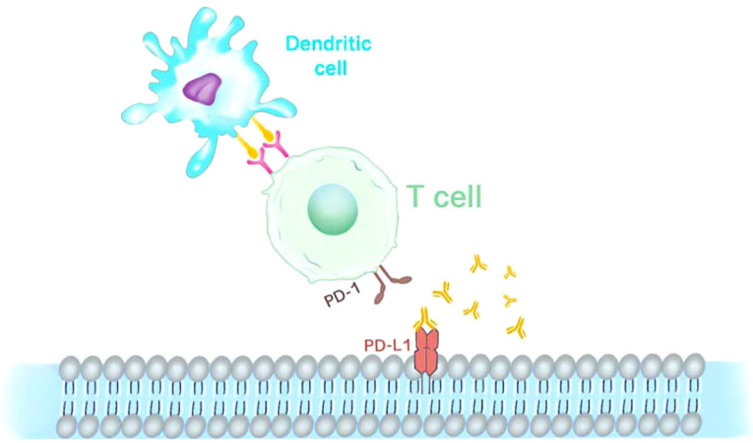

FIGURE 2
Immunotherapy anti PD-1 and PD-L1. PD-1 is expressed on the surface of CAR-T cells as an inhibitory receptor, while its ligands PD-L1 is mainly expressed in antigen-presenting cells and tumor cells.

The role of PD-1 in cancer immune evasion has been demonstrated because, as a ligand for PD-1, PD-L1 is highly expressed in some cancers (33). PD-L1 expression is not difficult to find in many tumor types, such as melanoma and glioblastoma, lung, kidney, head and neck, gastric, colon, pancreatic, breast, cervical, uterine, and ovarian cancers (34). PD-L1 is also expressed in hematological malignancies, such as multiple myeloma, lymphoma, and various leukemia types, and is associated with a worsening prognosis (35). However, the altered pattern of tumor microenvironment in primary and chemotherapeutic tumors has been documented in previous studies. However, the differences in histopathological findings and expression of immune markers in cases of primary retinoblastoma (group I) and chemotherapeutic retinoblastoma (group II) have remained to be studied to date. In Singh's study, the expression patterns of PD-1, PD-L1, and CTLA-4 proteins differed in both groups of retinoblastomas. There was increased expression of PD-L1 (46/144) and decreased expression of PD-1 (29/144) in primary retinoblastoma. A statistically significant overall survival rate was observed in PD-L1-expressing tumors (89.13%; P value = 0.015) compared to PD-1 expression (93.10%; P value = 0.394). In chemically induced retinoblastoma, on the other hand, the opposite pattern was observed, with increased expression of PD-1 (48/118) and decreased expression of PD-L1 (22/118). PD-1 expression was statistically found to correlate with overall survival in chemically induced patients (63.28%; P value = 0.003). While no clear correlation was found with patient outcomes, CTLA-4 protein expression revealed a similar pattern in both primary and chemically induced retinoblastoma. While evidence suggests that intrinsic expression of PD-1 promotes tumor growth independent of adaptive immunity in a variety of factors involving gene copy number alterations, epigenetic modifications, and the tumor microenvironment in tumor cell lines, the exact mechanism by which PD-1 may be expressed within tumor cells has not been clarified (32, 36–38).

B7H3

PD-L1 and PD-1, members of the B7 family, have been evaluated in many studies for both expressions in RB (39, 40). Researchers previously subjected primary retinoblastoma and retinal tissue to a membrane proteomics study (41). The study compared their expression of immunotherapeutic molecules, and one of the B7 family checkpoint molecules, B7-H3 (CD276), was overexpressed in RB tumors compared to retinal tissue. Many studies have shown that overexpression of B7H3 in some malignancies can cause metastasis or severe complications of cancer (42–47). B7H3 expression is highly heterogeneous. Interestingly, when B7H3 levels are high in the lobules, they are deficient in the blood vessels in the areas adjacent to the lobules and vice versa. Several studies have reported the expression of B7H3 in tumor vessels and tumor cells (48). In different diseases, B7H3 is differentially expressed in the stroma and tumor cells; for example, in colorectal and pancreatic cancers, a higher percentage of B7H3 was positive in stroma than in tumor cells, whereas in prostate cancer, B7H3 expression was higher in tumor cells than in stroma; in RB tumors, B7H3 was observed in mutually exclusive expression in tumors and blood vessels, which has not been reported in other cancer types. This result needs to be further investigated and examined whether it is related to cells in the vasculature, such as endothelial cells, or stromal cells surrounding the vasculature, such as pericytes and fibroblasts, or whether it is related to differences between pre-existing and newly generated vessels. Since the clinical importance of any target molecule in RB tumors depends on

certain histopathological features, the expression of B7H3 in terms of differentiation status, site of invasion, and degree of asexual reproduction of the tumor which is closely related to the prognosis of the disease were investigated. Among these, in terms of differentiation status, B7H3 is highly expressed in poorly differentiated RB and less expressed in moderately or well-differentiated RB tumors. A retrospective study of 326 primary RB tumors, showed that poorly differentiated tumors were significantly associated with more than three high-risk symptoms, particularly massive choroidal invasion (49). The high expression of B7H3 in such tumors is beneficial for targeted therapy.

The common metastatic areas of RB tumors are the central nervous system (CNS), regional lymph nodes, bone marrow, and bone (50). Its invasive status determines the areas where it metastasizes. The invasion sites are classified as neurological and non-neurological, depending on their prognosis and the area of metastasis. Neurological invasion leads mainly to CNS metastasis, whereas non-neurological invasion tends to metastasize more to other systemic sites (51). Among them, CNS metastasis has a poorer prognosis, probably because chemotherapeutic agents cannot cross the blood-brain barrier19, in which case adjuvant intrathecal or intracerebral chemotherapy is required (52, 53). Compared with neural tissue, B7H3 expression in invading non-neural tissue of RB tumors showed a significant increase (54). B7H3 expression may be suppressed when the tumor invades the optic nerve (40). However, we could not find any support from the published literature. One limitation is the number of samples that could be analyzed for this correlation; however, if built with a larger cohort, this finding may have clinical implications for the use of B7H3 as a therapeutic approach.

There is a significant anti-tumor activity demonstrated by B7-H3-targeted CAR-T cells against AML and melanoma for both *in vitro* and xenograft mouse models. In clinical trials, multiple therapeutic agents targeting B7-H3 have been conducted. As an Fc-optimized monoclonal antibody (mAb) against B7-H3, Enoblituzumab has been evaluated together with an anti-programmed death 1 (PD-1) monoclonal antibody in patients with B7-H3-expressing solid tumors during phase I clinical study (Figure 3A). Another B7-H3-targeting antibody for the treatment of brain and central nervous system tumors, neuroblastoma, and carcinoma, radiolabeled 8H9, was also evaluated in a phase I trial. (ClinicalTrials.gov: NCT00089245). MGD009 is a bispecific antibody developed by MacroGenics against B7-H3 and CD3, while the FDA partially shelved the two clinical studies on MGD009 due to hepatotoxic events in monotherapy trials, such as reversible transaminase level increases with or without concomitant bilirubin level increases (55) (Figure 3B).

The presence of B7H3 in RB tumors opens the way for developing targeted therapeutic and immunotherapeutic approaches. Furthermore, it is interesting to observe that the expression of B7H3 is reduced when the tumor enters the optic nerve, so the next step should focus on the presence of molecules that reduce B7H3 in the optic nerve bundle and their implications for clinical treatment. Clinical data with 1 to 4 years of follow-up did not show any significant correlation between patient survival and B7H3 expression. One with long-term follow-up data is needed further to understand the correlation between B7H3 expression and RB prognosis.

EpCAM

Epithelial cell adhesion molecule (EpCAM) was earlier considered as a marker for adult liver stem/progenitor cells and oval cells (56, 57), which is an epithelial cell adhesion molecule with all the characteristics of tumor stem cells (CSCs). EpCAM is highly expressed in aggressive tumors compared to RB, a non-invasive tumor. Damages to the EpCAM gene may result in a substantial decrease in cell proliferative capacity (58). Bispecific antibodies (bsAb) are artificial molecules with dual specificity for two separate antigens. The most common bsAb antigen on lymphocytes is an invariant CD3 signaling complex that induces the activation of polyclonal T cells. A number of anti-EpCAM bsAb and single-chain antibodies have been produced and tested as immunotherapeutics (Figure 4) (56, 59–62). The host antitumor immunity has a significant contribution to preventing the development of malignant tumors. However, when tumor cells lack tumor-associated antigens or various co-stimulatory or major histocompatibility complex molecules, the host mononuclear cells may become dysfunctional. Aggressive RB primary tumors express low levels of human leukocyte antigen (HLA) class I and II antigens, which may be an advantage for tumor cells to escape t-cell or natural killer (NK) cell-mediated attack (63). In this context, the potential of a novel therapeutic modality using the bispecific antibody-directed T-cell attack on tumor cells may become a promising treatment for retinoblastoma. The bispecific antibody can effectively induce lysis of tumor cells *in vitro*, thus reducing the production of malignant ascites in patients with advanced ovarian cancer (64). Mitra et al. studied the role and expression of EpCAM in the development of retinoblastoma (65). The study found that EpCAM+Y79 cells have strong proliferation and invasion ability and neurosphere formation ability. Using fresh retinoblastoma tissue, the co-expression of EpCAM and three other putative tumor stem cell markers CD44, CD24 and ABCG2 was examined. The results showed that not every tumor tissue expressed CD44, CD24 or ABCG2, but the expression of EpCAM could be detected. The use of preactivated PBMC and bispecific antibodies to EpCAM × CD3 can promote lysis of RB cells. Therefore, targeting CSC combined with conventional chemotherapy should be the basic therapeutic strategy for eradicating tumors. EpCAM is an attractive target for bsAb and bispecific single-chain antibodies for antitumor therapy (66–68).

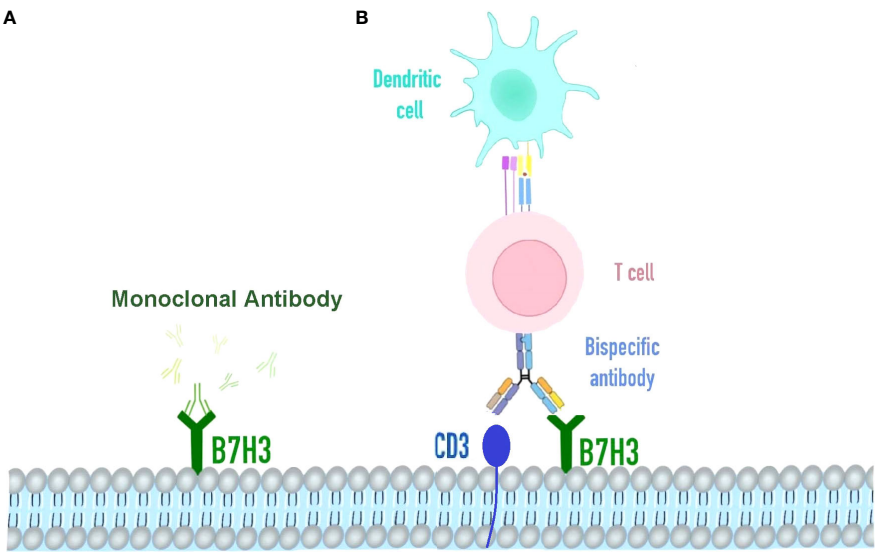

FIGURE 3
Immunotherapy strategy targeting B7H3. **(A)** Omburtamab is a radionuclide iodine-131-labeled monoclonal antibody targeting B7H3 cells in various solid tumors, including retinoblastoma. It binds to the FG cyclically dependent conformation, a key region of the biological function of the B7-H3 molecule. **(B)** Bispecific antibody of B7H3 and CD3, redirecting T cells and accessory immune cells.

Moreover, EpCAM×CD3 activity is dose-dependent and increases within 24 h. This effect was consistently observed in all five tumor types examined. The production of effector cytokines was raised in the supernatant of cultures containing EpCAM+ cells and pre-activated PBMC as well as EpCAM×CD3, as demonstrated by our ELISA assay. In summary, EpCAM×CD3 potently stimulates the secretion of effector cytokines by pre-activated lymphocytes in the presence of EpCAM-expressing tumor cells. Activated T cells secreting TNF-α, IFN-γ, and chemokines may increase efficacy by enhancing immune cell attraction and stimulation. It has been proven that high levels of IL-10 in the tumor microenvironment facilitate tumor rejection by potentiating the cytotoxicity of T lymphocytes (69). TGF-β functions as a tumor cell suppressor (70), suggesting that a bispecific antibody-mediated immunotherapeutic approach may potentially help manage the proliferation of RB tumor cells. A high percentage of cells in retinoblastoma express EpCAM, and especially tumors with optic nerve/choroidal invasion

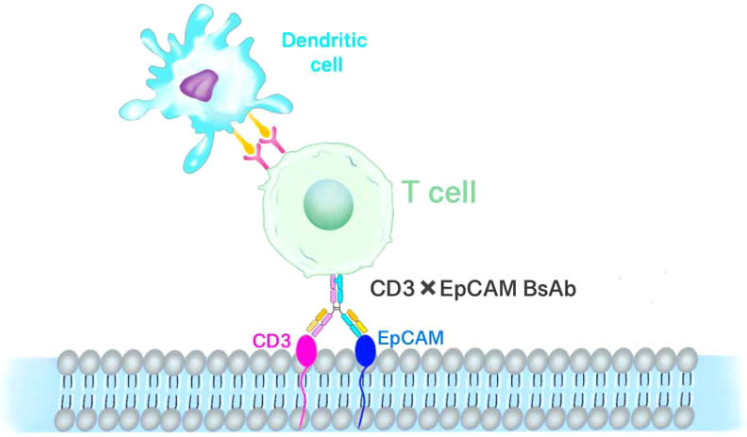

FIGURE 4
T-cell-mediated immunotherapy of EpCAM. EpCAM and CD3 bispecific antibodies redirect T lymphocytes to attack retinoblastoma cells.

demonstrate increased EpCAM expression (63). Therefore, the invasive retinoblastoma is an attractive tumor for therapeutic targeting using a bispecific antibody (EpCAM × CD3). In summary, EpCAM + RB cells behave *in vitro* similarly to tumor stem cells. In the presence of EpCAM expressing RB tumor cells, EpCAM×CD3 has potent anti-tumor activation *in vitro via* induction of interleukin and cytokine secretion by pre-activated lymphocytes.

SYK

The spleen tyrosine kinase (SYK) is one of the most dramatically upregulated kinase genes in RB cells (71). It is involved in signaling the inflammatory cell B-cell receptor complex in the inflammatory response and has also been associated with hematopoietic malignancies (72–74). There are two SYK isoforms in tumor cells, the full-length SYK (SYK-L) and the variable splice SYK transcript (SYK-S). Among them, SYK-L can enter the nucleus and prevent cancer cell invasion. At the same time, SYK-S is only found in the cytoplasm, where it can promote tumor development and is a proto-oncogene involved in the survival of RB cells. However, SYK is not expressed in retinal progenitor cells or neurons, and no function has been found in the developing visual system. ChIP-on-chip analysis revealed increased histone activation modifications (H3K4me3 and K3K9/14Ac) at the SYK promoter, whereas the histone repression marker (H3k9me3) was unchanged in human retinoblastoma *in situ* xenografts and cell lines (71). There was also an increase in RNA polymerase II bound to the SYK promoter. ChIP-on-chip results confirmed increased expression of the SYK gene. SYK protein was found at higher levels in human retinoblastoma *in situ* xenografts and cell lines than in human fetal retina. Retinoblastoma tissue microarrays (TMA) or whole eye sections were subjected to immunohistochemistry. The results indicated that SYK was heavily expressed (3+) in all tumor cells (82/82), while normal retinas had no expression of SYK. The kinase activity of SYK is regulated by autophosphorylation of the Tyr525/526 residues within its catalytic domain. In retinoblastoma cells, the sites are phosphorylated and reversed.

Although SYK was consistently immunonegative in non-neoplastic lesions and pseudo retinoblastoma eyes, conversely, it was histologically immunopositive in any RB eyes (75). Strong immunostaining of SYK is found in RB eyes - the nucleus and cytoplasm of RB cells. While SYK is silenced in benign retinas, it is activated in RB. In differentiating malignant tumors from benign diseases in the retina, SYK is also a good marker. SYK, an important promoter of tumorigenesis in RB, showed a more significant negative correlation between its expression and tumor necrosis. However, pseudo retinoblastoma is usually undetectable by clinical and diagnostic imaging techniques because its symptoms and clinical findings are comparable to those of RB. The above results suggest that SYK can be used in a protein-based or genetic approach to differentiate these disease possibilities and so is a useful clinical marker.

Since SYK expression is required for retinoblastoma growth and survival, X Chen et al. (76) synthesized SYK shRNA and cloned it into the lentivirus vector Lenti-SYK-9. In addition to accelerating apoptosis of retinoblastoma cells, Lenti-SYK-9 effectively removed SYK from retinoblastoma cell lines. Further to the previous efforts, the researchers used lentivirus to genetically modify dendritic cells (DC) to make cytotoxic T lymphocytes (CTL) express SYK antigens *in vitro*. SYK-negative cell lines (MDA-MB-231, MCF-10A, hTERT-RPE1) and SYK-positive cell lines (MCF-7 and RB-Y79) were used to assess the specificity and cytotoxicity of DCs expressing CTLs. The CTL toxicity triggered by SYK-high expression in DCs Figure 5 (SYK-DC-CTLs) elevated the killing effect on SYK-positive cells by more than three times compared to SYK-negative cells. SYK-modified DCS had a CTL cytotoxic effect on SYK-positive cell lines, but no killing effect on SYK-negative cell lines. Although SYK-silenced RB-Y79 cells potently bypassed the cytotoxic attack of SYK-DC-CTL, SYK-DC-CTLs were overexpressed in hTERT-RPE 1 cells, suggesting that SYK is a specific antigen for Rb. In addition, SYK-DC-CTL had specific cytotoxic effects on carboplatin-resistant RB-Y79 cells *in vitro*.

Exposure of Y79 cells to different doses of lymphocyte-derived microparticles (LMPs) was studied by Qian Q et al. (77). The results revealed that SYK mRNA was significantly diminished with 20 μg/ml of LMPs. For 24 h, treatment of human retinoblastoma cells with 20μg/ml LMPs was carried out and the expression of SYK protein was analyzed by Western blot. The results also showed that LMPs significantly inhibited the expression of SYK protein. LMPs can downregulate SYK and induce retinoblastoma cell death, as further supported by the immunohistochemical results of SYK expression.

These findings suggest that this gene may contribute to RB tumor development (71), and therefore SYK may be a potential target for RB therapy.

Discussion

The World Health Organization (WHO) has selected Retinoblastoma as a high-priority tumor for the Global Initiative for Childhood Cancer. The initial cure rate is high, yet it is potentially lethal when not treated promptly. Ocular palliative approaches have made great strides during the last few decades, making it the most treatable pediatric cancer for intraocular retinoblastoma in a high-income country. There have been developments in delivery methods locally enabling chemotherapy to maximize exposure in the retinal, subretinal, and vitreous spaces, i.e., improved techniques for safe ophthalmic artery chemosurgery (OAC) and intravitreous chemotherapy (IVi) injections which have

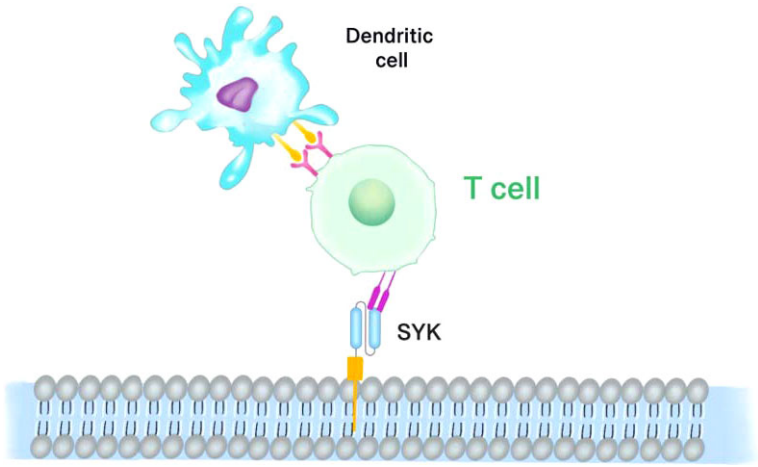

FIGURE 5
SYK-targeted dendritic cell-mediated CAR-T cells. Dendritic cells (DCs) which expressing and presenting the SYK peptide antigen are modified to cytotoxic T lymphocytes (CTL). SYK-overexpressing DCs induce the cytotoxicity of CTL.

led to the maintenance of ocular and visual acuity at levels never seen before. Critically, these new local therapies provide the retina and optic nerve access to chemotherapy at very high intensities, as seen in preclinical models, thus capable of blocking the spread of tumors to the central nervous system. After more than a decade of consistent access in major clinical centers worldwide and over 200 publications related to this field, the OAC and IVi have proven safe and reliable without increasing the risk of metastatic dissemination. By eliminating EBRT and systemic chemotherapy, long-term survival is improved with these therapies by reducing the incidence of treatment-related severe toxicities, the risk of secondary malignancies, and associated mortality.

Unfortunately, children suffering from disseminated retinoblastoma have virtually no options for treatment. New therapeutic strategies are expected to be highly effective for both intraocular and extraocular diseases, provided that the risk of toxicity is lower. In addition, the availability of more new non-chemotherapy therapies gives patients more options, such as targeted therapies, immunotherapy, and lysing viruses.

Author contributions

LW, JM and LY contributed to the conception of the manuscript. LW and SL wrote the manuscript and drew the pattern diagrams. All authors contributed to the article and approved the submitted version.

Funding

This study was funded by the National Natural Science Foundation of China (81870626), Science and Technology Plan Project of Shenzhen, China (JCYJ20170306123423907, JCYJ20210324125805012).

Conflict of interest

The authors declare that the research was conducted in the absence of any commercial or financial relationships that could be construed as a potential conflict of interest.

Publisher's note

References

1. Soliman SE, Racher H, Zhang C, MacDonald H, Gallie BL. Genetics and molecular diagnostics in retinoblastoma–an update. *Asia-Pac J Ophthalmol* (2017) 6(2):197–207. doi: 10.22608/APO.201711

2. Yanik O, Gunduz K, Yavuz K, Tacyildiz N, Unal E. Chemotherapy in retinoblastoma: Current approaches. *Turkish J Ophthalmol* (2015) 45(6):259–67. doi: 10.4274/tjo.06888

3. Temming P, Arendt M, Viehmann A, Eisele L, Le Guin CH, Schundeln MM, et al. Incidence of second cancers after radiotherapy and systemic chemotherapy in heritable retinoblastoma survivors: A report from the German reference center. *Pediatr Blood Cancer* (2017) 64(1):71–80. doi: 10.1002/pbc.26193

4. Clarissa A, Sutandi N, Fath AA. Stem-cell therapy following high-dose chemotherapy in advanced retinoblastoma: A systematic review. *Asia-Pac J Ophthalmol* (2021) 10(4):397–407. doi: 10.1097/APO.0000000000000372

5. Temming P, Lohmann D, Bornfeld N, Sauerwein W, Goericke SL, Eggert A. Current concepts for diagnosis and treatment of retinoblastoma in Germany: Aiming for safe tumor control and vision preservation. *Klin Padiatr* (2012) 224 (6):339–47. doi: 10.1055/s-0032-1327563

6. Shields CL, Shields JA, Baez KA, Cater J, De Potter PV. Choroidal invasion of retinoblastoma: Metastatic potential and clinical risk factors. *Br J Ophthalmol* (1993) 77(9):544–8. doi: 10.1136/bjo.77.9.544

7. Chen F, Zhuang X, Lin L, Yu P, Wang Y, Shi Y, et al. New horizons in tumor microenvironment biology: Challenges and opportunities. *BMC Med* (2015) 13:45. doi: 10.1186/s12916-015-0278-7

8. Wang M, Zhao J, Zhang L, Wei F, Lian Y, Wu Y, et al. Role of tumor microenvironment in tumorigenesis. *J Cancer* (2017) 8(5):761–73. doi: 10.7150/jca.17648

9. Sachdeva UM, O'Brien JM. Understanding pRb: toward the necessary development of targeted treatments for retinoblastoma. *J Clin Invest* (2012) 122 (2):425–34. doi: 10.1172/JCI57114

10. Quail DF, Joyce JA. Microenvironmental regulation of tumor progression and metastasis. *Nat Med* (2013) 19(11):1423–37. doi: 10.1038/nm.3394

11. Fang H, Declerck YA. Targeting the tumor microenvironment: From understanding pathways to effective clinical trials. *Cancer Res* (2013) 73 (16):4965–77. doi: 10.1158/0008-5472.CAN-13-0661

12. Suzuki M, Cheung NK. Disialoganglioside GD2 as a therapeutic target for human diseases. *Expert Opin Ther Targets* (2015) 19(3):349–62. doi: 10.1517/14728222.2014.986459

13. Durbas M, Horwacik I, Boratyn E, Kamycka E, Rokita H. GD2 ganglioside specific antibody treatment downregulates PI3K/Akt/mTOR signaling network in human neuroblastoma cell lines. *Int J Oncol* (2015) 47(3):1143–59. doi: 10.3892/ijo.2015.3070

14. Julien S, Bobowski M, Steenackers A, Le Bourhis X, Delannoy P. How do gangliosides regulate RTKs signaling? *Cells* (2013) 2(4):751–67. doi: 10.3390/cells2040751

15. Iwasawa T, Zhang P, Ohkawa Y, Momota H, Wakabayashi T, Ohmi Y, et al. Enhancement of malignant properties of human glioma cells by ganglioside GD3/GD2. *Int J Oncol* (2018) 52(4):1255–66. doi: 10.3892/ijo.2018.4266

16. Portoukalian J, David MJ, Gain P, Richard M. Shedding of GD2 ganglioside in patients with retinoblastoma. *Int J Cancer* (1993) 53(6):948–51. doi: 10.1002/ijc.2910530614

17. Roth M, Linkowski M, Tarim J, Piperdi S, Sowers R, Geller D, et al. Ganglioside GD2 as a therapeutic target for antibody-mediated therapy in patients with osteosarcoma. *Cancer* (2014) 120(4):548–54. doi: 10.1002/cncr.28461

18. Zugbi S, Ganiewich D, Bhattacharyya A, Aschero R, Ottaviani D, Sampor C, et al. Clinical, genomic, and pharmacological study of MYCN-amplified RB1 wild-type metastatic retinoblastoma. *Cancers* (2020) 12(9):2714. doi: 10.3390/cancers12092714

19. Eagle RC, Shields JA, Donoso L, Milner RS. Malignant transformation of spontaneously regressed retinoblastoma, Retinoma/Retinocytoma variant. *Ophthalmology* (1989) 96(9):1389–95. doi: 10.1016/S0161-6420(89)32714-X

20. Shen H, Tang Y, Xu X, Tang H. Detection of the GD2+/CD56+/CD45- immunophenotype by flow cytometry in cerebrospinal fluids from a patient with retinoblastoma. *Pediatr Hematol Oncol* (2013) 30(1):30–2. doi: 10.3109/08880018.2012.737094

21. Yu AL, Gilman AL, Ozkaynak MF, London WB, Kreissman SG, Chen HX, et al. Anti-GD2 antibody with GM-CSF, interleukin-2, and isotretinoin for neuroblastoma. *N Engl J Med* (2010) 363(14):1324–34. doi: 10.1056/NEJMoa0911123

22. Sadelain M, Brentjens R, Riviere I. The basic principles of chimeric antigen receptor design. *Cancer Discov* (2013) 3(4):388–98. doi: 10.1158/2159-8290.CD-12-0548

23. Nazha B, Inal C, Owonikoko TK. Disialoganglioside GD2 expression in solid tumors and role as a target for cancer therapy. *Front Oncol* (2020) 10:1000. doi: 10.3389/fonc.2020.01000

24. Michelle LT, Lisa WD, Marta F, Ronald RK, Miranda PD, Natasha KA, et al. Anti-GD2 based immunotherapy prevents late events in high-risk neuroblastoma patients over 18 months at diagnosis. *Cancers (Basel)* (2021) 13(19):4941. doi: 10.3390/cancers13194941

25. Wayne LF, Beth MC, Barry LS, Andrew D, Matthew K, Chia WH, et al. Improved outcome in children with newly diagnosed high-risk neuroblastoma treated with chemoimmunotherapy: Updated results of a phase II study using hu14.18K322A. *J Clin Oncol* (2022) 40(4):335–44. doi: 10.1200/JCO.21.01375

26. Jatuporn S, Elias S, Shih TT, Mongkol U, Kleebsabai S, Jassada B, et al. GD2-specific chimeric antigen receptor-modified T cells targeting retinoblastoma – assessing tumor and T cell interaction. *Trans Oncol* (2021) 14:100971. doi: 10.1016/j.tranon.2020.100971

27. Seidel JA, Otsuka A, Kabashima K. Anti-PD-1 and anti-CTLA-4 therapies in cancer: Mechanisms of action, efficacy, and limitations. *Front Oncol* (2018) 8:86. doi: 10.3389/fonc.2018.00086

28. Hanahan D, Weinberg RA. Hallmarks of cancer: the next generation. *Cell* (2011) 144(5):646–74. doi: 10.1016/j.cell.2011.02.013

29. Henick BS, Herbst RS, Goldberg SB. The PD-1 pathway as a therapeutic target to overcome immune escape mechanisms in cancer. *Expert Opin Ther Targets* (2014) 18(12):1407–20. doi: 10.1517/14728222.2014.955794

30. Yang W, Li H, Chen PW, Alizadeh H, He Y, Hogan RN, et al. PD-L1 expression on human ocular cells and its possible role in regulating immune-mediated ocular inflammation. *Invest Ophthalmol Visual Sci* (2009) 50(1):273–80. doi: 10.1167/iovs.08-2397

31. Alsaab HO, Sau S, Alzhrani R, Tatiparti K, Bhise K, Kashaw SK, et al. PD-1 and PD-L1 checkpoint signaling inhibition for cancer immunotherapy: Mechanism, combinations, and clinical outcome. *Front Pharmacol* (2017) 8:561. doi: 10.3389/fphar.2017.00561

32. Udall M, Rizzo M, Kenny J, Doherty J, Dahm S, Robbins P, et al. PD-L1 diagnostic tests: A systematic literature review of scoring algorithms and test-validation metrics. *Diagn Pathol* (2018) 13(1):12. doi: 10.1186/s13000-018-0689-9

33. Juneja VR, McGuire KA, Manguso RT, LaFleur MW, Collins N, Haining WN, et al. PD-L1 on tumor cells is sufficient for immune evasion in immunogenic tumors and inhibits CD8 T cell cytotoxicity. *J Exp Med* (2017) 214(4):895–904. doi: 10.1084/jem.20160801

34. Wang Q, Liu F, Liu L. Prognostic significance of PD-L1 in solid tumor: An updated meta-analysis. *Medicine* (2017) 96(18):e6369. doi: 10.1097/MD.0000000000006369

35. Pianko MJ, Liu Y, Bagchi S, Lesokhin AM. Immune checkpoint blockade for hematologic malignancies: A review. *Stem Cell Invest* (2017) 4:32. doi: 10.21037/sci.2017.03.04

36. Kleffel S, Posch C, Barthel SR, Mueller H, Schlapbach C, Guenova E, et al. Melanoma cell-intrinsic PD-1 receptor functions promote tumor growth. *Cell* (2015) 162(6):1242–56. doi: 10.1016/j.cell.2015.08.052

37. Du S, McCall N, Park K, Guan Q, Fontina P, Ertel A, et al. Blockade of tumor-expressed PD-1 promotes lung cancer growth. *Oncoimmunology* (2018) 7 (4):e1408747. doi: 10.1080/2162402X.2017.1408747

38. Yao H, Wang H, Li C, Fang JY, Xu J. Cancer cell-intrinsic PD-1 and implications in combinatorial immunotherapy. *Front Immunol* (2018) 9:1774. doi: 10.3389/fimmu.2018.01774

39. Shields CL, Manjandavida FP, Lally SE, Pieretti G, Arepalli SA, Caywood EH, et al. Intra-arterial chemotherapy for retinoblastoma in 70 eyes: Outcomes based on the international classification of retinoblastoma. *Ophthalmology* (2014) 121(7):1453–60. doi: 10.1016/j.ophtha.2014.01.026

40. Ganesan B, Parameswaran S, Sharma A, Krishnakumar S. Clinical relevance of B7H3 expression in retinoblastoma. *Sci Rep* (2020) 10(1):10185. doi: 10.1038/s41598-020-67101-7

41. Yousef YA, Soliman SE, Astudillo PPP, Durairaj P, Dimaras H, Chan HSL, et al. Intra-arterial chemotherapy for retinoblastoma: A systematic review. *JAMA Ophthalmol* (2016) 134(5):584–91. doi: 10.1001/jamaophthalmol.2016.0244

42. Zhao X, Li DC, Zhu XG, Gan WJ, Li Z, Xiong F, et al. B7-H3 overexpression in pancreatic cancer promotes tumor progression. *Int J Mol Med* (2013) 31(2):283–91. doi: 10.3892/ijmm.2012.1212

43. Tekle C, Nygren MK, Chen YW, Dybsjord I, Nesland JM, Maelandsmo GM, et al. B7-H3 contributes to the metastatic capacity of melanoma cells by modulation of known metastasis-associated genes. *Int J Cancer* (2012) 130 (10):2282–90. doi: 10.1002/ijc.26238

44. Zheng Y, Liao N, Wu Y, Gao J, Li Z, Liu W, et al. High expression of B7H2 or B7H3 is associated with poor prognosis in hepatocellular carcinoma. *Mol Med Rep* (2019) 19(5):4315–25. doi: 10.3892/mmr.2019.10080

45. Ye Z, Zheng Z, Li X, Zhu Y, Zhong Z, Peng L, et al. B7-H3 overexpression predicts poor survival of cancer patients: A meta-analysis. *Cell Physiol Biochem: Int J Exp Cell Physiol Biochem Pharmacol* (2016) 39(4):1568–80. doi: 10.1159/000447859

46. Han S, Shi X, Liu L, Zong L, Zhang J, Chen Q, et al. Roles of B7-H3 in cervical cancer and its prognostic value. *J Cancer* (2018) 9(15):2612–24. doi: 10.7150/jca.24959

47. Chen JT, Chen CH, Ku KL, Hsiao M, Chiang CP, Hsu TL, et al. Glycoprotein B7-H3 overexpression and aberrant glycosylation in oral cancer and immune response. *Proc Natl Acad Sci USA* (2015) 112(42):13057–62. doi: 10.1073/pnas.1516991112

48. Dimaras H, Corson TW. Retinoblastoma, the visible CNS tumor: A review. *J Neurosci Res* (2019) 97(1):29–44. doi: 10.1002/jnr.24213

49. Kashyap S, Meel R, Pushker N, Sen S, Bakhshi S, Sreenivas V, et al. Clinical predictors of high risk histopathology in retinoblastoma. *Pediatr Blood Cancer* (2012) 58(3):356–61. doi: 10.1002/pbc.23239

50. Raguraman R, Parameswaran S, Kanwar JR, Khetan V, Rishi P, Kanwar RK, et al. Evidence of tumour microenvironment and stromal cellular components in retinoblastoma. *Ocular Oncol Pathol* (2019) 5(2):85–93. doi: 10.1159/000488709

51. Dimaras H, Heon E, Budning A, Doyle JJ, Halliday W, Gallie BL, et al. Retinoblastoma CSF metastasis cured by multimodality chemotherapy without radiation. *Ophthal Genet* (2009) 30(3):121–6. doi: 10.1080/13816810902988780

52. Rodriguez A, Zugbi S, Requejo F, Deu A, Sampor C, Sgroi M, et al. Combined high-dose intra-arterial and intrathecal chemotherapy for the treatment of a case of extraocular retinoblastoma. *Pediatr Blood Cancer* (2018) 65(12):e27385. doi: 10.1002/pbc.27385

53. Bonaventura P, Shekarian T, Alcazer V, Valladeau-Guilemond J, Valsesia-Wittmann S, Amigorena S, et al. Cold tumors: A therapeutic challenge for immunotherapy. *Front Immunol* (2019) 10:168. doi: 10.3389/fimmu.2019.00168

54. Ravindran K, Dalvin LA, Pulido JS, Brinjikji W. Intra-arterial chemotherapy for retinoblastoma: An updated systematic review and meta-analysis. *J Neurointerv Surg* (2019) 11(12):1266–72. doi: 10.1136/neurintsurg-2019-014909

55. Zhang Z, Jiang C, Liu Z, Yang M, Tang X, Wang Y, et al. B7-H3-Targeted CAR-T cells exhibit potent antitumor effects on hematologic and solid tumors. *Mol Ther Oncol* (2020) 17:180–9. doi: 10.1016/j.omto.2020.03.019

56. Schmelzer E, Zhang L, Bruce A, Wauthier E, Ludlow J, Yao HL, et al. Human hepatic stem cells from fetal and postnatal donors. *J Exp Med* (2007) 204 (8):1973–87. doi: 10.1084/jem.20061603

57. Tanaka M, Okabe M, Suzuki K, Kamiya Y, Tsukahara Y, Saito S, et al. Mouse hepatoblasts at distinct developmental stages are characterized by expression of EpCAM and DLK1: Drastic change of EpCAM expression during liver development. *Mech Dev* (2009) 126(8-9):665–76. doi: 10.1016/j.mod.2009.06.939

58. Mitra M, Kandalam M, Verma RS, Maheswari KU, Krishnakumar S. Genome-wide changes accompanying the knockdown of ep-CAM in retinoblastoma. *Mol Vis* (2010) 16:828–42. doi: 10.1016/j.visres.2010.02.023

59. Morecki S, Lindhofer H, Yacovlev E, Gelfand Y, Ruf P, Slavin S. Induction of long-lasting antitumor immunity by concomitant cell therapy with allogeneic lymphocytes and trifunctional bispecific antibody. *Exp Hematol* (2008) 36 (8):997–1003. doi: 10.1016/j.exphem.2008.03.005

60. Wolf E, Hofmeister R, Kufer P, Schlereth B, Baeuerle PA. BiTEs: bispecific antibody constructs with unique anti-tumor activity. *Drug Discov Today* (2005) 10 (18):1237–44. doi: 10.1016/S1359-6446(05)03554-3

61. Burges A, Wimberger P, Kumper C, Gorbounova V, Sommer H, Schmalfeldt B, et al. Effective relief of malignant ascites in patients with advanced ovarian cancer by a trifunctional anti-EpCAM x anti-CD3 antibody: A phase I/II study. *Clin Cancer Res: Off J Am Assoc Cancer Res* (2007) 13(13):3899–905. doi: 10.1158/1078-0432.CCR-06-2769

62. Amann M, Brischwein K, Lutterbuese P, Parr L, Petersen L, Lorenczewski G, et al. Therapeutic window of MuS110, a single-chain antibody construct bispecific for murine EpCAM and murine CD3. *Cancer Res* (2008) 68(1):143–51. doi: 10.1158/0008-5472.CAN-07-2182

63. Krishnakumar S, Sundaram A, Abhyankar D, Krishnamurthy V, Shanmugam MP, Gopal L, et al. Major histocompatibility antigens and antigen-processing molecules in retinoblastoma. *Cancer* (2004) 100(5):1059–69. doi: 10.1002/cncr.20062

64. Marme A, Strauss G, Bastert G, Grischke EM, Moldenhauer G. Intraperitoneal bispecific antibody (HEA125xOKT3) therapy inhibits malignant ascites production in advanced ovarian carcinoma. *Int J Cancer* (2002) 101(2):183–9. doi: 10.1002/ijc.10562

65. Mitra M, Kandalam M, Harilal A, Verma RS, Krishnan UM. EpCAM is a putative stem marker in retinoblastoma and an effective target for T-cell-mediated immunotherapy. *Mol Vision* (2012) 18:290–308. doi: 10.1207/s15328023top0604_1

66. Dean M, Fojo T, Bates S. Tumour stem cells and drug resistance. *Nat Rev Cancer* (2005) 5(4):275–84. doi: 10.1038/nrc1590

67. Sebastian M, Passlick B, Friccius-Quecke H, Jager M, Lindhofer H, Kanniess F, et al. Treatment of non-small cell lung cancer patients with the trifunctional monoclonal antibody catumaxomab (anti-EpCAM x anti-CD3): A phase I study. *Cancer Immunol Immunother: CII* (2007) 56(10):1637–44. doi: 10.1007/s00262-007-0310-7

68. Brischwein K, Schlereth B, Guller B, Steiger C, Wolf A, Lutterbuese R, et al. MT110: A novel bispecific single-chain antibody construct with high efficacy in eradicating established tumors. *Mol Immunol* (2006) 43(8):1129–43. doi: 10.1016/j.molimm.2005.07.034

69. Kang SS, Allen PM. Priming in the presence of IL-10 results in direct enhancement of CD8+ T cell primary responses and inhibition of secondary responses. *J Immunol* (2005) 174(9):5382–9. doi: 10.4049/jimmunol.174.9.5382

70. Seoane J, Gomis RR. TGF-beta family signaling in tumor suppression and cancer progression. *Cold Spring Harbor Perspect Biol* (2017) 9(12):a022277. doi: 10.1101/cshperspect.a022277

71. Zhang J, Benavente CA, McEvoy J, Flores-Otero J, Ding L, Chen X, et al. A novel retinoblastoma therapy from genomic and epigenetic analyses. *Nature* (2012) 481(7381):329–34. doi: 10.1038/nature10733

72. Chen L, Monti S, Juszczynski P, Daley J, Chen W, Witzig TE, et al. SYK-dependent tonic b-cell receptor signaling is a rational treatment target in diffuse large b-cell lymphoma. *Blood* (2008) 111(4):2230–7. doi: 10.1182/blood-2007-07-100115

73. Feldman AL, Sun DX, Law ME, Novak AJ, Attygalle AD, Thorland EC, et al. Overexpression of syk tyrosine kinase in peripheral T-cell lymphomas. *Leukemia* (2008) 22(6):1139–43. doi: 10.1038/leu.2008.77

74. Young RM, Hardy IR, Clarke RL, Lundy N, Pine P, Turner BC, et al. Mouse models of non-Hodgkin lymphoma reveal syk as an important therapeutic target. *Blood* (2009) 113(11):2508–16. doi: 10.1182/blood-2008-05-158618

75. Yang YL, Zhou H, Yue LR, Shen H. Spleen tyrosine kinase expression and its correlation with necrosis and high-risk histopathologic features in retinoblastoma. *Chin Med J* (2020) 133(14):1752–3. doi: 10.1097/CM9.0000000000000889

76. Chen X, Patricia EK, Lin J, Zhou M, Huang J, Zhang H, et al. SYK-targeted dendritic cell-mediated cytotoxic T lymphocytes enhance the effect of immunotherapy on retinoblastoma. *J Cancer Res Clin Oncol* (2018) 144(4):675–84. doi: 10.1007/s00432-018-2584-x

77. Qiu Q, Yang C, Xiong W, Tahiri H, Payeur M, Rosanne S, et al. SYK is a target of lymphocyte-derived microparticles in the induction of apoptosis of human retinoblastoma cells. *Apoptosis* (2015) 20(12):1613–22. doi: 10.1007/s10495-015-1177-2

frontiers | Frontiers in Immunology

TYPE Review
PUBLISHED 08 September 2022
DOI 10.3389/fimmu.2022.978377

OPEN ACCESS

EDITED BY
Xuyao Zhang,
Fudan University, China

REVIEWED BY
Xuanjun Wang,
Yunnan Agricultural University, China
Ting Xu,
Alphamab Co. Ltd, China

*CORRESPONDENCE
Rong Fu
furong8369@tmu.edu.cn

†These authors have contributed equally to this work

SPECIALTY SECTION
This article was submitted to Cancer Immunity and Immunotherapy, a section of the journal Frontiers in Immunology

RECEIVED 26 June 2022
ACCEPTED 23 August 2022
PUBLISHED 08 September 2022

CITATION
Liu Z, Liu X, Shen H, Xu X, Zhao X and Fu R (2022) Adenosinergic axis and immune checkpoint combination therapy in tumor: A New perspective for immunotherapy strategy. *Front. Immunol.* 13:978377. doi: 10.3389/fimmu.2022.978377

Adenosinergic axis and immune checkpoint combination therapy in tumor: A new perspective for immunotherapy strategy

Zhaoyun Liu†, Xiaohan Liu†, Hongli Shen, Xintong Xu, Xianghong Zhao and Rong Fu*

Department of Hematology, Tianjin Medical University General Hospital, Tianjin, China

There are two figures and one table in this review, the review consists of 5823 words, without the description of figures and table, but including references.

Tumor cells escape anti-tumor immune responses in various ways, including functionally shaping the microenvironment through the secretion of various chemokines and, cytokines. Adenosine is a powerful immunosuppressive metabolite, that is frequently elevated in the extracellular tumor microenvironment (TME). Thus, it has recently been proposed as a novel antitumor immunoassay for targeting adenosine- generating enzymes, such as CD39, CD73, and adenosine receptors. In recent years, the discovery of the immune checkpoints, such as programmed cell death 1(PD-1) and cytotoxic T lymphocyte antigen 4 (CTLA-4), has also greatly changed treatment methods and ideas for malignant tumors. Malignant tumor immunotherapy has been developed from point-to-point therapy targeting immune checkpoints, combining different points of different pathways to create a therapy based on the macroscopic immune regulatory system network. This article reviews the theoretical basis of the adenosine energy axis and immune checkpoint combined therapy for malignant tumors and the latest advances in malignant tumors.

KEYWORDS

adenosine, CD39, CD73, adenosine receptor 2A, PD-1, CTLA- 4

Adenosinergic axis and tumor immunology

Adenosine is an important regulator of metabolism and a key immune checkpoint regulator associated with tumors evading the host immune system (1–4). Extracellular adenosine (eADO) inhibits immune function. One of the major mechanisms of tumor immune evasion is the production of high eADO levels *via* the overexpression of ectonucleotidases (5–7). An effective immunosuppressive microenvironment is

sustained when ADO functions synergistically or in combination with other immunosuppressive mechanisms (8). In 2006, high extracellular adenosine levels in tumors were discovered to play a key role in evading antitumor immune responses (9), and an environment rich in adenosine in the tumor may induce incompetent T cells (1, 10–12). The adenosine pathway is currently considered important for the effectiveness of immunotherapy and has become an important target for cancer therapy (1, 13).Endogenous ATP (eATP) can be released in large quantities through cell necrosis, apoptosis and mechanical damage (14), and can also be actively secreted by tumor cells, immunocytes, and other histocytes in the TME, triggered by various cell damage factors such as hypoxia, chronic inflammation, and cytotoxic drugs (2). The main source of eADO is the continuous degradation of eATP, which involves many different extracellular enzymes, including NTPDase1/CD39 and CD73 (2, 13, 14). CD39 is highly expressed in the tumor endothelium of the TME and on most immunocytes (including macrophages, myeloid cells, and FOXP3+ regulatory T cells (Treg) (3). The CD39 topological domain consists of two transmembrane domains, including short cytoplasmic N-and C-terminal segments and a large extracellular hydrophobic domain containing the active site (15).The extracellular domain contains five conserved propyrylase regions from ACR1 to ACR5, among which the amino acid sequences of ACR1 and ACR5 contain phosphate-binding motifs, which are believed to be critical for stabilizing the interaction between the enzyme and its nucleotide substrate during phosphate cleavage (4). CD39 can stabilize FOXP3+Tregs, contribute to their immunosuppressive function (16), promote type I Treg differentiation, produce IL-10, and restrict the activation of NLRP3 inflammatory bodies in dendritic cells (DCs) (2, 13, 14). CD73 can be found in different kinds of tissues, which includes the colon, liver, kidney, brain, lungs, and heart; leukocytes and endothelial cells of peripheral blood, lymph nodes, spleen and bone marrow (3). CD73 is now known as glycosyl phosphatidyl inositol (GPI)-anchored protein (17), which is a homodimeric disulfide linker protein of 548 amino acids, of which the N-terminus provides a binding site for two catalytic divalent metal ions and the C-terminus is a binding site for AMP (18). The expression and function of CD73 are elevated in the presence of hypoxia and inflammatory mediators (TGF- B, IFNs, TNF-α, IL-1B, PGE2, etc.), and the expression of CD73 is also increased in several tumor tissues, suggesting that CD73 is involved in tumor genesis and development (2, 13, 14, 19), eATP is decomposed into eADO through the sequence of CD39 and CD73, which bind to adenosine receptors on the cell membrane surface (2, 13, 14). Among several known adenosine receptors, adenosine receptor A2a (A2aR) is the predominant subtype and is mainly expressed in immunocytes (20). A2aR stimulation usually provides immunosuppressive signals that inhibit T cell proliferation, cytotoxicity, cytokine production, NK cell cytotoxicity, NKT cell cytokine production, CD40L upregulation, macrophage/DC antigen presentation, etc. (1, 19) (Figure 1). Based on the above background analysis, when we want to antagonize the immunosuppressive effect of eADO in the TME, we can start from the following three aspects: 1. It reduces the expression of CD39 in tumor cells and inhibits the conversion of eATP to AMP; 2. It reduces the expression of CD73 molecules on tumor cells and blocks the conversion of AMP into eADO, thereby reducing the binding of eADO to A2aR receptors on immune cells; 3. It reduces the expression of A2aR in immune cells, making them unable to combine with eADO to maintain their normal immune function.

Immune checkpoint

The immune system consists of innate and acquired immunity, which, once activated, clears infectious pathogens and tumor cells. Inhibitory pathways in antimicrobial or antitumor immune responses normally maintain auto-tolerance to avoid excessive damage and limit associated tissue damage (21, 22). This receptor and ligand inhibitory pathways are known as “Immune Checkpoint” and are used by tumor cells to avoid Immune attack. The development of monoclonal antibodies to inhibit these checkpoints, thereby removing the Inhibition of immunocytes and enabling them to recognize and kill tumor cells, is called “Immune Checkpoint Inhibition”. These drugs are called “ immune checkpoint inhibitors” (ICI) (23, 24). FDA-approved anti-CTLA-4 and anti-PD-1 antibodies for cancer treatment, which led to the belief that immunotherapy for cancer was realistic and further encouraged the development of other new ICIs (25–27). Immunotherapy is becoming an important treatment for cancer patients (1, 13). Immune checkpoint blocking (ICB) based on monoclonal antibody (mAb) has also proven to be a safe and effective treatment for hematologic malignancies in the past decade (22, 27). In oncology, checkpoints currently targeted by inhibitors to amplify the reactivity of T cells, NK cells and bone marrow cells include CTLA-4 (28), PD-1, PD-L1 (PD1 ligand 1/CD274), LAG-3 (CD223), TIM3 (T cell immunoglobulin-3), TIGIT(T cell immunoglobulin and ITIM domain) (29), VISTA (V-domain immunoglobulin suppressor of T cell activation) (30), B7/H3 (CD276), KIR (killer cell immunoglobulin-like receptors), NKG2A, A2AR, CD39, CD73, CSF1R, and CD47 (22, 31, 32) (Figure 2).

Each member of the adenosine signaling pathway constitutes a different drug target, meaning that it is possible for combined therapy with more than one drug to target this or complementary signaling pathway (33). Many of these combinations are currently in preclinical and clinical trials, such as anti-CD73 and anti-A2aR combinations, anti-CD73 and anti-PD-1 combinations, and anti-A2aR and anti-TIGIT antibody combinations (21, 31, 34–36) (Table 1).

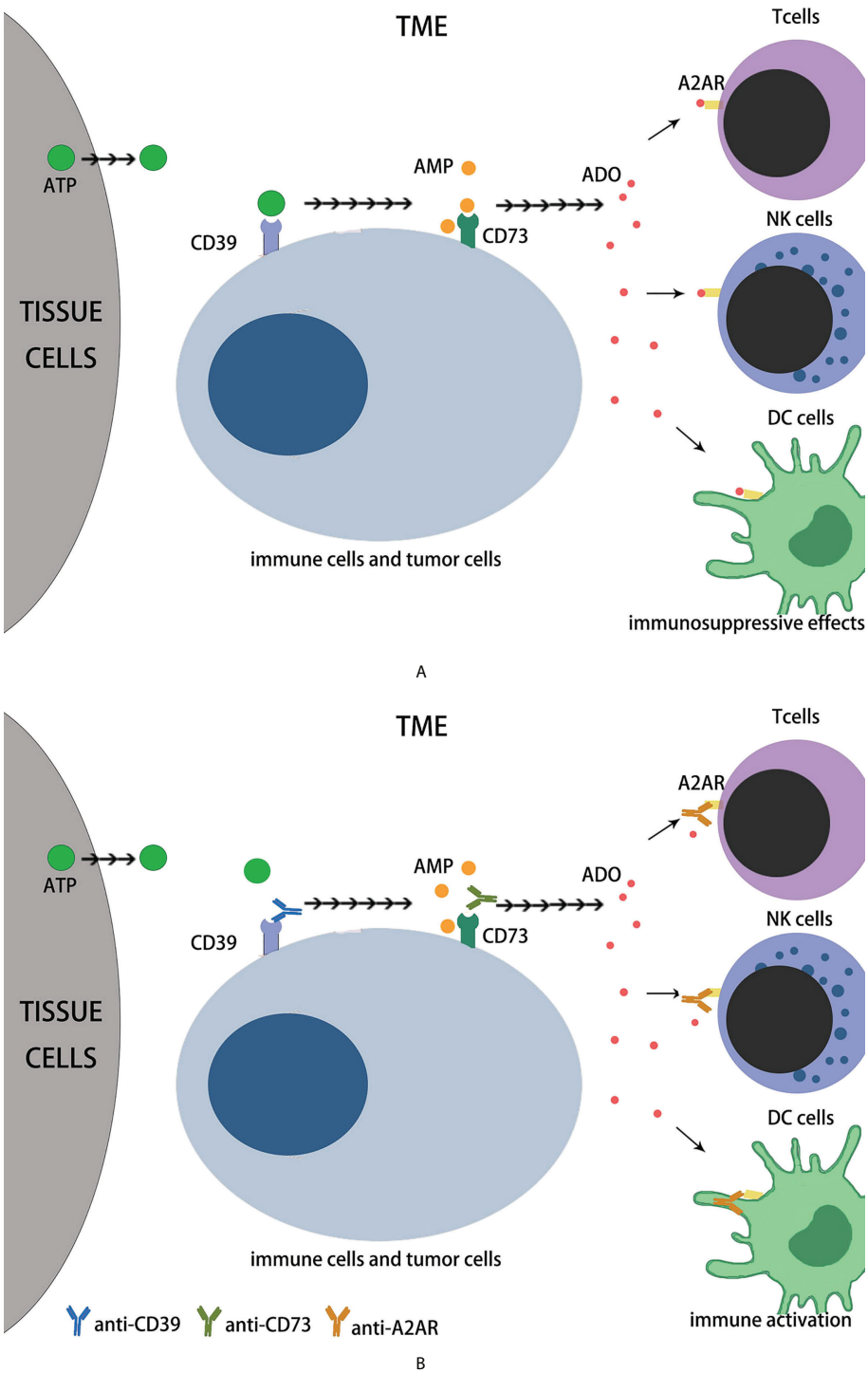

FIGURE 1
The immune effects of adenosine axis in TME. (**A**) The eATP can be released in large quantities during cell necrosis, apoptosis and mechanical damage, and can be actively secreted by tumor cells and other cells in the TME, which is triggered by hypoxia, chronic inflammation, nutrient deprivation, or cytotoxic drugs. Extracellular ATP is broken down by CD39 to AMP, then CD73 to adenosine. Extracellular adenosine binds to A2AR on immunocytes such as T cells, NK cells and DC cells, inhibiting their immune function. (**B**) Role of monoclonal antibodies in adenosine axis. CD39 mAb prevents eATP from binding to CD39 to reduce AMP production; CD73 mAb prevents AMP from binding to CD73 to reduce ADO production. A2AR mAb prevents ADO from binding to A2AR and inhibits its immunosuppressive effect.

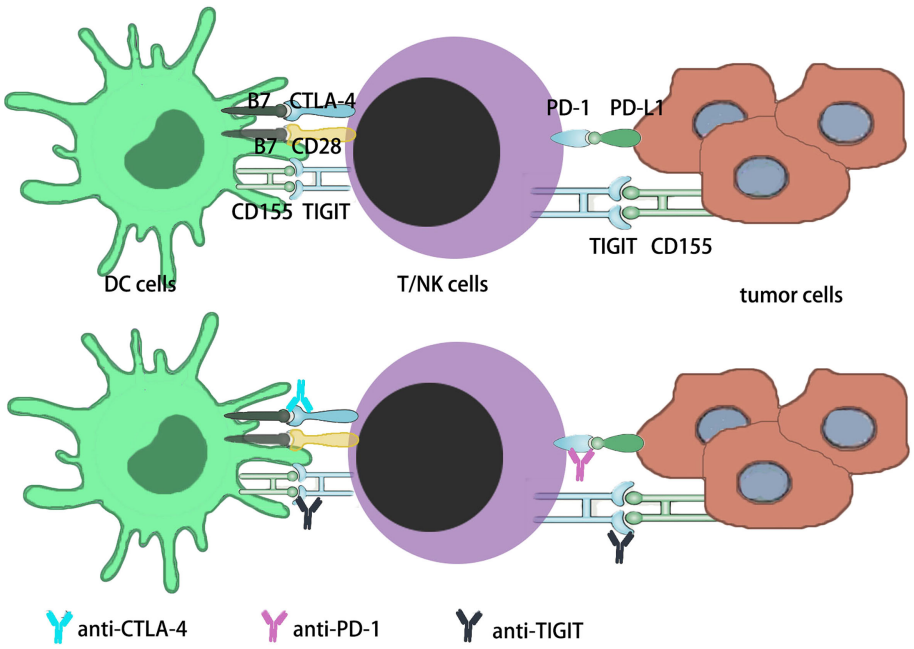

FIGURE 2
Immune checkpoints in current studies. i) The PD-1 is expressed on activated T cells in the early-stage lymph node as well as late-stage tumor tissues in the TME. In the early stage and late stage, PD-1 sustains immune homeostasis by decreasing activated T cells function. Tumors might become resistant to this suppression signaling, increasing the survival potential of the tumor cells. ii) The CTLA-4 is expressed on T cells that are activated by DCs in the lymph node. By MHC interaction with T cell receptor and B7 signal interaction with CD28 on T cells. In order to sustain immune homeostasis, CTLA-4 downregulates the function of activated T cells through the interaction of B7 signaling with CTLA-4 on T cells. Tumors may develop toleration to this inhibitory signal, thus improving the survival potential of tumor cells. iii) TIGIT is expressed both on NK cells and T cells, which includes CD4+ T cells, CD8+ T cells and Tregs. TIGIT has three ligands, CD155, CD112 and CD113, and the main ligand for TIGIT is CD155. The main effect of TIGIT is downregulating the function of NK cells and T cells.

Combination of CD39 with immune checkpoints

The rapid development of flow cytometry in recent years has further confirmed the expression of CD39 in tumor cells, particularly in melanoma, lymphoma, and chronic lymphocytic leukemia (CLL) cell lines (13, 14). In melanoma B16F10 mouse model and colorectal cancer Mc-38 mouse model, CD39-defective mice were resistant to tumor metastasis (31, 56). It has been documented that all cells expressing CD39 exhibit strong ATPase activity, which can be counterbalanced by CD39 inhibitors, such as ARL-67156 and POM-1, by measuring the degradation of eATP or releasing free phosphate from the cell culture supernatant. Treatment with BY40, a CD39 blocking antibody currently under preclinical development, reduces the inhibition of CD4+ and CD8+T cell proliferation, which is induced by tumor tissue and increases cytotoxicity mediated by cytotoxic T lymphocytes (CTL) and NK cells (16). At present, many studies have shown that human CD39+CD8+ T cells exhibited draining dysfunction or phenotype gene signature of T cells, including highly expressed inhibitory receptors, PD-1 and CTLA-4 (57). Thus targeted therapy of CD39 combined with other immune binding sites has great significance in the therapy of tumors. Currently, the main CD39 mAb used in clinical research is IPH5201, which blocks the hydrolysis of ATP by a membrane and soluble CD39, thus promoting DC maturation and macrophage activation (11); BY40 has been reported to block membrane-associated, but insoluble, human CD39 enzyme activity, but its clinical efficacy has not been evaluated (11, 58); POM1 is mainly used for experimental studies on mice and cell lines (11).

CD39 mAb combined with PD-1 mAb

PD-1 encodes immunoglobulin superfamily proteins and is focused on sustaining immune tolerance to autoantigens and preventing autoimmune diseases. PD-L1 is a PD-1 ligand blocking the interaction between the tumor cells expressing PD-L1 and tumor-specific T cells expressing PD-1 using PD-1 or PD-L1 antibodies enhance the cytolytic activity of T cells (25). It has strong therapeutic value and significance in solid tumors and hematologic malignancies (33, 59). However, during immunotherapy, many tumors show resistance to PD-1/PD-L1. The exhibition of resistance by patients might be due to the

TABLE 1 Application of different targets on adenosinergic axis combined with various immune checkpoints in tumor therapy.

Adenosine axis	*ICIs*	*Disease*	*Experimental subjects*	*Mechanism*	*References*
CD39	PD-1/PD-L1	Melanoma	Mouse model	Restored T cell proliferation	(11)
		Fibrosarcoma	Human tissue, Mouse model	Enhance CD8+T cells' activation	(37)
		HCC	Human tissue	Co-expression was detected	(38)
		NSCLC			
	CTLA-4	Melanoma	Mouse model	Enhance NK cells' activation	(39)
		HNSCC	Human tissue	Co-expression was detected	(40)
	TIGIT	AML	Human tissue	Enhance T/NK cells' activation	(41, 42)
CD73	PD-1/PD-L1	Breast cancer	Mouse model	Enhance T/NK cells' activation	(43, 44)
		Colon carcinoma	Human tissue	Enhance levels of secreted IFNγ and TNFα	(24, 45)
		Prostate carcinoma	Mouse model.	Enhance CD8+T cells' activation	(24)
		Fibrosarcoma	Cell line	Enhance CD8+T cells' activation	(24)
		Rectal cancer	Cell line	Enhance CD8+T cells' activation	(46)
			Cell line		
			Cell line		
			Mouse model		
	CTLA-4	Colon carcinoma	Cell line	Enhance CD8+T cells' activation	(24)
		Prostate carcinoma	Cell line	Enhance CD8+T cells' activation	(24)
		Melanoma	Mouse model	Enhance T cells' activation and levels of secreted IFNγ	(47)
A2aR	PD-1/PD-L1	Melanoma	Human T cell	Restore T cell activation; enhance T cell activation	(10, 48, 49)
		RCC	Mouse model	Associated with tumor prognosis	(50, 51)
		Breast cancer	Human tissue	Enhance CAR T cell efficacy and enhance the IFNγ production	(49, 52, 53)
			Clinical trial		
			Cell line and mouse model		
	CTLA-4	Colon carcinoma	Cell line and mouse model	Enhance survival, proliferation of T cells	(54)
	TIGIT	AML	Human tissue	Enhance T/NK cells' activation	(42)
		OAC	Human tissue	As evaluation standard of chemotherapy regimen	(55)

immunosuppressive TME, where ROS or nitrogen oxides (NO) released by bone marrow-derived suppressor cells (MDSC) tire T cells and no longer recognize tumor cells. PD1 resistance and poor prognosis in hepatocellular carcinoma (HCC) patients are associated with the upregulation of CD39 expression in macrophages, and CD39 can be used as a marker of unfavorable prognosis in HCC patients (37). This significantly improved through combination therapy with CD39 mAb. It has been reported that the therapy combining anti-CD39 and anti-PD1 mAbs can further slow tumor growth and that the inhibition of CD39 enzyme function can make the tumor model with inherent drug resistance sensitive to PD1 antibody (11, 38).This may be because CD39 mAb and PD-1 mAb can recover the ability of CD8+T cells to produce cytokines. CD39 mAb combined with PD-1 mAb has become one of the targets of many tumor therapies (37).

CD39 mAb combined with CTLA-4 mAb

CTLA-4 is a molecule belonging to the immunoglobulin superfamily. It was first discovered in the cDNA libraries of CTLs and expressed in activated T cells, Tregs, and acute myeloid leukemia cells (28, 33). Although CTLA-4 and its homologue CD28 bind to ligand B7 on B cells and APCs, stimulation of CTLA-4 does not result in T cell activation, but rather in T-cell-mediated antibodies that inhibit and prevent allograft rejection (23, 25). Blocking the CTLA-4-B7 interaction with anti-CTLA-4 mAb results in an enhanced alloantigen response that inhibits negative signaling to T cells (32). However, anti-CTLA-4 is rarely effective as a single drug for highly oncogenic and immunogenic tumors. Targeting CD39 with POM-1 has a synergistic effect on anti-CTLA-4 checkpoint blockade. Specifically, blocking CD39 with POM-1 significantly increased the antitumor activation of CTLA-4 mAb in a mouse model of lung metastasis, and showed better efficacy in a CD39-deficient mouse model of tumor transplanted with B16F10 (39). Recent research also showed that the expression of CTLA-4 and CD39 may be potential target molecules that inhibit Treg activity *in situ* (40). Although there is limited literature on the combination of CD39 mAb with CTLA-4 mAb, according to the current study, the combination of the two mAbs has great potential in tumor therapy, especially in the treatment of tumor metastasis.

CD39 mAb combined with TIGIT mAb

TIGIT is an inhibitory receptor expressed on lymphocytes that has recently attracted attention as the latest target for tumor immunotherapy. This shows the interplay between TIGHT and CD155, which is expressed on APCs or tumor cells, reducing T

and NK cell function. TIGIT, a significant inhibitor of antitumor responses, blocks the tumor immune cycle in multiple steps (60–62). Several studies have shown that blocking TIGIT can prevent various solid and hematologic malignancies. In AML, inhibition of CD39 combined with TIGIT can increase AML cell lysis in 2/3 cell lines, and the combined inhibition of TIGIT and CD39 significantly improved NK cell killing activity *in vitro*, thus further enhancing the NK cell killing effect on AML cells (41, 42, 63). Owing to the difference in the expression of the TIGIT/PVRIG axis and CD39 in different NK cell subsets, joint blocking of these pathways may enhance the cytotoxic function of different NK cell subsets *in vivo*. In addition, it has been preliminarily reported that RORγ agonists can simultaneously reduce the expression of CD39, TIGIT, and other immune checkpoints on lymphocytes, and integrate multiple antitumor mechanisms into one therapy. This enhances immune activity and reduces immunosuppression, thus effectively inhibiting tumor growth (64).

Association of CD73 with immune checkpoints

CD73 is expressed in various types of cancer and is known to promote tumor growth, metastasis, and drug tolerance in glioblastoma, melanoma, leukemia, colon, breast, ovarian, and bladder cancers (13, 19, 65). In human breast cancer cells, high expression of CD73 is related to low response and high resistance to anthracyclines (44, 46, 66). High levels of CD73 are associated with immunosuppression and tumor progression. The overexpression of CD73 in tumors not only leads to metastasis of tumor cells and anthracycline resistance but also leads to immune escape because of excess adenosine production (67, 68). Therefore, inhibitors of CD73 are currently used in combination with existing cancer therapies for cancer immunotherapy, including anti-PD-1/PD-L1 and anti-CTLA-4 therapies (44, 46, 67). Although blocking CD73 alone does not result in a cure, the inhibition of CD73 increases the antitumor effect of immune checkpoint therapies, including anti-CTLA-4 and anti-PD-1 (19, 24, 67). The synergistic effects of combined CTLA-4 mAb with CD73 mAb and combined PD-1 mAb with CD73 mAb immunotherapy have been observed in preclinical models of both breast cancer and colon cancer (24, 45, 68). Currently, MEDI9447(AstrazenecaMedimmune), a human IgG1CD73 mAb (46), can selectively inhibit the activity of CD73ECN and cross-react with mouse and human CD73. MEDI9447 internalized the desetting of CD73 from the cell surface, thereby inhibiting the conversion of AMP to adenosine and removing the inhibition of T cell proliferation mediated by AMP. In an immunoactive mouse tumor model, MEDI9447 reduces immunosuppressive effects and promotes antineoplastic function (45); BMS986179, a high affinity antibody, inhibits the activity of CD73 and mediates the internalization of CD73 (19, 69); CPI-006 (also known as CPX006) acts mainly by inhibiting CD73 activity and/or inducing CD73 downregulation; IPH5301, which blocks AMP from degrading to the immunosuppressant adenosine. At present, these antibodies are undergoing early-stage clinical trials (11, 70).

CD73 mAb combined with PD-1/PD-L1 mAb

As mentioned above, CD73-derived adenosine strongly mediates tumor immune status and metastasis, and weak patient response to PD-1 antibodies may also be associated with elevated intratomatous adenosine levels. In this context, the combination of CD73, mAb, and PD-1 mAb may be particularly effective in tumor immunotherapy. Currently, various studies have focused on the clinical effects of combining CD73 inhibition with PD-1 blockade. In melanoma, breast cancer, colon cancer, non-small cell lung cancer (NSCLC), prostate cancer, and other malignant tumors (24, 43, 45), combining the CD73 mAb with the PD-1 mAb has shown a more significant effect than these drugs alone. The high expression of CD73 on the surface of tumor cells shows a weaker effect of immunotherapy with a PD-1 antibody, and the combined use of PD-1 mAb and CD73 mAb prominently inhibited tumor growth (46), and increased gene expression related to inflammation and T cell function, causing an increase in the number and activity of tumor-infiltrating CD8+T cells and the production of IFN-γ and TNF-α (20, 46). It has also been reported that MEDI9447 when combined with anti-PD-1 antibodies, can produce a better antitumor effect, which is supported by multiple phases I/II trials based on MEDI9447. Preliminary phase I data for MEDI9447(NCT02503774) have recently been reported (24).The safety of MEDI9447 and duvacizumAb (anti-PD-L1) treatment is controllable, and PD-1 is consistent with its mechanism of function. BMS-986179 was also found to enhance the antineoplastic activity of anti-PD-1mAb in preclinical animal models (19, 71). Notably, the combination of A2aR antagonist and PD-1 antibody also showed an antimetastatic effect. However, the combination therapy with A2aR antagonists was effective only when tumors expressed high CD73 levels, suggesting that CD73 can also be used as a potential tumor indicator to assess the benefit of combination therapy (13, 19, 44).

CD73 mAb combined with CTLA-4 mAb

The combination of CD73 mAb and PD-1 mAb was more effective against both subcutaneous and metastatic tumors than that of CD73 mAb and CTLA-4 mAb (24). This may be due to the

stronger antineoplastic activity of PD-1 mAb itself than that of CTLA-4 mAb or the synergistic effect of CD73 mAb and PD-1 mAb on Tregs. However, CD73 mAb combined with CTLA-4 mAb still has clinical significance and cannot be ignored. CD73 mAb combined with CTLA-4 mAb significantly improved the median survival in a tumor metastasis mouse model (71). In melanoma, the efficacy of anti-CTLA-4 therapy can be enhanced by targeting various immunosuppressive mechanisms in tumor tissues, including CD73. CD73 antibody combined with CTLA-4 mAb significantly inhibited melanoma growth. In a mouse melanoma model, the percentage of infiltrated CD8+T and CD4+T cells significantly increased after the combination of the two antibodies, and the proportion of Tregs was also increased compared with that of the two antibodies alone, which may be due to the increase in CD4+T cells after the combination of the two monoclonal antibodies. At the same time, IFN-γ levels increased in melanoma tissues of mice treated with CD73 antibody in combination with CTLA-4 antibody (47). CTLA-4 mAb is also of great clinical significance in hematologic malignancies such as AML and MDS (22) and has great potential in combination with CD73 antibody in the treatment of malignant diseases of the blood.

Association of A2AR with immune checkpoints

The A2a receptor (A2aR) in the adenosinergic pathway is an important immune checkpoint. Adenosine levels in the extracellular fluid are increased in the TME because of the special metabolism of tumor cells, which contributes to tumor immune escape. Therefore, A2aR inhibitors are being investigated to enhance the effect of immunotherapy (2, 13). Several A2aR antagonists have been developed and tested in multiple preclinical studies. At least four drugs, CPI-444 (10) PBF-509 (Novartis/Pablobiofarma), MK-3814 (Merck), and AZD4635 (AstraZeneca/Heptares), are currently in phase I clinical trials (13). CPI-444 intensifies antineoplastic immunity and enhances anti-PD-L1 mAb activity in mice. CPI-444 has also been shown to intensify the antitumor effect of adoptive metastases of HER2-specific CD8+T cells in tumor-bearing mice treated with cyclophosphamide and a novel gene-expressed whole-cell vaccine (GVAX) (10). Vipatant (REDOX/Juno therapy) and Etradine (Kyowa Hakko Kirin) are other promising oral A2a antagonists that have previously gone through clinical trials for Parkinson's disease and may be effective in cancer patients. Recent research has shown that A2aR inhibits T cell proliferation and cytokine secretion and increases the expression of PD-1 and CTLA-4 on the surface (72, 73). Currently, combination therapy with A2aR and other immune checkpoints is also attracting attention (10, 13).

A2aR mAb combined with PD-1/PD-L1 mAb

As the expression of A2a is increased in antigen-activated T cells and PD-1 is involved in inhibiting T cell function, the combination of targeted blocking of these two molecules is considered a new direction in tumor therapy. Recent clinical studies have shown that in renal cell cancer (RCC) patients, A2aR and PD-L1 expression in the primary tumors may foresee the consequences of therapy with anti-VEGF agents and ICIs (51), and the A2aR antagonist ciforadenant showed monotherapy activity in patients who were resistant to or intractable to previous anti-PD-L1 therapy. Although this trial did not deliberately compare the effects of monotherapy with those of combination therapy, treatment with an A2aR antagonist plus anti-PD-L1 appeared to improve efficacy (50). Studies have shown that blocking A2aR with CPI-444 reduces the expression of checkpoints of various pathways in T-effs and Tregs, including PD-1 and LAG-3. By reducing the expression of immune checkpoints on these T cells, the threshold for anti-PD-1 treatment is lowered. In other words, there is a synergistic reaction with the combination of CPI-444 and PD-1 mAb (10, 48). Moreover, A2aR blockers significantly reduced the expression of PD-1 and LAG-3 in the draining lymph nodes of tumor-bearing mice (53). Another group successfully combined A2aR blockers with anti-PD-1 inhibitors in an anti-tumor regimen in a mouse model (35). Mittal et al. (49) also reported that combining SCH58261, the A2aR inhibitor, with anti-PD-1 therapy significantly reduced the burden of metastasis compared with either monotherapy alone. Uniting therapy with PD-1 mAbs and CPI-444 showed significant improvement in tumor regression and survival in CT26 and MC38 tumor models (more significant in CT26 tumor models) (48). In NSCLC mouse models, A2a receptor inhibition overcomes the resistance of tumor cells to PD-1/PD-L1 blocking treatment. Meanwhile, A2aR and CD73 were upregulated in mice treated with PD-1 or PD-L1 mAbs (52, 53). In mouse models of breast, colon, and hepatocellular carcinomas, drug resistance of tumor cells to PD-1/PD-L1 can be prevented through dual blocking of PD-1 and A2aR. Blocking A2aR after a viral attack also reduced the expression of PD-1, LAG-3, and TIM-3 on CD8+T cells and Tregs. These abundant *in vivo* and *in vitro* experiments suggest that the combination of A2aR blockers and PD-1/PD-L1 antibodies is of great significance in the clinical treatment of tumors (34, 71).

A2aR mAb combined with CTLA-4 mAb

Combining A2aR mAb CPI-444 with anti-CTLA-4 therapy eliminated tumors in up to 90% of the treated mice, including

restoring an immune response in a model against an incomplete response to CTLA-4 monotherapy. Moreover, tumor cells remained suppressed after re-inoculation of mice with tumor cells, suggesting that CPI-444 induces systemic antineoplastic immune memory and that the combination of CPI-444 with CTLA-4 mAb increases the presence of CD8+T cells and IFNγ and Gzm B levels in tumors (71). In a mouse melanoma model, inhibition of both CD73 and A2aR increased CTLA-4 the therapeutic effect. Blocking A2aR plays an important role in regulating T-cell function and significantly reduces melanoma growth (47). Most importantly, the combination of A2aR antagonists and anti-CTLA-4 therapy significantly restricts tumor growth and enhances the antitumor immune response (10, 71). Additionally, other studies have shown that the concomitant blocking of A2aR and CTLA-4 in T cells can synergistically enhance the antitumor response by downregulating PKA, SHP2, and PP2Aα signaling pathways, providing a theoretical basis for A2aR mAb combined with CTLA-4 mAb as a new treatment regimen for tumors (54).

A2aR mAb combined with TIGIT mAb

The frequency of TIGIT + NK cells in the blood of patients was negatively correlated with AML prognosis. Compared with healthy subjects, AML patients had abnormal NK cell populations in the peripheral blood (PB) and bone marrow (BM), which showed an increased frequency of TIGIT+, PVRIG +, CD39+, and CD69+NK cells. Thus, TIGIT is a potential target for AML treatment (42). The purinergic pathway also regulates NK cell functions. Proliferation and hypoxia of tumor cells increase the utilization of ATP and activate cancer-related CD39 and CD73, which catalyze the continuous dephosphorylation of ATP to AMP and then to eADO. Extracellular adenosine accumulation interacts with adenosine receptors expressed on the surface of NK cells and inhibits signaling through A2aR; therefore, A2aR antibodies are also important targets for tumor therapy (55). It has been demonstrated that the combined blocking of TIGIT and A2aR enhances NK-92 cell-mediated cytotoxicity in AML (42). In other tumors, the combination of TIGIT and A2aR mAbs is still being explored (55).

Comparison of the efficacy of CD39, CD73, A2AR and immune checkpoint inhibitors in clinical treatment

Studies have shown that A2AR mAb, Ciforadenant (CPI-144) has a good effect on RCC, and its combination with atezolizumab has a better effect than Ciforadenant alone (74). Taminadenant, another A2AR antagonist, has shown promising efficacy in NSCLC, either alone or in combination with the PD-1 mAb, Spartalizumab (75). There does not appear to be a significant difference in the efficacy of A2aR antagonists alone or in combination with immune checkpoint inhibitors for malignancy, but the number of clinical trials in this area is small, and the results of these two trials are not representative. The combination of A2aR antagonists and immune checkpoint inhibitors has been seriously considered in clinical practice and needs to be explored and validated in more clinical trials.

Although there are no cases of CD39 mAb used alone in clinical treatment, clinical studies have shown that the expression of CD39 in chronic lymphocytic leukemia patients is closely related to the stage of disease, the time of first treatment, and the prognosis of patients (76, 77). Similar results have been found in immune-related diseases, such as Crohn's disease and multiple sclerosis (78, 79). Due to various limitations, treatment with CD39 mAb combined with immune checkpoints such as PD-1, CTLA-4, and TIGIT has been limited to mouse models, cell lines, and human tissues. However, this combination therapy has been proved to have high clinical potential and value by a large number of *in vitro* experiments (11, 37–42).

CD73 is currently mainly used as a prognostic indicator for clinical tumors, including breast and rectal cancers (23, 24, 43–47). Few trials have applied the CD73 mAb in the clinical treatment of tumors. Recent *in vitro* experiments have confirmed that the CD73 mAb can enhance the efficacy of immune checkpoint inhibitors and reduce the formation of resistance. Its combination with immune checkpoint inhibitors is far more effective than either of them alone (23, 24, 43–47).

The efficacy of antagonists of CD39 and CD73, A2aR targets on the adenosinergic axis alone and in combination has been discussed in a study on multiple myeloma (80). *In vitro* experiments confirmed that the inhibitory effect of the three target antagonists alone on myeloma was not as good as that of the two target antagonists combined, while the combined use of three target antagonists, CD39, CD73, and A2aR, had the best inhibitory effect on myeloma.

Conclusion

In recent years, therapeutic advances in cancer immunotherapy (CIT) have emerged rapidly, reflecting the importance of human immune system interactions with cancer, as well as the complex and highly regulated nature of the immune system (81, 82). In the context of complex immune networks, point-to-point therapy has been unable to achieve satisfactory tumor treatment effects; therefore, combining various targeting axes or immune checkpoints will become a new direction of tumor treatment.

The role of the adenosine axis in the tumor microenvironment is mainly induced by hypoxia; therefore, some studies have also called this the hypoxia–adenosine axis. Extracellular adenosine

increases under hypoxic conditions, and simultaneously, the expression of CD39 and CD73 improves (8). Antihypoxia-adenosine therapy is synergistic with other immune checkpoint inhibitors such as CTLA-4 and PD-1 mAbs. The combination of anti-hypoxia-adenosine strategies may enhance the clinical response to other immunotherapies, chemotherapy, and radiotherapy (71). With advances in the treatment of tumors with immune checkpoint blockers such as CTLA-4 and PD-1/PDL1, more therapeutic targets have been sought, including but not limited to the immune targets in the adenosine energy axis mentioned above, to overcome the problems of incomplete tumor regression or recurrence after treatment (3). Immune checkpoint suppressor molecules are emerging as new potential targets for tumor therapy. In the TME, these molecular mechanisms may operate and may be supplementary to approved immunotherapies (26, 83, 84). When the immune escape of tumor cells makes the control of tumors difficult (85), the use of immune checkpoint inhibitors can offset the immune escape of tumor cells to a certain extent and further improve the response rate. Without increasing or even decreasing the adverse events related to excessive tissue damage, autoimmunity, and other immune-associated side reactions associated with the use of immune checkpoint inhibitors alone (22, 86–88). In the future, the treatment trend of malignant tumors will be developed from point-to-point therapy targeting individual immune checkpoints to a combination of immune networks composed of various signaling pathways, such as the adenosine axis. Non-traditional immunotherapies can induce or enhance antitumor immunity. Consequently, they may force tumors to upregulate immune checkpoints, which can be blocked as part of a combined strategy (87, 89–92).

Author contributions

ZL: Conceptualization, Writing - Review and Editing, Project administration. XL: Writing - Original Draft, Visualization, Resources. XX: Resources. HS: Resources. XZ: Resources. RF: Supervision, Funding acquisition, Project administration. All authors contributed to the article and approved the submitted version.

Funding

This work was supported by the National Natural Science Foundation of China Youth Project (grant no. 81900131,82000219), the National Natural Science Foundation of China Youth Project (grant no. 8210010129), the Tianjin Municipal Natural Science Foundation (grant no. 18JCQNJC80400, 19JCZDJC32900), the Tianjin Education Commission Research Project (grant no. 2018KJ043,20140118), the Tianjin Education Commission Research Project (grant no. 2018KJ045), and the Tianjin Science and Technology Planning Project (no. 20YFZCSY00060).Tianjin Municipal Health Commission Youth Project (grant no. TJWJ2021QN001); Medjaden Academy & Research Foundation for Young Scientists (Grant No. MJR20221011);Tianjin Key Medical Discipline(Specialty) Construction project(Grant TJYXZDXK-028A).

Conflict of interest

The authors declare that the research was conducted in the absence of any commercial or financial relationships that could be construed as a potential conflict of interest.

Publisher's note

References

1. Ohta A. A metabolic immune checkpoint: Adenosine in tumor microenvironment. *Front Immunol* (2016) 7:109. doi: 10.3389/fimmu.2016.00109

2. Boison D, Yegutkin GG. Adenosine metabolism: Emerging concepts for cancer therapy. *Cancer Cell* (2019) 36(6):582–96. doi: 10.1016/j.ccell.2019.10.007

3. Allard B, Allard D, Buisseret L, Stagg J. The adenosine pathway in immuno-oncology. *Nat Rev Clin Oncol* (2020) 17(10):611–29. doi: 10.1038/s41571-020-0382-2

4. Guo S, Han F, Zhu W. CD39 - a bright target for cancer immunotherapy. *BioMed Pharmacother* (2022) 151:113066. doi: 10.1016/j.biopha.2022.113066

5. Antonioli L, Blandizzi C, Pacher P, Haskó G. Immunity, inflammation and cancer: a leading role for adenosine. *Nat Rev Cancer* (2013) 13(12):842–57. doi: 10.1038/nrc3613

6. Stagg J, Smyth MJ. Extracellular adenosine triphosphate and adenosine in cancer. *Oncogene* (2010) 29(39):5346–58. doi: 10.1038/onc.2010.292

7. Beavis PA, Stagg J, Darcy PK, Smyth MJ. CD73: A potent suppressor of antitumor immune responses. *Trends Immunol* (2012) 33(5):231–7. doi: 10.1016/j.it.2012.02.009

8. Scheffel TB, Grave N, Vargas P, Diz FM, Rockenbach L, Morrone FB. Immunosuppression in gliomas *via* PD-1/PD-L1 axis and adenosine pathway. *Front Oncol* (2020) 10:617385. doi: 10.3389/fonc.2020.617385

9. Ohta A, Gorelik E, Prasad SJ, Ronchese F, Lukashev D, Wong MKK, et al. A2A adenosine receptor protects tumors from antitumor T cells. *Proc Natl Acad Sci USA* (2006) 103(35):13132–7. doi: 10.1073/pnas.0605251103

10. Willingham SB, Ho PY, Hotson A, Hill C, Piccione EC, Hsieh J, et al. A2AR antagonism with CPI-444 induces antitumor responses and augments efficacy to anti-PD-(L)1 and anti-CTLA-4 in preclinical models. *Cancer Immunol Res* (2018) 6(10):1136–49. doi: 10.1158/2326-6066.CIR-18-0056

11. Perrot I, Michaud H-A, Giraudon-Paoli M, Augier S, Docquier A, Gros L, et al. Blocking antibodies targeting the CD39/CD73 immunosuppressive pathway

unleash immune responses in combination cancer therapies. *Cell Rep* (2019) 27 (8):2411–2425.e9. doi: 10.1016/j.celrep.2019.04.091

12. Chew V, Toh HC, Abastado JP. Immune microenvironment in tumor progression: Characteristics and challenges for therapy. *J Oncol 2012* (2012) p:608406. doi: 10.1155/2012/608406

13. Leone RD, Emens LA. Targeting adenosine for cancer immunotherapy. *J Immunother Cancer* (2018) 6(1):57. doi: 10.1186/s40425-018-0360-8

14. Antonioli L, Pacher P, Vizi ES, Haskó G. CD39 and CD73 in immunity and inflammation. *Trends Mol Med* (2013) 19(6):355–67. doi: 10.1016/j.molmed.2013.03.005

15. Maliszewski CR, Delespesse GJ, Schoenborn MA, Armitage RJ, Fanslow WC, Nakajima T, et al. The CD39 lymphoid cell activation antigen. Molecular cloning and structural characterization. *J Immunol* (1994) 153(8):3574–83.

16. Bonnefoy N, Bastid J, Alberici G, Bensussan A, Eliaou J-F. CD39: A complementary target to immune checkpoints to counteract tumor-mediated immunosuppression. *Oncoimmunology* (2015) 4(5):e1003015. doi: 10.1080/2162402X.2014.1003015

17. Solyom A, Trams EG. Enzyme markers in characterization of isolated plasma membranes. *Enzyme* (1972) 13(5-6):329–72. doi: 10.1159/000459682

18. Strater N. Ecto-5'-nucleotidase: Structure function relationships. *Purinergic Signal* (2006) 2(2):343–50. doi: 10.1007/s11302-006-9000-8

19. Chen S, Wainwright DA, Wu JD, Wan Y, Matei DE, Zhang Y, et al. CD73: An emerging checkpoint for cancer immunotherapy. *Immunotherapy* (2019) 11 (11):983–97. doi: 10.2217/imt-2018-0200

20. Ghisoni G, Genta S, Scotto G, Tuninetti V, Turinetto M, et al. Immuno-metabolism and microenvironment in cancer: Key players for immunotherapy. *Int J Mol Sci* (2020) 21(12). doi: 10.3390/ijms21124414

21. Baghbani E, Noorolyai S, Shanehbandi D, Mokhtarzadeh A, Aghebati-Maleki L, Shahgoli VK, et al. Regulation of immune responses through CD39 and CD73 in cancer: Novel checkpoints. *Life Sci* (2021) 282:119826. doi: 10.1016/j.lfs.2021.119826

22. Kantarjian H, Garcia-Manero G, Allison J, Sharma P, Daver N. The emerging role of immune checkpoint based approaches in AML and MDS. *Leuk Lymphoma* (2018) 59(4):790–802. doi: 10.1080/10428194.2017.1344905

23. Antonia SJ, Vansteenkiste JF, Moon E. Immunotherapy: Beyond anti-PD-1 and anti-PD-L1 therapies. *Am Soc Clin Oncol Educ Book* (2016) 35:e450–8. doi: 10.1200/EDBK_158712

24. Allard B, Pommey S, Smyth MJ, Stagg J. Targeting CD73 enhances the antitumor activity of anti-PD-1 and anti-CTLA-4 mAbs. *Clin Cancer Res* (2013) 19 (20):5626–35. doi: 10.1158/1078-0432.CCR-13-0545

25. Khair DO, Bax HJ, Mele S, Crescioli S, Pellizzari G, Khiabany A, et al. Combining immune checkpoint inhibitors: Established and emerging targets and strategies to improve outcomes in melanoma. *Front Immunol* (2019) 10:453. doi: 10.3389/fimmu.2019.00453

26. Li B, Chan HL, Chen P. Immune checkpoint inhibitors: Basics and challenges. *Curr Med Chem* (2019) 26(17):3009–25. doi: 10.2174/0929867324666170804143706

27. DePeaux K, Delgoffe GM. Metabolic barriers to cancer immunotherapy. *Nat Rev Immunol* (2021) 21(12):785–97. doi: 10.1038/s41577-021-00541-y

28. Rowshanravan B, Halliday N, Sansom DM. CTLA-4: a moving target in immunotherapy. *Blood* (2018) 131(1):58–67. doi: 10.1182/blood-2017-06-741033

29. Joller N, Kuchroo VK. Tim-3, lag-3, and TIGIT. *Curr Top Microbiol Immunol* (2017) 410:127–56. doi: 10.1007/82_2017_62

30. Zhang X, Li E, Zhang G, Wang X, Tang X, et al. VISTA: an immune regulatory protein checking tumor and immune cells in cancer immunotherapy. *J Hematol Oncol* (2020) 13(1):83. doi: 10.1186/s13045-020-00917-y

31. Allard D, Allard B, Stagg J. On the mechanism of anti-CD39 immune checkpoint therapy. *J Immunother Cancer* (2020) 8(1). doi: 10.1136/jitc-2019-000186

32. Salik B, Smyth MJ, Nakamura K. Targeting immune checkpoints in hematological malignancies. *J Hematol Oncol* (2020) 13(1):111. doi: 10.1186/s13045-020-00947-6

33. Wang H, Kaur G, Sankin AI, Chen F, Guan F, Zang X, et al. Immune checkpoint blockade and CAR-T cell therapy in hematologic malignancies. *J Hematol Oncol* (2019) 12(1):59. doi: 10.1186/s13045-019-0746-1

34. Helms RS, Powell JD. Rethinking the adenosine-A2AR checkpoint: implications for enhancing anti-tumor immunotherapy. *Curr Opin Pharmacol* (2020) 53:77–83. doi: 10.1016/j.coph.2020.07.003

35. Allard D, Turcotte M, Stagg J. Targeting A2 adenosine receptors in cancer. *Immunol Cell Biol* (2017) 95(4):333–9. doi: 10.1038/icb.2017.8

36. Vijayan D, Young A, Teng MWL, Smyth MJ. Targeting immunosuppressive adenosine in cancer. *Nat Rev Cancer* (2017) 17(12):709–24. doi: 10.1038/nrc.2017.86

37. Lu J, Zhang P, Huang X, Guo X, Gao C, Zeng H, et al. Amplification of spatially isolated adenosine pathway by tumor-macrophage interaction induces anti-PD1 resistance in hepatocellular carcinoma. *J Hematol Oncol* (2021) 14 (1):200. doi: 10.1186/s13045-021-01207-x

38. Tøndell A, Wahl SGF, Sponaas A-M, Sørhaug S, Børset M, Haug M, et al. Ectonucleotidase CD39 and checkpoint signalling receptor programmed death 1 are highly elevated in intratumoral immune cells in non-small-cell lung cancer. *Transl Oncol* (2020) 13(1):17–24. doi: 10.1016/j.tranon.2019.09.003

39. Zhang H, Vijayan D, Li X-Y, Robson SC, Geetha N, Teng MWL. The role of NK cells and CD39 in the immunological control of tumor metastases. *Oncoimmunology* (2019) 8(6):e1593809. doi: 10.1080/2162402X.2019.1593809

40. Jie H-B, Gildener-Leapman N, Li J, Srivastava RM, Gibson SP, Whiteside TL, et al. Intratumoral regulatory T cells upregulate immunosuppressive molecules in head and neck cancer patients. *Br J Cancer* (2013) 109(10):2629–35. doi: 10.1038/bjc.2013.645

41. Brauneck F, Haag F, Woost R, Wildner N, Tolosa E, Rissiek A, et al. Increased frequency of TIGIT(+)CD73-CD8(+) T cells with a TOX(+) TCF-1low profile in patients with newly diagnosed and relapsed AML. *Oncoimmunology* (2021) 10(1):1930391. doi: 10.1080/2162402X.2021.1930391

42. Brauneck F, Seubert E, Wellbrock J, Schulze Zur Wiesch J, Duan Y, Magnus T, et al. Combined blockade of TIGIT and CD39 or A2AR enhances NK-92 cell-mediated cytotoxicity in AML. *Int J Mol Sci* (2021) 22(23). doi: 10.3390/ijms222312919

43. Liu S, Liu D, Wang H, Horecny I, Shen R, Zhang R, et al. A novel CD73 inhibitor SHR170008 suppresses adenosine in tumor and enhances anti-tumor activity with PD-1 blockade in a mouse model of breast cancer. *Onco Targets Ther* (2021) 14:4561–74. doi: 10.2147/OTT.S326178

44. Neo SY, Yang Y, Record J, Ma R, Chen X, Chen Z, et al. CD73 immune checkpoint defines regulatory NK cells within the tumor microenvironment. *J Clin Invest* (2020) 130(3):1185–98. doi: 10.1172/JCI128895

45. Hay CM, Sult E, Huang Q, Mulgrew K, Fuhrmann SR, McGlinchey KA. Targeting CD73 in the tumor microenvironment with MEDI9447. *Oncoimmunology* (2016) 5(8):e1208875. doi: 10.1080/2162402X.2016.1208875

46. Wurm M, Schaaf O, Reutner K, Ganesan R, Mostböck S, Pelster C, et al. A novel antagonistic CD73 antibody for inhibition of the immunosuppressive adenosine pathway. *Mol Cancer Ther* (2021) 20(11):2250–61. doi: 10.1158/1535-7163.MCT-21-0107

47. Iannone R, Miele L, Maiolino P, Pinto A, Morello S. Adenosine limits the therapeutic effectiveness of anti-CTLA4 mAb in a mouse melanoma model. *Am J Cancer Res* (2014) 4(2):172–81.

48. Leone RD, Sun I-M, Oh MH, Sun IH, Wen J, Englert J, et al. Inhibition of the adenosine A2a receptor modulates expression of T cell coinhibitory receptors and improves effector function for enhanced checkpoint blockade and ACT in murine cancer models. *Cancer Immunol Immunother* (2018) 67(8):1271–84. doi: 10.1007/s00262-018-2186-0

49. Mittal D, Young A, Stannard K, Yong M, Teng MWL, Allard B, et al. Antimetastatic effects of blocking PD-1 and the adenosine A2A receptor. *Cancer Res* (2014) 74(14):3652–8. doi: 10.1158/0008-5472.CAN-14-0957

50. Fong L, Hotson A, Powderly JD, Sznol M, Heist RS, Choueiri TK, et al. Adenosine 2A receptor blockade as an immunotherapy for treatment-refractory renal cell cancer. *Cancer Discov* (2020) 10(1):40–53. doi: 10.1158/2159-8290.CD-19-0980

51. Kamai T, Kijima T, Tsuzuki T, Nukui A, Abe H, Arai K. Increased expression of adenosine 2A receptors in metastatic renal cell carcinoma is associated with poorer response to anti-vascular endothelial growth factor agents and anti-PD-1/Anti-CTLA4 antibodies and shorter survival. *Cancer Immunol Immunother* (2021) 70(7):2009–21. doi: 10.1007/s00262-020-02843-x

52. Beavis PA, Henderson MA, Giuffrida L, Mills JK, Sek K, Cross RS, et al. Targeting the adenosine 2A receptor enhances chimeric antigen receptor T cell efficacy. *J Clin Invest* (2017) 127(3):929–41. doi: 10.1172/JCI89455

53. Beavis PA, Milenkovski N, Henderson MA, John LB, Allard B, Loi S, et al. Adenosine receptor 2A blockade increases the efficacy of anti-PD-1 through enhanced antitumor T-cell responses. *Cancer Immunol Res* (2015) 3(5):506–17. doi: 10.1158/2326-6066.CIR-14-0211

54. Ghasemi-Chaleshtari M, Kiaie SH, Irandoust M, Karami H, Afjadi MN, Ghani S, et al. Concomitant blockade of A2AR and CTLA-4 by siRNA-loaded polyethylene glycol-chitosan-alginate nanoparticles synergistically enhances antitumor T-cell responses. *J Cell Physiol* (2020) 235(12):10068–80. doi: 10.1002/jcp.29822

55. Davern M, Donlon NE, Sheppard A, O'Connell F, Hayes C, Bhardwaj A. Chemotherapy regimens induce inhibitory immune checkpoint protein expression on stem-like and senescent-like oesophageal adenocarcinoma cells. *Transl Oncol* (2021) 14(6):101062. doi: 10.1016/j.tranon.2021.101062

56. Sun X, Wu Y, Gao W, Enjyoji K, Muller CE, Murakami T. CD39/ENTPD1 expression by CD4+Foxp3+ regulatory T cells promotes hepatic metastatic tumor

growth in mice. *Gastroenterology* (2010) 139(3):1030–40. doi: 10.1053/j.gastro.2010.05.007

57. Gupta PK, Godec J, Wolski D, Adland E, Yates K, Pauken KE, et al. CD39 expression identifies terminally exhausted CD8+ T cells. *PloS Pathog* (2015) 11(10): e1005177. doi: 10.1371/journal.ppat.1005177

58. Nikolova M, Carriere M, Jenabian M-A, Limou S, Younas M, Kok A. CD39/adenosine pathway is involved in AIDS progression. *PloS Pathog* (2011) 7(7): e1002110. doi: 10.1371/journal.ppat.1002110

59. Jalali S, Price-Troska T, Paludo J, Villasboas J, Kim Yang H-J Z-Z. Soluble PD-1 ligands regulate T-cell function in waldenstrom macroglobulinemia. *Blood Adv* (2018) 2(15):1985–97. doi: 10.1182/bloodadvances.2018021113

60. Anderson AC, Joller N, Kuchroo VK. Lag-3, Tim-3, and TIGIT: Co-inhibitory receptors with specialized functions in immune regulation. *Immunity* (2016) 44(5):989–1004. doi: 10.1016/j.immuni.2016.05.001

61. Johnston RJ, Comps-Agrar L, Hackney J, Yu X, Huseni M, Yang Y, et al. The immunoreceptor TIGIT regulates antitumor and antiviral CD8(+) T cell effector function. *Cancer Cell* (2014) 26(6):923–37. doi: 10.1016/j.ccell.2014.10.018

62. Dougall WC, Kurtulus S, Smyth MJ, Anderson AC. TIGIT and CD96: new checkpoint receptor targets for cancer immunotherapy. *Immunol Rev* (2017) 276 (1):112–20. doi: 10.1111/imr.12518

63. Harjunpaa H, Guillerey C. TIGIT as an emerging immune checkpoint. *Clin Exp Immunol* (2020) 200(2):108–19. doi: 10.1111/cei.13407

64. Hu X , Liu X, Moisan J, Wang Y, Lesch CA, Spooner C, et al. Synthetic RORgamma agonists regulate multiple pathways to enhance antitumor immunity. *Oncoimmunology* (2016) 5(12):e1254854. doi: 10.1080/2162402X.2016.1254854.

65. Kong Y, Jia B, Zhao C, Claxton DF, Sharma A, Annageldiyev C, et al. Downregulation of CD73 associates with T cell exhaustion in AML patients. *J Hematol Oncol* (2019) 12(1):40. doi: 10.1186/s13045-019-0728-3

66. Loi Pommey S, Haibe-Kains S, Beavis B, Darcy PA, Smyth PK, MJ, et al. *CD73 promotes anthracycline resistance and poor prognosis in triple negative breast cancer. Proc Natl Acad Sci USA* (2013) 110(27):11091–6. doi: 10.1073/pnas.1222251110

67. Antonioli L, Yegutkin GG, Pacher P, Blandizzi C, Haskó G. Anti-CD73 in cancer immunotherapy: Awakening new opportunities. *Trends Cancer* (2016) 2 (2):95–109. doi: 10.1016/j.trecan.2016.01.003

68. Roh M, Wainwright DA, Wu JD, Wan Y, Zhang B. Targeting CD73 to augment cancer immunotherapy. *Curr Opin Pharmacol* (2020) 53:66–76. doi: 10.1016/j.coph.2020.07.001

69. Siu LL, Burris H, Le DT, Hollebecque A, Steeghs N, Delord JP, et al. Preliminary phase 1 profile of BMS-986179, an anti-CD73 antibody, in combination with nivolumab in patients with advanced solid tumors. *Cancer Res* (2018) 78(13). doi: 10.1158/1538-7445

70. Barnhart BC, Sega E, Yamniuk A, Hatcher S, Lei M, Ghermazien H, et al. A therapeutic antibody that inhibits CD73 activity by dual mechanisms. *Cancer Res* (2016) 76. doi: 10.1158/1538-7445.Am2016-1476.

71. Vigano S, Alatzoglou D, Irving M, Ménétrier-Caux C, Caux C, Romero P, et al. Targeting adenosine in cancer immunotherapy to enhance T-cell function. *Front Immunol* (2019) 10:925. doi: 10.3389/fimmu.2019.00925

72. Ohta A, Ohta Akiko, Madasu M, Kini R, Subramanian M, Goel N, et al. A2A adenosine receptor may allow expansion of T cells lacking effector functions in extracellular adenosine-rich microenvironments. *J Immunol* (2009) 183(9):5487–93. doi: 10.4049/jimmunol.0901247

73. Sevigny CP, Li L, Awad AS, Huang L, McDuffie M, Linden J, et al. Activation of adenosine 2A receptors attenuates allograft rejection and alloantigen recognition. *J Immunol* (2007) 178(7):4240–9. doi: 10.4049/jimmunol.178.7.4240

74. Fong L, Hotson A, Powderly JD, Sznol M, Heist RS, Choueiri TK, et al. Adenosine 2A receptor blockade as an immunotherapy for treatment-refractory renal cell cancer. *Cancer Discov* (2020) 10(1):40–53. doi: 10.1158/2159-8290.CD-19-0980

75. Chiappori AA, Creelan B, Tanvetyanon T, Gray JE, Haura EB, Thapa R, et al. Phase I study of taminadenant (PBF509/NIR178), an adenosine 2A receptor antagonist, with or without spartalizumab (PDR001), in patients with advanced non-small cell lung cancer. *Clin Cancer Res* (2022) 28(11):2313–20. doi: 10.1158/1078-0432.CCR-21-2742

76. Zaki EM, Zahran AM, Metwaly AA, Hafez R, Hussein S, Mohammed AE, et al. Impact of CD39 expression on CD4+ T lymphocytes and 6q deletion on outcome of patients with chronic lymphocytic leukemia. *Hematol Oncol Stem Cell Ther* (2019) 12(1):26–31. doi: 10.1016/j.hemonc.2018.09.002

77. Perry C, Hazan-Halevy I, Kay S, Cipok M, Grisaru D, Deutsch V, et al. Increased CD39 expression on CD4(+) T lymphocytes has clinical and prognostic significance in chronic lymphocytic leukemia. *Ann Hematol* (2012) 91(8):1271–9. doi: 10.1007/s00277-012-1425-2

78. Bai A, Moss A, Kokkotou E, Usheva A, Sun X, Cheifetz A, et al. CD39 and CD161 modulate Th17 responses in crohn's disease. *J Immunol* (2014) 193 (7):3366–77. doi: 10.4049/jimmunol.1400346

79. Visweswaran M, Hendrawan K, Massey JC, Khoo ML, Ford CD, Zaunders JJ, et al. Sustained immunotolerance in multiple sclerosis after stem cell transplant. *Ann Clin Transl Neurol* (2022) 9(2):206–20. doi: 10.1002/acn3.51510

80. Yang R, Elsaadi S, Misund K, Abdollahi P, Vandsemb EN, Moen SH, et al. Conversion of ATP to adenosine by CD39 and CD73 in multiple myeloma can be successfully targeted together with adenosine receptor A2A blockade. *J Immunother Cancer* (2020) 8(1). doi: 10.1136/jitc-2020-000610

81. Hegde PS, Chen DS. Top 10 challenges in cancer immunotherapy. *Immunity* (2020) 52(1):17–35. doi: 10.1016/j.immuni.2019.12.011

82. Galon J, Bruni D. Approaches to treat immune hot, altered and cold tumours with combination immunotherapies. *Nat Rev Drug Discov* (2019) 18 (3):197–218. doi: 10.1038/s41573-018-0007-y

83. Johnson DE, O'Keefe RA, Grandis JR. Targeting the IL-6/JAK/STAT3 signalling axis in cancer. *Nat Rev Clin Oncol* (2018) 15(4):234–48. doi: 10.1038/nrclinonc.2018.8

84. Llovet JM, Montal R, Sia D, Finn RS. Molecular therapies and precision medicine for hepatocellular carcinoma. *Nat Rev Clin Oncol* (2018) 15(10):599–616. doi: 10.1038/s41571-018-0073-4

85. Hinshaw DC, Shevde LA. The tumor microenvironment innately modulates cancer progression. *Cancer Res* (2019) 79(18):4557–66. doi: 10.1158/0008-5472.CAN-18-3962

86. Zhang Y, Zheng J. Functions of immune checkpoint molecules beyond immune evasion. *Adv Exp Med Biol 2020* (1248) p:201–26.

87. Yap TA, Parkes EE, Peng W, Moyers JT, Curran MA, Tawbi HA, et al. Development of immunotherapy combination strategies in cancer. *Cancer Discov* (2021) 11(6):1368–97. doi: 10.1158/2159-8290.CD-20-1209

88. Eschweiler S, Clarke J, Ramírez-Suástegui C, Panwar B, Madrigal A, Chee SJ, et al. Intratumoral follicular regulatory T cells curtail anti-PD-1 treatment efficacy. *Nat Immunol* (2021) 22(8):1052–63. doi: 10.1038/s41590-021-00958-6

89. Pardoll DM. The blockade of immune checkpoints in cancer immunotherapy. *Nat Rev Cancer* (2012) 12(4):252–64. doi: 10.1038/nrc3239

90. Bassez A, Vos H, Dyck LV, Floris G, Arijs I, Desmedt C, et al. A single-cell map of intratumoral changes during anti-PD1 treatment of patients with breast cancer. *Nat Med* (2021) 27(5):820–32. doi: 10.1038/s41591-021-01323-8

91. Simon B, Harrer DC, Thirion C, Schuler-Thurner B, Schuler G, Uslu U, et al. Enhancing lentiviral transduction to generate melanoma-specific human T cells for cancer immunotherapy. *J Immunol Methods* (2019) 472:55–64. doi: 10.1016/j.jim.2019.06.015

92. Banta KL, Xu X, Chitre AS, Au-Yeung A, Takahashi C, O'Gorman WE, et al. Mechanistic convergence of the TIGIT and PD-1 inhibitory pathways necessitates co-blockade to optimize anti-tumor CD8(+) T cell responses. *Immunity* (2022) 55 (3):512–26.e9. doi: 10.1016/j.immuni.2022.02.005

frontiers | Frontiers in Immunology

TYPE Original Research
PUBLISHED 13 September 2022
DOI 10.3389/fimmu.2022.956679

OPEN ACCESS

EDITED BY
Yubin Li,
University of Pennsylvania,
United States

REVIEWED BY
Raquibul Hannan,
University of Texas Southwestern Medical Center, United States
Kehua Jiang,
Guizhou Provincial People's Hospital, China

*CORRESPONDENCE
Jiawen Zhang
zhangjw2000@126.com
Haowen Jiang
urology_hs@163.com

†These authors have contributed equally to this work

SPECIALTY SECTION
This article was submitted to Cancer Immunity and Immunotherapy, a section of the journal Frontiers in Immunology

RECEIVED 30 May 2022
ACCEPTED 19 August 2022
PUBLISHED 13 September 2022

CITATION
Gao J, Ye F, Han F, Jiang H and Zhang J (2022) A radiogenomics biomarker based on immunological heterogeneity for non-invasive prognosis of renal clear cell carcinoma.
Front. Immunol. 13:956679.
doi: 10.3389/fimmu.2022.956679

A radiogenomics biomarker based on immunological heterogeneity for non-invasive prognosis of renal clear cell carcinoma

Jiahao Gao[1†], Fangdie Ye[2,3†], Fang Han[1†], Haowen Jiang[2,3,4*] and Jiawen Zhang[1*]

[1]Department of Radiology, Huashan Hospital, Fudan University, Shanghai, China, [2]Department of Urology, Huashan Hospital, Fudan University, Shanghai, China, [3]Fudan Institute of Urology, Huashan Hospital, Fudan University, Shanghai, China, [4]National Clinical Research Center for Aging and Medicine, Huashan Hospital, Fudan University, Shanghai, China

Background: Tumor immunological heterogeneity potentially influences the prognostic disparities among patients with clear cell renal cell carcinoma (ccRCC); however, there is a lack of macroscopic imaging tools that can be used to predict immune-related gene expression in ccRCC.

Methods: A novel non-invasive radiogenomics biomarker was constructed for immune-related gene expression in ccRCC. First, 520 ccRCC transcriptomic datasets from The Cancer Genome Atlas (TCGA) were analyzed using a non-negative matrix decomposition (NMF) clustering to identify immune-related molecular subtypes. Immune-related prognostic genes were analyzed through Cox regression and Gene Set Enrichment Analysis (GSEA). We then built a risk model based on an immune-related gene subset to predict prognosis in patients with ccRCC. CT images corresponding to the ccRCC patients in The Cancer Imaging Archive (TCIA) database were used to extract radiomic features. To stratify immune-related gene expression levels, extracted radiogenomics features were identified according to standard consecutive steps. A nomogram was built to combine radiogenomics and clinicopathological information through multivariate logistic regression to further enhance the radiogenomics model. Mann–Whitney U test and ROC curves were used to assess the effectiveness of the radiogenomics marker.

Results: NMF methods successfully clustered patients into diverse subtypes according to gene expression levels in the tumor microenvironment (TME). The relative abundance of 10 immune cell populations in each tissue was also analyzed. The immune-related genomic signature (consisting of eight genes) of the tumor was shown to be significantly associated with survival in patients with ccRCC in TCGA database. The immune-related genomic signature was delineated by grouping the signature expression as either low- or high-risk. Using TCIA database, we constructed a radiogenomics biomarker consisting of 11 radiomic features that were optimal predictors of immune-related gene

signature expression levels, which demonstrated AUC (area under the ROC curve) values of 0.76 and 0.72 in the training and validation groups, respectively. The nomogram built by combining radiomics and clinical pathological information could further improve the predictive efficacy of the radiogenomics model (AUC = 0.81, 074).

Conclusions: The novel prognostic radiogenomics biomarker achieved excellent correlation with the immune-related gene expression status of patients with ccRCC and could successfully stratify the survival status of patients in TCGA database. It is anticipated that this work will assist in selecting precise clinical treatment strategies. This study may also lead to precise theranostics for patients with ccRCC in the future.

KEYWORDS

clear cell renal cell carcinoma, radiogenomics, tumor heterogeneity, immune microenvironment (IME), contrast-enhanced computed tomography (CECT)

Introduction

Kidney cancer is one of the most common urological tumors, with the number of new patients with renal cancer reaching up to 90,0000 each year (1, 2). Clear cell renal cell carcinoma (ccRCC) is the most common pathological subtype of kidney cancer, accounting for 70%–80% (3, 4) of renal cancers. Early surgical intervention is currently the primary treatment for ccRCC (5, 6). Most patients who undergo early resection have an overall 5-year survival rate of >90%. Some patients with ccRCC have extremely high rates of recurrence and metastasis, which severely affects postoperative survival (7, 8). Some targeted therapies have shown decent treatment effects in ccRCC patients, including sorafenib and axitinib (9, 10). However, the indications for the application of targeted drugs remain highly controversial (11, 12). Therefore, there is an urgent need for non-invasive indicators to effectively diagnose ccRCC patients with different therapeutic reactions, thus enabling rational selection of clinical ccRCC treatment strategies.

Tumor heterogeneity is closely associated with the significant prognostic variability of current tumor therapies in ccRCC patients (13, 14). The synergy between tumor cells and the microenvironment is an important factor in tumor heterogeneity (15, 16). Immune and stromal cells, which represent important components of the TME, are considered to be closely related to the aggressiveness and the developmental potential of ccRCC. The heterogeneous expression of immune-related genes is thought to correlate with ccRCC prognosis (17, 18). Therefore, the exploitation of immune-related prognostic markers is considered an important tool to improve the diagnosis and treatment of ccRCC. Radiogenomics combines gene expression information with medical imaging features, thus enabling an in-depth understanding of tumor biology and capture of internal tumor heterogeneity information (19, 20). Traditional genetic analysis of the tumor based on invasive biopsy is costly and cannot fully reflect the heterogeneity of tumor microenvironment (TME) (21). Radiogenomics has the potential to become a promising non-invasive diagnostic method that can reflect gene expression information (22).

In this study, we constructed a novel radiogenomics method based on TME-related gene profiles. The immune-related gene expression risk score was calculated and predicted using the radiogenomics approach to build molecular markers for the non-invasive prognosis evaluation of ccRCC. Such a strategy may assist in making precise clinical treatment decisions and achieving precise theranostics for ccRCC.

Materials and methods

Data processing

Transcriptomic data and relevant clinical and pathological information were extracted from The Cancer Genomics Atlas (TCGA) for ccRCC patients, with a total of 539 samples. To obtain reliable conclusions, samples with a <30-day survival rate were excluded, leaving 520 ccRCC samples enrolled in the downstream analysis. In addition, immune-related (IR) gene symbol names were obtained from the Immunology Database and Analysis Portal (ImmPort). The corresponding enhanced CT digital images were

acquired from The Cancer Imaging Archive (TCIA) database. Initially, we collected 267 digital images, and some CT images were excluded based on set criteria for image collection (poor image quality or failure to identify the area of the lesion by the imaging physicians).

Identification of ccRCC subtypes

The obtained TME-related genes were used for non-negative matrix decomposition (NMF) clustering to identify ccRCC molecular subtypes, and the optimal cluster number K value was determined to be 2. Non-negative matrix factorization (NMF) is an unsupervised learning algorithm that extracts available features. NMF works similar to the principal component analysis and can be employed for dimensionality reduction. Principal component analysis (PCA) was performed to determine the robustness and reliability of ccRCC molecular subtypes.

Investigation of immune cell nfiltration status

To evaluate the status of immune cell infiltration in the TME, the R package "MCPcounter" was used to manage the relative abundance of 10 immune cell populations in each tissue according to the transcriptome data. The cell types included T cells, CD8+ T cells, cytotoxic lymphocytes, B lineage cells, NK cells, monocytic lineage cells, myeloid dendritic cells, neutrophils, endothelial cells, and fibroblasts. Wilcoxon rank-sum test analysis was performed to assess the differences in immune cell infiltration among the distinct molecular subtypes.

Construction and validation of the risk model

To quantify immune-related correlation patterns for individual tumors, we divided the patients into training and validation groups in a ratio of 7:3, and univariate Cox proportional hazard regression was conducted to identify immune-related prognostic markers. We further applied significant factors to Least Absolute Shrinkage and Selective Operator (LASSO) and univariate Cox proportional hazard regression analyses to construct the risk model. The risk score was calculated based on the coefficients of the candidate genes. According to the median risk score, patients were divided into low- and high-risk groups. To improve the accuracy and practicability of the clinical predictive model, we constructed a nomogram model that included the following parameters: risk score, clinical stage, TNM stage, age, and sex. A calibration curve of the nomogram model was established to assess the consistency between the predicted and observed results.

Gene Set Enrichment Analysis (GSEA) used predefined gene sets (gmt files C2 and C5) to rank genes according to their differential expression levels in the two risk groups using the clusterProfiler R package. Only items with a P-value < 0.05 were considered. GSEA was conducted to normalize the gene expression profile and to excavate GO and KEGG pathways.

Imaging protocol

In the radiogenomics section, the study initially included 245 patients, all of whom underwent preoperative abdominal CT or MRI, with ccRCC from TCGA-KIRC database. The patients underwent standard three-phase scans, including the cortical phase (25–30 s after contrast injection), parenchymal phase (60–70 s after contrast injection), and secretory phase (2–3 min after contrast injection). Iodine contrast injection standards were obtained from TCIA database for each hospital reference standard. The inclusion criteria were as follows: (1) confirmation of ccRCC with TNM staging obtained based on postoperative pathology; (2) preoperative contrast-enhanced CT (CECT) scan imaging data were complete, and a standard kidney CT triple enhancement scan protocol was used; and (3) recognizable mass lesions that could be detected in the kidney by parenchymal images with CE-CT scans. Exclusion criteria included the following: (1) a dissatisfactory quality of the CE-CT scans or the presence of large artifacts influencing the judgment of the lesion area; (2) radiomic features that cannot be successfully extracted through CECT scans. The detailed procedures of our study are shown in Figure S1.

Image preprocessing and region-of-interest acquisition

Based on previous studies on kidney-associated radiomics, we selected the parenchymal phase in CECT scans to extract the radiomics features most associated with immune heterogeneity (23, 24). In the process of image sketching, an imaging physician (with 15 years of work experience in diagnostic urologic CT imaging) identified and fragmented the lesion contours on each slice within the sequence using the 3D Slicer software (version 4.11.2; Boston, MA, USA). Features were then established using the radiomics extraction software Pyradiomics (3.0.0; https://github.com/Radiomics/pyradiomics). Following this, we processed the obtained feature data by utilizing the min–max approach.

Intra-class and inter-class correlation coefficients (ICC) were used to assess the stability of the acquired features. Fifty patients were randomly selected for repeat region-of-interest (ROI) fragmentation by both the previous radiologist and a new

radiologist (with 8 years of experience in urologic CT imaging) 30 days after the initial segmentation. Both physicians were unaware of the history of kidney disease and pathological diagnosis of the patients.

Preliminary construction of the radiogenomics biomarker

In TCGA-KIRC database, radiogenomics features extracted from CECT images were filtered, and radiogenomics models were constructed according to the following sequential steps. Firstly, features with both intra-class and inter-class correlation coefficients greater than 0.75 were allowed as components of the potential immune-related radiogenomics model. The minimum redundancy-maximum relevance (mRMR) method was used for further feature dimensionality reduction with sufficient stability. LASSO analysis was then used for the selection of optimal radiogenomics features. The selected optimal features were linearly combined with pass-through coefficients to construct radiogenomics labels associated with immune-related gene expression levels, also known as RADscores. Evaluation of the novel radiogenomics biomarker was performed using the Mann–Whitney U test, mainly to classify patients into high- or low-risk groups based on immune-related gene expression. ROC curves were calculated to assess the predictive efficacy of the preliminary radiogenomics model.

Nomogram construction based on the radiogenomics model

To further increase the credibility of the model, clinical and pathological information from the TCIA-KIRC database was combined in the radiogenomics model. Univariate analysis was performed to screen for elements associated with altered genetic subsets in the tumor microenvironment. In the training cohort, variables with $P < 0.1$ in the univariate regression were subsequently assigned to the multivariate logistic regression. A clinical model was constructed to include factors with $P < 0.1$ in the previous step of the multivariate analysis; backward stepwise selection was performed using the likelihood ratio test. We also compared the predictive power of the preliminary radiogenomics marker with clinical models for tumor immune-related gene risk model stratification. Finally, a combined multivariate logistic model was constructed using the RADscores and the selected clinicopathological factors. Variance inflation factor (VIF) analysis was performed on the combined model to further reduce the probability of overfitting. A nomogram was developed to visualize the final radiogenomics model, specifically to score each patient and quantify the levels of immune-related gene expression.

Radiogenomics biomarker validation

The combined model was evaluated in the patient cohort, including the training and testing groups. ROC curves and AUC values were adopted to assess the predictive recognition capability of the immune microenvironment in the combined model. Calibration curves and Hosmer–Lemeshow tests were used to estimate the agreement between the predicted outcomes and the expected probabilities in the radiogenomics model.

We also used decision curve analysis (DCA) to analyze the clinical potential of the radiogenomics biomarker and calculated the net benefit of the model for different threshold probabilities.

Statistical analysis

All statistical analyses were performed using the R software (version 3.6.3). The "survivalROC" package was employed to calculate the area under curve (AUC) of the ROC curve to assess the clinical utility of the prognostic model for clinical outcome. Kaplan–Meier (KM) analysis was conducted to assess survival differences among subtypes, with overall survival (OS) as the primary outcome. Disease-specific survival (DSS) and progression-free survival (PFS) were calculated as secondary outcomes. Continuous data were evaluated using the Wilcoxon rank-sum test. In addition, Fisher's exact test was used to calculate differences in categorical data. Statistical significance was set at P value < 0.1.

Results

Identification of molecular subtypes

To investigate the molecular subtypes of ccRCC, transcriptomic data of ccRCC patients from TCGA database were retrieved. The expression information of tumor microenvironment-related genes was extracted. The heatmap displayed a different distribution of TME-related genes between tumor tissues and normal tissues in ccRCC (Figure 1A). The NMF algorithm was used to cluster patients into diverse subtypes according to TME gene expression levels. To ensure robust clustering results, the cophenetic correlation coefficient was used to determine the optimal number of clusters, and $K = 2$ was selected as the optimal cluster number after comprehensive consideration (Figure 1B). When $k = 2$, we observed that the two subtypes (C1 and C2) had clear boundaries, indicating that the ccRCC samples had stable and reliable clustering (Figure 1C). The survival curve (Figures 1D, E) showed that the overall survival of cluster 1 was significantly better than that of cluster 2 ($P < 0.001$). In addition, C1 had a significant advantage in progression-free survival compared to C2 ($P < 0.001$).

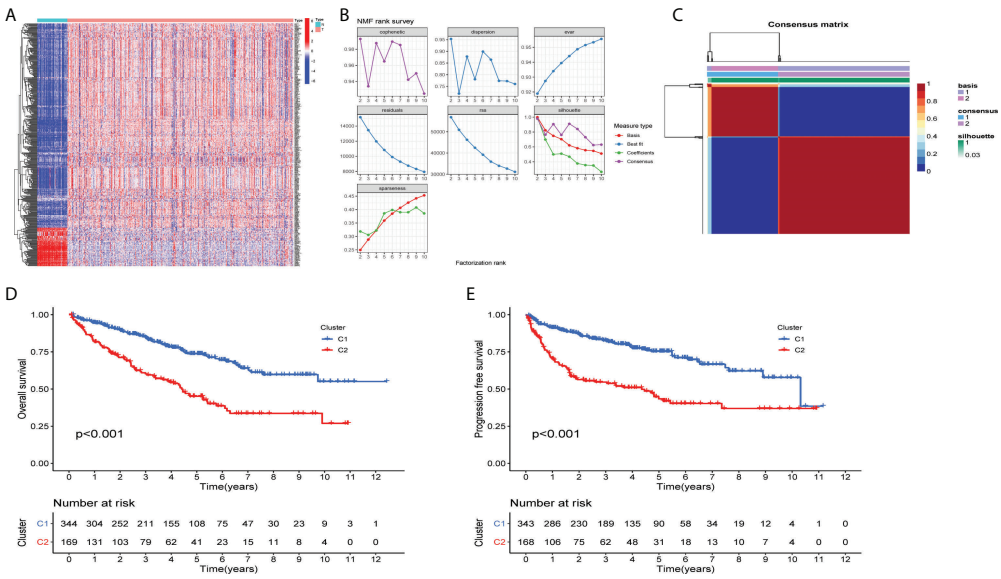

FIGURE 1
Two distinct TME-related molecular subtypes were identified by NMF analysis for ccRCC **(A)** The heatmap displays the expression patterns of TME-related genes in the tumors and normal tissues. N is equal to normal tissues, T is equal to tumor tissues. **(B)** Factorization rank for k = 2–10. **(C)** The heatmap of the consensus matrix when the consensus clustering k = 2. The value range is 0–1. The columns and rows are sorted through hierarchical clustering according to the Euclidean distance of the average link. **(D)** Kaplan–Meier OS curves and **(E)** PFS curve for the two clusters in TCGA-ccRCC dataset. The assessment of difference was achieved by log-rank test.

Relationship between molecular subtypes and the tumor microenvironment

To determine immune-related gene expression in the tumor microenvironment, we explored immune cell infiltration in the two ccRCC subtypes using the MCPcount algorithm. The degree of invasion of the 10 immune cell populations in each ccRCC patient was evaluated, as shown in Figure 2. Ten immune cell groups were variable between the two subtypes. The levels of T cells, myeloid dendritic cells, monocyte lineage cells, fibroblasts, and cytotoxic lymphocytes were significantly increased in cluster 2. In contrast, the numbers of endothelial cells and neutrophils were decreased in cluster 1. For each type of immune cell expression data, the FDR values (q-values) for statistical differences between the two groups are available in the supplementary material.

Identification of prognostic features in renal clear cell carcinoma

To further investigate the quantification of TME indicators for individual ccRCC patients, we performed in-group validation using TCGA datasets. The patients were divided into training and validation groups on a 7:3 scale. Univariate Cox regression analysis was performed to select genes with prognostic significance; 245 significant prognostic genes were retained. LASSO and Cox regression analyses were then performed to reduce redundancy. Fourteen genes were identified. Finally, in the prognostic model constructed by the multivariate regression method, a total of eight risk genes were selected, including PIMREG, CXCL5, UCN, KRBA1 PABPC1L RNASE2 IL4I1, and ABCB4. We then constructed a risk score formula based on the expression of specific genes and the coefficients calculated by multivariate Cox regression as follows: risk score = 0.461*PIMREG+0.11*CXCL5+0.526*UCN-0.465*KRBA1 +0.200*PABPC1L+0.254*RNASE2+0.261*IL4I1-0.595*ABCB4.

We further investigated the clinical outcomes of high-risk and low-risk patients using a risk prognostic model. Kaplan–Meier curves exhibited lower overall survival (OS) in the high-risk group in the training, validation, and TCGA datasets ($P < 0.001$, Figures 3A–C). We further investigated the clinical outcomes of patients with high or low expression of these eight risk genes alone as genomic markers through Kaplan–Meier analysis of OS, and the specific results are presented in the supplementary material. It should be noted that, although individual genes also have good survival prediction, the immune-related genetic risk model we constructed was able to significantly improve the predictive efficacy of survival stratification. We also adopted other survival times (including DSS and PFS) as the survival evaluation method, demonstrating

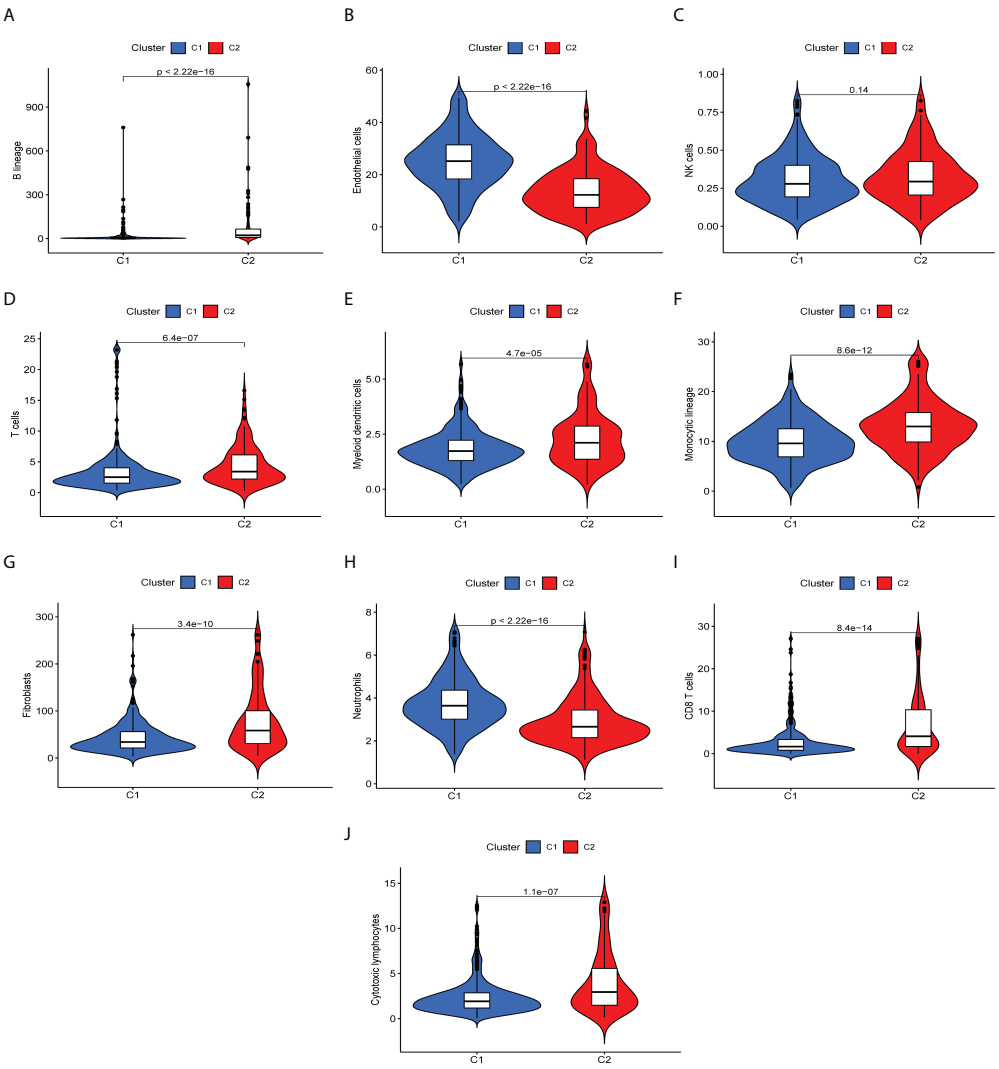

FIGURE 2
Differences of immune infiltrating cells in the immune microenvironment of two ccRCC molecular subtypes. **(A–I)** Levels of immune cell infiltration in the two subtypes. **(A)** B lineage, **(B)** endothelial cells, **(C)** NK cells, **(D)** T cells, **(E)** myeloid cells, **(F)** monocytic lineage, **(G)** fibroblasts, **(H)** neutrophils, **(I)** CD 8+T cells, **(J)** cytotoxic lymphocytes.

the predictive value of our immune-related genetic risk model for the clinical prognosis of ccRCC patients.

Validation of prognostic features in ccRCC

To evaluate the clinical applicability of the risk prognostic model as a tool to predict the survival probability of patients with renal clear cell carcinoma, receiver operating characteristic curve (ROC) analysis was performed. The area under the curve (AUC) values of the 1-year OS in the training, validation, and TCGA datasets were 0.804, 0.731, and 0.784, respectively. The AUC values of 3-year OS were 0.765, 0.738, and 0.757, respectively. The AUC values of 5-year OS were 0.782, 0.772, and 0.777, respectively (Figures 3E–G). Then, univariate Cox regression and multivariate Cox regression analyses demonstrated that the risk prognostic model was an independent predictive biomarker (Figures 3D, H). In addition, to improve the clinical applicability of the risk prognostic model, we constructed a nomogram, including TNM stage, sex, age, and clinical stage (Figure 4A). The calibration diagram shows a fair agreement between the prediction results and the actual observation results of the nomogram model (Figure 4B). In addition, we compared the advantages and disadvantages of the TME prognostic risk model and other reported prognostic risk models, including models

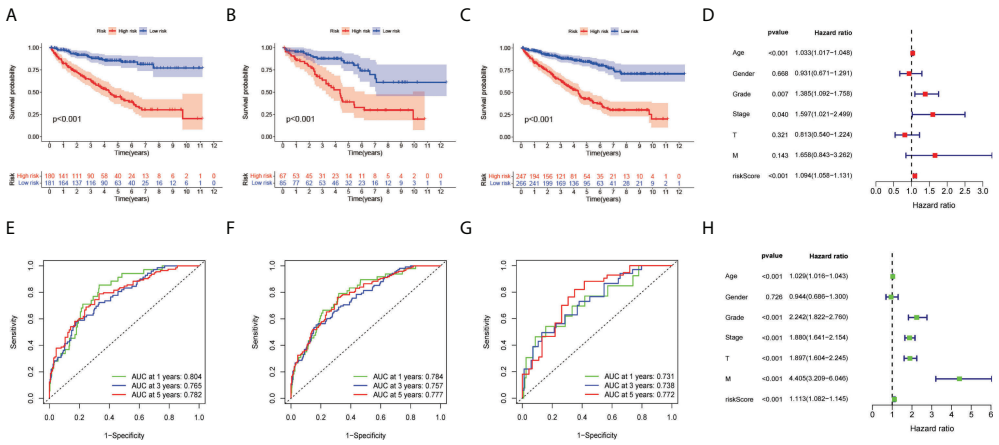

FIGURE 3
Development of eight risk genes for ccRCC. **(A-C)** Kaplan–Meier OS curve for high- and low-risk groups. **(A)** Training group, **(B)** validation group, and **(C)** TCGA dataset. **(D)** Forest plots displayed the univariate Cox regression analysis results of the risk score and clinical factors with OS. **(E-G)** Receiver operating characteristic curves (ROC curves) for the 1-, 3- and 5-year OS periods. **(E)** Training group, **(F)** validation group, and **(G)** TCGA dataset. **(H)** Forest plots display the multivariate Cox regression analyses results of the risk score and clinical factors with OS.

constructed in previous studies. The AUC values of 5-year OS were all higher than those of other known risk models (25–28) (Figures 5A–E). The K-M curve indicated that our immune-related prognostic risk model had the highest differentiation for patients' clinical outcomes (Figures 5F–J).

Comparison of clinicopathological features in high- and low-risk groups

We investigated the clinicopathological features of patients in the high-risk and low-risk groups, including T stage, N stage, lymphatic metastasis, and distant metastasis. The higher the clinical stage and T stage (Figures 4C, D), the more extensive the tumor lesion, and the higher the risk score ($P < 0.05$). In addition, there was a positive correlation between clinical stage and risk score ($P < 0.05$). Patients with lymphatic or distant metastasis had a higher risk factor ($P < 0.1$) (Figures 4E, F).

Preliminary radiogenomics biomarker construction and evaluation

The CT images of 193 patients corresponding to the above transcriptomic data were included based on defined criteria for image collection (poor image quality or failure to identify the area of lesion by the imaging physicians) in TCIA-KIRC database (Figure 6A). From the enhanced CT scans of all patients, 1,218 features were extracted separately. After ICC evaluation, a minimum criterion of 0.75 for intra- or inter-ICC values was applied, leaving 821 features for initial feature screening. The most influential 30 features were then retained using the mRMR algorithm. Thirteen radiomics features were selected using LASSO regression (Figure 6B) to construct a preliminary radiogenomics model; the specific features are shown in Figure 6C. The formula for RADscores is shown in Supplementary Material II.

From the Mann–Whitney U test (Figure 6D), there was a significant difference in expression between the subsets of tumor microenvironment gene composition in the training cohort ($P < 0.01$), which was confirmed in the independent validation cohort ($P < 0.05$). The AUC values of the preliminary radiogenomics model were 0.76 in the training cohort and 0.72 in the validation cohort (Figure 6E).

Nomogram construction based on the radiogenomics model

In the univariate analysis of the clinical model building, only grade was significantly associated with tumor microenvironment gene subset grouping ($P < 0.1$). It retained statistical significance in the multivariate logistic regression analysis ($P < 0.1$) and therefore constituted the clinical model. The combined model was constructed by combining RADScore and Grade. Finally, we visualized this ultimate radiogenomics marker in the form of a nomogram, as shown in Figure 6F.

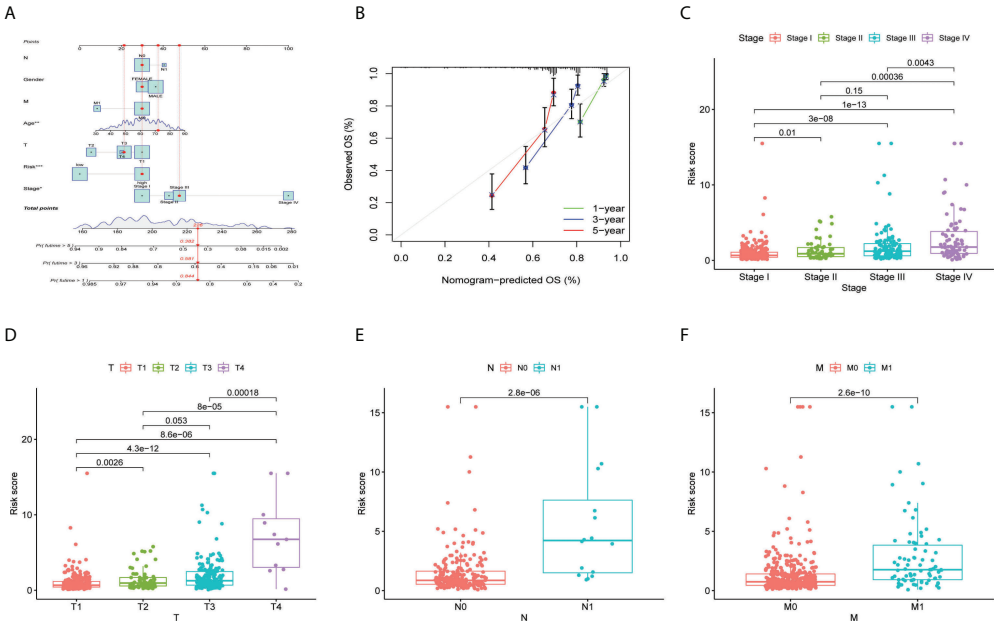

FIGURE 4
Validation of prognostic features in ccRCC. **(A)** Construction of a nomogram combining the risk prognostic signature and clinical features for prediction of OS. **(B)** Calibration plots display the actual and nomogram-predicted probability of the 1-, 3- and 5-year OS periods. **(C–F)** The box plot depicts the relationship between risk score and clinicopathology. **(C)** N stage, **(D)** M stage, **(E)** clinical stage, and **(F)** T stage. *$P < 0.05$; **$P < 0.01$; ***$P < 0.001$.

Final radiogenomics model validation and clinical use evaluation

The radiogenomics biomarker based on the subset of tumor immune-related gene expression showed good predictive performance (AUC of 0.81 and 0.74 in the training and validation cohorts, respectively) in reflecting tumor immune-related gene expression alterations (Figure 6G). The Delong test showed a statistically significant difference in AUC values between the combined nomogram and the clinical model ($P < 0.01$). The calibration curves (Figure 6H) showed good agreement between the predicted and the observed probabilities of the combined nomograms.

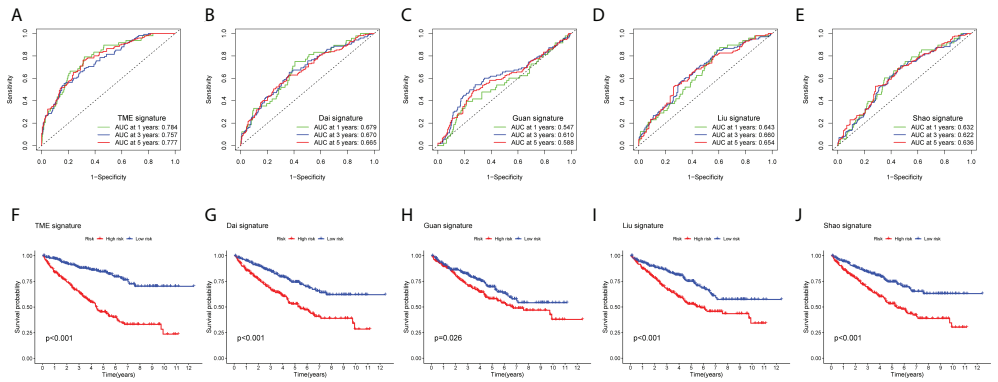

FIGURE 5
Comparison between prognostic models. **(A–E)** Receiver operating characteristic curves (ROC curves) for the 1-, 3-, and 5-year OS periods. **(A)** TME-related risk prognostic model, **(B)** Dai signature, **(C)** Guan signature, **(D)** Liu signature, and **(E)** Shao signature. **(F–J)** Kaplan–Meier OS curve for high- and low-risk groups. **(F)** TME-related risk prognostic model, **(G)** Dai signature, **(H)** Guan signature, **(I)** Liu signature, and **(J)** Shao signature.

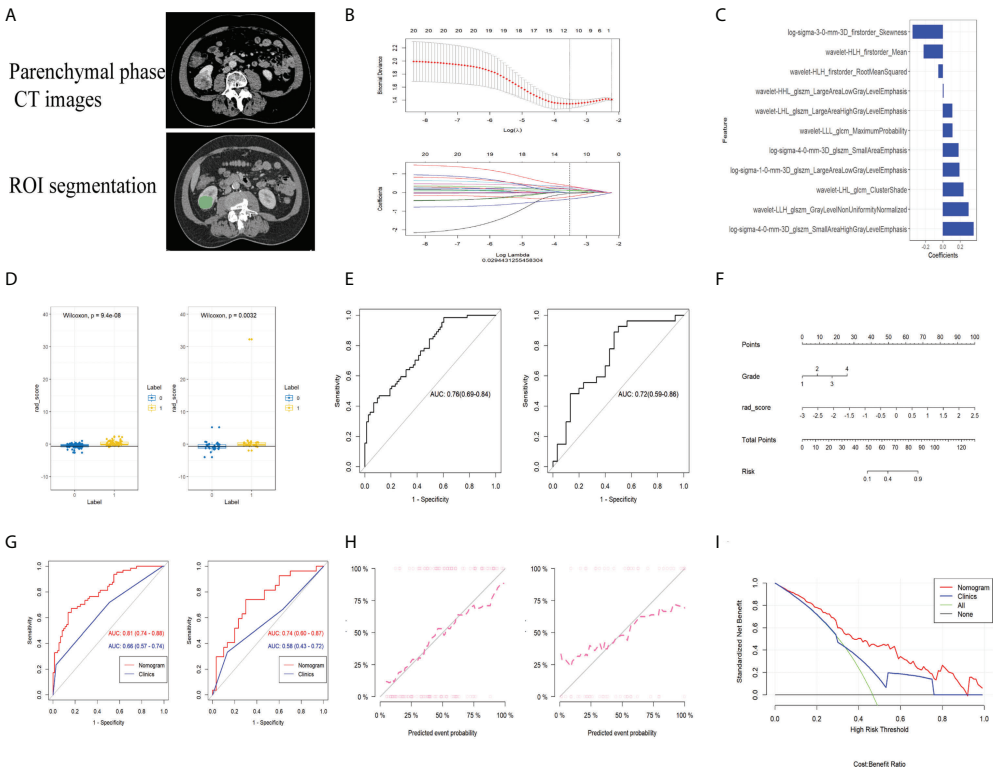

FIGURE 6
(A) CT image phase selection and ROI segmentation. **(B)** LASSO regression applied in the radiomics feature screening process. **(C)** The radiomics features finally screened for building the radiogenomics model. **(D)** M-W test showing that the radiomics model can effectively distinguish between the established gene subsets in both the training and validation groups. **(E)** ROC curves of the predictive power of the pure radiomics model for gene subsets in both the training and validation groups. **(F)** Nomogram built by combining radiomics as well as clinical and pathological information. **(G)** Predictive performance of the nomogram in both training and validation groups. **(H)** Calibration curves showing excellent fitting ability of the established radiogenomics model. **(I)** DCA curves of the established radiogenomics nomogram compared with the clinical model.

Decision curve analysis showed that the radiogenomics nomogram provided a net benefit compared to the "treat all" or "no treatment" strategy with a threshold probability of more than 10% for the clinical model (Figure 6I). This indicates that the radiogenomics nomogram has an excellent clinical utility.

Discussion

In this study, a novel radiogenomics biomarker was constructed to predict the prognosis of patients with ccRCC. Such a biomarker was built on its close relationship with immune-related gene expression detected by transcriptomic analysis in patients with ccRCC. Survival statistics demonstrated that it could effectively stratify the prognosis of ccRCC patients. We aim to improve the process of precise tumor diagnosis and treatment through radiogenomics and to promote the deep investigation and mining of genetic information by imaging methods.

As solid tumors exhibit completely different drug therapeutic efficacies and disease progression in different patients, the tumor microenvironment is increasingly becoming a scientific hotspot for research on therapeutic resistance of tumors as well as target selection. In clear cell renal cell carcinoma, large-scale genomic studies have identified somatic mutations that affect tumor progression and the response to immune checkpoint blockade therapy (29–31). Unfortunately, despite the large number of genetic markers currently constructed for the tumor microenvironment of kidney cancer and the good results they have achieved in prognosis prediction, their reliability and practical clinical application remain unconvincing; there are still major obstacles facing the use of multiple genetic markers in practical clinical application. Therefore, it is extremely important to identify the infiltration of TME and immune-related gene expression in ccRCC patients using non-invasive diagnostic methods.

Radiomics is different from the conventional perspective of image information interpretation, which uses high-level

algorithms and advanced image processors (32–34). The fundamental problems facing radiomics toward clinical applications, such as the poor interpretability of extracted features and the inability of more advanced deep learning methods to explain them in a completely "black box," have not received much attention from researchers. In our study, we found that a radiogenomics marker based on genetic information from the TME can reflect profound alterations in immune-related gene expression. Their expression levels are closely correlated with a variety of immune cells, such as T cells, myeloid dendritic cells, and fibroblasts. In addition, there were significant correlations between the alterations and pathways such as tumor fibrosis and microvascular infiltration. This suggests that the novel radiogenomics marker we constructed could adequately reflect the various profound modifications of the TME. Few previous studies have reported the application of radiogenomics approaches for the non-invasive monitoring of TME. This gives our study a unique advantage, although this research approach needs to be supported by further experimental data. However, it also provides a fresh and dynamic methodological guide for the optimal combination of imaging and genomic data. However, it must also be acknowledged that a direct association between the immune microenvironment of ccRCC and the clinical prognosis of patients has not been confirmed by large-scale clinical data. Therefore, our study was based on transcriptomic data, and it aimed to assess immune-related gene expression in tumors in a non-invasive manner. This way, prognostic differences in tumors can be explained from an immunological perspective. Notably, some ccRCC patients often suffer from a coexisting disease with abnormal autoimmune system function, which may have a confounding effect on the ultimate predictive efficacy of immune-based prediction models. We therefore recommend that immune-related clinical treatment decisions and predictive models be considered with caution in such patients. In our work, we have incorporated some valid clinical and pathological factors in addition to immune-related genes in the hope of diluting the adverse effects on model prediction in this subset of patients. However, specific predictive efficacy requires future clinical validation of transcriptomic data and imaging for this subset of immune abnormal ccRCC patients.

Some limitations exist in this study: (1) the images in the study were obtained from TCIA database, utilizing different imaging machines and image acquisition protocols. Although strict inclusion and exclusion criteria were used, the results need to be validated in future clinical trials in more centers. (2) Robust data on radiogenomics and specific phenotypes of the tumor microenvironment are still lacking, and we hope to deepen our understanding of this in the future by combining conventional methods with radiogenomics-based methods. (3) Concerning the comprehensiveness of clinical information in TCGA database, only select clinical and pathological factors were included in the radiogenomics model, and more factors, such as conventional markers, may be needed in the future to improve the predictive power and reliability of the model. (4) Radiomics analysis was based on the ROI of the entire tumor, while the biopsy was tumor-specific. Owing to the spatial resolution of the CT image and the unavailability of tumor sampling location information, it has not yet been possible to achieve a more accurate prediction between the two correspondences. We hope to make further breakthroughs on this problem in future work.

In conclusion, this study constructed a novel non-invasive radiogenomics marker for the prognostic stratification of ccRCC. Based on the contrast-enhanced CT scans and radiogenomics features in ccRCC patients, this biomarker achieved convergent prediction of immune-related gene risk model stratification and pathway alterations. Such a novel imaging-based approach, used to reveal tumor microenvironment alterations, may have great clinical value for future immunotherapy efficacy and individualized tumor treatment.

Data availability statement

The datasets presented in this study can be found in online repositories. The names of the repository/repositories and accession number(s) can be found in the article/Supplementary Material.

Ethics statement

This study was reviewed and approved by The institute review board of Huashan hospital, Fudan University. The patients/participants provided their written informed consent to participate in this study. Written informed consent was obtained from the individual(s) for the publication of any potentially identifiable images or data included in this article.

Author contributions

JG, FY, and FH contributed equally to this work. Research establishment, JG and FY. ROI outlining and image filtering, FH. Data analysis, JG. Supervision, JZ and HJ. All authors contributed to the article and approved the submitted version.

Funding

This work was funded by the National Key Research and Development Project in China (No. 2017YFC0113405), National Natural Science Foundation of China (82071877), and Natural Science Basic Research Plan of Shaanxi (No. 2022JQ-811).

Conflict of interest

The authors declare that the research was conducted in the absence of any commercial or financial relationships that could be construed as a potential conflict of interest.

Publisher's note

All claims expressed in this article are solely those of the authors and do not necessarily represent those of their affiliated organizations, or those of the publisher, the editors and the reviewers. Any product that may be evaluated in this article, or claim that may be made by its manufacturer, is not guaranteed or endorsed by the publisher.

Supplementary material

The Supplementary Material for this article can be found online at: https://www.frontiersin.org/articles/10.3389/fimmu.2022.956679/full#supplementary-material

References

1. Siegel RL, Miller KD, Fuchs HE, Jemal A. Cancer statistics, 2021. *CA: Cancer J Clin* (2021) 71(1):7–33. doi: 10.3322/caac.21654

2. Sung H, Ferlay J, Siegel RL, Laversanne M, Soerjomataram I, Jemal A, et al. Global cancer statistics 2020: GLOBOCAN estimates of incidence and mortality worldwide for 36 cancers in 185 countries. *CA: Cancer J Clin* (2021) 71(3):209–49. doi: 10.3322/caac.21660

3. Wettersten HI, Aboud OA, Lara PNJ, Weiss RH. Metabolic reprogramming in clear cell renal cell carcinoma. *Nat Rev Nephrol* (2017) 13(7):410–9. doi: 10.1038/nrneph.2017.59

4. Schödel J, Grampp S, Maher ER, Moch H, Ratcliffe PJ, Russo P, et al. Hypoxia, hypoxia-inducible transcription factors, and renal cancer. *Eur Urol* (2016) 69(4):646–57. doi: 10.1016/j.eururo.2015.08.007

5. Krishna C, DiNatale RG, Kuo F, Srivastava RM, Vuong L. Single-cell sequencing links multiregional immune landscapes and tissue-resident T cells in ccRCC to tumor topology and therapy efficacy. *Cancer Cell* (2021) 39(5):662–77. doi: 10.1016/j.ccell.2021.03.007

6. Turajlic S, Xu H, Litchfield K, Rowan A, Chambers T, Lopez JI, et al. Tracking cancer evolution reveals constrained routes to metastases: TRACERx renal. *CELL* (2018) 173(3):581–94. doi: 10.1016/j.cell.2018.03.057

7. Yong C, Stewart GD, Frezza C. Oncometabolites in renal cancer. *Nat Rev Nephrol* (2020) 16(3):156–72. doi: 10.1038/s41581-019-0210-z

8. Huang WC, Donin NM, Levey AS, Campbell SC. Chronic kidney disease and kidney cancer surgery: New perspectives. *J Urol* (2020) 203(3):475–85. doi: 10.1097/JU.0000000000000326

9. Kats-Ugurlu G, Oosterwijk E, Muselaers S. Neoadjuvant sorafenib treatment of clear cell renal cell carcinoma and release of circulating tumor fragments. *Neoplasia (New York, N.Y.)* (2014) 16(3):221–8. doi: 10.1016/j.neo.2014.03.007

10. Rini BI, Plimack ER, Stus V, Gafanov R. Pembrolizumab plus axitinib versus sunitinib for advanced renal-cell carcinoma. *N Eng J Med* (2019) 380(12):1116–27. doi: 10.1056/NEJMoa1816714

11. Motzer RJ, Penkov K, Haanen J, Rini B, Albiges L. Avelumab plus axitinib versus sunitinib for advanced renal-cell carcinoma. *N Eng J Med* (2019) 380(12):1103–15. doi: 10.1056/NEJMoa1816047

12. Motzer RJ, Robbins PB, Powles T, Albiges L, Haanen JB, Larkin J, et al. Avelumab plus axitinib versus sunitinib in advanced renal cell carcinoma: biomarker analysis of the phase 3 JAVELIN renal 101 trial. *Nature Med* (2020) 26(11):1733–41. doi: 10.1038/s41591-020-1044-8

13. Dagogo-Jack I, Shaw AT. Tumour heterogeneity and resistance to cancer therapies. *Nat Rev Clin Oncol* (2018) 15(2):81–94. doi: 10.1038/nrclinonc.2017.166

14. Pe'er D, Ogawa S, Elhanani O, Keren L, Oliver TG, Wedge D. Tumor heterogeneity. *Cancer Cell* (2021) 39(8):1015–7. doi: 10.1016/j.ccell.2021.07.009

15. Chen X, Song E. Turning foes to friends: targeting cancer-associated fibroblasts. *Nat Rev Drug Discov* (2019) 18(2):99–115. doi: 10.1038/s41573-018-0004-1

16. Chen Y, McAndrews KM, Kalluri R. Clinical and therapeutic relevance of cancer-associated fibroblasts. *Nat Rev Clin Oncol* (2021) 18(12):792–804. doi: 10.1038/s41571-021-00546-5

17. Gossage L, Eisen T, Maher ER. VHL, the story of a tumour suppressor gene. *Nat Rev Cancer* (2015) 15(1):55–64. doi: 10.1038/nrc3844

18. Choueiri TK, Kaelin WGJ. Targeting the HIF2-VEGF axis in renal cell carcinoma. *Nat Med* (2020) 26(10):1519–30. doi: 10.1038/s41591-020-1093-z

19. Moussa AM, Ziv E. Radiogenomics in interventional oncology. *Curr Oncol Rep* (2021) 23(1):9. doi: 10.1007/s11912-020-00994-9

20. Badic B, Tixier F, Cheze Le Rest C, Hatt M, Visvikis D. Radiogenomics in colorectal cancer. *Cancers* (2021) 13(5):973–81. doi: 10.3390/cancers13050973

21. Meng Y, Cai K, Zhao J, Huang K, Ma X, Song J, et al. Transcriptional profiling reveals kidney neutrophil heterogeneity in both healthy people and ccRCC patients. *J Immunol Res* (2021) 2021:5598627. doi: 10.1155/2021/5598627

22. Ursprung S, Beer L, Bruining A, Woitek R, Stewart GD, Gallagher FA, et al. Radiomics of computed tomography and magnetic resonance imaging in renal cell carcinoma-a systematic review and meta-analysis. *Eur Radiol* (2020) 30(6):3558–66. doi: 10.1007/s00330-020-06666-3

23. Rallis KS, Kleeman SO, Grant M, Ordidge KL, Sahdev A, Powles T. Radiomics for renal cell carcinoma: Predicting outcomes from immunotherapy and targeted therapies-a narrative review. *Eur Urol Focus* (2021) 7(4):717–21. doi: 10.1016/j.euf.2021.04.024

24. Suarez-Ibarrola R, Basulto-Martinez M, Heinze A, Gratzke C, Miernik A. Radiomics applications in renal tumor assessment: A comprehensive review of the literature. *Cancers* (2020) 12(6):1387–96. doi: 10.3390/cancers12061387

25. Dai S, Zeng H, Liu Z, Jin K. Intratumoral CXCL13(+)CD8(+)T cell infiltration determines poor clinical outcomes and immunoevasive contexture in patients with clear cell renal cell carcinoma. *J Immunother Cancer* (2021) 9 (2):1823–34. doi: 10.1136/jitc-2020-001823

26. Peng R, Wang Y, Mao L, Fang F, Guan H. Identification of core genes involved in the metastasis of clear cell renal cell carcinoma. *Cancer Manag Res* (2020) 12:13437–49. doi: 10.2147/CMAR.S276818

27. Chang K, Yuan C, Liu X. Ferroptosis-related gene signature accurately predicts survival outcomes in patients with clear-cell renal cell carcinoma. *Front Oncol* (2021) 11:649347. doi: 10.3389/fonc.2021.649347

28. Xu C, Chen L, Li D, Chen F, Sha M, Shao Y. Acyl-CoA thioesterase 8 and 11 as novel biomarkers for clear cell renal cell carcinoma. *Front Genet* (2020) 11:594969. doi: 10.3389/fgene.2020.594969

29. Miao D, Margolis CA, Gao W. Genomic correlates of response to immune checkpoint therapies in clear cell renal cell carcinoma. *Sci (New York N.Y.)* (2018) 359(6377):801–6. doi: 10.1126/science.aan5951

30. Clark DJ, Dhanasekaran SM, Petralia FZ. Integrated proteogenomic characterization of clear cell renal cell carcinoma. *Cell* (2019) 179(4):964–83. doi: 10.1016/j.cell.2019.10.007

31. Au L, Hatipoglu E, Robert de Massy M, Turajlic S. Determinants of anti-PD-1 response and resistance in clear cell renal cell carcinoma. *Cancer Cell* (2021) 39 (11):1497–518. doi: 10.1016/j.ccell.2021.10.001

32. Mayerhoefer ME, Materka A, Langs G, Häggström I, Szczypiński P, Gibbs P, et al. Introduction to radiomics. *J Nucl Med* (2020) 61(4):488–95. doi: 10.2967/jnumed.118.222893

33. Fiz F, Viganò L, Gennaro N, Costa G, La Bella L, Boichuk A, et al. Radiomics of liver metastases: A systematic review. *Cancers* (2020) 12(10):2881–902. doi: 10.3390/cancers12102881

34. van Timmeren JE, Cester D, Tanadini-Lang S, Alkadhi H, Baessler B. Radiomics in medical imaging-"how-to" guide and critical reflection. *Insights Imaging* (2020) 11(1):91. doi: 10.1186/s13244-020-00887-2

frontiers | Frontiers in Immunology

TYPE Original Research
PUBLISHED 15 September 2022
DOI 10.3389/fimmu.2022.954653

OPEN ACCESS

EDITED BY
Xuyao Zhang,
Fudan University, China

REVIEWED BY
Liangfang Shen,
Central South University, China
Wei Zhang,
Yantai Yuhuangding Hospital, China

*CORRESPONDENCE
Jia Li
18622663700@163.com

SPECIALTY SECTION
This article was submitted to Cancer Immunity and Immunotherapy, a section of the journal Frontiers in Immunology

RECEIVED 27 May 2022
ACCEPTED 23 August 2022
PUBLISHED 15 September 2022

CITATION
Chen S, Liu P, Zhao L, Han P, Liu J, Yang H and Li J (2022) A novel cuproptosis-related prognostic lncRNA signature for predicting immune and drug therapy response in hepatocellular carcinoma. *Front. Immunol.* 13:954653. doi: 10.3389/fimmu.2022.954653

A novel cuproptosis-related prognostic lncRNA signature for predicting immune and drug therapy response in hepatocellular carcinoma

Shujia Chen[1], Peiyan Liu[1], Lili Zhao[2], Ping Han[2], Jie Liu[2], Hang Yang[1] and Jia Li[2]*

[1]Clinical School of the Second People's Hospital, Tianjin Medical University, Tianjin, China, [2]Department of Hepatology, Tianjin Second People's Hospital, Tianjin, China

Intratumoral copper levels are closely associated with immune escape from diverse cancers. Cuproptosis-related lncRNAs (CRLs), however, have an unclear relationship with hepatocellular carcinoma (HCC). Gene expression data from 51 normal tissues and 373 liver cancer tissues from the Cancer Genome Atlas (TCGA) database were collected and analyzed. To identify CRLs, we employed differentially expressed protein-coding genes (DE-PCGs)/lncRNAs (DE-lncRNAs) analysis, Kaplan–Meier (K-M) analysis, and univariate regression. By univariate and Lasso Cox regression analyses, we screened 10 prognosis-related lncRNAs. Subsequently, five CRLs were identified by multivariable Cox regression analysis to construct the prognosis model. This feature is an independent prognostic indicator to forecast overall survival. According to Gene Set Variation Analysis (GSVA) and Gene Ontology (GO), both immune-related biological processes (BPS) and pathways have CRL participation. In addition, we found that the characteristics of CRLs were associated with the expression of the tumor microenvironment (TME) and crucial immune checkpoints. CRLs could predict the clinical response to immunotherapy based on the studies of tumor immune dysfunction and rejection (TIDE) analysis. Additionally, it was verified that tumor mutational burden survival and prognosis were greatly different between high-risk and low-risk groups. Finally, we screened potential sensitive drugs for HCC. In conclusion, this study provides insight into the TME status in patients with HCC and lays a basis for immunotherapy and the selection of sensitive drugs.

KEYWORDS

lncRNAs, immune, drug therapy, hepatocellular carcinoma, cuproptosis

Introduction

Hepatocellular carcinoma (HCC) is one of the most frequent malignancies worldwide and is the second dominant cause of cancer-related deaths (1, 2). More than 700,000 people die of liver cancer globally, with approximately 500,000 new cases annually (1). Hepatitis C virus (HCV) infection, chronic hepatitis B virus (HBV), non-alcoholic fatty liver disease, and alcoholic liver disease all contribute to HCC (2). Current therapy options for early-stage HCC include radiofrequency ablation surgery and liver transplantation (3–6). Recurrence, or the occurrence of distant metastases, occurs in most patients after surgery (7). Unfortunately, the diagnosis is advanced in more than 70% of patients. As a result, only restricted therapeutic help is available for a small number of patients. Thus, it is important to elucidate the molecular mechanism of HCC progression and set novel molecular goals for HCC diagnosis and treatment.

One of the fundamental mineral nutrients for all living things is copper (Cu), which is the foundation for many biological activities containing antioxidant/detoxification activities and mitochondrial respiration (8). Recently, cuproptosis has been considered as a copper-triggered mode of mitochondrial cell death (9). Moreover, many links between the disease status and Cu have been observed, and several studies have reported higher copper levels in cancer malignancies than in normal tissues. There is a relationship between copper accumulation and cell propagation, as well as angiogenesis. It can be seen that in cancer, copper imbalance exerts a dominant function. In particular, it has been found that there were great variations in the serum and tumor tissue levels of Cu in patients with diverse cancers such as ovarian cancer, pancreatic cancer, prostate cancer, cervical cancer, breast cancer, gastric cancer, lung cancer, and thyroid cancer (7, 10–18).

Long non-coding RNAs, or lncRNAs, are a family of transcripts of non-coding molecules over 200 nucleotides in length that are thought to exert important functions in diverse diseases (19, 20). Abnormal lncRNA presentation was greatly associated with tumor malignancy, including HCC (21–25). For example, according to previous reports, the lncRNA Miat family promotes the proliferation, invasion, and migration of HCC cells by sponging miR-214 (21); hepatoma cell propagation, migration, and chemoresistance could be virtually suppressed by lncRNA SNHG16 upregulation by functional cavernous hsa-mir-93 (22). Moreover, lncRNA HULC could cause autophagy. For instance, it has been reported that stabilizing SIRT1 lowered the sensitivity of HCC cells to chemotherapeutic drugs (23). However, the role of CRL imbalance in tumor progression is not well defined. Not much research had paid attention to the regulatory relationship between CRLs and HCC. Exploring the relationship between CRLs and HCC development could be useful for recognizing underlying indicators as therapeutic goals.

This paper performed a prognostic feature of lncRNAs related to cuproptosis (LINC01515, AC105020.5, AC019069.1, HCG15, AC079209.1). It is an independent prognostic indicator with high accuracy in forecasting overall survival (OS). This study shows that the characteristic is related to immune-related functional pathways, which exerted crucial function in HCC tumorigenesis, and is closely associated with the tumor microenvironment (TME), immunotherapy, and chemical drug response. Our study constructed a new prognosis model based on CRLs, which provides possible value in the prognosis of HCC patients and provides benefits in guiding individualized immune and drug therapy.

Materials and methods

Data sets and patients

From The Cancer Genome Atlas-Liver hepatocellular carcinoma (TCGA-LIHC) database (https://portal.gdc.cancer.gov/) RNA-seq, we collected transcriptome data from 373 HCC samples and 51 normal samples. In addition, we obtained the matching clinical and pathological characteristics, covering tumor grade, age, follow-up time, sex, Tumor, Node, Metastasis (TNM) phrase, and survival condition. We combined profiles from replicate samples from the same patient into an average. We further differentiated the transcriptomic data of TCGA-LIHC from mRNA and lncRNA and collected 19,323 mRNAs and 13,162 lncRNAs in HCC. We used TCGA-LIHC in the University of California Santa Cruz (UCSC) Xena (https://xena.ucsc.edu/) database to extract the copy number variation information of LIHC. As a public database, each case involved in TCGA has gained ethical agreement and is approved by TCGA. Individual researchers analyzed the database. Open-source data were the foundation of this work. We blinded related identifying data for all included cases, making the study plan ethical. We proceeded and reported this study based on the Declaration of Helsinki. Supplementary Figure 1 shows the data analysis process.

Identification of cuproptosis-related lncRNAs with prognostic significance in hepatocellular carcinoma

We first reviewed the literature and summarized the cuproptosis-related genes, and obtained a total of 19 genes (see Table S1). Next, the expression of cuproptosis-related genes was obtained by the R "limma" package (26). According to the correlation coefficient > 0.3, $P< 0.05$, 53 CRLs and their expression were identified. Finally, the coexpression of cuproptosis-related genes and CRLs were analyzed using the "ggplot2" and "ggalluvial" R package (27) to observe the interaction.

Construction of the risk score model based on prognostic cuproptosis-related lncRNAs in hepatocellular carcinoma

We collected 10 lncRNAs associated with cuproptosis by univariate Cox analysis. We employed Lasso Cox regression and applied the R package "glmnet" to remove highly correlated lncRNAs (28). Finally, this study recognized only five CRLs and entered into a fresh risk-scoring model. According to the prediction model, the CRLs of each HCC patient can be derived from the formula below:

$$CI\ (cuproptosisindex) = \Sigma Expi * \beta i$$

(βi stands for each lncRNA coefficient, and Expi stands for each lncRNA presentation).

Next, we randomly divided all patients into two sets (184 in the training group and 182 in the testing group). Patients were split into high-risk and low-risk groups based on risk scores within each cohort. We contrasted CRL median cutoff values and split patients into high-CRL and low-CRL groups. We used the R package "survival" (29) to perform a Kaplan–Meier (K-M) analysis of OS on the high- and low-CRL groups of the three data sets and evaluated model feasibility (30). Furthermore, through K-M analysis, there was no progression-free survival (PFS) in the training group between the high-CRL group and the low-CRL group.

A comprehensive evaluation of cuproptosis-related index and clinical parameters in patients with hepatocellular carcinoma

To further clarify the clinical practicality of CRLs, PCA analysis was carried out to prove whether the lncRNA involved in the model construction can distinguish these two groups of patients. In addition, through hierarchical analysis, the correlation between this formed model and many clinical markers containing the grade, gender, age, stage, and T was determined.

Development and evaluation of clinical pathological nomogram related to cuproptosis

We determined whether CRLs were independent prognostic HCC indicators by using univariate and multivariate Cox regression analyses. The mentioned findings showed "RMS" and the "regplot" R package, and a clinicopathological nomogram related to cuproptosis was exploited (31). We described the decision curve analysis (DCA) of HCC patients and the calibration curve (32) to verify that the nomogram prediction and recognition outcomes were content.

Functional enrichment analysis of differentially expressed genes related to cuproptosis

We deciphered the majorly enriched signaling pathways and biological roles between the high- and low-CRL groups in the training sets through GO and GSVA (33). $P< 0.05$, with $|NES| > 1.5$ and FDR q-value< 0.1, was statistically significant.

Tumor somatic mutation and differential tumor mutational burden and survival analysis

We utilized the "maftools" package (34) to assess and contrast the gene mutation frequencies between the two groups using the tumor somatic mutation waterfall method established in the high-risk and low-risk scores. For mutation type analysis, we selected the first few genes with high mutation frequencies. Secondly, we applied "limma" and "ggpubr" packages (26) to show the different analyses of survival analysis and tumor mutational burden (TMB) and then compared the prognosis and tumor mutation of the two groups.

The potential significance of immunotherapy based on characteristics and tumor immune microenvironment landscape estimation

Immunotherapy and targeted therapy techniques for HCC patients in recent years have been continuously improved. Consequently, this study evaluated the correlation between five lncRNAs and immune checkpoints (35) by using the Wilcoxon test and verified its accuracy with the Shapiro–Wilk normality test. We applied the single-sample gene set enrichment analysis (ssGSEA) method to calculate the four tumor immune-infiltrating cells' enrichment in the gene expression matrix of the TCGA-LIHC cohort in high-CRL and low-CRL HCC samples. The outcomes of immunoassays were represented by scatter plots, and $P< 0.05$ was regarded statistically significant by Spearman's test. The characteristics of CRLs in HCC and the differences in immune function, immune escape, and immunotherapy were analyzed, and the

effect of immunotherapy in high- and low-risk patients was evaluated.

Screening potential drugs for hepatocellular carcinoma

The "limma" and "ggpubr" packages (26) are used to predict which high-risk and low-risk groups have different susceptibilities to the drug. The filtration condition was $P< 0.05$. The lower the IC50 value, the more sensitive it is to drugs, to guide patients' clinical medication.

Statistical analysis

We used R software (version 4.0.2, http://www.R-project.org) to analyze all statistics. We used the log-rank test and compared each K-M curve included. Then, we utilized the Wilcoxon test to examine CRL expression levels in normal and HCC tissues in low- and high-CRL groups. In addition, we stratified the differences in the adjusted CRLs values for each clinicopathological parameter. Additionally, we screened CRLs and OS for independent prognostic indicators associated with OS by univariate and multivariate Cox regression analyses. The Spearman correlation test represented the correlation matrix. $P< 0.05$ was considered statistically significant, and the P-value was two sided.

Results

Identification and construction of cuproptosis-related lncRNAs

By comparing 373 HCC tumors and 51 normal tissues, we analyzed differentially expressed cuproptosis-related genes (Supplementary Table 1) in HCC and the expression of 53 CRLs (Figure 1A). We detected cuproptosis-related genes through the Human Protein Atlas (HPA) database (Supplementary Figure 2). Then, 10 CRLs with significant differential expression were obtained by univariate regression analysis (Figure 1B), Lasso Cox regression (Figures 1C, D), and multivariate Cox regression analysis. Five candidate OS-related CRLs were identified in the TCGA-LIHC cohort to find the best CRLs for establishing prognostic characteristics. Finally, the five key CRLs were extracted to construct the signature, which include LINC01515 and AC105020.5, AC019069.1, HCG15, and AC079209.1 (Figure 1E) showing the coexpression of cuproptosis-related genes (Figure 1F). Furthermore, we presented the box plots of expression levels (Figure 1G) and K-M curves of OS (Figure 1H) in the training set to study the expression levels and independent prognostic power of each characteristic CRLs. From the results, we found that the expression levels of LINC01515, HCG15, and AC079209.1 were significantly increased, while the expression levels of AC105020.5 and AC019069.1 were not significantly different between normal samples and HCC samples. In the separation K-

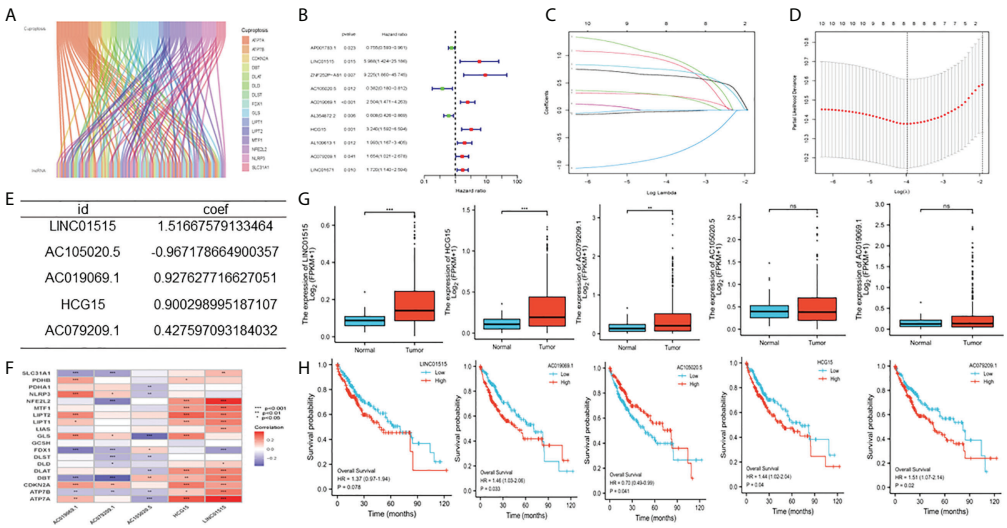

FIGURE 1
Construction of cuproptosis-related characteristics m TCGA-LIHC cohort **(A)** Co-expression analysis of cuproptosis related locRNAs, **(B)** Univariate Cox regression analysis **(C, D)** Lasso Cox regression analysis (lasso Lambda and lasso Cvfit), **(E)** Multivariate Cox regression analysis **(F)** Correlation between lncRNAs involved in model construction and cuproptosis-related genes **(G)** Expression level of five CDIs contained in signature **(H)** Kaplan-Meier (K-M) analyses OS based on the expression level of five CDIs TCGA, The Cancer Genome Atlas, CRLs, Cuproptosis related lncRNAs, OS overall survival. **Means P<0.01, ***means P<0.001, ns means no significance.

M analysis of OS, AC105020.5, AC019069.1, HCG15, and AC079209.1 high-risk and low-risk groups' survival had a significant difference, while LINC01515 was not statistically significant.

Construct the prognostic characteristics of cuproptosis in patients with hepatocellular carcinoma

Based on patient traits, we calculated the CI for each patient below: CI = expression of LINC01515 * 1.516676 – expression of AC1050205 * 0.967179 + AC0190691 expression * 0.927628 + HCG15 expression * 0.900299 + AC079209.1 * 0.427597. In addition, based on the CI median value, HCC patients in the training set can be separated into the high-CI group and low-CI group. The CI can be adjusted to make the data more direct (Figure 2A). In the TCGA-LIHC data set and compared to the low-CI group, the high-CI group patients had a higher rate of death (Figure 2B). To assess the prognostic feasibility of CI, a K-M analysis was performed to decipher that it can be seen that the high-CI group had a significantly lower OS than the low-CI group (Figure 2C). It was the same as the evaluation of PFS in the testing, training, and TCGA data set (Figure 2D).

PCA analysis and comprehensive evaluation of clinical parameters of cuproptosis-related lncRNA model in patients with hepatocellular carcinoma

PCA analysis was carried out on all genes, cuproptosis-related genes, cuproptosis-related lncRNAs, and risk lncRNAs of the model (Figures 3A–D), and the CRLs' clinical availability was further clarified. The lncRNAs involved in the model construction can effectively distinguish high-risk group patients and low-risk patients, proving the model's accuracy. The correlation between CI and clinical traits was further established, and the CI validity in predicting other clinical parameters was improved. Different levels of different clinical parameters (including age, sex, clinical stage, clinical grade, and pathological T) of the training set had remarkable deviations in

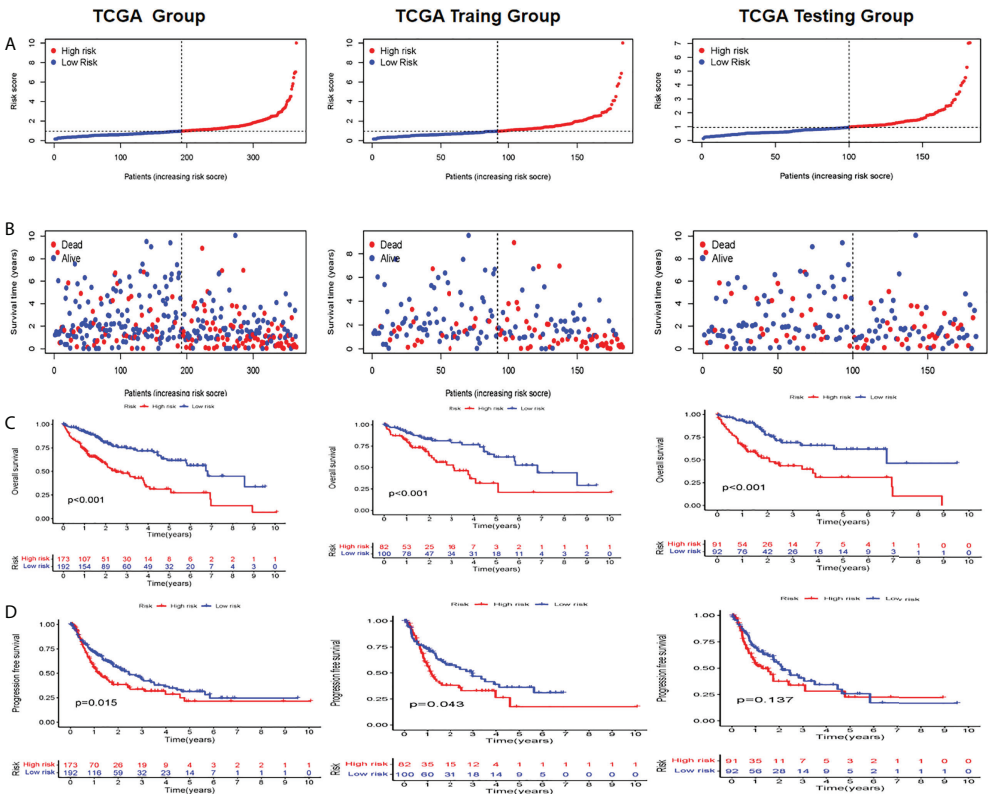

FIGURE 2
Evaluation and validation of the utility of CRLs in TCGA, training, and testing sets **(A)** Distribution of the patients normalized CRL scores **(B)** Patients' overall survival (OS) time along with their CRL score **(C)** K M analyses of OS between high- and low-CRL groups **(D)** K-M analyses of PFS between high- and low CRI. groups in the training set. C1 cuproptosis index, CRL suproptons related lncRNAs, K M Kaplan-Meier, OS overall survival PFS, progression-free survival.

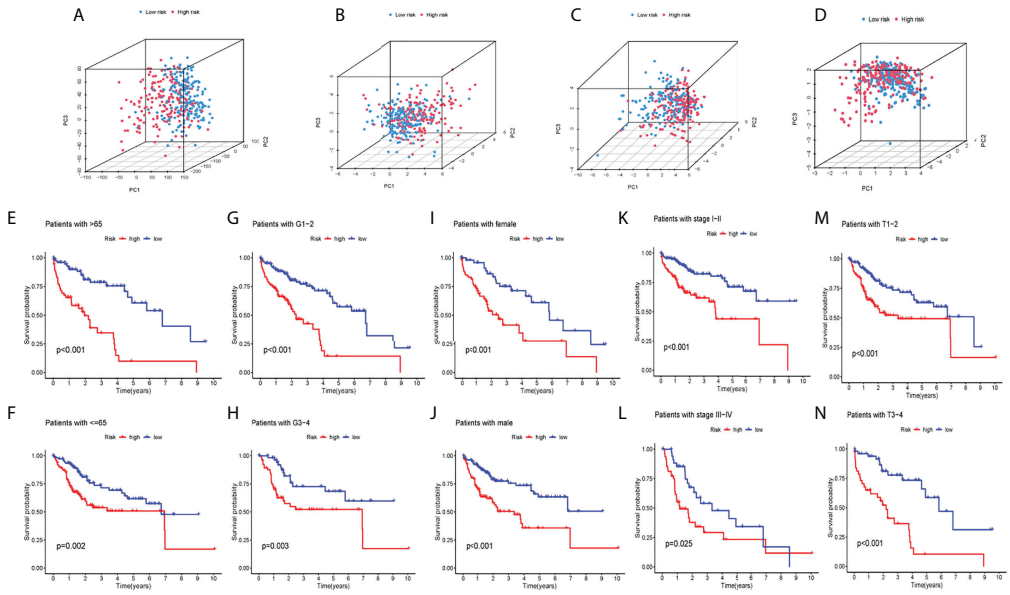

FIGURE 3
PCA analysis and systematic evaluation of CRLs and clinical parameters in HCC patients. **(A)** allGene PCA analysis; **(B)** cuproptosisLncRNA PCA analysis; **(C)** cuproptosisGene PCA analysis; **(D)** riskLnc PCA analysis; (E–N) Survival analyses of the risk score in different subgroups of various clinical factors: age (≤/>65years), pathological grade (1–2/3–4), sex (female/male),clinical stage (I–II/III–IV) and pathological T(T1-2/3-4).

adjusted CI ($P< 0.05$). Higher CI may be related to late clinical-stage, stage, and pathological T stage (Figures 3E–N), thus proving that our model department is used to distinguish patients with different clinical–pathological characteristics.

Development and evaluation of cuproptosis-related clinicopathological nomogram

Whether it was an independent prognostic indicator explored by conducting univariate and multivariate Cox regression analyses in the training set (Figures 4A, B). It was found that the age, risk score, and OS of HCC patients were markedly related in univariate and multivariate Cox analyses. The clinical ROC curve assessed the accuracy with an AUC value of 0.695 (Figure 4C). The result of the c-index curve is the same as the former (Figure 4D). In addition, the ROC curve had good results in evaluating the 1-, 3- and 5-year survival of patients (Figure 4E). Based on the above results, individual 1-, 3-, and 5-year OS was predicted by clinicopathological nomogram advance (Figure 4F). We performed survival descriptions on the calibration plots to confirm that the nomogram predictions were identified as satisfactory and the predictions were great (Figure 4G). In conclusion, multiple aspects illustrated the validity of prognostic maps.

Gene ontology function of risk differential genes and gene set variation analysis pathway analysis

First, we analyzed the difference of genes in high-risk and low-risk groups and found that the risk difference genes are based on their mean value in high-risk and low-risk groups (Supplementary Table 2). We then used the "clusterprofiler" software package to conduct enrichment analysis on differentially expressed genes (DEGs) to explore their biological characteristics (30). Biological process (BP) terminology indicates that DEGs are rich in the "emphasizing-activating MAPK cascade," "toxin metabolic process," and "cyclooxygenase P450 pathway." In terms of cell composition (CC), "glycoprotein complex" "astral microtubule" and "cytoplasmic microtubule" are significantly abundant. Therefore, we hypothesized that DEGs mainly play a role in the extracellular matrix. The main enrichment molecular function (MF) terms of DEGs are "oxidoreductase activity" "heme binding" and "sulfur compounds" (Figure 5A).

In addition, this study utilized the "clusterprofiler" software package for GSVA path enrichment analysis (30) for studying further roles of DEGs. According to the results, the following pathways were significantly enriched in DEGs: "cell cycle", "fatty acid metabolism" and "drug metabolism cytochrome P450" (Figure 5B). In conclusion, the results confirm that these central genes are involved in cellular metabolic processes.

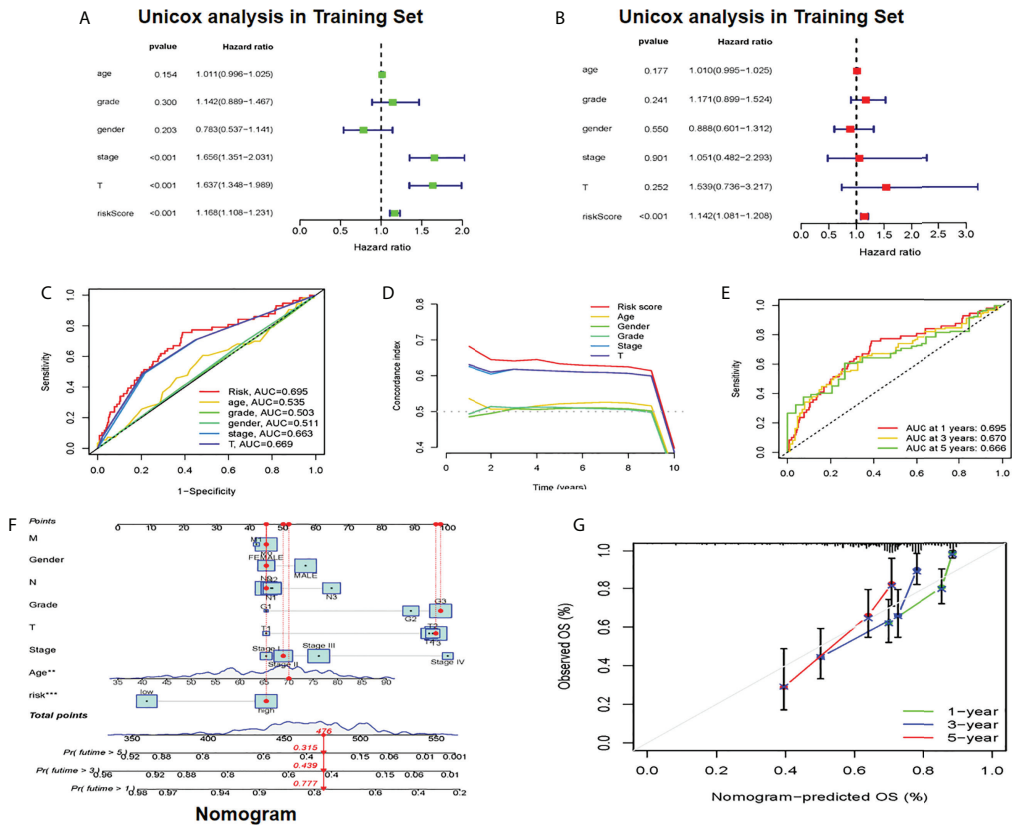

FIGURE 4
Establishment of cuproptosis-related clinicopathologic nomogram **(A)** Univariate Cox regression analysts of the signature CRLs and clinical parameters **(B)** Multivariate Cox regression analysis of the signature CRLs and clinical parameters **(C)** Development of a prognostic nomogram to predict 1-, 3- and 5-year OS in the HCC patients of the training set. **(D)** Clinical data c-index ROC curve **(E)** Characteristic CRLs to predict 1-, 3- and 5-OS of HCC patients in the traming set. **(F)** A prognostic nomogram was developed to predict the 1-, 3- and 5-year OS of HCC patients in the training set. **(G)** Prognostic nomogram predicted OS time, CRLs, cuproptosis-related lncRNAs; OS overall survival, HCC, hepatocellular carcinoma. *Means P<0.05, **Means P<0.01, ***means P<0.001.

Landscape of the hepatocellular carcinoma mutation profiles and survival analysis

In total, this study explored the somatic mutation spectrum of 371 HCC patients in a VCF format through the "maftools" software package (29) and selected the 20 genes with the highest mutation frequency for visualization. The waterfall plot showed that the first three mutated genes were TP53, CTNNB1, and TTN mutations in HCC samples. We not only counted the number of variants in each sample but also marked the HCC mutation kinds in box plots in different colors. Compared with the low-risk group, most high-risk group genes had higher mutation frequencies (Figures 6A, B). For TP53 and CTNNB1 with high mutation frequency, we found that the wild-type frequency in the high-risk and low-risk groups was higher than that of the mutant, and the difference was statistically significant (Figures 6C, D). In addition, we assessed TMB in both groups, meanwhile. We found that the high-risk group's TMB was not greatly different from that of the low-risk group (P = 0.89) (Figure 6E). Between the high and low mutation burden groups, however, there was a big difference in patient survival (P = 0.010). Compared with the high mutational burden group, patients in the low mutational burden group had a better prognosis (Figures 6F). Combining TMB with the risk score of patients, the survival rate of the four groups was also significantly different (P < 0.001) (Figures 6G).

Potential significance of immunotherapy based on characteristics and tumor immune microenvironment landscape estimation

We assessed the association of five CRLs with immune checkpoints (35) using the Wilcoxon test (Figure 7A) and found that they were significantly associated with PD1

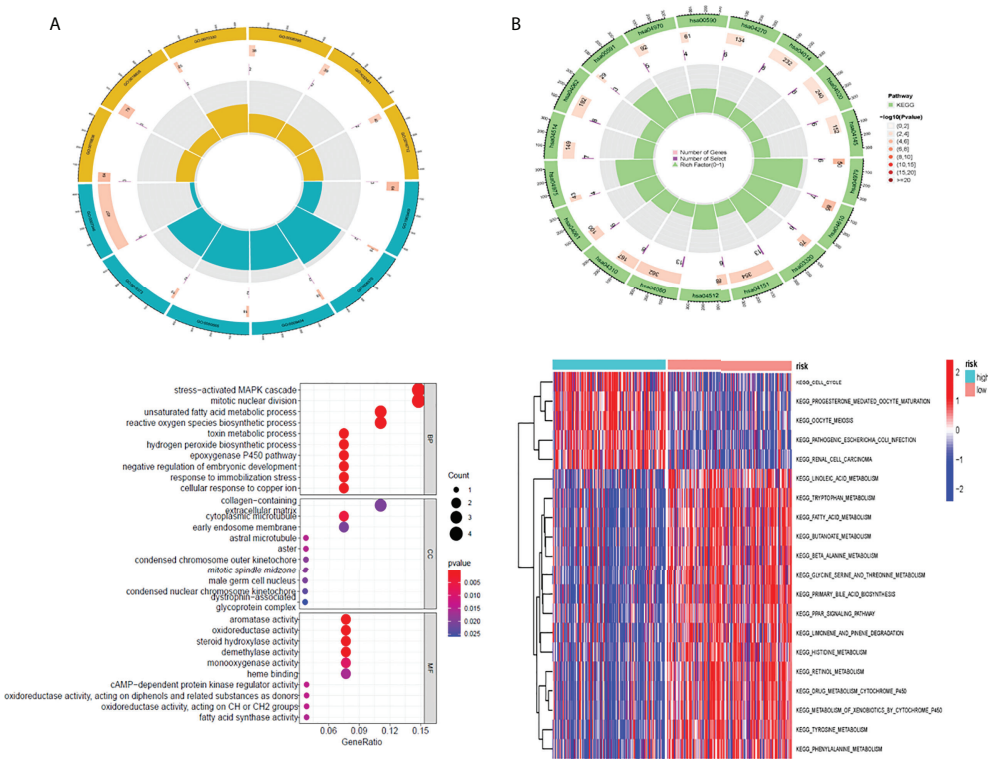

FIGURE 5
The result of GO and GSVA pathway enrichment analyses. The result of GO and GSVA pathway enrichment analyses **(A)** Biological process, cellular component, molecular function GO terms for risk DEGs **(B)** GSVA pathways for DEGs The top 10 sorted by the GeneRatio of GO terms and the top 20 sorted by GSVA pathways are shown. GO, Gene Ontology; GSVA, gene set variation analysis; DEGs, differentially expressed genes.

(PDCD1), PDL1 (CD274), CTLA4, and other common immune checkpoints. This is consistent with the Shapiro–Wilk Normality test (Supplementary Figure 3). In addition, we measured the content of four tumor immune-infiltrating cells (T cells, macrophages, NK cells, and CD8 T cells) in the gene expression matrix in the TCGA-LIHC cohort of HCC samples by using ssGSEA analysis. The scatter diagram was used to reveal the results of the immunoanalysis. Most of the results were statistically significant ($P< 0.05$) (Figure 7B). Additionally, we discussed the relationship between CRL characteristics and immune function in HCC. According to the heat map, some parameters were significantly different between high-risk and low-risk groups, such as APC_co_Stimulation, Type_I_IFN_Response, MHC_class_I, Type_II_IFN_Response, and CCR (Figure 7C). Finally, the effect of immunotherapy in high-risk and low-risk patients was assessed by assessing differences in immune escape and immunotherapy in high-risk and low-risk groups (Figure 7D). It was found that low-risk group TIDE (tumor immune dysfunction and exclusion) was higher, indicating that the greater the potential of immune escape, the worse the effect of immunotherapy ($P< 0.001$).

Screening potential drugs for hepatocellular carcinoma

We circulated the drugs and observed which drugs had different sensitivities between the two groups. The lower the IC50 value, the higher the sensitivity to the drugs. Finally, we screened five drugs with great differences in drug sensitivity between two groups, including sorafenib (Figures 8A, B), imatinib (Figures 8C, D), and saracatinib (Figures 8E, F), bortezomib (Figures 8G, H), and crizotinib (Figures 8I, J). In conclusion, this provides a great reference for clinical medication.

Discussion

HCC has a high recurrence rate and is one of the leading causes of tumor-related deaths. The prognosis of patients is seriously affected by the high recurrence rate, and there is currently no effective preventive method. With the rapid development of systemic therapy, after sorafenib treatment, more and more drugs are available but survival-enhancing

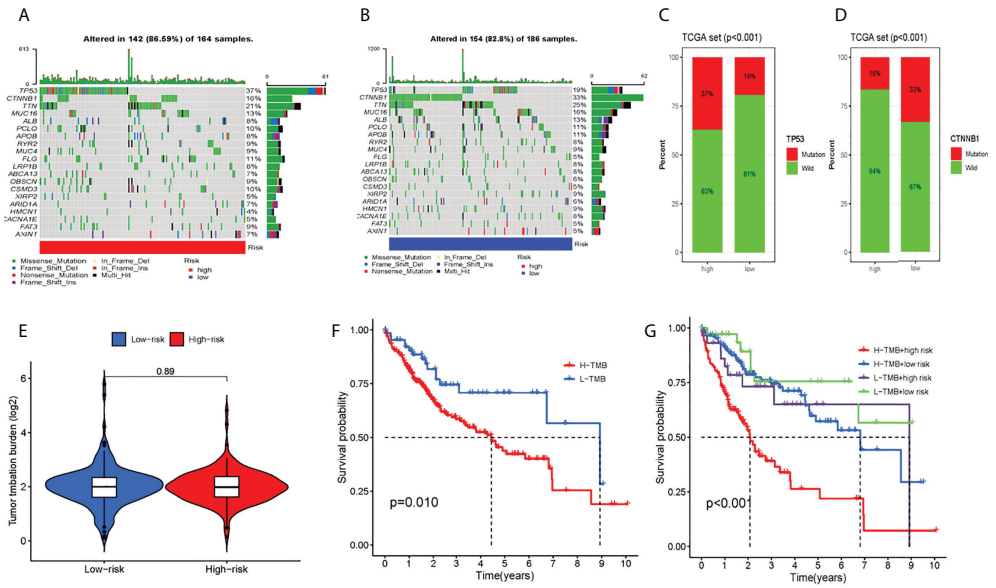

FIGURE 6
Tumor somatic mutation and differential tumor mutational burden (TMB) and survival analysis. The waterfall plot of tumor somatic mutation was established by those with high-risk scores **(A)** and low-risk scores **(B)**. **(C)** TP53 mutation, **(D)** CTNMBI mutation **(E)** Analysis of the difference of TMB; **(F)**TMB survival analysis; **(G)** Combined survival analysis of TMB and patient risk; Each column represented individual patients. The upper barplot showed TMB. The number on the right indicated the mutation frequency in each gene The right barplot showed the proportion of each variant type. TMB tumor mutational burden.

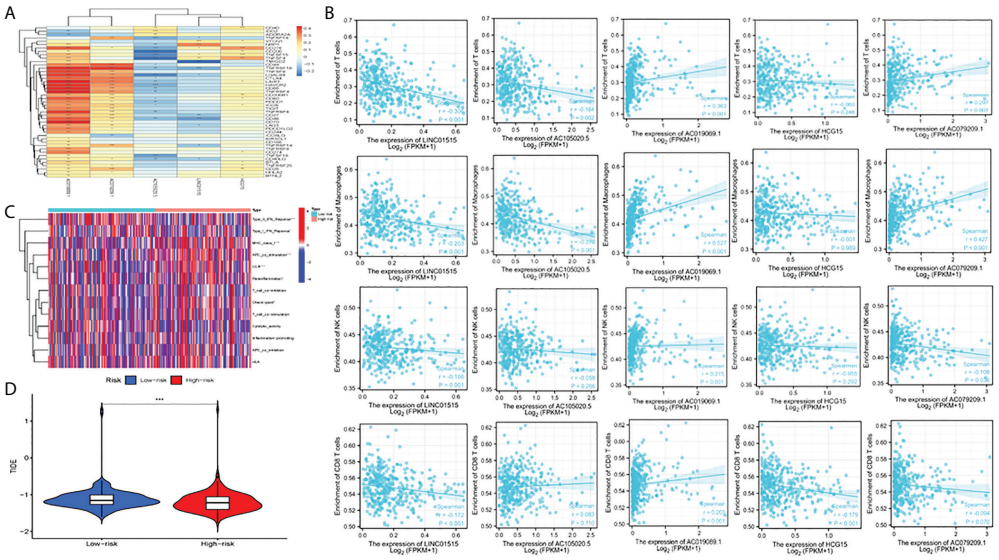

FIGURE 7
Analysis of immune function, escape, and immunotherapy. **(A)** Correlation analysis between CRLs and the immune checkpoint; **(B)** Correlation analysis between CRLs and immune cells (T cells, macrophage cells, NK cells and CD8 T cells); **(C)** Analysis of correlation and difference between high-risk and low-risk groups and immune function; **(D)** TIDE between high and low-risk groups; TIDE, tumor immune dysfunction and exclusion. *Means P<0.05, **Means P<0.01, ***means P<0.001.

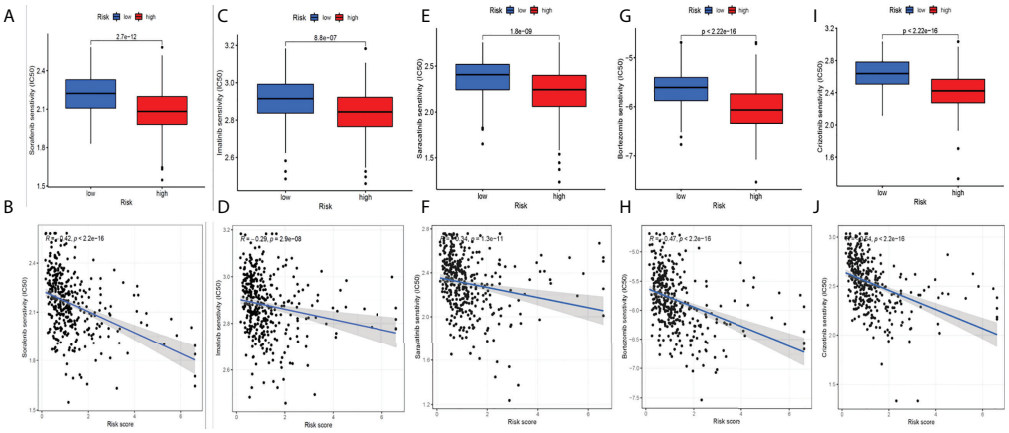

FIGURE 8
Screening potential drugs for HCC. Five drugs with great differences in drug sensitivity between two groups: sorafenib **(A-B)**, imatinib **(C-D)**, saracatinib **(E-F)**, bortezomib **(G-H)** and crizotinib **(I-J)**.

treatments remain unsatisfactory (36). Moreover, HCC treatments in recent years utilized the immunotherapy of immune checkpoints (32), but the therapeutic effect is not very ideal. Therefore, it is urgent to explore the occurrence, development, recurrence, migration, and HCC immunotherapy mechanism. Xing et al. have reported the diagnostic and prognostic value of genes related to the focal degeneration of HCC (37). In this way, key regulatory pathways or networks in HCC are further revealed, and the development and improvement of related therapeutic approaches are facilitated.

Recently, cuproptosis has been considered as a copper-triggered mode of mitochondrial cell death (9). In the case of the growth and severity of cancer, it was reported that Cu might exert an important function (33, 34). Related research supported this hypothesis. For instance, liver cancer in patients with Wilson's disease had an increased incidence. The relation between staging and Cu levels in colorectal cancer and breast cancer, Cu exposure, and the relation between pancreatic cancer and prostate cancer have also been observed (37–40). Studies have shown that the demand for NET (neutrophil extracellular trap) formation by different trace elements varies greatly; unlike zinc, low or negligible copper levels will not interfere with the NET formation and may even enhance NET formation. In contrast, high copper concentrations inhibit net release, but this was mainly due to cytotoxicity to neutrophils (41). Several mechanisms of copper-dependent tumor growth and development have been studied in recent years (8, 42, 43). Tsvetkov P et al. showed that the mechanism of copper-dependent regulation of cell death is different from the known death mechanism and depends on mitochondrial respiration. Copper-dependent death occurs through the direct combination of copper and the fatty acylation component of the tricarboxylic acid (TCA) cycle. This leads to the aggregation of acylated proteins and the subsequent loss of iron–sulfur cluster proteins, which lead to protein toxic stress and eventually cell death. These findings can explain the necessity of the steady-state mechanism of ancient copper (44). In addition, Cu can also promote angiogenesis, which is very important in tumor metastasis. In particular, more and more lines of evidence showed that several angiogenic factors could be stimulated by copper, including the vascular endothelial growth factor (VEGF), angiopoietin (hAng), and interleukin-1 (IL-1) (42, 45, 46). Additionally, Yang et al. found that the COMMD 10-inhibited HIF1α/CP loop can enhance the iron wire disease and radiosensitivity by destroying the Cu-Fe homeostasis in HCC. This work provided a new target and treatment strategy for overcoming the radioresistance of HCC (47). Our results were mostly consistent with most of the DEGs in their research. We, however, collected more DEGs because we registered more lncRNAs related to cuproptosis by reviewing the latest literature. It was found that cuproptosis studies are developing rapidly, and more and more discoveries are being revealed.

Based on the key role of cuproptosis in cancer and the close interaction between cuproptosis and lncRNA, we used TCGA transcriptome data to study the potential mechanism and prognostic value of CRLs in HCC. We identified five key CRLs (LINC01515, AC105020.5, AC019069.1, HCG15, AC079209.1). They were applied to develop a risk-scoring model. In this way, a patient's prognosis could be differentiated. Importantly, an independent prognostic HCC factor was the risk model. A prognostic nomogram with high precision was next established to provide 1-, 3-, and 5-year HCC OS prediction. This greatly improved the feasibility of CRLs in judging the prognosis of patients. Moreover, there was a significant correlation between CRLs and the immune-related function, immune escape, and immunotherapy of HCC. Given the

essential role of the TME in tumorigenesis and development, the interaction between cancer cells and immune cells regulates all links to tumor development. As a result, CRL-mediated variations may affect tumor progression (48) through immune-related mechanisms. In this study, we investigated that the expression of the immune checkpoint, containing PD-L1, PD-1, and CTLA-4, and five CRLs were significantly correlated with the above immune checkpoints. These findings suggest the potential role of CRLs in regulating immune checkpoint expression in the TME. In addition, differences between high- and low-risk groups in immune escape and immunotherapy were also assessed, and the influence of immunotherapy on high- and low-risk patients was then assessed. The results showed that the TIDE of the low-risk group was higher, and the greater the potential of immune escape in the low-risk group, the worse the effect of immune treatment. Based on this, we also screened the model-based sensitivity analysis of patients to chemotherapy drugs. Five drugs with significant expression differences were extracted, namely sorafenib, imatinib, saracatinib, bortezomib, and crizotinib, which provided a reliable choice for clinical medication.

A large number of studies have shown that lncRNA plays a very important role in the TME. For instance, Huang et al. showed that lncRNA can stimulate the differentiation of T regulatory cells, promote the immune escape of HCC cells, and can be used as a diagnostic biomarker of HCC (49). As for the five key CRLs, numerous studies explored the LINC01515 function and HCG15 function in cancer. Liu (50) et al. found that the expression of LINC01515 was increased in nasopharyngeal carcinoma, and the higher the expression of LINC01515, the worse its prognosis. This agreed with the findings of this study. In addition, earlier research (51) suggested that LINC01515 exerted a key function in the drug resistance of leukemia cells. However, in our study, LINC01515 was identified as the CRLs of HCC, while Liu reported lncRNA-related immunity. It was found in tumors that lncRNA had a complicated role. Yan (52) et al. found that HCG15 is a hypoxia-reactive lncRNA that improved HCC cell propagation and aggression by enhancing ZNF641 transcription. In addition, in the regulation of glioma formation, the PABPC5/HCG15/ZNF331 feedback loop involving HCG15 exerted a significant function, giving a novel target for glioma therapy (53). Additionally, the prognostic model involved in HCG15 is conducive to discovering the new mechanism of ivermectin-inhibiting ovarian cancer cells and the benefits of ivermectin-related molecular combination changes on its prediction in ovarian cancer, personalized drug treatment, and the prognostic evaluation of preventive and personalized drugs (PPPM) (54). Therefore, additional research on these newly discovered lncRNAs is essential.

There are some limitations on this study. First, the findings need to be further verified experimentally because the data and results of this study were based on TCGA transcriptomic, mutational, and clinical data. Then, the training and testing group were randomly grouped from the TCGA queue, which needs to be further verified by other databases.

Conclusion

In conclusion, a new model based on CRLs has been developed, which has an important potential to forecast HCC prognosis. This study is expected to give a novel perspective on the underlying mechanisms of CRLs in regulating the immune microenvironment and immunotherapy.

Data availability statement

The datasets presented in this study can be found in online repositories. The names of the repository/repositories and accession number(s) can be found in the article/Supplementary Material.

Ethics statement

Consent from all participants was obtained through The Cancer Genome Atlas (TCGA).

Author contributions

All authors participated in the present study, including conception and design (SC and PL), data collection (PH, JeL, LZ and HY), data analysis (SC and PL), drafting the article or critically revising (JaL) and study supervision (JaL). All authors contributed to the article and approved the submitted version.

Funding

This work was funded by the Natural Science Foundation of Tianjin City (20JCYBJC01150); Tianjin Health Science and Technology Project (No. TJWJ2021QN063, No. TJWJ2021ZD010 and No. TJWJ2021MS034) and Tianjin Key Medical Discipline (Specialty) Construction Project.

Acknowledgments

The authors are grateful to the contributors to the public databases used in this study and the reviewers for their constructive and helpful comments.

Conflict of interest

The authors declare that the research was conducted in the absence of any commercial or financial relationships that could be construed as a potential conflict of interest.

Publisher's note

Supplementary material

The Supplementary Material for this article can be found online at: https://www.frontiersin.org/articles/10.3389/fimmu.2022.954653/full#supplementary-material

SUPPLEMENTARY FIGURE 1
Flowchart of the data analysis procedures.

SUPPLEMENTARY FIGURE 2
Immunohistochemical staining of genes related to cuproptosis.

SUPPLEMENTARY FIGURE 3
Correlation analysis between CRLs and common immune checkpoints.

SUPPLEMENTARY TABLE 1
Identification of differentially expressed cuproptosis-related genes in HCC.

SUPPLEMENTARY TABLE 2
Screening of genes with different risks of cuproptosis.

References

1. Hartke J, Johnson M, Ghabril M. The diagnosis and treatment of hepatocellular carcinoma. *Semin Diagn Pathol* (2017) 34(2):153–9. doi: 10.1053/j.semdp.2016.12.011

2. Mcglynn KA, Petrick JL, London WT. Global epidemiology of hepatocellular carcinoma: An emphasis on demographic and regional variability. *Clin Liver Dis* (2015) 19(2):223–38. doi: 10.1016/j.cld.2015.01.001

3. Llovet JM, Zucman-Rossi J, Pikarsky E, Sangro B, Schwartz M, Sherman M, et al. Hepatocellular carcinoma. *Nat Rev Dis Primers* (2016) 14(2):16018. doi: 10.1038/nrdp.2016.18

4. Bruix J, Reig M, Sherman M. Evidence-based diagnosis, staging, and treatment of patients with hepatocellular carcinoma. *Gastroenterology* (2016) 150 (4):835–53. doi: 10.1053/j.gastro.2015.12.041

5. Vogel A, Cervantes A, Chau I, Daniele B, Llovet JM, Meyer T, et al. Hepatocellular carcinoma: ESMO clinical practice guidelines for diagnosis, treatment and follow-up. *Ann Oncol* (2018) 29(4):iv238–iv55. doi: 10.1093/annonc/mdy308

6. Galle PR, Forner A, Llovet JM, Mazzaferro V, Piscaglia F, Raoul J-L, et al. EASl clinical practice guidelines: Management of hepatocellular carcinoma. *J Hepatol* (2018) 69(1):182–236. doi: 10.1016/j.jhep.2018.03.019

7. Basu S, Singh MK, Singh TB, Bhartiya SK, Singh SP, Shukla VK. Heavy and trace metals in carcinoma of the gallbladder. *World J Surg* (2013) 37(11):2641–6. doi: 10.1007/s00268-013-2164-9

8. Ruiz LM, Libedinsky A, Elorza AA. Role of copper on mitochondrial function and metabolism. *Front Mol Biosci* (2021) 24:711227(8). doi: 10.3389/fmolb.2021.711227

9. Tang D, Chen X, Kroemer G. Cuproptosis: A copper-triggered modality of mitochondrial cell death. *Cell Res* (2022) 32(5):417–8. doi: 10.1038/s41422-022-00653-7

10. Ding X, Jiang M, Jing H, Sheng W, Wang X, Han J, et al. Analysis of serum levels of 15 trace elements in breast cancer patients in Shandong, China. *Environ Sci pollut Res Int* (2015) 22(10):7930–5. doi: 10.1007/s11356-014-3970-9

11. Pavithra V, Sathisha TG, Kasturi K, et al. Serum levels of metal ions in female patients with breast cancer. *J Clin Diagn Res* (2015) 9(1):BC25–Bc7. doi: 10.7860/JCDR/2015/11627.5476

12. Baltaci AK, Dundar TK, Aksoy F, Mallika DS, Amos SJ, Ragunatha S. Changes in the serum levels of trace elements before and after the operation in thyroid cancer patients. *Biol Trace Elem Res* (2017) 175(1):57–64. doi: 10.1007/s12011-016-0768-2

13. Stepien M, Jenab M, Freisling H, Becker NP, Czuban M, Tjønneland A. Pre-diagnostic copper and zinc biomarkers and colorectal cancer risk in the European prospective investigation into cancer and nutrition cohort. *Carcinogenesis* (2017) 38(7):699–707. doi: 10.1093/carcin/bgx051

14. Zhang X, Yang Q. Association between serum copper levels and lung cancer risk: A meta-analysis. *J Int Med Res* (2018) 46(12):4863–73. doi: 10.1177/0300060518798507

15. Chen F, Wang J, Chen J, Yan L, Hu Z, Wu J, et al. Serum copper and zinc levels and the risk of oral cancer: A new insight based on large-scale case-control study. *Oral Dis* (2019) 25(1):80–6. doi: 10.1111/odi.12957

16. Aubert L, Nandagopal N, Steinhart Z, Lavoie G, Nourreddine S, Berman J, et al. Copper bioavailability is a KRAS-specific vulnerability in colorectal cancer. *Nat Commun* (2020) 11(1):3701. doi: 10.1038/s41467-020-17549-y

17. Saleh SAK, Adly HM, Abdelkhaliq AA, Nassir AM. Serum levels of selenium, zinc, copper, manganese, and iron in prostate cancer patients. *Curr Urol* (2020) 14(1):44–9. doi: 10.1159/000499261

18. Michniewicz F, Saletta F, Rouaen JRC, Hewavisenti RV, Mercatelli D, Cirillo G, et al. Copper: An intracellular achilles' heel allowing the targeting of epigenetics, kinase pathways, and cell metabolism in cancer therapeutics. *ChemMedChem* (2021) 16(15):2315–29. doi: 10.1002/cmdc.202100172

19. Wapinski O, Chang HY. Long noncoding RNAs and human disease. *Trends Cell Biol* (2011) 21(6):354–61. doi: 10.1016/j.tcb.2011.04.001

20. Shi X, Sun M, Liu H, Yao Y, Song Y. Long non-coding RNAs: A new frontier in the study of human diseases. *Cancer Lett* (2013) 339(2):159–66. doi: 10.1016/j.canlet.2013.06.013

21. Huang X, Gao Y, Qin J, Lu S. lncRNA MIAT promotes proliferation and invasion of HCC cells via sponging miR-214. *Am J Physiol Gastrointest Liver Physiol* (2018) 314(5):G559–G65. doi: 10.1152/ajpgi.00242.2017

22. Xu F, Zha G, Wu Y. Overexpressing lncRNA inhibited HCC proliferation and chemoresistance by functionally sponging hsa-miR-93. *Onco Targets Ther* (2018) 11:8855–63. doi: 10.2147/OTT.S182005

23. Xiong H, Ni Z, He J, Jiang S, Li X, He J, et al. LncRNA HULC triggers autophagy *via* stabilizing Sirt1 and attenuates the chemosensitivity of HCC cells. *Oncogene* (2017) 36(25):3528–40. doi: 10.1038/onc.2016.521

24. Yan X, Zhang D, Wu W, Wu S, Qian J, Hao Y, et al. Mesenchymal stem cells promote hepatocarcinogenesis *via* lncRNA-MUF interaction with ANXA2 and miR-34a. *Cancer Res* (2017) 77(23):6704–16. doi: 10.1158/0008-5472.CAN-17-1915

25. Li B, Mao R, Liu C, Zhang W, Tang Y, Guo Z. LncRNA FAL1 promotes cell proliferation and migration by acting as a CeRNA of miR-1236 in hepatocellular carcinoma cells. *Life Sci* (2018) 15(197):122–9. doi: 10.1016/j.lfs.2018.02.006

26. Ritchie ME, Phipson B, Wu D, Hu Y, Law CW, Shi W, et al. Limma powers differential expression analyses for RNA-sequencing and microarray studies. *Nucleic Acids Res* (2015) 43(7):e47. doi: 10.1093/nar/gkv007

27. Liu S, Xie X, Lei H, Zou B, Xie L. Identification of key circRNAs/lncRNAs/miRNAs/mRNAs and pathways in preeclampsia using bioinformatics analysis. *Med Sci Monit* (2019) 5(25):1679–93. doi: 10.12659/MSM.912801

28. Yang LA, Qu Q, Hao Z, Sha K, Li Z, Li S. Powerful identification of Large quantitative trait loci using genome-wide r/glmnet-based regression. *J Hered* (2022). doi: 10.1093/jhered/esac006

29. Mayakonda A, Lin D-C, Assenov Y, Plass C, Koeffler HP. Maftools: Efficient and comprehensive analysis of somatic variants in cancer. *Genome Res* (2018) 28 (11):1747–56. doi: 10.1101/gr.239244.118

30. Zhou R-S, Zhang E-X, Sun Q-F, Ye ZJ, Liu JW, Zhou DH, et al. Integrated analysis of lncRNA-miRNA-mRNA ceRNA network in squamous cell carcinoma of tongue. *BMC Cancer* (2019) 19(1):779. doi: 10.1186/s12885-019-5983-8

31. Zhang Z, Kattan MW. Drawing nomograms with r: Applications to categorical outcome and survival data. *Ann Transl Med* (2017) 5(10):211. doi: 10.21037/atm.2017.04.01

32. Kalasekar SM, Garrido-Laguna I, Evason KJ. Immune checkpoint inhibitors in combinations for hepatocellular carcinoma. *Hepatology* (2021) 73(6):2591–3. doi: 10.1002/hep.31706

33. Ishida S, Andreux P, Poitry-Yamate C, Auwerx J, Hanahan D. Bioavailable copper modulates oxidative phosphorylation and growth of tumors. *Proc Natl Acad Sci U.S.A.* (2013) 110(48):19507–12. doi: 10.1073/pnas.1318431110

34. Shanbhag VC, Gudekar N, Jasmer K, Papageorgiou C, Singh K, Petris MJ. Copper metabolism as a unique vulnerability in cancer. *Biochim Biophys Acta Mol Cell Res* (2021) 1868(2):118893. doi: 10.1016/j.bbamcr.2020.118893

35. Gong Y, Ji P, Yang Y-S, Xie S, Yu TJ, Xiao Y, et al. Metabolic-Pathway-Based subtyping of triple-negative breast cancer reveals potential therapeutic targets. *Cell Metab* (2021) 33(1):51–64. doi: 10.1016/j.cmet.2020.10.012

36. Llovet JM, Montal R, Sia D, Finn RS. Molecular therapies and precision medicine for hepatocellular carcinoma. *Nat Rev Clin Oncol* (2018) 15(10):599–616. doi: 10.1038/s41571-018-0073-4

37. Vella V, Malaguarnera R, Lappano R, Maggiolini M, Belfiore A. Recent views of heavy metals as possible risk factors and potential preventive and therapeutic agents in prostate cancer. *Mol Cell Endocrinol* (2017) 457:57–72. doi: 10.1016/j.mce.2016.10.020

38. Guptta SK, Shukla VK, Vaidya MP, Roy SK, Gupta S. Serum and tissue trace elements in colorectal cancer. *J Surg Oncol* (1993) 52(3):172–5. doi: 10.1002/jso.2930520311

39. Sharma K, Mittal DK, Kesarwani RC, Kamboj VP, Chowdhery. Diagnostic and prognostic significance of serum and tissue trace elements in breast malignancy. *Indian J Med Sci* (1994) 48(10):227–32.

40. Gunjan D, Shalimar, Nadda N, Kedia S, Nayak B, Paul SB, et al. Hepatocellular carcinoma: An unusual complication of longstanding Wilson disease. *J Clin Exp Hepatol* (2017) 7(2):152–4. doi: 10.1016/j.jceh.2016.09.012

41. Masucci MT, Minopoli M, Del Vecchio S, Carriero MV. The emerging role of neutrophil extracellular traps (NETs) in tumor progression and metastasis. *Front Immunol* (2020) 11:1749. doi: 10.3389/fimmu.2020.01749

42. Lelievre P, Sancey L, Coll J-L, Deniaud A, Busser B. The multifaceted roles of copper in cancer: A trace metal element with dysregulated metabolism, but also a target or a bullet for therapy. *Cancers (Basel)* (2020) 12(12):3594. doi: 10.3390/cancers12123594

43. Ge EJ, Bush AI, Casini A, et al. Connecting copper and cancer: From transition metal signalling to metalloplasia. *Nat Rev Cancer* (2022) 22(2):102–13. doi: 10.1038/s41568-021-00417-2

44. Tsvetkov P, Coy S, Petrova B, Cobine PA, Cross JR, DeNicola GM, et al. Copper induces cell death by targeting lipoylated TCA cycle proteins. *Science* (2022) 375(6586):1254–61. doi: 10.1126/science.abf0529

45. Yang Y, Zhang M, Song H, Yu C. Silica-based nanoparticles for biomedical applications: From nanocarriers to biomodulators. *Acc Chem Res* (2020) 53 (8):1545–56. doi: 10.1021/acs.accounts.0c00280

46. Li H, Wang J, Wu C. The combination of disulfiram and copper for cancer treatment. *Drug Discovery Today* (2020) 25(6):1099–108. doi: 10.1016/j.drudis.2020.04.003

47. Yang M, Wu X, Hu J, Wang Y, Wang Y, Zhang L, et al. COMMD10 inhibits HIF1α/CP loop to enhance ferroptosis and radiosensitivity by disrupting Cu-fe balance in hepatocellular carcinoma. *J Hepatol* (2022) 76(5):1138–50. doi: 10.1016/j.jhep.2022.01.009

48. Shulman Z, Stern-Ginossar N. The RNA modification n-methyladenosine as a novel regulator of the immune system. *Nat Immunol* (2020) 21(5):501–12. doi: 10.1038/s41590-020-0650-4

49. Huang Z, Zhou J-K, Peng Y, He W, Huang C. The role of long noncoding RNAs in hepatocellular carcinoma. *Mol Cancer* (2020) 19(1):77. doi: 10.1186/s12943-020-01188-4

50. Liu D, Gong H, Tao Z, Chen S, Kong Y, Xiao B, et al. LINC01515 promotes nasopharyngeal carcinoma progression by serving as a sponge for miR-325 to up-regulate CDCA5. *J Mol Histol* (2021) 52(3):577–87. doi: 10.1007/s10735-021-09969-x

51. Liu Z, Wang Y, Xu Z, Yuan S, Ou Y, Luo Z, et al. Analysis of ceRNA networks and identification of potential drug targets for drug-resistant leukemia cell K562/ADR. *PeerJ* (2021) 9:e11429. doi: 10.7717/peerj.11429

52. Yan H, He N, He S. HCG15 is a hypoxia-responsive lncRNA and facilitates hepatocellular carcinoma cell proliferation and invasion by enhancing ZNF641 transcription. *Biochem Biophys Res Commun* (2022) 608:170–6. doi: 10.1016/j.bbrc.2022.03.143

53. Jing F, Ruan X, Liu X, Yang C, Wang D, Zheng J, et al. The PABPC5/HCG15/ZNF331 Feedback Loop Regulates Vasculogenic Mimicry of Glioma via STAU1-Mediated mRNA Decay. *Mol Ther Oncolytics* (2020) 30(17):216–31. doi: 10.1016/j.omto.2020.03.017

54. Li N, Zhan X. Anti-parasite drug ivermectin can suppress ovarian cancer by regulating lncRNA-EIF4A3-mRNA axes. *EPMA J* (2020) 11(2):289–309. doi: 10.1007/s13167-020-00209-y

frontiers | Frontiers in Immunology

TYPE Review
PUBLISHED 15 September 2022
DOI 10.3389/fimmu.2022.915094

OPEN ACCESS

EDITED BY
Xuyao Zhang,
Fudan University, China

REVIEWED BY
Chi-Ping Day,
National Cancer Institute (NIH), United States
Adeleye Oluwatosin Adeshakin,
St. Jude Children's Research Hospital, United States

*CORRESPONDENCE
Xia Zhao
xia-zhao@126.com

†These authors have contributed equally to this work and share first authorship

SPECIALTY SECTION
This article was submitted to Cancer Immunity and Immunotherapy, a section of the journal Frontiers in Immunology

RECEIVED 07 April 2022
ACCEPTED 19 August 2022
PUBLISHED 15 September 2022

CITATION
Zhou X, Ni Y, Liang X, Lin Y, An B, He X and Zhao X (2022) Mechanisms of tumor resistance to immune checkpoint blockade and combination strategies to overcome resistance. *Front. Immunol.* 13:915094. doi: 10.3389/fimmu.2022.915094

Mechanisms of tumor resistance to immune checkpoint blockade and combination strategies to overcome resistance

Xiaoting Zhou†, Yanghong Ni†, Xiao Liang, Yi Lin, Biao An, Xiang He and Xia Zhao*

Department of Gynecology and Obstetrics, Development and Related Disease of Women and Children Key Laboratory of Sichuan Province, Key Laboratory of Birth Defects and Related Diseases of Women and Children, Ministry of Education, West China Second Hospital, Sichuan University, Chengdu, China

Immune checkpoint blockade (ICB) has rapidly transformed the treatment paradigm for various cancer types. Multiple single or combinations of ICB treatments have been approved by the US Food and Drug Administration, providing more options for patients with advanced cancer. However, most patients could not benefit from these immunotherapies due to primary and acquired drug resistance. Thus, a better understanding of the mechanisms of ICB resistance is urgently needed to improve clinical outcomes. Here, we focused on the changes in the biological functions of $CD8^+$ T cells to elucidate the underlying resistance mechanisms of ICB therapies and summarized the advanced coping strategies to increase ICB efficacy. Combinational ICB approaches and individualized immunotherapies require further in-depth investigation to facilitate longer-lasting efficacy and a more excellent safety of ICB in a broader range of patients.

KEYWORDS

immune checkpoint blockade, combination therapy, T cell response, resistance mechanisms, immunotherapy

Introduction

The emergence of immune checkpoint blockade (ICB) has brought the oncology field to a new stage, offering renewed hope for patients with advanced cancer. Over the past decades, ICB, as one of the representative cancer immunotherapies, has produced the broadest impact on cancer treatment (1). ICB, including programmed cell death protein 1 (PD-1), programmed cell death ligand 1 (PD-L1), and cytotoxic T lymphocyte antigen 4 (CTLA-4) monoclonal antibodies, have shown antitumor efficacies in multiple advanced solid tumors since the initial approval of CTLA-4 inhibitors for metastatic melanoma in 2011 by the US

Food and Drug Administration (FDA) (2). There are currently three main classes of ICB approved by the FDA in the treatment of various solid tumors, including six drugs targeting the programmed cell death protein 1 (PD-1)/programmed cell death ligand 1 (PD-L1) checkpoint (nivolumab, pembrolizumab, cemiplimab, avelumab, durvalumab, atezolizumab), anti-CTLA-4 checkpoint (ipilimumab), and recently approved anti-LAG-3 (relatlimab) (3).

Unfortunately, most patients suffer primary resistance and do not respond to anti-PD-1/PD-L1 treatments. The limited efficacy of anti-PD1/PDL1 may be attributed to a range of mechanisms involving the whole immune response process. The most straightforward reasons for primary resistance are insufficient tumor immunogenicity, poor $CD8^+$ T-cell infiltration, and irreversible T-cell exhaustion. Moreover, some patients with the initial response develop resistance or relapse eventually, which is called acquired resistance (2, 4). The mechanisms accounting for either form of resistance are intricate and complex, which have not been fully cleared up yet. Golnaz Morad et al. systematically divided the factors that affect ICB response into host-intrinsic factors, including tumor cells, non-tumor cells, age, gender, obesity, and gut microbiota, and host-extrinsic factors such as environmental exposures, social pressure, and unhealthy lifestyles. According to their discussion, the role of host systemic and environmental factors should be noted in the study of ICB response (5). Similarly, Aldea et al. overviewed the tumor cell–intrinsic mechanisms and stromal mechanisms. Of note, the different locations of metastasis can lead to an opposite response to ICB (6). Bagchi et al. reviewed the mechanism of ICB resistance from primary and acquired resistance perspectives. Most cancer cell–intrinsic factors contribute to the primary resistance, for instance, the expression intensity of ICB biomarkers, tumor mutation burden, and epigenetic variations. However, the mechanisms of acquired resistance are not well understood, and some common mechanisms may be shared by both types of resistance (7). Genetic mutations are common during the process of tumor progression. Kobayashi et al. summarized six signaling pathways related to ICB resistance. Understanding these could provide potential combinational options for immunotherapy and molecular-targeted therapies. In addition, as a consequence of activating oncogenic drivers or in response to external stimuli, alteration in phenotype plasticity is another integral approach exploited by tumor cells to avoid immune surveillance, thus getting resistance to immunotherapy (8, 9). Based on the analysis of a panel of syngeneic melanoma mouse models, a melanocytic plasticity signature was uncovered to predict the response to ICB and the outcome of patients, implicating the core of plasticity in ICB resistance (10). Novel strategies targeting tumor cell plasticity could be beneficial for patients receiving immunotherapy (11).

A mounting number of preclinical and clinical studies are ongoing to reveal the mechanisms underlying immune checkpoint inhibitor resistance and offer abundant clues for potential combined therapeutic strategies (12, 13). Combination strategies, promising to solve the restrictions of anti-PD-1/PD-L1 treatment, include a combination with traditional chemotherapy and radiotherapy, other immune checkpoint inhibitors, CAR T therapy agonists of the costimulatory molecule, antiangiogenic agents, oncogenic pathway–targeted therapy, microbiota-centered interventions, and metabolic and epigenetic regulation (14–19). Overall, the higher response rates elicited by combination regimens are associated with boosting multiple phases in the cancer-immunity cycle.

This review will discuss the mechanisms underlying ICB resistance, focusing on the changes in the biological function of $CD8^+$ T cells. We then highlight existing and emerging strategies to overcome resistance to ICB and boost immunotherapy in preclinical and clinical studies.

Mechanisms of immune checkpoint blockade resistance from the perspective of immune response process

As is well known, $CD8^+$ cytotoxic T lymphocytes (CTLs) play a significant role in antitumor immunotherapy because they are directly lethal to cancer cells. The central theme of ICB immunotherapy lies in the generation or reactivation of this population of cells (20). Antitumor immunity can be described briefly as antigen presentation cells (APCs), such as dendritic cells (DCs), internalize and process tumor-associated antigens (TAAs) in peripheral tissue; then, DCs migrate to lymph nodes and present tumor-peptide-major histocompatibility complexes to naïve $CD8^+$ T cells (21). Meanwhile, mature DCs provide the second signal to naïve $CD8^+$ T cells by upregulating CD80 and CD86. Upon these efficient stimulations, naïve $CD8^+$ T cells differentiate into CTLs. Eventually, CTLs infiltrate lesion sites and kill cancer cells (22). Effective immunotherapy depends mainly on $CD8^+$ T cells as well as their successful activation (23). Therefore, we focused on the immune response procedures, especially changes in the biological function of $CD8^+$ T cells, for a deeper understanding of the mechanisms of immunotherapy resistance in ICB.

Drug resistance occurs in blocking the different phases of a cancer immunity cycle, from tumor-specific antigen recognition to presentation, from T-cell activation to recruitment. Overall, the mechanisms of resistance to ICB (Figure 1) can be summarized as the (1) failure of antigen recognition; (2) deficiency of antigen presentation; (3) poor $CD8^+$ T-cell infiltration; (4) inhibited activity of $CD8^+$ T cells; (5) exhaustion of $CD8^+$ T cells; and (6) insensitivity to CTL mediated killing.

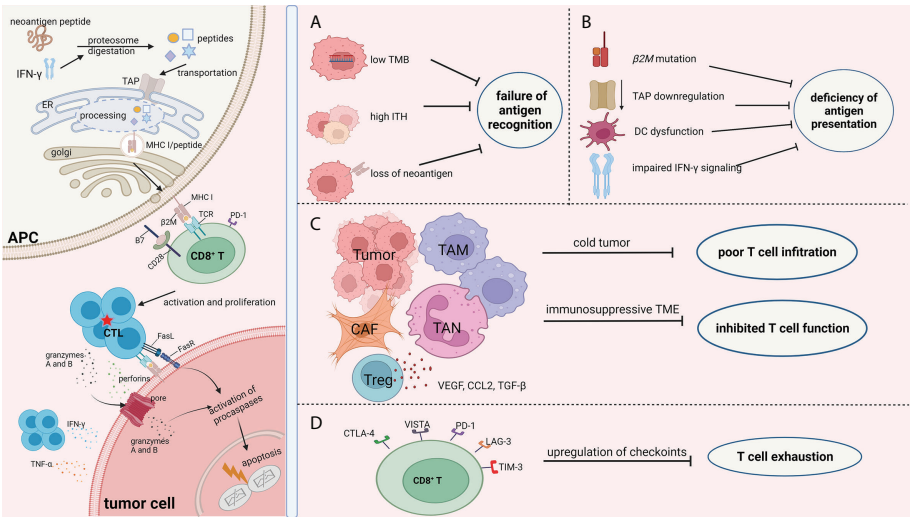

FIGURE 1
Mechanisms of ICB resistance from the perspective of immune response process. The success of ICB immunotherapy lies in the generation and/or reactivation of the population of CTL cells, which are also the central theme of immunotherapy. The left part of the picture depicts the normal immune response procedure which involves antigen processing and presentation, $CD8^+$T cell priming, and the efficient killing of tumor cells by CTLs. Failure of immunotherapy occurs when the different phases of the cancer immunity cycle are compromised and blocked. There are numerous factors that decrease the effect of the antitumor immunity during the fight between tumor cells and immune cells. Regardless of the complexity of the immunotherapy resistance mechanisms, the consequence of these factors can be summarized as **(A)** failure of antigen recognition; **(B)** deficiency of antigen presentation; **(C)** poor $CD8^+$ T cells infiltration and inhibited activity of $CD8^+$ T cells; and **(D)** exhaustion of $CD8^+$ T cells. Therefore, we focused on the immune response procedures, especially changes in biological function of $CD8^+$T cells, with an aim to better understand the resistance mechanisms of ICB. The picture was created with BioRender.com. APC, antigen presentation cell; TAP, transporters associated with neoantigen presentation; ER, endoplasmic reticulum; MHC I, major histocompatibility complex class I; TCR, T cell receptor; CTL, cytotoxic T lymphocytes; TMB, tumor mutation burden; ITH, intra-tumor heterogeneity; DC, dendritic cell; TAM, tumor associated macrophages; CAF, cancer associated fibroblasts; TAN, tumor associated neutrophil; CTLA-4, cytotoxic T-lymphocyte antigen 4; VISTA, V-domain Ig suppressor of T cell activation; LAG-3, lymphocyte activation gene-3; PD-1, programmed cell death protein -1; TIM-3, T-cell immunoglobulin mucin-3.

Failure of antigen recognition

The immune recognition of tumor cells depends on the HLA-presented antigenic peptide. During cancer progression, gene mutation occurs within cancer cells, resulting in the accumulation of mutated peptides. These neo-peptides are also termed neoantigens because they are different from self-antigens and can be immunogenic most of the time (24). Thus, increased expression of neoantigens within the tumor site can enhance antitumor immunity.

The concept of tumor mutation burden (TMB) has been introduced and utilized as a critical indicator to define tumor antigenicity and evaluate the clinical response to ICB (25). A considerable positive correlation was observed between TMB and the objective remission rate, with a correlation coefficient of 0.7 (26). Non-small lung cancer and melanoma have shown higher TMB and a better response to PD-1 inhibition. Conversely, sarcoma, prostate cancer, and ovarian cancer display lower TMB as well as primary resistance to PD-1inhibition (26, 27). Patients with high TMB (defined as "greater than or equal to 10mut/mb") were shown to have dramatically higher objective remission rates when treated with pembrolizumab (29%) than patients with low TMB treated with pembrolizumab (6%) in a clinical trial (NCT02628067) (28). On the other hand, tumors with microsatellite instability (MSI) phenotypes, or those with genetic defects in DNA repair enzymes, which is also called DNA mismatch repair deficiency (dMMR), display high mutation loads and more significant response to checkpoint inhibition immunotherapy (29). TMB alone is not a specific determinant of treatment efficacy. Differences in analytical methods, such as different sequencing coverage and depth, lead to differences in sensitivity and specificity when estimating TMB (30, 31). In fact, the durable efficacy of pembrolizumab was still obtained in patients with malignant rhabdoid tumors whose TMB was very low (31). Although high TMB plays a significant role in tumor response to ICB, the prediction of ICB response is far more than TMB estimation.

High intratumor heterogeneity (ITH) can also result in the ineffective recognition of tumor-specific neoantigen and decrease T-cell response to different subclones of tumor cells (32). Pan-cancer analysis indicated that a higher ITH level of tumors was associated with worse survival (33). Wolff et al. demonstrated that low intratumor heterogeneity was a prognosticator of overall survival (OS; $p = 0.046$) but not TMB

(p = 0.16), which suggested that tumors with high ITH were able to escape the immune system despite having high neoantigens (34). McGranahan et al. studied the impact of neoantigen load and neoantigen intratumor heterogeneity on OS in patients who were diagnosed with lung adenocarcinoma (LUAD) and lung squamous cell carcinoma (LUSC). No significant correlation between neoantigen load and neoantigen intratumor heterogeneity with OS in LUSC was discovered, even though the neoantigen burden of LUSC was equally high as LUAD, suggesting the importance of ITH (35).

The loss of neoantigens disturbs the recognition of tumor cells by T cells and causes resistance to ICB. Anagnostou et al. analyzed the data of NSCLC patients who developed required drug resistance after initial response. They discovered 7–18 assumed neoantigens in the resistant tumors. The mechanism of neoantigen loss lies in the deletion of chromosomal regions and the abolition of tumor subclones. The loss of neoantigens was correlated with changes in T-cell receptor clonality (36).

In summary, low TMB and/or high ITH, as well as neoantigen loss, can impact the antigen recognition by CTLs, causing primary or secondary drug resistance to ICBs. In general, tumors with elevated neoantigen expression at the onset of malignant cell cloning will respond better to ICB (37).

Deficiency of antigen presentation

The activation of $CD8^+$ T cells depends on the combination of the T-cell receptor (TCR) and major histocompatibility complex class I (MHC I) molecules (38). MHC I molecule–related neoantigen presentation is modulated by multiple proteins. Beta-2 microglobulin (β2M) is responsible for stabilizing MHC I molecules and promoting antigenic peptide loading (39). The mutations of *β2M* have been found in patients who have acquired resistance to ICBs. For example, in relapse melanoma patients with acquired resistance to pembrolizumab, it was found that a truncating mutation of *β2M* exists in biopsy analysis, leading to the loss of MHC I molecule expression (40). Point mutation, deletion, and the loss of heterozygosity (LOH) were also detected in metastatic melanoma tissues. The degree of *β2M* LOH was tripled in non-responders (approximately 30%) when compared with responders (approximately 10%) and was correlated with inferior OS (41). Apart from melanoma, the links between *β2M* alteration and acquired resistance have been reported in lung cancer (42), gastrointestinal adenocarcinoma (43), and colorectal cancer with a microsatellite instability–high (MSI-H) phenotype (44).

Reduced human leukocyte antigen (HLA) class I gene expression may lead to decreased antigen presentation, thus promoting immune evasion (45). There are up to six different HLA class I alleles in the genome. Highly polymorphic HLA class I genes, including HLA-A, HLA-B, and HLA-C, are responsible for encoding MHC I molecules (46). Eric et al. presented that resistance to KRAS G12D–specific T cell transfer therapy occurred in a patient with metastatic colorectal carcinoma after 9 months. The mechanism of this immunotherapy resistance lies in the deletion of chromosome HLA-C*08:02 in the resistant lesions. Since the existence of the HLA-C*08:02 allele was necessary for KRAS G12D neoantigen presentation and recognition by T cells, its loss directly caused immune evasion (47).

Transporters associated with neoantigen presentation (TAP) are critical players in the MHC I antigen presentation pathway. TAP is a heterodimer consisting of TAP1 and TAP2, both of which are required for peptide translocation (48). The loss or downregulation of TAP in cancers may result in immune evasion and is often associated with an unfavorable prognosis (49, 50). Zhang et al. reported that TAP deficiency resulted in resistance to anti-PD-1, while the efficacy was enhanced in patients lacking both TAP and the non-classical MHC I molecule $Qa\text{-}1^b$. The results suggested that the immune microenvironment can be altered by inhibiting Qa-1b, especially in the case of defective antigen processing (51). The accumulation of presentation defects may, in turn, lead to a reduced recognition of malignant cells by tumor-specific T cells.

The interruption of IFN-γ signaling, which facilitates MHC I molecule expression on the cell surface in normal conditions, influences neoantigen presentation. Specifically, IFN-γ is an essential signaling molecule for immune-proteasome formation during the degradation of intracellular proteins (52). The loss of IFN-γ signal causes reduced antigen presentation through compromising the coordinated upregulation of the antigen processing procedure (53). Decreased expression of elements in the MHC I antigen presentation pathway can usually be reversed by IFN-γ treatment (53, 54).

The dysfunction of DCs, the most potent antigen-presenting cells, plays a critical role in ICB resistance (55). The deletion of atypical chemokine receptor 4 (ACKR4) in colorectal tumor cells but not stromal cells inhibited the migration of DCs to tumor-draining lymph nodes and impaired antigen presentation. In addition, the knockdown of ACKR4 reduced tumor cells' sensitivity to ICB (56). High enrichment of myeloid dendritic cells in lung cancer tissues shows an immune activation state, and those patients may benefit from ICB treatment (57). Cytotoxic T-lymphocyte antigen 4 (CTLA4) has a higher affinity to CD80/86 than CD28. CTLA4-positive Treg cells impair the maturation of DCs by binding to CD80/86 and inhibit costimulatory signals (58). Antigen presentation by immature DC or CD80/86 low-expressed DC was unable to stimulate $CD8^+$ T cells potently, resulting in $CD8^+$ T cells being anergic with low proliferation and insufficient to produce cytokines (59).

Poor $CD8^+$ T-cell infiltration

Different tumor types exhibit various tumor-associated T-cell infiltration densities. The immune landscape of tumors can be divided into three types (1): hot tumor. It is characterized by

the enrichment of T cells and their infiltration into tumor tissues, such as lung cancer and melanoma (60) (2). Cold tumor, such as prostate cancer (61) and brain cancer (62), features fewer T cells in the tumor parenchyma or stroma (63). (3) "Immune excluded" tumor. Immune cells do not infiltrate the parenchyma of these tumors, even though there is an abundance of immune cells (64). Compared to hot tumors, the latter two phenotypes rarely respond to ICB immunotherapy, which results in primary drug resistance (65). The infiltration of $CD8^+$ T cells into the tumor tissues can be considered a good prognostic parameter for lung cancer and is associated with lymphocyte motility (66).

Genetic alterations within tumor cells have unfavorable effects on T-cell infiltration. *PTEN* loss was associated with reduced T-cell density, lower T-cell expansion, and poor response to PD-1 inhibited therapy in melanoma. Mechanically, the absence of *PTEN* in tumor cells enhances the level of immunosuppressive cytokines, including CCL2 and VEGF, causing less T-cell infiltration and inhibiting autophagy as well, thereby impairing CTL-mediated cell killing (67). *BRAF* mutations are common in melanoma (50%) (68), thyroid papillary cancers (approximately 35%) (69), and colorectal cancers (5%–10%) (70). The biopsy analysis of metastatic melanoma patients showed that selectively inhibiting BRAF with PLX4720 or GSK2118436 induced abundant $CD8^+$ T cells in tumors, which provided powerful support for combining BRAF inhibitors with immunotherapy (71). Skoulidis and colleagues showed that *STK11/LKB1* mutation is associated with less expression of PD-L1 and decreased infiltrative CTL density, resulting in primary resistance to PD-1-based immunotherapies in both human and murine *STK11/LKB1*-deficient lung adenocarcinoma (72). Additionally, the loss of *TET2*, which encodes ten-eleven translocation (TET) DNA dioxygenase, is correlated with reduced Th1-type chemokine generation, including CXCL9, CXCL10, and CXCL11, with the downregulated expression of PD-L1 and impaired T-cell attraction to tumor tissues, leading to immune escape and resistance to anti-PD-L1 therapy in the B16-OVA melanoma tumor model (73). NSCLC patients with *EGFR* mutations demonstrated an inadequate response to anti-PD-1 therapy than those with the EGFR wild type. *EGFR* mutation is associated with a reduction in PD-L1 expression, a deficiency in T-cell infiltration, and a decrease in TMB (74).

The elevated vascular endothelial growth factor (VEGF) within the tumor and the consequent aberrant vascular system with high interstitial pressure impair the recruitment of immune cells, correlated with decreased penetration of immune checkpoint inhibitors and increased drug resistance. VEGF inhibits T lymphocyte infiltration within the tumor microenvironment (TME) by suppressing NF-κB signals (75). Tumor-intrinsic STING signaling facilitates *BRCA-1* mutated ovarian cancer cells' resistance to both PD-L1 and CTLA-4 therapies by upregulating VEGF-A (76). In addition to VEGF, increased C-C motif chemokine ligand 2 (CCL2) was found to be correlated with primary resistance to ICB. CCL2 contributes to insensitivity to ICB by recruiting monocytes and reducing $CD8^+$ T-cell infiltration in pancreatic tumors. The poor efficacy of anti-PD-1 therapy can be reversed by CCL2 inhibition or monocyte neutralization (77). Meanwhile, transforming growth factor-beta (TGF-β) produced by cancer-associated fibroblasts (CAFs) was capable of preventing T cells from entering tumor tissue (78). The results from the transcriptional analysis of 298 metastatic urothelial carcinoma samples suggested that the enhanced TGF-β in CAFs was related to poor $CD8^+$ T-cell infiltration within tumor parenchyma and weak response to atezolizumab (79). Aside from CAFs, tumor-associated macrophages (TAMs) play an essential role in excluding T-cell infiltration from tumor sites. Interactions between CD8+ T cells and TAMs are durable (at least 20 min), resulting in slowed $CD8^+$ T-cell motility (66).

Inhibited activity of $CD8^+$ T cells

The TME is infiltrated by diverse innate and adaptive immune cells. The complex crosstalk between immune cells and tumor cells determines the immune status and the implementation of T-cell function, thus facilitating or inhibiting the tumor response to ICB (Figure 2). With the progression of tumors, the TME becomes progressively immunosuppressive. Immunosuppressive cells as well as their products facilitate tumor immune evasion and inevitable resistance to checkpoint inhibitors.

Tumor-associated neutrophils (TANs) are one of the critical characteristics of ICB resistance. Immunosuppressive neutrophils from blood and tumors are commonly named granulocyte–myeloid-derived suppressor cells (G-MDSCs) or polymorphonuclear MDSC (PMN-MDSC) (80). Neutrophil-enriched breast tumors display a required resistance to ICB, suggesting a direct suppressive effect on CTLs mediated by TANs (81). In colorectal cancer, the non-response group shows increased levels of MDSC infiltration than the response group treated with anti-PD-1 (82). Consistent with this, a smaller amount of MDSC was found to be linked with a more robust response to ipilimumab in melanoma patients (83). TANs can attenuate the activity of CD8+ T cells by secreting various mediators. One of the essential pathways participating in the immunosuppressive activity of MDSCs is STAT-1-dependent signaling. IFNγ-mediated signals generated by activated T cells can stimulate STAT-1, which subsequently induces the increased expression of immunosuppressive cytokines in MDSCs, such as arginase 1 (Arg-1) (84). Arg-1 results in the downregulation of the CD3ζ chain of T cells by L-arginine exhaustion, suppressing T-cell proliferation and function (85). In addition, the overexpression of fatty acid transporter protein 2 (FATP2) mediated by STAT5 signaling was associated with the enhanced uptake of arachidonic acid and the release of

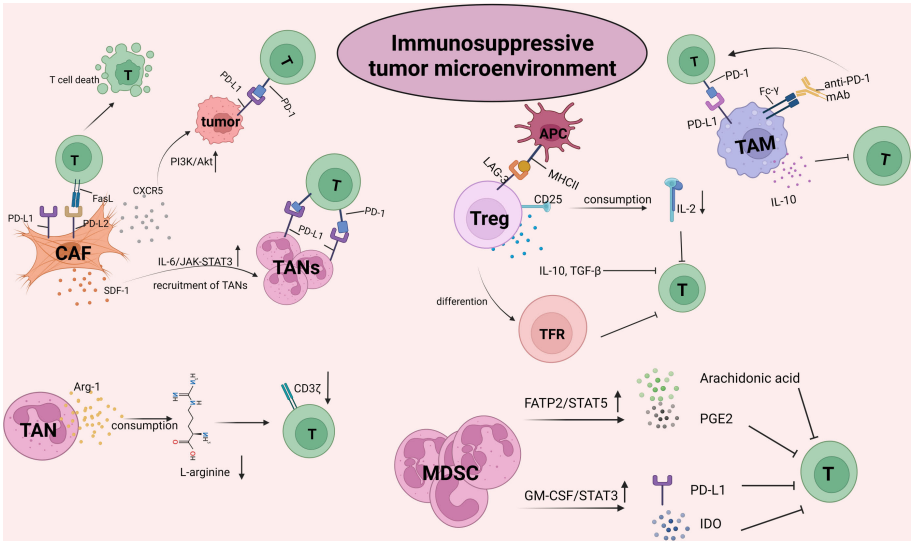

FIGURE 2
The crosstalk between CD8$^+$T cells and the other suppressive cells within tumor microenvironment (TME). TME is infiltrated by different types of innate and adaptive immune cells. The complex crosstalk between these immune cells and tumor cells determines the immune status and the implementation of T cell function, thus to facilitate or inhibit the tumor response to ICBs. With the progression of malignant cells, immune cells within TME, for example, macrophages and neutrophils, are educated into pro-tumor cells. As such, TME becomes progressively immunosuppressive. Immunosuppressive cells inhibit the activity of T cells by upregulating immune checkpoints, capturing anti-PD-1 antibodies and secreting pro-tumor soluble factors such as arg-1, IL-10, TGF-β, promoting tumor immune evasion and resulting in resistance to checkpoint inhibitors. The picture was created with BioRender.com. CAF, cancer associated fibroblasts; TAN, Tumor associated neutrophil; TAM, Tumor associated macrophage; MDSC, myeloid-derived suppressor cell; PGE2, prostaglandin E2; GM-CSF, granulocyte-macrophages colony-stimulating factor; IDO, indoleamine 2,3-dioxygenase; TFR, follicle-regulating T cell.

prostaglandin E2 (PGE2) in MDSCs (86). The interaction between tumor cells and MDSCs also plays a critical role in modulating the function of MDSCs. It is reported that MC38 cells secrete the granulocyte–macrophage colony-stimulating factor (GM-CSF) that binds with GM-CSF-R on MDSCs. The combination activates the STAT3 signal within MDSCs, which increases the immunosuppressive effect of MDSC by upregulating indoleamine 2,3-dioxygenase (IDO) and PD-L1, as well as FATP2 (87, 88). The combination of ICB and FATP2 inhibitors delays tumor progression and decreases the expression of PD-L1 on CD8+ T cells (86, 88).

TAMs also significantly contribute to ICB resistance by inducing immunosuppressive interactions within the TME. Notably, TAMs are one of the most enriched immune cells in TME and are involved in both immune stimulation and immunosuppression (89). There are two distinct functional groups of the TAM population, M1 cells (the antitumor macrophages) and M2 cells (the pro-tumor macrophages) (90). Phenotypes can be reversed dynamically between M1 and M2 mediated by cytokines and signals, which is called polarization (91). Firstly, TAMs attenuate T-cell activity by capturing ICB antibodies (mainly of the IgG1 subclass) through Fc-γ receptors, leading to ICB resistance. By using an *in vivo* image to monitor the activity of anti-PD-1 in real time, Arlauckas et al. proved that the anti-PD-1 monoclonal antibody (mAbs) could efficiently bind PD-1$^+$ tumor-infiltrating CD8$^+$ T cells initially after treatment. Nevertheless, this combination is transient because anti-PD-1 monoclonal antibody are removed by PD-1$^-$ TAMs from the T-cell surface within minutes. Measures to block Fc/FcγR binding inhibit the transfer of anti-PD-1 mAbs from CD8$^+$ T cells to macrophages *in vivo*, thereby strengthening the therapeutic effect of anti-PD-1 (92). Secondly, TAM reduces ICI efficacy by directly impeding the antitumor capacity of CD8+ T cells. It was found that TAMs directly or indirectly suppress CD8$^+$ T cells by secreting IL-10 (93). IL-10 inhibits CD8$^+$ T cells primarily by increasing N-glycan branching, thus upregulating the antigenic threshold needed for T-cell activation (94). Thirdly, TAM suppresses T-cell activity by expressing alternative immune checkpoints against ICI efficacy. On one hand, the majority of PD-L1$^+$ TAMs are M2 cells, constituting the major TAM population in advanced tumors (95). Thus, high expression of the inhibitory checkpoint on TAMs is inherently a crucial immunosuppressive factor in the TME. On the other hand, PD-L1 expression on TAMs plays a regulatory role during the interplay of TAMs presenting antigenic peptides to homologous effector T cells, which may restrict T-cell superactivation (96).

Under normal conditions, fibroblasts have a low proliferative capacity and metabolic state and are present in a relatively quiescent state in most tissues (97). However, within the TME, tumor cells

can promote fibroblast activation by secreting growth factors such as TGFβ, platelet-derived growth factor (PDGF), and fibroblast growth factor (FGF) (98, 99). The CAF-mediated inhibition of T-cell cytotoxic function can be achieved by the upregulation of immune checkpoint molecules. CAFs from melanoma patient biopsies showed the elevated expression of PD-L1 and PD-L2, which directly abrogated CD8+ T-cell function (100). It is suggested that enhanced expression of PD-L2 in CAFs results in antigen-specific T-cell death through PD-L2 and Fas ligand engagement, protecting tumor cells from immune destruction (101). Interestingly, some CAFs also participate in antigen presentation and thus can directly kill activated $CD8^+$ T cells *via* the involvement of PD-L2 and Fas ligands (101). PD-L1 and PD-L2 were simultaneously upregulated in CAFs in pancreatic cancer patients. Meanwhile, the CAFs facilitate inhibitory immune checkpoint receptor expression in proliferating T cells. However, the underlying mechanism is not fully understood (102). Apart from upregulating the immune checkpoint directly, CAFs can also indirectly increase the level of immune checkpoint molecules on malignant cells and other cells within the TME. Hepatocellular carcinoma– derived CAFs were demonstrated to recruit neutrophils by secreting SDF1a and facilitating neutrophils' activation *via* IL-6-JAK-STAT3 signaling. Then, the activated neutrophils upregulated the expression of PD-L1 and exerted a suppressive effect on T-cell immunity (103). CAF-derived CXCL5 is a potent cytokine, which mediates the upregulation of PD-L1 in a PI3K/AKT-dependent pathway within tumor cell lines, including B16, CT26, A375, and HCT116 (104). As such, it is essential to notice that the CAF-mediated dysfunction of $CD8^+$ T cells is not limited to a direct interplay of these two cell types.

Regulatory T lymphocytes (Tregs) are of vital importance in tumor progression and their resistance to immunotherapy. Increased infiltration of Tregs has been generally perceived as a biomarker of poor clinical outcomes such as high death hazards and decreased survival (105, 106). Tregs were initially identified as $CD4^+$ T cells with increased expression of CD25 (α chain for the IL-2 receptor). FoxP3 was then characterized as a specific marker and major regulator for the maintenance of the immunosuppressive functions of Treg cells (107, 108). Once activated, T cells begin to produce IL-2, which is essential for the sustained proliferation and activation of T cells (109). CD25 has a high affinity to IL-2. Tregs consume IL-2 by upregulating CD25, limiting the sustained activation and proliferation of effector T cells (110). Ren et al. reported that impaired T-cell immunity caused by IL-2 signaling obstruction could be restored by using a low-affinity IL-2 conjugated with anti-PD-1 (PD-1-laIL-2). PD-1-laIL-2, with a higher affinity to $PD\text{-}1^+CD8+$ T cells than to peripheral Treg cells, was able to amplify the dysfunctional tumor-specific $CD8^+$ T cells potently, thus overcoming tumor resistance to ICB (111). Moreover, Tregs suppress T-cell activity by upregulating the expression level of immune checkpoints. Activated Tregs can express lymphocyte activation gene-3 (LAG-3). $CD4^+CD25^{high}Foxp3^+LAG\text{-}3^+$ T cells possess robust inhibitory activity by releasing cytokines, including IL-10 and TGF-β1, without IL-2 (112). It has been proven that Tregs can differentiate into follicle-regulating T (TFR) cells with PD-1 expression, which inhibit the germinal center response (113). TFR cells are distinguished by the coexpression of CXCR5 and GITR2,5 or the transcription factors FOXP3 and BCL-6 (114, 115). TFR cells show advantageous suppressive capacity and *in vivo* persistence compared to conventional regulatory T cells, reducing the effect of an-PD-1 (116). Interestingly, Zappasodi et al. explored the role of a non-conventional subset of $CD4^+FOXP3^-PD\text{-}1^{high}$ T cells and found that this population of cells expresses a TFR-like phenotype and could limit the functions of the T-cell effector. However, in contrast to regulatory T cells, $CD4^+FOXP3^-PD\text{-}1^{high}$ T cells were helpful for B-cell activation (117).

T-cell exhaustion

T-cell exhaustion is characterized by an impaired tumor cell–killing function, the persistent and upregulated expression of inhibitory receptors, and the diverse transcriptional states of normal effector T cells or memory T cells. It is a status of T-cell dysfunction (118). Increased expression of immune checkpoints was reported to be associated with acquired resistance to ICB. *Ntrk1* has been proven to induce the upregulation of PD-L1 in mesenchymal Kras/p53 mutant lung cancer cells by stimulating Jak/Stat signaling, leading to the exhaustion of $CD8^+$ T cells within the TME (119). Enhanced expression of T-cell immunoglobulin mucin-3 (Tim-3) was observed in lung cancer patients who progressed after initially responding to anti-PD-1 therapy (120). The coexpression of PD-1 and Tim-3 in T cells was linked with an exhausted phenotype in head and neck squamous cell carcinoma (HNSCC) patients. Mechanically, the upregulated expression level of Tim-3 in T lymphocytes is dependent on the activation of the PI3K/Akt signaling pathway (121). Several checkpoints were coexpressed in TILs isolated from an ovarian tumor mouse model, including PD-1, CTLA-4, and lymphocyte activation gene-3 (LAG-3). The efficacy of single-agent blockade can be impaired by the compensatory enhancement of the other checkpoint molecules, resulting in poor response and resistance (122). With early PD-1 expression and late LAG-3/B- and T-cell lymphocyte attenuator (BTLA) expression, T cells gradually acquire the coexpression of these checkpoint receptors (123). The V-domain Ig suppressor of T-cell activation (VISTA) is another checkpoint of T cells. In melanoma patients with the initial response to anti-PD-1, the density of VISTA-positive T cells was significantly upregulated after treatment, which led to disease progression (124). Increased expression of these inhibitory coreceptors is associated with TCR signaling dysfunction and represents the initiation of negative regulatory signaling, leading to T-cell exhaustion and dysfunction (125). However, exhaustion does not mean the end of T cells' fate, and their function can be restored by blocking those overexpressed signals mentioned above.

Insensitivity to cytotoxic T lymphocyte–mediated killing

It is a consensus that CTLs kill tumor cells through two major pathways: granzymes A and B–mediated granule exocytosis and Fas/FasL conjugation–mediated apoptosis induction. Moreover, activated CTLs also secrete cytotoxic cytokines, including interferon-γ (IFN-γ) and tumor necrosis factor-α (TNF-α), to elicit cytotoxicity in tumor cells (126). From this perspective, the sensitive response of tumor cells to cytotoxic factors released by CTLs is vital in preventing immune evasion (127). On one hand, IFN-γ is quite essential for T cells' penetration into tumors. The effects of antigen-specific immunotherapy depend, to some extent, on tumor sensitivity to IFN-γ (128). The IFN-γ receptor (IFNGR) consists of two subunits, IFNGR1 and IFNGR2. The binding of IFN-γ to its receptor results in the activation of JAK1 and JAK2, which subsequently phosphorylates and dimerizes transcription factor STAT1. STAT1 homodimers then enter the nucleus, binding to specific promoters and initiating the transcription of IFN-γ-regulated genes (129). On the other hand, the release of IFN-γ also mediates the expression of PD-L1 and MHC class I molecules, which may be beneficial for anti-PD-L1 therapy (130).

The dysfunction of the IFN-γ signaling pathway was associated with the primary resistance to ipilimumab therapy in melanoma patients (131). The mutation of JAK1/JAK2 results in PD-L1 depletion and insensitivity to IFN-γ, ultimately causing the primary resistance to anti-PD-1 treatment in melanoma and colorectal cancer patients (40, 132). The depletion of the *IFNGR1* gene in B16 tumor cells suppressed IFN-γ mediated apoptosis and decreased the antitumor effects of anti-CTLA-4 therapy in a mouse model (131). However, the impact of additional IFN-γ pathway genomic alterations other than JAK1 and JAK2 on acquired drug resistance to ICB needs to be further investigated. Of note, the correlations between TNF mutations and survival were not discovered in any type of cancer by Cancer Genome Atlas (TCGA) analysis, indicating that although TNF acts as another cytotoxic factor, its effect is not as sufficient as IFN-γ (133).

Strategies in overcoming resistance to immune checkpoint blockade: Insights from preclinical cancer models

In accordance with the aforementioned proposed biological mechanisms of non-response to ICB, studies on potential therapeutic strategies addressing resistance mechanisms would be ideal for providing specific insights to improve clinical outcomes. Basically, strategies to reverse ICB tolerance are currently being explored (Table 1), which can be outlined as (1) releasing tumor antigens; (2) enhancing antigen presentation; (3) promoting T-cell infiltration; (4) reversing T-cell exhaustion; and (5) CD8+ T-cell stimulation.

Releasing tumor antigens

Low TMB and weak or unresponsive neoantigens contribute to the failure of antigen recognition, resulting in ICB resistance. Thus, elevating the release of tumor antigens appears to be a potentially effective approach to reversing ICB resistance (Figure 3).

Radiotherapy, as one of the most effective cytotoxic treatments, especially for localized solid cancers, has been considered to cause antitumor immune response apart from causing DNA damage to irradiated cancer cells (15). The abscopal response, originally described in 1953, referring to the shrinkage of tumors outside the irradiated area, has long been thought to involve the mechanisms of the immune response (162). Interestingly, this infrequently occurring abscopal effect could be strengthened by the addition of immunotherapy, which is, in turn, enhanced by radiotherapy (163). Increasing preclinical studies on radiotherapy combined with immunomodulators support the potential role of radiotherapy as an effective immune adjuvant (164). Mechanistically, radiation promotes the release of immunogenic neoantigens, known as TAAs, which play a vital role in *in situ* vaccination (134). Both *in vitro* and *in vivo* studies revealed that the irradiation effectively upregulates cancer testis antigens in the background of necrotic and apoptotic tumor cells and debris, followed with the promotion of the immunological recognition of the tumor (165).

Chemotherapy agents are the conventional treatment for various malignancies. As is known, cytotoxic chemotherapy primarily exerts an antitumor effect by blocking cell division (166). Apart from tumor debulking, chemotherapeutic agents have been demonstrated to promote immunogenic cell death (ICD), which is featured by the exposure of endoplasmic reticulum (ER) chaperones; lysosomal-secreting ATP; the aberrant accumulation of nucleic acids; the release of cytoplasmic and nuclear proteins such as high-mobility group box 1 (HMGB1), annexin A1; and the release of specific damage-associated molecular patterns (DAMPs) (14). Overall, this increasing antigenicity leads to on-target immunostimulatory effects in cancer (167). Recently, a bioresponsive doxorubicin (DOX)-based nanogel has been engineered to directionally release the loaded drugs after being internalized into the TME. These chemoimmunotherapies are promising to conquer the challenges of current ICB-based immunotherapy and provide a paradigm for developing immunomodulatory nanomedicines (168). Data from 12 NSCLC patients suggested that multiple non-mutated neoantigens released from cisplatin-induced apoptotic tumor cells elicited $CD8^+$ or $CD4^+$ Teff cell responses, which could notably be promoted by anti-PD-1

TABLE 1 Potential combination strategies to improve the antitumor effect of programmed cell death protein 1 (PD-1)/programmed cell death ligand 1 blockade.

Targeted process	Strategy	Mechanisms	Reference
Releasing tumor antigens	Radiotherapy	Promoting the release of immunogenic neoantigens	(134)
	Chemotherapy	Inducing the ICD	(14)
	Oncolytic viruses	Promoting tumor ICD and "in situ" vaccination	(135)
Enhancing antigen presentation	Histone deacetylase inhibitors	Epigenetically modulating the upregulation of the MHC pathway	(136)
	DNMTi	Elevating the expression of several antigen-presenting molecules	(137)
	STING agonists	Activating cGAS-STING to reverse MHC-I downregulation	(138)
	Polyinosinic:polycytidylic acid (poly I:C)	Inducing MHC I expression *via* NF-κB	(139)
	TLR9 agonists	Augmenting conventional DC (cDC) infiltration to increase antigen delivery	(140)
	Flt3L-poly I:C combined injection	Upregulating the expression levels of CD86, CD40, and MHC II of tumor-infiltrating CD103+ DC	(141)
Promoting T-cell infiltration	PI3K-AKT pathway inhibitors	Promoting T-cell infiltration in PTEN loss melanoma	(142)
Reversing T-cell exhaustion	PORCN inhibitors CGX-1321	Suppressing Wnt/β-catenin signaling to improve $CD8^+$ T-cell levels	(143)
	MEK inhibitors	Inhibiting the MAPK signaling pathway to increase T-cell infiltration	(144)
	CDK4/6 inhibitor abemaciclib	Increasing T-cell recruitment with elevated levels of TH1 cytokines/chemokines	(145)
	TGF-β inhibitors	Inducing potent and durable cytotoxic T-cell responses	(146)
	Antiangiogenic therapies	Elevating the expression of adhesion molecules, facilitating the adhesion and extravasation of T cells	(147)
	Low-dose radiotherapy	Reprogramming the TME and inducing T-cell infiltration	(148)
	Mesoporous silica nanoparticle	Eliciting T-cell-recruitment chemokine production and driving CTL infiltration	(149)
	CAR T therapy	Directly providing antigen-sensitive immune infiltration	(150)
	Dual checkpoint inhibitors	Blocking the alternative immune checkpoints to reverse T-cell exhaustion	(151)
	Costimulatory agonists	Reversing T-cell exhaustion and inducing the increase of effector $CD8^+$ T cells	(152)
	Targeting transcriptional regulator TOX	Downregulating TOX to ameliorate the exhaustion state of $CD8^+$ T cells	(153)
	DNMTi	Epigenetically inducing the rejuvenation of exhausted $CD8^+$ T cells	(154)
	Metabolic modulation	Instructing T-cell metabolic programming	(155)
CD8+ T-cell stimulation	Targeting TGF-β	Reducing tumor-infiltrating Tregs	(156)
	CSF1R inhibitors	Inhibiting the differentiation and accumulation of M2-like TAMs	(157)
	Carflzomib	Reprogramming M2 macrophages into the M1-like population through IRE1a-TRAF2-NF-κB signaling	(158)
	NOX4 inhibitors	Reversing TGF-β1-mediated CAF activation	(159)
	Radiotherapy	Increasing $CD8^+$ T cells with the reduction of MDSCs and Tregs	(160)
	Microbiota-centered interventions	Regulating the collaboration of microbiota with the TME to promote antitumor T-cell responses	(161)

ICD, immunogenic cell death; MAPK, mitogen-activated protein kinase; DNMTi, DNA methyltransferase inhibitors; NOX4, NADPH oxidase-4.

therapy, correlating with OS (167). Recent trial data on chemotherapy combined with PD-1/L1 inhibitors demonstrate the clinical benefit in patients with NSCLC, triple-negative breast cancer, gastric cancer, and HCC (166, 169, 170).

Oncolytic viruses (OVs) are another selective approach to promoting the release of antigens (171). Similarly, OVs induce tumor ICD and "in situ" vaccination. Subsequently, these soluble TAAs from dying tumor cells facilitate both innate and adaptive antitumor immune responses. Researchers found that in a model of disseminated lung cancer resistant to PD-1 immunotherapy, intratumoral virotherapy elicits $CD8^+$ T-cell responses against a set of cancer-specific neoepitopes, overcoming systemic resistance to PD-1 immunotherapy (135). However, different OVs are not capable of inducing ICD equally (172). Thus, incorporating ICD-related DAMP genes seems to be a further attractive option to enhance immunogenicity. In this way, OVs function as engineering platforms for combination immunotherapy. Still, challenges exist in allowing OVs to arrive at the directed primary and metastatic tumor position to perform systematic therapeutic effects (173).

Hopefully, many novel strategies for promoting tumor antigen release are under study. Minimally invasive thermal ablation treatments such as microwave ablation, cryoablation, radiofrequency ablation, or highintensity focused ultrasound

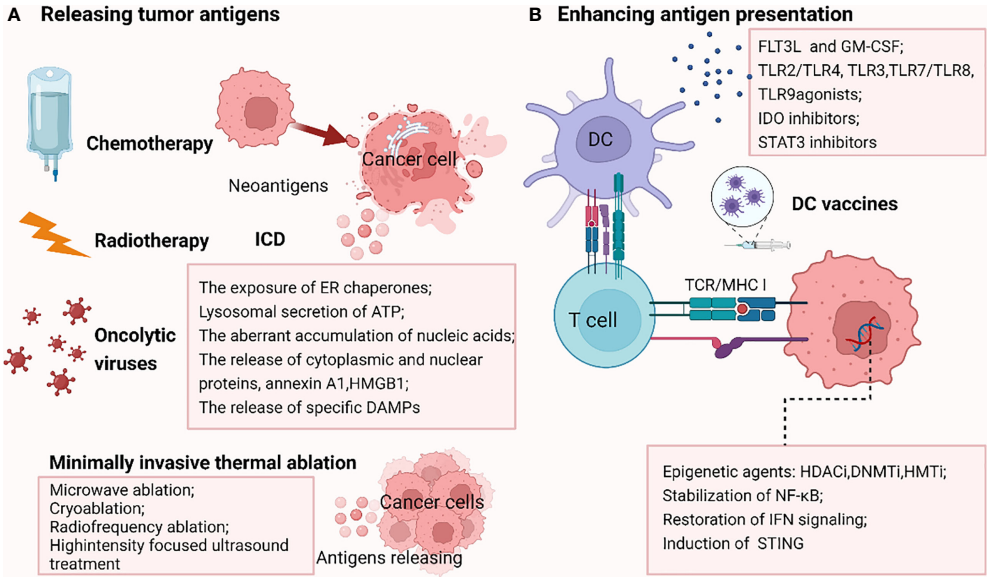

FIGURE 3
Strategies reversing PD-1/PDL1 blockade by releasing tumor antigens **(A)** and enhancing antigen presentation **(B)**. A.Chemotherapy, radiotherapy and oncolytic viruses could promote the immunogenic cell death (ICD), enhancing the liberation of immunogenic neoantigens, thus increasing the antigenicity in tumors resistant to ICB due to the failure of antigen recognition. In addition, some minimally invasive thermal ablation treatments lead to antigens release as well. **(B)** DNMTi, HDACi, HMTi epigenetically modulate the upregulation of MHC pathway. Stabilization of NF-κB, restoration of IFN signaling and induction of stimulator of interferon genes (STING) also reverse MHC-I downregulation. Besides, stimulation factors including cytokines such as FLT3L (FMS-like tyrosine kinase 3 ligand) and GM-CSF (granulocyte–macrophage colony-stimulating factor), Toll-like receptor (TLR2/TLR4, TLR3, TLR7/TLR8, TLR9) agonists, IDO inhibitors and STAT3 inhibitors could augment the infiltration, activation, and effector function of conventional DCs (cDCs), thus increasing antigen delivery. DC vaccines are also important tools boosting antigen presentation. The picture was created with BioRender.com. ICD, immunogenic cell death; STING, stimulator of interferon genes; FLT3L, FMS-like tyrosine kinase 3 ligand; GM-CSF, granulocyte–macrophage colony-stimulating factor; TLR, Toll-like receptor; IDO, indoleamine- (2,3)-dioxygenase; DC, dendritic cell.

treatment are the common selective therapies for patients with inoperable tumors. Interestingly, these local applications of extreme temperatures lead to the release of antigens from the necrotic tumor lesion, enhancing the activation of the tumor-specific immune response. However, the effect of single thermal ablation is too limited, and appropriate immunomodulators are required for promoting an effective therapeutical systemic antitumor immune response (174–176). Recently, a novel tumor microenvironment ROS/GSH dual-responsive nanoplatform consisting of chemophotodynamic therapy and synergistical control-release PTX has been designed to induce the release of DAMPs after tumor cell pyroptosis, boosting the curative effect of anti-PD-1 treatment in a CT26 tumor model (177).

Enhancing antigen presentation

The deficiency of antigen presentation represents another major challenge in ICB therapy, which is caused by multiple factors as stated above, including MHC I defects, β2M/HLA gene loss, deficient IFN signaling, and dysfunctional DCs (178). Aiming at these abnormalities is a promising strategy to improve the responsiveness to ICB regimens (Figure 3).

The epigenetic control of immune resistance has been implicated as associated with an overall loss of antigen presentation *via* the loss of antigen expression or downregulation of MHC I (179). Histone deacetylases (HDACs) are one class of epigenetic regulators, comprising four families (class I, IIa, IIb, and IV). HDACs appear to have crucial roles in both innate and adaptive immune responses. HDAC1 and HDAC2 have been reported to negatively mediate antigen presentation by inhibiting the main transcriptional regulator of MHC class II genes (180). Accordingly, histone deacetylase inhibitors (HDACis) can epigenetically modulate the upregulation of the MHC pathway, facilitating the immune targeting of cancer cells (136). Four HDACis (e.g., romidepsin, belinostat, vorinostat, and panobinostat) have been approved by the FDA for lymphoma and/or multiple myeloma treatment. In both colon and ovarian cancer cell lines, HDACi treatment promoted increased antigen processing and antigen presentation (181). The efficacy of combining HDACi with PD-1 inhibitors has been evaluated in multiple preclinical cancer models, including melanoma, ovarian cancer, breast cancer, and lung cancer, showing great promise (136,

182, 183). Other epigenetic agents such as DNA methyltransferase inhibitors (DNMTis) as well as histone methyltransferase inhibitors (HMTis) have also been indicated to improve antigen presentation by elevating the expression of several antigen-presenting molecules, thus enhancing the recognition and activation of immune cells (137). Based on these exciting preclinical results, a combination of DNMTi or/and HDACi with ICB has undergone clinical trials in advanced colorectal cancer (NCT02512172), non-small cell lung cancer (NCT01928576, NCT00387465), head and neck cancer (NCT03019003), and gastrointestinal cancers (NCT03812796) (184).

Apart from the epigenetic modification of MHC I antigen presentation, targeting pathways associated with MHC I expression has been described to reverse MHC I downregulation and boost immunotherapy efficacy. Potential therapeutic strategies include the stabilization of NF-κB, restoration of IFN signaling, and induction of stimulator of interferon genes (STING) (138, 139). Notably, the effects of NF-κB and IFNs are pro- or antitumorigenic in different stages and types of tumors. Accordingly, both negative and positive regulators of NF-κB and IFNs have been reported to upregulate MHC I expression (185).

Several strategies to augment conventional DC (cDC) infiltration, activation, or effective function have been proposed to increase antigen delivery and enhance the efficacy of ICB. The stimulation factors include Toll-like receptor (TLR2/TLR4, TLR3, TLR7/TLR8, TLR9) agonists, IDO (indoleamine-(2, 3)-dioxygenase) inhibitors, and STAT3 inhibitor cytokines such as GM-CSF, and FLT3L (FMS-like tyrosine kinase 3 ligand) (186). For example, combining pembrolizumab with a synthetic CpG oligonucleotide TLR9 agonist, SD-101, exhibited greater clinical efficacy than PD-1 blockade alone in a phase Ib trial, which was associated with elevated tumor-infiltrating DC characteristics (140). Similarly, Flt3L-poly I:C combined injection significantly induced the upregulating expression levels of CD86, CD40, and MHC II of tumor-infiltrating $CD103^+$ DC and promoted DC immunogenic function, eventually enhancing antitumor responses synergized with anti-PD-L1 Ab treatment in BRAF-mutant and B16 melanoma mouse models (141). Nanomaterials have recently been applied in facilitating the tumor antigen presentation of DCs. A cationic nanoscale metal–organic framework (nMOF) was designed to exert the effects of local immunogenic photodynamic therapy treatment and CpG stimulation, enhancing antigen presentation and synergizing with ICB to induce tumor regression in a breast cancer model (187). Moreover, "next-generation" DC vaccines, essential tools for anticancer therapy, have been suggested to be a desirable combinatorial counterpart for ICB, especially in tumors with low mutational burden (188).

Promoting T-cell infiltration

As a robust prognostic biomarker, tumor-infiltrating lymphocytes are influenced by multiple mechanisms, including genetic alterations within tumor cells, aberrant vasculature, and elevated immunosuppressive factors like TGF-β (12, 146, 189, 190). Low lymphocyte infiltration mainly accounts for the limited efficacy of ICB in many tumors, especially in the immune-infiltrated and -excluded phenotypes (191). Hence, promoting T-cell infiltration *via* targeting these factors provides an outlook on the future for improving ICB effectiveness (Figure 4).

mRNA nanoparticles reactivating the tumor suppressor PTEN have been proven to significantly elicit antitumor immune responses and restore the therapeutic effect of ICB in PTEN-null prostate cancer and a PTEN-mutated melanoma model by promoting $CD8^+$ T-cell infiltration (190). Furthermore, a drug candidate D18 could suppress the downregulation of PTEN expression by increasing KDM5A abundance, which also potentialized the efficacy of various ICBs in multiple tumor models (192). Moreover, targeting the PI3K-AKT pathway downstream of PTEN is a selective approach to elevate tumor-infiltrating T cells. For example, the PI3Kb inhibitor GSK2636771 sensitized PTEN-null melanomas to both CTLA-4 and PD-1 inhibitors and promoted T-cell infiltration to enhance the antitumor activity *in vivo* (142). Wnt/β-catenin signaling is another tumor-intrinsic pathway associated with poor spontaneous T-cell infiltration. Many inhibitors targeting WNT signaling have been developed to restore T-cell infiltration and reestablish anticancer immunity with ICB. In ovarian cancers, a typical "cold" immune phenotype, PORCN inhibitors CGX-1321 suppressing Wnt/β-catenin signaling, has been confirmed to improve $CD8^+$ T-cell levels in the omentum TME (143). Other Wnt signaling inhibitors such as the anti-FZD7 antibody, β-catenin inhibitor DCR-BCAT, DKK1 inhibitor, and WNT inhibitor have been suggested to exert immunomodulatory effects as well (193). Furthermore, clinical trials combining Wnt inhibitor and ICB are ongoing, including DKN-01 (DKK1 antibody) plus pembrolizumab (NCT02013154) and PORCN inhibitor WNT974 combined with spartalizumab (NCT01351103) (194, 195).

The mitogen-activated protein kinase (MAPK) signaling pathway, another oncogenic signaling pathway associated with shaping tumor immunogenicity, has been proposed to be a promising target combined with ICB therapies (12). In a preclinical model of BRAF(V600)-mutated metastatic melanoma, antiPD1 therapy in combination with BRAF and MEK inhibitors contributed to complete tumor regression with increasing T-cell infiltration into tumors (144). Similarly, it has been reported in colon cancer (the CT26 model) that MEK inhibition promotes the accumulation of TIL by preventing the death of CD8+ T cells triggered by chronic TCR stimulation (196). Clinical studies of MAPK signaling inhibitors plus ICB have shown encouraging results. In BRAF V600–mutated melanoma patients, treatment with the combination of atezolizumab (anti-PD-L1) plus vemurafenib (BRAF inhibitor) + cobimetinib (MEK inhibitor) promoted 71.8% objective responses (a complete

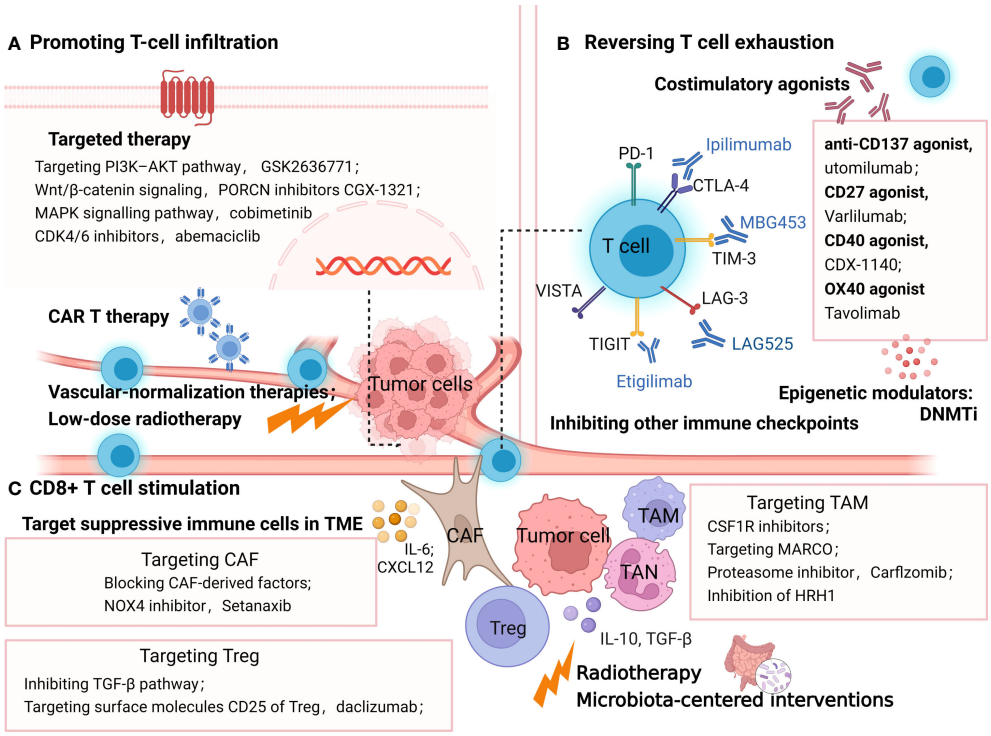

FIGURE 4
Strategies overcoming resistance to PD-1/PDL1 by promoting T-cell infiltration **(A)**, reversing T cell exhaustion **(B)**, and CD8+ T cell stimulation **(C)**. **(A)** methods promoting T-cell infiltration include targeted therapy, vascular-normalization therapies, CAR T therapy and low-dose radiotherapy; **(B)** treatment options to reinvigorate of T cell exhaustion include blocking the alternative immune checkpoints, targeting co-stimulatory receptors, inhibiting soluble immune suppressive mediators and epigenetically coordinating exhausted CD8+ T (Tex) cells. **(C)** strategies targeting immune-suppressive cells in TME such as TAM, Treg and CAF to stimulate T cells. In addition, radiotherapy and microbiota-centered interventions also reprogram the immunosuppressive TME, promoting antitumor T-cell responses. The picture was created with BioRender.com. CAR, chimeric antigen receptor, Treg, regulatory T lymphocytes; DC, dendritic cell; TAM, tumor associated macrophages; CAF, cancer associated fibroblasts; MARCO, macrophage receptor with collagenous structure; HRH1, histamine and histamine receptor H1.

response rate of 20%). Meanwhile, the run-in of cobimetinib and vemurafenib contributed to the increase of circulating proliferating CD4+ T-helper cells (197).

Cyclin-dependent kinases 4 and 6 (CDK4/6) inhibition has been highlighted to exert antitumor immune response *via* promoting antigen presentation and enhancing $CD8^+$ T-cell infiltration (145). The FDA-approved CDK4/6 inhibitor abemaciclib has shown preclinical synergistic antitumor effects with PD-1 inhibitor in breast cancer mouse models, the ID8 murine ovarian cancer model, and the colon adenocarcinoma murine model, which depends on increased T-cell recruitment with elevated levels of TH1 cytokines/chemokines (198–200).

Immunosuppressive cytokine TGFβ has received growing attention in cancer immunotherapy for its ability to block the antitumor immune response by limiting T- cell infiltration (201). Preclinical models suggested that coinhibiting TGF-β and PD-L1 induced potent and durable cytotoxic T-cell responses, transforming tumors from an excluded to an inflamed phenotype (146, 202). Strategies targeting TGF-β are under development, including the TGF-βRI kinase inhibitor galunisertib, neutralizing antibodies against the mature TGF-β cytokines, antibodies against TGF-βRII, and soluble TGF-β receptor traps, some of which are undergoing clinical trials in combination with anti-PD1 antibodies (203, 204).

As previously described, VEGF-induced immunosuppression inhibits T lymphocyte infiltration in the TME, hampering the therapeutic effect of ICB. In several earlier preclinical studies, vascular-normalization therapies have been proven to facilitate the transformation of the immunosuppressive TME toward an immune-supportive phenotype (205), which manifests as the aggregation of antitumor T cells and DC maturation inside tumors (206). In addition, the process of increased T lymphocyte infiltration induced by antiangiogenic therapies was partly associated with the elevated expression of adhesion molecules (intercellular adhesion molecule–1, vascular cell adhesion molecule-1), which facilitated the adhesion and extravasation of T cells (147). In preclinical mouse models and clinical trials, antiangiogenic agents significantly improved

immunotherapy outcomes (205, 207). The various antiangiogenic therapeutic agents mainly consist of anti-VEGFA monoclonal antibodies such as bevacizumab, inhibitors of angiopoietin-2, and VEGFR tyrosine kinase inhibitors (TKIs) such as sorafenib (207). Some of them are presently undergoing clinical trials combining with ICB, receiving more significant clinical benefits than monotherapy in some early data (19).

In addition to the combination of targeted therapies mentioned above, low-dose radiotherapy has been reported to reprogram the TME and induce T-cell infiltration in mouse models of immune-desert tumors (148). Meanwhile, in "inflamed" human tumors, the preexistent intratumoral T cells not only survived radiotherapy but also acquired improved antitumor effects with the increasing production of IFN-γ (208).

It is also noteworthy that biomaterials at the nanoscale have been explored to establish a T-cell-inflamed TME and overcome resistance to ICB. Mesoporous silica nanoparticles were reported to elicit T-cell-recruitment chemokine production and drive CTL infiltration in multiple tumor models resistant to PD-1 antibodies (149). A supramolecular gold nanorod has been reported to reprogram the TME and improve TILs, significantly augmenting ICB therapy, which depends on the hyperthermal activation of ICD and genome editing of PD-L1 (209).

Moreover, chimeric antigen receptor (CAR) T cells may be a direct approach to provide antigen-sensitive immune infiltrates, implying a new opportunity for patients with less immunogenic or "noninflamed" tumors. CAR-T therapy could target T cells directly to tumor cells by genetically modifying T cells (210). Since the initial proposition of CAR-T in 1989, its antitumor efficacy and persistence have been improved due to altering the construction in the advanced generations of CAR-T. Based on these remarkable clinical responses, the FDA has approved four anti-CD19 CAR T-cell products and one anti-BCMA CAR T-cell therapy in different hematological cancers (211). However, the clinical efficacy of CAR T cells in the solid tumor has shown much less satisfactory results. One of the major obstacles includes the fact that PD-1-mediated immunosuppression leads to the poor persistence and dysfunctions of CAR T cells (150). Therefore, ICB and CAR T-cell combination therapy holds promise to refresh the immune system and enhance therapeutic efficacy. A synergy effect has been reported in the combination of PD-1 blockade and CAR-T cell therapy (212). In a transgenic Her-2 recipient mice model, anti-PD-1 antibody combined with CAR T cells showed the enhanced activation and proliferation of anti-Her-2 T cells, with the significant regression of established tumor (213). Other preclinical studies have shown the synergistic antitumor activity of combination therapies in thyroid cancers (214) and pleural mesothelioma (215). Some encouraging clinical results suggested the safety, low toxicity, and clinical responses of combinatorial treatment. One case report demonstrated five patients with diffuse large B-cell lymphoma who endured progression/relapse post-CART19/20 therapy received anti-PD-1 treatment (sintilimab or camrelizumab). Three of five patients had objective responses, including two complete responses and one partial response (216). Similarly, E. A. Chong et al. reported that in 12 B-cell lymphoma patients who were relapsing after or refractory to CD19-directed CAR T-cell therapy, anti-PD1 ICB (pembrolizumab) treatment showed safety and clinical responses (217). Based on these promising preclinical results, a series of one-half of clinical trials exploring the combination immunotherapy of CAR T cells and PD-1 blockade agents for multiple malignancies are under investigation, including relapsed/refractory Hodgkin lymphoma (NCT04134325), classical Hodgkin lymphoma (NCT05352828), relapsed/refractory B-cell lymphoma (NCT04539444), HER2-positive sarcoma (NCT04995003), and glioblastoma (NCT03726515). Some early results of clinical trials suggested the safety and promising efficacy of this combination in patients with malignant pleural disease (218), relapsed/refractory (r/r) diffuse large B-cell lymphoma (219), and relapsed/refractory aggressive B-cell non-Hodgkin lymphoma (220). However, minimal response with no meaningful durability has also been reported in two relapsed, refractory (R/R) B-cell non-Hodgkin lymphoma patients receiving the combination therapy of bispecific CAR T cells and PD-1 inhibitors (221). Therefore, further research is needed to confirm the therapeutic efficacy and optimal administration method of this combination treatment.

Reversing T-cell exhaustion

As stated above, T-cell exhaustion is characterized by the increased expression of suppressive cytokines and inhibitory receptors, including PD-1, CTLA, LAG-3, TIM-3, VISTA and ITIM domain (TIGIT), hierarchical decreased cytokine production (IL-2, TNF, IFNγ), and reduced proliferative capacity, with underlying distinct epigenetic states (222, 223). Accordingly, upcoming treatment options to overcome ICB resistance by the reinvigoration of T-cell exhaustion (Figure 4) include blocking the alternative immune checkpoints, targeting costimulatory receptors, inhibiting soluble immune- suppressive mediators, and epigenetically coordinating exhausted $CD8^+$ T (Tex) cells (224–226).

Combining blockade treatments against multiple inhibitory receptors or combining checkpoint inhibitors with costimulatory agonists is a promising way to reinvigorate exhausted $CD8^+$ T cells. Desirable therapeutic outcomes have been indicated in the preclinical and clinical studies of many tumors (227). Alternative targeting IRs include anti-TIM-3(MBG453), anti-LAG-3 (LAG525), anti-TIGIT (etigilimab), anti-VISTA (JNJ-61,610,588), and anti-B7-H3 (enoblituzumab) (228–231). Accordingly, a wide range of combination strategies are

undergoing research in various malignancies both preclinically and clinically. For instance, ipilimumab (anti-CTLA-4) plus nivolumab (anti-PD-1) is the most well-studied immuno-oncology (IO) combination showing comparatively better efficacy in multiple advanced tumors. It has become the earliest dual ICB treatment that received FDA approval in September 2015 for the first-line therapy of metastatic melanoma. Currently, this combination has been approved for the treatment of advanced renal cell carcinoma (RCC), metastatic colorectal cancer with MMR/MSI-H aberrations, PD-L1-positive (≥1%) metastatic NSCLC, and HCC as well. Noteworthily, the increasing incidence and intensity of the adverse events have been reported in the combining blockade, which suggest the importance of further studies (151). Costimulatory agonists are another good choice for reversing T-cell exhaustion in treating ICB. For example, the anti-CD137 agonist utomilumab has been shown to induce the increase of effector CD8+ T cells and improve survival in synergy with ICB in an ovarian cancer model (232). Recently, a growing number of agonist antibodies targeting immune costimulatory receptors are in clinical development for cancer indications, such as CD27 agonist varlilumab (CDX−1127) and CD40 agonist CDX−1140, OX40 agonist tavolimab (MEDI0562). Although none have been approved to date, combination approaches are still full of therapeutic potential (152).

Pauken et al. demonstrated that PD-1 blockade alone minimally remodeled the Tex epigenetic landscape. Hence, epigenetic modifiers, or T-cell epigenomic engineering with checkpoint blockade, may help reacquire durable immune memory against tumors (233). The transcriptional regulator TOX has recently been highlighted to be involved in programming CD8+ T-cell exhaustion transcriptionally and epigenetically, which is associated with plenty of transcription-factor networks downstream of TCR signaling (225). The knockdown of TOX ameliorated the exhaustion state of CD8+ T cells, enhancing the response to ICB treatment in an HCC mouse model (234), suggesting a new strategy to maximize immunotherapeutic efficacy by the downregulation of TOX expression. Interestingly, coblocking PD-1 and TIGIT could reinvigorate TOX-expressing PD-1^{high}CD8+ TILs with better therapeutic outcomes in bladder cancer patients (153). Other modulators of the epigenetic landscape stated above, such as DNMTi, have also been found to induce the rejuvenation of exhausted CD8+ T cells, synergizing with a PD-1 inhibitor in a prostate adenocarcinoma mouse model (154).

Metabolic insufficiency play a crucial function in modulating T-cell exhaustion, implicating that metabolic modulation is a selective way to rejuvenate exhausted T cells, eliciting superior antitumor immunity (17, 155). In addition, ICB has been demonstrated to exert an inhibitory effect on immune cells' metabolism and suppress glycolysis while increasing FAO and lipolysis. Therefore, the combinations of ICB with metabolic interventions appear to be ideal opportunities to improve antitumor effects *via* reversing immune metabolic dysfunctions (235). Many metabolic interventions have been exploited, such as enhancing mitochondrial fitness, enforcing fatty acid oxidation, and ameliorating ER stress (236). For example, in a B16 melanoma mouse model, metformin combined with anti-PD-1 therapy promoted increasing tumor clearance with an elevated intratumoral T-cell function. In addition, this reinvigoration of T cells mediated by metformin is associated with modulating the oxygen tension of the TME (237).

$CD8^+$ T-cell stimulation

Various elements of the TME, including TANs, TAMs, CAFs, and Tregs, play critical immune-suppressive roles in mediating resistance to ICB. Correspondingly, therapies combined with ICB and strategies targeting these immune-suppressive cells appear to overcome resistance and improve clinical outcomes (Figure 4).

As is known, Tregs mediate tumor resistance against ICB in multiple ways, including upregulating the expression of other immune checkpoints including LAG-3, TIM-3, GITR, TIGIT, and VISTA; secreting high levels of TGF-β; and increasing the activation of the PI3K signaling pathway (238, 239). In glioblastoma, a typical immunologically 'cold' tumor, the suppressive Treg cells were converted toward CD4 effector T cells by an agonistic antibody (αGITR), which promoted the cure rates in GBM models combined with PD1 antibodies (240). Similar results have been reported in the coblockade of PD-1 and other immune checkpoints (241, 242). Importantly, this combined immunotherapy needs to be adapted to the specific immune environment for each tumor type. Targeting TGF-β is another appealing approach to reducing tumor-infiltrating Tregs and improving response to ICB treatment. R. Ravi et al. invented bifunctional antibody–ligand traps (Y-traps), simultaneously inhibiting the TGF-β pathway and CTLA-4 or PD-L1. This engineered antibody (a-CTLA4TGFβRIIecd and a-PDL1-TGFβRIIecd) significantly counteracted Tregs and restored beneficial TH1 cells in the TME, exhibiting superior antitumor efficacy than either the CTLA-4 antibody or PD-L1 antibodies in human melanoma (A375)–bearing NSG mice (156). Other strategies such as daclizumab, targeting the surface molecules CD25 of Treg, have been experimented both preclinically and clinically. Daclizumab administration reprogrammed Tregs. However, it also diminished activated Teff, showing no augmentation of T-cell responses in metastatic melanoma patients (243). Obviously, Treg-silencing strategies coupled with ICB require a deeper investigation of the crosstalk between the TME and Tregs.

As a vital source of PD-1, TAM has been demonstrated to hinder ICB efficacy by capturing ICB antibodies, secreting inhibitory cytokines, and expressing coinhibitory molecules. TAM-centered strategies are promising treatments to improve the efficacy of ICB agents (244, 245). CSF1R inhibitors enhanced the therapeutic efficacy of PD1 blockade by inhibiting the differentiation and accumulation of M2-like TAMs in melanoma models (157). Another monoclonal antibody targeting MARCO (macrophage receptor with collagenous structure) has also been reported to switch the TAM phenotype and boost checkpoint therapy effectively in melanoma tumor–bearing mice, which notably was induced by activating NK-cell-mediated killing other than T- cell-directed immunotherapy (246). Carfilzomib, a proteasome inhibitor approved by the FDA to treat relapsed/refractory multiple myeloma patients, has been supported to reprogram M2 macrophages into an M1-like population through IRE1a-TRAF2-NF-κB signaling and synergize with PD-1 inhibitors to reduce tumor growth in an autochthonous lung cancer model (158). Intriguingly, a recent study revealed that the high expression of histamine and histamine receptor H1 (HRH1) attenuated response to immunotherapies *via* polarizing TAMs toward an M2-like immunosuppressive phenotype. Hence, the HRH1 knockout or inhibition of HRH1 on macrophages with antihistamines reshaped the transcriptomic landscape of immune cells and blocked immune resistance when combined with anti-PD-1 treatment in mammary tumor and colon cancer mice models. In agreement with these results, the clinical data suggested that preexisting allergy or high histamine levels contributed to the inadequate immunotherapy responses in cancer patients (247). The similar antitumor properties of histamine dihydrochloride have been proven in MC-38 colon carcinoma and EL-4 lymphoma mouse model (248). However, in the murine cholangiocarcinoma (CAA) model, TAM blockade by anti-CSF1R failed to reduce CCA growth due to the compensatory infiltration of G-MDSCs. Meanwhile, the dual inhibition of TAMs and G-MDSCs was sufficient to enhance the efficiency of the PD-1 inhibitor in the orthotopic mouse model of CCA. Notably, the response rate to the ICB monotherapy of CAA patients is only 5.8% (249). Thus, targeting these immunosuppressive elements, particularly TAMs, is significant in potentiating PD-1 blockade.

Targeting CAF in the suppressive TME would be another valuable option to improve immunotherapy efficacy. Specifically, the targeted strategies include depleting CAF, interrupting their tumor-promoting ability, blocking CAF activation, and reverting CAF to a quiescent state (250). The inhibition of fibroblast activation protein (FAP)–positive CAF has disappointing results in metastatic colorectal cancer patients, possibly due to off-target effects (251). In recent years, single-cell RNA sequencing has characterized the heterogeneity of CAF in multiple tumor types, which suggests that targeting the subtype of CAF therapy may require a more nuanced approach (252). Blocking CAF-derived factors such as IL-6 and CXCL12 has been demonstrated to increase the accumulation of T cells and boost response to ICB in the models of multiple cancers (253). The ROS-producing enzyme NADPH oxidase-4 (NOX4) inhibition has been demonstrated as a well-studied approach to reversing TGF-β1-mediated CAF activation and promoting the transformation into a quiescent fibroblast-like phenotype (254). Using the NOX inhibitor GKT137831 (setanaxib) with immunotherapy can improve clinical outcomes in CAF-rich solid tumor models, indicating that reversing myofibroblastic CAFs to 'normalized' by setanaxib may be a considerable way to resensitize CAF-rich tumors to ICB, such as head and neck, colorectal, esophageal, and pancreatic cancers (255).

Apart from aiming at a specific group of cells or cytokines, radiotherapy is an appealing approach to shifting the immunosuppressive TME in the presence of immunotherapy. Combinatorial therapy has been shown to significantly increase $CD8^+$ T cells by reducing MDSCs and Tregs, compared with RT or immunotherapy alone (160, 256). However, the immunosuppression effect of RT was known as well. Those irradiated cells that died of apoptosis could release anti-inflammatory cytokines such as TGF-β and adenosine to reduce tumor tolerance (257). Therefore, the definition of the optimum dose, appropriate fraction, and suitable target site of RT is fundamental (258).

Microbiota-centered interventions have recently gained growing attention for the engagement of the gut microbiome in primary and acquired resistance to ICB in different tumors such as melanoma, RCC, NSCLC, pancreatic ductal adenocarcinoma, and colon cancer (18, 259). Studies have proposed that regulating the collaboration of microbiota with the TME could contribute to metabolic changes, promoting antitumor T-cell responses and ameliorating anti-PD-1 blockade resistance (161). B. Routy et al. revealed that *Akkermansia muciniphila* and *Enterococcus hirae* are the primary factors in eliciting immunological changes, increasing $CCR9^+CXCR3^+CD4^+$ T lymphocytes, which rely on interleukin-12 (18). Deep mechanisms accounting for the immunomodulatory effects of the gut microbiome remain to be explored. Nevertheless, manipulating the gut ecosystem is a profitable strategy to facilitate a better immune response (260). The specific interventions include supplementation with probiotics, the transfer of the fecal microbial content, microbiome-based metabolite therapy, and the depletion of the unfavorable bacterial taxa by proper oral antibiotics as well as dietary interventions, some of which have been evaluated in early phase clinical studies (261, 262). Intriguingly, researchers found that

orally supplementing camu-camu, a polyphenol-rich berry, could circumvent anti-PD-1 resistance by reprogramming the TME in a microbiome-dependent way (263).

Therapeutic trials to validate resistance mechanisms

Combining anti– programmed cell death protein 1 (PD-1)/programmed cell death ligand 1 with conventional cytotoxic chemotherapy

Based on the importance of chemotherapy in traditional cancer treatment and the beneficial immunomodulating effects of chemotherapy in the map of PD1/PDL1 therapy, chemotherapy has been the most widely used combination strategy approved in various indications so far and chemoimmunotherapy has become a standard of treatment for some cancer patients. The FDA granted pembrolizumab plus chemotherapy (pemetrexed and platinum) as the first-line therapy for advanced non-squamous NSCLC based on the clinical trial KEYNOTE-021 in 2017. Later in 2018, pembrolizumab plus carboplatin and either paclitaxel or nab-paclitaxel were approved as the first-line treatment of metastatic squamous NSCLC based on the results of KEYNOTE-407. On the strength of a series of successes in clinical trials, the approval of pembrolizumab plus chemotherapy covers more tumors, including gastroesophageal junction cancer (KEYNOTE-811), advanced triple-negative breast cancer (KEYNOTE-355), and esophageal cancer (KEYNOTE-590) (264–266). Meanwhile, anti-PD-L1-based chemoimmunotherapy such as atezolizumab plus chemotherapy and durvalumab combined with platinum plus etoposide treatment, has also received approval from the FDA in different tumors (170, 267). There is currently a rapidly growing number of clinical trials assessing chemoimmunotherapeutic regimens with the PD-1/PD-L1 inhibitor in clinical development but have not yet been approved by the FDA (166). The dose and sequence of administration require further evaluation to maximize the benefits of immunogenic chemotherapy.

Combining anti– programmed cell death protein 1 (PD-1)/programmed cell death ligand 1 with radiotherapy

Based on the above-mentioned preclinical data suggesting the potential synergistic effect of combining radiotherapy with anti–PD–1/PD–L1, a mounting number of translations into clinical trials are ongoing, most of which are still in phase I or II. In addition, the majority of radioimmunotherapy regimens are based on stereotactic body radiotherapy (SBRT). For instance, in PEMBRO-RT, a multicenter randomized phase 2 study of 92 patients with advanced NSCLC, patients who received SBRT (three doses of 8 Gy) before pembrolizumab showed improved trends in OS, progression-free survival (PFS), and objective response rate (ORR) compared with the non-irradiated group (268). However, in a single-center, randomized, phase II trial (NCT02684253) for patients with metastatic or recurrent HNSCC, nivolumab plus SBRT showed no improvement in response compared with nivolumab single arm (269). Further research is needed to explore the best radioimmunotherapy options, including the dose, volume, fractionation, and sequence.

Dual immune checkpoint blockade

The combination of ipilimumab (anti-CTLA-4) and nivolumab (anti-PD-1) is the first FDA-approved dual ICB treatment based on the results of CheckMate-067, CheckMate-069, and CheckMate-142 (151, 270). This combination is currently applied for the treatment of melanoma, RCC, HCC, PD-L1-positive NSCLC, MSI-H/dMMR colorectal cancer, and malignant pleural mesothelioma (3). Moreover, the FDA recently approved the first fixed-dose combination of nivolumab (Opdivo) and relatlimab (LAG-3 inhibitor) for unresectable or metastatic melanoma patients based on an appealing result from the phase-II/III RELATIVITY-047 trial. This trial demonstrated that the relatlimab–nivolumab combination yielded a progression-free survival rate of 10.1 months compared with 4.6 months in nivolumab monotherapy without new safety problems (271). Combinations of PD-1/PD-L1 blockers with other ICB are still in clinical trials. For instance, another CTLA-4 targeted monoclonal antibody, tremelimumab plus durvalumab, has entered phase 3 clinical trials in various malignancies, including small-cell lung cancer, high-risk urothelial carcinoma, advanced colorectal cancer, and advanced gastric and gastroesophageal junction adenocarcinoma, some of which received unsatisfactory results. No additional benefit was shown in combination (272–275). The severity and incidence of immune-related adverse events (irAEs), including colitis, thyroiditis, pneumonitis, and hypophysitis, have also been reported in the coblockade of PD-1/PD-L1 and CTLA-4 patients (276). In the primary analysis of the phase 2 CITYSCAPE trial, the TIGIT inhibitor tiragolumab plus atezolizumab (anti-PD-L1) showed improvement in PFS (stratified HR, 0.58; 95% CI, 0.38–0.89) in PD-L1-positive NSCLC patients (277).

Combining immune checkpoint blockade with targeted therapies in cancer treatment

Preclinical and clinical studies have verified the synergetic effect of the angiogenesis inhibitor with anti–PD–1/PD–L1. Based on studies 309/KEYNOTE-775 (NCT03517449) and KEYNOTE581 (NCT02811861), lenvatinib plus pembrolizumab has been

approved by the FDA in the treatment of advanced endometrial carcinoma and advanced RCC (278). The KEYNOTE-426 study revealed that patients receiving pembrolizumab plus axitinib gained statistically significant PFS, OS, and ORR improvement compared with sunitinib monotherapy, which promoted the approval of pembrolizumab plus axitinib as the first-line therapy for advanced RCC (279). In 2018, based on the IMpower150 trial (NCT02366143), atezolizumab with chemotherapy and bevacizumab was approved for the first-line treatment of metastatic non-squamous NSCLC (280). Additionally, atezolizumab combined with bevacizumab was approved in 2020 for unresectable hepatocellular carcinoma on the basis of the IMbrave150 trial (NCT03434379) (281). Moreover, the FDA approved axitinib plus avelumab (based on JAVELIN Renal 101) and cabozantinib plus nivolumab (based on CheckMate-9ER) for RCC initial-line treatment as well (282, 283).

Noteworthily, plenty of clinical trials are exploring the combination strategies of angiogenesis inhibitors and anti-PD-1/PD-L1 at present. The preliminary data of some combinations demonstrated favorable therapeutic effects such as camrelizumab plus apatinib in advanced triple-negative breast cancer (NCT03394287), advanced cervical cancer (NCT03816553), and advanced HCC (NCT03463876) and sintilimab plus anlotinib in advanced NSCLC (NCT03628521) and PD-L1-positive recurrent or metastatic cervical cancer (284). Subsequent phase 3 trials are necessary to confirm the effectiveness of these combination regimens.

Apart from angiogenesis inhibitors, various targeted therapies combined with anti-PD-1/PD-L1 are undergoing clinical trials, such as nivolumab plus erlotinib (EGFR) in NSCLC patients (NCT01454102), tislelizumab plus pamiparib (PARP) in solid tumor patients (NCT02660034), cobimetinib (MEK) plus atezolizumab in colorectal cancer patients (NCT02788279), nivolumab plus copanlisib (PI3K) in lymphoma and solid tumor patients (NCT03502733), and pembrolizumab plus abemaciclib (CDK4/6) in NSCLC and breast cancer patients (NCT02779751). Altogether, most clinical trials are still in phase I or II. Further research is needed to explore the efficacy of anti-PD-1/PD-L1-based combined strategies in phase 3 trials.

Concluding remarks

ICB has revolutionized the field of cancer treatment. However, the initial wave of success on ICB is challenged by primary and acquired resistance. The number of patients benefiting from ICB is limited. Thus, a more detailed map of resistant mechanisms is reasonably necessary to develop coping strategies to improve clinical outcomes. Firstly, in this context, we primarily focus on the changes in the biological functions of $CD8^+$ T cells to elucidate the underlying resistance mechanisms of ICB therapies. Based on the mechanical studies of both tumoral and systemic changes in the immune system, dozens of combinational regimens have been proposed, some of which exhibit potent antitumor activities in preclinical and clinical studies. Secondly, chemotherapy, VEGF/VEGFR-targeted therapy, and CTLA4-targeted treatment have been shown to be the most promising combinational options with anti-PD-1/PD-L1 therapy. They have great potential to improve the efficacy of ICB treatment in the condition of drug resistance. Nevertheless, only a tiny number of combinational strategies have been approved by the FDA, including anti-PD-1/PD-L1 plus chemotherapy, angiogenesis inhibitor, anti-CTLA-4, and anti-

TABLE 2 Approved combination strategies with the PD-1/PDL1 inhibitor.

Combined strategy	anti–PD–1/PD–L1	Cancer type	Clinical trial	Approval time
Chemotherapy	Pembrolizumab	Metastatic non-squamous NSCLC	KEYNOTE-189 (NCT02578680)	08/20/2018
		Metastatic squamous NSCLC	KEYNOTE-407 (NCT02775435)	10/30/2018
		Metastatic TNBC	KEYNOTE-355 (NCT02819518)	11/13/2020
		Esophageal or GEJ carcinoma	KEYNOTE-590 (NCT03189719)	03/22/2021
		Cervical cancer	KEYNOTE-826 (NCT03635567)	10/13/2021
	Nivolumab	Metastatic gastric cancer and esophageal adenocarcinoma	CHECKMATE-649 (NCT02872116)	04/16/2021
	Atezolizumab	PD-L1 positive unresectable locally advanced or metastatic TNBC	IMpassion130 (NCT02425891)	03/18/2019
		ES-SCLC	IMpower133 (NCT02763579)	03/18/2019
		Metastatic NSCLC without EGFR/ALK aberrations	IMpower130 (NCT02367781)	12/03/2019
	Durvalumab	ES-SCLC	NCT03043872	03/27/2020
Axitinib	Pembrolizumab	Advanced RCC	KEYNOTE–426 (NCT02853331)	04/19/2019
	Avelumab	RCC	JAVELIN Renal 101 (NCT02684006)	05/14/2019

(Continued)

TABLE 2 Continued

Combined strategy	anti–PD–1/PD–L1	Cancer type	Clinical trial	Approval time
Lenvatinib	Pembrolizumab	Advanced endometrial carcinoma	KEYNOTE-775 (NCT03517449)	06/21/2021
Bevacizumab	Atezolizumab	Unresectable HCC	IMbrave150 (NCT03434379)	05/29/2020
Cabozantinib	Nivolumab	Advanced RCC	CHECKMATE-9ER (NCT03141177)	01/22/2021
Ipilimumab (anti-CTLA-4)	Nivolumab (anti-PD-1)	Metastatic melanoma	CheckMate-069	10/01/2015
		Intermediate- or poor-risk advanced RCC	CheckMate 214 (NCT02231749)	04/16/2018
		MSI-H/dMMR colorectal cancer	CHECKMATE 142 (NCT02060188)	07/10/2018
		HCC	CHECKMATE-040, (NCT01658878)	03/10/2020
		PD-L1-positive NSCLC	CHECKMATE-227 (NCT02477826)	05/15/2020
		Malignant pleural mesothelioma	CHECKMATE-743 (NCT02899299)	10/02/2020
Relatlimab (LAG-3 inhibitor)	Nivolumab	Unresectable or metastatic melanoma	RELATIVITY-047 (NCT03470922)	03/18/2022

NSCLC, non-small cell lung cancer; TNBC, triple-negative breast cancer; GEJ, gastroesophageal; ES-SCLC, extensive-stage small cell lung cancer; RCC, renal cell carcinoma; HCC, hepatocellular carcinoma.

LAG-3 (Table 2). Overall, with a more profound elucidation of ICB resistance mechanisms, more novel clues of combinational strategies will emerge. Additional effort is needed to overcome barriers, including the occurrence of irAEs, the assessment of predictive biomarkers, and the definition of administration regimens such as dosage, timing, and sequence.

Author contributions

XTZ and YN jointly contributed to the first draft of the article, tables, and figures. XL provided assistance in making figures. YL, BA, and XH revised the manuscript. XZ conceived the presented idea, revised the manuscript again, and approved the final version. All authors approved this manuscript for publication.

Funding

This work was supported by the National Natural Science Foundation of China (No. 81902662), the National Natural Science Foundation of China (No. 81821002), Sichuan Science and Technology Program 2021YJ0011, and Sichuan Science and Technology Program 2018YJ0609.

Conflict of interest

The authors declare that the research was conducted in the absence of any commercial or financial relationships that could be construed as a potential conflict of interest.

Publisher's note

References

1. Postow MA, Callahan MK, Wolchok JD. Immune checkpoint blockade in cancer therapy. *J Clin Oncol* (2015) 33(17):1974–82. doi: 10.1200/JCO.2014.59.4358

2. Sharma P, Hu-Lieskovan S, Wargo JA, Ribas A. Primary, adaptive, and acquired resistance to cancer immunotherapy. *Cell* (2017) 168(4):707–23. doi: 10.1016/j.cell.2017.01.017

3. Vaddepally RK, Kharel P, Pandey R, Garje R, Chandra AB. Review of indications of fda-approved immune checkpoint inhibitors per nccn guidelines with the level of evidence. *Cancers (Basel)* (2020) 12(3):738. doi: 10.3390/cancers12030738

4. Schoenfeld AJ, Hellmann MD. Acquired resistance to immune checkpoint inhibitors. *Cancer Cell* (2020) 37(4):443–55. doi: 10.1016/j.ccell.2020.03.017

5. Morad G, Helmink BA, Sharma P, Wargo JA. Hallmarks of response, resistance, and toxicity to immune checkpoint blockade. *Cell* (2021) 184 (21):5309–37. doi: 10.1016/j.cell.2021.09.020

6. Aldea M, Andre F, Marabelle A, Dogan S, Barlesi F, Soria J-C. Overcoming resistance to tumor-targeted and immune-targeted therapies. *Cancer Discovery* (2021) 11(4):874–99. doi: 10.1158/2159-8290.CD-20-1638

7. Bagchi S, Yuan R, Engleman EG. Immune checkpoint inhibitors for the treatment of cancer: Clinical impact and mechanisms of response and resistance. *Annu Rev Pathol* (2021) 16:223–49. doi: 10.1146/annurev-pathol-042020-042741

8. Li J, Stanger BZ. How tumor cell dedifferentiation drives immune evasion and resistance to immunotherapy. *Cancer Res* (2020) 80(19):4037–41. doi: 10.1158/0008-5472.CAN-20-1420

9. Arozarena I, Wellbrock C. Phenotype plasticity as enabler of melanoma progression and therapy resistance. *Nat Rev Cancer* (2019) 19(7):377–91. doi: 10.1038/s41568-019-0154-4

10. Perez-Guijarro E, Yang HH, Araya RE, El Meskini R, Michael HT, Vodnala SK, et al. Multimodel preclinical platform predicts clinical response of melanoma to immunotherapy. *Nat Med* (2020) 26(5):781–91. doi: 10.1038/s41591-020-0818-3

11. Horn LA, Fousek K, Palena C. Tumor plasticity and resistance to immunotherapy. *Trends Cancer* (2020) 6(5):432–41. doi: 10.1016/j.trecan.2020.02.001

12. Kalbasi A, Ribas A. Tumour-intrinsic resistance to immune checkpoint blockade. *Nat Rev Immunol* (2020) 20(1):25–39. doi: 10.1038/s41577-019-0218-4

13. Horvath L, Thienpont B, Zhao L, Wolf D, Pircher A. Overcoming immunotherapy resistance in non-small cell lung cancer (Nsclc) - novel approaches and future outlook. *Mol Cancer* (2020) 19(1):141. doi: 10.1186/s12943-020-01260-z

14. Galluzzi L, Humeau J, Buque A, Zitvogel L, Kroemer G. Immunostimulation with chemotherapy in the era of immune checkpoint inhibitors. *Nat Rev Clin Oncol* (2020) 17(12):725–41. doi: 10.1038/s41571-020-0413-z

15. Schaue D, McBride WH. Opportunities and challenges of radiotherapy for treating cancer. *Nat Rev Clin Oncol* (2015) 12(9):527–40. doi: 10.1038/nrclinonc.2015.120

16. Morandi F, Airoldi I. Hla-G and other immune checkpoint molecules as targets for novel combined immunotherapies. *Int J Mol Sci* (2022) 23(6):2925. doi: 10.3390/ijms23062925

17. Franco F, Jaccard A, Romero P, Yu YR, Ho PC. Metabolic and epigenetic regulation of T-cell exhaustion. *Nat Metab* (2020) 2(10):1001–12. doi: 10.1038/s42255-020-00280-9

18. Routy B, Le Chatelier E, Derosa L, Duong CPM, Alou MT, Daillere R, et al. Gut microbiome influences efficacy of pd-1-Based immunotherapy against epithelial tumors. *Science* (2018) 359(6371):91–7. doi: 10.1126/science.aan3706

19. Yi M, Jiao D, Qin S, Chu Q, Wu K, Li A. Synergistic effect of immune checkpoint blockade and anti-angiogenesis in cancer treatment. *Mol Cancer* (2019) 18(1):60. doi: 10.1186/s12943-019-0974-6

20. Melief CJM. Mutation-specific T cells for immunotherapy of gliomas. *N Engl J Med* (2015) 372(20):1956–8. doi: 10.1056/NEJMcibr1501818

21. Huang Y, Shah S, Qiao L. Tumor resistance to Cd8+ T cell-based therapeutic vaccination. *Arch Immunol Ther Exp (Warsz)* (2007) 55(4):205–17. doi: 10.1007/s00005-007-0029-3

22. Lanzavecchia A, Sallusto F. Progressive differentiation and selection of the fittest in the immune response. *Nat Rev Immunol* (2002) 2(12):982–7. doi: 10.1038/nri959

23. Sade-Feldman M, Yizhak K, Bjorgaard SL, Ray JP, de Boer CG, Jenkins RW, et al. Defining T cell states associated with response to checkpoint immunotherapy in melanoma. *Cell* (2018) 175(4):998–1013.e20. doi: 10.1016/j.cell.2018.10.038

24. Li W, Sun T, Li M, He Y, Li L, Wang L, et al. Gnifdb: A neoantigen intrinsic feature database for glioma. *Database (Oxford)* (2022) 2022:baac004. doi: 10.1093/database/baac004

25. Strickler JH, Hanks BA, Khasraw M. Tumor mutational burden as a predictor of immunotherapy response: Is more always better? *Clin Cancer Res* (2021) 27(5):1236–41. doi: 10.1158/1078-0432.CCR-20-3054

26. Yarchoan M, Hopkins A, Jaffee EM. Tumor mutational burden and response rate to pd-1 inhibition. *N Engl J Med* (2017) 377(25):2500–1. doi: 10.1056/NEJMc1713444

27. Larkin J, Chiarion-Sileni V, Gonzalez R, Grob JJ, Cowey CL, Lao CD, et al. Combined nivolumab and ipilimumab or monotherapy in untreated melanoma. *N Engl J Med* (2015) 373(1):23–34. doi: 10.1056/NEJMoa1504030

28. Marabelle A, Fakih M, Lopez J, Shah M, Shapira-Frommer R, Nakagawa K, et al. Association of tumour mutational burden with outcomes in patients with advanced solid tumours treated with pembrolizumab: Prospective biomarker analysis of the multicohort, open-label, phase 2 keynote-158 study. *Lancet Oncol* (2020) 21(10):1353–65. doi: 10.1016/S1470-2045(20)30445-9

29. von Loga K, Woolston A, Punta M, Barber LJ, Griffiths B, Semiannikova M, et al. Extreme intratumour heterogeneity and driver evolution in mismatch repair deficient gastro-oesophageal cancer. *Nat Commun* (2020) 11(1):139. doi: 10.1038/s41467-019-13915-7

30. Strickler JH, Hanks BA, Khasraw M. Tumor mutational burden as a predictor of immunotherapy response: Is more always better? *Clin Cancer Res* (2021) 27(5):1236–41. doi: 10.1158/1078-0432.CCR-20-3054

31. Henon C, Blay JY, Massard C, Mir O, Bahleda R, Dumont S, et al. Long lasting major response to pembrolizumab in a thoracic malignant rhabdoid-like Smarca4-deficient tumor. *Ann Oncol* (2019) 30(8):1401–3. doi: 10.1093/annonc/mdz160

32. Gejman RS, Chang AY, Jones HF, DiKun K, Hakimi AA, Schietinger A, et al. Rejection of immunogenic tumor clones is limited by clonal fraction. *Elife* (2018) 7: e41090. doi: 10.7554/eLife.41090

33. Andor N, Graham TA, Jansen M, Xia LC, Aktipis CA, Petritsch C, et al. Pan-cancer analysis of the extent and consequences of intratumor heterogeneity. *Nat Med* (2016) 22(1):105–13. doi: 10.1038/nm.3984

34. Wolf Y, Bartok O, Patkar S, Eli GB, Cohen S, Litchfield K, et al. Uvb-induced tumor heterogeneity diminishes immune response in melanoma. *Cell* (2019) 179 (1):219–235.e21. doi: 10.1016/j.cell.2019.08.032

35. McGranahan N, Furness AJ, Rosenthal R, Ramskov S, Lyngaa R, Saini SK, et al. Clonal neoantigens elicit T cell immunoreactivity and sensitivity to immune checkpoint blockade. *Science* (2016) 351(6280):1463–9. doi: 10.1126/science.aaf1490

36. Anagnostou V, Smith KN, Forde PM, Niknafs N, Bhattacharya R, White J, et al. Evolution of neoantigen landscape during immune checkpoint blockade in non-small cell lung cancer. *Cancer Discovery* (2017) 7(3):264–76. doi: 10.1158/2159-8290.CD-16-0828

37. Jamal-Hanjani M, Wilson GA, McGranahan N, Birkbak NJ, Watkins TBK, Veeriah S, et al. Tracking the evolution of non-Small-Cell lung cancer. *N Engl J Med* (2017) 376(22):2109–21. doi: 10.1056/NEJMoa1616288

38. Blum JS, Wearsch PA, Cresswell P. Pathways of antigen processing. *Annu Rev Immunol* (2013) 31:443–73. doi: 10.1146/annurev-immunol-032712-095910

39. Hulpke S, Tampé R. The mhc I loading complex: A multitasking machinery in adaptive immunity. *Trends Biochem Sci* (2013) 38(8):412–20. doi: 10.1016/j.tibs.2013.06.003

40. Zaretsky JM, Garcia-Diaz A, Shin DS, Escuin-Ordinas H, Hugo W, Hu-Lieskovan S, et al. Mutations associated with acquired resistance to pd-1 blockade in melanoma. *N Engl J Med* (2016) 375(9):819–29. doi: 10.1056/NEJMoa1604958

41. Sade-Feldman M, Jiao YJ, Chen JH, Rooney MS, Barzily-Rokni M, Eliane J-P, et al. Resistance to checkpoint blockade therapy through inactivation of antigen presentation. *Nat Commun* (2017) 8(1):1136. doi: 10.1038/s41467-017-01062-w

42. Gettinger S, Choi J, Hastings K, Truini A, Datar I, Sowell R, et al. Impaired hla class I antigen processing and presentation as a mechanism of acquired resistance to immune checkpoint inhibitors in lung cancer. *Cancer Discovery* (2017) 7(12):1420–35. doi: 10.1158/2159-8290.CD-17-0593

43. Busch E, Ahadova A, Kosmalla K, Bohaumilitzky L, Pfuderer PL, Ballhausen A, et al. Mutations are linked to a distinct metastatic pattern and a favorable outcome in microsatellite-unstable stage iv gastrointestinal cancers. *Front Oncol* (2021) 11:669774. doi: 10.3389/fonc.2021.669774

44. Gurjao C, Liu D, Hofree M, AlDubayan SH, Wakiro I, Su M-J, et al. Intrinsic resistance to immune checkpoint blockade in a mismatch repair-deficient colorectal cancer. *Cancer Immunol Res* (2019) 7(8):1230–6. doi: 10.1158/2326-6066.CIR-18-0683

45. Kalbasi A, Ribas A. Antigen presentation keeps trending in immunotherapy resistance. *Clin Cancer Res* (2018) 24(14):3239–41. doi: 10.1158/1078-0432.CCR-18-0698

46. Sivapalan L, Anagnostou V. Genetic variation in antigen presentation and cancer immunotherapy. *Immunity* (2022) 55(1):3–6. doi: 10.1016/j.immuni.2021.12.010

47. Tran E, Robbins PF, Lu Y-C, Prickett TD, Gartner JJ, Jia L, et al. T-Cell transfer therapy targeting mutant kras in cancer. *N Engl J Med* (2016) 375 (23):2255–62. doi: 10.1056/NEJMoa1609279

48. Saveanu L, Carroll O, Hassainya Y, van Endert P. Complexity, contradictions, and conundrums: Studying post-proteasomal proteolysis in hla class I antigen presentation. *Immunol Rev* (2005) 207:42–59. doi: 10.1111/j.0105-2896.2005.00313.x

49. Cabrera CM, Jiménez P, Cabrera T, Esparza C, Ruiz-Cabello F, Garrido F. Total loss of mhc class I in colorectal tumors can be explained by two molecular pathways: Beta2-microglobulin inactivation in msi-positive tumors and Lmp7/Tap2 downregulation in msi-negative tumors. *Tissue Antigens* (2003) 61(3):211–9. doi: 10.1034/j.1399-0039.2003.00020.x

50. Vitale M, Rezzani R, Rodella L, Zauli G, Grigolato P, Cadei M, et al. Hla class I antigen and transporter associated with antigen processing (Tap1 and Tap2)

down-regulation in high-grade primary breast carcinoma lesions. *Cancer Res* (1998) 58(4):737–42.

51. Zhang X, Sabio E, Krishna C, Ma X, Wang J, Jiang H, et al. Qa-1 modulates resistance to anti-Pd-1 immune checkpoint blockade in tumors with defects in antigen processing. *Mol Cancer Res* (2021) 19(6):1076–84. doi: 10.1158/1541-7786.MCR-20-0652

52. Vigneron N, Ferrari V, Van den Eynde BJ, Cresswell P, Leonhardt RM. Cytosolic processing governs tap-independent presentation of a critical melanoma antigen. *J Immunol* (2018) 201(7):1875–88. doi: 10.4049/jimmunol.1701479

53. Romero JM, Jiménez P, Cabrera T, Cózar JM, Pedrinaci S, Tallada M, et al. Coordinated downregulation of the antigen presentation machinery and hla class I/Beta2-microglobulin complex is responsible for hla-abc loss in bladder cancer. *Int J Cancer* (2005) 113(4):605–10. doi: 10.1002/ijc.20499

54. López-Albaitero A, Nayak JV, Ogino T, Machandia A, Gooding W, DeLeo AB, et al. Role of antigen-processing machinery in the *in vitro* resistance of squamous cell carcinoma of the head and neck cells to recognition by ctl. *J Immunol* (2006) 176(6):3402–9. doi: 10.4049/jimmunol.176.6.3402

55. Okada M, Shimizu K, Iyoda T, Ueda S, Shinga J, Mochizuki Y, et al. Pd-L1 expression affects neoantigen presentation. *iScience* (2020) 23(6):101238. doi: 10.1016/j.isci.2020.101238

56. Wangmo D, Premsrirut PK, Yuan C, Morris WS, Zhao X, Subramanian S. Ackr4 in tumor cells regulates dendritic cell migration to tumor-draining lymph nodes and T-cell priming. *Cancers (Basel)* (2021) 13(19):5021. doi: 10.3390/cancers13195021

57. Liu X, Shang X, Li J, Zhang S. The prognosis and immune checkpoint blockade efficacy prediction of tumor-infiltrating immune cells in lung cancer. *Front Cell Dev Biol* (2021) 9:707143. doi: 10.3389/fcell.2021.707143

58. Walker LSK, Sansom DM. The emerging role of Ctla4 as a cell-extrinsic regulator of T cell responses. *Nat Rev Immunol* (2011) 11(12):852–63. doi: 10.1038/nri3108

59. Maeda Y, Nishikawa H, Sugiyama D, Ha D, Hamaguchi M, Saito T, et al. Detection of self-reactive $Cd8^+$T cells with an anergic phenotype in healthy individuals. *Science* (2014) 346(6216):1536–40. doi: 10.1126/science.aaa1292

60. Narayanan S, Vicent S, Ponz-Sarvisé M. Pdac as an immune evasive disease: Can 3d model systems aid to tackle this clinical problem? *Front Cell Dev Biol* (2021) 9:787249. doi: 10.3389/fcell.2021.787249

61. Annels NE, Simpson GR, Denyer M, Arif M, Coffey M, Melcher A, et al. Oncolytic reovirus-mediated recruitment of early innate immune responses reverses immunotherapy resistance in prostate tumors. *Mol Ther Oncolytics* (2021) 20:434–46. doi: 10.1016/j.omto.2020.09.010

62. Salemizadeh Parizi M, Salemizadeh Parizi F, Abdolhosseini S, Vanaei S, Manzouri A, Ebrahimzadeh F. Myeloid-derived suppressor cells (Mdscs) in brain cancer: Challenges and therapeutic strategies. *Inflammopharmacology* (2021) 29(6):1613–24. doi: 10.1007/s10787-021-00878-9

63. Gajewski TF, Woo S-R, Zha Y, Spaapen R, Zheng Y, Corrales L, et al. Cancer immunotherapy strategies based on overcoming barriers within the tumor microenvironment. *Curr Opin Immunol* (2013) 25(2):268–76. doi: 10.1016/j.coi.2013.02.009

64. Mühlberger M, Janko C, Unterweger H, Friedrich RP, Friedrich B, Band J, et al. Functionalization of T lymphocytes with citrate-coated superparamagnetic iron oxide nanoparticles for magnetically controlled immune therapy. *Int J Nanomedicine* (2019) 14:8421–32. doi: 10.2147/IJN.S218488

65. Chen DS, Mellman I. Elements of cancer immunity and the cancer-immune set point. *Nature* (2017) 541(7637):321–30. doi: 10.1038/nature21349

66. Peranzoni E, Lemoine J, Vimeux L, Feuillet V, Barrin S, Kantari-Mimoun C, et al. Macrophages impede Cd8 T cells from reaching tumor cells and limit the efficacy of anti-Pd-1 treatment. *Proc Natl Acad Sci U.S.A.* (2018) 115(17):E4041–E50. doi: 10.1073/pnas.1720948115

67. Peng W, Chen JQ, Liu C, Malu S, Creasy C, Tetzlaff MT, et al. Loss of pten promotes resistance to T cell-mediated immunotherapy. *Cancer Discovery* (2016) 6(2):202–16. doi: 10.1158/2159-8290.CD-15-0283

68. Karoulia Z, Gavathiotis E, Poulikakos PI. New perspectives for targeting raf kinase in human cancer. *Nat Rev Cancer* (2017) 17(11):676–91. doi: 10.1038/nrc.2017.79

69. Kimura ET, Nikiforova MN, Zhu Z, Knauf JA, Nikiforov YE, Fagin JA. High prevalence of braf mutations in thyroid cancer: Genetic evidence for constitutive activation of the Ret/Ptc-Ras-Braf signaling pathway in papillary thyroid carcinoma. *Cancer Res* (2003) 63(7):1454–7.

70. Rajagopalan H, Bardelli A, Lengauer C, Kinzler KW, Vogelstein B, Velculescu VE. Tumorigenesis: Raf/Ras oncogenes and mismatch-repair status. *Nature* (2002) 418(6901):934. doi: 10.1038/418934a

71. Wilmott JS, Long GV, Howle JR, Haydu LE, Sharma RN, Thompson JF, et al. Selective braf inhibitors induce marked T-cell infiltration into human metastatic melanoma. *Clin Cancer Res* (2012) 18(5):1386–94. doi: 10.1158/1078-0432.CCR-11-2479

72. Skoulidis F, Goldberg ME, Greenawalt DM, Hellmann MD, Awad MM, Gainor JF, et al. Mutations and pd-1 inhibitor resistance in -mutant lung adenocarcinoma. *Cancer Discovery* (2018) 8(7):822–35. doi: 10.1158/2159-8290.CD-18-0099

73. Xu Y-P, Lv L, Liu Y, Smith MD, Li W-C, Tan X-M, et al. Tumor suppressor Tet2 promotes cancer immunity and immunotherapy efficacy. *J Clin Invest* (2019) 129(10):4316–31. doi: 10.1172/JCI129317

74. Dong Z-Y, Zhang J-T, Liu S-Y, Su J, Zhang C, Xie Z, et al. Egfr mutation correlates with uninflamed phenotype and weak immunogenicity, causing impaired response to pd-1 blockade in non-small cell lung cancer. *Oncoimmunology* (2017) 6(11):e1356145. doi: 10.1080/2162402X.2017.1356145

75. Huang H, Langenkamp E, Georganaki M, Loskog A, Fuchs PF, Dieterich LC, et al. Vegf suppresses T-lymphocyte infiltration in the tumor microenvironment through inhibition of nf-κb-Induced endothelial activation. *FASEB J* (2015) 29(1):227–38. doi: 10.1096/fj.14-250985

76. Bruand M, Barras D, Mina M, Ghisoni E, Morotti M, Lanitis E, et al. Cell-autonomous inflammation of Brca1-deficient ovarian cancers drives both tumor-intrinsic immunoreactivity and immune resistance *Via* sting. *Cell Rep* (2021) 36(3):109412. doi: 10.1016/j.celrep.2021.109412

77. Li X, He G, Liu J, Yan M, Shen M, Xu L, et al. Ccl2-mediated monocytes regulate immune checkpoint blockade resistance in pancreatic cancer. *Int Immunopharmacol.* (2022) 106:108598. doi: 10.1016/j.intimp.2022.108598

78. Tauriello DVF, Palomo-Ponce S, Stork D, Berenguer-Llergo A, Badia-Ramentol J, Iglesias M, et al. Tgfβ drives immune evasion in genetically reconstituted colon cancer metastasis. *Nature* (2018) 554(7693):538–43. doi: 10.1038/nature25492

79. Mariathasan S, Turley SJ, Nickles D, Castiglioni A, Yuen K, Wang Y, et al. Tgfβ attenuates tumour response to pd-L1 blockade by contributing to exclusion of T cells. *Nature* (2018) 554(7693):544–8. doi: 10.1038/nature25501

80. Shaul ME, Fridlender ZG. The dual role of neutrophils in cancer. *Semin Immunol* (2021) 57:101582. doi: 10.1016/j.smim.2021.101582

81. Kim IS, Gao Y, Welte T, Wang H, Liu J, Janghorban M, et al. Immuno-subtyping of breast cancer reveals distinct myeloid cell profiles and immunotherapy resistance mechanisms. *Nat Cell Biol* (2019) 21(9):1113–26. doi: 10.1038/s41556-019-0373-7

82. Chen J, Sun H-W, Yang Y-Y, Chen H-T, Yu X-J, Wu W-C, et al. Reprogramming immunosuppressive myeloid cells by activated T cells promotes the response to anti-Pd-1 therapy in colorectal cancer. *Signal Transduct. Target Ther* (2021) 6(1):4. doi: 10.1038/s41392-020-00377-3

83. Meyer C, Cagnon L, Costa-Nunes CM, Baumgaertner P, Montandon N, Leyvraz L, et al. Frequencies of circulating mdsc correlate with clinical outcome of melanoma patients treated with ipilimumab. *Cancer Immunol Immunother.* (2014) 63(3):247–57. doi: 10.1007/s00262-013-1508-5

84. Movahedi K, Guilliams M, Van den Bossche J, Van den Bergh R, Gysemans C, Beschin A, et al. Identification of discrete tumor-induced myeloid-derived suppressor cell subpopulations with distinct T cell-suppressive activity. *Blood* (2008) 111(8):4233–44. doi: 10.1182/blood-2007-07-099226

85. Liu C-Y, Wang Y-M, Wang C-L, Feng P-H, Ko H-W, Liu Y-H, et al. Population alterations of l-arginase- and inducible nitric oxide synthase-expressed $Cd11b^+/Cd14^-/Cd15^+/Cd33^+$ myeloid-derived suppressor cells and Cd8+ T lymphocytes in patients with advanced-stage non-small cell lung cancer. *J Cancer Res Clin Oncol* (2010) 136(1):35–45. doi: 10.1007/s00432-009-0634-0

86. Veglia F, Tyurin VA, Blasi M, De Leo A, Kossenkov AV, Donthireddy L, et al. Fatty acid transport protein 2 reprograms neutrophils in cancer. *Nature* (2019) 569(7754):73–8. doi: 10.1038/s41586-019-1118-2

87. Thorn M, Guha P, Cunetta M, Espat NJ, Miller G, Junghans RP, et al. Tumor-associated gm-csf overexpression induces immunoinhibitory molecules *Via* Stat3 in myeloid-suppressor cells infiltrating liver metastases. *Cancer Gene Ther* (2016) 23(6):188–98. doi: 10.1038/cgt.2016.19

88. Adeshakin AO, Liu W, Adeshakin FO, Afolabi LO, Zhang M, Zhang G, et al. Regulation of ros in myeloid-derived suppressor cells through targeting fatty acid transport protein 2 enhanced anti-Pd-L1 tumor immunotherapy. *Cell Immunol* (2021) 362:104286. doi: 10.1016/j.cellimm.2021.104286

89. DeNardo DG, Ruffell B. Macrophages as regulators of tumour immunity and immunotherapy. *Nat Rev Immunol* (2019) 19(6):369–82. doi: 10.1038/s41577-019-0127-6

90. Orlikowsky T, Dannecker GE, Wang Z, Horowitz H, Niethammer D, Hoffmann MK. Activation or destruction of T cells. *Via Macrophages. Pathobiol.* (1999) 67(5-6):298–301. doi: 10.1159/000028084

91. Mantovani A, Sozzani S, Locati M, Allavena P, Sica A. Macrophage polarization: Tumor-associated macrophages as a paradigm for polarized M2 mononuclear phagocytes. *Trends Immunol* (2002) 23(11):549–55. doi: 10.1016/S1471-4906(02)02302-5

92. Arlauckas SP, Garris CS, Kohler RH, Kitaoka M, Cuccarese MF, Yang KS, et al. *In vivo* imaging reveals a tumor-associated macrophage-mediated resistance pathway in anti-Pd-1 therapy. *Sci Transl Med* (2017) 9(389):eaal3604. doi: 10.1126/scitranslmed.aal3604

93. Ruffell B, Chang-Strachan D, Chan V, Rosenbusch A, Ho CMT, Pryer N, et al. Macrophage il-10 blocks Cd8+ T cell-dependent responses to chemotherapy by suppressing il-12 expression in intratumoral dendritic cells. *Cancer Cell* (2014) 26(5):623–37. doi: 10.1016/j.ccell.2014.09.006

94. Smith LK, Boukhaled GM, Condotta SA, Mazouz S, Guthmiller JJ, Vijay R, et al. Interleukin-10 directly inhibits Cd8 T cell function by enhancing n-glycan branching to decrease antigen sensitivity. *Immunity* (2018) 48(2):299–312.e5. doi: 10.1016/j.immuni.2018.01.006

95. Zerdes I, Wallerius M, Sifakis EG, Wallmann T, Betts S, Bartish M, et al. Stat3 activity promotes programmed-death ligand 1 expression and suppresses immune responses in breast cancer. *Cancers (Basel)* (2019) 11(10):1479. doi: 10.3390/cancers11101479

96. Singhal S, Stadanlick J, Annunziata MJ, Rao AS, Bhojnagarwala PS, O'Brien S, et al. Human tumor-associated Monocytes/Macrophages and their regulation of T cell responses in early-stage lung cancer. *Sci Transl Med* (2019) 11(479):eaat1500. doi: 10.1126/scitranslmed.aat1500

97. Darby IA, Laverdet B, Bonté F, Desmoulière A. Fibroblasts and myofibroblasts in wound healing. *Clin Cosmet Investig Dermatol* (2014) 7:301–11. doi: 10.2147/CCID.S50046

98. Kuzet S-E, Gaggioli C. Fibroblast activation in cancer: When seed fertilizes soil. *Cell Tissue Res* (2016) 365(3):607–19. doi: 10.1007/s00441-016-2467-x

99. Gardner H, Strehlow D, Bradley L, Widom R, Farina A, de Fougerolles A, et al. Global expression analysis of the fibroblast transcriptional response to tgfbeta. *Clin Exp Rheumatol* (2004) 22(3 Suppl 33):S47–57.

100. Khalili JS, Liu S, Rodríguez-Cruz TG, Whittington M, Wardell S, Liu C, et al. Oncogenic Braf(V600e) promotes stromal cell-mediated immunosuppression *Via* induction of interleukin-1 in melanoma. *Clin Cancer Res* (2012) 18(19):5329–40. doi: 10.1158/1078-0432.CCR-12-1632

101. Lakins MA, Ghorani E, Munir H, Martins CP, Shields JD. Cancer-associated fibroblasts induce antigen-specific deletion of Cd8 T cells to protect tumour cells. *Nat Commun* (2018) 9(1):948. doi: 10.1038/s41467-018-03347-0

102. Gorchs L, Fernández Moro C, Bankhead P, Kern KP, Sadeak I, Meng Q, et al. Human pancreatic carcinoma-associated fibroblasts promote expression of Co-inhibitory markers on Cd4 and Cd8 T-cells. *Front Immunol* (2019) 10:847. doi: 10.3389/fimmu.2019.00847

103. Cheng Y, Li H, Deng Y, Tai Y, Zeng K, Zhang Y, et al. Cancer-associated fibroblasts induce Pdl1+ neutrophils through the Il6-Stat3 pathway that foster immune suppression in hepatocellular carcinoma. *Cell Death Dis* (2018) 9(4):422. doi: 10.1038/s41419-018-0458-4

104. Li Z, Zhou J, Zhang J, Li S, Wang H, Du J. Cancer-associated fibroblasts promote pd-L1 expression in mice cancer cells *Via* secreting Cxcl5. *Int J Cancer* (2019) 145(7):1946–57. doi: 10.1002/ijc.32278

105. Curiel TJ, Coukos G, Zou L, Alvarez X, Cheng P, Mottram P, et al. Specific recruitment of regulatory T cells in ovarian carcinoma fosters immune privilege and predicts reduced survival. *Nat Med* (2004) 10(9):942–9. doi: 10.1038/nm1093

106. Ma GF, Miao Q, Liu YM, Gao H, Lian JJ, Wang YN, et al. High Foxp3 expression in tumour cells predicts better survival in gastric cancer and its role in tumour microenvironment. *Br J Cancer* (2014) 110(6):1552–60. doi: 10.1038/bjc.2014.47

107. Shimizu J, Yamazaki S, Takahashi T, Ishida Y, Sakaguchi S. Stimulation of Cd25(+)Cd4(+) regulatory T cells through gitr breaks immunological self-tolerance. *Nat Immunol* (2002) 3(2):135–42. doi: 10.1038/ni759

108. Bennett CL, Christie J, Ramsdell F, Brunkow ME, Ferguson PJ, Whitesell L, et al. The immune dysregulation, polyendocrinopathy, enteropathy, X-linked syndrome (Ipex) is caused by mutations of Foxp3. *Nat Genet* (2001) 27(1):20–1. doi: 10.1038/83713

109. Zhang Y, Maksimovic J, Huang B, De Souza DP, Naselli G, Chen H, et al. Cord blood Cd8 T cells have a natural propensity to express il-4 in a fatty acid metabolism and caspase activation-dependent manner. *Front Immunol* (2018) 9:879. doi: 10.3389/fimmu.2018.00879

110. Pereira LMS, Gomes STM, Ishak R, Vallinoto ACR. Regulatory T cell and forkhead box protein 3 as modulators of immune homeostasis. *Front Immunol* (2017) 8:605. doi: 10.3389/fimmu.2017.00605

111. Ren Z, Zhang A, Sun Z, Liang Y, Ye J, Qiao J, et al. Selective delivery of low-affinity il-2 to pd-1+ T cells rejuvenates antitumor immunity with reduced toxicity. *J Clin Invest* (2022) 132(3):e153604. doi: 10.1172/JCI153604

112. Camisaschi C, Casati C, Rini F, Perego M, De Filippo A, Triebel F, et al. Lag-3 expression defines a subset of Cd4(+)Cd25(High)Foxp3(+) regulatory T cells that are expanded at tumor sites. *J Immunol* (2010) 184(11):6545–51. doi: 10.4049/jimmunol.0903879

113. Linterman MA, Pierson W, Lee SK, Kallies A, Kawamoto S, Rayner TF, et al. Foxp3+ follicular regulatory T cells control the germinal center response. *Nat Med* (2011) 17(8):975–82. doi: 10.1038/nm.2425

114. Sage PT, Francisco LM, Carman CV, Sharpe AH. The receptor pd-1 controls follicular regulatory T cells in the lymph nodes and blood. *Nat Immunol* (2013) 14(2):152–61. doi: 10.1038/ni.2496

115. Vanderleyden I, Fra-Bido SC, Innocentin S, Stebegg M, Okkenhaug H, Evans-Bailey N, et al. Follicular regulatory T cells can access the germinal center independently of Cxcr5. *Cell Rep* (2020) 30(3):611–619.e4. doi: 10.1016/j.celrep.2019.12.076

116. Eschweiler S, Clarke J, Ramírez-Suástegui C, Panwar B, Madrigal A, Chee SJ, et al. Intratumoral follicular regulatory T cells curtail anti-Pd-1 treatment efficacy. *Nat Immunol* (2021) 22(8):1052–63. doi: 10.1038/s41590-021-00958-6

117. Zappasodi R, Budhu S, Hellmann MD, Postow MA, Senbabaoglu Y, Manne S, et al. Non-conventional inhibitory Cd4foxp3pd-1 T cells as a biomarker of immune checkpoint blockade activity. *Cancer Cell* (2018) 33(6):1017–1032.e7. doi: 10.1016/j.ccell.2018.05.009

118. Wherry EJ. T Cell exhaustion. *Nat Immunol* (2011) 12(6):492–9. doi: 10.1038/ni.2035

119. Konen JM, Rodriguez BL, Fradette JJ, Gibson L, Davis D, Minelli R, et al. Ntrk1 promotes resistance to pd-1 checkpoint blockade in mesenchymal Kras/P53 mutant lung cancer. *Cancers (Basel)* (2019) 11(4):462. doi: 10.3390/cancers11040462

120. Koyama S, Akbay EA, Li YY, Herter-Sprie GS, Buczkowski KA, Richards WG, et al. Adaptive resistance to therapeutic pd-1 blockade is associated with upregulation of alternative immune checkpoints. *Nat Commun* (2016) 7:10501. doi: 10.1038/ncomms10501

121. Shayan G, Srivastava R, Li J, Schmitt N, Kane LP, Ferris RL. Adaptive resistance to anti-Pd1 therapy by Tim-3 upregulation is mediated by the Pi3k-akt pathway in head and neck cancer. *Oncoimmunology* (2017) 6(1):e1261779. doi: 10.1080/2162402X.2016.1261779

122. Huang R-Y, Francois A, McGray AR, Miliotto A, Odunsi K. Compensatory upregulation of pd-1, lag-3, and ctla-4 limits the efficacy of single-agent checkpoint blockade in metastatic ovarian cancer. *Oncoimmunology* (2017) 6(1):e1249561. doi: 10.1080/2162402X.2016.1249561

123. Thommen DS, Schreiner J, Müller P, Herzig P, Roller A, Belousov A, et al. Progression of lung cancer is associated with increased dysfunction of T cells defined by coexpression of multiple inhibitory receptors. *Cancer Immunol Res* (2015) 3(12):1344–55. doi: 10.1158/2326-6066.CIR-15-0097

124. Kakavand H, Jackett LA, Menzies AM, Gide TN, Carlino MS, Saw RPM, et al. Negative immune checkpoint regulation by vista: A mechanism of acquired resistance to anti-Pd-1 therapy in metastatic melanoma patients. *Mod Pathol* (2017) 30(12):1666–76. doi: 10.1038/modpathol.2017.89

125. Bauer C, Kühnemuth B, Duewell P, Ormanns S, Gress T, Schnurr M. Prevailing over T cell exhaustion: New developments in the immunotherapy of pancreatic cancer. *Cancer Lett* (2016) 381(1):259–68. doi: 10.1016/j.canlet.2016.02.057

126. Farhood B, Najafi M, Mortezaee K. Cd8 cytotoxic T lymphocytes in cancer immunotherapy: A review. *J Cell Physiol* (2019) 234(6):8509–21. doi: 10.1002/jcp.27782

127. Kearney CJ, Vervoort SJ, Hogg SJ, Ramsbottom KM, Freeman AJ, Lalaoui N, et al. Tumor immune evasion arises through loss of tnf sensitivity. *Sci Immunol* (2018) 3(23):eaar3451. doi: 10.1126/sciimmunol.aar3451

128. Dominiecki ME, Beatty GL, Pan Z-K, Neeson P, Paterson Y. Tumor sensitivity to ifn-gamma is required for successful antigen-specific immunotherapy of a transplantable mouse tumor model for hpv-transformed tumors. *Cancer Immunol Immunother* (2005) 54(5):477–88. doi: 10.1007/s00262-004-0610-0

129. Ikeda H, Old LJ, Schreiber RD. The roles of ifn gamma in protection against tumor development and cancer immunoediting. *Cytokine Growth Factor Rev* (2002) 13(2):95–109. doi: 10.1016/S1359-6101(01)00038-7

130. Bach EA, Aguet M, Schreiber RD. The ifn gamma receptor: A paradigm for cytokine receptor signaling. *Annu Rev Immunol* (1997) 15:563–91. doi: 10.1146/annurev.immunol.15.1.563

131. Gao J, Shi LZ, Zhao H, Chen J, Xiong L, He Q, et al. Loss of ifn-Γ pathway genes in tumor cells as a mechanism of resistance to anti-Ctla-4 therapy. *Cell* (2016) 167(2):397–404.e9. doi: 10.1016/j.cell.2016.08.069

132. Shin DS, Zaretsky JM, Escuin-Ordinas H, Garcia-Diaz A, Hu-Lieskovan S, Kalbasi A, et al. Primary resistance to pd-1 blockade mediated by Jak1/2 mutations. *Cancer Discovery* (2017) 7(2):188–201. doi: 10.1158/2159-8290.CD-16-1223

133. Vredevoogd DW, Kuilman T, Ligtenberg MA, Boshuizen J, Stecker KE, de Bruijn B, et al. Augmenting immunotherapy impact by lowering tumor tnf cytotoxicity threshold. *Cell* (2019) 178(3):585–599.e15. doi: 10.1016/j.cell.2019.06.014

134. Herrera FG, Bourhis J, Coukos G. Radiotherapy combination opportunities leveraging immunity for the next oncology practice. *CA Cancer J Clin* (2017) 67(1):65–85. doi: 10.3322/caac.21358

135. Woller N, Gurlevik E, Fleischmann-Mundt B, Schumacher A, Knocke S, Kloos AM, et al. Viral infection of tumors overcomes resistance to pd-1-Immunotherapy by broadening neoantigenome-directed T-cell responses. *Mol Ther* (2015) 23(10):1630–40. doi: 10.1038/mt.2015.115

136. Turner TB, Meza-Perez S, Londono A, Katre A, Peabody JE, Smith HJ, et al. Epigenetic modifiers upregulate mhc ii and impede ovarian cancer tumor growth. *Oncotarget* (2017) 8(27):44159–70. doi: 10.18632/oncotarget.17395

137. Mazzone R, Zwergel C, Mai A, Valente S. Epi-drugs in combination with immunotherapy: A new avenue to improve anticancer efficacy. *Clin Epigenet* (2017) 9:59. doi: 10.1186/s13148-017-0358-y

138. Lv M, Chen M, Zhang R, Zhang W, Wang C, Zhang Y, et al. Manganese is critical for antitumor immune responses *Via* cgas-sting and improves the efficacy of clinical immunotherapy. *Cell Res* (2020) 30(11):966–79. doi: 10.1038/s41422-020-00395-4

139. Kalbasi A, Tariveranmoshabad M, Hakimi K, Kremer S, Campbell KM, Funes JM, et al. Uncoupling interferon signaling and antigen presentation to overcome immunotherapy resistance due to Jak1 loss in melanoma. *Sci Transl Med* (2020) 12(565):eabb0152. doi: 10.1126/scitranslmed.abb0152

140. Ribas A, Medina T, Kummar S, Amin A, Kalbasi A, Drabick JJ, et al. Sd-101 in combination with pembrolizumab in advanced melanoma: Results of a phase ib, multicenter study. *Cancer Discovery* (2018) 8(10):1250–7. doi: 10.1158/2159-8290.CD-18-0280

141. Salmon H, Idoyaga J, Rahman A, Leboeuf M, Remark R, Jordan S, et al. Expansion and activation of Cd103(+) dendritic cell progenitors at the tumor site enhances tumor responses to therapeutic pd-L1 and braf inhibition. *Immunity* (2016) 44(4):924–38. doi: 10.1016/j.immuni.2016.03.012

142. Peng W, Chen JQ, Liu C, Malu S, Creasy C, Tetzlaff MT, et al. Loss of pten promotes resistance to T cell-mediated immunotherapy. *Cancer Discovery* (2016) 6 (2):202–16. doi: 10.1158/2159-8290.CD-15-0283

143. Wall JA, Meza-Perez S, Scalise CB, Katre A, Londoño AI, Turbitt WJ, et al. Manipulating the Wnt/β-catenin signaling pathway to promote anti-tumor immune infiltration into the tme to sensitize ovarian cancer to icb therapy. *Gynecol. Oncol* (2021) 160(1):285–94. doi: 10.1016/j.ygyno.2020.10.031

144. Ribas A, Lawrence D, Atkinson V, Agarwal S, Miller WHJr., Carlino MS, et al. Combined braf and mek inhibition with pd-1 blockade immunotherapy in braf-mutant melanoma. *Nat Med* (2019) 25(6):936–40. doi: 10.1038/s41591-019-0476-5

145. Goel S, DeCristo MJ, Watt AC, BrinJones H, Sceneay J, Li BB, et al. Cdk4/6 inhibition triggers anti-tumour immunity. *Nature* (2017) 548(7668):471–5. doi: 10.1038/nature23465

146. Mariathasan S, Turley SJ, Nickles D, Castiglioni A, Yuen K, Wang Y, et al. Tgfbeta attenuates tumour response to pd-L1 blockade by contributing to exclusion of T cells. *Nature* (2018) 554(7693):544–8. doi: 10.1038/nature25501

147. Schmittnaegel M, Rigamonti N, Kadioglu E, Cassara A, Wyser Rmili C, Kiialainen A, et al. Dual angiopoietin-2 and vegfa inhibition elicits antitumor immunity that is enhanced by pd-1 checkpoint blockade. *Sci Transl Med* (2017) 9 (385):eaak9670. doi: 10.1126/scitranslmed.aak9670

148. Klug F, Prakash H, Huber PE, Seibel T, Bender N, Halama N, et al. Low-dose irradiation programs macrophage differentiation to an Inos(+)/M1 phenotype that orchestrates effective T cell immunotherapy. *Cancer Cell* (2013) 24(5):589–602. doi: 10.1016/j.ccr.2013.09.014

149. Sun M, Gu P, Yang Y, Yu L, Jiang Z, Li J, et al. Mesoporous silica nanoparticles inflame tumors to overcome anti-Pd-1 resistance through Tlr4-nfkappab axis. *J Immunother Cancer* (2021) 9(6):e002508. doi: 10.1136/jitc-2021-002508

150. Grosser R, Cherkassky L, Chintala N, Adusumilli PS. Combination immunotherapy with car T cells and checkpoint blockade for the treatment of solid tumors. *Cancer Cell* (2019) 36(5):471–82. doi: 10.1016/j.ccell.2019.09.006

151. Rotte A. Combination of ctla-4 and pd-1 blockers for treatment of cancer. *J Exp Clin Cancer Res* (2019) 38(1):255. doi: 10.1186/s13046-019-1259-z

152. Mayes PA, Hance KW, Hoos A. The promise and challenges of immune agonist antibody development in cancer. *Nat Rev Drug Discovery* (2018) 17(7):509–27. doi: 10.1038/nrd.2018.75

153. Han HS, Jeong S, Kim H, Kim HD, Kim AR, Kwon M, et al. Tox-expressing terminally exhausted tumor-infiltrating Cd8(+) T cells are reinvigorated by Co-blockade of pd-1 and tigit in bladder cancer. *Cancer Lett* (2021) 499:137–47. doi: 10.1016/j.canlet.2020.11.035

154. Ghoneim HE, Fan Y, Moustaki A, Abdelsamed HA, Dash P, Dogra P, et al. *De novo* epigenetic programs inhibit pd-1 blockade-mediated T cell rejuvenation. *Cell* (2017) 170(1):142–57.e19. doi: 10.1016/j.cell.2017.06.007

155. Buck MD, O'Sullivan D, Klein Geltink RI, Curtis JD, Chang CH, Sanin DE, et al. Mitochondrial dynamics controls T cell fate through metabolic programming. *Cell* (2016) 166(1):63–76. doi: 10.1016/j.cell.2016.05.035

156. Ravi R, Noonan KA, Pham V, Bedi R, Zhavoronkov A, Ozerov IV, et al. Bifunctional immune checkpoint-targeted antibody-ligand traps that simultaneously disable tgfbeta enhance the efficacy of cancer immunotherapy. *Nat Commun* (2018) 9(1):741. doi: 10.1038/s41467-017-02696-6

157. Neubert NJ, Schmittnaegel M, Bordry N, Nassiri S, Wald N, Martignier C, et al. T Cell-induced Csf1 promotes melanoma resistance to Pd1 blockade. *Sci Transl Med* (2018) 10(436):eaan3311. doi: 10.1126/scitranslmed.aan3311

158. Zhou Q, Liang J, Yang T, Liu J, Li B, Li Y, et al. Carfilzomib modulates tumor microenvironment to potentiate immune checkpoint therapy for cancer. *EMBO Mol Med* (2022) 14(1):e14502. doi: 10.15252/emmm.202114502

159. Cheng Y, Li H, Deng Y, Tai Y, Zeng K, Zhang Y, et al. Cancer-associated fibroblasts induce Pdl1+ neutrophils through the Il6-Stat3 pathway that foster immune suppression in hepatocellular carcinoma. *Cell Death Dis* (2018) 9(4):422. doi: 10.1038/s41419-018-0458-4

160. Ji D, Song C, Li Y, Xia J, Wu Y, Jia J, et al. Combination of radiotherapy and suppression of tregs enhances abscopal antitumor effect and inhibits metastasis in rectal cancer. *J Immunother Cancer* (2020) 8(2):e000826. doi: 10.1136/jitc-2020-000826

161. Derosa L, Routy B, Desilets A, Daillère R, Terrisse S, Kroemer G, et al. Microbiota-centered interventions: The next breakthrough in immuno-oncology? *Cancer Discovery* (2021) 11(10):2396–412. doi: 10.1158/2159-8290.Cd-21-0236

162. Mole RH. Whole body irradiation; radiobiology or medicine? *Br J Radiol* (1953) 26(305):234–41. doi: 10.1259/0007-1285-26-305-234

163. Ngwa W, Irabor OC, Schoenfeld JD, Hesser J, Demaria S, Formenti SC. Using immunotherapy to boost the abscopal effect. *Nat Rev Cancer* (2018) 18 (5):313–22. doi: 10.1038/nrc.2018.6

164. Takahashi J, Nagasawa S. Immunostimulatory effects of radiotherapy for local and systemic control of melanoma: A review. *Int J Mol Sci* (2020) 21(23):9324. doi: 10.3390/ijms21239324

165. Sharma A, Bode B, Wenger RH, Lehmann K, Sartori AA, Moch H, et al. Gamma-radiation promotes immunological recognition of cancer cells through increased expression of cancer-testis antigens *in vitro* and *in vivo*. *PloS One* (2011) 6(11):e28217. doi: 10.1371/journal.pone.0028217

166. Salas-Benito D, Perez-Gracia JL, Ponz-Sarvise M, Rodriguez-Ruiz ME, Martinez-Forero I, Castanon E, et al. Paradigms on immunotherapy combinations with chemotherapy. *Cancer Discovery* (2021) 11(6):1353–67. doi: 10.1158/2159-8290.CD-20-1312

167. Grimaldi A, Cammarata I, Martire C, Focaccetti C, Piconese S, Buccilli M, et al. Combination of chemotherapy and pd-1 blockade induces T cell responses to tumor non-mutated neoantigens. *Commun Biol* (2020) 3(1):85. doi: 10.1038/s42003-020-0811-x

168. Ma X, Yang S, Zhang T, Wang S, Yang Q, Xiao Y, et al. Bioresponsive immune-Booster-Based prodrug nanogel for cancer immunotherapy. *Acta Pharm Sin B* (2022) 12(1):451–66. doi: 10.1016/j.apsb.2021.05.016

169. Mathew M, Enzler T, Shu CA, Rizvi NA. Combining chemotherapy with pd-1 blockade in nsclc. *Pharmacol Ther* (2018) 186:130–7. doi: 10.1016/j.pharmthera.2018.01.003

170. Schmid P, Rugo HS, Adams S, Schneeweiss A, Barrios CH, Iwata H, et al. Atezolizumab plus nab-paclitaxel as first-line treatment for unresectable, locally advanced or metastatic triple-negative breast cancer (Impassion130): Updated efficacy results from a randomised, double-blind, placebo-controlled, phase 3 trial. *Lancet Oncol* (2020) 21(1):44–59. doi: 10.1016/S1470-2045(19)30689-8

171. Russell L, Peng KW, Russell SJ, Diaz RM. Oncolytic viruses: Priming time for cancer immunotherapy. *BioDrugs* (2019) 33(5):485–501. doi: 10.1007/s40259-019-00367-0

172. Bommareddy PK, Shettigar M, Kaufman HL. Integrating oncolytic viruses in combination cancer immunotherapy. *Nat Rev Immunol* (2018) 18(8):498–513. doi: 10.1038/s41577-018-0014-6

173. Twumasi-Boateng K, Pettigrew JL, Kwok YYE, Bell JC, Nelson BH. Oncolytic viruses as engineering platforms for combination immunotherapy. *Nat Rev Cancer* (2018) 18(7):419–32. doi: 10.1038/s41568-018-0009-4

174. Takaki H, Cornelis F, Kako Y, Kobayashi K, Kamikonya N, Yamakado K. Thermal ablation and immunomodulation: From preclinical experiments to clinical trials. *Diagn Interv Imaging* (2017) 98(9):651–9. doi: 10.1016/j.diii.2017.04.008

175. Xing R, Gao J, Cui Q, Wang Q. Strategies to improve the antitumor effect of immunotherapy for hepatocellular carcinoma. *Front Immunol* (2021) 12:783236. doi: 10.3389/fimmu.2021.783236

176. Harari A, Graciotti M, Bassani-Sternberg M, Kandalaft LE. Antitumour dendritic cell vaccination in a priming and boosting approach. *Nat Rev Drug Discovery* (2020) 19(9):635–52. doi: 10.1038/s41573-020-0074-8

177. Xiao Y, Zhang T, Ma X, Yang QC, Yang LL, Yang SC, et al. Microenvironment-responsive prodrug-induced pyroptosis boosts cancer immunotherapy. *Adv Sci (Weinh)* (2021) 8(24):e2101840. doi: 10.1002/advs.202101840

178. Sade-Feldman M, Jiao YJ, Chen JH, Rooney MS, Barzily-Rokni M, Eliane JP, et al. Resistance to checkpoint blockade therapy through inactivation of antigen presentation. *Nat Commun* (2017) 8(1):1136. doi: 10.1038/s41467-017-01062-w

179. Gomez S, Tabernacki T, Kobyra J, Roberts P, Chiappinelli KB. Combining epigenetic and immune therapy to overcome cancer resistance. *Semin Cancer Biol* (2020) 65:99–113. doi: 10.1016/j.semcancer.2019.12.019

180. Falkenberg KJ, Johnstone RW. Histone deacetylases and their inhibitors in cancer, neurological diseases and immune disorders. *Nat Rev Drug Discovery* (2014) 13(9):673–91. doi: 10.1038/nrd4360

181. Siebenkas C, Chiappinelli KB, Guzzetta AA, Sharma A, Jeschke J, Vatapalli R, et al. Inhibiting DNA methylation activates cancer testis antigens and expression of the antigen processing and presentation machinery in colon and ovarian cancer cells. *PloS One* (2017) 12(6):e0179501. doi: 10.1371/journal.pone.0179501

182. Suraweera A, O'Byrne KJ, Richard DJ. Combination therapy with histone deacetylase inhibitors (Hdaci) for the treatment of cancer: Achieving the full therapeutic potential of hdaci. *Front Oncol* (2018) 8:92. doi: 10.3389/fonc.2018.00092

183. Zheng H, Zhao W, Yan C, Watson CC, Massengill M, Xie M, et al. Hdac inhibitors enhance T-cell chemokine expression and augment response to pd-1 immunotherapy in lung adenocarcinoma. *Clin Cancer Res* (2016) 22(16):4119–32. doi: 10.1158/1078-0432.CCR-15-2584

184. Chen X, Pan X, Zhang W, Guo H, Cheng S, He Q, et al. Epigenetic strategies synergize with pd-L1/Pd-1 targeted cancer immunotherapies to enhance antitumor responses. *Acta Pharm Sin B* (2020) 10(5):723–33. doi: 10.1016/j.apsb.2019.09.006

185. Cornel AM, Mimpen IL, Nierkens S. Mhc class I downregulation in cancer: Underlying mechanisms and potential targets for cancer immunotherapy. *Cancers (Basel)* (2020) 12(7):1760. doi: 10.3390/cancers12071760

186. Wculek SK, Cueto FJ, Mujal AM, Melero I, Krummel MF, Sancho D. Dendritic cells in cancer immunology and immunotherapy. *Nat Rev Immunol* (2020) 20(1):7–24. doi: 10.1038/s41577-019-0210-z

187. Ni K, Luo T, Lan G, Culbert A, Song Y, Wu T, et al. A nanoscale metal-organic framework to mediate photodynamic therapy and deliver cpg oligodeoxynucleotides to enhance antigen presentation and cancer immunotherapy. *Angew Chem Int Ed Engl* (2020) 59(3):1108–12. doi: 10.1002/anie.201911429

188. Garg AD, Coulie PG, Van den Eynde BJ, Agostinis P. Integrating next-generation dendritic cell vaccines into the current cancer immunotherapy landscape. *Trends Immunol* (2017) 38(8):577–93. doi: 10.1016/j.it.2017.05.006

189. Huang Y, Kim BYS, Chan CK, Hahn SM, Weissman IL, Jiang W. Improving immune-vascular crosstalk for cancer immunotherapy. *Nat Rev Immunol* (2018) 18(3):195–203. doi: 10.1038/nri.2017.145

190. Lin YX, Wang Y, Ding J, Jiang A, Wang J, Yu M, et al. Reactivation of the tumor suppressor pten by mrna nanoparticles enhances antitumor immunity in preclinical models. *Sci Transl Med* (2021) 13(599):eaba9772. doi: 10.1126/scitranslmed.aba9772

191. Liu YT, Sun ZJ. Turning cold tumors into hot tumors by improving T-cell infiltration. *Theranostics* (2021) 11(11):5365–86. doi: 10.7150/thno.58390

192. Wang L, Gao Y, Zhang G, Li D, Wang Z, Zhang J, et al. Enhancing Kdm5a and tlr activity improves the response to immune checkpoint blockade. *Sci Transl Med* (2020) 12(560):eaax2282. doi: 10.1126/scitranslmed.aax2282

193. Li X, Xiang Y, Li F, Yin C, Li B, Ke X. Wnt/Beta-catenin signaling pathway regulating T cell-inflammation in the tumor microenvironment. *Front Immunol* (2019) 10:2293. doi: 10.3389/fimmu.2019.02293

194. Klempner SJ, Bendell JC, Villaflor VM, Tenner LL, Stein SM, Rottman JB, et al. Safety, efficacy, and biomarker results from a phase ib study of the anti-Dkk1 antibody dkn-01 in combination with pembrolizumab in advanced esophagogastric cancers. *Mol Cancer Ther* (2021) 20(11):2240–9. doi: 10.1158/1535-7163.MCT-21-0273

195. Ganesh S, Shui X, Craig KP, Park J, Wang W, Brown BD, et al. Rnai-mediated beta-catenin inhibition promotes T cell infiltration and antitumor activity in combination with immune checkpoint blockade. *Mol Ther* (2018) 26(11):2567–79. doi: 10.1016/j.ymthe.2018.09.005

196. Ebert PJR, Cheung J, Yang Y, McNamara E, Hong R, Moskalenko M, et al. Map kinase inhibition promotes T cell and anti-tumor activity in combination with pd-L1 checkpoint blockade. *Immunity* (2016) 44(3):609–21. doi: 10.1016/j.immuni.2016.01.024

197. Sullivan RJ, Hamid O, Gonzalez R, Infante JR, Patel MR, Hodi FS, et al. Atezolizumab plus cobimetinib and vemurafenib in braf-mutated melanoma patients. *Nat Med* (2019) 25(6):929–35. doi: 10.1038/s41591-019-0474-7

198. Heckler M, Ali LR, Clancy-Thompson E, Qiang L, Ventre KS, Lenehan P, et al. Inhibition of Cdk4/6 promotes Cd8 T-cell memory formation. *Cancer Discovery* (2021) 11(10):2564–81. doi: 10.1158/2159-8290.CD-20-1540

199. Deng J, Wang ES, Jenkins RW, Li S, Dries R, Yates K, et al. Cdk4/6 inhibition augments antitumor immunity by enhancing T-cell activation. *Cancer Discovery* (2018) 8(2):216–33. doi: 10.1158/2159-8290.CD-17-0915

200. Zhang QF, Li J, Jiang K, Wang R, Ge JL, Yang H, et al. Cdk4/6 inhibition promotes immune infiltration in ovarian cancer and synergizes with pd-1 blockade in a b cell-dependent manner. *Theranostics* (2020) 10(23):10619–33. doi: 10.7150/thno.44871

201. Grauel AL, Nguyen B, Ruddy D, Laszewski T, Schwartz S, Chang J, et al. Tgfbeta-blockade uncovers stromal plasticity in tumors by revealing the existence of a subset of interferon-licensed fibroblasts. *Nat Commun* (2020) 11(1):6315. doi: 10.1038/s41467-020-19920-5

202. Chen X, Wang L, Li P, Song M, Qin G, Gao Q, et al. Dual tgf-beta and pd-1 blockade synergistically enhances mage-A3-Specific Cd8(+) T cell response in esophageal squamous cell carcinoma. *Int J Cancer* (2018) 143(10):2561–74. doi: 10.1002/ijc.31730

203. Batlle E, Massague J. Transforming growth factor-beta signaling in immunity and cancer. *Immunity* (2019) 50(4):924–40. doi: 10.1016/j.immuni.2019.03.024

204. Lind H, Gameiro SR, Jochems C, Donahue RN, Strauss J, Gulley JM, et al. Dual targeting of tgf-beta and pd-L1 *Via* a bifunctional anti-Pd-L1/Tgf-Betarii agent: Status of preclinical and clinical advances. *J Immunother Cancer* (2020) 8(1):e000433. doi: 10.1136/jitc-2019-000433

205. Huinen ZR, Huijbers EJM, van Beijnum JR, Nowak-Sliwinska P, Griffioen AW. Anti-angiogenic agents - overcoming tumour endothelial cell anergy and improving immunotherapy outcomes. *Nat Rev Clin Oncol* (2021) 18(8):527–40. doi: 10.1038/s41571-021-00496-y

206. Zhao Y, Ting KK, Li J, Cogger VC, Chen J, Johansson-Percival A, et al. Targeting vascular endothelial-cadherin in tumor-associated blood vessels promotes T-Cell-Mediated immunotherapy. *Cancer Res* (2017) 77(16):4434–47. doi: 10.1158/0008-5472.CAN-16-3129

207. Fukumura D, Kloepper J, Amoozgar Z, Duda DG, Jain RK. Enhancing cancer immunotherapy using antiangiogenics: Opportunities and challenges. *Nat Rev Clin Oncol* (2018) 15(5):325–40. doi: 10.1038/nrclinonc.2018.29

208. Arina A, Beckett M, Fernandez C, Zheng W, Pitroda S, Chmura SJ, et al. Tumor-reprogrammed resident T cells resist radiation to control tumors. *Nat Commun* (2019) 10(1):3959. doi: 10.1038/s41467-019-11906-2

209. Tang H, Xu X, Chen Y, Xin H, Wan T, Li B, et al. Reprogramming the tumor microenvironment through second-near-Infrared-Window photothermal genome editing of pd-L1 mediated by supramolecular gold nanorods for enhanced cancer immunotherapy. *Adv Mater* (2021) 33(12):e2006003. doi: 10.1002/adma.202006003

210. Depil S, Duchateau P, Grupp SA, Mufti G, Poirot L. 'Off-the-Shelf' allogeneic car T cells: Development and challenges. *Nat Rev Drug Discovery* (2020) 19(3):185–99. doi: 10.1038/s41573-019-0051-2

211. Gumber D, Wang LD. Improving car-T immunotherapy: Overcoming the challenges of T cell exhaustion. *EBioMedicine* (2022) 77:103941. doi: 10.1016/j.ebiom.2022.103941

212. Song W, Zhang M. Use of car-T cell therapy, pd-1 blockade, and their combination for the treatment of hematological malignancies. *Clin Immunol* (2020) 214:108382. doi: 10.1016/j.clim.2020.108382

213. John LB, Devaud C, Duong CPM, Yong CS, Beavis PA, Haynes NM, et al. Anti-Pd-1 antibody therapy potently enhances the eradication of established tumors by gene-modified T cells. *Clin Cancer Res* (2013) 19(20):5636–46. doi: 10.1158/1078-0432.Ccr-13-0458

214. Gray KD, McCloskey JE, Vedvyas Y, Kalloo OR, Eshaky SE, Yang Y, et al. Pd1 blockade enhances Icam1-directed car T therapeutic efficacy in advanced thyroid cancer. *Clin Cancer Res* (2020) 26(22):6003–16. doi: 10.1158/1078-0432.Ccr-20-1523

215. Cherkassky L, Morello A, Villena-Vargas J, Feng Y, Dimitrov DS, Jones DR, et al. Human car T cells with cell-intrinsic pd-1 checkpoint blockade resist tumor-mediated inhibition. *J Clin Invest* (2016) 126(8):3130–44. doi: 10.1172/jci83092

216. Wang C, Shi F, Liu Y, Zhang Y, Dong L, Li X, et al. Anti-Pd-1 antibodies as a salvage therapy for patients with diffuse Large b cell lymphoma who Progressed/Relapsed after Cart19/20 therapy. *J Hematol Oncol* (2021) 14(1):106. doi: 10.1186/s13045-021-01120-3

217. Chong EA, Alanio C, Svoboda J, Nasta SD, Landsburg DJ, Lacey SF, et al. Pembrolizumab for b-cell lymphomas relapsing after or refractory to Cd19-directed car T-cell therapy. *Blood* (2022) 139(7):1026–38. doi: 10.1182/blood.2021012634

218. Wang Z, Li N, Feng K, Chen M, Zhang Y, Liu Y, et al. Phase I study of car-T cells with pd-1 and tcr disruption in mesothelin-positive solid tumors. *Cell Mol Immunol* (2021) 18(9):2188–98. doi: 10.1038/s41423-021-00749-x

219. Osborne W, Chen R, Jonnaert M, Khokhar NZ, Peddareddigari VGR, Pule M, et al. Phase 1/2 study of Auto3 the first bicistronic chimeric antigen receptor (Car) targeting Cd19 and Cd22 followed by an anti-Pd1 in patients with Relapsed/Refractory (R/R) diffuse Large b cell lymphoma (Dlbcl): Results of cohort 1 and 2 of the Alexander study. *Blood* (2019) 134(Supplement_1):246. doi: 10.1182/blood-2019-122724

220. Hirayama AV, Gauthier J, Hay KA, Sheih A, Turtle CJ. Efficacy and toxicity of Jcar014 in combination with durvalumab for the treatment of patients with Relapsed/Refractory aggressive b-cell non-Hodgkin lymphoma. *Blood* (2018) 132(Suppl_1):1680. doi: 10.1182/blood-2018-99-116745

221. Zurko J, Chaney K, Astle JM, Johnson BD, Hari P, Shah NN. Pd-1 blockade after bispecific Lv20.19 car T modulates car T-cell immunophenotype without meaningful clinical response. *Haematologica*. (2021) 106(10):2788–90. doi: 10.3324/haematol.2021.278461

222. Thommen DS, Schumacher TN. T Cell dysfunction in cancer. *Cancer Cell* (2018) 33(4):547–62. doi: 10.1016/j.ccell.2018.03.012

223. Blank CU, Haining WN, Held W, Hogan PG, Kallies A, Lugli E, et al. Defining 'T cell exhaustion'. *Nat Rev Immunol* (2019) 19(11):665–74. doi: 10.1038/s41577-019-0221-9

224. Zarour HM. Reversing T-cell dysfunction and exhaustion in cancer. *Clin Cancer Res* (2016) 22(8):1856–64. doi: 10.1158/1078-0432.Ccr-15-1849

225. Khan O, Giles JR, McDonald S, Manne S, Ngiow SF, Patel KP, et al. Tox transcriptionally and epigenetically programs Cd8(+) T cell exhaustion. *Nature* (2019) 571(7764):211–8. doi: 10.1038/s41586-019-1325-x

226. Wherry EJ, Kurachi M. Molecular and cellular insights into T cell exhaustion. *Nat Rev Immunol* (2015) 15(8):486–99. doi: 10.1038/nri3862

227. Tabana Y, Moon TC, Siraki A, Elahi S, Barakat K. Reversing T-cell exhaustion in immunotherapy: A review on current approaches and limitations. *Expert Opin Ther Targets* (2021) 25(5):347–63. doi: 10.1080/14728222.2021.1937123

228. Schoffski P, Tan DSW, Martin M, Ochoa-de-Olza M, Sarantopoulos J, Carvajal RD, et al. Phase I/Ii study of the lag-3 inhibitor ieramilimab (Lag525) +/- anti-Pd-1 spartalizumab (Pdr001) in patients with advanced malignancies. *J Immunother Cancer* (2022) 10(2):e003776. doi: 10.1136/jitc-2021-003776

229. Curigliano G, Gelderblom H, Mach N, Doi T, Tai D, Forde PM, et al. Phase I/Ib clinical trial of sabatolimab, an anti-Tim-3 antibody, alone and in combination with spartalizumab, an anti-Pd-1 antibody, in advanced solid tumors. *Clin Cancer Res* (2021) 27(13):3620–9. doi: 10.1158/1078-0432.CCR-20-4746

230. Mettu NB, Ulahannan SV, Bendell JC, Garrido-Laguna I, Strickler JH, Moore KN, et al. A phase 1a/B open-label, dose-escalation study of etigilimab alone or in combination with nivolumab in patients with locally advanced or metastatic solid tumors. *Clin Cancer Res* (2022) 28(5):882–92. doi: 10.1158/1078-0432.CCR-21-2780

231. Benzon B, Zhao SG, Haffner MC, Takhar M, Erho N, Yousefi K, et al. Correlation of B7-H3 with androgen receptor, immune pathways and poor outcome in prostate cancer: An expression-based analysis. *Prostate Cancer Prostatic Dis* (2017) 20(1):28–35. doi: 10.1038/pcan.2016.49

232. Wei H, Zhao L, Hellstrom I, Hellstrom KE, Guo Y. Dual targeting of Cd137 Co-stimulatory and pd-1 Co-inhibitory molecules for ovarian cancer immunotherapy. *Oncoimmunology* (2014) 3:e28248. doi: 10.4161/onci.28248

233. Pauken KE, Sammons MA, Odorizzi PM, Manne S, Godec J, Khan O, et al. Epigenetic stability of exhausted T cells limits durability of reinvigoration by pd-1 blockade. *Science* (2016) 354(6316):1160–5. doi: 10.1126/science.aaf2807

234. Wang X, He Q, Shen H, Xia A, Tian W, Yu W, et al. Tox promotes the exhaustion of antitumor Cd8(+) T cells by preventing Pd1 degradation in hepatocellular carcinoma. *J Hepatol* (2019) 71(4):731–41. doi: 10.1016/j.jhep.2019.05.015

235. Qorraj M, Bruns H, Bottcher M, Weigand L, Saul D, Mackensen A, et al. The pd-1/Pd-L1 axis contributes to immune metabolic dysfunctions of monocytes in chronic lymphocytic leukemia. *Leukemia* (2017) 31(2):470–8. doi: 10.1038/leu.2016.214

236. Ho PC, Bihuniak JD, Macintyre AN, Staron M, Liu X, Amezquita R, et al. Phosphoenolpyruvate is a metabolic checkpoint of anti-tumor T cell responses. *Cell* (2015) 162(6):1217–28. doi: 10.1016/j.cell.2015.08.012

237. Scharping NE, Menk AV, Whetstone RD, Zeng X, Delgoffe GM. Efficacy of pd-1 blockade is potentiated by metformin-induced reduction of tumor hypoxia. *Cancer Immunol Res* (2017) 5(1):9–16. doi: 10.1158/2326-6066.CIR-16-0103

238. Ohue Y, Nishikawa H. (Treg) cells in cancer: Can treg cells be a new therapeutic target? *Cancer Sci* (2019) 110(7):2080–9. doi: 10.1111/cas.14069

239. Whiteside TL. The role of regulatory T cells in cancer immunology. *Immunotargets Ther* (2015) 4:159–71. doi: 10.2147/ITT.S55415

240. Amoozgar Z, Kloepper J, Ren J, Tay RE, Kazer SW, Kiner E, et al. Targeting treg cells with gitr activation alleviates resistance to immunotherapy in murine glioblastomas. *Nat Commun* (2021) 12(1):2582. doi: 10.1038/s41467-021-22885-8

241. Hung AL, Maxwell R, Theodros D, Belcaid Z, Mathios D, Luksik AS, et al. Tigit and pd-1 dual checkpoint blockade enhances antitumor immunity and survival in gbm. *Oncoimmunology* (2018) 7(8):e1466769. doi: 10.1080/2162402X.2018.1466769

242. Liu J, Yuan Y, Chen W, Putra J, Suriawinata AA, Schenk AD, et al. Immune-checkpoint proteins vista and pd-1 nonredundantly regulate murine T-cell responses. *Proc Natl Acad Sci U.S.A.* (2015) 112(21):6682–7. doi: 10.1073/pnas.1420370112

243. Jacobs JF, Punt CJ, Lesterhuis WJ, Sutmuller RP, Brouwer HM, Scharenborg NM, et al. Dendritic cell vaccination in combination with anti-Cd25 monoclonal antibody treatment: A phase I/Ii study in metastatic melanoma patients. *Clin Cancer Res* (2010) 16(20):5067–78. doi: 10.1158/1078-0432.CCR-10-1757

244. Santoni M, Romagnoli E, Saladino T, Foghini L, Guarino S, Capponi M, et al. Triple negative breast cancer: Key role of tumor-associated macrophages in regulating the activity of anti-Pd-1/Pd-L1 agents. *Biochim Biophys Acta Rev Cancer* (2018) 1869(1):78–84. doi: 10.1016/j.bbcan.2017.10.007

245. Gordon SR, Maute RL, Dulken BW, Hutter G, George BM, McCracken MN, et al. Pd-1 expression by tumour-associated macrophages inhibits phagocytosis and tumour immunity. *Nature* (2017) 545(7655):495–9. doi: 10.1038/nature22396

246. Eisinger S, Sarhan D, Boura VF, Ibarlucea-Benitez I, Tyystjarvi S, Oliynyk G, et al. Targeting a scavenger receptor on tumor-associated macrophages activates tumor cell killing by natural killer cells. *Proc Natl Acad Sci U.S.A.* (2020) 117(50):32005–16. doi: 10.1073/pnas.2015343117

247. Li H, Xiao Y, Li Q, Yao J, Yuan X, Zhang Y, et al. The allergy mediator histamine confers resistance to immunotherapy in cancer patients *Via* activation of the macrophage histamine receptor H1. *Cancer Cell* (2022) 40(1):36–52.e9. doi: 10.1016/j.ccell.2021.11.002

248. Grauers Wiktorin H, Nilsson MS, Kiffin R, Sander FE, Lenox B, Rydstrom A, et al. Histamine targets myeloid-derived suppressor cells and improves the anti-tumor efficacy of pd-1/Pd-L1 checkpoint blockade. *Cancer Immunol Immunother* (2019) 68(2):163–74. doi: 10.1007/s00262-018-2253-6

249. Loeuillard E, Yang J, Buckarma E, Wang J, Liu Y, Conboy C, et al. Targeting tumor-associated macrophages and granulocytic myeloid-derived suppressor cells augments pd-1 blockade in cholangiocarcinoma. *J Clin Invest* (2020) 130(10):5380–96. doi: 10.1172/JCI137110

250. Freeman P, Mielgo A. Cancer-associated fibroblast mediated inhibition of Cd8+ cytotoxic T cell accumulation in tumours: Mechanisms and therapeutic opportunities. *Cancers (Basel)* (2020) 12(9):2687. doi: 10.3390/cancers12092687

251. Narra K, Mullins SR, Lee HO, Strzemkowski-Brun B, Magalong K, Christiansen VJ, et al. Phase ii trial of single agent Val-boropro (Talabostat) inhibiting fibroblast activation protein in patients with metastatic colorectal cancer. *Cancer Biol Ther* (2007) 6(11):1691–9. doi: 10.4161/cbt.6.11.4874

252. Kieffer Y, Hocine HR, Gentric G, Pelon F, Bernard C, Bourachot B, et al. Single-cell analysis reveals fibroblast clusters linked to immunotherapy resistance in cancer. *Cancer Discovery* (2020) 10(9):1330–51. doi: 10.1158/2159-8290.CD-19-1384

253. Feig C, Jones JO, Kraman M, Wells RJ, Deonarine A, Chan DS, et al. Targeting Cxcl12 from fap-expressing carcinoma-associated fibroblasts synergizes with anti-Pd-L1 immunotherapy in pancreatic cancer. *Proc Natl Acad Sci U.S.A.* (2013) 110(50):20212–7. doi: 10.1073/pnas.1320318110

254. Hanley CJ, Mellone M, Ford K, Thirdborough SM, Mellows T, Frampton SJ, et al. Targeting the myofibroblastic cancer-associated fibroblast phenotype through inhibition of Nox4. *J Natl Cancer Inst* (2018) 110(1):10920. doi: 10.1093/jnci/djx121

255. Ford K, Hanley CJ, Mellone M, Szyndralewiez C, Heitz F, Wiesel P, et al. Nox4 inhibition potentiates immunotherapy by overcoming cancer-associated fibroblast-mediated Cd8 T-cell exclusion from tumors. *Cancer Res* (2020) 80(9):1846–60. doi: 10.1158/0008-5472.CAN-19-3158

256. Deng L, Liang H, Burnette B, Beckett M, Darga T, Weichselbaum RR, et al. Irradiation and anti-Pd-L1 treatment synergistically promote antitumor immunity in mice. *J Clin Invest* (2014) 124(2):687–95. doi: 10.1172/JCI67313

257. Mondini M, Levy A, Meziani L, Milliat F, Deutsch E. Radiotherapy-immunotherapy combinations - perspectives and challenges. *Mol Oncol* (2020) 14(7):1529–37. doi: 10.1002/1878-0261.12658

258. Teng F, Kong L, Meng X, Yang J, Yu J. Radiotherapy combined with immune checkpoint blockade immunotherapy: Achievements and challenges. *Cancer Lett* (2015) 365(1):23–9. doi: 10.1016/j.canlet.2015.05.012

259. Shui L, Yang X, Li J, Yi C, Sun Q, Zhu H. Gut microbiome as a potential factor for modulating resistance to cancer immunotherapy. *Front Immunol* (2019) 10:2989. doi: 10.3389/fimmu.2019.02989

260. Simpson RC, Shanahan E, Scolyer RA, Long GV. Targeting the microbiome to overcome resistance. *Cancer Cell* (2021) 39(2):151–3. doi: 10.1016/j.ccell.2021.01.016

261. Routy B, Gopalakrishnan V, Daillere R, Zitvogel L, Wargo JA, Kroemer G. The gut microbiota influences anticancer immunosurveillance and general health. *Nat Rev Clin Oncol* (2018) 15(6):382–96. doi: 10.1038/s41571-018-0006-2

262. Derosa L, Routy B, Fidelle M, Iebba V, Alla L, Pasolli E, et al. Gut bacteria composition drives primary resistance to cancer immunotherapy in renal cell carcinoma patients. *Eur Urol* (2020) 78(2):195–206. doi: 10.1016/j.eururo.2020.04.044

263. Messaoudene M, Pidgeon R, Richard C, Ponce M, Diop K, Benlaifaoui M, et al. A natural polyphenol exerts antitumor activity and circumvents anti-Pd-1 resistance through effects on the gut microbiota. *Cancer Discov* (2022) 12(4):1070–87. doi: 10.1158/2159-8290.CD-21-0808

264. Cortes J, Cescon DW, Rugo HS, Nowecki Z, Im SA, Yusof MM, et al. Pembrolizumab plus chemotherapy versus placebo plus chemotherapy for previously untreated locally recurrent inoperable or metastatic triple-negative breast cancer (Keynote-355): A randomised, placebo-controlled, double-blind, phase 3 clinical trial. *Lancet* (2020) 396(10265):1817–28. doi: 10.1016/S0140-6736(20)32531-9

265. Sun JM, Shen L, Shah MA, Enzinger P, Adenis A, Doi T, et al. Pembrolizumab plus chemotherapy versus chemotherapy alone for first-line treatment of advanced oesophageal cancer (Keynote-590): A randomised, placebo-controlled, phase 3 study. *Lancet* (2021) 398(10302):759–71. doi: 10.1016/S0140-6736(21)01234-4

266. Chung HC, Bang YJ, S Fuchs C, Qin SK, Satoh T, Shitara K, et al. First-line Pembrolizumab/Placebo plus trastuzumab and chemotherapy in Her2-positive advanced gastric cancer: Keynote-811. *Future Oncol* (2021) 17(5):491–501. doi: 10.2217/fon-2020-0737

267. Paz-Ares L, Dvorkin M, Chen Y, Reinmuth N, Hotta K, Trukhin D, et al. Durvalumab plus platinum-etoposide versus platinum-etoposide in first-line treatment of extensive-stage small-cell lung cancer (Caspian): A randomised, controlled, open-label, phase 3 trial. *Lancet* (2019) 394(10212):1929–39. doi: 10.1016/S0140-6736(19)32222-6

268. Theelen W, Peulen HMU, Lalezari F, van der Noort V, de Vries JF, Aerts J, et al. Effect of pembrolizumab after stereotactic body radiotherapy vs pembrolizumab alone on tumor response in patients with advanced non-small cell lung cancer: Results of the pembro-rt phase 2 randomized clinical trial. *JAMA Oncol* (2019) 5(9):1276–82. doi: 10.1001/jamaoncol.2019.1478

269. McBride S, Sherman E, Tsai CJ, Baxi S, Aghalar J, Eng J, et al. Randomized phase ii trial of nivolumab with stereotactic body radiotherapy versus nivolumab alone in metastatic head and neck squamous cell carcinoma. *J Clin Oncol* (2021) 39(1):30–7. doi: 10.1200/JCO.20.00290

270. Hodi FS, Chesney J, Pavlick AC, Robert C, Grossmann KF, McDermott DF, et al. Combined nivolumab and ipilimumab versus ipilimumab alone in patients with advanced melanoma: 2-year overall survival outcomes in a multicentre, randomised, controlled, phase 2 trial. *Lancet Oncol* (2016) 17(11):1558–68. doi: 10.1016/S1470-2045(16)30366-7

271. Tawbi HA, Schadendorf D, Lipson EJ, Ascierto PA, Matamala L, Castillo Gutierrez E, et al. Relatlimab and nivolumab versus nivolumab in untreated advanced melanoma. *N Engl J Med* (2022) 386(1):24–34. doi: 10.1056/NEJMoa2109970

272. Goldman JW, Dvorkin M, Chen Y, Reinmuth N, Hotta K, Trukhin D, et al. Durvalumab, with or without tremelimumab, plus platinum-etoposide versus platinum-etoposide alone in first-line treatment of extensive-stage small-cell lung cancer (Caspian): Updated results from a randomised, controlled, open-label, phase 3 trial. *Lancet Oncol* (2021) 22(1):51–65. doi: 10.1016/S1470-2045(20)30539-8

273. Kelly RJ, Lee J, Bang YJ, Almhanna K, Blum-Murphy M, Catenacci DVT, et al. Safety and efficacy of durvalumab and tremelimumab alone or in combination in patients with advanced gastric and gastroesophageal junction adenocarcinoma. *Clin Cancer Res* (2020) 26(4):846–54. doi: 10.1158/1078-0432.CCR-19-2443

274. Rizvi NA, Cho BC, Reinmuth N, Lee KH, Luft A, Ahn MJ, et al. Durvalumab with or without tremelimumab vs standard chemotherapy in first-line treatment of metastatic non-small cell lung cancer: The mystic phase 3 randomized clinical trial. *JAMA Oncol* (2020) 6(5):661–74. doi: 10.1001/jamaoncol.2020.0237

275. Ferris RL, Haddad R, Even C, Tahara M, Dvorkin M, Ciuleanu TE, et al. Durvalumab with or without tremelimumab in patients with recurrent or metastatic head and neck squamous cell carcinoma: Eagle, a randomized, open-label phase iii study. *Ann Oncol* (2020) 31(7):942–50. doi: 10.1016/j.annonc.2020.04.001

276. Postow MA, Sidlow R, Hellmann MD. Immune-related adverse events associated with immune checkpoint blockade. *N Engl J Med* (2018) 378(2):158–68. doi: 10.1056/NEJMra1703481

277. Horvath L, Pircher A. Asco 2020 non-small lung cancer (Nsclc) personal highlights. *Memo* (2021) 14(1):66–9. doi: 10.1007/s12254-020-00673-2

278. Nocera L, Karakiewicz PI, Wenzel M, Tian Z, Shariat SF, Saad F, et al. Clinical outcomes and adverse events after first-line treatment in metastatic renal cell carcinoma: A systematic review and network meta-analysis. *J Urol.* (2022) 207(1):16–24. doi: 10.1097/JU.0000000000002252

279. Powles T, Plimack ER, Soulieres D, Waddell T, Stus V, Gafanov R, et al. Pembrolizumab plus axitinib versus sunitinib monotherapy as first-line treatment of advanced renal cell carcinoma (Keynote-426): Extended follow-up from a randomised, open-label, phase 3 trial. *Lancet Oncol* (2020) 21(12):1563–73. doi: 10.1016/S1470-2045(20)30436-8

280. Reck M, Mok TSK, Nishio M, Jotte RM, Cappuzzo F, Orlandi F, et al. Atezolizumab plus bevacizumab and chemotherapy in non-Small-Cell lung cancer (Impower150): Key subgroup analyses of patients with egfr mutations or baseline liver metastases in a randomised, open-label phase 3 trial. *Lancet Respir Med* (2019) 7(5):387–401. doi: 10.1016/S2213-2600(19)30084-0

281. Galle PR, Finn RS, Qin S, Ikeda M, Zhu AX, Kim TY, et al. Patient-reported outcomes with atezolizumab plus bevacizumab versus sorafenib in patients with unresectable hepatocellular carcinoma (Imbrave150): An open-label, randomised, phase 3 trial. *Lancet Oncol* (2021) 22(7):991–1001. doi: 10.1016/S1470-2045(21)00151-0

282. Motzer RJ, Robbins PB, Powles T, Albiges L, Haanen JB, Larkin J, et al. Avelumab plus axitinib versus sunitinib in advanced renal cell carcinoma: Biomarker analysis of the phase 3 javelin renal 101 trial. *Nat Med* (2020) 26(11):1733–41. doi: 10.1038/s41591-020-1044-8

283. Choueiri TK, Powles T, Burotto M, Escudier B, Bourlon MT, Zurawski B, et al. Nivolumab plus cabozantinib versus sunitinib for advanced renal-cell carcinoma. *N Engl J Med* (2021) 384(9):829–41. doi: 10.1056/NEJMoa2026982

284. Xu Q, Wang J, Sun Y, Lin Y, Liu J, Zhuo Y, et al. Efficacy and safety of sintilimab plus anlotinib for pd-L1-Positive recurrent or metastatic cervical cancer: A multicenter, single-arm, prospective phase ii trial. *J Clin Oncol* (2022) 40(16)1795–1805. doi: 10.1200/JCO.21.02091

frontiers | Frontiers in Immunology

TYPE Original Research
PUBLISHED 16 September 2022
DOI 10.3389/fimmu.2022.933703

OPEN ACCESS

EDITED BY
Dianwen Ju,
Fudan University, China

REVIEWED BY
Benoit Paquette,
University of Sherbrooke, Canada
Xiyun Deng,
Hunan Normal University, China

*CORRESPONDENCE
Lixi Luo
luolixi1987@zju.edu.cn

SPECIALTY SECTION
This article was submitted to Cancer Immunity and Immunotherapy, a section of the journal Frontiers in Immunology

RECEIVED 08 July 2022
ACCEPTED 12 September 2022
PUBLISHED 16 September 2022

CITATION
Luo L, Wei Q, Xu C, Dong M and Zhao W (2022) Immune landscape and risk prediction based on pyroptosis-related molecular subtypes in triple-negative breast cancer.
Front. Immunol. 13:933703.
doi: 10.3389/fimmu.2022.933703

Immune landscape and risk prediction based on pyroptosis-related molecular subtypes in triple-negative breast cancer

Lixi Luo*, Qun Wei, Chenpu Xu, Minjun Dong and Wenhe Zhao

Department of Surgical Oncology, Sir Run Run Shaw Hospital, Zhejiang University School of Medicine, Hangzhou, China

The survival outcome of triple-negative breast cancer (TNBC) remains poor, with difficulties still existing in prognosis assessment and patient stratification. Pyroptosis, a newly discovered form of programmed cell death, is involved in cancer pathogenesis and progression. The role of pyroptosis in the tumor microenvironment (TME) of TNBC has not been fully elucidated. In this study, we disclosed global alterations in 58 pyroptosis-related genes at somatic mutation and transcriptional levels in TNBC samples collected from The Cancer Genome Atlas and Gene Expression Omnibus databases. Based on the expression patterns of genes related to pyroptosis, we identified two molecular subtypes that harbored different TME characteristics and survival outcomes. Then, based on differentially expressed genes between two subtypes, we established a 12-gene score with robust efficacy in predicting short- and long-term overall survival of TNBC. Patients at low risk exhibited a significantly better prognosis, more antitumor immune cell infiltration, and higher expression of immune checkpoints including PD-1, PD-L1, CTLA-4, and LAG3. The comprehensive analysis of the immune landscape in TNBC indicated that alterations in pyroptosis-related genes were closely related to the formation of the immune microenvironment and the intensity of the anticancer response. The 12-gene score provided new information on the risk stratification and immunotherapy strategy for highly heterogeneous patients with TNBC.

KEYWORDS

pyroptosis, tumor microenvironment, triple-negative breast cancer, prognosis, immune checkpoints

Introduction

Breast cancer (BC) is the leading cause of cancer death among women. Triple-negative breast cancer (TNBC), marked by negative expression of estrogen receptor (ER), progesterone receptor (PR), and human epidermal growth factor receptor-2 (HER2), is the most challenging subtype of BC due to its high heterogeneity and lack of effective target therapies (1). Tumor mutation burden (TMB) is higher in TNBC than in other subtypes, suggesting a higher probability of benefits from treatment with immune checkpoint inhibitors (ICIs) (2). Several clinical trials have investigated the feasibility of adding ICIs to chemotherapy in TNBC, and most of these studies focus on inhibitors of the PD-1/PD-L1 pathway. Pembrolizumab, an anti-PD-1 agent, has been demonstrated to be helpful in improving the survival of both metastatic and early stage TNBCs (3, 4). Meanwhile, the anti-PD-L1 agent atezolizumab shows discrepant efficacy in advanced TNBC when combined with paclitaxel or nab-paclitaxel (5, 6). Overexpression of CTLA-4, another immune checkpoint molecule, is observed in breast tumors (7). A single-arm pilot study suggested treatment responses to combined anti-CTLA-4 antibody tremelimumab and anti-PD-L1 durvalumab in three of the total of seven TNBC cases investigated (8). However, the study was terminated due to the low overall response rate that did not meet the required criteria. Currently, randomized trials exploring anti-CTLA-4 treatment in TNBC are ongoing, while no positive results have been reported (9, 10). It is worth mentioning that, compared to other cancers, the TMB or microsatellite instability (MSI) in BC is still notably low (11, 12), resulting in a less dramatic response to immunotherapy. The narrow therapeutic window and ultimate drug resistance also remain to be problems that need to be resolved.

Pyroptosis is a cytolytic and inflammatory form of programmed cell death mediated by proteins from the gasdermin family (13). It is characterized by pore formation and cell swelling, followed by rupture of the plasma membrane and release of cytokines, which trigger inflammatory responses and cell death (14). Increasing evidence reveals various roles for pyroptosis in cancer pathogenesis and progression (15). Pyroptosis that occurs in only a fraction of tumor cells can induce robust antitumor immunity and synergizes with anti-PD-1 blockade (16). Gasdermin E (GSDME) expression is inhibited in many types of cancer, including BC, and tumor GSDME can activate pyroptosis, improving tumor suppression through killer cytotoxic lymphocytes (17). The GSDME promoter was found to be methylated in primary BC tissues with high frequency, and the GSDME methylation status could increase the risk of lymph node metastasis in BC patients (18). In contrast, gasdermin B (GSDMB) is upregulated in breast carcinoma and is correlated with increased tumor cell invasiveness and poor survival in patients (19). Anti-GSDMB antibody loaded onto nanocapsules efficiently reduces the aggressiveness of HER2-positive BC (20).

There are emerging studies suggesting the crosstalk between pyroptosis and the tumor microenvironment (TME) (21). The expression of gasdermin D (GSDMD), accompanied by the upstream components of the NLRP3 inflammasome, is related to the activation of the inflammasome in the tumor. NLRP3 signaling in macrophages drives the establishment of an immune-suppressive TME in pancreatic ductal adenocarcinoma (22). GSDME expression suppresses tumor growth by enhancing the functionality of tumor-infiltrating natural-killer (NK) and CD8+ T lymphocytes (17). Currently, few studies have elucidated the collaborative effects of combined pyroptosis-related genes (PRG) on BC pathogenesis. Given the complex roles of PRGs in cancer, a comprehensive understanding of PGR-mediated TME alterations in TNBC is needed to provide new insights into patients' risk prediction and treatment decision.

This study disclosed the global characteristics of PRG alterations in TNBC and defined two distinct molecular subtypes based on 58 PRGs. Using differentially expressed genes (DEGs) between pyroptosis subtypes, we constructed a 12-gene-based risk score capable of predicting long-term overall survival (OS). A comprehensive characterization of the immune landscape in TNBC was performed based on the risk stratification system, paving the way for the identification of optimal candidates and potential regimens for efficient immunotherapy in TNBC.

Materials and methods

Data sources

Supplementary Figure S1 shows the workflow of this study. BC samples were obtained from The Cancer Genome Atlas (TCGA) (https://portal.gdc.cancer.gov/) and Gene Expression Omnibus (GEO) (https://www.ncbi.nlm.nih.gov/geo/) databases. A total of 1,366 samples were involved in this study (including 113 normal tissues and 1,253 primary BC tumors). The transcriptome profiling of 542 TNBC samples was collected from three cohorts, including 162 samples from the TCGA-BRCA program, 273 from the GSE96058 dataset, and 107 from the GSE58812 dataset. Of these, cases from TCGA-BRCA and GSE96058 were used as the development cohort for differential analysis, risk model establishment, and internal validation, while the GSE58812 dataset acted as an independent external validation cohort. The fragments per kilobase million (FPKM) values in the RNA sequencing data were transformed into transcripts per kilobase million (TPM). Gene expression data derived from both RNA sequencing and microarray were combined, with batch effects removed using the "ComBat" function in R. Clinicopathological information was collected, including patient phenotype (age, menopausal status, stage, and tumor grade) and survival endpoints (vital status, days to the last follow-up, and days to

death). Masked somatic mutation data of 144 TNBC samples and 986 all BC samples were retrieved from the TCGA-BRCA database.

Mutation analysis of PRGs

Fifty-eight PRGs were collected from the "REACTOME_PYROPTOSIS" gene set of the GSEA/MSigDB Team (http://www.broad.mit.edu/gsea/msigdb/) and published papers (23–25), as shown in Supplementary Table S1. The somatic mutations of the 58 PRGs were visualized using the "maftools" and "RCircos" packages in R software.

Identification of differentially expressed PRGs and prognostic PRGs

Package "limma" was used to identify differentially expressed PRGs between normal and TNBC samples. The correlations between PRG expression and OS of the patients were drawn using Kaplan–Meier curves using the "survival" and "survminer" packages.

Consensus clustering of PRGs and functional enrichment

To build a classification of molecular subtypes for TNBC, consensus clustering was performed based on patient PRG expression patterns using the package "ConsensusClusterPlus." The maximum number of clusters, K, was defined as 9 to draw the heatmaps from the consensus matrix. The optimal K was then determined from 2 to 9 according to the consensus matrix heatmap and the cumulative distribution function (CDF) curves. Principal component analysis (PCA) was performed to verify the disparity in pyroptosis transcription profiles among distinct subtypes. Differences in PRG expression levels, clinicopathological characteristics, and OS among different subtypes were compared. The expression of PD-1 and PD-L1 was also analyzed. The Kyoto Encyclopedia of Genes and Genomes (KEGG) signaling pathways in which different subtypes were involved were investigated by gene set variation analysis (GSVA) using the MSigDB curated gene set "c2.cp.kegg.v7.4." The abundance of immune cells infiltrating the TNBC TME was assessed by single-sample gene set enrichment analysis (ssGSEA).

Determination of DEGs among pyroptosis subtypes

DEGs among different pyroptosis subtypes were determined using a "limma" package with a log2-fold change > 1.5 and an adjusted p-value < 0.05. Functional enrichment of these subtype-related DEGs was performed using Gene Ontology (GO) annotation and KEGG pathway analysis with the "clusterProfiler" package.

Development of a DEG-based risk score and determination of prognostic predictors

Univariate Cox regression was conducted to identify OS-related genes from subtype-based DEGs. Consensus clustering, according to the expression of these prognostic DEGs, was conducted to categorize tumors into distinct gene subtypes. Relations between the OS of the patients and the gene subtypes were revealed by Kaplan–Meier curves. The expression patterns of prognostic DEGs among patients with different gene subtypes or different clinicopathological characteristics were visualized using a heatmap. The differential expression of PRGs between gene subtypes was also evaluated. We then randomly partitioned the TNBC samples from the development cohort into a training set (n=218) and a validation set (n=217) to build a risk model for OS of patients, based on the expression of prognostic DEGs related to pyroptosis. To improve the accuracy of the prediction and resolve the problem of overfitting, LASSO regression was used using the "glmnet" package in R. A 10-fold cross-validation for parameter selection of the LASSO model was performed with the minimum criteria (the value of lambda that gives a minimum mean cross-validated error). The candidate genes were finally selected by a multivariate Cox model regression analysis to generate a risk score in the training set. The OS-related risk score was calculated as:

$$Risk\ \ Score = \sum_{i=1}^{n} \beta_i * Exp_i$$

β_i and Exp_i represented the coefficients and expression levels of each candidate gene. Using the median score as a cutoff value, patients were divided into high- and low-risk subgroups. Kaplan–Meier curves were plotted to analyze survival differences between two groups. Receiver operating characteristic (ROC) curves were generated to assess the model efficacy for 2-, 3-, 5-, 7-, or 10-year OS. Both Kaplan–Meier curves and ROC curves were reanalyzed in the validation set and in the whole development set. Comparisons of risk scores between pyroptosis subtypes and gene subtypes are shown in boxplots. Differentially expressed PRGs were analyzed between high- and low-risk groups. Furthermore, 107 TNBC cases from the GSE58812 dataset were used as an independent external validation cohort to test the risk score model.

Tumor immunity analysis based on risk score stratification

CIBERSORT was used with the LM22 signature to assess the abundance of 22 immune cell types in the TME of TNBC between the high- and low-risk groups according to the gene

expression data (https://cibersort.stanford.edu/). Correlations between the risk score and the fractions of 22 immune cells infiltrating the tumor were analyzed separately. The "ESTIMATE" package was used to calculate the scores for tumor purity, the level of stromal cells, and the level of immune cells present in tumor tissues (https://bioinformatics.mdanderson.org/estimate/). The expression of 58 immune checkpoints was evaluated between two risk groups in all sample sets.

Somatic mutation and drug sensitivity analysis between risk groups

The somatic mutation information of the high- and low-risk groups was analyzed using the "maftools" package based on the TNBC cases from TCGA-BRCA dataset. TMB and MSI were compared. The MSI was calculated using the scoring system described in the study from Kautto et al., named Microsatellite Analysis for Normal Tumor InStability (MANTIS), which displayed superior performance compared to the previously published computational tools for MSI detection (26). Using the RNA-based stemness score (RNAss) signature from the UCSC XENA browser, we also investigated the relation between cancer stem cells and the risk score (https://xena.ucsc.edu/). To predict the chemotherapeutic response in TNBC patients of different risk groups, we compared the half maximum inhibitory concentration (IC50) of commonly used chemotherapy drugs through the "pRRophetic" package in R.

Statistical analysis

A two-sided probability value of $p<0.05$ was considered statistically significant. Data processing and data visualization were performed in RStudio (version 2021.09.1 + 372, https://www.rstudio.com/).

Results

Somatic mutation analysis of PRGs

The somatic mutation frequencies of 58 investigated PRGs were significantly higher in patients with TNBC (84.03%) than in all BC cohorts (40.67%) (Figures 1A, B). TP53 was the most frequently mutated PRG, which was seen in 82.64% of TNBC patients (119/144 samples) and in 34.18% of all BC patients (337/986 samples). CASP8 with somatic mutation was found in 2% of TNBC samples.

Copy number variations (CNVs) were detected in all 58 PRGs in both the TNBC set (Figure 1C) and the entire BC set (Figure 1D). Among patients with TNBC, AIM2 showed the highest frequency of increase in copy number (with 36.48% of the TNBC samples showing a higher copy number), followed by NLRP3 (32.08%), CHMP6 (32.08%), GSDMC (28.93%), and GSDMD (23.90%). Copy number loss was discovered more frequently in CASP9 (35.22%), ELANE (30.82%), GPX4 (30.19%), NLRP6 (18.24%), and TIRAP (17.61%). Different patterns of CNV were observed in all BC patients, among which GSDMC, CHMP6, GSDMD, NLRP3, and GSDMB exhibited the highest incidence of increased CNV, while CASP9, IL18, TIRAP, GPX4, and ELANE represented PRGs with the most frequent decrease in CNV. Copy number alteration loci of PRGs on chromosomes in TNBC patients are plotted in Figure 1E.

Identification of differentially expressed PRGs and OS-related PRGs

RNA sequencing data of 162 TNBC samples and 113 normal tissues from TCGA-BRCA were used to investigate differentially expressed PRGs. Different expression levels between cancer and normal samples were detected in 44 of the 58 PRGs (Figure 2A). PRGs showing significant CNV gain, including AIM2, GSDMC, and GSDMD, were significantly upregulated in TNBC samples. Similarly, PRGs with high CNV loss frequency, such as CASP9, ELANE, GPX4, and TIRAP, were also markedly downregulated in TNBC. However, there were other PRGs that showed a discrepancy between copy number alterations and mRNA expression (such as NLRP3 and TP63), indicating that CNV could contribute to the regulation of PRG mRNA levels in TNBC, but was not the only factor involved.

A total of 435 individuals with TNBC from the development cohort (162 cases of TCGA-BRCA and 273 of GSE96058) were included in the subsequent survival analysis. The differential expression of 31 PRGs was significantly associated with OS in these patients (Figures 2B–M, Supplementary Figure S2), suggesting the vital role of pyroptosis in the development of TNBC. The interactive network and the prognostic value of PRGs in TNBC are visualized in Figure 2N.

Classification of pyroptosis subtypes in TNBC

The PRG expression profile of 435 TNBC samples from the development cohort was recovered for consensus clustering analysis. Fifty-six PRGs, detected in both TCGA-BRCA and GSE96058 datasets, were included in the subtype clustering (Supplementary Table S2). The heatmap of the consensus matrix and the CDF curves identified k=2 as the optimal group number, which classified the TNBC samples into group A (n=211) and group B (n=224) (Figure 3A, Supplementary Figure S3). PCA verified the distinct features of the pyroptosis transcriptomes between two groups (Figure 3B). Furthermore,

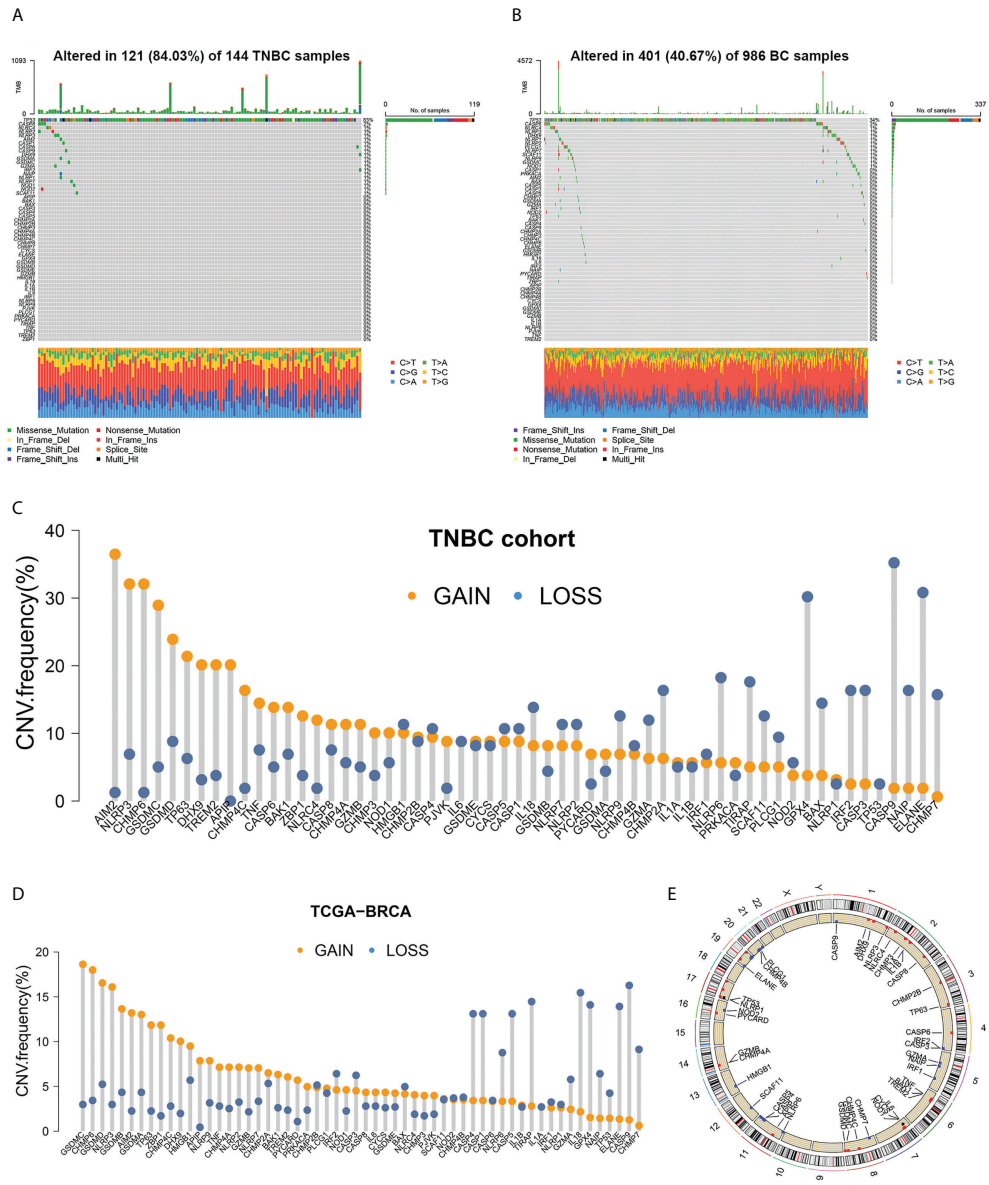

FIGURE 1
Somatic mutation analysis of PRGs. **(A, B)** Mutation frequencies of 58 PRGs in TNBC samples and all BC samples. **(C, D)** Copy number variations of 58 PRGs in TNBC samples and all BC samples. **(E)** Copy number alteration loci of PRGs on 23 chromosomes in TNBC patients.

Kaplan–Meier curves revealed markedly better OS in patients of subtype A than those of subtype B (p=0.003) (Figure 3C). The heatmap in Figure 3D also displayed disparate PRG expression patterns between two pyroptosis subtypes. The clinico pathological characteristics of different subtypes were further compared. The comparative proportions of T1, T2, and T3–T4 tumors between subtypes A and B were 50.98% vs. 39.64%, 41.67% vs. 50.45%, and 7.35% vs. 9.91%, respectively (p=0.040), suggesting that tumors of subtype A tended to have a lower T stage (Figure 3D).

TME characterization of pyroptosis subtypes

GSVA analysis of the canonical pathway of 435 TNBC samples distinguished subtype A as the subtype with dramatically higher enrichment in activated immune pathways, including NOD-like receptor signaling, cytosolic DNA sensing pathway, JAK-STAT signaling pathway, chemokine signaling pathway, cytokine–cytokine receptor interaction, antigen processing and presentation, T-cell receptor signaling, and B-cell

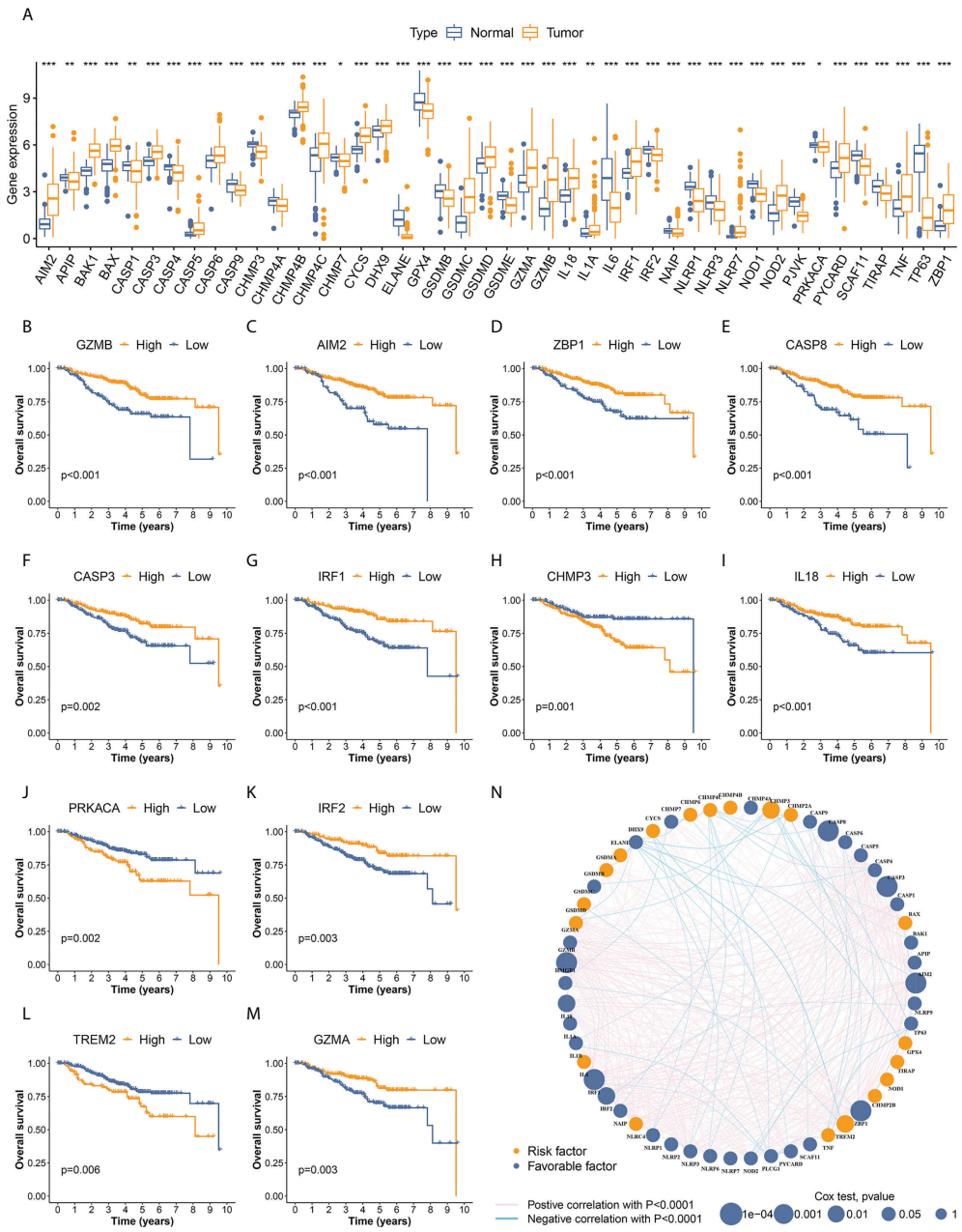

FIGURE 2
Identification of differentially expressed PRGs and OS-related PRGs in TNBC. **(A)** Differential expression was detected in 44 PRGs between cancer and normal samples. **(B–M)** PRGs significantly associated with overall survival of TNBC patients. Twelve OS-related PRGs showed statistical significance in both survival curves and Cox regression analyses. The other 19 OS-related PRGs with p<0.05 in Kaplan–Meier curves are illustrated in Supplementary Figure S1. **(N)** Interactive network and prognostic value of PRGs in TNBC. The thickness of green and pink lines represent the strength of interactive correlation between different PRGs. * p < 0.05, ** p < 0.01, *** p < 0.001.

receptor signaling pathway (Figure 3E). ssGSEA showed that 27 of the total 28 immune cell types investigated had markedly higher infiltration levels in the TME of subtype A compared to that of subtype B (Figure 3F). Furthermore, the expression of both PD-1 and PD-L1 was also remarkably elevated in subtype A samples compared to those of subtype B (Figures 3G, H). These results suggested a stronger immunogenicity and antitumor response in patients with TNBC of subtype A.

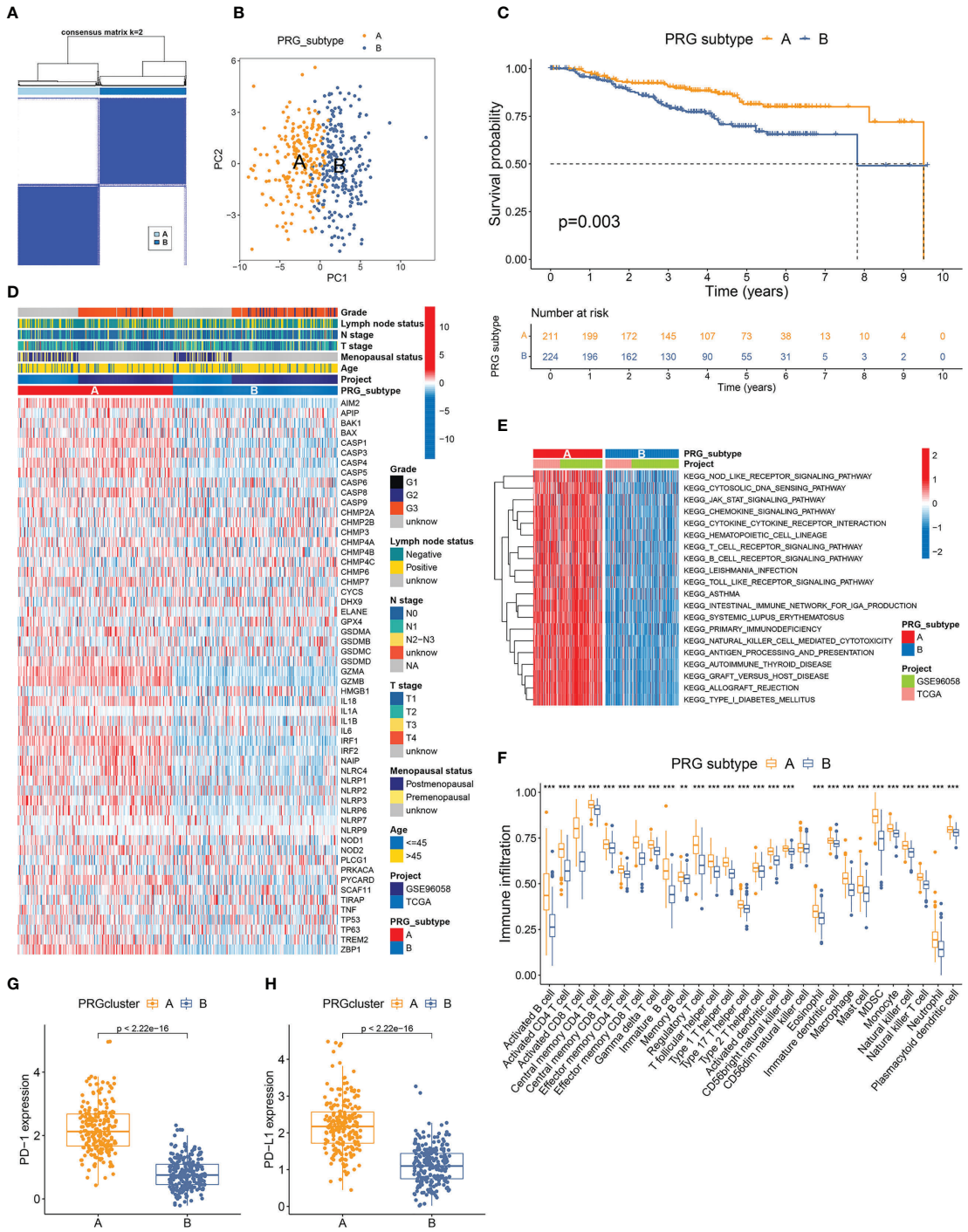

FIGURE 3
Classification and TME features of pyroptosis subtypes in TNBC. **(A)** Two pyroptosis-related subtypes and their correlation area defined by consensus matrix heatmap. Fifty-six PRGs listed in Supplementary Table S2 are included in the subtype clustering analyses. **(B)** PCA analysis verified the remarkable differences in pyroptosis transcription profiles between two subtypes. **(C)** TNBC patients defined as PRG subtype A exhibited significantly better OS compared to those from PRG subtype **(B, D)** Comparisons of PRG expression and clinicopathological features between two PRG subtypes. **(E)** GSVA canonical pathway analysis discovered PRG subtype A samples with dramatically higher enrichment in multiple immune-related pathways. **(F)** Twenty-seven immune cell types showed distinctly higher infiltration levels in the microenvironment of subtype **(A, G, H)** Expressions of PD-1 and PD-L1 were remarkably elevated in subtype A. ** $p < 0.01$, *** $p < 0.001$.

Identification of DEGs among pyroptosis subtypes and development of DEG-based gene subtypes

To disclose the biological differences related to different subtypes of pyroptosis, we identified 844 DEGs between subtype A and B tumors (Supplementary Table S3). The GO annotations of DEGs in terms of their biological process (BP), cellular component (CC), and molecular function (MF) are summarized in Figure 4A. The top-ranked GO terms were mostly related to hemopoietic cells and immunological processes, such as T-cell activation, leukocyte-mediated immunity, external side of the plasma membrane, immune receptor activity, and cytokine receptor activity. The pathway in which most DEGs were involved was the cytokine–cytokine receptor interaction, followed by multiple immune-related pathways including cell adhesion molecules and the chemokine signaling pathway (Figure 4B). The results of functional enrichment highlighted the potential role of pyroptosis in the immune response of TNBC.

To further differentiate TNBC patients with varied DEG patterns, we screened 346 genes that were significantly associated with OS from the 844 DEGs related to pyroptosis by univariate Cox regression (Supplementary Table S4). Among

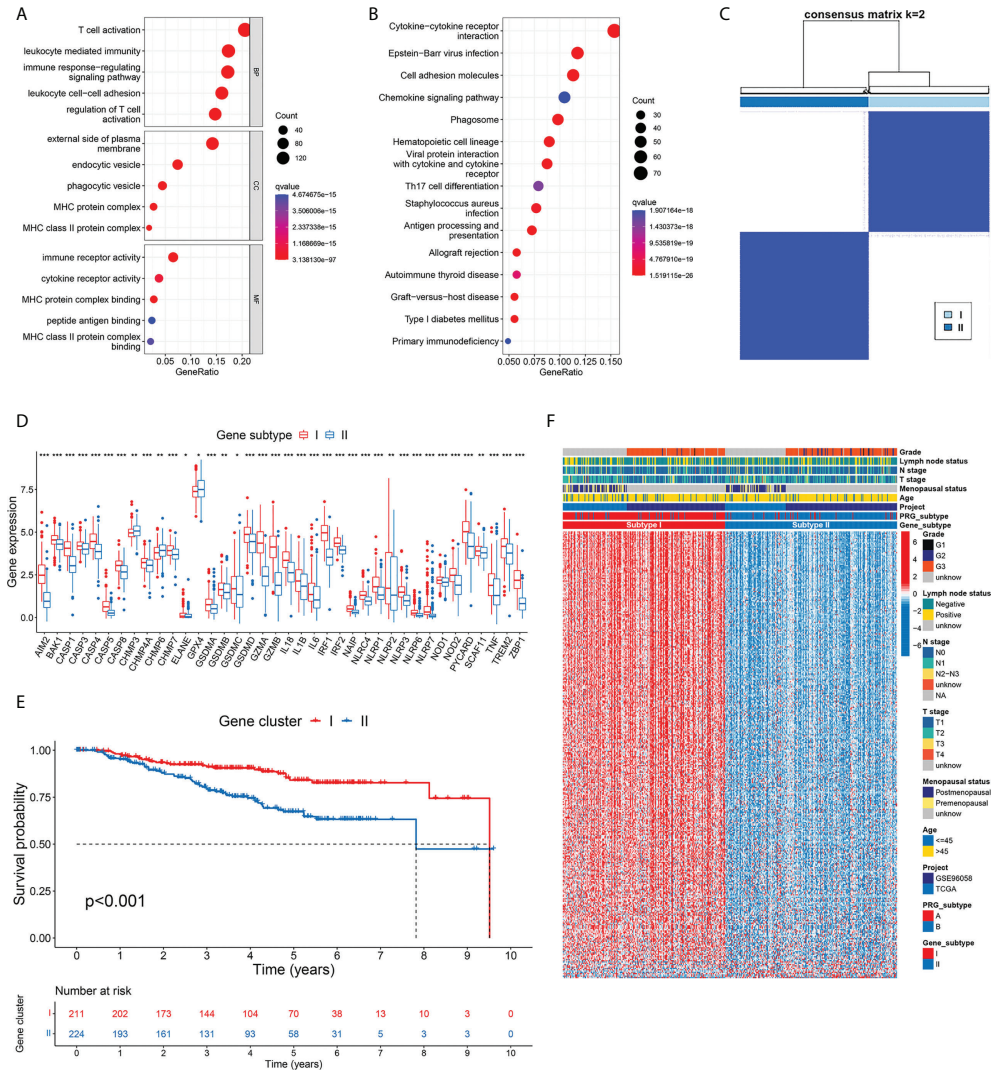

FIGURE 4
Development of gene subtypes based on differentially expressed genes between PRG subtypes. **(A, B)** GO and KEGG enrichment of DEGs identified between two PRG subtypes. **(C)** Consensus matrix heatmap defined two gene subtypes based on 346 prognostic DEGs. **(D)** Thirty-eight PRGs were differentially expressed between two gene subtypes. **(E)** TNBC patients defined as gene subtype I showed significantly better OS. **(F)** Comparison of gene expression and phenotype features between two gene subtypes. * $p < 0.05$, ** $p < 0.01$, *** $p < 0.001$.

them, 337 genes were favorable predictors, while 9 genes were risk factors. According to the 346 prognostic DEGs, we classified patients into two gene subtypes using the consensus clustering algorithm (Figure 4C; Supplementary Figure S4). Gene subtype I included 211 patients, while the other 224 cases were defined as gene subtype II. Consistent with the pyroptosis-based classification, differential expression of PRG was observed between gene subtypes (Figure 4D). Furthermore, survival analysis showed a worse OS in patients with gene subtype II tumors compared to those with gene cluster I tumors ($p<0.001$) (Figure 4E). The comparison of gene expression and phenotype characteristics between two gene subtypes is illustrated in Figure 4F. The pyroptosis subtypes and the gene subtypes exhibited high concordance in the patient distribution. In gene subtype I, 90.05% of the samples were from pyroptosis subtype A, while 90.63% of the samples from gene subtype II were from pyroptosis subtype B. As shown in the heatmap, a large proportion of DEGs, most of which were favorable predictors of OS, showed particularly higher expression in gene subtype I (consistent with the better survival outcome in subtype I patients). Similarly, subtype I samples had lower T stage ($p=0.028$).

Construction of a risk score based on pyroptosis-related prognostic DEGs

Four hundred thirty-five cases from the development cohort (composed of TCGA-BRCA and GSE96058) were included in the risk model exploration. The alluvial diagram in Figure 5A shows the patients' distribution between different subtypes, risk groups, and vital status. The patients were randomly partitioned into a training set (n=218) and an internal validation set (n=217). Based on the survival outcomes of the patients and the expression of 346 prognostic DEGs related to pyroptosis, we selected 12 candidate genes by LASSO regression and cross-validation (Figure 5B; Supplementary Figure S5). Using multivariate Cox regression analysis, we finally used the 12 DEGs (CCL13, CELF2, EFNA3, EGFL6, EMILIN3, FAM20A, FCGR2B, LGALS2, MCOLN2, RARRES1, SERPING1, and SNX10) and established the risk score with their coefficients and expression levels. Nine DEGs (CCL13, CELF2, EGFL6, FAM20A, LGALS2, MCOLN2, RARRES1, SERPING1, and SNX10) were favorable predictors, while the other three were high-risk factors (EFNA3, EMILIN3, and FCGR2B) (Supplementary Table S5). The expression heatmap of the 12 DEGs between the two risk groups is illustrated in Figure 5C.

A median score of −3.898 in the training set was defined as the cutoff value to distinguish high- and low-risk patients (Figure 5D). The vital status plot revealed that patients in the high-risk group had a higher death rate than those in the low-risk group (Figure 5E). The Kaplan–Meier curves confirmed significantly worse OS in high-risk individuals (Figure 5F): comparison of the 2-year OS rates between the high- and low-risk groups was 82.71% vs. 96.92%, while the 5-year OS rates were 53.72% vs. 85.45% ($p<0.001$). In ROC curve analysis, the areas under the curve (AUCs) for the prediction of 2-, 3-, 5-, and 7-year OS were 0.855, 0.834, 0.800, and 0.879, respectively (Figure 5G).

Risk stratification was repeated in the internal validation set using the median score of the training set (Supplementary Figure S6). Vital status and Kaplan–Meier curves verified favorable survival outcomes in the low-risk group with p-value <0.001 (Supplementary Figures S7, 8). The AUCs for the 2-, 3-, 5-, and 10-year OS prediction were 0.644, 0.719, 0.736, and 0.757, respectively, in the internal validation set (Supplementary Figure S9). Furthermore, differential expression of 32 PRGs was detected between high- and low-risk groups among all patients in the development cohort (Figure 5H). Among the 435 individuals in the entire development cohort, patients from both pyroptosis subtype A and gene subtype I, which represented activated cancer immunity and better OS, had a markedly lower risk score compared to subtype B and subtype II, respectively ($p<0.001$ in both tests) (Figures 5I, J), suggesting that the lower risk score could be associated with upregulated immune defense in the microenvironment of TNBC.

To further validate the prognostic value of the risk model, we performed the risk score calculation in an independent external validation cohort (GSE58812). A better long-term OS was observed in low-risk cases ($p=0.025$, Supplementary Figure S10), who had a significantly higher 5- and 10-year OS rate compared to high-risk patients (81.26% vs. 69.47 at 5 years, 78.80% vs. 59.47% at 10 years). The AUC for the prediction of OS at 3, 5, 7, and 10 years were 0.714, 0.766, 0.721, and 0.725, respectively (Supplementary Figure S11), demonstrating good performance of the 12-DEG-based risk score in the prediction of long-term prognosis for patients with TNBC.

Evaluation of tumor immune microenvironment based on risk stratification

To explore tumor immunity and the microenvironment in TNBC from different risk groups, we analyzed the correlation between risk score and immune cell abundance using the CIBERSORT algorithm. The risk score was positively related to the fraction of three non-activated or pro-tumorigenic cell types (resting CD4+ memory T cells, M0 macrophages, and M2 macrophages) and was negatively correlated with seven types of antitumor immune cell types (CD8+ T cells, gamma delta T cells, follicular helper T cells, activated CD4+ memory T cells, memory B cells, M1 macrophages, and activated dendritic cells) (Figure 6A). The 22 immune cell types analyzed exhibited a statistically significant correlation with at least one of the 12 DEGs of the scoring model (Figure 6B). The results of low-risk

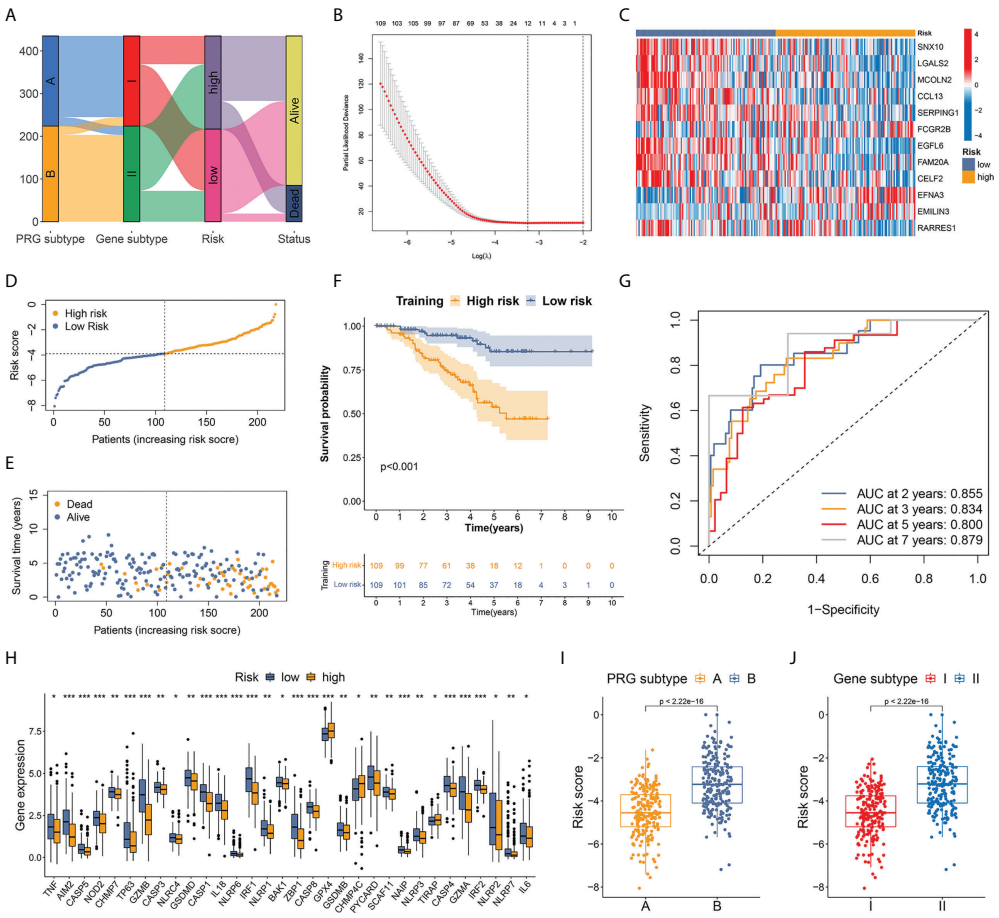

FIGURE 5
Establishment of a risk score based on pyroptosis-related prognostic DEGs. **(A)** Alluvial diagram of patients' distribution between different subtypes, risk groups, and vital status. **(B)** OS-related DEGs identified by univariate Cox analysis were screened by LASSO regression. **(C)** Expression heatmap of the 12 hub DEGs between two risk groups. **(D)** Risk score distribution in patients from training set. A median score of −3.898 was defined as the cutoff value. **(E)** Vital status plot showed higher death rate in patients from high-risk group in training set. **(F)** TNBC patients from high-risk group had markedly worse OS than low-risk patients. **(G)** AUC of ROC curves showed good performance of the 12-gene-based risk score in predicting 2-, 3-, 5-, and 7-year OS for patients in training set. **(H)** Differential expression of 32 PRGs between high- and low-risk groups. **(I, J)** Patients from both pyroptosis subtype A and gene subtype I, which represented activated anti-tumor immunity and better OS, had significantly lower risk score compared to subtype B and subtype II. * $p < 0.05$, ** $p < 0.01$, *** $p < 0.001$.

score samples with high abundance of antitumor immune cells were consistent with the finding that low-risk patients were more likely to exist in immune-activated subtypes.

The "ESTIMATE" package was utilized to calculate the TME score, containing a stromal score (capturing the presence of stromal cells in tumor tissue), an immune score (representing the infiltration of immune cells), and an ESTIMATE score (a combination of stromal and immune scores that inferred tumor purity). TNBC patients from the low-risk group scored higher in all three fields (Figure 6C), indicating a lower tumor purity with higher infiltration of both stromal cells and immune cells. Furthermore, the expression of immune checkpoints between different risk groups was compared. Thirty-three immune checkpoints, including PD-1 (PDCD1), PD-L1 (CD274), CTLA-4, and LAG3, showed markedly upregulated levels in low-risk samples (Figure 6D), implying better response to immunotherapy for low-risk patients with TNBC.

MSI and mutation analysis

The MSI status was investigated between the risk groups. More than 95% of patients with TNBC were defined as microsatellite stable (MSS) regardless of risk stratification (Figure 7A), consistent with previous reports that MSI incidence was rarely observed in BC compared to other types of cancer (12, 27). The MSI score values did not have statistical correlation with the pyroptosis-related risk scores (Figure 7B, p=0.33), and no difference in the distribution of the risk score was observed between the MSI and MSS cases (Supplementary

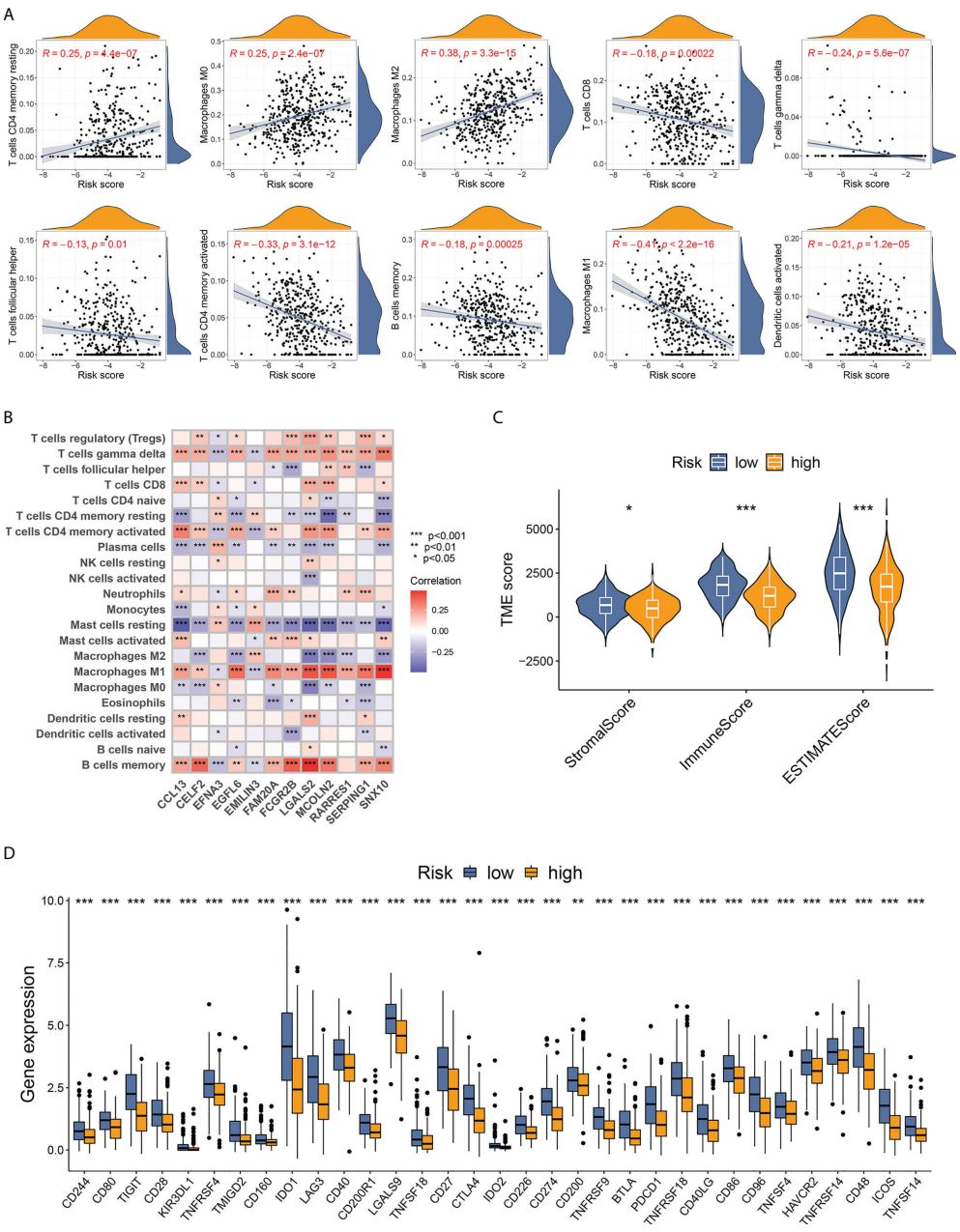

FIGURE 6
Evaluation of TME features based on the 12-DEG risk score. **(A)** Correlation between immune cell infiltrating fractions and the 12-DEG-based risk scores in TNBC samples. **(B)** Correlation between the 12 DEGs from the scoring system and the abundance of 22 analyzed immune cell types. **(C)** TNBC samples from low-risk patients showed higher stromal, immune, and ESTIMATE scores, indicating lower tumor purity with more stromal cells and immune cells in TME. **(D)** A total of 33 immune checkpoints were upregulated in low-risk TNBC patients. * p < 0.05, ** p < 0.01, *** p<0.001.

Figure S12). A trend of higher RNAss was observed with increasing risk score, while no statistical significance was observed (Figure 7C).

The TMB level was low in patients with TNBC and in all patients with BC (Supplementary Figure S13). No differences in TMB were observed between the two groups (Figure 7D). The waterfall graphs (Figures 7E, F) represented the characteristics of the somatic mutation between high- and low-risk individuals from the development cohort. A total of 143 patients with mutational data from TCGA-BRCA program were involved in the analysis. TP53, TTN, PIK3CA, PTEN, KMT2D, MUC16, MUC4, FAT3, CSMD3, and MUC17 ranked the top 10 most

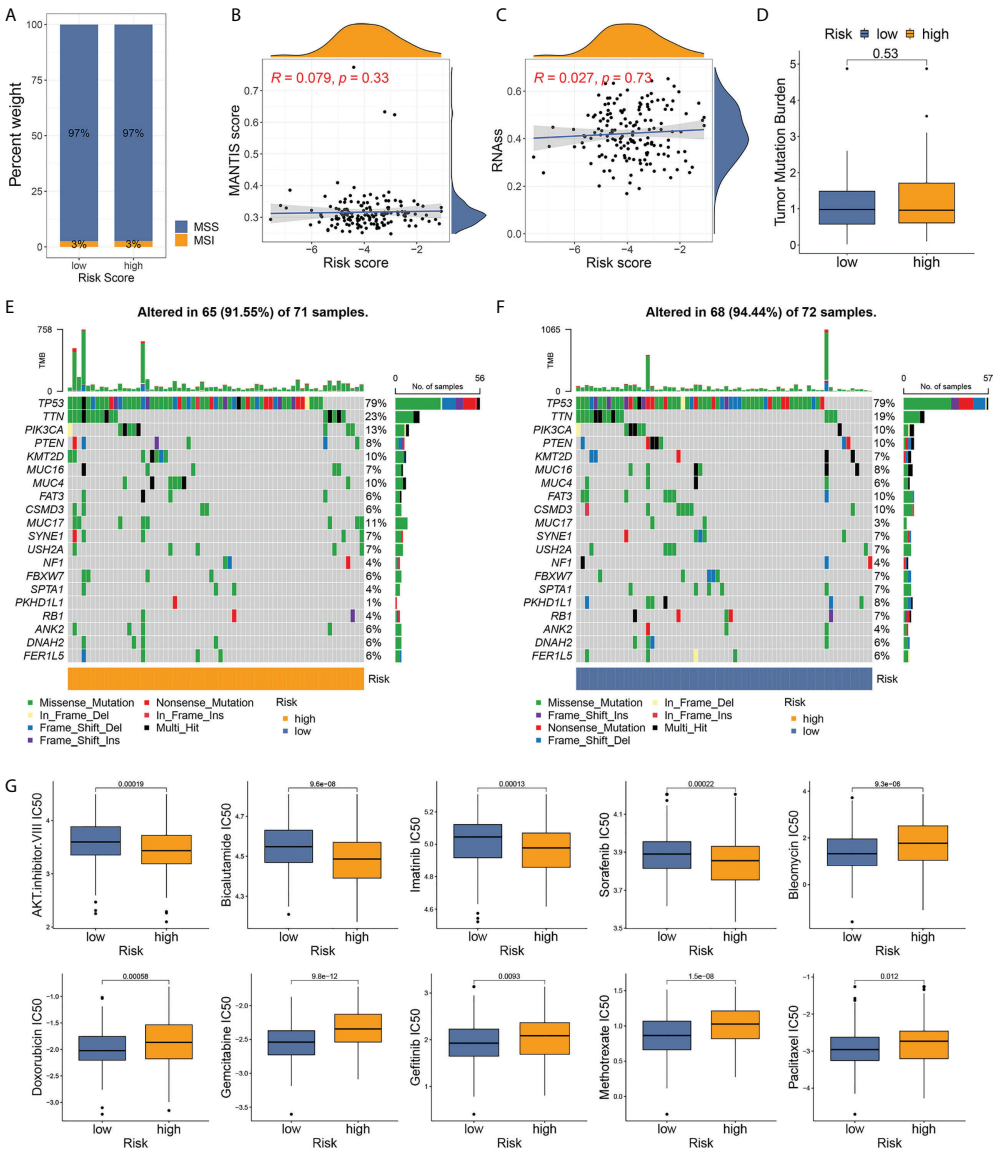

FIGURE 7
Analyses of microsatellite instability, somatic mutation, and drug susceptibility based on risk stratification. **(A)** Distribution of MSI incidence among high- and low-risk patients. **(B)** Correlation between MSI score and risk score of TNBC samples. **(C)** Correlation between RNA stemness score and risk score. **(D)** Comparison of TMB between risk groups. **(E, F)** Somatic mutation frequencies in high- and low-risk TNBC tumors. **(G)** Drug susceptibility analyses (IC50) of commonly used chemotherapy reagents between high- and low-risk patients.

frequently mutated genes in both groups. Among them, a higher mutation rate of TTN, PIK3CA, KMT2D, MUC4, and MUC17 was observed in high-risk patients.

Drug sensitivity analysis

To select the optimal treatment for patients with TNBC, we evaluated the susceptibility of commonly used chemotherapy drugs among high- and low-risk cases. Patients at high risk were more sensitive to the AKT inhibitor VIII, bicalutamide, imatinib, and sorafenib, while low-risk patients in low-risk groups had lower IC50 for bleomycin, doxorubicin, gemcitabine, gefitinib, methotrexate, and paclitaxel (Figure 7G). The drug susceptibility results implied that the classic regimen of chemotherapy based on taxane or anthracycline for BC could be avoided in patients with high-risk TNBC.

Discussion

Recent studies have unraveled the crucial role of genes associated with pyroptosis in breast tumor immunity, most of which elucidate the pro- or antitumor mechanism of a single PRG (28–30). Few studies have focused on the collaborative effects of multiple PRGs on the immune microenvironment specifically in TNBC. In the present study, we disclosed genetic alterations and expression patterns of more than 50 PRGs in patients with TNBC. It is worth mentioning that TP53 gene, mutated in over half of all human malignancies (31), showed frequent mutation (82.64%) in TNBC in this study, which was concordant with previous research results that TNBC had the highest prevalence of TP53 mutation among all breast cancers (32). However, the somatic mutation of TP53 did not cause its alteration in measured expression levels in TNBC compared to normal tissues (as shown in Figure 2A, TP53 was not among the differentially expressed PRGs). The role of TP53 in pyroptosis has not been fully studied. Expression of GSDME could be induced by p53, a tumor suppressor protein encoded by TP53 (33). Zhang et al. also discovered that the upregulation of p53 in non-small-cell lung cancer could prompt pyroptosis and produce antitumor effects (34). Further studies are needed to explore the association between TP53 mutation and pyroptosis in TNBC.

Based on PRG expression profiling, we identified two pyroptosis subtypes that harbored distinct characteristics of the TME and survival outcomes. Patients with pyroptosis subtype A had a lower T stage and notably better OS compared to patients with subtype B tumors. Additionally, subtype A TNBC samples exhibited fully activated immune microenvironments, with significantly higher infiltration levels of 27 types of immune cells, including B cells, CD4+ and CD8+ T cells, gamma delta T cells, and macrophages. Activation of multiple immune-related pathways was also detected in subtype A tumors, including NOD-like receptor signaling, chemokine signaling pathway, cytokine–cytokine receptor interaction, antigen processing and presentation, T-cell receptor signaling, and B-cell receptor signaling pathway. Furthermore, transcriptome profiling differed dramatically between pyroptosis subtypes, and DEGs identified between two subtypes were involved in immunological processes such as T-cell activation and immune receptor activity. Using the expression of DEGs associated with survival, we further classified TNBC patients into two gene subtypes. More than 97% of OS-related DEGs were survival benefiting, and most were distinctively elevated in gene subtype I. Furthermore, gene subtype I showed a high concordance in patient distribution with pyroptosis subtype A and a longer OS compared to subtype II. The above findings revealed that PRG alterations were closely related to the activation of the cancer immune microenvironment and the intensity of the antitumor response, which could lead to significant changes in OS of TNBC patients.

We utilized the pyroptosis-related prognostic DEGs and constructed a 12-gene-based score with reliable performance and robust efficacy in risk prediction. Remarkable differences were observed between high- and low-risk patients with respect to short- and long-term prognosis, TME characteristics, immune checkpoint expression, somatic mutation patterns, MSI scores, and susceptibility to chemotherapy.

Innate and adaptive immune cells in the TME modulate cancer progression and the therapeutic response (35). Evidence has shown the vital role of pyroptosis in maintaining the diversity and complexity of TME in breast tumors (36). Meanwhile, cytotoxic T cells and helper T cells are required for pyroptosis-induced tumor regression (16). In this study, TNBC samples from different pyroptosis subtypes and risk groups differed distinctly in the degree of immune cell infiltration. The presence of tumor-infiltrating lymphocytes (TILs) is predictive of a better response to immunotherapy and a favorable prognosis in BC (37–40). CD8+ T-cell infiltration in BC is independently associated with a reduced relative risk of cancer-related death (41), while TNBCs with CD8 positivity have greater possibilities to benefit from immunotherapy (42). These findings correspond to our results of more CD8+ T cells in the TME of pyroptosis subtype A and low-risk group that had higher expression of PD-1 and PD-L1 and better OS. Functional follicular helper T cells (Tfh) oriented by T-helper 1 (Th1) cells can promote humoral and cytotoxic immune responses in human breast cancer (43), and the presence of CXCL13-producing Tfh cells in tertiary lymphoid structures (TLS) of breast tumors robustly predicts positive clinical outcomes (44). Gamma delta T cells target tumor cells in TNBC (45), and their numbers in TME are positively related to the immunotherapy response of patients with advanced BC (46). Activated CD4+ memory T cells are also related to better survival in different cancer types (47–49). In this study, the above three types of T cells showed higher infiltration in subtype A patients and patients with low scores, indicating the potential of our pyroptosis-related risk score to identify TNBCs with greater sensitivity to immunotherapy. Tumor-infiltrating B cells (TIL-B) are another key component of TILs. TIL-B functions in anti-BC responses through antibody production, Th1 responses, and antigen presentation (50). CXCL13-producing Tfh cells can promote memory B-cell differentiation, thus facilitating humoral immune defense in BC (51). Hu et al. reported that memory B-cell transcription signatures were associated with improved overall and disease-free survival in patients with BC (52). Furthermore, memory B cells within TLS are associated with an improved response to immune checkpoint blockade (53). The sustained presence of memory B cells in TNBC is required for the control of myeloid-derived suppressor cells and for the durable efficacy of ICI treatment (54). Consistent with existing evidence, we observed a higher proportion of memory B cells within subtype A tumors and low-score samples, suggesting the role of memory B cells as an indicator of prognosis and ICI response in TNBC. Subpopulations of macrophage exhibit different functions in TME. Macrophages of the M1

phenotype, reprogrammed with the D2 dopamine receptor, can induce pyroptosis of GSDME-executed breast tumor cells (55). In our study, patients in the low-risk group, who had increased expression of nearly 30 PRGs compared to high-risk patients, showed a higher abundance of M1 macrophages in TME, suggesting the crosstalk between pyroptosis and macrophage-mediated cancer immunity. In contrast, M2 macrophages, the other polarized phenotype, are immunosuppressive and pro-tumorigenic. Zhang et al. revealed that TNBC cells induced an elevation of YAP expression in macrophages, which polarized macrophages to the M2 phenotype and increased the pro-metastatic potential of cancer cells *via* MCP-1/CCR2 pathway (56). In line with previous studies, we discovered a positive correlation between the increase in the risk score and the proportion of M2 macrophages in the immune microenvironment of TNBC, while the presence of M1 macrophages was negatively associated with the value of the risk score in patients. Dendritic cells, which are critical for T-cell activation and immunosurveillance in BC (57), also showed a lower infiltration rate as the risk score increased according to our findings. The correlation between immune cell abundance and pyroptosis-related risk stratification in our study implied the pivotal role of pyroptosis in shaping an activated antitumor microenvironment in TNBC.

BC has been defined as immunologically "cold" due to low T-cell infiltration and inefficient T-cell priming compared to other malignancies (58, 59). Non-synonymous DNA mutations, capable of increasing the presence of neoantigens and inducing the immune cell response, are also found with relatively low burden in breast tumors (60, 61). Despite the non-immunogenic nature, the magnitude of TILs varies within and between BC subtypes (37, 62). Increasing evidence has revealed that TNBC patients, previously termed the most aggressive subtype with a poor prognosis, have a higher abundance of TIL than non-TNBC patients, which could contribute to better survival after ICI treatment (37, 63, 64). However, extensive heterogeneity of the TME and biological behavior still exists within the TNBC cell population. In the present study, we identified individuals with "hot" immune status from TNBC patients based on the clustering of pyroptosis-related subtypes and stratification of risk scores. In addition to increased infiltration of tumor suppressor immune cells in TME, lower tumor purity calculated by the ESTIMATE algorithm was also observed in low-risk patients. A favorable OS has been found in patients with a high stromal score and an immune score in other cancer types (65). Similarly, our findings showed that TNBCs with low-risk score presented a higher immune score and lower tumor purity than high-risk cases. Hou et al. has discovered that PD-L1 can mediate GSDMC expression and trigger pyroptosis in BC cells (66). Beyond that, little is known about the interaction between pyroptosis and PD-1/PD-L1 function. In this study, we demonstrated higher expression of PD-1 and PD-L1 in both the pyroptosis subtype A and low-risk group. In addition, there were an additional 31 immune checkpoints showing a significantly higher level in low-risk-score TNBC, suggesting the ability of the pyroptosis-related risk score to predict the response of ICI therapy in TNBC. The results also provided a potential strategy of blocking other immune checkpoints for early-stage TNBC, including anti-CTLA-4 reagents, which are currently being used in mouse experiments and clinical trials for advanced BC (10, 67, 68). TMB and MSI predict a stronger response to ICI and prolonged survival in colorectal cancer, non-small cell lung cancer, and melanoma (69–72). However, no differences in TMB or MSI were detected between two risk groups, possibly due to the rare incidence of non-synonymous mutations and mismatch repair in BC patients (11, 12, 27). In line with existing research, the low-TMB/low-MSI nature of BC discovered in our study suggested that better predictive biomarkers for response to immunotherapy are needed for TNBC patients. Our findings also indicated the capacity of our scoring model to identify immune "hot" cases among the low-TMB/low-MSI TNBC population.

The major limitation of this study was that the data used for the analyses were derived from public databases, and some clinicopathological information, including patients' history of systemic treatment, was unavailable. Prospective studies and exploratory experiments are needed to further validate the efficacy of this pyroptosis-based risk stratification model.

Data availability statement

The datasets presented in this study can be found in online repositories. The names of the repository/repositories and accession number(s) can be found in the article/Supplementary Material.

Author contributions

LL and WZ designed and organized the study. LL, QW, and CX carried out bioinformatics analyses and drew figures. LL drafted the manuscript. QW and MD participated in the manuscript editing. All authors contributed to the article and approved the submitted version.

Funding

This work was supported by Zhejiang Provincial Natural Science Foundation of China (No. LQ19H160034) and Medical Health Science and Technology Project of Zhejiang Provincial Health Commission, China (No. 2018KY485).

Conflict of interest

The authors declare that the research was conducted in the absence of any commercial or financial relationships that could be construed as a potential conflict of interest.

Publisher's note

All claims expressed in this article are solely those of the authors and do not necessarily represent those of their affiliated organizations, or those of the publisher, the editors and the reviewers. Any product that may be evaluated in this article, or claim that may be made by its manufacturer, is not guaranteed or endorsed by the publisher.

Supplementary material

The Supplementary Material for this article can be found online at: https://www.frontiersin.org/articles/10.3389/fimmu.2022.933703/full#supplementary-material

References

1. Bianchini G, De Angelis C, Licata L, Gianni L. Treatment landscape of triple-negative breast cancer - expanded options, evolving needs. *Nat Rev Clin Oncol* (2022) 19(2):91–113. doi: 10.1038/s41571-021-00565-2

2. Barroso-Sousa R, Jain E, Cohen O, Kim D, Buendia-Buendia J, Winer E, et al. Prevalence and mutational determinants of high tumor mutation burden in breast cancer. *Ann Oncol* (2020) 31(3):387–94. doi: 10.1016/j.annonc.2019.11.010

3. Cortes J, Cescon DW, Rugo HS, Nowecki Z, Im SA, Yusof MM, et al. Pembrolizumab plus chemotherapy versus placebo plus chemotherapy for previously untreated locally recurrent inoperable or metastatic triple-negative breast cancer (Keynote-355): A randomised, placebo-controlled, double-blind, phase 3 clinical trial. *Lancet* (2020) 396(10265):1817–28. doi: 10.1016/s0140-6736(20)32531-9

4. Schmid P, Cortes J, Pusztai L, McArthur H, Kummel S, Bergh J, et al. Pembrolizumab for early triple-negative breast cancer. *N Engl J Med* (2020) 382 (9):810–21. doi: 10.1056/NEJMoa1910549

5. Miles D, Gligorov J, Andre F, Cameron D, Schneeweiss A, Barrios C, et al. Primary results from Impassion131, a double-blind, placebo-controlled, randomised phase iii trial of first-line paclitaxel with or without atezolizumab for unresectable locally Advanced/Metastatic triple-negative breast cancer. *Ann Oncol* (2021) 32(8):994–1004. doi: 10.1016/j.annonc.2021.05.801

6. Schmid P, Adams S, Rugo HS, Schneeweiss A, Barrios CH, Iwata H, et al. Atezolizumab and nab-paclitaxel in advanced triple-negative breast cancer. *N Engl J Med* (2018) 379(22):2108–21. doi: 10.1056/NEJMoa1809615

7. Kassardjian A, Shintaku PI, Moatamed NA. Expression of immune checkpoint regulators, cytotoxic T lymphocyte antigen 4 (Ctla-4) and programmed death-ligand 1 (Pd-L1), in female breast carcinomas. *PloS One* (2018) 13(4):e0195958. doi: 10.1371/journal.pone.0195958

8. Santa-Maria CA, Kato T, Park JH, Kiyotani K, Rademaker A, Shah AN, et al. A pilot study of durvalumab and tremelimumab and immunogenomic dynamics in metastatic breast cancer. *Oncotarget* (2018) 9(27):18985–96. doi: 10.18632/oncotarget.24867

9. McArthur HL, Comen EA, Bryce Y, Solomon SB, Leal JHS, Abaya CD, et al. A single-arm, phase 2 study of perioperative ipilimumab, nivolumab, and cryoablation in women with hormone receptor-negative, Her2-negative, early-Stage/Resectable breast cancer. *J Clin Oncol* (2022) 40(16_suppl):TPS617–TPS. doi: 10.1200/JCO.2022.40.16_suppl.TPS617

10. Kyte JA, Andresen NK, Russnes HG, Fretland SØ, Falk RS, Lingjærde OC, et al. Icon: A randomized phase iib study evaluating immunogenic chemotherapy combined with ipilimumab and nivolumab in patients with metastatic hormone receptor positive breast cancer. *J Transl Med* (2020) 18(1):269. doi: 10.1186/s12967-020-02421-w

11. Ding H, Zhao J, Zhang Y, Wang G, Cai S, Qiu F. Tumor mutational burden and prognosis across pan-cancers. *Ann Oncol* (2018) 29:viii16–viii7. doi: 10.1093/annonc/mdy269.055

12. Ding L, Bailey MH, Porta-Pardo E, Thorsson V, Colaprico A, Bertrand D, et al. Perspective on oncogenic processes at the end of the beginning of cancer genomics. *Cell* (2018) 173(2):305–20.e10. doi: 10.1016/j.cell.2018.03.033

13. Broz P, Pelegrin P, Shao F. The gasdermins, a protein family executing cell death and inflammation. *Nat Rev Immunol* (2020) 20(3):143–57. doi: 10.1038/s41577-019-0228-2

14. Liu X, Zhang Z, Ruan J, Pan Y, Magupalli VG, Wu H, et al. Inflammasome-activated gasdermin d causes pyroptosis by forming membrane pores. *Nature* (2016) 535(7610):153–8. doi: 10.1038/nature18629

15. Xia X, Wang X, Cheng Z, Qin W, Lei L, Jiang J, et al. The role of pyroptosis in cancer: Pro-cancer or pro-"Host"? *Cell Death Dis* (2019) 10(9):650. doi: 10.1038/s41419-019-1883-8

16. Wang Q, Wang Y, Ding J, Wang C, Zhou X, Gao W, et al. A bioorthogonal system reveals antitumour immune function of pyroptosis. *Nature* (2020) 579 (7799):421–6. doi: 10.1038/s41586-020-2079-1

17. Zhang Z, Zhang Y, Xia S, Kong Q, Li S, Liu X, et al. Gasdermin e suppresses tumour growth by activating anti-tumour immunity. *Nature* (2020) 579 (7799):415–20. doi: 10.1038/s41586-020-2071-9

18. Kim MS, Lebron C, Nagpal JK, Chae YK, Chang X, Huang Y, et al. Methylation of the Dfna5 increases risk of lymph node metastasis in human breast cancer. *Biochem Biophys Res Commun* (2008) 370(1):38–43. doi: 10.1016/j.bbrc.2008.03.026

19. Hergueta-Redondo M, Sarrio D, Molina-Crespo A, Megias D, Mota A, Rojo-Sebastian A, et al. Gasdermin-b promotes invasion and metastasis in breast cancer cells. *PLoS One* (2014) 9(3):e90099. doi: 10.1371/journal.pone.0090099

20. Molina-Crespo A, Cadete A, Sarrio D, Gamez-Chiachio M, Martinez L, Chao K, et al. Intracellular delivery of an antibody targeting gasdermin-b reduces Her2 breast cancer aggressiveness. *Clin Cancer Res* (2019) 25(15):4846–58. doi: 10.1158/1078-0432.CCR-18-2381

21. Scarpitta A, Hacker UT, Buning H, Boyer O, Adriouch S. Pyroptotic and necroptotic cell death in the tumor microenvironment and their potential to stimulate anti-tumor immune responses. *Front Oncol* (2021) 11:731598. doi: 10.3389/fonc.2021.731598

22. Daley D, Mani VR, Mohan N, Akkad N, Pandian G, Savadkar S, et al. Nlrp3 signaling drives macrophage-induced adaptive immune suppression in pancreatic carcinoma. *J Exp Med* (2017) 214(6):1711–24. doi: 10.1084/jem.20161707

23. Li X-Y, Zhang L-Y, Li X-Y, Yang X-T, Su L-X. A pyroptosis-related gene signature for predicting survival in glioblastoma. *Front Oncol* (2021) 11:697198. doi: 10.3389/fonc.2021.697198

24. Chen W, Zhang W, Zhou T, Cai J, Yu Z, Wu Z. A newly defined pyroptosis-related gene signature for the prognosis of bladder cancer. *Int J Gen Med* (2021) 14:8109–20. doi: 10.2147/IJGM.S337735

25. Xu D, Ji Z, Qiang L. Molecular characteristics, clinical implication, and cancer immunity interactions of pyroptosis-related genes in breast cancer. *Front Med (Lausanne)* (2021) 8:702638. doi: 10.3389/fmed.2021.702638

26. Kautto EA, Bonneville R, Miya J, Yu L, Krook MA, Reeser JW, et al. Performance evaluation for rapid detection of pan-cancer microsatellite instability with mantis. *Oncotarget* (2017) 8(5):7452–63. doi: 10.18632/oncotarget.13918

27. Wen YH, Brogi E, Zeng Z, Akram M, Catalano J, Paty PB, et al. DNA Mismatch repair deficiency in breast carcinoma: A pilot study of triple-negative and non-Triple-Negative tumors. *Am J Surg Pathol* (2012) 36(11):1700–8. doi: 10.1097/PAS.0b013e3182627787

28. Faria SS, Costantini S, de Lima VCC, de Andrade VP, Rialland M, Cedric R, et al. Nlrp3 inflammasome-mediated cytokine production and pyroptosis cell death in breast cancer. *J BioMed Sci* (2021) 28(1):26. doi: 10.1186/s12929-021-00724-8

29. An H, Heo JS, Kim P, Lian Z, Lee S, Park J, et al. Tetraarsenic hexoxide enhances generation of mitochondrial ros to promote pyroptosis by inducing the activation of caspase-3/Gsdme in triple-negative breast cancer cells. *Cell Death Dis* (2021) 12(2):159. doi: 10.1038/s41419-021-03454-9

30. Tamura Y, Morikawa M, Tanabe R, Miyazono K, Koinuma D. Anti-pyroptotic function of tgf-beta is suppressed by a synthetic dsrna analogue in

triple negative breast cancer cells. *Mol Oncol* (2021) 15(5):1289–307. doi: 10.1002/1878-0261.12890

31. Marei HE, Althani A, Afifi N, Hasan A, Caceci T, Pozzoli G, et al. P53 signaling in cancer progression and therapy. *Cancer Cell Int* (2021) 21(1):703. doi: 10.1186/s12935-021-02396-8

32. Shi Y, Jin J, Ji W, Guan X. Therapeutic landscape in mutational triple negative breast cancer. *Mol Cancer* (2018) 17(1):99. doi: 10.1186/s12943-018-0850-9

33. Masuda Y, Futamura M, Kamino H, Nakamura Y, Kitamura N, Ohnishi S, et al. The potential role of Dfna5, a hearing impairment gene, in P53-mediated cellular response to DNA damage. *J Hum Genet* (2006) 51(8):652–64. doi: 10.1007/s10038-006-0004-6

34. Zhang T, Li Y, Zhu R, Song P, Wei Y, Liang T, et al. Transcription factor P53 suppresses tumor growth by prompting pyroptosis in non-Small-Cell lung cancer. *Oxid Med Cell Longev* (2019) 2019:8746895. doi: 10.1155/2019/8746895

35. Hinshaw DC, Shevde LA. The tumor microenvironment innately modulates cancer progression. *Cancer Res* (2019) 79(18):4557–66. doi: 10.1158/0008-5472.CAN-18-3962

36. Wu J, Zhu Y, Luo M, Li L. Comprehensive analysis of pyroptosis-related genes and tumor microenvironment infiltration characterization in breast cancer. *Front Immunol* (2021) 12:748221. doi: 10.3389/fimmu.2021.748221

37. Stanton SE, Adams S, Disis ML. Variation in the incidence and magnitude of tumor-infiltrating lymphocytes in breast cancer subtypes: A systematic review. *JAMA Oncol* (2016) 2(10):1354–60. doi: 10.1001/jamaoncol.2016.1061

38. Dieci MV, Radosevic-Robin N, Fineberg S, van den Eynden G, Ternes N, Penault-Llorca F, et al. Update on tumor-infiltrating lymphocytes (Tils) in breast cancer, including recommendations to assess tils in residual disease after neoadjuvant therapy and in carcinoma in situ: A report of the international immuno-oncology biomarker working group on breast cancer. *Semin Cancer Biol* (2018) 52(Pt 2):16–25. doi: 10.1016/j.semcancer.2017.10.003

39. Yam C, Yen EY, Chang JT, Bassett RL, Alatrash G, Garber H, et al. Immune phenotype and response to neoadjuvant therapy in triple-negative breast cancer. *Clin Cancer Res* (2021) 27(19):5365–75. doi: 10.1158/1078-0432.CCR-21-0144

40. Adams S, Gray RJ, Demaria S, Goldstein L, Perez EA, Shulman LN, et al. Prognostic value of tumor-infiltrating lymphocytes in triple-negative breast cancers from two phase iii randomized adjuvant breast cancer trials: Ecog 2197 and ecog 1199. *J Clin Oncol* (2014) 32(27):2959–66. doi: 10.1200/JCO.2013.55.0491

41. Ali HR, Provenzano E, Dawson SJ, Blows FM, Liu B, Shah M, et al. Association between Cd8+ T-cell infiltration and breast cancer survival in 12,439 patients. *Ann Oncol* (2014) 25(8):1536–43. doi: 10.1093/annonc/mdu191

42. Wu SY, Xu Y, Chen L, Fan L, Ma XY, Zhao S, et al. Combined angiogenesis and pd-1 inhibition for immunomodulatory tnbc: Concept exploration and biomarker analysis in the future-C-Plus trial. *Mol Cancer* (2022) 21(1):84. doi: 10.1186/s12943-022-01536-6

43. Noel G, Fontsa ML, Garaud S, De Silva P, de Wind A, Van den Eynden GG, et al. Functional Th1-oriented T follicular helper cells that infiltrate human breast cancer promote effective adaptive immunity. *J Clin Invest* (2021) 131(19):e139905. doi: 10.1172/JCI139905

44. Gu-Trantien C, Loi S, Garaud S, Equeter C, Libin M, de Wind A, et al. Cd4 (+) follicular helper T cell infiltration predicts breast cancer survival. *J Clin Invest* (2013) 123(7):2873–92. doi: 10.1172/JCI67428

45. Siegers GM, Dutta I, Kang EY, Huang J, Kobel M, Postovit LM. Aberrantly expressed embryonic protein nodal alters breast cancer cell susceptibility to gammadelta T cell cytotoxicity. *Front Immunol* (2020) 11:1287. doi: 10.3389/fimmu.2020.01287

46. Meraviglia S, Eberl M, Vermijlen D, Todaro M, Buccheri S, Cicero G, et al. *In vivo* manipulation of Vgamma9vdelta2 T cells with zoledronate and low-dose interleukin-2 for immunotherapy of advanced breast cancer patients. *Clin Exp Immunol* (2010) 161(2):290–7. doi: 10.1111/j.1365-2249.2010.04167.x

47. Ju M, Qi A, Bi J, Zhao L, Jiang L, Zhang Q, et al. A five-mrna signature associated with post-translational modifications can better predict recurrence and survival in cervical cancer. *J Cell Mol Med* (2020) 24(11):6283–97. doi: 10.1111/jcmm.15270

48. Ning ZK, Hu CG, Huang C, Liu J, Zhou TC, Zong Z. Molecular subtypes and Cd4(+) memory T cell-based signature associated with clinical outcomes in gastric cancer. *Front Oncol* (2020) 10:626912. doi: 10.3389/fonc.2020.626912

49. Liu D, Vadgama J, Wu Y. Basal-like breast cancer with low tgfbeta and high tnfalpha pathway activity is rich in activated memory Cd4 T cells and has a good prognosis. *Int J Biol Sci* (2021) 17(3):670–82. doi: 10.7150/ijbs.56128

50. Garaud S, Buisseret L, Solinas C, Gu-Trantien C, de Wind A, Van den Eynden G, et al. Tumor infiltrating b-cells signal functional humoral immune responses in breast cancer. *JCI Insight* (2019) 5:e129641. doi: 10.1172/jci.insight.129641

51. Gu-Trantien C, Migliori E, Buisseret L, de Wind A, Brohee S, Garaud S, et al. Cxcl13-producing tfh cells link immune suppression and adaptive memory in human breast cancer. *JCI Insight* (2017) 2(11):e91487. doi: 10.1172/jci.insight.91487

52. Hu Q, Hong Y, Qi P, Lu G, Mai X, Xu S, et al. Atlas of breast cancer infiltrated b-lymphocytes revealed by paired single-cell rna-sequencing and antigen receptor profiling. *Nat Commun* (2021) 12(1):2186. doi: 10.1038/s41467-021-22300-2

53. Helmink BA, Reddy SM, Gao J, Zhang S, Basar R, Thakur R, et al. B cells and tertiary lymphoid structures promote immunotherapy response. *Nature* (2020) 577(7791):549–55. doi: 10.1038/s41586-019-1922-8

54. Vito A, Salem O, El-Sayes N, MacFawn IP, Portillo AL, Milne K, et al. Immune checkpoint blockade in triple negative breast cancer influenced by b cells through myeloid-derived suppressor cells. *Commun Biol* (2021) 4(1):859. doi: 10.1038/s42003-021-02375-9

55. Tan Y, Sun R, Liu L, Yang D, Xiang Q, Li L, et al. Tumor suppressor Drd2 facilitates M1 macrophages and restricts nf-kappab signaling to trigger pyroptosis in breast cancer. *Theranostics* (2021) 11(11):5214–31. doi: 10.7150/thno.58322

56. Zhang Y, Fan Y, Jing X, Zhao L, Liu T, Wang L, et al. Otud5-mediated deubiquitination of yap in macrophage promotes M2 phenotype polarization and favors triple-negative breast cancer progression. *Cancer Lett* (2021) 504:104–15. doi: 10.1016/j.canlet.2021.02.003

57. Mattiuz R, Brousse C, Ambrosini M, Cancel JC, Bessou G, Mussard J, et al. Type 1 conventional dendritic cells and interferons are required for spontaneous Cd4(+) and Cd8(+) T-cell protective responses to breast cancer. *Clin Transl Immunol* (2021) 10(7):e1305. doi: 10.1002/cti2.1305

58. Bates JP, Derakhshandeh R, Jones L, Webb TJ. Mechanisms of immune evasion in breast cancer. *BMC Cancer* (2018) 18(1):556. doi: 10.1186/s12885-018-4441-3

59. Thorsson V, Gibbs DL, Brown SD, Wolf D, Bortone DS, Ou Yang TH, et al. The immune landscape of cancer. *Immunity* (2018) 48(4):812–30.e14. doi: 10.1016/j.immuni.2018.03.023

60. Luen S, Virassamy B, Savas P, Salgado R, Loi S. The genomic landscape of breast cancer and its interaction with host immunity. *Breast* (2016) 29:241–50. doi: 10.1016/j.breast.2016.07.015

61. Stephens PJ, Tarpey PS, Davies H, Van Loo P, Greenman C, Wedge DC, et al. The landscape of cancer genes and mutational processes in breast cancer. *Nature* (2012) 486(7403):400–4. doi: 10.1038/nature11017

62. Tekpli X, Lien T, Rossevold AH, Nebdal D, Borgen E, Ohnstad HO, et al. An independent poor-prognosis subtype of breast cancer defined by a distinct tumor immune microenvironment. *Nat Commun* (2019) 10(1):5499. doi: 10.1038/s41467-019-13329-5

63. Denkert C, von Minckwitz G, Darb-Esfahani S, Lederer B, Heppner BI, Weber KE, et al. Tumour-infiltrating lymphocytes and prognosis in different subtypes of breast cancer: A pooled analysis of 3771 patients treated with neoadjuvant therapy. *Lancet Oncol* (2018) 19(1):40–50. doi: 10.1016/S1470-2045(17)30904-X

64. Loi S, Michiels S, Salgado R, Sirtaine N, Jose V, Fumagalli D, et al. Tumor infiltrating lymphocytes are prognostic in triple negative breast cancer and predictive for trastuzumab benefit in early breast cancer: Results from the finher trial. *Ann Oncol* (2014) 25(8):1544–50. doi: 10.1093/annonc/mdu112

65. Wang H, Wu X, Chen Y. Stromal-immune score-based gene signature: A prognosis stratification tool in gastric cancer. *Front Oncol* (2019) 9:1212. doi: 10.3389/fonc.2019.01212

66. Hou J, Zhao R, Xia W, Chang CW, You Y, Hsu JM, et al. Pd-L1-Mediated gasdermin c expression switches apoptosis to pyroptosis in cancer cells and facilitates tumour necrosis. *Nat Cell Biol* (2020) 22(10):1264–75. doi: 10.1038/s41556-020-0575-z

67. Vonderheide RH, LoRusso PM, Khalil M, Gartner EM, Khaira D, Soulieres D, et al. Tremelimumab in combination with exemestane in patients with advanced breast cancer and treatment-associated modulation of inducible costimulator expression on patient T cells. *Clin Cancer Res* (2010) 16(13):3485–94. doi: 10.1158/1078-0432.CCR-10-0505

68. Dongre A, Rashidian M, Eaton EN, Reinhardt F, Thiru P, Zagorulya M, et al. Direct and indirect regulators of epithelial-mesenchymal transition-mediated immunosuppression in breast carcinomas. *Cancer Discovery* (2021) 11(5):1286–305. doi: 10.1158/2159-8290.CD-20-0603

69. Popat S, Hubner R, Houlston RS. Systematic review of microsatellite instability and colorectal cancer prognosis. *J Clin Oncol* (2005) 23(3):609–18. doi: 10.1200/JCO.2005.01.086

70. Deng H, Zhao Y, Cai X, Chen H, Cheng B, Zhong R, et al. Pd-L1 expression and tumor mutation burden as pathological response biomarkers of neoadjuvant immunotherapy for early-stage non-small cell lung cancer: A systematic review and meta-analysis. *Crit Rev Oncol Hematol* (2022) 170:103582. doi: 10.1016/j.critrevonc.2022.103582

71. Ning B, Liu Y, Wang M, Li Y, Xu T, Wei Y. The predictive value of tumor mutation burden on clinical efficacy of immune checkpoint inhibitors in melanoma: A systematic review and meta-analysis. *Front Pharmacol* (2022) 13:748674. doi: 10.3389/fphar.2022.748674

72. Baretti M, Le DT. DNA mismatch repair in cancer. *Pharmacol Ther* (2018) 189:45–62. doi: 10.1016/j.pharmthera.2018.04.004

frontiers | Frontiers in Immunology

TYPE Review
PUBLISHED 16 September 2022
DOI 10.3389/fimmu.2022.975926

OPEN ACCESS

EDITED BY
Xuyao Zhang,
Fudan University, China

REVIEWED BY
Xin Han,
Zhejiang University, China
Shuai Wang,
Harvard Medical School, United States

*CORRESPONDENCE
Qi-Bing Liu
qibing.liu@hainmc.edu.cn
Kun-Feng Chen
chenkunfeng1972@126.com

†These authors have contributed equally to this work

SPECIALTY SECTION
This article was submitted to Cancer Immunity and Immunotherapy, a section of the journal Frontiers in Immunology

RECEIVED 22 June 2022
ACCEPTED 29 August 2022
PUBLISHED 16 September 2022

CITATION
Wang Y-T, Ji W-D, Jiao H-M, Lu A, Chen K-F and Liu Q-B (2022) Targeting 4-1BB for tumor immunotherapy from bench to bedside.
Front. Immunol. 13:975926.
doi: 10.3389/fimmu.2022.975926

Targeting 4-1BB for tumor immunotherapy from bench to bedside

Ya-Tao Wang[1†], Wei-Dong Ji[1†], Hong-Mei Jiao[1], Ang Lu[1], Kun-Feng Chen[1*] and Qi-Bing Liu[2,3*]

[1]First People's Hospital of Shangqiu, Henan Province, Shangqiu, China, [2]Department of Pharmacy, the First Affiliated Hospital of Hainan Medical University, Haikou, China, [3]Department of Pharmacology, School of Basic Medicine and Life Sciences, Hainan Medical University, Haikou, China

Immune dysfunction has been proposed as a factor that may contribute to disease progression. Emerging evidence suggests that immunotherapy aims to abolish cancer progression by modulating the balance of the tumor microenvironment. 4-1BB (also known as CD137 and TNFRS9), a member of tumor necrosis factor receptor superfamily, has been validated as an extremely attractive and promising target for immunotherapy due to the upregulated expression in the tumor environment and its involvement in tumor progression. More importantly, 4-1BB-based immunotherapy approaches have manifested powerful antitumor effects in clinical trials targeting 4-1BB alone or in combination with other immune checkpoints. In this review, we will summarize the structure and expression of 4-1BB and its ligand, discuss the role of 4-1BB in the microenvironment and tumor progression, and update the development of drugs targeting 4-1BB. The purpose of the review is to furnish a comprehensive overview of the potential of 4-1BB as an immunotherapeutic target and to discuss recent advances and prospects for 4-1BB in cancer therapy.

KEYWORDS

4-1BB, immunotherapy, cancer, immune checkpoint inhibitor, clinical trials

Introduction

Tumor immunotherapy exerts antitumor efficacy through the interaction of the host immune system with tumor-associated antigens (1). It can restore or enhance the body's immune system's natural defenses against tumors, which typically targets specific biomolecules on the surface of cancer cells, exemplified by tumor-associated antigens (2). Immunotherapy including immune checkpoint inhibitor (ICI) and CAR-T therapy

has made breakthroughs in tumor treatment, but the overall response rate is not high, and many patients cannot benefit from it (3–6). Therefore, the development of new immune checkpoints and biomarkers and expansion of the beneficiary population from immunotherapy are urgent problems to be solved.

Neoantigen epitopes generated by somatic mutations in cancer cells play an important role in T-cell immune responses, which have become an important driver of immune checkpoint discovery in immunotherapy. 4-1BB, also termed 4-1BB and TNFRSF9, was identified in 1989 and originally described as an inducible gene, which was expressed in T lymphocytes (7). 4-1BB exhibited an important effect in various cells and participated in the activation of multiple immune cells, such as CD8 T cells and cytotoxic T lymphocytes (CTL) (8). Emerging evidence has demonstrated that targeting 4-1BB is a uniquely attractive strategy for tumor immunotherapy (9–13). In this review, we discuss the recent advances and prospects of the cancer immunotherapy checkpoint 4-1BB from the aspects of structure, expression, role in tumor microenvironment, development of clinical drugs targeting 4-1BB, and their combination with traditional treatment methods.

Structure of 4-1BB and its ligand

4-1BB, a glycosylated type I membrane protein, contains four cysteine-rich pseudo repeats, which contribute to the formation of a cytoplasmic signaling domain, extracellular domain, and short helical transmembrane domain (7). An elongated structure was generally formed by the extracellular domain of TNFR (variation range: 1 to 4 CRDs). Based on this, antibodies can bind to these molecules through many modalities. Efficient binding of 4-1BB L to 4-1BB results in rapid receptor activation in response to antigenic stimulation. 4-1BBL (TNFSF9), a type II membrane protein of the TNF ligand superfamily, is the binding partner of 4-1BB (14, 15). TNFSF members, typically expressed on the cell membrane, exist in a homotrimeric complex (16–18), which can be divided into three parts: (a) LTα, TNF, RANKL, LIGHT, Apo2L/TRAIL, and CD40L (19, 20); (b) BAFF, APRIL, and EDA; and (c) GITRL, 4-1BBL, and OX40L, among which OX40L and GITRL exhibit a flatter conformation (19, 21). The sequences of 4-1BBL were poorly conserved in human and mouse.

As a member of the tumor necrosis factor superfamily, 4-1BB is mostly expressed on the surface of activated T cells but also on B cells, NK cells, and DC cells (22, 23). 4-1BB is widely distributed on various tumor cells (such as lung tumor cells, and leukemia cells) and has been identified in tissues (such as liver cancer tissue, and tumor vessel walls). Alfaro et al. found that 4-1BB is also expressed in tonsil and lymph node follicular structures. Thence, a comprehensive analysis of its distribution helps uncover potential roles and functions.

Role of 4-1BB in the tumor microenvironment

As shown in Figure 1, both IL-15 and IL-2 can promote the expression of 4-1BB on NK cells, which stimulates the proliferation of NK cells and produces IFN-γ, thus leading to the activation of T cells (24). 4-1BB facilitates the proliferation of $CD8^+$ T cells to produce memory T (Tm) cells (25, 26). Stimulation by 4-1BB will upregulate the expression IL-2 and IFN-γ in $CD4^+$ and $CD8^+$ T cells. However, 4-1BB expresses a controversial effect in T regulatory cells (Treg), which leads to Treg proliferation but alters Treg for cytotoxic or helper effects (27, 28). 4-1BBL inhibits the conversion of $CD4^+FOXP3^-$ cells to $CD4^+FOXP^+$ (29). 4-1BB is also expressed in monocytes, and it promotes upregulation of IL-8 and TNF-α but downregulation of IL-10. The differentiation of monocytes into dendritic cells can be promoted by 4-1BB, and dendritic cells then secrete IL-6 and IL-12 (30). However, 4-1BB stimulation differentiates monocytes into M2 macrophages and accelerates B-cell apoptosis, which also promotes the expression of TNF-α/β in B cells (31).

4-1BB in cancer progression

Through the PI3K/AKT/mTOR pathway, expression of 4-1BB was induced by EBV protein LMP1 to facilitate immune evasion in Hodgkin and Reed–Sternberg cells (32). Low levels of the soluble form of 4-1BBL in patients with AML were associated with better prognosis, especially longer disease-free survival (33). 4-1BB L and 4-1BB were abnormally expressed in tumor cells in hematopoietic malignancies, and their interaction promotes tumor growth in cutaneous T-cell lymphoma (34). Overexpression of 4-1BB on leukemic cells was significantly related to poor prognosis (35). Antitumor activity was enhanced in 4-1BB-knockout mice (36). Similarly, the tumor growth was seriously blocked in 4-1BB knockout mice subcutaneously injected with CT26 cells (37). The findings further proved the critical role of 4-1BB-4-1BBL in tumor development.

4-1BB-targeted drug development

The efficacy of the 4-1BB antibody in preventing cancer in animals has prompted clinical development. The use of monoclonal antibodies to treat cancer has achieved great success over the past few decades, many of which have been under evaluation in different clinical trials, as shown in Table 1.

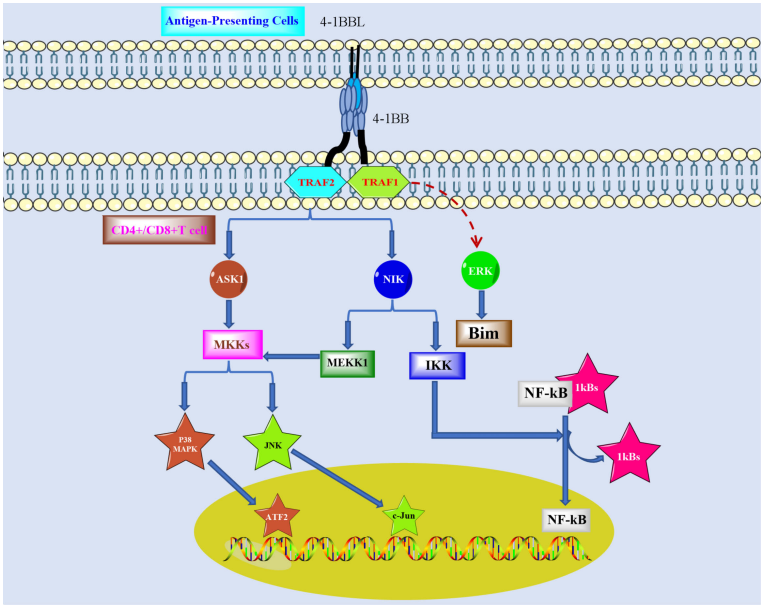

FIGURE 1
Role of 4-1BB in the tumor microenvironment.

Urelumab (BMS-663513), the first 4-1BB-targeted therapy to enter clinical trials developed by Bristol–Myers Squibb, is a human IgG4 human monoclonal antibody, which will not inhibit the interaction between 4-1BB with its ligand (38). Preliminary clinical results in phase 1/2 disclosed in 2008 showed encouraging efficacy, but further development was hindered by liver toxicity (39). Urelumab reentered clinical trials in 2012, which was combined with nivolumab, cetuximab, rituximab, and elotuzumab, respectively (12). However, hepatotoxicity of the antibody emerged shortly thereafter, causing the urelumab development program to be shelved. Currently, urelumab, a potent agonist mAb, is still under different clinical trials (Table 1), and strategies to avoid hepatotoxicity and achieve appropriate drug exposure levels are worth investigating. Utomilumab (PF-05082566) is a 4-1BB-humanized IgG2 monoclonal antibody developed by Pfizer (40). Compared with urelumab, it has a higher safety profile and is currently undergoing multiple clinical trials (41).

To reduce the hepatotoxicity of systemic 4-1BB agonists, the development of bispecific antibodies against 4-1BB has been recognized as a viable strategy, and some bispecific antibodies, including GEN1046 (PD-L1/4-1BB) and PRS343 (HER2/4-1BB), are currently being evaluated in different clinical trials (Table 1) (42, 43). ES101 (INBRX-105), a first-in-class tetravalent bispecific antibody targeting PD-L1/4-1BB, originally developed by Inhibrx, was introduced into its Greater China rights by Kewan Pharmaceuticals (44). It contains four domains, and two of them target PD-L1 while the other two target 4-1BB, which can alleviate PD-1/PD-L1-mediated immune checkpoint inhibition. The 4-1BB-binding domain may drive the aggregation of 4-1BB molecules on the surface of T cells, so that 4-1BB-mediated immune activation can be concentrated on T cells near the tumor, effectively reducing the potential off-target toxicity.

In addition to double-antibody drugs, the development of 4-1BB targets has been extended to tertiary and tetraspecific antibodies. NM21-1480 is a monovalent trispecific antibody fragment molecule against PD-L1, 4-1BB, and human serum protein (HSA) (45). NM21-1480 exerts a synergistic effect of 4-1BB agonism and PD-L1 blockade and shows an extended half-life by binding to HSA, thereby reducing the frequency of dosing. GNC-035 is a four-antibody drug targeting PD-L1/CD3/4-1BB/ROR1 while GNC-039 targets PD-L1/4-1BB/CD3/EGFR. In terms of design, both GNC-035 and GNC-039 build symmetrical tetraspecific antibodies based on IgG with three scFvs in series. Among them, PD-L1, 4-1BB, and CD3 are immunoregulatory functions, and the fourth target is tumor antigen. Both drugs are undergoing evaluation in different clinical trials (Table 1).

Future directions

Immunotherapy is known as the fourth cancer treatment after surgery, radiotherapy, and chemotherapy, which has changed the treatment patterns of patients with advanced

TABLE 1 4-1BB modulators in clinical trials.

Drug	Study Title	ClinicalTrials	Phase	Status
EU 101	A Study to Evaluate Safety, Efficacy, and Pharmacokinetics in Participants With Advanced Solid Tumors	NCT04903873	Phase 1 Phase 2	Recruiting
	Expanded Access Program Using IMM-101 for Patients With Advanced Pancreatic Cancer	NCT04137822	Unknown	No longer available
	A Study of Belinostat + Carboplatin or Paclitaxel or Both in Patients With Ovarian Cancer in Need of Relapse Treatment	NCT00421889	Phase 1 Phase 2	Completed
	Study of Lanreotide in Metastatic or Recurrent Grade I-II Hindgut NET	NCT03083210	Phase 4	Unknown
Urelumab	Urelumab (4-1BB mAb) With Rituximab for Relapsed, Refractory or High-risk Untreated Chronic Lymphocytic Leukemia (CLL) Patients	NCT02420938	Phase 2	Withdrawn
	Combination Study of Urelumab and Rituximab in Patients With B-cell Non-Hodgkins Lymphoma	NCT01775631	Phase 1	Completed
	Phase I-II Study of Intratumoral Urelumab Combined With Nivolumab in Patients With Solid Tumors	NCT03792724	Phase 1 Phase 2	Not yet recruiting
	Combination Study of Urelumab and Cetuximab in Patients With Advanced/Metastatic Colorectal Cancer or Advanced/Metastatic Head and Neck Cancer	NCT02110082	Phase 1	Completed
	Neoadjuvant Nivolumab With and Without Urelumab in Cisplatin-Ineligible or Chemotherapy-refusing Patients With Muscle-Invasive Urothelial Carcinoma of the Bladder	NCT02845323	Phase 2	Recruiting
	An Investigational Immuno-therapy Study to Determine the Safety of Urelumab Given in Combination With Nivolumab in Solid Tumors and B-cell Non-Hodgkin's Lymphoma	NCT02253992	Phase 1 Phase 2	Terminated
	A Phase I Open Label Study of the Safety and Tolerability of Elotuzumab (BMS-901608) Administered in Combination With Either Lirilumab (BMS-986015) or Urelumab (BMS-663513) in Subjects With Multiple Myeloma	NCT02252263	Phase 1	Completed
	Safety, Tolerability, Pharmacokinetics, and Immunoregulatory Study of Urelumab (BMS-663513) in Subjects With Advanced and/or Metastatic Solid Tumors and Relapsed/Refractory B-cell Non-Hodgkin's Lymphoma	NCT01471210	Phase 1	Completed
	Study of Urelumab in Subjects With Advanced and/or Metastatic Malignant Tumors	NCT02534506	Phase 1	Completed
	A Study of BMS-663513 Administered in Combination With Chemotherapy to Subjects With Advanced Solid Malignancies	NCT00351325	Phase 1	Terminated
	A Study of BMS-663513 in Combination With Chemoradiation in Subjects With Non Small Cell Lung Carcinoma (NSCLC)	NCT00461110	Phase 1	Terminated
	Study of BMS-663513 in Patients With Advanced Cancer	NCT00309023	Phase 1 Phase 2	Terminated
	Stereotactic Body Radiotherapy (SBRT) Plus Immunotherapy for Cancer	NCT03431948	Phase 1	Active, not recruiting
	Anti-LAG-3 Alone and in Combination w/Nivolumab Treating Patients w/Recurrent GBM (Anti-4-1BB Arm Closed 10/16/18)	NCT02658981	Phase 1	Active, not recruiting
	Phase II, 2nd Line Melanoma - RAND Monotherapy	NCT00612664	Phase 2	Completed
	Combination of Anti-4-1BB and Ipilimumab in Patients With Melanoma	NCT00803374	Phase 1	Withdrawn
	Platform Study of Neoadjuvant and Adjuvant Immunotherapy for Patients With Resectable Adenocarcinoma of the Pancreas	NCT02451982	Phase 2	Recruiting
	Combining PD-1 Blockade, 4-1BB Agonism and Adoptive Cell Therapy for Metastatic Melanoma	NCT02652455	Early Phase 1	Active, not recruiting
Sytalizumab	The Safety and Efficacy of TWP-101 in Patients With Advanced Solid Tumor	NCT04871347	Phase 1	Not yet recruiting
	Safety, Tolerability and Pharmacokinetics of TWP-101 in Patients With Advanced Melanoma and Urothelial Carcinoma	NCT04871334	Phase 1	Recruiting
LVGN-6051	A Study of LVGN6051 Combined With Anlotinib in Patient With Soft Tissue Sarcoma	NCT05301764	Phase 1 Phase 2	Recruiting
	Phase 1 Trial of LVGN6051 as Single Agent and in Combination With Keytruda (MK-3475-A31/ KEYNOTE-A31) in Advanced or Metastatic Malignancy	NCT04130542	Phase 1	Recruiting
	Study of LVGN6051 (4-1BB Agonist Antibody) in Advanced or Metastatic Malignancy	NCT04694781	Phase 1	Recruiting
	Study of LVGN3616 and LVGN6051 ± LVGN7409 in Combination With Nab-Paclitaxel or Bevacizumab and Cyclophosphamide in Metastatic Solid Tumors	NCT05075993	Phase 1	Recruiting
	Phase 1 Trial of LVGN7409 (CD40 Agonist Antibody) as Single Agent and Combination Therapies in Advanced or Metastatic Malignancy	NCT04635995	Phase 1	Recruiting

(Continued)

TABLE 1 Continued

Drug	Study Title	ClinicalTrials	Phase	Status
YH-004	Study of YH004 (4-1BB Agonist Antibody) in Advanced or Metastatic Malignancy	NCT05040932	Phase 1	Recruiting
GEN1046	GEN1046 Safety and PK in Subjects With Advanced Solid Malignancies	NCT04937153	Phase 1	Recruiting
	Safety and Efficacy Study of GEN1046 as a Single Agent or in Combination With Another Anti-cancer Therapy for Treatment of Recurrent (Non-small Cell) Lung Cancer	NCT05117242	Phase 2	Recruiting
	GEN1046 Safety Trial in Patients With Malignant Solid Tumors	NCT03917381	Phase 1 Phase 2	Recruiting
PRS343	PRS-343 in HER2-Positive Solid Tumors	NCT03330561	Phase 1	Completed
	PRS-343 in Combination With Atezolizumab in HER2-Positive Solid Tumors	NCT03650348	Phase 1	Active, not recruiting
	Cinrebafusp Alfa in Combination With Ramucirumab and Paclitaxel in HER2-High Gastric or GEJ Adenocarcinoma and in Combination With Tucatinib in HER2-Low Gastric or GEJ Andenocarinoma	NCT05190445	Phase 2	Recruiting
ES101	A Study of ES101 (PD-L1x4-1BB Bispecific Antibody) in Patients With Advanced Malignant Thoracic Tumors	NCT04841538	Phase 1 Phase 2	Withdrawn
	A Study of ES101 (PD-L1x4-1BB Bispecific Antibody) in Patients With Advanced Solid Tumors	NCT04009460	Phase 1	Terminated
	Ankle - Brachial Index Measurement in Atrial Fibrillation	NCT02986282	Not applicable	Completed
Cinrebafusp alfa	Cinrebafusp Alfa in Combination With Ramucirumab and Paclitaxel in HER2-High Gastric or GEJ Adenocarcinoma and in Combination With Tucatinib in HER2-Low Gastric or GEJ Andenocarinoma	NCT05190445	Phase 2	Recruiting
HLX-35	HLX35(EGFR×4-1BB Bispecific) in Patients With Advanced or Metastatic Solid Tumors	NCT05360381	Phase 1	Not yet recruiting
IBI319	Study of the Efficacy and Safety of IBI319 in Patients With Advanced Malignant Tumors	NCT04708210	Phase 1	Recruiting
TJ-033721	Study of TJ033721 in Subjects With Advanced or Metastatic Solid Tumors	NCT04900818	Phase 1	Recruiting
ATG 101	A Study of Evaluating the Safety and Efficacy of ATG-101 in Patients With Metastatic/Advanced Solid Tumors and Mature B-cell Non-Hodgkin Lymphomas	NCT04986865	Phase 1	Recruiting
	Study of ASC-101 in Patients With Hematologic Malignancies Who Receive Dual-cord Umbilical Cord Blood Transplantation	NCT01983761	Phase 1 Phase 2	Recruiting
	Safety and Efficacy of Two Doses of ATIR101, a T-lymphocyte Enriched Leukocyte Preparation Depleted of Host Alloreactive T-cells, in Patients With a Hematologic Malignancy Who Received a Hematopoietic Stem Cell Transplantation From a Haploidentical Donor	NCT02500550	Phase 2	Completed
	Antithymocyte Globulin and Cyclosporine in Preventing Graft-Versus-Host Disease in Patients Undergoing Chemotherapy With or Without Radiation Therapy Followed By Donor Stem Cell Transplant for Acute Lymphoblastic Leukemia or Acute Myeloid Leukemia	NCT00093587	Not applicable	Unknown
	Thymoglobulin to Prevent Acute Graft vs. Host Disease (GvHD) in Patients With Acute Lymphocytic Leukemia (ALL) or Acute Myelogenous Leukemia (AML) Receiving a Stem Cell Transplant	NCT00088543	Not applicable	Completed
LBL-024	A Phase I/II Clinical Study of LBL-024 in Patients With Advanced Malignant Tumors	NCT05170958	Phase 1 Phase 2	Recruiting
MCLA-145	A Study of Bispecific Antibody MCLA-145 in Patients With Advanced or Metastatic Malignancies	NCT03922204	Phase 1	Recruiting
ABL-503	This is a Study to Evaluate the Safety and Tolerability of ABL503, and to Determine the Maximum Tolerated Dose (MTD) and Recommended Phase 2 Dose (RP2D) of ABL503 in Subjects With Any Progressive Locally Advanced or Metastatic Solid Tumors	NCT04762641	Phase 1	Recruiting
PM 1032	A Study of Ramucirumab (IMC-1121B) and Paclitaxel in Participants With Solid Tumors	NCT01515306	Phase 2	Completed
QLF-31907	A Phase Ia Clinical Study of QLF31907 Injection in Patients With Advanced Malignant Tumors	NCT05150405	Phase 1	Recruiting
FS-120	FS120 First in Human Study in Patients With Advanced Malignancies	NCT04648202	Phase 1	Recruiting
RO-7227166	A Study to Evaluate the Safety, Pharmacokinetics and Preliminary Anti-Tumor Activity of RO7227166 in Combination With Obinutuzumab and in Combination With Glofitamab Following a Pre-Treatment Dose of Obinutuzumab Administered in Participants With Relapsed/Refractory B-Cell Non-Hodgkin's Lymphoma	NCT04077723	Phase 1	Recruiting
HBM-7008	HBM7008 -Study on Subjects With Advanced Solid Tumors	NCT05306444	Phase 1	Recruiting
ND-021	A Study of NM21-1480 in Adult Patients With Advanced Solid Tumors	NCT04442126	Phase 1 Phase 2	Recruiting
GNC-035	A Study of GNC-035, a Tetra-specific Antibody, in Participants With Locally Advanced or Metastatic Breast Cancer	NCT05160545	Phase 1	Recruiting
	A Study of GNC-035, a Tetra-specific Antibody, in Participants With Locally Advanced or Metastatic Solid Tumors	NCT05039931	Phase 1	Recruiting

(Continued)

TABLE 1 Continued

Drug	Study Title	ClinicalTrials	Phase	Status
	A Study of GNC-035, a Tetra-specific Antibody, in Participants With Relapsed/Refractory Hematologic Malignancy	NCT05104775	Phase 1	Recruiting
GNC-038	A Study of GNC-038, a Tetra-specific Antibody, in Participants With R/R Diffuse Large B-cell Lymphoma (DLBCL)	NCT05192486	Phase 1 Phase 2	Recruiting
	A Study of GNC-038, a Tetra-specific Antibody, in Participants With R/R Non-Hodgkin Lymphoma	NCT04606433	Phase 1	Recruiting
	Mechanism of Resistance to GNC-038 in Relapsed and Refractory Diffuse Large B-cell Lymphoma	NCT05189782	Unknown	Recruiting
GNC-039	A Study of GNC-039, a Tetra-specific Antibody, in Participants With Relapsed/Refractory or Metastatic Solid Tumors	NCT04794972	Phase 1	Recruiting
ADG-106	A Study to Evaluate the Combination of Nivolumab With ADG106 in Metastatic NSCLC	NCT05236608	Phase 1 Phase 2	Recruiting
	Study of ADG106 In Combination With PD-1 Antibody In Advanced or Metastatic Solid Tumors and/or Non Hodgkin Lymphoma	NCT04775680	Phase 1 Phase 2	Recruiting
	A Phase Ib Safety lead-in, Followed by Phase II Trial of ADG106 in Combination With Neoadjuvant Chemotherapy in HER2 Negative Breast Cancer	NCT05275777	Phase 1 Phase 2	Recruiting
	Study of ADG106 With Advanced or Metastatic Solid Tumors and/or Non-Hodgkin Lymphoma	NCT03802955	Phase 1	Active, not recruiting
	Study of 4-1BB Agonist ADG106 With Advanced or Metastatic Solid Tumors and/or Non-Hodgkin Lymphoma	NCT03707093	Phase 1	Active, not recruiting
	ADG126, ADG126 in Combination With Anti PD1 Antibody, and ADG126 in Combination With ADG106 in Advanced/Metastatic Solid Tumors	NCT04645069	Phase 1	Recruiting
	A Phase 1b Study of ADG116, ADG116 Combined With Anti-PD-1 Antibody or Anti-4-1BB Antibody in Solid Tumors Patients	NCT04501276	Phase 1	Recruiting
Utomilumab	Utomilumab and ISA101b Vaccination in Patients With HPV-16-Positive Incurable Oropharyngeal Cancer	NCT03258008	Phase 2	Completed
	T-Cell Infusion, Aldesleukin, and Utomilumab in Treating Patients With Recurrent Ovarian Cancer	NCT03318900	Phase 1	Active, not recruiting
	Safety and Efficacy of Axicabtagene Ciloleucel in Combination With Utomilumab in Adults With Refractory Large B-cell Lymphoma	NCT03704298	Phase 1	Active, not recruiting
	Avelumab, Utomilumab, Rituximab, Ibrutinib, and Combination Chemotherapy in Treating Patients With Relapsed or Refractory Diffuse Large B-Cell Lymphoma or Mantle Cell Lymphoma	NCT03440567	Phase 1	Active, not recruiting
	The AVIATOR Study: Trastuzumab and Vinorelbine With Avelumab OR Avelumab and Utomilumab in Advanced HER2+ Breast Cancer	NCT03414658	Phase 2	Recruiting
	4-1BB Agonist Monoclonal Antibody PF-05082566 With Trastuzumab Emtansine or Trastuzumab in Treating Patients With Advanced HER2-Positive Breast Cancer	NCT03364348	Phase 1	Active, not recruiting
	Utomilumab, Cetuximab, and Irinotecan Hydrochloride in Treating Patients With Metastatic Colorectal Cancer	NCT03290937	Phase 1	Active, not recruiting
	Avelumab, Utomilumab, Anti-OX40 Antibody PF-04518600, and Radiation Therapy in Treating Patients With Advanced Malignancies	NCT03217747	Phase 1 Phase 2	Active, not recruiting
	RITUXIMAB + IMMUNOTHERAPY IN FOLLICULAR LYMPHOMA	NCT03636503	Phase 1	Active, not recruiting
	A Study Of Avelumab In Combination With Other Cancer Immunotherapies In Advanced Malignancies (JAVELIN Medley)	NCT02554812	Phase 2	Active, not recruiting
	Avelumab In Combination Regimens That Include An Immune Agonist, Epigenetic Modulator, CD20 Antagonist and/or Conventional Chemotherapy in Patients With Relapsed or Refractory Diffuse Large B-cell Lymphoma (R/R DLBCL)	NCT02951156	Phase 3	Terminated
	Avelumab With Binimetinib, Sacituzumab Govitecan, or Liposomal Doxorubicin in Treating Patients With Stage IV or Unresectable, Recurrent Triple Negative Breast Cancer	NCT03971409	Phase 2	Recruiting
	Continued Access Study for Participants Deriving Benefit in Pfizer-Sponsored Avelumab Parent Studies That Are Closing	NCT05059522	Phase 3	Recruiting
	Study Of OX40 Agonist PF-04518600 Alone And In Combination With 4-1BB Agonist PF-05082566	NCT02315066	Phase 1	Completed

(Continued)

TABLE 1 Continued

Drug	Study Title	ClinicalTrials	Phase	Status
ATOR-1017	ATOR-1017 First-in-human Study	NCT04144842	Phase 1	Recruiting
AGEN-2373	Anti-4-1BB and Anti-CTLA-4 Monoclonal Antibody in Patient With Advanced Cancer	NCT04121676	Phase 1	Recruiting
CTX-471	Study of CTX-471 in Patients Post PD-1/PD-L1 Inhibitors in Metastatic or Locally Advanced Malignancies	NCT03881488	Phase 1	Recruiting
PRS-344	A Study of PRS-344/S095012 (PD-L1x4-1BB Bispecific Antibody-Anticalin Fusion) in Patients With Solid Tumors	NCT05159388	Phase 1 Phase 2	Recruiting
RO-7122290	Study To Evaluate Safety, Pharmacokinetics, Pharmacodynamics, And Preliminary Anti-Tumor Activity Of RO7122290 In Combination With Cibisatamab With Obinutuzumab Pre-Treatment	NCT04826003	Phase 1 Phase 2	Recruiting
	Study Evaluating the Efficacy and Safety of Multiple Immunotherapy-Based Treatments and Combinations in Patients With Urothelial Carcinoma (MORPHEUS-UC)	NCT03869190	Phase 1 Phase 2	Recruiting
Anti BCMA CART cell therapy	Anti-BCMA or/and Anti-CD19 CART Cells Treatment of Relapsed Multiple Myeloma	NCT03767725	Phase 1	Unknown
	BCMA Chimeric Antigen Receptor Expressing T Cells Therapy for Relapsed/Refractory Multiple Myeloma	NCT03943472	Early Phase 1	Recruiting
	Master Protocol for the Phase 1 Study of Cell Therapies in Multiple Myeloma	NCT04155749	Phase 1	Recruiting
	Study of T Cells Targeting CD19/BCMA (CART-19/BCMA) for High Risk Multiple Myeloma Followed With Auto-HSCT	NCT03455972	Phase 1 Phase 2	Recruiting
	A Study of BCMA-directed CAR-T Cells Treatment in Subjects With r/r Multiple Myeloma	NCT03751293	Phase 1	Unknown
	Clinical Trial Using Humanized CART Directed Against BCMA (ARI0002h) in Patients With Relapsed/Refractory Multiple Myeloma to Proteasome Inhibitors, Immunomodulators and Anti-CD38 Antibody.	NCT04309981	Phase 1 Phase 2	Recruiting
	A Study of BCMA-directed CAR-T Cells Treatment in Subjects With r/r Multiple Myeloma	NCT04322292	Phase 1	Unknown
	BCMA-directed CAR-T Cell Therapy in Adult Patients With Relapsed and/or Refractory Multiple Myeloma	NCT04318327	Phase 1	Recruiting
	Autologous CD8+ T-cells Expressing an Anti-BCMA CAR in Patients With Myeloma	NCT03448978	Phase 1 Phase 2	Completed
	CART-BCMA Cells for Multiple Myeloma	NCT02546167	Phase 1	Completed
	Humanized CAR-T Cells of Anti-BCAM and Anti-CD19 Against Relapsed and Refractory Multiple Myeloma	NCT04194931	Phase 1	Unknown
	BCMA Chimeric Antigen Receptor Expressing T Cells in Multiple Myeloma	NCT03093168	Phase 1	Unknown
	Safety and Efficacy Evaluation of BCMA-CART for Treating Multiple Myeloma	NCT03492268	Not applicable	Withdrawn
	Efficacy and Safety Evaluation of BCMA-UCART	NCT03752541	Not applicable	Suspended
HOT-1030	A Study of HOT1030 in Patients With Advanced Solid Tumors	NCT05060263	Phase 1	Recruiting
Delolimogene mupadenorepvec	A Phase I/II Trial Investigating LOAd703 in Combination With Atezolizumab in Malignant Melanoma	NCT04123470	Phase 1 Phase 2	Recruiting
	A Study Evaluating the Efficacy and Safety of Multiple Immunotherapy-Based Treatment Combinations in Patients With Metastatic Colorectal Cancer (Morpheus-CRC)	NCT03555149	Phase 1 Phase 2	Recruiting
	LOAd703 Oncolytic Virus Therapy for Pancreatic Cancer	NCT02705196	Phase 1 Phase 2	Recruiting
BT 7480	Study BT7480-100 in Patients With Advanced Malignancies Associated With Nectin-4 Expression	NCT05163041	Phase 1 Phase 2	Recruiting

tumors (46). However, only a minority of cancer patients can benefit from it. Treatment methods such as surgery, chemotherapy, radiotherapy, and targeted therapy can synergize with immunotherapy to enhance the curative effect. Guillerey et al. found that anti-4-1BB mAb combined with chemotherapy could prevent MM relapse and prolong survival in MM mice (47). A study undertaken by Newcomb et al. demonstrated that radiation could synergistically enhance the antitumor effect of anti-4-1BB therapy in a mouse glioma model (48). Moreover, anti-4-1BB mAbs could enhance the efficacy of other antitumor Abs (such as cetuximab, rituximab, and trastuzumab) and exert synergistic effects. Taken together, combination therapy for tumors may also be the future direction of tumor therapy.

Conclusion

To summarize, existing studies support immunotherapies targeting the 4-1BB pathway for the treatment of cancer. In the study, we have summarized the structure of 4-1BB and its ligand as well as the expression in various immune cells and tumor cells. More importantly, we discuss the role of 4-1BB in the microenvironment and tumor progression. Furthermore, the development of drug-targeted 4-1BB was summarized and updated, which exhibited tremendous potential in clinical trials. Although the anti-4-1BB therapy provides hope for cancer treatment, the effectiveness of drugs targeting 4-1BB in clinical antitumor therapy alone or in combination with other antitumor therapies still needs to be investigated in the future.

Author contributions

Y-TW, K-FC and Q-BL conceived the review. All authors contributed to the article and approved the submitted version.

Funding

This work was funded by the National Natural Science Foundation of China (No. 81960663).

Conflict of interest

The authors declare that the research was conducted in the absence of any commercial or financial relationships that could be construed as a potential conflict of interest.

Publisher's note

All claims expressed in this article are solely those of the authors and do not necessarily represent those of their affiliated organizations, or those of the publisher, the editors and the reviewers. Any product that may be evaluated in this article, or claim that may be made by its manufacturer, is not guaranteed or endorsed by the publisher.

References

1. Drake CG, Jaffee E, Pardoll DM. Mechanisms of immune evasion by tumors. *Adv Immunol* (2006) 90:51–81. doi: 10.1016/S0065-2776(06)90002-9

2. Yang Y. Cancer immunotherapy: harnessing the immune system to battle cancer. *J Clin Invest* (2015) 125:3335–7. doi: 10.1172/JCI83871

3. Wang R, Liu H, He P, An D, Guo X, Zhang X, et al. Inhibition of PCSK9 enhances the antitumor effect of PD-1 inhibitor in colorectal cancer by promoting the infiltration of CD8+ T cells and the exclusion of treg cells. *Front Immunol* (2022) 13:947756. doi: 10.3389/fimmu.2022.947756

4. Xu C, Ju D, Zhang X. Cell membrane-derived vesicle: A novel vehicle for cancer immunotherapy. *Front Immunol* (2022) 13:923598. doi: 10.3389/fimmu.2022.923598

5. Duan LJ, Wang Q, Zhang C, Yang DX, Zhang XY. Potentialities and challenges of mRNA vaccine in cancer immunotherapy. *Front Immunol* (2022) 13:923647. doi: 10.3389/fimmu.2022.923647

6. Xu C, Ju D, Zhang X. Chimeric antigen receptor T-cell therapy: challenges and opportunities in lung cancer. *Antib Ther* (2022) 5:73–83. doi: 10.1093/abt/tbac006

7. Kwon BS, Weissman SM. cDNA sequences of two inducible T-cell genes. *Proc Natl Acad Sci U.S.A.* (1989) 86:1963–7. doi: 10.1073/pnas.86.6.1963

8. Vinay DS, Kwon BS. 4-1BB (CD137), an inducible costimulatory receptor, as a specific target for cancer therapy. *BMB Rep* (2014) 47:122–9. doi: 10.5483/bmbrep.2014.47.3.283

9. Chu DT, Bac ND, Nguyen KH, Tien NLB, Thanh VV, Nga VT, et al. An update on anti-CD137 antibodies in immunotherapies for cancer. *Int J Mol Sci* (2019) 20:1822. doi: 10.3390/ijms20081822

10. Ye L, Jia K, Wang L, Li W, Chen B, Liu Y, et al. CD137, an attractive candidate for the immunotherapy of lung cancer. *Cancer Sci* (2020) 111:1461–7. doi: 10.1111/cas.14354

11. Wong HY, Schwarz H. CD137/CD137 ligand signalling regulates the immune balance: A potential target for novel immunotherapy of autoimmune diseases. *J Autoimmun* (2020) 112:102499. doi: 10.1016/j.jaut.2020.102499

12. Chester C, Sanmamed MF, Wang J, Melero I. Immunotherapy targeting 4-1BB: mechanistic rationale, clinical results, and future strategies. *Blood* (2018) 131:49–57. doi: 10.1182/blood-2017-06-741041

13. Etxeberria I, Glez-Vaz J, Teijeira A, Melero I. New emerging targets in cancer immunotherapy: CD137/4-1BB costimulatory axis. *ESMO Open* (2020) 4:e000733. doi: 10.1136/esmoopen-2020-000733

14. Armitage RJ. Tumor necrosis factor receptor superfamily members and their ligands. *Curr Opin Immunol* (1994) 6:407–13. doi: 10.1016/0952-7915(94)90119-8

15. Goodwin RG, Din WS, Davis-Smith T, Anderson DM, Gimpel SD, Sato TA, et al. Molecular cloning of a ligand for the inducible T cell gene 4-1BB: a member of an emerging family of cytokines with homology to tumor necrosis factor. *Eur J Immunol* (1993) 23:2631–41. doi: 10.1002/eji.1830231037

16. Lum L, Wong BR, Josien R, Becherer JD, Erdjument-Bromage H, Schlondorff J, et al. Evidence for a role of a tumor necrosis factor-alpha (TNF-alpha)-converting enzyme-like protease in shedding of TRANCE, a TNF family member involved in osteoclastogenesis and dendritic cell survival. *J Biol Chem* (1999) 274:13613–8. doi: 10.1074/jbc.274.19.13613

17. Powell WC, Fingleton B, Wilson CL, Boothby M, Matrisian LM. The metalloproteinase matrilysin proteolytically generates active soluble fas ligand and potentiates epithelial cell apoptosis. *Curr Biol* (1999) 9:1441–7. doi: 10.1016/s0960-9822(00)80113-x

18. Black RA, Rauch CT, Kozlosky CJ, Peschon JJ, Slack JL, Wolfson MF, et al. A metalloproteinase disintegrin that releases tumour-necrosis factor-alpha from cells. *Nature* (1997) 385:729–33. doi: 10.1038/385729a0

19. Compaan DM, Hymowitz SG. The crystal structure of the costimulatory OX40-OX40L complex. *Structure* (2006) 14:1321–30. doi: 10.1016/j.str.2006.06.015

20. Bodmer JL, Schneider P, Tschopp J. The molecular architecture of the TNF superfamily. *Trends Biochem Sci* (2002) 27:19–26. doi: 10.1016/s0968-0004(01)01995-8

21. Chattopadhyay K, Ramagopal UA, Mukhopadhaya A, Malashkevich VN, Dilorenzo TP, Brenowitz M, et al. Assembly and structural properties of glucocorticoid-induced TNF receptor ligand: Implications for function. *Proc Natl Acad Sci U.S.A.* (2007) 104:19452–7. doi: 10.1073/pnas.0709264104

22. Croft M. The role of TNF superfamily members in T-cell function and diseases. *Nat Rev Immunol* (2009) 9:271–85. doi: 10.1038/nri2526

23. Vinay DS, Kwon BS. Immunotherapy of cancer with 4-1BB. *Mol Cancer Ther* (2012) 11:1062–70. doi: 10.1158/1535-7163.MCT-11-0677

24. Wilcox RA, Tamada K, Strome SE, Chen L. Signaling through NK cell-associated CD137 promotes both helper function for CD8+ cytolytic T cells and responsiveness to IL-2 but not cytolytic activity. *J Immunol* (2002) 169:4230–6. doi: 10.4049/jimmunol.169.8.4230

25. Wortzman ME, Clouthier DL, McPherson AJ, Lin GH, Watts TH. The contextual role of TNFR family members in CD8(+) T-cell control of viral infections. *Immunol Rev* (2013) 255:125–48. doi: 10.1111/imr.12086

26. Willoughby JE, Kerr JP, Rogel A, Taraban VY, Buchan SL, Johnson PW, et al. Differential impact of CD27 and 4-1BB costimulation on effector and memory CD8 T cell generation following peptide immunization. *J Immunol* (2014) 193:244–51. doi: 10.4049/jimmunol.1301217

27. Akhmetzyanova I, Zelinskyy G, Littwitz-Salomon E, Malyshkina A, Dietze KK, Streeck H, et al. CD137 agonist therapy can reprogram regulatory T cells into cytotoxic CD4+ T cells with antitumor activity. *J Immunol* (2016) 196:484–92. doi: 10.4049/jimmunol.1403039

28. Zhang P, Gao F, Wang Q, Wang X, Zhu F, Ma C, et al. Agonistic anti-4-1BB antibody promotes the expansion of natural regulatory T cells while maintaining Foxp3 expression. *Scand J Immunol* (2007) 66:435–40. doi: 10.1111/j.1365-3083.2007.01994.x

29. Madireddi S, Schabowsky RH, Srivastava AK, Sharma RK, Yolcu ES, Shirwan H. SA-4-1BBL costimulation inhibits conversion of conventional CD4+ T cells into CD4+ FoxP3+ T regulatory cells by production of IFN-γ. *PloS One* (2012) 7:e42459. doi: 10.1371/journal.pone.0042459

30. Futagawa T, Akiba H, Kodama T, Takeda K, Hosoda Y, Yagita H, et al. Expression and function of 4-1BB and 4-1BB ligand on murine dendritic cells. *Int Immunol* (2002) 14:275–86. doi: 10.1093/intimm/14.3.275

31. Zhang X, Voskens CJ, Sallin M, Maniar A, Montes CL, Zhang Y, et al. CD137 promotes proliferation and survival of human b cells. *J Immunol* (2010) 184:787–95. doi: 10.4049/jimmunol.0901619

32. Aravinth SP, Rajendran S, Li Y, Wu M, Yi Wong AH, Schwarz H. Epstein-Barr Virus-encoded LMP1 induces ectopic CD137 expression on Hodgkin and reed-sternberg cells *via* the PI3K-AKT-mTOR pathway. *Leuk Lymphoma* (2019) 60:2697–704. doi: 10.1080/10428194.2019.1607330

33. Schmohl JU, Nuebling T, Wild J, Kroell T, Kanz L, Salih HR, et al. Expression of 4-1BB and its ligand on blasts correlates with prognosis of patients with AML. *J Investig Med* (2016) 64:1252–60. doi: 10.1136/jim-2016-000081

34. Kamijo H, Miyagaki T, Shishido-Takahashi N, Nakajima R, Oka T, Suga H, et al. Aberrant CD137 ligand expression induced by GATA6 overexpression promotes tumor progression in cutaneous T-cell lymphoma. *Blood* (2018) 132:1922–35. doi: 10.1182/blood-2018-04-845834

35. Kaban K, Greiner SM, Holzmayer S, Tandler C, Meyer S, Hinterleitner C, et al. Immunoprofiling of 4-1BB expression predicts outcome in chronic lymphocytic leukemia (CLL). *Diagnostics (Basel)* (2021) 11:2041. doi: 10.3390/diagnostics11112041

36. Choi BK, Kim YH, Kim CH, Kim MS, Kim KH, Oh HS, et al. Peripheral 4-1BB signaling negatively regulates NK cell development through IFN-gamma. *J Immunol* (2010) 185:1404–11. doi: 10.4049/jimmunol.1000850

37. Kang SW, Lee SC, Park SH, Kim J, Kim HH, Lee HW, et al. Anti-CD137 suppresses tumor growth by blocking reverse signaling by CD137 ligand. *Cancer Res* (2017) 77:5989–6000. doi: 10.1158/0008-5472.CAN-17-0610

38. Segal NH, Logan TF, Hodi FS, McDermott D, Melero I, Hamid O, et al. Results from an integrated safety analysis of urelumab, an agonist anti-CD137 monoclonal antibody. *Clin Cancer Res* (2017) 23:1929–36. doi: 10.1158/1078-0432.CCR-16-1272

39. Gordon MS, Sweeney CS, Mendelson DS, Eckhardt SG, Anderson A, Beaupre DM, et al. Safety, pharmacokinetics, and pharmacodynamics of AMG 102, a fully human hepatocyte growth factor-neutralizing monoclonal antibody, in a first-in-human study of patients with advanced solid tumors. *Clin Cancer Res* (2010) 16:699–710. doi: 10.1158/1078-0432.CCR-09-1365

40. Fisher TS, Kamperschroer C, Oliphant T, Love VA, Lira PD, Doyonnas R, et al. Targeting of 4-1BB by monoclonal antibody PF-05082566 enhances T-cell function and promotes anti-tumor activity. *Cancer Immunol Immunother* (2012) 61:1721–33. doi: 10.1007/s00262-012-1237-1

41. Gopal A, Bartlett N, Levy R, Houot R, Smith S, Segal N, et al. A phase I study of PF-05082566 (anti-4-1BB) + rituximab in patients with CD20+ NHL. *J Clin Oncol* (2015) 33:3004–4. doi: 10.1200/jco.2015.33.15_suppl.3004

42. Mayes PA, Hance KW, Hoos A. The promise and challenges of immune agonist antibody development in cancer. *Nat Rev Drug Discovery* (2018) 17:509–27. doi: 10.1038/nrd.2018.75

43. Goebeler ME, Bargou RC. T Cell-engaging therapies - BiTEs and beyond. *Nat Rev Clin Oncol* (2020) 17:418–34. doi: 10.1038/s41571-020-0347-5

44. Hashimoto K. CD137 as an attractive T cell Co-stimulatory target in the TNFRSF for immuno-oncology drug development. *Cancers (Basel)* (2021) 13:2288. doi: 10.3390/cancers13102288

45. Park DE, Cheng J, McGrath JP, Lim MY, Cushman C, Swanson SK, et al. Merkel cell polyomavirus activates LSD1-mediated blockade of non-canonical BAF to regulate transformation and tumorigenesis. *Nat Cell Biol* (2020) 22:603–15. doi: 10.1038/s41556-020-0503-2

46. Debela DT, Muzazu SG, Heraro KD, Ndalama MT, Mesele BW, Haile DC, et al. New approaches and procedures for cancer treatment: Current perspectives. *SAGE Open Med* (2021) 9:20503121211034366. doi: 10.1177/20503121211034366

47. Guillerey C, Nakamura K, Pichler AC, Barkauskas D, Krumeich S, Stannard K, et al. Chemotherapy followed by anti-CD137 mAb immunotherapy improves disease control in a mouse myeloma model. *JCI Insight* (2019) 5:e125932. doi: 10.1172/jci.insight.125932

48. Newcomb EW, Lukyanov Y, Kawashima N, Alonso-Basanta M, Wang SC, Liu M, et al. Radiotherapy enhances antitumor effect of anti-CD137 therapy in a mouse glioma model. *Radiat Res* (2010) 173:426–32. doi: 10.1667/RR1904.1

frontiers | Frontiers in Oncology

TYPE Case Report
PUBLISHED 23 September 2022
DOI 10.3389/fonc.2022.926480

OPEN ACCESS

EDITED BY
Dianwen Ju,
Fudan University, China

REVIEWED BY
Ruth Vera,
Complejo Hospitalario de Navarra, Spain
Jiang Chen,
Zhejiang University, China
Cibele Masotti,
Hospital Sirio Libanes, Brazil

*CORRESPONDENCE
Lina Zhao
zhaolina@fmmu.edu.cn
Lichun Wei
weilichun@fmmu.edu.cn

†These authors have contributed equally to this work

SPECIALTY SECTION
This article was submitted to Cancer Immunity and Immunotherapy, a section of the journal Frontiers in Oncology

RECEIVED 22 April 2022
ACCEPTED 24 August 2022
PUBLISHED 23 September 2022

CITATION
Zhang M, Yang H, Chen L, Du K, Zhao L and Wei L (2022) Pathological complete response in MMR-deficient/MSI-high and KRAS-mutant patient with locally advanced rectal cancer after neoadjuvant chemoradiation with immunotherapy: A case report. *Front. Oncol.* 12:926480. doi: 10.3389/fonc.2022.926480

Pathological complete response in MMR-deficient/MSI-high and KRAS-mutant patient with locally advanced rectal cancer after neoadjuvant chemoradiation with immunotherapy: A case report

Mai Zhang[1†], Hua Yang[1†], Ling Chen[2], Kunli Du[3], Lina Zhao[1*] and Lichun Wei[1*]

[1]Department of Radiation Oncology, The First Affiliated Hospital, Air Force Medical University, Xi an, China, [2]Department of Pathology, The First Affiliated Hospital, Air Force Medical University, Xi an, China, [3]Department of Gastrointestinal Surgery, The First Affiliated Hospital, Air Force Medical University, Xi an, China

To date, preoperative chemoradiation (CRT) is the standard of care for patients with locally advanced rectal cancer (LARC) regardless of status of mismatch repair. Immunotherapy showed promising results in the neoadjuvant treatment trials in patients with mismatch repair-deficient (dMMR) or high microsatellite instability (MSI-H) LARC. The efficacy of CRT plus programmed death 1 (PD-1) inhibitor in these patients with complex gene mutation remains unclear. Additionally, very few studies reported on whether such combination could induce abscopal effect. We report a case of dMMR and MSI-H LARC with KRAS mutation that achieved pathological complete response of primary lesion and liver metastases after neoadjuvant short-course radiotherapy followed by four cycles chemotherapy of XELOX plus PD-1 inhibitor tislelizumab and a subsequent total mesorectal excision. This case indicates that this combined treatment strategy has remarkable clinical response both in locoregional and distant diseases, which potentially leads to reduction in the risk of distant metastases and better locoregional control for this subgroup of population.

KEYWORDS

locally advanced rectal cancer, neoadjuvant chemoradiation, immunotherapy, pathological complete response, abscopal effect

Introduction

Preoperative chemoradiation (CRT) is the standard of care for patients with locally advanced rectal cancer (LARC). CRT before surgery could downstage tumors and increase local control rate, with a pCR rate of 30% in the RAPIDO trial. However, distant metastatic rate remains high, which was 20% at 3 years in the RAPIDO trial (1–3). The mismatch repair-deficient (dMMR) or high microsatellite instability (MSI-H) phenotype, accounting for approximately <10% of all rectal cancer, was considered to be sensitive to immunotherapy (4, 5). The NICHE trial showed a pathological complete response (pCR) rate of 60% in dMMR/MSI-H patients after surgery, with neoadjuvant immunotherapy of ipilimumab and nivolumab (6). The latter phase II trial investigated the efficacy of neoadjuvant programmed cell death protein 1 (PD-1) inhibitor with celecoxib and found that the pCR rate was 88% in dMMR/MSI-H colorectal cancer (7). These findings indicated that neoadjuvant immunotherapy could achieve a remarkable clinical response in downstaging tumors in dMMR/MSI-H rectal cancer. KRAS mutation occurred in approximately 40% of all colorectal cancer (8). For mCRC patients with KRAS mutations, the standard treatment is chemotherapy with or without bevacizumab. Meanwhile, chemoradiotherapy followed by surgery is the standard of care for patients with LARC irrespective of KRAS status. A previous study has revealed that MSI-H/dMMR metastatic colorectal cancer (mCRC) with KRAS or NRAS mutations could not benefit from single PD-1 inhibitor compared with chemotherapy in overall survival (9). Furthermore, whether the occurrence of locoregional recurrence and distant metastases could decrease with neoadjuvant immunotherapy remains unclear due to the immaturity of the data.

The clinical efficacy of CRT plus PD-1 inhibitor in dMMR/MSI-H LARC with KRAS mutation was rare, especially whether such combination could induce abscopal effect. Here, we present a LARC case with dMMR/MSI-H status and KRAS mutation who received short-course radiotherapy, followed by four cycles chemotherapy of XELOX plus PD-1 inhibitor tislelizumab and subsequently by a total mesorectal excision with pCR in primary tumor. Interestingly, during the treatment, a lesion was noted in the liver by imaging, and metastasis was rendered clinically; however, no tumor cells were identified by biopsy and pathological evaluation. To the best of our knowledge, this phenomenon has not been reported.

Case report

A 53-year-old man was diagnosed as having locally advanced rectal cancer in April 2021, which was 5.5 cm to the anal verge and staged as cT3N2 by magnetic resonance imaging (MRI) (Figure 1). Mesorectal fascia (MRF) was negative, and extramural vascular invasion (EMVI) was categorized as grade 3. Histopathologically, it was a moderately to poorly differentiated adenocarcinoma. The immunohistochemistry for protein of mismatch repair gene showed a deficiency of MLH1 and PMS2, which meant that it was mismatch repair gene deficient (dMMR) (Figures 2A–D). Multiplex PCR-microsatellite analysis also confirmed the MSI-H status in all markers, and the combined positive score of programmed cell death protein ligand 1 expression was grade 2 (Figure 2E). A next-generation sequencing (NGS) panel spanning 952 cancer-related genes was performed, and FBXW7, ERBB2, ERBB3, MLH1, APC, CDK12, PIK3CA, and KRAS mutations were observed. The tumor mutation burden was 52.94 mutations/megabase (the methods and the identified mutations can be seen in the Supplementary Material).

Therefore, the tumor was classified as MSI-H/dMMR rectal cancer. No evidence of liver or other distant metastases was found at initial diagnosis through contrast-enhanced computed tomography of the chest and abdomen and abdominal ultrasound examination. Reported data of LARC showed a higher likelihood of pCR rate with neoadjuvant immunotherapy in patients with dMMR/MSI-H tumor. Owing to the patient's persistent request for immunotherapy, and his dMMR/MSI-H LARC, we therefore decided within our multidisciplinary team to apply combined treatment strategy with PD-1 inhibitor tislelizumab and neoadjuvant chemoradiotherapy to enhance the efficacy of the anti-tumor therapy for his KRAS mutation. Short-course radiotherapy (5x5Gy) was performed at the beginning, and the patient then underwent four cycles of XELOX (capecitabine and oxaliplatin) with tislelizumab. Four weeks after completion of the treatment, restaging MRI showed a partial response of the rectal lesion (Figure 1). Biopsy pathology of the rectal lesion was negative.

Unfortunately, a liver lesion was detected on abdominal ultrasound examination and then clinically diagnosed as liver metastases (M1a) by dynamic-enhanced MRI and contrast-enhanced ultrasonography within our multidisciplinary team. The lesion size was 1.5 cm × 1.3 cm in MRI (Figures 3A, B). A reexamination of the baseline computed tomography of abdomen was performed and a nearly invisible, obscure lesion was detected at the corresponding location, which could represent the early stage of metastases (classified as suspicious metastases—Mx) (Figure 3C). Examination of fine-needle aspiration biopsy showed hepatic lobular structure with many lymphocyte infiltration, especially CD8-positive T cells (Figure 3D). No tumor cells were observed (Figure 3E).

We speculated that the possible reason of the new lesion in the liver was immunotherapy-related pseudoprogression. Meanwhile, radiofrequency ablation was delivered to the liver lesion for security purposes. One week later, total mesorectal excision was performed, the pathological result showed a complete response (Figure 1). Immunohistochemical analysis of the rectal tumor tissue after surgery showed that the tumor microenvironment was enriched with CD8+ T cells (Figures 2F, G). The timeline of this case is shown in Figure 4.

PD-1 inhibitor plus chemoradiation was tolerable in this patient, without significant toxicities except for grade 2 thyroid-

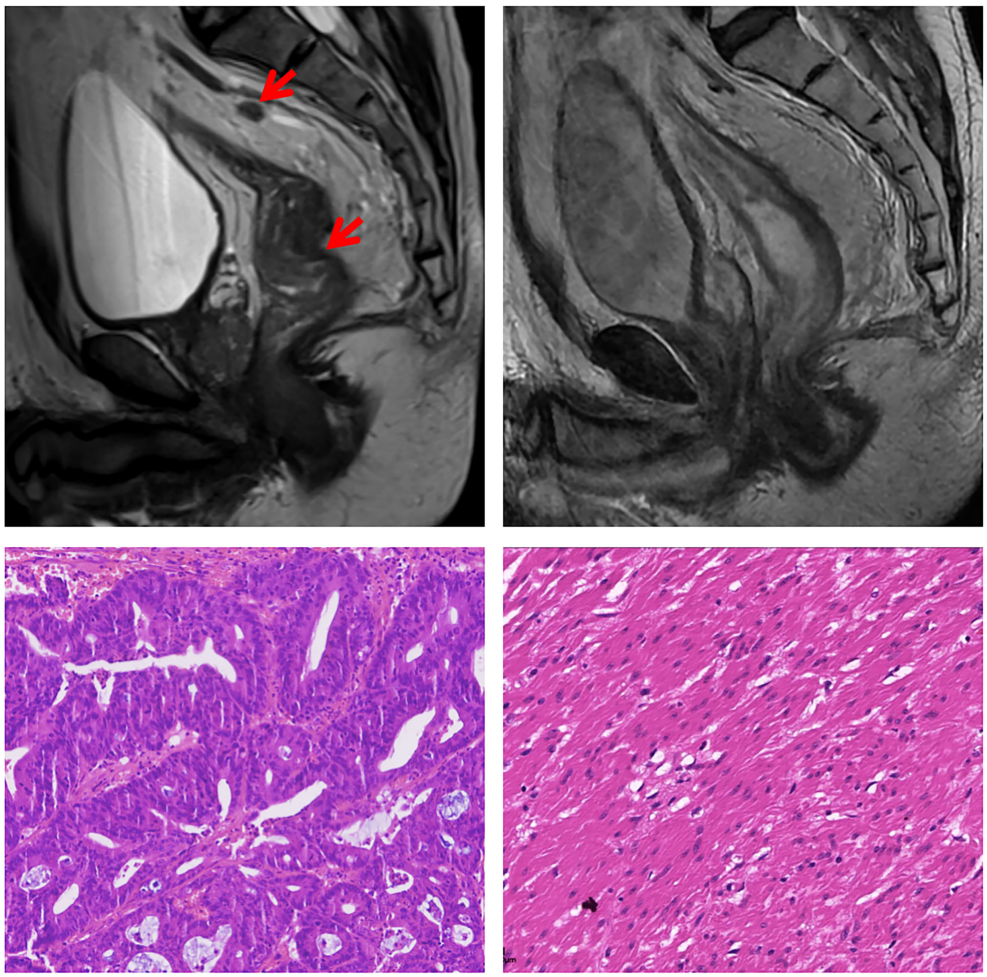

FIGURE 1
Magnetic resonance imaging and histological findings before and after treatment. In the upper row, Magnetic resonance imaging-T2 scans at diagnosis and before surgery showed partial response of the tumor. In the lower row, representative sections of tumor specimens before neoadjuvant treatment (left) and after the treatment (right) (hematoxylin and eosin staining × 200). This patient had pathological complete response of the primary tumor.

stimulating hormone increase. The surgery was delivered as scheduled without delay. Owing to the revised clinical stage, our multidisciplinary team planned to deliver adjuvant immunotherapy with single-agent tislelizumab for 6 months. The patient had finished adjuvant treatment. By the time of writing, this case has been followed up for 11 months and no evidence of disease recurrence was observed through regular re-examination (chest, abdominal, and pelvic computed tomography every 3 months, MRI of the rectum every 3 months, and CEA every 3 months).

Discussion

Increasing data on immunotherapy is challenging standard preoperative therapy of LARC patients with dMMR/MSI-H (6, 7, 10). The care regime could become even more complicated when KRAS mutation was identified in these patients. The experience in this case suggests that the novel combined strategy of CRT with immunotherapy could significantly downstage tumors. Meanwhile, it had the capacity to control distant metastases. There will be a significant trend for decision-making of neoadjuvant treatment in LARC stratified by mismatch repair or microsatellite instability and KRAS status.

A recent publication showed that single-agent PD-1 inhibitor has achieved remarkable efficacy in 12 LARC patients with dMMR/MSI-H. After neoadjuvant treatment with dostarlimab for 6 months, all patients in the trial had a clinical complete response (cCR), without subsequent chemoradiotherapy or surgery (10). However, the sustainability of disease remission needs to be verified *via* the follow-up. Regrettably, KRAS status and its

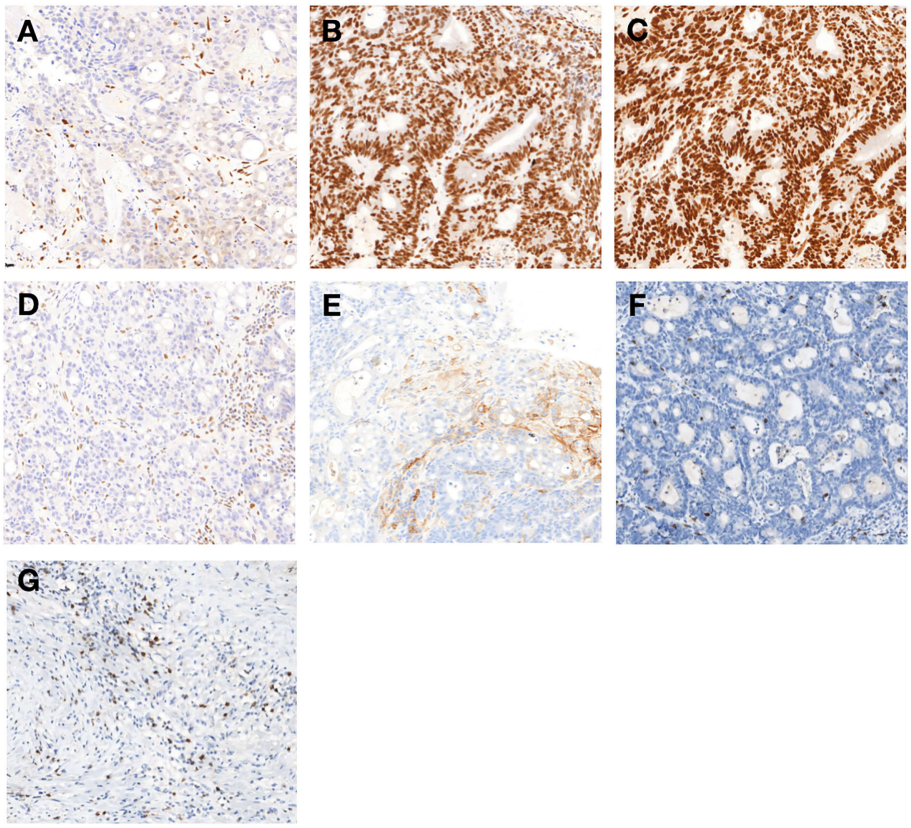

FIGURE 2
Immunohistochemical findings of primary tumor **(A–H)**: Immunohistochemistry of the protein MLH1 **(A)**, MSH2 **(B)**, MSH6 **(C)**, and PMS2 **(D)**. MSH2 and MSH6 were positively expressed, whereas MLH1 and PMS2 were lacking (200×). **(E)** The combined positive score of programmed cell death protein ligand 1 (PD-L1) expression in rectal tumor before treatment was grade 2 (200×). Immunohistochemical analysis of the rectal tumor microenvironment before treatment **(F)** and the tumor microenvironment was enriched with CD8+ T cells in primary tumor **(G)** after completion of treatment (200×).

potential implications for immunotherapy were not mentioned in the article. In the KEYNOTE-177 trial, which compared pembrolizumab versus chemotherapy dMMR/MSI-H metastatic colorectal cancer (mCRC), the forest plot of subgroup analysis revealed that no significant difference was seen in the survival benefit between PD-1 inhibitor versus chemotherapy in patients with KRAS or NRAS mutations (HR 0.92 [95% CI 0.48–1.75]) (9). The CheckMate 142 study showed that dMMR/MSI-H mCRC patients with KRAS mutation might benefit more from dual immunotherapy (11). In a pooled retrospective analysis of non-small cell lung cancer (NSCLC) patients (n = 1,430), NSCLC patients with KRAS mutation derived the greatest benefit from chemotherapy plus immunotherapy compared with either immunotherapy alone or chemotherapy alone (12). It could be seen that single PD-1 inhibitor might be insufficient, and a combined treatment would be needed for dMMR/MSI-H mCRC with KRAS mutation. In the future, it would be worth comparing the efficacy and long-term survival benefit of combined immunotherapy such as CRT plus PD-1 blockade versus single-agent immunotherapy, especially for patients with complicated gene status.

For patients with LARC after neoadjuvant therapy, organ preservation was an alternative to operation in patients who achieved cCR. Because the patient did not achieve cCR, organ preservation and subsequent watch-and-wait strategy might not be appropriate for this patient. Whether such combined treatment could improve the cCR rate and lead to subsequent organ preservation in patients with KRAS mutation still warrant further investigation. Besides, the relationship between clinical and pathological response was not equivalent. In patients who achieved cCR after neoadjuvant treatments, 74.3% of the patients were identified as pCR with local excision as reported (13). Although it still needs to be refined, such as consensus criteria of clinical assessment of cCR and management of tumor regrowth, the wait-and-see strategy still provided another option for LARC.

Radiation could remodulate the tumor microenvironment including the distant sites and enhance immune-cell recognition

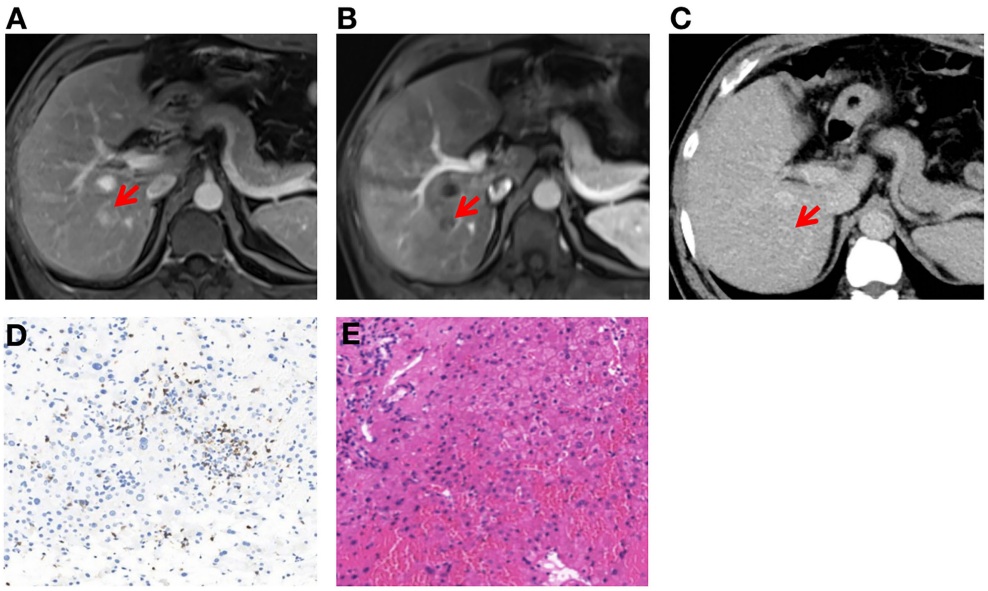

FIGURE 3
Clinical diagnosis and histological results of liver metastases **(A–E)**. **(A, B)** Dynamic-enhanced magnetic resonance imaging shows liver metastasis after neoadjuvant treatment and confirmed by contrast-enhanced ultrasonography. **(C)** Contrast-enhanced computed tomography shows no definite liver metastases before neoadjuvant treatment. **(D)** The tumor microenvironment was enriched with CD8+ T cells in liver metastases after completion of treatment (200×). **(E)** Post-treatment liver biopsy shows hepatic lobular structure with normal architecture, and no tumor cells were observed (200×).

and antigen release, which might lead to abscopal effect (14). The post-treatment specimen contained enriched CD8 + T cells, which was consistent with change in the immune microenvironment resulting from chemoradiotherapy. Neoadjuvant CRT has been shown to upregulate PD-L1 expression in rectal cancer (15). The clinical efficacy of such combination had also been confirmed. Luke et al. found that stereotactic body radiation therapy to metastatic lesions followed by pembrolizumab resulted in an abscopal response rate of 26.9% in a single-arm trial (16). Welsh et al. found that 42% of patients with lung metastases had abscopal responses in non-irradiated lesions treated with ipilimumab and sequential radiotherapy (17). Theelen et al. confirmed abscopal effect in metastatic NSCLC with a statistically significant difference. The incidence of abscopal response rate of radiotherapy with PD-1 inhibitor was significantly higher than that of single-agent PD-1 inhibitor (41.7% *vs.* 19.7%, p=0.0039) (18). Therefore, immunotherapy could synergize with CRT and had a potential to reduce the risk of distant metastasis. The surprising observation of the liver lesion in this case was perhaps attributed to the abscopal effect

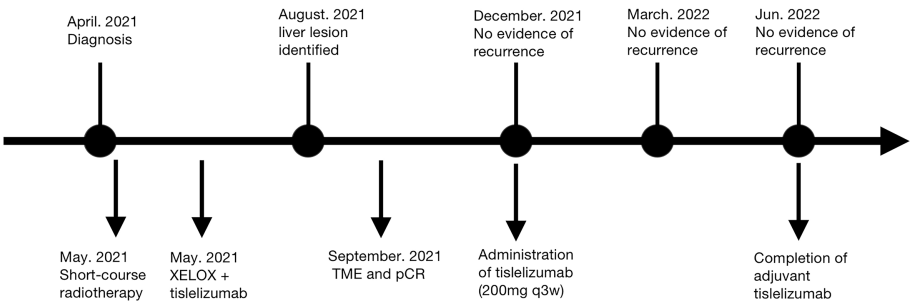

FIGURE 4
Timeline of disease status and corresponding treatment regimens. XELOX, capecitabine and oxaliplatin; TME, total mesorectal excision; pCR, pathological complete response.

enhanced by CRT-combined PD-1 inhibitor. However, the optimal pattern of dose fraction to efficiently induce an anti-tumor immune response or abscopal effect in rectal cancer remains ambiguous, and hypo-fractionated radiotherapy might have a noninferior therapeutic effect compared to conventional fractionated radiotherapy from the reported data (19, 20).

About 1% of patients with locally advanced rectal cancer will have distant metastasis during neoadjuvant treatment, which is a true progression (3). Different from true progression, pseudoprogression is an atypical response pattern of immunotherapy, observed in 10% of metastatic colorectal cancer patients with MSI-H/dMMR who received immunotherapy (21). Pseudoprogression is often followed by partial and complete responses and is considered to be associated with superior overall survival compared with real progression or stable disease (22). In this case, pseudoprogression of liver metastatic lesion was consistent with the pCR of the rectal lesion, demonstrating that the combined treatment had remarkable efficacy both in local and distant disease.

There were some limitations in this report. For example, the biopsy tissue from the liver did not represent the whole lesion sometimes. Second, follow-up duration was relatively short.

Collectively, CRT plus immunotherapy should be one option of neoadjuvant treatment for LARC patients with dMMR/MSI-H status and KRAS mutation. How to combine CRT with immunotherapy still warrants further investigation to improve the synergistic effect without significantly increased toxicity. Additional trials are underway.

Data availability statement

The raw data supporting the conclusions of this article will be made available by the authors, without undue reservation.

Ethics statement

This study was reviewed and approved by Ethics committee of Xijing Hospital. The patients/participants provided their written informed consent to participate in this study. Written informed consent was obtained from the individual(s) for the publication of any potentially identifiable images or data included in this article.

Author contributions

MZ, HY, LC, KD, LZ and LW are the members of multidisciplinary team. HY and LC collected the pathological, biological, and clinical data. MZ and LW drafted the initial manuscript. LZ and other authors reviewed or revised the manuscript and approved the final version. The corresponding author had full access to all data and had final responsibility for the decision to submit for publication. All authors contributed to the article and approved the submitted version.

Conflict of interest

The authors declare that the research was conducted in the absence of any commercial or financial relationships that could be construed as a potential conflict of interest.

Publisher's note

All claims expressed in this article are solely those of the authors and do not necessarily represent those of their affiliated organizations, or those of the publisher, the editors and the reviewers. Any product that may be evaluated in this article, or claim that may be made by its manufacturer, is not guaranteed or endorsed by the publisher.

Supplementary material

The Supplementary Material for this article can be found online at: https://www.frontiersin.org/articles/10.3389/fonc.2022.926480/full#supplementary-material

References

1. Braendengen M, Tveit KM, Berglund A, Birkemeyer E, Frykholm G, Påhlman L, et al. Randomized phase III study comparing preoperative radiotherapy with chemoradiotherapy in nonresectable rectal cancer. *J Clin Oncol* (2008) 26 (22):3687–94. doi: 10.1200/JCO.2007.15.3858

2. Sauer R, Liersch T, Merkel S, Fietkau R, Hohenberger W, Hess C, et al. Preoperative versus postoperative chemoradiotherapy for locally advanced rectal cancer: results of the German CAO/ARO/AIO-94 randomized phase III trial after a median follow-up of 11 years. *J Clin Oncol* (2012) 30(16):1926–33. doi: 10.1200/JCO.2011.40.1836

3. Bahadoer RR, Dijkstra EA, van Etten B, Marijnen CAM, Putter H, Kranenbarg EM, et al. Short-course radiotherapy followed by chemotherapy before total mesorectal excision (TME) versus preoperative chemoradiotherapy, TME, and optional adjuvant chemotherapy in locally advanced rectal cancer (RAPIDO): A randomised, open-label, phase 3 trial. *Lancet Oncol* (2021) 22 (1):29–42. doi: 10.1016/S1470-2045(20)30555-6

4. Cercek A, Dos Santos Fernandes G, Roxburgh CS, Ganesh K, Ng S, Sanchez-Vega F, et al. Mismatch repair-deficient rectal cancer and resistance to neoadjuvant chemotherapy. *Clin Cancer Res* (2020) 26:3271–9. doi: 10.1158/1078-0432.CCR-19-3728

5. Hasan S, Renz P, Wegner RE, Finley G, Raj M, Monga D, et al. Microsatellite instability (MSI) as an independent predictor of pathologic complete response (PCR) in locally advanced rectal cancer: A national cancer database (NCDB) analysis. *Ann Surg* (2020) 271:716–23. doi: 10.1097/SLA.0000000000003051

6. Chalabi M, Fanchi LF, Dijkstra KK, Van den Berg JG, Aalbers AG, Sikorska K, et al. Neoadjuvant immunotherapy leads to pathological responses in MMR-proficient and MMR-deficient early-stage colon cancers. *Nat Med* (2020) 26 (4):566–76. doi: 10.1038/s41591-020-0805-8

7. Hu H, Kang L, Zhang J, Wu Z, Wang H, Huang M, et al. Neoadjuvant PD-1 blockade with toripalimab, with or without celecoxib, in mismatch repair-deficient or microsatellite instability-high, locally advanced, colorectal cancer (PICC): A single-centre, parallel-group, non-comparative, randomised, phase 2 trial. *Lancet Gastroenterol Hepatol* (2022) 7(1):38–48. doi: 10.1016/S2468-1253(21)00348-4

8. Serebriiskii IG, Connelly C, Frampton G, Newberg J, Cooke M, Miller V, et al. Comprehensive characterization of RAS mutations in colon and rectal cancers in old and young patients. *Nat Commun* (2019) 10(1):3722. doi: 10.1038/s41467-019-11530-0

9. Diaz LAJr, KK S, Kim TW, Jensen BV, Jensen LH, Punt C, et al. KEYNOTE-177 investigators Pembrolizumab versus chemotherapy for microsatellite instability-high or mismatch repair-deficient metastatic colorectal cancer (KEYNOTE-177): Final analysis of a randomised, open-label, phase 3 study. *Lancet Oncol* (2022) 23(5):659–70. doi: 10.1016/S1470-2045(22)00197-8

10. Cercek A, Lumish M, Sinopoli J, Weiss J, Shia J, Lamendola-Essel M, et al. PD-1 blockade in mismatch repair-deficient, locally advanced rectal cancer. *N Engl J Med* (2022) 386(25):2363–76. doi: 10.1056/NEJMoa2201445

11. Overman MJ, Lonardi S, Wong KYM, Lenz HJ, Gelsomino F, Aglietta M, et al. Durable clinical benefit with nivolumab plus ipilimumab in DNA mismatch repair–Deficient/Microsatellite instability-high metastatic colorectal cancer. *J Clin Oncol* (2018) 36(8):773–9. doi: 10.1200/JCO.2017.76.9901

12. Nakajima E, Ren Y, Vallejo JJ, Akinboro O, Mishra-Kalyani PS, Larkins EA. Outcomes of first-line immune checkpoint inhibitors with or without chemotherapy according to KRAS mutational status and PD-L1 expression in patients with advanced NSCLC: FDA pooled analysis. *J Clin Oncol* (2022) 40(Suppl 16):9001. doi: 10.1200/JCO.2022.40.16_suppl.9001

13. Marchegiani F, Palatucci V, Capelli G, Guerrieri M, Belluco C, Rega D, et al. Rectal sparing approach after neoadjuvant therapy in patients with rectal cancer: The preliminary results of the ReSARCh trial. *Ann Surg Oncol* (2022) 29(3):1880–9. doi: 10.1245/s10434-021-11121-8

14. Menon H, Chen D, Ramapriyan R, Verma V, Barsoumian HB, Cushman TR, et al. Influence of low-dose radiation on abscopal responses in patients receiving high-dose radiation and immunotherapy. *J Immunother Cancer.* (2019) 7(1):237. doi: 10.1186/s40425-019-0718-6

15. Hecht M, Büttner-Herold M, Erlenbach-Wünsch K, Haderlein M, Croner R Grützmann R, et al. PD-L1 is upregulated by radiochemotherapy in rectal adenocarcinoma patients and associated with a favourable prognosis. *Eur J Cancer* (2016) 65:52–60. doi: 10.1016/j.ejca.2016.06.015

16. Luke JJ, Lemons JM, Karrison TG, Pitroda SP, Melotek JM, Zha Y, et al. Safety and clinical activity of pembrolizumab and multisite stereotactic body radiotherapy in patients with advanced solid tumors. *J Clin Oncol* (2018) 36:1611–8. doi: 10.1200/JCO.2017.76.2229

17. Welsh JW, Tang C, de Groot P, Naing A, Hess KR, Heymach JV, et al. Phase II trial of ipilimumab with stereotactic radiation therapy for metastatic disease: Outcomes, toxicities, and low-dose radiation-related abscopal responses. *Cancer Immunol Res* (2019) 7:1903–9. doi: 10.1158/2326-6066.CIR-18-0793

18. Theelen WSME, Chen D, Verma V, Hobbs BP, Peulen HMU, Aerts JGJV, et al. Pembrolizumab with or without radiotherapy for metastatic non-small-cell lung cancer: A pooled analysis of two randomised trials. *Lancet Respir Med* (2021) 9:467–75. doi: 10.1016/S2213-2600(20)30391-X

19. Morisada M, Clavijo PE, Moore E, Sun L, Chamberlin M, Van Waes C, et al. PD-1 blockade reverses adaptive immune resistance induced by high-dose hypofractionated but not low-dose daily fractionated radiation. *Oncoimmunology* (2018) 7(3):e1395996. doi: 10.1080/2162402X.2017.1395996

20. Grapin M, Richard C, Limagne E, Boidot R, Morgand V, Bertaut A, et al. Optimized fractionated radiotherapy with anti-PD-L1 and anti-TIGIT: A promising new combination. *J Immunother Cancer.* (2019) 7(1):160. doi: 10.1186/s40425-019-0634-9

21. Colle R, Radzik A, Cohen R, Pellat A, Lopez-Tabada D, Cachanado M, et al. Pseudoprogression in patients treated with immune checkpoint inhibitors for microsatellite instability-high/mismatch repair-deficient metastatic colorectal cancer. *Eur J Cancer.* (2021) 144:9–16. doi: 10.1016/j.ejca.2020.11.009

22. Jia W, Gao Q, Han A, Zhu H, Yu J. The potential mechanism, recognition and clinical significance of tumor pseudoprogression after immunotherapy. *Cancer Biol Med* (2019) 16(4):655–70. doi: 10.20892/j.issn.2095-3941.2019.0144

frontiers | Frontiers in Immunology

TYPE Case Report
PUBLISHED 05 October 2022
DOI 10.3389/fimmu.2022.983934

OPEN ACCESS

EDITED BY
Xian Zeng,
Fudan University, China

REVIEWED BY
Jian-Yong Li,
Nanjing Medical University, China
Reona Sakemura,
Mayo Clinic, United States

*CORRESPONDENCE
Lihong Liu
13831177920@163.com

SPECIALTY SECTION
This article was submitted to Cancer Immunity and Immunotherapy, a section of the journal Frontiers in Immunology

RECEIVED 01 July 2022
ACCEPTED 14 September 2022
PUBLISHED 05 October 2022

CITATION
Zhang W, Huang C, Liu R, Zhang H, Li W, Yin S, Wang L, Liu W and Liu L (2022) Case report: CD19-directed CAR-T cell therapy combined with BTK inhibitor and PD-1 antibody against secondary central nervous system lymphoma.
Front. Immunol. 13:983934.
doi: 10.3389/fimmu.2022.983934

Case report: CD19-directed CAR-T cell therapy combined with BTK inhibitor and PD-1 antibody against secondary central nervous system lymphoma

Wenqi Zhang[1], Chen Huang[1,2], Ruixia Liu[1], Huichao Zhang[3], Weijing Li[1], Shaoning Yin[1], Lianjing Wang[1], Wei Liu[1] and Lihong Liu[1,2]*

[1]Department of Hematology, The Fourth Hospital of Hebei Medical University, Shijiazhuang, China, [2]Hebei Provincial Key Laboratory of Tumor Microenvironment and Drug Resistance, Shijiazhuang, China, [3]Clinical Laboratory, The Fourth Hospital of Hebei Medical University, Shijiazhuang, China

Current therapeutic strategies for central nervous system (CNS) relapse of diffuse large B-cell lymphoma (DLBCL) are extremely limited. Secondary central nervous system lymphoma (SCNSL) also shows a grave prognosis and high mortality. This report describes a young female patient with DLBCL and CNS relapse who received low-dose CD19-directed chimeric antigen receptor T (CAR-T) cell therapy followed with Bruton's tyrosine kinase inhibitor and programmed cell death protein 1 antibody after several lines of chemotherapy. However, limited reports on CAR-T cell therapy are applied for SCNSL, particularly those in combination with targeted agents. The current treatment combination for this case provides a new regimen for CNS relapse from DLBCL.

Clinical Trial Registration: ClinicalTrials.gov number, NCT04666168.

KEYWORDS

SCNSL, CD19 CAR-T cell therapy, BTK inhibitor, PD-1 antibody, zanubrutinib, tislelizumab

Introduction

Central nervous system (CNS) relapse is one of the most devastating complications of diffuse large B-cell lymphoma (DLBCL). Studies show that CNS relapse in aggressive non-Hodgkin's lymphoma (NHL) patients accounts for 2%–27%, and the prognosis is poor with the median overall survival (OS) of only 3.9 months (1, 2). The existence of the blood–brain barrier (BBB) prevents immune and/or chemotherapeutic drugs from

penetrating into the brain and, thus, limits the therapeutic effect (3). Currently, the primary treatments for secondary central nervous system lymphoma (SCNSL) include whole brain radiation therapy (WBRT), high-dose chemotherapy–autologous stem-cell transplantation (HDCT-ASCT), or intravenous high-dose methotrexate. CD19-directed chimeric antigen receptor T (CAR-T) cell therapy, combined with novel agents, is one of the promising paradigm-changing options for CNS lymphoma (4). In 2017, the first successful case using CD19-directed CAR-T cell therapy was reported for CNS-DLBCL (5). Investigations and studies about CAR-T cell therapy in conjunction with other novel targeted agents, including Bruton's tyrosine kinase (BTK) inhibitor, programmed cell death protein 1 (PD-1) antibody revealed synergistic action for relapsed/refractory (R/R) DLBCL (6–8). BTK inhibitors could enhance the function and implantation of CAR-T cells (9). PD-1 antibody can promote their intracranial anticancer activity (10). However, TP53, as a tumor suppressor gene, modulates apoptosis in DNA-damaged cells and controls cell proliferation; the prognosis always becomes worse, and there is frequent chemotherapy resistance in DLBCL with this gene mutation (11). Promising treatment with an alternative mechanism, such as CAR-T cell therapy, could obtain a better prognosis than cytotoxic agents in a retrospective study observed by Edit Porpaczy et al. (12).

In this study, we report a case of DLBCL of CNS relapsed with TP53 mutation. The patient was enrolled in a clinical trial (ClinicalTrials.gov number, NCT04666168), which is a multicenter clinical study on the safety and efficacy of CAR-T cells in the treatment of R/R NHL as the third line therapy. In this case, we combined BTK inhibitor and PD-1 antibody with anti-CD19 CAR-T cell therapy. The patient achieved complete response (CR) for more than 18 months without any complication from this combination strategy and maintained an optimistic survival status.

Case description

A 38-year-old female patient initially presented with cough and expectoration for a month. The patient showed shortness of breath and chest tightness lasting 20 days without fever and dyspnea. The CT scan showed mediastinal masses, and treatment with antibiotics and glucocorticoid was ineffective in the local hospital. The symptoms worsened, and the patient was admitted to the emergency room at the Fourth Hospital of Hebei Medical University in October 2018. The positron emission tomography/computed tomography (PET/CT) showed several soft tissue masses, and multiple lymph nodes were found in the mediastinum, right axillary, around the thyroid, at thoracic entrance level, both internal mammary regions, behind the left diaphragmatic angle, retroperitoneum, and near right iliac vessels. The maximal standardized uptake value (SUV max) was 7.9. Some masses were distributed in the mediastinum and compressed the heart. The immunohistochemistry (IHC) from the mediastinal mass revealed CD3-, CD20+, CD21-, CD30-, Ki-67(90%+), AE/AE3-, BCL-2+, BCL-6+, CD10+, CD5-, CD23-, MUM1+, CMYC(5%), and TDT-, and the Han's algorithm was applied to determine germinal center B-cell-like (GCB) and non-GCB phenotypes according to IHC using anti-CD10, MUM1, and BCL6 antibodies (13). The result of fluorescence *in situ* hybridization (FISH) presented with EBER-. A complete blood count showed the white blood count was 10.26×10^9/L; the red blood count was 4.47×10^{12}/L; the platelet count was 339×10^9/L and hemoglobin was 124.9g/L. The patient's LDH and β2-microglobulin levels were 257 U/L and 1.37 mg/L, respectively. The patient did not present with fever, drenching night sweats, and loss of body weight, which were defined as "B symptoms" at initial diagnosis. Based on these examinations, the patient was diagnosed as stage III A GCB-DLBCL (international prognostic index (IPI) 3 points, KI-67 90%). Afterward, the patient received therapy with five cycles of rituximab combined with cyclophosphamide, liposomal doxorubicin, vincristine, and prednisone acetate (R-CHOP) in the General Hospital of the People's Liberation Army (PLAGH). The patient had a history of hepatitis B, and the HBV DNA level was detected at 5.88×10^6 IU/mL. Entecavir plus tenofovir disoproxil fumarate was used for antiviral therapy. Then, the patient obtained CR by PET/CT examination 4 months after the initial presentation. Another three cycles of R-CHOP were conducted for consolidation and maintenance treatment.

However, the first relapse occurred 4 months after the last chemotherapy (Figure 1). The patient developed lymphadenectasis in the right cervical and axillary regions and was admitted to the department of hematology in PLAGH. The PET/CT examination and CT scan indicated a large range of lesions with high metabolism, including endometrium and several parts of the bilateral diaphragm, except for the brain. The masses were considered to invade the spinal canal at T7 and T10 levels. There were also small nodules on the left breast without increased metabolism. Consequently, the patient was diagnosed with stage IV A relapse GCB-DLBCL and treated with five cycles of rituximab (600 mg on day 0) combined with ifosfamide, etoposide, carboplatin (R2-ICE), and oral lenalidomide. The mecapegfilgrastim injection was given to avoid agranulocytosis with fever after chemotherapy. Then, the patient received six cycles of methotrexate plus dexamethasone by intrathecal injection for CNS prevention. Several cerebrospinal fluid (CSF) laboratory tests revealed no abnormalities. Afterward, a PET/CT examination showed high-density enlarged lymph nodes in bilateral diaphragm regions, high metabolic parts in the endometrium, and a small nodule on the left breast disappeared. As a result, the patient was evaluated as CR2 on March 2020, but she refused consolidation chemotherapy and ASCT for further treatment.

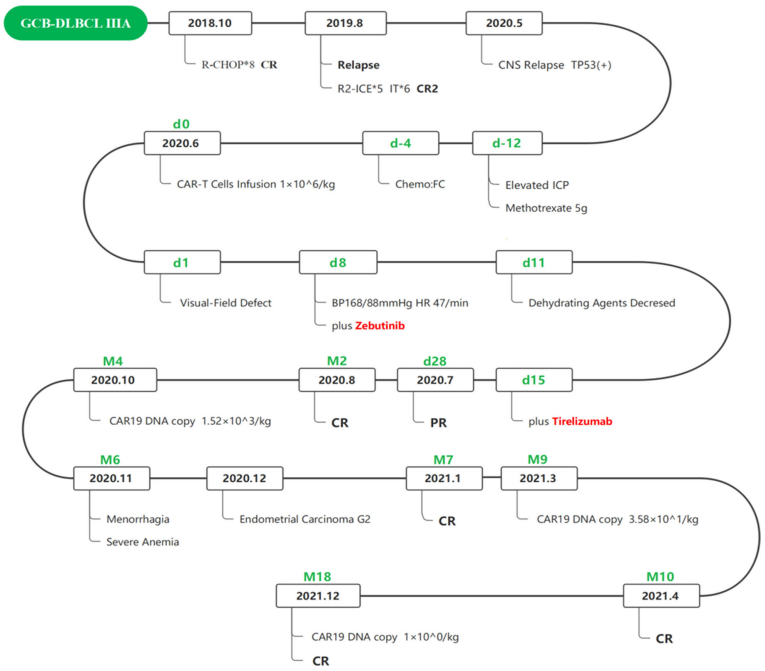

FIGURE 1
Flow chart of the disease process and therapeutic modalities.

Approximately 2 months later, the patient disease relapsed for the second time (Figure 1). The patient felt a headache for a week and was admitted to the department of hematology in the Fourth Hospital of Hebei Medical University. The compression in the right temporal and occipital lobes presented by cranial contrast-enhanced magnetic resonance imaging (MRI), and intracranial tumor infiltration was considered. The biopsy was performed by stereotactic surgery under general anesthesia. A right temporal lobe mass IHC revealed CD3-, CD20+, CD19+, CD21-, CD30-, KI-67 (80%+), CD10+, C-MYC(2%), BCL-2+, BCL-6+, MUM1+, CD38-, CD5-, and CyclinD1- (Figure 2A) and negative EBER by FISH test. Next-generation sequencing was conducted, which revealed the presence of a TP53 mutation (Table 1). Consequently, the patient was diagnosed with stage IV A CNS relapse GCB-DLBCL (TP53+), which implicated a poor prognosis.

The patient's disease was refractory to two previous lines of treatment and kept progressing. Therefore, she was enrolled in the clinical trial of CD19 CAR-T cell therapy in June 2020. Headache, dizziness, and unsteady walking presented on the fifth postoperative day, and the patient had a poor response to mannitol for dehydration and intracranial pressure reduction. Methotrexate was given at 5 g for CNS infiltration on day -12. Fludarabine (45.25 mg/m^2, days -3 to -1) and cyclophosphamide (925 mg/m^2, days -2 to -1) were administered daily for lymphodepletion. Anti-CD19 CAR-T cells were infused as 1.0×10^{6}cells/kg on day 0. Previous symptoms of this CNS relapse were not resolved, and visual-field defect occurred on the first day after anti-CD19 CAR-T cell infusion. Meanwhile, the patient's DNA copy level of the CD19 CAR-T cells in peripheral blood did not show obvious expansion, presenting as 4.6×10^1 copies/μg on day 4 and 5.65×10^1 copies/μg on day 7 (Figure 3). Neurological symptoms were not relieved and progressed on day 5 after a series of intracranial pressure reduction therapies, including administration of mannitol, glycerol fructose, and low-dose dexamethasone. However, the patient suffered a sharp increase in blood pressure at 168/88 mmHg and decreased heart rate at 47/min on day 8. The combination of BTK inhibitor (zanubrutinib; 160 mg) with CD19 CAR-T cell therapy was used to improve treatment efficacy (day 8). A week later, her elevated intracranial pressure (ICP) symptoms persisted with hypertension, heart rate reduction, intermittent dizziness, and headache with the support of dehydrating agents. DNA level of the CD19 CAR-T cells expanded slowly to 2.79×10^3 copies/μg on day 14. Therefore, a PD-1 inhibitor (tislelizumab; 200mg) was applied on day 15. The previous adverse events abated after a week without dehydrating agents, and the patient achieved partial response (PR) on day 28. Two months later, the patient was evaluated as CR by PET/CT; brain MRI; and neck, chest, and abdomen CT scan with significant clinical response (Figures 2B, C). The DNA expanded level of CD19 CAR-T cells increased but still remained low in the peripheral blood until 4 months after infusion.

After 5 months of CD19 CAR-T cell therapy combined with zanubrutinib and tislelizumab, the patient presented with menorrhagia and severe anemia. The patient received a red blood cell transfusion and responded poorly to hemostatic

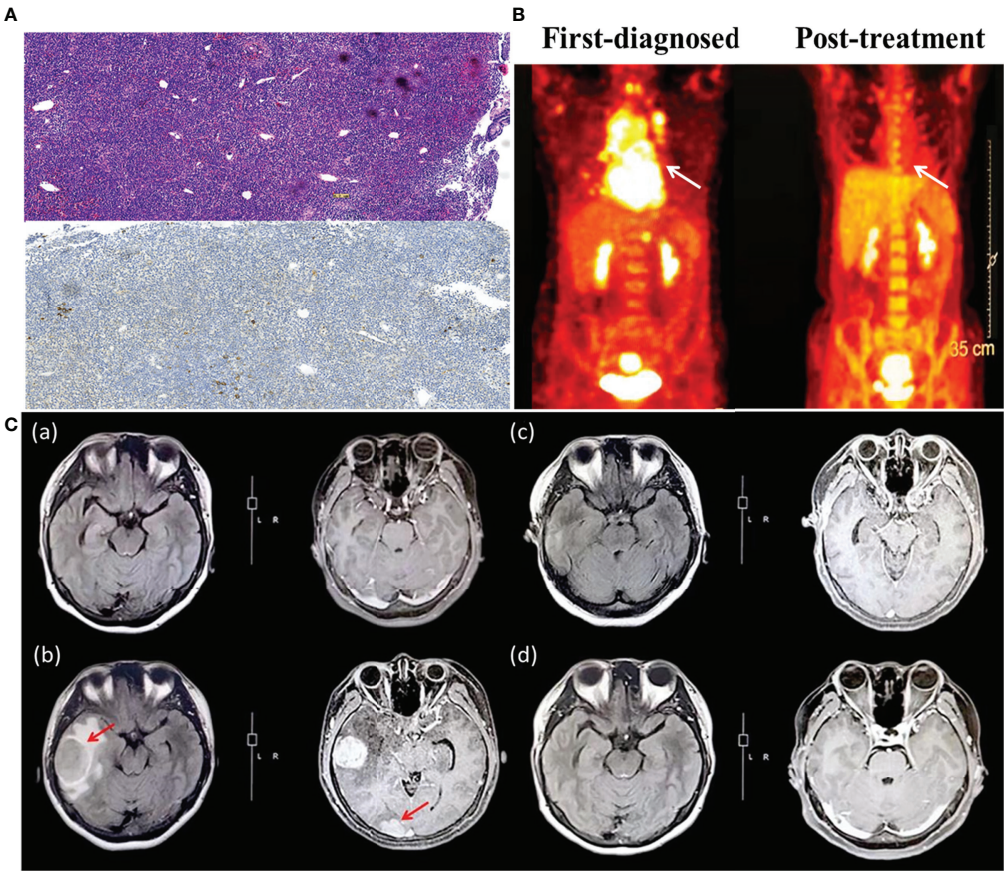

FIGURE 2
(A) The pathological section of mediastinum lymphatic tissue (upper panel: hematoxylin and eosin stain; lower panel: immunohistochemistry, CD30 negative). **(B)** Positron emission tomography assessment of patient first diagnosed (left) and after CAR-T cells infusion (right). The white arrow indicates the invasion of DLBCL on the mediastinum, which is the primary site. **(C)** Brain MRI images before and after CAR-T cell therapy. **(a)** Brain MRI on March 2020, after the second cycle of chemotherapy of R2-ICE*5 and evaluated as CR2. **(b)** Brain MRI on May 2020, when the patient showed CNS relapse. The size of the right temporal lobe and occipital lobe masses are 3.19 cm×4.03 cm and1.75 cm×2.4 cm, respectively. **(c)** The same region on October 2020, more than 4 months after CAR-T cells infusion. The mass almost disappeared and was evaluated as CR for 2 months. **(d)** The follow-up image on December 2020 with continuous CR.

agents in the local hospital. The PET/CT examination revealed complete molecular response (CMR) for DLBCL post-therapy but abnormally high metabolism in uterus (SUV max, 13.5). Afterward, the patient underwent hysterosalpingectomy and was confirmed with grade II endometrial carcinoma. The following radiotherapy for endometrial cancer was delayed because of the Covid-19 epidemic. Approximately 18 months after CD19 CAR-T cell treatment, no recurrence of symptoms was noted as stringent CR according to our follow-up (Figure 1).

Discussion

In the course of this case, the patient has failed previous multiline chemotherapy. This may be associated with TP53 mutation, which is always strongly associated with drug resistance and dismal prognosis as a negative indicator (11). Previous studies suggest CAR-T cells could potentially overcome the detrimental influence of TP53 expression (12). In addition, the disease aggressively progressed and rapidly relapsed with the longest interval shorter than 6 months. For DLBCL patients, the median survival time was less than one year if the disease recurrence interval was shorter than six months after remission and even worse in patients with CNS relapse (14). Thus, this patient had an extremely poor prognosis before CAR-T cell therapy. The administration of CAR-T cells was given only 1×10^6/kg, considering BBB was damaged due to the CNS relapse, and CAR-T cells became more permeable. However, anti-CD19 CAR-T cells initially expanded slowly in peripheral blood after infusion, but it may contribute to low toxicity and fewer adverse events. The peak level of CAR-T cells appeared on Day 14 (CAR19 DNA copies: 2.79×10^3 copies/μg; CAR-T cell expansion

TABLE 1 Gene mutation result from NGS report. The 55 hot spot genes of DLBCL were screened.

TP53	NM_000546:exon7:c.T687A :p.C229X	82.28%
DTX l	NM_004416:exon1:c.G99:p.E33D	40.30%
UBE2 A	NM_003336:exon6:c.G343A:p.El l5K	90.59%
BTGl	NM_00173 l:exon2:c.A2 17C:p.N73H	44.56%
DTX l	NM_004416:exon l:c.Al l9G:p.Y40C	43.04%
SOCSI	NM_003745:3xon2:c.C44T:p.T151	14.80%
PCLO	NM_033026 :exon3:c.G244 1C:p.S814T rs2877	99.24%
CCND3	NM_001760:exon5:c.T775G:p.S259A rsl 05 1130	99. l0%
PCLO	NM_033026:EXON5:c.G8410a:p.A2804T rs976714	98.76%
IDSTIHlC	NM_0053 19:exon l:c.C53T:p.A l 8V rs2230653	95.23%
PRDMl	NM_00 1198:exon2:c.G220A :p.G74S rs2185379	49.07%
TNFRSF14	NM_003820:exon l:c.A50G :p.K l 7R rs4870	53.67%
EZH2	NM_004456:exon6:c.G553C :p.D l 85H rs2302427	33.95%

TP53 was a primary variation, indicating a poor prognosis (December, 2021). SNP, single nucleotide polymorphism; NGS, next-generation sequence.

Primary variation Secondary variation Tertiary variation SNP.

was detected by flow cytometry: 3.64×10^7/L; CD3+CAR19 +/CD3+ T-cell: 8.55%), far from the ideal functional concentration (Figure 3). IL-6 and TNF-α were detected only on days 7 and day 14 at normal levels. The hematological indexes, cytokines, ferritin, and C-reaction protein (CRP) levels as well as temperature all remained normal (Supplementary Files, Figures S1–S4). Persisting neurological symptoms indicated disease progression rather than cytokine release syndrome (CRS) or immune effector cell associated neurotoxicity syndrome (ICANS). To the best of our knowledge, the patient's symptoms relieved rapidly after using tislelizumab. According to brain MRI, the patient's intracranial masses were significantly reduced after 5 months of the combination treatment (Figure 2C). The mechanism of incorporating of BTK inhibitor and PD-1 antibody may promote CAR-T cells' efficacy by improving the tumor

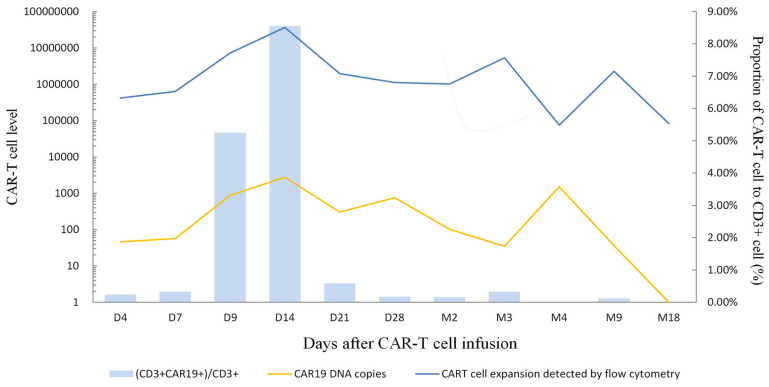

FIGURE 3
CAR19 DNA copies, CART cell expansion levels detected by flow cytometry and the proportion of CAR-T cell to CD3+ cell during treatment. The peak levels appeared on day 14 after CAR-T cell infusion, indicating CAR19 DNA copies were 2.79×103 copies/μg, CAR-T cells expansion detected by flow cytometry was 3.64×107/L and CD3+CAR19+/CD3+ T-cell was 8.55%.

microenvironment. This patient maintained great CR status with zanubrutinib and tislelizumab maintenance up to the latest follow-up (December 2021).

SCNSL has an extremely poor prognosis. Despite recent advances in treatment modalities, there is no standard and effective treatment guideline for SCNSL. Previously, a CD19 CAR-T cell therapy study emphasized a high complete remission rate and overall response rate in lymphoma patients, ranging from 40% to 60% and from 50% to 80%, respectively. However, a high relapse rate and failure risk remained elusive (15). In this case, we applied the second generation CARs containing the 4-1BB co-stimulatory signal for therapy. In most cases, CAR-T cells with 4-1BB domain possessed mild reactions with fewer ICANs and longer persistence for more than 6 months (16, 17). During R/R NHL treatment, CD19 CAR-T cells with 4-1BB co-stimulatory domain had superior safety profiles and fewer adverse events but was less effective to the disease compared with CD28 as a co-stimulatory molecule in numerous studies (18–21). Recently, a novel agent designed IM19 with 4-1BB-based co-stimulatory signal possessed durable antitumor activity to improve clinical efficacy (22).

Few reports are available on CAR-T cell therapy for SCNSL because most R/R B-cell lymphoma patients with CNS infiltration are excluded from CAR-T clinical trials. An immunosuppressive microenvironment could contribute to the escape of immune surveillance. The immunosuppressive factors, such as IL-10, TGF-β, and IDO, would possibly inhibit the activation of CAR-T cells and decrease the therapeutic effect (17). However, the immune checkpoint pathway plays a critical role in inhibitory signals to escape immune surveillance, especially the PD-1/PD-1 ligand (PD-L1) signaling pathway. It triggers T cell exhaustion and tumor tolerance. The tumor inhibitory microenvironment could be improved by blocking the PD-1/PD-L1 signaling pathway, leading to an increased T cell number and promoting antitumor efficacy. PD-1 was highly expressed in CAR-T cells, which caused weak antitumor immune response (6, 23, 24). The anti-PD-1 agent could be applied before CAR-T cell therapy or as a single agent for those extranodal relapsed DLBCL patients. PD-1 antibody enhanced CAR-T cells' function and prolonged their therapeutic effect by improving the immune microenvironment (25–29).

In terms of R/R B-cell NHL management, BTK inhibitors provide an opportunity to start a chemotherapy-free era as novel agents. Considerable research has been devoted to expanding its application for antitumor effects as targeted agents or combined with chemotherapy and immunotherapy in the last decades. Zanubrutinib is a next-generation BTK inhibitor that exhibits highly potent and less off-target toxicity (30). One pooled analysis of two clinical trials (BGB-3111-AU-003 and BGB-3111-206) revealed favorable efficacy of zanubrutinib monotherapy in R/R mantle cell lymphoma (MCL), produced an objective response rate (ORR) of 84.8% and a CR rate of 62.5% (31). In the CNS microenvironment, a hypothesis indicated that chronic antigen presentation and BCR stimulation could possibly promote BTK dependence. Zanubrutinib has superior target effects by blocking several essential molecular pathways, including BCR signaling, BTK or B-lymphocyte kinase, Toll-like receptor (TLR) signaling and downregulating exhaustion markers, such as PD-1, TIM-3, and LAG-3 (30). Zanubrutinib could cross the BBB to exert its effect, alleviating Bing–Neel syndrome with CNS lymphoplasmacytic cell infiltration among Waldenström macroglobulinemia (WM) patients and successfully applied to refractory PCNSL case (32, 33). Notably, emerging evidence has identified that zanubrutinib could modulate the immune system by inhibiting interleukin-2-inducible T-cell kinase (ITK) in T cells, which reduces T cell differentiation and shifting the balance of Th1/Th2 cells or enriches Th17 cell subsets. BTK inhibitor possesses complex interaction with CAR-T cells, which might optimize its proliferation and high tumor clearance effect under multiple preclinical trials. Narendranath et al. proposed the idea that administration of a BTK inhibitor before T cell collection could promote the level of IL-2 and IFNγ, which are associated with high self-renewal ability and production efficacy, respectively, as well as stronger cytotoxicity. Meanwhile, a case reported by Weiguo Zhu et al. considered dual inhibition of HDAC and BTK resulting in long-term remission with R/R DLBCL patients after failure of CAR-T cell therapy with TP53 mutation, which suggests underlying synergistic mechanism between BTK inhibitor and CAR-T cell therapy (7). Furthermore, BTK inhibitor enabled the reduction of PD-1 and cytotoxic T lymphocyte-associated protein 4 (CTLA-4) to overturn the exhausted T cell phenotype. Consequently, combining PD-1 antibody and BTK inhibitor was demonstrated to possess a stronger synergistic antitumor reaction than any single one of them with a manageable safety profile, resulting in 40% objective response rate (ORR) among GCB-DLBCL patients (30). However, the combination of PD-1 antibody or BTK inhibitor requires a novel approach to tackle their drug resistance and immune regulations such as CAR-T cell therapy, which could lead to a striking response (30).

Concluding remarks

This case report study describes a refractory DLBCL patient who developed CNS relapse and was successfully treated with anti-CD19 CAR-T cell therapy plus BTK inhibitor and PD-1 antibody. The therapy reversed the patient's dangerous condition and led to remarkable response without any ICANS. This patient sustained CR for more than 18 months without any adverse event by continuously taking zanubrutinib and tislelizumab. However, limitations still remain in our study. The BTK inhibitor and PD-1 antibody showed synergistic effects to CAR-T cell therapy, but we cannot figure out their mechanisms of action, respectively. Further research efforts

should focus on the potential treatment efficacy of CAR-T cell therapy with multimodality adjuvant protocol. Despite limitations, this treatment scheme provided an impetus and inspired-future strategies for similar disease. The successful experience with this case warrants further clinical studies.

Data availability statement

The original contributions presented in the study are included in the article/Supplementary Material. Further inquiries can be directed to the corresponding author.

Ethics statement

The studies involving human participants were reviewed and approved by the Institutional Ethics Committee of the Fourth Hospital of Hebei Medical University. The patients/participants provided their written informed consent to participate in this study. Written informed consent was obtained from the individual(s) for the publication of any potentially identifiable images or data included in this article.

Author contributions

RL was the physician-in-charge. WZ, LL designed the clinical protocol and wrote the manuscript. SY, WJL, LW and WL were the clinicians who participated in the treatment of the patient. HZ analyzed data. All authors contributed to the article and approved the submitted version.

Funding

This study was funded by the 2021 Hebei Provincial Department of Finance government-funded clinical medicine talent training project: Application of human CD19 CAR-T cells in recurrent, refractory B-cell lymphoma to L.L.H.

Conflict of interest

The authors declare that the research was conducted in the absence of any commercial or financial relationships that could be construed as a potential conflict of interest.

Publisher's note

All claims expressed in this article are solely those of the authors and do not necessarily represent those of their affiliated organizations, or those of the publisher, the editors and the reviewers. Any product that may be evaluated in this article, or claim that may be made by its manufacturer, is not guaranteed or endorsed by the publisher.

Supplementary material

The Supplementary Material for this article can be found online at: https://www.frontiersin.org/articles/10.3389/fimmu.2022.983934/full#supplementary-material

SUPPLEMENTARY FIGURE 1
Hematological indexes remained normal during the treatment process.

SUPPLEMENTARY FIGURE 2
Changes in Ferritin and C-reaction protein (CRP) levels before and after CAR-T cell infusion.

SUPPLEMENTARY FIGURE 3
Serum levels of cytokines were monitored after CAR-T cell infusions. Elevated serum of IL-18 was detected on day 21 and 28, respectively. IL-17A and MCP-1 reached peak level on day 7 and day 28, respectively.

SUPPLEMENTARY FIGURE 4
The temperature reached 37.8°C on the eighth day, accompanied by severe symptoms of intracranial hypertension, then recovered quickly and remained normal for the rest of the time.

References

1. Zhang J, Chen B and Xu X. Impact of rituximab on incidence of and risk factors for central nervous system relapse in patients with diffuse large b-cell lymphoma: A systematic review and meta-analysis. *Leuk. Lymphoma* (2013) 55:509–14. doi: 10.3109/10428194.2013.811239

2. El-Galaly TC, Cheah CY, Bendtsen MD, Nowakowski GS, Kansara R, Savage KJ, et al. Treatment strategies, outcomes and prognostic factors in 291 patients with secondary CNS involvement by diffuse large b-cell lymphoma. *Eur J Cancer* (2018) 93:57–68. doi: 10.1016/j.ejca.2018.01.073

3. Ayed AO, Chiappella A, Pederson L, Laplant BR, Congiu AG, Gaidano G, et al. CNS relapse in patients with DLBCL treated with lenalidomide plus r-CHOP (R2CHOP): Analysis from two phase 2 studies. *Blood Cancer J* (2018) 8(7):63. doi: 10.1038/s41408-018-0097-0

4. Ahmed G, Hamadani M and Shah NN. CAR T-cell therapy for secondary CNS DLBCL. *Blood Adv* (2021) 5:5626–30. doi: 10.1182/bloodadvances.2021005292

5. Abramson JS, McGree B, Noyes S. Anti-CD19 CAR T cells in CNS diffuse Large-B-Cell lymphoma. *N Engl J Med* (2017) 377(8):783–4. doi: 10.1056/NEJMc1704610

6. Niu Z, Sun L, Wen S, Song Z, Xing L, Wang Y, et al. Programmed cell death protein-1 inhibitor combined with chimeric antigen receptor T cells in the treatment of relapsed refractory non-Hodgkin lymphoma: A case report. *World J Clin cases.* (2021) 9:2394–9. doi: 10.12998/wjcc.v9.i10.2394

7. Zhu W, Tao S, Miao W, Liu H, Yuan X. Case report: Dual inhibition of HDAC and BTK for diffuse Large b-cell lymphoma after failure to CD19-targeted CAR-T therapy. *Front Immunol* (2022) 13:894787. doi: 10.3389/fimmu.2022.894787

8. Liu M, Wang X, Li Z, Zhang R, Mu J, Jiang Y, et al. Synergistic effect of ibrutinib and CD19 CAR-T cells on raji cells in vivo and *in vitro*. *Cancer Sci* (2020) 111(11):4051–60. doi: 10.1111/cas.14638

9. Mhibik M, Wiestner A and Sun C. Harnessing the effects of BTKi on T cells for effective immunotherapy against CLL. *Int J Mol Sci* (2020) 21:68. doi: 10.3390/ijms21010068

10. Xinfeng Chen XLYL, Huang HLFL, Sun HYZZ, Ying Zeng XWYH. A phase I clinical trial of chimeric antigen receptor-modified T cells in patients with relapsed and refractory lymphoma. *Immunotherapy-uk* (2020) 12(10):681–96. doi: 10.2217/imt-2020-0022

11. Bernard E, Nannya Y, Hasserjian RP, Devlin SM, Tuechler H, Juan S, Medina-Martinez JS, et al. Implications of TP53 allelic state for genome stability, clinical presentation and outcomes in myelodysplastic syndromes. *Nat Med* (2020) 26:1549–56. doi: 10.1038/s41591-020-1008-z

12. Porpaczy E, Wohlfarth P, Königsbrügge O, Rabitsch W, Skrabs C, Staber P, et al. Influence of TP53 mutation on survival of diffuse Large b-cell lymphoma in the CAR T-cell era. *Cancers* (2021) 13:5592. doi: 10.3390/cancers13225592

13. Cheson BD, Pfistner B, Juweid ME, Gascoyne RD, Specht L, Horning SJ, et al. Revised response criteria for malignant lymphoma. *J Clin Oncol* (2007) 25:579–86. doi: 10.1200/JCO.2006.09.2403

14. Spiegel JY, Dahiya S, Jain MD, Tamaresis J, Nastoupil LJ, Jacobs MT, et al. Outcomes of patients with Large b-cell lymphoma progressing after axicabtagene ciloleucel therapy. *Blood* (2021) 137(13):1832–5. doi: 10.1182/blood.2020006245

15. Chong EA, Ruella M, Schuster SJ. Five-year outcomes for refractory b-cell lymphomas with CAR T-cell therapy. *N Engl J Med* (2021) 384:673–4. doi: 10.1056/NEJMc2030164

16. Maude SLFN. Chimeric antigen receptor T cells for sustained remissions in leukemia. *N Engl J Med* (2014) 371(16), 1507–17. doi: 10.1056/NEJMoa1407222

17. Li X, Chen W. Mechanisms of failure of chimeric antigen receptor T-cell therapy. *Curr Opin Hematol* (2019) 26:427–33. doi: 10.1097/MOH.0000000000000548

18. Ying Z, He T, Wang X, Zheng W, Lin N, Tu M, et al. Parallel comparison of4-1BB or CD28 co-stimulated CD19-targeted CARTcells for b cell non-hodgkin's lymphoma. *Mol Ther Oncolytics* (2019) 15:60–8. doi: 10.1016/j.omto.2019.08.002

19. Zhao X, Yang J, Zhang X, Lu X, Xiong M, Zhang J, et al. Efficacy and safety of CD28- or 4-1BB-based CD19 CAR-T cells in b cellacute lymphoblastic leukemia. *Mol Ther Oncolytics* (2020) 18:272–81. doi: 10.1016/j.omto.2020.06.016

20. Locke FL, Neelapu SS, Bartlett NL, Siddiqi T, Chavez JC, Hosing CM, et al. Phase 1results of ZUMA-1: A multicenter study of KTE-C19anti-CD19 CAR T cell therapy in refractoryaggressive lymphoma. *Mol Ther* (2017) 25:285–95. doi: 10.1016/j.ymthe.2016.10.020

21. Westin JR, Kersten MJ, Salles G, Abramson JS, Schuster SJ, Locke FL, et al. Efficacy andsafety of CD19-directed CAR-T cell therapies inpatients with relapsed/refractory aggressive b-celllymphomas: Observations from the JULIET, ZUMA1, and TRANSCEND trials. *Am J Hematol* (2021) 96:1295–312. doi: 10.1002/ajh.26301

22. Ying Z, He T, Jin S, Wang X, Zheng W, Lin N, et al. A durable 4-1BB-based CD19 CAR-T cell for treatment of relapsed or refractory non-Hodgkin lymphoma. *Chin J Cancer Res* (2022) 34(1):53–62. doi: 10.21147/j.issn.1000-9604.2022.01.05

23. Parihar R, Rivas C, Huynh M, Rooney CM, Omer B, Lapteva N, et al. NK cells expressing a chimeric activating receptor eliminate MDSCs and rescue impaired CAR-T cell activity against solid tumors. *Cancer Immunol Res* (2019) 7:363–75. doi: 10.1158/2326-6066.CIR-18-0572

24. Shi X, Zhang D, Li F, Zhang Z, Wang S, Xuan Y, et al. Targeting glycosylation of PD-1 to enhance CAR-T cell cytotoxicity. *J Hematol Oncol* (2019) 12(1):127. doi: 10.1186/s13045-019-0831-5

25. McGowan. E, Lin. Q, Ma. G, Lin. Y, Yin H, Chen S, et al. PD-1 disrupted CAR-T cells in the treatment of solid tumors: Promises and challenges. *BioMed Pharmacother* (2020) 121:109625. doi: 10.1016/j.biopha.2019.109625

26. Hu. W, Zi. Z, Jin. Y, Li G, Shao K, Wei. F, et al. CRISPR/Cas9-mediated PD-1 disruption enhances human mesothelin-targeted CAR T cell effector functions. *Cancer Immunol Immunother* (2019) 68:365–77. doi: 10.1007/s00262-018-2281-2

27. Simon. B, Harrer. DC, Schuler-Thurner. B, Schaft N, Schuler G, Dorrie J, et al. The siRNA mediated down-regulation of PD-1 alone or simultaneously with CTLA-4 shows enhanced *in vitro* CAR-t-cell functionality for further clinical development towards the potential use in immunotherapy of melanoma. *Exp Dermatol* (2018) 27:769–78. doi: 10.1111/exd.13678

28. Heczey. A, Louis. CU, Savoldo. B, Dakhova O, Durett A, Grilley B, et al. CAR T cells administered in combination with lymphodepletion and PD-1 inhibition to patients with neuroblastoma. *Mol Ther* (2017) 25:2214–24. doi: 10.1016/j.ymthe.2017.05.012

29. Cherkassky L, Morello A, Villena-Vargas J, Feng Y, Dimitrov DS, Jones DR, et al. Human CAR T cells with cell-intrinsic PD-1 checkpoint blockade resist tumor-mediated inhibition. *J Clin Invest* (2016) 126:3130–44. doi: 10.1172/JCI83092

30. Wen T, Wang J, Shi Y, Qian H and Liu P. Inhibitors targeting bruton's tyrosine kinase in cancers: drug development advances. *Leukemia* (2021) 35:312–32. doi: 10.1038/s41375-020-01072-6

31. Zhou K, Zou D, Zhou J, Hu J, Yang H, Zhang H, et al. Zanubrutinib monotherapy in relapsed/refractory mantle cell lymphoma: A pooled analysis of two clinical trials. *J Hematol Oncol* (2021) 14:167. doi: 10.1186/s13045-021-01174-3

32. Cheng Q, Wang J, Lv C, Xu. J. Successful management of a patient with refractory primary central nervous system lymphoma by zanubrutinib. *Onco Targets Ther* (2021) 14:3367–72. doi: 10.2147/OTT.S309408

33. Wong J, Cher L, Griffiths J, Cohen A, Huang J, Wang L, et al. Efffcacy of zanubrutinib in the treatment of bing-neel syndrome. *Hemasphere* (2018) 2(6): e155. doi: 10.1097/HS9.0000000000000155

frontiers | Frontiers in Immunology

TYPE Original Research
PUBLISHED 07 October 2022
DOI 10.3389/fimmu.2022.970534

OPEN ACCESS

EDITED BY
Xian Zeng,
Fudan University, China

REVIEWED BY
Yan Zheng,
Henan Provincial Cancer Hospital, China
Wenwu He,
Sichuan Cancer Hospital, China

*CORRESPONDENCE
Jun Wang
wangjunzr@163.com
Jun-Feng Liu
13931152296@163.com

SPECIALTY SECTION
This article was submitted to Cancer Immunity and Immunotherapy, a section of the journal Frontiers in Immunology

RECEIVED 16 June 2022
ACCEPTED 22 September 2022
PUBLISHED 07 October 2022

CITATION
Jing S-W, Zhai C, Zhang W, He M, Liu Q-Y, Yao J-F, Wang R, Tian Z-Q, Wang J and Liu J-F (2022) Comparison of neoadjuvant immunotherapy plus chemotherapy versus chemotherapy alone for patients with locally advanced esophageal squamous cell carcinoma: A propensity score matching. *Front. Immunol.* 13:970534. doi: 10.3389/fimmu.2022.970534

Comparison of neoadjuvant immunotherapy plus chemotherapy versus chemotherapy alone for patients with locally advanced esophageal squamous cell carcinoma: A propensity score matching

Shao-Wu Jing[1], Chang Zhai[1], Wei Zhang[1], Ming He[2], Qing-Yi Liu[2], Ji-Fang Yao[2], Rui Wang[2], Zi-Qiang Tian[2], Jun Wang[1]* and Jun-Feng Liu[2]*

[1]Department of Radiation Oncology, Fourth Hospital of Hebei Medical University, Shijiazhuang, China, [2]Department of Cardiothoracic Surgery, Fourth Hospital of Hebei Medical University, Shijiazhuang, China

Objectives: Clinical studies on immune checkpoint inhibitors (ICIs) combined with neoadjuvant chemotherapy (nCT) have been carried out for the resectable esophageal squamous cell carcinoma (ESCC). So far, few studies have compared the survival outcomes of nCT plus ICIs and nCT alone. This study aimed to compare the efficacy and safety of neoadjuvant ICIs combined with nCT versus nCT followed by esophagectomy for patients with resectable locally advanced ESCC.

Methods: A retrospective analysis of ESCC patients underwent nCT or nCT combined with ICIs followed by esophagectomy (from March 2013 to April 2021) was performed. A 1:1 propensity score matching (PSM) with a caliper 0.01 was conducted to balance potential bias.

Results: A total of 47 comparable pairs of ESCC patients receiving nCT and nCT combined with ICIs were selected for the final analysis. The tumor regression grade (TRG) 0 and pathologic complete response (pCR) rates in the nCT+ICIs group were significantly higher than those of the nCT group (21.7% vs. 4.5%, P=0.016; and 17.0% vs. 2.1%, P=0.035, respectively). The rate of nerve invasion was 4.3% in the nCT+ICIs group, significantly lower than 23.4% of the nCT group (P=0.007). The incidences of adverse events in the nCT+ICIs group were similar compared with the nCT group and there was no grade 5 toxicity in either group. The 1-, 2-year disease-free survival rates (DFS) were 95.7%, 80.7% and 76.1%, 63.8% in the two groups (P=0.001, and P=0.046, respectively). The 1-

year OS was improved in the nCT+ICIs group, which was close to a statistical difference (95.7% vs. 84.8%, *P*=0.074). Local recurrence rate in the nCT+ICIs group was 6.4%, significantly lower than 21.3% of the nCT group (*P*=0.036), while there was no significant difference in the distant metastasis.

Conclusions: Compared with nCT alone, neoadjuvant immunotherapy plus nCT for patients with locally advanced ESCC has an advantage in pathological response, and could improve DFS with a good safety and feasibility, while long term survival validation is still needed further.

KEYWORDS

esophageal squamous cell carcinoma, neoadjuvant chemotherapy, immune checkpoint inhibitors, esophagectomy (or surgery), propensity score matching

Background

Esophageal carcinoma (EC) ranks seventh in terms of incidence (604, 000 new cases) and sixth in mortality overall (544, 000 deaths) in the world (1). In China, EC is the sixth leading type of cancer and the fourth most common cause of death from cancer, with approximately 320, 000 new cases and 300, 000 deaths in 2020 (2). For resectable locally advanced EC, the CROSS trial and NEOCRTEC 5010 have established neoadjuvant chemoradiotherapy (nCRT) followed by surgery as a cornerstone of the treatment strategy (3, 4). However, a meta analysis involving three randomized controlled trials showed that compared with neoadjuvant chemotherapy (nCT), the overall survival (OS) was not improved in nCRT group (HR: 0.749; 95% CI: 0.397-1.413; P=0.372), although R0 resection and pathologic complete response (pCR) rates are significantly increased (5). A network meta-analysis reveals that nCRT was associated with more postoperative complications and higher postoperative mortality (6). A three-arm randomized phase III study, JCOG 1109, was launched in 2013 to confirm the superiority of preoperative chemotherapy with docetaxel, cisplatin plus 5-fluorouracil (DCF), or chemoradiotherapy with CF (CF-RT) in overall survival over CF for locally advanced esophageal cancer. In 2022, JCOG 1109 demonstrates that nCRT could not significantly improved OS when compared to neoadjuvant CF, whereas DCF did (7). But real-world evidence has been reported that neoadjuvant DCF is not suitable for patients with poor lung function and elderly patients (8). It is urgent to explore novel pattern of neoadjuvant therapy for EC.

O, Reilly et al. (9) reviewed the role of immunotherapy (IO) agents in both early-stage and advanced-stage disease of EC with randomized phase III trials, they proposed that for advanced esophageal squamous cell carcinoma (ESCC) patients, immune checkpoint inhibitors (ICIs) in combination with chemotherapy should be offered in the first-line setting to IO-naive patients regardless of tumor programmed death receptor ligand-1 expression. Recently, a meta analysis revealed that neoadjuvant IO combined with nCT could be used as the recommended therapeutic option (10). However, there is no high quality evidence published for ESCC with neoadjuvant IO, and numerous clinical studies are ongoing for this promising therapy strategy (11, 12). A pilot study including 16 patients diagnosed with locally advanced ESCC had investigated the clinical value and tolerance of neoadjuvant camrelizumab plus paclitaxel and carboplatin, indicated that neoadjuvant IO plus chemotherapy exhibits good efficacy and acceptable tolerance (13). Till now, the most published reports are single-arm clinical trials, few studies compare the survival outcomes of nCT plus ICIs and nCT alone. Huang et al. (14) analyzed efficacy and safety between pembrolizumab combined with chemotherapy and simple chemotherapy in neoadjuvant therapy for ESCC. The pCR and objective response rate (ORR) in the combined group were significantly higher than those of the chemotherapy only group. Nevertheless, we still press for more clinical data including survival outcomes to stand in need of the role of neoadjuvant immunochemotherpay for ESCC. In this study, we aimed to compare the efficacy and safety of neoadjuvant ICIs combined with nCT versus nCT followed by esophagectomy for patients with resectable locally advanced ESCC.

Patients and methods

Patients selection

Data of ESCC patients who underwent esophagectomy followed nCT or nCT combined with ICIs in our hospital from March 2013 to April 2021 were retrospectively collected. Inclusion criteria were included: patients with locally advanced

resectable stage ESCC; the disease was histopathologically confirmed in tissue samples; receiving simple nCT or plus ICIs following esophagectomy; at least one of the following primary outcomes were reported: R0 resection rate; pCR; incidence of complications and survival. Exclusion criteria included patients with non-resectable tumors or metastases during exploratory surgery; patients receiving other neoadjuvant targeted therapy; patients receiving salvage or palliative surgery. The 8th edition of the International Union Against Cancer/American Joint Committee on Cancer (UICC/AJCC) TNM staging system was used. All procedures were performed in accordance with the 2013 edition of the Declaration of Helsinki. The study protocol was approved by the Ethic Committee of our Hospital. Due to the retrospective nature of the study, informed consent was waived.

Neoadjuvant treatment regimens

Patients in the nCT+ICIs group received 1-3 cycles of intravenous PD-1 inhibitor (pembrolizumab at a dose of 200mg, camrelizumab at a dose of 200mg, toripalimab at a dose of 240mg, or sintilimab at a dose of 200mg) every 3 weeks and simultaneous chemotherapy consisted of platinum-based drugs and 5-fluorouracil (FP) or docetaxel/paclitaxel (TP). The median usage cycle of neoadjuvant therapy was 2 in this group. Patients in the nCT group received 1-3 chemotherapy (FP or TP regimen) every 3 weeks, and the median usage cycle in this group was 2 either.

Surgical treatment

For patients suitable for radical esophagectomy after clinical evaluation, the surgery was performed after 4-8 weeks from the end of the last neoadjuvant therapy. Patients received thoracomy esophagectomy, or minimally invasive esophagectomy (MIE), including 2-field or 3-field lymphadenectomy and gastric reconstruction. Two-field lymphadenectomy was regularly conducted, and standard 3-field lymphadenectomy was performed in patients with suspected swollen lymph nodes in the neck.

Follow-up

The surveillance tests, including physical examination, chest computed tomography (CT), and barium scans were regularly performed during the follow-up, and ultrasonography, endoscopy or positron emission tomography (PET)/CT and magnetic resonance imaging (MRI) were employed if necessary. Toxicity was assessed according to the Common Terminology Criteria for Adverse Events (CTCAE; version 3.0). Surgical complications were recorded within 1 month after resection. All patients were followed up every 3 to 4 months in the first year, followed by an interval of 6 months in the next years.

Study endpoints

The primary endpoints were the tumor regression grade (TRG), R0 resection rate and pCR rate. The secondary endpoints included toxicities, disease-free survival (DFS), OS, and failure modes. The TRG was evaluated by the proportion of scar and residual tumor, and it was grading into 5 degrees according to Ryan, s TRG system (15): Grade 0 was no residual tumor, grade 1 was residual single tumor cells or small groups of tumor cells, grade 2 was residual partial of tumor, and grade 3 was no regression. pCR was defined as no evidence of residual tumor cells in the primary site and resected lymph nodes of operative specimens. DFS referred to the time from the date of neoadjuvant therapy to the first documentation of recurrence or metastasis. OS was defined as the time from the date of neoadjuvant therapy to death from any cause or lost follow-up.

Statistical analysis

A one-to-one matching analysis was performed using a caliper width of 0.01 between the nCT+ICIs and nCT groups. The propensity scores were calculated using a logistic regression model, which included age, gender, body mass index (BMI), tumor location, tumor length, clinical stage, surgical procedures and interval from neoadjuvant therapy to surgery. The rates of R0 resection, pCR, complications and failure modes were compared by the Kruskal-Wallis method or the independent-samples t-test. In order to indicate normality of the continuous and categorical variables, the Chi-square test and the Fisher's exact test were utilized, respectively. The DFS and OS were determined by the Kaplan-Meier method and were compared by the log-rank test. A P-value<0.05 was considered statistically significant. The statistical analysis was performed using SPSS 22.0 software (IBM, Armonk, NY, USA).

The propensity score matching (PSM) approach was used for the assembly of a well-balanced cohort using all available explanatory factors (16). Thus, PSM (nCT+ICIs group: nCT group in a 1:1 match) was conducted to adjust the available explanatory factors, including age, gender, BMI, tumor location, tumor length, stage T, stage N, TNM, surgical procedures and interval from neoadjuvant therapy to surgery, which might affect the results.

Results

Patients' baseline characteristics

According to the inclusion and exclusion criteria, 453 patients diagnosed with locally advanced ESCC from March

2013 to April 2021 were enrolled, of whom 48 patients were in the nCT+ICIs group, and 405 patients were in the nCT group. Then, to balance the potential bias, a 1:1 PSM was conducted, and eventually, 47 comparable pairs were matched for the final analysis. The baseline characteristics were listed in Table 1. After PSM, the clinical characteristics were well balanced, including age, gender, BMI, tumor location, tumor length, clinical stage T, clinical stage N, clinical stage TNM, chemotherapy regimen, neoadjuvant cycle, surgical approach and interval from neoadjuvant therapy to surgery.

Neoadjuvant treatment and surgical treatment outcome

Compared with the nCT group, the nCT+ICIs group had an advantage in pathological response. There were 10 cases (21.7%)

TABLE 1 Baseline characteristics before and after PSM.

Variables	Before PSM			After PSM		
	nCT+ICIs (n)	nCT(n)	*P*-value	nCT+ICIs(n)	nCT(n)	*P*-value
Age (years old)						
≤60	13	181	0.020	13	12	0.815
>60	35	224		34	35	
Gender						
Male	31	287	0.368	30	33	0.510
Female	17	118		17	14	
BMI (kg/m^2)						
≤22.9	23	208	0.652	22	26	0.409
>22.9	25	197		25	21	
Tumor location						
Upper-thoracic	4	38	0.935	4	1	0.170
Middle-thoracic	37	297		36	43	
Lower-thoracic	7	70		7	3	
Tumor length						
≤5cm	25	236	0.412	25	33	0.090
>5cm	23	169		22	14	
Clinical stage T						
T3	47	400	1.000	47	47	–
T4a	1	5		–	–	
Clinical stage N						
N0	27	225	0.953	26	30	0.661
N1	15	134		15	13	
N2	6	46		6	4	
Clinical stage TNM						
II	26	224	0.176	26	30	0.401
III	21	176		21	17	
IVA	1	5		–	–	
Chemotherapy regimen						
TP	38	333	0.603	37	38	0.797
FP	10	72		10	9	
Neoadjuvant cycle						
1	15	130	0.905	15	23	0.093
≥2	33	275		32	24	
Surgical approach						
Thoracotomy	27	314	0.001	26	33	0.135
MIE	21	91		21	14	
Interval to surgery	44.1±12.9	34.5±15.7	<0.001	40.0±11.2	39.5±10.2	0.766

PSM, propensity score matching; BMI, body mass index; nCT, neoadjuvant chemotherapy; ICIs, immune checkpoint inhibitors; MIE, minimally invasive esophagectomy.

of TRG 0 in the nCT+ICIs group, 2 (4.5%) in the nCT group, and statistically significant was found (*P*=0.016), seen in Table 2. The pCR rate was 17.0% in the nCT+ICIs group and 2.1% in the nCT group (*P*=0.035). The rate of nerve invasion was 4.3% in nCT+ICIs group, which was significantly lower than 23.4% of nCT group (*P*=0.007). The number lymph node removed in the nCT+ICIs group was 23.5 ± 10.9, while 19.2 ± 8.7 in the nCT group (*P*=0.032). Percentage of patients received adjuvant therapy followed surgery was 55.3% (26/47) in the nCT+ICIs group, lower than 76.6% (36/47) of nCT group (*P*=0.03), seen in Table 3.

Safety and complications

The complications after neoadjuvant therapy were summarized in Table 4. The incidence of bone marrow suppression, rash, myocardial enzyme elevation and transaminase elevation were comparable in both groups (all *P* value>0.05). The majority of patients experienced complications of grade 2 or less, and no grade 5 occurred. The incidence rates of postoperative complications, including anastomotic leakage, pneumonia and gastrointestinal bleeding were also similar in the two groups (all *P* value>0.05), seen in Table 5.

Follow-up

In the two groups, both 1 patient was lost in the follow-Up. The last follow-up time was April 30, 2022. It was shown that the 1-, 2-year DFS rates of the patients in nCT+ICIs group and in nCT groups were 95.7%, 80.7% and 76.1%, 63.8%, respectively (HR, 0.164, *P*=0.001; HR, 0.448, *P*=0.046). In terms of OS, the 1-, 2-year OS rates in the nCT+ICIs group was 95.7%, 83.2% and 84.8%, 72.3% in the nCT group (HR, 0.474, *P*=0.074; HR, 0.564, *P*=0.189). These results were shown in Figure 1A and Figure 1B.

We analyzed the failure modes of the two groups after surgery, and the results were shown that ESCC patients with recurrence in the nCT+ICIs group was 3 (6.4%), significantly lower than 10 (21.3%) of the nCT group (c^2, 4.374; *P*=0.036), and the mainly recurrence was regional lymph nodes, while there was no significant difference in the metastasis (c^2, 0.336; *P*=0.562) between the two groups, seen in Table 6.

Discussion

JCOG 9907 (17) confirmed the survival benefit of preoperative chemotherapy with CF over post-operative chemotherapy with the same regimen, which had become the

TABLE 2 Comparison of TRG between the two groups.

TRG	nCT+ICIs	nCT	*P*-value
0	21.7% (10/46)	4.5% (2/44)	0.016
1	6.5% (3/46)	4.5% (2/44)	1.000
2	32.6% (15/46)	40.9% (18/44)	0.414
3	39.1% (18/46)	50.0% (22/44)	0.300

TRG, tumor regression grade; nCT, neoadjuvant chemotherapy; ICIs, immune checkpoint inhibitors.

TABLE 3 Surgical treatment outcomes.

Variables	nCT+ICIs	nCT	*P*-value
R0 resection rate	87.2% (41/47)	91.5% (43/47)	0.503
pCR rate	17.0% (8/47)	2.1% (1/47)	0.035
Rate of nerve invasion	4.3% (2/47)	23.4% (11/47)	0.007
Rate of vascular tumor thrombus	6.4% (3/47)	4.3% (2/47)	1.000
Rate of positive lymph nodes	40.4% (19/47)	55.3% (26/47)	0.148
Thoracotom			
Left	80.8(21/26)	78.8% (26/33)	0.851
Right	19.2% (5/26)	21.2% (7/33)	
Lymph node moved number	23.5 ± 10.9	19.2 ± 8.7	0.032
Adjuvant therapy	55.3% (26/47)	76.6% (36/47)	0.030

nCT, neoadjuvant chemotherapy; ICIs, immune checkpoint inhibitors; pCR, pathologic complete response.

TABLE 4 Complications after neoadjuvant therapy.

Variables	nCT+ICIs (n)	nCT (n)	*P*-value
Bone marrow suppression			
Grade 1- 2	13	16	0.503
Grade 3-4	0	0	None
Rash		0	
Grade 1- 2	1	0	1.000
Grade 3-4	0		None
Myocardial enzyme elevation			
Grade 1- 2	5	1	0.206
Grade 3-4	1	0	1.000
Transaminase elevation			
Grade 1- 2	19	13	0.192
Grade 3-4	1	0	1.000

nCT, neoadjuvant chemotherapy; ICIs, immune checkpoint inhibitors.

current Japanese standard treatment for locally advanced esophageal cancer. Owing to the result, neoadjuvant chemotherapy could be applied as an approach for the treatment of resectable ESCC in China, but the survival benefit of this treatment was still limited. The preclinical studies demonstrated that chemotherapeutic agents could exert immunostimulatory effects, either by activating effector cells and/or inhibiting immunosuppressive cells in the tumor microenvironment or increasing immunogenicity and T-cell infiltration (18–20), a remarkable progress has been recently made in immunotherapy for the treatment of EC. The CheckMate 577 trial (21), of patients with R0 resected esophageal or gastroesophageal junction cancer with residual pathological disease had been conducted to evaluate nivolumab as adjuvant therapy. The median DFS among the patients who received nivolumab was 22.4 months, as compared with 11.0 months among the patients received placebo (HR, 0.69; $P<0.001$).

In the neoadjuvant setting, ICIs is deemed to eliminate micrometastasis and thus lead to superior survival by inducing system immune activation (22). Expansion of tumor resident T cell clones in the peripheral blood had been found in the neoadjuvant immunotherapy (23). In recent years, several studies have reported that nCT combined with ICIs followed by esophagectomy could be recognized as an effective treatment for locally advanced ESCC, and the pCR could be increased to 25%-39.2% (24–27). A multicenter, single-arm, phase II trial aimed to evaluate the safety and efficacy of camrelizumab and chemotherapy as neoadjuvant treatment for locally advanced ESCC had been reported (27). The R0 resection was achieved in 50 (98.0%) patients and pCR was identified in 20 (39.2%). Thirty-four patients (56.7%) had adverse events of grade 3 or worse, with the most common being leukocytopenia, demonstrated nCT combined with IO was a promising neoadjuvant treatment without unexpected safety signals. Up to now, there is no comparative data on the long-term survival between nCT group and nCT combined with ICIs group. In China, a phase III study (HCHTOG1909) comparing neoadjuvant toripalimab plus chemotherapy versus chemotherapy for patients with locally advanced ESCC is in progress (11).

TABLE 5 Complications after Surgery.

Variables	nCT+ICIs (n)	nCT (n)	*P*-value
Anastomotic leakage	0	3	0.240
Pneumonia	2	1	1.000
Gastrointestinal bleeding	0	1	1.000

nCT, neoadjuvant chemotherapy; ICIs, immune checkpoint inhibitors.

In the current study, 47 pairs of comparable patients with ESCC receiving nCT combined with ICIs and simple nCT were selected for the final analysis after PSM. Compared with the nCT group, the nCT+ICIs group had advantage in TRG and pCR. There were 10 cases (21.7%) of TRG 0 in the nCT+ICIs group, 2 (4.5%) in the nCT group ($P=0.016$). The pCR rates were 17.0%, 2.1% in the two groups ($P=0.035$). In addition, postoperative nerve invasion in the nCT+ICIs group was significantly lower than that of the nCT group ($P=0.007$). The R0 resection rate and the rate of vascular tumor thrombus were similar between the two groups. We observed the adverse effects of the patients. The complications after neoadjuvant therapy and postoperative (including bone marrow suppression, rash, myocardial enzyme elevation, transaminase elevation and anastomotic leakage, pneumonia, gastrointestinal bleeding) were comparable and the incidence of grade 5 was 0 in the two group, indicated that additional neoadjuvant ICIs to nCT was safe and feasible, and it was similar with other studies (4, 28).

To our knowledge, this is the first study to provide 2-year survival on ESCC patients receiving nCT plus ICIs versus nCT alone. The 1-, 2-year DFS rates were both significantly increased in the nCT+ICIs group ($P=0.001$, $P=0.046$, respectively), which might be related to the higher TRG 0 and pCR, lower nerve invasion rate and more lymph node dissections. In terms of OS, there was no significant difference in the 1-, 2-year OS rates between the two groups. However, the 1-year OS improved in the nCT+ICIs group, which was close to a statistical difference ($P=0.074$). Perhaps it was related to the relatively lower pCR rate (17.0%) and small sample size in our retrospective studies. After all, pCR rate was supposed to be strong associated with better survival in ESCC (29, 30). In addition, a more aggressive adjuvant therapy was conducted in the nCT group ($P=0.03$), which probably provided some survival benefits for patients with ESCC.

Regarding the failure modes, our results showed that nCT combined with ICIs could significantly reduce local recurrence ($P=0.036$), but there was no significant difference in terms of metastasis ($P=0.562$), indicated that systemic therapy might be

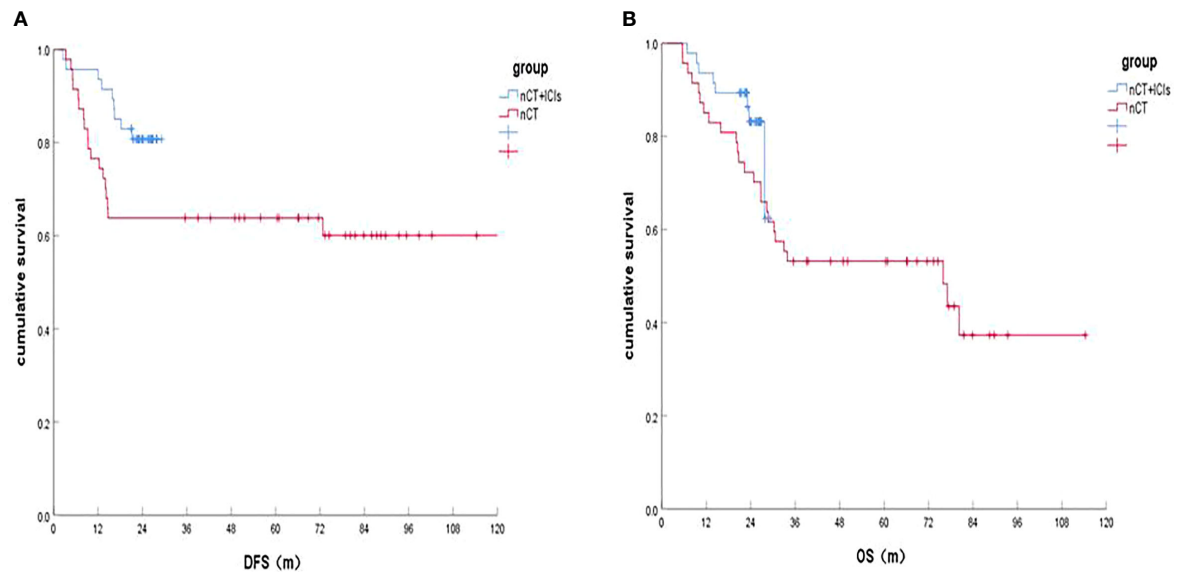

FIGURE 1
Survival of the nCT+ICIs group and nCT group after follow-up. **(A)** DFS rates between the two groups; **(B)** OS rate between the two groups.

TABLE 6 Failure modes after radical esophagectomy.

	nCT+ICIs (n)	nCT (n)	χ^2	*P*-value
Recurrence				
Regional lymph node	2	8	4.374	0.036
Anastomosis	1	2		
Metastasis				
Supraclaviclar lymph node	1	0	0.336	0.562
Abdominal lymph node	2	1		
Liver	2	0		
Bone	0	4		
Lung	1	1		
Brain	0	1		
Subcutaneous	0	1		

insufficient in the nCT+ICIs group and seemed need to be further strengthened. After all, 83.0% of the patients did not reach pCR in the nCIT group. This also reminds us higher pCR rate is still the focus of the neoadjuvant therapy strategy.

Some imitations were as followed: (1) It was a single-centered retrospective study, due to retrospective nature of the study, the treatment selection bias inevitably existed despite PSM; (2) In view of the almost 10 years span of the included cases, the lymph node dissection in the nCT+ICIs group was significantly more than that of the nCT group [(23.5 ± 10.9) vs. (19.2 ± 8.7), *P*=0.032], which might influence the results potentially; (3) The general information of the enrolled patients lacked data such as PD-L1 expression, so we could not make a detailed assessment of the expression of PD-L1 and the response to neoadjuvant therapy; (4) Lack of large cohort, and the follow-up period was short in the nCT+ICIs group; (5) Regarding times, changes had taken place in surgical techniques and chemotherapy regiments, all of these might affect the final results.

In conclusion, compared with nCT alone, neoadjuvant immunotherapy plus nCT for patients with locally advanced ESCC has an advantage in pathological response, and could improve DFS with a good safety and feasibility, while long term survival validation is still needed further.

Data availability statement

The raw data supporting the conclusions of this article will be made available by the authors, without undue reservation.

Ethics statement

The studies involving human participants were reviewed and approved by fourth hospital of Hebei medical university. Written informed consent for participation was not required for this study in accordance with the national legislation and the institutional requirements.

Author contributions

JW and J-FL conceived the concept and coordinated the design. S-WJ drafted the manuscript with significant contributions from CZ and WZ. MH, Q-YL, J-FY, RW, Z-QT were responsible of visualization, supervision and writing review. All authors listed have made a substantial and direct contribution to the work and approved to publication.

Funding

This work was supported by Hebei Clinical Research Center for Radiation Oncology (2057702D).

Conflict of interest

The authors declare that the research was conducted in the absence of any commercial or financial relationships that could be construed as a potential conflict of interest.

Publisher's note

References

1. Sung H, Ferlay J, Siegel RL, Laversanne M, Soerjomataram I, Jemal A, et al. Global cancer statistics 2020: GLOBOCAN estimates of incidence and mortality worldwide for 36 cancers in 185 countries. *CA Cancer J Clin* (2021) 71:209–49. doi: 10.3322/caac.21660

2. Cao W, Chen HD, Yu YW, Li N, Chen WQ. Changing profiles of cancer burden worldwide and in China: a secondary analysis of the global cancer statistics 2020. *Chin Med J (Engl)* (2021) 134:783–91. doi: 10.1097/CM9.0000000000001474

3. Van Heijl M, van Lanschot JJ, Koppert LB, van Berge Henegouwen M, Muller K. Neoadjuvant chemoradiation followed by surgery versus surgery alone for patients with adenocarcinoma or squamous cell carcinoma of the esophagus (CROSS). *BMC Surg* (2008) 8:21. doi: 10.1186/1471-2482-8-21

4. Yang H, Liu H, Chen YP, Zhu CC, Fang WT, Yu ZT, et al. Neoadjuvant chemoradiotherapy followed by surgery versus surgery alone for locally advanced squamous cell carcinoma of the esophagus (NEOCRTEC 5010): a phase III multicenter, randomized, open-label clinical trial. *J Clin Oncol* (2018) 36:2796–803. doi: 10.1200/JCO.2018.79.1483

5. Jing SW, Qin JJ, Liu Q, Zhai C, Wu YJ, Cheng YJ, et al. Comparison of neoadjuvant chemoradiotherapy and neoadjuvant chemotherapy for esophageal cancer: a meta-analysis. *Future Oncol* (2019) 15:2413–22. doi: 10.2217/fon-2019-0024

6. Chan KKW, Saluja R, Delos Santos K, Lien K, Shah K, Cramarossa G, et al. Neoadjuvant treatments for locally advanced, resectable esophageal cancer: a network meta-analysis. *Int J Cancer* (2018) 143:430–7. doi: 10.1002/ijc.31312

7. Kato K, Ito Y, Daiko H, Ozawa S, Ogata T, Hara H, et al. A randomized controlled phase III trial comparing two chemotherapy regimen and chemoradiotherapy regimen as neoadjuvant treatment for locally advanced esophageal cancer, JCOG 1109 NExT study. *J Clin Oncol* (2022) 40: suppl 238. doi: 10.1200/JCO/2022.40.4_suppl.238

8. Matsuda S, Kitagawa Y, Takemura R, Okui J, Okamura A, Kawakubo H. Real-world evaluation of the efficacy of neoadjuvant DCF over CF in esophageal squamous cell carcinoma: propensity score matched analysis from 85 authorized institutes for esophageal cancer in Japan. *Ann Surg* (2022). doi: 10.1097/SLA.0000000000005533

9. O'Reilly EM, Ko AH. Precision medicine and immunotherapy in GI cancers. *J Clin Oncol* (2022) 40:2659–61. doi: 10.1200/JCO.22.00601

10. Wang ZY, Shao CJ, Wang YY, Duan HT, Pan MH, Zhao JB, et al. Efficacy and safety of neoadjuvant immunotherapy in surgically resectable esophageal cancer: A systematic review and meta-analysis. *Int J Surg* (2022) 104:106767. doi: 10.1016/j.ijsu.2022.106767

11. Zheng Y, Liu XB, Sun HB, Xu JL, Shen SN, Ba YF, et al. A phase III study on neoadjuvant chemotherapy versus neoadjuvant toripalimab plus chemotherapy for locally advanced esophageal squamous cell carcinoma: Henan cancer hospital thoracic oncology group 1909 (HCHTOG1909). *Ann Transl Med* (2021) 9:73. doi: 10.21037/atm-20-5404

12. Xing WQ, Zhao LD, Fu XM, Liang GH, Zhang Y, Yuan DF, et al. A phase II, single-centre trial of neoadjuvant toripalimab plus chemotherapy in locally advanced esophageal squamous cell carcinoma. *J Thorac Dis* (2020) 12:6861–7. doi: 10.21037/jtd-20-2198

13. Yang P, Zhou X, Yang XF, Wang YF, Sun T, Feng SY, et al. Neoadjuvant camrelizumab plus chemotherapy in treating locally advanced esophageal squamous cell carcinoma patients: a pilot study. *World J Surg Oncol* (2021) 19:333. doi: 10.1186/s12957-021-02446-5

14. Huang BJ, Shi HY, Gong XH, Yu J, Xiao CX, Zhou B, et al. Comparison of efficacy and safety between pembrolizumab combined with chemotherapy and simple chemotherapy in neoadjuvant therapy for esophageal squamous cell carcinoma. *J Gastrointest Oncol* (2021) 12:2013–21. doi: 10.21037/jgo-21-610

15. Ryan R, Gibbons D, Hyland JM, Treanor D, White A, Mulcahy HE, et al. Pathological response following long-course neoadjuvant chemoradiotherapy for locally advanced rectal cancer. *Histopathology* (2005) 47:141–6. doi: 10.1111/j.1365-2559.2005.02176.x

16. Austin PC. An introduction to propensity score methods for reducing the effects of confounding in observational studies. *Multivariate Behav Res* (2011) 46:399–424. doi: 10.1080/00273171.2011.568786

17. Ando N, Kato H, Igaki H, Shinoda M, Ozawa S, Shimizu H, et al. A randomized trial comparing postoperative adjuvant chemotherapy with cisplatin and 5-fluorouracil versus preoperative chemotherapy for localized advanced squamous cell carcinoma of the thoracic esophagus (JCOG 9907). *Ann Surg Oncol* (2012) 19:68–74. doi: 10.1245/s10434-011-2049-9

18. Sakai H, Kokura S, Ishikawa T, Tsuchiya R, Okajima M, Matsuyama T, et al. Effects of anticancer agents on cell viability, proliferative activity and cytokine production of peripheral blood mononuclear cells. *J Clin Biochem Nutr* (2013) 52:64–71. doi: 10.3164/jcbn.12-60

19. Pol J, Vacchelli E, Aranda F, Castoldi F, Eggermont A, Cremer I, et al. Trial watch: Immunogenic cell death inducers for anticancer chemotherapy. *Oncoimmunology* (2015) 4:e1008866. doi: 10.1080/2162402X.2015.1008866

20. Heinhuis KM, Ros W, Kok M, Steeghs N, Beijinen JH, Schellens JHM. Enhancing antitumor response by combining immune checkpoint inhibitors with chemotherapy in solid tumors. *Ann Oncol* (2019) 30:219–35. doi: 10.1093/annonc/mdy551

21. Kelly RJ, Ajani JA, Kuzdzal J, Zander T, Van Cutsem E, Piessen G, et al. Adjuvant nivolumab in resected esophageal or gastroesophageal junction cancer. *N Engl J Med* (2021) 384:1191–203. doi: 10.1056/NEJMoa2032125

22. Lu Z, Zou J, Li S, Topper MJ, Tao Y, Zhang H, et al. Epigenetic therapy inhibits metastases by disrupting premetastatic niches. *Nature* (2020) 579:284–90. doi: 10.1038/s41586-020-2054-x

23. Rozeman EA, Menzies AM, van Akkooi ACJ, Adhikari C, Bierman C, van de Wiel BA, et al. Identification of the optimal combination dosing schedule of neoadjuvant ipilimumab plus nivolumab in macroscopic stage III melanoma (OpACIN-neo): A multicentre, phase 2, randomized, controlled trial. *Lancet Oncol* (2019) 20:948–60. doi: 10.1016/S1470-2045(19)30151-2

24. Yang WX, Xing XB, Yeung SJ, Wang SY, Chen WF, Bao Y, et al. Neoadjuvant programmed cell death 1 blockade combined with chemotherapy

for resectable esophageal squamous cell carcinoma. *J Immunother Cancer* (2022) 10:e003497. doi: 10.1136/jitc-2021-003497

25. Wu ZG, Zheng Q, Chen HQ, Xiang JQ, Hu H, Li H, et al. Efficacy and safety of neoadjuvant chemotherapy and immunotherapy in locally resectable advanced esophageal squamous cell carcinoma. *J Thorac Dis* (2021) 13:3518–28. doi: 10.21037/jtd-21-340

26. Shen DJ, Chen QX, Wu J, Li JQ, Tao KY, Jiang YH, et al. The safety and efficacy of neoadjuvant PD-1 inhibitor with chemotherapy for locally advanced esophageal squamous cell carcinoma. *J Gastrointest Oncol* (2021) 12:1–10. doi: 10.21037/jgo-20-599

27. Liu J, Yang Y, Liu ZC, Fu XL, Cai XY, Li HX, et al. Multicenter, single-arm, phase II trial of camrelizumab and chemotherapy as neoadjuvant treatment for locally advanced esophageal squamous cell carcinoma. *J Immunother Cancer* (2022) 10:e004291. doi: 10.1136/jitc-2021-004291

28. Lv HL, Tian Y, Li JC, Huang C, Sun BK, Gai CY, et al. Neoadjuvant sintilimab plus chemotherapy in resectable locally advanced esophageal squamous cell carcinoma. *Front Oncol* (2022) 29:864533. doi: 10.3389/fonc.2022.864533

29. Wan T, Zhang XF, Liang C, Liao CW, Li JY, Zhou YM, et al. The prognostic value of a pathologic complete response after neoadjuvant therapy for digestive cancer: Systematic review and meta-analysis of 21 studies. *Ann Surg Oncol* (2019) 26:1412–20. doi: 10.1245/s10434-018-07147-0

30. Soror T, Kho G, Zhao KL, Ismail M, Badakhshi H. Impact of pathological complete response following neoadjuvant chemoradiotherapy in esophageal cancer. *J Thorac Dis* (2018) 10:4069–76. doi: 10.21037/jtd.2018.06.85

frontiers | Frontiers in Immunology

TYPE Original Research
PUBLISHED 19 October 2022
DOI 10.3389/fimmu.2022.991790

OPEN ACCESS

EDITED BY
Xuyao Zhang,
Fudan University, China

REVIEWED BY
Howard Crawford,
Henry Ford Health System,
United States
Qiuju Han,
Shandong University, China

*CORRESPONDENCE
Anthony Sandler
ASandler@childrensnational.org

SPECIALTY SECTION
This article was submitted to Cancer Immunity and Immunotherapy, a section of the journal Frontiers in Immunology

RECEIVED 12 July 2022
ACCEPTED 28 September 2022
PUBLISHED 19 October 2022

CITATION
Wu X, Srinivasan P, Basu M, Zhang P, Saruwatari M, Thommandru B, Jacobi A, Behlke M and Sandler A (2022) Tumor Apolipoprotein E is a key checkpoint blocking anti-tumor immunity in mouse melanoma. *Front. Immunol.* 13:991790. doi: 10.3389/fimmu.2022.991790

Tumor Apolipoprotein E is a key checkpoint blocking anti-tumor immunity in mouse melanoma

Xiaofang Wu[1], Priya Srinivasan[1], Mousumi Basu[1], Peng Zhang[2], Michele Saruwatari[1], Bernice Thommandru[3], Ashley Jacobi[3], Mark Behlke[3] and Anthony Sandler[1]*

[1]The Joseph E. Robert Jr. Center for Surgical Care and The Sheikh Zayed Institute for Pediatric Surgical Innovation, Children's National Hospital, George Washington University, Washington, DC, United States, [2]Beijing Key Laboratory for Genetics of Birth Defects, Beijing Pediatric Research Institute, Beijing Children's Hospital, Capital Medical University, National Center for Children's Health, Beijing, China, [3]Integrated DNA Technologies, Inc., Coralville, IA, United States

Immunotherapy is a key modality in the treatment of cancer, but many tumors remain immune resistant. The classic mouse model of B16-F10 melanoma is immune resistant even in the face of checkpoint inhibition. Apolipoprotein E (apoE), a known immune suppressant is strikingly elevated in many human tumors, but its role in cancer immunology is not defined. We investigated the role of apoE in the immune micro-environment using a mouse melanoma model. We demonstrate that ApoE is -highly expressed in wild-type B16-F10 melanoma and serum levels progressively increase as tumors grow. The conditioned media from wild type ApoE secreting melanoma cells suppress T-cell activation *in vitro* while this suppressive effect is absent in conditioned media from ApoE knock out tumor cells. Mechanistically, apoE induces IL-10 secreting dendritic cells and stimulates T-cell apoptosis and arrest partially *via* the lrp8 receptor. Ablating ApoE in mice inoculated with tumor cells enabled tumor cell rejection and was associated with induction of immune pathway activation and immune cell infiltration. Tumor secreted apoE appears to be a potent immune cell checkpoint and targeting apoE is associated with enhanced tumor immunity in the mouse melanoma model.

KEYWORDS

apoE, immune-checkpoint, melanoma, T cells, dendritic cells

Introduction

The need for more effective therapy of tumors is evident in the poor outcomes of high-risk or advanced disease. Cancer vaccines and immune-based therapies hold great promise for malignant solid tumors, but despite robust immune activation with targeted checkpoint inhibitors, cure is often elusive. Immune based therapies (and specifically tumor vaccines) are frequently constrained by intrinsic tumor cell mechanisms enabling immune privilege/evasion. We identify tumor secreted apoE as a novel checkpoint enabling immune evasion in a mouse melanoma tumor model.

ApoE is a polymorphic multifunctional protein, classically considered to play a critical role in atherosclerosis and neurodegenerative diseases (1). Knockout mice fed an atherogenic diet develop pronounced hypercholesterolemia along with an immune-activated phenotype (2, 3). Experimental models reveal a critical function for myeloid derived apoE modulating DC antigen presentation and T-cell priming (2). ApoE attenuates inflammation by complex formation with activated C1q (4), while most recently it was shown that common germline variants of the human APOE gene modulate melanoma progression and survival (5).

In tumors, APOE itself is shown to act as an autocrine or paracrine modulator of carcinogenesis (6, 7). In several human cancers, APOE gene expression is significantly higher in cancer tissue than in adjacent non-cancer tissue (8–13) and higher levels of tumor APOE are associated with metastasis (14). In pancreatic ductal adenocarcinoma (PDA) patients, elevated plasma APOE protein levels are associated with poor survival, whereas tumor associated macrophages that are key drivers of immunosuppression are characterized by elevated levels of ApoE in both mouse and human PDA (15). Further studies reveal that apoE KO mice have less orthotopic mammary tumor development and pulmonary metastasis than wild type (WT) mice (16) and lung tumor development and metastasis are suppressed through enhancing anti-tumor activity of natural killer (NK) cells (6). In contrast, it is reported that apoE is involved in the inhibition of melanoma metastases and has anti-angiogenic properties (17). ApoE promoted anti-tumor immunity by targeting infiltrating innate myeloid derived suppressor cells (MDSC) *via* Liver X receptor (LXR) agonism (18). Furthermore, pretreating cancer cells with apoE inhibited their growth in mouse models. These conflicting observations suggest that the context in which apoE is engaged and the specific APOE genotype in humans may determine its effects, but apoE appears to inhibit its cellular target in most circumstances. The known association of apoE with immunosuppression and its conflicting observations described in tumor biology led us to examine the role of apoE in an immune resistant mouse melanoma model.

We investigated the expression of apoE in mouse melanoma and the role of apoE in the context of tumor growth and immunity. ApoE is abundantly present in B16-F10 melanoma tumors and serum levels of apoE increase dramatically with melanoma tumor growth. Mechanistically, apoE induces IL-10 secreting suppressive dendritic cells and directly inhibits T-cell function at least partially *via* the lrp8 receptor. Ablating ApoE in mouse melanoma enabled tumor cell rejection and induced robust immune activation and tumor immunity. The results reveal a critical role for tumor secreted apoE as a comprehensive checkpoint which appears to alter dendritic cell function and inhibit T-cell efficacy. ApoE is a novel checkpoint with extensive and potent suppressant effects in mouse melanoma. It is anticipated that targeting apoE will augment immune based therapy in apoE secreting immune resistant tumors.

Materials and methods

Animals

Female C57BL/6 mice and apoE$^{-/-}$ mice (B6.129P2-Apoe$^{tm1Unc/J}$) aged 6 weeks were purchased from Jackson Laboratories (Bar Harbor, Maine, United States). Lrp8$^{-/-}$ C57BL/6 breeder mice were generously provided by Dr. Sohail Tavazoie's laboratory from the Rockefeller University. Mice were housed five per cages and kept in a temperature-controlled environment (20 ± 2°C, 50 ± 5% relative humidity) with a 12-hour light/dark cycle in an air-conditioned room with free access to food and water. The animals were acclimated for 4–5 days prior to tumor challenge. All procedures were approved by the Institutional Animal Care and Use Committee (IACUC) of Children's National Hospital, Washington, DC.

Cells

The murine melanoma B16-F10 cell line (purchased from ATCC® CRL-6475, VA), were cultured in DMEM (Life Technologies, CA) supplemented with 10% heat-inactivated FBS (Sigma-Aldrich) and 100 IU/ml Penicillin, 100 µg/ml Streptomycin (Life Technologies).

Generation of apoE$^{-/-}$ cell lines *via* CRISPR genome editing in B16-F10 cells

Six guide RNAs (gRNAs) were designed using IDT's gRNA design tool, targeting the mouse apoE gene. gRNAs were synthesized as 2-part crRNA: tracrRNA gRNAs with chemical modifications (Integrated DNA Technologies, Inc., IA) and were functionally screened by next generation sequencing (NGS) for high INDEL (insertion/deletion) frequency and low in-frame INDEL rates. gRNAs were prepared by complexing a 1:1 molar ratio of the crRNA: tracrRNA at a final concentration of 100 µM, heating to 95°C and slowly cooling to room temperature.

Ribonucleoprotein complexes (RNPs) were formed by the addition of purified Alt-R HiFi Cas9 protein (IDT) to each gRNA at a 1.2:1 molar ratio in 1× PBS to a concentration of 5.6 µM. RNP complexes were allowed to form for 10 min at room temperature before electroporation. RNP complexes (5 µL), Alt-R Cas9 Electroporation Enhancer (3 µL), and 350,000 B16-F10 cells (20 µL) resuspended in Buffer SF were mixed and electroporated using the Lonza 96-well Shuttle System (Lonza, Basel, Switzerland) with electroporation protocol 96-DS-150. Final concentrations for RNP and Alt-R Cas9 Electroporation Enhancer were 1 µM and 4 µM, respectively. Genomic DNA was extracted 48 hours post-transfection using QuickExtract DNA extraction solution (Epicentre Biotechnologies, CA) according to the manufacturer's specifications. The targeting sequence for each ApoE crRNAs are listed in Supplementary Table 1.

Isolation of monocolonal apoE knockouts

The lead gRNA (Mm. Cas9.APOE.1-E) resulted in a 99% INDEL frequency with no in-frame INDELs and was electroporated into B16-F10 cells using the Lonza 96-well Shuttle System as previously described. The electroporated cells were plated in 1 well of a 6-well plate and allowed to grow until confluent. The cells were then dissociated by trypsinization, resuspended in media, and counted. The suspension was diluted to 20,000 cells/mL; 4000 cells were added to 1 well of a 96-well plate and then diluted by array dilution. After 5 days of growth, each well was visually screened for single colonies. Wells with only 1 colony were allowed to grow to confluency. Each well was progressively passaged to a larger well until confluent in a 100 mm dish, about 8.8 x 10^6 cells for genomic DNA extraction and further cell passaging. The genomic DNA from each well was subject to quantification of total editing and analysis of INDEL profile by NGS to confirm a monoclonal isolate.

Quantification of total editing and analysis of INDEL profiles by rhAmpSeq

Genomic DNA libraries for sequencing were prepared using IDT rhAmpSeq targeted amplification. In short, the first round of PCR was performed using target-specific primers with universal 5' tails (Supplementary Table 2); a second round of PCR incorporated P5 and P7 Illumina adapter sequences to the amplicon ends. Libraries were purified using Agencourt® AMPure® XP system (Beckman Coulter, Brea, CA, USA) with a 1:1 ratio of beads to reaction by volume and quantified with quantitative real-time PCR (qPCR) before loading onto the Illumina® MiSeq platform (Illumina, San Diego, CA, USA). Paired end 150 base pair reads were sequenced using V2 chemistry. A sequencing depth of at least 1000 reads was obtained for each sample. Total editing efficiency was calculated and INDEL profiles were evaluated using an IDT custom-built pipeline, CRISPAltRations.

Antibodies and reagents

Anti (α)-mouse CTLA-4, and mouse IgG2b isotype antibodies were purchased from BioXCell (West Lebanon, NH). COG133 and JQ1 were purchased from Tocris (Minneapolis, MN). Dynabeads™ Mouse T-Activator CD3/CD28 for T-Cell Expansion and Activation kit, Vybrant™ DyeCycle™ Violet Stain kit, SYTOX™ red dead cell stain kit, CellTrace™ far red cell proliferation kit, Live/Dead fixable aqua dead cell stain kit, Brilliant stain buffer and mouse IL-2 Carrier-Free recombinant protein were purchased from Thermo Fisher (Waltham, MA).

Multiplex cytokine/chemokine analysis

Cell culture supernatant was collected after centrifuge at 1,200 rpm for 10 min at 4°C. The concentrations of the following immune molecules were determined using the mouse Cytokine & Chemokine 36-plex ProcartaPlex Panel, a magnetic bead-based multiplex immunoassay (Thermo Scientific) following our previous protocol (19). Briefly, cell culture supernatant samples were mixed with antibody-linked polystyrene beads on a 96-well plate and incubated at room temperature (RT) for 2 h on an orbital shaker at 500 rpm. After washing, plates were incubated with biotinylated detection antibody for 30 min at RT. Plates were then washed twice and then labeled beads were re-suspended in streptavidin-PE. Each sample was measured in duplicate along with standards (8-point dilutions) and the buffer control. Plates were read using a Luminex Bio-plex 200 system (Bio-Rad Corp.) for quantitative analysis.

Isolating T cells from mouse spleen

Spleens were collected from mice euthanized by CO_2 narcosis and cervical dislocation. Spleens were pulverized through a 40-µm mesh cell strainer and treated with ACK lysing buffer (Thermo Fisher) for 10 seconds to remove erythrocytes. According to the manufacture's instruction of the Pan T Cell Isolation Kit (Miltenyi Biotec), 10 µL of Pan T Cell Biotin Antibody Cocktail was added per 10^7 splenocytes and incubated for 5 min at 4°C. Subsequently, 20 µL of Pan T Cell MicroBead Cocktail was added per 10^7 cells. Following incubation for 10 min at 4°C, the mixed cell suspension was applied onto the LS column (Miltenyi Biotec). The flow-through containing unlabeled cells, representing the enriched T cells were

collected. T cells were cultured in RPMI 1640 media containing 30 U/mL IL-2 (Thermo Fisher) and stimulated with Dynabeads® Mouse T-Activator CD3/CD28 magnetic beads (Thermo Fisher) at a 1:1 ratio (cell: bead).

IFNγ measurement

WT and apoE$^{-/-}$ mice or WT and lrp8$^{-/-}$ mice, were inoculated with either WT B16 or apoE$^{-/-}$ B16 cells, with anti-CTLA4 antibody on day 0. These vaccinated splenocytes (VS) were harvested on day 7 and co-cultured with either WT B16 or apoE$^{-/-}$ B16 cells for 48hr, following which IFNγ levels in media were compared with ELISA assay. To set up co-culture, a total of 5 × 10^5 freshly isolated mouse T cells or splenocytes were plated in a volume of 600 µl per well of 24-well plates, then they were co-cultured with 5 × 10^4 B16 cells and stimulated with or without CD3/CD28 Dynabeads. Cells were exposed to apoE agonist COG133 at 0, 0.3, 3, 9, 15, 30 µM or human anti-APOE antibody at 1 µg/ml, 10 µg/ml and 20 µg/ml at 37°C under 5% CO2 for 24 hr or 48 hr. Supernatants were collected from triplicate wells, and IFNγ was assayed using the mouse uncoated IFNγ ELISA kit from Invitrogen (Carlsbad, CA). Readings were measured at 450 nm using the EnSpire 2300 Multilabel plate reader (Perkin Elmer, Waltham, Massachusetts, US).

Cell lines and conditioned media

5x10^6 wild type (WT) and apoE$^{-/-}$ B16 cells were irradiated at 60 Gy and then cultured in 20 mL DMEM media supplemented with 10% FBS for 48 hr in T75 flask. The conditioned media (CM) was collected and centrifuged at 1100 rpm at room temperature for 5 min. The supernatant was aliquoted and stored at -80°C.

Cell cycle assay

For testing cell cycle, 1x10^6 T cells in 1 mL DMEM complete media were incubated with 5 µM Vybrant™ DyeCycle™ Violet Stain (Thermo Fisher) at 37˚C for 30 min. And then 5 µl 7AAD were added and incubated for 10 min prior to analysis. Total 25,000 cells were analyzed per measurement. The same forward and side scatter gates were applied to each sample, and within that gate we measured the intensity of vibrant cell cycle dye. Samples were analyzed on a flow cytometer using 405 nm excitation and 440 nm emission. To compare the growth rates of B16 WT and apoE$^{-/-}$ cells, the Click-iT Edu Alexa Fluor 488 flow cytometry assay kit was used in conjunction with the FxCycle Violet stain from Invitrogen (Carlsbad, CA). 50,000 cells were plated per well of a 6 well-plate and cell cycle was analyzed at 48 hr as per the manufacturer's directions.

Measurement of apoE in serum of mice

Mouse serum was collected from naïve WT C57/BL6 mice and also from both naïve and tumor-bearing C57/BL6 apoE$^{-/-}$ mice. ApoE levels in mouse sera were quantified using the mouse apoE ELISA^{PRO} kit from Mabtech (Cincinnati, OH) as per the manufacturer's directions.

Nanostring

RNA was extracted and gene expression was directly measured *via* counts of corresponding mRNA in each sample using an nCounter murine PanCancer Immune Profiling Panel (NanoString, Seattle, WA, USA). For full details, see our previous publication (19). Briefly, 100 ng of high-quality total RNA were hybridized with reporter probes, and then biotinylated capture probes at 65°C for 16–18 hr before being placed into the nCounter Prep station in which samples were affixed to a cartridge. Cartridges were then read by the nCounter Digital Analyzer optical scanner. Further advanced immune-profiling analysis was performed using nSolver 4.0 analysis software with nCounter advanced analysis package (NanoString Technologies) with identified immune cell types. Genes were grouped into 14 immune cell types and 39 immune functions according to the manufacturer's designation (19).

Quantitative real-time RT-PCR

Quantitative real-time PCR (qPCR) was performed using TaqMan® Gene Expression Master Mix (Life Technologies) in a QuantStudio 7 Flex Real-Time PCR System (Thermo Fisher Scientific, Waltham, MA) following the methods that we published previously (19). Each reaction was performed in triplicate, including no template controls and amplification of a housekeeping gene, GAPDH. Gene-specific assays were Mm01307192_m1 for apoE, Mm00464608_m1 for Lrp1, Mm01328171_m1 for Lrp2, Mm00474030_m1 for Lrp8, Mm01177349_m1 for Ldlr, Mm00443298_m1 for Vldlr, Mm99999915_g1 for Gapdh (Life Technologies, Thermo Fisher). Changes in relative gene expression normalized to GAPDH levels were determined using the ΔΔCt method. Results were averaged and statistically analyzed using t-tests.

Mouse melanoma models

C57BL/6 wild type (WT) mice, C57/BL6 apoE knockout (apoE$^{-/-}$) mice, and C57/BL6 lrp8 knockout (lrp8$^{-/-}$) mice were injected subcutaneously in the right flank with 1 × 10^4 freshly prepared B16 WT or apoE$^{-/-}$ tumor cells in 100 µl 1xPBS on day 0 and euthanized once the tumor reached 20mm in any

dimension. Tumor growth was recorded every day by measuring the diameter in 2 dimensions using a caliper when appropriate as we have previously published (19, 20). Briefly, tumor volume was calculated using the following formula: large diameter^2 × small diameter × 0.52. A tumor size of 20 mm in diameter in any dimension was designated as the endpoint, and mice were euthanized at that time. Euthanasia was achieved through cervical dislocation after CO2 narcosis. If a tumor impaired the mobility of an animal, became ulcerated, or appeared infected, or a mouse displayed signs of "sick mouse posture", the mouse was euthanized. All the procedures are approved by the IACUC at CNMC and are in accordance with the humane care of research animals.

Characterization of mouse tumors by immunohistochemistry (IHC)

Tumor was fixed in 10% neutral buffered formalin (pH 6.8–7.2; Richard-Allan Scientific, Kalamazoo, Michigan, US) for paraffin embedding and sectioning. Five µm tissue sections were cut with a microtome, and sample processing and IHC staining were performed as previously described (19) using rabbit polyclonal to CD45 and CD3 antibodies (1:200. Abcam, Cambridge, Massachusetts, US). Isotype-matched antibodies were used for negative controls.

Statistical analysis

Statistical analysis of nanostring gene expression, normalization, clustering, Pathview plots and fold-changes were performed using the Advanced Analysis Module in the nSolver™ Analysis Software version 4.0 from NanoString Technologies (NanoString Technologies, WA, USA) following our published methods (19). Briefly, raw data for each sample were normalized to the geometric mean of housekeeping genes using the geNorm algorithm. Pathway scores were calculated as the first principal component (PC) of the pathway genes' normalized expression. Each cell type score has been centered to have mean 0 and as abundance estimates (cell type scores) are calculated in log2 scale, an increase of 1 corresponds to a doubling in abundance. All differentially expressed genes were subjected to KEGG term analysis, with significance accepted at $p < 0.05$. The Benjamini-Yekutieli method was used to control the false discovery rate. All statistical analyses of nanostring data were carried out in R v3.4.3 software.

Statistical significance for each set of experiments was determined by the unpaired 2-tailed Student's t-test, and the specific tests were indicated in the figure legends. The data are expressed as the mean (± SD), with $p<0.05$ considered statistically significant.

Human melanoma RNA-seq analysis

We accessed the raw RNA-seq data of melanoma biopsies through the Gene Expression Omnibus database (accession number: GSE78220) (21) - Raw reads mapping to the reference genome (GRCh38) were performed on quality-checked and trimmed reads using STAR 2.4.1c (22). The reference annotation is Ensembl v86. The overlap of reads with annotation features found in the reference.gtf were calculated using HT-seq v0.6.1 (23). - The output computed for each sample (raw read counts) was then used as input for DESeq2 (24) analysis. Raw counts were normalized using DESeq2 function "rlog," and normalized counts were used for downstream analysis. Statistical calculations were performed using GraphPad Prism software (GraphPad Software, San Diego, CA, USA) or R Software (Version 4.0).

Results

ApoE is highly expressed in the melanoma B16-F10 cell lines and apoE serum levels rise with tumor growth *in vivo*

RNA was extracted and gene expression was directly measured *via* counts of corresponding mRNA in B16-F10 cells using an nCounter murine PanCancer Immune Profiling Panel (NanoString, Seattle, WA, USA). We evaluated the presence of multiple genes associated with immunosuppression in the B16-F10 melanoma cell line, ApoE was the most highly expressed immune-suppressive transcript in the cell line. (Figure 1A) ApoE is also constitutively detected in the serum of wild type (WT) C57/BL6 mice at high levels (Figure 1B). To evaluate the systemic levels secreted from the mouse melanoma tumor itself, we measured the level of serum apoE in apoE KO (apoE$^{-/-}$) C57/BL6 mice inoculated subcutaneously (s.c.) with 10^4 WT B16 (F10) cells injected in the right thigh. Blood and tumors were collected at various sizes until the tumors reached a max of 21 mm in any dimension. The serum levels of apoE in these tumor-baring apoE$^{-/-}$ mice increased progressively and considerably with tumor growth (Figure 1C).

To further investigate the function of apoE, we generated apoE$^{-/-}$ B16-F10 cell lines with CRISPR-Cas9 gene deletion. To confirm suppression or deletion of apoE protein, we performed western blot analysis on total protein lysates from B16 WT and apoE$^{-/-}$ single clones. Our data shows absent apoE expression in the apoE$^{-/-}$ single clones (Figure 1D). The apoE protein secreted from WT B16 and apoE knockout clones in culture media was quantified by ELISA assay and levels correlated with the protein expression pattern of western blot analysis confirming KO of apoE in the KO cell lines. (Figure 1E)

10.3389/fimmu.2022.991790

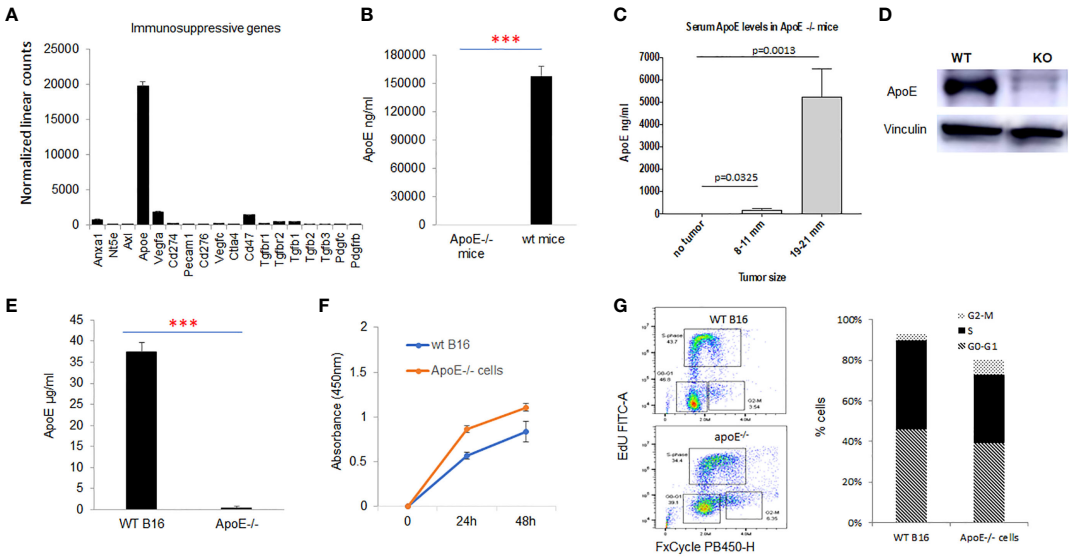

FIGURE 1
ApoE is the most highly expressed immune suppressive gene in the melanoma B16-F10 cell lines and apoE serum levels rise with tumor growth in vivo. **(A)** mRNA expression as revealed by nanostring nsolver Pancancer immune profiling, of the immune suppressive marker genes in B16F10 cells (n=6). **(B)** ApoE expression was undetectable in the serum of apoE knockout (apoE-/-) mice, but present at high levels in wild type (C57/BL6) mice with ELISA assay. **(C)** ApoE knockout mice were inoculated with 10^4 wild type (B16F10) cells and serum levels of apoE increased over time with increasing tumor size. **(D)** Validation of apoE gene knockout in B16F10 cells by CRISPR-Cas9 gene deletion. The level of apoE protein expression was measured in WT B16F10 and the corresponding apoE-/- clone by Western Blot. **(E)** Equivalent numbers of WT and apoE-/- B16 cells were plated and apoE levels released into culture media were quantified by ELISA at 48hr. ApoE is secreted at high levels in WT B16 cells and is not detectable in the apoE-/- cell line. **(F)** To evaluate whether targeting apoE influenced cell viability and proliferation, 5x10^4 WT (n=6) or apoE-/- B16 cells (n=6) were grown in 12-well plates and proliferation rates were measured at 24hr and 48hr by MTT assay. There is no statistically significant difference in cell proliferation rate between the two groups. **(G)** Cell cycle distribution was determined in WT and apoE-/- B16 cells. The various phases of the cell cycle are differentiated in the flow cytometry plot on the left: G0-G1 is the pre-synthesis phase, S-phase cells are undergoing active DNA synthesis and G2-M cells are preparing for mitosis. Bar graphs represents the percentage of cells in G0-G1, S and M phase of the cell cycle. Cell counts and cell cycle distribution indicate that WT and apoE-/- B16 cells proliferate at equivalent rates. Data are representative of three independent experiments. Results are expressed as mean score ±SD. ***p<0.001, determined by unpaired two-tailed Student's t-test.

We then evaluated the *in vitro* proliferation rate (Figure 1F) and cell cycling (Figure 1G) of the WT and KO cell lines to determine if targeting apoE influenced cell viability and proliferation. There is no statistically significant difference between WT and ApoE$^{-/-}$ cells in their proliferation rate or cell cycles (Figures 1F, G).

ApoE secreted into media from B16 melanoma tumor cells inhibits T-cell function

To investigate the effect of tumor cell secreted apoE on activated T cells, splenic derived C57/BL6 T cells were cultured in control media and melanoma B16 WT or apoE$^{-/-}$ conditioned media (CM) in which the T cells were activated with CD3/CD28 beads for 48 hr. Cytokine secretion, apoptosis and proliferation of the cultured mouse T cells were examined and compared to T cells cultured in the RPMI media that served as controls (Figure 2). IFNγ production (Figure 2A) and T cell viability (Figures 2B, C) were significantly ($P < 0.05$) suppressed when T cells were cultured in WT B16 CM at 48 hr of incubation as compared to the RPMI media control, whereas apoE$^{-/-}$ conditioned media was similar to RPMI control media alone and did not inhibit T cell activity nor viability (Figures 2A–C). In addition, cell cycle distribution showed that WT conditioned media arrested activated T cells in the G0/G1 phase while apoE$^{-/-}$ conditioned media-maintained T-cells in the S and G2M phase of the cell cycle, similar to control media without prior exposure to tumor cells. (Figures 2D, E). These results indicate that conditioned media derived from B16 tumor cells induces arrest of stimulated T cells in the G0/G1 phase of the cell cycle, resulting in apoptosis and suppression of cytokine production. In contrast, the singular absence of apoE in conditioned media rescues the activated T

10.3389/fimmu.2022.991790

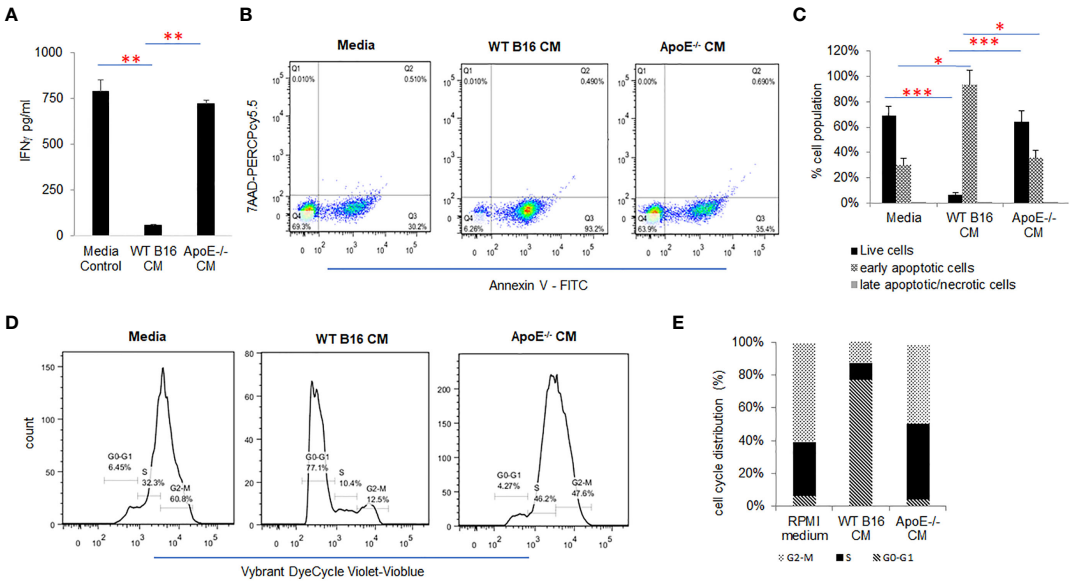

FIGURE 2
ApoE secreted into media from B16 melanoma tumor cells inhibits T-cell proliferation and function. **(A)** Conditioned media (CM) from WT or apoE$^{-/-}$ cells was cultured with T-cells activated by CD3/CD28 beads. Bar graphs depict IFNγ released under these conditions. The production of IFNγ was significantly suppressed when T cells were cultured in WT B16 CM, but this suppression was reversed in apoE free CM from apoE$^{-/-}$ cells. **(B)** Representative flow cytometry plots and **(C)** quantification of T cell apoptosis in CM. Results show that T cell viability is markedly reduced in the WT CM, whereas induction of apoptosis was reversed when cells were cultured in the apoE$^{-/-}$ medium, similar to RPMI control medium alone. **(D)** Representative flow cytometry plots and **(E)** quantification of cell cycle analysis of T cells in different media. Cell cycle distribution showed an arrest of activated T cells in the G0-G1 phase in the WT B16 medium, while in the apoE$^{-/-}$ medium most T cells were distributed in the S and G2-M phases, similar to the RPMI media control. Results are expressed as mean score ± SD. *p<0.05; **p<0.005; ***p<0.001, determined by unpaired two-tailed Student's t-test.

cell phenotype when stimulated with CD3/CD28 beads. To further define the cytokine response, we used a ProcartaPlex multiplex immunoassay, and quantified multiple cytokines/chemokines in the stimulated T-cell media from the same experiment. Ten out of 27 detectable cytokines suppressed by WT conditioned media returned to baseline levels or were upregulated when T cells were cultured in apoE$^{-/-}$ CM. These included effectors: IFNγ, IFNα, TNFα; stimulator, IL18; inflammatory factor: IL4, IL13; chemo attractive factor: MCP-1, MCP3, MIP-1α, MIP-1β; and regulatory factor: IL-10 ($P < 0.05$) cytokines. IL6, CCL-5 (Rantes) and GroαKC were downregulated (Supplement Figure 1A).

To further delineate the T-cell suppressive effect directly, COG133, a fragment of apoE peptide, which competes with the apoE holoprotein for binding the low-density lipoprotein (LDL) receptors and acts as an apoE mimetic, was tested to determine its effect on T cell activation. T cells were activated with CD3/CD28 dynabeads and the effects of COG133 (0, 3, 9, 15 and 30μM concentrations) on T cell apoptosis were evaluated. The T cell viability was diminished in a dose dependent manner (Supplement Figure 1B). These results confirm the immunomodulatory role of apoE on activation of T cells showing robust and extensive suppression of T cell function.

ApoE secreted from B16 melanoma tumor cells in culture may also impair activation of pro-inflammatory dendritic cells

Activation of innate antigen presenting cells like dendritic cells (DC) are critical for effective induction of immunity. We tested the effect of conditioned media on toll like receptor (TLR7/8) stimulated primary bone marrow derived dendritic cell activation. B16 WT conditioned media (CM) suppressed DC activation as determined by cytokine production, but this effect was absent in in media from apoE$^{-/-}$ B16-F10 cells (Supplement Figure 2). Multiplex results showed that secretion of the suppressive cytokine IL10 is diminished when DC were cultured in apoE$^{-/-}$ CM compared to culture in WT CM. In a pro-inflammatory fashion IL1α, IL1β, RANTES, MIP1α, MIP1β, IL28 are all increased with apoE$^{-/-}$ CM compared to WT CM (supplement Figure 2). To further delineate the DC suppressive effect directly, we tested the effect of the apoE peptide mimetic, COG133 on DC activation. In a dose dependent fashion, COG 133 induced secretion of the anti-inflammatory cytokine, IL-10 from activated DC. Furthermore, COG133 suppressed IL-1α, IL-1β and IL-23 in a dose dependent

manner suggesting the immune-modulatory role of ApoE on DC function (Supplement Figure 3).

ApoE peptide mimetic COG133 inhibits cytokine secretion induced by immunogenic tumor cells, while anti-APOE blocking antibody enhances cytokine secretion in tumor cell/splenocyte reactions

To further investigate the influence of tumor secreted apoE on immune cell function, immunogenic B16 tumor cells (B16 cells treated with Myc inhibitors (0.25μM BET+0.25μM JQ1 for 4 days) were irradiated at 60 Gray and co-cultured with naïve C57/BL6 splenocytes in the presence of either apoE mimetic COG133 at 0.3, 3 and 9 μM or anti-APOE blocking antibody at 1, 10 and 30 μg/ml concentrations. Prior work from our laboratory has shown the immunogenic effect of treating cancer cells with Myc inhibitors and irradiation (19). IFNγ production was quantified by ELISA at 48h. Splenocytes produced high levels of IFNγ when co-cultured with Myc-inhibited immunogenic B16 cells as shown in Figure 3. Exposure of these cells to apoE mimetic COG133 repressed IFNγ production (6-fold reduction) (Figure 3A), while the presence of Anti-APOE antibody enhanced IFNγ production (3-fold increase) (Figure 3B). We also tested IFNγ production from vaccinated splenocytes following co-culture with treated and untreated B16 cells in the presence of COG 133. To obtain vaccinated splenocytes, 10^4 WT B16 tumor cells and 100μg/ml anti-CTLA4 antibody were administered to C57BL/6 mice on day 0, and splenocytes were collected at day 7 after tumor cell inoculation. Compared with naïve splenocytes, vaccinated splenocytes produced dramatically greater level of IFNγ, especially when they were co-cultured with Myc inhibited B16 tumor cells. This high level IFNγ was also suppressed by COG 133 at a dose dependent manor (Figure 3C). In addition to IFNγ, we also quantified other cytokine/chemokines using ProcartaPlex multiplex immunoassay. Fourteen out of 23 detectable cytokines were significantly upregulated when splenocytes were co-cultured with Myc-inhibited B16 tumor cells, including effectors: IFNγ, TNFα; stimulators, IL18, G-CSF, M-CSF; inflammatory factor: IL6; chemo attractive factors: CCL-5 (Rantes), CXCL-1, CCL-2, CCL-7, CXCL-2, CCL3; and regulatory factors: IL-10, IL6 ($P < 0.05$). Within these 14 cytokines, four of them including IFNγ, IL6, IL18 and RANTES (CCL5) were suppressed after exposure to apoE peptide mimetic COG133 in a dose dependent manner (Supplement Figure 4).

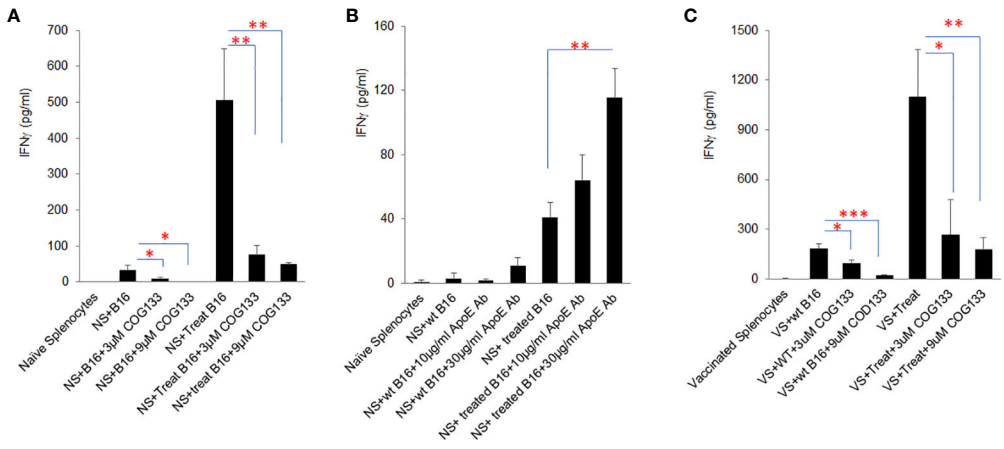

FIGURE 3
ApoE agonist peptide COG133 inhibits cytokine secretion induced by immunogenic tumor cells, while anti-APOE blocking antibody enhances cytokine secretion in tumor cell/splenocyte reactions. **(A)** Naïve and vaccinated splenocyte production of IFNγ was markedly reduced when splenocytes were co-cultured with immunogenic (BET/JQ1 treated) B16 tumor cells in the presence of the apoE agonist COG133. **(B)** Naïve splenocyte production of IFNγ was significantly increased when co-cultured with immunogenic B16 tumor cells with anti-APOE antibody. **(C)**. COG133 was also inhibitory of IFNγ production when vaccinated splenocytes were used for co-culture with treated immunogenic cancer cells. It is of interest to note that the levels of IFNγ production is significantly greater when vaccinated splenocytes were used for this experiment. NS: naïve splenocytes, splenocytes were collected from naïve C57BL/6 mice. Treated B16: B16 cells were expose to Myc inhibitor (0.25μM BET and 0.25μM JQ1) for 4 days, to induce immunogenicity. VS: vaccinated splenocytes. Irradiated 10^4 WT B16 tumor cells and 100ug/ml anti-CTLA4 antibody were administered to C57BL/6 mice on day 0, and splenocytes were collected at day 7 after tumor cell inoculation. Data are representative of three independent experiments. Results are expressed as mean score ± SD. *p<0.05; **p<0.005; ***p<0.001, determined by unpaired two-tailed Student's t-test.

The apoE receptors lrp8 and ldlr are dominantly expressed on activated T cells and dendritic cells and blocking lrp8 enhanced T-cell activation *in vitro*

The pattern of expression of apoE receptors on T cells and dendritic cells is not fully characterized. Here we examined the expression of apoE receptors on T cells, dendritic cells (DC) and macrophages using qPCR. All five of the receptor transcripts were shown to be expressed on T cells, DCs and macrophages. Ldlr and lrp8 were dominantly expressed on T cells (Figure 4A) whereas lrp1, lrp8 and ldlr are highly expressed on DC (Figure 4B). Lrp1 is highly expressed in macrophages (Figure 4C). Vldlr expression was relatively low, and lrp2 was barely detectable on these three cell types. We further examined the effect on expression of these receptors by stimulating T cells with CD3/CD28 beads and stimulating DCs and macrophages with a TLR7/8 agonist. Expression of lrp1, lrp8, ldlr and vldlr were all significantly upregulated on T cells following activation (Figure 4A), whereas only lrp2 and lrp8 were increased on DC after TLR stimulation (Figure 4B). This data together with previous studies (25, 26) suggest that ldlr and lrp8 (apoER2) are dominantly expressed and may be prominently engaged in apoE-mediated immune cell suppression.

To functionally define the role of the lrp8 receptor engagement in apoE suppression, we isolated vaccinated splenocytes from lrp8$^{-/-}$ mice. These cells were co-cultured with BET/JQ1 treated (Myc-suppressed) immunogenic B16 cells for 48hr with or without exposure to the apoE mimetic COG133. ELISA results show that IFNγ production from splenocytes was inhibited by COG133 in WT mice, however the inhibitory effect was lacking in splenocytes from the lrp8$^{-/-}$ mice (Figure 4D). In addition, using ProcartaPlex multiplex immunoassay, we also quantified other cytokines/chemokines produced in the reaction. Seventeen out of 27 detectable cytokines showed a similar pattern to IFNγ inhibition in WT mice that was reversed in lrp8$^{-/-}$ splenocytes. These included effector function: IFNγ; stimulator function, IL18, GM-CSF, G-CSF; inflammatory cytokines: IL2, IL3, IL4, IL5, IL9, IL13, IL23, IL12p70; chemo attractant factors: MCP-1, MCP3, MIP-1α, CCL-5 (Rantes); and regulatory factors: IL6, IL-10 ($P < 0.05$). Representative data are shown in Supplement Figure 5. These findings suggest that T-cell function is at least partially inhibited by apoE through the lrp8 receptor pathway.

Targeting apoE suppresses tumor growth with enhanced mouse survival in a murine melanoma model

To additionally investigate the role of apoE on melanoma tumor growth *in vivo*, 1x10^4 WT or apoE$^{-/-}$ B16 cells were injected into the right flank of WT, apoE$^{-/-}$ and lrp8$^{-/-}$mice (n=9). The mice from each group were monitored for tumor growth and survival. The results show that targeting apoE in both the tumor cells and the host (apoE$^{-/-}$ B16 cells injected into apoE$^{-/-}$ C57/BL6 mice) results in delayed tumor growth (Figure 5), and significant rejection of tumor cell inoculation

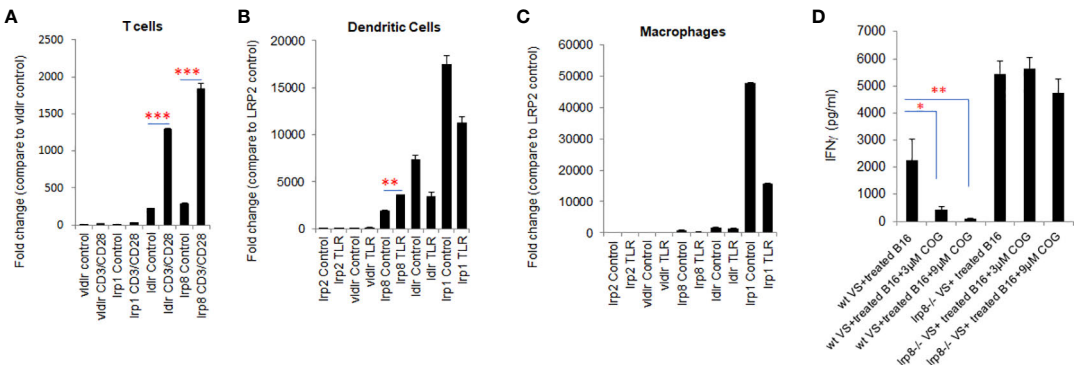

FIGURE 4
lrp8 is the most dominant receptor expressed on activated T cells and blocking lrp8 enhanced T-cell activation. **(A)** Expression of apoE receptors shows predominance of ldlr and lrp8 receptors on T cells, **(B)** lrp8, ldl and lrp1 receptors on dendritic cells, and **(C)** lrp1 receptors on macrophages as shown by quantitative real-time PCR (qPCR). Expression of ldlr and lrp8 was upregulated following T cell stimulation with CD3/CD28 beads. Expression of lrp8 was also upregulated following dendritic cell stimulation with TLR7/8. **(D)** The amount of IFNγ production from vaccinated splenocytes co-cultured with immunogenic WT B16 cells was quantified by ELISA assay. Results show that IFNγ production was significantly suppressed in the presence of the apoE agonist COG133, but suppression did not occur when splenocytes were harvested from lrp8$^{-/-}$ mice. These findings suggest that T-cell function is at least partially inhibited by apoE through the lrp8 receptor pathway. Results are expressed as mean score ± SD. *p<0.05; **p<0.005; ***p<0.001, determined by unpaired two-tailed Student's t-test.

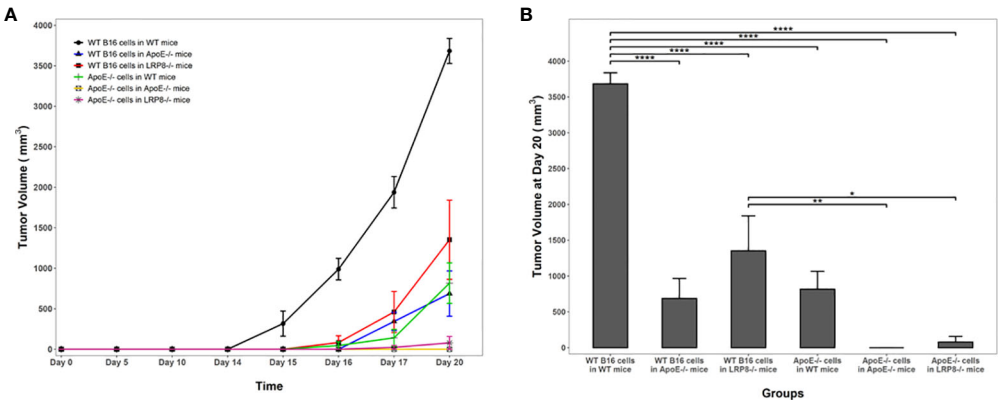

FIGURE 5
Knock out of apoE in both B16 tumor cells and in mice enhances host immunity and attenuates tumorigenicity. **(A)** In vivo, 104 WT or apoE-/- B16 cells were injected into the right leg of WT (n=9), apoE-/- (n=9) or lrp8-/- mice (n=9). The average tumor growth in each group (n=6) is compared. Tumor growth was significantly slower when apoE-/- B16 cells were injected into apoE-/- or lrp8-/- mice versus the other groups (two-way ANOVA; P <0.0001). **(B)** The final tumor volume between treatment groups at the end point of the experiment (Day 20) was also compared using a one-way ANOVA followed by Tukey HSD pairwise multiple comparisons between treatment groups. Tumor volumes at the end point of the experiment were significantly different between treatment groups (one-way ANOVA; P <0.0001). *p<0.05; **p<0.01; ****p<0.0001.

with improved overall survival (Figure 6). Tumor growth was also impaired when apoE$^{-/-}$ B16 cells were injected into lrp8$^{-/-}$ mice, suggesting apoE/LRP8 receptor engagement is important in mediating the apoE protective effect on tumor growth. Complete deletion of apoE in the tumor cells and in the host was most effective for inhibition of tumor growth, while apoE$^{-/-}$ B16 cells injected into WT mice, or WT B16 cells injected into apoE$^{-/-}$ mice or lrp8$^{-/-}$ mice partially suppressed tumor growth compared to control. The suppressive effect observed on tumor growth *in vivo* with apoE suppression appears indirect as apoE KO cells proliferate normally.

The combination of apoE$^{-/-}$ tumor cells administered to apoE$^{-/-}$ mice resulted in the most profound activation of immune pathway signaling and cell infiltrates in the tumor microenvironment

To evaluate if the protective effect against tumor growth with apoE targeting is immune mediated, we harvested the first 3 mice from each group that grew tumors to 15mm for tumor immune profiling. Nanostring analysis of immune cell infiltrates and activation of immune signaling pathways revealed that the

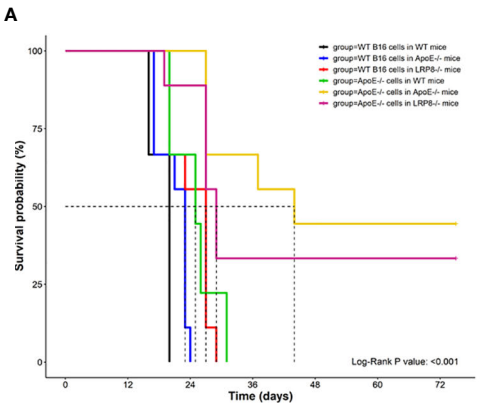

B

Groups (control vs. experimental)	Median Survival time (days)	Hazard Ratio (95% CI)	Log-Rank P value
WT B16 cells in WT mice vs. WT B16 cells in apoE -/- mice	20 vs. 23	0.374 (0.135, 1.040)	**0.020**
WT B16 cells in WT mice vs. WT B16 cells in lrp8 -/- mice	20 vs. 27	0.093 (0.028, 0.310)	**0.002**
WT B16 cells in WT mice vs. apoE -/- cells in WT mice	20 vs. 25	0.088 (0.026, 0.294)	**0.002**
WT B16 cells in WT mice vs. apoE -/- cells in apoE -/- mice	20 vs. 44	0.015 (0.003, 0.063)	**<0.001**
WT B16 cells in WT mice vs. apoE -/- cells in lrp8 -/- mice	20 vs. 29	0.024 (0.006, 0.095)	**<0.001**
WT B16 cells in apoE -/- mice vs. apoE -/- cells in apoE -/- mice	23 vs. 44	0.001 (NA)	**<0.001**
apoE -/- cells in WT mice vs. apoE -/- cells in apoE -/- mice	25 vs. 44	0.131 (0.034, 0.501)	**<0.001**
WT B16 cells in lrp8 -/- mice vs. apoE -/- cells in lrp8 -/- mice	27 vs. 29	0.299 (0.100, 0.894)	**0.030**
apoE -/- cells in apoE -/- mice vs. apoE -/- cells in lrp8 -/- mice	44 vs. 29	1.53 (0.463, 5.030)	0.500

FIGURE 6
Survival curve **(A)** Survival was significantly better (n=9) when apoE$^{-/-}$ B16 cells were injected into apoE$^{-/-}$ or lrp8$^{-/-}$ mice versus the other groups. **(B)** The median survival time and the cumulative survival probability were calculated and compared using the Kaplan-Meier survival estimator followed by a log-rank test, and the hazard ratio (HR) was calculated using the Cox proportional-hazards regression model. The comparison between the groups is shown in the table.

apoE$^{-/-}$ mice in which apoE$^{-/-}$ cells were inoculated, demonstrated the greatest number of immune cell infiltrates (Figure 7A) as well as the highest activation of immune signaling pathways (Figure 7B) based on the expression of signature marker gene transcripts when compared to the other groups. Wild type tumors in apoE$^{-/-}$ mice or WT mice receiving the apoE$^{-/-}$ cells demonstrated more activation of immune pathways and cellular infiltrates as determined by RNA transcripts than WT controls, but these effects were only partial and inferior to the immunity induced when apoE was abolished in the system (apoE$^{-/-}$ cells in apoE$^{-/-}$ B57/BL6 mice). The expression level of the gene transcripts of multiple activation markers for T cells (Figure 8A) and dendritic cells (DCs) (Figure 8B) were also compared within 6 tumor groups. Results showed that the markers for activation T cells including interleukin-2 receptor alpha chain (IL2RA, or CD25), CD69, CD8a, CD28, check point inhibitors PD-L1 and CTLA4, and T cell exhaustion marker Tim-3 were all significantly enhanced in the tumor from the apoE$^{-/-}$ mice in which apoE$^{-/-}$ cells were inoculated (apoE$^{-/-}$/apoE$^{-/-}$) compared with control group (wt/wt), PD1 and Lag 3 were slightly increased, but they were not statistically significant (data not shown). CD28 was also upregulated in the tumor from the apoE$^{-/-}$ mice in which wt tumor cells were inoculated (wt/apoE$^{-/-}$) (Figure 8A). For DCs, the activation genes including CD40, CD70, CD80, CD83, CD86, CD11b and CD11c were all significantly increased in

apoE$^{-/-}$/apoE$^{-/-}$ group compared with controls. CD70 was also increased in wt/apoE$^{-/-}$ and apoE$^{-/-}$/wt groups. (Figure 8B). These observations show that apoE secreted from the tumor or produced in the host impair immunity and establish the potent role that apoE plays in suppressing tumor immunity in the mouse melanoma model. Surprisingly, there was no upregulation of immune pathway scores nor enhanced immune cells scores in lrp8$^{-/-}$ mice. These observations do not correlate with *in vitro* findings nor *in vivo* growth rates, but this may have been specific to the three mice sampled that developed tumors early in this group. To validate nanostring RNA transcript results in the apoE targeted group, we performed immunohistochemistry staining of the immune cell marker CD45 (lymphocyte common antigen) and CD3 (T cell marker) on the same tumor samples that we used for nanostring analysis. Results showed that the apoE$^{-/-}$ mice in which apoE$^{-/-}$ cells were inoculated, have significantly more CD45 (Figures 9A, B) and CD3 (Figures 9C, D) positive immune cell infiltrates than WT control. The other groups were not studied as these gross observations do not have the same objectivity or power of analysis as the nanostring assay.

ApoE knock out in B16 tumor cells induces potent immunogenicity

In the mouse model, apoE appears to be an immune modulator critical for enabling tumor cell growth through suppression of immune activation. To determine if knocking out apoE in tumor cells induced immunogenicity, we vaccinated wild type and apoE$^{-/-}$ mice (Figure 10A) or wild type and lrp8$^{-/-}$ mice (Figure 10B) with WT B16 or apoE$^{-/-}$ B16 tumor cells and

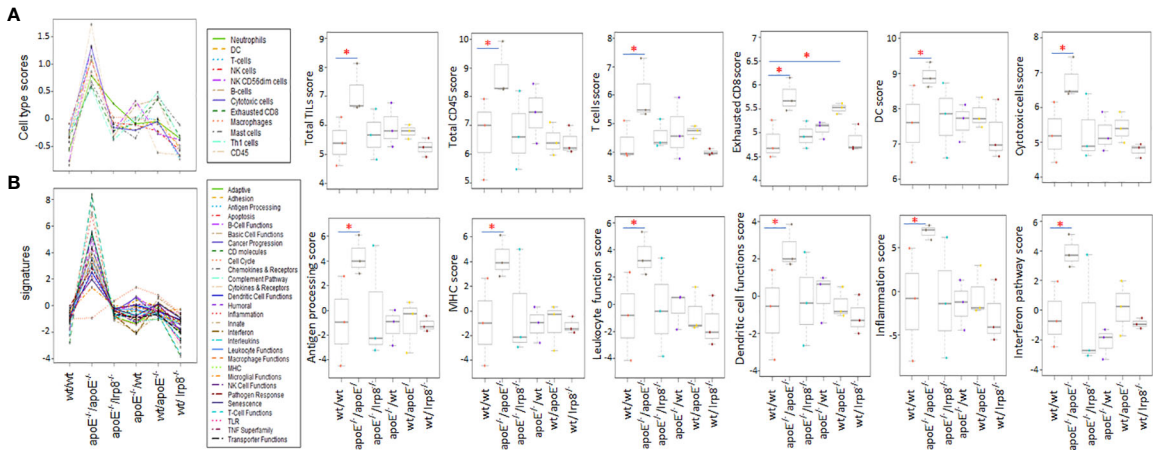

FIGURE 7
The first three tumors that reached 15mm in each of the experimental groups were harvested and the immune cell infiltrate and immune pathway activation was analyzed with nanostring Pancancer immune profiling. **(A)** Immune cell type scores and **(B)** immune pathway (signature) scores show that immune cell infiltrates and immune pathway activation were greatest when apoE-/- cells were injected into apoE-/- mice. Dot line plots show the score trends of 12 immune cell lines and 29 immune pathways. Box plots show selective representative score comparisons. Results are expressed as mean score ±SD. *p<0.05, determined by unpaired two-tailed Student's t-test. Wt/wt: wt B16 cells injected in wt mice; apoE-/-/apoE-/-: apoE-/- cells injected in apoE-/- mice; apoE-/-/lrp8-/-: apoE-/- cells injected in lrp8-/- mice; apoE-/-/wt: apoE-/- cells injected in wt mice; wt/apoE-/-: wt cells injected in apoE-/- mice; wt//lrp8-/-: wt cells injected in lrp8-/- mice.

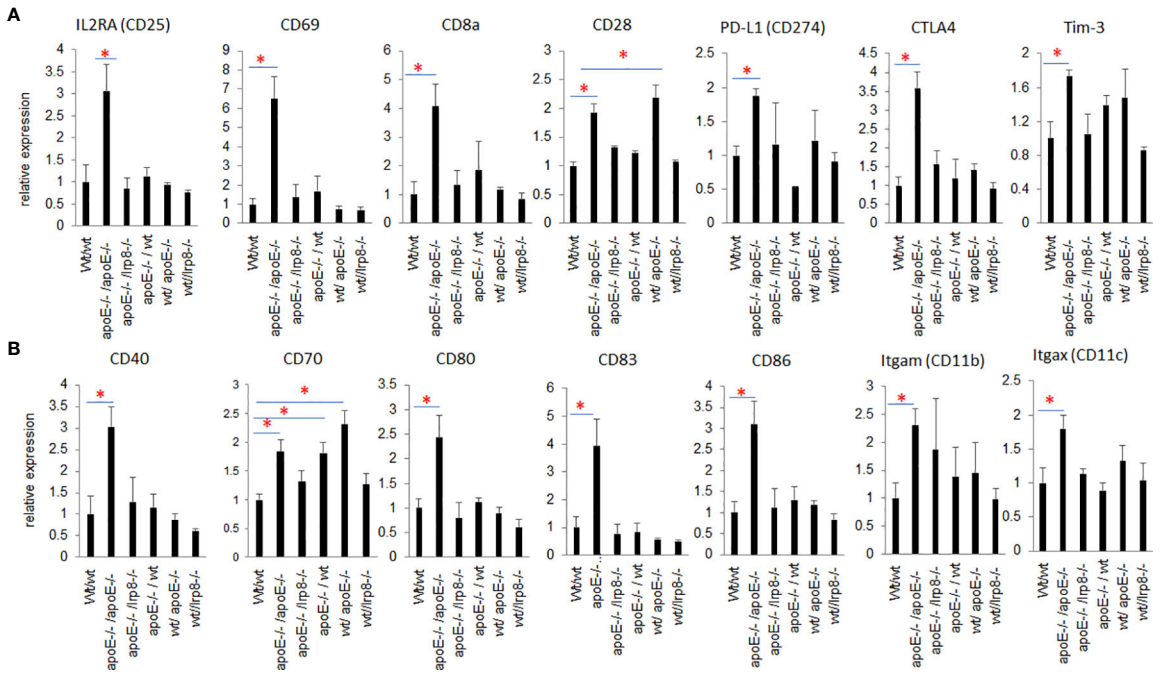

FIGURE 8
Nanostring PanCancer Immune Profiling analysis of RNAseq of activation markers for T cells and DCs that infiltrated into the tumors from the 6 different groups. **(A)** Activated T cell genes and **(B)** activated DC genes were all statistically significantly increased in the tumor from apoE-/-/ apoE-/- group when compared with wt/wt control groups. The relative gene expression level was indicated on the y-axis and tumor groups are listed along the x-axis. Results are expressed as mean score ±SE. *p<0.05, determined by unpaired two-tailed Student's t-test.

CTLA4 Ab and then collected splenocytes from these vaccinated mice 6 days later. We then co-cultured the splenocytes with WT B16 or apoE$^{-/-}$ B16 cells to evaluate IFNγ secretion as a marker of induced immunity. ApoE$^{-/-}$ B16 cells induced robust immunity in whatever circumstance they were tested either as the primary immunogen or with re-stimulation of splenocytes (Figures 10A, B). These findings re-iterate the potent inhibitory effect of apoE on immune cell activation and present an opportunity to exploit this pathway to enable tumor immunity and cancer immunotherapy.

ApoE RNA-seq expression is abundant in cutaneous melanoma but is not associated with PD1, PD-L1 or immune cell infiltrate RNA-seq expression

The potent immune-suppressive effects of ApoE in the melanoma mouse model suggests that APOE may be an important regulator of immunity in human melanoma. To evaluate its association with human melanoma, we analyzed TCGA melanoma datasets based on RNA-seq gene expression values (measured by RSEM algorithm) in 462 patient tumors. We evaluated expression and correlation with other checkpoints (Figure 11), immune cell infiltrates (Figure 12) and patient survival (Figure 13). APOE is abundantly present, however, it did not correlate with PD-L1 or PD1 expression, two checkpoints expressed on tumors, but did positively correlate with APOC1 expression APOC1 was used as a positive control in this analysis (Figure 11). APOE did not correlate with RNA-seq gene expression of T-cell, neutrophil and dendritic cells infiltrates whereas PD-L1 expression correlated with the presence of these three cell phenotypes (Figure 12). Also, APOE did not correlate with survival at a 30% bifurcate gene analysis, whereas the expression of PD-L1 and PD1 both positively correlated with survival of cutaneous melanoma (Figure 13). The high expression of checkpoints like PD-L1 and PD1 associated with cell infiltrates and survival curves, suggest that these genes are expressed in inflammatory tumors that have a better prognosis. APOE expression however appears to be independent of inflammatory phenotype in these tumors and may act as a separate and independent pathway in suppressing anti-tumor T-cell immunity.

Discussion

In prior published work, we showed a distinctly different response to the same tumor vaccine protocol in a mouse

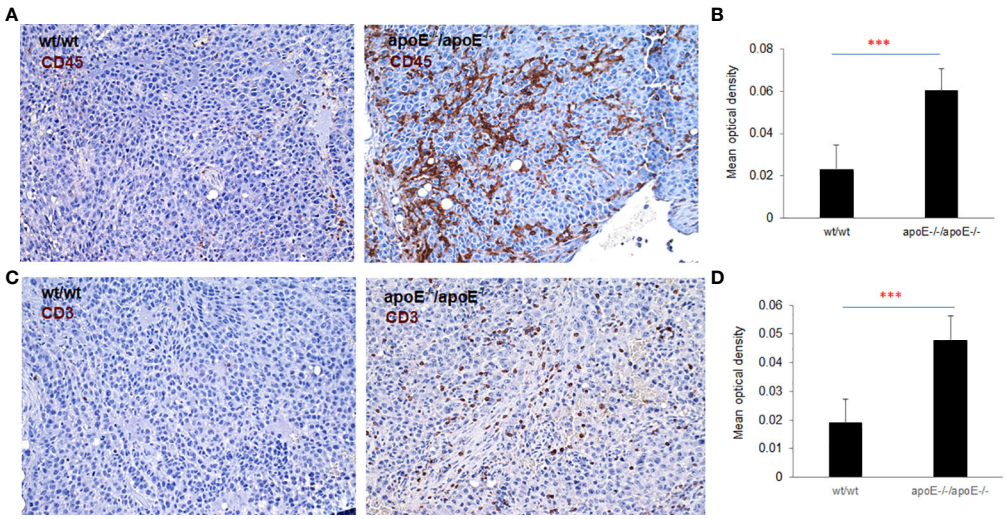

FIGURE 9
To validate nanostring results, both CD45 and CD3 expression were examined with IHC staining in the tumors from WT or apoE-/- mice following injection with WT or apoE-/- tumor cells. Representative images of CD45 **(A)** and CD3 **(C)** staining visualized with DAB (brown) and counterstained with hematoxylin (blue, nuclei). **(B, D)** Optical density (mean gray value) obtained by color deconvolution analysis. Optical density graph bars represent the mean ± SD (n = 30 images). ***p<0.001, determined by unpaired two-tailed Student's t-test. Wt/wt: wt B16 cells injected in wt mice; apoE-/- /apoE-/-: apoE-/- cells injected in apoE-/- mice.

neuroblastoma and melanoma tumor model (19). The neuroblastoma mouse model was remarkably sensitive to tumor vaccination even at a high dose of tumor cell inoculation whereas a low dose melanoma model was surprisingly resistant. This differential response could imply that intrinsic tumor cell characteristics and/or differences in tumor/host immunity are present that may account for differences in immune resistance.

In the current study we assess immunosuppressive modulators in the melanoma model and the modulator that was most highly expressed by qPCR in the B16-F10 melanoma is ApoE. We profiled over 700 immune associated gene transcripts

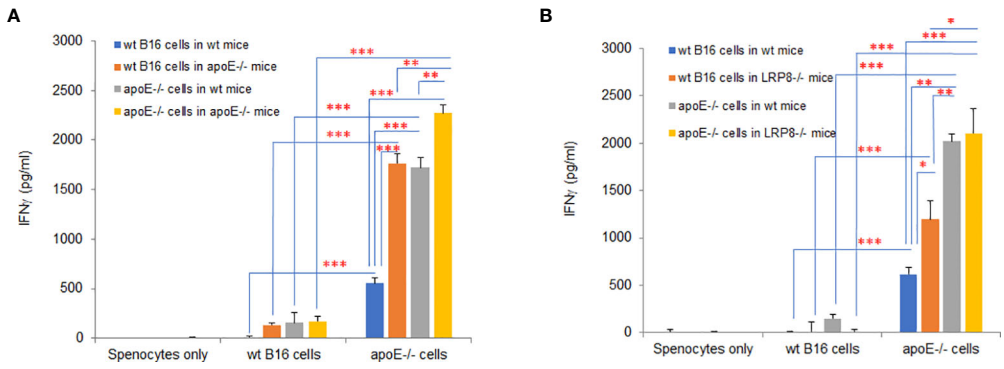

FIGURE 10
ApoE knock out in B16 tumor cells induces potent immunogenicity. Wild type and apoE$^{-/-}$ mice **(A)** or wild type and lrp8$^{-/-}$ mice **(B)**, were inoculated with either WT B16 or apoE$^{-/-}$ cells, with anti-CTLA4 antibody on day 0. Splenocytes were harvested on day 7 and co-cultured with either WT B16 or apoE$^{-/-}$ B16 cells for 48hr, following which IFNγ levels in media were compared with ELISA assay. Results show that IFNγ production is highest for all groups when apoE$^{-/-}$ cells are used. These findings re-iterate the potent inhibitory effect of apoE on immune cell activation in the cancer environment. Results are expressed as mean score ± SD. *p<0.05; **p<0.005; ***p<0.001, determined by unpaired two-tailed Student's t-test.

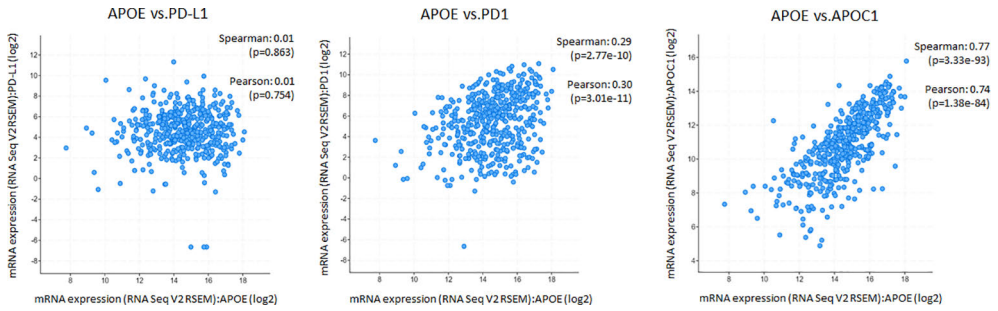

FIGURE 11
ApoE RNA-seq expression is abundant in cutaneous melanoma but is not associated with PD-L1 or PD1. Scatterplots showing mRNA expression correlation of APOE (x-axis) with PD-L1, PD1 and APOC1 from the TCGA melanoma datasets based on their RNA-seq gene expression values (measured by RSEM algorithm). APOE expression did not correlate with PD-L1 or PD1 but did positively correlate with APOC1 expression which was used as a control gene. The correlation was evaluated by the Spearman correlation coefficient with a cut-off value of 0.5 and P-value used a cut-off value of 0.05.

in the melanoma B16-F10 cells and identified 18 genes with known immunosuppressive characteristics that were detected. ApoE was notably detected and found to be more abundant than any of the other known immunosuppressive transcripts identified. Besides its role in cholesterol transport, Apolipoprotein E (apoE) has considerable immunomodulatory properties (4, 18, 27–29). ApoE is shown to suppress lymphocyte proliferation (30) and modulate immune activation by acting on antigen-presenting cells (2, 30), implicating apoE as a suppressant of immune function. We found ApoE to be abundantly expressed in the B16-F10 melanoma cell line and was actively secreted by these tumor cells into the serum of the host as the tumors establish and grow. These findings raised suspicion that apoE contributes to immune escape.

Both the expression of apoE as well as the secretion of apoE from the tumor cells seems to have clear immunosuppressive effects. Our studies show that tumor cells depleted of apoE can stimulate remarkable immune activation in co-culture experiments. The conditioned media from apoE$^{-/-}$ tumor melanoma cells alone did not suppress T-cell function like that of WT tumor cell conditioned media. To understand the mechanism by which apoE functions we investigated specific

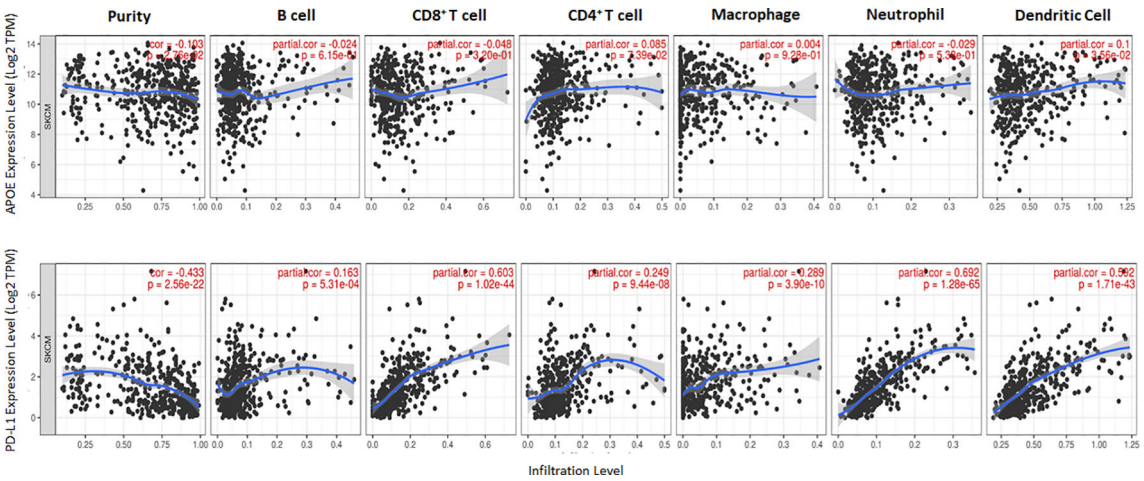

FIGURE 12
Scatterplots show the tumor purity-corrected partial Spearman's rho value and the correlation between gene expression with infiltration of six immune cell estimates. Top row is APOE expression while the bottom row depicts PD-L1. PD-L1 correlated with CD8 T cell and neutrophil infiltrates, while APOE does not correlate with immune cell infiltrates. The correlation was evaluated by the Spearman correlation coefficient with a cut-off value of 0.5 and P-value used a cut-off value of 0.05.

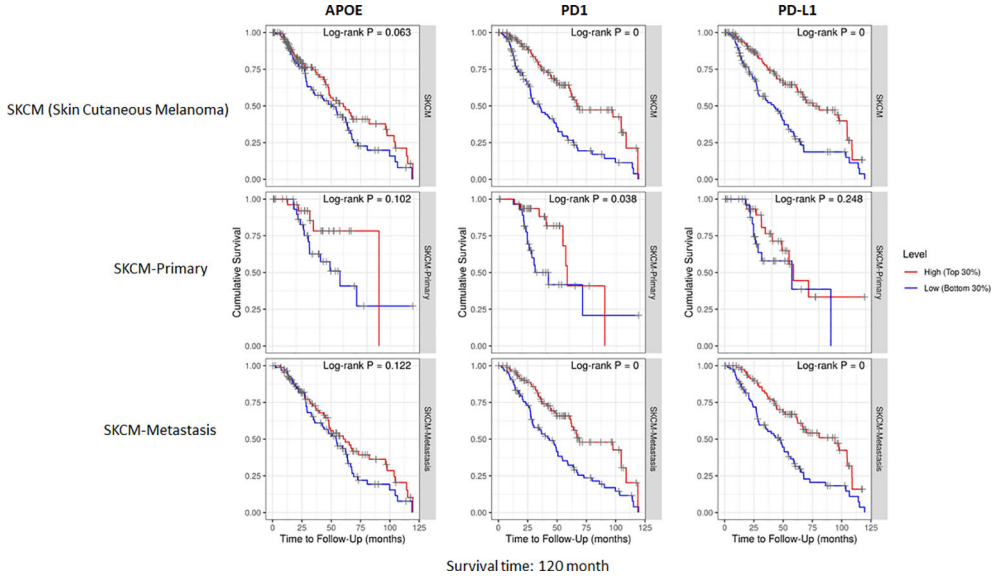

FIGURE 13
Cumulative survival of patients associated with bifurcate gene expression at 30%. TCGA database includes primary and metastasis samples (n=462). APOE expression did not associate with survival, while PD-L1 and PD1 was associated with survival at this level of analysis. The correlation was evaluated by the Spearman correlation coefficient with a cut-off value of 0.5 and P-value used a cut-off value of 0.05.

effects of the apoE peptide mimetic COG133 on T-cell and DC function. The suppressive effect appears to be evident on both stimulated DCs and T-cells as determined by cytokine secretion. We identified the dominant receptors on these cells showing that of the low-density lipoprotein (ldlr) receptor family evaluated, lrp8 and ldlr were most abundant and responsive to stimulation in T-cells while ldlr and lrp1 were present in DCs. In co-culture experiments, the suppressive effect of apoE on vaccinated splenocytes was absent when the splenocytes were harvested from lrp8$^{-/-}$ mice. These findings suggest that T-cell function is at least partially dependent on apoE-lrp8 receptor engagement.

To investigate the premise of ApoE being a potent immune checkpoint, we challenged WT, apoE$^{-/-}$ and lrp8$^{-/-}$ mice with WT and ApoE knock out B16-F10 melanoma tumor cells. Results show remarkable suppression of tumor growth when ApoE is absent from the system with significant tumor elimination when compared with WT controls. ApoE in tumor cells or endogenously produced in the mice was capable of suppressing tumor immunity and significant tumor immunity only occurred when ApoE was absent from both tumor cells and the murine host. Immuno-phenotyping of the tumor micro-environment in mice that grew tumors, revealed the highest levels of immune pathway activation and immune cell infiltrates in the apoE$^{-/-}$ mice that received apoE$^{-/-}$ B16 melanoma cells as detected by RNA transcripts. The effect of apoE seems to be at least partially mediated by its interaction with the Lrp8 receptor as this group also had slower tumor growth and rejection of tumor cells when apoE$^{-/-}$ melanoma cells were inoculated into Lrp8$^{-/-}$ mice, endorsing the *in vitro* findings in splenocyte studies. However, the immune mediated effect was not as apparent in the lrp8$^{-/-}$ mice, as activation of immune pathway and cellular RNA transcripts were not universally increased liked that observed in the complete apoE knock out tumor/mouse model. These findings may be limited and underestimate the ultimate tumor immunity as the tumor micro-environment was analyzed from the first three mice in each group that developed tumor and do not necessarily represent the mice with delayed or absent tumor growth.

Several potential shortfalls of our findings are evident considering prior literatureThe lack of myeloid-derived suppressor cells (MDSC) analysis in the B16-F10 mice models used is evident. Previous studies have shown that the liver-X nuclear receptor (LXR)/ApoE axis reduce MDSC abundance in murine melanoma models by binding to Lrp8 receptor on MDSC. MDSC blockade by LXR-induced ApoE enhanced cytotoxic T cell activation in B16-F10 bearing mice and patients, eventually leading to reduced melanoma growth (18). Hence, a further analysis of the innate and adaptive immune responses (including possibly depletion strategies to validate the model) is required to fully understand the implications of apoE in tumor immunity. Another potential limitation of our study is the assumption of cytokine responses observed. Cytokines have complex roles in immune response modulation, and it is also shown that IL-10 is considered to be immune-stimulatory as opposed to immune-suppressive (31) while IL-1a/b can be immune-suppressive. Thus, the results described for ApoE

secreted from B16 melanoma tumor cells may impair activation of pro-inflammatory DCs and can be interpreted in an opposite direction. Our results also add to a conflicted literature in which apoE can mediate either pro- or anti-tumor effects. We employ CRISPR gene editing to assess the tumor-intrinsic effects of ApoE. Previous studies have indicated that regardless of the gene being targeted, that CRISPR/Cas9 manipulation can yield tumor cells of increased immunogenicity based on expression of Cas9-derived xenoantigens (32). Thus, reduced growth rate and increased immunogenicity of ApoE-/- B16 melanoma cells *in vivo* could be more dependent on Cas9 than ApoE-deficiency, however several of our B16-F10 melanoma controls do have CRISPR/Cas9 expression alone that do not seem to alter immunogenicity.

Despite these contradictions, our findings suggest that apoE plays a substantial immunomodulatory role with multiple inhibitory effects on T cell function, inflammatory cytokine response, and activation of dendritic cells. ApoE also protects tumors by suppressing tumor cell immunogenicity. $ApoE^{-/-}$ B16 cells induced robust immunity in whatever circumstance they were tested either as the primary immunogen *in vivo* or with re-stimulation of splenocytes ex vivo. Together, the multiple experiments presented, establish the potent inhibitory effects of apoE on immune cell function and activation of immune signaling in the melanoma mouse model. These findings present an opportunity to exploit this pathway for enabling tumor immunity and cancer immunotherapy.

To understand the correlation between immunity and APOE expression in patients with melanoma, we accessed the raw RNA-seq data from the TCGA melanoma datasets (measured by RSEM algorithm) (n=462). Although APOE was abundantly present in the tumors, there was no correlation between APOE and PD1 or PD-L1 expression and there was also no association between APOE and cell infiltrates as there was between PD-L1 and T-cell/neutrophil expression. The findings do not take into consideration the serum levels of ApoE in the patients themselves. The observations from our mouse model imply that the absence of tumor ApoE alone is not sufficient to induce immunity in that the serum level of the host also has significant suppressive effects on induced immunity. In our patient analysis, we did not find any association with APOE and inflammatory tumors as we did for PD1 and PD-L1, nor did we find any association with patient survival. ApoE seems to be a potent suppressor of immunity and therefore may act independently of the classic well described checkpoints.

In summary, apoE plays a broad role in immune resistance observed in the WT B16 melanoma tumors. ApoE inhibits activation of immune cells, inflammatory signals, and tumor immunogenicity both locally and systemically *via* cellular secretion and host production. This work shows that tumor immunity can be restored and enhanced by targeting apoE. These findings identify apoE as a novel tumor checkpoint and an obvious target for improving tumor immunity with cancer immunotherapy.

Data availability statement

The datasets presented in this study can be found in online repositories. The names of the repository/repositories and accession number(s) can be found in the article/ Supplementary Material.

Ethics statement

The animal study was reviewed and approved by The Institutional Animal Care and Use Committee (IACUC) of Children's National Hospital, Washington, DC.

Author contributions

AS conceived the idea and acquired funding for the study. AS, XW and MS wrote the original draft, and all authors reviewed and edited the manuscript; XW, MBa, PS, BT, AJ, MBe, and AS interpreted the data, made the figures, planned the experiments, performed and analyzed the experiments. All authors reviewed, edited, and approved the final manuscript.

Funding

This work has been supported in part by the EVAN Foundation, the Catherine Blair foundation, and the Michael Sandler Research Fund as well as the Sheikh Zayed Institute for Pediatric Surgical Innovation. Author receiving: AS.

Acknowledgments

We thank Mrs Karuna Panchapakesan and Dr Susan Knoblach from the Children's National Genetic and Bioinformatics Core for helping with Nanostring experimental setup, and Dr. Christopher Lazarski for his assistance in flow cytometry experimental setup and data analysis.

Conflict of interest

Authors BT, AJ, and MBe were employed by Integrated DNA Technologies, Inc.

The remaining authors declare that the research was conducted in the absence of any commercial or financial

relationships that could be construed as a potential conflict of interest.

Publisher's note

All claims expressed in this article are solely those of the authors and do not necessarily represent those of their affiliated organizations, or those of the publisher, the editors and the reviewers. Any product that may be evaluated in this article, or claim that may be made by its manufacturer, is not guaranteed or endorsed by the publisher.

Supplementary material

The Supplementary Material for this article can be found online at: https://www.frontiersin.org/articles/10.3389/fimmu.2022.991790/full#supplementary-material

References

1. Stojakovic T, Scharnagl H, Marz W. ApoE: crossroads between alzheimer's disease and atherosclerosis. *Semin Vasc Med* (2004) 4(3):279–85. doi: 10.1055/s-2004-861496

2. Bonacina F, Coe D, Wang G, Longhi MP, Baragetti A, Moregola A, et al. Myeloid apolipoprotein e controls dendritic cell antigen presentation and T cell activation. *Nat Commun* (2018) 9(1):3083. doi: 10.1038/s41467-018-05322-1

3. Wang X, Huang R, Zhang L, Li S, Luo J, Gu Y, et al. A severe atherosclerosis mouse model on the resistant NOD background. *Dis Model Mech* (2018) 11(10): dmm033852. doi: 10.1242/dmm.033852

4. Yin C, Ackermann S, Ma Z, Mohanta SK, Zhang C, Li Y, et al. ApoE attenuates unresolvable inflammation by complex formation with activated C1q. *Nat Med* (2019) 25(3):496–506. doi: 10.1038/s41591-018-0336-8

5. Ostendorf BN, Bilanovic J, Adaku N, Tafreshian KN, Tavora B, Vaughan RD, et al. Common germline variants of the human APOE gene modulate melanoma progression and survival. *Nat Med* (2020) 26(7):1048–53. doi: 10.1038/s41591-020-0879-3

6. Lee YS, Yeo IJ, Kim KC, Han SB, Hong JT. Inhibition of lung tumor development in ApoE knockout mice *via* enhancement of TREM-1 dependent NK cell cytotoxicity. *Front Immunol* (2019) 10:1379. doi: 10.3389/fimmu.2019.01379

7. An HJ, Koh HM, Song DH. Apolipoprotein e is a predictive marker for assessing non-small cell lung cancer patients with lymph node metastasis. *Pathol Res Pract* (2019) 215(10):152607. doi: 10.1016/j.prp.2019.152607

8. Zhao Z, Zou S, Guan X, Wang M, Jiang Z, Liu Z, et al. Apolipoprotein e overexpression is associated with tumor progression and poor survival in colorectal cancer. *Front Genet* (2018) 9:650. doi: 10.3389/fgene.2018.00650

9. Fang Z, He M, Song M. Serum lipid profiles and risk of colorectal cancer: a prospective cohort study in the UK biobank. *Br J Cancer.* (2021) 124(3):663–70. doi: 10.1038/s41416-020-01143-6

10. Nicoll JA, Zunarelli E, Rampling R, Murray LS, Papanastassiou V, Stewart J. Involvement of apolipoprotein e in glioblastoma: immunohistochemistry and clinical outcome. *Neuroreport* (2003) 14(15):1923–6. doi: 10.1097/00001756-200310270-00008

11. Venanzoni MC, Giunta S, Muraro GB, Storari L, Crescini C, Mazzucchelli R, et al. Apolipoprotein e expression in localized prostate cancers. *Int J Oncol* (2003) 22(4):779–86. doi: 10.3892/ijo.22.4.779

12. Su WP, Chen YT, Lai WW, Lin CC, Yan JJ, Su WC. Apolipoprotein e expression promotes lung adenocarcinoma proliferation and migration and as a potential survival marker in lung cancer. *Lung Cancer.* (2011) 71(1):28–33. doi: 10.1016/j.lungcan.2010.04.009

13. Huvila J, Brandt A, Rojas CR, Pasanen S, Talve L, Hirsimaki P, et al. Gene expression profiling of endometrial adenocarcinomas reveals increased apolipoprotein e expression in poorly differentiated tumors. *Int J Gynecol Cancer.* (2009) 19(7):1226–31. doi: 10.1111/IGC.0b013e3181b33be0

14. Oue N, Hamai Y, Mitani Y, Matsumura S, Oshimo Y, Aung PP, et al. Gene expression profile of gastric carcinoma: identification of genes and tags potentially involved in invasion, metastasis, and carcinogenesis by serial analysis of gene expression. *Cancer Res* (2004) 64(7):2397–405. doi: 10.1158/0008-5472.CAN-03-3514

15. Kemp SB, Carpenter ES, Steele NG, Donahue KL, Nwosu ZC, Pacheco A, et al. Apolipoprotein e promotes immune suppression in pancreatic cancer through NF-kappaB-Mediated production of CXCL1. *Cancer Res* (2021) 81(16):4305–18. doi: 10.1158/0008-5472.CAN-20-3929

16. Alikhani N, Ferguson RD, Novosyadlyy R, Gallagher EJ, Scheinman EJ, Yakar S, et al. Mammary tumor growth and pulmonary metastasis are enhanced in a hyperlipidemic mouse model. *Oncogene* (2013) 32(8):961–7. doi: 10.1038/onc.2012.113

17. Pencheva N, Tran H, Buss C, Huh D, Drobnjak M, Busam K, et al. Convergent multi-miRNA targeting of ApoE drives LRP1/LRP8-dependent melanoma metastasis and angiogenesis. *Cell* (2012) 151(5):1068–82. doi: 10.1016/j.cell.2012.10.028

18. Tavazoie MF, Pollack I, Tanqueco R, Ostendorf BN, Reis BS, Gonsalves FC, et al. LXR/ApoE activation restricts innate immune suppression in cancer. *Cell* (2018) 172(4):825–40.e18. doi: 10.1016/j.cell.2017.12.026

19. Wu X, Nelson M, Basu M, Srinivasan P, Lazarski C, Zhang P, et al. MYC oncogene is associated with suppression of tumor immunity and targeting myc induces tumor cell immunogenicity for therapeutic whole cell vaccination. *J Immunother Cancer* (2021) 9(3):e001388. doi: 10.1136/jitc-2020-001388

20. Chakrabarti L, Morgan C, Sandler AD. Combination of Id2 knockdown whole tumor cells and checkpoint blockade: A potent vaccine strategy in a mouse neuroblastoma model. *PloS One* (2015) 10(6):e0129237. doi: 10.1371/journal.pone.0129237

21. Hugo W, Zaretsky JM, Sun L, Song C, Moreno BH, Hu-Lieskovan S, et al. Genomic and transcriptomic features of response to anti-PD-1 therapy in metastatic melanoma. *Cell* (2016) 165(1):35–44. doi: 10.1016/j.cell.2016.02.065

22. Dobin A, Davis CA, Schlesinger F, Drenkow J, Zaleski C, Jha S, et al. STAR: ultrafast universal RNA-seq aligner. *Bioinformatics* (2013) 29(1):15–21. doi: 10.1093/bioinformatics/bts635

23. Noble ML, Kelley DL. Accuracy of tri-axial cinematographic analysis in determining parameters of curvilinear motion. *Res Q* (1969) 40(3):643–5. doi: 10.1080/10671188.1969.10614893

24. Love MI, Huber W, Anders S. Moderated estimation of fold change and dispersion for RNA-seq data with DESeq2. *Genome Biol* (2014) 15(12):550. doi: 10.1186/s13059-014-0550-8

25. Bilousova T, Melnik M, Miyoshi E, Gonzalez BL, Poon WW, Vinters HV, et al. Apolipoprotein E/Amyloid-beta complex accumulates in Alzheimer disease cortical synapses *via* apolipoprotein e receptors and is enhanced by APOE4. *Am J Pathol* (2019) 189(8):1621–36. doi: 10.1016/j.ajpath.2019.04.010

26. Herz J. Apolipoprotein e receptors in the nervous system. *Curr Opin Lipidol.* (2009) 20(3):190–6. doi: 10.1097/MOL.0b013e32832d3a10

27. Laskowitz DT, Lee DM, Schmechel D, Staats HF. Altered immune responses in apolipoprotein e-deficient mice. *J Lipid Res* (2000) 41(4):613–20. doi: 10.1016/S0022-2275(20)32409-3

28. Baitsch D, Bock HH, Engel T, Telgmann R, Muller-Tidow C, Varga G, et al. Apolipoprotein e induces antiinflammatory phenotype in macrophages. *Arterioscler Thromb Vasc Biol* (2011) 31(5):1160–8. doi: 10.1161/ATVBAHA.111.222745

29. Zhu Y, Kodvawala A, Hui DY. Apolipoprotein e inhibits toll-like receptor (TLR)-3- and TLR-4-mediated macrophage activation through distinct mechanisms. *Biochem J* (2010) 428(1):47–54. doi: 10.1042/BJ20100016

30. Tenger C, Zhou X. Apolipoprotein e modulates immune activation by acting on the antigen-presenting cell. *Immunology* (2003) 109(3):392–7. doi: 10.1046/j.1365-2567.2003.01665.x

31. Wang Y, Sun SN, Liu Q, Yu YY, Guo J, Wang K, et al. Autocrine complement inhibits IL10-dependent T-cell-Mediated antitumor immunity to promote tumor progression. *Cancer Discovery* (2016) 6(9):1022–35. doi: 10.1158/2159-8290.CD-15-1412

32. Mehta A, Merkel OM. Immunogenicity of Cas9 protein. *J Pharm Sci* (2020) 109(1):62–7. doi: 10.1016/j.xphs.2019.10.003

frontiers | Frontiers in Immunology

TYPE Case Report
PUBLISHED 27 October 2022
DOI 10.3389/fimmu.2022.995496

OPEN ACCESS

EDITED BY
Yubin Li,
GlaxoSmithKline, United States

REVIEWED BY
Yasmin Mohseni,
University of Southern California, United States
Pooria Safarzadeh Kozani,
Tarbiat Modares University, Iran

*CORRESPONDENCE
Hui Liu
sylen@zju.edu.cn

†These authors have contributed equally to this work and share first authorship

SPECIALTY SECTION
This article was submitted to Cancer Immunity and Immunotherapy, a section of the journal Frontiers in Immunology

RECEIVED 15 July 2022
ACCEPTED 03 October 2022
PUBLISHED 27 October 2022

CITATION
Chen P, Xia Y, Lei W, Zhong S, Jiang H, Ren L, Qian W and Liu H (2022) Case report: Hashimoto's thyroiditis after CD19 chimeric antigen receptor T-cell therapy.
Front. Immunol. 13:995496.
doi: 10.3389/fimmu.2022.995496

Case report: Hashimoto's thyroiditis after CD19 chimeric antigen receptor T-cell therapy

Panpan Chen[1†], Yongming Xia[2†], Wen Lei[1], Shuhan Zhong[1], Huawei Jiang[1], Lingling Ren[1], Wenbin Qian[1] and Hui Liu[1*]

[1]Department of Hematology, The Second Affiliated Hospital, Zhejiang University School of Medicine, Hangzhou, China, [2]Department of Hematology, Yuyao People's Hospital of Zhejiang Province, The Affiliated Yangming Hospital of Ningbo University, Ningbo, China

Chimeric antigen receptor (CAR)-T cell therapy is a novel cell therapeutic approach that is increasingly being used to treat patients with relapsed refractory B-cell lymphoma. Despite the efficacy of CAR T cell therapy, it has various adverse effects that can affect any organ in the body. The application of immune checkpoint inhibitors such as programmed death 1 (PD-1), programmed death ligand 1 (PDL-1), and cytotoxic T-lymphocyte antigen 4 (CTLA-4) antibodies has previously been reported to be associated with immune-related adverse events such as thyroid dysfunction and thyroiditis. Reports of immune-related adverse reactions after CAR T therapy are currently extremely rare, with only one case of a cytokine storm (CRS) combined with severe arthritis in a patient with ALL after treatment. Here, we describe two cases of Hashimoto's thyroiditis secondary to CAR T therapy. Two patients with relapsed refractory diffuse large B-cell lymphoma developed elevated peroxidase and globulin antibodies secondary to CAR-T cell therapy and developed Hashimoto's thyroiditis. Complete remission was achieved in two patients at 1 and 3 months after CAR-T cell therapy. The inflammation of the thyroid tissue may be directly or indirectly related to CAR T cell therapy, and the mechanisms needs to be further investigated.

KEYWORDS

thyroditis, CAR T, lyphoma, TgAb, irAEs

Case presentation

Case 1

A 65-year-old male presented with dull pain and mass on the left side of the neck without significant fever or chills, no nausea or vomiting, no abdominal pain, bloating or diarrhea, and no hoarseness. thyroid puncture was performed in 2017 and pathology suggested diffuse large b-cell lymphoma, GCB type, high-grade B-cell lymphoma,

immunohistochemistry: CK-, EMA-, CD20+, CD79a+, CD3 little +, CD5 little +, CyclinD1-, BCL2-, BCL6 70%+, CD10 focal weak +, MUM1-, P53-, Kappa-, Lambda-, Ki-67 60%, CD19+, PD-L1-, FISH: MYC-, BCL2-, BCL6-. six times standard therapy with rituximab plus cyclophosphamide, doxorubicin, vincristine, and prednisone (R-CHOP), did not achieve partial remission (PR). Given rituximab plus gemcitabine, cisplatin and dexamethasone (R-GDP), the patient developed tinnitus in the right ear, so changed to rituximab plus gemcitabine oxaliplatin (R-Gemox) regimen chemotherapy. After four times of R-Gemox regimen chemotherapy, the patient performed autologous hemopoietic stem cell transplantation (HSCT) in April 2018. Subsequent PET-CT (Figure 1) suggested a hypodense thyroid nodule 1.8*2.7*3.4 cm^3 with unclear borders, localized at the anterior borders above the lesion invading the anterior vocal cord union, SUVmax 16.38. The patient was proposed for CAR T therapy, peripheral lymphocytes were collected (Table 1). On November 8, 2018 fludarabine and cyclophosphamide (FC) pretreatment regimen was performed to clearance of lymphocytes, and CAR T cells were infused back on November 12 (Table 2). The disease was evaluated in partial remission at one month and complete remission at three months (Table 3). Ultrasound suggested thyroid nodule of 0.8*0.6 cm (Figure 2), thyroid ultrasound suggested thyroid inflammation, thyroid function T3, T4, TSH within normal range, anti-thyroid peroxidase antibody and thyroglobulin antibody were elevated (Table 1). Consider secondary Hashimoto's thyroiditis.

Case 2

A 52-year-old female presented with right cervical lymph node enlargement without tenderness. A lymphoproliferative lesion was found during a neck biopsy at an outside hospital in October 2016. On reexamination 2 months later, the lymph node was enlarged by approximately 6* 8 cm without tenderness, with limited mobility, chest tightness, shortness of breath, no fever or chills, and no cough or sputum. A right cervical lymph node biopsy in December 2016 suggested (cervical lymph node) non-Hodgkin lymphoma, consistent with diffuse large b-cell lymphoma of germinal center origin, immunohistochemistry: CD3+, CD20+, Ki-67 60%+, CD79a+, CD30 partial+, CD5-, CD10+, BCL2+, BCL6 scattered +, MUM1-, PAX5+, CD21-, CyclinD1-, C-MYC-. ALK-, EBER-, CD15-. After the diagnosis was confirmed one course of chemotherapy with R-CHOP regimen, 3 courses of rituximab plus etoposide, cyclophosphamide, adriamycin, vincristine, prednisone (R-ECHOP) regimen, and 4 courses of R-CHOP regimen with partial remission assessed for efficacy. Lymph node enlargement 2 months after the end of chemotherapy and another lymph node biopsy in August 2018 suggested diffuse large b-cell lymphoma of germinal center origin and disease progression was

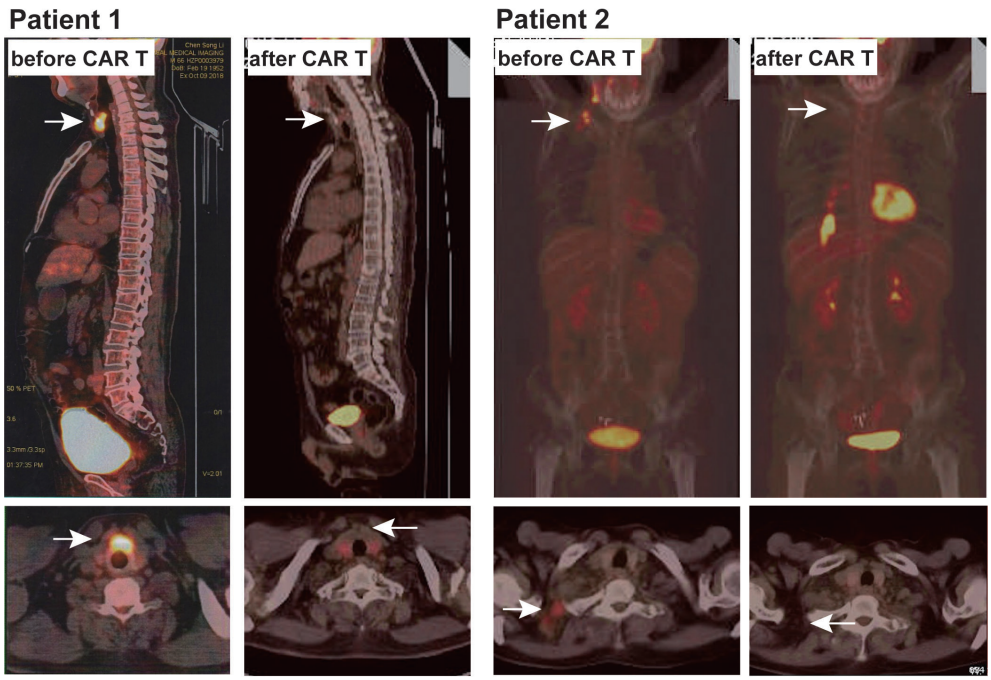

FIGURE 1
PET-CT images of two patients before and after CART treatment.

TABLE 1 Summary of the 2 cases with thyroid irAEs after CAR T cell therapy.

Case summaries		Following pembrolizumab therapy						Overview of 18 FDG-PET/CT imaging			
Patient	thyroiditis-related irAE	TSH	T3	FT3	T4	ATG Ab	TPO Ab	TG	Baseline	After abnormal TFTs	Time from CAR T infusion, mo
Patient 1	Thyroiditis, transient	2.06	1.57	4.32	94.5	171.8	31.48	NA	Increased	Increased	3
Patient 2	Thyroiditis, transient	–	1.74	5.58	125.6	13.29	33.83	6.02	No increase	Increased	3

NA, not available.
TSH, 0.35 to 4.94 mIU/L.
Total T3, 0.98 to 2.33 nmol/L.
FT3, 2.43 to 6.01 pmol/L.
Total T4, 58.1 to 140.6 nmol/L.
TPO Ab, <5.61 IU/mL.
ATG Ab, <4.11 IU/mL.
TG, 3.5-77.0 μg/L.

TABLE 2 Dynamic changes of serum cytokines after CAR T cell therapy.

Time from CAR T infusion, days	Patient 1			Patient 2		
	IL-6	TNF-α	INF-γ	IL-6	TNF-α	INF-γ
D1	3.84	1.14	9.51	14.22	8.57	0.1
D4	5.05	3.55	5.52	130.35	80.48	0.1
D8	10.33	2.32	12.28	8.98	18.73	0.1
D11	4.63	1.8	13.39			
D30	22.61	0.1	0.1	3.11	0.19	3.93
D90	1.82	0.95	2.56	1.67	0.87	0.1
D180	3.33	0.46	1.13	11.94	2.91	6

IL-6, Interleukin-6; TNF-α, tumor necrosis factor-α; INF-γ, Interferon-γ.
IL-6, 0.0 to 16.6 pg/ml.
TNF-α, 0.0 to 5.2 pg/ml.
INF-γ, 0.0 to 17.3 pg/ml.

TABLE 3 Timeline of Patient 1.

Day	Event
2017/5/10	Diagnosis as diffuse large b-cell lymphoma
2017/5/10	R-CHOP
2017/6/13	R-CHOP
2017/7/4	R-CHOP
2017/7/25	R-CHOP
2017/8/15	R-CHOP
2017/9/5	R-CHOP
2017/10/17	R-GDP
2017/11/29	R-GeMox
2017/12/22	R-GeMox
2018/1/15	R-GeMox
2018/2/9	R-GeMox
2018/3/1	R-GeMox
2018/4/2	autologous hemopoietic stem cell transplantation (HSCT)
2018/10/29	peripheral lymphocytes collection
2018/11/8	fludarabine and cyclophosphamide (FC) pretreatment
2018/11/12	CAR T cells infusion
2018/12/14	partial remission
2019/02/20	complete remission

considered. PET-CT (Figure 1) suggested lymphoma after chemotherapy: deep right sternocleidomastoid muscle and cervical sheath, right cervical root, left cervical sheath, bilateral supra- and inferior clavicular regions, mediastinal thoracic inlet and upper mediastinal vascular space, multiple deep axillary nodes of variable size on both sides Lymph nodes with varying degrees of increased FDG metabolism. Peripheral blood lymphocytes were collected on September 19, 2018. Pretreatment clearance of lympohcytes with FC protocol was performed on September 29, 2018 and CAR - t cell infusion was performed on October 4. One month later the disease was assessed to be in complete remission (Table 4). During follow-up, the patient had elevated TGAb, TMAb and TPOAb, but normal thyroid function (Table 2). Secondary Hashimoto's thyroiditis was considered.

Discussion

CAR - T cell therapy is a novel biological therapy in which T cells are genetically transduced to express specific CAR - T proteins that specifically recognize target antigens and kill target tumor cells (1). The major adverse effects of CAR - T cell therapy are cytokine

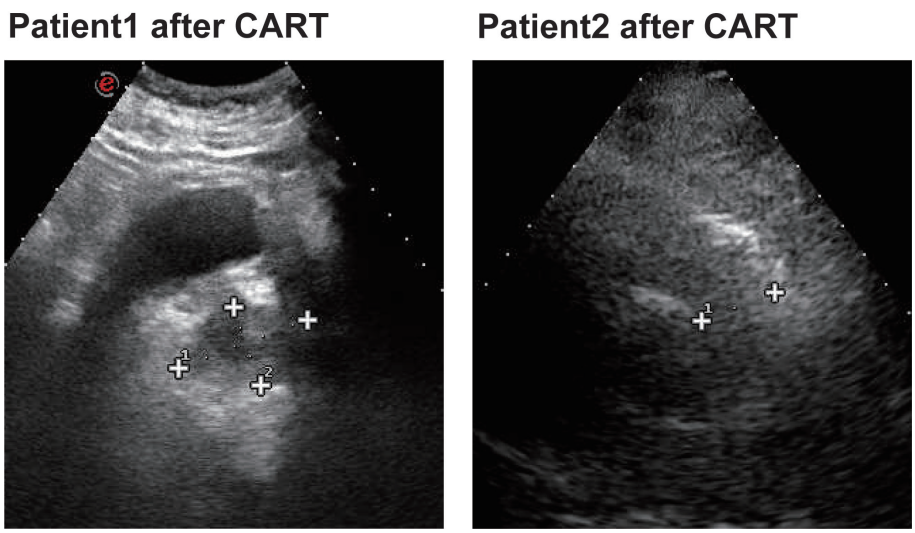

FIGURE 2
Ultrasound images of the thyroid gland after CART treatment in two patients.

release syndrome, neurotoxicity, and targeted and untargeted killing of healthy cells (2, 3). Li et al. reported a rare case of a patient with acute lymphoblastic leukemia who developed CRS with major arthritis after CAR T treatment and relief of joint symptoms after glucocorticoid therapy (4). No other immune-related adverse reactions (irAEs) were reported after CAR T cell therapy. Here, we report for the first time the progression of Hashimoto's thyroiditis (HT) in two patients with diffuse large B-cell lymphoma treated with CAR T cells.

Both patients had diffuse large B cell GCB subtype and elevated thyroid-associated antibodies after CAR - T treatment, but thyroid function remained within normal limits. Thyroid ultrasound suggested localized thyroid inflammation. We believe that these two patients developed complications of Hashimoto's thyroiditis (HT) after CAR - T treatment.

TABLE 4 Timeline of patient 2.

Day	Event
2017/1/5	Diagnosis as diffuse large b-cell lymphoma
2017/1/5	R-CHOP
2017/2/6	R-ECHOP
2017/3/3	R-ECHOP
2017/3/30	R-ECHOP
2017/4/28	R-CHOP
2017/5/19	R-CHOP
2017/6/13	R-CHOP
2017/7/4	R-CHOP
2018/9/19	peripheral lymphocytes collection
2018/9/29	fludarabine and cyclophosphamide (FC) pretreatment
2018/10/4	CAR T cells infusion
2018/11/6	complete remission
2019/01/9	complete remission

HT is a common autoimmune disease of the thyroid gland characterized by an enlarged or nodular thyroid gland with clinical manifestations of hyperthyroidism or hypothyroidism (5). In the pathophysiology of HT, B cells that produce inflammatory antibodies such as TGAb, TMAb, and TPOAb play a major role in thyroid tissue injury and are also involved in the infiltration of other lymphocytes, including plasma cells, natural killer cells, and macrophages (5). Several studies have shown that HT is an organ-specific autoimmune disease mediated by T cells (5). The relatively active function of helper T lymphocytes leads to decreased or even defective T lymphocyte function, resulting in a disruption of the balance between Th and T cells, leading to thyroid immune dysfunction (5). Several studies have reported the occurrence of HT after the use of immune checkpoint inhibitors (6). We report two cases of diffuse large B-cell lymphoma with HT after CAR T cell therapy. Ultimately, neither patient developed hypothyroidism and thyroid antibodies decreased at late follow-up. This is the first international report of HT complications after CAR T cell therapy.

In the previous literature, the use of immune checkpoint inhibitors has been reported to cause autoimmune associated inflammation in one organ or multiple systems throughout the body (7). Most immune responses occur in endocrine organs, particularly the thyroid (8). Related studies have shown that hypothyroidism occurs in 6-13% of patients receiving immunosuppressive therapy and hyperthyroidism in 3-16% (8). Adverse thyroid reactions occur over a wide range of time, from 1 day to 3 months after treatment, and even after cessation

of treatment. More patients with thyroiditis present with only elevated antibodies and normal thyroid function.

The mechanisms underlying immunotherapy for hypothyroidism is not fully understood. There may be thyroid inflammation, in which both T cells and natural killer cells may be involved (7, 9). The mechanism of thyroid inflammation after CAR T therapy have not been investigated. In conclusion, thyroid inflammation is associated with a combination of immunopathogenesis, with the entry of CAR - T cells into the bloodstream, the balance of T cells in the thyroid is disrupted, the role of T helper lymphocytes increases and the function of regulatory T cells decreases, which eventually leads to the production of antibodies by B lymphocytes and cytotoxic effects by antibody-dependent thyroid cells. On the other hand, when CAR - T cells enter the human body, cytotoxic CAR - T cells upregulate the expression of Fas and FasL in thyroid cells by releasing a large number of cytokines, thus promoting apoptosis and eventually leading to HT. the above are only speculations on the possible mechanisms, and the specific mechanisms need to be further investigated.

Conclusion

We reported for the first time the development of HT in two patients with diffuse large B-cell lymphoma treated with CAR T cells; these two patients presented only show elevated thyroid antibodies and no thyroid dysfunction was found, requiring no treatment.

Data availability statement

The original contributions presented in the study are included in the article/supplementary material. Further inquiries can be directed to the corresponding author.

Ethics statement

Written informed consent was not obtained from the individual(s) for the publication of any potentially identifiable images or data included in this article.

Author contributions

PC and YX performed the literature. WL performed CART cell detection after treatment. HL and SZ collected the data. WQ and HL revised the work. HJ and LR supported the study and reviewed the manuscript. All authors contributed to the article and approved the submitted version.

Conflict of interest

The authors declare that the research was conducted in the absence of any commercial or financial relationships that could be construed as a potential conflict of interest.

Publisher's note

References

1. June CH, Sadelain M. Chimeric antigen receptor therapy. *N Engl J Med* (2018) 379:64–73. doi: 10.1056/NEJMra1706169

2. Hirayama AV, Turtle CJ. Toxicities of CD19 CAR-T cell immunotherapy. *Am J Hematol* (2019) 94:S42–9. doi: 10.1002/ajh.25445

3. Siegler EL, Kenderian SS. Neurotoxicity and cytokine release syndrome after chimeric antigen receptor T cell therapy: Insights into mechanisms and novel therapies. *Front Immunol* (2020) 11:1973. doi: 10.3389/fimmu.2020.01973

4. Wang LX, Chen X, Jia M, Wang S, Shen J. Arthritis of large joints shown as a rare clinical feature of cytokine release syndrome after chimeric antigen receptor T cell therapy: A case report. *Med (Baltimore)* (2018) 97:e0455. doi: 10.1097/MD.0000000000010455

5. Ralli M, Angeletti D, Fiore M, D'Aguanno V, Lambiase A, Artico M, et al. Hashimoto's thyroiditis: An update on pathogenic mechanisms, diagnostic protocols, therapeutic strategies, and potential malignant transformation. *Autoimmun Rev* (2020) 19:102649. doi: 10.1016/j.autrev.2020.102649

6. Chang LS, Barroso-Sousa R, Tolaney SM, Hodi FS, Kaiser UB, Min L. Endocrine toxicity of cancer immunotherapy targeting immune checkpoints. *Endocr Rev* (2019) 40:17–65. doi: 10.1210/er.2018-00006

7. Byun DJ, Wolchok JD, Rosenberg LM, Girotra M. Cancer immunotherapy - immune checkpoint blockade and associated endocrinopathies. *Nat Rev Endocrinol* (2017) 13:195–207. doi: 10.1038/nrendo.2016.205

8. Barroso-Sousa R, Barry WT, Garrido-Castro AC, Hodi FS, Min L, Krop IE, et al. Incidence of endocrine dysfunction following the use of different immune checkpoint inhibitor regimens: A systematic review and meta-analysis. *JAMA Oncol* (2018) 4:173–82. doi: 10.1001/jamaoncol.2017.3064

9. Dougan M, Luoma AM, Dougan SK, Wucherpfennig KW. Understanding and treating the inflammatory adverse events of cancer immunotherapy. *Cell* (2021) 184:1575–88. doi: 10.1016/j.cell.2021.02.011

frontiers | Frontiers in Immunology

TYPE Case Report
PUBLISHED 15 November 2022
DOI 10.3389/fimmu.2022.978266

OPEN ACCESS

EDITED BY
Dianwen Ju,
Fudan University, China

REVIEWED BY
Chuanzhao Zhang,
Guangdong Provincial People's Hospital, China
Amin Nassar,
Yale New Haven Health System, United States

*CORRESPONDENCE
Yu Yang
yangyu@wchscu.cn

SPECIALTY SECTION
This article was submitted to Cancer Immunity and Immunotherapy, a section of the journal Frontiers in Immunology

RECEIVED 25 June 2022
ACCEPTED 26 October 2022
PUBLISHED 15 November 2022

CITATION
Xu Z, Ma J, Chen T and Yang Y (2022) Case report: The remarkable response of pembrolizumab combined with RC48 in the third-line treatment of metastatic urothelial carcinoma. *Front. Immunol.* 13:978266. doi: 10.3389/fimmu.2022.978266

Case report: The remarkable response of pembrolizumab combined with RC48 in the third-line treatment of metastatic urothelial carcinoma

Zhenying Xu, Jiaman Ma, Ting Chen and Yu Yang*

Department of Abdominal Oncology, West China Hospital, Sichuan University, Chengdu, China

Background: Systemic chemotherapy has been the mainstay treatment for locally advanced or metastatic urothelial carcinoma (UC). In the past few years, novel immune checkpoint inhibitors (ICIs) and antibody-drug conjugates (ADCs) have improved the treatment of advanced UC.

Case presentation: Here, we report systemic therapy of a 68-year-old male diagnosed with HER2 positive (immunohistochemistry 3+), programmed cell death ligand 1(PD-L1) negative metastatic UC, and renal insufficiency. He had encountered numerous metastases and failed first-line platinum-based chemotherapy and second-line treatment with pembrolizumab and trastuzumab. During third-line treatment with RC48 (a HER2 targeting ADC) combined with pembrolizumab, he achieved a rapid partial response (PR) in the first evaluation and subsequent complete response (CR) on PET/CT and long-term progression-free survival (>12 months) at the last follow-up on 25 August 2022. There are no grade 3 or 4 adverse events or aggravations of renal insufficiency during the third-line therapy.

Discussion: RC48 combined with pembrolizumab demonstrated outstanding efficacy and safety in this HER2-positive metastatic UC patient. ADC combined with ICI is a promising anti-tumor strategy that deserves further exploration in advanced UC.

KEYWORDS

urothelial carcinoma, human epidermal growth factor receptor 2 (HER2),trastuzumab (herceptin), pembrolizumab, antibody-drug conjugates, RC48-ADC

Introduction

Urothelial carcinoma (UC) is a multi-origin malignancy originating from the urinary tract epithelium, including the renal pelvis, ureter, bladder, and urethra. UC is the most common cancer type of the genitourinary system worldwide. Platinum-based chemotherapy is the primary clinical management for advanced UC, which has shown slow development over the past 30 years. New treatment options, including immune checkpoint inhibitors (ICIs) and antibody-drug conjugates (ADCs), have recently significantly improved the treatment of advanced UC. Up to this point, the Food and Drug Administration (FDA) has approved pembrolizumab and atezolizumab to treat patients with locally advanced or metastatic UC. *Human Epidermal Growth Factor Receptor 2 (HER2)*, a typical oncogene in humans, is relatively highly expressed in UC. Disitamab Vedotin (RC48), an ADC designed for HER2, has demonstrated promising therapeutic efficacy in advanced UC and has received Breakthrough Therapy Designation from the FDA as second-line treatment for patients with advanced UC with high HER2 expression, including immunohistochemistry (IHC) 2+ or 3+. In January 2022, RC48 was endorsed by China's National Medical Products Administration to treat locally advanced or metastatic UC patients with high HER2 expression (IHC 2+ or 3+) who have previously failed platinum-containing chemotherapy.

This article reported the excellent viability and well-being profile of pembrolizumab combined with RC48 as a third-line treatment for a patient with HER2 positive (IHC 3+) and programmed cell death ligand 1(PD-L1) negative metastatic UC and renal insufficiency who failed two cycles of second-line treatment with pembrolizumab plus trastuzumab.

Case presentation

A 68-year-old male presented to the outpatient unit in December 2020 with upper abdominal pain. He was diagnosed with high-grade bladder UC 12 years ago. He underwent radical total cystectomy on February 5, 2010, and total urethrectomy for recurrence in the urethra on 25 April 2012. In April 2018, the patient sought care for a swollen left lower limb. The positron emission tomography and computed tomography (PET/CT) scan showed partial invasion of soft tissue into the left iliac vessels in the left pelvis. Subsequently, the biopsy pathology report confirmed UC metastasis. After receiving six cycles of gemcitabine plus cisplatin (GP) chemotherapy, he achieved a complete response (CR). However, he did not follow up regularly for more than 2 years from August 2018. In December 2020, the patient presented to our hospital for abdominal pain with enhanced CT showing foci in the right kidney and right ureter indicative of UC (4.6 cm × 6 cm) accompanied by multiple metastases in the liver (maximum of 6.6 cm × 4.4 cm) and lymph nodes in the abdomen and retroperitoneum. The liver biopsy results confirmed metastatic UC. IHC exhibited PD-L1 (−), MSH-2 (+), MSH-6 (+), MLH-1 (+), PMS2 (+), and Her2 (+++). The patient also had renal insufficiency with a creatinine of 109 umol/L. The renogram showed mild functional impairment in the left kidney and moderate-to-severe impairment in the right kidney. After receiving first-line treatment with gemcitabine plus carboplatin (GCb) chemotherapy on 25 December 2020, he achieved a partial response (PR) as measured using Response Evaluation Criteria in Solid Tumors (RECIST) Version 1.1. However, the tumor progressed after five cycles of chemotherapy because of enlarged hepatic metastases.

The second-line treatment involved trastuzumab 8 mg/kg loading dose followed by 6 mg/kg Q3W and pembrolizumab 200 mg Q3W from 23 June 2021 (Figure 1A). After two cycles, a magnetic resonance imaging (MRI) scan showed the tumor had progressed. On MRI, tumor foci exhibited heterogeneity in efficacy. Notably, the hepatic metastasis in the right posterior upper lobe significantly increased in size (6.6 cm × 5 cm), whereas the rest of the metastases of the liver and lymph node were reduced (Figure 1B). Third-line treatment with RC48 115 mg Q2W and pembrolizumab 200 mg Q3W started on 20 August 2021. After three cycles of treatment, the first evaluation achieved PR with a significant reduction in metastases in the liver (maximum size of 2.5 cm × 2.4 cm) and abdominal lymph nodes on 29 October 2021 (Figure 1C). The time to response (TTR) was 70 days. Due to the inconvenience of admission from another city, subsequent treatment continued about every four weeks. Imaging reexamined every 2–3 months showed sustained PR (Figure 1D). At the last follow-up on 25 August 2022, PET/CT was performed again. The report showed no definite signs of the tumor throughout the body, and hepatic lesions with low density showed complete remission of metabolism after anti-tumor treatment (Figure 2). The patient achieved CR. At this moment, the progression-free survival (PFS) in the third-line treatment was more than 12 months. No grade 3 or 4 adverse events (Common Terminology Criteria for Adverse Events 5.0) or aggravation of renal insufficiency was observed during treatment with pembrolizumab combined with RC48. In the initial stage of treatment, the patient experienced grade 2 vomiting with a weight loss of 10 kg, which may be attributed to RC48. Considering that the antiemetic effect of 5-hydroxytryptamine receptor antagonist was not obvious, he was given olanzapine 5 mg qd orally for a short time. The vomiting symptoms were quickly controlled and the weight gradually recovered. During the third-line treatment, the patient maintained a good quality of life. Currently, the patient's performance status score was 0, and treatment is continuing. The main treatment steps for the patient are shown in Figure 3.

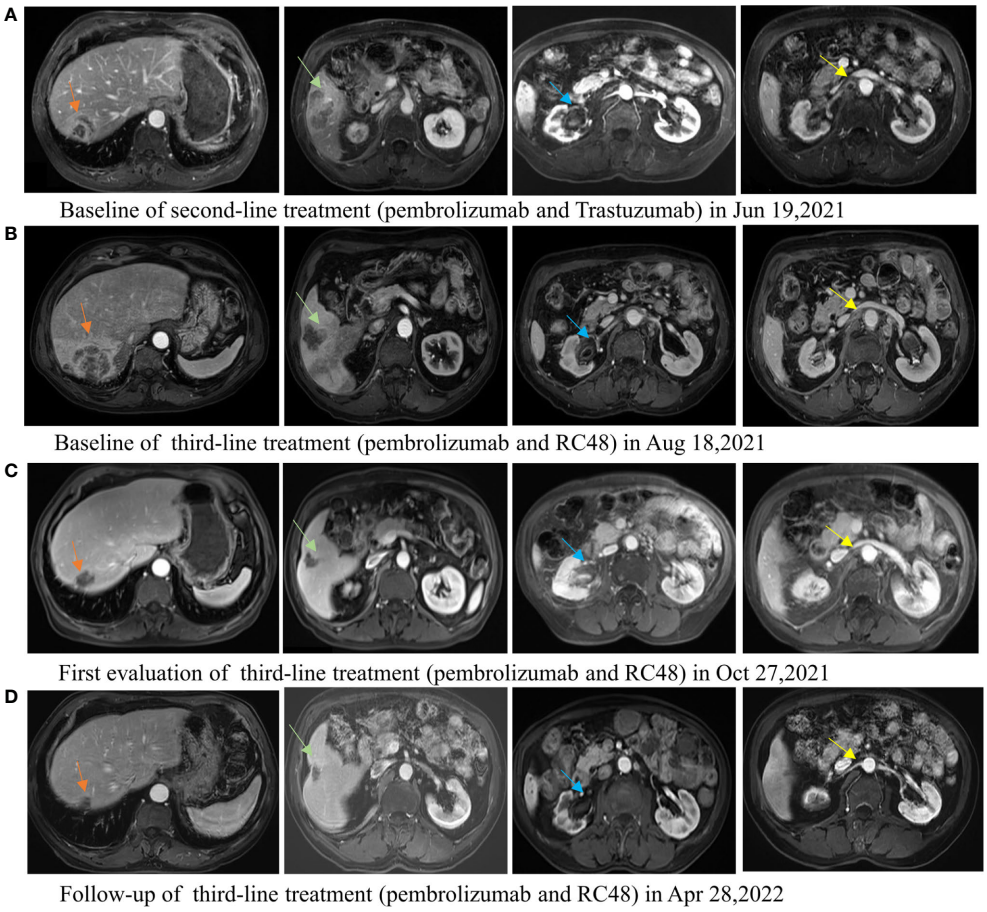

FIGURE 1
Lesions of the liver, ureteropelvic calyces, and lymph node change during the second-line treatment of pembrolizumab combined with trastuzumab and third-line treatment of pembrolizumab combined with RC48. **(A)** The baseline MRI image of the second-line treatment. **(B)** The image of tumor progression after second-line treatment, and the baseline image of the third-line treatment. The hepatic metastasis in the right posterior upper lobe was significantly enlarged and the other lesions reduced after second-line treatment. **(C)** The first efficacy evaluation after third-line treatment for 2 months: partial response. All tumor foci are reduced. **(D)** The image evaluation after third-line treatment for 8 months: partial response.

Discussion

This case was metachronous UC with multiple origins. The patient had previously been diagnosed with UC of the bladder and underwent surgery in 2010, but HER2 status was unknown. After about ten years, he was diagnosed with right kidney and ureteral UC with liver, abdominal, and retroperitoneal lymph node metastases and HER2 positive (IHC 3+) through imaging and liver biopsy in December 2020.

HER2 is an essential therapeutic target of anticancer drugs. For HER2-positive (IHC 3+ or 2+ and FISH +) advanced breast cancer and gastric cancer, chemotherapy combined with trastuzumab is the indicated first-line standard therapy (1, 2). Studies have reported 6%–17% HER2 mutations and amplification in UC (3). However, in first-line and maintenance treatment, monoclonal antibodies (mAbs) and tyrosine kinase inhibitors (TKIs) for HER2-positive UC failed. A phase II trial (4) compared gemcitabine plus platinum chemotherapy with or without trastuzumab in advanced UC overexpressing HER2. No significant difference was found in median PFS (10.2 *vs.* 8.2 months, p = 0.689) or median overall survival (mOS) (15.7 *vs* 14.1 months, p = 0.684) between the two treatment options. In a phase III trial, lapatinib maintenance therapy showed no significant improvements in OS after first-line chemotherapy for HER1 or HER2-positive metastatic urothelial bladder cancer. In addition, the difference in PFS or OS was not associated with HER status (HER1-positive only, HER2-positive only, and IHC 3+ for HER1/2) (5). Therefore, the current systemic treatment options for advanced UC are not stratified by HER2 expression. For cisplatinum-tolerant patients, GP or methotrexate, vinblastine, doxorubicin, and cisplatin (MVAC) combined with

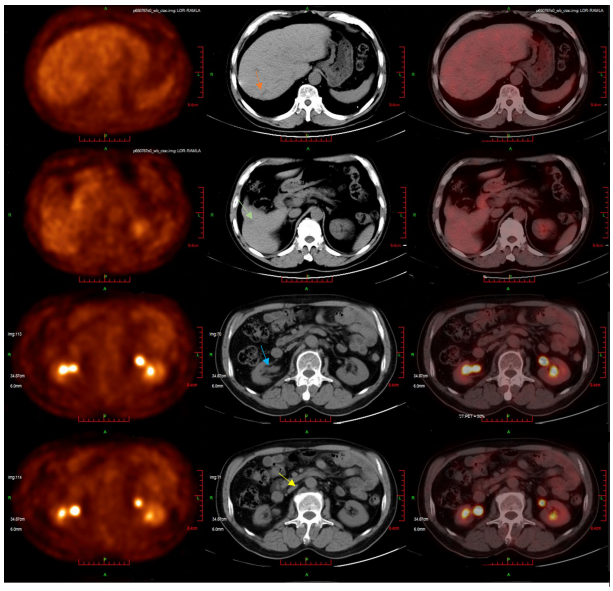

FIGURE 2
The patient's latest PET/CT showed a complete response on 25 August 2022. Several slightly hypodense shadows were seen in the liver parenchyma, none of which showed abnormally high ^{18}F-FDG uptake. No definite signs of residual tumors were seen throughout the body.

granulocyte colony-stimulating factor (G-CSF) is the recommended first-line chemotherapy, with mPFS of 7.7–8.3 months and mOS of 14–15.2 months (6). Cisplatinum-intolerant patients can receive GCb chemotherapy (7) or immunotherapy with pembrolizumab or atezolizumab (8, 9). Pembrolizumab is the standard second-line treatment for advanced UC after failing platinum-based chemotherapy, with an mOS of 10.3 months and an mPFS of 2.1 months reported in the KEYNOTE-045 trial (10).

Despite the shortage of data about immunotherapy combined with trastuzumab on UC, our ideas mainly referred to the treatment progress of gastric cancer. In preclinical studies, trastuzumab has been shown to stimulate HER2-specific T-cell responses (11) and

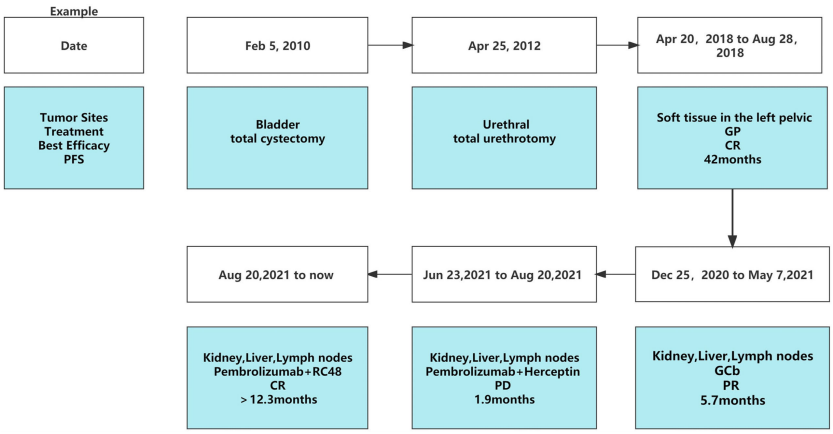

FIGURE 3
Timeline scheme of the major clinical events of the patient.

upregulate programmed cell death protein 1 (PD-1) and PD-L1 expression (12, 13). Coadministration of PD-1 inhibitors and trastuzumab enhances HER2-specific T-cell responses (11, 14). At the 2020 American Society of Clinical Oncology (ASCO) annual meeting, a Phase 1b/2 report combining pembrolizumab with trastuzumab and chemotherapy provided an ORR of 76.7% for advanced HER2-positive gastric cancer patients (15). Combining trastuzumab with pembrolizumab therapy was selected as the second-line treatment for our patient.

Unfortunately, in our patient with HER2-positive (IHC 3+) and PD-L1-negative UC, no synergistic effect was produced by combining trastuzumab with standard second-line pembrolizumab therapy. Interestingly, variable efficacy was observed between the enlarged right posterior superior hepatic metastasis and the reduced remaining hepatic and lymph node metastases (Figure 1B). Whether heterogeneity in HER2 expression existed among these metastases and affected the treatment response was unclear. Unfortunately, we could not verify this by biopsy of each metastasis. The short PFS of our case is also consistent with a later reported study (16). An analysis of 79 metastatic UC cases treated with second-line anti-PD-1 immunotherapy showed distinct differences in mPFS of 11, 3.7, and 1.8 months ($p = 0.001$) among HER2-negative (IHC 0), low-expression (IHC 2+7/FISH− and IHC 1+) and overexpression (IHC 3+ and IHC 2+/FISH+), respectively (16). HER2 expression levels increased from negative to overexpression with decreasing ORR (42.4% *vs.* 31.6% *vs.* 0%, $p = 0.08$). It was suggested that HER2 expression levels might influence second-line immunotherapy for UC. Also, in a phase 1b-2 trial, PANACEA (17) for trastuzumab-resistant, advanced, HER2-positive breast cancer, the synergistic efficacy of pembrolizumab plus trastuzumab was only observed in PD-L1-positive patients, with an ORR of 15% (6/40) and no remission in 12 PD-L1-negative patients. Therefore, the synergistic effect of pembrolizumab plus trastuzumab in HER2-positive cancers may differ depending on tumor type or expressed molecular marker.

RC48 (Disitamab vedotin) is a Chinese original HER2-targeting ADC, which has demonstrated excellent efficacy in advanced UC with HER2 IHC 2+/3+ in the phase II trials RC48-C005 (18) and RC48-C009 (19), reported in early 2021. For advanced UC patients who had failed at least one line of chemotherapy, the confirmed ORR was 46.9%–51.2%, and the mPFS was 4.3–6.9 months. The mOS was 13.9–14.8 months. In June 2021, RC48 was first approved in China for advanced HER2 overexpressing gastric cancer patients who have received at least two lines of systemic chemotherapy. In the phase II clinical study of advanced gastric cancer patients who were under at least second-line therapy, the ORR was 24.8%, the mPFS was 4.1 months, and the OS was 7.9 months (20). Subgroup analysis showed that the previous use of trastuzumab did not significantly affect the efficacy of RC48 for gastric cancer. Therefore, when our case progressed after trastuzumab combined with pembrolizumab in August 2021, RC48 was recommended. In the same period, the other two HER2-targeting ADC drugs, T-DM1 and T-DXd, had no relevant data on UC. The efficacy of apatinib for UC previously reported was not ideal. Besides that, considering the hepatic metastasis in the right posterior upper lobe was significantly enlarged and the other lesions reduced after treatment with trastuzumab combined with pembrolizumab, we also continued to use pembrolizumab in the third-line treatment.

Our case showed that RC48-ADC still works despite the failure of anti-HER2 monoclonal antibody therapy, which may be explained in several ways. Firstly, hertuzumab, a humanized anti-HER2 antibody, contained in RC48 is linked by a detachable linker to monomethyl auristatin E (MMAE) a microtubulin inhibitor. In addition to inhibiting the HER-2-receptor signal pathway, RC48 produces an anti-tumor effect *via* MMAE-induced cytotoxicity. Previous research also pointed to antibody-dependent cell-mediated cytotoxicity (ADCC) activity in *in vitro* assays (21–23). Secondly, compared with trastuzumab, hertuzumab has a higher affinity for HER2 (21). MMAE coupled with hertuzumab can potently kill HER-2 targeting tumor cells. Besides, MMAE released by enzymolysis has high membrane permeability, which can penetrate adjacent cells to produce a bystander effect and has a therapeutic effect on tumor cells with low or no expression of HER2 (24, 25). In the RC48-C011 study (26), for HER2-negative (IHC 0/1+) advanced UC patients treated with ≥1 prior systemic therapy, RC48 also showed promising efficacy, with an ORR of 26.3%. In the RC48-C008 study (20), the ORR of RC48 was 24.8% in trastuzumab-treated HER2-positive advanced gastric cancer patients who had received at least second-line therapy. Besides, RC48 and PD-1 inhibitors have a good synergistic effect, which is significantly higher than the efficacy of RC48 alone or PD-1 inhibitor alone (27).

As far as we know, this is the first report of RC48 combined with pembrolizumab in advanced UC. And more importantly, this case previously experienced failure of an anti-HER2 monoclonal antibody combined with pembrolizumab treatment. In our case, a phase Ib/II study (RC48-C014) reported a preliminary result showing promising synergistic efficacy of RC48 combined with toripalimab (an anti-PD-1 antibody) in advanced UC patients who were unable to tolerate or refused chemotherapy, or progressed after at least 1 prior systemic chemotherapy in 2021 (27). However, none of these patients received anti-HER2 monoclonal antibody treatment before enrollment. Seventeen patients enrolled (12 cases with HER2 IHC2+/3+ and five cases with HER2 IHC0/1+) achieved

an ORR of 94.1%. At the 2022 ASCO-GU annual meeting, a phase 1b study of T-DXd combined with nivolumab also showed antitumor activity in UC patients with HER-2 IHC2 +/3+ after the progression of chemotherapy, with an ORR of 36.7% (11/30) and mPFS of 6.9 months (28). For HER2-positive UC, HER-2-targeting ADCs combined with ICIs have shown good prospects, which deserve to be further investigated. Currently, a phase III study comparing RC48 in combination with toripalimab with chemotherapy in previously untreated HER2-expressing advanced UC is going on (NCT05302284).

Conclusion

In summary, we reported that a metastatic UC patient with HER2 positive (IHC 3+) achieved a remarkable response, excellent PFS, and good tolerance when treated with pembrolizumab combined with RC48 after the failure of second-line treatment with pembrolizumab combined with trastuzumab. Although our report was only a case, it showed a significant difference in the efficacy of anti-HER2 drugs for UC. RC48 combined with immunotherapy has shown a very good prospect in advanced UC. It is worth further exploring in patients with low or negative HER2 expression and evaluating the efficacy of front-line therapy.

Ethics statement

Written informed consent was obtained from the individual(s) for the publication of any potentially identifiable images or data included in this article.

Author contributions

ZX, JM, and TC contributed to the material preparation, data collection and manuscript writing. Thesis was reviewed and revised by YY. All authors contributed to the article and approved the submitted version.

Conflict of interest

The authors declare that the research was conducted in the absence of any commercial or financial relationships that could be construed as a potential conflict of interest.

Publisher's note

References

1. Bang Y, Van Cutsem E, Feyereislova A, Chung H, Shen L, Sawaki A, et al. Trastuzumab in combination with chemotherapy versus chemotherapy alone for treatment of HER2-positive advanced gastric or gastro-oesophageal junction cancer (ToGA): A phase 3, open-label, randomised controlled trial. *Lancet (London England)* (2010) 376:687–97. doi: 10.1016/S0140-6736(10)61121-X

2. Slamon DJ, Leyland-Jones B, Shak S, Fuchs H, Paton V, Bajamonde A, et al. Use of chemotherapy plus a monoclonal antibody against HER2 for metastatic breast cancer that overexpresses HER2. *New Engl J Med* (2001) 344:783–92. doi: 10.1056/NEJM200103153441101

3. Patelli G, Zeppellini A, Spina F, Righetti E, Stabile S, Amatu A, et al. The evolving panorama of HER2-targeted treatments in metastatic urothelial cancer: A systematic review and future perspectives. *Cancer Treat Rev* (2022) 104:102351. doi: 10.1016/j.ctrv.2022.102351

4. Oudard S, Culine S, Vano Y, Goldwasser F, Theodore C, Nguyen T, et al. Multicentre randomised phase II trial of gemcitabine+platinum, with or without trastuzumab, in advanced or metastatic urothelial carcinoma overexpressing Her2. *Eur J Cancer* (2015) 51:45–54. doi: 10.1016/j.ejca.2014.10.009

5. Powles T, Huddart RA, Elliott T, Sarker SJ, Ackerman C, Jones R, et al. Phase III, double-blind, randomized trial that compared maintenance lapatinib versus placebo after first-line chemotherapy in patients with human epidermal growth factor receptor 1/2-positive metastatic bladder cancer. *J Clin Oncol* (2017) 35:48–55. doi: 10.1200/JCO.2015.66.3468

6. von der Maase H, Sengelov L, Roberts JT, Ricci S, Dogliotti L, Oliver T, et al. Long-term survival results of a randomized trial comparing gemcitabine plus cisplatin, with methotrexate, vinblastine, doxorubicin, plus cisplatin in patients with bladder cancer. *J Clin Oncol* (2005) 23:4602–8. doi: 10.1200/JCO.2005.07.757

7. Dogliotti L, Carteni G, Siena S, Bertetto O, Martoni A, Bono A, et al. Gemcitabine plus cisplatin versus gemcitabine plus carboplatin as first-line chemotherapy in advanced transitional cell carcinoma of the urothelium: results of a randomized phase 2 trial. *Eur Urol* (2007) 52:134–41. doi: 10.1016/j.eururo.2006.12.029

8. Balar AV, Castellano D, O'Donnell PH, Grivas P, Vuky J, Powles T, et al. First-line pembrolizumab in cisplatin-ineligible patients with locally advanced and unresectable or metastatic urothelial cancer (KEYNOTE-052): A multicentre, single-arm, phase 2 study. *Lancet Oncol* (2017) 18:1483–92. doi: 10.1016/S1470-2045(17)30616-2

9. Balar AV, Galsky MD, Rosenberg JE, Powles T, Petrylak DP, Bellmunt J, et al. Atezolizumab as first-line treatment in cisplatin-ineligible patients with locally advanced and metastatic urothelial carcinoma: a single-arm, multicentre, phase 2 trial. *Lancet* (2017) 389:67–76. doi: 10.1016/S0140-6736(16)32455-2

10. Bellmunt J, de Wit R, Vaughn DJ, Fradet Y, Lee JL, Fong L, et al. Pembrolizumab as second-line therapy for advanced urothelial carcinoma. *New Engl J Med* (2017) 376:1015–26. doi: 10.1056/NEJMoa1613683

11. Park S, Jiang Z, Mortenson ED, Deng L, Radkevich-Brown O, Yang X, et al. The therapeutic effect of anti-HER2/neu antibody depends on both innate and adaptive immunity. *Cancer Cell* (2010) 18:160–70. doi: 10.1016/j.ccr.2010.06.014

12. Chaganty BKR, Qiu S, Gest A, Lu Y, Ivan C, Calin GA, et al. Trastuzumab upregulates PD-L1 as a potential mechanism of trastuzumab resistance through

engagement of immune effector cells and stimulation of IFNγ secretion. *Cancer Lett* (2018) 430:47–56. doi: 10.1016/j.canlet.2018.05.009

13. Triulzi T, Forte L, Regondi V, Di Modica M, Ghirelli C, Carcangiu ML, et al. HER2 signaling regulates the tumor immune microenvironment and trastuzumab efficacy. *Oncoimmunology* (2019) 8:e1512942. doi: 10.1080/2162402X.2018.1512942

14. Janjigian YY, Kawazoe A, Yanez P, Li N, Lonardi S, Kolesnik O, et al. The KEYNOTE-811 trial of dual PD-1 and HER2 blockade in HER2-positive gastric cancer. *Nature* (2021) 600:727–30. doi: 10.1038/s41586-021-04161-3

15. Rha SY, Lee C-K, Kim HS, Kang B, Jung M, Bae WK, et al. Targeting HER2 in combination with anti-PD-1 and chemotherapy confers a significant tumor shrinkage of gastric cancer: A multi-institutional phase Ib/II trial of first-line triplet regimen (pembrolizumab, trastuzumab, chemotherapy) for HER2-positive advanced gastric cancer (AGC). *J Clin Oncol* (2020) 38:3081–1. doi: 10.1200/JCO.2020.38.15_suppl.3081

16. Li S, Wu X, Yan X, Zhou L, Xu H, Li J, et al. Impact of different HER2 expression levels on the outcomes of second-line immunotherapy for metastatic urothelial carcinoma. *J Clin Oncol* (2022) 2022(40):524–4. doi: 10.1200/JCO.2022.40.6_suppl.524

17. Loi S, Giobbie-Hurder A, Gombos A, Bachelot T, Hui R, Curigliano G, et al. Pembrolizumab plus trastuzumab in trastuzumab-resistant, advanced, HER2-positive breast cancer (PANACEA): a single-arm, multicentre, phase 1b–2 trial. *Lancet Oncol* (2019) 20:371–82. doi: 10.1016/S1470-2045(18)30812-X

18. Sheng X, Yan X, Wang L, Shi Y, Yao X, Luo H, et al. Open-label, multicenter, phase II study of RC48-ADC, a HER2-targeting antibody-drug conjugate, in patients with locally advanced or metastatic urothelial carcinoma. *Clin Cancer Res* (2021) 27:43–51. doi: 10.1158/1078-0432.CCR-20-2488

19. Sheng X, He Z, Han W, Zhou A-P, Luo H, Shi Y, et al. An open-label, single-arm, multicenter, phase II study of RC48-ADC to evaluate the efficacy and safety of subjects with HER2 overexpressing locally advanced or metastatic urothelial cancer (RC48-C009). *J Clin Oncol* (2021) 2021(39):4584–4. doi: 10.1200/JCO.2021.39.15_suppl.4584

20. Peng Z, Liu T, Wei J, Wang A, He Y, Yang L, et al. Efficacy and safety of a novel anti-HER2 therapeutic antibody RC48 in patients with HER2-overexpressing, locally advanced or metastatic gastric or gastroesophageal junction cancer: A single-arm phase II study. *Cancer Commun (Lond)* (2021) 41:1173–82. doi: 10.1002/cac2.12214

21. Shi F, Liu Y, Zhou X, Shen P, Xue R, Zhang M. Disitamab vedotin: a novel antibody-drug conjugates for cancer therapy. *Drug Delivery* (2022) 29:1335–44. doi: 10.1080/10717544.2022.2069883

22. Diamantis N, Banerji U. Antibody-drug conjugates–an emerging class of cancer treatment. *Br J Cancer* (2016) 114:362–7. doi: 10.1038/bjc.2015.435

23. Lattanzi M, Rosenberg JE. The emerging role of antibody-drug conjugates in urothelial carcinoma. *Expert Rev Anticancer Ther* (2020) 20:551–61. doi: 10.1080/14737140.2020.1782201

24. Singh AP, Sharma S, Shah DK. Quantitative characterization of *in vitro* bystander effect of antibody-drug conjugates. *J Pharmacokinet Pharmacodyn* (2016) 43:567–82. doi: 10.1007/s10928-016-9495-8

25. Li L, Xu MZ, Wang L, Jiang J, Dong LH, Chen F, et al. Conjugating MMAE to a novel anti-HER2 antibody for selective targeted delivery. *Eur Rev Med Pharmacol Sci* (2020) 24:12929–37. doi: 10.26355/eurrev_202012_24196

26. Xu H, Sheng X, Zhou L, Yan X, Li S, Chi Z, et al. A phase II study of RC48-ADC in HER2-negative patients with locally advanced or metastatic urothelial carcinoma. *J Clin Oncol* (2022) 2022(40):4519–9. doi: 10.1200/JCO.2022.40.16_suppl.4519

27. Zhou L, Xu H, Yan X, Chi Z, Cui C, Si L, et al. RC48-ADC combined with toripalimab, an anti-PD-1 monoclonal antibody (Ab), in patients with locally advanced or metastatic urothelial carcinoma (UC): Preliminary results of a phase Ib/II study. *J Clin Oncol* (2021) 2021(39):4534–4. doi: 10.1200/JCO.2021.39.15_suppl.4534

28. Galsky MD, Conte GD, Foti S, Yu EY, Machiels J-PH, Doger B, et al. Primary analysis from DS8201-A-U105: A phase 1b, two-part, open-label study of trastuzumab deruxtecan (T-DXd) with nivolumab (nivo) in patients (pts) with HER2-expressing urothelial carcinoma (UC). *J Clin Oncol* (2022) 40:438–8. doi: 10.1200/JCO.2022.40.6_suppl.438

frontiers | Frontiers in Immunology

TYPE Original Research
PUBLISHED 16 November 2022
DOI 10.3389/fimmu.2022.1014638

OPEN ACCESS

EDITED BY
Dianwen Ju,
Fudan University, China

REVIEWED BY
Jian-Bo Wan,
University of Macau, China
Gang Zhang,
Zhejiang University, China

*CORRESPONDENCE
Xi Wang
xiwang@ccmu.edu.cn
Min Zhang
zhangm0601@ccmu.edu.cn
Xiaopeng Hu
xiaopeng_hu@sina.com

†These authors have contributed equally to this work and share first authorship

SPECIALTY SECTION
This article was submitted to Cancer Immunity and Immunotherapy, a section of the journal Frontiers in Immunology

RECEIVED 08 August 2022
ACCEPTED 18 October 2022
PUBLISHED 16 November 2022

CITATION
Zhang X, Zhang Y, Zhao L, Wang J, Li J, Wang X, Zhang M and Hu X (2022) Exploitation of tumor antigens and construction of immune subtype classifier for mRNA vaccine development in bladder cancer. *Front. Immunol.* 13:1014638. doi: 10.3389/fimmu.2022.1014638

Exploitation of tumor antigens and construction of immune subtype classifier for mRNA vaccine development in bladder cancer

Xin Zhang[1,2,3†], Yanlong Zhang[4†], Li Zhao[5†], Jiayu Wang[1,2], Jiaxing Li[1,2], Xi Wang[3,6,7*], Min Zhang[1,2,8*] and Xiaopeng Hu[1,2*]

[1]Department of Urology, Beijing Chao-Yang Hospital, Capital Medical University, Beijing, China, [2]Institute of Urology, Capital Medical University, Beijing, China, [3]Institute of Infectious Diseases, Beijing Key Laboratory of Emerging Infectious Diseases, Beijing Ditan Hospital, Capital Medical University, Beijing, China, [4]Department of Urology, Beijing Shijitan Hospital, Capital Medical University, Beijing, China, [5]School of Pharmacy, Shanxi Medical University, Taiyuan, Shanxi, China, [6]Department of Immunology, School of Basic Medical Sciences, Department of Oncology, Capital Medical University, Beijing, China, [7]Beijing Institute of Infectious Diseases, Beijing, China, [8]Department of Research Ward, Beijing Chao-Yang Hospital, Capital Medical University, Beijing, China

Background: Bladder cancer (BLCA) is one of the most prevalent urinary system malignancies, with high mortality and recurrence. The present study aimed to identify potential tumor antigens for mRNA vaccines in BLCA and patient subtypes suitable for different immunotherapy.

Methods: Gene expression profiles, mutation data, methylation data, and corresponding clinical information were obtained from the Cancer Genome Atlas (TCGA), Gene Expression Omnibus (GEO), and ArrayExpress databases. Immunohistochemical staining of microarrays was performed to assess protein expression levels of IGF2BP2 and MMP9. Differential gene analysis, survival analysis, correlation analysis, consensus clustering analysis, and immune cell infiltration analysis were conducted using R software. Finally, the R package "immcluster" was used based on Combat and eXtreme Gradient Boosting algorithms to predict immune clusters of BLCA samples.

Results: Two mutated, amplified, and over-expressed tumor antigens, IGF2BP2 and MMP9, were found to be associated with clinical outcomes and the abundance of antigen-presenting cells (APCs). Subsequently, three immune subtypes (BIS1, BIS2, and BIS3) were defined in the BLCA cohort. BIS3 subtype exhibited an "active" immune phenotype, while BIS1 and BIS2 subtypes have a "suppressive" immune phenotype. Patients in BIS1 and BIS2 had a poor prognosis compared to BIS3. BIS3 had a higher score in checkpoints or immunomodulators (CP) and immunophenoscore (IPS), while BIS1 and BIS2

scored higher in major histocompatibility complex-related molecules (MHC molecules). Meanwhile, BIS2 and BIS3 had a significantly higher tumor mutational burden (TMB) compared to patients with BIS1. Finally, the "immcluster" package was applied to the dataset, which has been shown to accurately predict the immune subtypes of BLCA samples in many cohorts.

Conclusions: IGF2BP2 and MMP9 were potential antigens for developing mRNA vaccines against BLCA. The results in the present study suggested that immunotherapy targeting these two antigens would be suitable for patients falling under the BIS2 subtype. R package "immcluster" could assist in screening suitable BLCA patients for antitumor therapy.

KEYWORDS

mRNA vaccine, tumor antigen, bladder cancer, immune subtypes, tumor immune infiltration

Introduction

Bladder cancer (BLCA) is one of the most prevalent urinary system malignancies, with more than 83,000 new cases and an estimated 17,200 deaths worldwide in 2020 (1). Risk factors associated with BLCA include advanced age, male, cigarette smoking, chronic inflammation, and occupational exposure containing benzene dyes and factory chemicals, among others (2, 3). BLCA can be generally categorized into non-muscle-invasive bladder cancer (NMIBC) and muscle-invasive bladder cancer (MIBC). In the former, the tumors are isolated in the urothelium (Ta stage) and lamina propria (T1 stage), accounting for approximately 75% of bladder cancers (2). MIBC invades the muscle (stage T2) or beyond (stages T3 and T4) (2). Up to 15% of patients with MIBC have a primary history of NMIBC, while the remaining patients are diagnosed with primary MIBC (4). Transurethral resection of the bladder tumor (TURBT) in combination with intravesical administration of chemotherapeutics or immunological pharmaceuticals is regarded as standard therapy for NMIBC (5). Treatments for MIBC consist of radical cystectomy, partial cystectomy, neoadjuvant therapy, cytotoxic chemotherapy, immune checkpoint inhibitors, or targeted therapies (2). However, a high proportion of patients with bladder cancer progress to high-grade or metastatic disease, with a 5-year progression rate ranging from 0.8% to 45% in various studies (2, 6). Therefore, effective therapeutics are needed to improve the prognosis of BLCA patients.

To date, cancer immunotherapy, especially immune checkpoint inhibitor (ICI) therapy, has gained considerable success as a cancer treatment (7–9). However, not all patients benefit from immunotherapy, both due to severe toxicity and high cost of treatment (9). In phase 3 IMvigor211 clinical trial of atezolizumab (PD-L1 inhibitor) targeting BLCA, the 24-mo survival rate was 23% with a median of 33 months of survival post-follow-up. Another phase 2 study, KEYNOTE-057, of pembrolizumab (PD-1 inhibitor) by Balar et al. showed that 39 of 96 patients (41%) with BCG-unresponsive carcinoma *in situ* in the bladder had a complete response at 3 months. 13 (13%) patients exhibited grade 3 or 4 treatment-related adverse events (10).

Tumor vaccines are another highly attractive alternative in cancer immunotherapy (11, 12). Tumor vaccines induce a sustained immune memory response that reactivates the patient's immune system to destroy cancer cells at the initial moment of disease recurrence (13). Currently, tumor vaccines that are applied either for bladder cancer indication or in the clinical trial phase include BCG vaccine, MTBVAC (a live attenuated vaccine derived from mycobacterium tuberculosis), VPM1002BC (a modified BCG vaccine), PANVAC (a poxvirus vector-based vaccine derived from two viral vectors), among others (14–16). mRNA vaccines have recently attracted attention with their application against SARS-CoV-2 (17). Several mRNA-based cancer vaccines have been developed and registered for various clinical trial stages, including prostate cancer, glioblastoma, melanoma, and renal cell carcinoma (18). However, the application of mRNA vaccines for bladder tumors still remains to be explored.

The objectives of this study were to explore novel BLCA antigens for the development of mRNA vaccines and to map the immune landscape of BLCA in order to identify suitable patients for vaccination. Two genes associated with poor survival and antigen-presenting cell infiltration were identified and validated in several databases. Based on prognostically immune-related genes, we defined three immune subtypes between all cohorts and explored the characteristics of the three different subtypes. Our results can inform mRNA vaccine development and patient selection for BLCA vaccination.

Methods

Data source and processing

Gene expression data including mRNA count, Fragments Per Kilobase per Million (FPKM), somatic gene mutations, and DNA methylation data (450k methylation array data) of patients with bladder cancer, were retrieved from the Cancer Genome Atlas (TCGA; https://tcga-data.nci.nih.gov/tcga/). Gene copy number variation (CNV) DNA mutation data were collected from cBioPortal for Cancer Genomics (cBioPortal; http://www.cbioportal.org). Gene expression or mRNA array expression data of other BLCA cohorts were downloaded from Gene Expression Omnibus (GEO, https://www.ncbi.nlm.nih.gov/geo/) and ArrayExpress (https://www.ebi.ac.uk/arrayexpress/). To avoid the impact of batch effects, we only collected the BLCA cohorts (GSE13507, GSE32894, and E-MTAB-4321) with more than 100 samples with survival information for further analysis.

Next, we used the "Combat" algorithm in the "sva" package to reduce batch effects between all BLCA cohorts and produce a Meta cohort, which included TCGA-BLCA, GSE13507, GSE32894, and E-MTAB-4321 cohort.

Finally, mRNA sequencing data and clinical information about BLCA PD-L1 treatment were extracted from the datasets using the R package "IMvigor210CoreBiologies" (IMvigor 210 cohort), and the mRNA sequencing data and clinical information about melanoma PD-1 treatment cohort were collected from GEO (GSE78220).

Gene differential expression analysis

To accurately select over-expressed genes and avoid data correction biases, we performed a differential analysis based on mRNA count data from the TCGA BLCA cohort and using the "DESeq2" algorithm. 1943 genes with log fold change (Log FC) > 2 and adjusted $P < 0.05$ were selected as over-expressed genes for further analysis.

Survival analysis

Samples with no more than 30 days of overall survival (OS), and disease-free survival (DFS) were excluded from the TCGA cohort. The univariable Cox was used to define the hazard ratio (HR) for genes based on mRNA expression data (log_2[TPM+1])) of the TCGA BLCA cohort. The statistical significance of survival data was tested by the log-rank test. A $P < 0.05$ was considered statistically significant.

Identification of subtypes by immune-related genes in BLCA

A total of 1,811 immune-related genes extracted from the import database (https://www.immport.org/) were used for Kaplan-Meier and univariable Cox analysis of the TCGA BLCA cohort. Then, 128 prognostic immune-related genes were screened for non-negative matrix factorization (NMF) analysis. Silhouette coefficient and three-dimensional principal component analysis (3D PCA) were then used to validate the subtype assignments based on the mRNA expression data.

Estimation of immune and stromal infiltration

To avoid bias of a single algorithm, the abundance of immune cell and stromal cell of BLCA sample were estimated by algorithms "xCell", "CIBERSORT", "Tumor Immune Estimation Resource (TIMER)", "MCP-counter", "EPIC", and "quanTIseq" based on the R package "immunedeconv". Single-sample Gene Set Enrichment Analysis (ssGSEA) was applied to assess the relative abundance of 23 immune cell types, stem cells, and active levels of other 15 signaling pathway ways for each sample. The list of genes corresponding to each immune cell type and the associated signaling pathways were obtained from recent publications (19, 20).

Functional enrichment analysis

Biological characteristics of each immune subtypes were identified by GSEA analysis and Metascape (https://metascape.org/) based on differential expression of the identified genes between three subtypes.

Building and publishing of R package "immcluster"

To predict the immune subtype of other BLCA cohorts not including in the meta cohort, we built a classifier based on XGBoost. First, 264 differential immune-related genes were identified by differential analysis ($P < 0.01$) based on training cohort (TCGA). Then, using the 10-fold cross-validation analysis of eXtreme Gradient Boosting (XGBoost), we optimized the parameters of the XGBoost model (max depth = 6, ta=0.4, and nround = 100) using the training cohort (TCGA). Next, we reduced batch effects between training and test cohorts using the "Combat" algorithm and predicted the immune subtype of each test cohort using the previously trained XGBoost model and TCGA cohort after batch correction. Finally, to facilitate other researchers using the model

and validating the proposed immune subtypes, we built the R package "immcluster" and released it on Github (https://github.com/ZylRpackage2022/immcluste).

Drug sensitivity analysis

The response of immunotherapy of the Meta cohort was predicted by Tumor Immune Dysfunction and Exclusion (TIDE, http://tide.dfci.harvard.edu/). The IC50 of chemotherapy of the TCGA BLCA cohort was predicted by R package "pRRophetic".

Immunohistochemistry

BLCA tissue with adjacent normal bladder tissue microarray (HBlaU050CS01) was purchased from Shanghai Outdo Biotech Co., Ltd., which contained 50 cases. Immunohistochemical staining of microarrays was performed by Wuhan Servicebio Technology Co., Ltd. (Wuhan, China). The primary antibodies used were IGF2BP2 (Proteintech, Chicago, USA; catalog no. 11601-1-AP; used at a 1:1000 dilution), and MMP9 (Servicebio, Wuhan, China catalog no. GB11132-2, using at a 1:200 dilution).

Histology score (H-score) analysis was used to assess the staining intensity using the AIpathwell Software (Servicebio Technology Co., Ltd.). The following formula was applied:

$$\text{H} - \text{score} = \sum(Pi \times \text{i}) = (\text{percentage of weak intensity cells} \times 1) + (\text{percentage of moderate intensity cells} \times 2) + (\text{percentage of strong intensity cells} \times 3)$$

(where Pi represents the percentage of positivity, and i represents intensity score)

Cell cultures and reagents

The mediums used for cell culture were listed in the Table S1. SiRNA for IGF2BP2 and negative control (NC) were provided by Genepharma (Shanghai, China). The siRNA sequences were shown in Table S1.

RNA extraction and RT-qPCR methods

The kit for RNA extraction and RT-qPCR was listed in Table S1.

Relative expression levels of IGF2BP2 were calculated using the comparative *Ct* ($\Delta\Delta Ct$) method, where *Ct* was the cycle threshold number and normalized to GAPDH. The primer sequences for RT-qPCR were shown in the Table S1.

Scratch assay method

After 48h of transfection, UMUC3 and T24 cells were seeded into 6-well plates (1×10^6 cells/well). When cells reached over 80-90% confluence, a single wound was made with a sterile plastic 20 µl pipette tip. After removing cellular debris, fresh serum-free medium was added. Next, the wound was photographed at 0, 6, and 24 hours after scraping. The cell migration rate was calculated by the formula as follows:

Migration rate (%) = (original distance − measured distance)/original distance×100%.

Western blot

The following antibodies were used: rabbit polyclonal anti-IGF2BP2 (Proteintech, Chicago, USA; catalog no. 11601-1-AP), and mouse monoclonal anti-β-actin (Proteintech, Chicago, USA; catalog no. 66009-1-Ig).

Transwell assay

The 24-well transwell chamber was used (Corning Inc.) to determine the cell migration capacity. After 48 h of transfection, UMUC3 and T24 cells ($1x10^5$ cells/well) were seeded into the upper chamber with a serum-free medium, and 500 µl medium with 10% FBS was added to the lower chamber to act as a chemoattractant. After incubation at 37°C for 48 h, migrated cells were fixed by 4% formaldehyde and then stained using 0.5% crystal violet.

Statistical analysis

Mann-Whitney U test was used to compare the two groups with non-normally distributed variables. As a nonparametric method, the Kruskal-Wallis test was adopted to compare multiple groups. Contingent variables were analyzed with the chi-square test or Fisher's exact test. Spearman's test was conducted to analyze the correlation between gene expression and immune cell abundance. Students t-test was used to compare the differences of the staining intensity between the normal tissue and bladder cancer groups after normality testing. The analyses were performed using R software (Version 4.1.2, https://www.r-project.org/) and Statistical Package for the Social Sciences Software (SPSS, version 23.0, Chicago, IL, USA.) The difference was considered statistically significant with $P < 0.05$.

10.3389/fimmu.2022.1014638

Results

Identification of potential antigens in BLCA

To detect potential tumor antigens of BLCA, we first identified 6,739 overexpressed genes between normal and tumor tissues and 11,978 genes exhibiting copy number amplification (amplified rate > 1%). Their distributions on the chromosomes were shown in Figures 1A, B. Then, a total of 9,413 mutated genes (mutation rate > 1%) were screened by altered genome fraction and mutation counts (Figures 1C, D). The most frequently mutated 15 genes were illustrated in Figures 1E, F. Mutational analysis identified TIN, TP53, MUC16, KMT2D, SYNE1, HMCN1, ARID1A, KDM6A, PIK3CA, KMT2C, MACF1, and RYR2 as the most frequently mutated genes in terms of both altered genome fraction and mutational counts. Overall, 196 overlapping genes from overexpressed, highly amplified, and frequently mutated genes included in the Meta cohort were identified in the TCGA dataset that could serve as potential tumor antigens (Table S2).

Identification of tumor antigens associated with BLCA prognosis and antigen presenting cells

The 196 aforementioned overlapping genes were used for survival analysis to develop prognostically relevant antigens. Eight genes were related to overall survival (OS) of BLCA patients, where five genes showed a strong correlation with DFS (Disease-free survival) (Figure 2A; Table S3). The survival curves in Figures 2B-F indicated that elevated expression of ZIC2, SLC6A17, PCSK9, MMP9, and IGF2BP2 in tumor tissues were associated with poor prognosis compared to the low expression group. The results of univariate COX regression analysis indicated that all five genes were risk factors for bladder cancer (HR > 1) (Figure 2G). In summary, these five genes were screened as prognostically-relevant antigens in BLCA.

Antigen-presenting cells (APCs), including dendritic cells (DCs), B cells, and macrophages, process and deliver antigens to T lymphocytes, which initiate an adaptive immune response. We next evaluated the relationship between the five overexpressed genes and antigen-presenting cell (APC) abundance using seven bioinformatic methods. As shown in Figure 2H, MMP9 and IGF2BP2 were positively correlated with levels of several APCs. We also explored the correlations between five overexpressed genes and markers of APCs through Spearman rank correlation and found that MMP9 and IGF2BP2 were significantly related to expressions of markers (Table S4). The results of tissue microarray-based immunohistochemical staining were shown in Figure 3A. The expression of IGF2BP2 and MMP9 was upregulated in tumor tissues compared with adjacent normal tissues (P<0.05) (Figures 3B, C).

Since MMP9 has been reported extensively in the field of oncology including BLCA, we chosen IGF2BP2 for further functional studies (21–24). As illustrated in Figure S1A, the relative expression levels of IGF2BP2 in common bladder cell lines were examined by RT-qPCR. Compared to urothelial cell line (SV-HUC-1 cells), the expression levels of IGF2BP2 were found to be relatively high in the bladder cancer cell lines UMUC3 and T24 cells. To further investigate the function of IGF2BP2 in bladder cells, we knocked down IGF2BP2 by specific interfering RNA (siRNA) in UMUC3 and T24 cells. Then, RT-qPCR and western blot analyses were performed to validate the knockdown efficiency of siRNA (Figures S1B, C). Compared to the NC group, the migration ability of the BLCA cells in the siRNA2 group was reduced significantly after interference with IGF2BP2 expression (Figures S1D, E). Taken together, two tumor antigens (MMP9 and IGF2BP2) were identified as promising candidates for developing mRNA vaccines against BLCA.

Definitions of the three immune subtypes of BLCA

Initially, a total of 1,811 immune-related genes were extracted from the import database to screen prognostically-related genes in the TCGA database. Consensus clustering was performed using Nonnegative Matrix Factorization (NMF) analysis based on the 128 prognostically immune-related genes in Meta cohort. Using the Total Within Sum of Square index (Figure 4A), we identified the optimal cluster number (n = 3) of BLCA patients in the Meta cohort and defined three immune subtypes, referred to as BIS1-BIS3 (Figure 4B). Silhouette plot (average silhouette width = 0.98) and 3D PCA analysis indicated distinct separations between the three subtypes (Figures 4C, D). We next compared the classifications defined in this study with previous classifications from the TCGA cohort (25). We found that bladder cancers of subtype BIS1 were mainly enriched in TP53-like and MS2b1 subtypes, samples of subtype BIS2 were mainly enriched in Basal and MS2b2, those with subtype BIS3 were primarily enriched in Luminal, MS1b and MS2a1 subtypes (Figure 4E). Subsequently, we explored the relationship between survival and BLCA subtype. BIS3 (n = 437) was associated with better prognosis (log-rank test, P< 0.001, Figures 4F, G), while BIS1 (n = 164) and BIS2 (n = 186) had poorer survival probability in the Meta cohort. Additionally, consistent results were obtained in each cohort (TCGA OS: log-rank test, P< 0.001; TCGA DFS: log-rank test, P = 0.002; GSE13507: log-rank test, P = 0.009; GSE32894: log-rank test, P< 0.001; E-MTAB-4321: log-rank test, P< 0.001) (Figure S2), indicating the reproducibility and stability of the subtypes identified in this study. Finally, we explored MMP9 and

10.3389/fimmu.2022.1014638

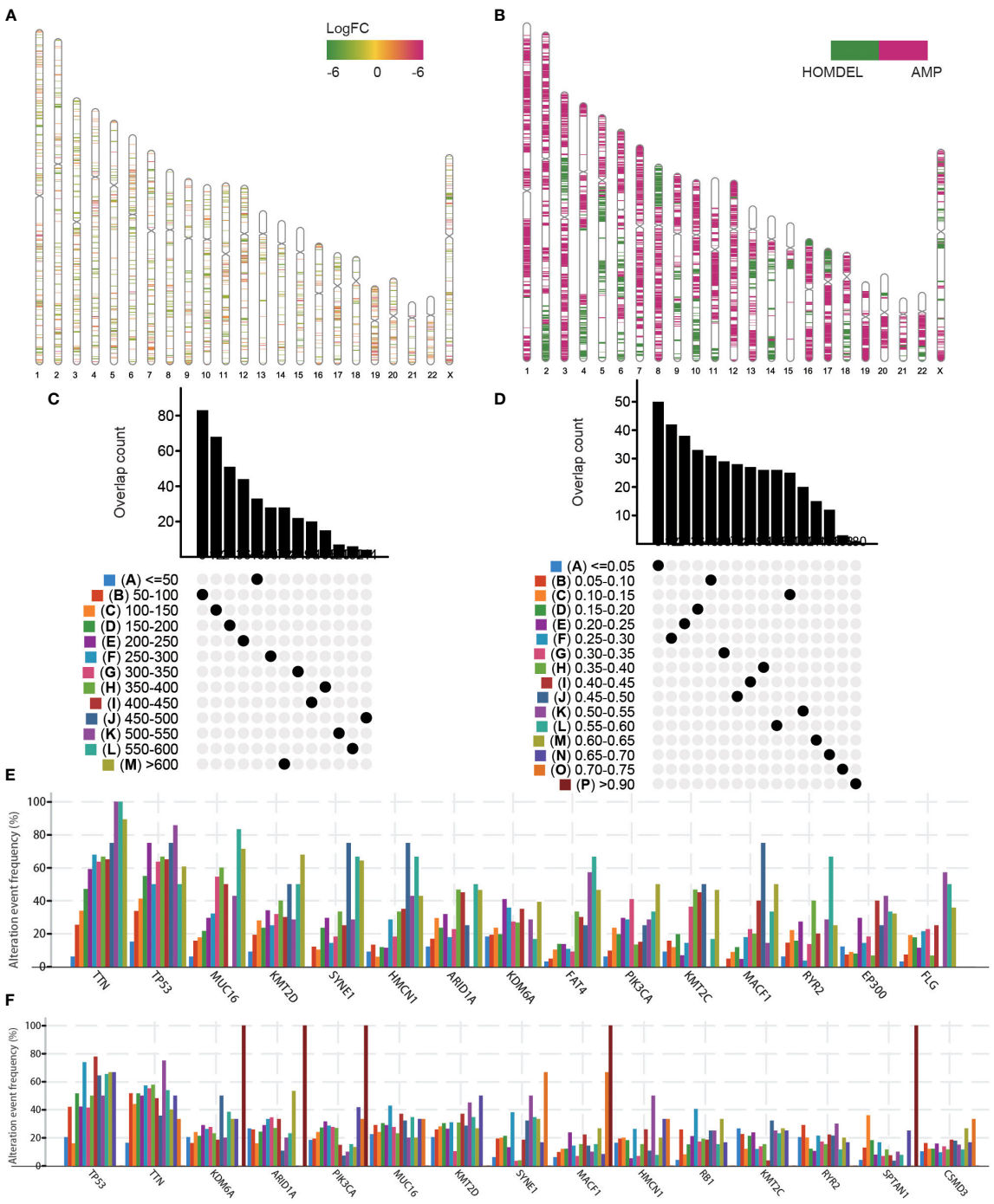

FIGURE 1
Identification of potential tumor antigens in BLCA. **(A)** Chromosomal distribution of the overexpressed genes in BLCA. **(B)** Chromosomal distribution of the aberrant copy number genes in BLCA. Overlapping mutated genes distributed in the fraction genome altered group **(C)** and mutation count group **(D)** were shown. Genes with the highest frequency in the fraction genome altered groups **(E)** and mutation count groups **(F)** were individually shown.

IGF2BP2 expression levels in the three subtypes and found that the two potential tumor antigens were lowest in BIS3 and highest in BIS2 (Kruskal-Wallis test, P< 0.001) (Figure 4H). In conclusion, immunotyping can be used to predict patient prognosis, and patients of the BIS3 subtype could potentially have better prognoses.

10.3389/fimmu.2022.1014638

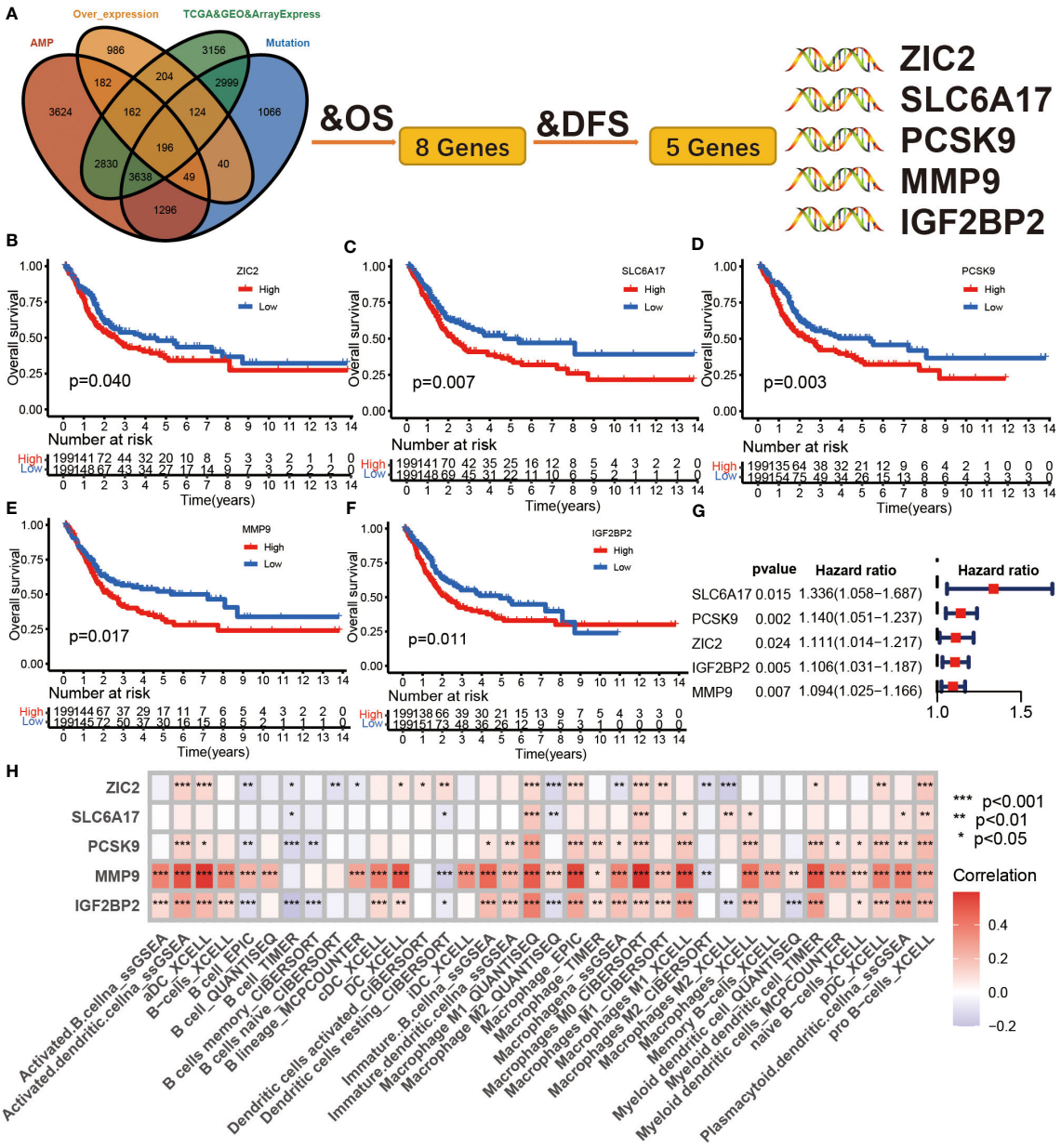

FIGURE 2
Identification of tumor antigens associated with clinical outcome in BLCA. **(A)** Tumor antigens significantly associated with OS and DFS from over expression, highly amplified, and mutated overlapping genes. **(B-F)** Kaplan-Meier survival curve analysis for ZIC2 **(B)**, SLC6A17 **(C)**, PCSK9 **(D)**, mmp9 **(E)**, and IGF2BP2 **(F)** genes in the TCGA BLCA cohort. The log-rank test was used to determine the statistical significance of the differences, and P< 0.05 was considered significant. **(G)** The univariable COX analysis of five potential tumor antigens in TCGA BLCA cohort. **(H)** The correlation between APCs and five tumor antigens in the Meta cohort.

The clinical, cellular and immune infiltration characteristics of BLCA tumor with the three subtypes

Subsequently, the clinical features of the three immune subtypes were investigated in the TCGA cohort (Figure S3). BIS3 was less malignant, considering pathological stage and histologic grade (x^2 test, P< 0.001) compared to the other two subtypes, consistent with survival outcome. In contrast, age (x^2 test, P = 0.2433) and gender (x^2 test, P = 0.5091) showed no significant difference among three subtypes (Table S5).

Figures S4A, B depicted the activated and inhibited pathways in the three subtypes based on the Kyoto Encyclopedia of Genes and Genomes (KEGG) functional enrichment analysis.

10.3389/fimmu.2022.1014638

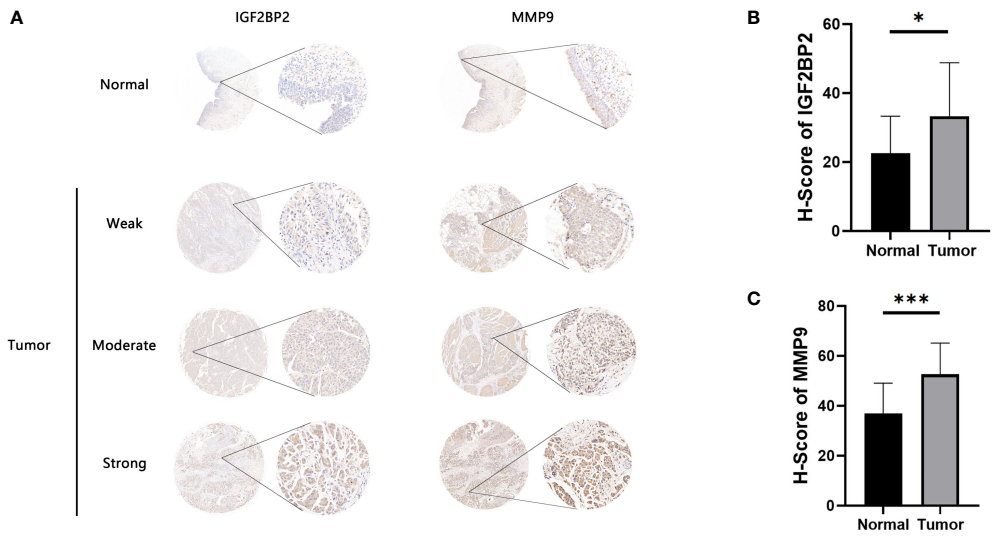

FIGURE 3
Immunohistochemical evaluation of IGF2BP2 and MMP9. **(A)** Weak, moderate, and strong immunohistochemical staining of IGF2BP2 shown respectively in normal and BLCA samples. **(B)**The H-scores of IGF2BP2 in BLCA tissues compared with normal tissues. **(C)** The H-scores of MMP9 in BLCA tissues compared with normal tissues. *P < 0.05, ***P < 0.001.

Additionally, we explored the signaling pathways critical for tumorigenesis and progression in three subgroups and found that the three groups were inconsistently expressed in all pathways (Figure S4C). To address the self-regenerating properties, we compared the ssGSEA scores of stem cell gene sets in three subtypes, and the results showed that BIS2 had the highest score among the three groups, followed by BIS1 and BIS3 (Figure S4D).

Since response to mRNA vaccines correlates with tumor immune status in the tumor microenvironment, the CIBERSORT algorithm was used to evaluate the proportions of 22 types of immune cell subpopulations among three subtypes (Figures 5A, B) (26). BIS3 displayed higher abundance of CD8+ T cells, B cells, and monocytes, while BIS3 showed lower proportions of immune inhibitory cells such as M2 macrophage. Therefore, we concluded that the BIS3 subtype exhibited an "active" immune phenotype, while BIS1 and BIS2 subtypes had a "suppressive" immune phenotype.

Figure 5C showed the expression of certain co-inhibitory and co-stimulatory molecules in the three subtypes. We found that the majority were differentially expressed in three subgroups.

Next, we characterized the immunogenicity of tumor subsets by immunophenoscore (IPS) (27) and visualized using an immunophenogram (Figure 5D). The results showed that BIS3 had a higher score in checkpoints or immunomodulators (CP) and IPS, while BIS1 and BIS2 had a higher score in major histocompatibility complex-related molecules (MHC molecules). These results indicated that the immune subtypes mirrored BLCA immune status and could stratify patients by suitability for mRNA vaccination. We hypothesized that mRNA vaccines targeting MMP9 and IGF2BP2 could induce immune infiltration in the tumor microenvironment of patients with immunologically "suppressive" BIS1 and BIS2 tumors.

The molecular and multi-omics characteristics of BLCA tumors within the three subtypes

High tumor mutational burden (TMB) is correlated with neo-antigen expression, which is presented by MHC proteins to T-cells and induce an effector T-cell response (28). High TMB also correlates with improved response to immune checkpoint inhibitors (ICIs) and mRNA vaccination (29). BLCA belonging to subtypes BIS3 and BIS2 had a significantly higher TMB compared to patients with BIS1 in TCGA cohort (Figure 6A; P< 0.05). When TMB was included as a variable, differences in overall survival between the three subtypes was highly significant (P< 0.001). BIS3 with high TMB showed the best prognosis, and BIS2 with low TMB displayed the worst prognosis (Figure 6B), consistent with our previous findings (Figures 4F, G). Among the three immune subtypes, BIS2 had the highest mutation rate (98.39%), followed by BIS3 (95.74%), and BIS1 (84.21%). The landscape of the 20 most frequently mutated genes between the three subtypes was displayed in Figure 6C. TP53 was the most frequently mutated gene in all three subgroups (Figures 6C, D; Table S6, P< 0.05). Overall, we found that TMB had a clear relationship with our three previously defined immune subtypes of BLCA, which remained to be explored further.

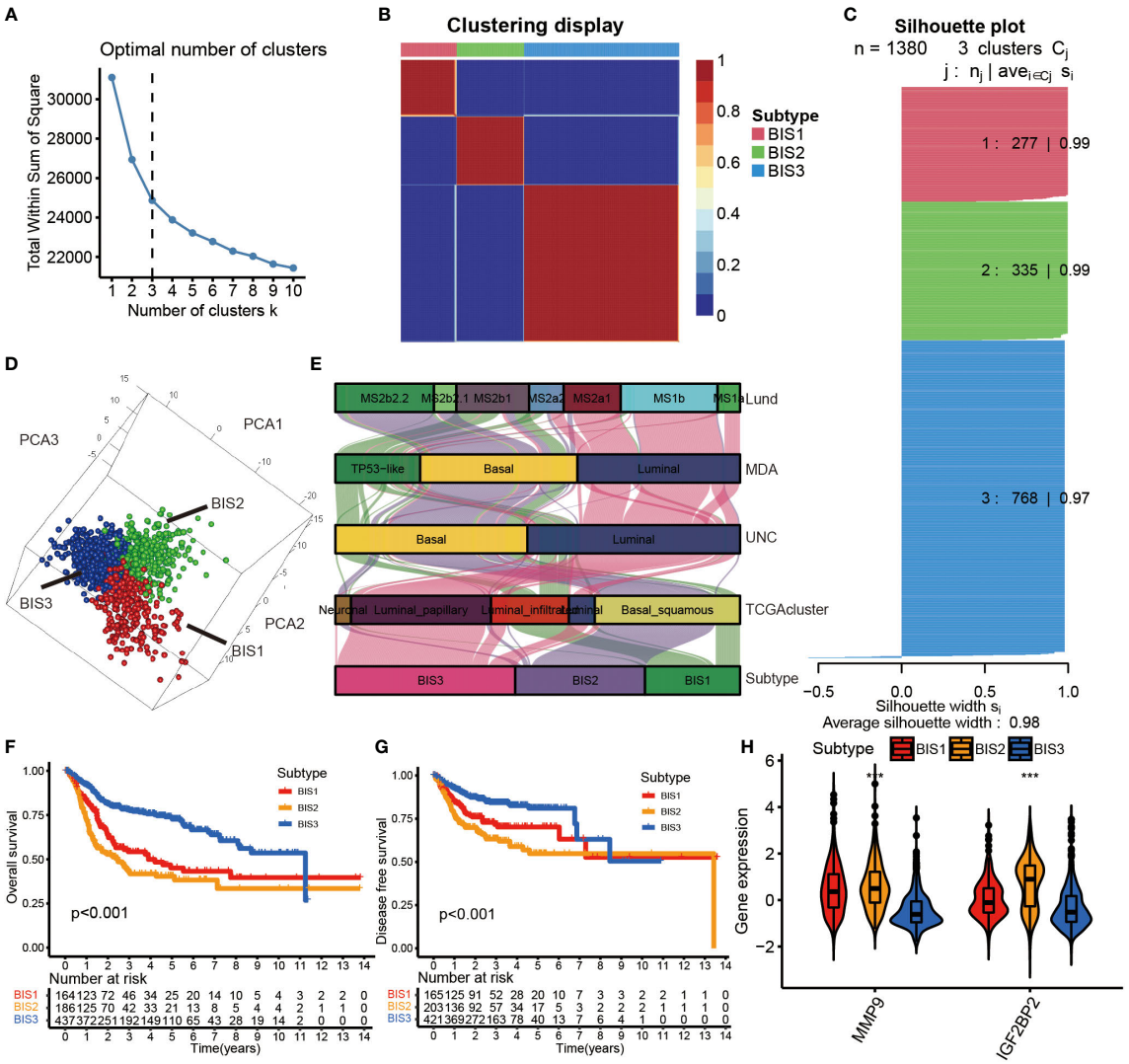

FIGURE 4
Identification of immune subtypes in BLCA. **(A)** The Total Whin Sum of Square of NMF analysis with varying cluster number (k=1-10). **(B)** Heatmap representing the consensus matrix in the Meta cohorts. **(C)** The Silhouette index of each sample after BLCA samples were divided into three clusters by NMF analysis. **(D)** Stratification into three subtypes validated by 3D PCA analysis in the Meta cohorts. **(E)** Correlation between immune subtypes and other molecular subtypes confirmed by previous studies in the TCGA cohort. **(F)** Survival analysis of OS for three subtypes in the Meta cohorts. **(G)** Survival analysis of DFS for three subtypes in the Meta cohorts. The log-rank test was used to determine the statistical significance of the differences, and P< 0.05 was considered significant. **(H)** IGF2BP2 and MMP9 gene expression levels in three subtypes. ***P < 0.001.

Related studies have found that DNA methylation can affect the immune status of BLCA (30, 31). To explore the relationship between DNA methylation in whole-genome and immune subtypes, we performed NMF analysis based on the top 500 genes of variance of DNA methylation level and characterized the DNA methylation status of the three immune subtypes (Figure S5). The results showed that BIS3 was corresponded with the cluster2 and cluster3 of DNA methylation subtypes (Figure 6E). BIS3 had reduced whole-genome DNA methylation compared to BIS1 and BIS2 (Figure 6F). This result suggested that the DNA methylation could directly affect the immune status of BLCA.

Developing a classifier to predict immune subtypes in the BLCA cohorts

To make our immune subtypes reproducible and generalizable, we developed a classifier to predict immune subtypes in new samples. First, we performed pairwise

10.3389/fimmu.2022.1014638

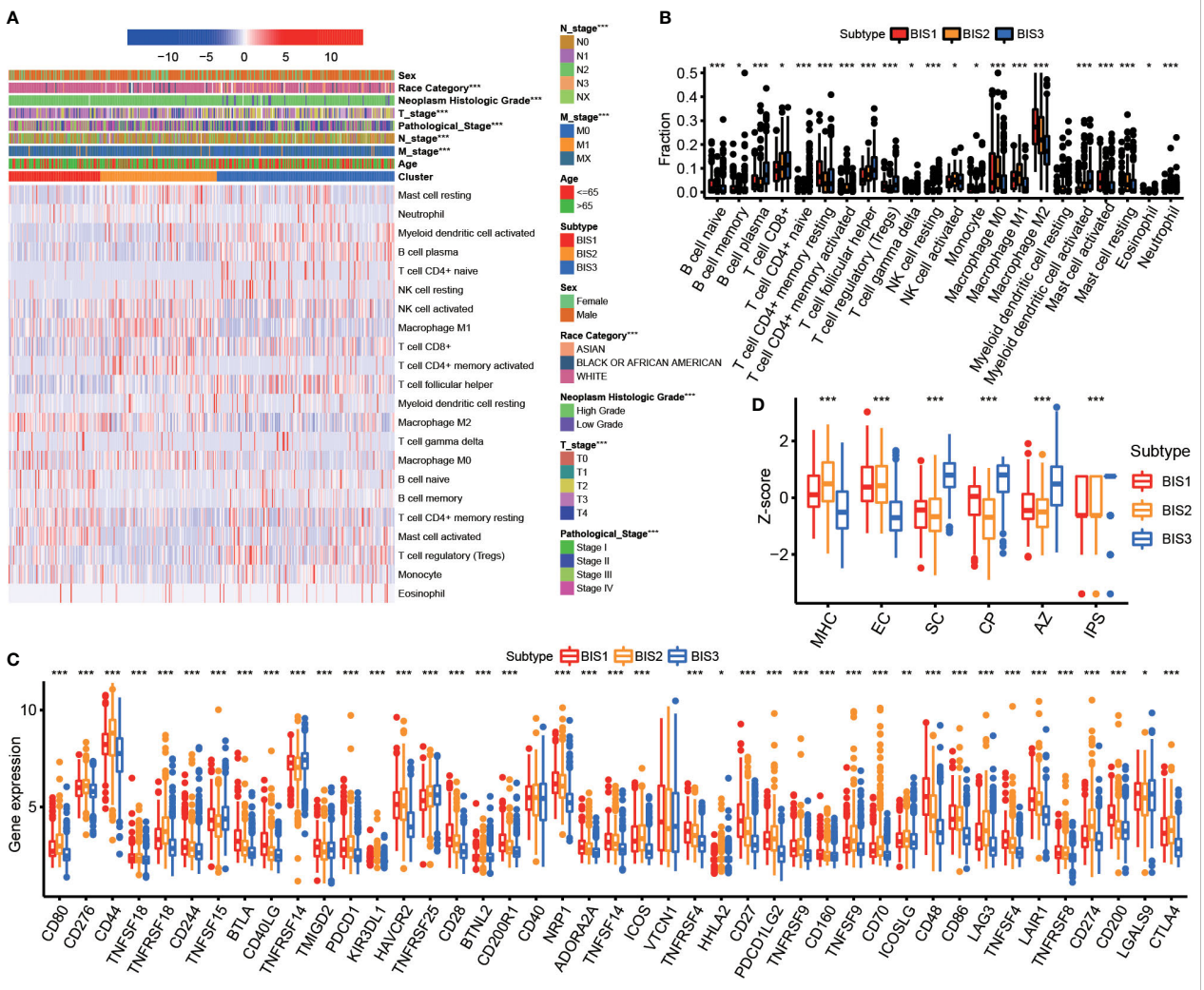

FIGURE 5
Immune characteristics of three subtypes. **(A)** Heatmap of immune cell fraction among three subtypes in TCGA BLCA cohort. **(B)** Boxplot of immune cell fraction among three subtypes in TCGA BLCA cohort. **(C)** Immune checkpoint of three subtypes in Meta cohort. **(D)** Immunophenogram for the visualization of the parameters determining immunogenicity. Boxplot showed the immune score of three subtypes in TCGA BLCA cohort (MHC, major histocompatibility complex-related molecules; EC, effector cells; SC, suppressor cells; CP, checkpoints or immunomodulators; AZ, averaged z-score; IPS, immunophenoscore). *P < 0.05, **P < 0.01, ***P < 0.001.

differential analysis across the immune subtypes in the training cohort (TCGA) based on 1,811 immune-related genes. A total of 264 overlapping differential expressed genes were prioritized as immune subtype-related genes for further analysis (Figure 7A; Table S7). Metascape analysis revealed that these genes were closely associated with the cell immune reactivity (Figure 7B; Table S8). Next, the XGBoost algorithm was used to create a classifier to predict immune subtypes, performing parameter optimization 10-fold cross-validation (Figure S6). Subsequently, we validated the accuracy of our classifier using the"immcluster" R package, applied to the TCGA (training) cohort, Meta cohort (excluding TCGA; testing cohort), (Figures 7C, D), and three independent cohorts (Figure S7; Table S9). Our classifier had accuracies of 1.000, 0.809, 0.803, 0.825, and 0.841, respectively, showing the robust performance of our package. Importantly, the "immcluster" R package can eliminate batch effects of data from multiple datasets to improve accuracy and predictive power on validation datasets.

Immune subtypes and classifier to help antitumor therapy in BLCA

Since immune characteristics of tumors correlate with treatment efficacy, we further explored the responsiveness of different immune subtypes to antitumor therapy. First, we used

10.3389/fimmu.2022.1014638

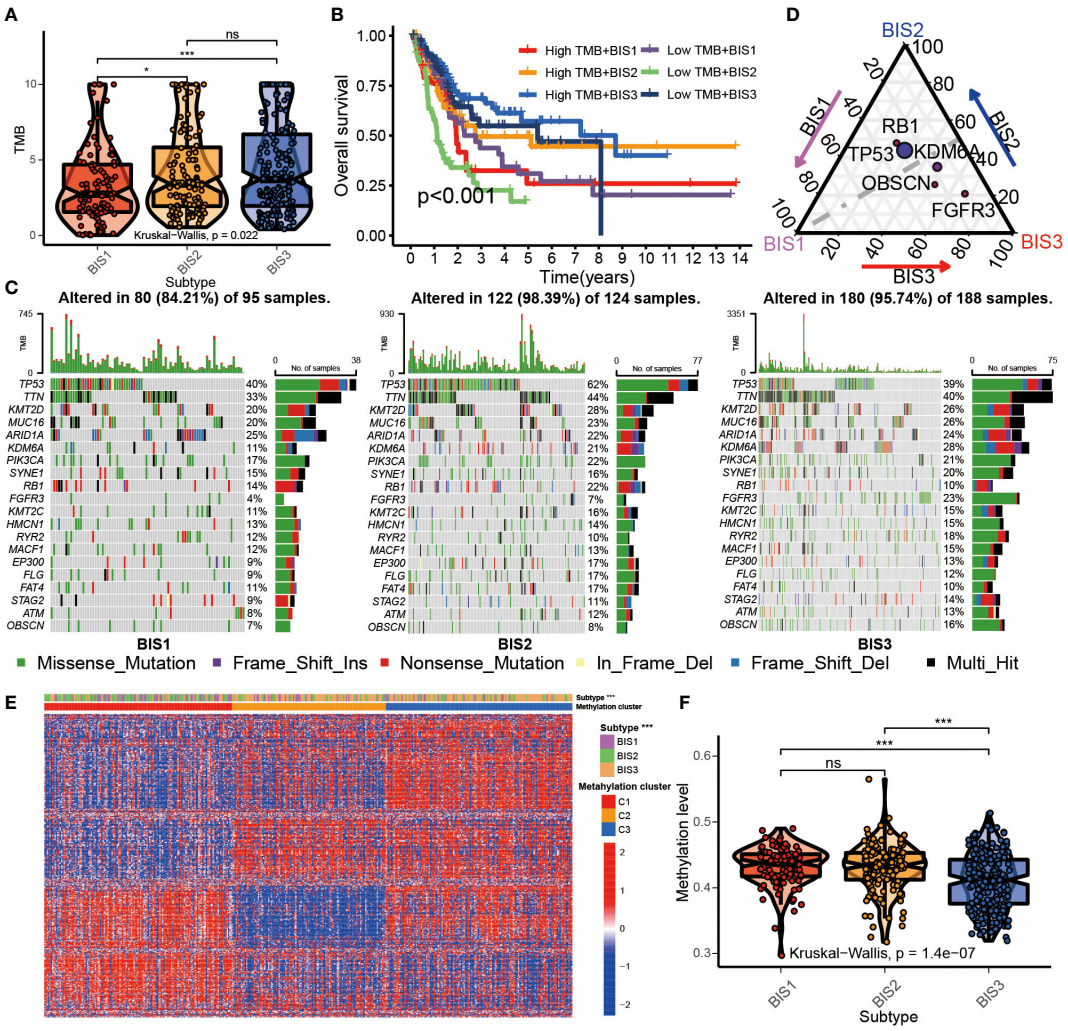

FIGURE 6
Multi-omics characteristics among three subtypes. **(A)** Boxplot of TMB in three subtypes in TCGA BLCA cohort. **(B)** Survival analysis for three subtypes and high/low TMB groups in the TCGA BLCA cohorts. **(C)** The waterfall plot of top 20 mutated genes among three subtypes in the TCGA BLCA cohorts. **(D)** Triangle plot of differential gene mutation among three subtypes in the TCGA BLCA cohorts. (Fisher's test, P< 0.05) **(E)** Heatmap of top 500 variance genes methylation level in three subtypes. **(F)** The average methylation level of immune-related genes in three subtypes in TCGA BLCA cohorts. *P < 0.05, ***P < 0.001; ns, no significance.

the TIDE algorithm to select patients who showed better responses to immune checkpoint blockade (ICB) (32). The results showed that patients in the BIS3 subtype had a lower TIDE score than those in BIS1 and BIS2, and BIS3 had the highest proportion of patients who responded to ICB, followed by BIS2 and BIS1 (Figures 8A-C, P< 0.001). We further validated the TIDE predictions in a large phase 2 trial (IMvigor210) (33), which investigated the clinical activity of PD-L1 blockade in metastatic urothelial cancer (Figures 8D-F). We found that BIS3 had the highest proportion of individuals responding to PD-L1 (27%), followed by BIS2 (24%), and BIS1 (15%), consistent with the TIDE predictions. In addition, we explored the response of patients within the three immune subtypes to PD-1 blockers in a GSE78220 (melanoma) cohort (34) and found a similar trend to the IMvigor210 cohort (Figures 8G, H; P< 0.05).

Finally, we predicted the IC50 of multiple chemotherapeutics in the TCGA BLCA cohort. The results indicated that the BIS2 subtype was most sensitive to drugs including mitomycin C, gemcitabine, cisplatin, vinblastine, and doxorubicin, and the BIS3 subtype was most sensitive to methotrexate treatment (Figure 8I, P< 0.001).

Discussion

Successful identification of tumor-associated antigens is the basis for vaccine development. Proteins dysregulated by genetic

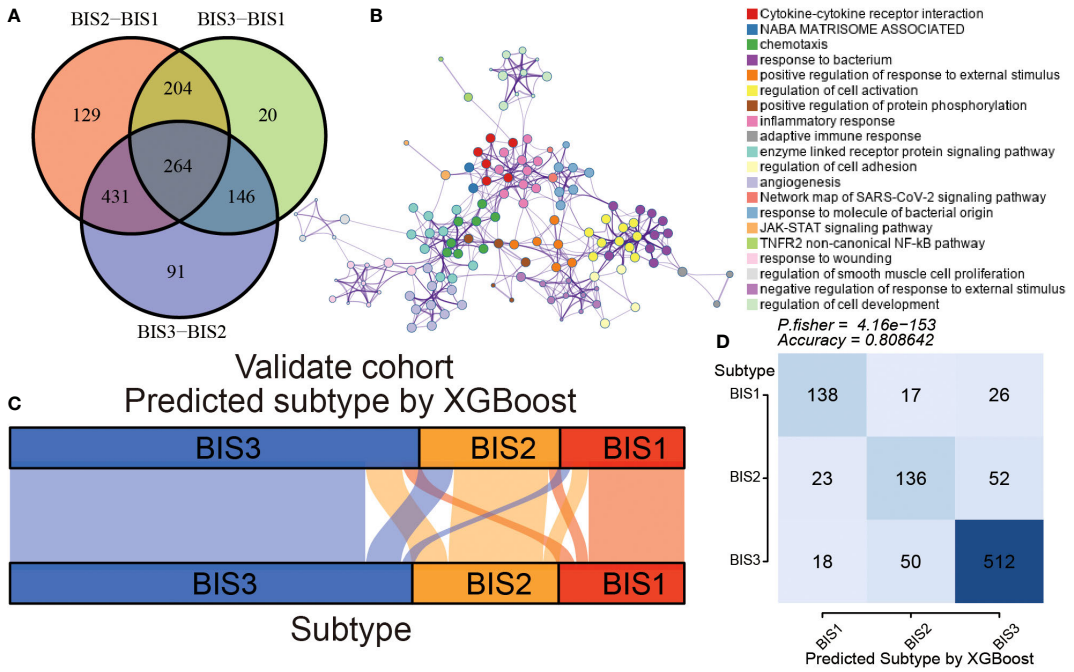

FIGURE 7
Construction and validation of an immune subtype classifier. **(A)** Venn diagram showing differential expression of immune-related gene between three subtypes in TCGA BLCA cohort. **(B)** The Metascape analysis of differential expression of immune-related genes. The alluvial diagram **(C)** and Fisher's test **(D)** of three subtypes samples in the validation cohort.

and epigenetic aberrations in tumor cells, when recognized by the immune system to attack cancer cells, can be classified as tumor antigens (35). In the present study, we identified five genes from overexpressed, highly amplified, and frequently mutated genes, which were significantly associated with worse prognosis in patients with BLCA in the Meta cohort and other cohorts. Further, we found that gene expression of MMP9 and IGF2BP2 was positively correlated with levels of several APCs, which processed tumor antigens and presented them to CD8+T cells. Additionally, we validated the expression of these two genes in clinical samples and found that MMP9 and IGF2BP2 genes were highly expressed in bladder cancer tissues compared to adjacent normal tissues, which meant they had the potential for the development of tumor vaccines. Though further preclinical evaluation and validation are still required, several previous studies have considered the potential of these two antigens as targets for mRNA vaccine targeting of BLCA. Owyong et al. reported that MMP9 played a key role in the early metastatic niche of tumorigenesis and promoted lung colonization of circulating tumor cells. In the MMTV-PyMT model, blocking the active form of MMP9 with a monoclonal antibody inhibited endogenous and experimental lung metastases (36). Andecaliximab (GS-5745, a monoclonal antibody targeting MMP9) had been evaluated in several clinical trials for indications including advanced gastric and gastroesophageal junction adenocarcinoma (37) and advanced pancreatic adenocarcinoma (38). IGF2BP2, an N6-methyladenosine (m6A) reader, participates in multiple biological processes by interacting with different RNAs (39). Overexpression of IGF2BP2 has been found to confer shorter survival and poor prognosis in multiple cancers (39), including breast cancer (40), hepatocellular carcinoma (41), and pancreatic ductal adenocarcinoma (42, 43).

Since the therapeutic response to an mRNA vaccine may be limited to a small subset of patients, it is essential to screen suitable populations for their suitability to vaccination (44). Using prognostically immune-related genes, we classified bladder cancer into three immune subtypes (BIS1, 2, and 3). Patients in BIS3 had the best survival among the three subtypes, while patients in BIS2 had shortened survival compared with those in other subtypes, suggesting that the immunophenotype can serve as a prognostic factor for BLCA. MMP9 and IGF2BP2 expression were lowest in BIS3 and highest in BIS2. In addition, immunophenoscore results of CP and IPS were highest in BIS3, while BIS1 and BIS2 had a higher score in MHC molecules.

Patients with subtype BIS3 and BIS2 had a substantially higher TMB compared to patients with BIS1 in TCGA cohort. These results indicated that patients in the BIS2 subgroup were

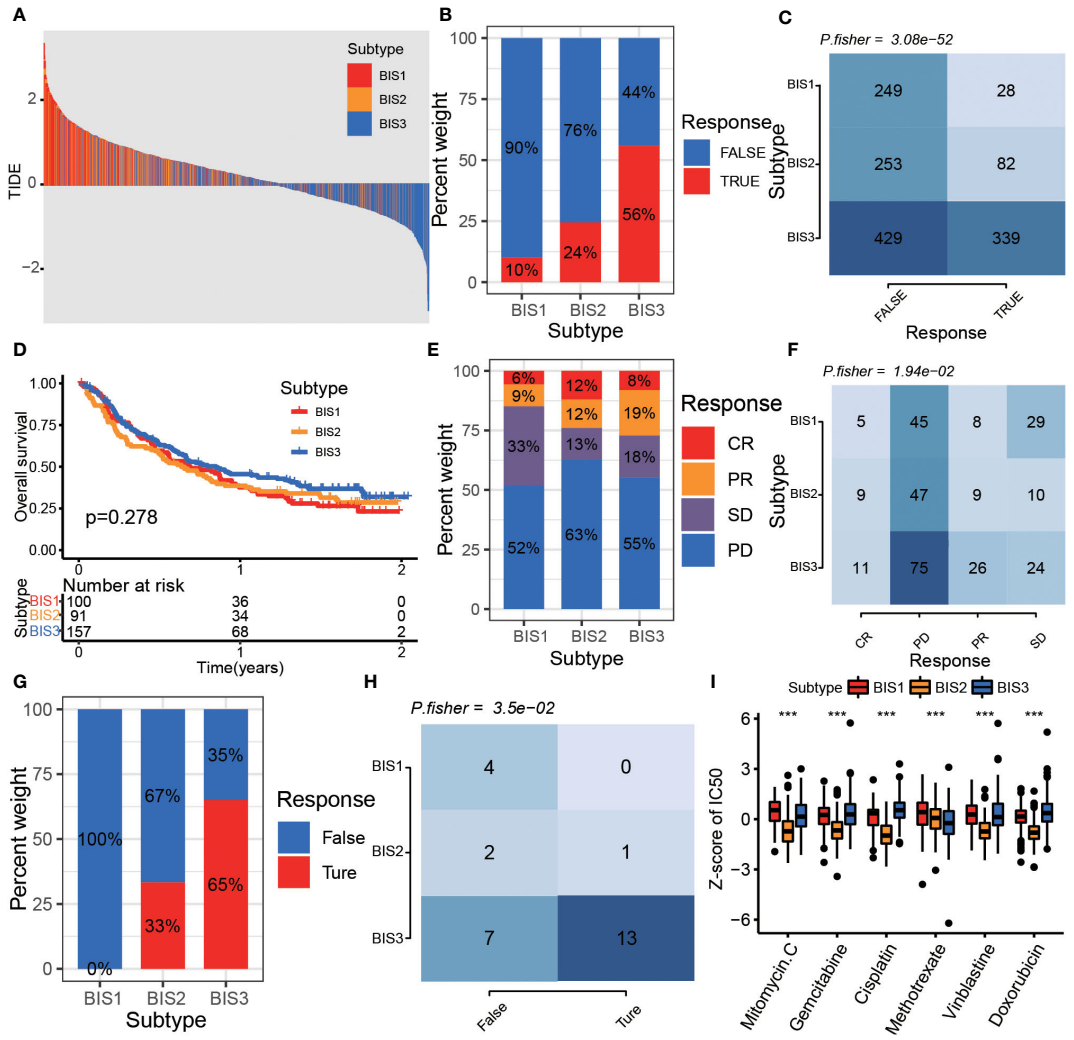

FIGURE 8
The drug sensitivity of different subtypes. **(A)** The distribution of TIDE score among the three subtypes in Meta cohort. The proportion **(B)** and Fisher's test **(C)** of immunotherapy response samples in different subtypes in Meta cohort. **(D)** Survival analysis for three subtypes in the IMvigor210 cohort. The proportion **(E)** and Fisher's test **(F)** of immunotherapy response samples in different subtypes in the IMvigor 210 cohort. The proportion **(G)** and Fisher's test **(H)** of immunotherapy response samples in different subtypes in GSE78220 cohort. **(I)** The boxplot of z-score of chemotherapy drug IC50 between three subtypes in the TCGA BLCA cohort. ***P < 0.001.

more likely to be responsive to mRNA vaccines targeting MMP9 and IGF2BP2, while immune checkpoint inhibitors were more suitable for patients in BIS3. Recently, McCann K et al. demonstrated that vaccination in non-small cell lung cancer with low mutational load was feasible and could be effective (45). Therefore, clinical trials of vaccination against the BIS2 subgroup, which had high MMP9 and IGF2BP2 expression and low TMB, is a promising future direction.

Compared to other types of vaccines, mRNA vaccines have several advantages. The risk of insertional mutations by integration into the host cell genome is unlikely to be a concern for mRNA vaccines. In addition, the manufacturing process of mRNA does not require cell culture or toxic chemicals; thus, mRNA vaccines are considered to be relatively safe (46). mRNA vaccines have the advantage of encoding different proteins or long peptides, enabling a wide range of polyclonal immune responses, thus avoiding possible immune escape owing to antigen loss or the restriction to a certain HLA molecule (47). Meanwhile, mRNA vaccines could deliver multiple antigens simultaneously, improving the efficiency and effectiveness of treatment (48, 49). Recently, several technical obstacles have been solved, including stability, delivery, and immunogenicity of mRNA, and efficient delivery has been achieved *in vivo* (46). In contrast to traditional protein subunit and viral vaccines, mRNA vaccine production is rapid and relatively

simple in production and manufacturing (46). In this study, we focused on MMP9 and IGF2BP2 genes, which were both elevated in BIS1 and BIS2 subtypes. Therefore, these two genes could be made into a bivalent vaccine composition, which could expand the vaccine population and enhance immune responses (48, 49). Alternatively, tumor-targeting mRNA vaccines could be combined with traditional chemotherapeutic agents or immune checkpoint inhibitors. A phase II trial investigated the combination of TriMixDC-MEL (autologous monocyte-derived dendritic cells electroporated with synthetic mRNA) and ipilimumab (CTLA-4 blocking monoclonal antibody) in patients with pretreated advanced melanoma. The results showed that this combination achieved a high rate of durable tumor responses in patients who achieved complete responses (50).

Several reports have explored the application of mRNA vaccines to urinary tumors, including bladder tumor (51). Gui C et al. established a ferroptosis-induced tumor microenvironment landscape in bladder cancer and identified six genes as potent antigens for developing an anti-BLCA mRNA vaccine (52). Wang G et al. identified AP2S1, P3H4, and RAC3 as three candidate genes of tumor-specific antigens in bladder cancer using the TCGA BLCA cohort and GSE13507 datasets (53). In contrast to these studies, we integrated four cohorts into a Meta cohort at the outset, including TCGA BLCA, GSE13507, GSE32894, and E-MTAB-4321 cohorts, which enhanced the robustness of our study. In addition, we validated the expression of MMP9 and IGF2BP2 in clinical samples, which was not done in other studies. Importantly, in order to perform immunotyping in new samples, we developed a classifier and released it for public use hosted on Github, which could eliminate batch effects from new datasets and make our immune subtypes reproducible and generalizable for other researchers. Furthermore, we validated the effect of various treatments on different subgroups in new datasets stratified by our classifier (IMvigor210 and GSE78220), which extended the value of the study.

Conclusions

In conclusion, this study identified IGF2BP2 and MMP9 as potential antigens for mRNA vaccine development targeting BLCA, which could highly benefit patients specifically in the BIS2 subtype. The findings in this study provide a theoretical foundation for developing mRNA vaccines against BLCA, predicting patient prognosis, and defining suitable patient populations for vaccination. mRNA vaccination therapy should be further explored in prospective clinical trials.

Data availability statement

The datasets presented in this study can be found in online repositories. The names of the repository/repositories and accession number(s) can be found in the article/Supplementary Material.

Ethics statement

The studies involving human participants were reviewed and approved by the ethics committee of Shanghai OUTDO Biotech Corporation Limited. The patients/participants provided their written informed consent to participate in this study.

Author contributions

XH, MZ and XW conducted this research study and revised the manuscript. XZ, YZ and LZ designed the research processes, exported the figures, wrote the first draft of the manuscript, and performed the verification experiments. JW and JL analyzed the experimental data. All authors contributed to the article and approved the submitted version.

Acknowledgments

The authors would like to express their gratitude to EditSprings (https://www.editsprings.cn) for the expert linguistic services provided.

Conflict of interest

The authors declare that the research was conducted in the absence of any commercial or financial relationships that could be construed as a potential conflict of interest.

Publisher's note

Supplementary material

The Supplementary Material for this article can be found online at: https://www.frontiersin.org/articles/10.3389/fimmu.2022.1014638/full#supplementary-material.

SUPPLEMENTARY FIGURE 1
Experimental verification of IGF2BP2. **(A)** Relative expression of IGF2BP2 in bladder cell lines. **(B)** The knockdown efficiency of siRNA in UMUC3 and T24. **(C)** The knockdown efficiency of siRNA2 in UMUC3 and T24. Transwell migration assay **(D)** and wound healing assay **(E)** show that interference with IGF2BP2 expression inhibits the migration of UMUC3 and T24.

SUPPLEMENTARY FIGURE 2
Survival analysis between three subtypes in GSE13507 **(A)**, GSE32894 **(B)**, TCGA OS **(C)**, TCGA DFS **(D)**, and E-MTAB-4321 **(E)** cohorts.

SUPPLEMENTARY FIGURE 3
The proportion of different age **(A)**, sex **(B)**, race category **(C)**, T stage **(D)**, N stage **(E)**, M stage **(F)**, neoplasm histologic grade **(G)**, and pathological stage **(H)** in three subtypes in TCGA cohort.

SUPPLEMENTARY FIGURE 4
The molecular characteristics of three subtypes. The keeg function enrichment analysis identifies the activated **(A)** and inhibited pathways **(B)** in each immune subtype. **(C)** The boxplot of ssGSEA score of signaling pathways between three immune clusters. **(D)** The boxplot of ssGSEA score of stem cell gene set between three immune clusters.

SUPPLEMENTARY FIGURE 5
Identification of methylation subtypes in BLCA. **(A)** The Total Whin Sum of Square of NMF analysis with different clusters number (k=1-10). **(B)** Stratification into three subtypes validated by PCA analysis in the Meta cohorts. **(C)** Heatmap representing the consensus matrix in the Meta cohorts. **(D)** The Silhouette index of each sample while BLCA samples were divided into three clusters by NMF analysis.

SUPPLEMENTARY FIGURE 6
Example R script of using "immcluster."

SUPPLEMENTARY FIGURE 7
The alluvial diagram of three subtypes predicted by XGBoost in TCGA **(A)**, E-MTAB-4321 **(B)**, GSE13507 **(C)**, and GSE32894 **(D)** cohorts. Survival analysis between three subtypes predicted by XGBoost in E-MTAB-4321 **(E)**, GSE13507 **(F)**, and GSE32894 **(G)** cohorts.

SUPPLEMENTARY TABLE 1
The mediums used for cell culture, the kit for RNA extraction and RT-qPCR, siRNA sequences, and RT-qPCR primer sequences.

SUPPLEMENTARY TABLE 2
The over-expression genes, mutation genes, and AMP genes.

SUPPLEMENTARY TABLE 3
Survival analysis of OS/DFS for overlapping genes.

SUPPLEMENTARY TABLE 4
Correlation between potential tumor antigens and APCs or APC markers.

SUPPLEMENTARY TABLE 5
Fisher's test of different age, sex, race category, T stage, N stage, M stage, neoplasm histologic grade, and pathological stage in three subtypes in the TCGA cohort.

SUPPLEMENTARY TABLE 6
Differential gene mutation in the three subtypes.

SUPPLEMENTARY TABLE 7
Differential expression of immune-related genes in three subtypes.

SUPPLEMENTARY TABLE 8
Metascape analysis of differential immune-related genes.

SUPPLEMENTARY TABLE 9
Model effectiveness of XGBoost in TCGA, E-MTAB-4321, GSE13507, and GSE32894 cohorts.

References

1. Siegel RL, Miller KD, Fuchs HE, Jemal A. Cancer statistics, 2021. *CA: Cancer J Clin* (2021) 71(1):7–33. doi: 10.3322/caac.21654

2. Lenis AT, Lec PM, Chamie K, Mshs MD. Bladder cancer: A review. *JAMA* (2020) 324(19):1980–91. doi: 10.1001/jama.2020.17598

3. Kirkali Z, Chan T, Manoharan M, Algaba F, Busch C, Cheng L, et al. Bladder cancer: Epidemiology, staging and grading, and diagnosis. *Urology* (2005) 66(6 Suppl 1):4–34. doi: 10.1016/j.urology.2005.07.062

4. Burger M, Catto JW, Dalbagni G, Grossman HB, Herr H, Karakiewicz P, et al. Epidemiology and risk factors of urothelial bladder cancer. *Eur Urol* (2013) 63 (2):234–41. doi: 10.1016/j.eururo.2012.07.033

5. Jordan B, Meeks JJ. T1 bladder cancer: Current considerations for diagnosis and management. *Nat Rev Urol* (2019) 16(1):23–34. doi: 10.1038/s41585-018-0105-y

6. Downes MR, Lajkosz K, Kuk C, Gao B, Kulkarni GS, van der Kwast TH. The impact of grading scheme on non-muscle invasive bladder cancer progression: Potential utility of hybrid grading schemes. *Pathology* (2022) 54(4):425–33. doi: 10.1016/j.pathol.2021.10.005

7. Zappasodi R, Merghoub T, Wolchok JD. Emerging concepts for immune checkpoint blockade-based combination therapies. *Cancer Cell* (2018) 33(4):581–98. doi: 10.1016/j.ccell.2018.03.005

8. Hargadon KM, Johnson CE, Williams CJ. Immune checkpoint blockade therapy for cancer: An overview of fda-approved immune checkpoint inhibitors. *Int Immunopharmacol* (2018) 62:29–39. doi: 10.1016/j.intimp.2018.06.001

9. Ribas A, Wolchok JD. Cancer immunotherapy using checkpoint blockade. *Science* (2018) 359(6382):1350–5. doi: 10.1126/science.aar4060

10. Balar AV, Kamat AM, Kulkarni GS, Uchio EM, Boormans JL, Roumiguie M, et al. Pembrolizumab monotherapy for the treatment of high-risk non-Muscle-Invasive bladder cancer unresponsive to bcg (Keynote-057): An open-label, single-arm, multicentre, phase 2 study. *Lancet Oncol* (2021) 22(7):919–30. doi: 10.1016/S1470-2045(21)00147-9

11. Sayour E, Mendez-Gomez H, Mitchell D. Cancer vaccine immunotherapy with rna-loaded liposomes. *Int J Mol Sci* (2018) 19(10):2890. doi: 10.3390/ijms19102890

12. Lang F, Schrors B, Lower M, Tureci O, Sahin U. Identification of neoantigens for individualized therapeutic cancer vaccines. *Nat Rev Drug Discovery* (2022) 21(4):261–82. doi: 10.1038/s41573-021-00387-y

13. Emens LA. Roadmap to a better therapeutic tumor vaccine. *Int Rev Immunol* (2009) 25(5-6):415–43. doi: 10.1080/08830180600992423

14. Tameris M, Mearns H, Penn-Nicholson A, Gregg Y, Bilek N, Mabwe S, et al. Live-attenuated mycobacterium tuberculosis vaccine mtbvac versus bcg in adults and neonates: A randomised controlled, double-blind dose-escalation trial. *Lancet Respir Med* (2019) 7(9):757–70. doi: 10.1016/S2213-2600(19)30251-6

15. Rentsch CA, Bosshard P, Mayor G, Rieken M, Puschel H, Wirth G, et al. Results of the phase I open label clinical trial sakk 06/14 assessing safety of intravesical instillation of Vpm1002bc, a recombinant mycobacterium bacillus calmette guerin (Bcg), in patients with non-muscle invasive bladder cancer and previous failure of conventional bcg therapy. *Oncoimmunology* (2020) 9 (1):1748981. doi: 10.1080/2162402X.2020.1748981

16. Gulley JL, Arlen PM, Tsang KY, Yokokawa J, Palena C, Poole DJ, et al. Pilot study of vaccination with recombinant cea-Muc-1-Tricom poxviral-based vaccines in patients with metastatic carcinoma. *Clin Cancer Res* (2008) 14(10):3060–9. doi: 10.1158/1078-0432.Ccr-08-0126

17. Chakraborty C, Sharma AR, Bhattacharya M, Lee SS. From covid-19 to cancer mrna vaccines: Moving from bench to clinic in the vaccine landscape. *Front Immunol* (2021) 12:679344. doi: 10.3389/fimmu.2021.679344

18. Jackson N, Kester KE, Casimiro D, Gurunathan S, DeRosa F. The promise of mrna vaccines: A biotech and industrial perspective. *NPJ Vaccines* (2020) 5:11. doi: 10.1038/s41541-020-0159-8

19. Cao R, Ma B, Wang G, Xiong Y, Tian Y, Yuan L. Characterization of hypoxia response patterns identified prognosis and immunotherapy response in bladder cancer. *Mol Ther Oncolytics* (2021) 22:277–93. doi: 10.1016/j.omto.2021.06.011

20. Miranda A, Hamilton PT, Zhang AW, Pattnaik S, Becht E, Mezheyeuski A, et al. Cancer stemness, intratumoral heterogeneity, and immune response across cancers. *Proc Natl Acad Sci United States America* (2019) 116(18):9020–9. doi: 10.1073/pnas.1818210116

21. Liu F, Zhang H, Xie F, Tao D, Xiao X, Huang C, et al. Hsa_Circ_0001361 promotes bladder cancer invasion and metastasis through mir-491-5p/Mmp9 axis. *Oncogene* (2020) 39(8):1696–709. doi: 10.1038/s41388-019-1092-z

22. Wong JPC, Wei R, Lyu P, Tong OLH, Zhang SD, Wen Q, et al. Clinical and analysis of osteopontin as a prognostic indicator and unveil its potential downstream targets in bladder cancer. *Int J Biol Sci* (2017) 13(11):1373–86. doi: 10.7150/ijbs.21457

23. Augoff K, Hryniewicz-Jankowska A, Tabola R, Stach K. Mmp9: A tough target for targeted therapy for cancer. *Cancers* (2022) 14(7):1847. doi: 10.3390/cancers14071847

24. Mondal S, Adhikari N, Banerjee S, Amin SA, Jha T. Matrix metalloproteinase-9 (Mmp-9) and its inhibitors in cancer: A minireview. *Eur J Med Chem* (2020) 194:112260. doi: 10.1016/j.ejmech.2020.112260

25. Robertson AG, Kim J, Al-Ahmadie H, Bellmunt J, Guo G, Cherniack AD, et al. Comprehensive molecular characterization of muscle-invasive bladder cancer. *Cell* (2017) 171(3):540–56.e25. doi: 10.1016/j.cell.2017.09.007

26. Newman AM, Liu CL, Green MR, Gentles AJ, Feng W, Xu Y, et al. Robust enumeration of cell subsets from tissue expression profiles. *Nat Methods* (2015) 12 (5):453–7. doi: 10.1038/nmeth.3337

27. Charoentong P, Finotello F, Angelova M, Mayer C, Efremova M, Rieder D, et al. Pan-cancer immunogenomic analyses reveal genotype-immunophenotype relationships and predictors of response to checkpoint blockade. *Cell Rep* (2017) 18 (1):248–62. doi: 10.1016/j.celrep.2016.12.019

28. Jardim DL, Goodman A, de Melo GD, Kurzrock R. The challenges of tumor mutational burden as an immunotherapy biomarker. *Cancer Cell* (2021) 39 (2):154–73. doi: 10.1016/j.ccell.2020.10.001

29. Choucair K, Morand S, Stanbery L, Edelman G, Dworkin L, Nemunaitis J. Tmb: A promising immune-response biomarker, and potential spearhead in advancing targeted therapy trials. *Cancer Gene Ther* (2020) 27(12):841–53. doi: 10.1038/s41417-020-0174-y

30. Chen J-Q, Salas LA, Wiencke JK, Koestler DC, Molinaro AM, Andrew AS, et al. Immune profiles and DNA methylation alterations related with non-Muscle-Invasive bladder cancer outcomes. *Clin Epigenet* (2022) 14(1):14. doi: 10.1186/s13148-022-01234-6

31. Su X, Lu X, Bazai SK, Compérat E, Mouawad R, Yao H, et al. Comprehensive integrative profiling of upper tract urothelial carcinomas. *Genome Biol* (2021) 22(1):7. doi: 10.1186/s13059-020-02230-w

32. Jiang P, Gu S, Pan D, Fu J, Sahu A, Hu X, et al. Signatures of T cell dysfunction and exclusion predict cancer immunotherapy response. *Nat Med* (2018) 24(10):1550–8. doi: 10.1038/s41591-018-0136-1

33. Mariathasan S, Turley SJ, Nickles D, Castiglioni A, Yuen K, Wang Y, et al. Tgfβ attenuates tumour response to pd-L1 blockade by contributing to exclusion of T cells. *Nature* (2018) 554(7693):544–8. doi: 10.1038/nature25501

34. Hugo W, Zaretsky JM, Sun L, Song C, Moreno BH, Hu-Lieskovan S, et al. Genomic and transcriptomic features of response to anti-Pd-1 therapy in metastatic melanoma. *Cell* (2016) 165(1):35–44. doi: 10.1016/j.cell.2016.02.065

35. Leko V, Rosenberg SA. Identifying and targeting human tumor antigens for T cell-based immunotherapy of solid tumors. *Cancer Cell* (2020) 38(4):454–72. doi: 10.1016/j.ccell.2020.07.013

36. Owyong M, Chou J, van den Bijgaart RJ, Kong N, Efe G, Maynard C, et al. Mmp9 modulates the metastatic cascade and immune landscape for breast cancer anti-metastatic therapy. *Life Sci Alliance* (2019) 2(6):e201800226. doi: 10.26508/lsa.201800226

37. Shah MA, Starodub A, Sharma S, Berlin J, Patel M, Wainberg ZA, et al. Andecaliximab/Gs-5745 alone and combined with Mfolfox6 in advanced gastric and gastroesophageal junction adenocarcinoma: Results from a phase I study. *Clin Cancer Res* (2018) 24(16):3829–37. doi: 10.1158/1078-0432.CCR-17-2469

38. Bendell J, Sharma S, Patel MR, Windsor KS, Wainberg ZA, Gordon M, et al. Safety and efficacy of andecaliximab (Gs-5745) plus gemcitabine and nab-paclitaxel in patients with advanced pancreatic adenocarcinoma: Results from a phase I study. *Oncologist* (2020) 25(11):954–62. doi: 10.1634/theoncologist.2020-0474

39. Wang J, Chen L, Qiang P. The role of Igf2bp2, an M6a reader gene, in human metabolic diseases and cancers. *Cancer Cell Int* (2021) 21(1):99. doi: 10.1186/s12935-021-01799-x

40. Barghash A, Helms V, Kessler SM. Overexpression of Igf2 mrna-binding protein 2 (Imp2/P62) as a feature of basal-like breast cancer correlates with short survival. *Scand J Immunol* (2015) 82(2):142–3. doi: 10.1111/sji.12307

41. Pu J, Wang J, Qin Z, Wang A, Zhang Y, Wu X, et al. Igf2bp2 promotes liver cancer growth through an M6a-Fen1-Dependent mechanism. *Front Oncol* (2020) 10:578816. doi: 10.3389/fonc.2020.578816

42. Hu X, Peng WX, Zhou H, Jiang J, Zhou X, Huang D, et al. Igf2bp2 regulates dancr by serving as an N6-methyladenosine reader. *Cell Death Differ* (2020) 27 (6):1782–94. doi: 10.1038/s41418-019-0461-z

43. Dahlem C, Barghash A, Puchas P, Haybaeck J, Kessler SM. The insulin-like growth factor 2 mrna binding protein Imp2/Igf2bp2 is overexpressed and correlates with poor survival in pancreatic cancer. *Int J Mol Sci* (2019) 20 (13):3204. doi: 10.3390/ijms20133204

44. Han S, Lee SY, Wang WW, Tan YB, Sim R, Cheong R, et al. A perspective on cell therapy and cancer vaccine in biliary tract cancers (Btcs). *Cancers (Basel)* (2020) 12(11):3404. doi: 10.3390/cancers12113404

45. McCann K, von Witzleben A, Thomas J, Wang C, Wood O, Singh D, et al. Targeting the tumor mutanome for personalized vaccination in a tmb low non-small cell lung cancer. *J ImmunoTherapy Cancer* (2022) 10(3):e003821. doi: 10.1136/jitc-2021-003821

46. Pardi N, Hogan MJ, Porter FW, Weissman D. Mrna vaccines - a new era in vaccinology. *Nat Rev Drug Discovery* (2018) 17(4):261–79. doi: 10.1038/nrd.2017.243

47. Heine A, Juranek S, Brossart P. Clinical and immunological effects of mrna vaccines in malignant diseases. *Mol Cancer* (2021) 20(1):52. doi: 10.1186/s12943-021-01339-1

48. Miao L, Zhang Y, Huang L. Mrna vaccine for cancer immunotherapy. *Mol Cancer* (2021) 20(1):41. doi: 10.1186/s12943-021-01335-5

49. Chivukula S, Plitnik T, Tibbitts T, Karve S, Dias A, Zhang D, et al. Development of multivalent mrna vaccine candidates for seasonal or pandemic influenza. *NPJ Vaccines* (2021) 6(1):153. doi: 10.1038/s41541-021-00420-6

50. Wilgenhof S, Corthals J, Heirman C, van Baren N, Lucas S, Kvistborg P, et al. Phase ii study of autologous monocyte-derived mrna electroporated dendritic cells (Trimixdc-Mel) plus ipilimumab in patients with pretreated advanced melanoma. *J Clin Oncol* (2016) 34(12):1330–8. doi: 10.1200/jco.2015.63.4121

51. Xu H, Zheng X, Zhang S, Yi X, Zhang T, Wei Q, et al. Tumor antigens and immune subtypes guided mrna vaccine development for kidney renal clear cell carcinoma. *Mol Cancer* (2021) 20(1):159. doi: 10.1186/s12943-021-01465-w

52. Gui C-P, Li J-Y, Fu L-M, Luo C-G, Zhang C, Tang Y-M, et al. Identification of mrna vaccines and conserved ferroptosis related immune landscape for individual precision treatment in bladder cancer. *J Big Data* (2022) 9(1):88. doi: 10.1186/s40537-022-00641-z

53. Wang G, Gao Y, Chen Y, Wang K, Zhang S, Li G. Identification of novel tumor antigens and the immune landscapes of bladder cancer patients for mrna vaccine development. *Front Oncol* (2022) 12:921711. doi: 10.3389/fonc.2022.921711

frontiers | Frontiers in Immunology

TYPE Original Research
PUBLISHED 24 November 2022
DOI 10.3389/fimmu.2022.1015081

OPEN ACCESS

EDITED BY
Dianwen Ju,
Fudan University, China

REVIEWED BY
Qi Deng,
Tianjin First Central Hospital, China
Xianhuo Wang,
Tianjin Medical University Cancer Institute and Hospital, China
Wei Sang,
The Affiliated Hospital of Xuzhou Medical University, China

*CORRESPONDENCE
Yun Liang
liangyun@zju.edu.cn
Wenbin Qian
qianwb@zju.edu.cn
Weiping Zhang
15325715566@163.com

†These authors have contributed equally to this work

SPECIALTY SECTION
This article was submitted to Cancer Immunity and Immunotherapy, a section of the journal Frontiers in Immunology

RECEIVED 09 August 2022
ACCEPTED 07 November 2022
PUBLISHED 24 November 2022

CITATION
Yuan X, Li X, Huang Y, Jin X, Liu H, Zhao A, Zhang W, Qian W and Liang Y (2022) Zanubrutinib plus salvage chemotherapy for relapsed or refractory diffuse large B-cell lymphoma. *Front. Immunol.* 13:1015081. doi: 10.3389/fimmu.2022.1015081

Zanubrutinib plus salvage chemotherapy for relapsed or refractory diffuse large B-cell lymphoma

Xianggui Yuan[1†], Xian Li[1†], Yurong Huang[1†], Xueli Jin[1], Hui Liu[1], Aiqi Zhao[1], Weiping Zhang[2*], Wenbin Qian[1,3*] and Yun Liang[1*]

[1]Department of Hematology, the Second Affiliated Hospital, Zhejiang University School of Medicine, Hangzhou, China, [2]Department of Oncology, The Third Affiliated Hospital of Zhejiang Chinese Medical University, Hangzhou, China, [3]National Clinical Research Center for Hematologic Diseases, the First Affiliated Hospital of Soochow University, Hangzhou, China

Introduction: Relapsed or refractory diffuse large B-cell lymphoma (R/R DLBCL) has poor clinical outcomes when treated with conventional salvage chemotherapy. Monotherapy using zanubrutinib, a selective Bruton's tyrosine kinase (BTK) inhibitor, has achieved modest antitumor effect in R/R DLBCL. Here we aimed to evaluate the efficacy and safety of zanubrutinib plus salvage chemotherapy in R/R DLBCL patients.

Methods: We retrospectively reviewed R/R DLBCL patients who were administered with zanubrutinib plus salvage chemotherapy in our center between January, 2019 and December, 2021. Targeted panel sequencing of 11 lymphoma-related genes was performed on 8 patients with poor responses to zanubrutinib-based chemotherapy.

Results: 27 R/R DLBCL patients were enrolled. Median age at this study was 59 years (range, 15-72). The best overall response rate (ORR) was 74.1% and complete remission rate was 33.3%. With a median follow-up of 11 months (range, 1-17), the median progression-free survival (PFS) was 8.1 months, and the overall survival (OS) was not achieved. The most common grade-3/4 adverse events were neutropenia (70.4%), thrombocytopenia (66.7%), and febrile neutropenia (33.3%). In multivariate analysis, early treatment and overall response after chemotherapy were independent favorable prognostic factors for PFS. Overall response after chemotherapy was an independent favorable factor for OS. Among the 8 patients with poor response to zanubrutinib-based treatment, the majority of patients had *NOTCH2* mutations (n=8, 100%) and *TP53* mutations (n=7, 87.5%). However, these patients achieved an ORR of 75% at 3 months after CD19-CAR-T cell therapy (including 4 cases of complete remission and 2 cases of partial remission). With a median follow-up of 9 months from CAR-T cell infusion (range, 1-16 months), the median PFS was 14.5 months, and the median OS was not reached.

10.3389/fimmu.2022.1015081

Conclusion: With high efficacy and manageable tolerability, zanubrutinib plus salvage chemotherapy may be a potential treatment option for R/R DLBCL. CAR-T cell therapy may be a priority strategy for these poor responders to BTKi-based treatment.

KEYWORDS

relapsed or refractory diffuse large B-cell lymphoma, zanubrutinib, Bruton's tyrosine kinase inhibitor, combination chemotherapy, TP53, chimeric antigen receptor T-cell (CAR-T)

Introduction

Diffuse large B-cell lymphoma (DLBCL) is the most common aggressive lymphoma, accounting for 30% to 40% of non-Hodgkin lymphomas (NHLs) (1, 2). R-CHOP (rituximab, cyclophosphamide, doxorubicin, vincristine, and prednisone) has been the standard first-line treatment, achieving approximately 50%-60% of long-term remission. Unfortunately, up to 50% of patients are ultimately refractory to, or relapse after initial remission (3, 4). Salvage chemotherapy followed by autologous stem cell transplantation (auto-SCT) is effective for relapsed or refractory DLBCL (R/R DLBCL). But only 26% of patients respond to next-line salvage therapy and the median overall survival (OS) is only 6.3 months in the SCHOLAR-1 study (5). Currently there is no preferred salvage chemotherapy for R/R DLBCL.

Bruton tyrosine kinase (BTK) inhibitor has been proven highly effective for diverse B-cell malignancies. Ibrutinib, the first-in-class BTK inhibitor, has achieved an overall response rate (ORR) of 23% with modest activity in R/R DLBCL (6). Zanubrutinib (BGB-3111), a next-generation BTK inhibitor with minimal off-target effects, has demonstrated higher efficacy and safety for treating Waldenström macroglobulinemia, compared with ibrutinib (7). The phase 2 BGB-3111-207 study revealed that zanubrutinib monotherapy produced modest antitumor activity and favorable safety in R/R DLBCL, with an ORR of 29.3% and a complete remission (CR) rate of 17.1%. Developing mechanistically-based synergistic combinations may open a way to increase response rates and durability of zanubrutinib.

Over the last 2 years, our institution had integrated zanubrutinib into conventional salvage chemotherapy for R/R DLBCL. Therefore, we conducted a retrospective study to evaluate the efficacy and safety of zanubrutinib plus salvage chemotherapy for R/R DLBCL.

Materials and methods

Patients

This was a retrospective study of R/R DLBCL patients who received zanubrutinib plus conventional chemotherapy at our center. Patients were enrolled from January 2019 to December 2021. Clinicopathological data were collected using electronic medical records. Follow-up data was obtained from patients' records or by telephone.

Patients were enrolled in this study who met the criteria as follows: age ≥14 years and histologically diagnosed CD20-positive DLBCL with relapsed or refractory disease. The excluded criteria were: central nervous system lymphoma, HIV-positive DLBCL, post-transplant lymphoproliferative disorders, or prior exposure to a BTK inhibitor. Refractory disease was defined as progressive disease (PD) or stable disease (SD) as the best response to chemotherapy or relapse ≤12 months after auto-SCT. Primary refractory DLBCL was defined as non-responders to first-line treatment or patients who relapsed within 3 months of CR or partial remission (PR). Relapse was defined as recurrence of progressive disease after achieving a CR through last-line therapy. Patients with incomplete medical data or those lost to follow-up were excluded from this study. The day of the last follow-up was January, 6th, 2022. The Ethics Committee of the Second Affiliated Hospital, Zhejiang University approved this study, which was conducted in accordance with the Declaration of Helsinki.

Treatment

Salvage chemotherapy regimens included the ICE regimen (ifosfamide, carboplatin and etoposide), GDP regimen (gemcitabine, dexamethasone, and cisplatin) and GemOx regimen (oxaliplatin and gemcitabine). Salvage chemotherapy was selected by treating investigator and the same salvage chemotherapy had not been ever applied before they were enrolled in this study. Patients received rituximab when the patients relapsed >6 months after rituximab-containing treatment or based on their willingness. The dose was reduced by 20%-50% after patients experienced grade-4 adverse events (AEs). Prophylactic pegylated granulocyte colony-stimulating factor (Peg-G-CSF) was administered if grade-4 neutropenia

or grade-3 neutropenia with fever developed in previous cycles of treatment. Zanubrutinib,160 mg orally, twice a day was initially given and the dose was reduced by 50% after patients experienced grade-4 neutropenia or grade-3 neutropenia with fever again in previous cycles of treatment after prophylactic Peg-G-CSF used. The number of cycles was up to 6 cycles with response. Autologous stem cell transplantation (auto-SCT) consolidation was recommended for transplant-eligible patients who achieved remission from combination therapy. Prophylactic antifungal therapy was not routinely used.

Outcomes and toxicity assessments

Patients' responses were assessed according to the revised response criteria for malignant lymphoma every two cycles (8). ^{18}F-fluorodeoxyglucose positron-emission tomography and computed tomography (PET/CT) were used to assess responses after 4 cycles of treatment and upon suspected CR. Patients were regularly followed every 3 to 6 months thereafter. Overall response was defined as a PR or a CR. Covariates including disease stage, B symptoms, cell of origin, and results of immunohistochemical analysis were identified upon diagnosis. The nongerminal center B-cell like (non-GCB) or germinal center B-cell like (GCB) subtype was identified according to Hans's algorithm. Eastern Cooperative Oncology Group (ECOG), Lactate dehydrogenase (LDH), extranodal sites, previous line of therapy, performance status, and disease status were determined before initiating treatment. Adverse events were evaluated according to the National Cancer Institute Common Terminology Criteria for Adverse Events version 5.0.

Targeted panel sequencing

Targeted panel sequencing was performed using a selected panel that contained 11 genes related to DLBCL (NOTCH2, TP53, KMT2D, CD79B, TRAF3, PRDM1, MYD88, CD79A, CXCR4, ARIDIA and LYN). Genomic DNA was extracted from the formalin-fixed paraffin-embedded tumor tissue samples at recurrence or refractory disease. The detailed methods were carried out as described previously (9). The aimed average sequencing depth for all targeted regions was 2000×. Targeted panel sequencing and sequencing data analysis were performed by Idtbio Biotechnology Co. LTD (Hangzhou, China).

Statistical analysis

Patients' characteristics were summarized using descriptive statistical methods. Statistical analyses were performed using SPSS version 17. Statistical values were reported as medians. PFS was defined as initiation of zanubrutinib-based chemotherapy to disease progression or relapse, death of any cause, or last follow-up. OS was defined as initiation of zanubrutinib-based chemotherapy to death from any cause or last follow-up. PFS and OS were plotted according to the Kaplan-Meier method. Survival distributions were compared with the log-rank test. Multivariate analysis was performed using the Cox's proportional hazards model. A two-sided P value <0.05 was considered a significant difference.

Results

Patients' characteristics

We identified 27 patients who received zanubrutinib combined with salvage chemotherapies between January 2019 and December 2021. Patients' baseline data are presented in Table 1. At the time of diagnosis, 74.1% (n=20) patients were presented with Ann-Arbor stages III-IV, 82.5% (n=23) were identified with the non-GCB subtype, 51.9% (n=14) patients exhibited double expression, and 14.8% (n=4) patients exhibited double-hit status. At the time of this study, the median age was 59 (range, 15-72 years), 55.6% (n=15) had an ECOG score of 2-4, 70.5% (n=19) had elevated LDH levels, 66.7% (n=18) had extra-nodal disease, 14.8% (n=4) had relapsed disease, and 85.2% (n=23) had refractory diseases, among which 48.1% (n=13) had primary refractory diseases. The median lines of prior chemotherapies were 2 (range, 1-4). Two patients received prior auto-SCT and one received prior CD19-targeted chimeric antigen receptor T-Cell (CAR-T) immunotherapy.

Efficacy

Overall, 17, 7, and 3 patients received the ICE-based regimen, the GDP-based regimen, or the GemOx-based regimen, respectively. Swimmer plots of all patients evaluable for response are shown in Figure 1A. At the end of follow-up, 3 patients continued treatments, and 24 discontinued treatments. A total of 88 cycles of chemotherapy were administered. The median cycles of treatment were 4 (range, 1-6 cycles). 66.7% (n=18) patients received rituximab treatment.

The final responses and best responses to different combination regimens are shown in Figures 1B, C, respectively. At the end of treatment, 59.3% (n=16) patients had an overall response and 33.3% (n=9) achieved a CR. The best ORR was 74.1% (n=20) with 33.3% (n=9) of CR. Responses were observed in most subgroups (Figure 2), although there was a lower ORR trend in heavily pretreated patients (4-5 lines *vs.* 2-3 lines, 50.0% *vs.* 63.2%) and refractory patients (refractory *vs.* relapsed, 56.5% *vs.* 75%). Furthermore, 46.2% (6/13) patients with primary refractory DLBCL responded. The final ORR of the ICE-based, GDP-based, and GemOx-based groups were 70.6%, 57.1%, and 0%, respectively. The GemOx-based combination regimen was not as

10.3389/fimmu.2022.1015081

TABLE 1 Demographics and baseline characteristics.

Demographic or Characteristic		Cases (%), n=27	
Gender	Male	20	(74.1)
	Female	7	(25.9)
Age (years) at study entry	Median 59 (Range,15-72)		
	<60y	14	(51.9)
	≥60y	13	(48.1)
Hans classification	GCB	4	(14.8)
	Non-GCB	23	(85.2)
Double expression	Yes	14	(51.9)
	No	13	(48.1)
Double hit	Yes	4	(14.8)
	No	23	(85.2)
Ann arbor stage at diagnosis	I-II	7	(25.9)
	III-IV	20	(74.1)
B symptom at diagnosis	Yes	4	(14.8)
	No	23	(85.2)
ECOG at study entry	0-1	12	(44.4)
	2-4	15	(55.6)
LDH at study entry	Elevated	19	(70.5)
	Normal	8	(29.6)
Extra-nodal disease at study entry	Bone	8	(29.6)
	Lung	6	(22.2)
	Liver	3	(11.1)
	Uterus	2	(7.4)
	Breast	2	(7.4)
Prior lines of therapy	1 line	7	(25.9)
	2 lines	12	(44.4)
	3 lines	6	(22.2)
	4 lines	2	(7.4)
Disease status	Refractory	23	(85.1)
	Primary refractory	13	(48.1)
	Relapsed	4	(14.8)
Prior auto-SCT		2	(7.4)
Prior CAR-T treatment		1	(3.7)

ECOG, Eastern Cooperative Oncology Group; LDH, Lactate dehydrogenase; auto-SCT, Autologous stem cell transplantation; CAR-T, Chimeric Antigen Receptor T-Cell; GCB, Germinal center B-cell like.

effective as the other two regimens. Overall, 7.1% (1/14) of transplant-eligible patients proceeded to auto-SCT, and 60% (6/10) of unresponsive patients as well as 2 PR patients proceeded to CD19-targeted CAR-T cell therapy with costimulatory 4-1BB endodomain (ClinicalTrials.gov ID: NCT04833504).

With a median follow-up of 11 months (range, 1-17 months), 15 patients progressed and 7 died. The median PFS was 8.1 months (95%CI, 0.2-15.8) (Figure 3A), but the median OS was not reached (Figure 3B). Univariate and multivariate analyses of PFS and OS are described in Table 2. PFS and OS did not differ significantly regarding cell of origin, age, serum LDH, ECOG, disease status, combination regimen (Figures 3G, H), and subsequent treatment. Univariate analysis revealed that PFS was significantly longer in patients with early treatment (2-3 lines vs 4-5 lines, p=0.029) (Figure 3C) and in those with overall response after chemotherapy (p<0.001) (Figure 3E). Furthermore, univariate analysis revealed that OS was significantly longer in patients with overall response after chemotherapy (p=0.041) (Figure 3F) but not with prior lines of chemotherapies(p=0.819) (Figure 3D). Multivariate analysis revealed that early treatment (HR=0.27, p=0.032) and overall response after chemotherapy (HR=0.06, p<0.001) were independent factors for favorable PFS. Overall response after chemotherapy (HR=0.11, p=0.036) was an independent indicator for favorable OS.

Safety

Treatment-related adverse events are described in Table 3. Neutropenia (n=19, 70.4%) and thrombocytopenia (n=18, 66.7%) were the most common grade 3/4 adverse events. Febrile neutropenia was observed in 33.3% patients (n=9). Platelet transfusion was required for 7.4% (n=2) of patients. The most non-hematologic adverse events were fatigue (n=13, 48.1%), nausea and vomiting (n=14, 51.9%), and bleeding (n=5, 18.5%). One patient developed Grade 4 thrombocytopenia and gastrointestinal bleeding, which were resolved with active symptomatic treatments. Two patients developed grade 1 hematuria and the remaining 2 patients developed grade 1 petechiae when the platelet count was normal. These bleeding disappeared after symptomatic treatments. Atrial fibrillation, aspergillosis, and tumor lysis syndrome were not observed. All toxicities were manageable and reversible. No treatment-related deaths were observed. The categories and severities of adverse events did not significantly vary among the different combination regimens.

Targeted panel sequencing

The gene panel was performed on 8 patients (6 PD and 2 PR with prior zanubrutinib- based chemotherapy), who proceeded to CD19-CAR-T cell therapy. Genomic DNA was extracted from the formalin-fixed paraffin-embedded tumor tissue samples at recurrence or refractory disease. In total, 52 somatic alterations were detected. The patients presented a median of 6 mutations per sample (range 2–9). Missense mutations were the most frequent at 50/52 (96.2%). Figure 4A present the gene mutation frequencies. The most frequently mutated gene was NOTCH2 (8/8) and TP53 (7/8). Mutation location of NOTCH2 and TP53 at the protein level are shown in Figures 4D, E, respectively. The next were mutations of KMT2D and CD79B, which observed simultaneously in 5 cases. MYD88 mutation was identified in only one case, who achieved partial response with zanubrutinib-based chemotherapy. The ORR at 3 months after

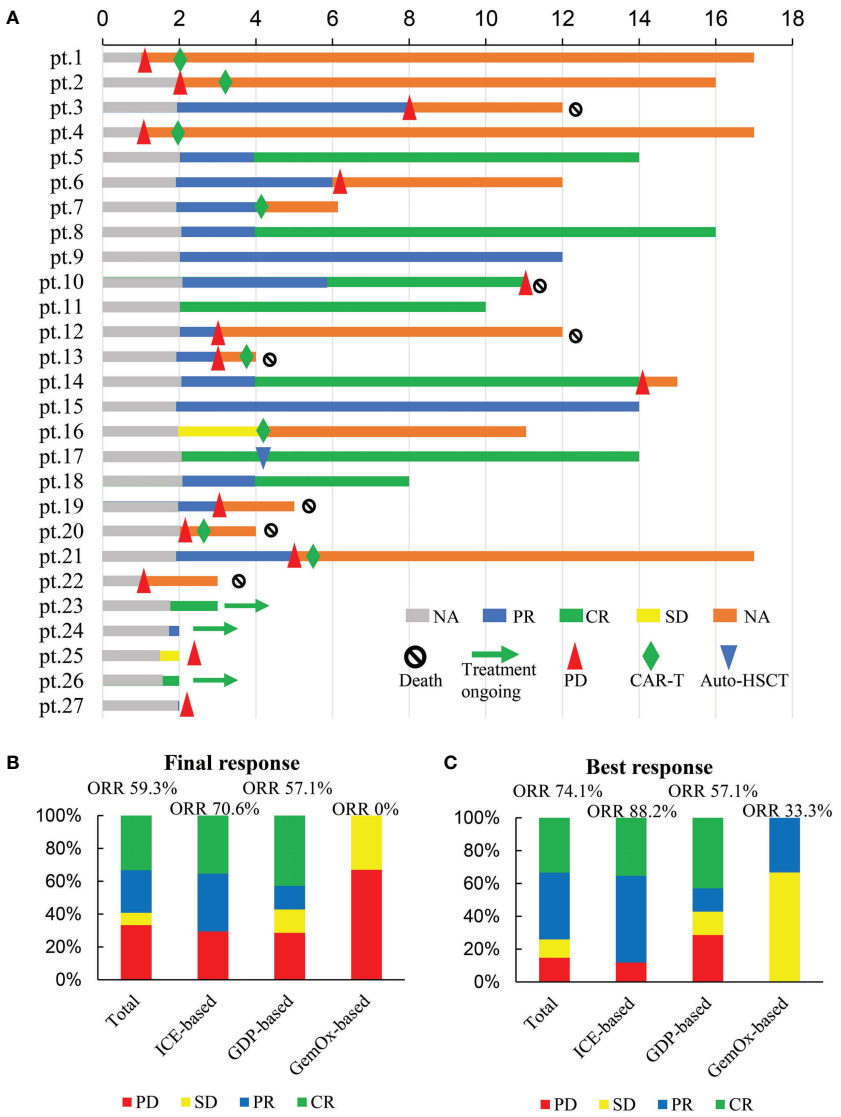

FIGURE 1
Responses to treatment. **(A)** swimmer plots of all patients evaluable for response; **(B)** Final responses to treatment; **(C)** Best responses to treatment.

CAR-T cell therapy were 75% (including 4 cases of CR and 2 cases of PR). With a median follow-up of 9 months from CAR-T cell infusion (range, 1-16 months), the median PFS was 14.5 months (Figure 4B), but the median OS was not reached (Figure 4C).

Discussion

Zanubrutinib (BGB-3111) is a next-generation BTK inhibitor. Previous studies shows that zanubrutinib is more selective and active than ibrutinib in inhibiting BTK activity, with lower off-target activity against the follow protein tyrosine kinases: tyrosine kinase interleukin-2-inducible T-cell kinase (ITK), epidermal growth factor receptor (EGFR), and other kinases expressed in hepatocellular carcinoma (TEC) (10). In the present study, patients benefited from the encouraging efficacy of zanubrutinib plus salvage chemotherapy. The ORR of the present study was 74.1% and the CR rate was 33.3%. The median PFS was 8.1 months, but the median OS was not reached.

The responses and outcomes of BTK inhibitor monotherapy are unsatisfactory (6, 11). Developing mechanistically-based synergistic combinations may open a way to increase response rates and durability of BTK inhibitor. A study employing a high-throughput screening platform found that ibrutinib acted

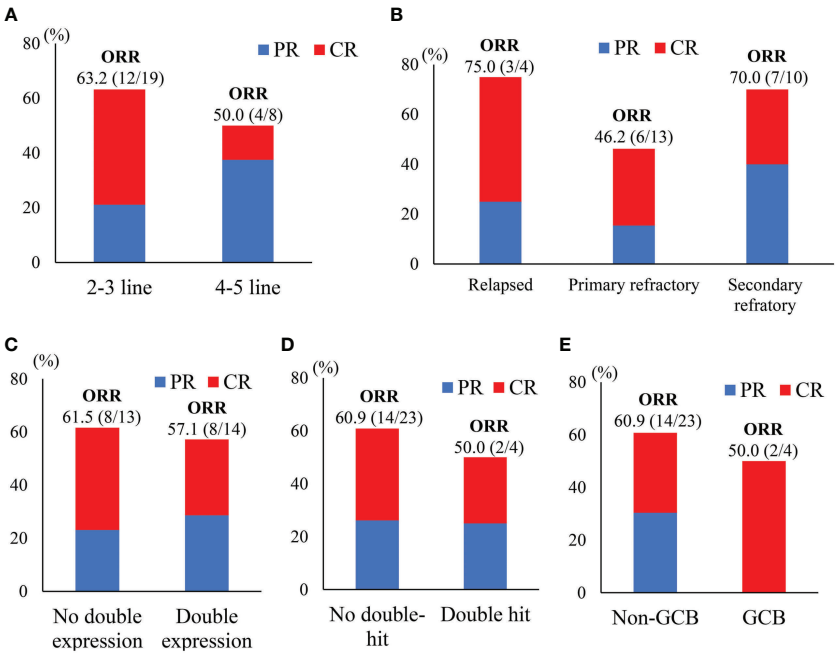

FIGURE 2
Subgroups responses to treatment. **(A)**Treatment lines; **(B)** disease status; **(C)** immunohistochemical analysis; **(D)** with or without double-hit; **(E)** cell of origin based on Hans's algorithm.

synergistically, additively, or both, with standard chemotherapeutic agents (12). A phase 1 study of ibrutinib plus R-ICE in R/R DLBCL demonstrated favorable tolerability and encouraging efficacies with 90% ORR and 55% CR (13). A phase 1/1b study of ibrutinib plus BR (rituximab, and bendamustine) induced 37% ORR and 31% CR in R/R DLBCL. Two patients with R/R DLBCL who received zanubrutinib plus R-DICE or R-DHAP respectively, also achieved a CR (14). Besides conventional salvage chemotherapy regimens, novel agents as BCL-2 inhibitors (venetoclax), immunomodulator(lenalidomide), PI3K inhibitors, XPO1 inhibitors(selinexor), IRAK4 inhibitors, immune checkpoint inhibitors, monoclonal/bispecific antibodies, CAR-T cell therapy and antibody-drug conjugates show strong synergistic activities with BTK inhibitors (12, 15, 16). A phase Ib study evaluated the combination of ibrutinib, lenalidomide, and rituximab for R/R DLBCL. The ORR was 44%, CR rate was 28%, and DOR was 15.9 months (17). Ibrutinib plus durvalumab achieved an ORR of 13% and 38% in GCB and non-GCB DLBCL, respectively (18). Ibrutinib plus venetoclax achieved an ORR of 53.8% after 4 cycles of treatment, and the median DOR、PFS and OS were 11 months, 5.6 months and 11.3 months, respectively (19). Acalabrutinib plus vistusertib (mTORC1/2 inhibitor) accomplished an ORR of 12% for R/R DLBCL (20). Ibrutinib plus buparlisib (a pan-PI3K inhibitor) for 37 patients with R/R DLBCL achieved an ORR of 31% (21). In the REAL-TREND study (22), a real-world retrospective analysis of treatment response of R/R DLBCL from 8 centers in China (including our center), the pooled ORR of salvage chemotherapy was 30% and the CRR was 9%. Our results with high efficacy indicated that zanubrutinib may act synergistically with conventional chemotherapeutic regimens.

DLBCL behaves genetic heterogeneity. Multiple studies have been made to identify sensitive patients who may potentially benefit from BTK inhibitors, based on tumor genetics, clinicopathology features, or both. Ibrutinib proves more effective in ABC-DLBCL (ORR=36.8%) than GCB (ORR=5%) (6). MCD, a genetic subtype of DLBCL with double mutant of *CD79B* and *MYD88*L265P, have inferior outcomes (23). The MCD subtype are more responsive to ibrutinib or zanubrutinib treatment (6, 11). *CD79B* and *MYD88*L265P double mutation are more responsive to ibrutinib, while single mutation is refractory (24, 25). Ibrutinib responders frequently harbor mutations in *KLHL14*, *RNF213*, and *LRP1B*, while non-responders commonly harbor mutations in *EBF1*, *ADAMTS20*, and *AKAP9* (26). Furthermore, mutation of *CARD11* and inactivation of TNFAIP3 (a negative regulator of NF-κB) predict no response to ibrutinib (6, 27). For non-responders to BTK inhibitors, *BTK* mutation are the best-described mechanisms (28). Third-generation non-covalent BTK inhibitors and CAR-T cell therapy, are promising strategies to overcome BTK inhibitor-resistance (29, 30). In the present

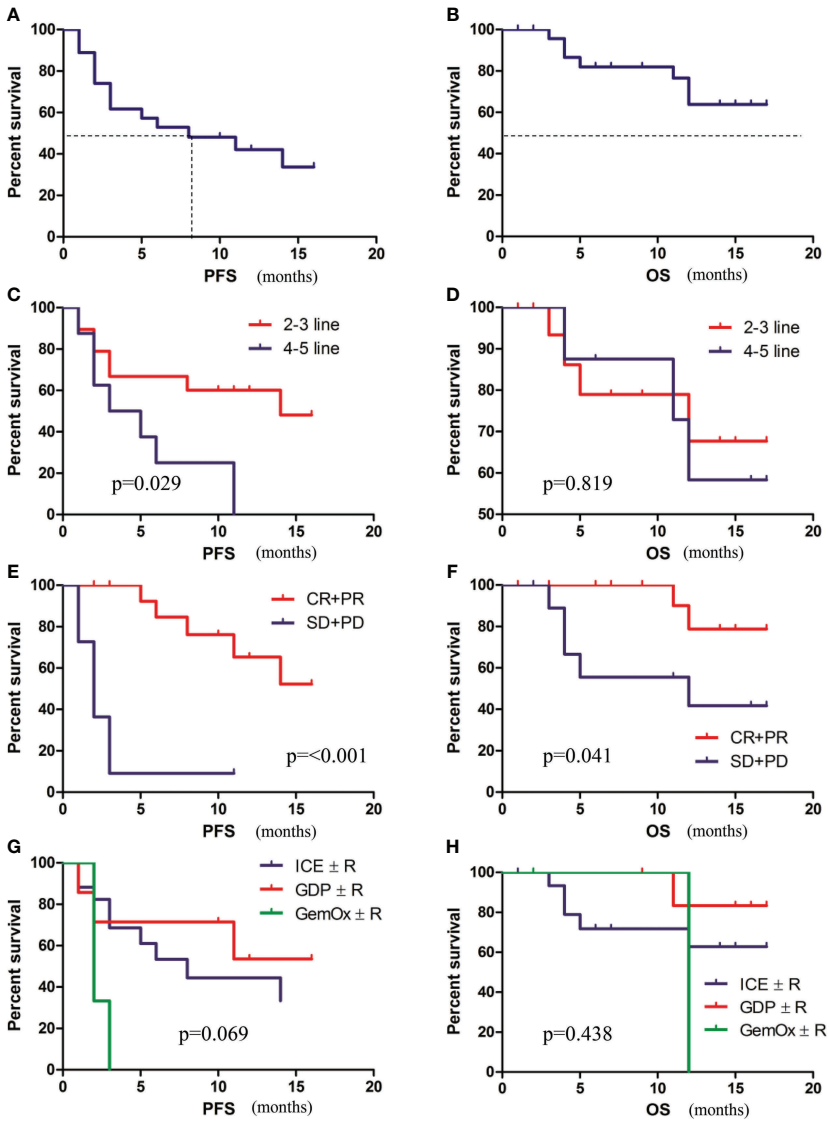

FIGURE 3
Survival analysis of patients. **(A)** PFS of patients. **(B)** OS of patients. **(C)** PFS of patients with early treatment (2-3 lines) versus late treatment (4-5 lines). **(D)** OS of patients with early treatment (2-3 lines) versus late treatment (4-5 lines). **(E)** PFS of patients with or without an overall response. **(F)** OS of patients with or without an overall response. **(G)** PFS according to combination regimens. **(H)** OS PFS according to combination regimens.

study, the majority of the poor responders to zanubrutinib-based treatment had *NOTCH2* mutations and *TP53* mutations, while none was of MCD subtype, indicating that patients without MCD subtype maybe not benefit from BTKi-based treatment. *TP53* is a tumor suppressor gene and *TP53* mutation was an independent prognostic factor for survival in R/R DLBCL. In a retrospective study, in R/R DLBCL patients not treated with CAR-T cells, *TP53* mutation was an independent inferior prognostic factor for OS, but in the CAR-T cell group, this significance could not be shown (31). CAR19/22 T-cell therapy combined with ASCT is efficacious in r/r aggressive B-NHL with *TP53* alterations, producing a best ORR and CRR of 92.9% and 82.1%, respectively (32). However, in another retrospective study, *TP53* alterations (mutations and/or copy number alterations) were still associated with inferior CR and OS rates in R/R DLBCL treated with CD19-CAR-T treatment (33). In our study, among the 7 patients with *TP53* mutations, The ORR at 3 months after CAR-T cell therapy was 85.7% and the CRR was 57.1%. Compared with the results of TRANSCEND NHL 001study (Liso-cell) with the same costimulatory endodomain and similar follow-up time (ORR of 73% and CRR of 53%) (34), it seemed that the CAR-T cell therapy for patients with *TP53* mutations was still highly effective. Although the prognostic value of *TP53* mutations in R/R DLBCL patients receiving

10.3389/fimmu.2022.1015081

TABLE 2 Univariate and multivariate analyses of overall and progression-free survival.

Variable	PFS						OS					
	Univariate analysis			Multivariate analysis			Univariate analysis			Multivariate analysis		
	HR	95%CI	P-value	HR	95%CI	P-value	HR	95%CI	P-value	HR	95%CI	P-value
Age ≥60y	0.75	0.24-2.13	0.573				1.19	0.26-5.33	0.819			
ECOG 2-4	1.45	0.51-4.09	0.468				5.39	0.65-44.9	0.075	5.17	0.50-53.1	0.162
Elevated LDH	1.46	0.41-5.21	0.544				1.42	0.14-3.75	0.694			
Double expression	1.04	0.37-2.87	0.943				2.68	0.52-12.9	0.214			
Non-GCB cell of origin	0.42	0.13-1.35	0.927				0.49	0.09-2.54	0.604			
Combination Regimen	0.28	0.69-1.13	0.069	0.59	0.13-2.66	0.253	0.38	0.04-3.30	0.438	0.27	0.01-5.43	0.386
Early treatment (2-3 line)	0.34	0.12-0.98	0.029	0.27	0.08-0.89	0.032	0.84	0.19-3.77	0.819	0.88	0.14-5.67	0.895
Overall response at the end of treatment	0.11	0.03-0.38	<0.001	0.06	0.01-0.28	<0.001	0.22	0.04-1.12	0.041	0.11	0.02-0.87	0.036
Subsequent CAR-T cell therapy or auto-SCT	0.96	0.34-2.70	0.633				0.36	0.07-1.84	0.323			

CI, confidential interval; HR, hazard ratio; ECOG, Eastern Cooperative Oncology Group; non-GCB, non-germinal center B-cell; LDH, lactate dehydrogenase; ORR, overall response rate; OS, overall survival; PFS, progression-free survival.

CAR-T cells is still undefined, CAR-T cell therapy may be a priority strategy for these patients.

As we expected, grade 3 and higher hematological toxicities were the major concern during and after zanubrutinib plus chemotherapy for patients with R/R DLBCL. Grade 3/4 neutropenia and thrombocytopenia of sole R-ICE regimen for R/R DLBCL occurred in 16% and 17.8% patients, respectively (35). Grade 3/4 neutropenia and thrombocytopenia of single

TABLE 3 Main adverse effects by treatment group.

Toxicities	Total (n=27)	ICE-based (n=17)	GDP-based (n=7)	GemOx-based (n=3)
Hematologic, n (%)				
Neutropenia	26 (96.3%)	17 (100%)	6 (85.7%)	3 (100%)
Grade 1-2	7 (25.9%)	3 (17.6%)	2 (28.6%)	2 (66.7%)
Grade 3-4	19 (70.4%)	14 (82.4%)	4 (57.1%)	1 (33.3%)
Anemia	24 (88.9%)	15 (88.2%)	6 (85.7%)	3 (100%)
Grade 1-2	16 (59.3%)	9 (52.9%)	4 (57.91%)	3 (100%)
Grade 3-4	8 (29.6%)	6 (35.3%)	2 (28.6%)	0 (0%)
Thrombopenia	24 (88.9%)	15 (88.2%)	7 (100%)	2 (66.7%)
Grade1-2	6 (22.2%)	5 (29.4%)	1 (14.3%)	0 (0%)
Grade3-4	18 (66.7%)	10 (58.8%)	6 (85.7%)	2 (66.7%)
Febrile neutropenia	9 (33.3%)	5 (29.4%)	4 (57.1%)	0 (0%)
Non-hematologic, n (%)				
Fatigue	13 (48.1%)	9 (52.9%)	3 (42.9%)	1 (33.3%)
Grade1-2	12 (44.4%)	8 (47.1%)	3 (42.9%)	1 (33.3%)
Grade3-4	1 (3.7%)	1 (5.8%)	0 (0%)	0 (0%)
Nausea and vomiting	14 (51.9%)	11 (64.7%)	2 (28.6%)	1 (33.3%)
Grade1-2	14 (51.9%)	11 (64.7%)	2 (28.6%)	1 (33.3%)
Grade3-4	0 (0%)	0 (0%)	0 (0%)	0 (0%)
Hepatotoxicity	1 (3.7%)	1 (14.3%)	0 (0%)	0 (0%)
Grade1-2	1 (3.7%)	1 (14.3%)	0 (0%)	0 (0%)
Grade3-4	0 (0%)	0 (0%)	0 (0%)	0 (0%)
Bleeding	5 (18.5%)	5 (71.4)	0 (0%)	0 (0%)
Grade1-2	4 (14.8%)	4 (57.1%)	0 (0%)	0 (0%)
Grade3-4	1 (3.7%)	1 (14.3%)	0 (0%)	0 (0%)
Atrial fibrillation	0 (0%)	0 (0%)	0 (0%)	0 (0%)
Diarrhea	0 (0%)	0 (0%)	0 (0%)	0 (0%)

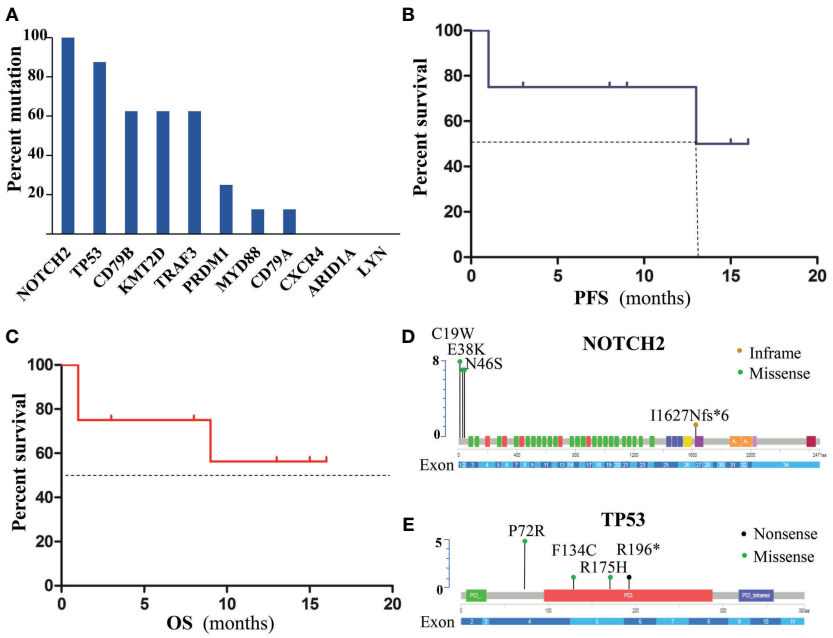

FIGURE 4
Gene mutations of patients with poor response to treatment. **(A)**Frequency of gene mutations. **(B)** PFS of patients. **(C)** OS of patients. **(D)** mutation location of NOTCH2 at the protein level. **(E)** TP53 Mutations at the protein level.

zanubrutinib for R/R DLBCL occurred in 7.3% and 2.4% patients, respectively. In our present study, grade 3/4 neutropenia and thrombocytopenia of by zanubrutinib plus chemotherapy occurred in 70.4% and 66.7% of patients, respectively. Higher rates of hemorrhage were observed in 18.5% patients, which may be explained by thrombocytopenia and off-target activity of zanubrutinib. All above safety data showed that zanubrutinib plus chemotherapy increased myelosuppression. Fortunately, all hematological toxicities are manageable and reversible. There were no serious infectious complications or treatment-related mortality. To relieve bone marrow suppression, prophylactic Peg-G-CSF and recombinant human thrombopoietin (rhTPO) are required, and dose-modified salvage chemotherapy may also reduce hematologic toxicities. Regarding different BTK inhibitors, a phase 3 study demonstrated that the incidence and severity of BTK inhibitor toxicities were lower with zanubrutinib than ibrutinib in Waldenström macroglobulinemia (7). The efficacy and safety of zanubrutinib versus ibrutinib for CLL/SLL is ongoing in a head-to-head phase 3 study (36).

Our current study has several limitations. First, this study was insufficiently powered limited by the small sample size and short follow-up. Second, there were variations in prior therapies, which limit comparability. For example, only two patients received upfront auto-SCT in our study. Third, there were no genetic data available to demonstrate the underlying mechanisms of such synergistic combination. Nevertheless, the high activity of zanubrutinib combined with conventional chemotherapy, provides a new strategy for R/R DLBCL, and may serve as a bridge treatment to CAR-T cell therapy.

In conclusion, our study showed that zanubrutinib combined with salvage chemotherapy may serve as an effective salvage therapy for R/R DLBCL with manageable toxicity. Patients without MCD subtype maybe not benefit from BTKi-based treatment. CAR-T cell therapy may be a priority strategy for these poor responders to BTKi-based treatment. Further investigations of larger study populations are warranted to identify the most effective combination regimens and to precisely select patients.

Data availability statement

The original contributions presented in the study are included in the article/supplementary material. Further inquiries can be directed to the corresponding authors.

Ethics statement

The studies involving human participants were reviewed and approved by The Ethics Committee of the Second Affiliated

Hospital, Zhejiang University. The patients/participants provided their written informed consent to participate in this study.

Author contributions

Conceptualization, YL and WQ; Methodology, XY; Software, YH and XL; Validation, XL; Formal Analysis, YH and HL; Investigation, XY, XL, and YH; Resources, YL and WQ; Data Curation, HL and AZ; Writing – Original Draft Preparation, XY; Writing -Review and Editing, WZ, WQ and YL: Visualization, XJ; Supervision, YL and WQ; Project Administration, XY; Funding Acquisition, WQ. All authors contributed to the article and approved the submitted version.

Funding

This work was supported by funds from Translational Research Grant of HCRCH (2020ZKZC01), the National Natural Science Foundation of China (No. 81830006), and the Natural Science Foundation of Zhejiang Province of China (No. LY15H160038).

Conflict of interest

The authors declare that the research was conducted in the absence of any commercial or financial relationships that could be construed as a potential conflict of interest.

Publisher's note

References

1. Teras LR, DeSantis CE, Cerhan JR, Morton LM, Jemal A, Flowers CR. US Lymphoid malignancy statistics by world health organization subtypes. *CA: Cancer J Clin* (20162016) 66(6):443–59. doi: 10.3322/caac.21357

2. Sun J, Yang Q, Lu Z, He M, Gao L, Zhu M, et al. Distribution of lymphoid neoplasms in China: analysis of 4,638 cases according to the world health organization classification. *Am J Clin Pathol* (2012) 138(3):429–34. doi: 10.1309/AJCP7YLTQPUSDQ5C

3. Habermann TM, Weller EA, Morrison VA, Gascoyne RD, Cassileth PA, Cohn JB, et al. Rituximab-CHOP versus CHOP alone or with maintenance rituximab in older patients with diffuse large b-cell lymphoma. *J Clin Oncol* (2006) 24(19):3121–7. doi: 10.1200/JCO.2005.05.1003

4. Coiffier B, Thieblemont C, Van Den Neste E, Lepeu G, Plantier I, Castaigne S, et al. Long-term outcome of patients in the LNH-98.5 trial, the first randomized study comparing rituximab-CHOP to standard CHOP chemotherapy in DLBCL patients: a study by the groupe d'Etudes des lymphomes de l'Adulte. *Blood* (2010) 116(12):2040–5. doi: 10.1182/blood-2010-03-276246

5. Crump M, Neelapu SS, Farooq U, Van Den Neste E, Kuruvilla J, Westin J, et al. Outcomes in refractory diffuse large b-cell lymphoma: results from the international SCHOLAR-1 study. *Blood* (2017) 130(16):1800–8. doi: 10.1182/blood-2017-03-769620

6. Wilson WH, Young RM, Schmitz R, Yang Y, Pittaluga S, Wright G, et al. Targeting b cell receptor signaling with ibrutinib in diffuse large b cell lymphoma. *Nat Med* (2015) 21(8):922–6. doi: 10.1038/nm.3884

7. Tam CS, Opat S, D'Sa S, Jurczak W, Lee H-P, Cull G, et al. A randomized phase 3 trial of zanubrutinib vs ibrutinib in symptomatic waldenström macroglobulinemia: the ASPEN study. *Blood* (2020) 136(18):2038–50. doi: 10.1182/blood.2020006844

8. Cheson BD, Pfistner B, Juweid ME, Gascoyne RD, Specht L, Horning SJ, et al. Revised response criteria for malignant lymphoma. *J Clin Oncol* (2007) 25(5):579–86. doi: 10.1200/JCO.2006.09.2403

9. Jiang S, Qin Y, Jiang H, Liu B, Shi J, Meng F, et al. Molecular profiling of Chinese r-CHOP treated DLBCL patients: Identifying a high-risk subgroup. *Int J Cancer* (2020) 147(9):2611–20. doi: 10.1002/ijc.33049

10. Tam CS, Trotman J, Opat S, Burger JA, Cull G, Gottlieb D, et al. Phase 1 study of the selective BTK inhibitor zanubrutinib in b-cell malignancies and safety and efficacy evaluation in CLL. *Blood* (2019) 134(11):851–9. doi: 10.1182/blood.2019001160

11. Yang H, Xiang B, Song Y, Zhang H, Zhao W, Zou D-H, et al. Zanubrutinib monotherapy for relapsed or refractory non-germinal center diffuse Large b-cell lymphoma. *Blood Adv* (2022) 6(6):1629–36. doi: 10.1182/bloodadvances.2020003698

12. Mathews Griner LA, Guha R, Shinn P, Young RM, Keller JM, Liu D, et al. High-throughput combinatorial screening identifies drugs that cooperate with ibrutinib to kill activated b-cell-like diffuse large b-cell lymphoma cells. *P Natl Acad Sci USA* (2014) 111(6):2349–54. doi: 10.1073/pnas.1311846111

13. Sauter CS, Matasar MJ, Schoder H, Devlin SM, Drullinsky P, Gerecitano J, et al. A phase 1 study of ibrutinib in combination with r-ICE in patients with relapsed or primary refractory DLBCL. *Blood* (2018) 131(16):1805–8. doi: 10.1182/blood-2017-08-802561

14. Zhang Y, Li Y, Zhuang Z, Wang W, Wei C, Zhao D, et al. Preliminary evaluation of zanubrutinib-containing regimens in DLBCL and the cerebrospinal fluid distribution of zanubrutinib: A 13-case series. *Front Oncol* (2021) 11:760405. doi: 10.3389/fonc.2021.760405

15. Schaffer M, Chaturvedi S, Davis C, Aquino R, Stepanchick E, Versele M, et al. Identification of potential ibrutinib combinations in hematological malignancies using a combination high-throughput screen. *Leukemia Lymphoma* (2018) 59(4):931–40. doi: 10.1080/10428194.2017.1349899

16. Sehn LH, Salles G. Diffuse Large b-cell lymphoma. *N Engl J Med* (2021) 384 (9):842–58. doi: 10.1056/NEJMra2027612

17. Goy A, Ramchandren R, Ghosh N, Munoz J, Morgan DS, Dang NH, et al. Ibrutinib plus lenalidomide and rituximab has promising activity in relapsed/refractory non-germinal center b-cell-like DLBCL. *Blood* (2019) 134(13):1024–36. doi: 10.1182/blood.2018891598

18. Herrera AF, Goy A, Mehta A, Ramchandren R, Pagel JM, Svoboda J, et al. Safety and activity of ibrutinib in combination with durvalumab in patients with relapsed or refractory follicular lymphoma or diffuse large b-cell lymphoma. *Am J hematology* (2020) 95(1):18–27. doi: 10.1002/ajh.25659

19. Zhou Z, Zhang L, Wang X, Li X, Li L, Fu X, et al. Ibrutinib combined with venetoclax for the treatment of relapsed/refractory diffuse large b cell lymphoma. *Ann hematology* (2021) 100(6):1509–16. doi: 10.1007/s00277-021-04535-7

20. Collins GP, Clevenger TN, Burke KA, Yang B, MacDonald A, Cunningham D, et al. A phase 1/2 study of the combination of acalabrutinib and vistusertib in patients with relapsed/refractory b-cell malignancies. *Leukemia Lymphoma* (2021) 62(11):2625–36. doi: 10.1080/10428194.2021.1938027

21. Stewart CM, Michaud L, Whiting K, Nakajima R, Nichols C, De Frank S, et al. Phase I/Ib study of the efficacy and safety of buparlisib and ibrutinib therapy in MCL, FL, and DLBCL with serial cell-free DNA monitoring. *Clin Cancer Res* (2022) 28(1):45–56. doi: 10.1158/1078-0432.CCR-21-2183

22. Wang S, Wang L, Hu J, Qian W, Zhang X, Hu Y, et al. Outcomes in refractory diffuse large b-cell lymphoma: results from a multicenter real-world study in China. *Cancer Commun (Lond)* (2021) 41(3):229–39. doi: 10.1002/cac2.12126

23. Schmitz R, Wright GW, Huang DW, Johnson CA, Phelan JD, Wang JQ, et al. Genetics and pathogenesis of diffuse Large b-cell lymphoma. *New Engl J Med* (2018) 378(15):1396–407. doi: 10.1056/NEJMoa1801445

24. Wang YL. MYD88 mutations and sensitivity to ibrutinib therapy. *J Mol Diagn* (2018) 20(2):264–6. doi: 10.1016/j.jmoldx.2017.11.006

25. Younes A, Sehn LH, Johnson P, Zinzani PL, Hong X, Zhu J, et al. Randomized phase III trial of ibrutinib and rituximab plus cyclophosphamide, doxorubicin, vincristine, and prednisone in non-germinal center b-cell diffuse Large b-cell lymphoma. *J Clin Oncol* (2019) 37(15):1285–95. doi: 10.1200/JCO.18.02403

26. Hodkinson BP, Schaffer M, Brody JD, Jurczak W, Carpio C, Ben-Yehuda D, et al. Biomarkers of response to ibrutinib plus nivolumab in relapsed diffuse large b-cell lymphoma, follicular lymphoma, or richter's transformation. *Transl Oncol* (2021) 14(1):100977. doi: 10.1016/j.tranon.2020.100977

27. Bartlett NL, Costello BA, LaPlant BR, Ansell SM, Kuruvilla JG, Reeder CB, et al. Single-agent ibrutinib in relapsed or refractory follicular lymphoma: a phase 2 consortium trial. *Blood* (2018) 131(2):182–90. doi: 10.1182/blood-2017-09-804641

28. Woyach JA, Furman RR, Liu T-M, Ozer HG, Zapatka M, Ruppert AS, et al. Resistance mechanisms for the bruton's tyrosine kinase inhibitor ibrutinib. *New Engl J Med* (2014) 370(24):2286–94. doi: 10.1056/NEJMoa1400029

29. Ondrisova L, Mraz M. Genetic and non-genetic mechanisms of resistance to BCR signaling inhibitors in b cell malignancies. *Front Oncol* (2020) 10:591577. doi: 10.3389/fonc.2020.591577

30. Gauthier J, Hirayama AV, Purushe J, Hay KA, Lymp J, Li DH, et al. Feasibility and efficacy of CD19-targeted CAR T cells with concurrent ibrutinib for CLL after ibrutinib failure. *Blood* (2020) 135(19):1650–60. doi: 10.1182/blood.2019002936

31. Porpaczy E, Wohlfarth P, Königsbrügge O, Rabitsch W, Skrabs C, Staber P, et al. Influence of mutation on survival of diffuse Large b-cell lymphoma in the CAR T-cell era. *Cancers (Basel)* (2021) 13(22):5592. doi: 10.3390/cancers13225592

32. Wei J, Xiao M, Mao Z, Wang N, Cao Y, Xiao Y, et al. Outcome of aggressive b-cell lymphoma with TP53 alterations administered with CAR T-cell cocktail alone or in combination with ASCT. *Signal Transduct Target Ther* (2022) 7(1):101. doi: 10.1038/s41392-022-00924-0

33. Shouval R, Alarcon Tomas A, Fein JA, Flynn JR, Markovits E, Mayer S, et al. Impact of genomic alterations in Large b-cell lymphoma treated with CD19-chimeric antigen receptor T-cell therapy. *J Clin Oncol* (2022) 40(4):369–81. doi: 10.1200/JCO.21.02143

34. Abramson JS, Palomba ML, Gordon LI, Lunning MA, Wang M, Arnason J, et al. Lisocabtagene maraleucel for patients with relapsed or refractory large b-cell lymphomas (TRANSCEND NHL 001): A multicentre seamless design study. *Lancet (London England)* (2020) 396(10254):839–52. doi: 10.1016/S0140-6736(20)31366-0

35. Gisselbrecht C, Glass B, Mounier N, Singh Gill D, Linch DC, Trneny M, et al. Salvage regimens with autologous transplantation for relapsed large b-cell lymphoma in the rituximab era. *J Clin Oncol* (2010) 28(27):4184–90. doi: 10.1200/JCO.2010.28.1618

36. Hillmen P, Brown JR, Eichhorst BF, Lamanna N, O'Brien SM, Qiu L, et al. ALPINE: zanubrutinib versus ibrutinib in relapsed/refractory chronic lymphocytic leukemia/small lymphocytic lymphoma. *Future Oncol (London England)* (2020) 16(10):517–23. doi: 10.2217/fon-2019-0844

frontiers | Frontiers in Oncology

TYPE Original Research
PUBLISHED 16 January 2023
DOI 10.3389/fonc.2022.977251

OPEN ACCESS

EDITED BY
Xuyao Zhang,
Fudan University, China

REVIEWED BY
Tao Xin,
The First Affiliated Hospital of Shandong First Medical University, China
Chongming Jiang,
Baylor College of Medicine, United States

*CORRESPONDENCE
Shaoshan Hu
shaoshanhu421@163.com
Hang Ji
jih723@hrbmu.edu.cn

†These authors have contributed equally to this work

SPECIALTY SECTION
This article was submitted to Cancer Immunity and Immunotherapy, a section of the journal Frontiers in Oncology

RECEIVED 24 June 2022
ACCEPTED 28 December 2022
PUBLISHED 16 January 2023

CITATION
Dong J, Wang F, Gao X, Zhao H, Zhang J, Wang N, Liu Z, Yan X, Jin J, Ba Y, Ma S, Du J, Ji H and Hu S (2023) Integrated analysis of genome-wide DNA methylation and cancer-associated fibroblasts identified prognostic biomarkers and immune checkpoint blockade in lower grade gliomas. *Front. Oncol.* 12:977251. doi: 10.3389/fonc.2022.977251

Integrated analysis of genome-wide DNA methylation and cancer-associated fibroblasts identified prognostic biomarkers and immune checkpoint blockade in lower grade gliomas

Jiawei Dong[1,2†], Fang Wang[1,2†], Xin Gao[1], Hongtao Zhao[1,2], Jiheng Zhang[1,2], Nan Wang[1,2], Zhihui Liu[1,2], Xiuwei Yan[1,2], Jiaqi Jin[1,2], Yixu Ba[1,2], Shuai Ma[1,2], Jianyang Du[1], Hang Ji[1,2*] and Shaoshan Hu[1,2*]

[1]Cancer Center, Department of Neurosurgery, Zhejiang Provincial People's Hospital, Affiliated People's Hospital, Hangzhou Medical College, Hangzhou, Zhejiang, China, [2]Department of Neurosurgery, The Second Affiliated Hospital of Harbin Medical University, Harbin, China

Background: Cancer-associated fibroblasts (CAFs) are vital components of prominent cellular components in lower-grade gliomas (LGGs) that contribute to LGGs' progression, treatment resistance, and immunosuppression. Epigenetic modification and immunity have significant implications for tumorigenesis and development.

Methods: We combined aberrant methylation and CAFs abundances to build a prognostic model and the impact on the biological properties of LGGs. Grouping based on the median CAFs abundances score of samples in the TCGA-LGGs dataset, differentially expressed genes and aberrantly methylated genes were combined for subsequent analysis.

Results: We identified five differentially methylated and expressed genes (LAT32, SWAP70, GSAP, EMP3, and SLC2A10) and established a prognostic gene signature validated in the CGGA-LGGs dataset. Immunohistochemistry (IHC) and in vitro tests were performed to verify these expressions. The high-risk group increased in tumor-promoting immune cells and tumor mutational burden. Notably, risk stratification had different ICB sensitivities in LGGs, and there were also significant sensitivity differences for temozolomide and the other three novel chemotherapeutic agents.

Conclusion: Our study reveals characteristics of CAFs in LGGs, refines the direct link between epigenetics and tumor stroma, and might provide clinical implications for guiding tailored anti-CAFs therapy in combination with immunotherapy for LGGs patients.

KEYWORDS

DNA methylation, cancer-associated fibroblasts, lower-grade gliomas, prognosis, immune checkpoint blockade

1 Introduction

Lower-grade gliomas (LGGs) including World Health Organization (WHO) grade II and III diffuse gliomas are slow-growing infiltrative brain tumors (1). Although the survival of LGGs patients after standardized treatment is better than that of glioblastoma (GBM), recurrent LGGs inevitably progress to GBM (2). With advances in the 2021 WHO Classification of Tumors of the Central nervous system, the understanding of molecular typing for glioma is gradually increasing. Exploration of epigenetics can help us better understand LGGs' immunity and prognosis.

DNA methylation and gene expression are promising sources for identifying glioma's molecular biomarkers. For instance, the promoter hypermethylation and epigenetic silencing of the O6-methylguanine-DNA methyltransferase (MGMT) gene have become a classical biomarker for temozolomide resistance glioma (3, 4). DNA demethylation and upregulation of IGF2BP3 can be involved in the malignant progression of glioma (5). Alternated DNA methylation in ZDHHC12 is associated with migration and invasion capabilities in glioma cell lines (6). GPX8 expression was correlated to the reduced DNA methylation at the promoter region and might be related to cancer-associated fibroblasts and immune infiltration levels in glioma (7). However, the clinical impact of these studies remains limited. Either due to the lack of drugs targeting these potential biomarkers or because of a breakthrough in immunotherapy.

Cancer-associated fibroblasts (CAFs) are the significant members of tumor stroma cells in the tumor microenvironment (TME) (8). Research on the significance of CAFs in cancer has recently gained momentum. Accumulating evidence has indicated that CAFs significantly affect tumor progression and migration, promote epithelial-mesenchymal transition (EMT), and induce chemoresistance and immunosuppression (9–12). On the other hand, CAFs and extracellular matrices constitute the tumor immune escape initiation mechanism (13). In response to this problem, harnessing CAFs-related immunosuppressive stromal environment has been proposed to ameliorate the response to immune checkpoint inhibitors (14, 15). However, whether CAFs are associated with the predictive value and immunotherapy of LGGs patients has not been elucidated.

We reasoned that LGGs samples with different CAFs scores broadly alter methylation levels and immune infiltration patterns. To verify the conjecture, we used a median of CAFs score as the grouping basis for the sample to gather genome-wide methylation and gene expression data to locate the altered methylations coupled with altered expression of the same genes. Then we constructed a risk score system containing five risk genes and validated them at tissue-level and cell-level. We found the risk score is an excellent predictive value for survival and a potential factor for immune checkpoint blockade (ICB) therapies. Applying this prognostic gene signature, the sensitivity of GDC0941, Bleomycin, and Axitinib showed a significant difference in sensitivity within the subgroups. These drugs may have different effects on patients with different levels of CAFs infiltration.

2 Material and methods

2.1 Data acquisition

RNA-seq data and clinical data on LGGs were extracted from The Cancer Genome Atlas (TCGA, https://portal.gdc.cancer.gov/) and Chinese Glioma Genome Atlas (CGGA, http://www.cgga.org.cn/). After transcripts per million (TPM) conversion, we held genes with expression levels larger than 0.1 TPM for analysis. Matched Normal data: 105 cortex tissues were obtained from the GTEx project (https://commonfund.nih.gov/GTEx/). We downloaded both methylation data (Illumina Infinium HumanMethylation450 BeadChip) and somatic mutation data generated by TCGA from the UCSC Xena browser (https://xenabrowser.net/hub/) (16). Fibroblast and glioma cell lines from The Cancer Cell Line Encyclopedia (CCLE) (https://portals.broadinstitute.org/ccle) (17). Infiltration Estimation for TCGA-LGGs was collected from TIMER2.0 (http://timer.comp-genomics.org/). The STRING (https://www.string-db.org) database produced the protein-protein interaction network and reconstructed them *via* Cytoscape software. A flowchart of the entire procedure can be shown in Figure 1.

2.3 Analysis of DNA methylation data

The Illumina HumanMethylation450 BeadChip array contains probes covering 99% of reference sequence genes and 96% of CpG islands. The raw methylation intensities for each probe were represented as β-values, which were converted into M-values with R package Lumi for statistics analysis (18). 5'-C-phosphate-G-3' (CpG) methylation data between different groups were compared with R package limma to identify differentially methylated CpG sites. Benjamini-Hochberg (BH) method was used to adjust p-value as a false discovery rate (FDR). The CpG site and gene mapping files were downloaded from illumine (https://www.illumina.com/). CpGs span various gene regions, including 1500 bp and 200 bp upstream of the transcription start sites (TSS1500 and TSS200, respectively). The average β-values for each region were calculated according to all CpG sites at the corresponding region, and the average β-value was converted to an M-value. Average regional methylation data between different groups were compared with R package limma to identify differentially methylated regions (DMRs). The hypermethylated DMRs with a threshold of adjusted p-value< 0.05 combined a delta β-value > 0.2, and the hypomethylated DMRs with a threshold of adjusted p-value< 0.05 combined a delta β-value< −0.2. Genes harboring DMRs in any part of the gene features were differentially methylated genes (DMGs). The equations described above are listed below.

$$M_i = \log_2\left(\frac{\beta_i}{1-\beta_i}\right) \tag{1}$$

$$\beta_{region} = 2^{\left(\sum_{i=1}^{k} \log 2(\beta_i)\right)/k} \tag{2}$$

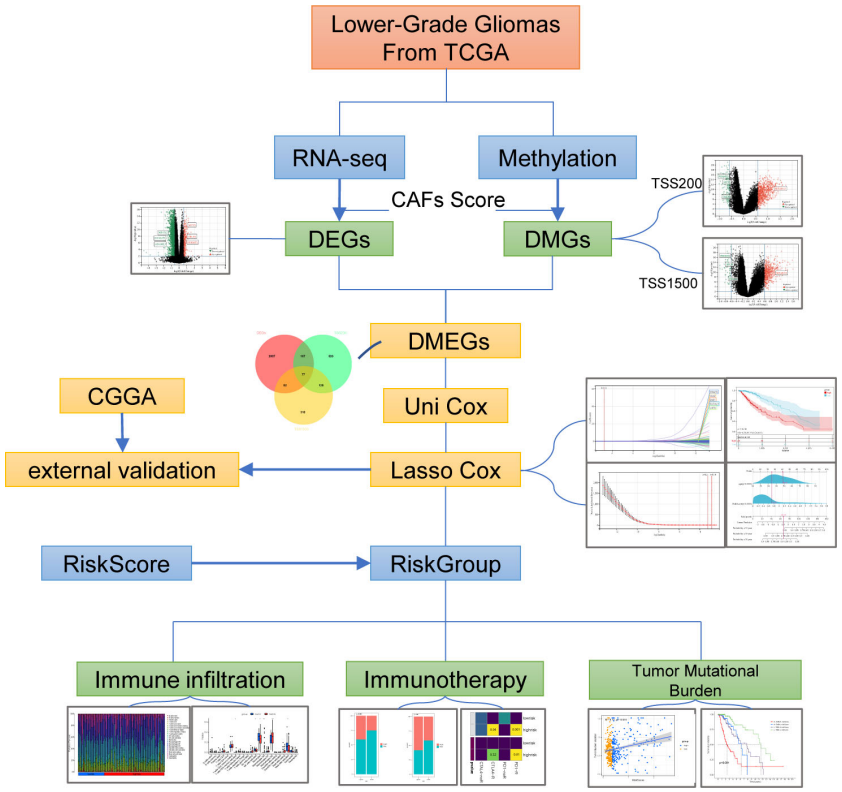

FIGURE 1
Study Flow Chart.

where M is the intensity of the methylated allele, i = 1, 2, 3,…, k, and k is the number of CpG sites in a region.

2.4 Cancer-associated fibroblasts (CAFs) infiltration estimation and immune score calculation

CAFs abundances were separately estimated *via* Estimate the Proportion of Immune and Cancer cells (EPIC) algorithm using the R package Immunedeconv (19). TCGA-LGGs were divided into a high-CAFs-score group and a low-CAFs-score group according to the median score. The estimated immune and stromal scores were computed using the R package ESTIMATE.

2.5 Analysis of DEGs and DMGs

Differential expression between the high-CAFs-score and low-CAF-score group samples was analyzed with the R package limma. False discovery rate (FDR) as adjusted p-value using the Benjamini-Hochberg (BH) method. The fold change was log2-transformed. Differentially expressed genes (DEGs) were calculated with a difference > 1.5-fold and p< 0.01. Methylation analysis results were carried out for joint analysis. Venn diagram analyses were performed to calculate the intersection of DMGs and DEGs and explored the differentially methylated and expressed genes (DMEGs). DMEGs were grouped according to four expression patterns: HypoUp, HypoDown, HyperUp, and HyperDown.

2.6 Functional enrichment analyses

To functionally annotate DMEGs of this study, Gene Ontology (GO) including biological process (BP), cellular component (CC), and molecular function (MF) analysis was performed in the R package ClusterProfiler (20). A p-value of< 0.05 and an FDR of< 0.05 were used for the cutoff value. The ClueGO Plugin version 2.5.8 in Cytoscape Version 3.8.2 was employed to identify hub genes and functional analysis (21).

2.7 Construction and validation of the risk score system

We selected HypoDown and HyperUp genes in TSS200 and TSS1500 for univariate cox regression analysis and filtrated the prognostic-related genes. Subsequently, we used the R package glmnet to conduct the least absolute shrinkage and selection operator (LASSO) Cox regression algorithm and develop a potential risk signature. The minimum value of lambda was derived from 1,000 cross-validations ('1-se' lambda), and which corresponding partial likelihood deviance value was the smallest for the risk model. Coefficients with regression were confirmed by the "cvfit" function with 1000 repeats. The risk score calculating equation, which contains five risk genes, is:

$$Riskscore = \sum_{i=1}^{n} Coef_i * x_i \quad (3)$$

where $Coef_i$ means the coefficients, x_i is the expression value of each gene.

The predictive power of the prognostic signature was evaluated by the receiver-operating characteristic (ROC) curve. The independent clinical factor was validated by multivariate Cox regression analysis. Finally, a nomogram was constructed according to independent predictors. The calibration of the nomogram was evaluated by the calibration curve to assess the goodness of 1-, 3-, and 5-year overall survival.

2.8 Analysis of immunological characteristics

In this study, the mRNA expression matrix of LGGs was analyzed using the CIBERSORT R script downloaded from http://cibersort.stanford.edu. Based on deconvolution, we estimated the abundance of immune cell populations. The relationship between each immune cell and survival was measured by Kaplan-Meier (KM) survival analysis. We evaluated a total of 60 immune checkpoints (ICP) genes in two categories (Inhibitory ICP (22) and Stimulatory ICP (23)) from widely recognized literature (24). Then we assessed the expression and survival of these ICP in the TCGA-LGGs cohort for a comprehensive overview of the immunosuppressive landscape.

The Tumor Immunophenotype Profiling (TIP) was performed to quantify the extent of infiltrating immune cells and anticancer immunity (25). Assessment of antitumor immunity was conceptually divided into seven steps, including tumor cell antigen release (step 1), cancer antigen presentation (step 2), priming and activation (step 3), trafficking of immune cells to tumors (step 4), infiltration of immune cells (step 5), T cell recognition of cancer cells (step 6), and killing of cancer cells (step 7).

TIDE (http://tide.dfci.harvard.edu/), an excellent algorithm, was used to explore the prediction of clinical response to immune checkpoint blockade (ICB) therapy (22). The TIDE score was calculated to simulate two mechanisms of tumor immune evasion: the induction of T cell dysfunction with high infiltration of cytotoxic T lymphocytes and the retard of T cell infiltration in tumors with low cytotoxic T lymphocyte infiltration. The TIDE score is a good reflection of the responsiveness of the ICB. The SubMap (https://www.genepattern.org/) was carried out to validate the reliability of the prediction of TIDE.

The R package pRRophetic was used to predict chemotherapeutic response in LGGs patients (26). In addition to temozolomide, which patients with glioma widely used, we included three drugs with the therapeutic potential for glioma in this study: Axitinib, GDC-0941 (PI3K inhibitor), and Bleomycin.

2.9 Verification of gene expression at cellular level and tissue level

H4, SW1783, and HMF cell lines were purchased from ATCC. According to the manufacturer's instructions, total RNA was isolated using Trizol reagent (Invitrogen, USA). 2μg of the total RNA was transcribed into cDNA. SYBR Green PCR kit (Takara, Japan) was used for qRT-PCR. We selected the $2-\Delta\Delta Cq$ method to calculate gene transcription level, with β-actin mRNA as control. Data represent the mean ± SD of triplicate real-time PCR. The primers were synthesized by Tsingke Biotechnology (Shanghai, China) and displayed in Supplementary Table S1. Immunohistochemistry (IHC) analyzed the protein expression levels. GSAP (ab106630), LATS2 (ab111054), SWAP70 (ab228846), and SLC2A10 (ab110528) antibody was purchased from Abcam. EMP3 (sc-81797) antibody was purchased from Santa Cruz Biotechnology. Clinical characteristics of LGGs patients cohort are displayed in Supplementary Table S2. All the patients and the hospital's Ethics Committee approved this research. LGGs tissues were formalin-fixed, paraffin-embedded, and sectioned at 4 μm. Immune complexes were detected with the SP Kit (Solarbio, Beijing, China) and DAB Substrate Kit (Solarbio, Beijing, China). Signals were detected using an Olympus BX41 microscope. Quantification of Immunohistochemistry (IHC) staining was performed in a blinded fashion.

2.10 Statistical analysis

All the data were analyzed using the R software version 4.1.0. The overall survival (OS) between different groups was analyzed using Kaplan-Meier curves. Kruskal–Wallis tests were applied to compare gene expression in two groups. The Fisher test assessed different groups' responses to ICB treatment. Somatic mutation data sorted in the form of Mutation Annotation Format (MAF) was analyzed using the R package maftools. ImageJ and ImageJ plugin IHC profiler was applied to quantify IHC staining analysis. IHC scoring data and qRT-PCR data were analyzed using GraphPad/Prism 9.0. In addition, tumor mutational burden (TMB) and mutation counts were computed from somatic mutation frequencies. $p< 0.05$ was marked as '*', $p< 0.01$ was marked as '**', $p< 0.001$ was marked as '***'. and $p< 0.0001$ was marked as '****'.

3 Results

3.1 Differentially methylated and expressed genes (DMEGs) in LGG

To identify DMEGs in LGGs, we first extracted the gene expression and DNA methylation data of TCGA-LGGs and performed a comparative analysis. Samples were divided into high- and low-CAFs-score groups according to the median CAFs score. From the summary estimate, 2393 statistically significant Differentially Expressed Genes (DEGs) were identified (difference > 1.5-fold, p-value< 0.01), including 263 upregulated and 2131 downregulated genes (Figure 2A, Table S3). Promoter regions (TSS200 and TSS1500) were enrolled in the primary study. As shown in volcano plots, 1276 DMGs were identified from two regions, including 896 DMGs in the TSS200 region (Figure 2B, Table S4) and 583 DMGs in the TSS1500 region (Figure 2C, Table S5).

We analyzed the relationship between methylation and gene expression by integrating DMGs and DEGs in two promoter regions (TSS1500 and TSS200). A total of 77 DMEGs were identified (Figure 2D), and then we performed a principal component analysis (PCA) of the DMEGs in normal tissue and LGGs (Figure 2E). The

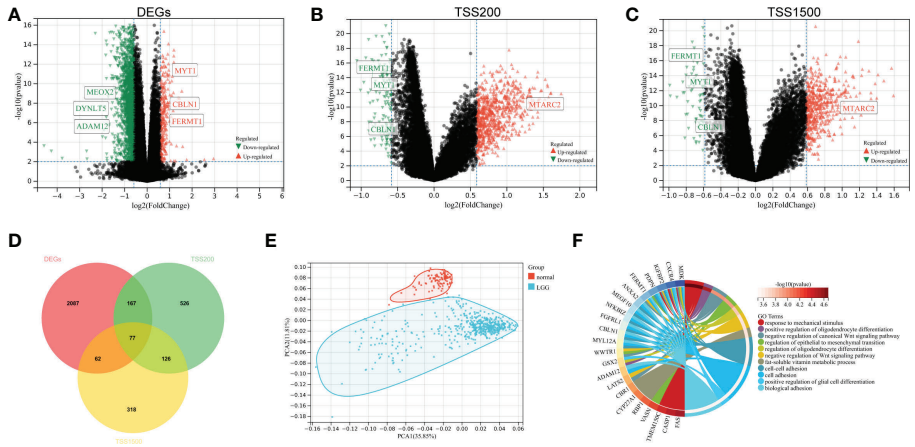

FIGURE 2
Identification and functional enrichment of DMEGs. **(A)** Volcano plot presenting the DEGs (difference > 1.5-fold, p-value< 0.01) between two groups. **(B)** DMGs (difference > 1.5-fold, p-value< 0.01) volcano plot of TSS200 region. **(C)** DMGs (difference > 1.5-fold, p-value< 0.01) volcano plot of TSS1500 region. **(D)** Venn diagram exhibiting DMEGs expressed in the TCGA dataset. **(E)** The profiles of DMEGs and principal component analysis (PCA) between tumor and normal cortex tissues. **(F)** GO analysis shows significant GO terms in DMEGs.

PCA profile revealed a clear separation of normal samples from LGGs. Afterwards, GO enrichment analysis was performed on these DMEGs, and the result indicated that DMEGs were significantly enriched in positive regulation of oligodendrocyte differentiation, negative regulation of canonical Wnt signaling pathway, and regulation of epithelial to mesenchymal transition (Figure 2F). These functions were closely related to the oncogenesis and progression of glioma.

3.2 DMEGs analysis in two promoter regions

To investigate the differences in DMEGs within each region, we classified these DMEGs into four groups (HypoUp, HyperUp, HyperDown, and HypoDown) for TSS200 and TSS1500, respectively (Figures 3A, B). The HyperDown group was the most prevalent in TSS200 and TSS1500 regions, and the HypoUp group had the second-highest proportion in the two regions (Figure 3C). After extracting the HyperDown and HypoUp DMEGs in TSS200 and TSS1500 regions separately, we used STRING to construct PPI networks. These genes were analyzed by GO enrichment using the "ClueGO" plugin for Cytoscape software (p< 0.01, Kappa score = 0.5). Functional enrichment analysis revealed that these DMEGs participated in critical biological processes. In the TSS200 region, DMEGs are mainly associated with response to mechanical stimulus, regulation of cell-substrate adhesion, and positive regulation of macrophage migration (Figure 3D). As shown in Figure 3D,

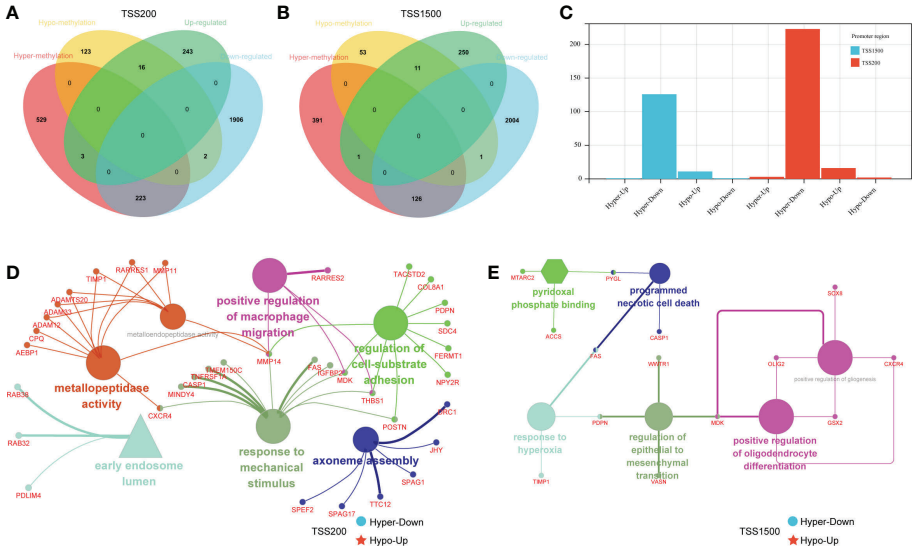

FIGURE 3
Grouping and functional analysis of DMEGs. **(A, B)** Venn diagram showed four different groups (HypoDown, HyperUp, and HyperDown) of DMEGs in the TSS200 region **(A)** and TSS1500 region **(B)**. **(C)** The bar chart shows the different groups of DMEGs in the two regions. **(D, E)** ClueGO Cytoscape network of statistically DMEGs in two regions.

MMP14 is critically involved in various immune-related functions. Meanwhile, DMEGs in the TSS1500 region are mainly related to regulating epithelial to mesenchymal transition, programmed necrotic cell death, and positive regulation of gliogenesis (Figure 3E). These simultaneous differential DEGs and DMGs pooled to DMEGs may be the main factor causing the altered biological function of LGGs.

3.3 Construct the DMEGs prognostic signature

Among the DMEGs in HyperDown and HypoUp groups, Univariate Cox regression analysis screened 203 DMEGs with prognostic values. Then a Lasso-penalized Cox analysis was performed to shrink further the scope of DMEGs screening (Figure 4A) and lambda. Min was regarded as the optimal value in the cross-validation process (Figure 4B). Five DMEGs (GSAP, EMP3, LATS2, SWAP70, and SLC2A10) and corresponding coefficients (Table S6) were identified. We used TCGA-LGGs as the train set CGGA-325 and CGGA-693 as the test sets, and samples were split into high- and low-risk groups by the median value of the risk score. KM survival curves depicted that LGG patients with increased risk scores had worse clinical outcomes in both train set and test sets (Figures 4C, D, and Figure S1A). Statistical analysis was performed using a log-rank test (train set $p< 0.001$, test set $p< 0.001$). After that, we established ROC curves of the risk score model with 1-year, 3-year, and 5-year. The results revealed that the risk score could effectively distinguish LGGs patients with different survival statuses (Figure 4E 1-yer AUC = 0.86, 3-year AUC = 0.83, and 5-year AUC = 0.80). The results were similar and slightly lower in the test set (Figure 4F 1-yer AUC = 0.73, 3-year AUC = 0.79, and 5-year AUC = 0.77). Multivariate Cox regression analysis showed the independent prognostic value of this risk score (Figure 4G, $p< 0.001$, HR = 3.844). Then we examined the mRNA expression of five risk genes in the glioma cell lines and fibroblast cell lines with CCLE (Figure 4H). Although glioma lines are not representative of LGGs, we found the expression of GSAP was consistent with that of

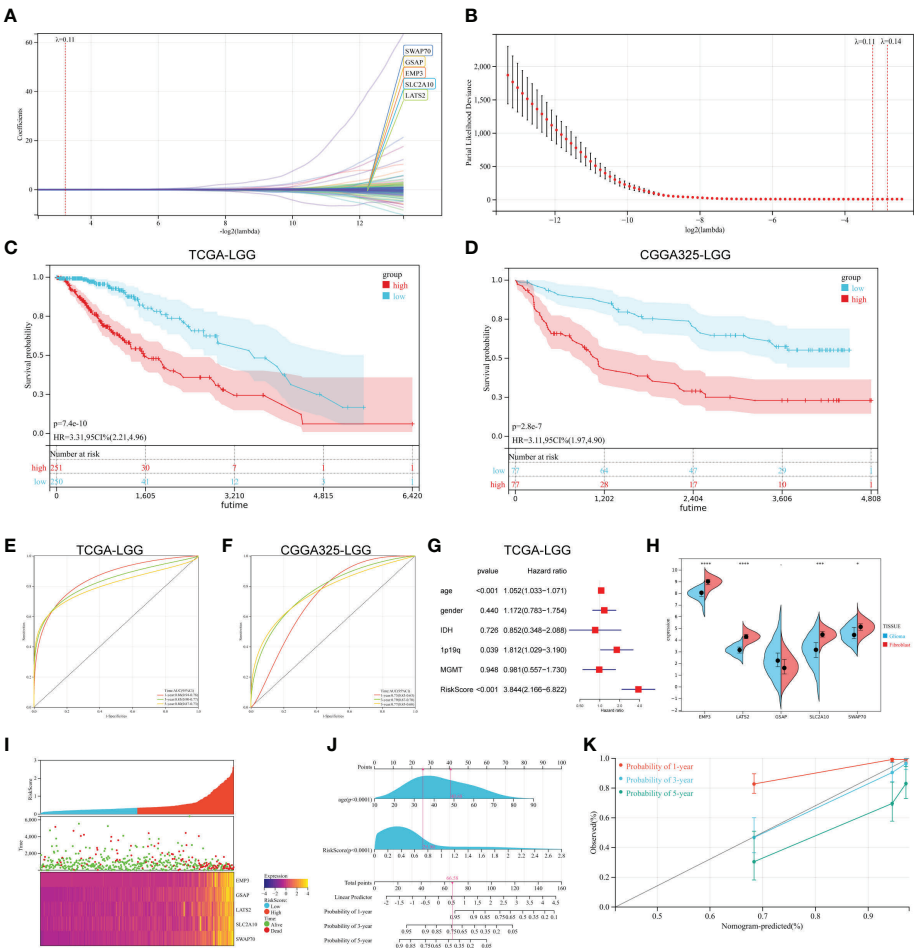

FIGURE 4
Construction of prognostic signature. **(A, B)** The process of building the signature. The least absolute shrinkage and selection operator (LASSO) regression was performed, calculating the minimum criteria. **(C, D)** K-M curves showed that the high-risk subgroup had worse overall survival than the subgroup in the train set ($p< 0.001$) and test set ($p< 0.001$). **(E, F)** ROC curves showed the predictive efficiency of the risk signature on the 1-, 3- and 5-year survival rates of train set **(E)** and test set **(F)**. **(G)** Independent prognostic factors were determined by the multivariate Cox regression analyses. **(H)** Expression of five risk genes in fibroblast cell lines and glioma cell lines in the CCLE dataset. **(I)** The heatmap was based on the expression of the five genes in the high- and low-risk group. **(J, K)** A nomogram **(J)** and decision curve analysis **(K)** of the risk score for predicting 1-, 3- and 5-year survival. (*p < 0.05, **p <0.01, ***p <0.001, ****p <0.0001).

fibroblasts, and the expression of the other four risk genes was lower than that of fibroblasts in glioma cell lines. The mortality of patients increased with the increase in the risk score (Figure 4I). Finally, we established the Nomogram model, which contained risk score and age to assess the survival prediction in LGGs patients (Figure 4J) and calibration curves for nomogram predicted 1-, 3- and 5-year overall survival performed well with the risk model (Figure 4K).

3.4 Correlation between risk score and clinical characteristics

Clinical variables were introduced into the risk score system to analyze the relationship between risk scores and clinical characteristics. We initially compared the CAFs' scores concerning the risk score. As shown in Figure 5A, the risk score was mildly positively associated with the CAFs score ($r = 0.42$, $p< 0.01$). In contrast, tumor purity was negatively correlated with the risk score (Figure 5B $r = -0.56$, $p < 0.01$). Other clinical features were then introduced. WHO grade III LGGs have a higher risk score than WHO grade II LGGs, which is consistent with their poor prognosis (Figures 5C, D, Figure S1B). The risk score in MGMT promoter methylated LGGs were significantly lower than that in MGMT promoter unmethylated LGGs samples (Figures 5E, F, Figure S1C). It is widely accepted that glioblastoma patients with MGMT promoter methylated are sensitive to temozolomide and suitable for TMZ chemotherapy. For another crucial molecular marker 1p19q codeletion status, the risk score was significantly higher in 1p19q-non-codeletion samples compared to codeletion samples in both datasets (Figures 5G, H, Figure S1D). Correspondingly, IDH1/2 wild-type cases showed a valid increased risk score compared to IDH1/2 mutant cases (Figures 5I, J, Figure S1E). The high-risk scores were seen in cases aged > 45 years. (Figures 5K, L, Figure S1F). Overall, some important molecular markers and clinical features of LGGs responded well to this risk score system.

3.5 Prognostic signature and immune landscape

To investigate the relationship between the prognostic signature and immune cell infiltration in LGGs. We evaluated immune scores, immune cell infiltration, and immune checkpoints separately. CAFs are the most prominent tumor stroma cell type in the TME. Comparing the stromal score and immune score of the LGGs datasets, we found a significantly positive correlation between the risk score and stromal score, and the same was true of the immune score (Figures 6A, B, stromal score $p< 0.001$ and Figures 6C, D immune score $p< 0.001$). CIBERSORT algorithm showed the proportions of distinct immune cell subpopulations in different risk groups (Figure 6E). The relative expression is shown in bar diagrams. The proportions of Macrophages M0 and Macrophages M2 in the high-risk group were significantly higher than in the low-risk group (Figure 6F). By contrast, the proportions of Monocytes, activated NK-cell and activated Mast-cells were higher in the low-risk group. Subsequently, we performed KM survival analysis to evaluate the OS with differing immunocytes infiltration samples (Figures 6G–I). High proportions of activated NK-cell and activated Mast-cell had a better OS (Figures 6G, I). Conversely, the level of macrophage M0 expression is inversely related to OS (Figure 6H). We next examined whether the risk score is associated with the expression of inhibitory and stimulatory immune checkpoint (ICP) molecules. Fortunately, the expression of many immune checkpoint molecules showed significant differences between high and low-risk groups (Figure 6J Inhibitory ICP and Figure 6K stimulatory ICP). The KM curves for survival analysis of these immune checkpoints were presented in

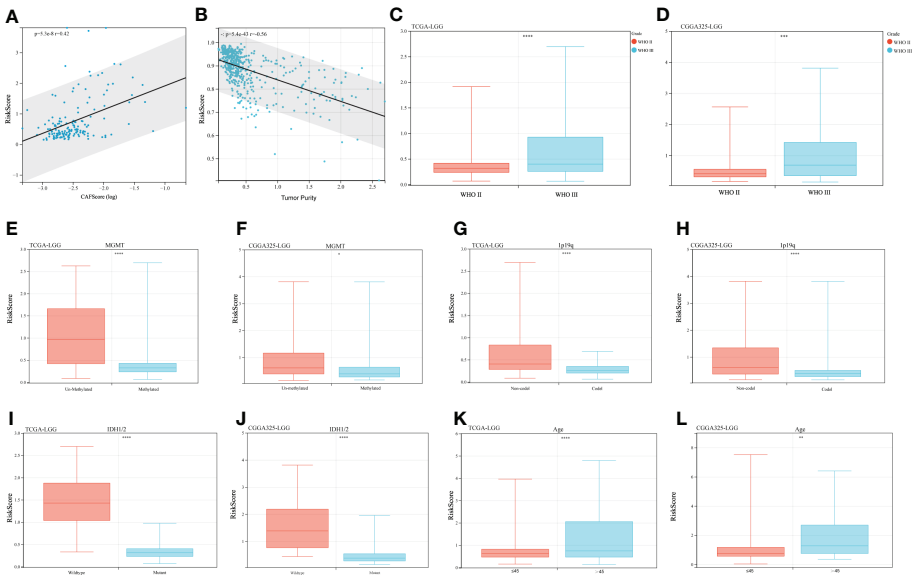

FIGURE 5
Clinical characteristics and risk scores. **(A)** Correlation of risk scores with CAFs scores, $r = 0.42$ $p< 0.001$. **(B)** Correlation of risk scores with tumor purity, $r = -0.56$, $p< 0.001$. **(C, D)** Risk scores for different WHO-graded samples, **(E, F)** MGMT promoter status, **(G, H)** 1p19q codeletion status, **(I, J)** IDH mutation status, and **(K, L)** Age effect. (*p < 0.05, **p <0.01, ***p <0.001, ****p <0.0001).

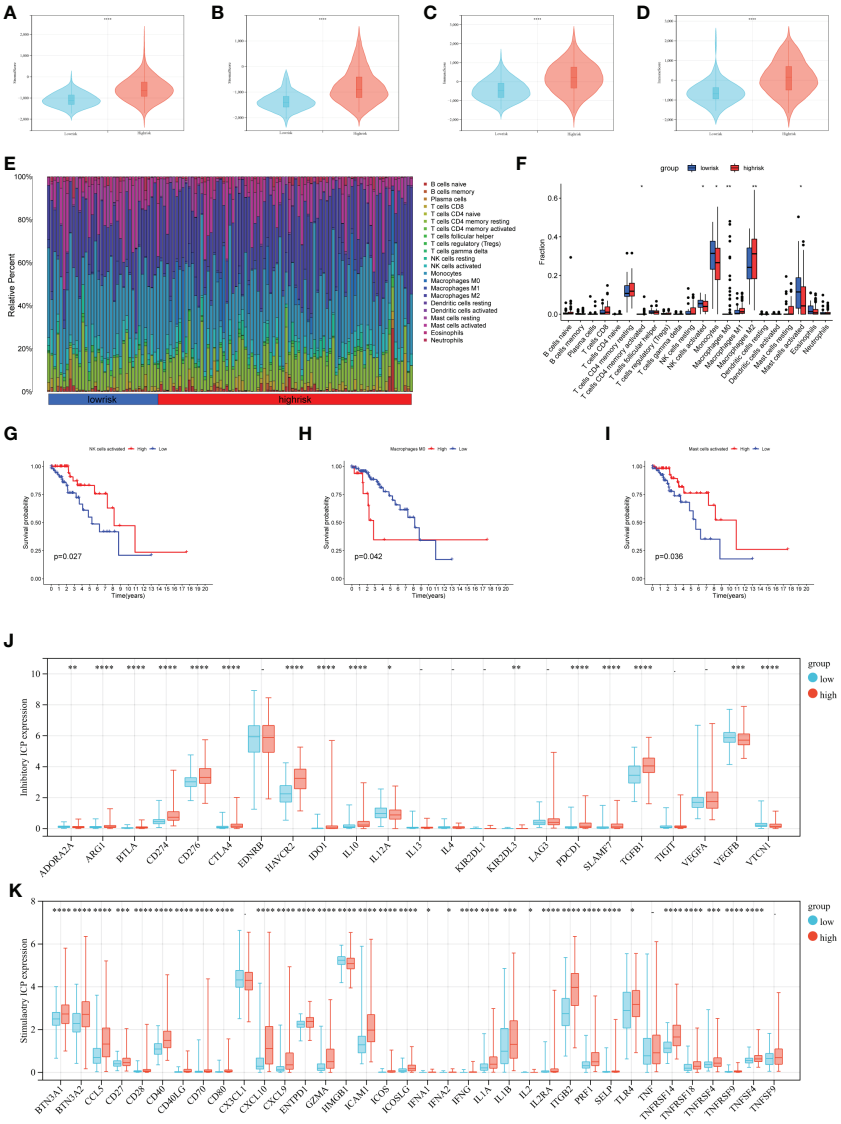

FIGURE 6
Analysis of immune infiltration in different risk groups. **(A–D)** Immune score and stromal score calculated by ESTIMATE in different groups **(A, C** TCGA data set, and **B, D** CGGA data set**)**. **(E, F)** The relative infiltrating proportion of 22 immune cells in high- and low-risk groups. **(G–I)** KM curves of infiltrating immune cells associated with survival in LGGs patients (p< 0.05). **(J, K)** Immune checkpoints expression in the LGGs microenvironment, inhibitory ICP **(J)**, and stimulatory ICP **(K)**. (*p < 0.05, **p <0.01, ***p <0.001, ****p <0.0001).

Figure S2. In summary, the risk score was associated with the expression of these immune checkpoint molecules.

3.6 Risk score-based stratification predicts the immune response and chemotherapy efficacy

To explore the risk score stratification and the associated characteristics of the antitumor immune response, we introduced the Tracking Tumor Immunophenotype (TIP) system, which analyzed the status of anticancer immunity and the proportion of tumor-infiltrating immune cells across seven-step Cancer-Immunity Cycle. As shown in Figure 7A, the scores of the high-risk group were significantly higher in tumor antigen release (step 1), immune cell recruitment (step 4), and immune cell infiltration into the tumor (step 5). Conversely, the low-risk group scored significantly higher in T cell priming and activation (step 3), T cell recognition of cancer cells (step 6), and killing of cancer cells (step 7). Then, we used the CGGA dataset to validate these results (Figure S3A). Next, we introduce the TIDE algorithm to assess the efficacy of risk score in predicting ICB responsiveness. We found there was a significant difference in response to ICB treatment between the two groups (p< 0.001), and the response to ICB treatment was more sensitive in the low-risk group (Figures 7B, C). SubMap was used to compare the prediction response to anti-PD1 and anti-CTLA4 therapy results with another dataset containing 47 patients with melanoma that responded to immunotherapies. Using this tool, we found that the high-risk group in the train and test sets showed comparable performance in predicting the LGGs' response to anti-PD1 therapy (Figures 7D, E p< 0.05). Anti-CTLA4 therapy also showed a partial response in the TCGA train set (Figure 7D Bonferroni corrected p = 0.32).

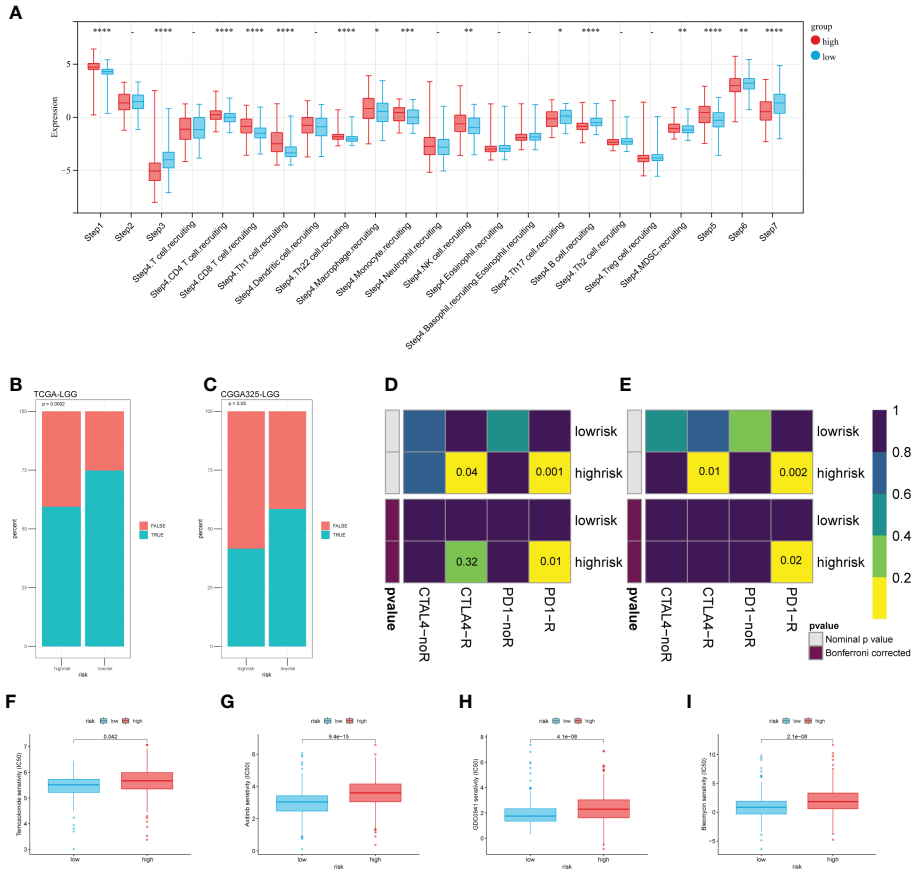

FIGURE 7
Risk score-based analysis of the stratifiable immune response and chemotherapy efficacy. **(A)** The TIP system quantified seven steps of the antitumor immune response. **(B, C)** Predicted response of TIDE to immune checkpoint inhibitors. **(D, E)** Comparing the effectiveness of PD1 and CTLA4 in response to different risk groups. **(F–I)** The sensibility of chemotherapeutic drugs **(F)** Temozolomide, **(G)** Axitinib, **(H)** GDC0941, and **(I)** Bleomycin. (*p < 0.05, **p <0.01, ***p <0.001, ****p <0.0001).

We tried to analyze the response of two risk groups to chemo-drug efficacy. Here, in addition to TMZ, we selected three other chemo drugs from the literature that may have therapeutic potential for glioma. As expected, the sensitivity in the low-risk group was slightly better than that in the high-risk group (Figure 7F). That may be related to the level of MGMT promoter methylation in the low-risk group (Figure 5E). For the other three drugs, the estimated IC50 was significantly better in the low-risk group (Figures 7G–I). These results were validated using the CGGA325 dataset (Figure S3B–E). Although these drugs have not been used in clinical treatment on a large-scale, differences in sensitivity suggest that they have potential as novel therapeutic agents.

3.7 Genomic alterations of prognostic signature

Tumor genomic alterations have profound effects on immunity and drug therapy. We investigated the mutation frequencies of different risk groups and showed the top ten most frequently mutated genes (Figures 8A, B). As we expected, IDH1 had the highest mutation frequency, predominantly missense. Remarkably, some genes were associated with the immune microenvironment and immunotherapy. These genes were more prominent in the high-risk group, such as ATRX, EGFR, and PTEN. We targeted IDH1, the most frequently mutated of the two groups in our study and analyzed the relationship between the expression of five risk genes and IDH1 mutations. The results were shown in Figures 8C–G. The expression of all risk genes was higher in samples with wild-type IDH1 than in mutant IDH1. These risk genes and corresponding risk scores are consistent with the findings summarized in the preceding text (Figure 5I). In addition, we analyzed correlations between tumor mutational burden (TMB) and risk score. Like previous research, LGGs patients in the high TMB group have a poorer prognosis. Hence, we introduced the risk score and analyzed it jointly with TMB. Our results show that the risk score had a low positive correlation with TMB values (Figure 8H). Meanwhile, the high-risk group with a poorer prognosis corresponded to high TMB values (Figure 8I). Combining the two elements in the analysis, we found that LGGs samples with high-risk scores and high TMB values had the worst prognosis (Figure 8J). Finally, we compared the TIDE, dysfunction, and exclusion scores between the different risk groups. The TIDE score in patients with low-risk scores was significantly higher than those with high-risk scores (Figure 8K $p< 0.01$). In parallel, patients in the high-risk group had higher dysfunction scores constructed using dysregulated immune genes (Figure 8L $p< 0.001$). No difference was

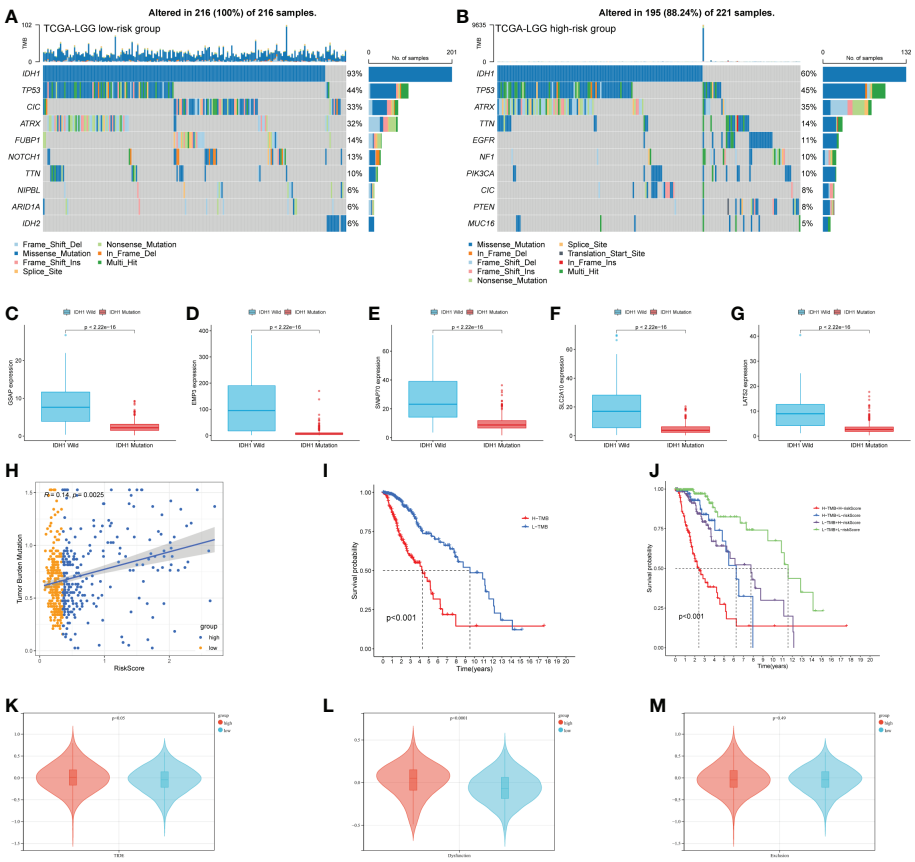

FIGURE 8
Epigenetic analysis of risk genes. **(A, B)** The mutation of high- and low-risk groups (Top 10 mutated genes). **(C–G)** Expression of 5 risk genes in the presence of different IDH1 mutations status. **(H)** Correlation analysis of risk score and TMB. **(I)** K-M curves of the high-TMB and low-TMB groups **(p< 0.001)**. **(J)**The combined risk score and TMB analysis of K-M curves in LGGs patients. **(K–M)** TIDE algorithm to model tumor immune evasion, **(K)** TIDE score, **(L)** Dysfunction score, and **(M)** Exclusion score.

found between the two groups for exclusion scores constructed using immune rejection genes (Figure 8M). The mechanism of immune escape in these high-risk LGGs samples may be immune dysfunction rather than immune exclusion. These epigenetic alterations may affect the prognostic model for the therapeutic assessment of LGGs patients.

3.8 Experimental verification in cell lines and tissues

After obtaining the above five risk genes, we identified them at the cellular and protein levels. Given the rarity of fibroblasts in brain tissue, we chose a stable human mammary fibroblast (HMF) cell line as a control group. T98G and U251 cell lines are commonly used glioma cell lines for experiments. GSAP and SWAP70 expressed similar levels in different cell lines, and the expression of the remaining three genes was lower in glioma cell lines (Figures 9A–E). For protein expression, three patients were analyzed with IHC. LGGs tissues were obtained from the tumor center (TC) and tumor periphery (TP). We found the expression of five proteins was highly expressed in tumor periphery (Figure 9F). After a 4-step grading system was quantified, except for LATS2, other proteins showed high expression in the TP group (Figures 9G–K). This founding may be related to the research that tumor cells can influence the recruitment of CAFs precursors and induce the activation of normal fibroblasts into CAFs.

4 Discussion

Abnormal epigenetic alterations contribute to tumorigenesis and progression, as reflected in the latest guidelines for glioma classification (27). DNA methylation has been found to regulate microRNAs and predict overall survival in glioma (28, 29). Recurrence of LGGs occurs mainly within a few centimeters of the resected cavity, even in complete tumor resection and adjuvant chemotherapy (30, 31). Glioma recurrence and prognosis are closely related to alterations of TME (32, 33). Immune cells and CAFs are essential components of the TME. Here, we combined abnormal methylation and CAFs abundance for an in-depth analysis of LGGs, which is essential for a more comprehensive understanding of TME and developing stromal CAFs-targeted therapies.

Herein, we analyzed DMEGs in different CAFs abundance groups, and we found that the functional annotations of these DMEGs were enriched in pathways of tumorigenesis, progression, and malignant transformation. Compelling evidence shows that the extracellular matrix acts as the “soil” for malignant tumor progression and immune resistance (34). Among them, functions closely related

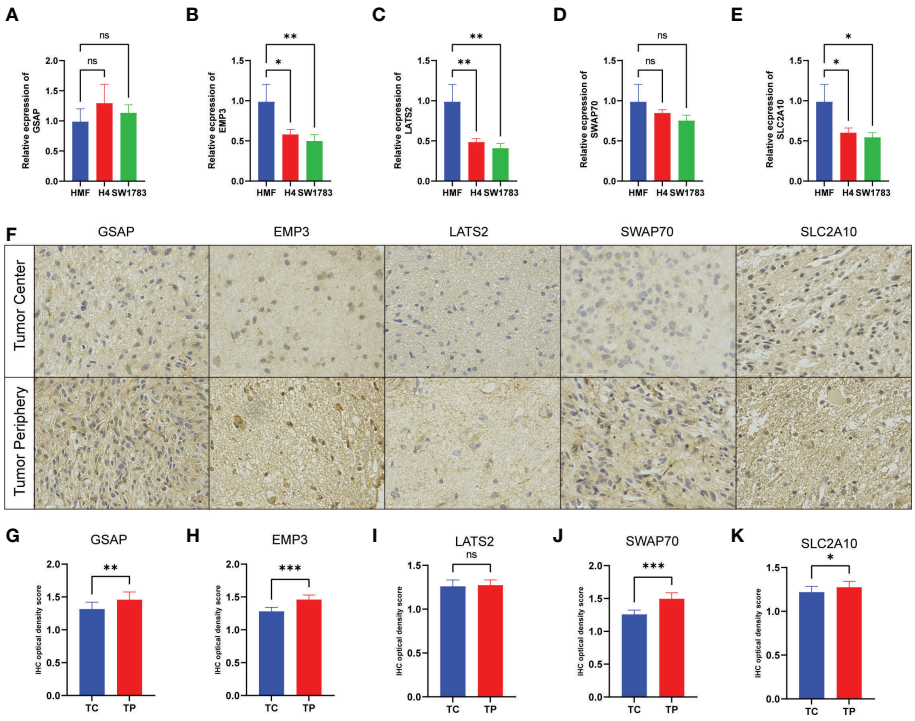

FIGURE 9
Experimental verification in cell lines and tissues. **(A–E)** The mRNA levels were determined by qRT-PCR in three cell lines. **(F)** The expression of five protein comparison of tumor center (TC) vs tumor periphery (TP) sites. **(G–K)** Bar graph showing the five protein levels obtained by quantification of immunohistochemical images. (*p< 0.05, **p < 0.01, and ***p < 0.001).

to CAFs, such as the Wnt signaling pathway plays a vital role in the carcinogenic activity of LGGs (35). Oligodendrocyte differentiation reflects the stemness of glioma cells (36). EMT has been implicated in cancer stemness, invasiveness, and drug resistance (23). The genes with simultaneous alterations in gene expression and methylation levels may be factors that alter LGGs functions through CAFs. DNA methylation at these promoter regions is widely known to correlate negatively with gene expression levels (37). GO enrichment analysis revealed the main functions and hub genes involved in DMEGs. It is worth noting that in TSS200 and TSS1500 regions, MDK is a critical player in cancer progression and immune microenvironment (38). MMP14 regulates the activity of multiple extracellular and plasma membrane proteins, influencing cell-cell and cell-extracellular matrix communication (39).

After integrating clinical information, we constructed a prognostic signature based on five genes (EMP3, GSAP, LATS2, SLC2A10, and SWAP70). Compared to fibroblast cell lines and glioma cell lines using the CCLE database, we found that the expression of GSAP was similar. In the validation of *in vitro* cell experiments, in addition to GSAP, SWAP70 expression was also similar to fibroblasts. However, no evidence exists that any glioma cell line can represent LGGs or GBM. Its predictive value appears to be quite weak. In order to test protein expression, we performed sampling and IHC analysis in the center and periphery of LGGs. The expression of EMP3, GSAP, SLC2A10, and SWAP70 was higher in tumor periphery. This finding suggests that there may be more activated fibroblasts at the TP, and CAFs could function at tumor periphery. However, there is no significant difference in LATS2 expression between TC and TP. Despite LATS2 having been recognized as a target gene of CAFs-derived exosome microRNA-92 in breast cancer (40). SLC2A10 regulated fibroblasts in arterial tortuosity syndrome by encoding glucose transporter 10 (41). The PI3K-dependent recruitment of SWAP70 to the plasma membrane has been observed in growth factor-stimulated fibroblasts (42). EMP3 plays an important role in the regulation of membrane receptors associated with IDH-Wild type glioblastoma (43).

More and more research focused on the immuno-phenotype and immunotherapy of glioma cells. The high-risk scoring group showed increased antitumor immune cells macrophage M2 and M0. Despite glioma being defined as a cold tumor, proportions of macrophages can still constitute up to 30–50% of the TME (44–46). Surprisingly, mast cells activated were higher in the low-risk group. We quantified antitumor immunity in seven steps and further evaluated the antitumor immune process. Increased risk in the LGGs sample was accompanied by a decrease in the score of T cell priming and activation (step3) and destruction of tumor cells (step6, 7). It corresponds to a higher density of antitumor immune infiltration in the high-risk group. Immunotherapy, especially ICB, has brought paradigm shifts to cancer treatment. We found that the specific inhibitory immune checkpoints PD1 and CTLA4 were significantly overexpressed in the high-risk group (Figure 6J), while the Submap approach suggests that the high-risk group showed promising performance in predicting LGGs predicted response to anti-PD1 and anti-CTLA4 therapies (Figures 7D, E). Other immune checkpoints that are highly expressed in high-risk groups are also being studied in an expanding way, such as the inhibitory immune

checkpoints CD276 (47) and IL-10 (48), and the stimulatory checkpoints ICOS (49) and CD40 (50) are involved in the regulation of T cell function. TGFB1 can increase endothelial and epithelial permeability. It is more inclined to promote GBM cell invasion (51). SLAMF7 is a cell surface receptor involved in natural killer cell activation that received approval for treating multiple myeloma (52). Treatment by blocking or stimulating these new checkpoints in LGGs holds the promise of going beyond traditional PD1 therapies. Although our risk score distinguished the expression of ICPs of LGGs and predicted anti-ICB therapy, it still lacks elucidation of the interaction mechanism between CAFs and ICB. We hope to provide new ideas on the relationship between the treatment of immune checkpoints and CAFs.

TMZ has become the conventional chemotherapeutic agent for glioma however, TMZ resistance is the main factor that leads to current studies aimed at expanding multiple chemotherapeutic agents for glioma (53). Besides TMZ, three promising drugs were introduced in this study (Figures 7G–I). Axitinib induces senescence-associated cell death and necrosis in glioma (54). The PI3K inhibitor GDC-0941 enhances radiosensitization and reduces chemoresistance to temozolomide in GBM (55). Bleomycin inhibits proliferation and promotes apoptosis of glioma *via* the TGF-β/Smad signaling pathway (56). All three drugs showed promising IC50 in the low-risk group, and we hope this study will provide potential directions for the relationship between new chemotherapeutic agents and CAFs. However, these speculations are still at the level of data analysis, and whether these drugs can be applied to LGGs still needs a lot of experimental verification, such as molecular docking.

Solid evidence suggests that TMB plays a vital role in tumor immune escape (57). TP53 was frequently mutated in the high-risk subtype, and its mutation was reported to be associated with a poorer prognosis. Mutations in IDH1 characterize the majority of lower-grade gliomas in adults and define a subtype associated with a favorable prognosis (58, 59). Glioma shows a markedly elevated mutation burden, referred to as TMB-H (60). A study suggests that some gliomas with high TMB may benefit from PD-1 blockade therapy (61). Interestingly, MMR deficiency gliomas with TMB-H also lack significant inflammatory CD8+ infiltrates (62). On the other hand, TIDE algorithm analysis revealed that the mechanism of immune escape in LGGs samples might be immune dysfunction (Figure 8L). Even in the presence of a high level of infiltration by cytotoxic T cells, immune escape is still inevitable (63). However, it is worth noting that our study also has some limitations. Although our study identified five risk genes, they could not directly serve as CAFs marker genes in LGGs. We should further confirm the role of these CAFs risk genes on glioma cells using *in vitro* co-culture or single-cell multi-omics. Bioinformatics has always been used to research CAFs, but how gliomas induce the production of CAFs and exercise their functions in TME still requires extensive *in vivo* or *in vitro* experimental studies. These efforts will be included in our future studies.

Data availability statement

The original contributions presented in the study are included in the article/Supplementary Materials. Further inquiries can be directed to the corresponding authors.

Ethics statement

The studies involving human participants were reviewed and approved by The Animal Ethical and Welfare Committee of Zhejiang Provincial People's Hospital. The patients/participants provided their written informed consent to participate in this study.

Author contributions

SH, JWD, and HJ conceived and designed the study and revised the manuscript. JWD, HZ, JJ, XG, and XY provided analytical technical support. ZL, NW, and JZ participated in the production of charts and pictures. JWD and FW designed and completed qRT-PCR and IHC experiments. YB, JYD, and SM revised the manuscript. SH supervised the study. All authors contributed to the article and approved the submitted version.

Funding

This work was funded by the National Natural Science Foundation of China (No. 61575058).

Acknowledgments

The authors gratefully acknowledge TCGA, CGGA, and other public databases for their facilitation of data analysis.

Conflict of interest

The authors declare that the research was conducted in the absence of any commercial or financial relationships that could be construed as a potential conflict of interest.

Publisher's note

Supplementary material

The Supplementary Material for this article can be found online at: https://www.frontiersin.org/articles/10.3389/fonc.2022.977251/full#supplementary-material

SUPPLEMENTARY FIGURE 1
Clinical characteristics and risk scores in CGGA-693 LGGs test set. **(A)** K-M curves showed that the high-risk subgroup had worse overall survival than the subgroup in the test set (p< 0.001). **(B)** K-M curves of different risk groups in WHO II and WHO III gliomas, **(C)** MGMT promoter status, **(D)** 1p19q codeletion status, **(E)** IDH mutation status, and **(F)** age effect.

SUPPLEMENTARY FIGURE 2
Overall survival analysis on immune checkpoint for LGGs patients. Grouping by median expression of immune checkpoint genes.

SUPPLEMENTARY FIGURE 3
Immunotherapy response and chemotherapy sensitivity in the CGGA. **(A)** TIP system analyzed the status of anticancer immunity and the proportion of tumor-infiltrating immune cells across the seven-step Cancer-Immunity Cycle. **(B)** Chemosensitivity of TMZ, p = 0.11. **(C)** Chemosensitivity of Axitinib, p< 0.001. **(D)** Chemosensitivity of GDC0941, p< 0.001. **(E)** Chemosensitivity of Bleomycin, p = 0.004.

SUPPLEMENTARY TABLE 1
The primers used in this study.

SUPPLEMENTARY TABLE 2
Clinical characteristics of patient cohort.

SUPPLEMENTARY TABLE 3
DEGs in TCGA.

SUPPLEMENTARY TABLE 4
DMGs in TSS200 region

SUPPLEMENTARY TABLE 5
DMGs in TSS1500 region

SUPPLEMENTARY TABLE 6
The formula of calculate risk score.

References

1. Ostrom QT, Cioffi G, Waite K, Kruchko C, Barnholtz-Sloan JS. CBTRUS statistical report: Primary brain and other central nervous system tumors diagnosed in the united states in 2014-2018. *Neuro-oncology* (2021) 23(12 Suppl 2):iii1–iii105. doi: 10.1093/neuonc/noab200

2. Weller M, van den Bent M, Tonn JC, Stupp R, Preusser M, Cohen-Jonathan-Moyal E, et al. European Association for neuro-oncology (EANO) guideline on the diagnosis and treatment of adult astrocytic and oligodendroglial gliomas. *Lancet Oncol* (2017) 18(6): e315–e29. doi: 10.1016/s1470-2045(17)30194-8

3. Yin D, Xie D, Hofmann WK, Zhang W, Asotra K, Wong R, et al. DNA Repair gene O6-methylguanine-DNA methyltransferase: promoter hypermethylation associated with decreased expression and G:C to A:T mutations of p53 in brain tumors. *Mol carcinogenesis.* (2003) 36(1):23–31. doi: 10.1002/mc.10094

4. Hegi ME, Diserens AC, Godard S, Dietrich PY, Regli L, Ostermann S, et al. Clinical trial substantiates the predictive value of O-6-methylguanine-DNA methyltransferase promoter methylation in glioblastoma patients treated with temozolomide. *Clin Cancer research: An Off J Am Assoc Cancer Res* (2004) 10(6):1871–4. doi: 10.1158/1078-0432.ccr-03-0384

5. Nomura M, Saito K, Aihara K, Nagae G, Yamamoto S, Tatsuno K, et al. DNA Demethylation is associated with malignant progression of lower-grade gliomas. *Sci Rep* (2019) 9(1):1903. doi: 10.1038/s41598-019-38510-0

6. Lu F, Shen SH, Wu S, Zheng P, Lin K, Liao J, et al. Hypomethylation-induced prognostic marker zinc finger DHHC-type palmitoyltransferase 12 contributes to glioblastoma progression. *Ann Trans Med* (2022) 10(6):334. doi: 10.21037/atm-22-520

7. Ren Z, He Y, Yang Q, Guo J, Huang H, Li B, et al. A comprehensive analysis of the glutathione peroxidase 8 (GPX8) in human cancer. *Front Oncol* (2022) 12:812811. doi: 10.3389/fonc.2022.812811

8. Tommelein J, Verset L, Boterberg T, Demetter P, Bracke M, De Wever O. Cancer-associated fibroblasts connect metastasis-promoting communication in colorectal cancer. *Front Oncol* (2015) 5:63. doi: 10.3389/fonc.2015.00063

9. Fiori ME, Di Franco S, Villanova L, Bianca P, Stassi G, De Maria R. Cancer-associated fibroblasts as abettors of tumor progression at the crossroads of EMT and therapy resistance. *Mol cancer.* (2019) 18(1):70. doi: 10.1186/s12943-019-0994-2

10. Wu X, Tao P, Zhou Q, Li J, Yu Z, Wang X, et al. IL-6 secreted by cancer-associated fibroblasts promotes epithelial-mesenchymal transition and metastasis of gastric cancer *via* JAK2/STAT3 signaling pathway. *Oncotarget* (2017) 8(13):20741–50. doi: 10.18632/oncotarget.15119

11. Lotti F, Jarrar AM, Pai RK, Hitomi M, Lathia J, Mace A, et al. Chemotherapy activates cancer-associated fibroblasts to maintain colorectal cancer-initiating cells by IL-17A. *J Exp Med* (2013) 210(13):2851–72. doi: 10.1084/jem.20131195

12. Monteran L, Erez N. The dark side of fibroblasts: Cancer-associated fibroblasts as mediators of immunosuppression in the tumor microenvironment. *Front Immunol* (2019) 10:1835. doi: 10.3389/fimmu.2019.01835

13. Gamradt P, De La Fouchardière C, Hennino A. Stromal protein-mediated immune regulation in digestive cancers. *Cancers* (2021) 13(1):146. doi: 10.3390/cancers13010146

14. Miyai Y, Sugiyama D, Hase T, Asai N, Taki T, Nishida K, et al. Meflin-positive cancer-associated fibroblasts enhance tumor response to immune checkpoint blockade. *Life Sci alliance.* (2022) 5(6):e202101230. doi: 10.26508/lsa.202101230

15. Bienkowska KJ, Hanley CJ, Thomas GJ. Cancer-associated fibroblasts in oral cancer: A current perspective on function and potential for therapeutic targeting. *Front Oral Health* (2021) 2:686337. doi: 10.3389/froh.2021.686337

16. Goldman M, Craft B, Hastie M, Repečka K, McDade F, Kamath A, et al. The UCSC xena platform for public and private cancer genomics data visualization and interpretation. *bioRxiv* (2019), 326470. doi: 10.1101/326470

17. Barretina J, Caponigro G, Stransky N, Venkatesan K, Margolin AA, Kim S, et al. The cancer cell line encyclopedia enables predictive modelling of anticancer drug sensitivity. *Nature* (2012) 483(7391):603–7. doi: 10.1038/nature11003

18. Du P, Zhang X, Huang CC, Jafari N, Kibbe WA, Hou L, et al. Comparison of beta-value and m-value methods for quantifying methylation levels by microarray analysis. *BMC Bioinf* (2010) 11:587. doi: 10.1186/1471-2105-11-587

19. Sturm G, Finotello F, List M. Immunedeconv: An r package for unified access to computational methods for estimating immune cell fractions from bulk RNA-sequencing data. *Methods Mol Biol (Clifton NJ).* (2020) 2120:223–32. doi: 10.1007/978-1-0716-0327-7_16

20. Yu G, Wang LG, Han Y, He QY. clusterProfiler: an r package for comparing biological themes among gene clusters. *Omics: J Integr Biol* (2012) 16(5):284–7. doi: 10.1089/omi.2011.0118

21. Bindea G, Mlecnik B, Hackl H, Charoentong P, Tosolini M, Kirilovsky A, et al. ClueGO: A cytoscape plug-in to decipher functionally grouped gene ontology and pathway annotation networks. *Bioinf (Oxford England).* (2009) 25(8):1091–3. doi: 10.1093/bioinformatics/btp101

22. Jiang P, Gu S, Pan D, Fu J, Sahu A, Hu X, et al. Signatures of T cell dysfunction and exclusion predict cancer immunotherapy response. *Nat Med* (2018) 24(10):1550–8. doi: 10.1038/s41591-018-0136-1

23. Zhang Y, Weinberg RA. Epithelial-to-mesenchymal transition in cancer: complexity and opportunities. *Front Med* (2018) 12(4):361–73. doi: 10.1007/s11684-018-0656-6

24. Thorsson V, Gibbs DL, Brown SD, Wolf D, Bortone DS, Ou Yang TH, et al. The immune landscape of cancer. *Immunity* (2018) 48(4):812–30.e14. doi: 10.1016/j.immuni.2018.03.023

25. Xu L, Deng C, Pang B, Zhang X, Liu W, Liao G, et al. TIP: A web server for resolving tumor immunophenotype profiling. *Cancer Res* (2018) 78(23):6575–80. doi: 10.1158/0008-5472.can-18-0689

26. Geeleher P, Cox N, Huang RS. pRRophetic: an r package for prediction of clinical chemotherapeutic response from tumor gene expression levels. *PloS One* (2014) 9(9): e107468. doi: 10.1371/journal.pone.0107468

27. Louis DN, Perry A, Wesseling P, Brat DJ, Cree IA, Figarella-Branger D, et al. The 2021 WHO classification of tumors of the central nervous system: a summary. *Neuro-oncology* (2021) 23(8):1231–51. doi: 10.1093/neuonc/noab106

28. Kang EM, Yin AA, He YL, Chen WJ, Etcheverry A, Aubry M, et al. A five-CpG signature of microRNA methylation in non-G-CIMP glioblastoma. *CNS Neurosci Ther* (2019) 25(9):937–50. doi: 10.1111/cns.13133

29. Guo W, Ma S, Zhang Y, Liu H, Li Y, Xu JT, et al. Genome-wide methylomic analyses identify prognostic epigenetic signature in lower grade glioma. *J Cell Mol Med* (2022) 26(2):449–61. doi: 10.1111/jcmm.17101

30. Lemée JM, Clavreul A, Menei P. Intratumoral heterogeneity in glioblastoma: don't forget the peritumoral brain zone. *Neuro-oncology* (2015) 17(10):1322–32. doi: 10.1093/neuonc/nov119

31. Niyazi M, Brada M, Chalmers AJ, Combs SE, Erridge SC, Fiorentino A, et al. ESTRO-ACROP guideline "target delineation of glioblastomas". *Radiotherapy oncology: J Eur Soc Ther Radiol Oncol* (2016) 118(1):35–42. doi: 10.1016/j.radonc.2015.12.003

32. Shen Y, Chi H, Xu K, Li Y, Yin X, Chen S, et al. A novel classification model for lower-grade glioma patients based on pyroptosis-related genes. *Brain Sci* (2022) 12(6):700. doi: 10.3390/brainsci12060700

33. Schaafsma E, Jiang C, Nguyen T, Zhu K, Cheng C. Microglia-based gene expression signature highly associated with prognosis in low-grade glioma. *Cancers* (2022) 14(19):4802. doi: 10.3390/cancers14194802

34. Kalluri R. The biology and function of fibroblasts in cancer. *Nat Rev Cancer.* (2016) 16(9):582–98. doi: 10.1038/nrc.2016.73

35. Zhang M, Wang D, Su L, Ma J, Wang S, Cui M, et al. Activity of Wnt/PCP regulation pathway classifies patients of low-grade glioma into molecularly distinct subgroups with prognostic difference. *Front Oncol* (2021) 11:726034. doi: 10.3389/fonc.2021.726034

36. Hashemi M, Abbasiazam A, Oraee-Yazdani S, Lenzer J. Response of human glioblastoma cells to hyperthermia: Cellular apoptosis and molecular events. *Tissue Cell* (2022) 75:101751. doi: 10.1016/j.tice.2022.101751

37. Jones PA. Functions of DNA methylation: islands, start sites, gene bodies and beyond. *Nat Rev Genet* (2012) 13(7):484–92. doi: 10.1038/nrg3230

38. Filippou PS, Karagiannis GS, Constantinidou A. Midkine (MDK) growth factor: a key player in cancer progression and a promising therapeutic target. *Oncogene* (2020) 39 (10):2040–54. doi: 10.1038/s41388-019-1124-8

39. Gonzalez-Molina J, Gramolelli S, Liao Z, Carlson JW, Ojala PM, Lehti K. MMP14 in sarcoma: A regulator of tumor microenvironment communication in connective tissues. *Cells* (2019) 8(9):991. doi: 10.3390/cells8090991

40. Dou D, Ren X, Han M, Xu X, Ge X, Gu Y, et al. Cancer-associated fibroblasts-derived exosomes suppress immune cell function in breast cancer via the miR-92/PD-L1 pathway. *Front Immunol* (2020) 11:2026. doi: 10.3389/fimmu.2020.02026

41. Zoppi N, Chiarelli N, Cinquina V, Ritelli M, Colombi M. GLUT10 deficiency leads to oxidative stress and non-canonical αvβ3 integrin-mediated TGFβ signalling associated with extracellular matrix disarray in arterial tortuosity syndrome skin fibroblasts. *Hum Mol Genet* (2015) 24(23):6769–87. doi: 10.1093/hmg/ddv382

42. Kriplani N, Duncan RR, Leslie NR. SWAP70 undergoes dynamic conformational regulation at the leading edge of migrating cells. *FEBS letters.* (2019) 593(4):395–405. doi: 10.1002/1873-3468.13326

43. Martija AA, Pusch S. The multifunctional role of EMP3 in the regulation of membrane receptors associated with IDH-Wild-Type glioblastoma. *Int J Mol Sci* (2021) 22(10):5261. doi: 10.3390/ijms22105261

44. Huang L, Wang Z, Chang Y, Wang K, Kang X, Huang R, et al. EFEMP2 indicates assembly of M0 macrophage and more malignant phenotypes of glioma. *Aging* (2020) 12 (9):8397–412. doi: 10.18632/aging.103147

45. Grabowski MM, Sankey EW, Ryan KJ, Chongsathidkiet P, Lorrey SJ, Wilkinson DS, et al. Immune suppression in gliomas. *J neuro-oncology.* (2021) 151(1):3–12. doi: 10.1007/s11060-020-03483-y

46. Guadagno E, Presta I, Maisano D, Donato A, Pirrone CK, Cardillo G, et al. Role of macrophages in brain tumor growth and progression. *Int J Mol Sci* (2018) 19(4):1005. doi: 10.3390/ijms19041005

47. Picarda E, Ohaegbulam KC, Zang X. Molecular pathways: Targeting B7-H3 (CD276) for human cancer immunotherapy. *Clin Cancer research: an Off J Am Assoc Cancer Res* (2016) 22(14):3425–31. doi: 10.1158/1078-0432.ccr-15-2428

48. Porichis F, Hart MG, Massa A, Everett HL, Morou A, Richard J, et al. Immune checkpoint blockade restores HIV-specific CD4 T cell help for NK cells. *J Immunol (Baltimore Md: 1950)* (2018) 201(3):971–81. doi: 10.4049/jimmunol.1701551

49. Marin-Acevedo JA, Dholaria B, Soyano AE, Knutson KL, Chumsri S, Lou Y. Next generation of immune checkpoint therapy in cancer: new developments and challenges. *J Hematol Oncol* (2018) 11(1):39. doi: 10.1186/s13045-018-0582-8

50. Tang T, Cheng X, Truong B, Sun L, Yang X, Wang H. Molecular basis and therapeutic implications of CD40/CD40L immune checkpoint. *Pharmacol Ther* (2021) 219:107709. doi: 10.1016/j.pharmthera.2020.107709

51. Chen Y, Liu P, Sun P, Jiang J, Zhu Y, Dong T, et al. Oncogenic MSH6-CXCR4-TGFB1 feedback loop: A novel therapeutic target of photothermal therapy in glioblastoma multiforme. *Theranostics* (2019) 9(5):1453–73. doi: 10.7150/thno.29987

52. Sherbenou DW, Mark TM, Forsberg P. Monoclonal antibodies in multiple myeloma: A new wave of the future. *Clin lymphoma myeloma leukemia.* (2017) 17 (9):545–54. doi: 10.1016/j.clml.2017.06.030

53. Liu B, Zhou J, Wang C, Chi Y, Wei Q, Fu Z, et al. LncRNA SOX2OT promotes temozolomide resistance by elevating SOX2 expression *via* ALKBH5-mediated epigenetic regulation in glioblastoma. *Cell Death disease.* (2020) 11(5):384. doi: 10.1038/s41419-020-2540-y

54. Morelli MB, Amantini C, Nabissi M, Cardinali C, Santoni M, Bernardini G, et al. Axitinib induces senescence-associated cell death and necrosis in glioma cell lines: The proteasome inhibitor, bortezomib, potentiates axitinib-induced cytotoxicity in a p21 (Waf/Cip1) dependent manner. *Oncotarget* (2017) 8(2):3380–95. doi: 10.18632/oncotarget.13769

55. Shi F, Guo H, Zhang R, Liu H, Wu L, Wu Q, et al. The PI3K inhibitor GDC-0941 enhances radiosensitization and reduces chemoresistance to temozolomide in GBM cell lines. *Neuroscience* (2017) 346:298–308. doi: 10.1016/j.neuroscience.2017.01.032

56. Jin H, Luo C. Bleomycin inhibits proliferation and promotes apoptosis of brain glioma cells *via* TGF-β/Smad signaling pathway. *J BUON: Off J Balkan Union Oncol* (2020) 25(2):1076–83.

57. Chan TA, Yarchoan M, Jaffee E, Swanton C, Quezada SA, Stenzinger A, et al. Development of tumor mutation burden as an immunotherapy biomarker: Utility for the oncology clinic. *Ann oncology: Off J Eur Soc Med Oncol* (2019) 30(1):44–56. doi: 10.1093/annonc/mdy495

58. Jiao Y, Killela PJ, Reitman ZJ, Rasheed AB, Heaphy CM, de Wilde RF, et al. CIC, FUBP1 and IDH1 mutations refine the classification of malignant gliomas. *Oncotarget* (2012) 3(7):709–22. doi: 10.18632/oncotarget.588

59. Yan H, Parsons DW, Jin G, McLendon R, Rasheed BA, Yuan W, et al. IDH1 and IDH2 mutations in gliomas. *New Engl J Med* (2009) 360(8):765–73. doi: 10.1056/NEJMoa0808710

60. Teter Z, Śliwczyński A, Brzozowska M, Świerkowski M, Jacyna A, Pinkas J, et al. The assessment of overall survival (OS) after adjuvant chemotherapy for patients with malignant endometrial cancer in Poland. *Ginekologia polska.* (2017) 88(6):296–301. doi: 10.5603/GP.a2017.0056

61. Bouffet E, Larouche V, Campbell BB, Merico D, de Borja R, Aronson M, et al. Immune checkpoint inhibition for hypermutant glioblastoma multiforme resulting from germline biallelic mismatch repair deficiency. *J Clin oncology: Off J Am Soc Clin Oncol* (2016) 34(19):2206–11. doi: 10.1200/jco.2016.66.6552

62. Touat M, Li YY, Boynton AN, Spurr LF, Iorgulescu JB, Bohrson CL, et al. Mechanisms and therapeutic implications of hypermutation in gliomas. *Nature* (2020) 580(7804):517–23. doi: 10.1038/s41586-020-2209-9

63. Joyce JA, Fearon DT. T Cell exclusion, immune privilege, and the tumor microenvironment. *Sci (New York NY).* (2015) 348(6230):74–80. doi: 10.1126/science.aaa6204

frontiers | Frontiers in Immunology

TYPE Original Research
PUBLISHED 19 January 2023
DOI 10.3389/fimmu.2022.1074644

OPEN ACCESS

EDITED BY
Dianwen Ju,
Fudan University, China

REVIEWED BY
Amaia Martinez Usatorre,
Swiss Federal Institute of Technology Lausanne, Switzerland
Trupti Vardam-Kaur,
Omeros Corporation, United States

*CORRESPONDENCE
Richard B. Markham
RMarkha1@jhu.edu

†These authors have contributed equally to this work and share first authorship

SPECIALTY SECTION
This article was submitted to Cancer Immunity and Immunotherapy, a section of the journal Frontiers in Immunology

RECEIVED 19 October 2022
ACCEPTED 29 December 2022
PUBLISHED 19 January 2023

CITATION
Gordy JT, Sandhu AK, Fessler K, Luo K, Kapoor AR, Ayeh SK, Hui Y, Schill C, Chen F, Wang T, Karanika S, Sunshine JC, Karakousis PC and Markham RB (2023) IFNα and 5-Aza-2′-deoxycytidine combined with a dendritic-cell targeting DNA vaccine alter tumor immune cell infiltration in the B16F10 melanoma model. *Front. Immunol.* 13:1074644. doi: 10.3389/fimmu.2022.1074644

IFNα and 5-Aza-2′-deoxycytidine combined with a dendritic-cell targeting DNA vaccine alter tumor immune cell infiltration in the B16F10 melanoma model

James T. Gordy[1†], Avinaash K. Sandhu[1†], Kaitlyn Fessler[1], Kun Luo[1], Aakanksha R. Kapoor[2], Samuel K. Ayeh[2], Yinan Hui[1], Courtney Schill[1], Fengyixin Chen[1], Tianyin Wang[1], Styliani Karanika[2], Joel C. Sunshine[3], Petros C. Karakousis[2] and Richard B. Markham[1*]

[1]Department of Molecular Microbiology and Immunology, Johns Hopkins Bloomberg School of Public Health, Baltimore, MD, United States, [2]Division of Infectious Diseases, Center for Tuberculosis Research, Department of Medicine, The Johns Hopkins Hospital, Baltimore, MD, United States, [3]The Departments of Dermatology, Pathology, and Biomedical Engineering, Johns Hopkins University School of Medicine, Baltimore, MD, United States

Introduction: DNA vaccines containing a fusion of the gene encoding chemokine MIP-3α (CCL20), the ligand for CCR6 on immature dendritic cells (DCs), to melanoma-associated antigen genes have enhanced anti-tumor immunity and efficacy compared to those lacking the chemokine gene. Previous work has shown that type-I interferon (IFNα or IFN) and 5-Aza-2′-deoxycytidine (5Aza) significantly enhance the therapeutic benefit of DNA vaccines as measured by reduced tumor burden and improved mouse survival.

Methods: Here, we explored mouse intratumoral immune correlates underlying the therapeutic benefit of this combination regimen (vaccine, IFN, and 5Aza) as compared to vaccine alone and IFN and 5Aza without vaccine, focusing on chemokine mRNA expression by qRT-PCR and inflammatory cellular infiltration into the tumor microenvironment (TME) by flow cytometry and immunohistochemistry (IHC).

Results: The combination group significantly upregulated intratumoral mRNA expression of key immune infiltration chemokines XCL1 and CXCL10. Flow cytometric analyses of tumor suspensions exhibited greater tumor infiltration of CD8+ DCs, CCR7+ DCs, and NK cells in the combination group, as well as reduced levels of myeloid-derived suppressor cells (MDSCs) in vaccinated groups. The mice receiving combination therapy also had greater proportions of effector/memory T-cells (Tem), in addition to showing an enhanced infiltration of Tem and central memory CD8+ T-cells, (Tcm). Tem and Tcm populations both correlated with smaller tumor size. Immunohistochemical analysis of tumors confirmed that CD8+ cells were more abundant overall and especially in the tumor parenchyma with combination therapy.

Discussion: Efficient targeting of antigen to immature DCs with a chemokine-fusion vaccine offers a potential alternative approach to classic and dendritic cell-based vaccines. Combining this approach with IFNα and 5Aza treatments significantly improved vaccine efficacy. This treatment creates an environment of increased inflammatory chemokines that facilitates the trafficking of CD8+ DCs, NK cells, and CD8+ T-cells, especially memory cells, while reducing the number of MDSCs. Importantly, in the combination group, CD8+ cells were more able to penetrate the tumor mass in addition to being more numerous. Further analysis of the pathways engaged by our combination therapy is expected to provide additional insights into melanoma pathogenesis and facilitate the development of novel treatment strategies.

KEYWORDS

interferon, 5-Aza-2'-deoxycitidine, dendritic cell, vaccine, B16F10 melanoma, chemokine, CCL20, CD8+ T-cells

Introduction

Despite advances in medical innovation and treatment, cancer resulted in nearly 10 million deaths globally in 2020 (1). Of these deaths, over 57,000 were from melanoma (2). Traditional treatments like surgery and chemotherapy aid in early stages of the disease but treating late-stage metastatic melanoma remains a challenge. Recently, immunotherapies such as immune checkpoint blockades (ICB) targeting the markers CTLA-4 and PD-1/PD-L1 have shown promise, but their use is limited by the severity of their associated side effects and a high frequency of non-responsiveness and relapse (3). The limited success of these treatments has prompted the deployment of combination therapies, which often include traditional anticancer drugs such as decitabine and immunotherapeutic agents such as interferon-α, ICB, and CAR-T-cells (3–6).

Two bottlenecks in the development of cancer immunotherapy are activation of sufficient numbers of effector cells targeting tumor antigens and ensuring that those effector cells enter the tumor environment. Cancer vaccines have been employed to expand populations of cancer antigen specific T-cells (7) frequently employing approaches that recognize the importance of dendritic cell (DC) recruitment in T-cell activation (8, 9). We have previously reported marked enhancement of anti-tumor efficacy of a DC-targeting melanoma vaccine by the addition of Interferon α (IFN) and 5'aza-2 deoxycytidine (5Aza) to the therapeutic regimen. Of note, the enhanced efficacy of this regimen was dependent on the presence of all components and was not attributable to additive effects of individual components. In the current studies we have explored the intratumoral immune parameters of the regimen components IFN +5Aza, Vaccine, and the combination to define their roles in overcoming the treatment bottlenecks. Our findings provide a basis for understanding the requirement for all treatment components to achieve the synergistic efficacy observed with this treatment regimen.

This study investigated the intratumoral immune mechanisms associated with the enhanced therapeutic efficacy of combinatorial treatment seen in previous studies (10, 11). In line with previous findings, CD8+ T-cells were enriched in tumors from mice receiving combination therapy relative to mice receiving IFN and 5Aza or mice receiving vaccine alone. Chemokines important for attracting inflammatory cells, such as CCL19 (11), CXCL10, and XCL1, were significantly upregulated. Inflammatory cell types such as natural killer (NK) cells, CD8+ DCs, and memory CD8+ T-cells were also significantly enriched, whereas levels of myeloid-derived suppressor cells (MDSCs) were greatly reduced. Importantly, the IHC results highlight that the CD8+ cells in the combination group are of greater number and are infiltrating into the tumor mass as compared to the other groups where they remain primarily on the periphery. The findings here elucidate a system where the IFN with 5Aza and vaccine components act in tandem to create a microenvironment more conducive to immune activity.

Abbreviations: 5Aza, 5-Aza-2'-Deoxycytidine; ICB, Immune checkpoint blockade; IFN, Interferon alpha; IHC, Immunohistochemistry; MIP3α, Macrophage inflammatory protein 3-alpha; M-MDSC, Monocytic myeloid-derived suppressor cell; PMN-MDSC, Granulocytic or poly-morphonuclear myeloid-derived suppressor cell; TME, Tumor microenvironment.

Materials and methods

Tumor model

6–12-week-old female C57BL/6 (Charles River, Wilmington, MA) mice were challenged with a lethal dose of B16F10 melanoma (5×10^4 cells, >95% viability) administered intradermally on the mouse flank on day 0 of therapy (10, 11). Tumor size was recorded by calipers every 1–3 days as square mm (L × W). Mice were monitored for signs of distress in accordance with IACUC protocols.

Vaccinations and therapeutics

Vaccine antigen is the MIP-3α-Gp100-Trp2 (tyrosinase-related protein 2) DNA construct in the pCMVe mammalian expression

plasmid published here (11). Vaccination-grade plasmids were extracted from *E. coli* DH5-α (Invitrogen™ ThermoFisher Scientific, Waltham, MA) using Qiagen® (Germantown, MD) EndoFree® Plasmid Kits and were diluted with endotoxin-free 1xPBS. Vaccine DNA preps were verified by insert sequencing (JHMI Synthesis and Sequencing Facility, Baltimore, MD), spectrophotometry, and gel electrophoresis, and then administered at 50 µg/dose into the gasctocnemius muscle followed by *in vivo* electroporation, pulsing the muscle with the ECM 830 Electro Square Porator with 2-Needle Array Electrode (BTX Harvard Apparatus; Holliston, MA) under the following parameters: 106 V; 20 ms pulse length; 200 ms pulse interval; 8 total pulses (10). 50 µg ODN2395 Type C CpG (Innaxon LPS Biosciences, Tewkesbury, UK) was administered intramuscularly 2 days post-vaccination into vaccinated muscle. Recombinant mouse interferon alpha-A (IFNα, R&D Systems, Inc. Minneapolis, MN) was administered intratumorally as a series of doses: one high dose (10,000 units) followed by 2-3 days of low doses (1000-2000 units). InSolution™ 5 Aza 2′-deoxycytidine (5Aza, CalBiochem®, MilliporeSigma, Burlington, MA) was administered intraperitoneally at 1 mg/kg in 50 µl, at approximately 20 µg/mouse. Figure 1A outlines the therapy schedule.

Lymphocyte extraction and flow cytometry

Tumor cell suspensions were prepared as previously described, with or without the Lympholyte M (Cedarlane Labs, Burlington, NC) purification step (10, 11). Briefly, tissue was extracted, kept cold, ground through a filter, washed, either purified or processed to lyse red blood cells, and used for downstream applications. In one experiment, the tumor cells were cryopreserved in 90% FBS 10% DMSO freezing media using isopropanol baths at -80°C prior to moving the samples to -150°C. Cells were quick-thawed and allowed to rest for 4 hours at 37°C before proceeding. Cells undergoing a freeze-thaw were only utilized for T-cell subtype analyses. If fewer than 10 live CD8+ T cells were measured, the samples were not included due to poor cell viability. Results of T-cell subtypes from cryopreserved cells were not significantly different from the remainder of the datasets. Tumor cell suspensions were stained in a 96-well V-bottom plate (Sarstedt, Inc., Newton, NC), with combinations of the following anti-mouse mAbs: PercPCy5.5 conjugated anti-CD3, CD11b-APC, Ly6G-FITC, Ly6C-Percp-Cy5.5 (eBioscience, Inc., San Diego, CA), FITC-CD8, NK1.1-PE, Live/Dead Near-IR (Invitrogen by Thermo Fisher Scientific, Carlsbad, CA), CD8-AF700, CD62L-APC, CD44-AF700, NK1.1 AF700, CD11c-PE, and CCR7 PE-Cy7 (Biolegend, San Diego, CA). The Attune™ NxT (Thermo Fisher Scientific, Waltham, MA) flow cytometer was utilized. Flow data were analyzed by FlowJo Software (FlowJo, LLC Ashland, OR) or Attune NxT Software v3.2.1 (Thermo Fisher Scientific, Waltham, MA). Tumors smaller than 25mm^2 were not analyzed due to an insufficient amount of tissue. Figure 1B shows common initial gates: cells were gated on potential immune cells by FSCxSSC, screened out doublets and clumps, and selected for alive cells. %Alive refers to the percentage of all cells passing through these first three gates. Gates were formulated using full-minus-one (FMO) staining controls as reference.

RNA extraction and qRT-PCR

Cross-sections of tumor weighing less than 100 mg were harvested. Tumor was minced as finely as possible, added to 1 ml Trizol® (Ambion® by Life Technologies, Carlsbad, Ca), and then homogenized by the Fisher Scientific™ PowerGen125 (Thermo Fisher Scientific, Waltham, MA). RNA was extracted according to the manufacturer's protocol. The cDNA reverse transcription reaction utilized the SuperScript™ III First-Strand Synthesis System

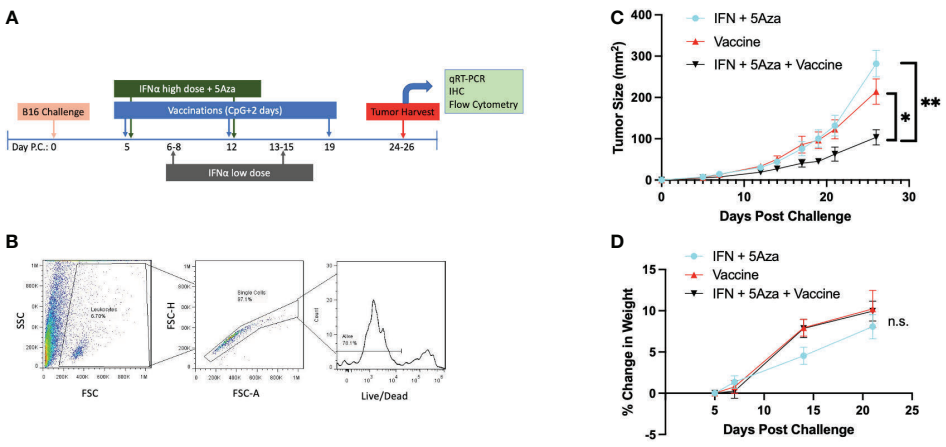

FIGURE 1
Experimental Design and General Characteristics. **(A)** Challenge and treatment outline. **(B)** Flow cytometry initial gating strategy. Potential leukocytes are gated by FSC vs SSC, followed by doublet discrimination, and live cell selection. All flow cytometry data in these studies utilize these three gates. **(C)** Tumor size over time across treatments. Data are represented as average of experimental means across all experiments that have data referenced in this study (N=5). Day 26 time point has significant differences by 2-Way Anova with Tukey's test. *p<0.05; **p<0.01. **(D)** Change in mouse weight across groups and time. Analysis stopped at day 21 before tumor masses became a significant proportion of mouse weight. Data are representative of 6-14 mice across 2-3 independent experiments. Data analyzed by Mixed Effects Analysis with Tukey's test. Relationships are not significant (n.s.).

(Invitrogen ™, Waltham, MA), as per the manufacturer's protocol. Real-time quantitative reverse transcription-PCR (qRT-PCR) was performed utilizing TaqMan® Gene Expression Master Mix or Fast Advanced Master Mix and TaqMan®Gene Expression Assays (Applied Biosystems™ by Thermo Fisher, Halethorpe, MD) with probes specific for mouse GAPDH, XCL1, and CXCL10, utilizing the manufacturer's protocols. Ct threshold was standardized across experiments, and the Ct statistic equated to the average of triplicate technical replicates. For analysis, ΔCt is calculated by subtracting the Ct value of the housekeeping gene GAPDH from that of the gene of interest. qRT-PCR was performed utilizing the StepOnePlus™ machine and software (Applied Biosystems™ by Thermo Fisher, Halethorpe, MD).

Histology

Tumor cross-sections or whole tumors were fixed in 10% neutral buffered formalin. The samples were embedded in paraffin, cut in levels and adhered to slides, and then cuts from the same level were stained with hematoxylin and eosin (H&E) or labelled CD8 by immunohistochemistry (IHC) in parallel by the Sydney Kimmel Comprehensive Cancer Center Histology Core Facility (Baltimore, MD). All H&E and CD8 IHC cases were reviewed by a board-certified dermatopathologist (JCS) who was blinded during histologic scoring and evaluated for overall histologic appearance and degree of immune response. Immune infiltration was scored semi-quantitatively, with 0 for no inflammation, 1 for mild, 2 for moderate, and 3 for strong peripheral and intratumoral T-cell infiltration. Images were digitally brightened by 10%. Images are presented from the 10x objective, and zoomed images were digitally zoomed an additional 2x. Quantitative analysis of the infiltrating CD8+ cells was performed by two individuals blinded to the groups, each counting stained CD8+ cells across 10 random fields per sample (40x objective). The mean value of the 20 fields counted was utilized as the data point for analysis.

Statistics and data

Tumor size, qRT-PCR, and flow cytometric analyses were statistically tested by one-way ANOVA with Tukey's multiple comparison test if dataset distributions were approximately normal or with Dunn's multiple comparison test if not. Normality was assessed by D'Agostino & Pearson test primarily or by Shapiro-Wilk test if the sample size was too small. Scatter plots were analyzed by simple linear regression with Spearman correlation coefficient test. Grouped experiments were analyzed by 2-way ANOVA with Sidak multiple comparison test. Microsoft® Excel (Microsoft Corp, Redmond, WA) was used for database management. Prism 9 (GraphPad Software, Inc. San Diego, CA) was utilized for statistical analyses and figure creation. All error bars represent the estimation of the standard error of the mean, and all midlines represent the group mean. The significance level of $\alpha \leq 0.05$ was set for all experiments. Data provided in (Supplementary file 1).

Results

Tumor model

Figure 1A outlines the therapy schedule utilized both in this study and our prior work (10, 11). Importantly, the tumor growth phenotype remains consistent across experiments (Figure 1C), allowing the studies here to expand on previous work. Since our prior studies found that mice receiving no treatment did not survive to days 24-26 (10, 11), in the current study we decided to compare the three treatment groups to each other. At select time points, mouse weight was measured to ensure the therapeutic regimen did not induce excessive stress. A representative gating strategy indicating the initial steps of gating for samples is shown here as well (Figure 1B). All groups consistently gained weight over time, and there was no significant difference in weight change across the groups (Figure 1D).

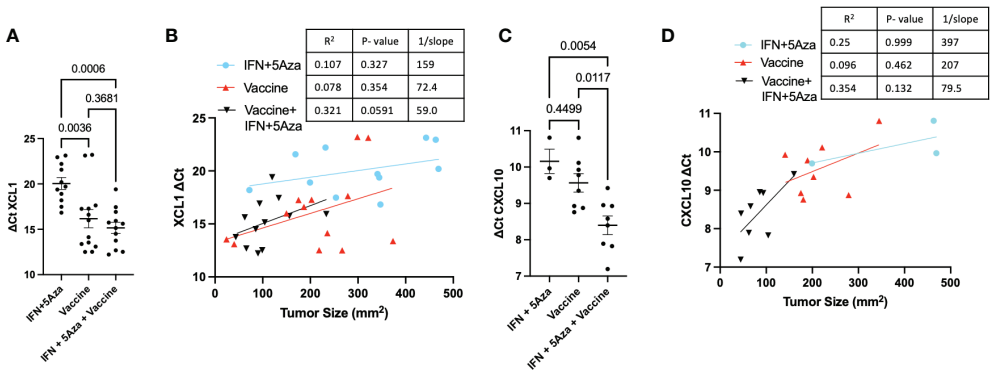

FIGURE 2
Tumor Lysate Chemokine RNA Expression. At harvest, RNA was Extracted from all or a cross-section of tumor and analyzed by qRT-PCR. Values are expressed as ΔCT normalized to GAPDH expression. **(A)** Expression of XCL1 across groups and **(B)** correlated to tumor size. **(C)** Expression of CXCL10 across groups and **(D)** correlated to tumor size. All data represent 2-3 independent experiments with sample sizes ranging from 3-5 per group per experiment. Group comparisons were tested by One-Way Anova with Tukey's multiple comparisons test. Correlations analyzed by Spearman correlation coefficient test.

Tumor lysate chemokine expression

Our previously published data showed significant upregulation of CCL19 in mice receiving combination therapy (11). Since CCL19 has been implicated in homing CCR7+ immune cells to the lymph nodes (12), additional chemokines associated with immune cell infiltration were chosen for qRT-PCR analysis. XCL1, essential in attracting cross-presenting DCs (13), showed higher expression in the vaccine alone ($p = 0.0036$) and combination ($p = 0.0006$) groups compared to IFN + 5Aza (Figure 2A). XCL1 expression was also correlated with trends of reduced tumor size in the combination group ($p = 0.0591$, $R^2 = 0.321$) (Figure 2B). CXCL10 is a primary recruiter of T cells (14), and its transcription levels were also significantly elevated in the combination group compared to both vaccine alone ($p = 0.0117$) and to IFN + 5Aza ($p = 0.0054$) (Figure 2C). Additionally, levels were correlated with trends of reduced tumor size in the combination group ($p = 0.132$; $R^2 = 0.354$) (Figure 2D). In both cases, the combination group is the only group with an R^2 above 0.3. Across all groups, XCL1 (R^2: 0.53, $p<0.001$) and CXCL10 (R^2: 0.584; $p<0.001$) also showed significant overall correlations.

Natural killer and dendritic cells

Emerging evidence suggests that DC- and NK- cell infiltration into the TME aids in mounting an effective anti-tumor response (15, 16). To understand the cellular makeup of the TME, we performed flow cytometric analysis on tumor lysates. Figure 3A shows the gating strategy of representative samples. While there was too much variation to achieve statistical significance, a trend of increased intratumoral infiltration of CD3-CD11c+ DCs was observed between the combination group and the IFN + 5Aza ($p = 0.1138$) and vaccine alone ($p = 0.0738$) groups (Figure 3B). Interestingly, the percentage of CD8+ DCs, representing inflammatory and cross-presenting DCs (17), was modestly increased following vaccination alone ($p = 0.0672$), and significantly increased following combination treatment ($p = 0.0012$) relative to IFN+5Aza (Figure 3C). However, only the combination group had enhanced levels infiltrating the tumor compared to the IFN + 5Aza group ($p = 0.0003$; Figure 3D). Correlation between XCL1 expression and the presence of CD8+ DCs was also highly significant ($p = 0.0055$, $R2 = 0.443$) (Figure 3E). Additionally, the upregulation of CCL19 and CCR7 (11) seen in the combination group, and the fact that CCL19 binds CCR7 directed us to investigate the percent of CCR7+ DCs present in the tumor lysate (Figure 3F), which were significantly higher in the combination group ($p = 0.037$) when compared to the vaccine group. NK cell numbers were also analyzed (representative gating in Figure 3G) and were significantly higher in the combination therapy group when compared to vaccine alone (Figure 3H, $p = 0.0202$).

Myeloid-derived suppressor cells

A category of innate immune cells known as MDSCs (myeloid derived suppressor cells) is often present in the TME and disables an effective anti-tumoral response by potentiating immunosuppressive activity (17). To analyze whether these cells were present in the TME, we performed flow cytometry on the tumor lysate; both classes

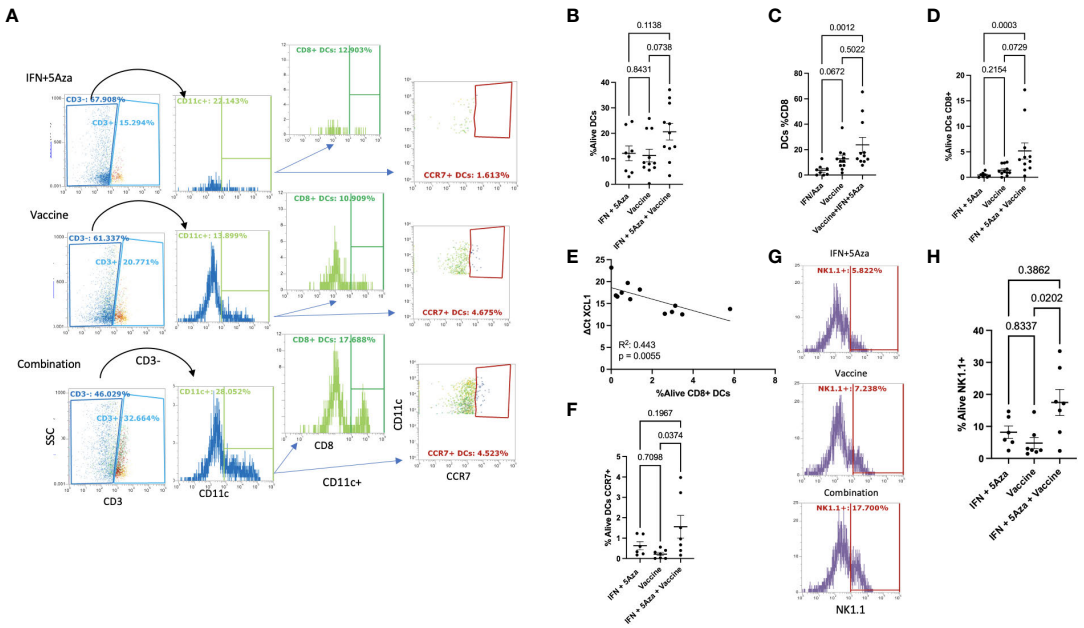

FIGURE 3
Dendritic Cell and Natural Killer Cell Tumor Infiltration. **(A)** Gating of DCs. Single, live, leukocytes (Figure 1B) were selected for CD3 negativity and CD11c positivity to determine the DC population. DC's were analyzed for CD8 and CCR7 expression. Plots shown are representative samples from their groups. **(B)** %Alive analysis of total DCs. **(C)** Analysis of the percentage of DC's that are CD8+ per group. **(D)** %Alive analysis of CD8+ DCs. **(E)** Correlation of XCL1 expression versus %Alive analysis of DC's expressing CD8. **(F)** %Alive DC's expressing CCR7. **(G)** Representative gating of NK1.1 positivity. **(H)** %Alive of NK1.1 positive cells. All data represent 2-3 independent experiments with sample sizes ranging from 3-5 per group per experiment, except panel E, which represents one experiment. Group comparisons were tested by One-Way Anova with multiple comparisons test (Tukey's if approximately Gaussian **(F)** or Dunn's if not **(B–D, H)**. Correlations analyzed by Spearman **(E)** correlation coefficient test.

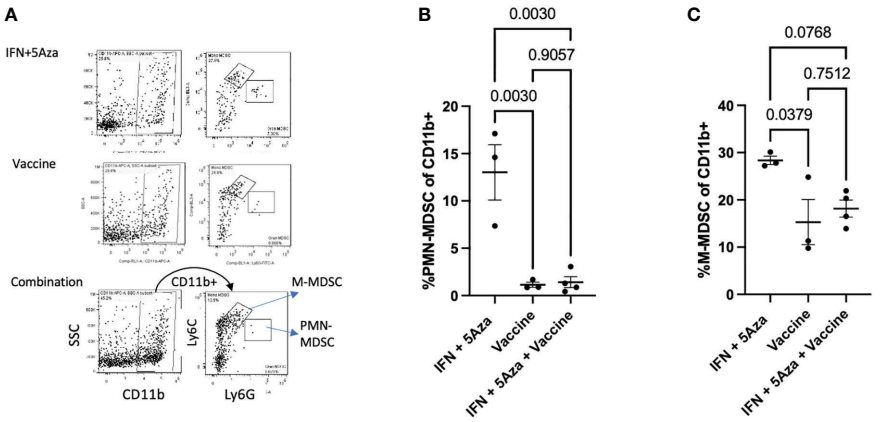

FIGURE 4
MDSC analysis. **(A)** Gating structure. Cells were selected as CD11b+ and then divided into PMN-MDSCs (Ly6G hi/Ly6C lo) and G-MDSCs (Ly6C hi, Ly6G lo). Plots shown are representative samples from their groups. **(B, C)** Grouped analysis as a percentage of CD11b+ cells of **(B)** PMN-MDSCs and **(C)** M-MDSCs. Data are representative of one experiment with 3-4 mice per group and are tested by by One-Way Anova with Tukey's multiple comparisons test.

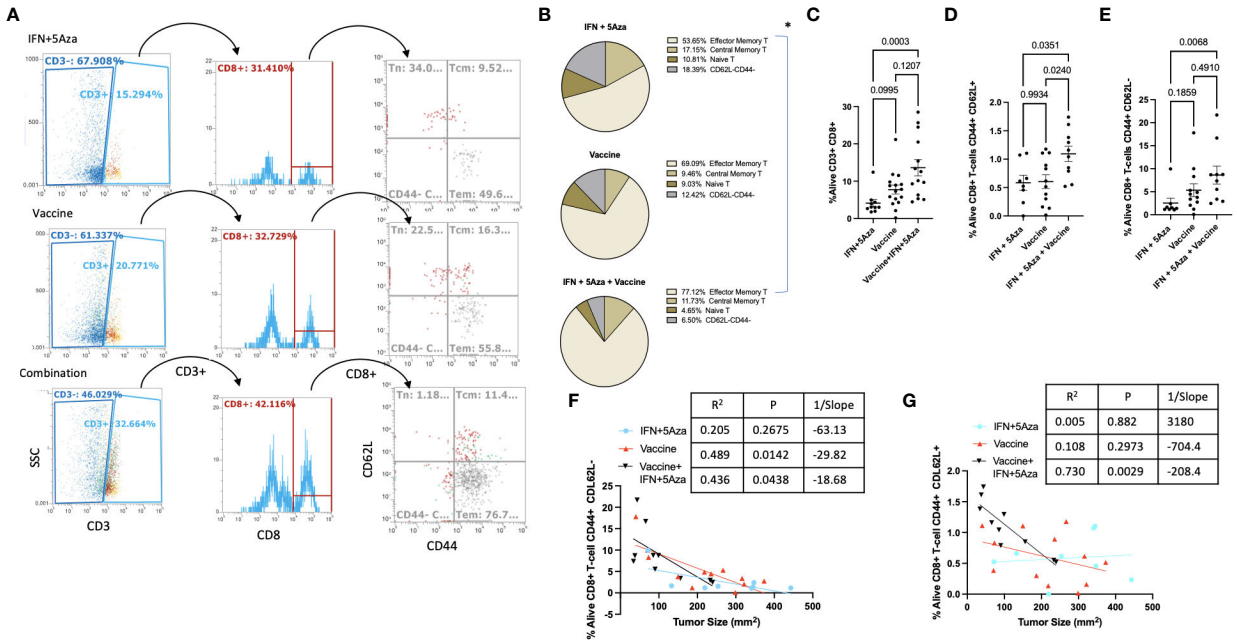

FIGURE 5
T-cell subtype analysis. **(A)** Gating structure. CD3+CD8+ cells are divided by CD44 and CD62L expression patterns. CD44+CD62L- are T effector/effector memory cells, CD44+CD62L+ are central memory T-cells, and CD44-CD62L+ are naïve T-cells. Plots shown are representative samples from their groups. **(B)** For each group, proportions of the three primary subtypes are plotted by pie chart. **(C–E)** %Alive analysis of tumor infiltrating populations of **(C)** all CD8+ T-cells, **(D)** Central Memory CD8+ T-cells, and **(E)** effector/effector memory CD8+ T-cells. **(F, G)** Correlation analysis between **(F)** CD8+ Tem or **(G)** CD8+ Tcm and tumor size. Data are representative of 3-4 independent experiments with 10-16 total mice per group. Groups were tested by One-Way Anova with multiple comparisons: Tukey's test **(B–D)** or Dunn's test **(E)**. Correlations tested by Spearman correlation coefficient test.

of murine MDSCs were analyzed and included M-MDSC (monocytic MDSCs) and PMN-MDSC (polymorphonuclear or granulocytic MDSCs). Figure 4A shows the representative gating strategy. The percent of both PMN-MDSCs (Figure 4B) and M-MDSCs (Figure 4C) were reduced in the vaccine alone and combination therapy groups. The differences between mice receiving the vaccine alone compared to IFN + 5Aza were significant for PMN-MDSCs ($p = 0.003$) and M-MDSCs ($p = 0.0379$). When comparing combination therapy to IFN + 5Aza, there was significant reduction of PMN-MDSCs ($p = 0.003$) and a trend towards reduction of M-MDSCs ($p = 0.0768$).

Tumor infiltrating lymphocytes

Our previous data indicated increased levels of CD8+ T cells in the combination therapy group (10, 11), and findings from this

study confirmed those results. Figure 5A shows the representative gating strategy used to stratify CD8+ T cells, and total CD8+ T cells were significantly enriched in the combination group compared to IFN + 5Aza (Figure 5C, p = 0.0003) and trending towards significance in vaccine alone (p=0.1207). To understand differences in CD8+ T-cell composition, CD3+ CD8+ T cells were further gated on CD44 and CD62L to categorize effector (CD44+ CD62L-), naive (CD44- CD62L+), and central memory (CD44+ CD62L+) T cells (Figure 5A). When total CD8+ T cells were stratified based on percentage, naïve and double negative (CD44- CD62L-) T cells were qualitatively lower in the combination therapy group compared to mice receiving either IFN + 5Aza or vaccine alone, and the combination group was primarily composed of central memory and effector memory T cells (Figure 5B). Importantly, the combination therapy group showed significantly higher amounts of effector memory CD8+ T cells (Figure 5E, p = 0.0068) compared to mice receiving IFN + 5Aza, and also showed increased numbers of central memory T cells relative to both mice receiving vaccine alone (p = 0.024) and IFN+ 5Aza (p = 0.0351) (Figure 5D). Furthermore, the correlations between decreased tumor size and increased CD8+ T effector memory cell or CD8+ T central memory cell infiltration into the TME in the combination treatment group (p = 0.0438, R^2 = 0.436; Figure 5F, p = 0.0029, R^2 = 0.73; Figure 5G respectively) were significant.

Immunohistochemistry

A representative sample of four tumors per group across two experiments were selected for microscopy analysis. Tumor cross-sections were mounted onto slides and stained for H&E and CD8 by immunohistochemical methods. Figure 6A shows representative images with selected clusters of CD8+ cells pointed to with arrows, with areas of interest outlined in boxes and zoomed an additional 2-fold to more clearly show the stained cells. In all the IFN + 5Aza samples and three out of four vaccine-only samples, CD8+ cells were visualized primarily around peritumoral vessels but not infiltrating the tumor mass (arrows, Figure 6A left and middle). Three out of four samples from the combination group showed substantial infiltration of CD8+ cells into the tumor mass (arrows, Figure 6A right). Figure 6B provides evidence that our sampling was representative, as the tumor size averages did not significantly differ from across group means.

Additionally, the samples were scored in a group-blinded fashion for level of inflammation ranging from 0-3 (Figure 6C). The IFN + 5Aza group showed little inflammation with one out of four samples scored as 0, and three with minimal inflammation, scored as 0+ to 1. The vaccine alone group showed higher variability, with one tumor lacking any inflammation (scored 0), two showing only peripheral CD8+ cell accumulation (scored 0+ to 1), and one with peripheral accumulation and intratumoral penetration (scored 2). The combination group resulted in the highest proportion of cases with both peripheral CD8+ cell accumulation and CD8+ cell penetration, with three out of four samples scored at 2.

To provide quantitative analysis of the infiltration of CD8+ cells into the tumor mass, twenty total randomly selected parenchymal 40X objective microscope fields per sample were counted by two group-blinded individuals. Figure 6D shows that the combination group had significantly more CD8+ cells that infiltrated the tumor parenchyma as compared to IFN+5Aza (p=0.0266) and to vaccine alone (p=0.0316).

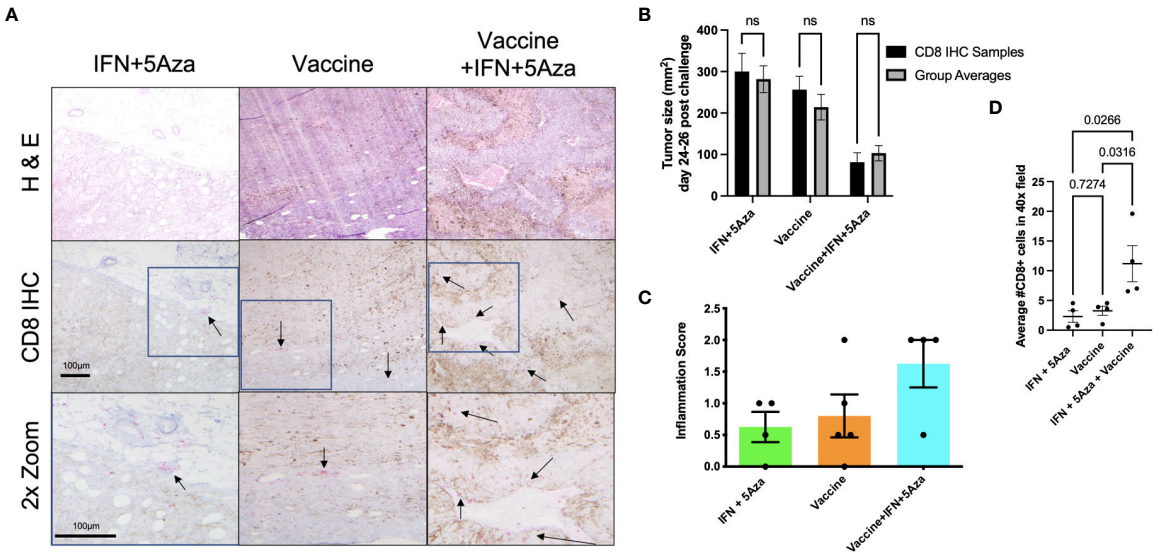

FIGURE 6
CD8 Immunohistochemistry (IHC). **(A)** IHC of tumor sections. CD8+ cells were stained with pink color to differentiate from brown melanin background. Representative images were selected and scored by group-blinded dermatopathologist from slides stained from 4 samples per group across two independent experiments. Top two rows utilized 10x objective. Bottom row images were digitally zoomed 2x from boxes in middle row. Arrows are pointing to select clusters of CD8+ cells. **(B)** Tumor size comparison of CD8 IHC samples to group averages across experiments, tested by 2-way Anova with Sidak multiple comparison test; n.s. = not significant. **(C)** Semi-quantitative tumor inflammation scores. **(D)** Average of CD8+ cell counts from twenty random and blinded fields per sample from parenchymal regions using a 40x objective, tested by One-way Anova with Tukey's multiple comparison test.

Discussion

Treatment of late-stage tumors, including metastatic melanoma, has historically been challenging as elements within the TME interfere with immune cell infiltration and limit an effective anti-tumoral response (18). Combining traditional therapies with other treatment options including immunotherapy, however, has yielded impressive results and improved prognosis (19–21).

In our study, we utilized a MIP3α fused vaccine targeting two common melanoma antigens, gp100 and trp2, in combination with 5Aza and IFN. Previously published data indicated high efficacy of this combination therapy compared to vaccine or 5Aza and IFN alone, as manifested by greater median survival time and reduced tumor burden in mice given the combination therapy. Our work also indicated that this group had greater CD8+ T-cell infiltration into the TME, as well as significant CCL19 upregulation (11). These findings prompted this study, which reinforced the CD8+ T-cell data (Figure 5C), but also introduced the possibility of DC and NK cell anti-tumoral action in the TME (Figure 3) and highlighted the immunosuppressive role MDSCs may play in dampening immune responses (Figure 4). Additionally, we also noted upregulation of the chemokines CXCL10 and XCL1 (Figure 2); XCL1 in the combination group was upregulated relative to the IFN+5Aza group, and CXCL10 in the combination group was upregulated relative to both vaccine alone and IFN + 5Aza groups. Furthermore, stratification of CD8+ T-cells revealed increased percentages of effector memory and central memory T-cells in the combination group (Figures 5E, D), which were highly correlated with decreased tumor burden (Figures 5F, G). Importantly, results from this study further define immunological mechanisms underlying the synergism seen previously of all combination therapy components in enhancing survival and anti-tumoral activity (11).

Optimally activated CD8+ T cells are critical to tumor control, and the presence of both effector memory and central memory CD8+ T cells has also been correlated with an effective anti-tumoral response. Our findings indicate that the combination therapy can elicit an effective memory response, which is critical to remission (22, 23). In many solid tumors including melanoma, immune infiltration into the TME is depressed and leads to a limited immune response ineffective in killing the cancer cells (18). A high expression of chemokines related to DC, NK, and T-cell recruitment within the TME has been associated with greater influx of these cells into the tumor and consequently, better prognosis (15, 16, 24). We saw heightened expression of CCL19 (11), CXCL10, and XCL1 in mice treated with the combination therapy, suggesting the creation of an environment favoring greater immune cell influx. CCL19 binds to CCR7 on a multitude of cell types including DCs and T-cells, whereas CXCL10 is a is a canonical chemokine for attracting T-cells (14), and its upregulation is correlated with smaller tumor size. XCL1, on the other hand, is secreted by activated NK cells and CD8+ T-cells and is part of the Th1 response. It binds XCR1, present on conventional DCs type 1 (cDC1), NK cells, and CD8+ T-cells (13). Bottcher et al. (25) found that XCL-1 and CCL5 secreting NK cells promoted cDC1 infiltration into the TME, which was correlated with higher survival and better prognosis, and other studies have also noted the anti-tumoral role facilitated by DC-NK crosstalk (26). It is possible that these processes are also occurring in our system.

These results, when taken together, indicate that the combination therapy is integral in creating an effective anti-tumoral environment composed overall of CD8+ T-cells of memory phenotypes, CD8+ DCs, and NK cells. We believe that this occurs primarily by increased immune cell trafficking into the TME, as seen by the IHC (Figure 6). This increased immune infiltration into the TME requires the presence of all three components of the combination therapy and is likely not attributed to a singular element. This is best demonstrated by the IHC data, where the combination group has consistently higher levels of inflammation and of CD8+ cells infiltrating the tumor parenchyma compared to the IFN+5Aza and vaccine alone groups. The recruitment of these cells is likely due to the upregulation of CCL19, CXCL10 and XCL1, among other potential untested targets, which enable cells to respond to the chemokine gradient and infiltrate the TME.

Overall, our results suggest that the establishment of an effective tumor-killing environment composed of favorable cell types, such as DCs, CD8+ memory T-cells, and NK cells, as well as important chemokines, including CCL19, CXCL10, and XCL1 relies on all aspects of the combination therapy. This study provides evidence for well-designed cancer vaccines as an important arm of combined therapy and supports the use of combination therapies in the clinic for metastatic tumors. Future studies will aim to further define the TME, and the protective immune responses elicited by combination treatment. A lung metastatic model of the disease will also be incorporated to extend our knowledge of treatment efficacy.

Data availability statement

The original contributions presented in the study are included in the article/supplementary material. Further inquiries can be directed to the corresponding author.

Ethics statement

The animal study was reviewed and approved by the IACUC of the Johns Hopkins University under Protocols #MO16H147 and MO19H139.

Author contributions

JG and AS performed and analyzed the experimental studies and co-wrote the manuscript. KF performed confirmatory studies and XCL1 qRT-PCR. KL, AK, SA, YH, and SK assisted with animal studies, tissue processing, and assays. CS, IC, and TW assisted with manuscript revision and microscope analyses. JS performed the immunohistochemical analysis. PK and RM contributed to the conception and design of the experiments and the writing of the manuscript. All authors contributed to the article and approved the submitted version.

Funding

This study was supported by NIH grants R01AI148710 to PK and RM and K24AI143447 to PK, by discretionary funds available to RM, and by the Dermatology Foundation Dermatopathology Career Development Award to JS.

Acknowledgments

We would like to acknowledge the staff at JHU Research Animal Resources for their assistance with animal care. We would also like to acknowledge the JHU Oncology Tissue Services core facility for embedding tumor tissue in paraffin and making and staining slides (partially supported by the SKCCC Cancer Center Support Grant (CCSG; P30 CA006973)). The StepOne Plus Real-time qPCR systems and the Attune Flow Cytometer were provided and supported by Johns Hopkins Malaria Research Institute and Department of Molecular Microbiology and Immunology (MMI). We thank Anne Jedlicka and Amanda Dziedzic in the JHSPH Genomic Analysis and Sequencing Core and Dr. Prakash Srinivasan (MMI) for core facility management, technological expertise, and instrument support.

Conflict of interest

Authors RM and JG are inventors on a patent 11419928 for the vaccine that has been issued to Johns Hopkins University.

The remaining authors declare that the research was conducted in the absence of any further commercial or financial relationships that could be construed as a potential conflict of interest.

Publisher's note

Supplementary material

The Supplementary Material for this article can be found online at: https://www.frontiersin.org/articles/10.3389/fimmu.2022.1074644/full#supplementary-material

References

1. Sung H, Ferlay J, Siegel RL, Laversanne M, Soerjomataram I, Jemal A, et al. Global cancer statistics 2020: Globocan estimates of incidence and mortality worldwide for 36 cancers in 185 countries. *CA: A Cancer J Clin* (2021) 71:209–49. doi: 10.3322/caac.21660

2. Siegel R, Miller K, Fuchs H, Jemal A. Cancer statistics, 2022. *Cancer Journal for Clinicians* (2022) 72(1):7–33. doi: 10.3322/caac.21708

3. Jenkins RW, Barbie DA, Flaherty KT. Mechanisms of resistance to immune checkpoint inhibitors. *Br J Cancer* (2018) 118:9–16. doi: 10.1038/bjc.2017.434

4. Aricò E, Castiello L, Capone I, Gabriele L, Belardelli F. Type I interferons and cancer: An evolving story demanding novel clinical applications. *Cancers* (2019) 11:1043. doi: 10.3390/cancers11121943

5. Grosser R, Cherkassky L, Chintala N, Adusumilli PS. Combination immunotherapy with CAR T cells and checkpoint blockade for the treatment of solid tumors. *Cancer Cell* (2019) 36:471–82. doi: 10.1016/J.CCELL.2019.09.006

6. Hu C, Liu X, Zeng Y, Liu J, Wu F. DNA Methyltransferase inhibitors combination therapy for the treatment of solid tumor: Mechanism and clinical application. *Clin Epigenet* (2021) 13:1–16. doi: 10.1186/S13148-021-01154-X

7. Saxena M, van der Burg SH, Melief CJ, Bhardwaj N. Therapeutic cancer vaccines. *Nat Rev Cancer* (2021) 21:360–78. doi: 10.1038/s41568-021-00346-0

8. Alfei F, Ho P-C, Lo W-L. DCision-making in tumors governs T cell anti-tumor immunity. *Oncogene* (2021) 40:5253–261. doi: 10.1038/s41388-021-01946-8

9. le Borgne M, Etchart N, Goubier A, Lira SA, Sirard JC, van Rooijen N, et al. Dendritic cells rapidly recruited into epithelial tissues *via* CCR6/CCL20 are responsible for CD8+ T cell crosspriming *in vivo*. *Immunity* (2006) 24:191–201. doi: 10.1016/J.IMMUNI.2006.01.005

10. Gordy JT, Luo K, Zhang H, Biragyn A, Markham RB. Fusion of the dendritic cell-targeting chemokine MIP3α to melanoma antigen Gp100 in a therapeutic DNA vaccine significantly enhances immunogenicity and survival in a mouse melanoma model. *J Immunother Cancer* (2016) 4:96. doi: 10.1186/s40425-016-0189-y

11. Gordy JT, Luo K, Kapoor A, Kim ES, Ayeh SK, Karakousis PC, et al. Treatment with an immature dendritic cell-targeting vaccine supplemented with IFN-α and an inhibitor of DNA methylation markedly enhances survival in a murine melanoma model. *Cancer Immunol Immunother* (2020) 69(4):569–80. doi: 10.1007/s00262-019-02471-0

12. Yan Y, Chen R, Wang X, Hu K, Huang L, Lu M, et al. CCL19 and CCR7 expression, signaling pathways, and adjuvant functions in viral infection and prevention. *Front Cell Dev Biol* (2019) 7:212. doi: 10.3389/fcell.2019.00212

13. Kroczek RA, Henn V. The role of XCR1 and its ligand XCL1 in antigen cross-presentation by murine and human dendritic cells. *Front Immunol* (2012) 3:14. doi: 10.3389/fimmu.2012.00014

14. Karin N. CXCR3 ligands in cancer and autoimmunity, chemoattraction of effector T cells, and beyond. *Front Immunol* (2020) 11:976/BIBTEX. doi: 10.3389/FIMMU.2020.00976/BIBTEX

15. Nersesian S, Schwartz SL, Grantham SR, MacLean LK, Lee SN, Pugh-Toole M, et al. NK cell infiltration is associated with improved overall survival in solid cancers: A systematic review and meta-analysis. *Transl Oncol* (2021) 14. doi: 10.1016/J.TRANON.2020.100930

16. Szpor J, Streb J, Glajcar A, Fraczek P, Winiarska A, Tyrak KE, et al. Dendritic cells are associated with prognosis and survival in breast cancer. *Diagnostics* (2021) 11:702. doi: 10.3390/diagnostics11040702

17. Kumar V, Patel S, Tcyganov E, Gabrilovich DI. The nature of myeloid-derived suppressor cells in the tumor microenvironment. *Trends Immunol* (2016) 37:208–20. doi: 10.1016/j.it.2016.01.004

18. Jiang Y, Li Y, Zhu B T-cell exhaustion in the tumor microenvironment. *Cell Death and Disease* (2015) 6(6):e1792. doi: 10.1038/cddis.2015.162

19. Pérez-Romero K, Rodríguez RM, Amedei A, Barceló-Coblijn G, Lopez DH. Immune landscape in tumor microenvironment: Implications for biomarker development and immunotherapy. *Int J Mol Sci* (2020) 21:1–14. doi: 10.3390/IJMS21155521

20. Sodergren MH, Mangal N, Wasan H, Sadanandam A, Balachandran VP, Jiao LR, et al. Immunological combination treatment holds the key to improving survival in pancreatic cancer. *J Cancer Res Clin Oncol* (2020) 146:2897–911. doi: 10.1007/s00432-020-03332-5

21. Lucarini V, Buccione C, Zicchedda G, Peschiaroli F, Sestili P, Puglisi R, et al. Combining type I interferons and 5-Aza-2′-Deoxycitidine to improve anti-tumor response against melanoma. *J Invest Dermatol* (2017) 137:159–69. doi: 10.1016/J.JID.2016.08.024

22. Ayoub NM. Editorial: Novel combination therapies for the treatment of solid cancers. *Front Oncol* (2021) 11:708943. doi: 10.3389/fonc.2021.708943

23. Perret R, Ronchese F. Memory T cells in cancer immunotherapy: Which CD8+ T-cell population provides the best protection against tumours? *Tissue Antigens* (2008) 72:187–94. doi: 10.1111/J.1399-0039.2008.01088.X

24. Shortman K, Heath WR. The CD8+ dendritic cell subset. *Immunol Rev* (2010) 234:18–31. doi: 10.1111/J.0105-2896.2009.00870.X

25. Böttcher JP, Bonavita E, Chakravarty P, Blees H, Cabeza-Cabrerizo M, Sammicheli S, et al. NK cells stimulate recruitment of cDC1 into the tumor microenvironment promoting cancer immune control. *Cell* (2018) 172:1022–037.e14. doi: 10.1016/J.CELL.2018.01.004

26. Peterson EE, Barry KC. The natural killer–dendritic cell immune axis in anti-cancer immunity and immunotherapy. *Front Immunol* (2021) 11:621254/BIBTEX. doi: 10.3389/FIMMU.2020.621254/BIBTEX

Frontiers in Immunology

Explores novel approaches and diagnoses to treat immune disorders.

The official journal of the International Union of Immunological Societies (IUIS) and the most cited in its field, leading the way for research across basic, translational and clinical immunology.

Discover the latest Research Topics

See more →

Frontiers

Avenue du Tribunal-Fédéral 34
1005 Lausanne, Switzerland
frontiersin.org

Contact us

+41 (0)21 510 17 00
frontiersin.org/about/contact